International Mine Water Association Conference 2026

Sustainability & Efficiency

Jeongseon, Gangwon Province
South Korea

5 – 10 July 2026

Duk-Min Kim
Ritva Mühlbauer
Christian Wolkersdorfer

IMWA 2026
Jeongseon

IMWA 2026

Jeongseon

International Mine Water Association Conference – Sustainability & Efficiency

IMWA 2026
Jeongseon

International Mine Water Association Conference – Sustainability & Efficiency

Proceedings of the International Mine Water Association Conference

July 5–10, 2026

Jeongseon, South Korea

Editors

Duk-Min Kim

Ritva Mühlbauer

Christian Wolkersdorfer

International Mine Water Association Conference 2026 – Sustainability & Efficiency
2026, Jeongseon, South Korea

ISBN 978-3-9825293-4-9

© International Mine Water Association 2026

Editors
Duk-Min Kim, Ritva Mühlbauer, Christian Wolkersdorfer

Cover design
Christian Wolkersdorfer, ChatGPT

Layout and Typesetting
Jigsaw Graphic Design & Christian Wolkersdorfer

Cover Photographs
ChatGPT generated, Duk-Min Kim, Mathew Schwartz at Unsplash

All abstracts were reviewed by 2–6 experts of the International Scientific Committee.

All full papers were peer-reviewed by 2–3 experts from the International Scientific Committee. Authors were asked to correct their papers after the review and those that did not meet the requirements of the IMWA proceedings were rejected.

www.IMWA.info

Organizers

International Mine Water Association

SANGJI UNIVERSITY

Sangji University, South Korea

International Scientific Committee (ISC)

Rodrigo Alvarez
John George Annandale
Margarida Horta Antunes
Norberto Jr Aquino
David Arcos
Tim Aubel
Okan Aygün
Mattias Bäckström
Abie Badhurahman
Jeff Bain
Felipe Barbosa
Fernando Barrio-Parra
Zuzana Bártová
MaryBeth Berkes
Melanie Lise Blanchette
Dantie Claudia Butar Butar
Joanna Butlanska
Paula Carvalho
Devin Castendyk
Patricia Sekina Chagonda
Youngwook Cheong
Frances Chikanda
Vitalis Chipakwe
Yosoon Choi
Eunhyea Chung
Lucie Coudert
Ronan Courtney
Roberto Pereira da Silva
Priyal Dama-Fakir
Matthew John Damhuis
Camilo Raul de los Hoyos
Julia Dent
Nathan Cory DePriest
Ramón Díaz
Gareth Digges La Touche
Yanqing Ding
Donglin Dong
Lucila Dunnington
Nuno Durães
Sendy Dwiki
Elnaz Eghlidi
Mariana Erasmus
Marcus Fahle
Marlese Fairgray
Hernan Flores
Alfredo Gallardo
Peter Goerke-Mallet
Andres Gonzalez Quiros
Jabulani Gumbo
Lenka Hagarová
Florian Hahn
Takaya Hamai
Edmund Kevin Hardwick
Robert S Hedin
Benjamin Hedin
Asieh Hekmat
Xiaotong Huang
Paul Hubbard
Imane Hzikar
Suhaina Ismail
Judith Liliana Jaeger Collantes
Sajjad Jannesar Malakooti
Sangwoo Ji
Myung Chae Jung
Ohene Karikari-Yeboah
Uzair Akbar Khan
Recardo Derely Sibusiso Khumalo
Duk-Min Kim
Robert Lawrence Kleinmann
Petr Kuznetsov
Alsu Kuznetsova
Stéphane Lafortune
Soonjae Lee
Jae Myung Lee
Tiina Leiviskä
Colin A Lennox
Simon Antony Lorentz
Paul Joel Lourens
Mark Lund
Rudzani Lusunzi
Joseph Ddumba Lwanyaga
Liyuan Ma
Ann Maest
Mamile Belina Mahlohla
Saeid Maknooni Gilani
Malibongwe Shadrach Manono
Abdelkabir Maqsoud
Genevieve Marchand

Mokhinabonu Mardonova
Paula Marinho Reis
Antonio Luis Marqués Sierra
Khodani Matshusa
Cherie McCullough
Matthew P. McGann
Hsan Youssef Mehdaoui
Ryan David Merckel
Broder Merkel
Kym Lesley Morton
Ritva Muhlbauer
Ronald H Mullennex
Kevin Myers
Amirhossein Najafabadipour
combined
Aracelis Narayan
Sofia Angelina Nazaruk
Carmen Mihaela Neculita
Gustavo Neira-Arenas
Helene Flore Nguemgaing
Katarzyna Niedbalska
Emma-Tuulia Katariina Nurmesniemi
Maria Almudena Ordóñez Alonso
Oscar Osores
Sheyla Palomino Ore
Ilhwan Park
Benoît Plante
Nele Pollmann
Bolormaa Purevjav
Mokabolane Innocent Rabohale
Aicha Rahmouni
Jill Leighanne Riddell
Pierre Rousseau
Tobias Rudolph
Carlos Ruiz Cánovas
Netramani Sagar
David Anthony Salmon
Ralph Schöpke
Logan Schultz
Yon-Sik Shim
Albert Shumba
Alison Sinclair
Givarn Singh
Viktor Sjöberg
Stephanie Somot
Gideon Steyl
Roald Alexander Strand
Wanghua Sui
Małgorzata Szlachta
Salamatu Joana Tannor
Barbara M.A. Teichert
Mark John Thomasson
Craig Thompson
Heather Thomson
Tuan Quang Tran
Viswanath Ravi Kumar Vadapalli
Teresa Maria Valente
Rob Van Hille
Stéphane Vaxelaire
Rens Verburg
Danie Vermeulen
Dickson Wachira
Xingjie Wang
John Douglass Waterhouse
Thomas Wenzel
Godfred Williams-Nanyaa
Christian Wolkersdorfer
Peter Woods
Magdalena Worsa-Kozak
Qiang Wu
Yang Xiang
Tetsuo Yasutaka
Sergio Yi
Huichao Yin
John Ngoni Zvimba

Local Organizing Committee (LOC)

Duk-Min Kim
Christian Wolkersdorfer
Elke Mugova
Seong-Jun Cho
Myung-Chae Jung
Gil-Jae Yim
Sang-Woo Ji
Youngwook Cheong
Dong-Kil Lee
Seong-Sook Park
Tae-Heok Kim
Young-Kook Jung
Ju-In Ko
Tackhyun Kim
Jay-Hyun Park
Youn-Soo Oh
Joon-Hak Lee
Jin-Soo Lee
Ye-Ji Kim
Yon-Sik Shim
Kwang-Soo Nam
Changhee Lee
Yeong-Hwan Kim
Shin-Yeong Kong
Kirim Lee
Young-Min Kim
Dae-Gyu Im
Da-Som Kim
Jae-Hyun Park

IMWA 2026
Jeongseon

Sponsors

Silver

Korea Mine Rehabilitation and Mineral Resources Corp.
KOMIR

srk consulting

(주) 이앤켐솔루션
Environment Energy & Chemical Solution

Bronze

HUESKER
Ideen. Ingenieure. Innovationen.

BYUCKSAN ENGINEERING

SANHA E&C

Supported by

KOREA TOURISM ORGANIZATION

GWTO Gangwon Tourism Organization

한국자원공학회
The Korean Society of Mineral and Energy Resources Engineers

정선군
JEONGSEON COUNTY

SANGJI UNIVERSITY

high1 RESORT

KIGAM 한국지질자원연구원
Korea Institute of Geoscience and Mineral Resources

Contents

Conference Papers – Peer Reviewed

Abfertiawan, Muhammad Sonny; Edytya, Agventy Nuranis; Syafila, Mindriany; Hasan, Faiz
Leaching behavior of hexavalent chromium from nickel processing residues: a free draining column study on dry tailings and nickel slag 1

Aquino, Norberto Jr; Salifu, Musah; Novikova, Ksenia; Månsson, Erik; Ronne, Erik; Alakangas, Lena
Mechanisms of Arsenic (As) release and retention during Fenton treatment of mine wastewater 7

Bäckström, Mattias; Sartz, Lotta; Johansson, Thomas; Säfström, Maria; Sädbom, Stefan
Abandoned mines as pumped hydro storage power plants – a strategy for geochemical characterization of mine water before operation 12

Bamforth, Selina Mary; Potter, Hugh; Cox, Nick; Sapsford, Devin
Innovative passive treatment technologies for UK metal mine waters 18

Barrio-Parra, Fernando; Montalvo-Piñeiro, Jaime; Álvarez-Mejías, Lucía; Serrano-García, Humberto; Izquierdo-Díaz, Miguel; Ordoñez, Almudena; Álvarez, Rodrigo; De Miguel, Eduardo
Predicting contamination pathways in mining-affected watersheds using a cellular automaton 23

Barroso, Ana Raquel; Vasques, Isabela; Antelo, Juan; Fiol, Sarah; Carabante, Ivan; Horta Ribeiro Antunes, Isabel Margarida; Marinho Reis, Amélia Paula; Valente, Teresa Maria
The role of secondary iron phases in acid mine drainage: implications for contaminant mobilization 28

Bártová, Zuzana; Fabián, Martin; Briančin, Jaroslav
From AMD to pigments: Biological iron oxidation and characterization of recovered iron precipitates 35

Bazardorj, Sod-Erdene; Puntsag, Tamir; Batbayar, Uugankhuu; Purevsuren, Uuganbayar
Water management sustainable implementation at a remote water-scarce mine site of Mongolia 41

Benson, David; Miller, Savannah
Probabilistic estimation of aquifer properties and non-linear well losses to support dewatering forecasts and planning 47

Bettoni, Laura Nina; Hellman, Maria; Hallin, Sara; Johansson, Maria Elisa; Salmi, Tomas; Sokolova, Ekaterina; Tuncer, Elif; Ylipää, Mattias; Herbert, Roger B.
Performance of a sulfate-reducing bioreactor for sulfate removal under cold climate conditions 54

Chikanda, Frances; Nakamura, Fugo; San, Hkaung; Otake, Tsubasa; Sato, Tsutomu
Simultaneous acid mine drainage remediation and carbon sequestration via enhanced rock weathering in Japan and Zambia 60

Chipakwe, Vitalis; Berry, Luke; Lundell, Peter; Ronne, Ksenia; Novikova, Ksenia; Suup, Malin
Electrochemical treatment of Maurliden mine AMD using Clean&Recover ECR™ technology 66

Choe, Yonghwan; Lee, Seon-Yong; Yim, Gil-Jae; Lee, Hayeon; Kwon, Soondong; Park, Jeong Sik; Hwang, Huijeong; Ji, Sangwoo
Valorization of manganese sludge from mine drainage treatment facility: development of alginate-based adsorbent beads for dissolved manganese removal 72

Choi, Euna; Kim, Duk-Min; Rodriguez-Vasquez, Carmen; Bottger-Gamarra, Joyce Carol; Santos-Conde, Alina Liliana; Requena-Mendizabal, Manuel; Rivera Blanco, Edward; Anaya-Hilario, Isabel Magaly; Torres-Aguilar, Carlos Cheito; Servan-Vargas, Mario; Jeon, Jong-Wook; Kim, Yo-Han; Kang, Seyoung; Jung, Youngkook
Pilot-scale passive treatment including slag reactors, As adsorption reactors, and vertical flow reactors for mine drainages in Peru 74

Choo, Yeon Moon; Oh, Jung Geun; Hwang, Dong Shin; Kim, Hee Dae; Yoon, Daewan; Choo, Tai Ho
Neutralization and metal stabilization of acid mine drainage using an inorganic–mineral–polymer composite system 76

Choo, Yeon Moon; Oh, Jung Geun; Hwang, Dong Shin; Kim, Hee Dae; Yoon, Daewan; Choo, Tai Ho
Soil neutralization and trace metal stabilization in abandoned mine areas using a composite soil stabilization system 80

Chun, Chan Lan; Larson, Britta; Thompson, John; Castillo, Mariel; Washburn, Spencer; Dufresne, Kevin; Kolka, Randy
Design and operation of a scalable electrochemical–biological sulfur bioreactor for mine water treatment 85

Čičáková, Claudia; Bártová, Zuzana; Hagarová, Lenka; Mačingová, Eva; Zeman, Josef; Kupka, Daniel
Geochemical pathways and kinetic controls of Fe(II) oxidation and secondary mineral formation in acid sulfate waters from siderite deposit (Slovakia) 91

Conde, Eduardo; Reina, Pablo; Serrano-García, Humberto; Barrio-Parra, Fernando; Izquierdo-Díaz, Miguel; Fernández-Gutiérrez del Álamo, Luis; Mazadiego, Luis; De Miguel, Eduardo
Low-Cost Environmental Monitoring System for water parameters measurement in mining 97

Dano, Dayle Tranz; Park, Ilhwan; Ito, Mayumi; Tabelin, Carlito; Resabal, Vannie Joy
Treatment of Simulated Copper-Zinc-Bearing Acid Mine Drainage Using Scrap-Derived Aluminum–Iron Bimetals and Implications for Downstream Metal Recovery 98

de los Hoyos, Camilo Raúl; González, Claudina; Canavessi, Juana María; Leybourne, Matthew; Layton-Matthews, Daniel; Verri Kozlowski, Alejandro; Bowell, Robert
Natural and mining-related sulfate sources at two high-sulfidation deposits constrained by a triple-tracer Bayesian isotope mixing model 104

Dendup, Tshewang; Lund, Mark; Bernasconi, Rachele
Source water characterization in a rehabilitated mine pit lake using natural tracers and mixing model – a pilot study 110

DePriest, Nathan; Spirnak, Rachel
Implementing the watershed-scale approach to remediation of acid mine drainage from abandoned mine lands in West Virginia, USA 117

Ding, Jia; Dong, Shuning; Guo, Xiaoming; Liu, Feng; Zhang, Wenzhong
Study on water quality evolution of water inrush from typical coal mine roof Cretaceous aquifer in western china mining area 124

Dong, Shuning; Zhang, Xiyu; Shi, Hongjie; Wu, Qiang; Guo, Xiaoming; Wang, Tiantian; Liu, Feng; Dong, Donglin; Sun, Wenjie; Zeng, Yifan; Li, Peitao
Geochemical responses and environmental feasibility of managed aquifer recharge with mine water in coal mining areas 129

du Preez, Kerri; Merckel, Ryan
Demonstration of a biological sulfate reduction process at scale, treating acidic, sulfate-laden mining-influenced water 136

Du, Guri; Ho, Hsing-Jung; Kondo, Masataka; Masaki, Yusei; Hamai, Takaya; Iizuka, Atsushi
Development of a CO2 accounting methodology for acid mine drainage treatment processes and CO2 emission assessment of real sites 142

Dzimbanhete, Vimbainashe Lorraine; Karlsson, Torbjörn; Paulsson, Oscar; Alakangas, Lena
Elemental and isotopic tracers as tools for understanding mine water geochemistry – insights from an iron ore mine site in Northern Sweden 149

Fahle, Marcus; Lau, Maximilian P.; Röder, Eric; Licht, Gero; Weber, Anne; Zug, Sebastian
Improving pit lake monitoring by using a combination of autonomous robotic devices and drones 156

Fairgray, Marlese; du Plessis, Gert
Advances in pit lake water quality monitoring using Unmanned Aerial Vehicles 157

Febriana, Adithyanti; Gunathunga, Samadhi; Ñancucheo, Iván; Southam, Gordon; Gomez, Denys Villa
Bioremediation of acid and metalliferous drainage using sulfate-reducing bacteria 162

Flores, Hernan; Reker, Bastian; Dogan, Tansel; Marquez, Antonio; Krzemień, Alicja; Păsculescu, Vlad Mihai
Revalorization of coal waste facilities: The CRMsDataSpace EU Approach 169

Flores, Hernan; Teichert, Barbara M.A; Nikutta, Simon; Rudolph, Tobias
Multi-Temporal UAV hyperspectral monitoring of a mine-water influenced pond system: Harpener Teiche (Germany) 176

Gautrey, Simon; Boucher, Sebastien; Desjardin, Mathieu
Groundwater flow interactions in a seven-layer meromictic pit lake at the former Victor Diamond Mine, Ontario Canada 182

Gebrekristos, Robel; Trusler, Graham
Saving money and improving data collection when drilling on mining projects 189

Golian, Saeed; Carruth, David; Raynor, Mark
Improving catchment yield and low-flow estimation using HEC-HMS: Application of loss methods in a case study in Gabon 195

Grab, Thomas; Ebel, Tom; Oppelt, Lukas; Wunderlich, Timm; Raithel, Fritz; Fieback, Tobias
Categorisation and analysis of flooded mines with regard to their geothermal potential 202

Hagarová, Lenka; Kupka, Daniel
Chemical Characterization of Mine Water and Microbial Communities from the Mária Mine (Rožňava, Slovakia): Assessment of Autotrophic and Heterotrophic Bacteria after Cultivation on Liquid and Solid Media 208

Hu, Yunhao; Wu, Jinxin; Dong, Shuning; Yu, Qingchun; Guo, Xiaoming; Zhang, Wenzhong; Zhang, Xiyu
A study on the permeability evolution of self-healing mudstone fracture under long-term stress 213

Hubbard, Paul
The value of holistic water quality assessment to support pit lake closure decisions 219

Hugman, Rui; Ortega, Pablo; White, Jeremy
Efficient data assimilation for reactive transport models using data-space inversion 225

Hwang, Hyoun-Tae; Park, Young-Jin; Berg, Steven; Jones, Jon; Miller, Killian; Sudicky, Edward
Integrated modeling innovations for mining and underground infrastructure: dynamic mesh adaptation and tunnel boundary conditions for surface–groundwater systems 231

Im, Dae Gyu; Kim, Duk-Min; Kwon, Hye-Lim; Lee, Joon-Hak; Yun, Seong-Taek
Assessing Mn and Ni removal from mine drainage using a bench-scale slag reactor 237

Ji, Sangwoo; Pak, Seungil; Oh, Chamteut; Yim, Gil-Jae
Field demonstration of solar-powered iron electrocoagulation for arsenic-contaminated mine drainage at the Geumjeong abandoned mine, South Korea 243

Kasmon, Umar; Abfertiawan, Muhammad Sonny; Hasan, Faiz; Ristiaramdani, Nur Latifa; Butar Butar, Lionie; Darojat, Irfa
Electrocoagulation as alternative active treatment for hexavalent chromium removal from nickel mine water in Indonesia 248

Kim, Duk-Min; Kwon, Oh-Hun
Development of design software for mine drainage treatment facilities 254

Kim, Hyeseong; In, Hyunjin; Jeong, Jiyun; Lee, Sang Yun; Choi, Uikyu; Oh, Youn Soo
Facile synthesis of zeolite A from molybdenum mine tailings and its potential application in mine reclamation 260

Kim, Young-Min; Kim, Duk-Min; Lee, Ki-Rim; Jung, Jee-Hyun; Park, Seong-Sook; Kwon, Oh-Hun; Park, Jung-Sik
Factors influencing difference between theoretical and actual lime dosages including lime concentration and dosing rate 267

Ko, Myoung-Soo; Kim, Su-Jin; Kwon, Oh-Hun
Sorption of Arsenic and Fluoride in Neutral Mine Drainage Using Fe-Based sorbents 272

Kunze, Katja; Bilek, Felix
In-lake water treatment of post-mining lakes – reactivity of lime products 276

Lee, Dong-Kil; Cheong, Youngwook; Ji, Sangwoo; Yim, Giljae
Advanced continuous-monitoring column test for sedimentation analysis of mine drainage sludge 281

Lee, Ki-Rim; Kim, Duk-Min; Kim, Young-Min; Jung, Jee-Hyun; Park, Jae-Hyun; Kim, Da-Som; Kwon, Joon-Uk; Park, Jung-Sik
Hydrogeochemical and isotope-based assessment of level-specific mine water and rock characteristics in a recently closed coal mine 286

Lourens, Paul Joël Havemann; Vermeulen, Petrus Daniël; Zielke-Olivier, Josepha Simone Doris Renata; De Lange, Stephanus Steyn
The Influence of a Graben Structure on Pollution Migration from Mining and Industrial Waste Facilities 292

Madiseng, Lesego; Annandale, John; Tanner, Philip; van der Burgh, Gerhard; Delport, Marion; Ottermann, Helga; Witthüser., Kai; Zielke–Olivier, Josepha
Approach for assessing the feasibility of large-scale irrigation with mining-influenced water and guidance for implementation 298

Magwaza, Siboniso; Annandale, John; Madiseng, Lesego; Steyn, Martin; Tanner, Phil; Sukati, Sakhiwo
Crop response to irrigation with untreated and partially treated mine waters 305

Mannke, Kevin; Hahn, Florian; Klein, Stefan; Nikolov, Alexander; Ignacy, Roman
Feasibility study for geothermal mine water usage at the mine water drainage site Haus Aden, Bergkamen, Germany 310

Manono, Malibongwe Shadrach; October, Lisa Louise; Corin, Kirsten Claire
Exploring the effects of seawater use in Cu-Ni-PGM flotation against recycled mine water 315

Mardonova, Mokhinabonu; Mainali, Bandita; Abbassi, Rouzbeh; Shahid, Muhammad Kashif; Arzaghi, Ehsan
Site-specific Ecological Risk Assessment of metal mixtures in a mining influenced river: A case study of the Loddon River Basin, Australia 322

McGann, Matthew P.
Tailings Storage in a disused open pit - the conundrum of explaining the concept of a terminal groundwater sink 328

Merckel, Ryan David; du Preez, Kerri
Technoeconomics of the industrial-scale cloSURE® biological treatment process 335

Mugova, Elke; Klein, Stefan; Hahn, Florian
Repurposing Flooded Underground Mines for Seasonal Heat Storage: Insights from the EU project PUSH-IT 342

Mugova, Elke; Klein, Stefan; Lehmann, Jonas Enno
Mine thermal energy storage in flooded mine workings: Current status and next development Steps for a Pilot Site in Bochum, Germany 347

Nikutta, Simon Elias; Teichert, Barbara M. A.; Strauss, Harald
Modeling of pyrite oxidation and sulfate reduction in former German hard coal mines 348

Nordstrom, Darrell Kirk
Redox in mine waters - still misunderstood 354

Oh, Youn Soo; Park, Hyun-Sung; Kang, Chan-Ung; Kim, Kang Ho
Arsenic removal from alkaline mine drainage using waste sludge: pilot-scale experiments at an abandoned mine in South Korea 360

Ortega, Pablo; Aufdenkampe, Anthony; Prieto-Estrada, Andres; Foster, Allan; Tomasula, Paul; Mancewicz, Lauren; White, Jeremy
MF6RTM: flexible reactive transport modeling for mining applications via MODFLOW 6 and PHREEQC 365

Pinka, Jana; Jannneck, Eberhard; Hedrich, Sabrina
MindMontan – reduction of pollution in the Freiberger Mulde river in the Erzgebirge/Krušnohoří mining region through a passive water treatment plant 370

Pinto, Mariana; Diamantino, Catarina; Arán, Diego; Martins, Carlos; Santos, Erika; Carvalho, Edgar
Case study of an Environmental Remediation project using Technosols in São Domingos mining area (Portugal) 377

Pradhana, Adhika Catra; Saputra, Yudha Hadiyanto Eka
Wastewater management in coal mining operations: a geotextile-based semi-active treatment system in South Kalimantan, Indonesia 384

Puntsag, Tamir; Yadamsuren, Oyunchuluun; Tulganyam, Samdanjigmed; Sededpurev, Otgonbaatar; Bazardorj, Sod-Erdene; Myagmar, Bilguun; Bayanzul, Batdemberel; Munkhzorig, Munkhtuya; Ganzorig, Sunderiya; Nyambuu, Purevsuren; Naranbaatar, Enkhjin
Stable isotope evidence for hydro-chemical processes in groundwater of the Oyu Tolgoi copper mine, Mongolia 390

Roberts, Mark; Pearce, Steven; Grohs, Ken; Liu, Michael; Satriawan, Azwar
Inference of green rust formation and Fe^{2+}/Fe^{3+} redox cycling in treatment of acid metalliferous drainage 397

Rousseau, Pierre; Vernengo Lezica, Ignacio; Boniecki, Zip; Murton, Steven; Stimpfl, Marilena
Pit lake water balance modelling – detail matters 404

Sajid, Abeer; Taghavi, Seyed Mostafa; Hamedi, Moeen; Anticoi, Hernán; Bascompta, Marc
A quantitative ESG based framework for evaluating tailings reprocessing and resource recovery 411

Sartz, Lotta; Bäckström, Mattias; Sädbom, Stefan; Geiger, Veronika; Andersson, Monika
Fallen Rocks: A participatory land art installation for community engagement in Bergslagen's past and present mining landscape 418

Schmidt, Nadja; Eulenberger, Sven; Jenk, Ulf
Implementation of operative monitoring during flooding of the Königstein mine – first experiences from hydraulic test 2 425

Skifa, Nadia; McKenna, James; Glenis, Vassilis
Modelling a moving disaster: A novel approach to modelling non-Newtonian flow post tailings dam breach 432

Sugiura, Itsuki; Park, Ilhwan; Jeon, Sanghee; Tabelin, Carlito; Ito, Mayumi
Microencapsulation for suppressing acid mine drainage formation: Applications in mineral processing and metallurgical operations 439

Taghavi, Seyed Mostafa; Sajid, Abeer; Hamedi, Moeen; Anticoi Sudzuki, Hernan Francisco; Bascompta Massanes, Marc
Identifying the sustainability efficiency peak in tailings reprocessing: An entropy–TOPSIS assessment of restorative mining 445

Taki, Mariam; Flipo, Nicolas; Goetz, Damien
Global copper supply under climate-driven water stress: a proof of concept 452

Teichert, Barbara M.A.; Nikutta, Simon E.; Strauss, Harald; Weinand, Svenja; Westermann, Sebastian
Impacts of extreme precipitation on abandoned mines: a case study from North Rhine-Westphalia, Germany 458

Thomson, Heather; So, Joanna; Walls, Justin
How long is long enough? Assessing the critical storm duration for non-discharge TSFs 463

Tran, Tuan Quang; Vu, Hien Thu; Dao, Bang Duc; Nguyen, Thao Bach
Hydrogeological and hydrogeochemical characteristics of the Lo Tri coal mine in Cam Pha, Vietnam 469

Ulrich, Maik; Totsche, Oliver
The Lusatian Mining Area Water Management Centre: a case study in successful, forward-looking, cross-border water management in a mining region with limited water resources 477

Villa Gomez, Denys; Gillane, Rosie; Webster, Luke; Soto, Fernanda; Marcellin, Esteban
Microbial systems for sustainable resource recovery 483

Witbooi, Jan Bonakele; Mkhize, Innocentia Gugulethu; Waanders, Frans Boudewijn; Eloka-Eboka, Andrew; Ntwampe, Seteno Karabo Obed
A linear flow channel reactor for high sulphate water treatment: A simple and practicable AMD treatment system for rural communities in South Africa 487

Wolkersdorfer, Christian; Mugova, Elke; More, Kagiso; Molaba, Leshego; Botha, Joané; Utkin, Valentina
Hydrodynamic investigations in the abandoned Havelock asbestos mine, eSwatini, by means of tracer tests 494

Worsa-Kozak, Magdalena; Chudy, Krzysztof; Kasza, Damian; Wajs, Jarosław
From Pit to Lake: UAV-assisted tracking of hydrological and geomorphological transformation in the Stanisław-Południe clay mine, SW Poland 501

Yasya, Heksantia Rahmadinda; Abfertiawan, Muhammad Sonny; Arfan, Aditia Adyanugraha; Ristiaramdani, Nur Latifa; Mulyana, Bagja
Designing the post-mining future: hydrological modeling as a foundation for sustainable pit lake management 509

Zhou, Wanfang
Hydrogeological significance of a buried polje on dewatering of karst aquifers for a diamond mine in Northern Ontario, Canada 516

Ziukelis, Laurence; Colston, Rob
Integrating geochemical and hydro(geo)logical modelling to predict long-term water quality 517

Zvimba, John Ngoni; Holtzhausen, Pieter; Morton, Kym
Mine Water Sharing for Sustainable Water Security - A strategy for a water-scarce region 524

Zvimba, John Ngoni; Makate, Mavis Dineo; Macquela, Resego Bernice
Exploring a new water economy post mining in coal mining zones 530

IMWA 2026
Jeongseon

Leaching Behavior of Hexavalent Chromium from Nickel Processing Residues: A Free Draining Column Study on Dry Tailings and Nickel Slag

Muhammad Sonny Abfertiawan[1*], Agventy Nuranis Edytya[2], Mindriany Syafila[1], Faiz Hasan[1]

[1]*Water and Wastewater Engineering Research Group, Faculty of Civil and Environmental Engineering, Bandung Institute of Technology, Bandung, Indonesia*

[2]*Bachelor of Environmental Engineering Program, Faculty of Civil and Environmental Engineering, Institut Teknologi Bandung, Bandung 40132, Indonesia*

Abstract

Nickel processing using High Pressure Acid Leaching (HPAL) and Rotary Kiln Electric Furnace (RKEF) generates large volumes of dry tailings and nickel slag that may release metals through leaching. This study evaluates their kinetic leaching behavior using Free Draining Column Leaching (FDCL) tests over 12 weekly cycles in five single and combined configurations. Dry tailings produced oxidative conditions under which hexavalent chromium (Cr^{6+}) reached 0.512 mg/L. In contrast, nickel slag generated alkaline and reductive conditions that suppressed Cr^{6+} mobility. The 50% tailings–50% slag mixture showed the lowest metal concentrations, highlighting the potential of slag-based co-disposal to mitigate chromium leaching risks.

Keywords: Dry tailings, free draining column leaching, chromium, mine waste management

Introduction

According to the Ministry of Energy and Mineral Resources (ESDM, 2023), Indonesia possesses approximately 17.7 billion tons of nickel ore resources, corresponding to 177.8 million tons of contained metal, with total reserves estimated at 5.2 billion tons of ore and 57 million tons of metal. National nickel production increased from 1.58 million tons in 2022 to 1.8 million tons in 2023, reflecting the rapid expansion of downstream nickel processing. To support this development, integrated utilization of limonite and saprolite laterite ores is increasingly promoted to supply raw materials for both nickel grade 1 and nickel grade 2 products, resulting in the continuous generation of large volumes of processing residues.

High Pressure Acid Leaching (HPAL) is commonly applied to process limonite laterite ores with nickel grades of approximately 1.1–1.4%, producing tailings as a major residual by-product (Gultom & Sianipar, 2020). In contrast, saprolite ores with higher nickel grades (Ni > 1.8%) are generally processed using Rotary Kiln Electric Furnace (RKEF) technology, generating substantial amounts of nickel slag (Setiabudi et al., 2012). These two processing routes produce waste materials with distinct physical and geochemical characteristics.

HPAL tailings may contain elevated concentrations of potentially hazardous elements, including Fe, Mg, Mn, S, and Cr prior to neutralization (Gultom & Sianipar, 2020). After dewatering processes such as filter pressing, tailings are commonly managed as dry tailings that may remain geochemically reactive when exposed to oxygen and infiltrating water. Nickel slag, although generally alkaline and classified as non-acid forming, may also undergo leaching under long-term weathering conditions. Under rainfall infiltration, both tailings and slag can release dissolved metals, posing potential risks to surrounding soil and water systems (Wang et al., 2024).

Evaluation of the leaching behavior of nickel processing residues is therefore essential to assess their environmental performance. Kinetic methods such as Free

Draining Column Leaching (FDCL) tests are widely used to characterize mineral reactivity, oxidation processes, and temporal changes in leachate quality under conditions that better represent field exposure than static tests (AMIRA International, 2002). Accordingly, FDCL testing provides a relevant approach for assessing the long-term leaching behavior of dry tailings, nickel slag, and their potential interactions under realistic hydrological conditions.

Methods

The kinetic test is conducted to observe the behavior of metals in leachate water. In this study, the kinetic test was carried out over 12 cycles, equivalent to 12 weeks. Each cycle used deionized water. The simulation of the kinetic test is shown in Fig 1

Kinetic tests aim for further geochemical identification based on previous physical, mineralogical, and static tests as well as based on SNI 6597:2021. The kinetic test was conducted with an acrylic reactor with a diameter of 15 cm and a total height of 35 cm. The kinetic test used 2–3 kg of dry tailing and slag samples, with the soil samples homogenized beforehand to a size of less than 75 µm. The leachate that passes through the samples will be tested for several parameters as listed in Table 1.

Results and Discussion

The kinetic tests presented in this study were conducted over 12 cycles (weekly cycles), and the samples analyzed included reactor 1 (100% dry tailings), reactor 2 (100% slag), reactor 3 (layering of 75% dry tailings and 25% slag), reactor 4 (layering of 50% dry tailings and 50% slag), and reactor 5 (mixing of 50% dry tailings and 50% slag).

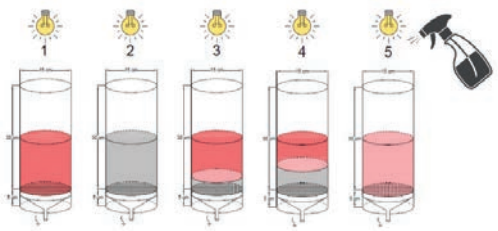

Figure 1 *Kinetic test simulation: 1) 100% dry tailing; 2) 100% slag; 3) 75% dry tailing & 25% slag (layering); 4) 50% dry tailing & 50% slag (layering); 5) 50% dry tailing & 50% slag (mixing).*

Characteristics of Deionized Water Used

The characterization of deionized water or distilled water in kinetic testing is necessary because this water serves as a neutral and pure dissolving medium that does not contain interfering ions which could affect the leaching or mineral dissolution reactions during testing. By ensuring that the characteristics of the deionized water, such as pH, conductivity, and initial ion concentrations, are very low or nearly zero, the kinetic test results will represent the true leaching rates of the samples without any additional interactions from ions already present in the water. This is crucial to obtain well-controlled leachate data.

Overall, the deionized water used was in a generally neutral condition based on the parameters tested, including pH, ORP, conductivity, salinity, DO, and TDS, indicating that it can accurately represent leachate water in the testing.

Temperature and Conductivity

The temperature graph in Figure 2a and the conductivity graph in Figure 2b are closely related, as ion mobility increases with rising temperature, allowing ions to move more rapidly, which indicates a faster electrical conduction process. The indicator in the process of conducting electricity can be assessed as conductivity. The measured leachate water temperature is around room temperature while the conductivity has decreased over time indicating that the ions in the leachate water are decreasing.

pH and ORP

pH and ORP parameters are related to each other and represented in the Pourbaix diagram to determine the chemical stability of an element or compound in water. Figure 3a shows that the pH of dry tailing tends to be neutral to alkaline, while the pH of slag is alkaline. These results are in line with the static test results which show that slag belongs to the NAF and dry tailing UC (tends to NAF). Then the ORP result in Figure 3b show that

Table 1 Leachate water test parameters and analysis procedure.

Parameters	Analysis Procedure	Standar Methods
TDS	Gravimetry	SNI 6989.3 : 2019
TSS	Gravimetry	SNI 6989.3 : 2019
Temperature	Thermometer	SNI 6989.23 : 2005
pH	pH meter	SNI 6989.11 : 2019
Oxidation Reduction Potential (ORP)	ORP meter	SNI 06-6989.2:2004
Conductivity	Conductivity meter	SNI 6989.1 : 2019
Total Cr	ICP-MS AAS	APHA 3125 SNI 6989.84 : 2019
Cr^{6+}	Spectofotometry	SNI 6989.71:2009
Other metals	ICP-MS AAS	APHA 3125 SNI 6989.84 : 2019

Table 2 Characteristics of deionized water used on weekly cycle.

Parameter	Value	Unit
pH	6,45	–
ORP	2,63	mV
Conductivity	0,01	µS/m
Salinity	0,01	psu
DO	7,5	mg/L
TDS	0	mg/L

the ORP value of dry tailing is higher than that of slag (negative value) which indicates that dry tailing tend to be oxidative and slag tends to be reductive.

TSS (Total Suspended Solid) and TDS (Total Dissolved Solid)

The TSS parameter shown in Figure 4a indicates a relatively high value only at the

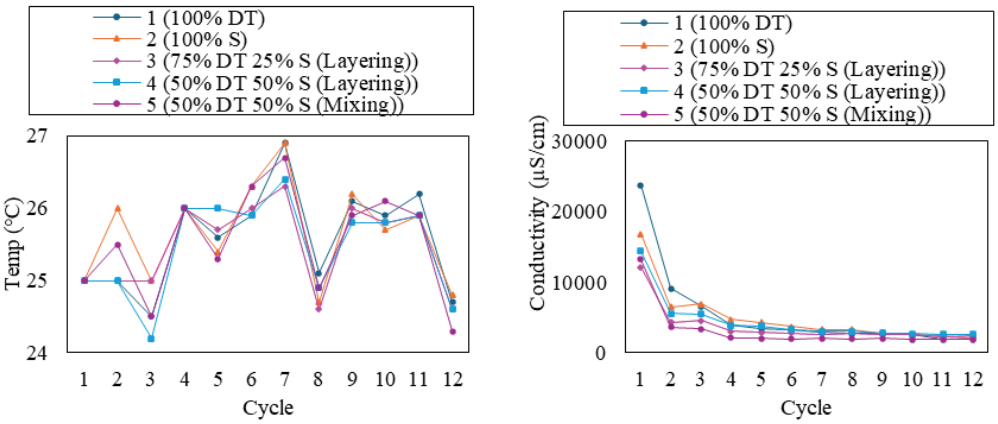

Figure 2 Leachate water (a) temperature and (b) conductivity.

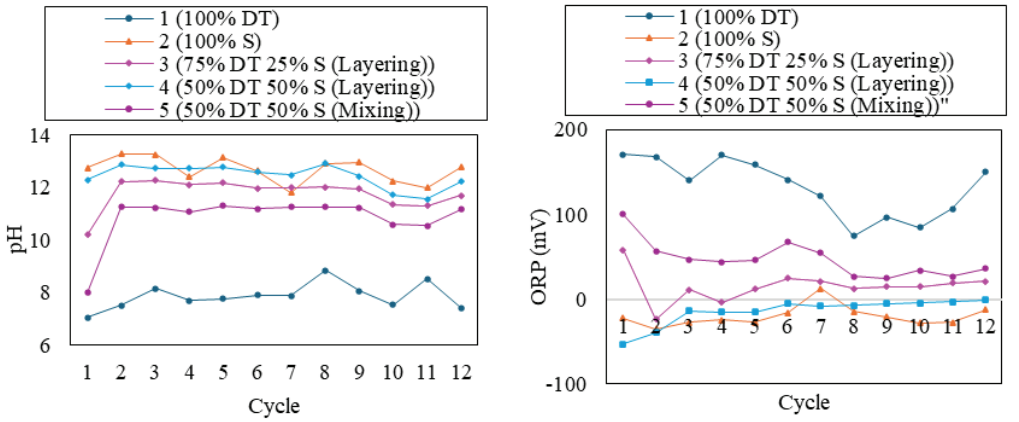

Figure 3 *Leachate water (a) pH and (b) ORP.*

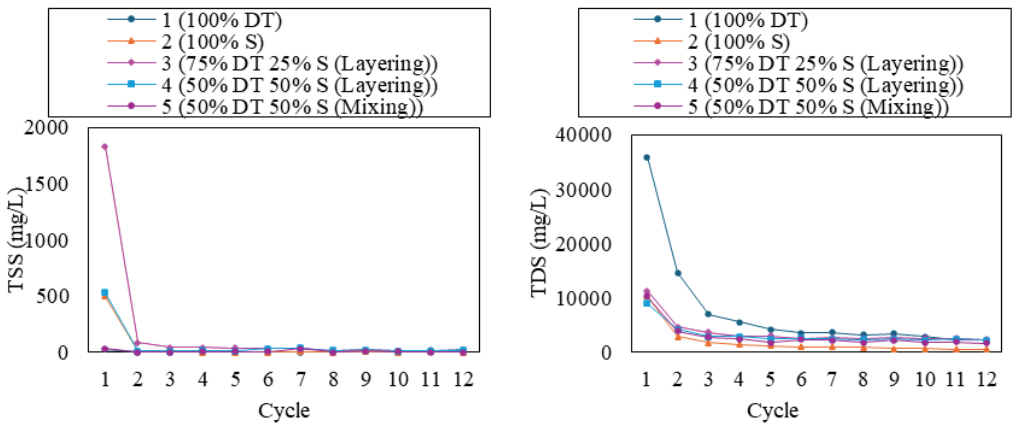

Figure 4 *Leachate water (a) TSS and (b) TDS test result.*

beginning, due to the release of fine particles during the initial dry condition of the sample. In the subsequent cycles, the TSS values are very low because a 10-micron filter paper was used during the kinetic test simulation to prevent fine particles (especially from the dry tailing) from being significantly leached into the water. Furthermore, the TDS parameter in Figure 4b shows a decreasing trend, as dissolved substances are gradually leached out over time.

Cr Metal Concentration

The most common oxidation states of chromium in the environment are Cr^{3+}, or trivalent chromium, and Cr^{6+}, or hexavalent chromium. Cr^{3+} species are more stable and less mobile, and they are less soluble in water compared to Cr^{6+}. Cr^{3+} tends to adsorb onto soil particles or organic matter and precipitate, whereas Cr^{6+} is highly soluble in water and more mobile, making it easier to spread in groundwater and surface water. Figures 5 shows an increase in total Cr and Cr^{6+} concentrations, with the peak Cr^{6+} concentration in reactor 1 occurring in week 9.

The concentration trends of total Cr and Cr^{6+} in the leachate show fluctuating values. This fluctuation is related to the properties of Cr_2O_3, which tends to be stable and therefore leaches into the environment gradually.

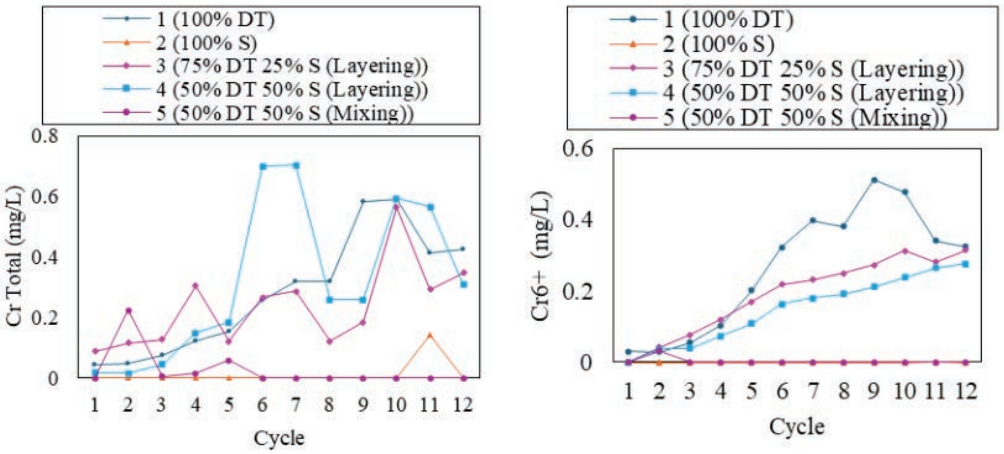

Figure 5 (a) Total Cr test result and (b) Cr6+ test result.

Table 3 Summary of pH, ORP, and Cr^{6+} concentrations in leachate.

Reactor	pH		ORP (mV)		Cr^{6+} (mg/L)	
	Min	Maks	Min	Maks	Min	Maks
1	7,05	8,85	75	171	0,028	0,512
2	11,80	13,28	-35	12,5	0	0,001
3	10,20	12,26	-23,5	58	0	0,314
4	11,55	12,90	-52,5	-1	0	0,275
5	7,99	11,29	25	100,5	0	0,032

Concentrations of Other Metals

The metal analysis focused on dissolved metals in accordance with the quality standards stated in the Indonesian Ministry of Environment Regulation No. 9 of 2009, except for chromium, which was analyzed separately. Before conducting periodic monitoring of these metals in each test cycle, an initial analysis was performed on the leachate from the first cycle (week 1) to determine the concentrations of dissolved metals using the ICP-MS method. Table 4 below presents a comparison between the dissolved metal concentrations and the quality standards.

Based on these results, it was found that the concentrations of dissolved Ni and Fe were still relatively high in the leachate. To further identify the behavior of these two metals, additional testing was conducted for Ni and Fe in the subsequent cycles.

Figure 6a above shows that dissolved nickel concentrations in the leachate were only detected in reactor 1 (100% dry tailings) and reactor 2 (100% slag) during the first week (cycle 1), while in reactors 3, 4, and 5, dissolved nickel concentrations remained at 0 mg/L throughout the testing cycles. The highest concentration of dissolved Ni was found in reactor 2, slightly exceeding the quality standard. For dissolved Fe testing in the leachate, Figure 6b shows that dissolved Fe was only detected in weeks one and two, with the highest concentration observed in reactor 2, exceeding the nickel mining wastewater quality standard.

Conclusions

Leachate from dry tailings exhibited neutral to slightly alkaline conditions (pH up to 8.55) and oxidative behavior (ORP up to 171 mV), whereas nickel slag produced strongly alkaline

Table 4 Comparison of week 1 leachate concentrations with quality standards.

Metals	Quality Standard (mg/L)	Reactor (mg/L)				
		1	2	3	4	5
Cu*	2	ND	0,03	ND	0,05	0,02
Cd*	0,05	ND	ND	ND	ND	ND
Zn*	5	0,19	0,05	ND	ND	ND
Pb*	0,1	ND	0,006	ND	ND	ND
Ni*	0,5	0,02	0,53	ND	ND	ND
Fe*	5	0,84	22,40	0,47	0,19	0,09
Co*	0,4	0,02	ND	ND	ND	ND

*) Dissolved Metals ND = Not Detected

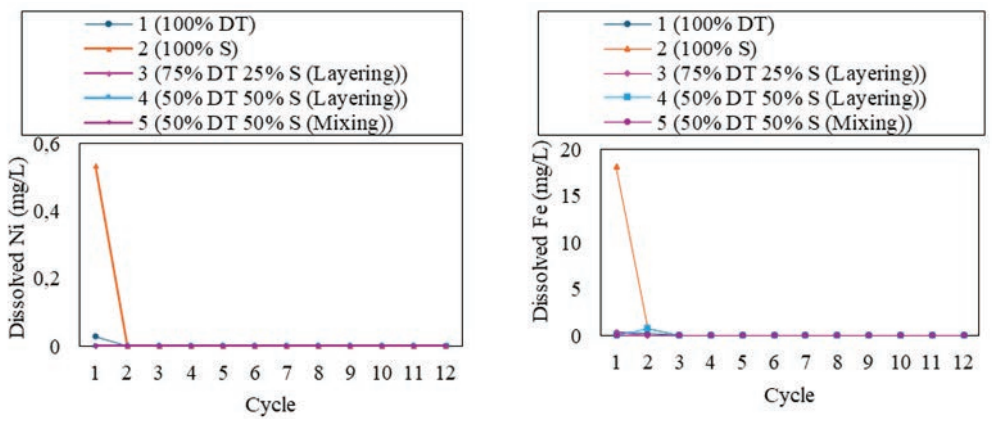

Figure 6 Dissolved (a) Ni and (b) Fe test result.

and predominantly reductive conditions (pH up to 13.28). Hexavalent chromium (Cr^{6+}) was more frequently detected in dry tailings leachate, reaching a maximum concentration of 0.512 mg/L. In contrast, the mixed system comprising 50% dry tailings and 50% slag showed the lowest concentrations of Cr^{6+}, total Cr, dissolved Fe, and dissolved Ni, all meeting mining wastewater quality standards. These results demonstrate that nickel slag effectively suppresses metal mobility and highlight its potential use in integrated waste management strategies to mitigate leaching risks from nickel processing residues.

Acknowledgements

This study was supported by the Bandung Institute of Technology through the Water and Wastewater Engineering Research Group (KK-RALC) and the Environment Department of Harita Nickel, Indonesia

References

AMIRA International (2002) ARD Test Handbook. Ian Wark Research Institute, New Zealand

ESDM (2023) Potensi Menjanjikan, Nikel RI Bakal Laris Manis Pikat Investor. https://www.esdm.go.id/id/media-center/arsip-berita/potensi-menjanjikan-nikel-ri-bakal-laris-manis-pikat-investor-. Accessed 20 Jan 2025

Gultom T, Sianipar A (2020) High pressure acid leaching: A newly introduced technology in Indonesia. In: IOP Conference Series: Earth and Environmental Science. Institute of Physics Publishing

Setiabudi A, Hardian R, Mudzakir A (2012) Karakterisasi Material : Prinsip dan Aplikasinya dalam Penelitian Kimia. UPI PRESS

Wang F, Li W, Wang H, et al (2024) The leaching behavior of heavy metal from contaminated mining soil: The effect of rainfall conditions and the impact on surrounding agricultural lands. Science of the Total Environment 914:. https://doi.org/10.1016/j.scitotenv.2024.169877

IMWA 2026
Jeongseon

Mechanisms of Arsenic (As) Release and Retention During Fenton Rreatment of Nine Wastewater

Norberto Jr Aquino[1], Musah Salifu[1], Ksenia Novikova[2], Erik Månsson[2], Erik Ronne[2], Lena Alakangas[1]

[1]*Department of Civil, Environmental and Natural Resources Engineering, Luleå University of Technology, SE-971 87 Luleå, Sweden*

[2]*Boliden AB, SE-101 20 Stockholm, Sweden*

Abstract

This study investigates the mechanisms controlling arsenic (As) removal and retention during Fenton treatment of mine wastewater from 2015 to 2025. Results show a substantial decrease (sevenfold) in dissolved As concentrations during treatment accompanied by an increase in particulate As (sixfold), indicating transfer of As from aqueous to the solid phase. Sequential extraction results suggest that As is proportionally associated with Fe oxide phases (≈13.2%). These observations indicate that As removal is primarily controlled by adsorption and co-precipitation with Fe(III) (oxyhydr)oxide precipitates formed during the Fenton reaction and subsequent liming. The findings provide insights into the geochemical processes governing As stabilization in mine wastewater treatment systems and highlight implications for the long-term management of treatment residues.

Keywords: Arsenic, Fenton reaction, wastewater, sludge, adsorption, co-precipitation

Introduction

Arsenic (As) is a toxic and carcinogenic metalloid commonly released from mining activities, posing risks to aquatic ecosystems and human health. The environmental behavior, mobility, and toxicity of As are generally governed by its speciation and geochemical conditions, particularly pH and redox state (Jomova *et al.* 2011). In aqueous systems, As primarily occurs as arsenite [As(III)] and arsenate [As(V)], with As(III) generally being more mobile and toxic (Wang *et al.* 2015), while As(V) exhibits stronger affinity for adsorption onto iron (Fe) hydroxides (Liu *et al.* 2024).

Mine wastewaters often contain elevated concentrations of As with complex mixtures of dissolved metals and reduced sulfur species (i.e. thiosalts). Treatment of such waters remains challenging at full scale due to the complexity of geochemical characteristics and interactions among multiple contaminants. For wastewaters with high thiosalts concentration, advance oxidation processes (AOPs), such as Fenton treatment (addition of H_2O_2 and $FeSO_4$), have been applied to promote oxidation and degradation (Olvera-Vargas *et al.* 2021). Fenton reactions generate reactive oxidants (e.g., hydroxyl radicals) and Fe(III) species, while subsequently form iron hydroxide precipitates upon pH adjustments and flocculation (liming and clarification).

While Fenton treatment is primarily implemented for oxidation of thiosalts, the simultaneous redox cycling of iron and formation of Fe(III) solids can influence As mobility. Acidic conditions during the Fenton stage may promote temporary As release, whereas subsequent liming and precipitation of Fe(III) hydroxides may enhance As retention through sorption and co-precipitation. In addition, Fenton reaction may oxidize As(III) to As(V), reducing its toxicity (Hug and Leupin 2003; Wang *et al.* 2015). With these complex mechanisms of As release and retention, it is therefore important to understand its behaviour, especially during full-scale Fenton treatment that will contribute to long-term management of As contamination in mine wastewater.

This study investigates the mechanisms controlling As release and retention during full-scale Fenton treatment and subsequent liming of mine wastewater by integrating long-term water quality monitoring data (2015–2025) with As partitioning and stability in the sludge.

Methods

Fenton Wastewater Treatment Process

Inflow wastewater originating from the mine tailings impoundment was subjected to full-scale Fenton treatment. Hydrogen peroxide (H_2O_2) was added with ferrous sulfate ($FeSO_4$), where Fe^{2+} catalyzed the decomposition of H_2O_2 and generated reactive oxidants. Following oxidation stage, slaked lime ($Ca(OH)_2$) was added to increase the pH and promote precipitation of iron hydroxides. The outflow water was then passed through a clarification area to enhance solid-liquid separation. The treated water was discharged to receiving tributaries, with a portion recycled within the mine site. The separated solids were classified as sludge.

Water Quality Monitoring

From 2015 to 2025, water samples were collected at three locations within the treatment system: (i) inflow (prior to Fenton treatment), (ii) outflow (after Fenton treatment and liming), and (iii) final discharge (after clarification). Samples were filtered (0.45 μm) to determine dissolved concentrations and analyzed unfiltered for total concentrations. Arsenic concentrations were quantified using Inductively Coupled Plasma Sector Field Mass Spectrometry (ICP-SFMS) at ALS Scandinavia, Luleå, Sweden.

Sequential Extraction for Sludge Sample

Arsenic partitioning in sludge was determined using a six-step sequential extraction procedure (Dold 2003; Hall *et al.* 1996). One gram of dried and powdered sludge was subjected to a sequential extraction procedure to operationally define As partitioning among different geochemical fractions. The extraction steps targeted the following fractions: (1) water-soluble fraction extracted with ultrapure water (MQ-H_2O); (2) acetate-soluble fraction extracted with 1 M $NH_4CH_3CO_2$, representing exchangeable and carbonate-bound phases; (3) easily reducible fraction extracted with 0.25 M $NH_2OH{\cdot}HCl$, corresponding to amorphous oxide phases; (4) moderately reducible fraction extracted with 1 M $NH_2OH{\cdot}HCl$, representing crystalline oxide phases; (5) oxidizable fraction extracted using 0.75 g $KClO_3$ and 12 M HCl to target sulfide-bound phases; and (6) residual fraction determined by complete digestion of the remaining solids using HCl, HNO_3, and HF.

Results and Discussion

Arsenic Behavior during Fenton Wastewater Treatment Process

Changes in As concentrations were evaluated across the treatment process (Figure 1) to assess As removal and retention in the wastewater. The untreated inflow wastewater contained dissolved As concentrations averaging around 14 μg/L, with an average pH of approximately 8.7 prior to entering the Fenton reactor. Following Fenton treatment and subsequent liming (pH ≈ 10), average dissolved As concentrations decreased by about seven (7) times compared to the inflow. In contrast, average particulate As concentrations increased substantially during this stage (from 3 μg/L to 18 μg/L), likely reflecting the formation and suspension of newly precipitated solid phases. After clarification, the final discharge waters (pH≈ 8.4) exhibited a decrease in particulate As concentrations, indicating effective removal of suspended particles. Dissolved As concentrations remained relatively similar between the outflow and discharge stages despite pH differences (from ≈10 to 8). This behavior suggests that remobilization of As from the particulate phase was limited during the clarification step, indicating relatively stable retention of As within the solid phases formed during the treatment.

The distribution of As in the sludge sample was evaluated using a six-step sequential extraction procedure targeting operationally defined geochemical phases (Figure 2) to assess the stability of As in the treatment sludge. The results indicate that As is predominantly associated with the residual (58.2%) and sulfide-bound (15.8%)

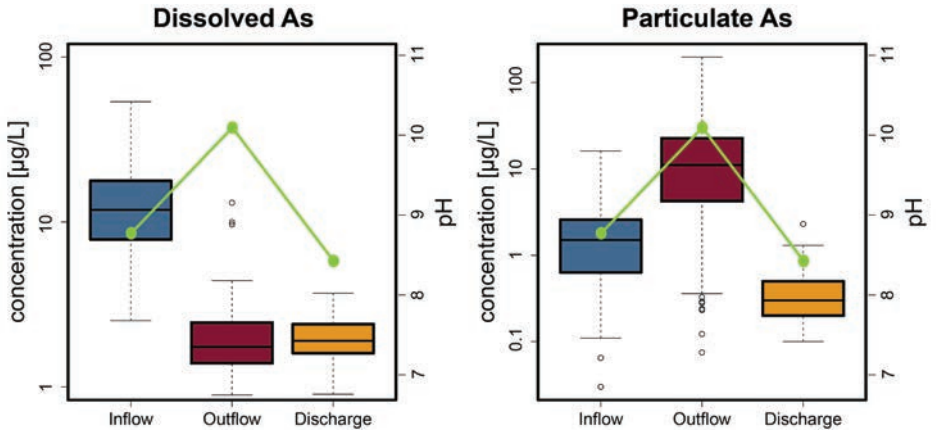

Figure 1 Dissolved and particulate arsenic (As) concentrations across treatment stages. Boxplots show dissolved (left) and estimated particulate (right; calculated as total minus dissolved) As concentrations in inflow, post-treatment outflow, and final discharge waters. Boxes represent interquartile range (IQR), center lines indicate medians, whiskers denote 1.5x IQR, and empty circles represent outliers. Green circles and lines represent average pH across treatment stages (right Y-axis). Note the logarithmic left Y-axis scaling.

fractions, suggesting its potential association with structurally stable mineral phases such as silicates and sulfide minerals (e.g., Arsenopyrite) likely from the mine tailings. This indicates that it is not only water that enters the Fenton reactor but also includes particulates and sand from the mine tailings impoundment. Comparable proportions of As were also associated with the crystalline oxide (12.6%) and carbonate-bound (12.8%) fractions, suggesting adsorption and co-precipitation with secondary iron hydroxide minerals formed during treatment as well as incorporation into carbonate phases generated during the liming step. Only minor amounts of As were detected in the amorphous oxide fraction (0.6%), while the water-soluble fraction was negligible (<0.1%).

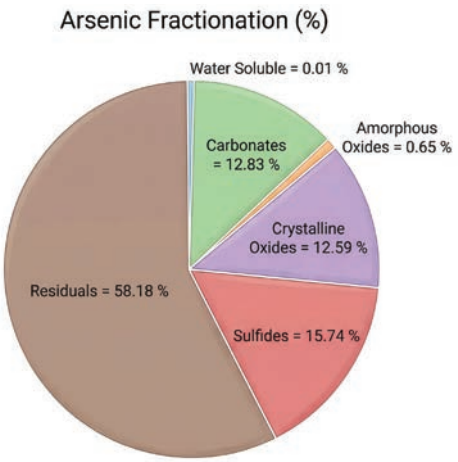

Figure 2 Distribution of As among operationally defined geochemical fractions in sludge determined by sequential extraction.

Potential Controls on Arsenic Removal and Retention from Mine Wastewater

Fenton reaction supports the oxidation of metastable sulfur species (e.g., thiosulfate) into a more stable form (e.g., sulfate). Moreover, it may also support oxidation of other species such as As(III) to As(V) as well as oxidation of sulfidic minerals hosting As (Noor *et al.* 2011). The behavior of As in a lab-scale Fenton system has been investigated by Hug and Leupin (2003), who demonstrated that the reaction between Fe(II) and H2O2 produces oxidizing species (e.g., hydroxyl radicals) capable of oxidizing As(III) to As(V). The oxidation of As(III) occurs in parallel with Fe(II) oxidation, facilitating removal through adsorption and co-precipitation with Fe(III) (oxyhydr) oxides. However, in the current study, almost all dissolved As concentration is in the form

of As(V), which is estimated and calculated through PHREEQC (wateq4f.dat). Thus, the Fenton oxidation process has a minimal control on As stabilization in the wastewater. It should be noted that the presence of H2O2 during the Fenton process creates strongly oxidizing conditions that favor the formation of As(V). Consequently, the dominance of As(V) predicted by the PHREEQC calculations is consistent with the expected redox environment of the treatment system. However, because measured redox potential (Eh) data were not available, the PHREEQC model assumes equilibrium conditions, which may not fully represent the actual As(III)/As(V) distribution in the system.

Assuming that the system is dominated by As(V), this may suggest that dissolved As has a high affinity of adsorption to Fe(III) (oxyhyd)oxide surface (Liu *et al.* 2024). In the Fenton wastewater treatment system, Fe^{2+} oxidizes to Fe^{3+} (Zeliger 2022), which then go through hydrolysis and eventually form Fe(III) (oxyhydr)oxides precipitates (Figure 3) under alkaline conditions (pH ≈10). These newly formed Fe precipitates can provide sorption sites for different As species (Liu *et al.* 2024) (Figure 3). For instance, As(III) can adsorb onto Fe(III) hydroxide surfaces through inner-sphere surface complexation (e.g., adsorption to micropore, macropore, mesoporous). In contrast, As(V) occurs mainly as negatively charged oxyanions (e.g., $H_2AsO_4^-$ and $HAsO_4^{2-}$) that bind to positively charged surface sites on Fe (oxyhydr)oxide through electrostatic attraction in addition to its inner-sphere surface complexation. Due to its anionic property, As(V) generally exhibits a higher adsorption affinity to Fe (oxyhydr)oxide compared to As(III) under several environmental conditions. This interpretation is somehow reflected in the calculated average dissolved Fe/As ratios across the treatment stages. In the untreated inflow water, dissolved Fe/As is relatively low (≈1.76), suggesting limited availability of Fe sorption sites relative to dissolved As. Following Fenton reaction and liming treatment, the dissolved Fe/As ratio increases to ≈46, indicating a large excess of dissolved Fe that can hydrolyze and precipitate as Fe(III) hydroxides, thereby providing sorption sites for As. After flocculation, the dissolved Fe/As ratio decreases to ≈10, reflecting removal of Fe-bearing particulates from the water column, but still remains in a concentration sufficient to maintain As co-precipitation with Fe phases as compared to the inflow ratio. This is further supported by the sequential extraction result where a substantial proportion of As was associated with amorphous and crystalline Fe oxide phases (≈13.2%). Although As is mostly associated with the sulfide and residual phases, this does not necessarily indicate that all As in these fractions occurs exclusively as discrete sulfide or silicate minerals. Sequential extraction technique is a qualitative method and is operationally defined (Dold 2003; Hall *et al.* 1996). This may lead to challenges like non-specificity and incomplete dissolution. As a result, the residual and sulfide fractions

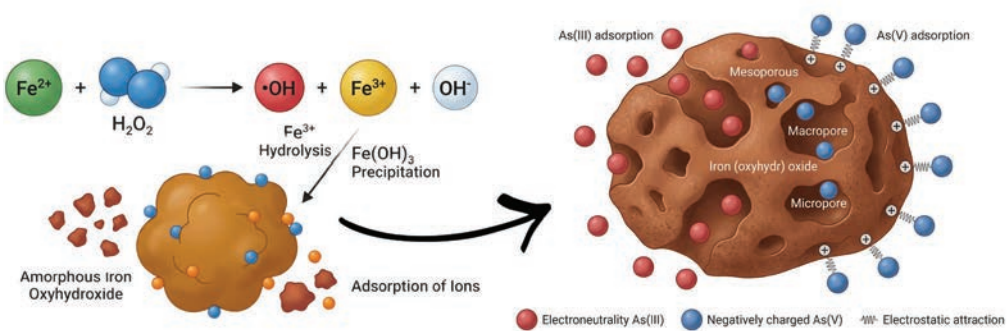

Figure 3 *Conceptual illustrations of arsenic removal and retention mechanisms during Fenton treatment of mine wastewater. Fenton reaction is modified and adapted from (Zeliger 2022) and As adsorption in Fe (oxyhydr)oxide is adapted from (Liu et al. 2024).*

may also include As incorporated within complex mineral matrices or strongly bound to mineral surfaces (e.g., strongly bound As to Fe hydroxide surface) that are not readily dissolved by earlier extraction reagents. Therefore, while the sequential extraction results suggest relative stability of As in the sludge, they should be interpreted cautiously and together with mineralogical analysis (e.g., SEM and XRD) after each extraction step.

Conclusions

Fenton treatment ideally promotes the oxidation of As(III) to As(V) in wastewater treatment system, although in the present system the untreated wastewater is already dominated by As(V) based on PHREEQC calculations. The addition of Fe during the Fenton process followed by the addition of lime leads to the precipitation of Fe(III) (oxyhydr)oxide which facilitates the removal of dissolved As in the system through adsorption and surface complexation. This process effectively removed dissolved As from the wastewater and transfer it to the resulting solid which is the treatment sludge.

Although this treatment reduced dissolved As concentrations in the treated effluent, the long-term stability of As retained in the sludge remains an important challenge. Arsenic associated with the Fe-rich sludge may remain stable under certain environmental conditions (e.g., alkaline with pH ≈8) but could potentially remobilized under changing environmental conditions such as strong reducing and oxidizing environments, pH fluctuations, or mineral transformation processes.

These findings highlight the importance of not only treating contaminated wastewater but also addressing potential As mobilization at the early stages of mine waste system. For instance, As stabilization or removal at the source can be considered through improved management of mine tailings, extraction of contaminated wastewaters, or early treatment of drainage streams. While such approaches do not eliminate the formation of As-bearing sludge, they can reduce the overall As load entering treatment systems and enable better-controlled handling of sludge, thereby lowering the risk of re-dissolution and unintended environmental release, particularly near discharge points. Nevertheless, treatment sludge generated from mine wastewater remains an ongoing environmental management challenge. Thus, sustainable stabilization and valorization techniques for sludge handling should be explored.

Acknowledgements

This project is co-funded by the European Union, the Swedish Agency for Economic and Regional Growth, and the Center of Advance Mining and Metallurgy (CAMM) at Luleå University of Technology.

References

for geochemical studies of copper sulfide mine waste. J Geochem Explor 80:55–68

Hall GEM, Vaive JE, Beer R, Hoashi M (1996) Selective leaches revisited, with emphasis on the amorphous Fe oxyhydroxide phase extraction. J Geochem Explor 56:59–78

Hug SJ, Leupin O (2003) Iron-catalyzed oxidation of arsenic (III) by oxygen and by hydrogen peroxide: pH-dependent formation of oxidants in the Fenton reaction. Environ Sci Technol 37:2734–2742

Jomova K, Jenisova Z, Feszterova M, et al (2011) Arsenic: toxicity, oxidative stress and human disease. J Appl Toxicol 31:95–107. https://doi.org/10.1002/jat.1649

Liu J, Duan Y, Chen H, et al (2024) Extent of As(III) versus As(V) adsorption on iron (oxyhydr) oxides depends on the presence of vacancy cluster-like micropore sites: Insights into a seesaw effect. Sci Total Environ 954:176376. https://doi.org/10.1016/j.scitotenv.2024.176376

Noor M, Hassan A, Noor ZZ, Aris A (2011) Performance of fenton oxidation towards sulfide removal for spent caustic remediation. In: 2011 National Postgraduate Conference. pp 1–6

Olvera-Vargas H, Dubuc J, Wang Z, et al (2021) Electro-Fenton beyond the degradation of organics: Treatment of thiosalts in contaminated mine water. Environ Sci Technol 55:2564–2574

Wang Y, Wang S, Xu P, et al (2015) Review of arsenic speciation, toxicity and metabolism in microalgae. Rev Environ Sci Biotechnol 14:427–451. https://doi.org/10.1007/s11157-015-9371-9

Zeliger H (2022) Oxidative stress: its mechanisms and impacts on human health and disease onset. Academic press

IMWA 2026
Jeongseon

Abandoned Mines as Pumped Hydro Storage Power Plants – A Strategy for Geochemical Characterisation of Mine Water Before Operation

Mattias Bäckström[1], Lotta Sartz[1,2], Thomas Johansson[3], Maria Säfström[3], Stefan Sädbom[1]

[1]*Bergskraft Bergslagen AB, Södra Kungsvägen 49, 692 30 Kumla, Sweden, mattias.backstrom@bergskraft.se, ORCID 0000-0002-2674-4994, stefan.sadbom@bergskraft.se, ORCID 0000-0003-2384-4188*

[2]*Örebro University, 701 82 Örebro, Sweden, lotta.sartz@oru.se, ORCID 0000-0001-9348-6481*

[3]*Mine Storage International AB, Torsgatan 11, 111 23 Stockholm, Sweden, thomas.johansson@minestorage.com, maria.safstrom@minestorage.com*

Abstract

Pumped hydro storage (PHS) is a suitable method for storing energy, and abandoned mines are often suitable due to the large elevational differences between potential upper and lower storage reservoirs. Several geochemically related issues have been identified regarding the selection of abandoned mines: (i) initial lowering of the mine water level to obtain a suitable elevational difference, (ii) discharge of excess water during operation, and (iii) water quality during operation.

It is suggested that detailed chemical profiles and underground water volumes be determined. It is also important to determine the water quality and water flows in the recipient in order to avoid breaching environmental quality standards during both the initial and the operational discharge of excess water.

Keywords: Mine water, geochemical evolution, sampling, acid rock drainage

Introduction

Abandoned mining sites are common around the world. Underground mine infrastructure can, however, continue to deliver value after active mining has ceased. As intermittent electricity production increases, the need for energy storage and energy balancing services increases as well. Pumped hydro storage (PHS) is a suitable method for energy storage, as it requires fewer finite resources and provides substantially longer lifecycles compared to battery storage systems. Pumped hydro storage also contributes to grid stability and security through, e.g., inertia and black start capabilities. Several studies have been published regarding issues surrounding pumped hydro storage (Morabito *et al.*, 2020; Lyu *et al.*, 2022; Colas *et al.*, 2023), but few have focused on issues related to the geochemical composition of the mine water and the resulting effect on potential projects.

The elevational difference in some underground mines is well suited for pumped hydro storage. With an elevational difference of 100–150 m or more, even small volumes of water (0.5 Mm^3) can be used to produce electricity and provide balancing services for an extended period (several hours).

In Sweden, there are several abandoned mining sites with deep underground infrastructure suitable as the lower reservoir, in combination with a suitable upper reservoir either above or below ground. The upper reservoir can, for instance, be an adjacent open pit, an aggregate quarry, or a large cavity in the upper parts of the underground mine.

There are, however, several geochemical challenges when repurposing an abandoned underground mine. The geochemical issues are at least threefold: (i) discharge of existing mine water in an abandoned mine, (ii) discharge of excess water during operation, and (iii) quality of water during operation.

Abandoned underground mines are often water-filled, and water needs to be discharged to obtain a sufficient elevational difference between the upper and lower reservoirs. Depending on the mineralisation (base

metals or iron ore), the initial water quality might be an issue (ARD in sulfide base metal mines and, for instance, molybdenum or uranium in iron ore mines). Lowering the water level by 100–150 m may require draining several Mm^3 of mine water into a suitable recipient.

During injection from the upper reservoir to the lower reservoir in the mine, large amounts of dissolved oxygen will also be introduced into the underground mine system. Increased oxygen saturation might lead to increased oxidation of any sulfide minerals present and of dissolved ferrous iron, resulting in lower water quality (Pujades *et al.*, 2018; Pujades *et al.*, 2019). The groundwater cone of depression will draw additional drainage water into the mine, requiring continuous discharge and potentially treatment if the water quality is poor. Moreover, injection and pumping activities during operation can alter groundwater levels in the surrounding area (Pujades *et al.*, 2016), potentially enhancing the leaching of trace elements from remaining mineralisation.

Water quality during operation may also affect scaling or corrosion of the turbine and pumping equipment (Roy *et al.*, 2016).

We have developed a strategy, from a geochemical perspective, for determining whether a mine site can be developed into a pumped hydro storage facility. The strategy will be illustrated using a water-filled abandoned iron ore mine in Norberg, Sweden, where minor parts were also mined for silver and lead.

Methods

It is important to properly sample and characterise the underground mine water through depth profiles in several parts of the mine in order to determine the likely quality of the entire water volume and, based on this, to determine proper management and suitable discharge points into the recipient. It is important to understand both the underground and the surface water quality in order to avoid breaching any environmental water quality standards in the recipient during discharge.

Norberg field site

The municipality of Norberg, in the historical mining district of Bergslagen, Sweden, has had active mining for around 1 500 years. Mining started around 500 AD and stopped in the early 1980s. Iron ore has been the major product, while small amounts of silver ore have been produced in one of the oldest parts, around Silvergruvan (Fig. 1). One of the largest underground mines in Norberg is today water-filled and contains, in total, around 10 Mm^3 of water. The natural discharge point is currently located somewhere south of Centralschaktet (C), in an abandoned area with several open or poorly covered shafts and building remains. The current natural discharge from the underground mine is estimated to be around 10–20 L/s.

Prior to the installation of equipment (turbines and pumps) in the underground mine, the current water level needs to be lowered to around 100 m, requiring an estimated 3 Mm^3 of water to be pumped and discharged into the recipient. It is planned to be discharged into the recipient over 1 year at an average rate of 100 L/s.

A disused aggregate quarry will be used as the upper reservoir, and the entire underground mine will act as the lower reservoir. A penstock will transfer water between the quarry (upper reservoir) and Skakelbergsschaktet (Sk in Fig. 1) (lower reservoir). The upper reservoir will have a maximum capacity of around 0.5 Mm^3, allowing for 5–6 hours of continuous electricity production at 25 m^3/s.

Sampling

Sampling has been performed in the accessible shafts: Silvergruvan, Skakelbergsschaktet, and Centralschaktet (see Fig. 1 for a map and Fig. 2 for the depth profiles). Depth profile sampling was performed using both a depth sampler and a continuously logging diver for temperature and electrical conductivity. Surface water was sampled at selected recipient points around the old mine (Fig. 1). The surface water sampling points were selected both to generate a water quality baseline prior to operation and to determine the most suitable discharge points

Table 1 Surface water sampling points.

	Description
N1	Present outlet from the quarry, the upper reservoir.
N3	Into lake Bålsjön. Between N1 and N3 the creek is affected by historical sulfidic mining waste. Potential recipient for discharge of excess water during operation (10-20 L/s).
N15	Outlet lake Bålsjön.
N11	Inlet lake Dammsjön. Potential recipient for discharge of excess water during operation (10-20 L/s).
N14	Outlet lake Dammsjön. Lake Dammsjön also affected by a reprocessed stainless steel slag deposit.
N5	Potential current discharge from the underground mine.
N18	Potential current discharge from the underground mine.
N16	Downstream N18. Between N18 and N16 the water passes through another underground mine. Potential recipient for discharge of excess water during operation (10-20 L/s).
N8	Outlet lake Noren (major recipient in Norberg). Potential recipient for the initial draining of the underground mine (100 L/s).

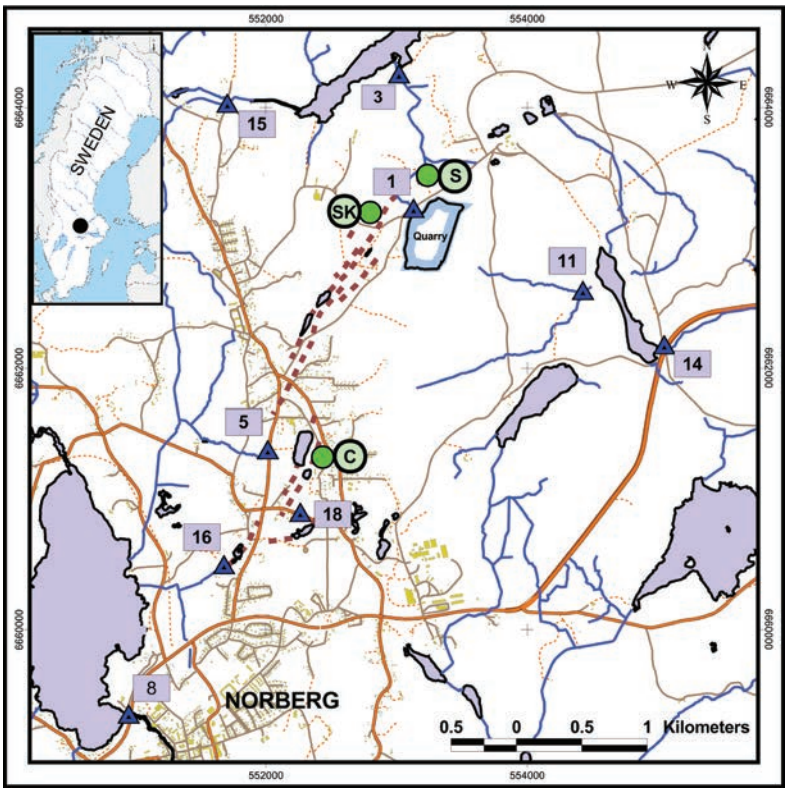

Figure 1 Illustration of the Norberg underground mining system. Silvergruvan (S), Skakelbergsschaktet (Sk), the upper reservoir (Quarry) and Centralschaktet (C). Skakelbergsschaktet (C) is the shaft planned to be used for turbines and pumps. Surface water sampling points 1, 3, 5, 8, 11, 14, 15, 16 and 18. Red dotted line indicates the extension of the underground mine between shaft Silvergruvan (S) and Centralschaktet (C).

for emptying the underground mine and for the discharge of excess water (rain on the upper reservoir and groundwater seepage into the lower reservoir) during operation. During water sampling, the water flow was also estimated at each point. The surface water sampling points are described in more detail in Tab. 1.

Chemical analysis

Water samples were analysed for pH, electrical conductivity, alkalinity, sulfate, chloride, fluoride, nitrate and ammonia as well as base cations (Na, K, Mg, Ca, Fe and Mn) and trace elements including molybdenum and uranium.

Results and discussion

The results from the water sampling in the mining shafts are presented in Tab. 2. The mine water in the Silvergruvan (S) shaft is affected by the sulfide mineralisation in that part of the underground mine. Sulfate, lead, copper and zinc concentrations are elevated. In the more modern parts of the mine, represented by the Skakelbergsschaktet (Sk) and Centralschaktet (C) shafts, concentrations of molybdenum and uranium are elevated instead. Both molybdenum and uranium concentrations increase with depth, along with increasing dissolved iron concentrations, while decreasing sulfate concentrations indicate slightly more reducing conditions with depth. To avoid drawing water from Silvergruvan (S) during the emptying of the underground mine, the most likely draw point for the initial lowering of the water level is Centralschaktet (C). Since the exact water volumes in the underground mine as a function of depth are not fully understood, it is not possible to determine exactly the average water quality during the initial pumping. The large mined-out voids underground are not accessible, and the water quality for a large fraction of the underground mine water is thus not known. At this stage, it

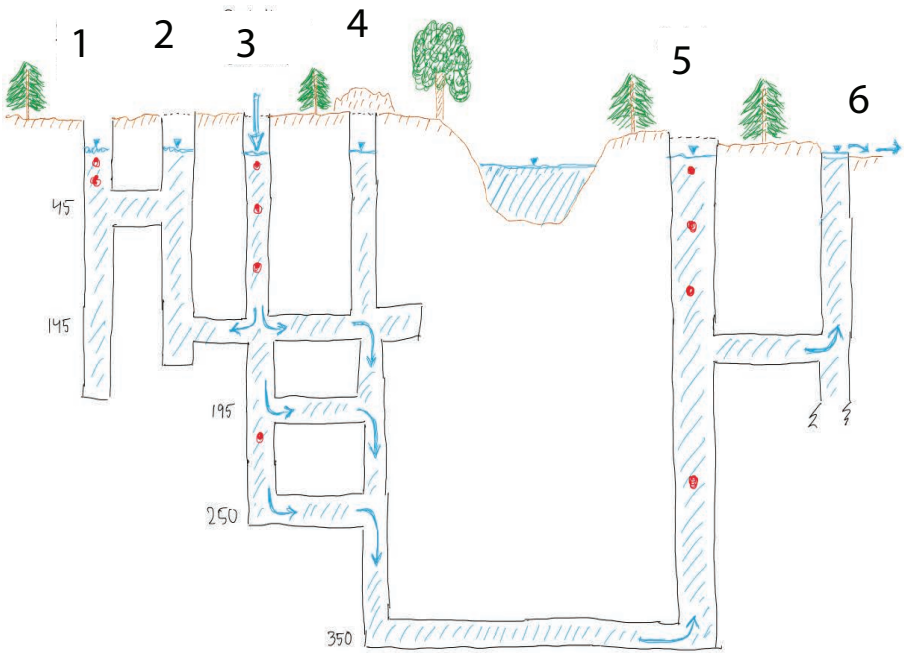

Figure 2 *Illustration of the Norberg underground mining system. Shafts are numbered; Silvergruvan (1), Nya Månsgruvan (2), Skakelbergsschaktet (3), Gustaf Adolfsschaktet (4), Centralschaktet (5) and discharge area (6). Red dots illustrate sampling points and numbers in black are depth below the surface. Skakelbergsschaktet (3) is the shaft planned to be used for installation of turbines and pumps. Blue arrows indicate possible waterways for injected water during operation. Also note that the actual stoping chambers (larger voids) are not included in the illustration.*

Table 2 Concentrations in the mine shafts. All concentrations in µg/L except for sulfate and fluoride (mg/L). S, Silvergruvan; Sk, Skakelbergsschaktet and C, Centralschaktet (shaft numbers 1, 3 and 5 in Fig. 2). Numbers indicate depth (m) below water surface.

	S1	S20	Sk5	Sk43	Sk100	Sk208	C5	C48	C96	C228
pH	6.20	6.60	6.70	6.60	6.70	7.20	7.40	7.40	7.40	7.40
Pb	1 300	180	7.3	7.5	7.1	4.4	0.12	0.38	0.49	1.6
Cd	0.62	0.11	0.019	0.011	0.011	0.013	0.013	0.014	0.016	<0.01
Cu	150	12	24	15	13	4.5	8.4	9.1	6.9	4.1
Mo	-	-	1.6	1.3	1.6	6.9	7.0	6.8	7.1	8.6
U	0.10	0.48	0.88	1.0	1.4	8.9	3.6	3.6	4.8	8.1
Zn	88	19	25	5.6	7.2	9.5	24	25	22	12
Fe	680	7 300	11 000	12 000	11 000	5 000	65	380	700	2 800
Sulfate	99	130	56	56	54	31	15	15	19	20
Fluoride	4.0	3.2	3.5	3.4	3.4	2.5	0.75	0.74	1.5	1.6

Table 3 Average concentrations of trace elements in selected recipient sampling points. All concentrations in µg/L except for sulfate and fluoride (mg/L). Average flow calculated from the size of the drainage area and an annual runoff of 260 mm.

	N1	N3	N15	N11	N14	N5	N18	N16	N8
Av flow (L/s)	0.2	13	48	13	35	1.2	-	15	1 390
pH	7.15	7.43	7.27	6.27	7.60	7.73	7.70	7.90	6.93
Pb	2.89	15.9	0.57	0.34	0.39	0.09	0.31	<0.02	0.27
Cd	0.02	0.02	<0.01	0.02	0.02	<0.01	0.01	<0.01	<0.01
Cu	2.75	12.8	3.93	1.01	4.57	1.90	7.80	3.77	1.20
Mo	10.5	4.90	2.50	<1	26.0	<1	6.30	18.0	<1
U	41.0	4.07	0.87	0.29	1.93	0.48	7.0	11.0	0.40
Zn	<1	2.80	1.25	2.67	1.73	<1	2.90	<1	1.87
Fe	71.3	3 000	427	1 250	800	60.0	1 300	60.0	407
Sulfate	35.0	10.6	6.60	3.37	53.7	7.13	19.0	30.0	3.93
Fluoride	2.18	1.90	0.89	0.26	0.99	0.85	2.10	1.90	0.19

is therefore assumed that the water quality in the large voids is similar to the water quality in the closest shaft at a similar depth.

The results for concentrations in selected surface waters are presented in Tab. 3. Elevated concentrations of molybdenum and uranium indicate a major influence from mine water (N16 and N18). The local granite is also a likely source of molybdenum and uranium, as the discharge from the disused aggregate quarry (N1) contains the highest concentrations. Leaching from the remaining crushed aggregate in the disused quarry might thus also be a problem during operation. It is also likely that the surface water at N18 originates from the discharge of underground mine water close to Centralschaktet. After passing through another underground mine,

sample N16 has even higher concentrations of molybdenum and uranium, confirming the fact that the iron ore in the area contributes these trace elements to the leachates.

The relatively small water volumes in the Silvergruvan (S) shaft (Fig. 2) indicate that the sulfide-affected water will not create an issue, as it will most likely drain into the Skakelbergsschakt (Sk) shaft, where the reduced iron will precipitate. The major issue when it comes to discharging the initial volume of water (around 5 Mm^3) is the effect on the recipient, given a flow of 100 L/s over a full calendar year and the elevated concentrations of molybdenum and uranium. A high discharge flow from the underground mine requires a recipient with a decent water flow, where the concentrations of the relevant trace elements will not be significantly affected by the discharged water. If a suitable discharge point cannot be found, water treatment or a lower pumping rate might be required to decrease the amount of trace elements being discharged and thus avoid breaching the environmental quality standards.

Conclusions

The initial lowering of the water level in the underground mine, prior to the installation of turbines and pumps, requires detailed knowledge of the water chemistry as well as of the water volume in the mine as a function of depth, in order to determine the actual concentrations during pumping and to select a suitable draw point in one of the shafts. Knowledge of the water flow and concentrations in the recipient is required, in combination with the quality of the underground mine water, in order to select a suitable discharge point into the recipient.

Leaching from the upper reservoir also needs to be investigated, as frequent repeated cycles of pumping and discharge might create conditions leading to increased leaching of naturally occurring trace elements.

The water quality during operation is a function of the original mine water quality, the leachability of the surrounding rock, and the injection of oxygen, as well as of potential leaching from the upper reservoir.

Acknowledgements

The authors thank the municipality of Norberg for access to sampling sites at the historical mining area.

References

Colas E, Klopries E-M, Tian D, Kroll M, Selzner M, Bruecker C, Khaledi K, Kukla P, Preuße A, Sabarny C, Schüttrumpf, Amann F (2023) Overview of converting abandoned coal mines to underground pumped storage systems: Focus on the underground reservoir. J Ener Stor 109153, doi:10.1016/j.est.2023.109153

Lyu X, Yang K, Fang J, Tang J, Wang Y (2023) Feasibility study of construction of pumped storage power station using abandoned mines: A case study of the Shitai mine. Energies 16:314, doi:10.3390/en16010314

Morabito A, Spriet J, Vagnoni E, Hendrick P (2020) Underground pumped storage hydropower case studies in Belgium: Perspectives and challenges. Energies 13:4000, doi:10.3390/en13154000

Pujades E, Willems T, Bodeux S, Orban P, Dassargues A (2016) Underground pumped storage hydroelectricity using abandoned works (deep mines or open pits) and the impact on groundwater flow. Hydrogeol J 24:1531-1546, doi:10.1007/s10040-016-1413z

Pujades E, Jurado A, Orban P, Dassargues A (2018) Hydrochemical changes induced by underground pumped storage hydropower: influence of aquifer parameters in coal mine environments. Adv Geosc 45:45-49

Pujades E, Jurado A, Orban P, Dassargues A (2019) Parametric assessment of hydrochemical changes associated to underground pumped hydropower storage. Sci Tot Environ 659:599-611, doi:10.1016/j.scitotenv.2018.12.103

Roy JM, Preston R, Bewick RP (2016) Classification of aqueous corrosion in underground mines. Rock Mech Rock Eng 49:3387-3391

Innovative Passive Treatment Technologies for UK Metal Mine Water

Selina Mary Bamforth[1], Hugh Potter[2], Nick Cox[1], Devin Sapsford[3]

[1]*Mining Remediation Authority, United Kingdom*
[2]*The Environment Agency, United Kingdom*
[3]*Cardiff University, School of Engineering, United Kingdom*

Abstract

UK metal mine waters are challenging to treat due to highly variable chemistry, the need for very low residual metal concentrations and system footprints constrained by limited land availability. This paper presents results from the first 300 days of operation of three 50 m^2 Vertical Flow Reactors (VFRs) treating mildly acidic mine water. Excellent Fe and Mn removal and effective polishing of Cu, Ni and Cd were observed. Zn removal was more variable and dependent on pH with seasonal effects noted. Findings inform design, optimisation and media reuse for passive treatment schemes.

Keywords: Vertical flow reactors, metal mine waters, pilot-scale trials

Introduction

The Water and Abandoned Metal Mines (WAMM) programme was established in 2011 to address pollution from abandoned metal mines, which affects approximately 1,500 km of rivers across England. These mines, once central to Britain's industrial heritage, now release harmful metals into waterways, damaging aquatic ecosystems and impacting economic activity. The programme is a partnership between the Mining Remediation Authority (formerly the Coal Authority), the Environment Agency and the Department for Environment, Food and Rural Affairs (Defra). It is primarily funded by Defra to support delivery of the statutory Environment Act target: to halve the length of rivers polluted by harmful metals from abandoned metal mines by 2038.

Many mine sites are located in rural and/or upland landscapes where the availability or suitability of land can be limited, restricting the feasibility of more conventional passive treatment technologies. To address this, the WAMM Programme has initiated pilot-scale research trials across the UK, including the Coombe Mine Water Treatment Scheme (MWTS), where pilot-scale Vertical Flow Reactors (VFRs) are being investigated to treat mine water from Coombe Adit. The mine water is net-acidic and contains Fe, Mn, Zn, Cu, As, Ni and Cd at concentrations sufficient to pollute the receiving river. The Coombe MWTS consists of four pilot-scale VFRs, each with an area of 50 m2 (5 m × 10 m) and a depth of 2 m. These were constructed utilising the findings from small-scale field trials (Okeme *et al.* 2025). Treatment media tested include granite and limestone, enabling investigation of both oxidation-driven and alkalinity-driven removal pathways. The nature and thickness of the media in the VFRs are described in Table 1. Target retention times (RT) in the limestone portion of VFR 2 and VFR 3 are broadly reflective of the RT in the limestone reactors of the original trial (Okeme *et al.* 2025), with a nominal RT on average of 2.8 and 2.5 hrs in the limestone section of VFR 2 and 3 respectively compared to ≈ 3 hrs in the limestone reactors of the METAL-SoLVER trial. Average flow rates over the trial were of 0.4 L/s for VFRs 1 and 2 and 0.5 l/s for VFR 3. VFR 4 was not in use for this trial.

Results and Discussion

CO_2 degassing is an important phenomenon in VFRs, in common with coal mine waters (see Geroni *et al.* 2012). This is most clearly demonstrated by the data for VFR 1 which contained only granite media. A pH rise is observed as water passes through VFR 1,

Table 1 Vertical Flow Reactor (VFR) configuration and media details.

	Media type and size	Media layers and depth
VFR 1	Granite gravel 6 mm	Top layer: Depth of 200 mm
	Granite gravel 20 mm	Bottom layer: Depth of 150 mm
VFR 2	Granite gravel 6 mm	Top layer: Depth of 200 mm
	Limestone gravel 2-6 mm	Middle layer: Depth of 200 mm
	Granite gravel 20 mm	Bottom layer: Depth of 150 mm
VFR 3	Limestone gravel 2-6 mm	Top layer: Depth of 400 mm

***Figure 1** General arrangement of the four VFRs at Coombe MWTS.*

***Figure 2** VFR 1 and its aeration rose, showing iron accumulation on the surface of the media layer.*

with loss of the temporary acidity due to CO_2 degassing (compare "raw" influent mine water and ''VFR 1" effluent in Figure 3). Bubbles were clearly seen escaping from the influent water for all VFRs and from the VFR media, leaving small holes visible in accumulated ochre. It is not known whether these are due to entrained air subsequently escaping, but it is feasible that these could be evidence of CO_2 degassing. In VFRs 2 and 3 the more substantial pH rise is due also to reaction with limestone.

Iron is a secondary contaminant of concern for this system, but its removal as a filter cake on top of the upper layer of granular granite media (see Figure 2) also allows the use of limestone in subsequent treatment, which otherwise has a tendency to become armoured/blinded with iron precipitates (as has been demonstrated in

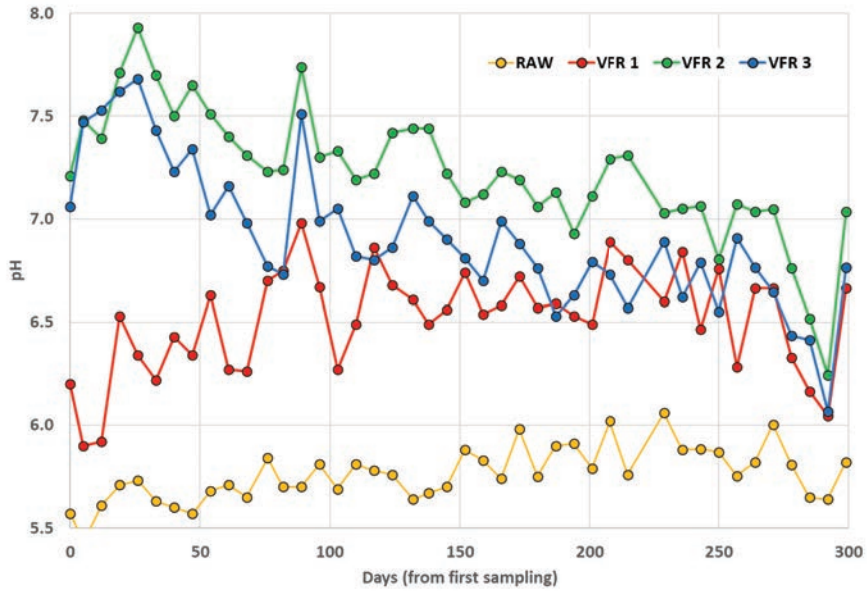

Figure 3 *A plot of pH versus time for raw mine water and the effluent from VFRs 1–3.*

many mine water treatment systems). Iron removal was excellent, with effluent total iron concentrations for VFRs 1–3 being commonly lower than the detection of the analysis used (<0.01 mg/l)) over the entire period of the trial. That the same Fe removal results were obtained for VFR 1 (no limestone) shows that the effectiveness of iron removal in VFRs for this mine water does not require the further pH increase from limestone dissolution. It is interesting to note that at the pH of the influent (pH 5.5-6) the literature reported rates of homogenous Fe(II) oxidation suggest an expected half-life of days (Stumm and Morgan 1997), whereas the Fe(II) oxidation and precipitation is observed here are happening in hours. This is likely due to heterogenous catalysis by ochre considerably enhancing Fe(II) oxidation kinetics (Barnes *et al.* 2009). These findings are important evidence for the application of VFRs for Fe removal in coal and metal mine water treatment schemes. Despite the excellent iron removal and consequent accumulation of ochre on top of the media, sufficient hydraulic conductivity of the VFRs was maintained allowing for continuous operation over the trial.

Mn removal versus time is shown in Figure 4. Mn is not removed in VFR 1, likely due to relatively low pH impeding the oxidation kinetics. In VFRs 2 and 3 Mn is removed from almost the beginning of the trial. The removal is attributed to the limestone layers in VFR 2 and 3 acting to boost the pH of the mine water upon contact through dissolution of calcite. A plot of effluent Mn concentration versus pH (not shown) indicates that at pH> 6 the Mn is effectively removed. The rapid removal might have initially involved sorption, but Mn(II) oxidation and precipitation of MnO2 was rapidly established, evidenced by accumulation of black precipitate in the limestone of VFR 3 and subsequent analyses (not shown). Once MnO_2 precipitate has accumulated, the well-known autocatalytic oxidation mechanism (Stumm & Morgan 1997) and additional biotic effects become more important. The establishment of a zone of catalysing MnO_2 precipitate during early operation of VFR 2 and 3 may explain why VFR 2 and 3 continue to remove Mn later in the trial when compared to the lack of removal in VFR 1, which is of comparable pH (Figure 3). Differences in pH dependence of sorption to calcite surfaces present in VFR 2 & 3 (but not

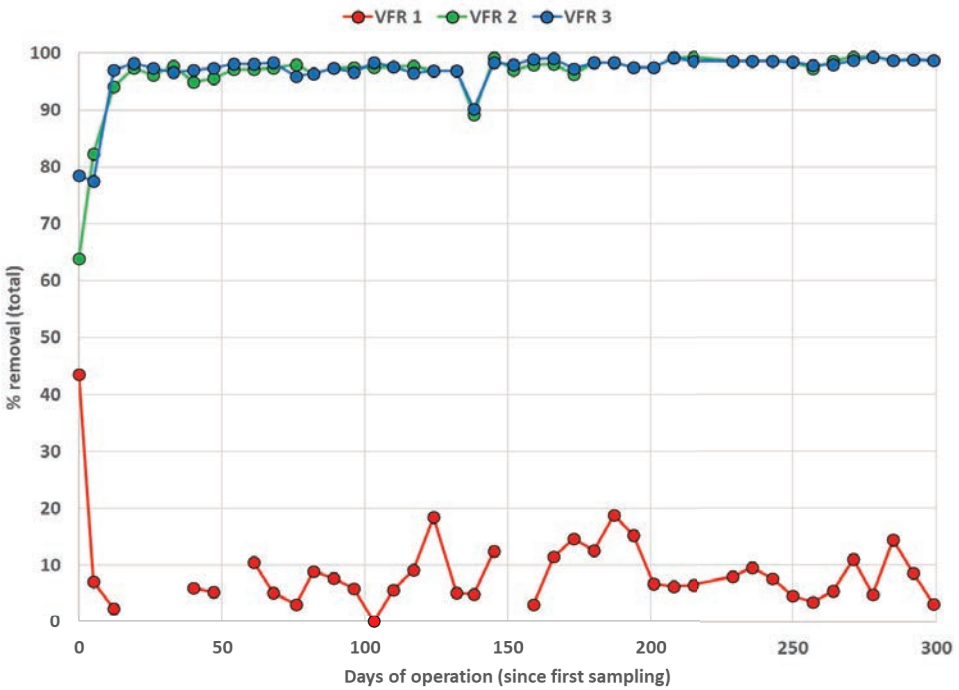

Figure 4 *A plot of Mn removal % versus time in VFRs 1–3*

VFR 1) and/or formation of $MnCO_3$ may also be important in the continued removal.

Zn removal with time is shown in Figure 5. This shows excellent removal at the beginning of the trial for VFRs 2 and 3, and then a decrease over time, with the latest data suggesting a stabilisation in the range of 20–50% removal. In terms of load removal (by calculation combining flow data) over the 300 days, 50% and 51% of the Zn load has been removed for VFR 2 and 3 respectively. Whilst this is promising removal for a simple granite/limestone bed, the system is not performing as well as in the previous small-scale trial (Okeme *et al.* 2025). The likely explanation is that unlike in the original trials, the CO_2 content of the water was not fully degassed in VFRs 2 and 3 which constrains the pH rise upon contact with limestone. Interestingly, this is in-line with the sorption edge for Zn adsorption on to amorphous or hydrous manganese oxides (Pretorius & Linder 2001; Gadde & Laitinen 1974). The most recent data for the system (not shown) shows increasing recovery of Zn removal rates indicating possible seasonal effects in the system.

The VFRs also displayed excellent polishing of Cu, Ni and Cd. Cu was removed from a mean of 64 µg/l in the influent to a mean of 1 and 2 µg/l in the effluents from VFRs 2 and 3 respectively. Ni was removed from a mean of 60 µg/l in the influent to a mean of 2 µg/l for both VFRs 2 and 3. Cd was removed from a mean of 2 µg/l in the influent to a mean of 0.5 µg/l for both VFR 2 and 3.

Conclusions

The VFR trials have shown remarkable removal of Fe and Mn which may have very important implications for mine water treatment in general. The VFR trials have also demonstrated that permeability of the ochre layer was not an issue for the duration of the trial. Furthermore, excellent removal of Ni and Cu was noted despite the very low concentrations in the influent, showing that the system can polish these effectively to very low levels. Zn removal was not as high, with 50–51% of the total influent Zn load removed (in VFRs 2 and 3), although still notable given these are very simple aerobic granite/limestone reactors. However, effluent concentrations of Zn were generally not as low

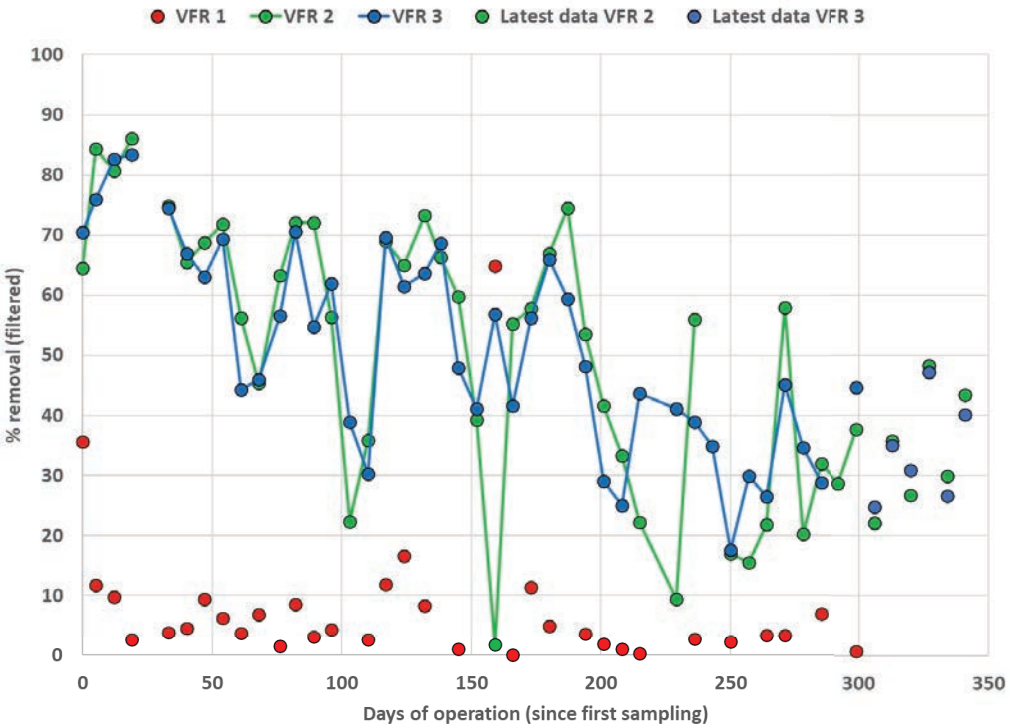

Figure 5 A plot of Zn removal versus time for VFRs 1 – 3, including latest data from VFRs 2 and 3.

as those achieved during earlier trials because of dissolved CO_2 restricting the pH rise when contacting limestone. It is important that CO_2 is degassed as this will lead to higher pH and better co-removal of Zn by adsorption to MnO_2 precipitated on the VFR media.

References

Barnes A, Sapsford DJ, Dey M, Williams KP (2009). Heterogeneous Fe (II) oxidation and zeta potential. Journal of Geochemical Exploration, 100(2–3), 192–198.

Gadde RR and Laitinen HA (1974) Heavy metal adsorption by hydrous iron and manganese oxides. Analytical Chemistry, 46(13), pp.2022–2026.

Geroni JN, Cravotta III CA. and Sapsford DJ (2012) Evolution of the chemistry of Fe bearing waters during CO2 degassing. Applied geochemistry, 27(12), pp.2335–2347.

Okeme IC, Srivastava P, Sapsford DJ (2025) Highly efficient co-removal of zinc and manganese during passive treatment of mine drainage: Mechanisms, microbiology and application. Ecological Engineering. 219:107681.

Pretorius PJ and Linder PW (2001). The adsorption characteristics of δ-manganese dioxide: a collection of diffuse double layer constants for the adsorption of H^+, Cu^{2+}, Ni^{2+}, Zn^{2+}, Cd^{2+} and Pb^{2+}. Applied Geochemistry, 16(9-10), pp.1067–1082.

Stumm W, Morgan JJ (1997) Aquatic chemistry: chemical equilibria and rates in natural waters. John Wiley & Sons.

Predicting Contamination Pathways in Mining-Affected Watersheds Using a Cellular Automaton

Fernando Barrio-Parra[1], Jaime Montalvo-Piñeiro[1], Lucía Álvarez-Mejías[1], Humberto Serrano-García[1], Miguel Izquierdo-Díaz[1], Almudena Ordoñez[2], Rodrigo Álvarez[2], Eduardo De Miguel[1]

[1]*Prospecting & Environment Laboratory (PROMEDIAM), ETS de Ingenieros de Minas y Energía, Universidad Politécnica de Madrid, Alenza 4, Madrid 28003, Spain*

[2]*ISYMA Group, Department of Mining Exploitation and Prospecting, University of Oviedo, Independencia 13, Oviedo, Asturias 33004, Spain*

Abstract

Historical mining has introduced trace elements and acid mine drainage into river systems via surface-runoff pathways from waste deposits and abandoned workings, altering sediment geochemistry and posing ecological and health risks. This study evaluates the Contaminant Mass Transfer Cellular Automaton (CMTCA), a probabilistic model that simulates slope-driven runoff trajectories using minimal inputs. Applied to the Nalón River basin (Spain), The results support CMTCA as a low-cost tool to prioritise risk assessment, guide background-sampling design by identifying non-affected reaches and inform early-stage environmental management in mining-influenced watersheds.

Keywords: Mining contamination, acid mine drainage, cellular automaton, risk assessment

Introduction

Historical and active mining activities release trace elements and generate acid mine drainage (AMD); these processes enhance metal mobilisation by surface runoff and fluvial transport, favouring their accumulation in river sediments, posing ecological and human-health risks (Álvarez *et al.*, 2018; Ordóñez *et al.*, 2013). Beyond direct releases, trace elements naturally cycle through weathering and biogeochemical processes (Izquierdo *et al.*, 2015), but mining increases metal availability and disrupts environmental equilibria (Kobina Mensah & Amoakwah, 2024). Landscape alteration exposes mineralised materials to erosion and chemical transport, often promoting soil and water acidification and enhancing metal mobility; residues such as waste rock and tailings become long-term sources affecting soils, sediments, and waters (Kim *et al.*, 2008; Álvarez *et al.*, 2018). Exposure may occur through contaminated crops (Gallego *et al.*, 2002; Hu & Ding, 2009), inhalation, dermal contact, or accidental ingestion (Han *et al.*, 2005). Also, in aquatic systems downstream of mining areas, bioaccumulation and biomagnification of trace elements along food chains may constitute a relevant exposure pathway for ecological and human receptors.

Because trace elements concentrate in the upper soil centimetres, surface runoff is the principal mechanism for lateral transfer from sources to river corridors and sediments, especially in mountainous basins with steep slopes and intense or torrential precipitation; under favourable conditions, transfer distances may reach ≈3 km before entering surface waters (Álvarez *et al.*, 2018; Giuliano *et al.*, 2007; Larios *et al.*, 2012; Sims *et al.*, 2022). Delineating likely influence areas therefore requires tools that incorporate topographic control and runoff routing.

Robust risk assessment further depends on distinguishing natural variability from anthropogenic enrichment via background levels (and derived reference values) representative of unaffected conditions (De Miguel *et al.*, 2002). Background can be obtained from generic compilations, site-specific literature, or dedicated basin sampling (Garcia-Ordiales *et al.*, 2019;

Nude *et al.*, 2011; Gallego *et al.*, 2002; Garcia-Ordiales *et al.*, 2018, Barrio-Parra *et al.*, 2025).

Within this context, the Contaminant Mass Transfer Cellular Automaton (CMTCA) offers a probabilistic, computationally efficient framework to simulate runoff-driven transport from mining/industrial sources to river receptors using minimal inputs (Barrio-Parra *et al.*, 2020). This study evaluates the suitability of CMTCA to delineate potential influence areas of historical mining on sediment trace-element concentrations in the Nalón River basin (Asturias, Spain).

Methods

Study area

The Nalón River basin (5,442 km^2) is characterised by steep geomorphology (mean slope 41%), abundant precipitation (>970 mm/year), and a dense network of 614 rivers. The basin also hosts over 800 historical mining sites (coal, iron, mercury, fluorite, kaolin) that are distributed across the basin (Álvarez *et al.*, 2018). These extractive and industrial operations have generated waste rock, tailings, and acid mine drainage over time, making them potential sources of trace-element mobilisation. Their spatial distribution and topographic context are key factors influencing the potential transfer of contaminants toward river sediments.

Modelling of transport by surface runoff

The transport modelling was carried out using the Contaminant Mass Transfer Cellular Automaton (CMTCA), a probabilistic and slope-driven algorithm designed to simulate the surface-runoff-mediated movement of particles from source points to river receptors (Barrio-Parra et al., 2020). The model operates on four essential input layers—Digital Elevation Model (DEM), influence points (source cells), receptors, and optional barriers—all discretized into a regular grid. For each source cell, the automaton evaluates downslope gradients toward the eight neighbouring cells and assigns transition probabilities proportional to local slope. A stochastic selection identifies the next cell in the trajectory, and the process iterates successively until a receptor is reached.

This procedure represents a single simulation; in this study, 1000 simulations were performed per source cell, and the resulting ensemble was aggregated into a pathway-frequency surface in which each cell value corresponds to the number of realisations in which it was traversed, thus providing a probabilistic estimate of runoff-driven transport likelihood (Figure 1). A 5 m × 5 m grid was used as the baseline spatial resolution, and an additional 200 m grid was evaluated to assess scale effects. For comparison, two simplified approaches were also incorporated: the Trace Downstream tool in ArcGIS Pro - based in the maximum slope preference path from an origin point - and a 3 km fixed influence buffer, representing a conservative upper-bound assumption for maximum transport distance by runoff.

Results

The initial output consisted of the compilation of a basinwide database, which made it possible to visualise the large number of historical and operational activities potentially influencing trace element concentrations in sediments. Most of these activities correspond to mining operations, although several industrial facilities are also present. Even prior to the application of any modelling technique, the spatial distribution of influence points provides a valuable qualitative overview of possible anthropogenic pressures. While the specific objective of this study concerns the alteration of sediment trace element concentrations, the typology and location of human activities across the basin are relevant for a wide range of environmental assessments.

As shown in Figure 2, the maps of sediments affected or non-affected that has been obtained with the different methodologies. In this case, the influence of all activity types is jointly considered; however, the complete analysis was also carried out for each mining and industrial category separately.

A key outcome observable in these maps is the identification of sediment reaches that remain unaffected under all methodologies. These areas are of particular interest because they represent suitable locations for establishing geochemical background

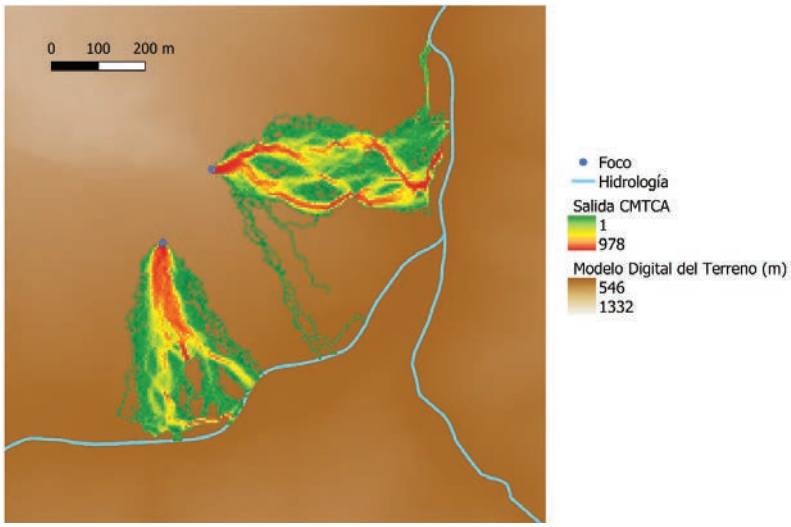

Figure 1 *Example of surface runoff pathways predicted with CMTCA for two source zones (blue dots).*

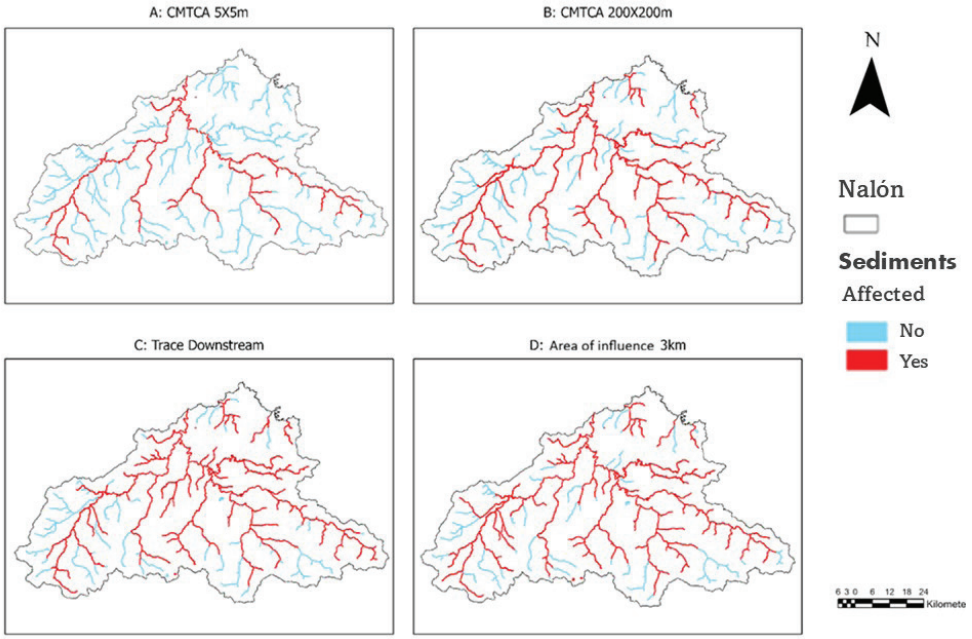

Figure 2: *Maps of sediments potentially affected (red) and non-affected (blue) by legacy mining and industrial activities, obtained through different methodologies.*

samples. Another relevant observation concerns the activities associated with the greatest potential influence—namely coal, fluorite, iron and mercury mining, together with thermal power plants. This behaviour can be attributed to two factors: (i) the high density of these activity types, and (ii) their preferential location in the upper basin, resulting in a large proportion of downstream sediment being potentially affected.

Notable differences arise when comparing the 5 × 5 m CMTCA model (Figure 1A) with the alternative methods. Using the 5 m-resolution DEM, sediments in 36% of the streams in the river basin could be affected by human activity. This proportion increased to 61% when the automaton was applied at 200 × 200 m DEM and reached 74% when using both the Trace Downstream tool and the 3 km influence-area criterion. Differences were also evident in the diversity of activities identified as potential sources: the application of CMTCA with a 5 m resolution DEM yield that only coal, mercury, iron, fluorite and magnesite sites could have a potential effect to river sediments, whereas all three complementary methods attributed a potential influence on every activity type.

These discrepancies stem from the operational logic of the automaton, which excludes flat or upslope cells (zero or positive slope), as they do not contribute to surface-runoff transport. Consequently, the model avoids overestimating influence in areas where runoff cannot realistically occur.

The application of the Trace Downstream tool resulted in the largest proportion of potentially affected sediment (reaches 74%), a value identical to that obtained using the fixed 3 km influence area. This outcome reflects the intrinsic conservatism of Trace Downstream, which assigns a deterministic downstream pathway from each source point, systematically reaching the fluvial network and marking all downstream segments as potentially affected. The 3 km buffer assumes maximum influence regardless of topographic constraints – potentially marking as "potentially affected" sediments of water streams located upslope from influence points, which is physically implausible and must therefore be interpreted with caution.

The probabilistic nature of the CMTCA also provides additional insight by indicating areas where runoff pathways diverge or converge, which is not captured by deterministic approaches. This approach account for key geomorphological constraints on surface-runoff transport, such as the presence of flat or inverse-slope areas, depositional zones, or attenuation processes that limit sediment delivery. This information is particularly relevant for studies aimed at evaluating contaminant accumulation zones, as the automaton highlights the areas where surface runoff is more likely to decelerate or terminate, thus favouring deposition.

Conclusions

The CMTCA proves to be an interesting approach to characterise the potential influence of anthropogenic activities on sediment trace-element concentrations. Its advantages are threefold: (i) parsimony of inputs (DEM, hydrological network, and locations of influence points), (ii) a probabilistic representation of transport (multiple plausible pathways rather than a single deterministic route), and (iii) more accurate delineation of influence zones by incorporating slope both to weight transitions and to exclude flat/upslope cells that do not contribute to surface runoff. While flat areas may favour contaminant accumulation, they are not involved in downstream transfer toward sediment-sampling reaches.

Applied to the Nalón basin at 5 × 5 m resolution, the CMTCA indicates that approximately 64% of sediment reaches remain unaffected by anthropogenic pressure and are therefore appropriate candidates for establishing background values. The remaining 36% appears potentially affected, mainly in association with coal, fluorite, iron, magnesite and mercury mining, in line with the spatial distribution of activities and their known geochemical signatures.

Beyond the modelling exercise, the compiled database evidences a high density of abandoned mining sites, many lacking adequate restorations. This pattern—observed in the Nalón basin and common elsewhere—reinforces the need for continued investigation and management actions to protect ecosystems and nearby communities.

Acknowledgments

This study was financed by the EU-funded ROTATE–CIRCULAR ECOLOGICAL ESSENTIAL & CRITICAL RAW MATERIALS [Grant Agreement ID: 101058651].

References

Álvarez, R., Ordóñez, A., Pérez, A., De Miguel, E., & Charlesworth, S. (2018). Mineralogical and environmental features of the asturian copper mining district (Spain): A review. Engineering Geology, 243, 206–217. https://doi.org/10.1016/j.enggeo.2018.07.007

Barrio-Parra, F., Izquierdo-Díaz, M., Del Álamo, L. J. F. G., Biosca, B., & De Miguel, E. (2020). Modelling the transference of trace elements between environmental compartments in abandoned mining areas. International Journal of Environmental Research and Public Health, 17(14), 1–14. https://doi.org/10.3390/ijerph17145117

Barrio-Parra, F., Álvarez, R., Serrano-García, H., Izquierdo-Díaz, M., Ordóñez, A., García-Fernández, C.C., De Miguel, E. (2025). A proposed methodology for the definition of background and reference values for trace elements in fluvial sediments. Ecotoxicology and Environmental Safety, 290, 117517. https://doi.org/10.1016/j.ecoenv.2024.117517

De Miguel, E., Callaba, A., Arranz, J. C., Cala, V., Chacón, E., Alberruche, E., Fdez.-Canteli, P., Iribarren, I., & Palacios, H. (2002). Determinación de niveles de fondo y niveles de referencia de metales pesados y otros elementos traza en suelos de la Comunidad de Madrid. Instituto Geológico y Minero de España.

Gallego, J. L. R., Ordóñez, A., & Loredo, J. (2002). Investigation of trace element sources from an industrialized area (Avilés, northern Spain) using multivariate statistical methods. Environment International, 27, 589–596. https://doi.org/10.1016/S0160-4120(01)00115-5

Garcia-Ordiales, E., Cienfuegos, P., Roqueñí, N., Covelli, S., Flor-Blanco, G., Fontolan, G., & Loredo, J. (2019). Historical accumulation of potentially toxic trace elements resulting from mining activities in estuarine salt marshes sediments of the Asturias coastline (northern Spain). Environmental Science and Pollution Research, 26(4), 3115–3128. https://doi.org/10.1007/s11356-017-0449-5

Garcia-Ordiales, E., Covelli, S., Rico, J. M., Roqueñí, N., Fontolan, G., Flor-Blanco, G., Cienfuegos, P., & Loredo, J. (2018). Occurrence and speciation of arsenic and mercury in estuarine sediments affected by mining activities (Asturias, northern Spain). Chemosphere, 198, 281–289. https://doi.org/10.1016/j.chemosphere.2018.01.146

Giuliano, V., Pagnanelli, F., Bornoroni, L., Toro, L., & Abbruzzese, C. (2007). Toxic elements at a disused mine district: Particle size distribution and total concentration in stream sediments and mine tailings. Journal of Hazardous Materials, 148(1–2), 409–418. https://doi.org/10.1016/j.jhazmat.2007.02.063

Han, Y., Zhang, S., Kang, D. et al. A Decade Review of Human Health Risks from Heavy Metal Contamination in Industrial Sites. Water Air Soil Pollut 236, 144 (2025). https://doi.org/10.1007/s11270-025-07759-9

Hu, X., & Ding, Z. (2009). Lead/cadmium contamination and lead isotopic ratios in vegetables grown in peri-urban and mining/smelting contaminated sites in Nanjing, China. Bulletin of Environmental Contamination and Toxicology, 82(1), 80–84. https://doi.org/10.1007/s00128-008-9562-y

Izquierdo, M., De Miguel, E., Ortega, M.F., & Mingot, J. (2015). Bioaccessibility of metals and human health risk assessment in community urban gardens. Chemosphere, 135, 312–318. https://doi.org/10.1016/j.chemosphere.2015.04.079

Kobina Mensah, A., & Amoakwah, E. (2024). Soil Biogeochemical Factors Influencing Mobilization of Toxic Elements in Mine-Contaminated Soils and Remediation Potential of Plants. In Environmental Sciences. https://doi.org/10.5772/intechopen.1005487

Kim, S., Kwon, H. J., Cheong, H. K., Choi, K., Jang, J. Y., Jeong, W. C., Kim, D. S., Yu, S., Kim, Y. W., Lee, K. Y., Yang, S. O., Ik, J. J., Yang, W. H., & Hong, Y. C. (2008). Investigation on health effects of an abandoned metal mine. Journal of Korean Medical Science, 23(3), 452–458. https://doi.org/10.3346/jkms.2008.23.3.452

Larios, R., Fernández-Martínez, R., Álvarez, R., & Rucandio, I. (2012). Arsenic pollution and fractionation in sediments and mine waste samples from different mine sites. Science of the Total Environment, 431, 426–435. https://doi.org/10.1016/j.scitotenv.2012.04.057

Nude, P. M., Foli, G., & Yidana, S. M. (2011). Geochemical Assessment of Impact of Mine Spoils on the Quality of Stream Sediments within the Obuasi Mines Environment, Ghana. International Journal of Geosciences, 02(03), 259–266. https://doi.org/10.4236/ijg.2011.23028

Ordóñez, A., Álvarez, R., & Loredo, J. (2013). Asturian mercury mining district (Spain) and the environment: A review. Environmental Science and Pollution Research, 20(11), 7490–7508. https://doi.org/10.1007/s11356-013-1663-4

Sims, D. B., Hudson, A. C., Keller, J. E., Strange, M., Buch, A. C., Ferrari, D., Fernandez, G. M., Garcia-Hernandez, J., Kesl, B. D., & Torres, S. (2022). Trace elements migrating from tailings to rock varnish laminated sediments in an old mining region from Nelson, Nevada, USA. International Journal of Sediment Research, 37(2), 202–213. https://doi.org/10.1016/j.ijsrc.2021.08.001

The Role of Secondary Iron Phases in Acid Mine Drainage: Implications for Contaminant Mobilization

Ana Barroso[1], Isabela Vasques[2], Juan Antelo[3], Sarah Fiol[3], Ivan Carabante[4], Isabel Margarida Horta RibeiroAntunes[1], Amélia Paula Marinho Reis[1,5], Teresa Maria Valente[1]

[1]*Institute of Earth Sciences (ICT), University of Minho, Braga, Portugal*

[2]*Soils Department, Universidade Federal de Viçosa, Minas Gerais, Brazil*

[3]*Cross-disciplinary Research Center in Environmental Technologies (CRETUS), University of Santiago de Compostela, Santiago de Compostela, Spain,*

[4]*Civil Department, Environmental and Natural Resources Engineering, Lulea University of Technology, Lulea, Sweden.*

[5]*GEOBIOTEC, Geosciences Department, University of Aveiro, Campus Universitário de Santiago, 3810–193 Aveiro, Portugal*

Abstract

This study investigates the role of secondary Fe phases in controlling arsenate retention under conditions of acid mine drainage (AMD). Natural samples collected from the Valdarcas mine and laboratory-synthesized goethite and schwertmannite were compared to evaluate the arsenate adsorption capacity. Mineralogical and chemical characterization was performed using XRD, SEM, TEM, and ICP-MS, followed by batch adsorption experiments at pH 3, 5, and 7. Natural goethite showed high arsenate removal (>98%), whereas synthetic goethite showed lower efficiency (36–41%). Natural and synthetic schwertmannite exhibited moderate adsorption (50–57%). Results indicate that schwertmannite acts as a short-term arsenate reservoir, while goethite promotes long-term immobilization in AMD-affected environments.

Keywords: Goethite, schwertmannite, adsorption, arsenate, Valdarcas mine

Introduction

Acid mine drainage (AMD) is a global environmental problem associated with mining activities, particularly in areas where sulfide-rich ores are exposed to atmospheric conditions. The oxidation of sulfide minerals, such as pyrite, releases acidity, sulfate and dissolved metal(loid)s into surrounding waters (Jönsson *et al.*, 2006; Valente *et al.*, 2012). As Fe(II) released during sulfide oxidation is further oxidized to Fe(III), secondary iron minerals precipitate, forming characteristic ferruginous coatings and sediments in AMD-affected environments (Jönsson *et al.*, 2006; Valente & Gomes, 2009).

The composition and stability of these secondary Fe(III) precipitates are strongly controlled by environmental factors such as pH, sulfate concentration and redox conditions. Under highly acidic conditions (pH < 3), minerals such as jarosite may precipitate, whereas at slightly higher pH values schwertmannite and ferrihydrite are commonly observed. With increasing pH and time, more crystalline and thermodynamically stable phases such as goethite may develop (Jönsson *et al.*, 2006; Antelo *et al.*, 2012). In several AMD-systems these precipitates occur as mixtures of poorly crystalline and more stable phases due to ongoing mineral transformations and geochemical variations.

Secondary Fe-minerals play a key role in controlling the mobility of metal(loid) s in AMD environments. Due to their high specific surface area and reactive sites, these minerals can remove contaminants from solution through adsorption, coprecipitation or surface complexation processes (Antelo *et al.*, 2012). Among these contaminants, arsenic is of environmental concern due to its toxicity and common association with sulfide mineral deposits. Several studies have

shown that schwertmannite can efficiently retain arsenate under acidic conditions (Regenspurg, and Peiffer, 2005; Song *et al.*, 2015; Lee et a., 2023), while more crystalline iron oxides such as goethite also exhibit moderate sorption capacities for oxyanions (Antelo *et al.*, 2021). However, the stability and transformation of these phases may affect the long-term mobility of contaminants in AMD-systems, highlighting the importance of understanding their mineralogical proprieties and adsorption behavior.

The present study focuses on the Valdarcas mine, a former tungsten and tin mine hosted in a skarn-type deposit with abundant pyrrhotite (Valente and Gomes, 2009). Although the site was rehabilitated in 2007, AMD persists due to the presence of residual sulfide-rich wastes in the drainage system (Alves *et al.*, 2011; Barroso *et al.*, 2023). The aim of this study is to investigate the mineralogical characteristics and arsenate adsorption behavior of secondary Fe-precipitates collected from this AMD-affected mining area. Natural Fe-precipitates were characterized using mineralogical, microscopic and wet chemical techniques and compared with synthetic schwertmannite and goethite. Adsorption experiments were conducted to evaluate the role of these phases in arsenic retention.

Methods

Two natural samples of secondary Fe-phases were collected from Valdarcas mine (Covas, in Northern Portugal NW Portugal), a rehabilitated site affected by AMD, where the precipitation of Fe-oxyhydroxides and hydroxysulfates is commonly observed. The samples correspond to ferruginous precipitates and iridescent films formed in AMD environments. After field collection, the samples were transported to the laboratory, dried at room temperature, and carefully examined under a binocular microscope to obtain subsamples composed of a reduced number of mineral phases suitable for mineralogical and chemical characterization. A set of complementary analytical techniques was used to identify the mineral phases and assess their physicochemical properties. Mineralogical identification was performed by X-ray diffraction (XRD). Particle size and morphology characteristics were investigated by scanning electron microscopy (SEM) and transmission electron microscopy (TEM), whereas the chemical composition, including major and trace elements, was determined by inductively coupled plasma mass spectrometry (ICP-MS) following total digestion. These analyses were performed at Activation Laboratories (Actlabs, Canada). Quality assurance and quality control (QA/QC) protocols included the systematic analysis of procedural blanks, laboratory duplicates, internal standards, and certified reference materials. All QC results strictly met the laboratory acceptance criteria, with duplicates yielding a relative percent difference (RPD) of ≤5% for major elements and ≤10% for trace elements.

To compare the adsorption behavior of the natural samples with that of pure mineral phases, synthetic schwertmannite and goethite were prepared in the laboratory. Schwertmannite was synthesized following the hydrogen peroxide oxidation method described by Regenspurg *et al.* (2004), in which $FeSO_4$ dissolved in distilled water reacts with H_2O_2 to produce a red-orange precipitate under acidic conditions. After approximately 24 h, the precipitated material was separated by filtration and freeze-dried. Goethite was prepared following a procedure analogous to that described by Schwertmann and Cornell (2008), by adding a NaOH solution dropwise to a $Fe(NO_3)_3{\cdot}9H_2O$ solution under continuous stirring and N_2 bubbling to prevent contamination by atmospheric CO_2. The resulted precipitate was aged at 60 °C for 72 h, dialyzed against double-distilled water, and finally oven-dried at 50 °C for two days to obtain a dry powder.

Batch experiments were conducted to evaluate the arsenate adsorption capacity of both natural and synthetic samples of goethite and schwertmannite. Arsenate solutions were prepared from KH_2AsO_4 and added to the mineral suspensions at a concentration of 400 µM AsO_4^{3-}, for goethite and 1200 µM for shwertmannite. Immediately after arsenate addition, the pH of the suspensions was adjusted using standard HNO_3 or KOH solutions within the

range of pH 3–7, and all experiments were conducted under constant ionic strength conditions (0.1 M KNO_3). For goethite samples, the suspensions were agitated for 24 h, with pH adjustments performed every 2 h to maintain stable experimental conditions. In the case of schwertmannite, adsorption experiments lasted 72 h, with pH adjustments carried out every 6 h. After equilibration, the suspensions were filtered through 0.45 µm Millipore membrane filters, and the filtrates were stored at 4 °C until analysis. The concentration of arsenic remaining in solution was subsequently determined by ICP-MS.

Reagents used in the experiments were of analytical grade; arsenic reagents were purchased as potassium salts from Sigma-Aldrich, whereas all other chemicals were obtained from Merck. All experiments were performed using double-distilled, CO_2-free water at 25 ± 1 °C. Polycarbonate materials were used throughout the preparation of stock solutions, synthesis procedures, and adsorption experiments to avoid contamination by dissolved silica, and all laboratory equipment was previously washed with 10% HNO_3 and thoroughly rinsed with ultrapure water.

Results and discussion

Field observations revealed two distinct types of Fe-precipitates associated with acidic drainage water in the rehabilitated mining area (Figure 1). One sample corresponds to iridescent films precipitate at acidic surface water, which, after drying, develop fragile orange-brown crusts. The other sample occurs as powdery to crusty ferruginous precipitates accumulated in drainage channels constructed during the mine rehabilitation process.

The XRD patterns of the samples confirm the presence of two main mineral phases with markedly different degrees of crystallinity. The sample corresponding to the iridescent precipitates exhibits broad and poorly defined reflections at approximately 3.39 Å, 2.55 Å, 2.28 Å, 1.95 Å, 1.66 Å, and 1.52 Å, which are characteristic of schwertmannite (Figure 2 a). In contrast, the second sample shows well-defined and intense diffraction peaks at 4.18 Å, 2.68 Å, 2.44 Å, 2.18 Å, 1.71 Å, and 1.55 Å, consistent with the presence of goethite (Figure 2b). The sharpness and intensity of these reflections indicate a more crystalline and structurally ordered mineral phase. Microscopic observations further support these mineralogical differences. SEM and TEM analyses reveal that schwertmannite occurs as aggregates of spheroidal particles with diameters ranging from approximately 350 nm to 1.3 µm. These aggregates display rough surfaces and radial acicular projections, producing the characteristic "hedgehog-like" morphology frequently described for schwertmannite (Cornell and Schwertmann, 2003) (Figure 2c). In contrast, the goethite

Figure 1 *Images of the sampling sites of the two samples studied. Each panel shows a field photograph of the material, together with a binocular microscope image of the sample.*

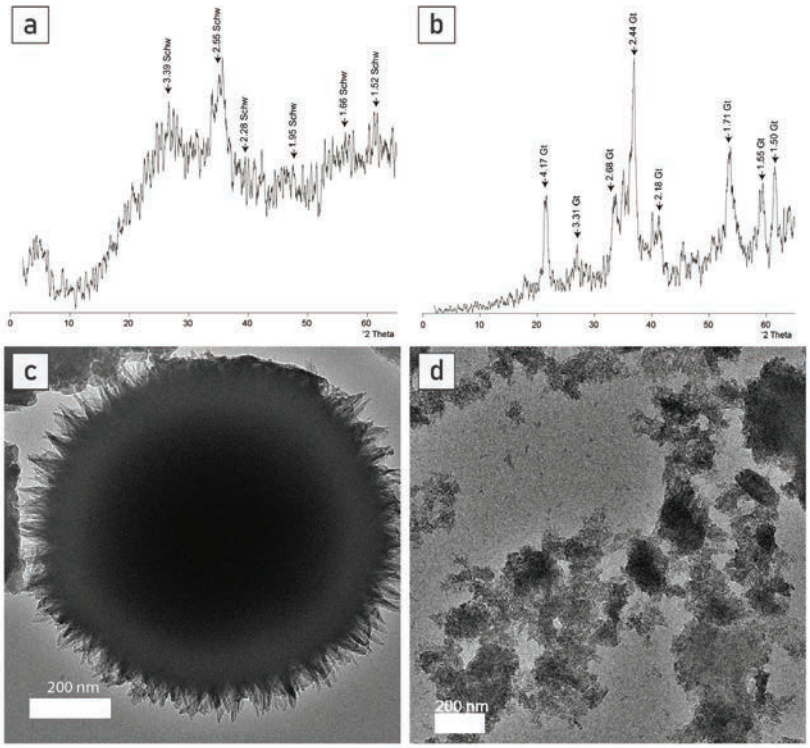

Figure 2 *XRD patterns of schwertmannite (a) and goethite (b), and TEM images showing the morphology of schwertmannite (c) and goethite (d).*

sample is composed of elongated and acicular aggregated particles (Figure 2d).

The chemical composition determined by ICP-MS reveals clear differences between the goethite and schwertmannite natural samples (Figure 3). Iron is the dominant element in both phases, as expected for secondary precipitates formed in AMD environments. However, the relative abundance of the remaining elements differs between the two samples, reflecting distinct mineralogical compositions. The schwertmannite sample is characterized by comparatively higher proportions of Al and several trace elements, particularly Mn, Ni, Zn, and Pb, suggesting a greater capacity to incorporate or retain these elements during precipitation under acidic conditions. In contrast, the goethite sample shows a composition strongly dominated by Fe and relatively higher proportions of Cu and Sb when compared with the schwertmannite. Cr and Co occur in both samples in comparable proportions, whereas Cd is only present at very low levels. Arsenic was detected in both mineral phases, confirming that these secondary iron precipitates can act as relevant sinks for this metalloid in AMD-affected environments. Overall, the chemical data indicate that, although both phases are Fe dominated, they differ in their minor and trace element signatures, which is consistent with their distinct crystal chemistry, formation pathways and environmental behavior.

The arsenate adsorption experiments revealed differences in adsorption behavior between natural and synthetic samples (Figure 4). Schwertmannite exhibited intermediate adsorption efficiencies. The natural schwertmannite sample (V4W_Sch) removed approximately 54–56% of arsenate, whereas the synthetic sample showed slightly lower values, around 50–52%. In both cases, adsorption was only weakly affected by

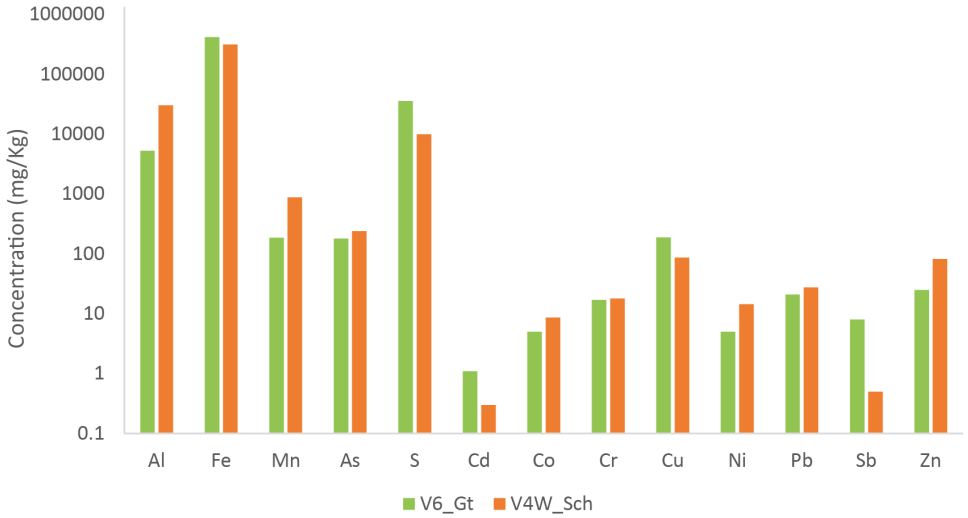

Figure 3 *Relative distribution of metal(loid)s in the natural goethite (V6_Gt) and schwertmannite (V4W_Schw) natural samples determined by ICP-MS. Values are plotted on a logarithmic scale.*

pH, with a slight increase towards neutral conditions for the natural sample. This slight difference in adsorption capacity may be associated with the presence of Al in the natural schwertmannite (V4W_Schw). Previous studies (e.g., Carrero *et al.*, 2022) suggest that Al incorporation can slightly enhance arsenate adsorption. However, this effect is generally moderate, and other factors, such as surface area, structural order, and the presence of impurities, may also play an important role in the observed differences.

On the other hand, the natural goethite sample (V6_Gt) showed the highest adsorption efficiency, with arsenate removal consistently around 98% at all tested pH values (pH 3, 5, and 7). In contrast, the synthetic goethite sample displayed substantially lower adsorption efficiencies, ranging from approximately 36 to 41%. Although the adsorption capacity remained relatively stable with pH, the marked difference relative to the natural sample suggests that the surface properties of the natural goethite are more favorable for arsenate retention. This behavior may reflect the greater mineralogical and structural complexity of the natural material, including the presence of defects, poor crystalline domains, minor element substitutions, or residual associated phases, all of which may increase the number and reactivity of available adsorption sites.

Conclusions

The results obtained in this study highlight the importance of secondary Fe minerals in AMD environments. The combined mineralogical, microscopic, and chemical characterization confirmed the presence of schwertmannite and goethite, two representative Fe phases formed under distinct geochemical conditions.

The adsorption experiments demonstrated that both minerals can retain arsenate, although with different efficiencies. Schwertmannite, both natural (V4W_Schw) and synthetic (Sch_syn), exhibited moderate adsorption capacity, with the natural sample showing slightly higher performance. In contrast, natural goethite (V6_Gt) exhibited a higher adsorption capacity than its synthetic counterpart (Gt_syn).

These distinct behaviors underscore that laboratory-synthesized minerals may not always act as accurate proxies for natural specimens when evaluating geochemical controls. The enhanced performance of the natural samples is driven by mineralogical

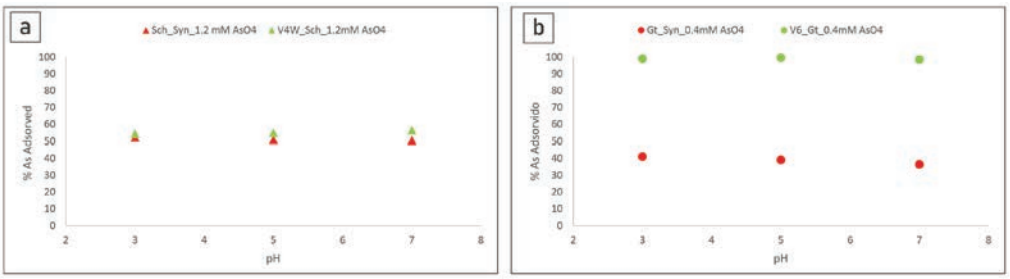

Figure 4 *Arsenate adsorption as a function of pH for natural and synthetic schwertmannite (a) and goethite (b) samples.*

heterogeneity and surface reactivity, features that remain difficult to fully replicate in the lab. Specifically, natural phases possess greater structural and compositional complexity, often including crystal defects, minor-element substitutions, varying crystallinity, and associated minor phases, which can increase the number and reactivity of adsorption sites.

Overall, these findings suggest that secondary iron phases play a key role in controlling arsenic mobility in AMD-affected and rehabilitated mining environments. Consequently, this study suggests that while synthetic phases remain fundamental benchmarks for understanding baseline mechanisms, relying solely on them may not fully capture the complexity of real-world scenarios. This highlights the clear benefit of combining both synthetic and natural materials in environmental assessments. Furthermore, these discrepancies point to the need for a more in-depth mineralogical and structural characterization of these phases, which is essential to better understand how specific chemical and structural differences influence arsenic retention capacities. Therefore, their formation, transformation, and physicochemical properties should be carefully considered when assessing contaminant behavior and predicting the long-term stability of arsenic in these systems.

Acknowledgements

Ana Barroso acknowledges the financial support of FCT – Foundation for Science and Technology, I.P., through the ICT research fellowship with reference UI/BD/151330/2021. This work was also co-funded by FCT through the Instituto de Ciências da Terra in the framework of the project UIDB/04683/2025, https://doi.org/10.54499/UID/04683/2025, and through the NanoMINENV project (PTDC/CTA-AMB/29259/2017).

References

Alves, R. C., Valente, T. M. F., Braga, M. A., & Gomes, C. L. (2011). Mineralogical composition and metals retention in the fine-fraction streambed precipitates of on AMD affected system. In Proceedings of the International Mine Water Association Congress-IMWA, Aachen, Germany, 4–11 September 2011.

Antelo, J., Fiol, S., Carabante, I., Arroyo, A., Lezama-Pacheco, J. S., Josevska, N., ... & Kumpiene, J. (2021). Stability of naturally occurring AMD–schwertmannite in the presence of arsenic and reducing agents. Journal of Geochemical Exploration, 220, 106677.

Antelo, J., Fiol, S., Gondar, D., López, R., & Arce, F. (2012). Comparison of arsenate, chromate and molybdate binding on schwertmannite: surface adsorption vs anion-exchange. Journal of colloid and interface science, 386(1), 338–343.

Barroso, A., Valente, T., Marinho Reis, A. P., & Antunes, I. M. H. (2023). A new acidity-based approach for estimating total dissolved solids in acidic mining influenced water. Water, 15(16), 2995. https://doi.org/10.3390/w15162995

Carrero, S., Fernandez-Martinez, A., Pérez-López, R., Cama, J., Dejoie, C., & Nieto, J. M. (2022). Effects of aluminum incorporation on the schwertmannite structure and surface properties. Environmental Science: Processes & Impacts, 24(9), 1383–1391.

Cornell, R. M., & Schwertmann, U. (2003). The iron oxides: structure, properties, reactions, occurrences and uses. John Wiley & Sons.

Jönsson, J., Jönsson, J., & Lövgren, L. (2006). Precipitation of secondary Fe (III) minerals from acid mine drainage. Applied Geochemistry, 21(3), 437–445.

Lee, S. Y., Kim, Y., Kang, S. A., Chang, B., Hur, H., & Lee, Y. J. (2023). Characterization of arsenic (III and V)

adsorption on natural schwertmannite formed in acid coal mine drainage: Batch studies and spectroscopic observations. Journal of Environmental Chemical Engineering, 11(1), 109170.

Regenspurg, S., & Peiffer, S. (2005). Arsenate and chromate incorporation in schwertmannite. Applied Geochemistry, 20(6), 1226–1239.

Regenspurg, S., Brand, A., & Peiffer, S. (2004). Formation and stability of schwertmannite in acidic mining lakes. Geochimica et Cosmochimica Acta, 68(6), 1185–1197.

Schwertmann, U., & Cornell, R. M. (2008). Iron oxides in the laboratory: preparation and characterization. John Wiley & Sons.

Song, J., Jia, S. Y., Ren, H. T., Wu, S. H., & Han, X. (2015). Application of a high-surface-area schwertmannite in the removal of arsenate and arsenite. International Journal of Environmental Science and Technology, 12(5), 1559–1568.

Valente, T. M., & Gomes, C. L. (2009). Occurrence, properties and pollution potential of environmental minerals in acid mine drainage. Science of the total environment, 407(3), 1135–1152.

From AMD to Pigments: Biological Iron Oxidation and Characterization of Recovered Iron Precipitates

Zuzana Bártová[1], Jaroslav Briančin[1], Martin Fabián[1]

[1]*Institute of geotechnics, Slovak Academy of Sciences, Slovak Republic*

Abstract

This study investigates biological iron removal and recovery from the real mine water at the Smolnik site (Slovakia). Ferrous iron oxidation was enhanced using native acidophilic microbial consortia, achieving over 99% removal within 30 hours under acidic conditions. A sequential process combining aeration, microbial oxidation, and controlled pH adjustment enabled the formation of iron precipitates such as schwertmannite and ferrihydrite. Elemental and structural analyses confirmed low arsenic content in biologically produced precipitates, meeting regulatory limits for pigment use. This approach highlights a sustainable strategy focusing on contaminant removal with value-added material recovery.

Keywords: Mining influenced water, acidophiles, mineral pigments, circular economy, iron oxidation

Introduction

Iron is a common contaminant in natural and industrial waters, particularly in effluent associated with mining and metallurgical activities, where elevated concentrations can adversely affect aquatic ecosystems and technical infrastructure. At the same time, iron constitutes a valuable secondary resource, as its precipitate forms can be reutilized as mineral pigments in a wide range of industrial applications, including paints, ceramics, plastics, and construction materials.

In nature, iron occurs mainly in two oxidation states, as ferrous (Fe^{2+}) and ferric (Fe^{3+}) ions. The prevailing form is dependent on pH, oxygen concentration, and redox conditions (Stumm and Morgan 1996).

The oxidation of ferrous iron to ferric iron by dissolved oxygen is a complex and multi-step process. It involves the formation of partially oxidized intermediate phases which are metastable and challenging to characterize or predict. Over time, these intermediates undergo transformation into more thermodynamically stable iron oxide minerals, including hematite, magnetite, goethite, and lepidocrocite (Morgan and Lahav 2007).

Mining influenced waters are commonly acidic due to the oxidation of certain sulfide minerals exposed during mining activities, which generates acidity and lowers the pH of the drainage waters (Johnson and Hallberg 2005; Singer and Stumm 1970; Wolkersdorfer 2022).

In acidic environments, the abiotic oxidation of ferrous iron by dissolved oxygen is kinetically limited, as Fe^{2+} remains relatively stable at low pH (Morgan and Lahav 2007). Consequently, spontaneous chemical oxidation proceeds slowly and is insufficient to account for the rapid iron cycling observed in acid mine drainage (AMD) systems. Instead, this process is largely driven by the metabolic activity of acidophilic iron-oxidizing microorganisms, which catalyze the oxidation of ferrous to ferric iron at rates several orders of magnitude higher than abiotic reactions (Johnson *et al.* 2012).

The microbial oxidation of iron plays a central role in both natural and engineered systems, enabling efficient iron removal and influencing the formation of secondary iron minerals. Biohydrometallurgical studies have demonstrated that near-complete ferrous iron oxidation can be achieved at pH values as low as 1.5 without the need for chemical

neutralization, highlighting the advantages of biological processes over conventional chemical treatments (Kaksonen *et al.*, 2014). These processes promote the formation of iron precipitates such as schwertmannite, jarosite, and goethite, which are critical for the removal of iron and associated contaminants from mine waters.

This study focuses on iron removal regarding acid mine drainage from the historical mining site in Smolnik, Slovakia. In the recent years, pH of the mining influenced water from the main drainage shaft Pech, ranges from 3.95 to 4.12 and produces a high volume of mine water (approximately 6.5–10 L/s). Concentration of metals analysed in the water ranges according to the weather conditions and rainfall volumes (Bártová 2025).

The purpose of this study was to optimize Fe^{2+} oxidation processes and characterize iron precipitates formed from real mine water under laboratory conditions. Mine water samples were either inoculated with iron-oxidizing acidophiles (pre-grown cultures of native strains) or left uninoculated, allowing a comparison of products formed by biological and chemical oxidation.

Methods

Bacterial strains and incubation conditions

For the purposes of the experiment, native microbial consortia were cultivated in mine water from the main discharge shaft (Pech), supplemented with 9K salts (1.6 mmol/L $MgSO_4 \cdot 7H_2O$, 0.76 mmol/L $(NH_4)_2SO_4$, 0.23 mmol/L K_2HPO_4, and 120 mmol/L $FeSO_4 \cdot 7H_2O$). Cultivation was carried out in magnetically stirred, aerated baffled reactors (0.5 L working volume) at 25 °C and 240 rpm.

Mine water parameters

pH/ ORP analysis

A combined glass electrode (InLab Micro, Mettler Toledo) was used for pH measurement, and oxidation–reduction potential (ORP) was monitored using a Pt–Ag/AgCl redox electrode (InLab Redox Micro, Mettler Toledo). Measurements were performed with a Seven2Go S2 meter (Mettler Toledo).

Iron speciation

Ferric iron was determined with a UV-spectrophotometric method at 300 nm (Basaran and Tuovinen 1986). Ferrous iron concentrations were determined by a modified o-phenantroline spectrophotometric method, insensitive to Fe3+ interference (Herrera *et al.* 1989).

Chemical analyses

Elemental analysis of the water was done using AAS (Varian AA240Z, AA240FS) and ICP-MS 7700 (Agilent). Sulfate concentration was analyzed by ion chromatography (Dionex ICS 5000).

The microstructure and morphology

Iron powders were investigated by MIRA 3 FE-SEM scanning electron microscope (TESCAN GROUP, a.s., Czech Republic) with an EDX detector (Oxford Instruments, Abingdon, UK).

XRPD patterns were obtained using a D8 Advance diffractometer (Bruker) operating with Cu Kα radiation in the Bragg–Brentano configuration.

Elemental composition was determined using a handheld X-ray fluorescence (XRF) analyzer (X-MET8000 Expert Geo, Hitachi High-Tech).

Color measurements

Color was measured using a Nix™ Spectro 2 sensor (D50, 2°), with results expressed in the CIELab* color space (Robertson 1977).

Results and discussion

Mine water from the Smolnik site was analyzed and treated in order to remove dissolved iron and recover precipitates usable as mineral pigments in form of powders. Air-dried precipitates were then characterized using X-ray diffraction (XRD), X-ray fluorescence (XRF), scanning electron microscopy (SEM), energy-dispersive X-ray spectroscopy (EDX), and NIX™ color determination instruments. Liquid samples and resulting mine water after Fe-precipitates removal were analyzed using atomic absorption spectroscopy (AAS).

Initial composition of the mine water is given in Tab. 1. During the experiment, concentrations of Fe, As, Al, Mg, Mn, Cu, Co and SO_4^{2-} were followed, as these elements

Table 1 Parameter sand composition of the Smolnik mine water (2026).

pH	ORP	Conductivity	Temperature	Flow rate
	mV	mS/cm	°C	L/s
3.95	286	2.53	11.7	n.a.

Shaft Pech mg/L	SO_4^{2-}	Fe	Al	Mn	Zn	Mg	Ca
2026	2871	238	40.7	12.9	50.3	275	111

Shaft Pech mg/L	Cu	Co	Pb	As	Cd	Cr	Ni
2026	1750	360	47.1	39.4	5.8	0.6	90

either form a pigment structure (Fe, Al, S) or they are considered an unwanted impurity, often exhibiting toxic characteristics (As) or they are considered a valuable component of the water (Cu, Co, Mg, Mn) where leaving them in the water might lead to possibilities of their subsequent recovery from already iron-free solutions.

Iron precipitate (pigment) formation in mine water was carried out as a sequential three-stage process: (i) initial aeration of MIW (30 h) to lower pH and partially oxidize and precipitate Fe, removing phases that can sorb arsenic; (ii) bacterial inoculation to accelerate ferrous iron oxidation; and (iii) pH adjustment to promote precipitation of poorly crystalline phases such as ferrihydrite or schwertmannite. Between stages, Fe precipitates were removed by filtration using a 0.22 µm PES filter.

Iron oxidation

Ferrous iron oxidation is limited at pH below 4 (Jones *et al.* 2014; Morgan and Lahav 2007). As the pH of Smolník MIW fluctuates around this value and decreases below 3.5 after aeration, acidophilic microbial consortia were introduced to enhance oxidation. Despite genotypic differences, many acidophilic iron oxidizers share similar physiological traits (Kupka *et al.* 2023). Therefore, native microbial species were preferred over pure collection species, which can be costly and their purity needs to be confirmed over a longer period of time to ensure that we are still working with the declared species. Native consortia isolated from Smolník MIW were pre-cultivated and subsequently used for iron oxidation.

A 2 L of Smolník MIW were aerated for 30 h and subsequently filtered to collect the initial iron phase (A). The filtrate was transferred to a 5 L flask, and 50 mL of actively growing microbial culture (exponential phase; ≈2.0×10^6 cells/mL) was added. Iron introduced with the growth medium was not considered. Iron oxidation was monitored for 29 h, with a substantial decrease in Fe^{2+} concentration observed within the first 21 h. After 29 h, Fe^{2+} levels dropped below 2 mg/L, corresponding to a removal efficiency exceeding 99%. The solution was then filtered again to collect the resulting iron precipitates (B) for further analysis.

After filtration, the water was divided into separate flasks for the final pH adjustment. Starting from pH 2.6, the pH was increased to (i) 3.2 (optimal for schwertmannite formation), (ii) 4.1 (natural Smolník MIW pH), (iii) 5.5 (favorable for Al precipitation), and (iv) 6.2 (rapid ferrihydrite formation) using 20% NaOH. After each adjustment, precipitates were removed by filtration, and the water was either subjected to further treatment or stabilized with concentrated HNO_3 for AAS analysis (Tab. 2). Note that a pH level of 5.5 was achieved using the remaining water after filtering water that had already been adjusted to a pH of 3.2, as a high iron concentration was still present in the sample.

As table 2 shows, majority of Fe was effectively removed already after the bacterial oxidation, without any further pH adjustments. Applying pH levels above 4.1 the Fe concentration complied with the Regulation of the Government of the Slovak

Table 2 Final elemental composition of mine water after the pH adjustment; n.d.: below detection limit.

	Name	Fe	Al	Mn	Mg	Cu	As	Co
		mg/L	mg/L	mg/L	mg/L	mg/L	mg/L	mg/L
–	**Initial MIW**	238.8	40.7	12.88	275.3	1750	39.4	359.9
A	**30 hours aeration**	196.5	40.9	13.12	277	1740	15.7	369.4
B	**Bacterial oxidation**	15.68	42.2	13.22	273.1	1780	3.3	368.3
C	**pH 3.2**	8.39	38.8	13.18	246.3	1750	2.3	404.2
D	**pH 4.1**	0.21	32.7	13.03	236	1610	1.9	394.1
E	**pH 5.5**	0.05	n.d.	11.7	216.3	210	1.8	400.2
F	**pH 6.2**	0.05	n.d.	10.99	210.9	60	1.8	334.6

Republic (2010), which sets a limit of 2 mg/L. Aluminum was effectively removed from the solution at pH 5.5, as it was expected. Co, Cu, Mg and Mn did not co-precipitate from the water at pH below 4.1 and such water can be subject for their later recovery. The majority of arsenic was removed during the first aeration step, and the remaining concentration already complied with the Regulation of the Government of the Slovak Republic (2010), which sets a limit of 0.02 mg/L.

Pigments obtained from the first two steps (i, ii) of iron precipitation were analyzed using SEM-EDS and a handheld X-ray fluorescence (XRF) analyzer to confirm their elemental composition and to ensure that the resulting products did not contain high concentrations of arsenic or other potentially toxic elements. XRF analysis showed that Product A (30-hour aeration) contained a high arsenic concentration of above 350 mg/kg. In contrast, Product B (bacterial oxidation) exhibited minor arsenic levels of less than 30 mg/kg. This value complies with the European Commission criteria, which state that pigments must not be based on Cd, Pb, Cr (VI), Hg, As, Se, Sb, or Co, and that impurities from these elements must not exceed 100 mg/kg in the final product formulation (European Commission 2025). Based on these criteria, Sample B can be considered suitable for use as a pigment.

All samples were characterized using XRPD. The diffraction patterns indicated poorly crystalline iron phases consistent with schwertmannite or ferrihydrite-like materials, clearly in samples A and B and less distinctly in sample C. Samples E and F exhibited predominantly amorphous characteristics, while sample D showed intermediate properties. EDS analysis revealed a transition from Fe-rich oxyhydroxysulfate phases (schwertmannite-like) at low pH to Al-rich hydroxide phases at higher pH, confirming a sequential precipitation mechanism controlled by microbial oxidation and pH adjustment.

The color of iron precipitates is a key parameter for their potential use as pigments because it directly determines their aesthetic and commercial value. Variations in color are closely linked to mineral phase, crystallinity, particle size, and chemical composition, all of which influence optical properties such as light absorption and scattering (Cornell and Schwertmann 2003). In addition, impurities and substitutions (e.g., Al, sulfate, or trace metals) can modify hue and stability, affecting pigment performance (Bigham *et al.* 1990; Schwertmann and Cornell 2000). To quantitatively evaluate these properties, it is convenient to express color values in the CIE L*a*b* color space system, which provides a standardized, device-independent framework based on lightness (L*) and chromatic coordinates (a*, b*). This system correlates well with human visual perception and enables precise comparison between samples making it particularly suitable for pigment characterization and quality control (Mclaren 1976; Robertson 1977). To determine color, Nix™ Spectro 2 Color Sensor was used.

The synthesized iron precipitates (Tab. 3) exhibited a wide range of color coordinates in the CIE L*a*b* space (L* = 14.81–48.80, a* =

Table 3 Final elemental composition of mine water after the pH adjustment; n.d.: below detection limit.

		CIE L*a*b*	Nix Color
A	30 hours aeration	CIELAB: 32.84, 16.42, 34.09	
B	Bacterial oxidation	CIELAB: 46.63, 18.09, 47.59	
C	pH 3.2	CIELAB: 34.16, 14.59, 26.14	
D	pH 4.1	CIELAB: 14.81, 5.94, 10.97	
E	pH 5.5	CIELAB: 48.80, 8.82, 26.42	
F	pH 6.2	CIELAB: 18.80, 6.78, 11.48	

5.94–18.09, b* = 10.97–47.59), corresponding to dark brown, brown, and yellow- to orange-brown (ochre-like) hues typical of iron-based pigments. These color differences can be related to the identified mineral phases and compositions, where Fe-rich oxyhydroxides (ferrihydrite- to schwertmannite-like) tend to produce darker brown to orange-brown hues, while Al-rich hydroxide/hydroxysulfate phases are associated with lighter, more yellowish tones (Cornell and Schwertmann 2003; Schwertmann and Cornell 2000). In addition, sulfate incorporation and the presence of trace elements can influence color intensity and saturation, particularly in poorly crystalline Fe phases such as schwertmannite (Bigham *et al.* 1990).

Conclusions

Despite extensive research on AMD treatment, most studies address iron removal, microbial oxidation, or mineral formation separately. The integration of biological iron oxidation with controlled precipitation for simultaneous contaminant removal and resource recovery remains insufficiently explored, particularly in real AMD systems. In addition, the performance of native microbial consortia under field-relevant conditions has received limited attention.

This study demonstrates that coupling microbial Fe^{2+} oxidation with staged pH adjustment enables efficient iron removal from authentic mine water while producing iron-rich precipitates suitable for use as mineral pigments. The use of native acidophilic microorganisms proved effective under acidic conditions without the need for extensive chemical inputs.

Beyond iron removal, the process preserves dissolved metals such as Cu, Co, Mn, and Mg in solution, allowing their potential downstream recovery. Overall, this approach represents a sustainable and economically attractive strategy that links wastewater treatment with the production of value-added materials.

Acknowledgements

This study was funded by the EU NextGenerationEU through the Recovery and Resilience Plan for Slovakia under the projects No. 09I03-03-V04-00697

References

Bártová Z (2025) The Smolnik Mining Site in Slovakia: its Potential Use for the Production of Mineral Pigments. Paper presented at the 2025 International Mine Water Association Conference.

Basaran AH, Tuovinen OH (1986) An ultraviolet spectrophotometric method for the determination of pyrite and ferrous ion oxidation by Thiobacillus ferrooxidans. Applied Microbiology and Biotechnology 24(4):338-341. https://doi.org/10.1007/BF00257060

Bigham JM, Schwertmann U, Carlson L, Murad E (1990) A poorly crystallized oxyhydroxysulfate of iron formed by bacterial oxidation of Fe(II) in acid mine waters. Geochimica et Cosmochimica Acta 54(10):2743-2758. https://doi.org/https://doi.org/10.1016/0016-7037(90)90009-A

Cornell RM, Schwertmann U (2003) The Iron Oxides: Structure, Properties, Reactions, Occurrences and Uses. Wiley-VCH, Weinheim. https://doi.org/10.1002/3527602097

European Commission D-GfIM, Industry, Entrepreneurship and SMEs (2025) Commission Decision (EU) 2025/2607 establishing EU Ecolabel criteria, Report №. European Commission, Brussels,

Herrera L, Ruiz P, Aguillon JC, Fehrmann A (1989) A new spectrophotometric method for the determination of ferrous iron in the presence of ferric iron. Journal of Chemical Technology & Biotechnology 44(3):171–181. https://doi.org/https://doi.org/10.1002/jctb.280440302

Johnson DB, Hallberg KB (2005) Acid mine drainage remediation options: a review. Science of The Total Environment 338(1):3-14. https://doi.org/https://doi.org/10.1016/j.scitotenv.2004.09.002

Johnson DB, Kanao T, Hedrich S (2012) Redox Transformations of Iron at Extremely Low pH: Fundamental and Applied Aspects. Frontiers in Microbiology 3:96. https://doi.org/10.3389/fmicb.2012.00096

Jones AM, Griffin PJ, Collins RN, Waite TD (2014) Ferrous iron oxidation under acidic conditions – The effect of ferric oxide surfaces. Geochimica et Cosmochimica Acta 145:1-12. https://doi.org/https://doi.org/10.1016/j.gca.2014.09.020

Kaksonen AH, Morris C, Rea S, Li J, Wylie J, Usher KM, Ginige MP, Cheng KY, Hilario F, du Plessis CA (2014) Biohydrometallurgical iron oxidation and precipitation: Part I – Effect of pH on process performance. Hydrometallurgy 147-148:255-263. https://doi.org/https://doi.org/10.1016/j.hydromet.2014.04.016

Kupka D, Bártová Z, Hagarová L (2023) Kinetics study comparing bacterial growth and iron oxidation kinetics over a range of temperatures 5–45 °C. Hydrometallurgy 222:106181. https://doi.org/https://doi.org/10.1016/j.hydromet.2023.106181

Mclaren K (1976) XIII—The Development of the CIE 1976 (L* a* b*) Uniform Colour Space and Colour-difference Formula. Journal of the Society of Dyers and Colourists 92(9):338-341. https://doi.org/https://doi.org/10.1111/j.1478-4408.1976.tb03301.x

Morgan B, Lahav O (2007) The effect of pH on the kinetics of spontaneous Fe(II) oxidation by O2 in aqueous solution – basic principles and a simple heuristic description. Chemosphere 68(11):2080-2084. https://doi.org/https://doi.org/10.1016/j.chemosphere.2007.02.015

Robertson AR (1977) The CIE 1976 Color-Difference Formulae. Color Research & Application 2(1):7-11. https://doi.org/https://doi.org/10.1002/j.1520-6378.1977.tb00104.x

Schwertmann U, Cornell RM (2000) Iron Oxides in the Laboratory: Preparation and Characterization. Wiley-VCH, Weinheim. https://doi.org/10.1002/9783527613229

Singer PC, Stumm W (1970) Acidic Mine Drainage: The Rate-Determining Step. Science 167(3921):1121-1123. https://doi.org/10.1126/science.167.3921.1121

Stumm W, Morgan JJ (1996) Aquatic Chemistry: Chemical Equilibria and Rates in Natural Waters. 3 edn. John Wiley & Sons

Wolkersdorfer C (2022) Mine Water Treatment – Active and Passive Methods. https://doi.org/10.1007/978-3-662-65770-6

Water Management Sustainable Implementation at a Remote Water-Scarce Mine Site of Mongolia

Sod-Erdene Bazardorj, Tamir Puntsag, Uugankhuu Batbayar, Uuganbayar Purevsuren

Oyu Tolgoi LLC, Mongolia

Abstract

Oyu Tolgoi mine, located in the remote and water-scarce Gobi Desert region of Mongolia, began operations in 2013 to produce copper concentrate. Prior to mining, extensive water exploration identified the Gunii Khooloi aquifer as the primary water source to sustain the large-scale operation. Also to support mining activities, critical water infrastructure was established, including a Water Treatment & Bottling Plant, Wastewater Treatment Plants, and Tailings Storage Facilities. To address complex water issues in-situ operation and also acquire the license to operate, an integrated Water Management system was successfully implemented.

The purpose of this study is to describe the water management practices at Oyu Tolgoi mine, focusing on the development and implementation of the Water Resources Management Plan (WRMP) ensuring sustainable water use, compliance with standards, and environmental protection in a water-scarce gobi region by managing water abstraction, quality, and monitoring across the site.

The WRMP was introduced and adjusted in relation to operations defining scope, roles, standards, procedures, monitoring, training, and references for effective water management. Mongolian and international water quality standards were compared, and the most stringent values were adopted as project standards. Water monitoring were implemented at multiple water points around the mine to assess environmental impacts and support compliance reporting. Over a decade of water quality and level data were collected from monitoring bores, springs, and herder wells, forming the basis for regulatory reports shared with Mongolian authorities and local communities. Additionally, institutional domestic water standards were introduced to close gaps between local and international requirements, enabling safe domestic water consumption at the mine site.

The successful implementation of an integrated water management system and supporting documentation has enabled Oyu Tolgoi to maintain compliance, adapt to legislative changes, and ensure sustainable water use in one of the most challenging environments globally. Continuous monitoring and timely updates to management plans have supported uninterrupted copper production while minimizing environmental impacts and fostering trust with regulators and local stakeholders.

Keywords: Oyu Tolgoi mine, water resources management plan, water monitoring

Introduction

Oyu tolgoi is a copper-gold mine situated in Khanbogd soum of the Southgobi province in Mongolia. The international Rio Tinto Group started the mining operation in 2013 of Open-pit method. After years of construction, the underground mining infrastructure started in 2023. The Oyu Tolgoi mine is currently operating in full capacity by Open pit and Underground mines and is one of the biggest copper mines in the world.

The Oyu Tolgoi mine abstracts water for its operation, from the Gunii Khooloi aquifer, located southeast of the mine license area, through 28 borewells drilled to depths of 150–400 meters. The water is temporarily stored in lagoons, from which it is supplied to the concentrator for the flotation process through process water ponds. The water

recycled from the flotation process passes through the thickener, and the remaining tailings water is also recycled through the Tailings Storage Facilities.

In 2025, a total of 123,219,539 cubic meters of process water was used in the Concentrator, 86.73% water was recovered and reused from the Thickener and the Tailings Storage Facilities. 17 million cubic meter of water was abstracted from Gunii Khooloi as replenishment.

In the Gunii Khooloi abstraction area, local herders practice a traditional pastoral lifestyle, watering livestock from hand-dug wells. Because the region has very limited surface potable water—aside from a few springs and occasional short-lived flash-flood pools—these hand-dug wells serve as the primary source of drinking water for herders.

The fundamental purpose of the WRMP is to provide scientifically supported answers based on regular monitoring data to current and potential questions related to operational impacts and possible negative effects on the surrounding environment. One key issue raised by local communities, was declining changes in the shallow groundwater regime in connection to water abstraction from the deep aquifer, which is critical for their livelihoods. This paper aims to examine the potential connection between deep and shallow groundwater systems by using long-term monitoring data combined with statistical analysis with water abstraction volume and precipitation.

Methods

Prior to the start of the mining operation the Water Monitoring Procedure was introduced and implemented to study the general patterns of the natural groundwater regime, the key factors that influence it, and any actual or potential influence from mine water use and mining operations, including technogenic influences. As part of the monitoring activities, water-level fluctuations, water quality, and changes in chemical composition are monitored at observation boreholes, herder hand-dug wells, and springs located in the around Oyu Tolgoi and including Gunii Khooloi area. The collected data are compiled into a database and analyzed to support optimal groundwater resource management, to determine the extent of mining impacts on groundwater quantity, quality, and natural dynamics, and to plan mitigation measures

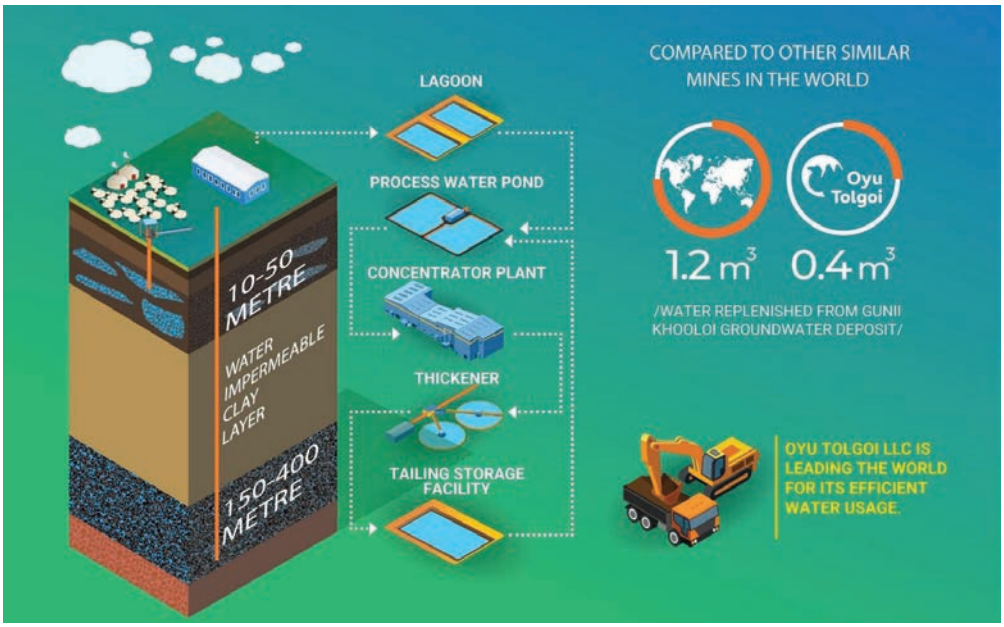

Figure 1 *Closed loop water management scheme in Oyu Tolgoi mining.*

for potential negative impacts.

The monitoring program for Oyu Tolgoi Mine includes a total 406 water points comprises of 348 boreholes, 47 hand-dug wells, and 11 springs. At these water monitoring points the water level measurements are conducted, in-situ water-quality parameters are recorded, and water samples are collected for comprehensive laboratory analysis accordance to monitoring program schedule. In the Gunii Khooloi area there are 13 herder wells are included in the active water-monitoring program. These wells are typically located within shallow, dry riverbeds and generally range from 2 to 7 meters in depth (Figure 2).

Results and discussion

The groundwater water levels of herder hand-dug wells fluctuate seasonally as a direct result of precipitation. When precipitation is high, the water level in the loose sediments of the dry riverbeds rises, and during drought periods, the water level decreases. In summer, sudden rainstorms and prolonged rainfall often cause flash floods that create temporary surface runoff, which strongly influences the water level and water quality composition of the shallow aquifer.

Figure 3 shows the long-term groundwater level measurements, expressed in meters below ground level (mbgl), for 13 herder wells situated in the Gunii Khooloi recharge zone, presented in relation to daily precipitation. The herders' wells located in the distant recharge-zone riverbeds are shown in Figure 3a, while the middle-distance and close-distance zones are illustrated in Figures 3b and 3c, respectively.

Oyu Tolgoi area total precipitation in 2025 was 97.5 mm, which is slightly below the long-term average of 102.8 mm. In 2018 following the heavy rainfall totalling 218 mm, particularly the flood event on August 3, 2018 – the water levels of hand-dug wells along dry riverbeds around the Oyu Tolgoi area incluing Gunii Khooloi abstraction area reached the highest levels recorded since the start of monitoring. During 2022–2023, precipitation was significantly below the

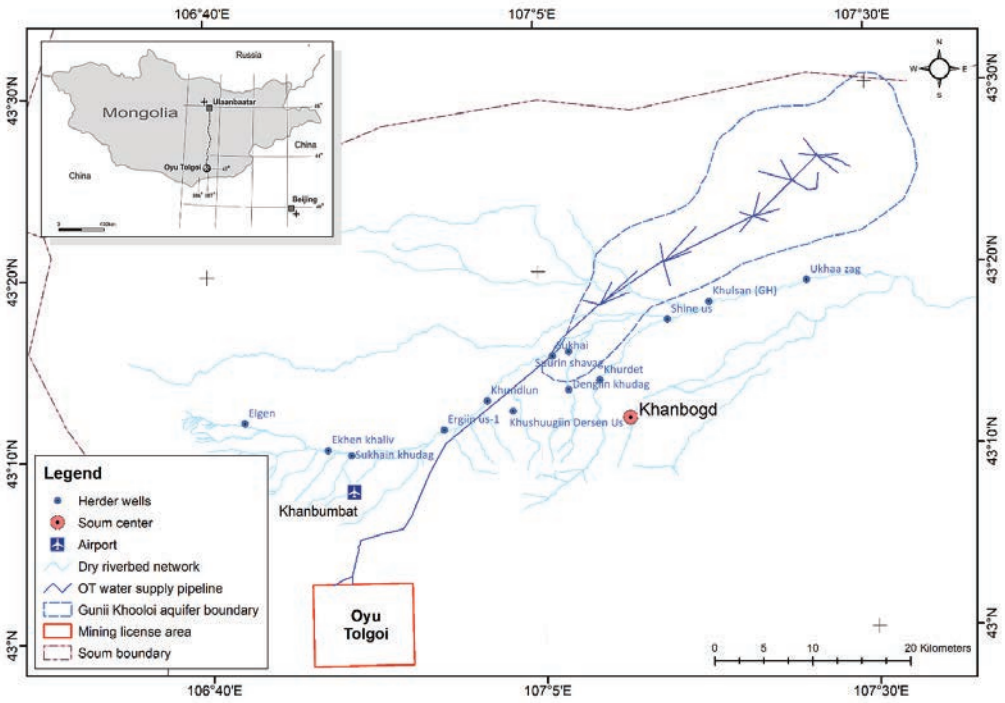

Figure 2 Herder Well Locations in dry riverbeds of the Gunii Khooloi area.

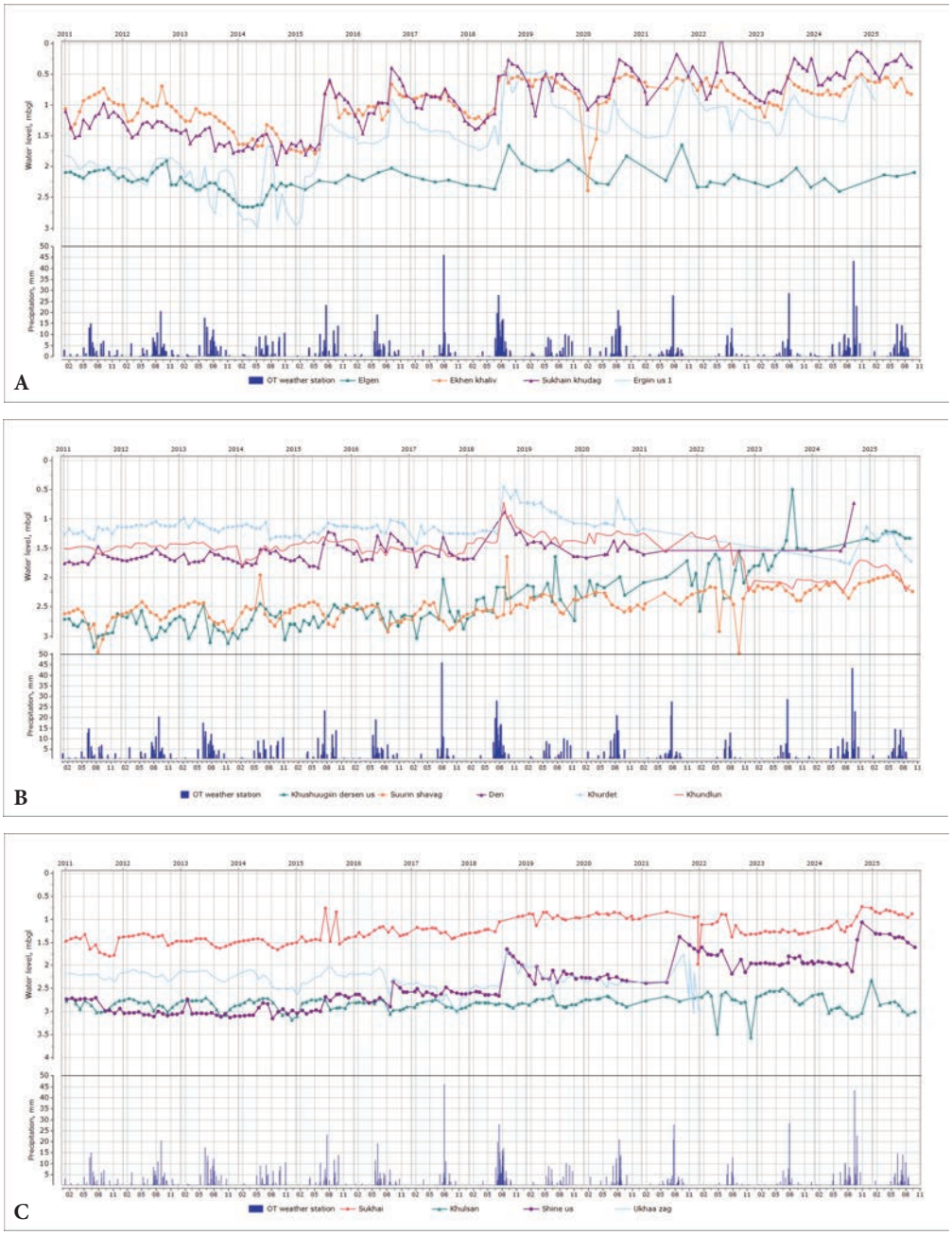

Figure 3 *Herder wells long term water monitoring data versus precipitation in Gunii Khooloi area.*

average and drought conditions prevailed, leading to a gradual decline in groundwater water levels. (Figure 3).

The figure 4 is a box-and-whisker plot showing the distribution of Static Water Levels (SWLs) measured in herder wells across the Gunii Khooloi area. The SWL values are expressed in meters below ground level (mbgl – meaning lower values represent shallower water (closer to surface).

Ergiin Us-1 and Sukhain khudag has the widest water level fluctuation, because it is

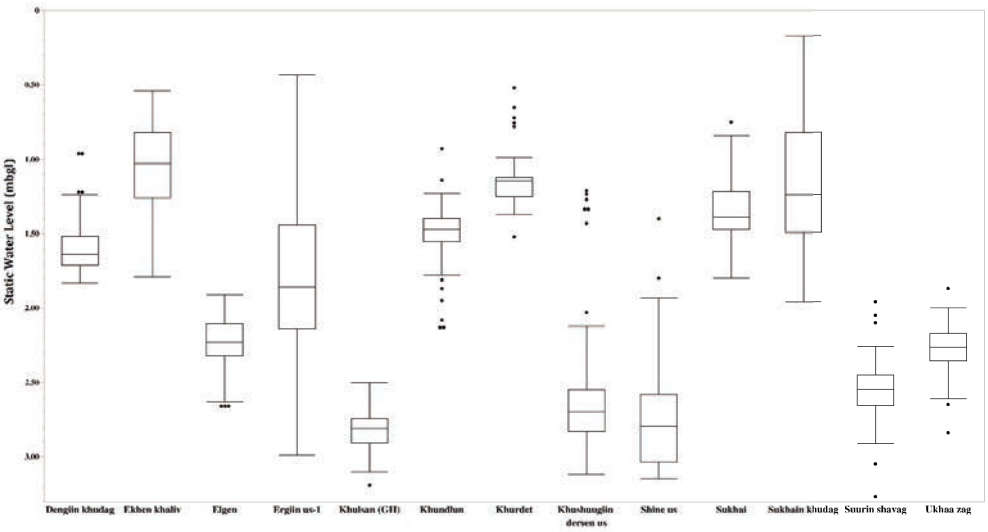

Figure 4 *Distribution of Static Water Levels in Herder Wells across the Gunii Khooloi area.*

Table 1 *Statistical Summary of Groundwater Levels in Herder Wells (*significant).*

No	Herder well name	N	Depth (mbgl)	Min	Max	Mean	Std Dev	Slope (cm)	R2	P value
1	Suurin shavag	85	6.84	1.96	3.27	2.56	0.19	0.32	0.42	<.0001*
2	Khulsan (GH)	70	6.43	2.5	3.19	2.83	0.12	0.04	0.02	0.11
3	Ekhen khaliv	102	5.43	0.54	1.79	1.07	0.34	0.34	0.25	<.0001*
4	Shine us	70	4.66	1.4	3.15	2.73	0.38	0.92	0.81	<.0001*
5	Khushuugiin dersen us	74	3.82	1.21	3.12	2.58	0.44	0.98	0.75	<.0001*
6	Elgen	68	3.75	1.91	2.66	2.24	0.18	0.13	0.06	0.0260*
7	Ergiin us-1	92	3.72	0.43	2.99	1.83	0.57	0.85	0.51	<.0001*
8	Ukhaa zag	70	3.09	1.87	2.84	2.28	0.17	-0.16	0.07	0.0025*
9	Khundlun	95	2.72	0.93	2.13	1.5	0.18	-0.26	0.24	<.0001*
10	Sukhai	86	2.69	0.75	1.8	1.33	0.24	0.33	0.47	<.0001*
11	Dengiin khudag	78	2.66	0.96	1.83	1.59	0.18	0.27	0.41	<.0001*
12	Sukhain khudag	101	2.65	0.17	1.96	1.14	0.44	0.72	0.62	<.0001*
13	Khurdet	79	1.9	0.52	1.52	1.15	0.15	-0.07	0.02	0.09

located in a highly recharge-responsive shallow alluvial setting, active dry riverbed with high permeability. This makes the well more sensitive to seasonal rainfall, flash-flood events and local usage compared to other herder wells in the Gunii Khooloi area. Khurdet shows the narrowest water-level fluctuation, which corresponds to its shallowest depth.

Based on monthly data from 2011, ten of thirteen herder wells' water level show a slight increasing trend in over time, with monthly slopes ranging from 0.98 cm to 0.04 cm monthly, and with explanatory power (R^2) varying from strong to weak (0.81 to 0.02).

The remaining three wells; Ukhaa zag has a significant but weak decreasing trend (R^2 = 0.07, p = 0.0025), while Khurdet's slight decrease is not statistically significant (R^2 = 0.02, p=0.092). Long-term monthly monitoring data indicate a

statistically significant decreasing trend in the groundwater level at the Khundlun herder well.

Based on long-term water level and water abstraction volume datasets, statistical analyses were done for all herder wells (Table 2). For the Khundlun herder well, the linear relationship between water abstraction and well water level is weak and not statistically significant (R^2 = 0.02, p = 0.09).

Based on the statistical analysis of the long-term water level and abstraction datasets, three close-distance herder wells and two far-distance herder wells showed statistically significant relationships ($p < 0.05$) between water abstraction and well water level; however, the explanatory power of these models remained low (R^2 = 0.03–0.09).

Conclusion

Long-term monitoring results from the Oyu Tolgoi Water Resources Management Program demonstrate that shallow groundwater used by herder communities in the Gunii Khooloi region is primarily controlled by **natural climatic conditions**, especially precipitation and episodic flood events. Water-level fluctuations in the 13 monitored herder wells consistently correlate with rainfall patterns, rising during wet years and declining during drought periods. Statistical analyses show **no strong or widespread evidence** that deep-aquifer abstraction for mining operations has caused significant declines in shallow groundwater levels.

Although five herder wells exhibit statistically significant relationships with abstraction volume, the explanatory power of these correlations remains **very low (R^2 = 0.03–0.09)**, indicating that abstraction is not a dominant factor influencing shallow groundwater behavior. In contrast, most wells show slight increasing long-term trends or stable conditions, with only one well (Khundlun) presenting a statistically significant decreasing trend.

Overall, the combined hydrological data, water-level trends, and statistical evaluations indicate that **deep-aquifer pumping for Oyu Tolgoi operations has minimal measurable impact on the shallow hand-dug wells relied upon by herders**. The shallow aquifer continues to respond mainly to **natural recharge processes**, seasonal variability, and riverbed hydrodynamics. Continuous monitoring remains essential to ensure sustainable water management and to address ongoing community concerns.

References

B.Shikhtulga, G.Dolgorsuren, U.Borchuluun et all (2021), 2021 audit report on "Oyu Tolgoi" mine's water utilization

Otgonbaatar. S, Batdemberel.B, Tamir.P et all (2025), Oyu Tolgoi LLC water usage report 2025.

Uugankhuu.B, Tamir. P, Sod-Erdene.B et all (2025), Oyu Tolgoi LLC water monitoring report 2025.

Tseveenjav.B, Bataa.D (2025), OT mine site general condition report

Mijiddorj. P. (1992). Climate characteristics of Gobi desert of Mongolia. Ulaanbaatar.

Buyankhishig. N, Jadambaa.N, Oyun.D. (2008). Impact of Water compumption of Gunii khooloi groundwater deposits. Geology journal, 18, p 28-140.

*Table 2 Statistical relationship of herder water level between Gunii Khooloi water abstraction volume (*significant).*

N	Herder well name	P value	R^2	N	Herder well name	P value	R^2
1	Khundlun	0.09	0.02	8	Elgen	0.98	0
2	Khushuugiin dersen us	0.13	0.02	9	Ukhaa zag	0.003*	0.09
3	Khurdet	0.15	0.02	10	Shine us	0.007*	0.05
4	Ekhen khaliv	0.19	0.01	11	Sukhain khudag	0.016*	0.04
5	Suurin shavag	0.2	0.01	12	Ergiin us	0.017*	0.04
6	Dengiin khudag	0.24	0.02	13	Khulsan	0.038*	0.03
7	Sukhai	0.24	0.01				

IMWA 2026
Jeongseon

Probabilistic Estimation of Aquifer Properties and Non-Linear Well Losses to Support Dewatering Forecasts and Planning

Savannah Miller[1], David Benson[2]

[1]*INTERA Geosciences, Perth, Western Australia, smiller@intera.com, ORCID 0009-0009-2887-9815*

[2]*Hydrologic Science and Engineering, Colorado School of Mines, Colorado, USA, dbenson@mines.edu, ORCID 0000-0001-5652-5197*

Abstract

We review and apply the methods used by Benson *et al.* (2026) who use a Bayesian Markov-chain Monte Carlo (MCMC) framework to estimate aquifer properties and non-linear well losses from pumping. Results show strong parameter correlation and non-Gaussian uncertainty, which are not captured by conventional deterministic methods. A synthetic dewatering example links parameter uncertainty to operating costs across a range of pumping rates. A volume-price risk analysis directly links pumping targets to the probability of meeting budget constraints, enabling rapid and transparent evaluation of production-cost trade-offs. The approach is implemented in Python and provides a fast, low-cost tool for risk-informed planning.

Keywords: MCMC, pump-test, uncertainty, well efficiency

Introduction

Reliable estimation of aquifer and well performance parameters is critical for the design and planning of mine dewatering systems. Conventional pumping test interpretation typically relies on deterministic calibration, producing single-value estimates of transmissivity, storativity (or specific yield), and well-loss coefficients. These parameters are often highly correlated and non-unique, which can lead to overconfident predictions of drawdown, well efficiency, and associated pumping costs. In mine dewatering applications, where pumping may be sustained over the life of a project, pumping energy can represent a substantial fraction of total operating expenditure, making parameter uncertainty directly consequential to project economics. Where aquifer parameters are poorly constrained, uncertainty in drawdown and well efficiency predictions translate directly into uncertainty in energy consumption and operation costs. This financial sensitivity is greatest during feasibility and pre-feasibility studies, where design decisions are made under high uncertainty. A probabilistic framework for pump test interpretation that quantifies uncertainty in pumping costs as a function of production rate allows mine planners to better understand the potential range in dewatering costs. This is particularly valuable when: (1) electricity cost represents a large fraction of total mine operating expenditure; (2) aquifer parameters are poorly constrained due to limited pumping test data, resulting in a wide range of plausible drawdown and cost outcomes; or (3) a go/no-go planning decision depends on whether a target pumping rate can be sustained within acceptable cost bounds.

Benson *et al.* (2026) present a Bayesian Markov-chain Monte Carlo (MCMC) framework for estimating aquifer parameters and non-linear well-loss coefficients from variable-rate pumping tests. Their results show that parameter estimates are frequently non-Gaussian and strongly correlated, particularly between transmissivity and storativity, and between linear and non-linear well-loss parameters. This correlation reflects the nonlinear relationship between parameters and the drawdown response and gives rise to non-uniqueness: multiple distinct parameter combinations can reproduce the observed data equally well. The framework

links parameter uncertainty to uncertainty in well efficiency (the ratio of theoretical to actual drawdown at a given pumping rate) and pumping costs.

Methods

Aquifer Response and Non-Linear Well Losses

The model is based on the Theis (1935) solution for radial flow to a well:

$$s(t) = \frac{Q}{4\pi T} W(u),$$

where drawdown $s(t)$ depends linearly on pumping rate Q, transmissivity T, and the well function $W(u)$, that depends on $u = r^2 S/(4Tt)$, where r is the radius of measurement and S is aquifer storativity (Kruseman and Ridder 2000). For variable-rate pumping, the linear response is expressed using convolution (denoted by *):

$$s(t) = B(t) \star Q(t) \text{ where } B(t) = \frac{1}{4\pi T}\frac{d}{dt} W(u).$$

Step-drawdown tests commonly exhibit additional drawdown that increases non-linearly with pumping rate due to turbulent flow near the well. This is represented as: $s(t) = B(t)^*Q(t) + CQ^p(t)$ where C is a non-linear well-loss coefficient and p is typically greater than 2 (Cooper and Jacob 1946; Rorabaugh 1953; Benson 2024). This equation generalises the classical quadratic well-loss model and better captures observed behaviour in step tests.

Benson *et al.* (2026) introduce a discharge correction to account for wellbore storage effects, improving early-time model fit and parameter estimation. The corrected discharge is:

$$Q_c = sign(Q)(Q - \pi r_w^2 \frac{ds}{dt})$$

where r_w is pumping well radius and the drawdown rate is best estimated by backward finite differences of the measured data. Drawdown is now:

$$s(t) = B(t) \star Q(t) + sign(Q) C Q_c^p(t).$$

Bayesian Inference and MCMC Sampling

Bayesian inference is applied using MCMC sampling to estimate posterior distributions of model parameters. The Bayesian framework updates prior parameter distributions using observed data via Bayes' theorem:

$$p(M|D) \propto p(D|M)p(M)$$

where $p(M|D)$ is the posterior probability density function (PDF) of model M given the data D, $p(D|M)$ is the likelihood that the data D came from model M and $p(M)$ is the prior PDF of model M. Sampling is performed with an ensemble sampler from emcee (Foreman-Mackey *et al.* 2013, https://emcee.readthedocs.io/en/stable/). This sampler was designed to handle correlated and non-Gaussian parameter values with multiple walkers simultaneously. Convergence is assessed using chain length relative to autocorrelation time and diagnostics such as the Gelman-Rubin statistic (Gelman and Rubin 1992).

Cost Estimation and risk analysis

Hydraulic uncertainty is linked to operational costs through energy requirements for pumping. Power demand is calculated from total dynamic head (static lift plus losses), following methodology in the State of Colorado Water Plan (Starosta *et al.* 2019). Parameter sets drawn from the posterior distribution are used to estimate annual operating costs for standardized pumping scenarios.

Synthetic Mine Dewatering Example

The framework is applied to a synthetic high-capacity dewatering well. Posterior distributions of S, T, C, and p are used to simulate drawdown across a range of pumping rates, which are converted to annual production volumes. These are used to estimate energy consumption and operating costs with uncertainty bounds. A volume–price risk analysis is conducted to quantify the probability of operating below specified cost thresholds and the risk of exceeding

them, providing a decision-support framework for selecting pumping strategies under uncertainty.

Results

Benson *et al.* (2026) show that aquifer and well-loss parameters may exhibit strong correlation and non-uniqueness. The posterior distributions for a typical pumping well (Figure 1) demonstrate:

- Negative correlation between transmissivity and storativity;
- Strong negative correlation between nonlinear well-loss parameters (C and p);
- Non-gaussian, elongated ("banana-shaped") posterior parameter distributions;

These results indicate that multiple parameter combinations can produce observed data equally well, limiting the reliability of single best-fit solutions.

Accounting for wellbore storage improves early-time model fit and reduces bias by preventing wellbore storage effects from being incorrectly attributed to non-linear well losses. This leads to more realistic distributions of well efficiency and operating cost. Bayesian assessment of well efficiency

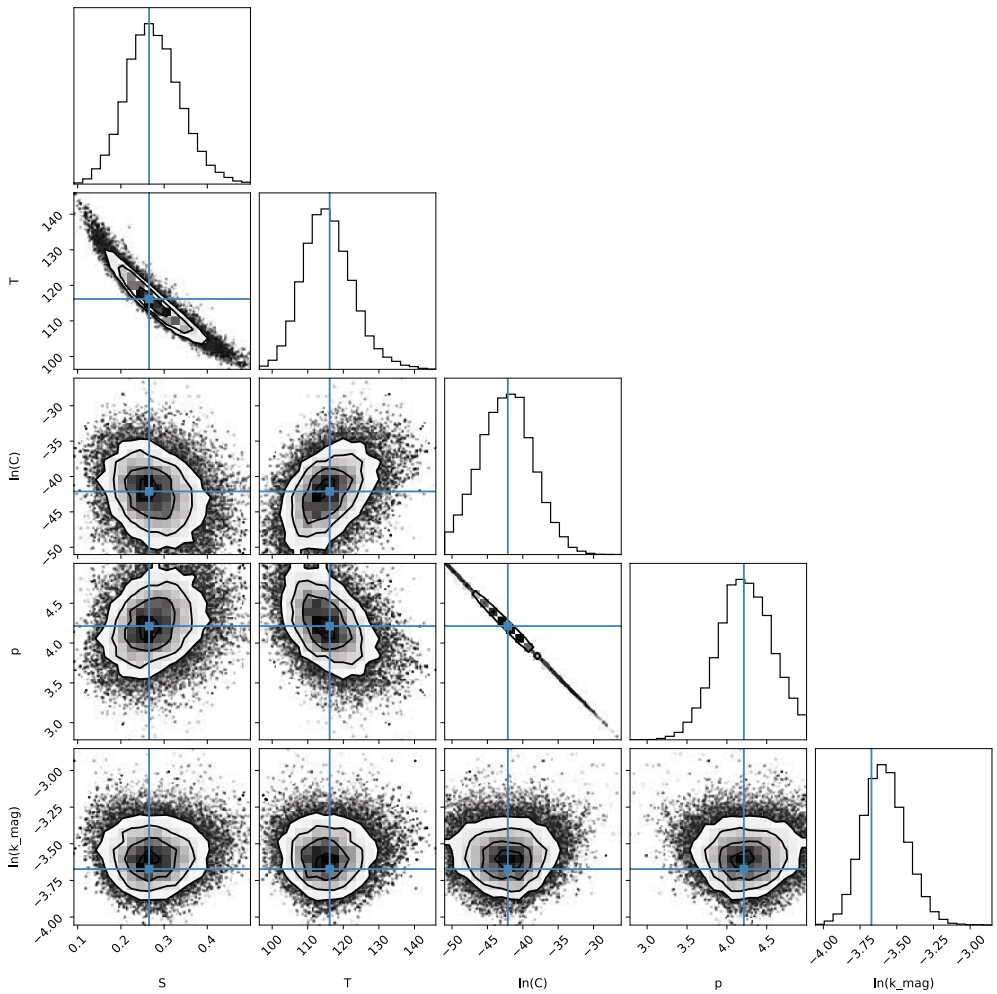

Figure 1 *Corner plot of 1-D and 2-D marginal densities of each parameter with all others for well CR-226. "Best-fit" values from Marquardt-Levenberg optimization are shown in blue. Taken from Benson* et al. *(2026).*

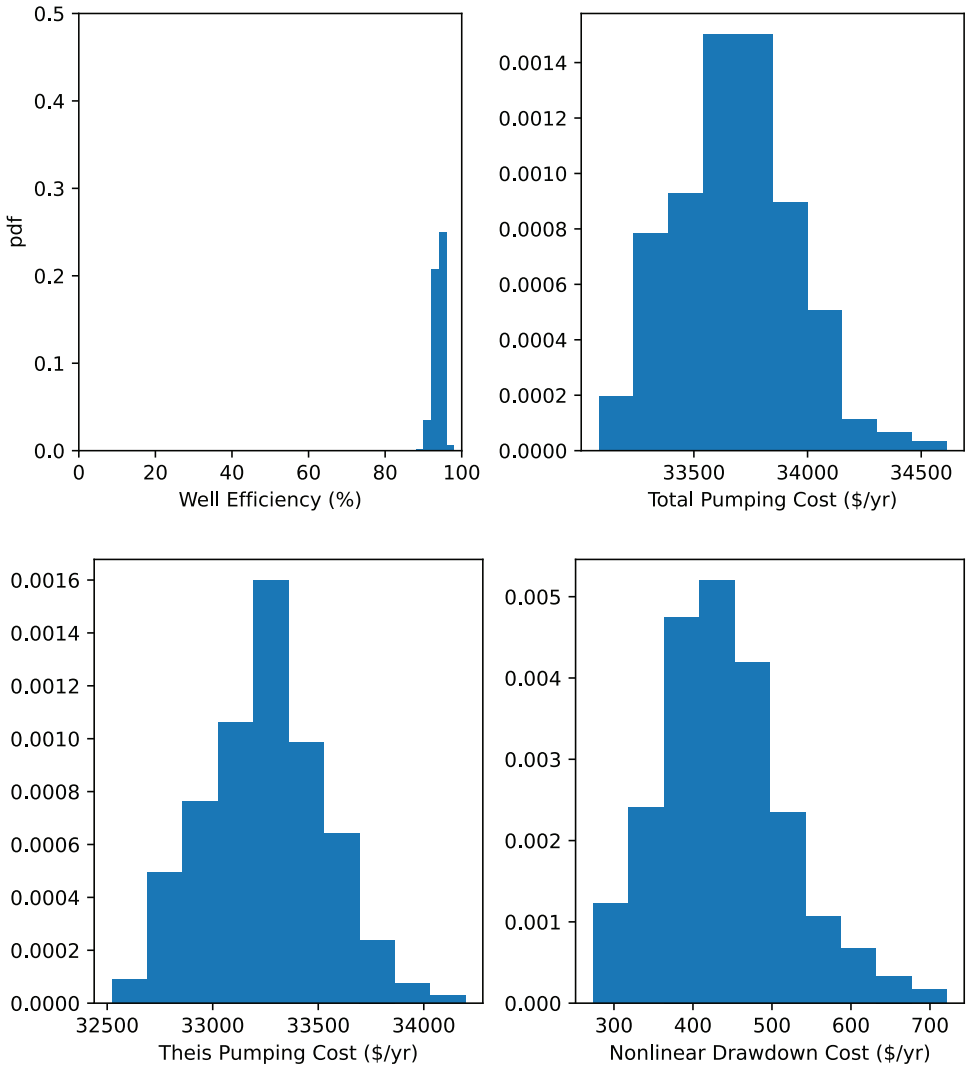

Figure 2 *Example histograms of forward runs taken from the Markov chain for well CR-226. Taken from Benson* et al. *(2026).*

and associated cost distributions can be seen in Figure 2 (Benson *et al.* 2026).

Application to Mine Dewatering: Synthetic Evaluation

A synthetic dewatering well was analysed with representative characteristics (e.g., 300 m depth, 73 m screen interval, 0.15 m radius). Posterior parameter distributions derived from the well CR 226 step-drawdown test but revised well design parameters were used to simulate system performance. Results (Figure 3) show that both energy use and cost increase non-linearly with pumping rate due to:

- Increased drawdown at higher extraction rates;
- Non-linear well losses;
- Frictional head losses;

Cost uncertainty also increases with production rate, leading to a widening spread of possible outcomes.

The volume-price risk analysis (Figure 4) shows the probability of maintaining a

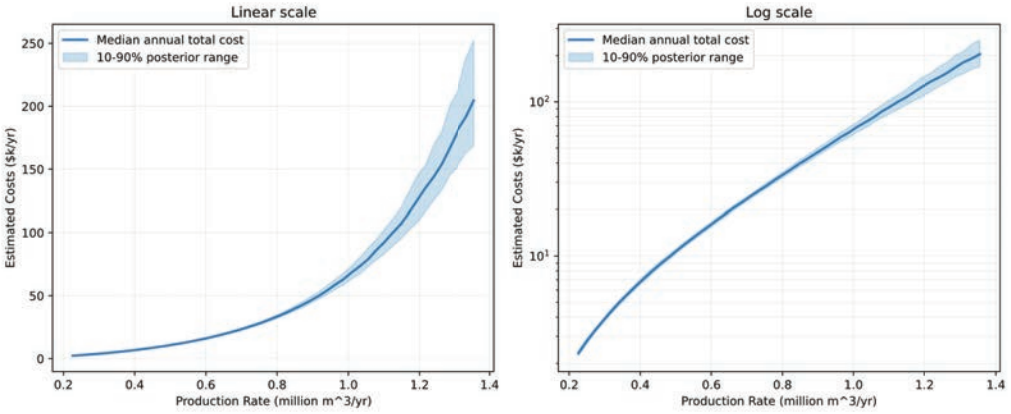

Figure 3 Estimated costs for a range in production rates under uncertainty.

cost threshold for different annual pumping volumes. For example, at a threshold of approximately $105.8k/year, the probability of meeting the threshold for different annual pumping targets is:

- At 0.89 million m³/year: ~100% probability of meeting the threshold;
- At 1.12 million m³/year: ~74% probability of success;
- At 1.24 million m³/year: ~0.25% probability of success;

The analysis shows a rapid change in the probability of meeting a cost threshold over a relatively narrow range of pumping rates. Note, this example assumes that the aquifer and pumping system can sustain the required discharge rates.

Discussion

These results highlight the limitations of deterministic pumping test interpretation for dewatering design, where parameter correlation and non-uniqueness can lead to underestimation of uncertainty in system performance. Conventional pumping test analyses produce a single best-fit parameter set and therefore a single predicted outcome for each pumping rate, with no indication of the confidence that should be placed in those estimates. In contrast, the Bayesian MCMC framework captures the full range of plausible parameter combinations and translates this uncertainty into predictions of drawdown, energy use, and cost. For the synthetic example presented here, the

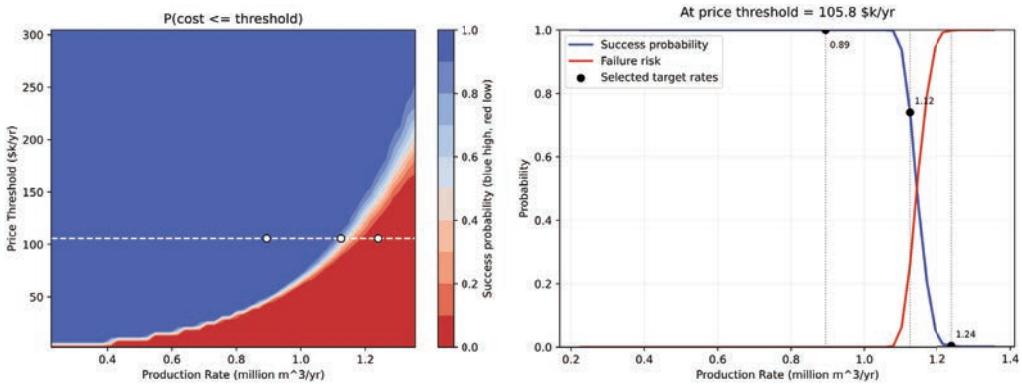

Figure 4 Estimated costs for a range in production rates under uncertainty.

deterministic approach would suggest a single annual cost at each pumping rate, for example, $85,700 at a pumping rate of 1.08 Mm3/year, whereas the MCMC framework reveals that the true cost could range from approximately $70,000 to $102,000 at that same rate, representing a 37% spread around the deterministic estimate (see Figure 3). This range reflects the combined influence of parameter correlation and non-uniqueness, neither of which is captured by a single best-fit solution. The synthetic example shows that cost uncertainty grows non-linearly with production, leading to increasing financial risk. At low pumping rates, cost predictions are relatively constrained. However, as production increases, both expected costs and uncertainty grow rapidly. This behaviour reflects the combined influence of aquifer response, well losses, and system hydraulics. The volume-price risk analysis provides a practical and quick tool for comparing cost to operational demand by linking production targets directly to financial risk. Rather than selecting a single "optimal" pumping rate, operators can evaluate trade-offs between production and the probability of exceeding budget constraints.

The current analysis assumes sufficient hydraulic capacity to meet target pumping rates. In practice, constraints such as pump performance, well interference, and aquifer limits would need to be included for full system evaluation. Additionally, the results are sensitive to the choice of prior distributions: poorly specified priors can bias posterior estimates, particularly when data are limited or noisy. The cost calculation depends on the assumed pump efficiency curve, which introduces an additional source of uncertainty not propagated through the current analysis. It should be noted that the posterior parameter distributions used in the synthetic example are derived from a single field well (CR-226) and are therefore site-specific; the absolute cost values presented are intended to be illustrative of the methodology rather than representative of a particular dewatering scenario.

Recommended Additional Analysis and Next Steps

Building on the methodology in Benson *et al.* (2026) and the synthetic evaluation presented here, several extensions are recommended to further improve applicability and robustness:

- Extend the framework to multi-well systems to capture interference effects and system-scale behaviour.
- Apply the method to field data and compare results with conventional deterministic approaches.
- Compare MCMC with alternative Bayesian methods (e.g., iterative ensemble smoothing) to evaluate trade-offs between computation cost and accuracy.
- Incorporate operational constraints such as pump capacity and aquifer limits.
- Integrate capital costs and energy price variability for more comprehensive economic evaluation.

Conclusions

Bayesian MCMC methods provide a robust framework for estimating aquifer and well parameters while accounting for uncertainty and parameter correlation. Parameter estimates derived from pumping tests are often highly correlated and non-unique, leading to non-Gaussian posterior distributions that cannot be adequately represented by single deterministic values. Application to a synthetic mine dewatering scenario shows that uncertainty in hydraulic parameters translates directly into uncertainty in energy consumption and operating costs. Both expected costs and their variability increase non-linearly with production. The volume-price risk analysis provides a practical means of linking pumping decisions to financial risk. The method is straightforward to implement, computationally efficient, and based on free, open-source Python tools. As such, it offers a practical and accessible approach for initial risk-informed dewatering planning. The ability to quantify the probability of meeting cost targets at different pumping rates, derived directly from pumping test data and

requiring no commercial software, makes this framework well suited to early-stage mine planning where budget uncertainty has the greatest consequence.

References

Benson D.A. (2024). Automated estimation of aquifer parameters from arbitrary-rate pumping tests in Python and MATLAB. Groundwater 62(2):285–294. https://doi.org/10.1111/gwat.13338

Benson D.A., Miller, S., & Barber, J. (2026). Markov-chain Monte Carlo estimation of aquifer parameters, non-linear well losses, and probable costs of water extraction. Journal of Hydrology, 668: 134952. https://doi.org/10.1016/j.jhydrol.2026.134952

Cooper H.H. and Jacob C.E. (1946). A generalized graphical method of evaluating formation constants and summarizing well-field history. Transactions, American Geophysical Union 27(4):526–534.

Foreman-Mackey, D., Hogg, D.W., Lang, D., and Goodman, J. (2013). Emcee: the MCMC hammer, Publ. Astron. Soc. Pac. 125, 306–312, https://doi.org/10.1086/670067.arXiv:1202.3665

Gelman, A and Rubin, D.B. (1992). Inference from iterative simulation using multiple sequences. Statistical Science., 7(4):457–472. https://www.semanticscholar.org/paper/Inference-from-Iterative-Simulation-Using-Multiple-Gelman-Rubin/9c67f30235a47e305dc57c9f185d5587faca4236

Kruseman G.P., and Ridder N.A.D (2000). Analysis and evaluation of pumping test data. 2nd edn. International Institute for Land Reclamation and Improvement (ILRI), Wageningen, The Netherlands, 47:377.

Rorabaugh M. I. (1953). Graphical and theoretical analysis of step-drawdown test of artesian wells. Proceedings of the American Society of Civil Engineers 79:1–23.

Starosta L., Gruber E., Schultze D. (2019). Colorado Water Project Cost Estimating Tool Documentation. Technical Report Technical Memorandum. Analysis and Technical Update to the Colorado Water Plan.

Theis CV (1935) The relation between the lowering of the piezometric surface and the rate and duration of discharge of a well using groundwater storage. Transactions, American Geophysical Union 16(2):519–524. https://doi.org/10.1029/TR016i002p00519

Performance of a Sulfate-Reducing Bioreactor for Sulfate Removal under Cold Climate Conditions

Laura Nina Bettoni[1], Maria Hellman[2], Sara Hallin[2], Maria Elisa Johansson[3], Tomas Salmi[3], Ekaterina Sokolova[1], Elif Tuncer[3], Mattias Ylipää[3], Roger Herbert[1]

[1]*Department of Earth Sciences, Uppsala University, Uppsala, Sweden, lauranina.bettoni@geo.uu.se, ekaterina.sokolova@geo.uu.se, roger.herbert@geo.uu.se*

[2]*Department of Forest Mycology and Plant Pathology, Swedish University of Agricultural Sciences, Uppsala, Sweden, maria.hellman@slu.se, sara.hallin@slu.se*

[3]*Research and development, Luossavaara-Kiirunavaara Aktiebolag (LKAB), Kiruna, Sweden, mariaelisa.johansson@lkab.com, tomas.salmi@lkab.com, elif.tuncer@lkab.com, mattias.ylipaa@lkab.com*

Abstract

Mining activities can elevate sulfate levels in freshwater recipients, prompting stricter discharge limits in Sweden and increasing the need for effective treatment of mine leachate. This study evaluates a pilot-scale sulfate-reducing bioreactor operated under subarctic conditions at the Kiruna mine, examining the effects of temperature, flow rate, and lactate dosing. The woodchip-filled bioreactor achieved up to 88% sulfate removal, with performance strongly driven by lactate availability and enhanced at higher temperatures. Initial DOC release, pipe fouling, and high nitrate levels influenced system behavior. Overall, sulfate-reducing bioreactors show promising potential for sulfate removal in cold climates when properly optimized.

Keywords: Biological sulfate reduction, bioreactor efficiency, field operation, temperature, woodchips

Introduction

In mining areas, waste materials that contain sulfide or sulfate-rich minerals may, under certain environmental conditions, release sulfate (SO_4^{2-}) into nearby freshwater systems. Long-term exposure to elevated sulfate levels can be harmful to freshwater organisms (Soucek and Kennedy 2005; Karjalainen *et al.* 2023). Additionally, rising sulfate concentrations can indirectly impact aquatic ecosystems by enhancing phosphorus availability and increasing the risk of eutrophication (Lamers *et al.* 1998; Smolders *et al.* 2006; Zak *et al.* 2006; Geurts *et al.* 2009), as well as by stimulating mercury methylation (Han *et al.* 2007; Wang *et al.* 2022). In Sweden, recent environmental court decisions have introduced limits on sulfate discharges to surface waters, creating a need for reliable and efficient removal technologies (Swedish Agency for Marine and Water Management 2018).

One example of a removal technology is the woodchip bioreactor, which has previously been applied in mining settings to remove nitrate through denitrification (Nordström and Herbert 2018; Hellman *et al.* 2024). With appropriate modifications, this type of system could also be utilized for sulfate removal (e.g. Parvage and Herbert 2023). In such a configuration, the initial step for sulfate removal would involve dissimilatory sulfate reduction (reaction 1), carried out by sulfate-reducing bacteria (SRB) under anaerobic conditions. When sufficient organic carbon (CH_2O) is available, these microorganisms reduce sulfate to sulfide (H_2S). The produced sulfide can subsequently be immobilized through different pathways, such as by precipitation with metal ions or chemical or biological oxidation, depending on the desired product (Pudi *et al.* 2022).

$$SO_4^{2-} + 2\ CH_2O \rightarrow H_2S + 2\ HCO^{3-} \quad (1)$$

This study evaluates the influence of temperature, flow rate and an external carbon source on sulfate removal in an on-site SRB-

woodchip treatment system at the Kiruna mine in northern Sweden under subarctic conditions.

Methods

Experimental setup

The treatment system was constructed at LKAB's Kiruna iron ore mine located in northern Sweden (67°85′ N, 20°14′ E) and operated from June 2024 to December 2025. During this period, the hourly atmospheric temperature from a nearby weather station ranged from –28.5 to +28.1 °C with an average of +2.7 °C (Swedish Meteorological and Hydrological Institute (SMHI), n.d.). The treatment consists of four main units: (1) a water reservoir, (2) a sulfate-reducing bioreactor, (3) a sulfide precipitation tank, and (4) a sedimentation tank (Fig. 1).

The water reservoir continuously received outflow from a denitrifying woodchip bioreactor treating mine leachate from a nearby waste rock pile (described in Hellman *et al.*, 2024). The collected water was subsequently pumped at rates of 3.45–9.50 m^3/d (Fig. 2) to the SRB bioreactor. Prior to reaching the bioreactor, the mine water was amended with lactate at a dosing rate of 4.5–40 kg/d (Fig. 2); lactate was added as a labile carbon source to enhance microbial sulfate reduction (reaction 2).

$$SO_4^{2-} + 2\ CH_3CH(OH)COO^- \rightarrow H_2S + 2\ CH_3COO^- + 2HCO^{3-} \quad (2)$$

In addition to lactate dosing, the inlet water was also heated before entering the bioreactor (Fig. 1). A 2000 W inline electrical heater installed in the inlet pipeline was used for this purpose.

The sulfate-reducing bioreactor consisted of a subsurface concrete cylindrical tank (2.4 m diameter × 5.4 m height) filled with pine woodchips (size approximately 30 × 30 × 10 mm). A downward flow direction and a 50 cm water layer on top were implemented to limit sulfide emissions. Sampling wells were installed into the bioreactor for chemical profiling at six depths (A and B, Fig. 1). Three weeks after the start of operations, the woodchips were inoculated by adding 500 L of active sewage sludge (100:1 woodchip: sludge volume ratio) at a high lactate dose (27.2 kg/d) to promote the establishment of a microbial community. Flow rate (3.5–9.5 m^3/d), lactate dosing (0–40 kg/d), and inflow temperature (10–25 °C), were systematically varied to assess process responses (Fig. 2).

The effluent from the bioreactor was directed to the precipitation tank (Fig. 1), where sodium hydroxide (NaOH) and iron chloride ($FeCl_3$) were added to

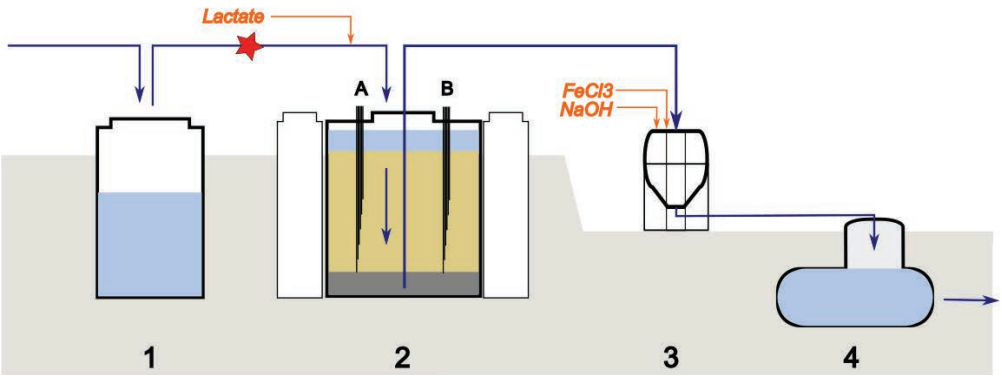

Figure 1 *Cross-section representation of the SRB–woodchip treatment system, consisting of: (1) water reservoir, (2) sulfate-reducing bioreactor including water-sampling wells (A and B), (3) sulfide precipitation tank, and (4) sedimentation tank. The red star indicates the heating apparatus, blue arrows show the flow direction, and orange arrows denote points of chemical addition. The figure is not drawn to scale.*

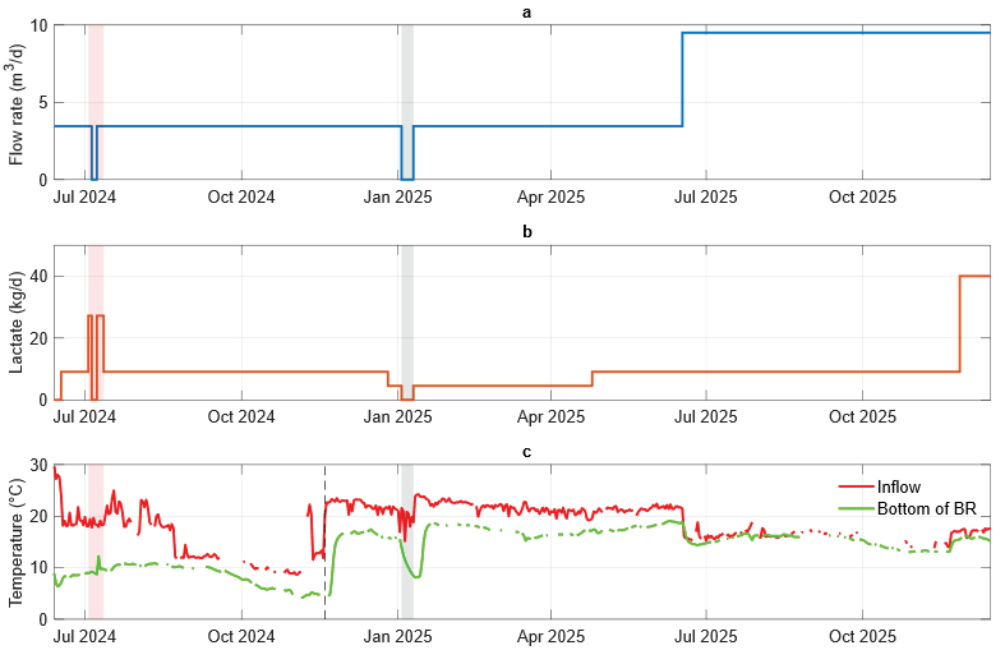

Figure 2 Flow rate (a), lactate dosing (b), and water temperature (c) of the inflow and the bottom of the SRB bioreactor (BR). The red vertical highlight represents the inoculation period while the grey vertical highlight displays a stop of operation.

precipitate dissolved sulfide as iron sulfide (FeS) and elemental sulfur (S^0) prior to the sedimentation tank (reactions 3 and 4). The $FeCl^{3-}$ driven precipitation generates acidity, but in the presence of alkalinity (HCO^{3-}), this acidity can be neutralized through the formation of carbonic acid (reaction 4).

$$H_2S + NaOH \rightarrow HS^- + H_2O + Na^+ \quad (3)$$

$$2\ FeCl_3 + 3\ HS^- + 3\ HCO^{3-} \rightarrow S^0_{(s)} + 2\ FeS_{(s)} + 3\ H_2CO_3 + 6\ Cl^- \quad (4)$$

Sampling procedure and chemical analysis

Water samples (2 L) were collected weekly by LKAB personnel from the inflow and outflow of the sulfate-reducing bioreactor. For the outflow samples, a $ZnCl_2$ solution (50 mL, 117 mM) was added to precipitate sulfide to ensure safe handling during analysis. All water samples were analyzed by LKAB, which has an accredited laboratory for chemical analyses. Depth profiles of chemical parameters in the bioreactor were obtained during regular sampling campaigns and included analyses of sulfate, sulfide, nitrate, nitrite, and ammonium. Water samples were collected from each sampling well (see Fig. 1) using a peristaltic pump, and approximately 2 L were purged to ensure representative sampling prior to filling 50 mL collection bottles. All analyses were performed within 4 hours of collection to prevent oxidation, using a spectrophotometer (HACH DR1900) in combination with HACH pre-dosed reagent kits.

Sulfate removal was evaluated through the calculation of sulfate removal efficiency based on outlet sulfate sulfur concentrations (C_{out}) relative to their corresponding inlet concentrations (C_{in}) (equation 5).

$$Sulfate\ removal\ efficiency\ (\%) = \frac{C_{in} - C_{out}}{C_{in}} \times 100$$

Results and discussion

During the operational period, the average inflow concentrations were 385 mg/L for SO_4^{2-}–S and 34 mg/L for NO_3^- -N (Tab. 1). The large standard deviations (Tab. 1) were closely linked to seasonal variations.

Table 1 Mean concentrations at the inflow and outflow of the sulfate-reducing bioreactor. All values are expressed in mg/L, except Al, Cu, Fe, Mn, P, and Zn, which are expressed in µg/L. An asterisk (*) indicates a statistically significant difference (P < 0.05) between the median inflow and outflow concentrations, determined using an unpaired Wilcoxon signed-rank test.

Compound	Inflow	Outflow	Compound	Inflow	Outflow
pH*	7.2 ± 0.2	6.9 ± 0.3	NO_2^- –N*	3.5 ± 2.7	0.5 ± 1.3
Alkalinity*	208.2 ± 42.6	403.3 ± 124.3	NH_4^+ –N*	0.1 ± 0.0	3.7 ± 4.4
DOC*	7.0 ± 19.0	192.3 ± 105.7	Al*	11.1 ± 3.1	6.1 ± 3.9
SO_4^{2-} –S*	384.7 ± 79.6	343.1 ± 123.8	Cu*	1.2 ± 0.7	0.4 ± 0.9
NO_3^- – N*	34.2 ± 19.0	1.2 ± 2.1	Fe*	0.01 ± 0.01	0.08 ± 0.23
Ca	457.8 ± 89.6	453.2 ± 77.9	Mn*	6.2 ± 3.3	13.4 ± 19.6
K	51.4 ± 13.0	51.7 ± 12.0	P	7.8 ± 4.8	8.0 ± 4.3
Mg	51.4 ± 12.8	51.2 ± 12.0	Zn*	22.2 ± 13.5	3.2 ± 10.5

Both SO_4^{2-}–S and NO_3^-–N concentrations decreased following the snowmelt period, which diluted the inflow water (Fig. 3a and c). Similar dilution effects, while not displayed in this article, were observed for major ions (e.g. K, Mg, Ca), whose concentrations did not differ before and after treatment (Tab. 1).

The highest sulfate removal efficiency (88%) was achieved during summer 2025 under low flow (3.45 m^3/d), medium lactate dosing (9.1 kg/d), and heating conditions (Fig. 3a). Sulfate concentrations were inversely related to sulfide concentrations, which is consistent with sulfide being produced through sulfate reduction (Fig. 3a and b). At low water inflow, lactate addition played a critical role, with higher dosages corresponding to higher sulfate removal.

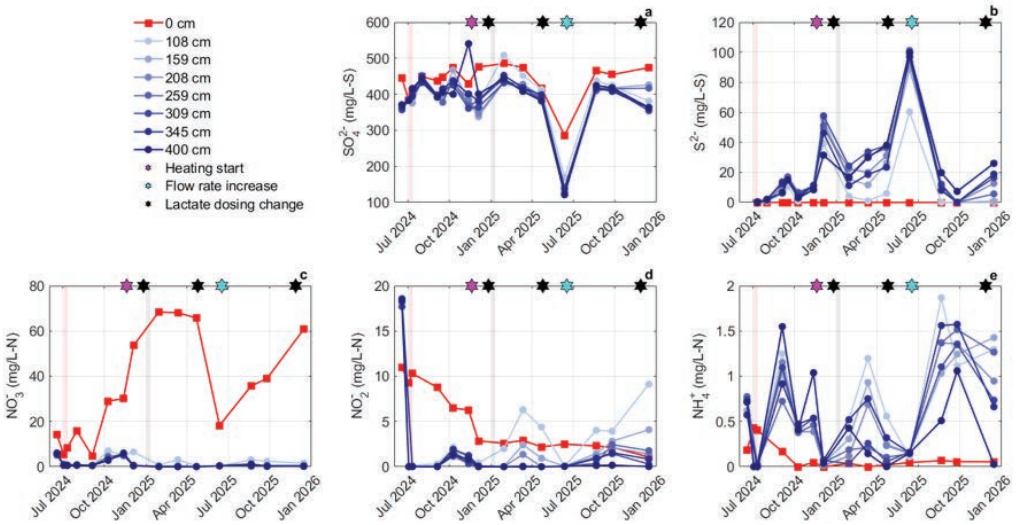

Figure 3 Change in average A-B wells concentrations with depth in bioreactor for sulfate (a), sulfide (b), nitrate (c), nitrite (d) and ammonium (e). Red squares represent the inflow concentration while blue circles are concentrations at different bioreactor depths (from top light blue to bottom dark blue). The purple star marks the beginning of heating, the blue star indicates a flow increase, and the black stars display main lactate dosage changes (more details in Fig. 2). The red vertical highlight represents the inoculation period while the grey vertical highlight indicates a stop of operation.

These results indicate that increasing lactate availability directly enhanced sulfate reduction under longer hydraulic retention times. However, when the inflow rate increased, high lactate dosage did not substantially improve sulfate reduction. Whereas low-flow operations provided approximately three days of residence time, increasing the flow reduced this to roughly one day, which likely did not allow sufficient time for sulfate-reducing bacteria to carry out complete reduction.

Despite considerable nitrate loads entering the system, nitrate removal efficiency consistently exceeded 75% throughout the monitoring period. These values indicate strong and stable denitrification performance, highlighting the bioreactor's potential as an effective treatment option for enhanced nitrate removal. Nitrite removal was similarly efficient (Fig. 3d), with low nitrite accumulation (< 10 mg/L–N) observed in the system. In contrast, ammonium concentrations increased within the bioreactor, suggesting net ammonium production. While these values remain low (< 2 mg/L–N), this trend is likely associated with dissimilatory nitrate reduction to ammonium (DNRA). The addition of lactate elevated the C:N ratio, creating conditions favorable for DNRA. Previous studies show that under anaerobic conditions, high availability of electron donors relative to nitrate or nitrite concentration promotes DNRA (Burgin and Hamilton 2007; Parvage and Herbert, 2023).

Additionally, vertical profiling showed that most sulfate and nitrate removal occurred in the upper layers of the bioreactor (Fig. 3), with minimal variation in compound concentrations across the sampling wells. However, at higher flow rates, this variation increased, suggesting a possible shift in removal activity into the deeper layers of the bioreactor. The sulfide precipitation tank achieved complete sulfide removal and maintained a pH of 6.9 ± 0.3.

A significant removal in several trace metals, including Cu, Zn, and Mo, was observed, while Mn, and Fe exhibited net release (Tab. 1). However, the relatively high standard deviation observed for Mn and Fe suggests concentration spikes within the system rather than a continuous release. The removal of selected trace metals is likely attributable to sulfide precipitation, whereas the release of others appears to originate primarily from the woodchips used as the reactive substrate (Lepine *et al.* 2021).

Although the SRB bioreactor was intended to function in a semi-passive manner, it still relied on pumps, chemical inputs, and periodic maintenance, which further complicated operation in an area with limited infrastructure. Continuous carbon dosing was essential to sustain sulfate reduction, reinforcing that the system cannot operate reliably without supplemental electron donors (Bettoni and Herbert 2024). For this reason, adding the carbon source directly within the bioreactor is recommended, as upstream dosing can stimulate biomass growth in the pipes and lead to fouling. In the presence of nitrate, denitrifying bacteria outcompete SRB for the available carbon source. This competition limits the carbon available for SRB and contributes to lower sulfate removal efficiency. Consequently, more effective or complete nitrate removal is required before the bioreactor, which introduces additional operational costs and highlights the need for more sustainable and affordable pre-treatment strategies.

Conclusions

This study demonstrates that SRB-based bioreactors can effectively remove sulfate from carbon-limited mine water under subarctic conditions when key operational parameters (flow rate, lactate dosing, and temperature) are properly optimized. The results provide valuable operational insights for the design and implementation of biological sulfate removal systems in cold mining regions, supporting more sustainable compliance with sulfate discharge standards.

Acknowledgements

This study is part of the SULFREM project, conducted within the strategic innovation program Swedish Mining Innovation, a collaboration between the Swedish Innovation Agency, Formas, and the Swedish Energy Agency. Funding was provided through the Swedish Innovation Agency (VINNOVA, project number 2021-04669), Boliden Mineral AB and LKAB.

References

Bettoni LN, Herbert RB (2024) Sulfate removal from mine drainage at low temperature: effects of three reactive porous media on microbial sulfate reduction. In: Kleinmann, B., Skousen, J., Wolkersdorfer, Ch.: West Virginia Mine Drainage Task Force Symposium & 15th International Mine Water Association Congress. Morgantown, WV, USA (International Mine Water Association), pp 50–56

Burgin AJ, Hamilton SK (2007) Have we overemphasized the role of denitrification in aquatic ecosystems? A review of nitrate removal pathways. Frontiers in Ecology and the Environment 5:89–96. doi.org/10.1890/1540-9295(2007)5[89:HWOTRO]2.0.CO;2

Geurts JJM, Sarneel JM, Willers BJC, et al (2009) Interacting effects of sulphate pollution, sulphide toxicity and eutrophication on vegetation development in fens: A mesocosm experiment. Environmental Pollution 157:2072–2081. doi.org/10.1016/j.envpol.2009.02.024

Han S, Obraztsova A, Pretto P, et al (2007) Biogeochemical factors affecting mercury methylation in sediments of the Venice Lagoon, Italy. Environmental Toxicology and Chemistry 26:655–663. doi.org/10.1897/06-392R.1

Hellman M, Juhanson J, Wallnäs F, et al (2024) Microbial succession and denitrifying woodchip bioreactor performance at low water temperatures. Journal of Environmental Management 356:120607. doi.org/10.1016/j.jenvman.2024.120607

Karjalainen J, Hu X, Mäkinen M, et al (2023) Sulfate sensitivity of aquatic organism in soft freshwaters explored by toxicity tests and species sensitivity distribution. Ecotoxicol Environ Saf 258:114984. doi.org/10.1016/j.ecoenv.2023.114984

Lamers LPM, Tomassen HBM, Roelofs JGM (1998) Sulfate-Induced Eutrophication and Phytotoxicity in Freshwater Wetlands. Environ Sci Technol 32:199–205. doi.org/10.1021/es970362f

Lepine C, Christianson L, Soucek D, et al (2021) Metal leaching and toxicity of denitrifying woodchip bioreactor outflow—Potential reuse application. Aquacultural Engineering 93:102129. doi.org/10.1016/j.aquaeng.2020.102129

Nordström A, Herbert RB (2018) Determination of major biogeochemical processes in a denitrifying woodchip bioreactor for treating mine drainage. Ecological Engineering 110:54–66. doi.org/10.1016/j.ecoleng.2017.09.018

Parvage MM, Herbert R (2023) Sequential removal of nitrate and sulfate in woodchip and hematite – coated biochar bioreactor. Environ Sci: Water Res Technol. doi.org/10.1039/D2EW00499B

Pudi A, Rezaei M, Signorini V, et al (2022) Hydrogen sulfide capture and removal technologies: A comprehensive review of recent developments and emerging trends. Separation and Purification Technology 298:121448. doi.org/10.1016/j.seppur.2022.121448

Swedish Meteorological and Hydrological Institute (SMHI) (n.d). Lufttemperatur (h) from station ID 180940. Retrieved 2026-05-18, from https://www.smhi.seSmolders AJP, Lamers LPM, Lucassen ECHET, et al (2006) Internal eutrophication: How it works and what to do about it—a review. Chemistry and Ecology 22:93–111. doi.org/10.1080/02757540600579730

Soucek DJ, Kennedy AJ (2005) Effects of hardness, chloride, and acclimation on the acute toxicity of sulfate to freshwater invertebrates. Environmental Toxicology and Chemistry 24:1204–1210. doi.org/10.1897/04-142.1

Swedish Agency for Marine and Water Management (2018) Remittance on the revision of regulations (HVMFS 2013:19) on the classification on environmental quality standards with regard to surface water

Wang J, Dai J, Chen G, Jiang F (2022) Role of sulfur biogeochemical cycle in mercury methylation in estuarine sediments: A review. Journal of Hazardous Materials 423:. doi.org/10.1016/j.jhazmat.2021.126964

Zak D, Kleeberg A, Hupfer M (2006) Sulphate-mediated phosphorus mobilization in riverine sediments at increasing sulphate concentration, River Spree, NE Germany. Biogeochemistry 80:109–119. doi.org/10.1007/s10533-006-0003-x

Geochemical Safety of Enhanced Rock Weathering for Acid Mine Drainage Remediation in Japan and Zambia

Frances Chikanda[1,2], Fugo Nakamura[3], Hkaung Htut San[3], Ryosuke Kikuchi[1], Tsubasa Otake[1]

[1]*Faculty of Engineering, Hokkaido University, 060-0813, Sapporo, Japan. franceschikanda2@eng.hokudai.ac.jp, https://orcid.org/0000-0003-2596-2743*

totake@eng.hokudai.ac.jp, https://orcid.org/0000-0001-9596-4141

tomsato@eng.hokudai.ac.jp, https://orcid.org/0000-0002-3279-3696

[3]*Graduate School of Engineering, Hokkaido University, 060-0813, Sapporo, Japan*

Abstract

Enhanced rock weathering (ERW) has recently been proposed as a strategy to couple mine drainage remediation with carbon dioxide removal. However, the geochemical safety of applying mafic rocks to acidic mine drainage systems remains insufficiently understood. This study evaluates the release and subsequent attenuation of nickel (Ni) and chromium (Cr) during basalt dissolution under acidic conditions representative of mine drainage. Batch experiments show that Ni and Cr concentrations initially increase but subsequently decline as pH rises, indicating natural sequestration through secondary iron mineral formation. In addition, tailings from Zambia were characterized to evaluate their potential suitability as carbon-reactive substrates, with basalt identified as a promising additive to enhance reactive Ca and Mg availability.

Keywords: Mine drainage, enhanced rock weathering, Ni, Cr, carbon dioxide removal, mine tailings

Introduction

Mine drainage from abandoned mines remains a long-term environmental challenge due to persistent acidity and dissolved metal release (Nordstrom, 2011). Although passive treatment systems such as wetlands and limestone drains are widely used because of their low operational requirements, they often provide limited alkalinity generation and do not contribute to climate-related goals such as carbon dioxide removal.

Enhanced rock weathering (ERW) has emerged as a promising approach for atmospheric CO_2 removal through accelerated silicate dissolution (Beerling *et al.*, 2020). While most ERW studies have focused on agricultural soils, acidic mine drainage systems may offer favourable geochemical conditions because low pH and high water–rock interaction rates can enhance silicate dissolution, consume acidity, and generate bicarbonate alkalinity. However, the use of mafic rocks such as basalt raises safety concerns because they may contain elevated nickel (Ni) and chromium (Cr) concentrations (Flipkens *et al.*, 2021). Under acidic conditions, dissolution of these minerals may release trace metals into already impacted waters, making it essential to evaluate whether Ni and Cr remain mobile or become naturally attenuated through secondary mineral formation.

This study assesses the geochemical safety of basalt application in acidic mine drainage systems in Japan by examining the release and subsequent behaviour of Ni and Cr during basalt dissolution. In addition, because mine tailings storage facilities are increasingly being considered as potential carbon sinks due to their large volumes and reactive surface areas (Bullock *et al.*, 2022), Zambian mine tailings were characterized to evaluate their suitability for carbon sequestration. The study further investigates whether blending tailings with basalt can enhance carbonation reactions by increasing reactive Ca and Mg availability. The specific objectives are to: (i) evaluate Ni and Cr release during basalt dissolution

under acidic mine drainage conditions, (ii) determine whether natural geochemical processes promote their sequestration over time, and (iii) assess the potential of mine tailings for carbon reduction and the role of basalt in enhancing carbonation reactions.

Materials and Methodology

Basalt Characterization

Basalt samples from Hokkaido, Japan were crushed and sieved to approximately 75 µm particle size. Bulk mineralogy was determined using X-ray diffraction (XRD), while major element composition was measured by X-ray fluorescence (XRF). Surface morphology and mineral textures were examined using scanning electron microscopy (SEM) with energy dispersive spectroscopy (EDS). Basalt serves as the primary reactive material for the experimental dissolution study, both in the lab and in the field.

Batch Dissolution Experiments

Batch dissolution experiments were conducted to simulate basalt weathering under acidic mine drainage conditions (Figure 1). Basalt powders were reacted with deionized water adjusted to pH 3.5 with sulfuric acid, which represents typical acidic mine drainage conditions. Experiments were performed at a solid-to-liquid ratio of 1:8 and maintained at approximately 25 °C with constant agitation. Samples were collected periodically over a 50-day period. Filtered solutions were analyzed using ICP-MS to determine concentrations of Ca, Mg, Ni and Cr.

To validate the laboratory findings, field-scale trials were conducted by applying 1 tonne of basalt material to two separate river systems. In the field trials, basalt was applied as a passive reactive amendment. The material was placed directly in selected river systems, packaged in 5 kg nylon filter bags, allowing water–rock contact under natural flow conditions while minimizing environmental impacts (Figure 1). The crushed basalt had a coarser particle-size distribution (1~2cm) than the laboratory powders, reflecting practical field deployment conditions and reducing the likelihood of rapid downstream transport. Water samples were collected upstream of the application zone, immediately downstream of the amended zone, and at a downstream mixing point to distinguish basalt-related geochemical effects from background river chemistry. Flow rates at Shojin and Amemasu were ~0.19 and ~0.16 m3 /s, respectively. Conditions were monitored qualitatively during each sampling event, and the results are interpreted as field-scale geochemical trends under dynamic hydrological conditions.

Tailings Characterization

Mine tailings collected from Zambia were characterized using XRD and XRF to determine mineral composition and elemental content. Particular attention was given to minerals containing Ca and Mg that could contribute to carbonation reactions. To evaluate methods of enhancing carbonation potential, the tailings were conceptually

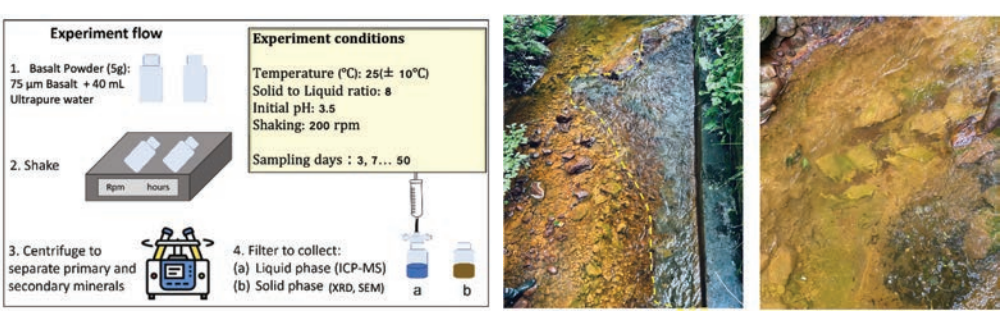

Figure 1 *(a) Experiment conditions for the basalt dissolution and (b) pictures of the field-scale trial in one of the rivers, upon installation on the left, and one month later to the right.*

assessed by mixing with basalt, a by-product rich in reactive Ca and Mg. In this study, carbon sequestration was assessed as a geochemical potential rather than directly quantified CO_2 removal. Therefore, the carbon-removal component is interpreted from mineralogical and geochemical indicators, particularly the availability of reactive Ca- and Mg-bearing silicates, pH evolution, and the potential for alkalinity generation during basalt dissolution.

Results and Discussion

Basalt Dissolution and Acid Neutralization

Silicate rocks from Japan, including nineteen mafic rocks (basalt) and one ultramafic rock (harzburgite), were assessed for enhanced rock weathering (ERW) in acidic mine drainage systems. Whole-rock XRF results showed clear lithological differences in trace metals (Figure 2). The ultramafic sample contained very high Ni and Cr concentrations, exceeding 500 mg/L for both elements, while the basalts had much lower contents, with Cr below 250 mg/L and Ni below 150 mg/L. Because Ni and Cr may be released during dissolution under acidic conditions, the ultramafic rock was considered less suitable for direct ERW application. Basalt, however, is widely regarded as a suitable ERW feedstock due to its relatively rapid dissolution, lower trace-metal risk, and ability to release Ca and Mg for neutralization and carbon sequestration (Linke *et al.*, 2024).

Batch experiments showed that basalt dissolution progressively increased pH from about 3.5 to approximately 7.5–8.5. This reflects proton-promoted dissolution of mafic silicate minerals such as olivine and pyroxene, during which acidity is consumed and Mg^{2+}, Ca^{2+}, and dissolved silica are released (Equation 1). These reactions act as a geochemical buffer and represent the main mechanism by which basalt can neutralize acidic mine drainage (Rimstidt *et al.*, 2012). The released Ca and Mg also support carbon sequestration by reacting with atmospheric or dissolved CO_2 to form bicarbonate alkalinity and, potentially, carbonate minerals or enhanced ocean alkalinity (Beerling *et al.*, 2020; Hartmann *et al.*, 2023). Thus, basalt weathering may provide a dual benefit by coupling AMD remediation with long-term carbon storage.

$$(Mg,Ca)_2SiO_4 + 2\ H_2SO_4 \rightarrow 2\ (Mg,Ca)^{2+} + 2\ SO_4^{2+} + H_4SiO_4 \quad (1)$$

Environmental Risk Assessment: Nickel and Chromium mobility and attenuation

A primary environmental concern regarding the application of basalt for mine drainage

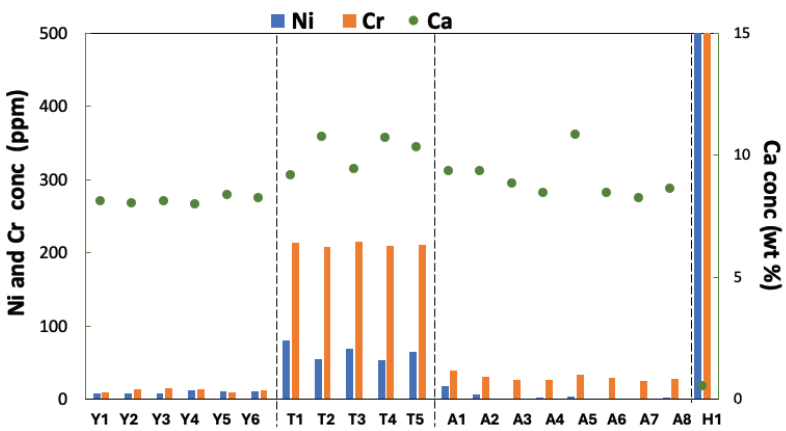

Figure 2 (a) Experiment conditions for the basalt dissolution and (b) pictures of the field-scale trial in one of the rivers, upon installation on the left, and one month later to the right.

remediation is the potential mobilization of trace elements, specifically nickel (Ni) and chromium (Cr), which are inherent to mafic minerals. As shown in the 50-day batch experiments (Figure 3), dissolved Ni and Cr concentrations exhibited a distinct peak and decline trend across all samples (A1, T1, Y1, and H1).

During the early stages of the batch experiment (Days 3–28), dissolved Ni and Cr concentrations increased markedly, with sample H1 reaching peak values of approximately 65 µg/L Ni and 125 µg/L Cr. This initial release is attributed to the rapid proton-promoted dissolution of primary basaltic silicate minerals, including olivine, pyroxene, plagioclase, augite, and smectite, in which Ni commonly substitutes for Mg and Cr may occur within the mineral lattice (White, 2017). However, between Day 28 and Day 50, both Ni and Cr concentrations declined sharply, returning to near-baseline levels. This pattern suggests that trace-metal release during basalt dissolution was transient and became increasingly controlled by natural attenuation as silicate weathering consumed acidity and increased solution pH toward circumneutral to alkaline conditions.

To assess environmental relevance, measured concentrations were compared with selected international water-quality guidelines. The maximum dissolved Ni concentration in the batch experiment, approximately 65 µg/L, remained below the WHO drinking-water guideline value of 70 µg/L. In contrast, the maximum total Cr concentration of approximately 125 µg/L exceeded both the WHO guideline value of 50 µg/L for total Cr and the Japanese environmental standard of 20 µg/L for Cr(VI). However, this Cr peak occurred under closed-system, high water–rock interaction conditions and declined substantially by Day 50. Importantly, field monitoring over 78 days in two rivers, River S and River A, and at a downstream mixing point showed that these elevated batch concentrations were not reproduced under dynamic environmental conditions. Ni concentrations in River S remained relatively stable at approximately 20 µg/L, while River A showed very low concentrations. At the downstream monitoring point, Ni remained consistently low, below 5 µg/L, throughout the monitoring period. Chromium concentrations were negligible across all field sites and remained below 10 µg/L, indicating that dilution and geochemical attenuation effectively limited trace-metal accumulation in the river system.

The observed decline in dissolved Ni and Cr concentrations in both laboratory and field settings suggests that trace-metal release during basalt dissolution is transient and partly self-limiting. During the early reaction stage, proton-promoted dissolution of primary basaltic minerals such as plagioclase, pyroxene, and augite likely promoted the release of divalent cations and trace elements hosted within the mineral structure. However, as basalt dissolution progressed, acidity was consumed and solution pH increased toward circumneutral to alkaline conditions. Under these conditions, Fe released from basaltic minerals can hydrolyse and precipitate as secondary Fe-bearing phases, which provide high-surface-area sites for trace-

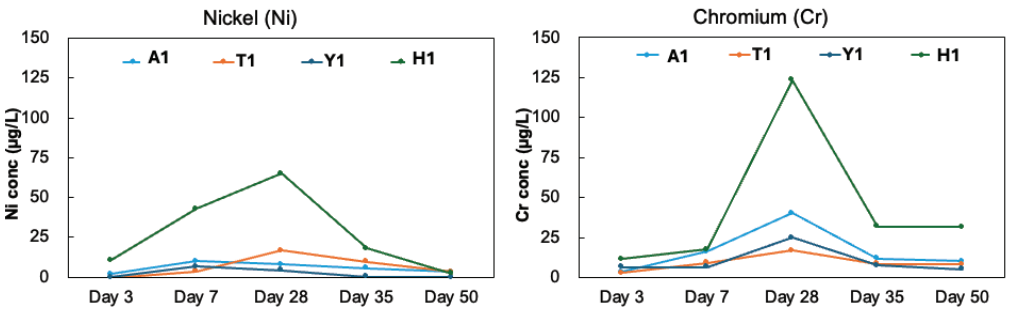

Figure 3 *Trends of Ni and Cr during batch experiments for a 50 day period.*

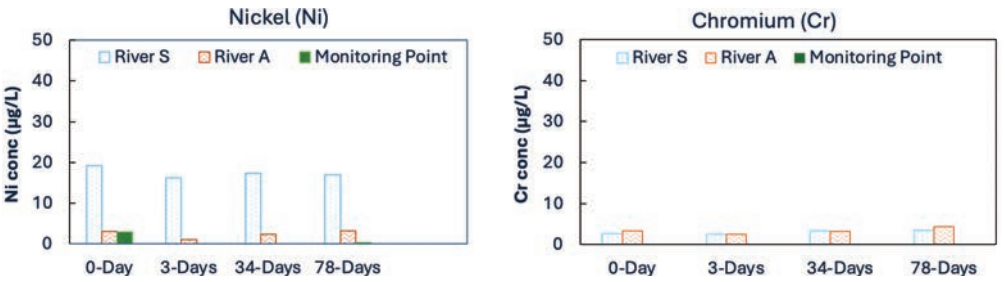

Figure 4 *Long-term field monitoring of Ni and Cr concentrations (µg/L) in River S, River A, and the downstream mixing point.*

metal attenuation through adsorption, co-precipitation, or structural incorporation. Secondary Fe minerals formed during AMD neutralization are widely recognized as important controls on trace-metal mobility because they can scavenge metals from solution and limit their downstream transport (Nordstrom, 2011; Baleeiro *et al.*, 2018).

The increase in pH alongside declining dissolved Ni and Cr indicates that basalt weathering neutralized acidity while promoting trace-metal sequestration. Fe released during dissolution likely precipitated as secondary Fe-bearing phases, providing sites for Ni and Cr removal through adsorption, co-precipitation, or structural incorporation. Post-reaction XRD (Figure 5) supports this mechanism, showing the persistence of basaltic minerals and increased clay mineral formation. As Fe oxyhydroxides are common in AMD systems, secondary Fe minerals can retain trace metals and have been shown to adsorb Ni(II) and Cr(VI), depending on pH, ionic strength, and competing ions (Kim and Kim, 2021; Zhao *et al.*, 2022).

Overall, the laboratory and field results indicate that Ni and Cr release during basalt-enhanced weathering is initially enhanced under acidic conditions but becomes partly self-limiting as pH increases and secondary Fe-bearing minerals form. Nevertheless, because Cr was measured only as total dissolved Cr, future work should distinguish Cr(III) from Cr(VI), particularly because Cr(VI) is more mobile and toxic under oxidizing conditions. In addition, since XRD may not fully resolve poorly crystalline Fe phases such as ferrihydrite, complementary SEM–EDS, selective extraction, or spectroscopic analyses would further strengthen confirmation of the trace-metal attenuation mechanism.

Potential of Tailings Ponds as Carbon Sinks

Beyond basalt use in mine drainage, Zambia's mine tailings were evaluated as potential substrates for carbon sequestration. XRD analysis showed that the tailings are mainly composed of silicate minerals with minor sulfide remnants, while XRF results identified measurable Cu and Co, reflecting the original ore signature. Their fine-grained nature provides a high reactive surface area, but limited Ca- and Mg-bearing phases may constrain carbonation.

To improve carbonation potential, blending tailings with basalt was considered because basalt supplies reactive Ca and Mg silicates that dissolve to generate alkalinity. This hybrid approach could support both

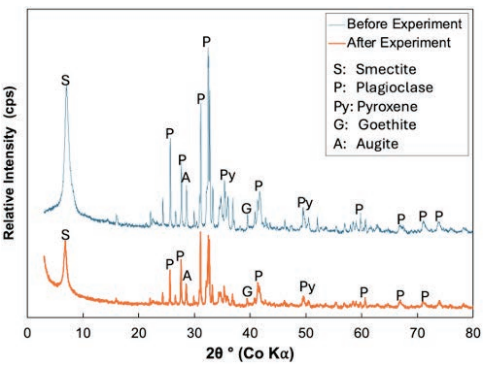

Figure 5 *XRD patterns of basaltic material before and after the batch dissolution experiment.*

metal stabilization and carbon sequestration, allowing tailings storage facilities to act as long-term carbon sinks when combined with water management systems that enhance water–rock interaction (Bullock *et al.*, 2022).

Conclusions

This study shows that basalt can effectively neutralize AMD while releasing Ca and Mg that may support carbon sequestration. Although Ni and Cr were initially released during dissolution, their concentrations declined as pH increased, suggesting transient and self-limiting metal mobility through secondary Fe-phase adsorption or co-precipitation. Zambian mine tailings also showed potential as carbon sinks, especially when blended with basalt to enhance reactive Ca and Mg availability. Overall, basalt-enhanced weathering offers a promising approach for combined mine water remediation, mine waste management, and carbon removal.

Acknowledgements

This research was supported by the New Energy and Industrial Technology Development Organization (NEDO) program in Japan.

References

Baleeiro, A., Fiol, S., Otero-Fariña, A., & Antelo, J. (2018). Surface chemistry of iron oxides formed by neutralization of acidic mine waters: Removal of trace metals. Applied Geochemistry, 89, 129–137. https://doi.org/10.1016/j.apgeochem.2017.12.003

Beerling, D. J., Kantzas, E. P., Lomas, M. R., Wade, P., Eufrasio, R. M., Renforth, P., Sarkar, B., Andrews, M. G., James, R. H., Pearce, C. R., Mercure, J. F., Pollitt, H., Holden, P. B., Edwards, N. R., Khanna, M., Koh, L., Quegan, S., Pidgeon, N. F., Janssens, I. A., … Banwart, S. A. (2020). Potential for large-scale CO2 removal via enhanced rock weathering with croplands. Nature, 583(7815), 242–248. https://doi.org/10.1038/s41586-020-2448-9

Bullock, L. A., Yang, A., & Darton, R. C. (2022). Kinetics-informed global assessment of mine tailings for CO2 removal. Science of the Total Environment, 808. https://doi.org/10.1016/j.scitotenv.2021.152111

Flipkens, G., Blust, R., & Town, R. M. (2021). Deriving Nickel (Ni(II)) and Chromium (Cr(III)) Based Environmentally Safe Olivine Guidelines for Coastal Enhanced Silicate Weathering. Environmental Science and Technology, 55(18), 12362–12371. https://doi.org/10.1021/acs.est.1c02974

Hartmann, J., Suitner, N., Lim, C., Schneider, J., Marín-Samper, L., Arístegui, J., Renforth, P., Taucher, J., & Riebesell, U. (2023). Stability of alkalinity in ocean alkalinity enhancement (OAE) approaches – consequences for durability of CO2storage. Biogeosciences, 20(4), 781–802. https://doi.org/10.5194/bg-20-781-2023

Linke, T., Oelkers, E. H., Dideriksen, K., Möckel, S. C., Nilabh, S., Grandia, F., & Gislason, S. R. (2024). The geochemical evolution of basalt Enhanced Rock Weathering systems quantified from a natural analogue. Geochimica et Cosmochimica Acta, 370, 66–77. https://doi.org/10.1016/j.gca.2024.02.005

Noor, N., Zhou, Z., Latta, D. E., Scherer, M. M., Borch, T., Thompson, A., & Plante, A. (2020). Aerobic Microbial Respiration of Fe (II) Reacted Ferrihydrite-Natural Organic Matter Coprecipitates. (Ii), 1945–1945. https://doi.org/10.46427/gold2020.1945

Nordstrom, D. K. (2011). Mine Waters : Acidic to Circumneutral. 393–398. https://doi.org/10.2113/gselements.7.6.393

Rimstidt, J. D., Brantley, S. L., & Olsen, A. A. (2012). Systematic review of forsterite dissolution rate data. Geochimica et Cosmochimica Acta, 99, 159–178. https://doi.org/10.1016/j.gca.2012.09.019

White, W. M. (2020). Geochemistry. Wiley-Blackwell.

Zhao, X., Wang, H., Zhu, M., & Li, W. (2022). Competitive kinetics of Ni(II)/Co(II) and Cr(VI)/P(V) adsorption and desorption on goethite: A unified thermodynamically based model. Journal of Hazardous Materials, 424, 127338. https://doi.org/10.1016/j.jhazmat.2021.12733

Electrochemical Treatment of Maurliden Mine AMD using Clean&Recover ECR™ Technology

Vitalis Chipakwe[1], Luke Berry[2], Peter Lundell[1], Erik Ronne[1], Ksenia Novikova[1], Malin Suup[1]

[1]*Boliden, Finnforsvägen 4, 936 81 Boliden, Sweden*

[2]*Clean & Recover, 531 Gympie Rd, Kedron, 4031, Australia*

Abstract

Acid mine drainage (AMD) from the Maurliden mine presents substantial environmental challenges due to low pH and elevated sulfate and metal concentrations. This study evaluates the ElectroClear Reactor™ (ECR), a modified electrodialysis-based electrochemical process, for AMD treatment at mini-pilot scale. ECR achieved >98% removal of Zn, Ni, Cu, Al, As, Cd, Co, Mn, and Fe, together with 76% sulfate removal, producing discharge-compliant water and a sulfuric acid by-product. Optimal operation was achieved at 17 A and 0.5 $m^3 h^{-1}$, with an energy demand of 8.7–15.6 kWh m^{-3}. Compared to lime treatment, ECR provided equivalent neutralisation (pH 9.8), substantially reduced sludge generation, produced Zn-enriched sludge, and improved settling behaviour, demonstrating a pathway toward electrified, lower-carbon AMD treatment.

Keywords: Acid mine drainage, electrodialysis, resource utilisation, neutralisation, electrochemical treatment

Introduction

Acid mine drainage (AMD) remains a major challenge for mine remediation due to the acidity and elevated sulfate and metal concentrations, as exemplified at Boliden's closed Maurliden mine in northern Sweden Fig. 1. Current lime-based neutralisation effectively reduces acidity and metals but generates large sludge volumes, incurs high operational costs, and carries a substantial CO_2 footprint, highlighting the need for alternative treatment technologies.

Non-chemical active water treatment technologies have gained increasing attention, with electro- and membrane-based processes such as reverse osmosis, nanofiltration, ion exchange, electrocoagulation, and electro-oxidation widely investigated for AMD treatment (Arana Juve *et al.* 2022). However, these technologies typically require extensive pretreatment – and/or post-treatment - steps, including pH adjustment and removal of metals such as Fe and Mn, leading to increased process complexity and high CAPEX/OPEX. Electrodialysis (ED), combining electrical driving forces with ion-selective membranes, has been proposed as a cleaner alternative (Arahman *et al.* 2017; Aydin *et al.* 2019; Liu *et al.* 2022; Hopsort *et al.* 2024). ED has demonstrated high metal removal efficiencies (>97–99%) for ions such as Fe^{3+}, Zn^{2+}, Ni^{2+}, Mg^{2+}, and Mn^{2+} (Buzzi *et al.* 2013; Liu *et al.* 2022); however, it generates concentrated ion streams that require further treatment. Proposed solutions, including electrowinning or chemical precipitation, often overlook the economic implications of downstream recovery, complicating water treatment and mine closure strategies (Arana Juve *et al.* 2022; Cerrillo-Gonzalez *et al.* 2023).

To address limitations, Clean&Recover developed the ElectroClear Reactor (ECR™), a modified electrodialysis system employing a single sulfate-selective anion-exchange membrane rather than paired anion and cation membranes. Unlike conventional ED, which generates a concentrated brine that requires secondary treatment, ECR™ selectively isolates sulfate ions without producing a reject stream. In this study, a mini-pilot ECR was evaluated for treatment of Maurliden AMD, assessing the effects of current (11–20 A) and flow rate (0.1–0.5 $m^3 h^{-1}$) on water recovery and energy

consumption, alongside sludge production and characterisation benchmarked against conventional lime treatment.

Methods

AMD was collected from the Boliden's Maurliden mine in Fig.1. The ECR comprised 10 paired chambers, each containing an anionic membrane positioned between a titanium-based cathode and a mixed-metal-oxide-coated anode (iridium and ruthenium), with an effective total membrane area of 10000 cm^2. The water treatment tests were carried out on a mini-pilot ECR plant installed at the Boliden pilot plant facilities in Boliden, Sweden, Fig. 2. For all experiments, pH and Eh were measured and corrected using an Ag/AgCl reference electrode. All the water and sludge samples analysed using ICP-OES and ion chromatography, as presented in Table 1.

A Box–Behnken design (BBD) was applied for the parametric study. 15 experiments were conducted at varying voltage (27–63 V), current (11–20 A), and catholyte-to-anolyte (CA:AN) flow-rate ratio (0.6–1.4), while the final pH was fixed to ensure target removal. The responses were energy consumption (kWh m^{-3}) and runtime, allowing minimisation of energy demand and processing time. Operational parameters (flow rate, temperature, pH, redox potential, current, and voltage) were recorded at 10-min intervals, and selected streams were chemically analysed. In addition to the parametric study, the selected parameters were used for the next study, where the analyte was recycled for different AMD batches and summarised in Table 2.

Results and Discussion

Maurliden AMD was treated in the ECR, and samples were taken at different pH values. The starting pH for AMD was 2.8 with a redox potential of 546 mV and the pH increased to 11.5 while the redox change from oxidising to reducing conditions as the test progressed. The redox decreases sharply from 546 mV to 134 mV at pH 4 decreasing to -205 mV at pH 11.5. Most elements reach >95 % removal at pH 6 except for sulfate, Ba, Ca, and Cl. Beyond pH 10 as expected signs of Al resolubilising start, and the removal rate decreases to 92,8 % from >95 % level.

Based on the initial pH test presented in Fig. 3, pH 9.8 was selected as the optimum for metal removal. For the optimised case, the energy consumption for the 5 runs is

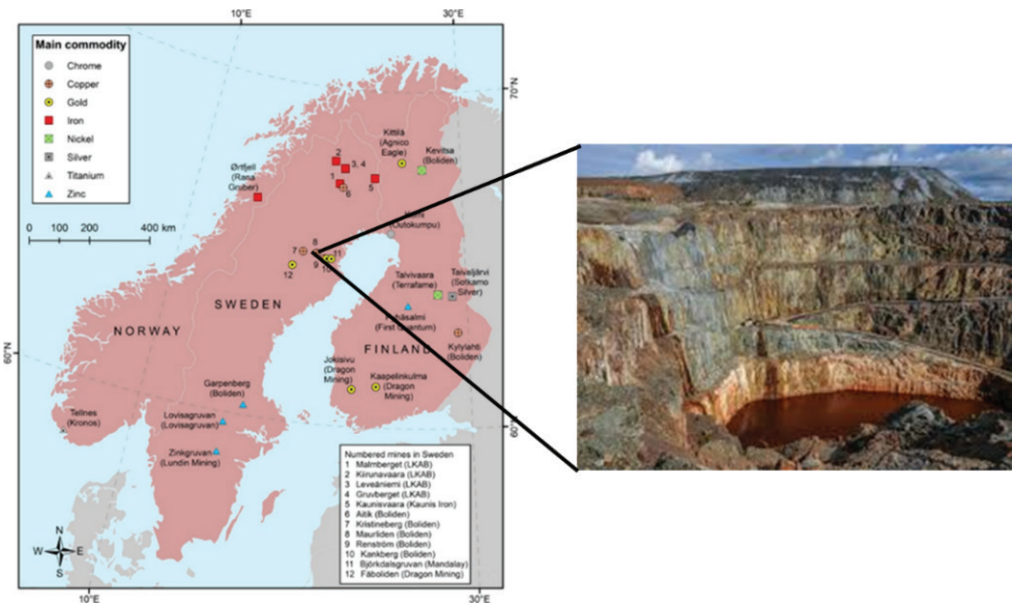

Figure 1 Maurliden mine located in northern Sweden (adapted from (Klein et al. *2022)).*

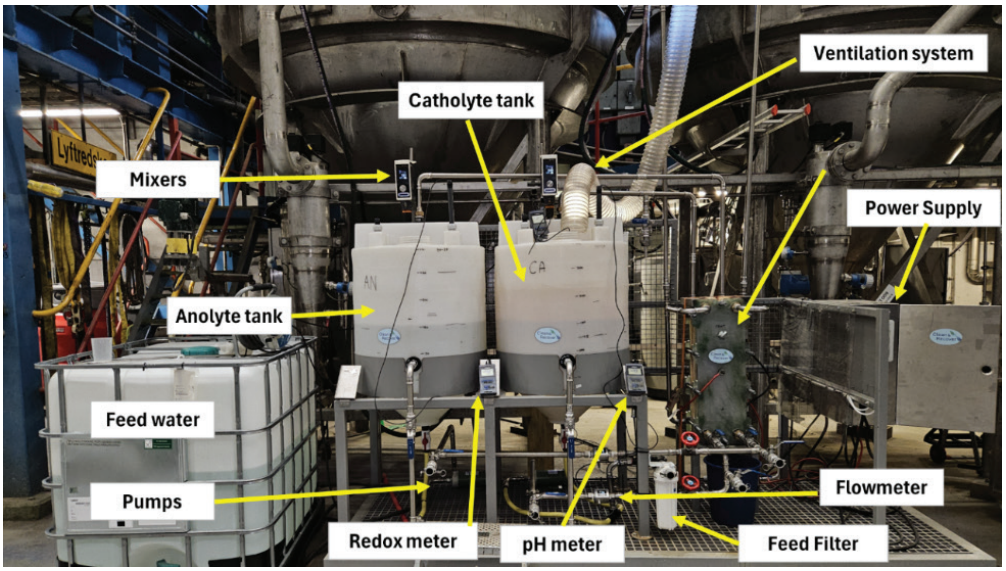

Figure 2 ECR™ setup at the pilot plant in Boliden.

Table 1 Chemical characterisation of the Maurliden AMD.

Parameter	Units	Maurliden AMD	Treated water	% Removal
Fe	mg/L	205	0.04	99.9
Mg	mg/L	157	21.6	86.2
Al	mg/L	79.3	0.79	99.0
Zn	µg/L	136000	2.0	99.9
Mn	µg/L	28000	61.1	99.8
Cu	µg/L	5040	1.0	99.9
As	µg/L	1010	5,2	99.5
Ni	µg/L	157	0,5	99.7
Pb	µg/L	28,8	0.2	99.3
U	µg/L	19.9	0.01	99.9
Cr	µg/L	13	0.5	96.2
SO4	mg/L	4020	968	75.9
Cl	mg/L	15.8	4.0	74.9
F	mg/L	8.69	2.05	76.4
pH	-	2,8	9.8	
Electrical conductivity	µS/cm	3478	121	
ORP	mV	546	52	

presented in Fig. 5. In these runs, the anolyte was recycled.

The trends in energy consumption (Fig. 4) reflect the increase in cycle times from 1.50 h (run #1-1) to 3.33 h (run #1-5). At constant current, the voltage decreased with anolyte recycling as a result of increased conductivity; however, energy use increased, likely from elevated sulfate levels altering membrane diffusion gradients. At pH 9.8, the removal of

Table 2 Experiments with anolyte recirculation.

Run	#1-1	#1-2	#1-3	#1-4	#1-5
Energy, kWh/m³	10.2	11.6	12.5	13.1	18.3
Voltage, V	50	45	42	39	40
Amps, A	17	17	17	17	17
CA flowrate, m³/h	0.5	0.4	0.3	0.3	0.3
AN flowrate, m³/h	0.3	0.4	0.4	0.4	0.4
CA:AN flowrate ratio	1.4	1,0	0,8	0,8	0,6
Final pH	9.8	9.8	9.8	9.8	9.88
Running time, h	1.50	1.92	2.17	2.50	3.33

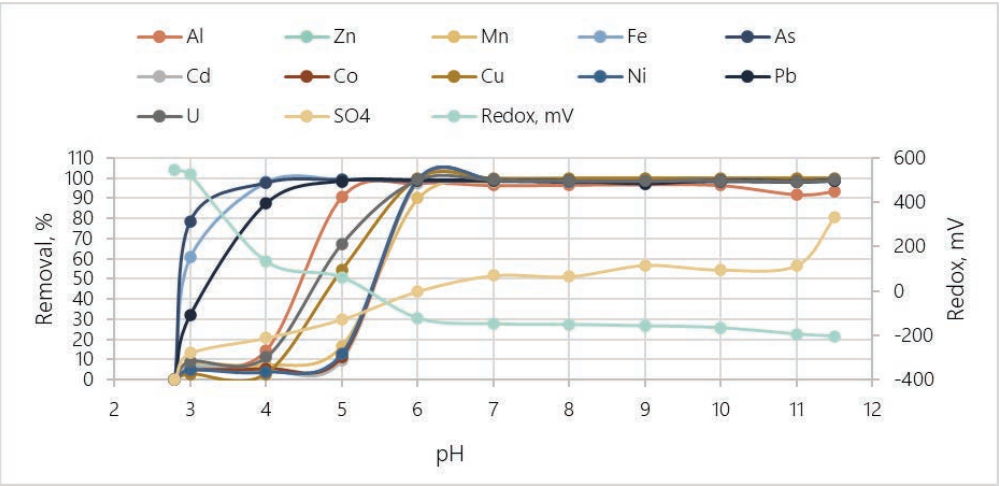

Figure 3 Variation of element removal as a function of pH.

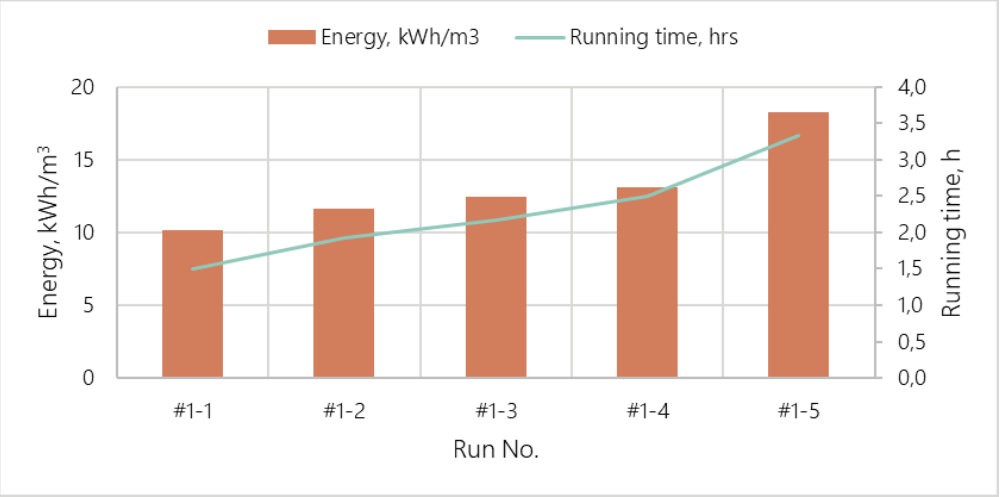

Figure 4 Energy use for the at pH 9.8 and 17 A.

cations exceeded 99 % at 80% water recovery, while Ca and Ba removal was minimal (0–15 %), attributed to low pH and short operation time, Fig. 5. Anion removal reached 70 % (Cl^-), 40 % (F^-), and 76 % (SO_4^{2-}). Low efficiency is attributed to reduced anolyte pH and sulfate loading, which limit sulfate ion transport due to a weakened diffusion gradient (Hopsort *et al.* 2024).

As expected from the design, the removal of the anions mainly sulfate is observed from the catholyte side. All sulfate ions migrated to the anolyte chamber to give a sulfuric acid by-product (1220 mg/L SO_4, pH 1.3) with some minor cations transported via the inevitable leakage (Hopsort *et al.* 2024). As the anolyte represents about 20 % of the total flow, feasibility is contingent on local utilisation, with nearby applications such as pH control in Fenton-based thiosalt treatment offering a practical integration option into existing operations.

Chemical characterisation and settling tests were conducted in the sludge. Sludge production was 1.4 kg m^{-3} of AMD treated for ECR, compared to 6.7 kg m^{-3} for lime treatment. The zinc content increased to 9.82% relative to 3.62 % in lime sludge (Table 3), indicating potential for sludge valorisation. This enrichment is attributed to reduced lime addition, reflected by lower calcium content in ECR sludge.

The stabilisation tests of the ECR™ catholyte sludges, benchmarked against the lime sludge of the Maurliden plant without flocculant, showed markedly faster settling for the ECR (Fig. 6), with clarification largely complete within 20 min and plateauing at 60 min versus 90 min for the lime sludge. This behaviour reflects the denser mineral-like nature of metal-enriched galvanic sludges compared to gelatinous flocs from lime precipitation (Yu Makoskaya *et al.* 2020). Consequently, ECR enables reduced retention times and smaller solid–liquid separation units, reducing the size of the equipment and the footprint of the process.

ECR™ offers an improved approach for AMD treatment, characterised by reduced sludge production and generation of a sulfuric acid by-product. In contrast, conventional electrochemical processes and membrane

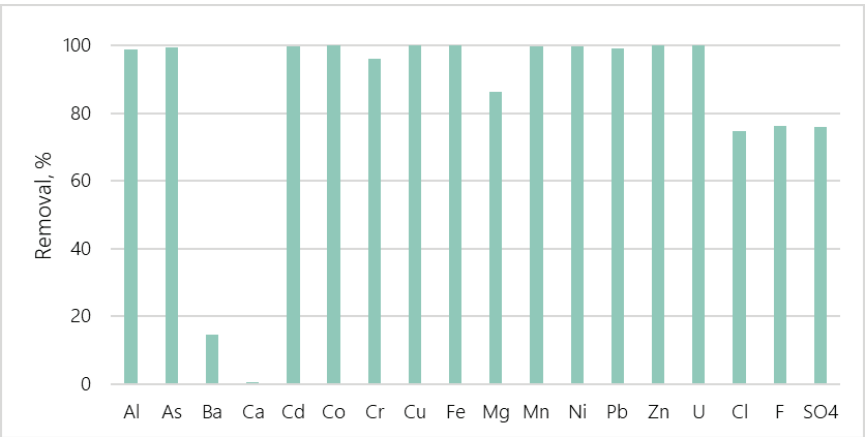

Figure 5 *Removal rates under optimised conditions.*

Table 3 *Sludge analysis.*

Process	Sludge (kg/m³)	Zn (%)	Cu (%)	Fe (%)	Ca (%)	Al_2O_3 (%)
Maurliden liming	6.7	3.62	0.18	9.16	21.3	4.64
ECR	1.4	9.82	0.31	14.75	2.91	10.07

– require extensive pretreatment, including pH adjustment and removal of organics and foulants. This work demonstrates a path toward electrified and decarbonised AMD treatment, reducing the reliance on bulk lime logistics and lowering overall water treatment costs.

Conclusions

This study demonstrates that mini-pilot-scale ECR effectively treats Maurliden AMD, producing effluent that meets discharge permit requirements. The process achieved >98 % removal of target metals (Zn, Ni, Cu, Al, As, Cd, Co, Mn) and up to 76% sulfate removal. Optimal operation was obtained at 17 A and 0.5 $m^3 h^{-1}$, with an average energy demand of 8.7–15.6 kWh m^{-3}. Compared to conventional lime treatment, ECR provided comparable neutralisation (pH 9.8) without lime addition, substantially reduced sludge production (1.4 vs 6.7 kg m^{-3}), generated a Zn-enriched sludge (9.8 wt.% Zn), and exhibited improved settling characteristics.

Acknowledgements

The authors acknowledge financial and logistic support provided by Boliden and Clean & Recover to conduct this research. The authors thank the assistance provided by the Pilot plant and Maurliden personnel.

References

Arahman N, Mulyati S, Lubis MR, et al (2017) Removal profile of sulfate ion from mix ion solution with different type and configuration of anion exchange membrane in elctrodialysis. J Water Process Eng 20:173–179. https://doi.org/10.1016/j.jwpe.2017.10.007

Arana Juve J-M, Christensen FMS, Wang Y, Wei Z (2022) Electrodialysis for metal removal and recovery: A review. Chem Eng J 435:134857. https://doi.org/10.1016/j.cej.2022.134857

Aydin MI, Yuzer B, Hasancebi B, Selcuk H (2019) Application of electrodialysis membrane process to recovery sulfuric acid and wastewater in the chalcopyrite mining industry. Desalination Water Treat 172:206–211. https://doi.org/10.5004/dwt.2019.25051

Buzzi DC, Viegas LS, Rodrigues MAS, et al (2013) Water recovery from acid mine drainage by electrodialysis. Miner Eng 40:82–89. https://doi.org/10.1016/j.mineng.2012.08.005

Cerrillo-Gonzalez MDM, Villen-Guzman M, Rodriguez-Maroto JM, Paz-Garcia JM (2023) Metal Recovery from Wastewater Using Electrodialysis Separation. Metals 14:38. https://doi.org/10.3390/met14010038

Hopsort G, Cacciuttolo Q, Pasquier D (2024) Electrodialysis as a key operating unit in chemical processes: From lab to pilot scale of latest breakthroughs. Chem Eng J 494:153111. https://doi.org/10.1016/j.cej.2024.153111

Klein J, Käyhkö J, Räsänen A, et al (2022) Climate risk perception, management, and adaptation in the Nordic mining sector. Extr Ind Soc 10:101092. https://doi.org/10.1016/j.exis.2022.101092

Liu W, Zhao Y, Hu X, et al (2022) A combined electrodialysis and coal dust suppression system for acid mine drainage treatment and high mechanical hydrogel dust suppressant generation. Water Cycle 3:126–132. https://doi.org/10.1016/j.watcyc.2022.09.001

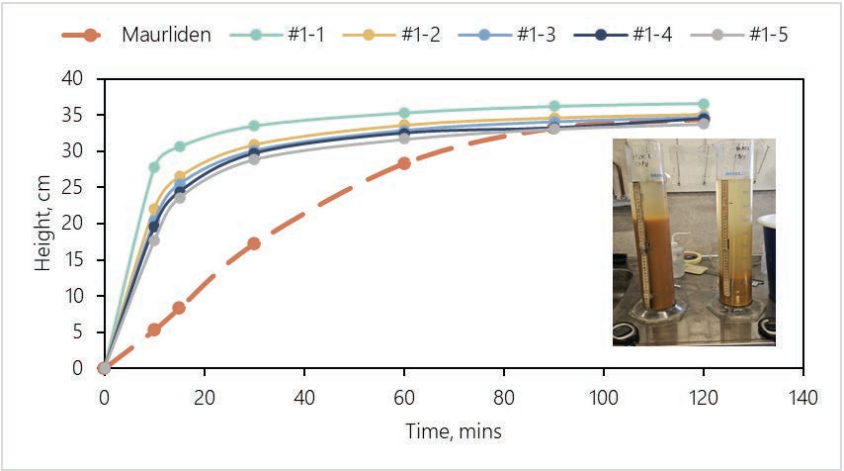

Figure 6 *Settling test showing liming sludge (left) and ECR sludge (right).*

Valorization of Manganese Sludge from Mine Drainage Treatment Facility: Development of Alginate-Based Adsorbent Beads for Dissolved Manganese Removal

Yonghwan Choe[1,2], Seon-Yong Lee[2], Gil-Jae Yim[2], Hayeon Lee[2], Soondong Kwon[3], Jeong Sik Park[3], Huijeong Hwang[1], Sangwoo Ji[2]

[1]*Gwangju Institute of Science and Technology (GIST), 123 Cheomdangwagi-ro, Buk-gu, Gwangju, 61005, Republic of Korea*

[2]*Korea Institute Geoscience And Mineral Resources (KIGAM), 124 Gwahak-ro, Yuseong-gu, Daejeon, 34132, Republic of Korea*

[3]*Korea Mine Rehabilitation and Mineral Resources Corporation (KOMIR), 199 Hyeoksin-ro, Wonju-si, Gangwon-do, 26464, Republic of Korea*

Abstract

Manganese (Mn) contamination in water systems presents considerable environmental and public health challenges. Although manganese is an essential trace element for human metabolism, chronic exposure can cause nervous system damage similar to Parkinson's disease, while also causing aesthetic problems such as water discoloration and unpleasant taste. Mine drainage treatment facilities often receive influent with high manganese concentrations, requiring treatment to comply with effluent discharge standards (typically ≤ 2 mg/L for dissolved manganese in clean areas). Conventional treatment using lime addition to achieve pH > 10 for manganese precipitation is energy-intensive and generates substantial sludge waste, particularly problematic for acid mine drainage (AMD) systems. The effective utilization of sludge waste generated during treatment processes represents both an environmental imperative and an opportunity for sustainable resource management in the mining sector.

This study aimed to valorize manganese sludge generated from mine drainage treatment facilities by developing alginate-based adsorbent beads through ionic cross-linking with Ca^{2+}. The effect of different drying methods (freeze-drying, oven-drying, and air-drying) on adsorption characteristics was evaluated via batch adsorption experiments. The specific surface areas of the fabricated beads were determined by nitrogen (N2) adsorption-desorption isotherm analysis using the Brunauer-Emmett-Teller (BET) equation. Bead fabrication conditions were optimized by evaluating manganese leaching behaviour and adsorption performance under varying cross-linking times (30 min, 1 h, 2 h, 6 h, 12 h) and initial pH conditions. The raw manganese sludge was characterized by X-ray powder diffraction (XPRD) for mineralogical composition and X-ray fluorescence (XRF) for elemental composition. The morphology of fabricated beads was observed by scanning electron microscopy (SEM). The maximum adsorption capacity was determined from adsorption isotherm experiments, and the adsorption mechanism and optimal contact time were elucidated through kinetic studies.

Freeze-drying preserved the porous structure and yielded both the highest specific surface area and the highest manganese removal efficiency among the tested drying methods. Leaching tests showed no manganese release at pH ≥ 4 across all cross-linking times. The optimized beads effectively removed manganese under weakly acidic pH conditions similar to actual influent, substantially improving upon conventional precipitation methods requiring pH > 10. Kinetic and isotherm analyses revealed efficient removal capacity through combined mechanisms including ion exchange, precipitation, and intraparticle diffusion.

This study presents a dual-benefit approach that simultaneously achieves waste valorization and enhanced water treatment performance. By converting manganese sludge waste from treatment facilities into functional adsorbents, this method addresses waste management challenges while reducing chemical consumption for manganese removal. The bead format enables recovery and potential reuse, facilitating practical implementation in mining wastewater treatment systems. This approach offers a sustainable solution for addressing manganese contamination in mining-affected water resources.

Keywords: Acid mine drainage (AMD), manganese sludge, alginate beads, sorption, valorization

Acknowledgements

This study was supported by the Basic Research Project of Korea Institute of Geoscience and Mineral Resources (Project code: 26-3414).

Pilot-Scale Passive Treatment Including Slag Reactors, as Adsorption Reactors, and Vertical Flow Reactors for Mine Drainages in Peru

Euna Choi[1,2] (presenting author), Duk-Min Kim[2*], Carmen Rodriguez-Vasquez[3], Joyce Carol Bottger-Gamarra[3], Alina Liliana Santos-Conde[3], Manuel Requena-Mendizabal[3], Edward Rivera Blanco[3], Isabel Magaly Anaya-Hilario[3], Carlos Cheito Torres-Aguilar[3], Mario Servan-Vargas[3], Jong-Wook Jeon[1], Yo-Han Kim[1], Seyoung Kang[4], Youngkook Jung[4]

[1]*Byucksan Engineering, Republic of Korea*

[2]*Sangji University, Republic of Korea*

[3]*Ministerio de Energía y Minas, Peru*

[4]*Korea Mine Rehabilitation and Mineral Resources Corporation, Republic of Korea*

Abstract

Peru is the world's second-largest producer of Cu and Zn. Its porphyry copper deposits and hydrothermal multimetal ores contain a wide range of metals, which can lead to water contamination by Al, As, Cd, Fe, Mn, and Zn. To mitigate these impacts, eco-friendly, low-carbon, and cost-efficient treatment technologies are necessary for metalliferous mines.

Two mine drainages located in the Ancash Region, Peru, were investigated: the El Triunfo 1 (ET) adit drainage exhibited elevated concentrations of As (10.6 mg/L), Cd (0.042 mg/L), Cu (0.576 mg/L), Fe (64.3 mg/L), Mn (5.27 mg/L), and Zn (11.2 mg/L), and the Santa Teresita (ST) adit drainage contained elevated concentrations of Al (22.44 mg/L), Cu (0.346 mg/L), Fe (3.44 mg/L), Mn (41.3 mg/L), and Zn (7.89 mg/L). Pilot-scale passive treatment facilities — including successive alkalinity producing systems (SAPS) units, oxidation-settling ponds, a slag reactor, an aerobic wetland, and an As adsorption pond — were constructed and operated for approximately one year under varying flow rate conditions; optimal treatment performance was achieved at flow rates of 1.08 m^3/d (ET) and 2.31 m^3/d (ST). Additionally, the oxidation-settling ponds were converted into vertical flow reactors (VFR) to evaluate its As-removal performance.

Through the SAPS and oxidation-settling pond sequence effectively decreased Al and Fe concentrations, with removal efficiencies exceeding 99% for both elements. During treatment, Cu, Zn, and Cd concentrations were also reduced — Cu to below detection limit, Zn by >98%, and Cd by >99% — indicating effective coprecipitation with and adsorption onto freshly formed Fe (oxy)hydroxides. This coprecipitation–adsorption effect was also confirmed in adit drainage samples stored in a laboratory. Although the first-phase slag reactor did not sufficiently raise pH to remove Mn, the second-phase slag reactor — using a different type of steel slag — successfully increased pH to >11, enabling efficient Mn precipitation. Following a stabilization period of approximately 5–6 months, the pilot-scale slag reactor at the ET mine achieved Mn concentrations below 1.0 mg/L at hydraulic retention times (HRT) ≥17.6 h, while the ST mine achieved the same target at HRT ≥15.7 h. In the As adsorption unit containing adsorbent synthesized from coal mine drainage sludge, As concentrations were reduced to ≤0.1 mg/L at the ET mine at HRT of approximately 7 h or longer. Furthermore, the VFR installed at the ET site decreased As concentrations from 1.9 mg/L to 0.08 mg/L, demonstrating its effectiveness for As removal in Fe-rich mine drainage.

Given the diverse contaminants present in these mine drainages, the passive treatment technologies demonstrated here show strong potential for broader application to other mine sites affected by Al, As, Cd, Cu, Fe, Mn, and Zn. Under optimised flow rate and HRT conditions — specifically HRT ≥17.6 h for the slag reactor and HRT ≈7 h for the As adsorption unit — effluent quality met Peruvian regulatory discharge limits for the target metals, supporting the feasibility of scale-up at similar polymetallic mine drainage sites.

Keywords: Coal mining, irrigation, green hydrogen, coal-fired power, water reuse

Neutralization and Metal Stabilization of Acid Mine Drainage Using an Inorganic–Mineral–Polymer Composite System

Yeon Moon, Choo– Director, CJ Carbon Neutrality Research Institute (Korea) | Email: chooyean@naver.com
Joong Geun Oh– CEO, IO Geotech (Korea) | Email: geod1968@gmail.com
Dong Shin Hwang– Director, IO Geotech (Korea) | Email: 7karma@naver.com
Hee Dae Kim– CEO, NTC Co., Ltd. (Korea) | Email: ceokhd@naver.com
Daewan Yoon– Kyungpook National University (Korea)
| Email: koreanyoon@daum.net
(Corresponding Author) Tai Ho, Choo– Emeritus Professor, Department of Civil & Environmental Engineering, Pusan National University (Korea) | Email: thchoo@pusan.ac.kr

Abstract

Acid mine drainage (AMD) remains a critical challenge in abandoned mine areas due to its low pH, elevated sulfate concentrations, and high mobility of dissolved metals. Conventional alkaline neutralization methods, typically based on lime or sodium hydroxide, provide rapid pH adjustment but are often associated with excessive sludge generation, limited long-term stability, and secondary environmental burdens. This study presents an inorganic–mineral–polymer composite system designed to achieve rapid neutralization of AMD while simultaneously promoting stabilization of dissolved metals.

Laboratory-scale experiments demonstrated that strongly acidic AMD (initial pH 2–3) was rapidly neutralized to near-neutral conditions (pH 6–8) within several minutes. Concurrently, significant reductions in dissolved iron, manganese, and zinc were observed compared to untreated AMD. The immobilization of metals is attributed to a combination of pH-induced precipitation, co-precipitation and incorporation into mineral phases, and physical stabilization within polymer-enhanced solid matrices.

Unlike conventional single-step alkaline treatment, the proposed system explicitly separates rapid neutralization from long-term stabilization within a single composite framework. Preliminary stability assessments under repeated equilibration conditions indicate reduced susceptibility to metal re-dissolution, suggesting improved long-term performance. The system is compatible with modular and mobile treatment configurations, making it particularly suitable for remote or inaccessible abandoned mine sites. The results demonstrate the potential of the composite approach as a practical and sustainable alternative for active AMD treatment, with clear relevance to the International Mine Water Association community.

Keywords: Acid mine drainage (AMD); AMD neutralization, metal stabilization, composite treatment system, mine water treatment, trace metal immobilization, sustainable mine water management

Introduction

Acid mine drainage (AMD) is one of the most persistent environmental problems associated with mining activities, particularly in abandoned mine areas where active management has ceased [1–3]. The oxidation of sulfide minerals generates acidic waters enriched with sulfate and dissolved metals, which can contaminate surface water and groundwater over extended periods [4].

Conventional AMD treatment relies primarily on alkaline reagents such as lime or sodium hydroxide to increase pH and induce metal precipitation [5]. While effective in the short term, these approaches often generate large volumes of hydroxide sludge with limited chemical

stability [6]. Under fluctuating pH or redox conditions, metals immobilized as hydroxides may be re-dissolved, leading to renewed contamination [7].

Recent research has highlighted the potential of composite and multi-functional treatment systems that combine chemical, mineralogical, and physical stabilization mechanisms [8–10]. Such systems are increasingly considered promising alternatives for sustainable AMD management, particularly in remote or abandoned mine environments [11].

Conceptual Basis of the Composite AMD Treatment System

The composite system investigated in this study integrates three functional components: an inorganic alkaline fraction, mineral-based components, and polymeric stabilizing agents. Each component contributes a distinct function while operating synergistically within the overall treatment process.

The inorganic alkaline fraction provides immediate neutralization capacity, allowing rapid correction of AMD acidity. Mineral components supply reactive surfaces and phases that facilitate co-precipitation and incorporation of dissolved metals into solid matrices. The polymeric component enhances the physical integrity of the resulting solids by binding fine precipitates and reducing their susceptibility to dispersion and leaching.

A key feature of the proposed system is the explicit distinction between rapid neutralization and longer-term stabilization processes. While neutralization occurs almost instantaneously following application, stabilization mechanisms continue to operate as metals interact with mineral phases and polymer-enhanced matrices. This conceptual separation differentiates the composite system from conventional single-step alkaline treatments. The conceptual framework of the proposed AMD treatment system is illustrated in Figure 1. The composite approach distinguishes between two interconnected processes: rapid neutralization of AMD acidity and subsequent long-term stabilization of dissolved metals. While

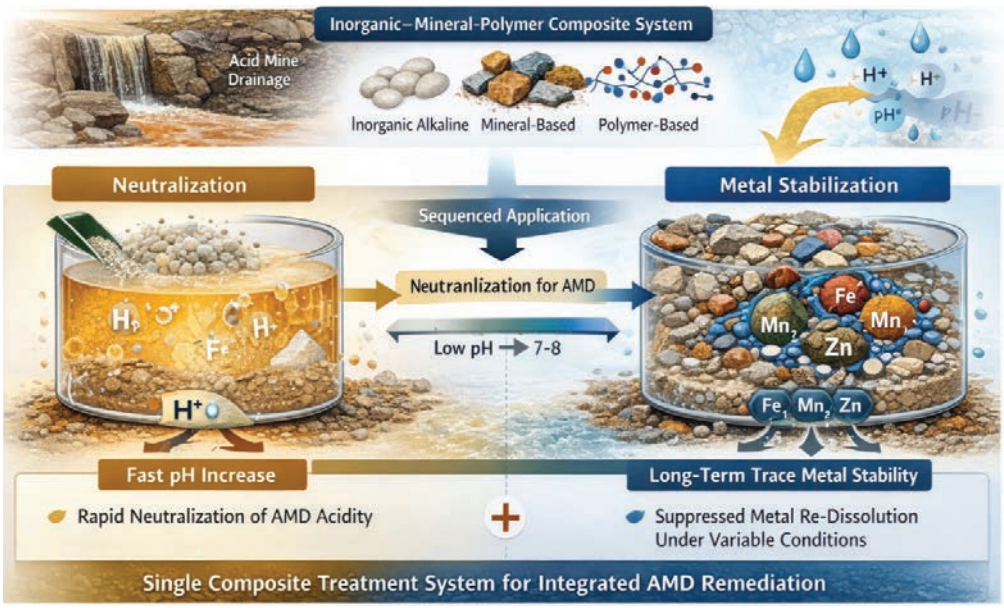

Figure 1 *Conceptual separation of AMD neutralization and metal stabilization processes using an inorganic–mineral–polymer composite system. The composite treatment system achieves rapid pH neutralization of acid mine drainage while simultaneously promoting long-term stabilization of dissolved metals through mineral-phase interactions and polymer-enhanced solid matrices.*

the alkaline fraction induces immediate pH elevation, mineral-based components promote co-precipitation and incorporation of metals into solid matrices. Simultaneously, polymeric stabilizers enhance the structural integrity of the resulting solids, reducing particle dispersion and suppressing metal re-dissolution under variable environmental conditions.

Experimental Approach

AMD characteristics and treatment procedure

AMD samples were obtained from abandoned mine settings characterized by strongly acidic conditions and elevated concentrations of dissolved iron, manganese, and zinc. The AMD exhibited initial pH values in the range of approximately 2–3.

Composite treatment materials were applied under controlled laboratory conditions. AMD samples were mixed with the composite system and monitored for pH evolution to assess neutralization kinetics. Following neutralization, treated waters were allowed to equilibrate, and dissolved metal concentrations were analyzed to evaluate removal performance.

Assessment of stabilization behavior

To investigate stability beyond immediate neutralization, treated AMD samples were subjected to repeated equilibration under neutral and mildly acidic conditions. This procedure was intended to simulate environmental fluctuations that may occur in field settings and to evaluate susceptibility to metal re-dissolution.

Results and Discussion

Rapid neutralization performance

The composite system achieved rapid neutralization of AMD, increasing pH from strongly acidic levels to near-neutral conditions within minutes. This rapid response is comparable to conventional alkaline treatments and satisfies operational requirements for active AMD management, particularly in high-flow or episodic discharge scenarios.

Importantly, pH levels remained relatively stable during subsequent equilibration, indicating that the neutralization capacity was not immediately exhausted and that buffering effects were present.

Metal removal and immobilization

Following treatment, dissolved concentrations of iron, manganese, and zinc were substantially reduced. While pH elevation played a critical role in decreasing metal solubility, the observed reductions cannot be explained solely by hydroxide precipitation.

Mineral components within the composite promoted co-precipitation and incorporation of metals into solid phases, while the polymeric fraction enhanced physical stabilization by binding precipitates and limiting particle mobility. This multi-mechanistic immobilization contrasts with conventional treatments, where metals are often retained as relatively unstable hydroxide solids. The composite system also exhibited reduced sludge-generation tendencies compared with conventional lime-based treatment systems.

Stability under repeated equilibration

During repeated equilibration under neutral and mildly acidic conditions, treated samples did not exhibit significant increases in dissolved metal concentrations. This behavior suggests resistance to re-dissolution and indicates that metals were stabilized within more robust solid matrices rather than being temporarily precipitated.

Such stability is essential for long-term AMD treatment, where treated waters may be exposed to varying chemical conditions over time.

Implications for field application

The composite system is compatible with modular and mobile treatment configurations, allowing deployment at remote or inaccessible abandoned mine sites. The use of widely available material categories supports scalability and reduces dependence on specialized reagents.

By integrating rapid neutralization with stabilization mechanisms in a single system, the proposed approach simplifies operational requirements while enhancing environmental protection.

Conclusions

The inorganic–mineral–polymer composite system evaluated in this study provides an effective approach for the treatment of acid mine drainage. Rapid neutralization of strongly acidic AMD was achieved alongside substantial reductions in dissolved iron, manganese, and zinc.

The improved performance relative to conventional alkaline treatments is attributed to the combined effects of pH-induced precipitation, mineral-phase co-precipitation, and polymer-enhanced physical stabilization. Preliminary stability assessments indicate resistance to metal re-dissolution under variable conditions, highlighting the potential for long-term effectiveness.

Overall, the composite approach represents a potentially practical and sustainable alternative for active AMD treatment, with strong relevance to abandoned mine remediation and the objectives of the International Mine Water Association.

Reference

Nordstrom DK (2011) Mine waters: acidic to circumneutral. *Elements*

Johnson DB, Hallberg KB (2005) Acid mine drainage remediation options. *Science of the Total Environment*

Akcil A, Koldas S (2006) Acid mine drainage treatment. *Journal of Cleaner Production*

Younger PL (2001) Mine water pollution. *Engineering Geology*

Skousen J *et al.* (2017) Passive and active treatment of AMD. *Mine Water and the Environment*

Hedin RS, Nairn RW (1994) Passive treatment of coal mine drainage. *US Bureau of Mines*

Evangelou VP (1998) Pyrite oxidation and its control. CRC Press

Sheoran AS, Sheoran V (2006) Heavy metal removal mechanisms. *Minerals Engineering*

Bolan N *et al.* (2014) Environmental remediation of metals. *Environmental International*

Beesley L *et al.* (2011) Biochar and stabilization mechanisms. *Environmental Pollution*

Wolkersdorfer C (2008) Mine water management. Springer

Soil Neutralization and Trace Metal Stabilization in Acid-Impacted Mine Soils Using a Composite Soil Stabilization System

Yeon Moon, Choo– Director, CJ Carbon Neutrality Research Institute (Korea) | Email: chooyean@naver.com

Joong Geun Oh– CEO, IO Geotech (Korea) | Email: geod1968@gmail.com

Dong Shin Hwang– Director, IO Geotech (Korea) | Email: 7karma@naver.com

Hee Dae Kim– CEO, NTC Co., Ltd. (Korea) | Email: ceokhd@naver.com

Daewan Yoon– Kyungpook National University (Korea)

| Email: koreanyoon@daum.net

(Corresponding Author) Tai Ho, Choo– Emeritus Professor, Department of Civil & Environmental Engineering, Pusan National University (Korea) | Email: thchoo@pusan.ac.kr

Abstract

Soils in abandoned mine areas are frequently affected by prolonged exposure to acid mine drainage (AMD), resulting in severe acidification, increased mobility of trace metals, and deterioration of soil physical structure. These acid-impacted mine soils can act as long-term secondary sources of contamination to surrounding surface water and groundwater. Effective remediation therefore requires not only rapid neutralization of soil acidity but also long-term stabilization of trace metals to prevent re-mobilization under variable environmental conditions.

This study evaluates a composite soil stabilization system designed to simultaneously achieve soil neutralization and trace metal immobilization in AMD-affected mine soils. The system integrates three functional material categories: inorganic alkaline components, mineral-based industrial by-products, and polymeric stabilizing agents. Laboratory experiments were conducted using soils collected from abandoned mine areas characterized by low pH and elevated concentrations of iron, manganese, and zinc.

Application of the composite stabilization system resulted in rapid neutralization of strongly acidic soils toward near-neutral pH conditions. Leaching-oriented tests demonstrated substantial reductions in the mobile fractions of trace metals. The improved performance is attributed to a combination of pH-induced precipitation, mineral-phase co-precipitation and incorporation of metals into solid matrices, and polymer-enhanced physical stabilization that reduces particle dispersion.

Repeated equilibration experiments under neutral and mildly acidic conditions indicated resistance to re-acidification and secondary metal release, suggesting improved long-term stability compared with conventional single-component alkaline amendments. By integrating multiple stabilization mechanisms within a single treatment framework using widely available materials, the proposed approach provides a practical and scalable solution for remediation of acid-impacted mine soils. The findings contribute to the development of sustainable mine land remediation technologies relevant to the objectives of the International Mine Water Association.

Keywords: Acid-impacted mine soils; soil neutralization; trace metal stabilization, composite soil stabilization, mine land remediation, trace metal immobilization, sustainable soil remediation

Introduction

Soils in abandoned mine areas are frequently subjected to prolonged exposure to acid mine drainage (AMD), resulting in severe acidification, enhanced mobility of trace metals, and progressive degradation of soil physical structure [1–3]. These acid-impacted mine soils represent a persistent source of secondary contamination to surface water and groundwater, particularly during rainfall events or changes in redox and pH conditions [4]. Effective remediation therefore requires not only neutralization of soil acidity, but also long-term stabilization of trace metals to prevent re-mobilization and recontamination.

Conventional soil remediation practices in mine-affected areas often rely on the application of alkaline amendments such as lime or other calcium-based materials to increase soil pH [5]. While such approaches can temporarily reduce acidity, numerous studies have shown that pH adjustment alone does not guarantee sustained immobilization of trace metals [6–8]. Under fluctuating environmental conditions, metals initially precipitated or adsorbed may be released again, undermining the long-term effectiveness of remediation efforts [9]. Furthermore, single-component soil amendments typically provide limited control over soil structure and fine particle mobility, which are critical factors influencing metal transport [10].

In response to these limitations, increasing attention has been given to composite and multi-functional soil stabilization systems that integrate chemical neutralization with physical and mineralogical stabilization mechanisms [11–13]. The International Mine Water Association (IMWA) has highlighted the importance of remediation technologies that are field-applicable, scalable, and capable of providing long-term environmental protection rather than short-term compliance [14].

Materials and Experimental Approach

Composite soil stabilization system

The composite soil stabilization system investigated in this study consists of three functional material categories: inorganic alkaline components, mineral-based industrial by-products, and polymeric stabilizing agents. These components were selected based on their complementary roles in soil neutralization and stabilization, as well as their widespread industrial availability.

The inorganic alkaline fraction provides rapid neutralization capacity, enabling efficient correction of soil acidity. The mineral-based components, derived from commonly available industrial by-products, contribute reactive surfaces and mineral phases that promote co-precipitation and incorporation of trace metals into relatively stable solid matrices. The polymeric component enhances microstructural integrity by binding fine soil particles and precipitates, thereby reducing dispersion and improving resistance to leaching.

Importantly, all components belong to material categories that are produced at industrial scales and are commercially available, allowing practical implementation in large-scale remediation projects without reliance on specialized or limited-supply reagents.

Soil samples and treatment procedure

Soil samples were collected from abandoned mine areas characterized by long-term AMD influence, exhibiting low pH and elevated concentrations of iron, manganese, and zinc. The soils were air-dried, homogenized, and sieved prior to treatment.

Composite stabilization materials were mixed with the soils at predetermined application rates. Treated soils were conditioned under controlled laboratory conditions to allow equilibration. Soil pH was monitored to evaluate neutralization performance, and leaching-oriented tests were conducted to assess changes in trace metal mobility.

To evaluate stability beyond immediate neutralization, treated soils were subjected to repeated equilibration cycles under neutral and mildly acidic conditions. This approach was designed to simulate environmental fluctuations and to assess resistance to re-acidification and secondary metal release.

Results and Discussion

Soil neutralization performance

Application of the composite stabilization system resulted in rapid neutralization of strongly acidic mine soils toward near-neutral pH conditions. For example, soil pH increased from approximately 2–3 to near-neutral conditions (pH 6–8) following treatment. Compared with untreated soils, which maintained persistently acidic pH values, treated soils exhibited stable pH levels after equilibration, indicating effective consumption of soil acidity by the alkaline fraction of the composite.

Unlike conventional single-component alkaline amendments, the composite system maintained pH stability during subsequent equilibration cycles, suggesting that buffering capacity was not exhausted immediately after treatment. This behavior is particularly relevant for mine soils exposed to episodic acid inputs from residual sulfide oxidation or acidic pore water migration.

Reduction of trace metal mobility

Leaching-oriented analyses demonstrated a relevant reduction in the mobile fractions of iron, manganese, and zinc following treatment. The decrease in trace metal mobility cannot be attributed solely to pH increase. Instead, the results indicate the combined influence of multiple stabilization mechanisms.

The initial rise in pH reduced metal solubility and promoted precipitation reactions. Simultaneously, mineral components within the composite provided surfaces and reactive phases that facilitated co-precipitation and incorporation of metals into solid matrices. The polymeric stabilizer further enhanced retention by physically binding fine particles and precipitates, reducing their susceptibility to transport.

This multi-mechanistic stabilization contrasts with conventional treatments, where metals are often immobilized primarily as loosely bound hydroxide precipitates that may dissolve under changing conditions. The conceptual stabilization mechanisms of the composite system are illustrated in Figure 1. The system integrates three complementary functional components: an inorganic alkaline fraction responsible for rapid pH adjustment, mineral-based materials that promote co-precipitation and incorporation of metals into solid phases, and polymeric stabilizers that enhance microstructural integrity and reduce particle dispersion. Through the interaction of these mechanisms, trace metals become incorporated into stable soil matrices, substantially reducing their mobility and susceptibility to re-leaching.

Long-term stability and resistance to re-acidification

A key concern in mine soil remediation is the potential for recontamination following environmental changes. In this study, treated soils subjected to repeated equilibration under neutral and mildly acidic conditions exhibited sustained reductions in leachable metal concentrations. No abrupt increases in iron, manganese, or zinc mobility were observed during these cycles.

These findings suggest that trace metals were not merely temporarily precipitated but were incorporated into more stable solid phases and physically constrained within the soil matrix. The polymer-enhanced microstructure appears to play an important role in limiting particle dispersion and maintaining metal immobilization even when external conditions become less favorable.

Implications for field-scale application

The use of industrially available alkaline materials, mineral by-products, and polymeric stabilizers offers clear advantages for large-scale implementation. The composite system can be adapted to site-specific soil conditions by adjusting application rates, while maintaining the same fundamental stabilization mechanisms.

From a sustainability perspective, the incorporation of mineral by-products aligns with circular economy principles and reduces reliance on virgin materials. The ability to achieve both neutralization and stabilization within a single treatment framework simplifies field operations and reduces the likelihood of performance decline over time.

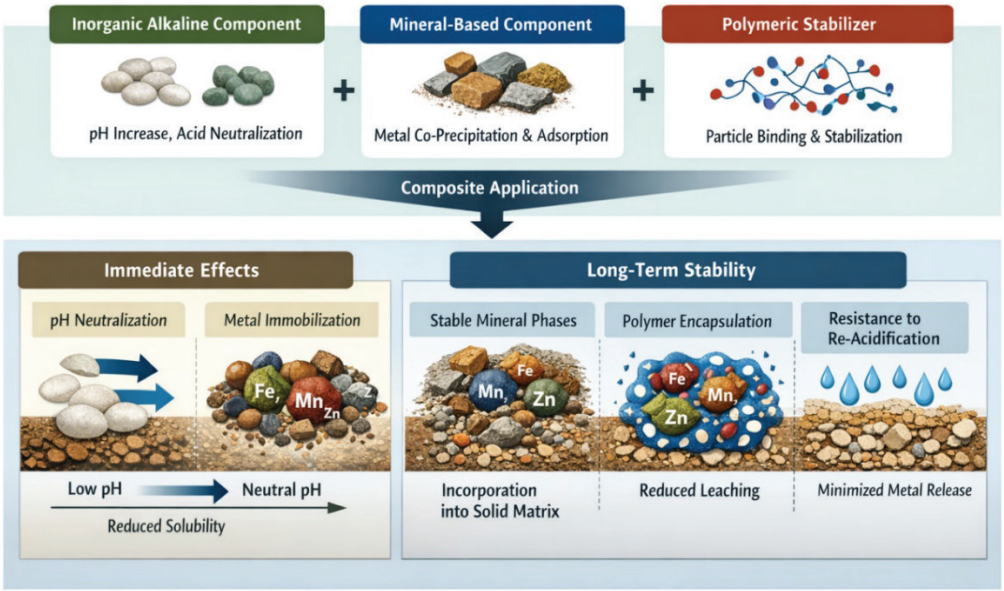

Figure 1 Composite soil stabilization mechanism for acid-impacted mine soils. Conceptual stabilization mechanism of the composite soil stabilization system for acid-impacted mine soils.

Conclusions

This study demonstrates that effective remediation of acid-impacted mine soils requires an integrated approach that combines soil neutralization with long-term trace metal stabilization. The composite soil stabilization system evaluated here successfully neutralized acidic mine soils while substantially reducing the mobility of iron, manganese, and zinc.

The observed performance is attributed to the synergistic action of pH-induced precipitation, mineral-phase co-precipitation, and polymer-enhanced physical stabilization. Importantly, the treated soils exhibited resistance to re-acidification and secondary metal release during repeated equilibration, indicating potential for long-term environmental protection.

By utilizing widely available material categories and integrating multiple stabilization mechanisms within a single framework, the proposed system offers a practical, scalable, and sustainable solution for the remediation of acid-impacted mine soils. The findings are directly relevant to the objectives of the International Mine Water Association and provide a solid foundation for further field validation and long-term monitoring studies.

Reference

Johnson DB, Hallberg KB (2005) Acid mine drainage remediation options: A review. Sci Total Environ 338:3–14. https://doi.org/10.1016/j.scitotenv.2004.09.002

Nordstrom DK (2011) Mine waters: acidic to circumneutral. Elements 7:393–398. https://doi.org/10.2113/gselements.7.6.393

Akcil A, Koldas S (2006) Acid mine drainage (AMD): causes, treatment and case studies. J Clean Prod 14:1139–1145. https://doi.org/10.1016/j.jclepro.2004.09.006

Younger PL (2001) Mine water pollution: the remarkable recovery of the River Tyne. Eng Geol 60:41–59. https://doi.org/10.1016/S0013-7952(00)00108-9

Skousen J, Ziemkiewicz P, McDonald LM (2017) Acid mine drainage formation, control and treatment: approaches and strategies. Mine Water Environ 36:241–249. https://doi.org/10.1007/s10230-017-0447-5

Evangelou VP (1998) Pyrite oxidation and its control. CRC Press, Boca Raton

Park JH, Lamb D, Paneerselvam P, Choppala G, Bolan N, Chung JW (2011) Role of organic amendments on enhanced bioremediation of heavy metal(loid) contaminated soils. J Hazard Mater 185:549–574. https://doi.org/10.1016/j.jhazmat.2010.09.082

Bolan N, Kunhikrishnan A, Thangarajan R *et al.* (2014) Remediation of heavy metal(loid)s contaminated soils – To mobilize or to immobilize? J Hazard Mater 266:141–166. https://doi.org/10.1016/j.jhazmat.2013.12.018

Violante A, Cozzolino V, Perelomov L, Caporale AG, Pigna M (2010) Mobility and bioavailability of heavy metals and metalloids in soil environments. J Soil Sci Plant Nutr 10:268–292. https://doi.org/10.4067/S0718-95162010000100005

Adriano DC (2001) Trace elements in terrestrial environments: biogeochemistry, bioavailability, and risks of metals. Springer, New York

Dermatas D, Meng X (2003) Utilization of fly ash for stabilization/solidification of heavy metal contaminated soils. Eng Geol 70:377–394. https://doi.org/10.1016/S0013-7952(03)00105-4

Bolan NS, Park JH, Robinson B, Naidu R, Huh KY (2011) Phytostabilization: a green approach to contaminant containment. Adv Agron 112:145–204. https://doi.org/10.1016/B978-0-12-385538-1.00004-4

Beesley L, Moreno-Jiménez E, Gomez-Eyles JL *et al.* (2011) A review of biochars' potential role in the remediation, revegetation and restoration of contaminated soils. Environ Pollut 159:3269–3282. https://doi.org/10.1016/j.envpol.2011.07.023

Wolkersdorfer C (2008) Water management at abandoned flooded underground mines: fundamentals, tracer tests, modelling, water treatment. Springer, Berlin Heidelberg

Design and Operation of a Scalable Electrochemical–Biological Sulfur Bioreactor for Mine Water Treatment

Chan Lan Chun[1,2], Britta Larson[2], Jack Thompson[1], Mariel Castillo[1], Spencer Washburn[3], Kevin Dufresne[4], and Randall Kolka[5]

[1]*Department of Civil and Environmental Engineering, University of Minnesota Duluth, Duluth, MN 55812*

[2]*Natural Resources Research Institute, University of Minnesota, Duluth, MN 55811*

[3]*Geosyntec Consultants, Minneapolis, MN 55402*

[4]*Geosyntec Consultants, Waterloo, ON N2L 6R5*

[5]*Northern Research Station, United States Department of Agriculture Forest Service, Grand Rapids MN 55744*

Abstract

Sulfur management poses environmental and economic challenges for mining due to complex sulfur chemistry and its ecological impacts, especially in low sulfate freshwater systems. Improving sulfur recovery remains a key need. We developed a low-current, electrode-integrated sulfate bioreactor that promotes microbial sulfate reduction and sulfide removal, offering an in-situ remediation option. Bench and pilot studies demonstrate sulfate removal performance from mine pit lake water with concurrent recovery of solid elemental sulfur. This work presents the engineering design for an upscaled system, outlining operational and maintenance considerations needed for next-stage treatment development. These efforts advance sustainable, interdisciplinary solutions for sulfur management.

Keywords: Sulfate, in situ bioremediation, bioreactor, pilot-scale, and sulfur recovery

Introduction

Sulfate-laden water is a biogeochemical stressor in freshwater environments and is a burden to many industries and municipalities, both in Minnesota and globally. Although natural sources of sulfate exist, elevated concentrations in freshwater ecosystems are often linked to anthropogenic sources such as industrial and municipal waste streams, or mining drainage (Zak *et al.*, 2021 and Berndt *et al.*, 2016). Introducing sulfate into ecosystems that naturally have low background levels can alter natural biochemical processes and, under certain conditions, cause adverse ecological consequences such as mercury methylation and methane production (Zak *et al.*, 2021 and Weiss *et al.*, 2024). Globally, sulfate limits for freshwater aquatic ecosystems and drinking water typically range from 10 mg/L to 250 mg/L (Weiss *et al.*, 2024 and Xiao *et al.*, 2024). With increasing demand for critical minerals and the expansion of green technologies, managing sulfate loading has become even more challenging. These ecological, industrial, and regulatory pressures have driven interest in developing low-cost and efficient approaches to reduce sulfate levels.

Current treatment technologies for sulfate removal remain hindered largely by high costs, intensive maintenance, and sludge management requirements of membrane-based treatment technologies (Andrews *et al.*, 2018). Moreover, sulfate concentration levels and water chemistry in mine waste streams vary widely from processing water to drainage, requiring a treatment train approach. Among currently available options, biological treatment processes have been applied beneficially for waters with a wide sulfate concentration range (250-2000 mg/L) in both active and passive treatment systems.

In situ remediation is an engineered approach being deployed directly at contaminated sites for treating and managing pollutants, often as passive treatment systems such as constructed wetlands, permeable reactive barriers, and biofiltration units. Passive or semi-passive treatment systems rely on natural processes (physical, chemical,

biological, hydrological) to transport and reduce contaminants in a targeted treatment zone, thus requiring relatively little infrastructure and routine maintenance. However, their treatment performance has been reported to vary depending on site characteristics, season, or substrate availability.

One promising treatment technology that addresses limitations of current technologies for sulfate treatment is the use of bioelectrochemical systems. These systems enable controlled and direct delivery of substrates, which provides design and operational flexibility. Our recent work has developed a treatment approach which low-voltage electrical potential is used to promote and sustain biological sulfate reduction and to support chemical and biological sulfide immobilization by providing electrolytic hydrogen and oxygen in a controlled manner for in-situ remediation. The system has been evaluated with sulfate-rich mine pit lake water and industrial wastewater at a bench scale (Johnson *et al.* 2019) and through mathematical modelling (Berens *et al.* 2024). Those results indicate that sulfate removal efficiency in bioelectrochemical systems is determined by both hydraulic residence and the rate of electrochemical hydrogen generation (Berens *et al.* 2024).

Building on these findings, **this project aims to evaluate an upscaled bioelectrochemical treatment system for sulfur management for mine water, providing key operational and maintenance considerations needed for reliable, full-scale treatment.** This will help establish an engineering foundation and increase confidence in the technology for the management of sulfate-rich mine water.

Conceptual Bioelectrochemical Treatment

To evaluate an upscaled bioelectrochemical treatment system, a pilot-scale electrochemical biofiltration was designed and constructed. Successful sulfate bioremediation relies on both biological sulfate reduction [Equation 2] and sulfide immobilization [Equations 3 & 5]. The bioelectrochemical treatment system integrates two major pathways mediated by water electrolysis [Equations 1 & 4]. Figure 1 shows the conceptual reaction pathways through the pilot-scale system. Specifically, sulfate reduction is stimulated by providing electrolytic hydrogen to sulfate-reducing bacteria (SRB) at the cathode [Equation 1] while oxygen or other oxidants generated at the anode are involved in both chemical and biologically-mediated sulfide immobilization to either elemental sulfur or iron sulfide. In this pilot-scale treatment system, elemental sulfur is the desired solid-phase sulfur species for recovery.

$$2H_2O + 2e^- \rightarrow H_2 + 2OH^- \quad [1]$$
$$4H_2 + SO_4^{2-} + H^+ \rightarrow HS^- + 4H_2O \quad [2]$$
$$HS^- + Fe^{2+} \rightarrow FeS(s) + H^+ \quad [3]$$
$$2H_2O \rightarrow O_2 + 4H^+ + 4e^- \quad [4]$$
$$2HS^- + O_2 + 2H^+ \rightarrow 2S^0 + 2H_2O \quad [5]$$

Methods

Electrode-integrated biofiltration system

The pilot-scale treatment system is comprised of a series of individual circular bioreactor columns made of clear PVC with an upflow design. The column is modular, allowing for up to 3 1-ft paired electrode columnar sections (Figure 1), totalling a maximum height of about 5 ft. Each column is equipped with an underdrain at the base, a gas vent at the top, and porewater collection ports between each electrode pair to allow for accessible sampling points. A twisted-titanium wire carbon fiber brush (Surface area: ~2 m2, Mill Rose, Inc.) was used for the cathode, and a carbon fiber cloth (Surface area: ~0.18 m2; Composite Envisions, Inc.) was chosen for the anode. The electrode system was powered by a BK Precision Model 9130 Triple-Output Programmable DC Power Supply. The bioreactor columns are filled with a variety of conductive geomedia compositions for operational comparison. Media is composed of varying volume ratios of C-33 washed sand (particle size range, 0.075-4.75 mm), pea gravel (6.35-12.2 mm), and biochar (0.1-2.0mm; Wakefield Biochar, GA, USA) for biofilm formation and filtration.

Mine Pit Lake Water

The performance of the electrode-integrated biofiltration system has been evaluated with

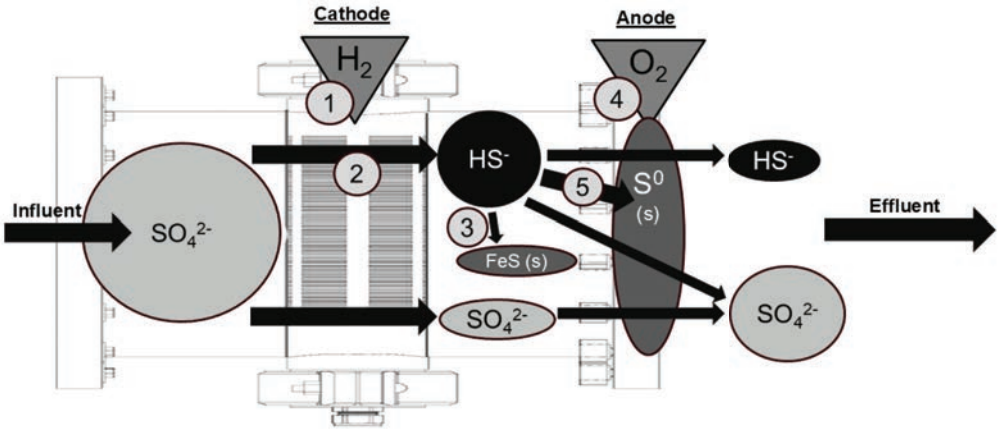

Figure 1 *Conceptual diagram of sulfur transformation and water electrolysis reactions in the electrode-integrated biofiltration system, including: [1] electrolytic hydrogen (H_2) generation at the carbon brush cathode; [2] sulfate (SO_4^{2-}) reduction to sulfide (HS^-) by sulfate reducing bacteria; [3] precipitation of iron sulfide (FeS); [4] electrolytic oxygen (O_2) generation at the carbon cloth anode; and [5] partial oxidation of sulfide (HS^-) to elemental sulfur (S^0)*

water associated with a mine pit lake as a result of historic iron ore mining in Aurora, Minnesota (USA). The lake water contained elevated levels of dissolved solids, primarily sulfate (300-400 mg/L), calcium, and magnesium. Low concentrations of nitrogen, phosphorus, and organic carbon within the pit lake water indicate the predominance of oligotrophic conditions (Table 1). Water is circumneutral pH with moderate alkalinity levels, suggesting a well-buffered system. For the pilot-scale operation, both unaltered pit lake water and pit lake water amended with calcium sulfate and magnesium sulfate to create elevated sulfate concentrations (up to 1200 mg/L) were used.

Pilot System Operation

Initially, the treatment system was operated in a batch mode to establish the microbial community responsible for sulfur transformation, accomplished by inoculating SRB culture enriched with the mine pit lake water and a nutrient solution composed of a 100:10:1 C:N:P. Sufficient biological activity was verified by measuring sulfate and sulfide levels in sampling port between two electrodes. After verification, the systems were operated to evaluate key operational parameters, including different geomedia compositions (7:3 sand to biochar and 7:3 gravel to biochar v/v), hydraulic retention times (HRT; 1-5 days), and applied currents (5-50 mA).

Table 1 *Water chemistry of the mine pit lake water.*

Parameters	Unit	Value
Total organic carbon	mg/L	1.6
Total hardness	mg/L as $CaCO_3$	531
Total alkalinity	mg/L as $CaCO_3$	177
Total sulfur	mg/L	123
SO_4^{2-}	mg/L	370
Ca^{2+}	mg/L	37.9
Mg^{2+}	mg/L	91.1

The amount of biochar amendment was based on amounts previously determined in microcosm biokinetic experiments of sulfate reduction.

To evaluate the performance of sulfur transformation, aqueous samples were collected at three locations within the treatment system (influent, sampling ports, and effluent) for measurement of sulfur speciation (SO_4^{2-}, $S_2O_3^{2-}$, HS-, and S^0). Sulfate concentration was determined by Ion Chromatography (Dionex ICS 2000; EPA Method 300.0). For sulfide measurements, samples were immediately preserved in a zinc acetate and sodium hydroxide solution and subsequently quantified using Methylene Blue (EPA Method 376.2). Elemental sulfur was extracted with chloroform and quantified using High Performance Liquid Chromatography (Dionex UltiMateTM 3000; Aliboni et al, 2015).

Results

Preliminary sulfate treatment performance at pilot scale

Upon the establishment of sulfur-transforming biofilm in batch mode, the gravel–biochar biofiltration systems were operated in a regime with a 3-day HRT and a constant current of 10 mA (applied voltage: 1.5-4.0 V). Influent water containing ~400 mg/L as S (1200 mg/L sulfate) was pumped into the system. Sulfate concentrations in samples collected between the electrode pair and at the effluent decreased during operation, with net removal ranging from 100 to 300 mg/L as S (Figure 2). These reductions were presumably supported by the continuous production of electrolytic hydrogen. Although sulfide was observed to accumulate in the effluent during operation, concentrations remained below 30 mg/L as S, a level approximately tenfold lower than the net sulfate removal, indicating substantial sulfide immobilization by the geomedia and/or conversion to other sulfur species.

To verify sulfide immobilization by geomedia, sorption isotherm experiments were conducted for both sulfate and sulfide using the fresh biochar used in this study. Sulfide solutions with different concentrations were added to biochar masses ranging from

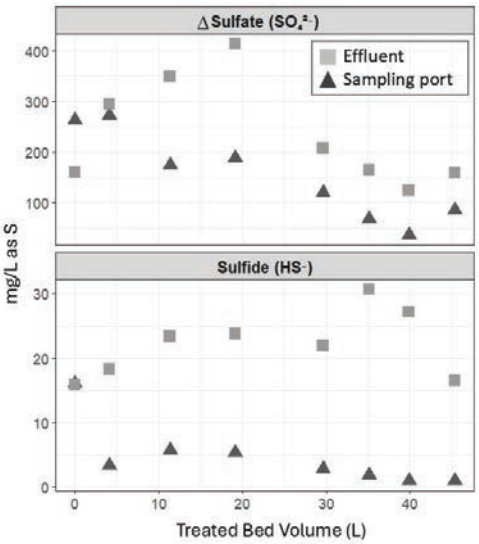

Figure 2 *The change of sulfate concentration from influent and sulfide concentration in sampling port between each electrode pair and effluent of the electrode-integrated biofiltration filled with gravel-biochar (7:3 v/v) operated with 10 mA of constant current application and 3-day HRT. Concentration unit is mg/L as S (on a sulfur mass basis).*

0.01 to 1.0 grams. The mixtures were placed on a shaker for 24 hours to reach equilibrium. We observed high sorption affinity of sulfide onto the biochar. Using the Freundlich isotherm, the sorption capacity constant (Kf) was estimated as 238±1.15 L/Kg, which is much greater than observed for sulfate (35-85 L/kg). This enhanced affinity for sulfide compared to sulfate is likely attributable to the iron content of the biochar, consistent with metal sulfide precipitation (Equation 3). These results suggest that biochar used in this study not only supports biofilm development and enhances biokinetics but also effectively sequesters dissolved sulfide produced during biological sulfate reduction.

During the operation of the pilot-scale system, white-yellow film-like solids were visually observed on the surfaces of the carbon-cloth anode, suggesting the formation of elemental sulfur was occurring, in addition to sulfide immobilization on the geomedia. Through Scanning Electron Microscopy–Energy Dispersive X-ray Spectroscopy (Hitachi TM3030), we verified the solids

were largely crystalline elemental sulfur. Comprehensive characterization of these solid-phase materials will be conducted at the conclusion of the pilot-scale operation.

Effect of geomedia types on the performance

Concurrently, we operated treatment systems filled with either sand alone or a sand–biochar mixture (7:3 v/v) at 3–5-day HRT and constant current applications up to 50 mA. Compared with the gravel–biochar system, sulfate reduction was initially observed in both the sand alone and sand-biochar configurations but declined over time. At the same time, the voltage required to maintain a 50-mA current increased to as high as 30 V, indicating unfavorable conditions for both water electrolysis and biological activity. This performance decline was attributed to substantial gas accumulation within the biofiltration beds, which required periodic manual release by tapping the reactors. Gas buildup increased electrical resistance by insulating electrolytic reactions. This behavior was more pronounced at higher current applications, where excess H_2 and O_2 were generated beyond the amounts needed to sustain biomass activity on the geomedia.

Additionally, geomedia with smaller particle sizes and heterogeneous composition exhibited higher internal electrochemical resistance due to limited hydraulic conductivity and mass transfer. As reported by Quejigo *et al.* (2019), such conditions require higher voltages to achieve target water-electrolysis reactions. These observations suggest that larger pore spaces and more fluidic bed structures may be important design considerations for optimizing system performance. In consideration of the current findings, a treatment system with geomedia with greater fluidic bed structure characteristics is under investigation.

Relationship of net sulfate removal and current density

As the pilot-scale treatment systems have been operated under various combinations of HRTs and applied currents, these results will be used to develop a relationship between required current and target sulfate removal to guide future system design and operational parameters. To enable broader applicability across treatment scales, a theoretical relationship between applied current density and sulfate load reduction was developed based on the stoichiometric electron balance of the biochemical reactions (Reactions 1–5; red line in Figure 3). Net sulfate load reduction is a function of the magnitude of sulfate concentration change from influent to effluent and HRT. As pilot-scale system evaluation progresses, this theoretical relationship will be compared with the emerging empirical relationship (green line in Figure 3).

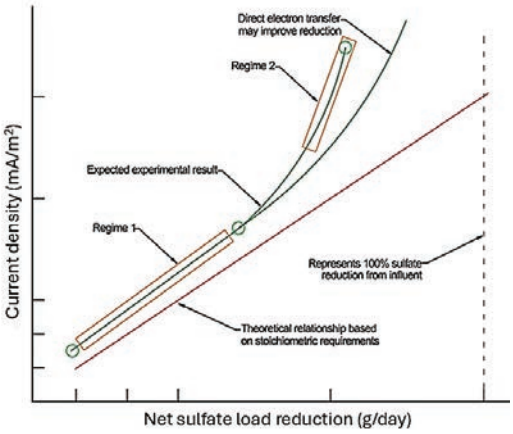

Figure 3 *Theoretical and empirical relationship of current density and sulfate load reduction.*

Based on current testing, the empirical trend is expected to exhibit two regimes: When biomass and sulfate are abundant relative to available electron donors, increasing current density increases electrolytic H_2 production, which proportionally enhances sulfate reduction by SRB (Regime 1 of green line in Figure 3). When influent sulfate concentrations fall below the threshold needed to sustain biological activity or when sulfate is limiting, further increases in current are expected to yield diminishing or no additional sulfate reduction. In this range, sulfate reduction may approach thermodynamic or biological limits, and excess H_2 may instead be consumed by competing side reactions (e.g., iron reduction, methanogenesis). This relationship will help

define the effective treatment window and inform optimal electron donor delivery at given biomass levels, which can be influenced through biochar amendment.

Conclusions

Bioelectrochemical systems provide a promising treatment approach for sulfate remediation and sulfur recovery, with the potential to reduce some of the costs associated with existing technologies. Pilot scale operation has helped identify essential design considerations for a future field deployable system. Ongoing work is focused on refining hydraulic retention time and current application to better target sulfate removal. At the pilot scale, managing electrical resistance and biomass sensitivity has emerged as an important factor for informing next stage design. Overall, this study demonstrates the capabilities of pilot scale bioelectrochemical systems for sulfur remediation and offers an engineering basis to guide further treatment development.

Acknowledgements

This study was supported by the United State Department of Agricultural Forest Service (21-JV-11242307) and Minnesota Pollution Control Agency (279573). We thank Intuitech Inc. (USA) for technical support and collaboration on fabrication of the pilot-scale treatment system and Marissa Trombley for technical assistance on microcosm experiments.

References

Aliboni, A, Lona L, Felici C, Corsaro N, Izzo G, De Luca E (2015) Analytical protocols for the determination of sulphur compounds characteristic of the metabolism of *Chlorobium limicola*, Analytical Chemistry Research 5: 9–13

Andrews EJ, Richard DE, Dharmarajah HA, and Hanson AT (2018) Analysing Alternatives for Sulfate Treatment in Municipal Wastewater. Minnesota Pollution Control Agency Wq-rule4-15pp

Berens MJ, Deen TW, and Chun CL (2024) Bioelectrochemical reactor to manage anthropogenic sulfate pollution for freshwater ecosystems: Mathematical modelling and experiment validation. Chemosphere 357:142054

Berndt ME, Rutelonis W, and Regan CP (2016) A comparison of results from a hydrologic transport model (HSPF) with distributions of sulfate and mercury in a mine-impacted watershed in northeastern Minnesota. Journal of environmental management 181: 74–79.

Johnson LB, Cai M, Chun CL, Hanson A, Hudak G, Kolomitsyn I, Rao S, Bernhardt B, Deen TW, Henneck J (2019) Responding to Minnesota's Regulatory Sulfate Standard for Wild Rice Waters Responding to Minnesota's Regulatory Sulfate Standard for Wild Rice Waters. International Mine Water Association 2019 Conference Proceedings "Mine Water: Technological and Ecological Challenges" Wolkersdorfer, Ch.; Khayrulina, E.; Polyakova, S.; Bogush, A. (Editors)

Quejigo JR, Tejegor-Sanz S, Esteve-Nunex A and Harnisch F (2019) Bed electrodes in microbial electrochemistry: setup, operation and characterization. ChemText. 5:4

U.S. Environmental Protection Agency (1993) Method 300.0: Determination of Inorganic Anions by Ion Chromatography (Revision 2.1). Environmental Monitoring Systems Laboratory, Office of Research and Development, U.S. Environmental Protection Agency, Cincinnati, Ohio 45268.

U.S. Environmental Protection Agency (1983) Method 376.2: *Sulfide (Colorimetric, Methylene Blue)*. In Methods for Chemical Analysis of Water and Wastes (EPA-600/4-79-020). Cincinnati, OH: Environmental Monitoring and Support Laboratory.

Weiss S, Kyser S, Lindon M, Wasley D, and Brault E (2024) Procedures for implementing the Class 4A wild rice sulfate standards in NPDES wastewater permit in Minnesota. Minnesota Pollution Control Agency wq-wwprm2-109

Xiao, C., S. Qu, Z.J. Ren, Y. Chen, X. Zou, G. Chen, Z. Zhange 2024 Understanding the global distribution of groundwater sulfate and assessing population at risk. Environmental Science & Technology 58(47): 21002–21014

Zak D, Hupfer M, Cabezas A, Jurasinski G, Audet J, Kleeberg A, McInnes R, Kristiansen SM, Petersen RJ, Lui H, and Coldhammer T (2021) Sulphate in freshwater ecosystems: A review of sources, biogeochemical cycles, ecotoxicological effects and bioremediation. Earth-Science Reviews 212: 103446

IMWA 2026
Jeongseon

Geochemical Pathways and Kinetic Controls of Fe(II) Oxidation and Secondary Mineral Formation in Acid Sulfate Waters from Siderite Deposit (Slovakia)

Claudia Čičáková[1], Zuzana Bártová[1], Lenka Hagarová[1], Eva Mačingová[1], Josef Zeman[2], Daniel Kupka[1]

[1]*Institute of Geotechnics, Slovak Academy of Sciences, Watsonova 45, Košice 040 01, Slovak Republic, cicakova@saske.sk, ORCID 0000-0002-3016-5397*

[2]*Institute of Geological Sciences, Faculty of Science, Masaryk University in Brno, Kotlárská 2, CZ-611 37 Brno, Czech Republic, jzeman@sci.muni.cz, ORCID 0000-0001-6567-0222*

Abstract

This study examines indigenous iron-oxidizing bacteria in the initial stage of acid mine drainage treatment, focusing on selective iron removal for subsequent base metal recovery. Slightly acidic mine water (pH 5.6; net acidity ≈ 160 mmol/L) from siderite deposit in the Spiš–Gemer Ore Mountains - Slovakia was used. Under aerobic conditions, abiotic Fe^{2+} oxidation was followed by accelerated oxidation driven by indigenous bacteria, resulting in complete oxidation of Fe^{2+} to Fe^{3+}. Subsequent Fe^{3+} hydrolysis and precipitation, coupled with pH decrease <2.6, enabled selective iron removal while retaining Ni, Co, Mn, and Mg in solution for potential recovery in the following steps.

Keywords: Fe-oxidizing bacteria, iron oxidation, metals recovery, acid mine drainage, mining influenced water

Introduction

The mining industry plays a major role in global economic development. However, it is also associated with environmental challenges, most notably the formation of acid mine drainage (AMD) (Yang *et al.* 2020). Although the chemical composition of AMD differs across sites, it is typically characterized by high concentrations of sulfuric acid, metals, and metalloids such as Fe, Mn, Al, and As, which represent a valuable secondary source of mineral resources (Wang *et al.* 2019; Kelly 1999; Singovszka *et al.* 2020). The pH of AMD is usually defined as pH below 5.6 (Nordstrom 2011) and/or between pH 2 and 6 (Nordstrom *et al.* 2000, 2015; Rakotonimaro *et al.* 2017). The more acidic the effluents, the higher the concentrations of metals, particularly Cu, Zn, Ni, Co, and REEs (Plumlee 1999). In general, AMD can be treated using active and passive technologies (García *et al.* 2001). Active treatment involves the addition of alkaline reagents to increase pH and promote metal precipitation (Moodley *et al.* 2018). Passive treatment systems utilise natural biological and geochemical processes, including microbial-mediated Fe and Mn oxidation, sulfate reduction, alkalinity generation, and reactions with alkaline materials such as limestone or steel slag (Skousen *et al.* 2017). The biological oxidation of ferrous sulfate by acidophilic iron and sulfur-oxidising bacteria has been broadly studied (Jensen and Webb 1995; Nemati *et al.* 1998). After oxidation of Fe^{2+} to Fe^{3+}, which subsequently precipitates at substantially lower pH values compared to ferrous iron, enabling selective iron removal (Sandström and Mattsson 2001). While passive systems are generally more sustainable and cost-effective than active treatments, their application is often constrained by larger spatial requirements, longer hydraulic retention times, and reduced efficiency under fluctuating or high contaminant loads (Johnson and Hallberg 2005). Slovakia has a long-standing, historically relevant mining tradition, which has played a key role in the economic development of several regions. In

the 1990s, dozens of ore mines were closed in Slovakia due to a state reduction program in the ore mining sector, most of which are located just in the Spiš-Gemer Ore Mountains (Bajtoš 2025). Smolník and Nižná Slaná sites are two well-known mining influenced sites in the Spiš-Gemer Ore Mountains. Mining influenced water utilised in this paper is coming from flooded mine from area Spiš-Gemer Ore Mountains and represents a model mining influenced water sample. The water is highly supersaturated with respect to ferric hydroxide. In this paper, only the initial stage of bacterial oxidation of ferrous iron will be discussed. Biologically mediated Fe^{2+} oxidation under acidic conditions enables the selective precipitation of Fe-jarosite while retaining divalent metals (Mn^{2+}, Ni^{2+}, Co^{2+}, Mg^{2+}) in solution for potential recovery and minimizing sludge production.

Methods

Sampling and Chemical analyses

Samples of mine water were collected from the main shaft that receives the majority of water draining the flooded mine area. The water sample intended for the experiment was processed immediately upon transport to the laboratory to minimize physicochemical and microbiological alterations. The mine water was poured into four sterile 500 mL magnetically stirred reactors equipped with the pH and oxidation–reduction potential (ORP) probes. Air supplied to the reactors was sterilised by filtration through 0.2 µm membrane filters. All experiments were conducted at 30 °C, corresponding to the in-situ temperature of the mine water at the time of sampling. Regarding iron monitoring, the experiments were performed in quadruplicate. In two reactors, pH probes were inserted, and in the other two, ORP electrodes were used. Concentration of metals in mine water was determined using atomic absorption spectrometer VARIAN AA240FS. Sulfate, magnesium, calcium and potassium concentrations were analysed by ion chromatography Dionex ICS 5000. Ferric iron was determined by a UV-spectrophotometric method at 300 nm (Basaran and Tuovinen 1986). Ferrous iron concentrations were determined using a modified o-phenanthroline spectrophotometric method insensitive to Fe^{3+} interference (Herrera *et al.* 1989). Physical-chemical parameters, such as pH and ORP were measured using probes Radiometer Analytical/HACH Lange for pH and Mettler Toledo InLab Redox-L type for ORP.

Gas analysis

The rates of chemical (abiotic) and bacterial ferrous iron oxidation, as well as bacterial growth, were monitored by online measurements of gas-phase oxygen consumption and carbon dioxide production/consumption. Oxygen and carbon dioxide concentrations in the inlet and outlet air were measured using a paramagnetic oxygen analyzer and an infrared carbon dioxide analyzer (Sable Systems, USA), respectively. The analyzers were calibrated using high-purity nitrogen (99.99% N_2) for zero point and ambient outdoor air for span calibration of O_2 (20.95%) and CO_2 (0.042%) concentrations. Air of the same quality was used to aerate the reactors. The data acquisition was performed by a software application developed in LabVIEW ® (National Instruments).

Results and discussion

Characterisation of water

The real acid mine water originating from a flooded siderite ore deposit in the Spiš-Gemer Ore Mountain was used as a model system for the biological iron-oxidation step. The slightly acidic pH of the mine water (pH values ≈ 5.7) was influenced by the siderite buffering system (Wolkersdorfer 2008). The mine water effluent transported substantial quantities of potentially toxic metals and metalloids into the river system. Elevated iron concentrations (1261.5 mg/L) caused intense reddish-brown discoloration of the water (Zeman *et al.* 2022). The retention of these metals in soluble form enables their potential recovery from the treated mine water. Characterisation of the AMD sample is summarised in Table 1.

For the potential recovery of divalent metals (such as Mn, Ni, Co and/or Mg), it is necessary to first remove the major element Fe from the solution (Sandström and Mattsson 2001). This can be achieved

Table 1 Characterisation of the initial sample of acid mine drainage.

Parameter	Concentration	Parameter	Concentration
Al	0.785 mg/L	Net acidity	160 – 190 mmol/L
As	15.4 mg/L	Ni	2.88 mg/L
Ca^{2+}	565.4 mg/L	Sb	0.0082 mg/L
Cd	<0.1 mg/L	Pb	0.035 mg/L
Co	0.370 mg/L	SO_4^{2-}	30,162 mg/L
Fe	1261.5 mg/L	Zn	0.87 mg/L
K^+	90.87 mg/L	TDS	53 g/L
Mg^{2+}	5460 mg/L	t	30.9 °C
Mn	97.5 mg/L	pH	5.7
Na^+	69.85 mg/L	Eh	182 mV

through the biological oxidation of Fe^{2+} to Fe^{3+} by iron-oxidizing bacteria, followed by the precipitation of Fe^{3+} as Fe-hydroxysulfates under low-pH conditions. This process operates without the addition of neutralizing agents, allowing divalent metal cations (Mn^{2+}, Ni^{2+}, Co^{2+} and Mg^{2+}) to remain in solution (Johnson and Hallberg 2005).

Upon discharge from the anoxic underground environment into the surface, mine water commonly undergoes rapid physico-chemical transformations driven by the degassing of dissolved CO_2, oxidation of Fe^{2+} and Mn^{2+}, and hydrolysis of Fe^{3+} and Mn^{4+} as the system equilibrates with atmospheric conditions (Geroni *et al.* 2012; Cravotta *et al.* 2013). The chemical oxidation rate of Fe^{2+} by molecular oxygen is strongly pH-dependent (Singer and Stumm 1970; Lowson 1982). The initial rapid abiotic oxidation of Fe^{2+} in aerated water progressively slows down as pH decreases, particularly below pH 3.5. Consequently, a substantial amount of ferrous iron remained in solution. The onset of exponential growth of indigenous iron-oxidising bacteria was observed up to 72 h after the mine water equilibrated with atmospheric conditions (Fig. 1). The rate of Fe^{2+} oxidation increased proportionally with the exponential growth of bacterial biomass. Subsequently, the oxidation-reduction potential (Eh) rose in parallel with a further decrease in solution pH (Fig. 3). The exponential increase in O_2 consumption rate (Fig. 1a) accompanied by CO_2 consumption, indicates the activity of indigenous autotrophic iron-oxidizing bacteria naturally present in mine water (Johnson and Hallberg 2005). Isolation of bacterial strains and methanogenic analysis of biodiversity in the mine water before and after treatment are currently underway. The bacteria completely oxidized ferrous iron to ferric iron within the next 80 h. The maximum iron oxidation rate reached ca. 30 mg L^{-1} h^{-1} (Fig.1B). Due to Fe^{3+} hydrolysis the pH decreased to ≈ 2.6. At this low pH, Fe^{3+} precipitation was less pronounced because hydrolysis reactions were limited (Johnson and Hallberg 2005). Part of the oxidized iron precipitated as secondary Fe-minerals, while approximately half of the Fe^{3+} remained in solution as a sulfate complex (Fig. 2A, B). Variations in pH, redox potential (Eh), O_2 consumption and CO_2 production/consumption values were recorded online. The rate of iron oxidation was continuously monitored using online gas analysis, based on oxygen consumption (Fig. 1), and calculated according to the stoichiometry of Eq. 1.

$$4FeSO_4 + O_2(aq) + 2H_2SO_4 \rightarrow 2Fe_2(SO_4)_3 + 2H_2O \quad (1)$$

The Fe^{2+} oxidation rate derived from O_2 and CO_2 consumption rates (Fig. 1), was used to calculate the decline in Fe^{2+} concentration by integrating r_{Fe2+} over time. The Fe^{2+} concentration decline calculated from gas analysis showed good agreement with the data obtained from chemical determination of ferrous iron in the liquid phase (Fig. 2A).

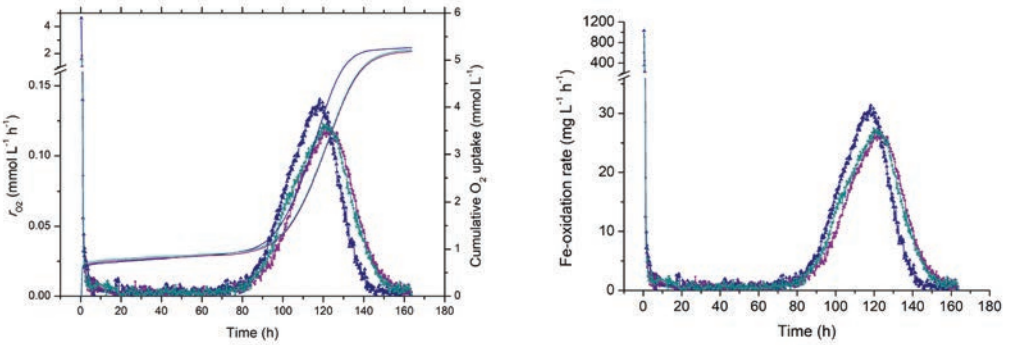

Figure 1 Oxidation of ferrous iron in the mine water under aerobic conditions. A) O_2 consumption rate and cumulative O_2 consumption related to Fe^{2+} oxidation. Chemical iron oxidation was followed by increased O_2 consumption due to exponential growth of indigenous Fe-oxidizing bacteria. B) Fe^{2+} oxidation rate derived from gas analysis based on O_2 and CO_2 consumption.

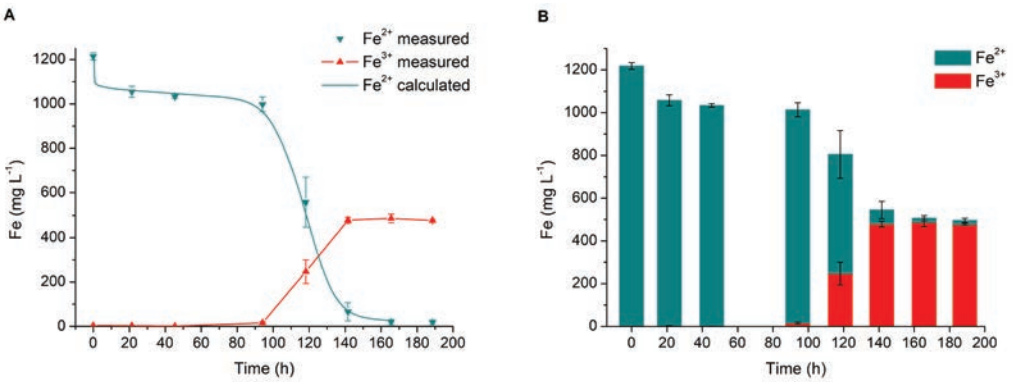

Figure 2 Iron speciation in mine water during oxidation. A) Concentrations of Fe^{2+} and soluble Fe^{3+} determined chemically in the liquid phase and the Fe^{2+} concentration decline calculated by integrating of r_{Fe2+} over time. B) cumulative amounts of dissolved iron species (Fe^{2+}, Fe^{3+}).

After approx. 180 h of experiments, almost all ferrous iron was oxidised into ferric form.

In acidic aqueous solutions, biological Fe^{2+} oxidation exceeds the rate of chemical oxidation by six orders of magnitude, as chemical oxidation is inhibited by low pH (<3.5) (Kupka 2002; Singer and Stumm 1970). Water in contact with air can exhibit biological activity due to the natural presence of bacteria in the acid-mine-water environment (Johnson and Hallberg 2005). The process also enables partial control of pH and the targeted addition of monovalent cations, both of which are critical in governing the solubility and precipitation behavior of iron and sulfate species under acidic conditions. Such control is essential for optimizing mineral formation pathways and achieving predictable iron speciation during treatment. During Fe oxidation, the Eh of the mine water increases from approximately 182 mV at the beginning to 832 mV (Fig. 3).

Alkali and alkaline earth cations were monitored during the experiment. Magnesium and calcium remained stable, while minor potassium fluctuations occurred in pH and ORP probed reactors, likely from KCl release. Biologically mediated Fe^{2+} oxidation under acidic conditions enables the selective precipitation of iron as secondary minerals without the need for neutralizing agents. This allows divalent metal cations, such as Mn^{2+}, Ni^{2+}, Co^{2+}, and Mg^{2+}, to remain in solution without notable changes after

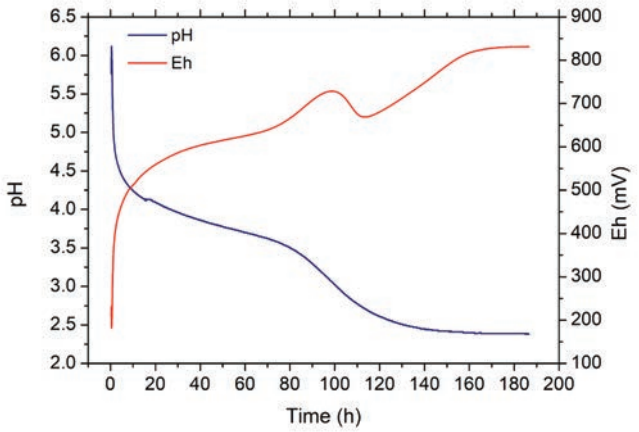

Figure 3 *pH and Eh profiles during iron oxidation in the mine water.*

Fe-oxidation, which enables their potential recovery in subsequent treatment steps. The concentration of sulfates remained constant during the experiment.

Conclusions

The results demonstrate that indigenous iron-oxidizing bacteria present in AMD can effectively catalyse the oxidation of ferrous iron under acidic conditions. Following an initial phase of rapid abiotic oxidation, biological activity significantly enhanced the overall oxidation rate, leading to complete conversion of Fe^{2+} to Fe^{3+} within approximately 80 hours. The course of Fe^{2+} concentration calculated from online gas analysis agrees with the values of Fe^{2+} concentration measured by offline chemical analysis (Fig. 2a). The study confirms that chemical iron oxidation is strongly influenced by pH, with lower pH values limiting abiotic iron oxidation rate. As a result, a substantial fraction of Fe^{3+} remained in solution under highly acidic conditions (pH ≈ 2.6). Nevertheless, this process enables selective iron transformation without the addition of neutralizing agents, allowing divalent metals such as Mn, Ni, Co, and Mg to remain dissolved and available for subsequent recovery. These findings support the applicability of biologically driven processes as an initial step in AMD treatment, particularly in systems aiming to recover metals rather than achieve complete neutralization. The research is ongoing and focuses on optimizing conditions for Fe^{3+} precipitation as oxyhydroxides or hydroxysulfates to improve treatment efficiency and resource utilization.

Acknowledgements

The authors would like to thank the European Commission and Slovak Academy of Sciences for funding in the frame of the collaborative international consortium HydroShift financed under the 2024 Joint call of the European Partnership 101060874 - Water4All

References

Bajtoš P (2025) Podmienky a charakteristika vývoja chemického zloženia vysoko mineralizovanej banskej vody počas troch rokov po zatopení sideritovej bane Manó – Gabriela v Nižnej Slanej. Engl. Conditions and characterstics of the development of the chemical composition of highly mineralised mine water from the Manó – Gabriela siderite mine in Nižná Slaná during three years after flooding. Podzemná voda, 31(1) 47–70

Basaran AH, Tuovinen OH (1986) An ultraviolet spectrophotometric method for the determination of pyrite and ferrous ion oxidation by Thiobacillus ferrooxidans. Appl Microbiol Biotechnol 24:. https://doi.org/10.1007/BF00257060

Cravotta CA, III, Geroni JN (2013) Effects of CO2 Degassing on pH and Fe(II) Oxidation Rates in Coal Mine Effluents. In: Brown A, Figueroa L, Wolkersdorfer C (eds) IMWA 2013 Reliable Mine Water Technology. Golden CO. USA, pp 949–954

García C, Moreno DA, Ballester A, Blázquez ML, González F (2001) Bioremediation of an industrial acid mine water by metal-tolerant sulphate-reducing bacteria. Miner Eng 14:997–1008. https://doi.org/10.1016/S0892-6875(01)00107-8

Geroni JN, Cravotta CA, Sapsford DJ (2012) Evolution of the chemistry of Fe bearing waters during CO2 degassing. Appl Geochemistry 27:2335–2347. https://doi.org/10.1016/j.apgeochem.2012.07.017

Herrera L, Ruiz P, Aguillon JC, Fehrmann A (1989) A new spectrophotometric method for the determination of ferrous iron in the presence of ferric iron. J Chem TechnolBiotechnol 44:171–181. https://doi.org/10.1002/jctb.280440302

Jensen AB, Webb C (1995) Ferrous sulphate oxidation using Thiobacillus ferrooxidans: a review. Process Biochemistry 30:225–236. https://doi.org/10.1016/0032-9592(95)85003-1

Johnson DB, Hallberg KB (2005) Acid mine drainage remediation options: a review. Sci Total Environ 338:3–14. https://doi.org/10.1016/j.scitotenv.2004.09.002

Kelly MG (1999) Effects of Heavy Metals on the Aquatic Biota. In: The Environmental Geochemistry of Mineral Deposits. In: Plumlee GS, Logsdon MJ (eds) The Environmental Geochemistry of Mineral Deposits. vol 6A. Society of Economic Geologists, Littleton. Society of Economic Geologists, pp 363–371

Kupka D (2002) Ferrous iron oxidation by bacteria Thiobacillus ferrooxidans. PhD. Thesis, Techni Univ in Kosice. Institute of Geotechnics, Slovak Academy of Sciences.

Lowson RT (1982) Aqueous oxidation of pyrite by molecular oxygen. Chem Rev 82:461–497. https://doi.org/10.1021/cr00051a001

Moodley I, Sheridan CM, Kappelmeyer U, Akcil A (2018) Environmentally sustainable acid mine drainage remediation: Research developments with a focus on waste/by-products. Miner Eng 126:207–220. https://doi.org/10.1016/j.mineng.2017.08.008

Nemati M, Harrison STL, Hansford GS, Webb C (1998) Biological oxidation of ferrous sulphate by Thiobacillus ferrooxidans: a review on the kinetic aspects. Biochem Eng J 1:171–190. https://doi.org/10.1016/S1369-703X(98)00006-0

Nordstrom DK, Alpers CN, Ptacek CJ, Blowes DW (2000) Negative pH and Extremely Acidic Mine Waters from Iron Mountain, California. Environ Sci Technol 34:254–258. https://doi.org/10.1021/es990646v

Nordstrom DK (2011) Mine Waters: Acidic to Circumneutral. Elements 7(6):393–398. https://doi.org/10.2113/gselements.7.6.393

Nordstrom DK, Blowes DW, Ptacek CJ (2015) Hydrogeochemistry and microbiology of mine drainage: An update. Appl Geochem 57:3–16. https://doi.org/10.1016/j.apgeochem.2015.02.008

Plumlee GS (1999) The Environmental Geology of Mineral Deposits. In: The Environmental Geochemistry of Mineral Deposits. Society of Economic Geologists, pp 71–116

Rakotonimaro TV, Neculita CM, Bussière B, Benzaazoua M, Zagury GJ (2017) Recovery and reuse of sludge from active and passive treatment of mine drainage-impacted waters: a review. Environ Sci Pollut Res 24:73–91. https://doi.org/10.1007/s11356-016-7733-7

Sandström Å, Mattsson E (2001) Bacterial ferrous iron oxidation of acid mine drainage as pre-treatment for subsequent metal recovery. Int J Miner Process 62:309–320. https://doi.org/10.1016/S0301-7516(00)00062-4

Singer PC, Stumm W (1970) Acidic Mine Drainage: The Rate-Determining Step. Science (1979) 167:1121–1123. https://doi.org/10.1126/science.167.3921.1121

Singovszka E, Balintova M, Junakova N (2020) The impact of heavy metals in water from abandoned mine on human health. SN Appl Sci 2:934. https://doi.org/10.1007/s42452-020-2731-2

Skousen JG, Zipper CE, Rose A, Ziemkiewicz PF, Nairn R, McDonald LM, Kleinmann RL (2017) Review of Passive Systems for Acid Mine Drainage Treatment. Mine Water Environ 36:133–153. https://doi.org/10.1007/s10230-016-0417-1

Wang Y, Dong R, Zhou Y, Luo X (2019) Characteristics of groundwater discharge to river and related heavy metal transportation in a mountain mining area of Dabaoshan, Southern China. Sci Total Environ 679:346–358. https://doi.org/10.1016/j.scitotenv.2019.04.273

Wolkersdorfer C (2008) Water Management at Abandoned Flooded Underground Mines – Fundamentals, Tracer Tests, Modelling, Water Treatment. Springer, Heidelberg. https://doi.org/10.1007/978-3-540-77331-3

Yang B, Luo W, Wang X, *et al* (2020) The use of biochar for controlling acid mine drainage through the inhibition of chalcopyrite biodissolution. Sci Total Environ 737:139485. https://doi.org/10.1016/j.scitotenv.2020.139485

Zeman J, Kupka D, Bártová Z, Hagarová L (2022) Chemizmus banskej vody zo šachty Gabriela v Nižnej Slanej a návrh technológií na jej úpravu [Chemistry of mine water from the Gabriela shaft in Nižná Slaná and proposal of technologies for its treatment]. In: Jurkovič Ľ, Kordík J, Čičáková C (eds) Geochémia 2022. ŠGUDŠ Bratislava, Piešťany, pp 118–121.

Low-Cost Environmental Monitoring System for Water Parameters Measurement in Mining

Eduardo Conde, Pablo Reina, Humberto Serrano-García, Fernando Barrio-Parra, Miguel Izquierdo-Díaz, Luis Fernández-Gutiérrez del Álamo, Luis Mazadiego, Eduardo De Miguel

E.T.S.I. de Minas y Energía, Universidad Politécnica de Madrid

Extended Abstract

Mining activities pose various environmental risks that necessitate effective monitoring and mitigation strategies. This work presents a novel low-cost environmental monitoring system designed to support risk assessment and enable real-time control actions for mining and quarrying (M&Q) sites. The system is designed to offer an accessible and easily adaptable solution for monitoring water parameters, as part of a broader environmental framework that may include other receiving matrices such as air and soil. Telemetry allows for the remote, continuous monitoring of key water quality indicators, facilitating prompt control actions.

This study delineates the requisite components for implementing an online monitoring system for environmental parameters, such as pH, Turbidity, and Total Dissolved Solids (TDS), utilizing low-cost and commercially available hardware (e.g., Arduino and ESP32 boards). This affordable system enables measurements which, while lacking high precision, effectively allow for the observation of trend shifts, as well as the acquisition of real-time, semi-quantitative data to aid in undertaking the necessary actions to mitigate adverse environmental effects as soon as possible, reducing the need for high-cost instrumentation. The sensor network communication is established via the LoRa protocol, facilitating the wide-area deployment of sensor nodes around the mining operation.

The pH sensors were calibrated using standard buffer solutions (pH 4, 7, and 10). Due to the complexity of the measured variable, turbidity sensor calibration required a more intensive process; a HANNA HI93703 turbidimeter, calibrated with 0, 10, and 500 NTU standards, served as the reference. Final calibration was performed by comparison with the HI93703 using water samples from 'El Tomillar' gravel pit (Hormisoria). This work was conducted within the framework of the EU-funded project ROTATE [Grant Agreement ID: 101058651].

A prototype was engineered to acquire readings of pH, Turbidity, and Total Dissolved Solids (TDS) in waters near mining operations, utilizing a network based on Arduino MKR 1310 microcontrollers and LoRa communication. To mitigate data loss, measurements are also stored on microSD cards, given that many locations may lack a Wi-Fi network for cloud data upload. The estimated cost per sensing node is approximately €300 (≈ $350). The study demonstrates the viability of developing and implementing a data acquisition and measurement system at a reasonable cost. Leveraging open-source code available in the cloud, as well as the code generation capabilities of AI tools, the prototype development does not require deep electronic knowledge. The derived measurements facilitate the real-time monitoring of water quality adjacent to the quarry and streamline decision-making for environmental variable control.

The prototype can be scaled to multipoint measurements, as well as to monitoring other environmental variables, such as Suspended Particulate Matter (SPM), using low-cost components. Furthermore, this can be implemented by the mining or industrial operation's own personnel, obviating the need for high-cost instrumentation.

Keywords: Mining-Influenced water, testing, acid mine drainage measure, data acquisition systems

Treatment of Simulated Copper-Zinc-Bearing Acid Mine Drainage Using Scrap-Derived Aluminum–Iron Bimetals and Implications For Downstream Metal Recovery

Dayle Tranz Dano[1], Ilhwan Park[1], Mayumi Ito[1], Carlito Tabelin[2], Vannie Joy Resabal[2]

[1]*Division of Sustainable Resources Engineering, Hokkaido University, Sapporo 060-8628, Japan, dayletranz.dano@gmail.com*

[2]*Department of Materials and Resources Engineering and Technology, College of Engineering, Mindanao State University-Iligan Institute of Technology, Iligan City 9200, Philippines*

Abstract

Acid mine drainage (AMD) is widely managed as an environmental liability, yet the same dissolved metals that drive its toxicity make it an untapped secondary resource. This study evaluated Al–Fe bimetallic particles synthesized directly from scrap aluminum filings for the capture of Cu and Zn from simulated AMD. At 20 g/L and 120 min, the bimetal removed essentially all Cu and 98% of Zn while raising pH from 2.12 to 5.7. Surface analyses indicated Cu capture proceeded mainly by electrochemical reduction, whereas Zn involved combined reduction and co-precipitation with in situ Al/Fe oxyhydroxides – establishing groundwork for downstream metal recovery.

Keywords: AMD treatment, metal removal, circular remediation

Introduction

Acid mine drainage (AMD), an acidic and metal-rich effluent generated by mining activities, remains one of the most enduring legacies of the industry. Its consequences are far-reaching, degrading water quality, damaging ecosystems, and posing risks to human health. For this reason, AMD has traditionally been treated primarily as an environmental liability that requires containment, neutralization, and continuous management – a persistent economic burden alongside its environmental cost (Johnson and Hallberg 2005). In recent years, however, a paradigm shift in the approach to AMD is emerging. The same dissolved constituents that make AMD problematic position it as a viable secondary source of valuable metals.

Conventional AMD treatment has been essential for protecting downstream water systems, yet most approaches remain centered on contaminant removal rather than resource recovery. Neutralization and precipitation methods can effectively lower dissolved metal concentrations, but they often rely on continuous reagent input and generate mixed sludge with limited direct commercial value (Fu and Wang 2011). Additionally, AMD is not an easy resource to valorize because metals are present in relatively dilute concentrations within chemically complex aqueous matrices, where acidity, sulfate, and coexisting ions can strongly influence selectivity and reaction pathways (Aghaei *et al.* 2021). This complexity helps explain why many proposed recovery technologies, although promising under controlled laboratory conditions, remain challenging to justify in practice. For mine water applications, a useful recovery method must be more than chemically effective; it must also be sustainable from both environmental and economic perspectives.

In this context, reactive bimetallic materials offer a promising alternative. Bimetals are composite materials composed of two dissimilar metals with different electrochemical behavior, allowing them to exhibit reactivity distinct from that of their individual components. Owing to their strong reductive potential, such materials have been widely explored in wastewater treatment applications (Aghaei *et al.* 2022). Their effectiveness arises from localized

galvanic interactions formed between the coupled metals, in which the more active metal functions as a sacrificial anode and the more noble metal serves as the cathodic site. This galvanic coupling enhances electron transfer, sustains reductive recovery, and can improve contaminant removal efficiency (Xiang *et al.* 2018). In acidic and metal-laden systems such as AMD, these characteristics make bimetals particularly attractive as reactive materials for metal recovery.

In selecting the bimetal composition, Al and Fe are particularly attractive because they are widely available, relatively inexpensive, and electrochemically complementary compared with more noble metals. Individually, both aluminum- and iron-based materials have been applied in wastewater treatment, but their reactivity is often limited by rapid oxide passivation at the surface (Plessl *et al.* 2023). When synthesized as a bimetal, however, this drawback can be partly overcome through galvanic interaction between the two metals. In the Al–Fe system, Al, with its more negative standard reduction potential (Al^{3+}/Al: E^0 = -1.66 V), acts as the sacrificial anode, whereas Fe (Fe^{3+}/Fe: E^0 = -0.04 V) serves as the cathodic partner that facilitates electron transfer and reductive reactions at the surface. As a result, the coupled system exhibits a reactivity distinct from that of either metal alone, making Al–Fe bimetals a promising low-cost candidate for metal recovery applications.

Building on these considerations, this study examines scrap-derived Al–Fe bimetallic particles – synthesized directly from waste aluminum filings – for the capture of Cu and Zn from simulated AMD. This dual-waste framing couples the upcycling of an industrial waste stream with the treatment of a persistent mining effluent, addressing both within a single material system. The effects of contact time and bimetal dosage on metal removal and solution pH are evaluated alongside the surface reactions and resulting metal speciation that govern capture. Together, these results establish the mechanistic basis on which downstream metal recovery from mine-affected waters can be developed in future work.

Methods

Preparation of Simulated Acid Mine Drainage

In this study, synthetic AMD was chemically prepared to replicate the composition of real AMD obtained from an operating copper mine in the Philippines. Table 1 presents the assayed concentrations (mg/L) of individual metals in the real AMD. Preparation of the synthetic AMD involved the use of metal sulfate forms of Ni, Cu, Zn, and Mn, as well as sodium chloride (NaCl), calcium chloride ($CaCl_2$), and sodium sulfate (Na_2SO_4). To achieve the target pH (2.0–2.2) similar to AMD, dilute hydrochloric acid (HCl) was added to the synthetic AMD.

Synthesis of Al–Fe Bimetals using Scrap Aluminum

Al–Fe bimetallic particles were synthesized following a published two-stage mechanical–chemical method using scrap Al (Tabelin *et al.* 2021). Unlike the reference study, shredded aluminum filings from Iligan City, Philippines were used instead of aluminum cuboids, thereby eliminating the need for surface mechanical polishing and likely enhancing reactivity because of the higher surface area. The scrap was sieved, washed with deionized water, and vacuum dried before a pre-weighed sample was placed in an Erlenmeyer flask. An HCl–NaCl–$FeCl_3$ reagent mixture was then added to remove the native oxide/anodized layer and supply Fe^{3+} ions for reduction at the aluminum surface. The reagent mixture consisted of 0.125 M HCl, 0.125 M NaCl, and 1.25 M $FeCl_3$.

Table 1 *Initial solute concentrations (mg/L) in the real AMD.*

Components	Cu	Fe	Mn	Ni	Zn	Al	Mg	Ca	SO_4^{2-}
Concentration (mg/L)	10.4	17.1	6.9	1.5	7.4	27.8	25.8	352.2	1,752.0

Batch Removal Experiments of Cu and Zn from Simulated AMD

The performance of Al–Fe bimetallic materials in removing Cu and Zn from synthetic AMD was investigated through batch removal experiments conducted in triplicate. A predetermined dosage of the bimetallic material (5, 10, and 20 g/L) was placed in an Erlenmeyer flask and mixed with simulated AMD. This suspension was then placed in a thermostat water bath shaker with 40 mm of shaking amplitude and 110 min−1 of shaking frequency at 25 °C for 5–120 min. After the predetermined reaction time, the filtrates were collected, filtered through syringe-driven membrane filters (pore size: 0.2 μm), and analyzed by ICP-AES (ICPE-9820, Shimadzu Corporation, Japan; instrument error ±2%) to quantify the concentrations of Cu and Zn. The removal of target metal ions (%R) was determined in percentage using the equation:

$$\%R = [(C_0 - C) / C_0] \times 100$$

where C_0 is the initial metal concentration in mg/L, and C is the residual metal ion concentration in mg/L. This metric quantifies the loss of dissolved Cu and Zn from the aqueous phase and does not represent the mass of metal recovered as a separable product; downstream recovery is treated here as a future implication informed by the observed surface speciation.

Results

Characterization of Synthesized Al–Fe Bimetal from Scrap Al

Scrap Al and the synthesized bimetal were characterized using XRF, SEM-EDS, and XPS. Scrap Al was mainly Al (>95%) with minor Si, Fe, and Mg typical of Al alloys. After synthesis, Fe content increased from 0.6% to 40.4% (Figure 1), and XPS confirmed zero-valent Fe (ZVI) deposited on the Al surface.

Copper and Zinc Removal from Synthetic Acid Mine Drainage and pH Changes

Figure 2 shows that the Al–Fe bimetal removed both Cu and Zn from simulated AMD under all tested conditions, with removal rates improving at longer times and higher dosages. Cu was removed faster and more completely, reaching full removal within 20 min at 20 g/L, while Zn required 120 min at the same dosage to approach 98% removal – indicating Cu is more readily removed than Zn.

This difference reflects electrochemical favorability: Cu, the more noble metal, has a larger electrode-potential difference relative to Al than Zn, making its reduction thermodynamically more favorable. Longer treatment times and higher dosages increased exposure and reactive-site availability, driving progressively higher removals for both metals.

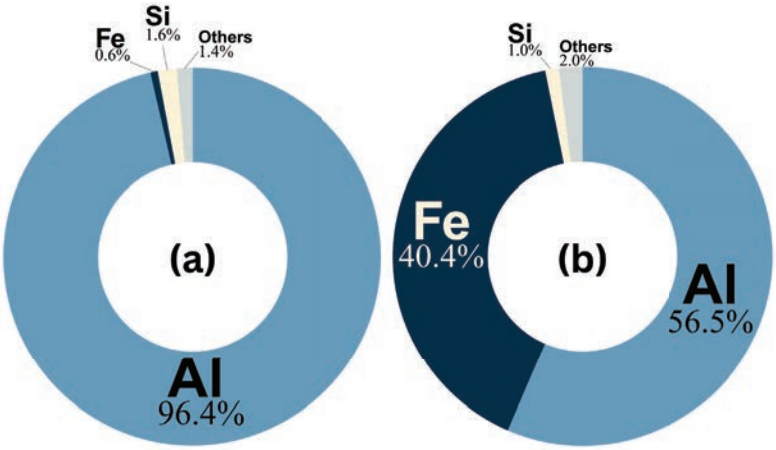

Figure 1 *Elemental composition of (a) scrap Al and (b) synthesized Al–Fe bimetal.*

Solution pH also increased concurrently from 2.12 to a maximum of 5.7 at the maximum conditions (Figure 2), indicating that the removal process consumed acidity and promoted hydroxide generation (Lien *et al.* 2019; Teng *et al.* 2023). The Al–Fe bimetal thus captures dissolved metals while partially self-neutralizing the treated solution. From a mine-water perspective, this is an important result because it suggests that the Al–Fe bimetal offers a dual function of metal capture and partial acid neutralization in a single step, reducing the downstream burden of pH correction.

Mechanistic Investigation of Cu and Zn Removal

Copper and zinc removal are governed by surface electrochemical processes activated under acidic AMD conditions. At pH ≈ 2.1, high proton activity dissolves pre-existing oxide/oxyhydroxide layers, exposing reactive Al and Fe sites. As illustrated in Figure 3, two parallel pathways then operate: (1) galvanic reduction, where Al acts as the sacrificial anode and supplies electrons to Fe-rich cathodic regions that reduce dissolved metal ions, and (2) direct reduction at exposed Al and Fe surfaces.

XPS of the reacted bimetal showed no distinct Cu 2p or Zn 2p signals initially, while Al 2p and Fe 2p regions became dominated by Al(III) and Fe(II/III) oxide/oxyhydroxide species with zero-valent Al and Fe no longer evident. As XPS probes only the top few nanometers, this corrosion-product overlayer – consistent with the observed pH rise – likely masks earlier-formed metallic deposits, especially given that Cu removal was complete well before the reaction ended. To resolve the captured metal speciation, a more concentrated Cu–Zn–Fe model solution was examined by XPS (Figure 4).

The Cu 2p spectra confirm Cu capture predominantly via electrochemical reduction, with Cu(0) on the reacted surface and Cu(I) (Cu2O) suggesting a sequential Cu2+ → Cu+ → Cu0 route; the Cu(II) signal (CuO) is attributable to subsequent oxidation of deposited Cu during the prolonged reactive period rather than to capture itself. Zn showed a different speciation: Zn(0) confirms reductive deposition, but the simultaneous Zn(II) signals (likely ZnO and Zn(OH)2), together with Al/Fe oxide–oxyhydroxide enrichment in the Al 2p and Fe 2p spectra, indicate a mixed mechanism of reduction plus secondary co-precipitation with Al–Fe corrosion products — a well-documented Zn-removal pathway in wastewater systems. Overall, Cu capture is dominated by electrochemical reduction, whereas Zn proceeds through combined reduction and surface-mediated retention, consistent with the faster, more favorable Cu removal (Wang *et al.* 2014; Passos *et al.* 2021).

Preliminary investigation of bimetal reusability and implications for downstream recovery

A preliminary reusability test applied a single batch of Al–Fe bimetals to five successive sets of fresh synthetic AMD (20 g/L, 120 min per cycle). Cu removal remained consistently high across all five runs, whereas Zn removal began to decline after the third cycle. This divergence is likely driven by progressive surface passivation: with each cycle, deposited metallic Cu and accumulating Al/Fe corrosion products build up on the

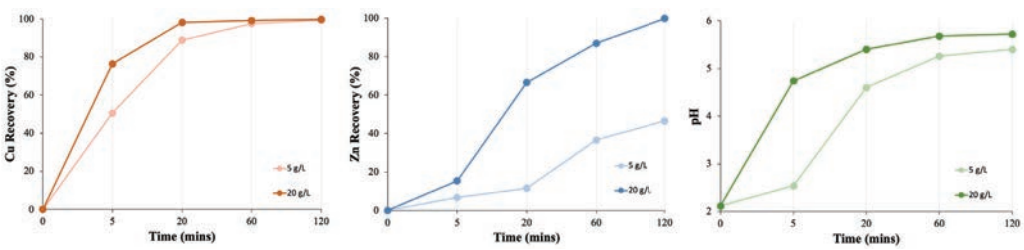

Figure 2 *Removal of Cu and Zn, and pH changes in varying bimetal dosages and contact time.*

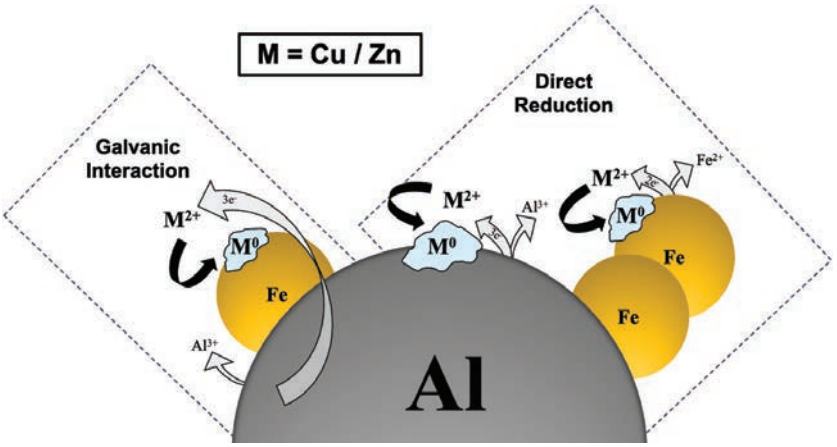

Figure 3 Schematic illustration of the surface electrochemical processes in the Al–Fe bimetal.

bimetal and gradually mask the reactive Al^0 and Fe^0 sites that drive galvanic activity. Cu can still be reduced because residual Fe at the surface remains sufficiently reducing toward Cu^{2+} even as the galvanic system weakens. For Zn, however, removal depends on the combined action of galvanic reduction and co-precipitation with freshly formed Al/Fe oxyhydroxides – both of which are diminished once the surface is passivated – explaining why Zn is the first to drop off with repeated use.

The kinetics and speciation observed for Cu and Zn point to several possibilities for post-recovery valorization that future work can pursue using this study as groundwork. One possibility lies in the kinetic window between the two metals: Cu reached complete removal within 20 min while Zn still required 120 min at the same dosage, suggesting that contact time could be used as a selectivity lever – a short-contact stage to preferentially load Cu, followed by a longer-contact stage on a separate batch to target Zn. Another possibility is to design downstream processing around the differing surface speciation of the loaded metals – Cu captured largely as Cu(0) on a discrete metallic layer, and Zn distributed between Zn(0) and Zn(II) phases co-precipitated with Al/Fe oxyhydroxides – with leaching and recovery schemes tailored to each form. These directions can be pursued in parallel, alongside regeneration strategies that restore reactive sites and testing on

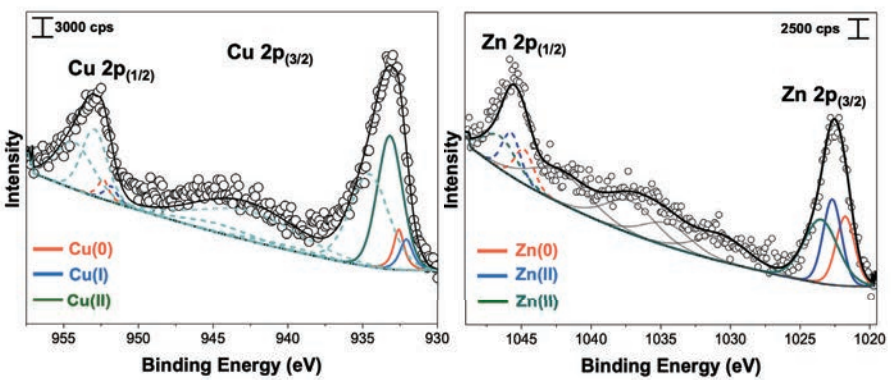

Figure 4 XPS narrow-scan spectra of the loaded Al–Fe bimetal after reaction with model solutions, acquired at Cu 2p and Zn 2p regions.

real AMD matrices with techno-economic evaluation to assess practical deployment.

Conclusions

The broader significance of this work lies in its dual-waste reuse concept. By simultaneously repurposing scrap aluminum filings and applying them to acid mine drainage for metal capture, this work demonstrates a concrete pathway toward circular mine water management. Unlike conventional AMD treatment approaches that generate mixed sludge of limited commercial value, the Al–Fe bimetal captures Cu and Zn onto a concentrated solid substrate amenable to downstream recovery while partially self-neutralizing the treated solution, reducing the downstream burden of pH correction. These characteristics make the approach particularly attractive for application in active or legacy mining sites in developing regions where access to high-purity reagents and complex infrastructure is limited. Taken together, these findings establish scrap-derived Al–Fe bimetals as a promising AMD treatment platform with downstream recovery potential. Future work should focus on isolating the captured metals as separable, usable products, alongside testing on real AMD matrices, extended reusability assessment, and techno-economic evaluation for practical deployment.

References

Aghaei E, Tadesse B, Tabelin CB, Alorro RD (2022) Mercury sequestration from synthetic and real gold processing wastewaters using Fe–Al bimetallic particles. J Clean Prod 372:133482. https://doi.org/10.1016/j.jclepro.2022.133482

Aghaei E, Wang Z, Tadesse B, et al (2021) Performance evaluation of fe-al bimetallic particles for the removal of potentially toxic elements from combined acid mine drainage-effluents from refractory gold ore processing. Minerals 11:1–13. https://doi.org/10.3390/min11060590

Fu F, Wang Q (2011) Removal of heavy metal ions from wastewaters: A review. J Environ Manage 92:407–418. https://doi.org/10.1016/j.jenvman.2010.11.011

Johnson DB, Hallberg KB (2005) Acid mine drainage remediation options: A review. Science of the Total Environment 338:3–14. https://doi.org/10.1016/j.scitotenv.2004.09.002

Lien HL, Yu CH, Kamali S, Sahu RS (2019) Bimetallic Fe/Al system: An all-in-one solid-phase Fenton reagent for generation of hydroxyl radicals under oxic conditions. Science of the Total Environment 673:480–488. https://doi.org/10.1016/j.scitotenv.2019.04.116

Passos H, Cruz B, Schaeffer N, et al (2021) Selective Sequential Recovery of Zinc and Copper from Acid Mine Drainage. ACS Sustain Chem Eng 9:3647–3657. https://doi.org/10.1021/acssuschemeng.0c07549

Plessl K, Russ A, Vollprecht D (2023) Application and development of zero-valent iron (ZVI) for groundwater and wastewater treatment. International Journal of Environmental Science and Technology 20:6913–6928. https://doi.org/10.1007/s13762-022-04536-7

Tabelin CB, Resabal VJT, Park I, et al (2021) Repurposing of aluminum scrap into magnetic Al0/ZVI bimetallic materials: Two-stage mechanical-chemical synthesis and characterization of products. J Clean Prod 317:128285. https://doi.org/10.1016/j.jclepro.2021.128285

Teng R, Jiang J, Shi D, Li H (2023) Synthesis of Acid Mine Drainage (AMD) Sludge-Derived Al-Fe3O4 as Fenton-like Catalysts for the Efficient Degradation of Tetracycline. Langmuir 39:14275–14283. https://doi.org/10.1021/acs.langmuir.3c01555

Wang LP, Ponou J, Matsuo S, et al (2014) Selective precipitation of copper and zinc over iron from acid mine drainage by neutralization and sulfidization for recovery. International Journal of the Society of Material Engineering for Resources 20:136–140. https://doi.org/10.5188/ijsmer.20.136

Xiang S, Cheng W, Nie X, et al (2018) Zero-valent iron-aluminum for the fast and effective U(VI) removal. J Taiwan Inst Chem Eng 85:186–192. https://doi.org/10.1016/j.jtice.2018.01.039

IMWA 2026
Jeongseon

Natural and Mining-Related Sulfate Sources at Two High-Sulfidation Deposits Constrained by a Triple-Tracer Bayesian Isotope Mixing Model

Camilo Raúl de los Hoyos[1], Claudina González[1], Juana María Canavessi[1], Matthew Leybourne[2], Daniel Layton-Matthews[2], Alejandro Verri Kozlowski[1], Robert Bowell[3]

[1]*SRK Consulting (Argentina) S.A., Salta, Argentina, cdeloshoyos@srk.com.ar*

[2]*Queen's Facility for Isotope Research, Kingston, Canada*

[3]*SRK Consulting (UK) Ltd., Cardiff, Wales*

Abstract

Distinguishing natural from mining-derived sulfate in surface water is particularly challenging in high-altitude catchments hosted in intensely hydrothermally altered lithologies. Two compliance monitoring stations downstream of two high-sulfidation epithermal deposits (VD and PL) were investigated using a triple-tracer Bayesian isotope mixing model (δ^{34}SSO4, δ^{18}OSO4, δ^{18}Owater; MixSIAR). Natural hydrothermal and geothermal sources dominate sulfate loading at both stations: at TAG_mid (VD), DPB and TAG_sup account for ~66% of the sulfate budget, with mining-related contributions (~8%) smaller than the unaccounted source fraction. At TAG_low (PL), the upstream TAG_mid reach contributes ~74%, propagating the predominantly natural signal downstream. In contrast to sulfate, dissolved As decreases ~600-fold between TAG_mid and TAG_low, while total As loads remain near-conservative (~4.5% decrease), indicating phase transfer to the particulate fraction through Fe-hydroxide co-precipitation induced by lime treatment rather than mass removal from the system.

Keywords: Sulfate source proportions, stable isotopes, Bayesian isotope mixing, high-sulfidation

Introduction

Characterizing sources of sulfate, arsenic (As), and potentially toxic metals is essential for accurate water quality monitoring, regulatory compliance, and remediation. Distinguishing anthropogenic from natural sulfate sources in catchments associated with high-sulfidation epithermal mine sites is challenging, as natural weathering of sulfur-bearing minerals in hydrothermal alteration zones produces hydrochemical signatures similar to those from mining activities. Sulfur and oxygen stable isotopes (δ^{34}S and δ^{18}OSO4) provide a useful tool for assessing sulfate source contributions (e.g., Pellicori *et al.*, 2005). Combined with hydrochemical data and Bayesian mixing models, this multi-tracer approach offers a robust statistical framework for quantifying source proportions with full uncertainty characterization (Stock *et al.*, 2018; Zhang *et al.*, 2024).

This study focuses on the origin of sulfate in surface water at two compliance monitoring stations, located downstream of two high-sulfidation epithermal deposits (hereinafter VD and PL; site identities and operational details are withheld under a non-disclosure agreement between SRK and the Client).

Methods

Hydrochemical characterisation and sulfate load estimations drew on the client's monitoring database (>20 years), with a baseline period from 1999/2000 until 2004. Water samples were analyzed for stable isotopes and dissolved constituents. δ^{18}Owater and δ^{2}H were measured by IRMS (CO_2 equilibration and thermo-chemical reduction, respectively; VSMOW reference). δ^{34}S and δ^{18}OSO4 were determined after $BaSO_4$ precipitation by IRMS (VCDT and VSMOW references). Analytical precision: ±0.2‰ for δ^{18}O and δ^{34}S; ±3‰

for δ^2H. Major anions were measured by ion chromatography; major and trace cations by ICP-MS.

Bayesian mixing models were implemented in MixSIAR v3.1 (Stock *et al.* 2018) using three simultaneous tracers ($\delta^{34}S$, $\delta^{18}OSO4$, $\delta^{18}Owater$). Concentration-dependent mixing was applied using sulfate as the weighting variable. Informative priors were constructed from log_{10}-transformed sulfate mass loads per source (prior strength = 1.5). Sensitivity to prior specification was evaluated against a uniform prior. Markov Chain Monte Carlo (MCMC) convergence was assessed with the Gelman-Rubin diagnostic ($\hat{R} < 1.1$).

Site, sources and mixtures characterisation

Geological, and hydrochemical setting

The study area occupies a high-altitude mountainous region (4,000–5,000 m.a.s.l.) spanning two Köppen climate zones: cold arid steppe (BSk) and polar tundra (ET). Precipitation is scarce and predominantly in the form of snowfall during winter; surface runoff is consequently driven by snowmelt, with peak streamflow occurring between October and February.

VD is a high-sulfidation epithermal deposit that is almost completely oxidized. The district lithology comprises felsic intrusive bodies (granites and monzonites) at the margins, andesitic rocks and volcanic breccias in the interior, and rhyolites within the open pit areas. Hydrothermal alteration is intense and pervasively zoned. Silicic cores bearing jarosite and alunite correspond to the mineralized zones and are surrounded by advanced argillic assemblages, with distal propylitic alteration (chlorite–epidote) developed at the outer margins. Gold is associated with iron oxides (hematite and goethite) and jarosite, whereas hypogene sulfides are rare or absent.

PL is a high-sulfidation epithermal deposit dominated by primary hypogene mineralization. Lithology is dominated by porphyritic granite and dacitic porphyry, with felsic tuffs at the margins and diorite stocks intruding the sequence. Hydrothermal alteration is pervasive and multistage. Silicic alteration (vuggy quartz) characterizes the mineralized breccia cores, which are surrounded by advanced argillic assemblages, with distal propylitic alteration at the outer margins. Gold and silver are primarily hosted within a hypogene alunite–pyrite–enargite assemblage, occurring as trace constituents within the enargite and pyrite structure.

Surface water chemistry is strongly controlled by the hydrothermal alteration zones within each sub-catchment. Waters draining silicic and advanced argillic zones are naturally acidic and sulfate-rich, enriched in aluminum and trace metals, with jarosite dissolution as the primary natural source of acidity in VD and PL, the latter involving pyrite oxidation. Catchments influenced by propylitic alteration (source PT) produce Ca-SO_4-type waters at near-neutral pH, while sectors draining unaltered primary volcanic lithologies yield Na–Cl signatures. The geothermal system southeast of the project represents the dominant natural sulfate and As to the downstream monitoring points (source DPB). Contribution from groundwater and minor springs was not considered in this study.

Sources and mixture sites

Sources were characterized from water samples collected during three field campaigns to capture temporal variability, whereas solid-phase isotopic data for alunite and jarosite were compiled from the literature (Deyell *et al.*, 2005; Holley *et al.*, 2017). All sources and mixing sites are summarized in Table 1 and Figure 2. For VD, five sources were defined: three natural – geothermal spring tributary DPB, upper main collector TAG_sup, and the sub-catchment PT – and two mining-related: the Valley Leach Facility (VLF) and the Open Pit (OP). Contribution assessment from VLF and OP was included using a highly conservative approach: fixed flow rates of 7 L/s (VLF) and 10 L/s (OP) were assigned to represent hypothetical seepage scenarios. This intentionally biases the model toward maximizing mining-related inputs. For PL, four sources were characterized: one predominantly natural upstream source, TAG_mid; one natural acid rock drainage source, Turbio_head which also includes groundwater originating from the tunnel (pH ~3.3; $\delta^{34}S$ = −0.7‰) that is captured

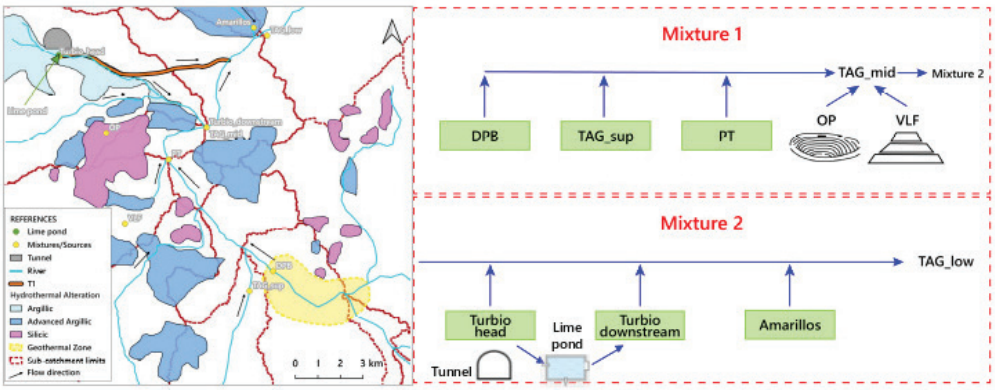

Figure 1 *Sketch map of hydrothermal alteration zones (a) and sources-mixtures scheme (b).*

and conveyed through a pipe system (T1 in Figure 1) and discharged near TAG_low; one partially mining-influenced source, Turbio_downstream, which consists of lime-treated drainage from a mining tunnel intercepting the Turbio_head aquifer, supplemented by minor natural tributaries; and one natural drainage from the PL argillic alteration zone, Amarillos ($\delta^{34}S$ = −5.4‰). Despite both Turbio_head and Amarillos being sourced from the PL alteration zone, their contrasting isotopic signatures likely reflect different alteration assemblages or sulfide oxidation pathways (Deyell *et al.*, 2005). The heavier $\delta^{34}S$ of Turbio_downstream relative to Turbio_head may reflect kinetic fractionation during lime-induced gypsum precipitation. Table 1 combines data from high- and low-flow campaigns; seasonal disaggregation was beyond the scope of this study but would allow identification of gaining and losing reaches and is recommended for future work.

Results and discussion

Isotopic mixing space for sources and mixtures and model results

The $\delta^{34}S$ vs. $\delta^{18}OSO4$ biplots (Figure 2a and c) suggest differentiation among sources at both sites. At VD, solid-phase analyses define two distinct mineral fields: VD_jar ($\delta^{34}S$: −3.8 to −0.8‰; $\delta^{18}O\text{-}SO_4$: −4 to +0.7‰) and VD_aln ($\delta^{34}S$: +5.9 to +17.5‰; $\delta^{18}OSO4$: +2 to +9‰), separated by ~15‰ in $\delta^{34}S$ and consistent with the contrasting formation mechanisms of these phases (Deyell *et al.*, 2005). $\delta^{34}S$ values for VLF are similar to those for VD_jar, suggesting jarosite dissolution as a plausible sulfate source by dissolution. OP shows broader scatter although closer to VD_aln field, suggesting predominance of alunite mineralogy of the pit walls; the highest $\delta^{34}S$ sample (~12.9‰) plots to VD_aln, likely reflecting dominant alunite dissolution at that sampling station. The $\delta^{34}S$ vs. $\delta^{18}OSO4$ (Figure 2c) shows some overlapping between DPB and OP, although both sources plot clearly distinguished within the mixing space $\delta^{34}S$ vs. $\delta^{18}Owater$ (Figure 2b).

At PL, the PL_py $\delta^{34}S$ range (−6 to −3.4‰) plots towards the lightest portion of the system (Figure 2c). Amarillos is clearly distinguished in the $\delta^{34}S$ vs. $\delta^{18}OSO4$ biplot, and plots within the PL_py $\delta^{34}S$ range. Turbio_head tends to plot towards PL_jar $\delta^{34}S$ range. TAG_mid (which is now a source) is plotted almost together with TAG_low (mixture) both in the $\delta^{34}S$ vs. $\delta^{18}OSO4$ and the $\delta^{34}S$ vs. $\delta^{18}Owater$ mixing spaces (Figure 2d). The PL_aln field ($\delta^{34}S$ = +12.6 to +24.5‰; $\delta^{18}OSO4$ = +13.8–+20.7‰) lies entirely outside the PL mixing space, indicating that alunite dissolution does not constitute an important dissolved sulfate source at this monitoring station (TAG_low) under sampled conditions. All VD and PL samples plot within the isotope mixing space of their respective end-member sets, validating the source framework.

MCMC convergence was confirmed, with $\hat{R} < 1.1$ for all modeled parameters. Sensitivity analysis showed differences between informative and uniform prior models for all

Table 1 Isotopic composition (mean ± 1SD) and classification of end-members and mixing sites. pH values are averaged. Sulfate and As are dissolved contents. n = number of isotope results.

Source/Mixture	pH	$\delta^{34}S_{SO4}$ (‰)	$\delta^{18}O_{SO4}$ (‰)	$\delta^{18}O_{water}$ (‰)	Sulfate (mg/L)	As[1] (µg/L)	Flow (L/s)
VD sources							
DPB (n = 7)	7.6	3.8 ± 1.1	2.2 ± 1.4	−15.6 ± 0.7	299 ± 72	1479 ± 455	583 ± 406
TAG_sup (n = 6)	8.1	2.6 ± 0.6	1.1 ± 1.2	−16.0 ± 0.5	706 ± 7	489 ± 574	325 ± 236
PT (n = 9)	9	1.5 ± 0.6	0.2 ± 0.9	−17.0 ± 0.4	397 ± 15	66 ± 78	35 ± 41
VLF (n =4)	10.1	−1.2 ± 1.4	3.0 ± 1.0	−15.8 ± 1.3	1060 ± 26	348 ± 35	7 ± 1
OP (n = 13)	3.4	4.3 ± 3.4	3.9 ± 1.5	−17.9 ± 0.6	28 ± 3	0.63 ± 0.62	10 ± 1
TAG_mid (n = 4)	8.1	2.3 ± 0.4	0.6 ± 1.2	−15.8 ± 0.5	500 ± 45	813 ± 328	969 ± 615
PL sources							
TAG_mid (n = 4)	8.1	2.0 ± 0.6	0.7 ± 1.1	−15.8 ± 0.4	500 ± 45	813 ± 328	969 ± 615
Turbio_head (n = 6)	3.3	−0.7 ± 1.3	−0.5 ± 1.9	−16.7 ± 1.1	2600 ± 1570	224 ± 181	59 ± 66
Turbio_downstream (n = 6)	4.1	2.9 ± 1.0	−0.7 ± 1.5	−16.7 ± 0.3	895 ± 34	0.45 ± 0.24	122 ± 70
Amarillos (n = 6)	4.9	−5.4 ± 0.8	−7.3 ± 1.6	−16.4 ± 0.2	805 ± 317	0.78 ± 1.03	126 ± 105
TAG_low (n = 6)	5.1	1.6 ± 0.6	−0.9 ± 1.4	−15.6 ± 0.2	704 ± 27	1.26 ± 2.75	1141 ± 745

[1]Arsenic contents are reported in µg/L, given their low values relative to sulfate and their wide variability across sources.

sources of less than 15% for VD and less than 5% for PL, indicating that the three-tracer isotopic system carries sufficient information to constrain the posteriors without excessive dependence on the prior.

Source proportional contribution at VD

Natural sources dominate sulfate at TAG_mid (Fig. 3a). TAG_sup and DPB are the main contributors (~66% combined posterior median; 95% credible interval or CI), reflecting the substantial hydrothermal sulfate background characteristic of high-sulfidation systems. PT contributes ~19%, acting mainly as a dilution end-member. Mining contributions from VLF and OP are 4.9% and 2.9% respectively (~8% combined), smaller than the unaccounted fraction of 6.5% (100% - Σsource-proportions), even though assigned sulfate loads were highly conservative. Wide CIs reflect uncertainty inherent to a five-source system with n = 4 mixture samples. Predicted sulfate concentrations agree reasonably with observed values at TAG_mid.

Source proportional contribution at PL

TAG_mid is the dominant source at TAG_low (~74% posterior median; 95% CI; Fig. 3b), robust to prior specification and reflecting the physical dominance of the main river collector. Since TAG_mid is predominantly natural, a strong natural signature propagates to TAG_low. Turbio_head and Turbio_downstream contribute ~16% combined, where Turbio_downstream (~8.8%) represents a partially mining-related pathway to TAG_low. Amarillos, the isotopically most distinguishable source, contributes ~6%. Overall mining influence is small relative to the natural geothermal and hydrothermal background. TAG_mid remains distinguishable as the dominant source, with a lower credible limit (~27%) exceeding the medians of all other sources. Credible intervals are wide for TAG_mid and Turbio_head, reflecting inherent uncertainty due to the limited number of samples in the mixture (n=6). The predicted sulfate concentration at TAG_low (~950 mg/L) exceeds measured contents (~700 mg/L), suggesting active sulfate removal in the confluence and consistent with gypsum precipitation when Ca^{2+}-rich lime-treated water from Turbio_downstream contacts the sulfate-rich TAG_mid water, a process supported by the isotopic fractionation observed in Turbio_downstream.

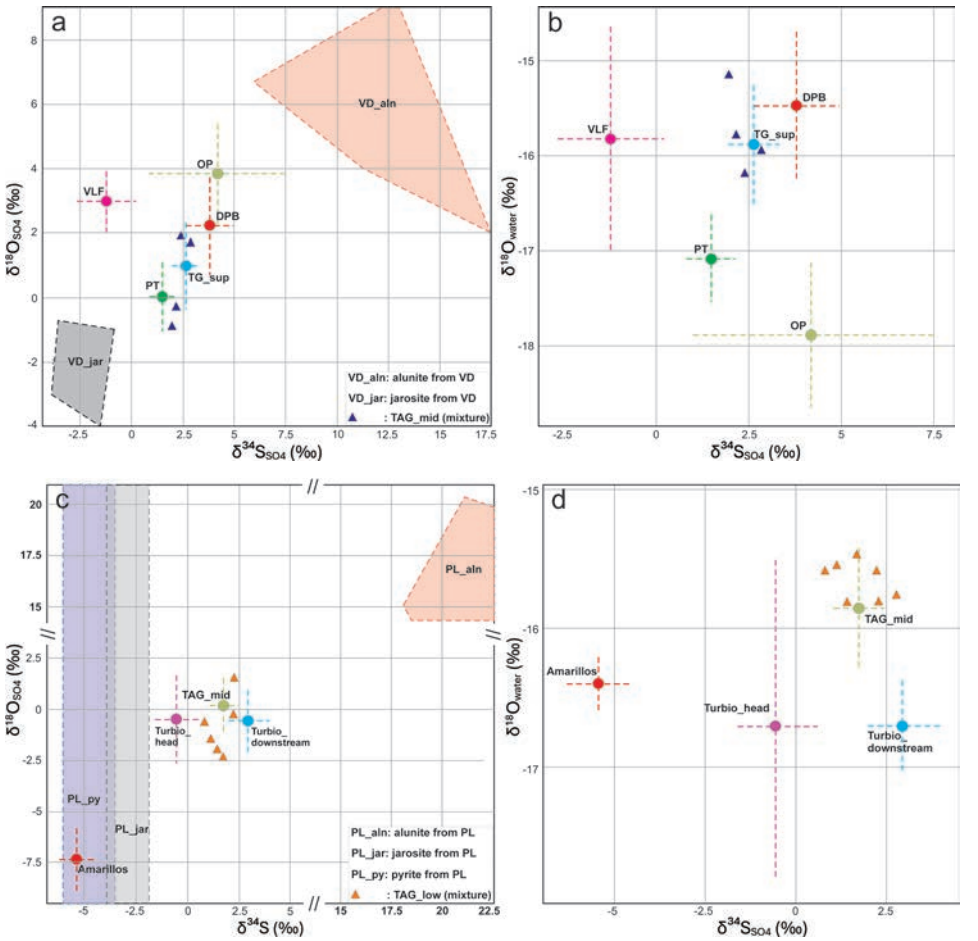

Figure 2 *Biplots for the triple-tracer $\delta^{34}S$ – $\delta^{18}O_{SO4}$ – $\delta^{18}O_{water}$ system including sources, mixtures and solid-phase isotopic signatures for VD (a and b) and PL (c and d).*

Dissolved arsenic non-conservativity between TAG_mid and TAG_low

The most notable feature of the TAG_mid–TAG_low segment is the behavior of As. Dissolved As shows strongly non-conservative behavior between the two compliance stations (Table 1). At TAG_mid (pH 8.1), dissolved As averages 813 ± 328 µg/L, dominated by the geothermal source DPB (1,479 ± 455 µg/L at pH 7.6), while mining-related sources contribute negligibly. Total As at TAG_mid averages 1,289 µg/L, indicating that ~37% of As is already particulate at this station, likely associated with Fe and Al hydroxide colloids stable at near-neutral pH.

At TAG_low (pH 5.1), dissolved As drops to 1.26 ± 2.75 µg/L, which is a ~600-fold decrease relative to TAG_mid, while total As remains at 1,045 µg/L, implying that >99% of As at TAG_low is particulate. Total As loads are near-conservative between stations (TAG_mid: ~1,249,000 µg/s; TAG_low: ~1,192,000 µg/s; ~4.5% difference), suggesting that this decrease does not represent mass removal but rather phase change to the particulate fraction, likely through adsorption onto Fe-hydroxide flocs. The contrast between Turbio_head (224 ± 181 µg/L; pH 3.3) and Turbio_downstream (0.45 ± 0.24 µg/L; pH 4.1) suggests that lime treatment efficiently removes great part of the dissolved As prior to confluence. Thus, the decrease in dissolved As (V) between TAG_mid and TAG_low may rather represent adsorption

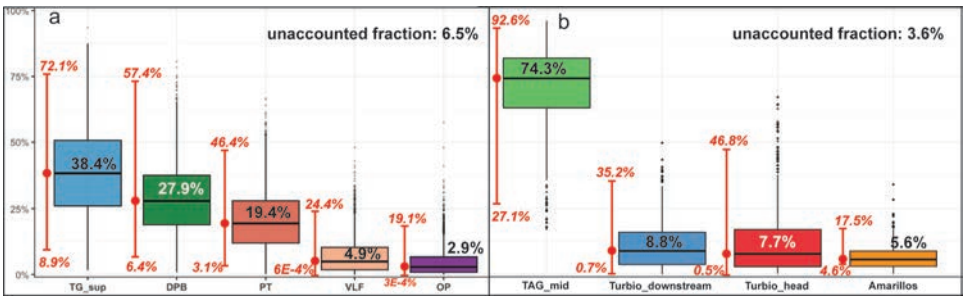

Figure 3 Boxplots of source contributions at VD (a) and PL (b). Median values are indicated within the boxplots. 95% credible intervals (2.5 to 97.5% CI) are shown in red to the left of each boxplot, with red points indicating the position of the median.

onto Fe-hydroxide flocs generated by lime treatment in the Turbio_downstream source. Speciation of As was not considered in this study, although it is strongly recommended for future work.

Conclusions

Sulfate load proportions were estimated considering combined high-flow and low-flow conditions. A triple-tracer Bayesian isotope mixing approach successfully quantified sulfate source contributions, in terms of mass, at two compliance monitoring sites within high-sulfidation epithermal catchments. At TAG_mid (VD), hydrothermal inputs (DPB and TAG_sup) dominate the sulfate budget (~66%), with PT acting primarily as a dilution source; mining-related contributions from the OP and VLF are quantifiable but minor (~8%), smaller than the unaccounted source fraction. At TAG_low (PL), upstream inputs dominate (~74% from TAG_mid); the Turbio system accounts for ~16% of the sulfate load, with Turbio_downstream as the primary mining-related pathway. In both cases, the sulfate budget is predominantly controlled by natural hydrothermal sources.

In contrast to sulfate, dissolved As shows non-conservative behavior along the TAG_mid–TAG_low segment. Total As loads are near-conservative (~4.5% decrease), whereas dissolved As decreases ~600-fold, suggesting phase transfer to the particulate fraction through Fe-hydroxide co-precipitation induced by lime treatment rather than removal from the system.

These results have direct implications for environmental monitoring in high-sulfidation deposits, where sulfate concentrations may be predominantly natural and might be misattributed to mining environmental affectation. The combined use of multiple isotopic tracers and Bayesian mixing models provides a robust and transferable framework for source apportionment in complex systems, particularly where overlapping source signatures and non-conservative behavior may complicate interpretation.

References

Deyell, C.L., Rye, R.O., Landis, G.P. & Bissig, T. (2005). Alunite and the role of magmatic fluids in the Tambo high-sulfidation deposit, El Indio–Pascua belt, Chile. Chemical Geology, 215, 185–218.

Holley, E.A., Monecke, T., Bissig, T., & Reynolds, J. (2017). Evolution of High-Level Magmatic-Hydrothermal Systems: New Insights from Ore Paragenesis of the Veladero High-Sulfidation Epithermal Au-Ag Deposit, El Indio-Pascua Belt, Argentina. Economic Geology, 112, 1747-1771.

Pellicori, D.A., Gammons, C.H. & Poulson, S.R. (2005). Geochemistry and stable isotope composition of the Berkeley pit lake and surrounding mine waters, Butte, Montana. Applied Geochemistry, 20, 2116–2137.

Smedley, P.L. & Kinniburgh, D.G. (2002). A review of the source, behaviour and distribution of arsenic in natural waters. Applied Geochemistry, 17, 517–568.

Stock, B.C., Jackson, A.L., Ward, E.J., Parnell, A.C., Phillips, D.L. & Semmens, B.X. (2018). Analyzing mixing systems using a new generation of Bayesian tracer mixing models. PeerJ, 6, e5096.

Zhang, K.; Shi, Z.; Ding, X.; Ge, L.; Xiong, M.; Zhang, Q.; Lai, W.; Ge, L (2024). Identification of Anthropogenic and Natural Inputs of Sulfate into River System of Carbonate Zn-Pb Mining Area in Southwest China: Evidence from Hydrochemical Composition, δ34SSO4 and δ18OSO4. Water 2024, 16, 2311.

IMWA 2026
Jeongseon

Exploring a New Water Economy Post Mining in a Coal Mining Region

Tshewang Dendup[1,2], Mark A. Lund[1,2], Rachele Bernasconi[1,2,3]

[1]*School of Science, Edith Cowan University, Joondalup, Western Australia 6027, Australia, t.dendup@ecu.edu.au, ORCID 0000-0001-8079-4952*

[2]*Mine Water and Environment Research Centre (MiWER), School of Science, Edith Cowan University, Joondalup, Western Australia 6027, Australia, m.lund@ecu.edu.au, ORCID 0000-0002-2047-3476*

[3]*Mine Water and Environment Research Centre (MiWER), School of Science, Edith Cowan University, Joondalup, Western Australia 6027, Australia, r.bernasconi@ecu.edu.au*

Abstract

Pit lakes are shaped by interactions between water sources. Understanding these interactions is essential for managing water quality and ecological risks post-mining. We studied Lake Kepwari, a rehabilitated coal mine void in Collie, Western Australia. To quantify relative contributions of source waters and evaluate hydrologic controls on lake chemistry, we used diagnostic tools of mixing models (DTMM) and end-member mixing analysis (EMMA). Water samples collected were analysed for isotopic and geochemical compositions. EMMA solutions determined the dominant source waters highlighting potential in determining the sources of salinity or acidity, evaluating lake-groundwater interactions, and impacts on downstream waters.

Keywords: mining lakes, endmember mixing analysis, conservative tracers, groundwater, hydro-geochemistry

Introduction

The successful closure of mine voids as stable, non-polluting water bodies remains a major economic and environmental challenge. In the Collie Coal Basin, Western Australia, Lake Kepwari, a former coal pit, stands as a pioneering example pit lake rehabilitation that lead to the lake being formally relinquished back to the state. After mining ceased in 1997, the void was filled largely with diverted flows from the seasonal Collie River South Branch (CRSB). Since an accidental river breach in 2011, a permanent connection to the CRSB as part of the closure strategy has maintained lake water levels and transformed the system into a flow-through lake, providing intermittent but effective neutralisation of acidity, reduction of dissolved metals, and nutrient inputs (Lund *et al*. 2020; Lund *et al*. 2018). Like many post-mining pit lakes, Kepwari's long-term hydrogeochemical behaviour is governed by intricate interactions between groundwater, surface runoff, spoil geochemistry, submerged sediments, and pit-wall erosion. Hydrogeology is complex due to faulting, mining disturbances, and groundwater abstraction. The pit void intersects the Permian Muja coal measures aquifer hydraulically connecting to the larger regional groundwater system (Varma, 2002).

Geochemical modelling (PHREEQC) and mass balance framework by Salmon *et al*. (2008) suggested that acidity in Lake Kepwari was potentially controlled by iron-rich regional groundwater inflows or internal sources like pyrite oxidation, while river water supplied alkalinity. Later, Salmon *et al*. (2017) using a coupled hydrodynamic-bio-geochemical model (DYRESM–CAEDYM) further demonstrated that water quality evolution was governed by externally driven acidity loading and Fe–Al solubility-controlled processes. The model inferred that the external acidity loading delivered by groundwater throughflow exerted primary geochemical control over the long-term evolution of water quality. PITLAKQ modelling by Müller *et al*. (2010) predicted that besides groundwater exchange, high acidity surface runoff and bank erosion may

explain the lake's re-acidification following the neutral river inflow. Both models were completed prior to river flow through, only including river contributions used to fill the lake. Recent work by Lund *et al.* (2018) suggests that groundwater inflow (based on estimates from Varma, 2002) has declined markedly from ≈2.1 GL per year in 1999 to <0.3 GL per year by 2016, yet internal acidity generation persists and is currently neutralised primarily by river inflows. None of the previous investigations into Lake Kepwari have empirically quantified the proportional contribution of dominant source waters to the lake. Water budget analysis for 2010–2016 indicate that inputs are dominated by highly variable river inflow (28–10,793 ML yr^{-1}), followed by rainfall (397–1,011 ML yr^{-1}), groundwater (≈220–293 ML yr^{-1}), and surface runoff (58–133 ML yr^{-1}). However, large residual errors (−2,244 to +941 ML yr^{-1}) indicate substantial uncertainty in flux estimates and data gaps (Lund *et al.*, 2018).

Environmental tracer techniques have been acknowledged as a powerful tool in understanding the interactions between surface waters and groundwaters including mixing dynamics within the lakes. Specifically, naturally occurring isotopes of water and conservative geochemical tracers are routinely used to quantify source water contributions and track flow path. The literature points to a limited application of these tracer approach within pit lake systems and where it is used, the mixing model and tracers selected can heavily influence the interpretation of the data. This study directly addresses that gap and provides a preliminary first order understanding of mixing processes in the lake, offering new insight into the hydrological controls on acidity generation, solute dynamics, and seasonal transitions.

Methods

Grab water samples were collected in September and October 2025 from all the potential source waters contributing to Lake Kepwari: CRSB inflow and CRSB outflow or lake outflow (n = 4); Groundwater samples (n = 10) from 5 monitoring bore wells (depth ranging from 13 to >100 m below top of casing); Shallow subsurface matrix flow was characterised using drainage lysimeters (n = 3) installed around the lake to intercept near-surface runoff generated during storm events. Additionally, piezometers (n = 3) were installed around the lake perimeter to intercept bank seepage before it entered the lake, enabling characterisation of water derived from wall erosion, subsurface leaching, and near-shore spoil material. A rain sample (n = 2) was obtained from a monthly bulk precipitation collector within the lake catchment. Lake-water samples (n = 12) were collected from surface and bottom waters at three sites located near the inflow, outflow, and mid-lake sections. At each site, full-depth physicochemical profiling was conducted throughout the water column to characterise thermal structure, stratification, and vertical chemical gradients.

Water samples were collected in new 1 L high-density polyethylene (HDPE) bottles and divided into three aliquots for geochemical analysis and one for isotopic analysis. Nutrients and metals/metalloids samples were filtered through disposable 0.45 µm polypropylene syringe filter with glass microfiber (GMF) membrane (Thermo Scientific, USA) within 24 h of collection and stored in 60 mL clean HDPE bottles. Metal samples were acidified to pH <2 using 70% nitric acid and stored at 4 °C. Nutrient and major anion samples were frozen at -20 °C before analysis. Isotope samples were stored in 30 mL glass bottles and sealed with screw caps with no headspace to avoid fractionation and stored at 4 °C until analysis.

Filtered water samples were analysed at Edith Cowan University (ECU) Analytical Facility for dissolved trace metals and metalloids (Al, As, Ba, Cd, Co, Cr, Cs, Cu, Fe, Pb, Mn, Hg, In, Li, Ni, Rb, Sb, Se, Si, Sr, Ti, U, V, and Zn) and common metals (Na^+, K^+, Ca^{2+}, and Mg^{2+}) using inductively coupled plasma-mass spectrometry (ICP-MS) and Inductively Coupled Plasma Optical Emission spectroscopy (ICP-OES). Common ions (Cl^- and SO_4^{2-}) were analysed by Ion Chromatography. Nutrients (NO_X and NH/NH_4) were measured on a Lachat autoanalyser (Hach, USA) and carbon (non-purgeable organic carbon (NPOC) and dissolved inorganic carbon (DIC)) were

measured using a total carbon analyser (Shimadzu, Japan). Total alkalinity was determined by titration using a mini-titrator (Hanna Instruments, USA) on an unfiltered aliquot of the sample to a pH endpoint of 4.5. Samples were also analysed for water isotopes including oxygen-18 (^{18}O) and deuterium (^{2}H) by a L2130-*i* Picarro Cavity Ringdown Spectrometer, at Australian Biogeochemistry Centre, University of Western Australia.

Following the EMMA procedure of Liu *et al.* (2008), end-members (or source waters) and their relative contributions to the lake and river outflow were determined. The conservative tracers and number of end-members were determined without any information from end-members based on the DTMM developed by Hooper (2003). To achieve that, principal component analysis (PCA) was applied on the correlation matrix of standardised lake and river outflow chemistry. Eigenvectors extracted were then used to project lake and river outflow chemistry into mixing U-space following Christophersen and Hooper (1992). This analysis helps identify tracers that exhibit linear mixing behaviour (conservative mixing of end-members with unique chemistry is a linear process), and to determine the dimensionality of the mixing subspace, where the number of U-space dimensions is one less than the number of end-members required (Liu *et al.* 2008; Liu *et al.* 2013). The residuals between the reprojected pit lake chemistry and original values were then examined to evaluate tracer suitability: no structure or trend, randomly distributed residuals ($p>0.05$) indicate conservative behaviour, while systemic trends indicate non-conservative processes. The relative root-mean-square error (RRMSE) was also used to assess the appropriate number of dimensions and to screen out non-conservative tracers; in a well-posed model, RRMSE typically decreases from a one-dimensional (1-D, two–end member) subspace to higher-dimensional subspaces (Frisbee *et al.* 2011; Liu *et al.* 2008).

After defining the conservative tracers and mixing dimensionality, PCA was again performed to extract eigenvectors using a correlation matrix of the standardized conservative tracer set. The lake and river outflow chemistry data were then orthogonally projected using the eigenvectors along with all the end-members. The first two principal components of these tracers were used to construct mixing diagrams in U-space, and candidate end-members were evaluated based on (a) whether they form a polygon that encloses all pit-lake samples, and (b) how well their predicted fractions and concentrations reproduce observed lake chemistry. Final end-member fractions were then solved using the simultaneous-equation approach of Liu *et al.* (2020).

Results and Discussion

All the chemical data of lake and river outflow samples were included in DTMM to identify conservative tracers and the number of end-members. The residuals analysis showed a random distribution for Na^{+}, Mg^{2+}, Ca^{2+}, K^{+}, Cl^{-}, NO_x, Fe, Co, Ni, Sr and U under two dimensions (2-D) ($R^2 \approx 0$; $p > 0.05$) suggesting their conservative behaviour upon mixing of three end-members in lake waters. However, their RRMSE in 2-D mixing spaces exhibited conservative behaviour only for Na^{+}, Mg^{2+}, Ca^{2+}, K^{+}, Cl^{-}, Ni, Sr and U. U was excluded from the conservative tracer set considering its instability in the pit lake system (Gunten *et al.* 2018). The first two eigenvectors (PC1 and PC2) of selected conservative tracers explained 98% of variance confirming that the conservative mixing space is effectively two-dimensional and consistent with a three end-member mixing model. A mixing diagram (Fig. 1a) was constructed in U-space using PC1 and PC2 for the geometric evaluation of end-member mixing. Multiple combinations of three candidate end-members could form a geometrically viable mixing triangle in U-space. However, the mixing triangle that best circumscribed the lake and river outflow sample cloud defined by three vertices were: A groundwater (GW3), river inflow (CRSB-In), and hypolimnetic water (K2 Bottom). The K2 Bottom is not a source water *per se*; rather, it represented a distinct geochemically evolved water mass likely evolved due to evapo-concentration and stratification de-coupling itself from a volumetric mixture of inflow waters.

Persistent stratification is evident from temperature contrasts between surface waters (14.2-16.9 °C in September; 17.5-17.8 °C in October) and bottom waters (12.6-12.7 °C), while electrical conductivity increases systematically with depth (2,280-2,390 µS cm^{-1} at the surface versus 2,930-2,980 µS cm^{-1} at depth), indicating solute accumulation and prolonged hypolimnetic residence times. Dissolved oxygen declines with depth (e.g. 11.36 mg L^{-1} at K1 Top versus 8.34 mg L^{-1} at K1 Bottom in September, and 95% versus 73-77% saturation in October).

EMMA demonstrates a pronounced vertical separation of water sources within Lake Kepwari during initial stratified conditions (Fig. 1b). Surface waters (K1-K3 Top) comprise mixed proportions of groundwater (41-45%) and river inflow (27-58%), with hypolimnetic fraction of 1-30%. The K2 Top consisted of 45% groundwater and 38% river inflow in September, shifting towards relatively higher river influence in October (56-58% river inflow at K1-K3 Top). In contrast, bottom waters (K1–K3 Bottom) are consistently dominated by the hypolimnetic fraction (41-83%), with moderate groundwater input (<33%) and negligible river influence in September but considerably higher river fraction in October (38-39%). The river outflow (CRSB-Out) had a mixed river–groundwater signature in both months (river 32-51%; groundwater 41-43%), while hypolimnetic fractions declined from 24% in September to 8% in October.

This finding quantitatively confirms earlier qualitative assessments that river reconnection improves surface-water quality without substantial export of hypolimnetic water during stratification (McCullough 2015; Salmon *et al.* 2017). Notably, EMMA resolves a key ambiguity in previous modelling by showing that groundwater can constitute nearly half of epilimnion volume even when surface-water quality remains favourable. The lake-water chemistry was well reproduced using the end-member fractions derived from EMMA and the ionic compositions of the identified end-members. Recreated versus measured concentrations had their R^2 values over 0.90 for all selected tracers giving confidence in the EMMA solution (Fig. 2).

The mean δ^2H and $\delta^{18}O$ of the water samples in September were -3.80±1.56‰ and -18.06±7.46‰, respectively. The δ^2H and $\delta^{18}O$ values were plotted with Global Meteoric Water Line (GMWL: $\delta^2H = 8\delta^{18}O + 10$) and Local Evaporation Line (LEL) was established using regression line of surface water samples as shown in Fig. 3. The Local Meteoric Water Line (LMWL) of Perth (WA) is shown as a reference (Griffiths *et al.* 2022). Precipitation and groundwater plot close to each other above the GMWL and along LMWL, confirming a meteoric origin with minimal evaporative modification prior to recharge (Priestley *et al.* 2020). Whereas lake waters plot below the GMWL along a LEL, indicating evaporation is also an important process controlling lake chemistry. The slope of 4.5 in LEL is indicative of

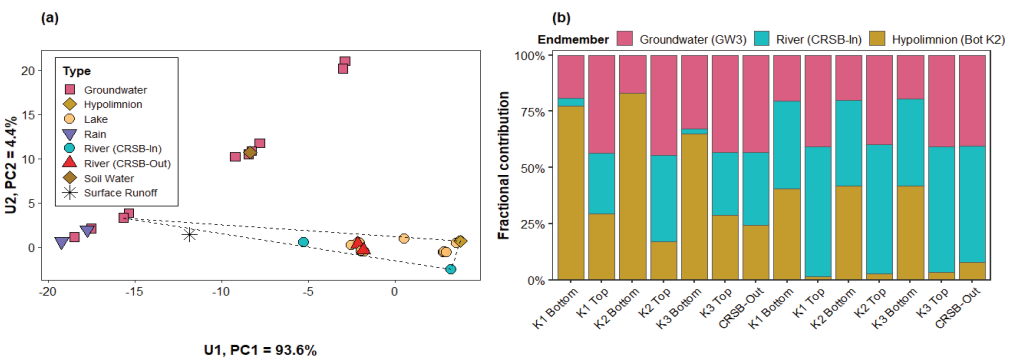

Figure 1 *(a) Mixing diagram using the first two principal components (PC1 and PC2) constructed from 7 tracers; (b) The fractional contributions of three end-members to the Lake Kepwari.*

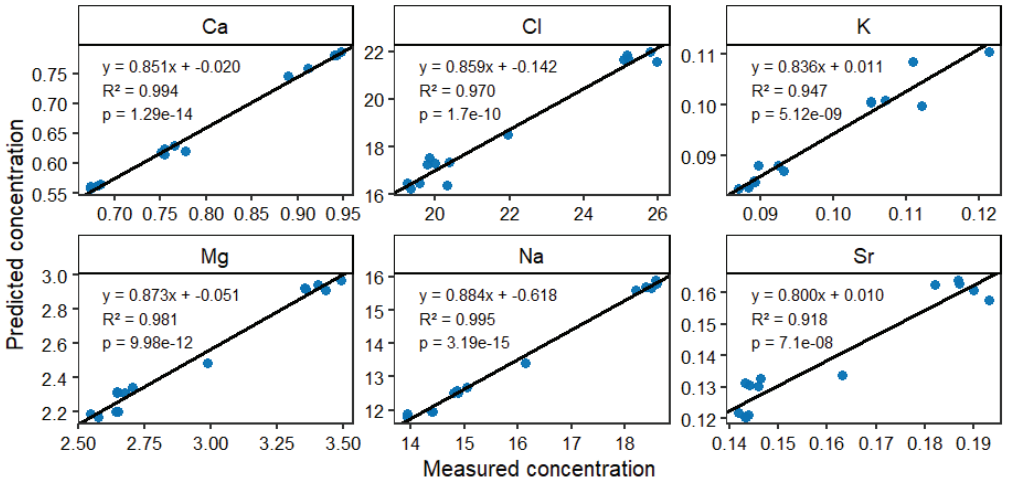

Figure 2 Recreation of ionic concentrations in lake waters based on relative contributions of endmembers determined by endmember mixing analysis (EMMA) and ionic concentrations in endmembers.

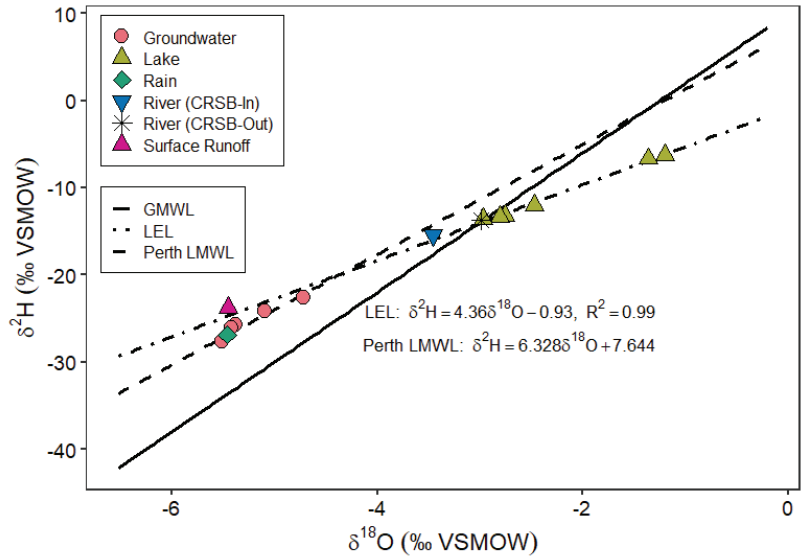

Figure 3 δ^2H–$\delta^{18}O$ stable-isotope cross-plot of lake waters and potential source waters in Lake Kepwari.

evaporation processes in free water bodies within arid or semi-arid regions with low relative humidity (Gibson *et al.* 2008). The K1–K3 Top samples are moderately enriched ($\delta^{18}O$ = −2.97 to −2.76‰; δ^2H = −13.60 to −13.18‰) and plot closer to river inflow (CRSB-In; $\delta^{18}O$ = −3.46‰, δ^2H = −15.44‰), consistent with EMMA results showing considerable river fraction and active renewal of the epilimnion during early stratification. Active surface-water renewal can promote oxygenation and buffering, favouring the oxidation and attenuation of dissolved metals like Fe(II). In contrast, K1–K3 Bottom are relatively more enriched ($\delta^{18}O$ = −2.47 to −1.20‰; δ^2H = −12.01 to −6.23‰), reflecting longer residence times and a stronger cumulative evaporative signal

prior to isolation. Among bottom samples, K1 and K2 were the most highly evaporated plotting furthest from LMWL on a LEL. These isotopic characteristics align with EMMA results indicating hypolimnetic dominance, supporting the interpretation of chemically evolved bottom waters during stratified conditions. The river CRSB-Out plots along the LEL and overlaps surface-lake values, corroborating EMMA results showing mixed river and groundwater contributions and negligible hypolimnetic export.

Conclusions

These preliminary findings demonstrate the applicability of the conjunctive use of tracer-based DTMM and EMMA for determining source waters and their relative contributions in flow-through pit lakes, as supported by stable isotope results. Our results highlight the critical roles of hydrologic controls and evaporative enrichment in shaping the water quality of Lake Kepwari. Consequently, EMMA can provide a robust empirical tool for understanding hydrogeochemical processes that govern pit lake water quality and quantity, thereby guiding effective mine closure strategies.

Acknowledgements

The authors thank Premier Coal Ltd (managed by Yancoal Australia Ltd) for their support. The authors also thank Mark Bannister at ECU and other volunteers for their support.

References

Andrys J, Kala J, Lyons TJ (2017) Regional climate projections of mean and extreme climate for the southwest of Western Australia (1970–1999 compared to 2030–2059). Climate Dynamics 48(5):1723-1747. https://doi.org/10.1007/s00382-016-3169-5

Christophersen N, Hooper RP (1992) Multivariate analysis of stream water chemical data: The use of principal components analysis for the end-member mixing problem. Water Resources Research 28(1):99-107. https://doi.org/https://doi.org/10.1029/91WR02518

Frisbee MD, Phillips FM, Campbell AR, Liu F, Sanchez SA (2011) Streamflow generation in a large, alpine watershed in the southern Rocky Mountains of Colorado: Is streamflow generation simply the aggregation of hillslope runoff responses? Water Resources Research 47(6). https://doi.org/https://doi.org/10.1029/2010WR009391

Gibson JJ, Birks SJ, Edwards TWD (2008) Global prediction of δA and δ2H-δ18O evaporation slopes for lakes and soil water accounting for seasonality. Global Biogeochemical Cycles 22(2). https://doi.org/https://doi.org/10.1029/2007GB002997

Griffiths AD, Treble PC, Hope P, Rudeva I (2022) Rainfall Stable Water Isotope Variability in Coastal Southwestern Western Australia and Its Relationship to Climate on Multiple Timescales. Journal of Geophysical Research: Atmospheres 127(1):e2021JD035433. https://doi.org/https://doi.org/10.1029/2021JD035433

Gunten Kv, Warchola T, Donner MW, Cossio M, Hao W, Boothman C, Lloyd J, Siddique T, Partin CA, Flynn SL, Rosaasen A, Konhauser KO, Alessi DS (2018) Biogeochemistry of U, Ni, and As in two meromictic pit lakes at the Cluff Lake uranium mine, northern Saskatchewan. Canadian Journal of Earth Sciences 55(5):463-474. https://doi.org/10.1139/cjes-2017-0149

Hooper RP (2003) Diagnostic tools for mixing models of stream water chemistry. Water Resources Research 39(3). https://doi.org/https://doi.org/10.1029/2002WR001528

Liu F, Bales RC, Conklin MH, Conrad ME (2008) Streamflow generation from snowmelt in semi-arid, seasonally snow-covered, forested catchments, Valles Caldera, New Mexico. Water Resources Research 44(12)

Liu F, Hunsaker C, Bales RC (2013) Controls of streamflow generation in small catchments across the snow–rain transition in the Southern Sierra Nevada, California. Hydrological Processes 27(14):1959-1972. https://doi.org/https://doi.org/10.1002/hyp.9304

Liu F, Lerch RN, Yang J, Peters G (2020) Determining hydrologic pathways of streamflow using geochemical tracers in a claypan watershed. Hydrological Processes 34(11):2494-2509. https://doi.org/https://doi.org/10.1002/hyp.13743

Lund M, van Etten E, Polifka J, Vasquez MQ, Ramessur R, Yangzom D, Blanchette ML (2020) The importance of catchments to mine-pit lakes: Implications for closure. Mine Water and the Environment 39(3):572-588

Lund MA, Blanchette ML, Harkin C Seasonal river flow-through as a pit lake closure strategy: is it a sustainable option in a drying climate. In: Proceedings, 11th ICARD| IMWA| MWD conference: risk to opportunity, 2018. vol 1. 34-41 p

McCullough CD (2015) Consequences and opportunities from river breach and decant of an acidic mine pit lake. Ecological Engineering 85:328-338. https://doi.org/https://doi.org/10.1016/j.ecoleng.2015.10.001

Müller M, Eulitz K, McCullough C, Lund M (2010) Mine voids management strategy (V): water quality modelling of Collie Basin Pit Lakes. MiWER/Centre for Ecosystem Management Report 10

Priestley SC, Meredith KT, Treble PC, Cendón DI, Griffiths AD, Hollins SE, Baker A, Pigois J-P (2020) A 35 ka record of groundwater recharge in south-west Australia using stable water isotopes. Science of The Total Environment 717:135105. https://doi.org/https://doi.org/10.1016/j.scitotenv.2019.135105

Salmon SU, Hipsey MR, Wake GW, Ivey GN, Oldham CE (2017) Quantifying Lake Water Quality Evolution: Coupled Geochemistry, Hydrodynamics, and Aquatic Ecology in an Acidic Pit Lake. Environmental Science & Technology 51(17):9864-9875. https://doi.org/10.1021/acs.est.7b01432

Salmon SU, Oldham CE, Ivey GN (2008) Assessing internal and external controls on lake water quality: Limitations on organic carbon-driven alkalinity generation in acidic pit lakes. Water Resources Research 44(10). https://doi.org/https://doi.org/10.1029/2007WR005959

Varma, S. (2002). Hydrogeology and groundwater resources of the Collie Basin, Western Australia. Resource Science Division, Water and Rivers Commission.

Implementing the Watershed-Scale Approach to Remediation of Acid Mine Drainage from Abandoned Mine Lands in West Virginia, USA

Nathan DePriest[1], Rachel Spirnak[2]

[1]*West Virginia Water Research Institute, West Virginia University, Morgantown, WV, USA, nate.depriest@mail.wvu.edu, ORCID 0009-0008-2965-4733*

[2]*West Virginia Water Research Institute, West Virginia University, Morgantown, WV, USA, rachel.spirnak@mail.wvu.edu, ORCID 0000-0003-2999-198X*

Abstract

The West Virginia Water Research Institute (WVWRI) characterized watersheds in West Virginia (WV), USA, with water quality impairment from acid mine drainage (AMD) from abandoned mine lands (AML), prioritized such watersheds for watershed-scale AMD remediation, and developed conceptual plans for remediation. The characterization and prioritization procedures developed in the project provided a valuable blueprint for evaluating AMD impairments at a watershed scale. Prioritization of watersheds promoted informed decisions on remediation implementation. Designs documented critical considerations for remediation planning. Successful demonstration of the approach through this project aims to promote widespread implementation.

Keywords: Mine drainage, remediation, restoration, watersheds, abandoned mine lands

Introduction

Acid mine drainage (AMD) affects approximately 4,000 stream km in West Virginia (WV), USA (Skousen *et al.* 2019). Remediation of AMD in WV has historically utilized a point-source approach focused on treatment of individual regulated discharges, including active mining operations and bond forfeiture (BF) sites. Limitations to the approach are evident in restoration efficacy and cost, as the majority of AMD impairment in WV watersheds is often from unregulated abandoned mine land (AML) discharges. AML discharges remediation typically utilizes at-source passive treatment due to limited funding. Recent funding of approximately $140 million allocated to WV through the Infrastructure Investment and Jobs Act (IIJA) in each fiscal year 2022 through 2025 provides an unprecedented opportunity to remediate AMD from AML in WV at a larger scale.

The watershed-scale approach to AMD remediation aims to comprehensively address AMD throughout a watershed to balance restoration outcomes with long-term treatment cost. Implementation of the approach has been limited in WV, but a project in the Muddy Creek watershed demonstrated favorable economic and restoration outcomes by using combined in-stream and centralized treatment (Spirnak *et al.* 2025). Beyond Muddy Creek, watershed-scale projects in WV have been limited to in-stream treatment (e.g., Three Forks Creek Watershed) (Petty *et al.* 2008). Case studies, particularly using the centralized approach, are limited even at a conceptual or preliminary design level. Design of new watershed-scale AMD remediation projects is necessary to better understand implementation of the approach and to determine the most efficacious AMD remediation strategy in WV.

Implementation, financial, and environmental factors contribute to a watershed's suitability for watershed-scale remediation. While the spatial distribution of AML and associated AMD impairments is somewhat well known (WVDEP 2024a), the severity of impairment is not understood well enough to inform allocation of remediation funding. Widespread characterization efforts are necessary to support remediation decisions. WV also has unique jurisdictional concerns that have not been adequately

evaluated. BF sites in WV, which are forfeited to the State when companies can no longer meet their treatment liability, must be treated to regulatory compliance. Watershed projects that require remediation of AMD sources of different jurisdictions (active regulated, BF regulated, AML unregulated) are difficult to pursue under current policies. Watersheds with AMD primarily or exclusively from AML are desirable targets because they do not require a discharge permit for treatment.

Methods

Watershed Characterization

Characterization efforts were focused in northern WV, where coal mine drainage is particularly acidic, causes widespread stream impairment, and is commonly associated with AML. Desktop evaluations considered watershed hydrology, stream impairment, AMD source jurisdiction (active, BF, and AML), mining history, and pollutant load. From November 2023 to December 2025, over 1,700 water quality samples were collected in over 50 watersheds. Four (4) were identified as priority watersheds for routine sampling: Robinson Run (HUC 050200030309), Greens Run (050200040705), Heather-Lick Run (HUC 50200040702), and Headwaters Deckers Creek (050200030201). All four watersheds are located within the Monongahela River basin in Monongalia and Preston Counties. Samples were classified according to type (in-stream, at-source AML, at-source BF, at-source active). Typical field parameters were monitored: flow, pH, temperature, conductivity, total dissolved solids (TDS), dissolved oxygen (DO), and oxidation reduction potential (ORP). Samples were collected for laboratory analysis of a full suite of AMD parameters, including alkalinity, acidity, and total and dissolved individual major metals.

Project Prioritization

Preliminary project prioritization considered treatment feasibility, restoration potential, existing data, and West Virginia Department of Environmental Protection (WVDEP) priorities. Preliminary subjective prioritization through informal mechanisms was necessary to identify watersheds of interest for initial and routine sampling. In parallel, a Watershed-Scale AMD Remediation Decision Tool was developed to promote objective watershed project prioritization by AMD treatment operators and decision-makers moving forward (Marino 2025). The tool used Multi-Criteria Decision Analysis (MCDA) and specifically the Analytical Hierarchy Process (AHP) method. MCDA is a useful decision-making tool when alternatives have multiple, often conflicting, variables to consider (Al-Bayati and Al-Zubaid 2020; Kozlov and Norek 2021). AHP is appropriate for both quantitative and qualitative assessments and has been successfully applied in site suitability, prioritization of research areas, and funding allocation decisions (Elghazouly *et al.* 2022). The Decision Tool was constructed in three levels: categories, subcategories, and criteria. Decision Tool criteria were developed using the Delphi Method (Okoli and Pawlowski 2004). A long list of criteria was developed by a multi-disciplinary team of engineers, geologists, chemists, biologists, and environmental scientists at WVWRI, then refined to a short list based on feedback from stakeholders and decision makers (e.g., local watershed groups, WVDEP). A rubric was developed to provide objective measures for scoring individual criteria on a scale of 1 to 5. Individual criteria scores were summed to develop subcategory scores. Weights were assigned to categories and subcategories based on feedback from stakeholders and decision makers. Criteria scores were combined with subcategory and category weights to determine a score for a given watershed on a scale of 0 to 1, with 1 corresponding to the highest priority. The Decision Tool was applied to one existing and one proposed watershed-scale AMD remediation project for validation and refinement. Additional details on tool development, criteria development and weighting, rubric development, and scoring are provided by Marino (2025).

Remediation Design

Conceptual designs were developed for four priority watersheds. Designs focused on centralized treatment as the remediation

mechanism whenever possible. Designs identified the primary AMD sources of concern and methods for at-source treatment, elimination, or capture and conveyance to a centralized treatment location. Hydrologic and hydraulic constraints were used to evaluate treatment feasibility and identify a centralized treatment location. Designs focused on gravity conveyance of consolidated sources whenever possible to avoid operational and maintenance concerns associated with pumping AMD. Consolidation of sources and conveyance via the underground mines themselves was promoted to limit hydraulic conveyance lines. Preliminary designs are in progress. In preliminary designs, detailed methods for source capture and conveyance, active treatment, and sludge disposal are being evaluated.

Results and Discussion

Watershed Characterization

The four priority watersheds account for approximately 117 km of stream impaired by AMD and are 69-81% impaired by length (WVDEP 2016). Total underground coal mining in these watersheds was 6,855 hectares (ha); 42% of mining was classified as AML, and most mining occurred in the Upper Freeport (46%) or Pittsburgh (44%) coal seams (R. Toth, WVGES, personal communication, 2025). Over 90% of AMD discharges were classified as unregulated AML in all watersheds, except for Robinson Run, in which 39% of AMD discharges were from active regulated mining. Total acidity, iron, and aluminum loads for all watersheds from desktop evaluations of Total Maximum Daily Load (TMDL) reports were 3,514, 1,029, and 465 metric tons per year (tpy), respectively (WVDEP 2014, WVDEP 2024b).

Of the over 1,700 water quality samples collected in the project, 1,138 were collected in the four priority watersheds. At-source and in-stream samples accounted for 855 and 162 samples, respectively. Sampled AMD sources confirmed low pH and high acidity, iron, and aluminum (Tab. 1). Pollutant loads based on source sampling were similar but higher than those obtained via desktop analysis of TMDL reports. Preference was given to the data gathered from extensive sampling rather than TMDL reports, as the TMDL reports utilized modeling of less refined and recent data.

Project Prioritization

The Decision Tool was constructed in three levels (Fig. 1). Level 1 categories consisted of Implementation, Financial, and Environmental considerations. Implementation subcategories were Technical Feasibility and Community Engagement, financial subcategories were Cost and Benefit, and environmental subcategories were Impairments and Restoration. Weights for categories 1, 2, and 3 were assigned as 35, 30, and 35%, respectively, and subcategory weights were evenly split within each category. Decision-makers preferred an even distribution of weights to a higher weight for one category over the other.

Muddy Creek is the most robust existing watershed-scale AMD remediation project in WV and provided the opportunity to validate the tool and inform criteria scoring using existing data. Application of the tool

Table 1 *Summary of hydrologic and water quality data for sampled AMD sources in priority watersheds.*

Watershed	Stream length impaired by AMD (km)	No. AMD sources	Percent AML sources (%)	Flow (m^3/s), total	Acidity load (tpy), total	Iron load (tpy), total	Aluminum load (tpy), total
Greens Run	24.5	19	95	0.150	2,563	429	156
Robinson Run	16.7	24	61	0.052	1,175	285	72
Heather-Lick Run	15.4	51	98	0.202	2,104	261	175
Headwaters Deckers Creek	60.5	36	92	0.111	1,107	314	55
Total	117.1	130	–	0.515	6,949	1,289	458

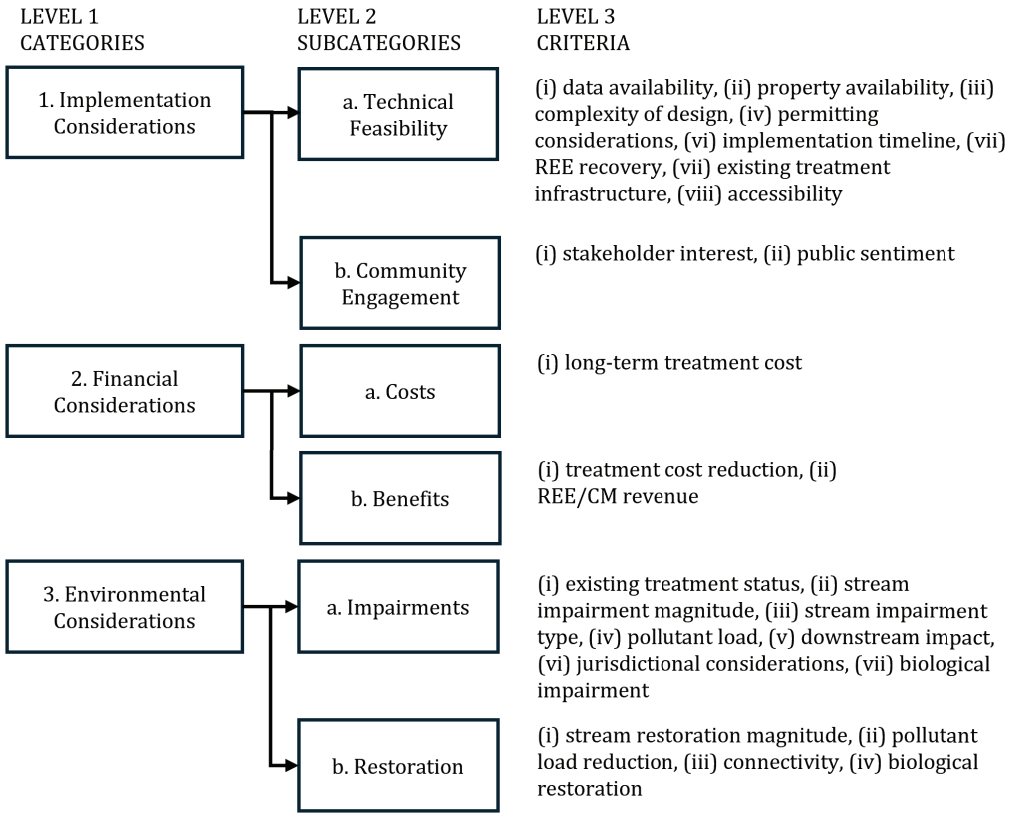

Figure 1 *Watershed-Scale AMD Remediation Decision Tool hierarchical structure and criteria.*

to Greens Run also evaluated the tool's effectiveness when evaluating a proposed project. The final scores for Muddy Creek and Greens Run were 0.622 and 0.654, respectively. Both watersheds have a similar level of impairment, restoration potential, and community engagement. Pollutant sources in Greens Run, however, are clustered more closely together, which improved technical feasibility and stream restoration magnitude. Proposed treatment in Greens Run would use centralized treatment, while treatment in Muddy Creek relied on a combination of centralized treatment for clustered sources and isolated in-stream treatment for sources in headwaters.

Preliminary application of the Decision Tool highlighted the following valuable considerations for scoring additional proposed projects moving forward: i) watershed size and pollutant spatial distribution were key factors in technical feasibility and stream restoration magnitude and should be considered closely; ii) quantitative criteria and scoring should be implemented whenever possible, as qualitative criteria (e.g., community engagement, public sentiment) are important but difficult to judge objectively; ii) databases should be built out as the tool is applied to more watersheds, as some quantitative criteria (e.g., treatment cost, biological impairment/restoration) lacked comprehensive data to easily score; iii) weighting of criteria is dependent on the number of criteria within that subcategory, so criteria should be limited to the minimum amount needed to adequately assess a watershed. Revisions to the Decision Tool based on the above considerations will be completed in future work. The Decision Tool will then be applied to a larger project dataset to produce a prioritized list based on Decision Tool output.

Remediation Design

Conceptual designs highlighted the importance of a watershed-specific approach to AMD remediation. Three of the four watersheds focused on centralized treatment, while one watershed (Headwaters Deckers Creek) required a network of at-source passive treatment systems due to the dispersed nature of the AMD. Most watersheds using the centralized approach can address all AMD discharges of interest with one centralized plant (Greens Run [Fig.2], Robinson Run), while one will need to complement centralized treatment with at-source passive or in-stream active treatment in the headwaters (Heather-Lick Run). Due to regulatory challenges, conceptual designs focused on AML sources only. When possible, however, design contingencies were recommended to account for regulated discharges (BF and active sites). These regulated discharges may be integrated into treatment if future policy allows.

In-progress preliminary plans for Greens Run and Robinson Run estimate total project costs at $9.5 and $11.2 million, respectively. Many design considerations were consistent across both watersheds and can inform remediation design in other watersheds. Priority considerations were as follows: i) pumping of AMD was limited by prioritizing gravity conveyance whenever possible through gravity lines or conveyance within the underground mines themselves; ii) a reliable location for long-term sludge disposal was identified at an early stage; iii) to minimize required maintenance for conveyance lines, pretreatment was installed where possible to convert any ferrous iron to ferric iron prior to collection; and, iv) extraneous surface water was separated from AMD wherever possible to limit treated flow to AMD only.

Treatment plant locations aimed to promote gravity flow and limit hydraulic conveyance lines. In Greens Run, this can be more easily accomplished due to proximity

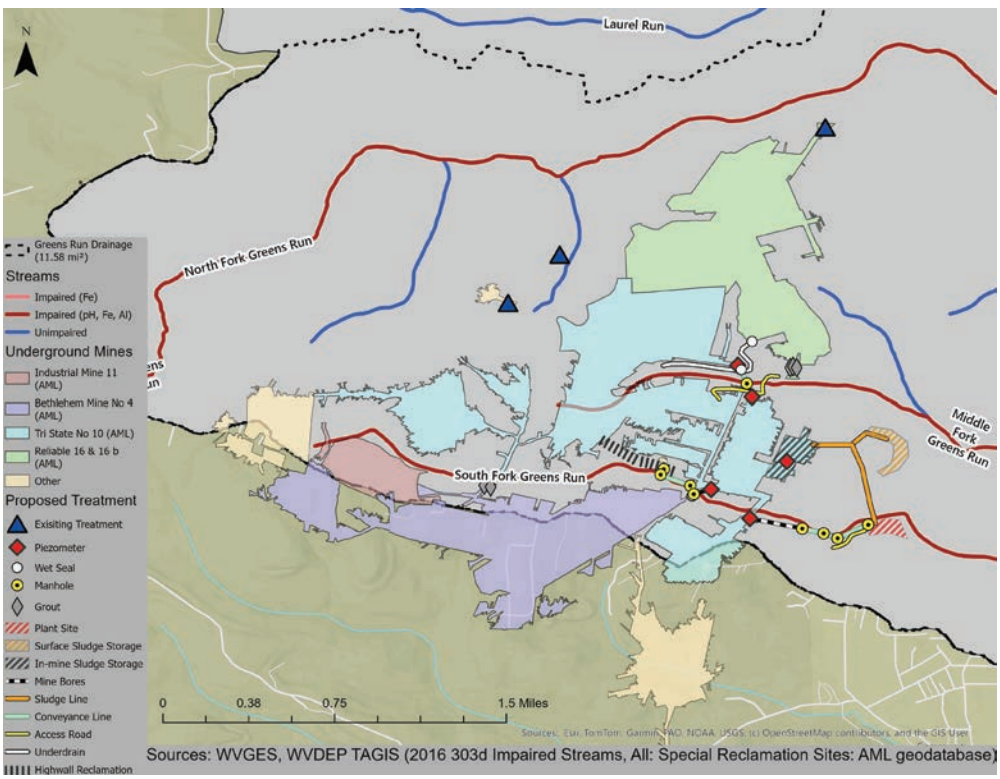

Figure 2 *Conceptual design for watershed-scale AMD remediation in the Greens Run watershed.*

of the sources to each other. In Robinson Run, pumping some sources to a centralized location is unavoidable due to limited locations for the plant site. Sludge disposal was a primary challenge, as almost all mines are up-dip and free-draining. Isolated sections of mines are limited but will be utilized for underground disposal, as surface storage is not feasible due to space constraints. Treatment plants will use rectangular clarifiers. This uncommon alternative to conventional circular clarifiers has been successfully implemented by WVDEP at multiple AMD treatment plants and has benefits in construction and maintenance; concrete clarifier structures can be pre-cast, smaller mechanical components can perform better in acidic conditions and be more easily replaced, and a rectangular footprint can be easily covered to mitigate weather concerns. Landowner considerations played a critical role in both projects. A network of individual private landowners who are supportive of the project was necessary to prove the feasibility of Greens Run, while the support of one to two private corporation landowners were instrumental in Robinson Run. Even with widespread landowner support, the scale of these projects (15 properties in Greens, 22 properties in Robinson) resulted in tailoring treatment plans to specifically avoid individual landowners not amenable to the project.

Conclusions

Watersheds across northern WV with impairments from AML AMD were identified as candidates for watershed-scale AMD remediation. Conceptual designs demonstrated the watershed-specific nature of evaluating remediation alternatives while also highlighting remediation mechanisms and design constraints that can be considered across all watershed projects. A Watershed-Scale AMD Remediation Decision Tool was developed to promote objective project prioritization and remediation funding allocations moving forward. Decision Tool development highlighted the importance of technical feasibility and restoration potential The multi-faceted, iterative approach utilized in this study can be employed in other regions to characterize, prioritize, and design watershed-scale AMD treatment with favorable economic and restoration outcomes.

Acknowledgements

The authors thank our colleagues at the West Virginia Water Research Institute (WVWRI) and West Virginia University (WVU) who contributed to this project and the West Virginia Department of Environmental Protection Office of Abandoned Mine Lands and Reclamation (WVDEP AML) for sponsoring this project.

References

Al-Bayati, II, Al-Zubaidy SS (2020) Applying the analytical hierarchy process and weighted sum model for small project selection in Iraq." IOP Conf. Ser.: Mater. Sci. Eng. 671 (1): 012158, doi:10.1088/1757-899X/671/1/012158

Elghazouly HG, Elnaggar AM, Ayaad SM, Nassar, ET (2022) Framework for integrating multi-criteria decision analysis and geographic information system (MCDA-GIS) for improving slums interventions policies in Cairo, Egypt. Alexandria Engr J 86, 277–288, doi:10.1016/j.aej.2023.11.059

Kozlov V, Norek T (2021) Towards objective multi-criteria drone evaluation based on VIKOR and COMET methods. Procedia Comput Sci. 192: 4522–4531, doi:10.1016/j.procs.2021.09.230

Okoli C, Pawlowski SD (2004) The Delphi method as a research tool: An example, design considerations and applications. Info & Mgmt 42(1), 15–29, doi:10.1016/j.im.2003.11.002

Marino JN (2025) Prioritizing AMD impaired watersheds for watershed-scale restoration using multi-criteria decision analysis. Graduate Theses, Dissertations, and Problem Reports. 12853. https://researchrepository.wvu.edu/etd/12853, doi:10.33915/etd.12853

Petty JT, Gutta B, Herd R, Fulton F, Stiles J, Strager M, Svetlick J, Ziemkiewicz P (2008) Identifying cost-effective restoration strategies in mining impacted West Virginia watersheds. In: Barnhisel RI (Ed), Proceedings of 2008 national meeting of the American Society of Mining and Reclamation: new opportunities to apply our science. Richard, VA p 837—355, doi:10.21000/JASMR08010837

Skousen JG, Ziemkiewicz PF, McDonald LM (2019) Acid mine drainage formation, control and treatment: approaches and strategies. Extr Ind Soc 6(1):241-249, doi:10.1007/s10230-025-01052-1

Spirnak R, Shafer M, Risch C, O'Neal M, Ziemkiewicz P (2025) Evaluation of watershed-scale acid mine drainage treatment in the Muddy Creek Watershed, West Virginia. Mine Water Environ 44:579-594, doi:10.1007/s10230-025-01052-1

WVDEP (2014) Total Maximum Daily Loads for Selected Streams in the Monongahela River Watershed, West Virginia. West Virginia Department of Environmental

Protection, Division of Water and Waste Management, Charleston, WV, US

WVDEP (2016) 2016 West Virginia Integrated Water Quality Monitoring and Assessment Report. West Virginia Department of Environmental Protection, Division of Water and Waste Management, Charleston, WV, US

WVDEP (2024a) SHP WVDEP GIS Data Abandoned Mine Lands Problem Inventory Point. https://tagis.dep.wv.gov/data/vector/SHP_WVDEP_GIS_data_abandoned_mine_lands_problem_inventory_point.zip Accessed 2026-03-06

WVDEP (2024b) Cheat TMDL 2010 Metals and pH Allocations Spreadsheet. Division of Water and Waste Management Water Quality Standards and Assessment Section, Charleston, WV, US

Study on Water Quality Evolution of Water Inrush from Typical Coal Mine Roof Cretaceous Aquifer in WesternChina Mining Area

Jia Ding[1,2], Shuning Dong[1,2], Xiaoming Guo[1,2], Feng Liu[1,2], Wenzhong Zhang[1,2]

[1]*CCTEG Xi'an Research Institute (Group) Co., Ltd., Xi'an 710077, China*

[2]*State Key Laboratory of Coal Mine Disaster Prevention and Control, Xi'an 710077, China*

Abstract

To clarify the hydrogeochemical evolution mechanism of roof inflow water in Cretaceous aquifers of western China coal mines, this study takes Dafosi Coal Mine as the research object, combining field sampling, laboratory testing and PHREEQC geochemical modeling to analyze the water-rock interaction process during the migration of Luohe Formation aquifer water through Jurassic strata to the mining face. The results show that silicate mineral dissolution and cation exchange are the dominant processes altering inflow water quality: Ca^{2+}/Mg^{2+} in groundwater are adsorbed by clay minerals and exchanged with Na^{+}, leading to a sharp increase in Na^{+} and a significant decrease in Ca^{2+}/Mg^{2+}; silicate weathering consumes CO_2/H^{+}, keeping water slightly alkaline and increasing TDS by ~50%. The water type evolves from HCO_3–Mg·Na·(Ca) to HCO_3–Na (actual inrush water is HCO_3·SO_4–Na). A field roof water inrush event verifies the simulation results, and neglecting such evolution will reduce the reliability of traditional static hydrochemical fingerprint methods for water source identification. It is recommended to incorporate water quality evolution analysis into mine water hazard assessment.

Keywords: Western China coal mine; cretaceous aquifer; roof water inflow; hydrogeochemical evolution; water-rock interaction; PHREEQC

Introduction

Coal is the core energy source for China's energy security, and mining activities are accelerating westward with the depletion of eastern coal resources (Wu *et al.* 2022). Western China coal basins are faced with complex hydrogeological conditions, and roof water inrush from Cretaceous Luohe Formation sandstone aquifers above Jurassic coal seams has become a major hidden danger restricting safe mining (Zeng *et al.* 2023).

Rapid and accurate identification of water inrush sources is the key to mine water hazard control (Motyka *et al.* 2024). Traditional methods rely on the static "hydrochemical fingerprint" of aquifers, but groundwater undergoes continuous water-rock interaction during migration along fracture paths in mining environments, leading to dynamic changes in chemical composition (Jiang *et al.* 2024). In the Ordos Basin and other western mining areas, Luohe Formation groundwater migrates downward through Jurassic strata after the roof fracture zone is connected, and its hydrochemical characteristics are altered by dissolution and ion exchange (Hao *et al.* 2021; Samborska-Goik *et al.* 2024), which may cause misidentification of water sources if ignored.

This study selects Dafosi Coal Mine (Binchang mining area, Shaanxi Province) with typical Cretaceous roof water inrush as the research site, collects water/rock samples for laboratory analysis, and uses PHREEQC to simulate the hydrochemical evolution process. The research results provide a scientific basis for the accurate identification of roof water inrush sources in western China coal mines.

Study Area and Hydrogeological Setting

Dafosi Coal Mine is located in the southern Binchang mining area of the Huanglong Jurassic coal basin, a national high-risk area for mine water disasters. The mine mainly mines the No.4 coal seam of the Jurassic Yan'an Formation at a depth of ~400 m, with prominent roof water inrush hazard from the Cretaceous Luohe Formation.

The study area has a layered aquifer system, and the Huanhe Formation aquitard effectively isolates the shallow Quaternary aquifer, so the roof inflow water is mainly from the Cretaceous Luohe Formation aquifer directly overlying the Jurassic coal measures (Fig.1). The Luohe Formation is composed of loosely cemented sandstone with high porosity, permeability and water yield capacity; the underlying Jurassic strata (Anding, Zhiluo, Yan'an Formations) are fractured and easy to cave in during mining.

When the No.4 coal seam is mined, the roof forms a caved zone and a fissure zone. Once the fissure zone is connected with the Luohe aquifer, pressurized groundwater migrates downward along fractures through Jurassic strata to the mining face, and undergoes full water-rock interaction with broken rock mass during migration, leading to hydrochemical changes. This hydrogeological characteristic makes Dafosi Coal Mine an ideal object for studying water quality evolution of roof inflow water.

Materials and Methods

Sampling and Laboratory Analysis

Groundwater sampling was carried out in the pre-drained borehole above the 40203 longwall panel of Dafosi Coal Mine on March 20 and 22, 2025. After sufficient purging, samples were filtered, stored and acidified in aliquots, and in-situ pH/temperature were measured. Cations (K^+, Na^+, Ca^{2+}, Mg^{2+}) were determined by ICP-OES, anions (Cl^-, SO_4^{2-}, HCO_3^-) by ion chromatography, and HCO_3^- was cross-checked by titration. The average values of the two samples were taken as the initial hydrochemical data (Tab.1).

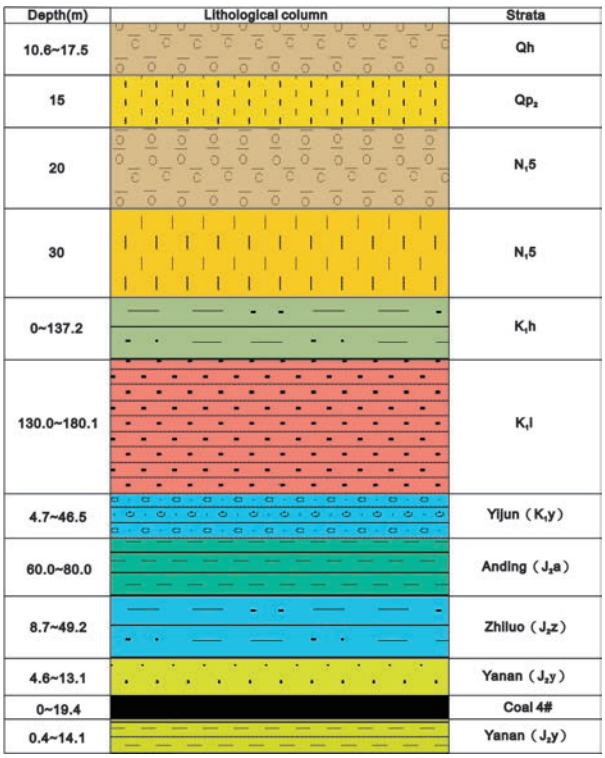

Figure 1 *Generalized hydrogeological column of Dafosi Coal Mine area.*

Table 1 Major ion concentrations of Luohe Formation aquifer water.

Date	K^+ (mg/L)	Na^+ (mg/L)	Ca^{2+} (mg/L)	Mg^{2+} (mg/L)	Cl^- (mg/L)	SO_4^{2-} (mg/L)	HCO^{3-} (mg/L)	TDS (mg/L)	pH
2025/03/20	1.16	53.18	32.36	30.63	6.12	347.24	347.24	516.53	8.00
2025/03/22	1.56	74.2	34.18	31.89	32.65	308.57	308.57	551.75	8.22
Average	1.36	63.69	33.27	31.26	19.385	50.99	327.905	534.14	8.11

Table 2 Mineral composition of roof strata rock samples (Only a portion is displayed due to space constraints).

Sample number	X-ray diffraction analysis results	Mineral composition and content
	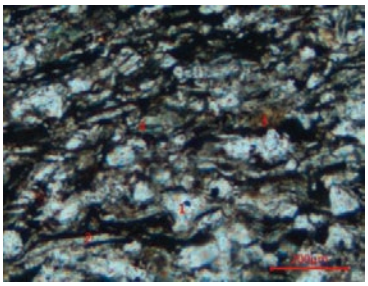	Clay minerals ~45% Muscovite ~30% Quartz ~15% Mica ~6% Chlorite ~4% Metal minerals <1%
	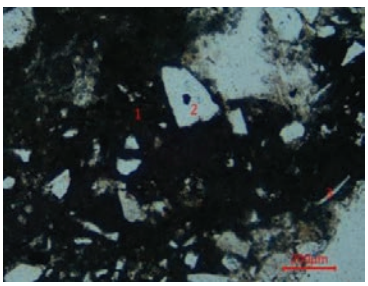	Clay minerals ~70% Muscovite ~3% Quartz ~10% Sericite ~12% Chalcedony ~4% Calcite ~1%

Eight representative core samples were collected from the Jurassic Anding/Zhiluo Formations between the Luohe aquifer and the No.4 coal seam. XRD analysis was performed on air-dried and crushed samples to determine mineral composition. The results show that the roof strata are dominated by silicate minerals: clay minerals (illite/chlorite) account for 45%~85% of most samples (strong cation exchange capacity), followed by quartz (10%~50%), with small amounts of muscovite, feldspar and trace calcite cement. The high clay content provides material conditions for water-rock interaction.

Geochemical Modeling

PHREEQC hydrogeochemical simulation software was used to construct the reaction path model of Luohe aquifer water reacting with Jurassic roof rocks. The initial solution was the average hydrochemical composition of Luohe aquifer water, and the reaction mineral phases included illite, chlorite, K-feldspar, plagioclase, quartz, calcite and pyrite (based on XRD results, Tab 2).

The model set reaction control conditions: calcite/gypsum for equilibrium dissolution-precipitation, silicate minerals for kinetic dissolution (literature rate parameters), and clay surface cation exchange for equilibrium

reaction (literature ion exchange capacity). The simulation was carried out with reaction progress from 0 (initial aquifer water) to 1 (full equilibrium with rock mass), and the changes of pH, major ion concentration and TDS were calculated to identify the dominant geochemical processes and water chemistry evolution trends.

Results and Discussion

Simulated Water Chemistry Evolution by Water-Rock Interaction

PHREEQC simulation results show that silicate mineral dissolution and cation exchange are the two dominant geochemical processes driving hydrochemical evolution, and water chemistry indicators change regularly with reaction progress. Cation exchange is the core process of cation composition change: Na^+ concentration rises sharply from 63.69 mg/L to ~230 mg/L, while Ca^{2+} and Mg^{2+} decrease to near zero. The essence is the exchange between Ca^{2+}/Mg^{2+}in water and Na^+ on clay minerals, with the reaction equation:

Silicate mineral dissolution releases K^+/Na^+ and produces H_4SiO_4, and its weathering consumes H^+/CO_2 to generate additional HCO_3^-, keeping HCO_3^- concentration high and water slightly alkaline (pH rises from 8.11 to 8.2~8.7). Ion release from cation exchange and silicate dissolution leads to a ~50% increase in TDS (from 534.14 mg/L to ~795 mg/L). With the progress of water-rock interaction, the original HCO_3–Mg·Na·(Ca) type water gradually evolves into HCO_3–Na type water with high Na^+, high SiO_2, low $Ca^{2+}$and low Mg^{2+}.

Field Validation by Roof Water Inrush Event

On October 15~16, 2024, a roof water inrush event occurred in the 40103 longwall panel of Dafosi Coal Mine (maximum inflow ~200 m^3/h). Water samples were collected from the fault inflow point for hydrochemical testing, and the results were compared with the simulation data and original aquifer water characteristics, as shown in Tab. 3.

The hydrochemical characteristics of actual inrush water are highly consistent with the simulation results: Na^+ concentration increases sharply, Ca^{2+}/Mg^{2+} decrease significantly (Mg^{2+} is nearly completely depleted), pH rises and TDS increases by ~50%. The actual water type is HCO_3·SO_4–Na, and the high SO_4^{2-} is related to pyrite oxidation under mining disturbance and residual pore water

Table 3 *Comparison of hydrochemical characteristics of original aquifer water.*

Index	Initial aquifer water sample (simulation initial)	Simulate the water sample after the reaction	Actual water sample(2024/10/16)
Hydrochemical type	HCO_3-Mg·Na·(Ca)	HCO_3-Na	HCO_3·SO_4-Na
pH	8.11	8.72	8.68
TDS (mg/L)	534	795	813~819
Na^+ (mg/L)	63.7	233	233~240
Ca^{2+} (mg/L)	33.3	9.1	6.5~11.6
Mg^{2+} (mg/L)	31.3	1.4	1.1~1.5
K^+ (mg/L)	1.36	2.5	2.3~2.7
HCO_3^- (mg/L)	328	330	333~335
Cl^- (mg/L)	19.4	19(initial)	52~67
SO_4^{2-} (mg/L)	51.0	51(initial)	116~141

mixing in Jurassic strata. The consistency verifies the reliability of the simulated water-rock interaction process and evolution trend.

Impact on Mine Water Source Identification

The hydrochemical evolution of roof inflow water has a critical impact on traditional static hydrochemical fingerprint identification: the original Luohe aquifer water is HCO_3–Mg·Na·(Ca) type, while the actual inrush water is HCO_3·SO_4–Na type with high Na^+ and low Ca^{2+}/Mg^{2+}. If the evolution process is ignored, the hydrochemical characteristics of inrush water will be inconsistent with the aquifer baseline data, which may lead to misjudgment that the inrush water is a mixture of Luohe aquifer and other deep aquifers.

In western China Jurassic coal mines with developed roof fractures and strong water-rock interaction, the aquifer hydrochemical fingerprint is a dynamic characteristic changing with groundwater migration. The traditional direct comparison method is difficult to meet the accuracy requirements, and it is necessary to incorporate hydro-geochemical evolution analysis into the identification system and combine geochemical modeling to predict water chemistry variation, so as to improve the reliability of water source identification.

Conclusions

The original water of the Cretaceous Luohe Formation aquifer in Dafosi Coal Mine is HCO_3–Mg·Na·(Ca) type with moderate mineralization (TDS=534.14 mg/L) and slightly alkaline (pH=8.11). The Jurassic roof strata are dominated by clay minerals (illite/chlorite) with high cation exchange capacity, which provides the material basis for water-rock interaction. Silicate mineral dissolution and cation exchange are the dominant geochemical processes of water quality evolution: cation exchange leads to a sharp increase of Na^+ and a significant decrease of Ca^{2+}/Mg^{2+}; silicate weathering maintains the slight alkalinity of groundwater (pH=8.2~8.7) and increases TDS by about 50%, and the water type evolves to HCO_3–Na type with high SiO_2 content.

The field roof water inrush event verifies the simulation results: the inrush water is HCO_3·SO_4–Na type, with Na^+ increased to 233.33 mg/L, Ca^{2+}/Mg^{2+} decreased to 9.09/1.36 mg/L, TDS increased to 795.23 mg/L and pH rose to 8.72, which is highly consistent with the predicted evolution trend. Neglecting hydrogeochemical evolution will reduce the accuracy of traditional static hydrochemical fingerprint methods. For western China coal mines with complex hydrogeological conditions, it is necessary to incorporate water quality evolution analysis into mine water hazard assessment and combine geochemical modeling to predict the dynamic variation of water chemistry, so as to improve the reliability of water inrush source identification and the scientificity of mine water hazard prevention and control.

References

Wu M, Hu N, Ye Y, *et al* (2022) Multi-hazard risk characterization and collaborative control oriented to space in non-coal underground mines. Scientific Reports 12:. https://doi.org/10.1038/s41598-022-20437-8

Zeng Y, Mei A, Wu Q, *et al*. Double verification and quantitative traceability for mixed mine water sources[J]. Journal of Hydrology, 2024, 630: 130725.

Motyka J, Cień D, d'Obyrn K. The Use of Hydrochemical Zoning to Predict Water Hazards[J]. Mine Water and the Environment, 2024, 43(2): 198-209.

Jiang Y, Liu H, Liang T, *et al* (2024) Impact of water-rock interaction on natural fractures and shale permeabilities under the closure stress. Geoenergy Science and Engineering 243:213357. https://doi.org/10.1016/j.geoen.2024.213357

Hao C, Gui H, Sheng L, *et al* (2021) Contrasting water–rock interaction behaviors of antimony and arsenic in contaminated rivers around an antimony mine, Hunan Province, China. Geochemistry 81:125748. https://doi.org/10.1016/j.chemer.2021.125748

Rivas S, Sanchez-Alfaro P, Alvarez-Amado F, *et al* (2024) Water-rock interaction and magmatic contribution in thermal fluids of the Southern Volcanic Zone, Chile: Insights from Li, B and Sr isotopes. Journal of Volcanology and Geothermal Research 453:108149. https://doi.org/10.1016/j.jvolgeores.2024.108149

Samborska-Goik K, Ulańczyk R, Krupanek J, Pogrzeba M (2024) A PHREEQC-Based Tool for Planning and Control of In Situ Chemical Oxidation Treatment. Applied Sciences 14:3600. https://doi.org/10.3390/app14093600

Geochemical Responses and Environmental Feasibility of Managed Aquifer Recharge with Mine Water in Coal Mining Areas

Shuning Dong[1,2,3], Xiyu Zhang[1,2,3], Hongjie Shi[1,2], Qiang, Wu[4], Xiaoming Guo[1,2], Tiantian Wang[1,2],Feng Liu[1,2], Donglin Dong[4], Wenjie Sun[4], Yifan Zeng[4], Peitao Li[4]

[1]*CCTEG Xi'an Research Institute (Group) Co., Ltd., Xi'an 710054, China*

[2]*Coal Mine Hazard Prevention and Control National Key Laboratory, Xi'an 710054, China*

[3]*School of Energy and Power Engineering, Xi'an Jiaotong University, Xi'an, 710049, China*

[4]*China University of Mining & Technology (Beijing), Beijing 100083, China*

Abstract

The coal-water mismatch in China induces severe groundwater depletion in arid mining regions. This study proposes Mine Water Managed Aquifer Recharge (MMAR), a source-treatment-storage framework that returns treated mine water to aquifers for near-zero discharge. In-situ trials at Mindong No.1 Mine revealed that near-field processes involved cation exchange, mineral dissolution, and organic carbon mobilization, whereas the far-field accumulated refractory organics and microbial protein-like substances. Cross-zonal cation bridging exacerbates bio-chemical clogging. Low-disturbance pretreatment and zonal monitoring are recommended to ensure long-term groundwater sustainability.

Keywords: Mine water Managed Aquifer Recharge (MMAR), hydrochemical evolution, dissolved organic matter, secondary mobilization

Introduction

Coal remains fundamental to China's energy security, yet its distribution exhibits a severe spatial mismatch with water resources. The central and western regions hold nearly 90% of the national coal resources but possess limited water, situating coal-abundant areas predominantly in arid and semi-arid zones (Peng *et al.* 2015; Yuan 2023). As coal exploitation shifts westward, intensive deep mining severely disturbs overlying aquifers, leading to massive groundwater ingress and the loss of over 6 billion tons of groundwater through drainage-dominated hazard control measures (Gu *et al.* 2021). While current management emphasizes source protection and surface reuse, limited industrial water demand in western mining areas causes large volumes of treated mine water to be discharged as surface runoff. This permanent conversion of groundwater to surface water causes sustained depletion of regional groundwater systems. In ecologically fragile zones, this depletion manifests as persistent water level drawdowns, vegetation degradation, and severe spring desiccation (Wang *et al.* 2025). In intensely dewatered regions like the Huanglong mining area, maximum local drawdowns reaching 194.87 m compress aquifer storage space and diminish hydraulic conductivity, leading to the functional attenuation of the entire groundwater system (Fan *et al.* 2020).

To address these insidious environmental risks, this study proposes the Mine Water Managed Aquifer Recharge (MMAR) conceptual framework. By constructing a circulation pathway, MMAR aims to achieve sustainable water circulation by returning mine water to underground aquifers. Focusing on the complex biogeochemical risks associated with this system, an in-situ recharge trial was conducted at the Mindong No. 1 Mine. This study elucidates the mechanisms of environmental responses within the MMAR system, providing a scientific basis for developing risk management strategies based on geo-

chemical compatibility and facilitating the green transformation of water conservation technologies.

Mine water Managed Aquifer Recharge

To sustain the groundwater eco-environment amid the coal-water mismatch, this study proposes the Mine Water Managed Aquifer Recharge (MMAR) conceptual framework. MMAR utilizes engineering measures—including surface ecological infiltration, pressurized well-field recharge, and underground cross-aquifer redistribution—to construct a "Source-Treatment-Storage" closed loop. This approach returns mine water to underground systems, minimizing surface discharge (Fig. 1).

MMAR encompasses three primary recharge modes: (1) diverting and reallocating threatening, unentered groundwater in-situ via underground boreholes; (2) treating ingressed mine water for surface infiltration to sustain shallow ecological aquifers; and (3) injecting treated mine water ex-situ into primary water-supply aquifers via pressurized well fields. By reconstructing impaired flow fields, MMAR strives for near-zero discharge and the simultaneous remediation of mining hazards and ecosystems (Miao et al. 2025).

However, implementing MMAR in deep, complex environments creates a coupled system involving stress, flow, and geochemical processes, introducing multiple risks. Macroscopically, artificial flow field reconstruction may threaten underlying coal extraction. Microscopically, MMAR faces highly concealed biogeochemical environmental risks (Fakhreddine *et al.* 2021; Imig *et al.* 2022). Injecting treated mine water with different hydrochemical characteristics inevitably disrupts the native aquifer's dynamic equilibrium (Sun *et al.* 2020; Fakhreddine *et al.* 2021). This incompatibility makes the system susceptible to recharge pathway clogging and secondary hydrogeochemical deterioration (Antoniou *et al.* 2014; Fakhreddine *et al.* 2021). While hydrodynamic threats are manageable, delayed and potentially irreversible biogeochemical risks present a critical barrier.

Given the limited understanding of these water-rock interactions, conducting whole-process water quality evolution studies based on in-situ field trials is essential for scientifically identifying and managing MMAR environmental risks.

Materials and Methods

The Mindong No. 1 Coal Mine in the Yimin Coalfield experiences a considerable inflow of 500 to 600 m^3/h. The lack of effective recycling, juxtaposed against an arid climate with an annual evaporation of 1166 to 1284 mm, causes substantial resource wastage. The study area is underlain by two major aquifer systems: the Cretaceous Yimin Formation aquifer and the Quaternary pore aquifer

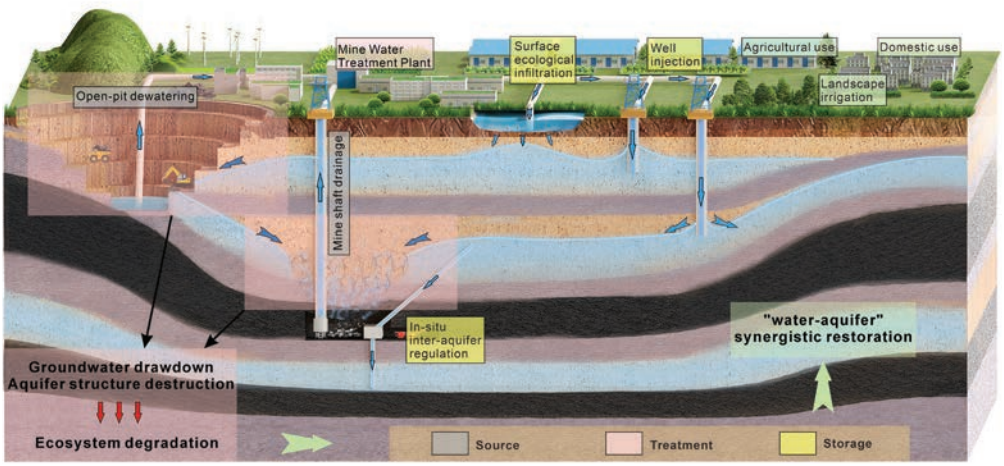

Figure 1 Conceptual model of the M-MAR system.

(average thickness 29.80 m). The Quaternary strata comprise upper silty-fine sands and lower sandy gravels. Hydraulic conductivity ranges from 58.17 to 114.09 m/d, and specific capacity ranges from 0.582 to 23.669 L/ (s·m). The phreatic groundwater flows from southeast to northwest (Fig. 2).

The Quaternary aquifer was selected for the recharge experiment. The system comprised an injection well (R1) and five monitoring wells (M2 to M6), supplied by a reservoir 350 m away. Continuous injection lasted 173.5 h, followed by a 65.5 h recovery period. Upon stabilization, the water level depth in R1 was 701.84 m. The monitoring wells achieved dynamic stability within 9 to 12 h, with water level increases of 0.75 to 1.39 m. Groundwater was sampled daily in triplicate, filtered (0.45 μm), stored in brown glass bottles, and analyzed within 24 h.

Water quality parameters, including pH, total hardness, turbidity, total dissolved solids, chloride, nitrate, nitrite, and ammonia nitrogen, were measured (Table 1). Dissolved organic matter was characterized using three-dimensional Excitation-Emission Matrix (EEM) fluorescence spectroscopy. The fluorescence dataset was subsequently decomposed using a three-component Parallel Factor Analysis (PARAFAC) model in MATLAB to identify underlying fluorescence components.

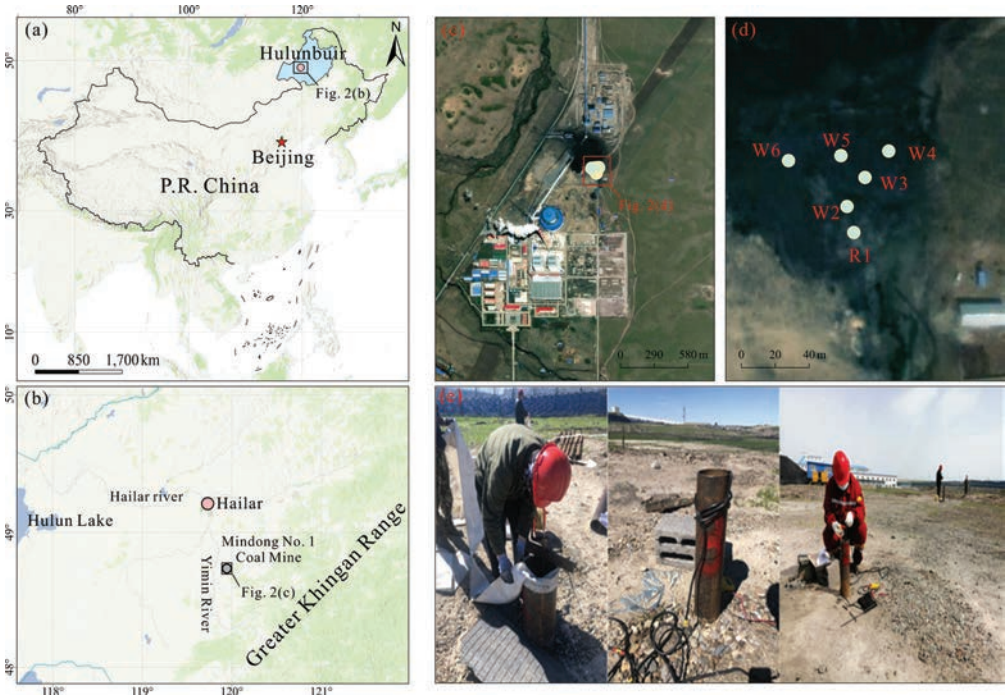

Figure 2 *Conceptual model of the M-MAR system.*

Table 1 *Determination methods of physical and chemical parameters.*

Test items	Unit	Testing method	Reference standard
pH		glass electrode method	DZ/T0064-1993/5
Total hardness	mg/L	Disodium EDTA titration	DZ/T0064-1993/15
TDS	mg/L	105 °C drying method	DZ/T0064-1993/9
Chloride	mg/L	silver nitrate titration	DZ/T0064-1993/50
Nitrate	mg/L	Thyme Powder Spectrophotometry	GB/T5750.5-2006/5.1

Results

Inorganic Hydrochemistry

Initially, pH in all monitoring wells declined, rebounding variably after 5 d. Pre-treated recharge water exhibited low total hardness (≈15 mg/L), whereas ambient groundwater exhibited high hardness. Hardness in most monitoring wells initially exceeded the source water, subsequently declining and stabilizing from 5 d onwards. Conversely, well W2 exhibited increasing hardness from 3 d, peaking at 155 mg/L on 7 d. Total dissolved solids followed an identical pattern, with W3 to W6 remaining low while W2 reached 316 mg/L by 7 d. Chloride concentrations remained below 250 mg/L (4 to 16 mg/L), though W2 maintained higher levels. Nitrate was low in the recharge water, but W2 displayed a short-term nitrate enrichment (peak 4.36 mg/L), likely originating from ammonium desorption and rapid nitrification.

Organic Composition

Dissolved organic carbon and chemical oxygen demand exhibited spatial disparities. After 2 d, dissolved organic carbon in W2 exceeded the recharge water but subsequently declined, while other wells displayed daily increases. Chemical oxygen demand in W2 was initially anomalously high before decreasing; conversely, levels in W2 to W5 increased from 4 d. These spatiotemporal patterns indicate the secondary mobilization of endogenous organic matter triggered by injection. Parallel factor analysis of excitation-emission matrix data identified three primary fluorescent components. Component C1 (Ex/Em = 240/380 nm) corresponds to a highly mobile, terrestrial fulvic acid-like substance (Harjung *et al.* 2019). Component C2 (Ex/Em = 265/440 nm) is a terrestrial humic-like component characterized by high aromaticity (Chen *et al.* 2017; Tang *et al.*

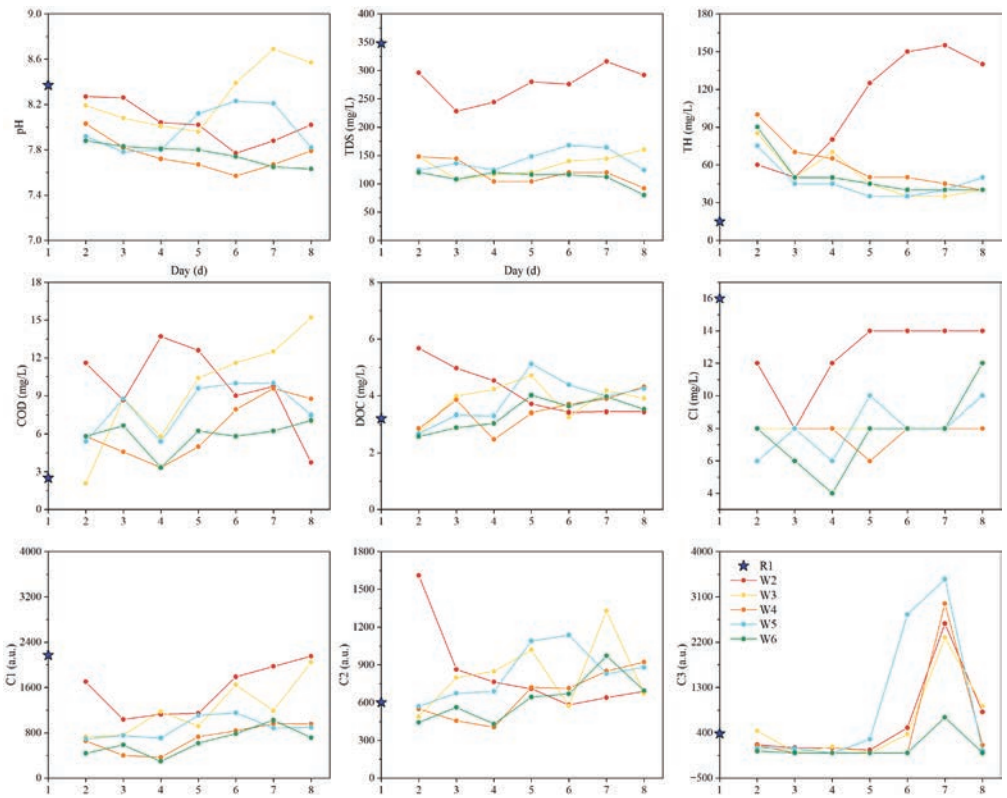

Figure 3 Temporal variations of major hydrochemical components.

2024). Component C3 (Ex peak ≈300 nm, Em peak ≈340 nm) is a protein-like component derived from biological activity (Yamashita *et al*. 2010; Eder *et al*. 2022).

Discussion

Hydrochemical Response Characteristics

Maintaining a constant recharge rate of 12 L/ min in the injection well (R1) raised the groundwater level from 702 to 715 m, inducing a substantial hydraulic gradient. Wells W2 to W6 exhibited a synchronous rapid rise on the first day, followed by a slower ascent governed by the superimposed native flow field and recharge mound. Hydrochemical evolution demonstrated a spatiotemporal lag between pressure propagation and solute transport (Fig. 3). Based on chloride and total dissolved solids variations, the aquifer comprises two distinct regions. The rapid response zone (near-field, R1 to W2) showed immediate chloride and total dissolved solids responses, indicating advection-dominated rapid mixing where near-field hydrochemistry became controlled by the injectant. The transitional zone (far-field, W3 to W6) showed solute concentrations remaining low and increasing only around 5 d, demonstrating that the solute transport front lagged the pressure wave. Intense hydraulic disturbance induced anomalous geochemical responses. In the transitional zone, total hardness declined due to dilution by the injected soft water (≈15 mg/L). Conversely, in the rapid response zone (W2), total hardness rapidly spiked to 150 mg/L between 5 d and 8 d. This anomaly, alongside a rapid surge of nitrate, is attributed to intensified cation exchange (displacing adsorbed Ca^{2+} and Mg^{2+}) and carbonate mineral dissolution driven by high flow velocities and the Na-rich, carbonate-undersaturated injectant. Consequently, near-field hydrochemistry is dominated by mineral leaching and cation exchange, masking physical dilution.

Spatiotemporal Evolution of DOM

Dissolved organic matter evolution diverged markedly from theoretical mixing predictions. Component C1 (fulvic acid-like) maintained high levels in the rapid response zone and accumulated in the transitional zone, eventually approaching source water levels (>2000 a.u.) and dominating the aquifer background (>50%). Component C2 (humic-like) mirrored this accumulation. Initially, C2 in W2 exceeded source water levels, indicating that hydraulic scouring caused the secondary mobilization of adsorbed humic acids. While mixing influences organic content, the accumulation of C1 and C2 over time and distance dominates. Conversely, the protein-like component C3 exhibited reactive generation, surging in both zones around 5 d to 6 d (reaching 3451 a.u. in W5). Because C3 was negligible in the source water, this burst precludes physical mixing. Initially, hydraulic disturbance mobilized endogenous organic carbon in the near-field (chemical oxygen demand reached 11.6 mg/L). This mobilized carbon was transported downstream, providing abundant substrate for microbes in the transitional zone. Furthermore, the upstream release of Ca^{2+} and Mg^{2+} stimulated microbial extracellular polymeric substance secretion. Therefore, the release of hardness components and endogenous organic carbon jointly drove the explosive growth of metabolic by-products (C3), marking a shift to microbially dominated processes.

Conceptual Model of Environmental Response in MMAR

Based on these findings, a conceptual model of the MMAR groundwater environmental response was established (Fig. 4). Discharged mine water, despite pre-treatment, retains ionic and organic disparities compared to native groundwater. This incompatibility creates two spatial response zones. In the rapid response zone, forced convection and inorganic re-equilibration dominate. The injection of Na-dominated, carbonate-undersaturated water triggers vigorous cation exchange and mineral dissolution, displacing Ca^{2+} and Mg^{2+}. Concurrently, hydraulic scouring desorbs endogenous organic carbon, causing an instantaneous release of organic load. This secondary mobilization masks dilution, creating a near-field hydrogeochemical anomaly. In the transitional zone, the dominant process shifts to organic accumulation and biogeochemical transformations. Refractory humic

substances (C1/C2) migrate to the far-field, while endogenous organics from the near-field fuel microbial activity, leading to an explosive growth of protein-like components (C3). A critical cross-zonal coupling occurs where high concentrations of Ca^{2+} and Mg^{2+} from the near-field interact with C1 and C3 via cation bridging, promoting organic colloid flocculation and biofilm consolidation. This exposes the far-field to severe bio-chemical composite clogging risks.

Environmental Implications and Risk Control Strategies

In-situ trials validate MMAR's hydraulic feasibility for elevating groundwater levels without irreversible flow field alterations. However, geochemical incompatibility necessitates a paradigm shift to prioritize geochemical compatibility alongside hydraulic loading. Pre-treatment should adhere to a minimal interference principle. Rather than pursuing absolute purity, it should modulate the ionic strength and sodium adsorption ratio of the recharge water to match the receiving aquifer, minimizing matrix dissolution and pollutant desorption driven by cation exchange. Enhanced removal of colloids and dissolved organic matter is also recommended to eliminate carriers that facilitate pollutant co-transport. Furthermore, long-term MMAR operation is threatened by deep bio-chemical composite clogging. Divalent cations (Ca^{2+}/Mg^{2+}) promote suspended particle flocculation and stimulate microbial extracellular polymeric substance secretion, forming recalcitrant clogging layers. Consequently, operational management requires a zonal warning strategy. In the near-field, abrupt changes in hardness and total dissolved solids should trigger interventions, such as adjusting injection rates, to suppress cation exchange. In the far-field, lagged peaks in protein-like fluorescence (C3) or chemical oxygen demand serve as precursors to deep bio-clogging, necessitating timely responses like backwashing or applying bacteriostats to destabilize biofilms.

Conclusion

This study proposes the Mine Water Managed Aquifer Recharge (MMAR) theoretical framework, utilizing in-situ trials, hydrochemical analysis, and three-dimensional fluorescence spectroscopy to reveal groundwater evolutionary mechanisms. By integrating multiple geoscientific disciplines, this "source–treatment–storage" pathway enables near-zero mine water discharge, addressing regional coal-water constraints. Field trials at the Mindong No. 1 Mine elucidated specific biogeochemical patterns during MMAR implementation. In

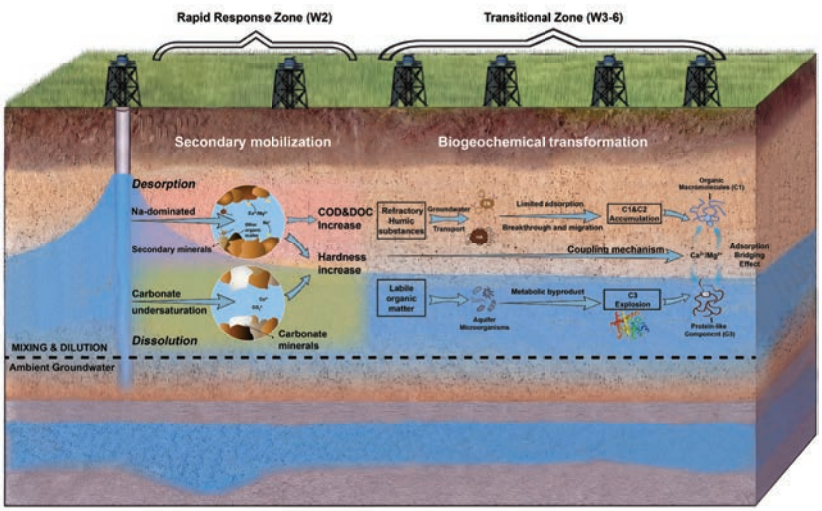

Figure 4 *Conceptual model of environmental responses to M-MAR.*

the near-field region, strong ion exchange and the secondary mobilization of inorganic and organic components occur. Conversely, in the far-field region, hardness ions interact with protein-like components via complexation and bridging, synergistically contributing to bio-chemical clogging. These mechanisms highlight the necessity of coupled water quality and quantity regulation. Implementing low-disturbance pre-treatment alongside zonal monitoring strategies effectively mitigates clogging risks, ensuring the long-term stability and groundwater sustainability of MMAR systems.

References

Antoniou EA, Hartog N, Van Breukelen BM, Stuyfzand PJ (2014) Aquifer pre-oxidation using permanganate to mitigate water quality deterioration during aquifer storage and recovery. Appl Geochem 50:25–36. https://doi.org/10.1016/j.apgeochem.2014.08.006

Chen M, Kim S-H, Jung H-J, *et al* (2017) Dynamics of dissolved organic matter in riverine sediments affected by weir impoundments: Production, benthic flux, and environmental implications. Water Res 121:150–161. https://doi.org/10.1016/j.watres.2017.05.022

Eder A, Weigelhofer G, Pucher M, *et al* (2022) Pathways and composition of dissolved organic carbon in a small agricultural catchment during base flow conditions. Ecohydrol Hydrobiol 22:96–112. https://doi.org/10.1016/j.ecohyd.2021.07.012

Fakhreddine S, Prommer H, Scanlon BR, *et al* (2021) Mobilization of arsenic and other naturally occurring contaminants during managed aquifer recharge: A critical review. Environ Sci Technol 55:2208–2223. https://doi.org/10.1021/acs.est.0c07492

Fan L, Sun K, Li C, *et al* (2020) Background, thought and method of groundwater monitoring in large coal base of northwest China. J China Coal Soc 45(1): 317–329. https://doi.org/10.13225/j.cnki.jccs.YG19.1617. (In Chinese)

Gu D, Li T, Li J, *et al* (2021) Current status and prospects of coal mine water treatment technology in China. Coal Sci Technol 2021; 49(1): 11–18. https://doi.org/10.13199/j.cnki.cst.2021.01.002. (In Chinese)

Harjung A, Ejarque E, Battin T, *et al* (2019) Experimental evidence reveals impact of drought periods on dissolved organic matter quality and ecosystem metabolism in subalpine streams. Limnol Oceanogr 64:46–60. https://doi.org/10.1002/lno.11018

Imig A, Szabó Z, Halytsia O, *et al* (2022) A review on risk assessment in managed aquifer recharge. Integr Environ Assess Manag 18:1513–1529. https://doi.org/10.1002/ieam.4584

Miao H, Dong S, Wang H, *et al* (2025) Multi-objective allocation optimization model for water resources from a coal mine in the Inner Mongolia-Shaanxi contiguous area. Coal Geol Explor 53(7): 166–176. (In Chinese)

Peng S, Zhang B, Wang T (2015) China's Coal Resources: Octothorpe shaped distribution characteristics and sustainable development strategies. Strateg Stud CAE 17(9): 29–35. (In Chinese)

Sun J, Donn MJ, Gerber P, *et al* (2020) Assessing and managing large-scale geochemical impacts from groundwater replenishment with highly treated reclaimed wastewater. Water Resour Res 56(11):1–24. https://doi.org/10.1029/2020WR028066

Tang T, Zhang L, Tang S, *et al* (2024) Molecular insights into pilot-scale selective removal of emerging contaminants in hospital wastewater. Chem Eng J 500:157097. https://doi.org/10.1016/j.cej.2024.157097

Wang H, Wang Q, Dong S, *et al* (2025) Hydroecological effects of mining and its restoration ways in coal mining areas of Western China. J China Coal Soc 50(1):610–622. https://doi.org/10.13225/j.cnki.jccs.YG24.1527. (In Chinese)

Yamashita Y, Scinto LJ, Maie N, Jaffé R (2010) Dissolved organic matter characteristics across a subtropical wetland's landscape: Application of optical properties in the assessment of environmental dynamics. Ecosystems 13:1006–1019. https://doi.org/10.1007/s10021-010-9370-1

Yuan L (2023) Theory and technology considerations on high-quality development of coal main energy security in China. Bull Chin Acad Sci 2023; 38(1):11–22. https://doi.org/10.16418/j.issn.1000-3045.20220819002. (In Chinese)

Demonstration of a Biological Sulfate Reduction Process at Scale, Treating Acidic, Sulfate-Laden Mining-Influenced Water

Kerri du Preez[1], Ryan Merckel[2]

[1]*Biometallurgy Division, Mintek, 200 Malibongwe Drive, Randburg, Johannesburg 2194, South Africa, kerrid@mintek.co.za, ORCID 0009-0000-5097-9112*

[2]*Biometallurgy Division, Mintek, 200 Malibongwe Drive, Randburg, Johannesburg 2194, South Africa, ryanm@mintek.co.za, ORCID 0000-0002-1289-1598*

Abstract

Mintek's cloSURE® technology treats acidic, sulfate-laden mine-influenced water through biological sulfate reduction followed by sulfide oxidation, producing treated water suitable for re-use. Demonstration-scale operation, treating mine influenced water at 25 m^{-3} d^{-1} achieved sulfate-reduction rates greater than 250 g m^{-3} d^{-1}, and the treated water met South Africa's Target Water Requirements for re-use in irrigated agriculture. However, the water had high concentrations of alkalinity and carbonate minerals, limiting its reuse opportunities. Operation of the plant provided insights into key engineering aspects relating to scale-up and recovery after feed disruptions. Results to date suggest that cloSURE® will be a technically feasible and economically sustainable biological treatment process for sulfate-laden mine waters at field-scale.

Keywords: cloSURE®, mine-influenced water, biological sulfate reduction, sulfide oxidation, trace analysis, residence-time distribution, process scale-up, effluent quality

Introduction

South Africa's coal and goldfields are associated with high amounts of pyrite, resulting in mining influenced water (MIW) that ranges from acidic with high concentrations of sulfate to circum-neutral water. Sulfate concentrations can range from 1 000 mg L^{-1} to above 10 000 mg L^{-1}. Metal concentrations are typically low, leaving almost no opportunity for value recovery. Mintek has been developing and scaling up a semi passive biological sulfate reduction treatment process, cloSURE®, targeting MIW with elevated concentrations of sulfate between 3 000 mg L^{-1} and 4 500 mg L^{-1}. Given the concentrations of sulfate, sulfide management has been an important part of the research and development, and a sulfide oxidation step follows biological sulfate reduction for the production of biosulfur. The aim of the treatment technology is reuse of the treated water in irrigated agriculture, or as an alternate resource to promote post mining activities.

There is only one operating passive biological sulfate reduction plant in South Africa, treating 50 m^3 d^{-1} mine-influenced water emanating from a closed colliery, with sulfate concentrations between 1 200 mg L^{-1} and 1 600 mg L^{-1} (Pulles & Heath, 2009; Pulles *et al.* 2016). The aim of the treatment process is sufficient sulfate reduction for bioneutralisation and precipitation of key metals, in order to meet the discharge requirements to release the treated water to the environment. There have been two active demonstration plants operated in South Africa, which were ultimately terminated despite positive results being reported in the literature (Rode *et al.*, 2004). It is understood by the authors that these active sulfate reduction processes were not sustainable over the long term due to the high costs of the process and the provision of sufficient organic carbon for reduction of elevated sulfate concentrations.

Pulles and Heath (2009) demonstrated that reliance solely on a packed bed of organic

material to provide the electron donor for sulfate reduction did not provide consistently available organic carbon and once the readily hydrolysable carbon was consumed, the bed entered a crash phase, capable of sustaining only limited sulfate reduction. A key focus of the cloSURE® demonstration plant project is on a semi passive process with an inert packed bed (woodchips or waste plastic) coupled with a continuous liquid organic carbon feed, sourced from local waste materials. This is intended to increase the longevity and long-term hydraulic conductivity of the bed, minimising interventions such as churning the bed to release organic carbon which also risks solubilising metal precipitates trapped in the bed. Furthermore, co-treatment of difficult-to-treat organic wastes is realised, such as abattoir wash water or landfill leachate.

This paper evaluates the operational performance of the cloSURE® process at demonstration scale under real mine-water conditions and focuses on treatment efficiency, effluent quality, and process stability.

Process Overview and Operational Conditions

The cloSURE® process consists of two stages. The first step entails biological sulfate reduction, which employs sulfate reducing microbes that use sulfate as the terminal electron acceptor for respiration and organic carbon as an electron donor in energy metabolism. This results in the production of sulfide which binds to bivalent metals forming metal sulfide precipitates, and hydrogencarbonate which generates alkalinity and increases pH values. The sulfate reduction ponds are operated in a down-flow configuration which is intended to simulate a plug-flow reactor and prevent loss of sulfide to the atmosphere. The reactions are as follows:

$$2CH_2O + SO_4^{2-} \rightarrow 2HCO_3^- + H_2S \quad (1)$$

$$H_2S + Me^{2+} \rightarrow MeS + 2H^+ \quad (2)$$

The second step of the process involves the development of a floating biofilm containing sulfur oxidising bacteria which partially oxidise sulfide to biosulfur under conditions where the stoichiometric ratio of sulfide to oxygen is greater than 2:1 (Buisman *et al.* 1990; van Hille and Mooruth 2011). When well established, the floating biofilm minimises oxygen dissolution and maintains low oxygen conditions in the reactor to prevent oxidation of sulfide to sulfate, and it minimises losses of sulfide to the environment. The floating biofilm is harvested to provide a value product containing elemental sulfur which could be used as a fertiliser, and is continuously formed according to the following reaction:

$$2HS^- + O_2 \rightarrow 2S^0 + 2OH^- \quad (3)$$

The layout of the demonstration plant is shown in Figure 1, with two systems each incorporating a biological sulfate reduction pond with an operating volume of 250 m^3 followed by six sulfide oxidation channels each with an operating volume of 45 m^3. The plant was operated continuously, with each system flow rate set at 25 $m^3\ d^{-1}$. Each biological sulfate reduction pond consisted of a packed bed of waste woodchips and was inoculated with effluent collected from prior sulfate reduction piloting studies at the same site. Abattoir wash water was introduced as a carbon and nutrient source to start-up the ponds, and the carbon source was changed to ethanol for continuous operation, due to logistical practicality under demonstration conditions. The pond had a target residence time of 10 d and the ethanol was fed at a molar ratio of 0.67 g chemical oxygen demand to 1.00 g sulfate.

Treated water flowed by gravity to the sulfide oxidation channels, which had a volume of 24 m^3 and a target hydraulic residence time of 7.5 d. Organic carbon and nutrients were introduced for development and maintenance of the sulfur biofilm. The resulting biofilm was harvested periodically. Treated water was routed to a sump and to a mine water storage dam, as well as to irrigation plots for testing of the suitability of the water for re-use in irrigation. The irrigation results are not included in this paper.

The feed water was acidic with an average pH value of 2.7 and variable concentrations of sulfate, between 2 300 mg L^{-1} and 5 900 mg L^{-1}, averaging 2670 mg L^{-1}.

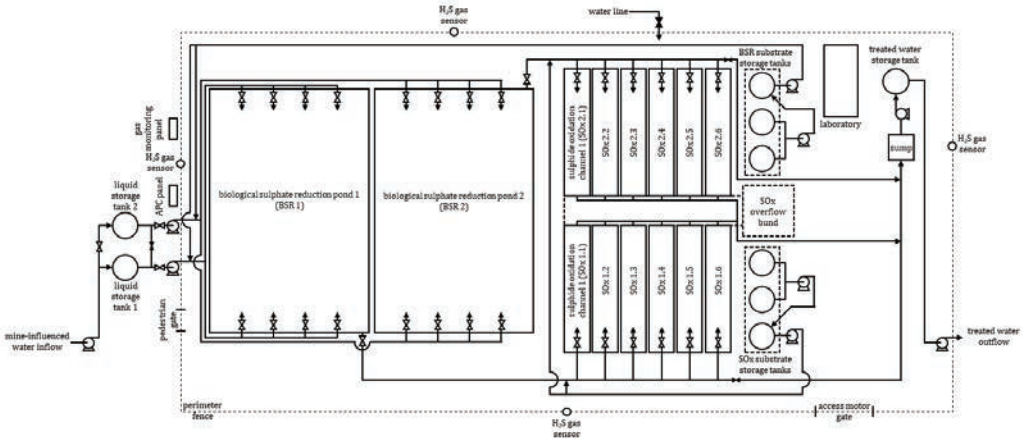

Figure 1 *Schematic showing the cloSURE® demonstration plant layout.*

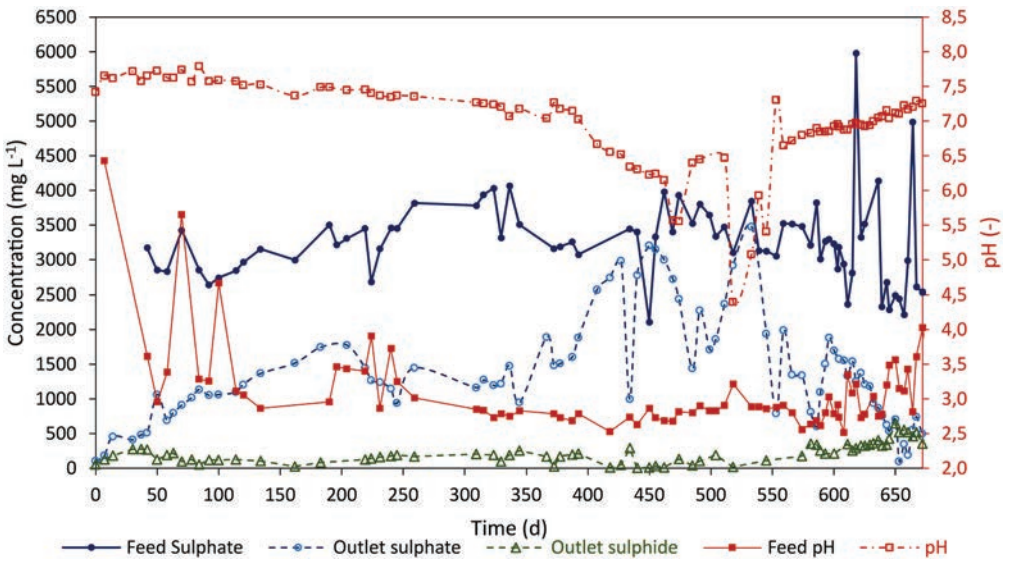

Figure 2 *Time series data for operation of the biological sulfate reduction pond at the cloSURE® demonstration plant.*

Operational Performance

Figure 2 shows the time series data for the biological sulfate reduction pond for the duration of continuous operation. For the first 18 months, of operation, there were a number of challenges with feed availability and consistent flows, blockages of inlets and outlets, scaling of feed lines with iron precipitate, as well as challenges with supplementation of organic carbon. The results during that period show up to 77% removal of sulfate, increases the pH value to 7.2, but inconsistent flows resulted in uncertainties about true sulfate reduction rates and performance. On Day 504 there was a change in the feed quality, likely due to an unknown contaminant from the mine upstream from the dam, resulting in a sudden increase in redox potential -373 mV to -20 mV, and a sudden decrease in pH value from 6.5 to 4.4 in the biological sulfate reduction pond. This indicated microbial activity had ceased. A cell count of an effluent sample showed there were 10^6 cells mL^{-1},

with the cells observed to be active under the microscope. The plant was stopped and the biological sulfate reduction pond allowed to recover in batch mode, while feeding additional organic carbon (abattoir wash water) each week. Over the next six weeks, key operational parameters (pH, sulfate, redox, alkalinity and sulfide) returned to normal in the pond and continuous operation resumed. This disruption indicated that the sulfate reduction step was robust and the microbial consortia were able to tolerate inhibitory conditions with appropriate maintenance measures.

In the remaining three months of operation, feed flows and organic carbon addition were more consistent, and the data suggest the pond was approaching steady state towards the end of the study period. The pH values in the effluent were between 7.0 and 7.5, redox potential decreased to -390 mV, and sulfate concentrations were between 100 mg L^{-1} and 600 mg L^{-1}. The average sulfate reduction rate for the period was 229 g m^{-3} d^{-1} with a maximum of 290 g m^{-3} d^{-1}. Typical values for passive treatment processes range between 28 mg m^{-3} d^{-1} and 76 mg m^{-3} d^{-1} (Pulles, 2009). cloSURE® is not strictly passive as it is intended for treatment of elevated sulfate concentrations and therefore requires addition of an organic carbon source on a regular basis, which enables the higher sulfate reduction rates. Sulfide concentrations in the effluent increased to a maximum of 652 mg L^{-1}, with an average of 397 mg L^{-1}.

Two channels were used to demonstrate the sulfide oxidation step. The data (Figure 3) indicate that at least 274 mg L^{-1} feed sulfide concentration is required before the biofilm and biosulfur product are formed. An average sulfide removal of 56% was achieved, up to a maximum of 80%, indicating there is room for further optimisation, particularly of the type of carbon source and amount of organic carbon and nutrients required. The pH remains stable in this step, and Figure 3 shows that the results are highly reproducible.

At the end of the operating period, the channels were approaching stable operation. A biosulfur product was formed on the surface of the channels, consisting of 59% total sulfur. Other major compounds in the biosulfur product included magnesium, calcium and carbonate compounds.

Final Treated Effluent Quality

Table 1 and 2 compare the average feed water quality with the average treated effluent quality, indicating removal of metals and sulfate and neutralisation of the water. The tables compare the treated water parameters with the most stringent Target Water Quality Requirements (TWQR) from South Africa's Irrigation Water Quality Guidelines, showing that all parameters except manganese meet the requirements for re-use of the treated water in irrigated agriculture.

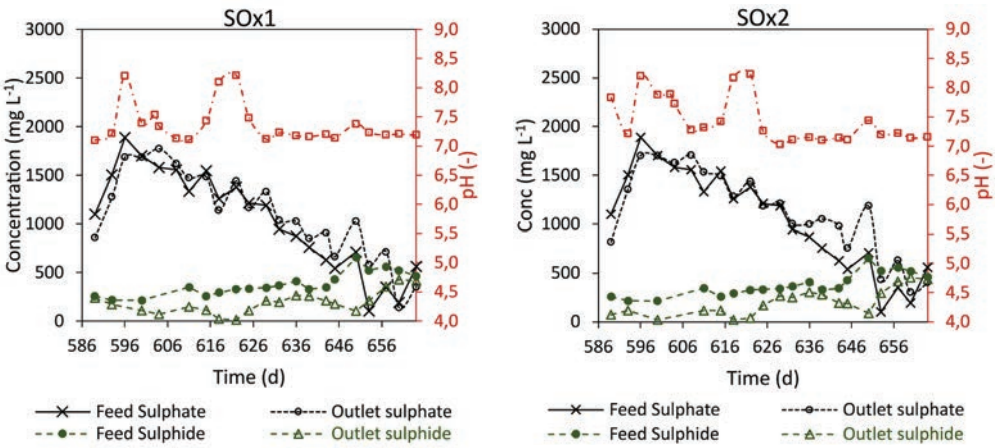

Figure 3 Time series data for the sulfide oxidation (SO×) channels, processing effluent from the biological sufate reduction ponds.

Table 1 Average metals concentrations in the feed and effluent, compared to South Africa's Water Quality Guidelines for Irrigation (red: exceeds TWQR, green: below TWQR).

	Al	Co	Cu	Fe	Mn	Ni	Zn
				mg L^{-1}			
AMD Feed	44	0.2	0.05	240	20	0.2	1
Treated Water	<0.001	<0.001	<0.001	5	18	<0.001	<0.001
TWQR	5	0.05	0.2	5	0.02	0.2	1

Table 2 Average water quality parameters in the feed and effluent, compared to South Africa's Water Quality Guidelines for Irrigation (red: exceeds TWQR, green: below TWQR).

	SO_4	pH	EC	Alkalinity	Cl	F	Na	Ca	Mg	Total N
	mg L^{-1}	–	mS m^{-1}				mg L^{-1}			
AMD Feed	2 670	2.7	29	0	22	3	113	613	277	9
Treated Water	657	7.6	386	1200	22	1	75	-	187	3
TWQR	-	6.5-8.5	-		100	2	-	-	-	-

Table 3 High level comparative costs of the cloSURE® process and reverse osmosis.

Financial Indicator	cloSURE® Plant*	Reverse Osmosis**
Total Fixed Capital Investment	USD 5,760,656	USD 16,304,765
Total operational expenditure	USD 1,177,010	USD 4,602,578
Treatment cost per m^3	USD 0.68	USD 2.67

Exchange rate: USD 1.0000 = ZAR 16.4995, based on the South African Reserve Bank Selected Historical Rates as of 5 March 2026.
* Includes waste management costs ** Excludes waste management and brine treatment/disposal costs

The general assumption is that hydrogencarbonate and carbonate concentrations should be less than 120 mg L^{-1} and 15 mg L^{-1} respectively. As-yet unpublished irrigation trial data have shown poor plant development with the treated water from the cloSURE® process, likely due to the presence of elevated hydrogencarbonate alkalinity. A softening or hydrogencarbonate precipitation step would expand the opportunities for re-use of the treated water.

High-Level Costing

A high-level cost analysis was conducted based on the Guthrie method and the performance data of the demonstration plant, and compared to a reverse osmosis plant treating the same quality water and daily flows (Merckel & du Preez, 2026). A field scale-cloSURE® plant, treating 5 ML d^{-1} with sulfate concentrations between 5000 mg L^{-1} and 7000 mg L^{-1} is expected to have approximately a third of the capital expenditure of a reverse osmosis plant at USD 5.76 million, and operating costs of a quarter of that of reverse osmosis at USD 0.68 m^{-3}, as indicated in Table 3. These costs are a best case scenario, assuming only transport costs for organic waste feedstocks and low cost inert materials for the packed bed. If sulphur sales are incorporated into the cost analysis there is potential for the process to breakeven or make a marginal profit.

Conclusions

The results of the cloSURE® demonstration plant excellent performance in the last three months of operation due to continuous feed and management of reactor in- and outflows. The data suggest that the biological sulfate reduction pond and the sulfide oxidation

channels were approaching steady state, with an average sulfate reduction rate of 229 g $m^{-3}d^{-1}$. Further, no neutralisation or pretreatment of the mine water feed was required, and due to the alkalinity generated in the process, the pH value remains stable post treatment. Metals were removed to within South African Target Water Quality Requirements, except for manganese, and the process is robust and quickly recovered after feed disruptions. A high-level cost analysis indicates the process will be economically feasible over the long term. Further optimization of the process is still required, specifically to reduce the residence time in the biological sulfate reduction ponds, to improve sulfur production in the sulfide oxidation step, and to soften the treated water for improved re-use opportunities. Operation of the demonstration plant provided insights into key engineering aspects relating to scale-up, and transfer and storage of large volumes of mine water for treatment, that are required to develop a technically feasible and economically sustainable biological mine water treatment process.

Acknowledgements

The authors acknowledge and are grateful for the financial support provided by Mintek, the Technology Innovation Agency (TIA), and Thungela Resources for the research presented in this study. Other research partners included in the study are The Moss Group and University of Pretoria.

References

Department of Water Affairs (1996) South African Water Quality Guidelines Volume 4: Agricultural Use – Irrigation. Second edition.

Du Preez, K (2021) Mintek's Integrated cloSURETM Technology for Treatment of Acid Mine Drainage. In International Mine Water Association Conference Proceedings 2021 – Mine Water Management for Future Generations.

Du Preez, K, Marumo, M (2024) Feasibility of the scale-up of a semi-passive biological sulfate reduction process treating high sulfate mine-influenced water. – In: Kleinmann, B., Skousen, J., Wolkersdorfer, Ch.: West Virginia Mine Drainage Task Force Symposium & 15th International Mine Water Association Congress. – p. 157 – 162; Morgantown, WV, USA (International Mine Water Association).

Merckel R. and Du Preez K. (2026) Technoeconomics of the industrial-scale cloSURE® biological treatment process In International Mine Water Association Conference Proceedings 2026 – Sustainability & Efficiency, South Korea.

Molwantwa J., Coetser S., Heath R., Pulles W., Bowker M., Rose P. (2010) Monitoring, evaluation and long-term verification of the passive water treatment plant at VCC. Report no. 1623/1/10, WRC, South Africa.

Neculita, C.M. and Zagury, G.J., 2008. Biological treatment of highly contaminated acid mine drainage in batch reactors: long-term treatment and reactive mixture characterization. Journal of Hazardous Materials, 157(2-3), pp.358-366.

Neale, J.; Gericke, M.; Mühlbauer, R. (2018): On-Site Pilot-Scale Demonstration of a Low-Cost Biological Process for the Treatment of High-Sulfate Mine Waters. Paper presented at 11th ICARD and IMWA Congress – Risk to Opportunity

Pulles, W., Lodewijks, H.M., Toerien, A., Muhlbauer, R., van Niekerk, J.A. & Richardt, A. 2016, 'Passive treatment of acid mine drainage at Vryheid Coronation Colliery, South Africa', in AB Fourie & M Tibbett (eds), Mine Closure 2016: Proceedings of the 11th International Conference on Mine Closure, Australian Centre for Geomechanics, Perth, pp. 425-438, https://doi.org/10.36487/ACG_rep/1608_31_Pulles

Rose P.D., Corbett C.J., Whittington-JonesS K. and Hart O.O. (2004) The Rhodes BioSURE Process. Part 1: Biodesalination of mine drainage wastewaters. WRC Report No. TT 195/04, Water Research Commission, Pretoria.

van Hille, R., Marais, T., Huddy, R., Johnson-Robertson, M., Smart, M., Couperthwaite, J., Horn, E., Pott, E., Naidoo, N., Burke, M., Jian, J. and Harrison, S. (2019) An integrated bioprocess for ARD remediation and renewable energy generation. WRC Report No. K5-2392.

IMWA 2026
Jeongseon

Development of a CO_2 Accounting Methodology for Acid Mine Drainage Treatment Processes and CO_2 Emission Assessment of Real Sites

Guri Du[1], Hsing-Jung Ho[1], Masataka Kondo[2], Yusei Masaki[3], Takaya Hamai[3], Atsushi Iizuka[1]

[1]*Department of Environmental Studies for Advanced Society, Graduate School of Environmental Studies, Tohoku University, 468-1 Aoba-Aramaki, Aoba-ku, Sendai, Miyagi 980-8527, Japan, du.guri.t1@dc.tohoku.ac.jp*

[2]*Metals Technology Center, Japan Organization for Metals and Energy Security, 9-3 Furudate Kosaka-kozan, Kosaka, Akita, Japan*

[3]*Metals Environment Management Department, Japan Organization for Metals and Energy Security, 2-10-1 Toranomon, Minato-ku, Tokyo, Japan*

Abstract

A comprehensive CO_2 accounting method based on carbon mass balance was developed for active acid mine drainage treatment plants. Five emission scopes are defined, covering treatment, internal and external transport, power, and chemical production. Applied to four Japanese plants ranging in scale and using different neutralizers, the results show that calcium-based neutralizers and electricity use dominate emissions. $Ca(OH)_2$ systems can absorb CO_2 under high pH conditions. The method enables plant-specific and cross-plant comparisons, providing a practical framework for decarbonization strategies in the acid mine drainage treatment sector. A CO_2 calculation method was developed and applied to AMD passive treatment system.

Keywords: Acid mine drainage, treatment, CO_2 emission, carbon neutrality

Introduction

Acid mine drainage (AMD) is generated by the oxidation of sulfide minerals during mining activities. These solutions are characterized by low pH and elevated metal concentrations, necessitating their long-term treatment prior to discharge. Active treatment systems that employ alkaline neutralizers, such as limestone ($CaCO_3$) and hydrated lime ($Ca(OH)_2$), are widely used due to their operational reliability and high capacity. These processes are, however, inherently carbon-intensive, because CO_2 is emitted during lime production (calcination), in the neutralization reactions, and owing to electricity generation. Active AMD treatment plants are therefore potential long-term point sources of CO_2 emissions.

Globally, many countries have committed to achieving carbon neutrality by 2050 (IEA 2023). The Japanese government has proposed policies for economic treatment of AMD and aims to achieve carbon neutrality in this industry by 2050 (Ministry of Economy 2023).

Previous studies in South Korea and Germany reported substantial CO_2 emissions from AMD treatment, mainly associated with neutralizer production and application (Kim *et al.* 2025; Totsche *et al.* 2025). Emissions have also been estimated using life cycle assessment and standardized inventory methodologies provided by the Intergovernmental Panel on Climate Change (IPCC 2006). While these approaches offer useful estimates, they rely on generalized emission factors or national-level accounting frameworks that do not fully capture plant-specific operational conditions and inorganic carbon (IC) transformations. To achieve carbon neutrality in the AMD treatment sector, facility-level and process-resolved CO_2 accounting is essential.

This study developed a site-specific CO_2 accounting framework for active AMD

treatment plants based on carbon mass balance, enabling precise quantification of direct and indirect emissions. Unlike conventional methods, it explicitly captures IC transformations and plant-specific operational characteristics, evaluated at four representative active AMD treatment plants in Japan. Its implications for achieving carbon neutrality in the AMD treatment sector are discussed.

Methods

System boundaries

System boundaries were defined to quantify CO_2 emissions from active AMD treatment processes by distinguishing direct and indirect sources (Figure 1). Direct emissions (Scope 1) include CO_2 released during neutralization reactions and biological processes occurring between AMD inflow and treated effluent discharge. Indirect emissions (Scopes 2 and 3) comprise electricity generation and emissions associated with production and transportation of the alkaline neutralizers.

Because flocculant dosage is minor and their manufacturing data are limited, flocculant production is excluded, but its transportation is included. CO_2 exchange during treatment is governed by pH-dependent carbonate equilibria, and direct measurement of gas fluxes is rarely conducted in AMD plants; therefore, CO_2 emissions within the defined boundary were estimated using a carbon mass balance approach that accounts for IC transformations during the neutralization process.

Calculation formula

Active AMD treatment site

CO_2 emissions for active AMD treatment were calculated using the difference between the carbonate inputs and outputs. CO_2 emissions related to transportation, electricity consumption, fossil fuel combustion, and chemical reagent production were calculated using the respective total masses and their specific emission factors (EF).

1. Direct emissions

Total inorganic carbon (TIC) values of the influent (in), effluent (out), and sludge (S) were used to represent IC distribution within the system:

$$M_{T-CO_2} = [(V_{in} \times C_{in-C} \times m_{CO_2}/m_C \times 10^{-6}) + (M_N \times P_N/100 \times m_{CO_2}/m_N)] - [(V_{out} \times C_{out-C} \times m_{CO_2}/m_C \times 10^{-6}) + (M_S \times C_{S-TIC} \times m_{CO_2}/m_C \times 10^{-3})], \quad (1)$$

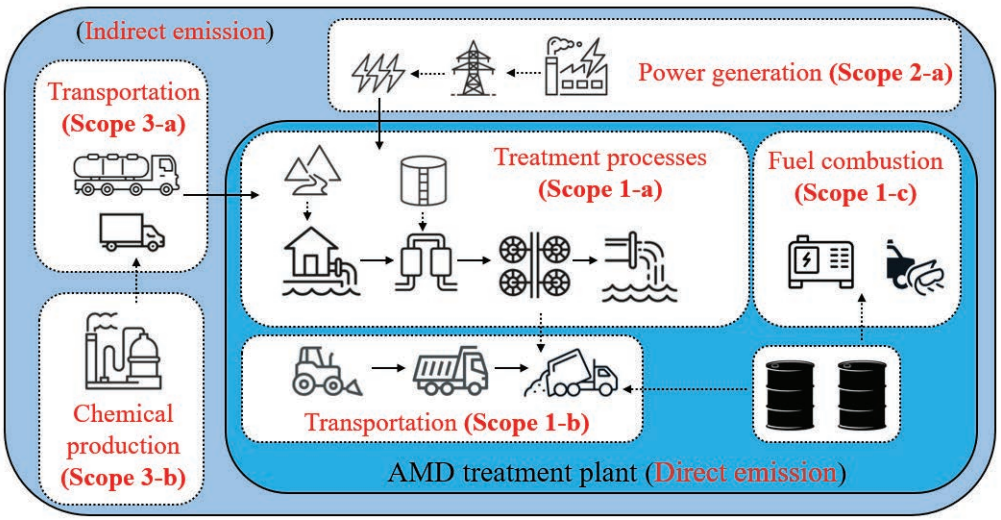

Figure 1 System boundaries for CO_2 emission scopes from an acid mine drainage (AMD) treatment plant.

where V_i(m³), C_i(mg/L), m_i(g/mol), M_i(t) and P_i(%) represent volume of influent and effluent, concentration of IC in influent, effluent and sludge, molar mass, weight of neutralizer and sludge and purity of neutralizer respectively.

Emissions from on-site fuel combustion (vehicles and machinery) were calculated as:

$$M_{fuel-CO_2} = \sum_i V_{\text{fuel}-i} \times EF_{\text{fuel}-i}, \quad (2)$$

where V(L) and EF(kg – CO_2/L) represent volume of fuel and emission factor of each fuel type respectively.

2. Indirect emissions

Indirect emissions include electricity consumption and upstream processes. EF were obtained from national inventory databases and supplier-specific data.

Electricity consumption-related emissions were estimated by:

$$M_{power-CO_2} = P_{\text{Total}} \times EF_{\text{Power}}, \quad (3)$$

where P(kWh) and EF(kg – CO_2/kWh) represent amount of purchased electricity and emission factor of each grid respectively.

Emissions from transportation of reagents were calculated as:

$$M_{vehicle-CO_2} = \sum_i D_{\text{vehicle}-i} \times EF_{\text{vehicle}-i}, \quad (4)$$

where D(km) and EF(kg – CO_2/ km) represent distance of transportation and emission factor of each vehicle type respectively.

Emissions from chemical manufacturing were estimated by:

$$M_{con.-CO_2} = \sum_i M_{\text{con.}-i} \times EF_{\text{con}-i}, \quad (5)$$

where M(t) and EF(t – CO_2/t) represent weight of each chemical reagent and emission factor of its production respectively.

Passive AMD treatment site

Carbon fluxes within a passive AMD treatment system are defined as shown in Figure 2. AMD enters the system carrying dissolved inorganic carbon (DIC), which is transported along the flow path and transformed through gas exchange, carbonate precipitation, and biological processes. Elevated pH promotes CO_2 absorption and carbonate formation in the substrate; plants and microorganisms convert DIC into organic carbon (OC) and mediate its mineralization. These processes govern carbon partitioning between aqueous DIC, biomass, carbonate solids, and atmospheric CO_2 within the passive treatment system.

Annual CO_2 emissions from passive AMD treatment systems were estimated using a system-boundary carbon mass balance approach. The calculation integrates: (i) DIC fluxes associated with influent and effluent AMD, (ii) temporal changes in solid-phase carbon stocks, including substrates and accumulated sludge, and (iii) biomass carbon accumulation and removal due to plant growth and harvesting. Total emissions from

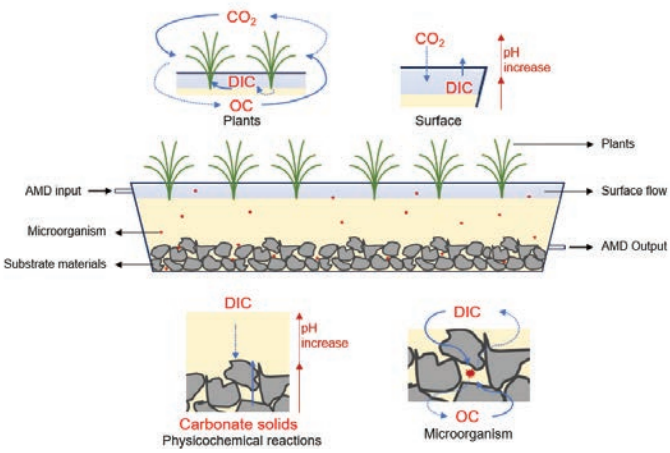

Figure 2 Carbon flow in a passive acid mine drainage treatment system.

n years were annualized based on the total operational duration:

$$M_{T-CO_2} = \left[(V_{in} \times C_{in-IC} + V_{out} \times C_{out-IC}) + \frac{(M_{S-initial} \times C_{S-initial-TC} - M_{S-final} \times C_{S-final-TC})}{n} + (M_{P-initial} \times C_{P-initial-TC} - \sum_i M_{P-cut} \times C_{P-cut-TC})/n\right] \times \frac{m_{CO_2}}{m_C} \times 10^{-6}, \quad (6)$$

where V_i(m³), C_i(mg/L), M_i (t), n and m_i(g/mol) represent volume of influent and effluent, concentration of C in influent, effluent, substrates and plants, weight of substrates and plants, molar mass and total operation year respectively.

The framework is applicable to typical passive AMD treatment configurations, including open drains and constructed wetlands, where hydraulic inflow–outflow, sediment accumulation, and optional vegetation constitute the carbon fluxes.

Study sites and data sources

Four full-scale active AMD treatment plants in Japan (Plants A–D) were selected to evaluate plant-level CO_2 emissions. All facilities apply neutralization–sedimentation processes but differ in operational scale, neutralizer type, and sludge management practices. Plants A and D use $Ca(OH)_2$, Plant C uses ground $CaCO_3$, and Plant B applies both materials. These variations reflect differences in influent flow rate, initial water chemistry, and site-specific design, making the selected plants representative of typical active AMD treatment systems currently operating in Japan. One passive AMD treatment site in Japan was evaluated. This site treats AMD in open drain flow and precipitation pools. The volumes treated and metals concentrations are much lower than those of the active treatment plants.

Operational data, including AMD flow rate, electricity consumption, chemical usage, and sludge production, were obtained from official governmental records (JOGMEC 2025). Carbon-related parameters of the water and sludge were determined by on-site sampling and laboratory analysis of TC. The combination of operational records and measured carbon data ensured consistent and reliable input for the plant-specific CO_2 accounting framework.

Results and discussion

Yearly CO_2 emissions from active acid mine drainage treatment plants

1. Yearly total and average emissions

Annual CO_2 emissions for April 2023–March 2024 were calculated using this accounting framework. Total emissions differed substantially between the four plants due to variations in treatment scale, influent chemistry, neutralizer type, and electricity consumption.

Table 1 *Annual CO_2 emissions by scope in different active acid mine drainage treatment plants (Unit: t).*

Scope	Plant A	Plant B	Plant C	Plant D
1a Treatment	–0.34	942.62	2602	–4.04
1b and 1c Internal transportation and other	3.76	59.63	99.13	1.15
2a Power generation	56.92	761.02	1582	27.86
3a External transportation	1.71	8.11	33.93	0.22
3b Chemical production	103.1	275.71	16.89	3.43
Total	165.1	2047	4334	28.62

As shown in Table 1, Plant C had the highest total annual emissions; Plant D had the lowest. Emission ranking generally followed neutralizer type and consumption: Plants B and C, which used powdered $CaCO_3$, exhibited significant direct emissions from carbonate decomposition under acidic conditions, plant B utilized both $CaCO_3$ and $Ca(OH)_2$ and resulted in higher emissions from chemical production than Plant C; in contrast, Plants A and D used $Ca(OH)_2$, and negative values were observed for Scope 1a, indicating net CO_2 uptake during treatment. This uptake was attributed to high pH conditions that promote atmospheric CO_2 dissolution and potential microbial fixation (Vesper *et al.* 2016). The treated water showed a pH comparable to that of the receiving natural water bodies, and most sludge is managed within the treatment facility. Therefore, the risk of immediate CO_2 re-release is considered limited, although its long-term stability remains uncertain.

2. Distribution of CO_2 emissions by scope

The distribution of emissions by scope reveals that indirect emissions dominated in most cases. For Plant A, approximately 98% of total emissions originated from electricity consumption and chemical production. In Plants B and C, direct emissions from neutralization contributed 46%–56% of total emissions, reflecting the influence of carbonate-based reagents.

When neutralizer-related emissions (Scopes 1a and 3b) were combined, they accounted for approximately 60% of total emissions in Plants A–C. Electricity consumption contributed about 36% on average, while transportation and other activities represented less than 5%. In Plant D, high final pH and low neutralizer demand resulted in net negative neutralizer-derived emissions, and electricity became the dominant source.

Overall, neutralizer selection was the primary determinant of emission structure, followed by electricity consumption. Transportation contributed minimally in all cases. The relative contribution of electricity-related emissions would vary depending on the electricity mix, and it would decrease substantially with transition toward a low-carbon grid.

Carbon flow during active acid mine drainage treatment

Carbon flux analysis (Table 2) shows that IC conversion to OC occurred in all plants; however, the influence on total direct emission estimates was limited. Differences between the simplified mass balance calculation and detailed carbon flux analysis were below 9% except for Plant A, where higher microbial conversion affected net direct emissions (Ishii *et al.* 2015; Huang *et al.* 2025).

Plants using $CaCO_3$ (B and C) showed increased dissolved TIC in the effluent due to carbonate dissolution, whereas Plants A and D exhibited greater potential for atmospheric CO_2 uptake under higher pH conditions. Although IC conversion introduces minor uncertainty, its contribution is small relative to emissions from electricity and neutralizer production. Therefore, excluding detailed IC–OC conversion has limited influence on total emission estimates for most plants.

In the passive treatment system, CO_2 is emitted in the open drain flow from the generating point source to the precipitation tank; however, CO_2 is absorbed during the precipitation process. This result indicates

Table 2 *Mass distributions of total carbon (TC), total inorganic carbon (TIC), and total organic carbon (TOC) in active acid mine drainage treatment plants (Unit: t).*

Plant	A			B			C			D		
Carbon	TIC	TOC	TC	TIC	TOC	TC	TIC	TOC	TC	TIC	TOC	TC
Output	0.56	1.93	2.48	20.39	18.47	38.86	33.12	23.83	56.95	1.12	0.18	1.29
Input	0.47	0.28	0.76	277.5	4.51	282.0	743.8	16.86	760.7	0.02	0.07	0.09

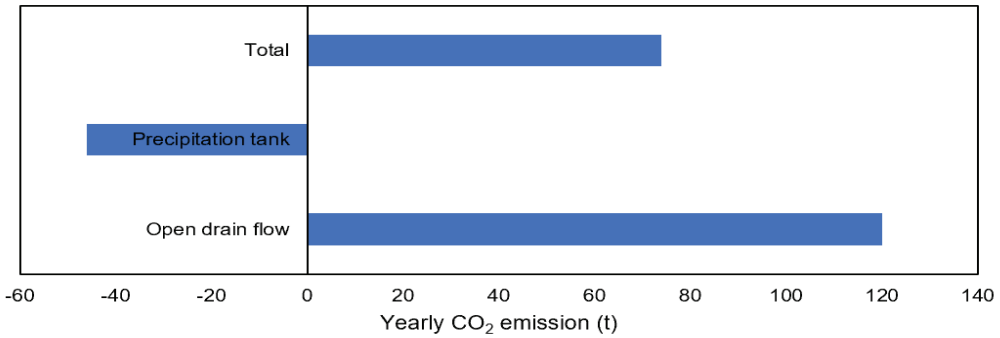

Figure 3 *Yearly CO_2 emissions of passive acid mine drainage treatment site.*

that oversaturated CO_2 in the original AMD would be released during open drain flow. In the precipitation tank, CO_2 would be absorbed due to the higher pH value and possible microbial activities. The treatment duration is much longer than active treatments, which allows potential for absorption of more CO_2 from the atmosphere and its storage in effluent and sludge.

For passive treatment systems without open drain flow (not including the treatment process), the total CO_2 emissions could be lower and may even have the possibility of achieving CO_2 absorption.

Conclusions

Carbon neutrality in all industries is essential, and decarbonizing AMD treatment is a key step. This study developed a CO_2 accounting method for active AMD treatment plants, covering five emission scopes: treatment, internal and external transportation, power generation, and chemical production. Applied to four operating plants of ranging scales and using different neutralizers, the method identified calcium-based neutralizers and electricity use as dominant emission sources, with indirect emissions prevailing. Inter-plant differences mainly reflect neutralizer type and operational configuration. In $Ca(OH)_2$-based systems, CO_2 alternated between emission and uptake: IC–OC conversion could cause overestimation. To achieve the carbon neutrality target for power generation by 2050, decarbonization should focus on use of alternative low-carbon neutralizers and optimized treatment capacity. This plant-specific framework enables cross-plant comparison and longitudinal analysis, supporting evidence-based mitigation strategies for AMD treatment. Passive treatment systems have lower CO_2 emissions than active systems and have higher possibility of achieving zero emission or even absorption.

Acknowledgements

This work was supported by Japan Science and Technology Agency for the establishment of university fellowships towards the creation of science technology innovation, Grant Number JPMJFS2102. We thank Kathryn Sole, PhD, from Edanz (https://jp.edanz.com/ac) for editing a draft of this manuscript.

References

Huang Y, Li X-T, Jiang Z, Liang Z-L, Liu W, Liu Z-H, Li L-Z, Yang Z-N, Zhang G-Q, Yin H-Q, Liang J-L, Zhou N, Liu S-J, Jiang C-Y (2025) Mineral types dominate microbiomes and biogeochemical cycling in acid mine drainage. Water Research 278:123367. https://doi.org/10.1016/j.watres.2025.123367

Ishii T, Kawaichi S, Nakagawa H, Hashimoto K, Nakamura R (2015) From chemolithoautotrophs to electrolithoautotrophs: CO_2 fixation by Fe(II)-oxidizing bacteria coupled with direct uptake of electrons from solid electron sources. Frontiers in Microbiology 6:994. https://doi.org/10.3389/fmicb.2015.00994

Kim DM, Lee KR, Park MS (2025) Potential generation and consumption of carbon dioxide during treatment of mine drainages in South Korea. Science of the Total Environment 975:179270. https://doi.org/10.1016/j.scitotenv.2025.179270

International Energy Agency (IEA) (2023) Net zero roadmap: A global pathway to keep the 1.5 °C goal in reach. International Energy Agency, Paris.

Intergovernmental Panel on Climate Change (IPCC) (2006) 2006 IPCC Guidelines for national greenhouse gas inventories, Volume 5, Waste. Intergovernmental Panel on Climate Change, Geneva.

Japan Organization for Metals and Energy Security (JOGMEC) Mine pollution control: JOGMEC's activities in Japan. Available at: https://www.jogmec.go.jp/english/mp_control/mp_control_metal_10_000005.html (accessed 28 Feb 2026).

Ministry of Economy (2023) Overview of the "Basic Policy for the Implementation of Mine Pollution Prevention Projects for Specified Facilities (FY2023–FY2032)". Available at: https://www.meti.go.jp/policy/safety_security/industrial_safety/sangyo/mine/seisaku/pdf/20230417_01-1.pdf (accessed 28 Feb 2026).

Totsche O, Kunze K, Bilek F (2025) Carbon footprinting of mine water treatment for future CO_2 emission reduction. In: Proceedings of the 2025 International Mine Water Association Conference, Portugal, Spain.

Vesper DJ, Moore JE, Adams JP (2016) Inorganic carbon dynamics and CO_2 flux associated with coal-mine drainage sites in Blythedale PA and Lambert WV, USA. Environmental Earth Sciences 75(4): 10.1007/s12665-015-5191-z

Elemental and Isotopic Tracers as Tools for Understanding Mine Water Geochemistry – Insights from an Iron Ore Mine Site in Northern Sweden

Vimbainashe Lorraine Dzimbanhete[1], Torbjörn Karlsson[2], Oscar Paulsson[1], Lena Alakangas[1]

[1]*Luleå University of Technology;* [2]*Luossavaara-Kiirunavaara AB Gällivare*

Abstract

Understanding the geochemical controls on uranium (U) release and mobility in mining environments is essential for predicting water quality and supporting proactive management. This study integrates minewall and laboratory leaching experiments with $^{234}U/^{238}U$ activity ratios (AR) to identify U sources and mobilization regimes at an iron ore mine in Northern Sweden. Uraninite was the most reactive U-bearing mineral. Carbonate complexation enhanced U mobility under circumneutral conditions. Groundwater AR values distinguished low U recoil-dominated flow paths from high U, dissolution, and complexation-enhanced flow paths. The high U end member contributes the highest U loads and should be prioritized for monitoring and mitigation.

Keywords: Uranium, $^{234}U/^{238}U$ activity ratios, elemental tracers, carbonate complexation, weathering regimes, mine water

Introduction

Uranium (U) mobility in mining environments is controlled by mineralogical composition and reactivity, water-rock interaction processes, redox conditions, and aqueous complexation reactions. Although U commonly occurs at low concentrations in many host rocks, mining activities expose fresh mineral surfaces and fracture networks, increasing contact with oxygenated groundwater and enhancing U-mineral dissolution. Oxidation of U(IV) bearing minerals such as uraninite (UO_{2+X}) converts relatively insoluble U(IV) to the more soluble U(VI) oxidation state, which readily forms aqueous complexes with ligands including CO_3^{2-}, SO_4^{2-}, and PO_4^{3-} over a wide pH range (Smedley and Kinniburgh 2023). Groundwater U concentrations and associated elemental signatures may therefore reflect the geochemical characteristics of the underlying bedrock or dominant groundwater flow paths. Identifying such geochemical fingerprints is particularly important in mining environments where multiple lithologies and flow systems may contribute differently to dissolved U loads.

U isotopes provide an additional tracer for evaluating U mobilization in groundwater systems. The $^{234}U/^{238}U$ activity ratio (AR) can be used to distinguish between different U mobilization mechanisms in the subsurface (Basu *et al.* 2015). In undisturbed systems, secular equilibrium results in $^{234}U/^{238}U$ AR = 1. Deviations arise from the combined effects of alpha recoil and mineral dissolution. During the radioactive decay of ^{238}U, emission of an alpha particle may displace the ^{234}Th daughter nuclide (precursor to ^{234}U), within the crystal lattice or into adjacent pore water if decay occurs near a grain boundary (Brown *et al.* 2016). Recoil-damaged lattice sites enriched in ^{234}U are more susceptible to leaching during oxidative dissolution, therefore groundwater may become enriched in ^{234}U ($^{234}U/^{238}U$ AR > 1), while the solid phase comes depleted in ^{234}U ($^{234}U/^{238}U$ AR < 1).

Leveäniemi open pit in Northern Sweden is comprised of several rock types with variable U content and differing U-bearing mineral assemblages. U concentrations of up to 100 µg/L have been detected in groundwater entering the open pit through drainage pipes installed at different elevations for pit slope stability. This groundwater mixes with surface water runoff and is pumped to the processing plant, influencing U concentrations in process water and U loads

discharged to a downstream recipient river. This study combines field observations with controlled laboratory leaching experiments and $^{234}U/^{238}U$ AR systematics to improve the understanding of mineral phase reactivity and groundwater mobilization regimes controlling U mobility. The objectives of the study were to (1) evaluate the reactivity of U-bearing mineral phases, (2) define lithology-specific elemental fingerprints, and (3) distinguish groundwater weathering regimes using $^{234}U/^{238}U$ AR.

Methods

Minewall weathering stations and field sampling

Different rock types, including pegmatite and trachyandesite, were collected from Leveäniemi open pit to assess their potential for U release (Fig.1). To estimate U leaching rates per unit surface area in µg/m2/week, minewall weathering stations were installed on selected rock faces following the established field protocols (Morin and Hutt 2004; Dzimbanhete *et al.* 2025). The rock surfaces were cleaned with Milli-Q water before installation. A sealed frame was constructed using inert silicone, and a transparent cover was installed to allow for sunlight exposure and atmospheric exchange while preventing direct rainfall, wind disturbance, and dust contamination (Fig.1C). During sampling campaigns, each station was flushed with Milli-Q water proportional to its surface area to collect leachates for analysis. Leachates were filtered through 0.22 µm nitrocellulose membrane filters into lab-controlled HDPE bottles and submitted to ALS Scandinavia in Luleå for elemental and isotope analysis.

Groundwater and drainage ditch sampling

Groundwater was sampled from drainage pipes drilled approximately 150 m into the open-pit walls for slope stability (Fig.1C). Discharged groundwater mixes with seepage and precipitation runoff in drainage ditches that run alongside open-pit benches (Fig.1C). All collected water flows towards a central sump at the base of the open pit and is subsequently pumped to the processing plant. Sampling campaigns were conducted between 2021 and 2023 at selected drainage pipe and drainage ditch locations (Fig.1B). Field parameters, including pH, temperature, and electrical conductivity (EC), were measured on site with a calibrated VWR multimeter. Water samples were filtered on-site using a 0.22 µm nitrocellulose membrane filter before storage and subsequent elemental and isotope analysis at ALS.

Batch leaching experiments

Batch leaching experiments were conducted on crushed pegmatite and trachyandesite samples to evaluate the reactivity of U-bearing minerals under controlled geochemical conditions. Acid leaching tests were performed over 24 hours using H_2SO_4, and HNO_3 (pH 0.7 to 3.3), whereas alkaline conditions were simulated using Na2CO3 and $NaHCO_3$ (pH 9.8 to 10). Additional experiments at circumneutral pH (7 to 8) were performed using solutions replicating mine water chemistry containing SO_4^{2-}, NO^{3-}, Cl^-, and HCO^{3-} at representative average and maximum concentrations. A constant solid-to-liquid ratio was maintained for all the experiments. Leachate and residual solids samples were sent to ALS for element and isotopic analysis.

Elemental and uranium isotope analysis

Element concentrations in groundwater, drainage ditch water, minewall leachates, batch leachates, and residual solids were determined using sector field inductively coupled plasma mass spectrometry (ICP-SFMS) at ALS. Solid samples were analysed following lithium metaborate fusion and acid digestion. Quality control included blank correction and analysis of certified reference materials. U isotope ratios were measured using multi-collector inductively coupled plasma mass spectrometry (ICP-MS) after chemical separation of U. The $^{234}U/^{238}U$ AR was calculated from measured isotope ratios ($^{238}U/^{235}U$ and $^{235}U/^{234}U$) using decay constants. The $^{234}U/^{238}U$ AR were used to distinguish between recoil-dominated U release and dissolution-driven U mobilization processes. To identify lithology-specific elemental fingerprints, Spearman rank correlation analysis (ioGAS) and hierarchical

cluster analysis (IBM SPSS) were applied to the batch leaching data.

Results and Discussion

U release from minewall weathering stations

Pegmatite minewall stations exhibited the highest U leaching rates overall, although substantial variation was observed between them. At minewall station 2, where uraninite was the dominant U-bearing mineral, U leaching reached approximately 1800 µg/m²/week. In contrast, the other pegmatite station, dominated by pyrochlore, showed lower leaching rates of up to 400 µg/m²/week (Fig.2). Trachyandesite (stations 3 and 4) displayed lower but consistent U release rates with uraninite identified as the main U-bearing phase. The elevated leaching rate in pegmatite (station 2) reflects both its higher bulk U content and the accessibility of uraninite within the rock matrix. Trachyandesite, although lower in U, covers an extensive surface area in the open pit as it is the main rock type in the hanging and footwall and therefore represents an important cumulative source of U. Based on their release rates and surface area coverage, pegmatite and trachyandesite were selected for subsequent batch leaching tests.

U mineral dissolution and pH influence

Batch leaching experiments at acidic and alkaline pH demonstrate that uraninite is the reactive U-bearing mineral in both pegmatite and trachyandesite, whereas other U-bearing minerals, including fergusonite, thorite, and xenotime, were largely refractory. Under circumneutral conditions representative of open pit mine water (pH 7 to 8), bulk mineral dissolution was limited (Fig.3). However, dissolved U concentrations increased in carbonate-bearing solutions relative to sulfate, nitrate, and chloride-dominated systems. This enhanced mobilization likely reflects the formation of stable aqueous uranyl–carbonate complexes, which increase U(VI) solubility and inhibit reprecipitation at circumneutral pH. Consequently, groundwater chemistry, particularly carbonate availability, exerts strong control on U mobility.

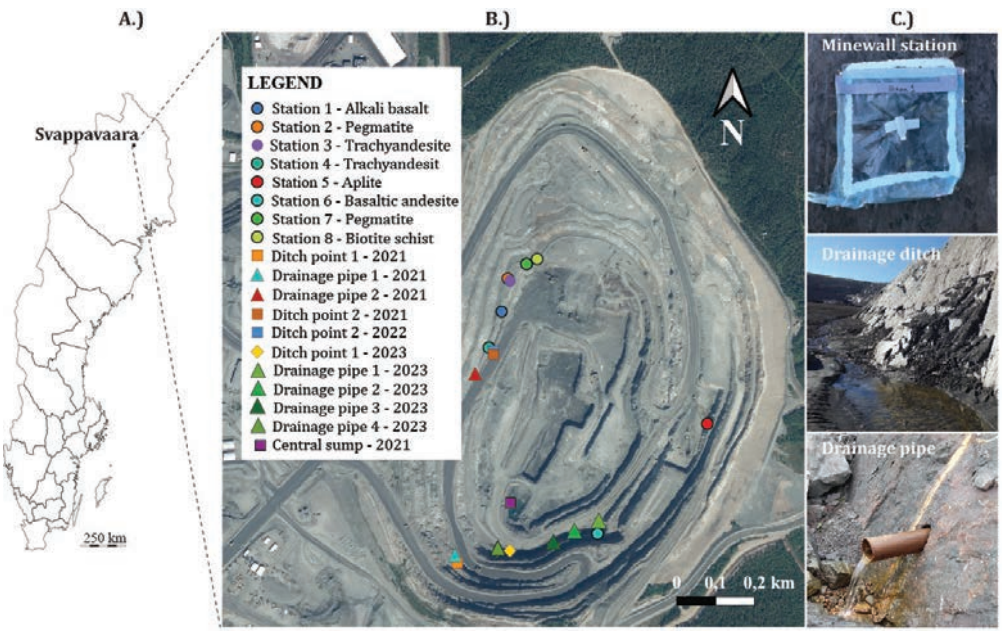

Figure 1 *Orthophoto of Leveäniemi open pit showing minewall station, drainage pipe, and drainage ditch locations, and photographs showing minewall weathering station, drainage ditch, and drainage pipe in the open pit.*

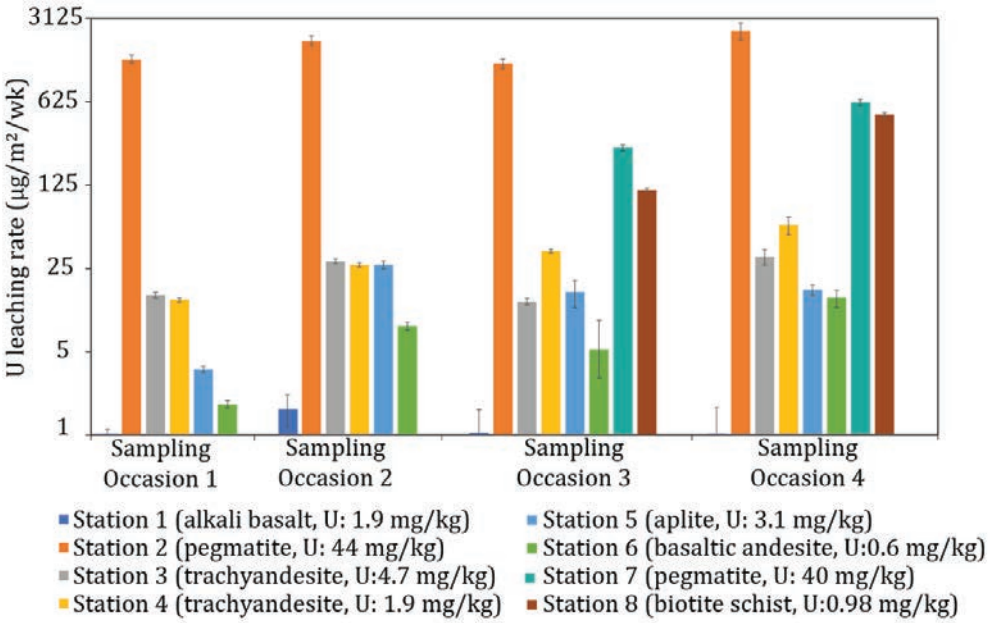

Figure 2 *Uranium leaching rates at minewall stations 1 – 8. Stations 7 and 8 could not be sampled on occasions 1 and 2 due to open-pit bench safety concerns.*

Batch leaching at circumneutral pH and element associations

At circumneutral pH, HCO_3^- was the most effective ligand for U mobilization in pegmatite (Fig.4A), whereas the groundwater solution containing multiple complexing ligands produced the highest release in trachyandesite (Fig.4B). Speciation modelling indicated that uranyl-carbonate and Ca-U-CO_3 complexes dominated under groundwater conditions, confirming carbonate complexation as the primary control on U mobility at around pH 8. In the groundwater solution, pegmatite exhibited a clear U-Pb-Th association reflecting release from uraninite and associated trace elements hosted within this mineral. Electron microprobe analyses showed that uraninite in pegmatite contains 63–68 wt.% UO_2, together with significant PbO (18–20 wt.%), ThO2 (4–7 wt.%) and Y_2O_3 (3–8 wt.%) (Dzimbanhete *et al.* 2025). In contrast, uraninite in trachyandesite contained 70–73 wt.% UO2, 19–22 wt.% PbO but lower ThO_2 (<1.5 wt.%) and Y2O3 (<2.5 wt.%). In the groundwater solution, trachyandesite showed U mobilization primarily associated with Ca rather than Pb and Th, indicating that Ca-U-

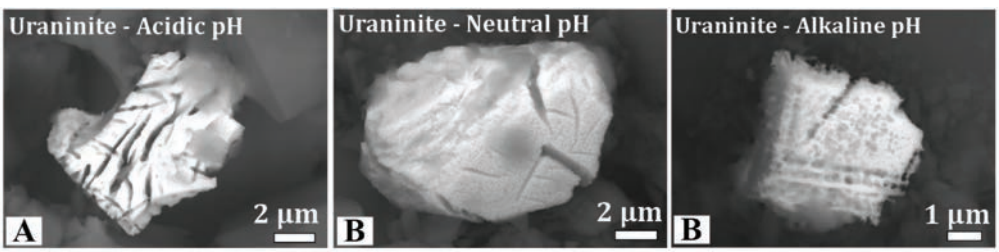

Figure 3 *SEM images of uraninite in residual solids after leaching at acidic pH (0.5 M H_2SO_4), neutral pH (203 mg/L $NaHCO_3$), and alkaline pH (0.5 M $NaHCO_3$/Na_2CO_3).*

CO_3 complex formation can exert a stronger influence on dissolved U concentrations than dissolution of U-bearing minerals. These results demonstrate that elemental associations derived under groundwater solution conditions can reflect mineral-host signatures in pegmatite, whereas in trachyandesite, aqueous complexation processes may partially overprint mineralogical signals.

Uranium isotopes and groundwater mobilization regimes

Groundwater discharged from the drainage pipes exhibited $^{234}U/^{238}U$ activity ratios (AR) consistently greater than one, indicating isotopic disequilibrium and active water-rock interaction processes. Two groundwater mobilization regimes were identified based on combined U concentrations and $^{234}U/^{238}U$ AR values (Tab.1): a low U recoil-dominated regime and a high U dissolution and complexation enhanced regime. Samples with intermediate U concentrations are interpreted as mixed or transitional waters.

The low U end member is characterized by U concentrations (< 20 µg/L) and high AR values of 2.7 to 3.8, consistent with preferential release of 234U from alpha-recoil damaged lattice sites or mineral surfaces under limited bulk dissolution(Kronfeld 1974; Cowart and Osmond 1977). The high U end member is characterized by U concentrations >30 µg/L, reaching up to 100 µg/L) and a moderately elevated AR value of 2.6. This pattern is interpreted as dissolution or complexation-enhanced U mobilization, where oxidative dissolution of uraninite and other U-bearing minerals increases dissolved U, while carbonate/Ca complexation promotes U(VI) transport and preferential ^{234}U release maintains isotope disequilibrium (Andersen *et al.* 2009; Coyte *et al.* 2018). Pegmatite and biotite schist produced high U minewall leachates with lower AR values of 1.1 to 1.5, and the corresponding rocks

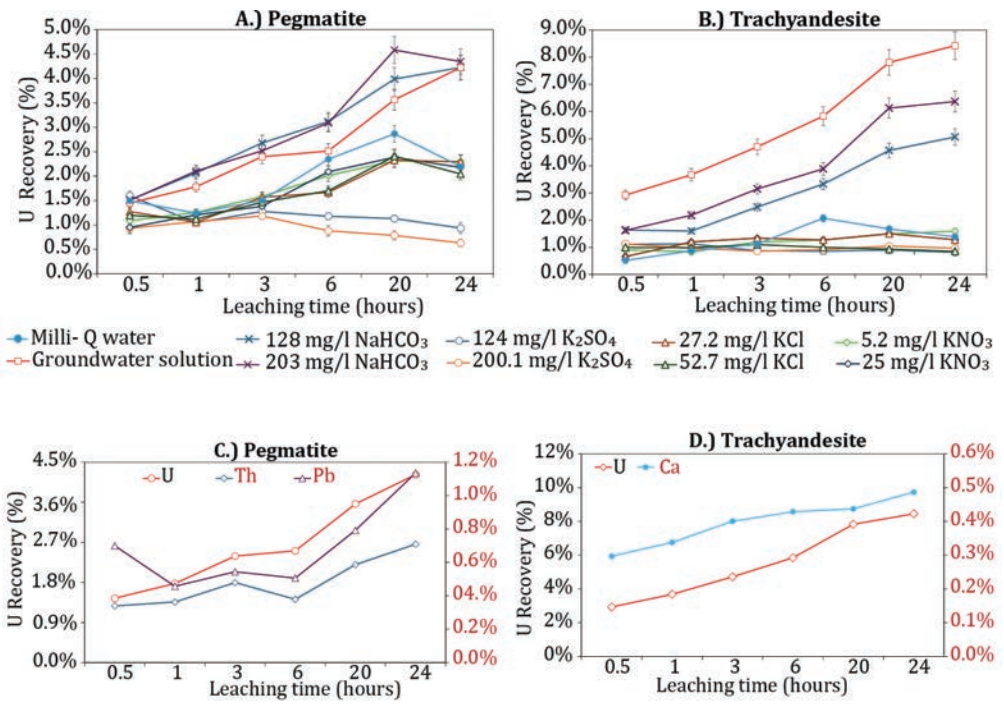

Figure 4 *A and B: U recovery vs leaching time for pegmatite and trachyandesite for batch leaching with $NaHCO_3$, KCl, K_2SO_4, MQ water, and groundwater solution at neutral pH, C and D: U recovery vs leaching time for elements showing similar leaching behavior to U in pegmatite and trachyandesite.*

Table 1 Groundwater mobilization regimes identified using U concentrations and $^{234}U/^{238}U$ AR.

Parameter	Recoil-dominated, low-U regime	Dissolution and complexation enhanced, high U regime
U concentration (µg/L)	<20 µg/L	>30 µg/L, up to 100 µg/L
$^{234}U/^{238}U$ (AR)	High, 2.7 – 3.8	Moderately elevated, 2.6 in the high-end member
U mobilization process	Preferential ^{234}U release by alpha recoil; limited bulk dissolution	Oxidative dissolution of U-bearing minerals, U(VI)-carbonate/Ca complexation
Relative U load contribution/ management priority	Low	High

were ^{234}U-depleted, supporting bulk mineral dissolution as the dominant process in high U-source materials. Drainage ditch waters had intermediate U concentrations and AR values consistent with mixing between drainage pipe groundwater and surface runoff. Since the high U end member contributes most to dissolved U loads, it represents the main target for monitoring and management.

Implications for environmental management

The combined minewall, batch leaching, and isotope results indicate that management should focus on the high U dissolution or complexation enhanced end member. Flow paths with elevated U concentrations and moderately enriched AR values contribute most to dissolved U loads and should therefore be prioritized for monitoring and mitigation. In contrast, recoil-dominated groundwater is isotopically distinct but has lower U concentrations and represents a lower immediate management priority.

Minewall weathering data identify pegmatite and biotite schist as important U source rocks, particularly where uraninite is the main U-bearing mineral. These rocks produced high U leaching rates and relatively low leachate AR values, supporting bulk dissolution of U-bearing minerals as the main process of U release. The corresponding rocks are also ^{234}U-depleted, supporting the interpretation that preferential ^{234}U loss and active U release have occurred in these rocks. Uraninite-bearing rocks should therefore be prioritized during waste rock characterization and, where possible, managed to limit exposure to limit water exposure, excessive particle-size reduction, and co-storage with acid-generating rocks.

Batch-leaching results further show that carbonate-rich, circumneutral waters enhance U mobility through uranyl-carbonate and Ca-U-carbonate complexation. Mine water management should therefore consider both mineralogical source control and groundwater chemistry, particularly alkalinity, Ca, and bicarbonate concentrations. Although direct control of carbonate and calcium may be difficult at the field scale, monitoring alkalinity, Ca, bicarbonate, and U along key drainage-pipe flow paths can help identify conditions that favour U transport. Overall, the results show that combining mineralogical observations, elemental tracers, and $^{234}U/^{238}U$ AR values provides a practical framework for identifying high-risk U sources and reactive flow paths in the mine water system.

References

Andersen MB, Erel Y, Bourdon B (2009) Experimental evidence for 234U–238U fractionation during granite weathering with implications for 234U/238U in natural waters. Geochim Cosmochim Acta 73:4124–4141. https://doi.org/10.1016/j.gca.2009.04.020

Basu A, Brown ST, Christensen JN, et al (2015) Isotopic and Geochemical Tracers for U(VI) Reduction and U Mobility at an in-Situ Recovery U Mine. Environ Sci Technol 49:5939–5947. https://doi.org/10.1021/acs.est.5b00701

Brown ST, Basu A, Christensen JN, et al (2016) Isotopic Evidence for Reductive Immobilization of Uranium Across a Roll-Front Mineral Deposit. Environ Sci Technol 50:6189–6198. https://doi.org/10.1021/acs.est.6b00626

Cowart JB, Osmond JK (1977) Uranium isotopes in groundwater: Their use in prospecting for sandstone-type uranium deposits. J Geochem Explor 8:365–379. https://doi.org/10.1016/0375-6742(77)90062-0

Coyte RM, Jain RC, Srivastava SK, et al (2018) Large-Scale Uranium Contamination of Groundwater Resources in India. Environ Sci Technol Lett 5:341–347. https://doi.org/10.1021/acs.estlett.8b00215

Dzimbanhete V, Paulsson O, Karlsson T, et al (2025). Identifying Key Uranium Sources in Mine Water: Open-pit Wall Rock Leaching and Groundwater Contributions in Leveäniemi Open Pit. J Geochem Explor 107773. https://doi.org/https://doi.org/10.1016/j.gexplo.2025.107773

Kronfeld J (1974) Uranium deposition and Th-234 alpha-recoil: An explanation for extreme U-234/U-238 fractionation within the Trinity aquifer. Earth Planet Sci Lett 21:327–330. https://doi.org/10.1016/0012-821X(74)90169-1

Morin KA, Hutt NM (2004) The Minewall approach for Estimating the Geochemical Effects of Mine Walls on Pit Lakes. In: Pit Lakes 2004. United States Environmental Protection Agency, Reno, Nevada, pp 1–19

Smedley PL, Kinniburgh DG (2023) Uranium in natural waters and the environment: Distribution, speciation and impact. Applied Geochemistry 148:105534. https://doi.org/10.1016/J.APGEOCHEM.2022.105534

Improving Pit Lake Monitoring by Using a Combination of Autonomous Robotic Devices and Drones

Marcus Fahle[1], Maximilian P. Lau[2], Eric Röder[2], Gero Licht[2], Anne Weber[3], Sebastian Zug[2]

[1]*Federal Institute for Geosciences and Natural Resources (BGR), Cottbus, Germany*

[2]*Freiberg University of Mining and Technology, Freiberg, Germany;* [3]*Lausitz and Central German Mining Administration Company, Leipzig, Germany*

Abstract

Pit lakes are formed from the voids that remain after surface mining has ended. They are filled either due to groundwater recovery or artificial flooding. These very young water bodies often have water quality issues. To understand the ongoing processes leading to the observed problems and finding ways to address them, monitoring of these lakes is an essential first step. Yet water levels far from the surface or restricted access to the shores due to unstable embankments can complicate the measurements. Not only in the Lusatia region of Germany, even helicopters are being used to collect water samples from such lakes. Due to the associated costs, monitoring is often restricted to multiple depths at a single point. However, it is questionable whether the obtained measurements are representative of the entire water body. Advanced monitoring systems offer the possibility of improving data gathering and considering spatial differences in more detail.

An autonomous surface vehicle (ASV), developed at the Technical University Bergakademie in Freiberg, was used at Lake Runstedt, a lignite mining pit lake in Germany, in 2023. The ASV was equipped with a multiparameter probe to perform automated in-situ measurements. The aim was to capture three-dimensional distributions of parameters such as pH and oxygen during three separate campaigns. Lake Runstedt (maximum depth: 32 m) had previously been used as a dumping site for fly ash and industrial waste. Since 2002, after flooding, its hypolimnion has been artificially aerated to mitigate contaminant release. Using the ASV, up to 13 in-situ measurement profiles were obtained during one day without causing any disturbance due to anchoring. The data revealed spatial differences in oxygen depletion and the effects of aeration. For example, in October 2023 the 6 mg L-1 oxygen isocline occurred at depths between 16 m and 24 m, with higher depths near the aerators.

In a new project, we will complement the ASV monitoring with an uncrewed aerial vehicle (UAV), i.e. a drone. The UAV will gather two-dimensional multispectral data that will be correlated with in-situ measurements, providing spatial distributions of turbidity, temperature and chlorophyll content in the uppermost layer of the lake. These data will then be used as input to design an ASV monitoring strategy that covers the most relevant areas. Additionally, technical adjustments will enable both the ASV and the UAV to collect water samples.

Besides the 2023 results, the poster will outline the planned project activities and present initial findings. A primary objective of the joint monitoring approach is to evaluate the effectiveness of (pit) lake treatments aimed at improving the water quality, such as in-lake neutralisation. Furthermore, the obtained data will be used to develop a lake model, which could help to predict and optimise such water quality treatments.

Keywords: Pit lake, uncrewed aerial vehicle (UAV), autonomous surface vehicle (ASV), environmental monitoring

Advances in Pit Lake Water Quality Monitoring Using Unmanned Aerial Vehicles

Marlese Fairgray[1], Gert du Plessis[1]

[1]*WSP Australia Pty Ltd. 250 St Georges Terrace, Perth WA*

Abstract

Sampling of pit lake water quality by unmanned aerial vehicle (UAV; i.e., drone) presents an emerging technology in the monitoring and management of mine-affected waterbodies. The use of UAV for data and sample collection mitigates the need for persons to enter a non-operational pit void or be in contact with a waterbody, thereby increasing the safety of the monitoring program.

Experienced gained through conducting sampling programs at both open and closed sites, and repeated sampling events at individual sites have allowed for refinement of the sampling procedure to improve health and safety outcomes and increase the efficiency of the sampling procedure.

Samples are taken at different water depths, as determined using sonar to measure water depth, and *in-situ* water chemistry measurements made using a multi-parameter probe. Both sonar and probe are suspended from the UAV. Samples for laboratory analysis are collected by bailers and Hydrasleeves® housed within an upright structure, for surface and sub-surface water samples, respectively.

Ongoing refinements to the sampling methodology are improving the efficiency in sample collection and enabling more robust monitoring programs to support mine waste and tailings management objectives through to closure.

Keywords: UAV, drone sampling, pit lake, monitoring

Introduction

Following the cessation of dewatering within a mined-out pit void where excavation extended to below the pre-mining groundwater level, the water table rebound commonly results in the formation of a pit lake. Such voids may also be repurposed for in-pit disposal of mine waste material, reducing reliance on external waste rock dumps or a designated tailings storage facility (McCullough *et al*. 2024, 2010; Obermeyer *et al*. 2025). The introduction of waste rock or tailings into a pit lake as backfill, can alter pit lake water quality through geochemical interactions between the waste materials and lake water (Schultze *et al*. 2011). Vertical stratification can develop when density gradients form between surface and bottom waters, driven by differences in salinity and temperature. Stratification can have an influence on dissolved oxygen concentrations and redox conditions within stratified layers of pit lake water. This can cause water chemistry to change as a function of depth, especially for redox-sensitive chemical species. Recent studies (Gammons and Icopini (2020); Vandenberg and Litke (2017); and Obermeyer *et al*. (2025)) indicate that the depth of tailings and/or sludge deposition within a pit lake can influence pit lake behaviour such as stratification. Consequently, at sites undergoing active material deposition, systematic monitoring of pit lake water quality is important to track the evolution of water chemistry relative to water quality objectives and validate water quality modelling (Schultze *et al*. 2024). Furthermore, regulatory agencies often require pit lake water quality to be monitored and reported, thus creating an external requirement for ongoing pit lake water quality monitoring.

Traditional (grab) sampling and sampling from surface water vehicles both require direct access to the pit lake and present a risk of drowning associated with working on or near the waterbody. Moreover, grab sampling from the shore only allows for a small, and

often unrepresentative, portion of the lake to be sampled, and sampling from surface water vehicles involves considerable efforts to transport equipment to site (Banerjee et al. 2018; Ross and McCullough 2011). Pit geometry and water quality conditions can oftentimes create unsafe environments such as steep, unstable pit walls with the potential for slope failure and restricted access, making direct sampling hazardous to site personnel. Furthermore, several sample locations, and multiple depths may need to be sampled to account for differences in water quality at different depths due to stratification (Castendyk *et al.* 2019), and different areas of the pit lake influenced by pit wall geology.

Sampling of pit lake water by UAV is becoming the preferred method of water quality monitoring for pit lakes owing to its benefit to personnel health and safety. Our team have enhanced an established methodology (Castendyk *et al.* 2020, 2019; Straight *et al.* 2021) to undertake both surface and sub-surface *in-situ* monitoring and sampling at target depths.

Methods

An overview of sampling programs conducted are presented in Table 1. The number of locations within a pit was dependant on pit size and bathymetry. Sampling points (*in-situ* measurements and water samples collected) were taken at either 5 m intervals or 10 m intervals, with the number of sampling points at each location dependant on the total pit lake depth at that location. A typical cross-section of a pit lake indicating locations and sampling points is presented in Figure 1.

Table 1 *Pit lake sampling program overview.*

Program	Pits	Locations	Sampling points	Total number of sampling points	Monitoring events
A	11	41 (1-6 per pit)	1-6 depths at each location. Surface to 30 m	145	1
B	1	3	4 depths at each location. Surface to 30 m	12	4

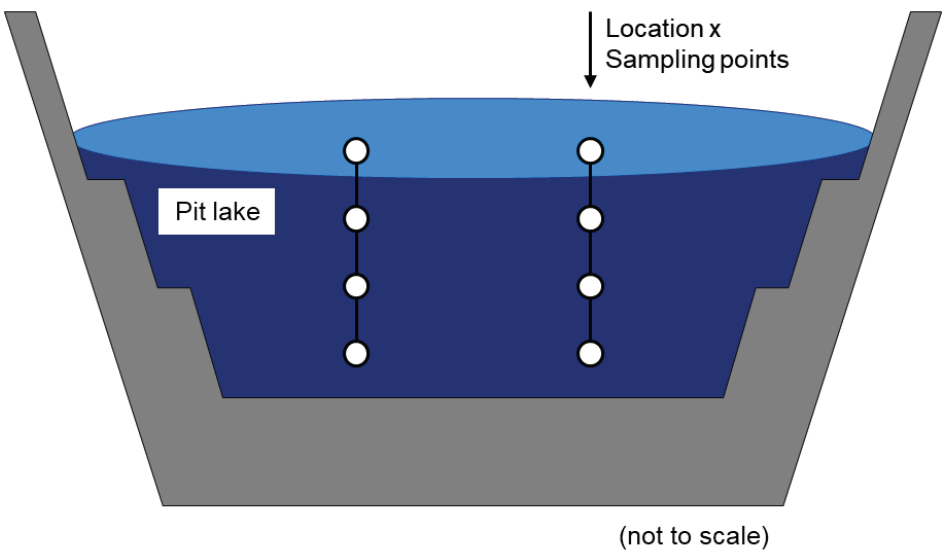

Figure 1 *Typical pit lake with n locations and x sampling points at depth intervals per location.*

Under a typical pit lake sampling program, depth and *in-situ* water chemistry measurements are taken by instruments suspended from the UAV (DJI Matrice 300 RTK; Figure 2). Samples for laboratory analysis are collected by bailers and Hydrasleeves® for surface and sub-surface water samples, respectively.

During each sampling event, the following tasks were undertaken for multiple locations within a pit lake:

- Pit lake water depth was measured using either a tether-mounted CastAway conductivity-temperature-depth (CTD) sonde (Program A), or a tether-mounted custom-built sonar which recorded depth, GPS location, time and date, and certainty (Program B).
- A YSI EXO Sonde multi-parameter data logger was used to collect *in-situ* measurements of pH, electrical conductivity (EC), oxidation-reduction potential (ORP), dissolved oxygen (DO), and temperature.
- Water samples were submitted for laboratory testing of physico-chemical parameters, major ions, total and dissolved trace metal(loids), nutrients, and total organic carbon (TOC). Samples for dissolved metal(loid) analysis were filtered in the field, and all samples were preserved in the field.

Outcomes

Health and Safety Considerations

UAV-based sampling eliminated the need for personnel to enter the pit void and work on or near water, thereby reducing exposure to slope failure, drowning hazards and potentially harmful water (Castendyk *et al.* 2019).

Key health and safety risks associated with UAVs, such as falling object/material and battery fire or explosions were controlled by the following protocols and procedures:

- Risk of falling object/material controlled by:
  - Demarcating an exclusion zone for UAV pilot and sampling personnel only;

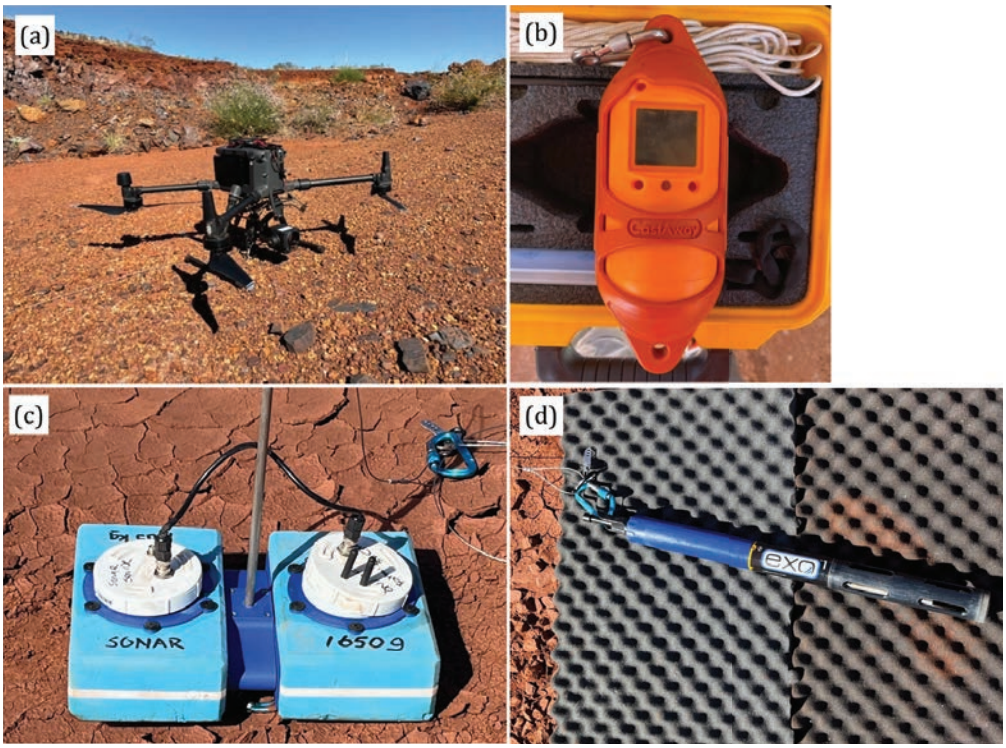

Figure 2 *Equipment set-up: (a) UAV (DJI M300 RTK), (b) CastAway conductivity-temperature-depth (CTD) sensor, (c) sonar device, and (d) EXO sonde multi-parameter probe.*

  - Personnel working within the exclusion zone were briefed on hazards and protocols in place to control for hazards, and at an operational site, a site-wide notice was issued regarding UAV operations including date, time and location of operations;
  - Zero access below the UAV and suspended was allowed load during take-off and landing;
  - Consideration that weather conditions were within allowable flight tolerances;
  - Adhering to payload limitations such that instruments and/or sampling equipment, water sample and tether were within the lift capacity of the UAV used; and
  - Return to home (RTH) procedures were initiated when battery level reduced to 30%.

- Risk of battery fire or explosions controlled by:
  - Batteries were stored, transported and managed according to documented policies and charged in accordance with manufacturer recommendations; and
  - RTH procedures at low battery level.

These controls safeguarded the health and safety of the sampling team whilst in the field.

Sampling Methodology

Sampling events were conducted with three persons; one UAV pilot, and two samplers/spotters.

UAV flight times to collect water samples varied depending on distance to location, difference in vertical elevation between take-off/landing zone and lake level, and depth to sampling points. Travel distance between pit lakes and respective take-off/landing zones should also be considered for a program with multiple pit lakes.

Approximate times for each task were as follows:

- Depth by sonar: 15 minutes for a pit with three locations.
- *In-situ* measurements: 20 minutes for flights that recorded data at three sampling points to 20 minutes for flights that recorded data at four sampling points. Measurements were recorded at 2 second intervals such that the UAV hovering with the sonde at the specified depth three minutes in order for the pH measurements to settle allowed for a minimum of 90 measurements at each data collection point.
- Water sample collection: Up for six minutes for a sampling location at a distance of 850 m from the take-off/landing zone, and 30 m depth. With the UAV model used, a single water sample was collected per flight. However, with a larger UAV capable of handling a larger payload, multiple water samples may be collected in a single flight.

UAV flights were limited by battery discharge time, and in some cases the *in-situ* measurements needed to be collected with more than one flight. Reliable access to an electrical supply for battery charging should be considered.

Measurement of pit lake depth by a sonar device that floated on the water surface eliminated the need to lower instruments, suspended from the UAV, to the depth of the pit lake where there is the possibility for instruments to become entangled with or damaged by aquatic plants, unconsolidated material or uneven surface at the base of the pit lake. This reduced the risk of instruments being lost or damaged and minimised the cost and program feasibility impacts.

Several methods for retrieving the water sample from the UAV were trialled to optimise the volume of sample collected with consideration of health and safety and flight capacity limitations. Detaching the sample from the tether whilst the UAV was airborne did not align with health and safety protocols. Landing the Hydrasleeve® on a tarpaulin mat permitted safe UAV landing before the sample was retrieved, but substantial sample was lost through the unsealed valve such that this technique was not suitable. Use of a custom-built, lightweight tripod to house the Hydrasleeves® in a contained way allowed the full Hydrasleeve® to remain upright on landing, achieving minimal sample loss and retrieval of the sample upon landing of the UAV. Retention of a full sample on landing, allowed for a reduced number of sampling

vessels to be filled at each flight. Fewer sample vessels initially filled offset the weight of the tripod to retain a low payload weight. Further to this, sampler skill in transferring the water sample from Hydrasleeves® with minimal loss of sample allowed for a single Hydrasleeve® (1L capacity) to be used for each flight, further reducing the payload weight.

Discussion

Improvements to the sampling methodology allowed for a reduction in bailer or Hydrasleeve® needed for collecting each sample, reducing effort for each UAV flight. By measuring *in-situ* water quality for surface and subsurface sample points, the stratification status of the pit lake could be demonstrated for repeated monitoring events.

Further enhancements to the sampling technique that we aim to realise in future sampling events include the use of larger UAV's with a higher payload capable of retrieving multiple samples in one flight. These changes will further improve drone flight time efficiencies and battery usage.

Besides water quality monitoring, this methodology and the use of UAVs in a mine water context can be modified for other applications such as depth profiling and evaluating water depth to backfilled materials, mounting of sediment samplers to collect pit lake sediments for characterisation. Additionally, UAVs can be used to collect high resolution imagery, for example evaluating the geology of pit walls, mounting other environmental sensors for site-specific applications, or deploying long-term monitoring stations.

Conclusions

Improvements to sampling by UAV methodologies enabled depth, *in-situ* data and samples to be collected in a safe and efficient manner emphasizing the benefits of using UAVs to monitoring pit lake water quality. We continue to make improvements to the sampling by UAV methodology with a focus on safety and efficiency.

Acknowledgements

The authors would like to thank our clients for the opportunity to conduct water sampling by UAV at their sites, the drone pilots who accompanied us for sampling events, and reviewers who provided constructive feedback.

References

Banerjee BP, Raval S, Maslin TJ, Timms W (2018) Development of a UAV-mounted system for remotely collecting mine water samples. International Journal of Mining, Reclamation and Environment, 34(6), 385–396. https://doi.org/10.1080/17480930.2018.154952

Castendyk D, Voorhis J. Kucera B (2020) A Validated Method for Pit Lake Water Sampling Using Aerial Drones and Sampling Devices. Mine Water Environ 39, 440–454. https://doi.org/10.1007/s10230-020-00673-y

Castendyk DN, Straight BJ, Voorhis JC, Somogyi MK, Jepson WE, Kucera BL (2019) Using aerial drones to select sample depths in pit lakes. In Fourie AB, Tibbett M (eds), Mine Closure 2019: Proceedings of the 13th International Conference on Mine Closure. Perth, p 1113-1126, https://doi.org/10.36487/ACG_rep/1915_89_Castendyk

McCullough CD, Schultze M, Vandenberg J, Castendyk D (2024). Mine waste disposal in pit lakes: a good practice guide. In Fourie AB. Tibbett M, Boggs G (eds.), Mine Closure 2024: Proceedings of the 17th International Conference on Mine Closure. Perth, p 1,063-1,076.

McCullough CD, Lund MA, Zhao LYL (2010). Mine Voids Management Strategy (III): A Monitoring Strategy for Pit Lakes and Connected Waters. Department of Water Project Report MiWER/Centre for Ecosystem Management Report 2010-2, Edith Cowan University, Perth, Australia. Unpublished report to Department of Water, Government of Western Australia.

Obermeyer J, Staton H, Castendyk D, Sitler K (2025). Eagle Mine case study: methods and monitoring for subaqueous tailings deposition in a pit lake. Proceedings of Tailings and Mine Waste 2025. Banff, p 2159-2168.

Schultze M, Vandenberg J, Castendyk D, Schleußner H-P, McCullough C (2024). Monitoring for pit lake planning, filling and use: What? When? Why? Mine Closure 2024. Perth, Australia. Fourie, A.; Tibbett, M. and Boggs, G. (eds.), Australian Centre for Geomechanics (ACG), p 1,049-1,062.

Schultze M, Boehrer B, Friese K, Stasik S, Wendt-Potthoff K (2011) Disposal of waste materials at the bottom of pit lakes, in AB Fourie and M Tibbett (eds), Mine Closure 2011: Proceedings of the 6th International Conference on Mine Closure. Alberta, p 555-564.

Straight B, Castendyk D, Mcknight D, Newman C, Filiatreault P, Pino A (2021). Using an unmanned aerial vehicle water sampler to gather data in a pit-lake mining environment to assess closure and monitoring. Environmental Monitoring and Assessment. 193. 10.1007/s10661-021-09316-3.

Bioremediation of Acid and Metalliferous Drainage using Sulfate-Reducing Bacteria

Adithyanti Febriana[1], Samadhi Gunathunga[2], Iván Ñancucheo[3], Gordon Southam[2,4], and Denys Villa Gomez[5]

[1]*Centre for Environmental Responsibility in Mining, Sustainable Minerals Institute, the University of Queensland, Australia, a.febriana@uq.edu.au, ORCID 0009-0008-7586-5697*

[2]*School of the Environment, the University of Queensland, Australia, samadhi.gunathunga@uq.edu.au, ORCID 0000-0003-3637-0946*

[3]*Universidad San Sebastián, Concepción, Chile, ivan.nancucheo@uss.cl, ORCID 0000-0001-9289-9399*

[4]*W.H. Bryan Mining and Geology Research Centre, Sustainable Minerals Institute, The University of Queensland, Australia, g.southam@uq.edu.au, ORCID 0000-0002-8941-1249*

[5]*School of Civil Engineering and the Australian Institute for Bioengineering and Nanotechnology, The University of Queensland, Australia, d.villagomez@uq.edu.au, ORCID 0000-0002-4329-311X*

Abstract

This study examined acid-tolerant sulfate-reducing bacteria (SRB)-based AMD treatment using an inoculum cultured from sediment exposed to a pH 3.5 AMD stream at the Mt. Morgan gold and copper legacy mine site in Central Queensland, Australia. The SRB-consortium was enriched in a selective growth medium and inoculated into a continuously running anaerobic-bioreactor operated for 290 days at 33 hours hydraulic retention time with gradually increased synthetic AMD load. Ethanol was used as the carbon source at a 0.67 COD:sulfate ratio by mass and 2–4 mm size porous beads were added for SRB colonization. Following bioreactor stabilisation, the effluent analysis showed Desulfobacterota as the most abundant bacterial phylum (almost 45% relative abundance) in the bioreactor system. Operation at 0.2 mL/min synthetic AMD feed achieved a maximum sulfate removal of 71% accompanied by acetate and sulfide production (600 mg/L sulfide). Increasing COD:sulfate ratio to 1 at 0.5 mL/min synthetic AMD feed resulted in enhanced sulfate removal and a pH increased from 5.7 to 6.5. Moreover, dissolved Cu, Fe, and Zn in the synthetic AMD were fully removed as metal sulfides, highlighting the potential for both AMD remediation and metal recovery valorisation.

Keywords: Acid Metalliferous Drainage (AMD), bioremediation, sulfate-reducing bacteria

Introduction

Acid and Metalliferous Drainage (AMD) remains an enduring challenge for the mining sector. A study by Werner *et al.* (2020) estimated that Australia has approximately 80,000 abandoned mines, and around 2,825 of them are located in Queensland. One of the mine sites with AMD issue in Queensland is the Mount Morgan gold and copper legacy mine site in Central Queensland (Kaur *et al.* 2018). Mining operations at the site ceased in 1990 and remediation efforts applied at the historic mine site including operation of a lime-dosing water treatment plant (Queensland Government, 2021). Despite the state government efforts, environmental concerns related to AMD generated from the site persist until today.

Limestone or lime addition is among the most widely used AMD treatment methods. While effective in neutralizing acidity and precipitating most metals, it generates chemical sludge requiring further management (Villa Gomez *et al.* 2023) and contributes to greenhouse gas emissions through limestone production and CO_2 release during the acid-neutralization process (Iizuka *et al.* 2022). Nature-based treatments,

such as biologically mediated sulfate reduction, offer advantages over conventional alkaline methods, including lower CO_2 footprint and maintenance cost (Kim *et al.* 2025), as well as the potential for sustained sulfate reduction and metal recovery through metal sulfide formation (Liu *et al.* 2021). Extensive research on sulfate-reducing bacteria (SRB)-mediated AMD treatment have been conducted with focus on non-native or model SRB strains to mediate AMD bioremediation. However, comparatively little attention has been given to the potential of indigenous, in situ microbial communities to drive AMD bioremediation. Investigating these naturally adapted communities could provide significant advantages, as their intrinsic tolerance to acidic and metal-rich environments may reduce the need for pH buffering and enable sustained bioprocess performance under variable AMD loading conditions.

This study aims to evaluate the potential of indigenous, acid-tolerant SRB to sustain sulfate reduction and metal recovery under variable carbon, acidity, and metal loading conditions typical of AMD systems.

Methods

Study Location and Sample Collection.

The Mt. Morgan site is a legacy gold and copper mine located 35 km southwest of Rockhampton in Central Queensland (Queensland Government, 2021). Water, sediment, and biofilm samples were collected in March 2023 and June 2024 from the Mine Pit, Frog Hollow Tailing Dump, Linda Gully, and Dee River Downstream (Figure 1). AMD collected from Frog Hollow Tailing Dump was used to prepare synthetic AMD for this study.

Enrichment of Sulfate Reducing Bacterial Consortium

One (1) mg of sediment sample collected from underneath a pH 3.5 AMD stream at Frog Hollow Outlet was inoculated into enrichment media consist of 6 mL/L lactate (60% w/w), 10 g/L tryptone, 1 g/L yeast, 2 g/L $MgSO_4.7H_2O$, 0.5 g/L $FeSO_4.7H_2O$, and 0.75 g/L ascorbic acid to enrich sulfate reducing bacterial consortium.

Experimental Set-Up

The enriched SRB culture was used as inoculum in a 2L working volume anaerobic bioreactor supplemented with ethanol as a carbon source (indicated as Chemical Oxygen Demand/COD loading) and 2–4 mm Poraver® porous beads for SRB colonization. The experiment was operated for 290 days at 33-hour hydraulic retention time (HRT) and 1 mL/min inlet flow rate. The reactor inlet solution was growth media consisting of 0.5 g/L KH_2PO_4, 0.2 g/L NH_4Cl, 2.5 g/L

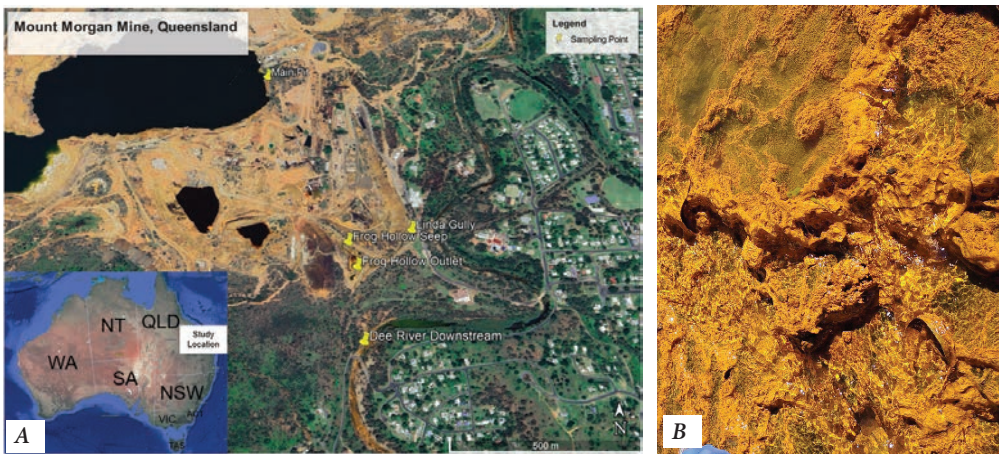

Figure 1 *Mt. Morgan gold and copper mine site sampling locations: (A) Frog Hollow Seep, Frog Hollow Outlet, Main Pit, Linda Gully, and Dee River Downstream. Source: Mt. Morgan Ltd. (Queensland Government Department of Resources, 2023), (B) Frog Hollow Outlet AMD stream SRB inoculum collection point.*

$CaCl_2.2H_2O$, 2.5 g/L $MgSO_4.7H_2O$, 1.51 g/L $FeSO_4.7H_2O$, an d 0.75 g/L ascorbic acid. The inlet solution was gradually transitioned from 100% growth media to increasing load of synthetic AMD, applied sequentially as 0.2, 0.5, and 1 mL/min AMD, with the remainder of each mixture consisting of growth media. The acidity and metal concentration in the bioreactor system were gradually increased along with increasing synthetic AMD in the feed solution over the experiment (Table 1). The synthetic AMD consisted of 1.5 g/L $CaSO_4.2H_2O$, 0.3 g/L $CuSO_4.5H_2O$, 5 g/L $MgSO_4.7H_2O$, 0.4 g/L Na_2SO_4, 6.8 g/L $Al_2K(SO_4)2.12H_2O$, 3.7 $FeSO_4.7H_2O$, 0.3 g/L $MnSO_4.H_2O$, and 0.1 g/L $ZnSO_4.7H_2O$ adjusted to pH 3.5 with 0.5M H_2SO_4.

Chemistry and Electron Microscopy Analysis

Triplicate influent and effluent samples were collected for pH, metals, ethanol, acetic acid, sulfate, sulfide and total organic carbon (TOC) analyses. pH values were measured using an Eutech Instruments pH 700 pH meter. Metal samples were filtered using 0.2 µm syringe filters, then analysed using Inductively Coupled Plasma Optical Emission Spectroscopy (ICP-OES) analysis using Thermo Fisher iCAP PRO XP Duo. Ethanol and acetic acid analysis was conducted using gas chromatography system with Agilent Technologies 7890A. Sulfate concentrations were measured using Dionex ICS 2000 IC. Sulfide concentrations were determined using colorimetric method as described by Cord-Ruwisch (1985). TOC and bicarbonate (measured as total inorganic carbon) was determined using the difference method on a Shimadzu TOC-L analyzer Inoculated porous beads were fixed with 2.5% glutaraldehyde and dehydrated and dried according to Jones *et al.* (2023), and analysed using a Secondary Electron Microscopy Energy (SEM) using a JEOLJSM – 7800F.

Molecular Identification using Amplicon Sequencing

Biomass pellets from the SRB enrichment culture and bioreactor effluent were submitted for DNA extraction and amplicon sequencing at the Australian Centre for Ecogenomics employing Polymerase Chain Reaction (PCR) amplification of 16S rRNA gene using universal primers (Jones *et al.*, 2023). The resulting raw DNA sequences were then processed using MOTHUR software version 1.48.0 (Schloss *et al.*, 2009) following the pipeline reported in Gagen *et al.* (2018).

Results and Discussion

SEM analysis showed extensive microbial colonization and growth within the porous beads, indicating that the beads matrix

Table 1 *SRB bioreactor operating conditions.*

Phase	Day of Experiment	Inlet pH	COD loading (g/L)	Sulfate loading (g/L)	COD:sulfate	Synthetic AMD flow rate (mL/m)	Note
I	0-7	7.0	1	1.4	0.67	0	Batch
II	8-56	7.0	1	1.4	0.67	0	Continuous
III	57-70	6.0	1	1.4	0.67	0	Continuous
IV	71-114	7.0	1	1.4	0.67	0	Continuous
V	115-134	7.0	1.5	2.0	0.67	0	Continuous
VI	135-156	6.7	1.5	2.0	0.67	0	Continuous
VII	157-184	6.4	2.3	3.4.	0.67	0.2	Continuous
VIII	185-194	6.4	1.6	1.6	1	0.2	Continuous
IX	195-215	5.8	4.1	4.1	1	0.5	Continuous
X	216-243	5.8	6.1	4.1	1.5	0.5	Continuous
XI	244-268	5.8	4.1	4.1	1	0.5	Continuous
XII	269-290	3.6	8.1	8.1	1	1	Continuous

provides effective attachment surface and protected microenvironment for biofilm development. This condition likely contributed to the SRB community ability to maintain their dominance under acidic AMD conditions throughout the long-term bioreactor operation (Figure 2). Microbial community development was further confirmed through 16S rRNA sequencing (Figure 3), which showed that microbial diversity grew from predominantly sulfate-reducing bacteria to including fermentative bacteria over time, consistent with an AMD environment. After more than 100 days of bioreactor operation, *Desulfobacterota*, the incomplete carbon-oxidizing SRB (Dyksma & Pester, 2024), thrive and became the most abundant microbial group in the system. Their dominance was consistent with the observed incomplete ethanol oxidation to acetic acid in the system.

The bioreactor stabilized after approximately 70 days of operation (stage I-III), marking the transition from SRB community acclimation to a steady sulfate-reduction system (stage IV-IX). During 200 days of bioreactor operation, SRB metabolic activity generated bicarbonates that buffered the system and maintained neutral pH (Figure 3). A stress-response phase was evident during stages X-XII. After stage IX (0.5 mL/min synthetic AMD), increased acidity and dissolved metal concentrations likely inhibited SRB metabolic activity, reducing bicarbonate production, and driving the effluent pH below 6. Increasing the COD:sulfate ratio in stage X did not restore the system performance, demonstrating that increasing the carbon load alone is insufficient to overcome inhibition caused by acidity and metal stress. Therefore, the COD:sulfate ratio was returned to the prior level in stage XI. At the highest synthetic AMD loading tested (stage XII, 1 mL/min synthetic AMD), effluent pH was higher than the influent pH, suggesting an improved SRB metabolic activity due to reduced H_2S toxicity as a result of increased metal loading that consumed sulfide through precipitation.

Despite the stress response observed during stage X-XII, operation at stage IX with 0.5 mL/min synthetic AMD flow rate and COD:sulfate ratio 1 enhanced sulfate removal, peaking at 1.3 g sulfate removed/L/day (Figure 4). This performace is comparable to sulfate removal rates reported in recent studies with similar AMD inflow rate, lower sulfate loading, and shorter experimental durations (Hernandez *et al.* 2022; Liu *et al.* 2021). Metal analysis under optimum bioreactor performance (stage 9) showed complete removal of dissolved iron, aluminium, copper, and zinc, suggesting effective precipitation as metal sulfides (Figure 5). In contrast, the SRB bioreactor removed only about half of the dissolved manganese, consistent with the relatively high solubility of Mn compared with metal sulfides such as FeS, ZnS, and CuS, (Clark *et al.* 1998). Overall, these results demonstrated the potential of the indigenous, acid-tolerant SRB adapted to high acidity and metal concentrations for site-specific AMD remediation, while also indicating the opportunity to further system performance optimization through SRB community amendments and carbon loading control. While the experiment was conducted at a maximum synthetic AMD rate of

1 mL/min under laboratory conditions, practical applications would require scaling to much higher flow rates (e.g., on the order of m3/s), potentially through multi-unit operation or reactor redesign.

Conclusions

This study demonstrated that indigenous, acid-tolerant SRB can be successfully enriched and sustain sulfate reduction and metal recovery within a bioreactor system under prolonged and variable carbon, acid, and metal loading conditions to treat AMD. The findings also highlight opportunities for performance optimization through microbial community diversity amendments, reduced AMD loading, and improved control of COD:sulfate ratio and sulfide levels. Effective removal of iron, alumunium, copper, and zinc demonstrated sulfide-driven metal recovery, while incomplete manganese removal indicated the need for staged or integrated treatment process for comprehensive metal recovery.

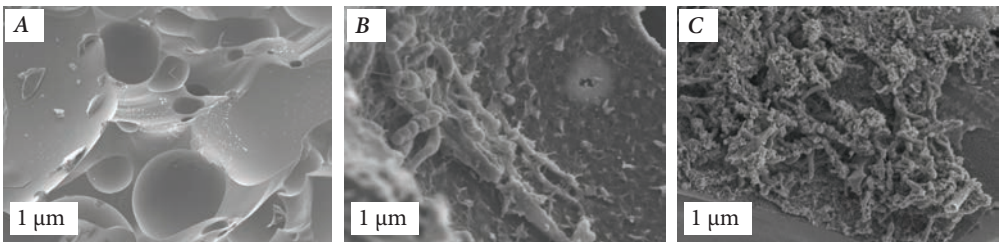

Figure 2 *Secondary images of porous beads from (A) day 0, (B) 71, and (C) 290 of SRB bioreactor operation showing development of microbial community in the system.*

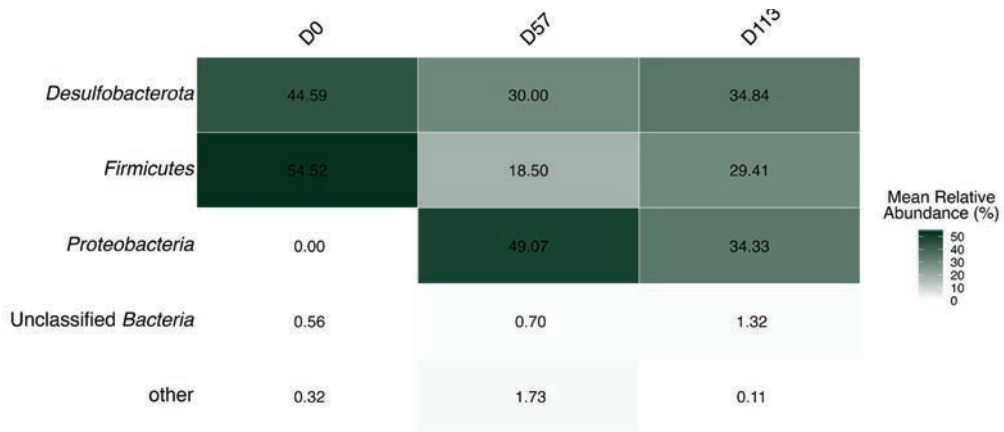

Figure 3 *Microbial community composition at phylum level in the bioreactor system at day 0, 57, and 113 shows Desulfobacterota as the most abundant phyla in the bioreactor system.*

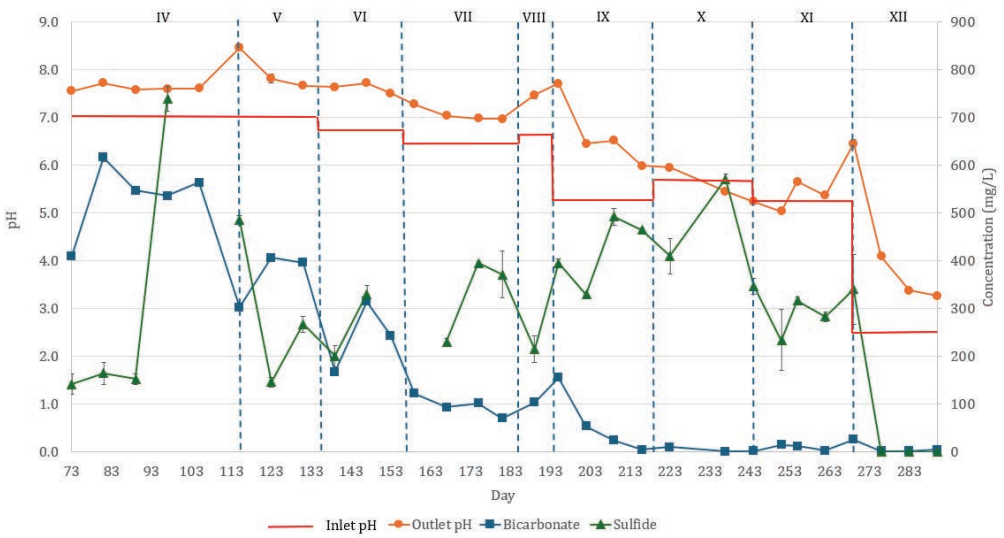

Figure 4 *Bicarbonate production influence on bioreactor effluent pH after bioreactor system stabilization.*

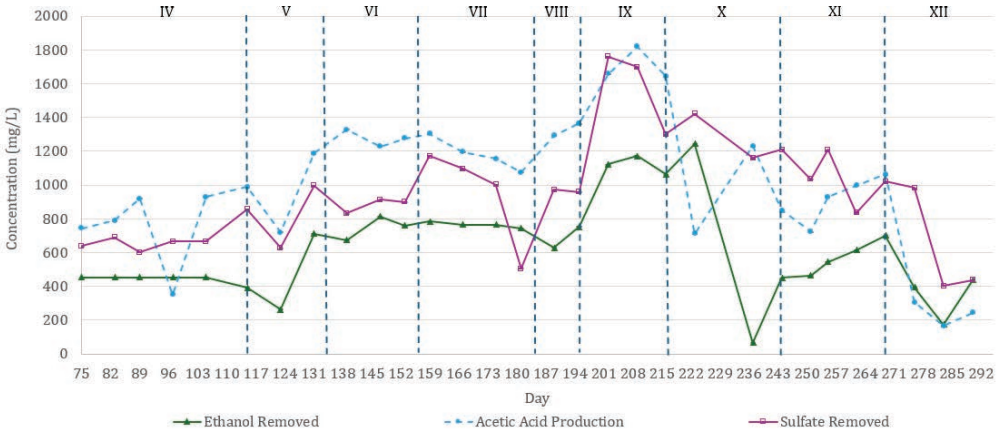

Figure 5 *Bioreactor system dynamic over experiment time after bioreactor system stabilization showing acetic acid production as by product of incomplete ethanol oxidation. The chemical parameters dynamic also shows that increased in ethanol loading did not always correspond to sulfate removal improvements.*

Acknowledgements

The authors thank the Indonesia Endowment Fund for Education (LPDP) scholarship and the support of the Australian Government through the Cooperative Research Centre for Transformations in Mining Economies (CRC TiME) in funding this research. The Queensland Department of Natural Resources, and Mines, Manufacturing and Regional and Rural Development provided access to the site and field assistance.

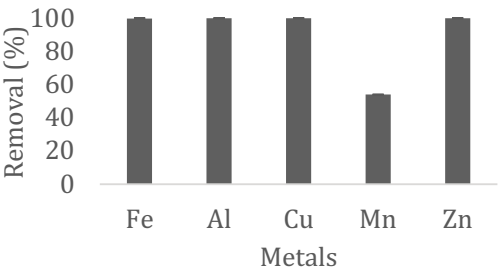

Figure 6 *Metals removal efficiency at 0.5 mL/min AMD highlight effectiveness of SRB bioreactor system in recovering Fe, Al, Cu, and Zn as metal sulfide precipitates.*

References

Clark RW, Bonicamp JM (1998) The Ksp-solubility conundrum. J Chem Educ 75(9):1182–1185. https://doi.org/10.1021/ed075p1182

Cord-Ruwisch R (1985) A quick method for the determination of dissolved and precipitated sulfides in cultures of sulfate-reducing bacteria. J Microbiol Methods 4(1):33–36. https://doi.org/10.1016/0167-7012(85)90005-3

Dyksma S, Pester M (2024) Growth of sulfate-reducing Desulfobacterota and Bacillota at periodic oxygen stress of 50% air-O2 saturation. Microbiome 12(1):191–116. https://doi.org/10.1186/s40168-024-01909-7

Gagen EJ, Levett A, Shuster J, Fortin D, Vasconcelos PM, Southam G (2018) Microbial diversity in actively forming iron oxides from weathered banded iron formation systems. Microbes Environ 33(4):385–393. https://doi.org/10.1264/jsme2.ME18019

Hernández P, Recio G, Canales C, Schwarz A, Villa-Gomez D, Southam G, Nancucheo I (2022) Evaluation of operating conditions on sulfate reduction from acidic wastewater in a fixed-bed bioreactor. Miner Eng 177:107370. https://doi.org/10.1016/j.mineng.2021.107370

Iizuka A, Ho H-J, Sasaki T, Yoshida H, Hayakawa Y, Yamasaki A (2022) Comparative study of acid mine drainage neutralization by calcium hydroxide and concrete sludge–derived material. Miner Eng 188:107819. https://doi.org/10.1016/j.mineng.2022.107819

Jones TR, Poitras J, Gagen E, Paterson DJ, Southam G (2023) Accelerated mineral bio-carbonation of coarse residue kimberlite material by inoculation with photosynthetic microbial mats. Geochem Trans 24:1. https://doi.org/10.1186/s12932-023-00082-4

Kaur G, Couperthwaite SJ, Hatton-Jones BW, Millar GJ (2018) Alternative neutralisation materials for acid mine drainage treatment. J Water Process Eng 22:46–58. https://doi.org/10.1016/j.jwpe.2018.01.004

Kim D-M, Lee K-R, Park M-S (2025) Potential generation and consumption of carbon dioxide during treatment of mine drainages in South Korea. Sci Total Environ 975:179270. https://doi.org/10.1016/j.scitotenv.2025.179270

Liu Y, Vaughan J, Southam G, Serrano A, Marcellin E, Nancucheo I, Villa-Gomez DK (2021) Enhanced metal recovery by efficient agglomeration of precipitates in an up-flow fixed-bed bioreactor. Chem Eng J 416:127662. https://doi.org/10.1016/j.cej.2020.127662

Queensland Government (2021) Mount Morgan remediation project. Retrieved 12 May 2025, from https://www.qld.gov.au/environment/land/management/abandoned-mines/remediation-projects/mount-morgan

Queensland Government Department of Resources (2023) Queensland Globe. Retrieved 24 December 2023 from https://qldglobe.information.qld.gov.au/qldglobe/private/proposed-sampling-points

Schloss PD, Westcott SL, Ryabin T, Hall JR, Hartmann M, Hollister EB, Lesniewski RA, Oakley BB, Parks DH, Robinson CJ, Sahl JW, Stres B, Thallinger GG, Van Horn DJ, Weber CF (2009) Introducing mothur: open-source, platform-independent, community-supported software for describing and comparing microbial communities. Appl Environ Microbiol 75(23):7537–7541. https://doi.org/10.1128/AEM.01541-09

Villa Gomez D, Hong P, Berry L, Liu D, Edraki M (2023). Element distribution in electrochemically treated mine wastewater for efficient resource recovery and water treatment: A pilot study. Chemosphere (Oxford) 339: 139536-139536. https://doi.org/10.1016/j.chemosphere.2023.139536

Werner TT, Bach PM, Yellishetty M, Amirpoorsaeed F, Walsh S, Miller A, Roach M, Schnapp A, Solly P, Tan Y et al (2020) A geospatial database for effective mine rehabilitation in Australia. Minerals 10:745. https://doi.org/10.3390/min10090745

IMWA 2026
Jeongseon

Multi-Temporal UAV Hyperspectral Monitoring of a Mine-Water Influenced Pond System: Harpener Teiche (Germany)

Hernan Flores[1,2], Barbara M.A. Teichert[1], Simon Nikutta[1], Tobias Rudolph[1]

[1]*Research Center of Post-Mining, University of Applied Sciences Georg Agricola (THGA), Herner Straße 45, 44787 Bochum, Germany*

[2]*Institute of Mine Surveying and Geodesy, TU Bergakademie Freiberg, Fuchsmühlenweg 9B, 09599 Freiberg, Germany*

Correspondence author: hernan.flores@thga.de

Abstract

This study evaluates UAV-based hyperspectral imaging for multi-temporal monitoring of a mine-water influenced pond system at Harpener Teiche, Bochum, Germany. Three campaigns between October 2025 and February 2026 were processed to reflectance and analysed using a normalized four-band VNIR brightness metric. The resulting maps and transect profiles reveal recurrent optical patterns associated with the mine-water inflow and plume dispersion. Spectral reflectance profiles distinguish optical signatures of inflow, mixing zone, and background pond water, while in-situ electrical conductivity and temperature measurements provide hydrochemical context. The approach complements point-based monitoring with spatially continuous observations.

Keywords: UAV; hyperspectral sensing; mine-water; environmental monitoring; post-mining; remote sensing

Introduction

Mine-water discharge is one of the most persistent environmental challenges associated with the legacy of underground mining. After mine closure, active water management is required to prevent groundwater rebound and flooding of underground workings, resulting in large volumes of mine-water being continuously pumped and discharged into nearby rivers, streams, or artificial lakes.

Conventional monitoring of these discharges relies on in-situ sampling and laboratory analysis, which provide detailed chemical information but are limited to discrete sampling points. Consequently, spatial patterns and mixing processes within receiving water bodies often remain poorly characterized. Remote sensing offers complementary capabilities: hyperspectral imaging provides near-continuous spectral information across many narrow bands, while recent advances in uncrewed aerial vehicle (UAV) platforms enable flexible, high-resolution deployment over targeted areas. Previous studies have demonstrated the potential of UAV-based hyperspectral sensing for monitoring aquatic environments affected by acid mine drainage (Flores *et al.*, 2021), mine-water sludge in tailings ponds (Flores *et al.*, 2024), and variations in water optical properties related to turbidity and mixing processes (Cui *et al.*, 2022). However, its application for tracking environmental changes on a multi-temporal basis remains limited.

In this study, we evaluate the capability of UAV-based hyperspectral imaging for multi-temporal monitoring of a mine-water influenced pond system at Harpener Teiche (Bochum, Germany). By integrating UAV hyperspectral imagery with in-situ water measurements, the study demonstrates how high-resolution remote sensing can complement conventional monitoring and improve the understanding of spatial environmental processes within mine-water systems.

Study Area

The study area is located at Harpener Teiche (Fig. 1), a system of artificial ponds situated in the city of Bochum within the Ruhr mining region in western Germany. The ponds form part of a local surface water system influenced by historical coal mining activities in the region.

Previous studies have shown that mine-water inflows represent a major component of the water balance in the Harpener Teiche and the downstream hydrological

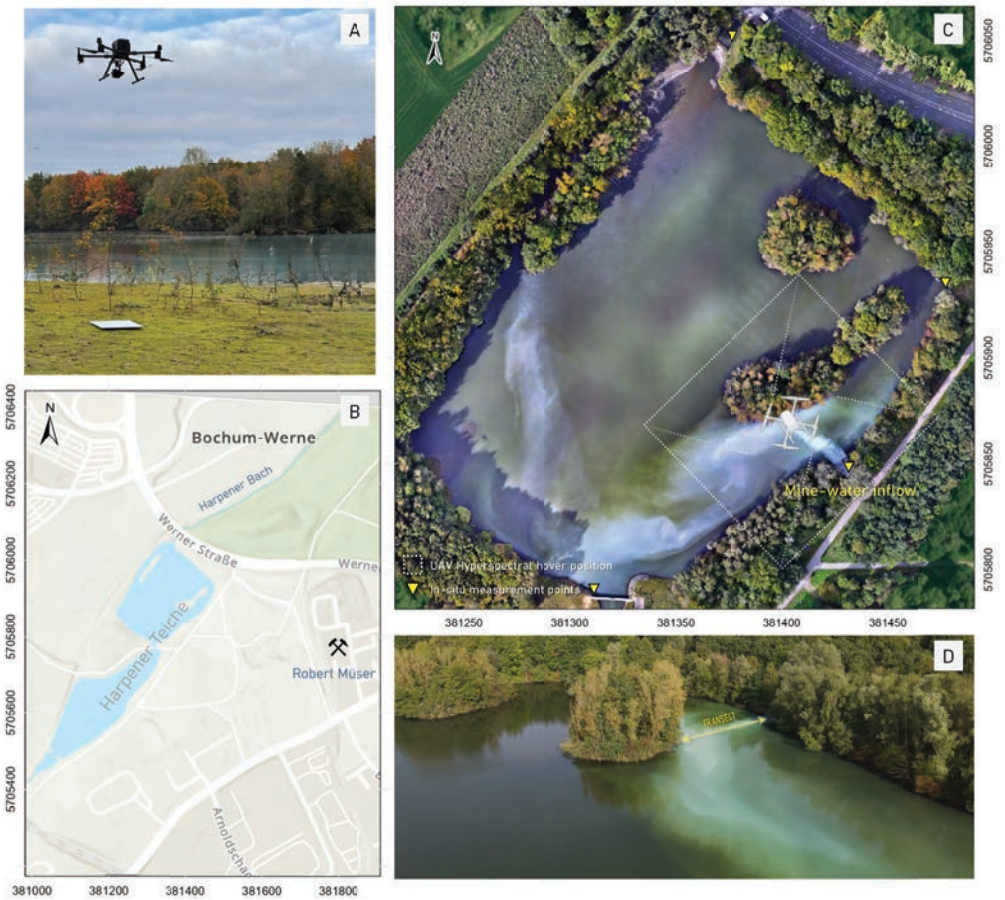

Figure 1 *Study area and UAV monitoring configuration at Harpener Teiche (Bochum, Germany). (A) UAV system used for hyperspectral data acquisition. (B) Location within Bochum. (C) UAV orthomosaic showing the mine-water inflow, hover acquisition area, and in-situ measurement points (yellow markers). (D) Oblique image of the visible plume and the A–B transect used for spatial analysis. Coordinates in panels B and C: ETRS89 / UTM Zone 32N (EPSG:25832), in meters.*

network (Schneider *et al.*, 2008). The discharged mine-water originates from the former Robert Müser coal mine and is characterized by elevated mineralization, increased temperature, and sulfur-related treatment products, which influence the physical and chemical conditions of the receiving water body. In the present field campaigns, electrical conductivity measured near the mine-water inflow ranged between approximately 5.36 and 5.87 mS cm^{-1}, while water temperature ranged between 17.9 and 20.4 °C. These values are consistent with a highly mineralized mine-water influence. Sulfur species were not quantified in this study; however, the whitish coloration of the inflow is linked to the mine-water treatment process, where hydrogen peroxide is added to oxidize hydrogen sulfide. This process can produce sulfur-related suspended particles that contribute to the visible plume.

The Harpener Teiche system consists of two main shallow artificial ponds connected to a small stream network (Fig. 1B). Mine-water is discharged into the pond through a controlled inflow structure connected to the regional mine-water management infrastructure (Fig. 1C). The inflow generates a visible plume within the pond due to differences in turbidity and suspended particles, likely including sulfur-related treatment products, between mine-water and the surrounding pond water (Fig. 1D).

Aerial and field measurements were collected during three monitoring campaigns in October 2025, December 2025, and February 2026. During each campaign, in-situ measurements of water temperature, electrical conductivity (EC), and pH were obtained at four accessible shoreline locations within the pond system, including the mine-water inflow area and three additional points around the pond. These locations are indicated by yellow markers in Fig. 1C. Water parameters were measured using a multi-parameter portable meter (WTW ProfiLine Multi 3320). The pH meter was calibrated using Hanna standard solutions (pH 4.01 and pH 7.01). The probes were placed directly into the water from the shoreline with gentle agitation, and measurements were recorded once the readings stabilized.

Methods

UAV hyperspectral data acquisition

Hyperspectral data were collected using a UAV-mounted BlackBird V2 hyperspectral camera (HAIP Solutions GmbH, 2022) operating in the visible to near-infrared (VNIR) spectral range. The sensor was mounted on a DJI Matrice M350 RTK platform (Fig. 1A) and includes a hyperspectral (HSI) sensor and a separate RGB camera for livestreaming on the remote controller. The hyperspectral sensor captures images at a native resolution of 540 × 540 pixels and records 100 spectral bands across the 500–1000 nm wavelength range, with a spectral resolution and spectral sampling interval of 5 nm according to the manufacturer specifications. The sensor was deployed in a hover acquisition configuration above the mine-water inflow zone to maximize spatial resolution and minimize geometric distortions. The UAV was operated at a flight height of 120 m above ground level with constant sensor orientation, resulting in an approximate ground sampling distance of 0.13 m per pixel. Georeferencing was based on the integrated positioning system of the RTK-enabled UAV platform. Camera settings were adjusted slightly between campaigns to account for changing illumination conditions.

Hyperspectral preprocessing

Hyperspectral datasets were preprocessed using a custom Python-based preprocessing workflow developed by the first author, comprising dark frame correction, radiometric calibration, reflectance calibration using a reference panel, and spectral smoothing. A water mask was applied to isolate the pond surface and exclude surrounding vegetation and land areas from the analysis.

To compare spatial patterns between campaigns, a four-band brightness metric was calculated as the arithmetic mean of reflectance at 557, 667, 752, and 852 nm. These wavelengths were selected to represent visible, red-edge, and near-infrared regions sensitive to suspended particles, turbidity-related scattering, and plume visibility, while avoiding major atmospheric and water absorption features near 760 nm and 970 nm (Wu *et al.*, 2014; Cui *et al.*, 2022). The metric

was used as a relative brightness proxy, not as a physically based turbidity index. Brightness values were then normalized to a 0–1 range using min–max scaling.

Results

Multi-temporal hyperspectral monitoring

Normalized brightness maps derived from the hyperspectral datasets reveal a recurrent optical pattern associated with the mine-water inflow during the three monitoring campaigns. In all datasets, the inflow area is characterized by increased normalized brightness relative to the surrounding pond water, indicating enhanced reflectance linked to suspended particles, turbidity-related effects, and plume dispersion.

Figure 2 illustrates the spatial distribution of normalized brightness values across the water surface during the three monitoring dates. The brightness maps consistently identify the mine-water inflow and the associated plume-like dispersion pattern. While the exact spatial extent and intensity of the high-brightness zone vary between campaigns, the inflow signature remains detectable in all three datasets. These variations likely reflect differences in illumination, local hydrodynamic conditions, and short-term mixing behaviour at the time of acquisition.

The repeated detection of this optical anomaly demonstrates that UAV hyperspectral imagery can capture spatial patterns related to mine-water dispersion within the pond system. The brightness metric should therefore be interpreted as a relative optical proxy for plume visibility and turbidity-related spatial variability, rather than as a direct measurement of water chemistry.

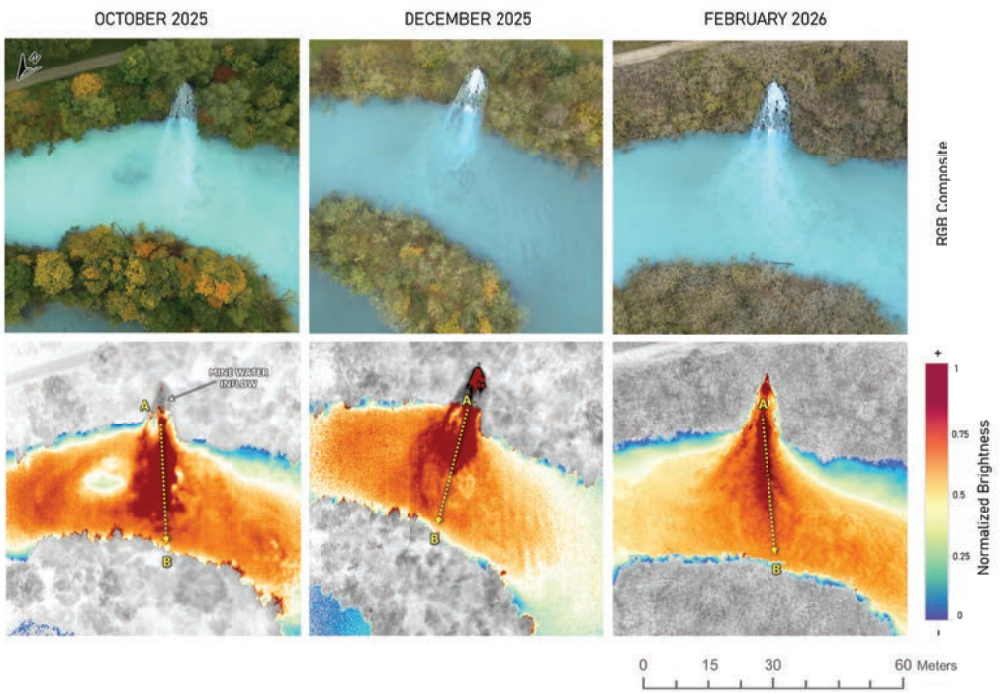

Figure 2 *Multi-temporal UAV monitoring of the mine-water inflow at Harpener Teiche. The upper row shows RGB composites acquired during the October 2025, December 2025, and February 2026 campaigns. The lower row shows min–max normalized hyperspectral brightness maps derived from selected VNIR bands. The A–B transects indicate the plume-axis profiles used for the brightness analysis shown in Fig. 3.*

Spatial gradients in optical properties

To quantify spatial variations in brightness across the mixing zone, A–B transects were extracted from the mine-water inflow toward the pond interior for each monitoring campaign, as shown in Figure 2. The resulting profiles in Figure 3 show clear gradients in normalized brightness associated with the transition from the inflow-dominated zone toward areas of lower optical influence.

The brightness profiles show high normalized brightness values near the inflow, corresponding to the visible mine-water plume entering the pond. Along the transect, brightness values generally decrease with distance from the inflow, reflecting changes in water optical properties related to plume dispersion, suspended particles, and mixing with the surrounding pond water.

Differences between the three profiles indicate campaign-specific variations in the spatial extent and intensity of the optical plume. The October profile shows a more gradual decrease along the transect, suggesting a more extended high-brightness zone. In contrast, the December profile decreases more sharply, indicating a more localized optical signal near the inflow. The February profile shows an intermediate pattern, with high brightness near the inflow followed by a progressive decrease toward the pond interior. Overall, these observations indicate that normalized hyperspectral brightness profiles can capture recurring spatial gradients and short-term temporal differences in mine-water plume dispersion under varying environmental conditions.

Spectral reflectance characteristics

Spectral reflectance profiles were extracted from three regions of interest (ROIs) representing the mine-water inflow, the mixing zone, and background pond water (Fig. 4A). The mean spectra show a systematic decrease in reflectance magnitude from the mine-water inflow to the mixing zone and finally to pond water (Fig. 4B). The inflow spectrum exhibits the highest reflectance values across the visible wavelengths, particularly in the green spectral region around 550 nm, which is consistent with increased turbidity and suspended particle concentrations in aquatic environments (Cui *et al.*, 2022). The mixing-zone spectrum

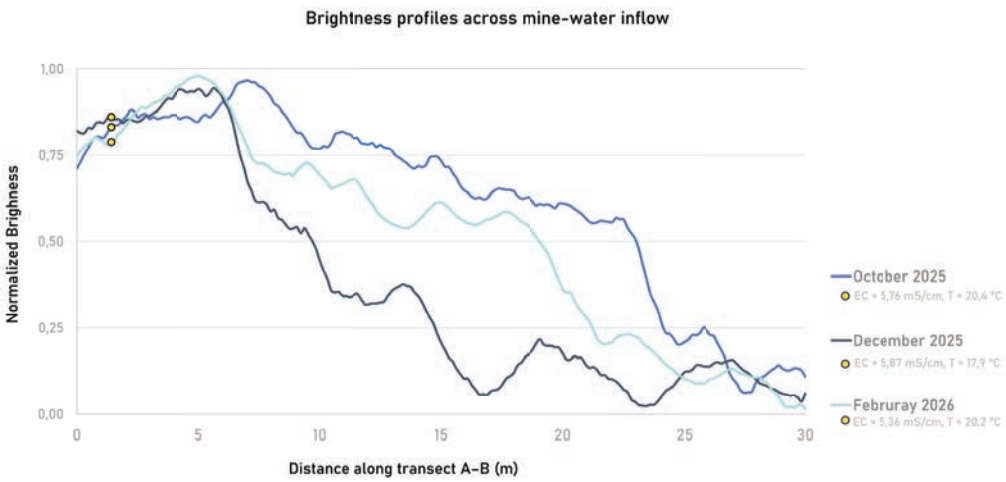

Figure 3 *Normalized brightness profiles extracted along the A–B transects shown in Fig. 2. Distance is measured from the mine-water inflow toward the pond interior over approximately 30 m. All campaigns show a general decrease in normalized brightness away from the inflow, reflecting changes in optical properties across the mixing zone. Yellow markers indicate near-inflow in-situ measurements of electrical conductivity (EC) and water temperature (T), which are shown for hydrochemical context.*

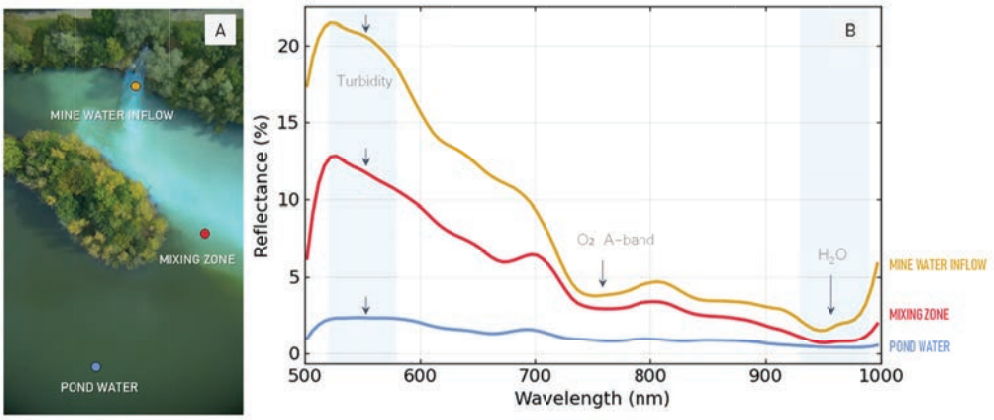

Figure 4 Spectral reflectance profiles from selected regions of interest (ROIs) within the Harpener pond system. (A) Orthoimage showing ROIs for the mine-water inflow, mixing zone, and background pond water. (B) Mean VNIR reflectance spectra (500–1000 nm) extracted from the ROIs. Shaded regions indicate turbidity-sensitive visible wavelengths and atmospheric or water-related absorption features, including the O_2 A-band and H_2O absorption.

shows intermediate reflectance values, while the pond-water spectrum exhibits the lowest overall reflectance.

The spectra are largely featureless across most of the VNIR range, as expected for surface water, but show a narrow absorption feature near 760 nm corresponding to the atmospheric O_2 A-band and a broader decrease around 970 nm associated with liquid-water absorption (Green *et al.*, 2006; Flores *et al.*, 2021). These spectral patterns support the interpretation that the hyperspectral data capture relative optical differences between the inflow, mixing zone, and surrounding pond water, rather than directly measuring water chemistry.

In-situ measurements collected at the four accessible shoreline locations provide hydrochemical context for the hyperspectral observations. Electrical conductivity values measured during the campaigns ranged between approximately 5.3 and 5.9 mS cm^{-1} at the sampled shoreline points, confirming the strong mine-water influence of the pond system. However, because measurements were limited to accessible shoreline locations, these values should not be interpreted as a full spatial validation of electrical conductivity across the pond. In contrast, measurements from the nearby Harpener Bach showed substantially lower electrical conductivity values (< 1 mS cm^{-1}), indicating freshwater primarily derived from precipitation and shallow surface runoff.

Conclusions

This study demonstrates the potential of UAV-based hyperspectral imaging for multi-temporal monitoring of mine-water influenced pond systems. The datasets captured recurrent brightness gradients across the inflow and mixing zone, while spectral reflectance profiles distinguished optical signatures of inflow, mixing zone, and background pond water. In-situ measurements of electrical conductivity and temperature provided hydrochemical context for the mine-water influence at the site.

In practical terms, UAV hyperspectral monitoring can complement conventional sampling by mapping plume extent, guiding sampling locations, and documenting temporal changes in mixing patterns, particularly useful in post-mining water bodies where discharge points are spatially heterogeneous. Future work should exploit the full 100-band dataset and combine UAV observations with denser in-situ measurements collected away from the shoreline, enabling empirical reflectance–turbidity relationships and more quantitative monitoring of mine-water dispersion.

Acknowledgements

The authors thank the Research Center of Post-Mining (FZN), THGA Bochum, for providing the UAV platform and sensor systems, and Dr. Marcin Pawlik for fieldwork support.

References

Cui, M., Sun, Y., Huang, C. and Li, M. 2022. Water turbidity retrieval based on UAV hyperspectral remote sensing. Water, 14(1), 128. https://doi.org/10.3390/w14010128

Flores, H., Lorenz, S., Jackisch, R., Tusa, L., Contreras, I.C., Zimmermann, R. and Gloaguen, R. 2021. UAS-based hyperspectral environmental monitoring of acid mine drainage affected waters. Minerals, 11(2), 182. https://doi.org/10.3390/min11020182

Flores, H., Reker, B., Pawlik, M., Haske, B. and Rudolph, T. 2024. Hyperspectral UAS-sensing for tailing ponds monitoring: Towards responsible resource repurposing. In: Kleinmann, B., Skousen, J. and Wolkersdorfer, C. (eds), Proceedings of the West Virginia Mine Drainage Task Force Symposium & 15th International Mine Water Association Congress, Morgantown, WV, USA, pp. 196–202.

Green, R.O., Painter, T.H., Roberts, D.A. and Dozier, J. 2006. Measuring the expressed abundance of the three phases of water with an imaging spectrometer over melting snow. Water Resources Research, 42. https://doi.org/10.1029/2005WR004509

HAIP Solutions GmbH. 2022. BlackBird V2 hyperspectral camera: Product data sheet. Hannover, Germany.

Schneider, Y., Grube, S. and Weilandt, M. 2008. Determination and evaluation of the phosphorus load of an artificial shallow lake. Water Science and Technology, 58(10), 1993–2000. https://doi.org/10.2166/wst.2008.747

Wu, J.-L., Ho, C.-R., Huang, C.-C., Srivastav, A., Tzeng, J.-H. and Lin, Y.-T. 2014. Hyperspectral sensing for turbid water quality monitoring in freshwater rivers: Empirical relationship between reflectance and turbidity and total solids. Sensors, 14, 22670–22688. https://doi.org/10.3390/s141222670

IMWA 2026
Jeongseon

Revalorization of Coal Waste Facilities: The CRMsDataSpace EU Approach

Hernan Flores[1,5], Bastian Reker[1], Tansel Dogan[1], Antonio Marquez[2] Alicja Krzemień[3], Vlad Mihai Păsculescu[4]

[1]*Research Center of Post-Mining, University of Applied Sciences Georg Agricola (THGA), Herner Straße 45, 44787 Bochum, Germany*

[2]*University of Oviedo, Department of Mining Exploitation and Prospecting, 13 Independencia Street – 33004 Oviedo, Spain*

[3]*Central Mining Institute, Department of Extraction Technologies, Rockbursts and Risk Assessment, 40-166 Katowice, Poland*

[4]*National Institute for Research and Development in Mine Safety and Protection to Explosion - INSEMEX, 32-34 G-ral Vasile Milea Street, 332047 Petroșani, Romania*

[5]*Institute of Mine Surveying and Geodesy, TU Bergakademie Freiberg, Fuchsmühlenweg 9B, 09599 Freiberg, Germany*

Correspondence author: hernan.flores@thga.de

Abstract

Europe's coal mining legacy is often viewed as an environmental burden, yet closed coal waste facilities may also represent overlooked secondary sources of critical raw materials. The CRMsDataSpace project responds to this challenge by developing a harmonized European data infrastructure to assess CRM potential in closed extractive coal waste facilities. This paper presents the project framework, pilot sites in Germany, Spain, Romania and Poland, and the German case study of iron-rich mine water treatment sludge from the former Ibbenbüren coalfield. It shows how standardized data and material characterization can support more transparent revalorization strategies for post-mining regions.

Keywords: Critical raw materials, mine waste, tailings sludge, data space, data integration, land reuse, resource estimation

Introduction

Historical coal mining activities across Europe have generated large volumes of waste materials, including waste rock dumps, tailings from coal processing, and residues derived from mine water treatment. These deposits form extensive anthropogenic accumulations distributed throughout historical coal basins and represent long-term environmental and management challenges in post-mining regions.

At the same time, Europe faces an increasing demand for critical raw materials (CRMs) required for the energy transition, including renewable energy technologies, digital systems, and advanced manufacturing. In response to growing supply risks and geopolitical dependencies, the European Union has introduced new policy instruments to strengthen resource security, including the Critical Raw Materials Act (CRMA) (European Union, 2024).

Within this context, increasing attention is being given to secondary anthropogenic deposits generated by historical mining activities. Mine wastes are increasingly investigated as potential sources of valuable metals and critical raw materials. These materials, often historically considered non-valuable, may still contain relevant concentrations of rare earth elements and other critical metals that could be recovered through reprocessing and circular economy strategies (Vitti & Arnold, 2022; Tayebi-Khorami *et al.*, 2019; Flores *et al.*, 2025). Furthermore, mine-water treatment

residues represent a particularly relevant case, especially in regions where mine water management continues after mine closure. During treatment processes, dissolved iron and other metals precipitate as hydroxides and oxides, forming sludge deposits that may act as effective sorption phases for trace metals and rare earth elements (Reker *et al.*, 2022; Reker & Westermann, 2025).

In this context, several research initiatives are exploring the potential revalorisation of mining wastes through re-mining approaches and integrated resource assessments. The CRMsDataSpace project, funded by the EU Research Fund for Coal and Steel (RFCS), aims to assess the recovery potential of critical raw materials from closed extractive coal waste facilities across several European coal regions while developing a harmonized digital data infrastructure to support resource assessment and sustainable post-mining land management.

The CRMsDataSpace Project

The project *"Common European Data Space on Critical Raw Materials for the Green Deal: Recovery Potential from Closed Extractive Coal Waste Facilities" (CRMsDataSpace)* focuses on the identification, characterization, and evaluation of coal-related waste facilities that may host critical raw materials.

The main objective is to develop a standardized European framework for assessing CRM potential in closed extractive coal waste facilities and to establish a structured data space integrating geological, geochemical, environmental, and technical information related to these sites.

The methodological framework combines several components: (1) identification and inventory of coal-related waste facilities, (2) field sampling and material characterization, (3) geochemical and mineralogical analyses, (4) evaluation of environmental and technical constraints, and (5) integration of results into a European data space.

These activities aim to support the development of circular economy strategies for mining regions undergoing post-mining transition while improving the management of legacy mining wastes. As illustrated in Figure 1, the CRMsDataSpace methodological framework operates on two complementary levels: the development of a harmonized data infrastructure and the application of integrated datasets for resource assessment, AI-assisted analysis, and circular economy strategies.

The upper level of Figure 1 represents the development of the data infrastructure, including data collection from closed extractive coal waste facilities, creation of a harmonized data catalogue, and the implementation of a Minimum Viable Data Space (MVDS) contributing to the future European Data Space on Critical Raw Materials. The lower level illustrates the application layer, where integrated datasets support AI-assisted resource estimation, development of business models, and knowledge transfer activities for the sustainable revalorisation of coal mining wastes.

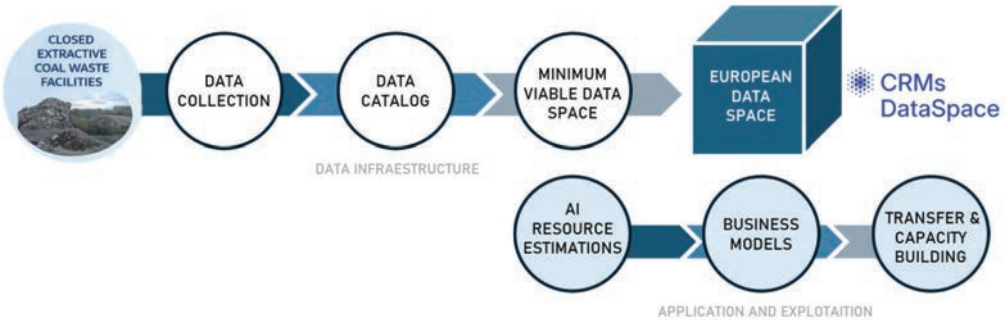

Figure 1 *Conceptual framework of the CRMsDataSpace project showing two complementary levels.*

Pilot Sites Across European Coal Regions

The CRMsDataSpace project currently investigates several pilot sites representing different types of coal-related waste facilities. These include mine waste dumps, coal processing residues, and sludge deposits generated during mine water treatment. Figure 2 illustrates the general investigation workflow applied across the pilot sites. The assessment typically begins with field reconnaissance and surface sampling aimed at obtaining an initial geochemical screening of the waste materials. Based on this preliminary evaluation, additional investigations such as hydrometallurgical testing and, where applicable, exploration drilling may be carried out to characterize deeper waste layers and support resource estimation. The final stage consists of integrating the generated datasets into the CRMsDataSpace data infrastructure.

In Germany, the project investigates sludge deposits generated at the Gravenhorst mine water treatment plant in the former Ibbenbüren coalfield. These deposits consist of iron-rich sludge accumulated during several decades of mine water treatment operations.

In Spain, investigations focus on historical coal waste heaps located in the Asturias mining region. The San Nicolás waste dump is currently being evaluated through exploratory drilling campaigns and systematic sampling to characterize the geochemical composition of the deposited materials.

In Romania, the project includes the Petrila mine waste dump located in the Jiu Valley coal basin. This deposit represents a large accumulation of coal mining waste generated during decades of underground mining activities.

In Poland, several coal-related waste deposits from the Upper Silesian coal basin are being investigated to evaluate their potential as secondary sources of critical raw materials.

These pilot sites represent different geological settings, waste formation processes, and environmental conditions, providing a test framework for the standardized methodology developed within the project.

Case Study: Mine Water Treatment Sludge at Ibbenbüren (Germany)

The German case study focuses on sludge deposits at the Gravenhorst mine water treatment plant, located near Hörstel in the former Ibbenbüren coal mining district in North Rhine-Westphalia. Following the closure of the Ibbenbüren hard coal mine in 2018, long-term mine water management became part of the perpetual post-mining obligations, managed by RAG Foundation, associated with former underground coal mining operations in Germany (RAG-Stiftung, 2022).

At the Gravenhorst facility, mine water emerging from underground workings is treated before its discharge into the regional river system. During treatment, dissolved iron and other metals precipitate as hydroxides and oxides. These precipitates are separated from the treated water and deposited in nearby sludge tailing ponds. Over several decades

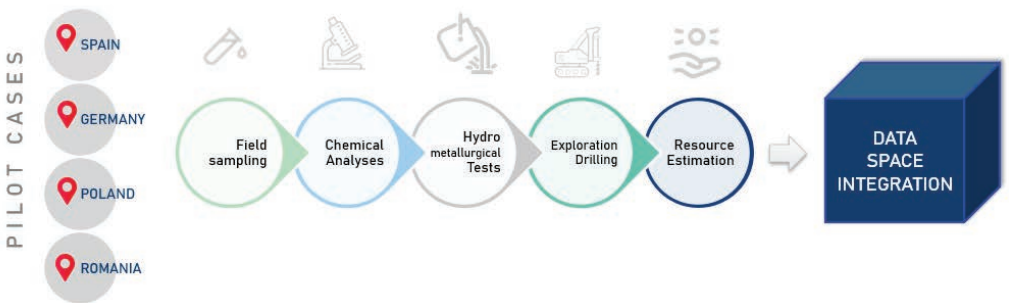

Figure 2 Investigation workflow applied across the CRMsDataSpace pilot sites.

of operation, this process has resulted in the accumulation of substantial volumes of iron-rich sludge.

The sludge deposition complex consists of four main ponds with a combined surface area of approximately 257,000 m², with estimated sludge thicknesses ranging between 2 and 4 m (Reker & Westermann, 2025). This corresponds to an estimated total sludge volume between 472,000 and 944,000 m³, representing a substantial accumulation of mine water treatment residues associated with long-term mine water management.

These materials are mainly composed of ferric hydroxides, iron oxides, manganese oxides, gypsum, and fine-grained clay particles (Flores *et al.*, 2024). Such mineral phases are known to efficiently adsorb trace metals and potentially concentrate elements of economic interest (Reker *et al.*, 2022). Previous studies have suggested that these sludge deposits may host recoverable quantities of several metals, including iron, manganese, aluminium, and trace amounts of critical raw materials such as cobalt and rare earth elements. Estimated recoverable quantities reported for the Ibbenbüren sludge deposits are summarized in Table 1 (adapted from Reker & Westermann, 2025).

These estimates represent a conservative scenario, as the deeper layers of the sludge deposits may contain higher metal concentrations. This enrichment may be related to the first flush effect, a process commonly observed during the early stages of mine flooding and mine water discharge, where elevated concentrations of dissolved metals are mobilized and subsequently precipitated during treatment (Younger, 1997).

An overview of the sludge tailing ponds associated with the Gravenhorst mine water treatment plant is shown in Figure 3.

Planned Sampling and Characterization

Sampling activities are planned within the CRMsDataSpace project to characterize the geochemical and mineralogical composition of the Ibbenbüren sludge deposits. Laboratory analyses will focus on trace metals and potential critical raw materials associated with iron-rich mine water treatment residues, supporting the evaluation of their potential role as secondary resources.

Conclusions

Coal mining waste deposits represent an important, yet largely underexplored potential source of critical raw materials in Europe. The CRMsDataSpace project represents one of the first coordinated European initiatives aimed at developing a standardized framework for assessing the CRM potential of coal-related waste facilities. The investigation of pilot sites in Germany, Spain, Romania, and Poland provides a unique opportunity to evaluate the applicability of common methodologies across diverse geological settings, waste formation processes, and environmental conditions.

The German case study at Ibbenbüren highlights the potential importance of mine water treatment sludges as secondary anthropogenic deposits enriched in iron hydroxides and associated trace metals. Ongoing sampling and laboratory characterization will provide further insights

Table 1 *Estimated recoverable metals from Ibbenbüren mine water sludge deposits (adapted from Reker & Westermann, 2025).*

Element	Estimated Recoverable Amount (t)
Fe	88,000 – 176,000
Mn	3,000 – 6,000
Al	2,400 – 4,800
Ni	90 – 180
Ti	75 – 150
Co	65 – 130
REEs	20 – 40

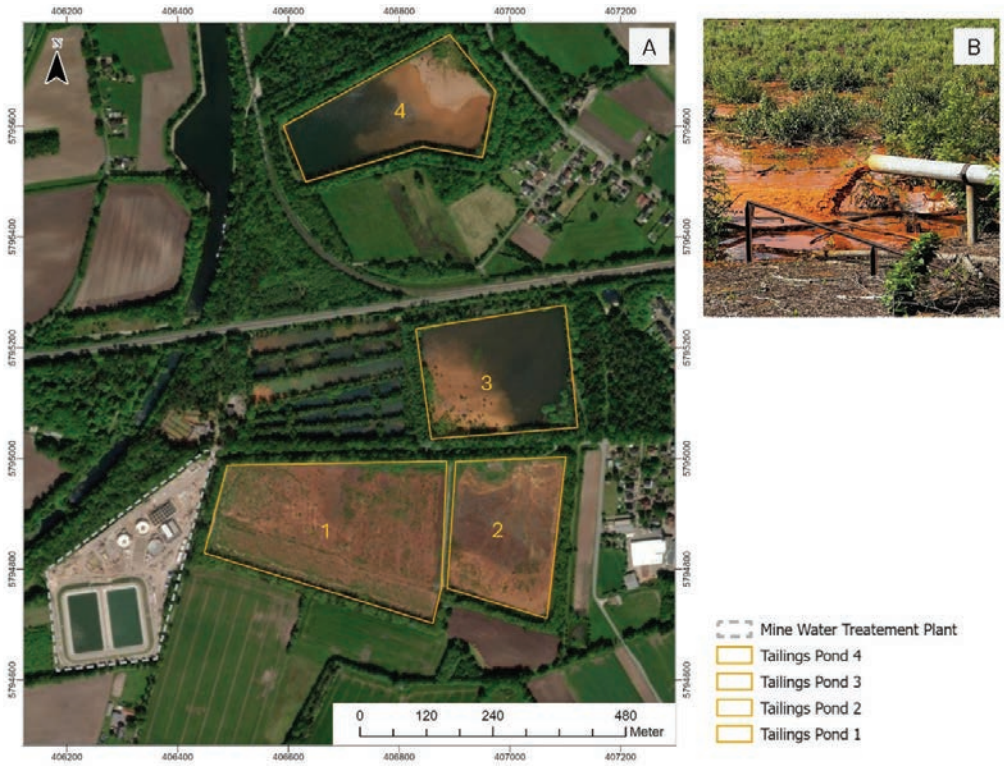

Figure 3 *Overview of mine water treatment residues investigated in Germany. (A) Orthophoto showing the sludge tailing ponds associated with the Gravenhorst mine water treatment plant from the former Ibbenbüren coalfield. (B) Field photograph illustrating iron-rich sediments produced during mine water treatment (Photography by Hernan Flores).*

into the geochemical composition of these materials and their potential contribution to future circular resource strategies and the sustainable recovery of critical raw materials from legacy coal mining wastes.

Acknowledgements

This work has been developed within the framework of the RFCS project CRMsDataSpace, funded by the European Union under Grant Agreement No. 101216677. The authors gratefully acknowledge the collaboration and contributions of all CRMsDataSpace consortium partners: GIG-PIB, Universidad de Oviedo, SATEC Group, University of Burgos, INSEMEX, Grupo DEX, THGA, and EURACOAL.

References

European Union, 2024. Regulation (EU) 2024/1252 of the European Parliament and of the Council of 11 April 2024 establishing a framework for ensuring a secure and sustainable supply of critical raw materials (Critical Raw Materials Act). Official Journal of the European Union. Available at: https://eur-lex.europa.eu/legal-content/EN/TXT/?uri=CELEX:32024R1252

Flores, H., Reker, B., Pawlik, M., Haske, B., Rudolph, T., 2024. Hyperspectral UAS-sensing for tailing ponds monitoring: Towards responsible resource repurposing. In: Kleinmann, B., Skousen, J., Wolkersdorfer, C. (Eds.), West Virginia Mine Drainage Task Force Symposium & 15th International Mine Water Association Congress. Morgantown, WV, USA, pp. 196–202.

Flores, H., Rudolph, T., Benndorf, J., 2025. Multi-scale characterization of mine waste in a circular economy: Challenges and opportunities. In: Valente, T., Mühlbauer, R., Ordóñez, A., Wolkersdorfer, C. (Eds.), Internatioal Mine Water Association Conference – Time to Come. Braga, Portugal, pp. 319–325.

RAG-Stiftung, 2022. The RAG Foundation at a glance. Available at: https://anrep.rag-stiftung.de/2022/the-rag-stiftung-at-a-glance.html accessed 05 March 2026).

Reker, B., Westermann, S., Melchers, C., 2022. Mine waters as a resource of critical raw materials in

Germany. GeoResources, 4, 43–47. Available at: https://www.georesources.net/cms.php/de/journals/865/Grubenwaesser-als-Ressource-kritischer-Rohstoffe-in-Deutschland

Reker, B., Westermann, S., 2025. Re-mining of mine water sludges in Germany: An opportunity? In: Valente, T., Mühlbauer, R., Ordóñez, A., Wolkersdorfer, C. (Eds.), International Mine Water Association Conference – Time to Come. Braga, Portugal, pp. 807–812.

Tayebi-Khorami, M., Edraki, M., Corder, G., Golev, A., 2019. Re-thinking mining waste through an integrative approach led by circular economy aspirations. Minerals, 9(5), 286. https://doi.org/10.3390/min9050286

Vitti, C., Arnold, T., 2022. Mine waste as a potential source of critical raw materials: A review. Mineral Economics, 35, 1–14. https://doi.org/10.1007/s13563-021-00264-0

Younger, P.L., 1997. The longevity of mine water pollution: A basis for decision-making. Science of the Total Environment, 194–195, 457–466. https://doi.org/10.1016/S0048-9697(96)05383-1

Groundwater Flow Interactions in a Seven-Layer Meromictic Pit Lake at the Former Victor Diamond Mine, Ontario Canada

Simon Gautrey[1], Mathieu Desjardins[2], Sebastien Boucher[2]

[1]*WSP Canada Inc., Hamilton, Ontario Canada, simon.gautrey@WSP.com*

[2]*De Beers Canada Inc., mathieu.desjardins@debeersgroup.com*

Abstract

Groundwater interactions with a meromictic pit lake were investigated at the former Victor Diamond Mine, Ontario, Canada, through a comparison of pit lake and pre-mining groundwater conductivity and temperature profiles. The study provides an example of a pit lake where groundwater interactions from thin, flat-lying, bedding-plane aquifers containing waters of differing chemistry create measurable stratification.

Keywords: Pit Lake, meromictic, groundwater, Victor diamond mine, diamond mine

Introduction

The former Victor Diamond Mine (VDM) is located in the James Bay portion of the Hudson Bay Lowlands, approximately 90 km west of Attawapiskat (Fig. 1a). Mining ended in early 2019 after 12 years of operation, allowing the pit to flood (Fig. 1b). Flooding was assisted by pumping freshwater from the nearby Attawapiskat River between April 2020 and December 2022. Most of the water was pumped during the non-winter months because of seasonal pumping constraints. Using this strategy, flooding of the 280 m deep pit ended in 2022. Pit lake levels stabilized by mid-2023.

This paper presents a case study of a pit lake at a non-metallic mine in sedimentary bedrock containing several flat-lying bedding-plane aquifers of differing water quality. The study shows that groundwater flow can produce measurable stratification in the pit lake water quality profile, coincident with aquifer locations. This case study may assist future scientists in assessing pit lake conditions in similar environments, including prospective open pit mines in sedimentary bedrock settings such as the Hudson Bay Lowlands portion of the Ring of Fire area.

Methods

This study compares pit lake water quality data, including profiles and sampling, with similar groundwater datasets collected prior to and during mining to examine the role of groundwater flow interactions with the pit lake. The data for this study come from De Beers Canada (De Beers), which has been responsible for operation and monitoring of the former VDM site. These data include more than 23 years of climate, hydrology, and groundwater information, including drilling records, groundwater and pit lake water quality data, groundwater levels, pumping records, groundwater modelling, and aquifer assessments. They are the primary source of information for this study.

The pit lake profiles were collected between the onset of pit lake flooding in 2019 and 2026 using a YSI EXO3 Sonde. The profile data include total dissolved solids (TDS), electrical conductivity, temperature, pH, and turbidity. A conversion factor is not available for the TDS data. The profiles were collected two to four times per year by lowering the instrument from a boat using approximately 200 m of line. The line length is insufficient to reach the full 280 m depth of the pit lake. Therefore, profiles from two profiling events are used to represent the entire lake profile. The longest profile available, collected in September 2024 after lake levels stabilized in 2023, is used to represent conditions in the upper portion of the pit lake. A profile from 2020, collected at a lower lake level and before

Figure 1 *a) Location of former Victor Diamond Mine (left), b) pit lake in 2025 (top right) and c) example of local peat land environment adjacent to the Attawapiskat River (bottom right).*

significant augmentation of the pit lake with river water, is used to represent the deepest portion of the pit lake.

The comparable groundwater profiles include electrical conductivity and temperature profiles from a downhole geophysical program completed in 2007, before large-scale dewatering, in drillholes located around the open pit. Available groundwater profiles were screened to select longer profiles showing minimal vertical water movement that would influence water quality. In addition, electrical conductivity profiles from drillholes located downgradient of the kimberlite were excluded to avoid its effects on water quality. The residual dataset included electrical conductivity from two profiles located cross-gradient or upgradient of the kimberlite (drillholes VDW-11 and VDW-17) and one longer temperature profile (VDW-22). Additional groundwater temperature data were taken from depth-specific measurements made in vibrating wire piezometers (VWPs) installed in the country rock around the pit prior to flooding.

Water quality sampling data include discrete-depth samples from the pit lake collected at the same frequency as the pit lake profiles, and depth-specific groundwater quality samples collected during drilling in 12 regional drillholes from 2003 to 2006 (HCI 2003 and 2007).

The site and hydrogeologic setting are summarized from several sources. These include previous research (Gautrey 2018; Gautrey and Desjardins 2025), pre-mining groundwater investigations (HCI 2003 and 2007), a hydrogeologic and pit lake model developed prior to the end of dewatering (Itasca 2019), author observations from involvement at the mine site from 2004 to 2026, including during mine operations from 2007 to 2019, annual groundwater reporting, and other materials.

Site Setting

The Hudson Bay Lowlands are a vast peatland with thousands of ponds and small lakes that is drained by numerous creeks and a few large rivers. Near the former mine, the terrain is flat and includes one large river, the Attawapiskat River (Fig. 1c). The area has cold winters (mean January temperature of -22.2 °C) and cool summers (mean July temperature of 16.1 °C), and it is relatively dry, with average annual precipitation and evaporation totals of 540.8 mm/year and 462.9 mm/year, respectively (Golder 2020).

Prior to mining, the diamond-bearing kimberlite at the former mine site consisted of two intertwined kimberlite pipes that intruded through the country rock approximately 170 million years ago (Kong *et al.* 1999). Several other kimberlites occur in the region but have not been mined.

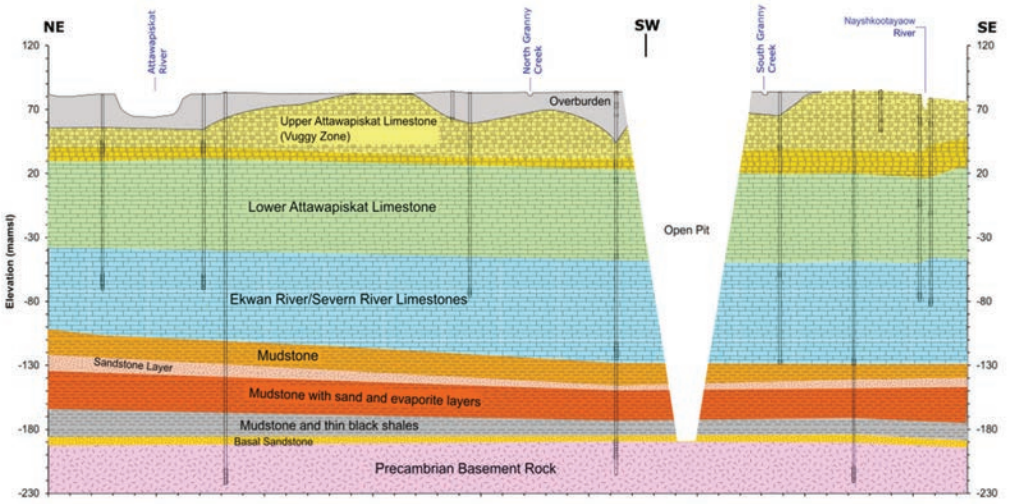

Figure 2 a) cross section illustrating general stratigraphy at the open pit (above), and b) 2019 picture from open pit showing inflow from individual water producing zones in lower portion of open pit (right).

At the VDM, the country rock consists of up to approximately 270 m of Paleozoic sedimentary rock that overlies Precambrian crystalline bedrock of the Superior Craton (Fig. 2a). Most groundwater flow occurs through near-flat-lying, thin, bedding-plane aquifers in the Paleozoic rock. These bedding-plane aquifers developed in bedrock layers that were slightly more prone to dissolution than others. They also developed where flat-lying aquitards, usually mudstones, concentrate horizontal groundwater flow and hence dissolution of the carbonate rock. In total, ten such horizons were identified in the sedimentary bedrock sequence at the VDM (Gautrey and Desjardins 2025). During mining, when there was sufficient groundwater to support the inflows, curtains of water were observed to ring the open pit at the horizons of these aquifers (Fig. 2b). The crystalline bedrock at the base of the sedimentary sequence and the overburden, consisting mostly of clayey silt Tyrrell Sea deposits and till, are not considered aquifers.

In terms of groundwater chemistry, some groundwater is in equilibrium with the carbonate bedrock, including gypsum layers in the deeper mudstone layers. Previous investigators (Mahoney and Howell 2006) also hypothesized that relic Tyrrell Sea water was trapped in some deeper aquifers and within Quaternary sediments laid down before the retreat of the Tyrrell Sea. Following the retreat of the sea between ≈8.2 ka BP and ≈6.1 ka BP (Gao and Turon 2025), this former seawater has been progressively flushed by freshwater recharge. As a result, groundwater occurs in layers of differing water quality depending on regional groundwater flow patterns.

The crystalline bedrock holds ancient, pre-Quaternary water. Tyrrell Sea deposits containing relic seawater and kimberlite intrusions can also influence groundwater quality downgradient of these features.

Pit Lake Development

The pit lake was created following the end of mining in 2019, when the open pit was

allowed to flood. During the mine life, a large-scale dewatering operation was required to operate the mine. Upon initial cessation of dewatering, groundwater was the primary source of water flooding the pit lake. Beginning in 2020 and continuing until late 2022, the mine site's dewatering infrastructure was repurposed to pump water from the Attawapiskat River to the open pit. The rapid pit-filling pumping system was turned off after pit lake levels exceeded the anticipated final steady-state level. Filling the pit lake above its final level was intended to assist in aquifer recovery.

Approximately 28,000,000 m^3 of freshwater from the Attawapiskat River and 1,400,000 m^3 of freshwater from an onsite pond were pumped to the pit lake during flooding. Based on site sampling data, the average concentrations of TDS and chloride in the river water were 121 mg/L and 10.5 mg/L, respectively. The temperature of the pumped water would vary seasonally; however, given that most of the water was pumped during the summer, it is anticipated that the pumped water was largely representative of warmer months.

Based on a stage storage curve for the pit lake developed by De Beers, the stabilized pit lake contains approximately 36,982,000 m^3 of water. A total of 29,400,000 m^3 of freshwater was added to the pit, representing 79.5% of the lake's total volume if all the water remained in the pit lake.A comparison of pit lake levels with the stage storage relationship and recorded pumping rates indicates that net inward groundwater gradients were maintained during flooding until May 2021 (Piteau 2025). At that time, the pit lake elevation reached 46.5 metres above mean sea level (mamsl). After this point, pit lake pumping exceeded groundwater inflows, leading to a net loss of water from the lake to the aquifers. Data reported by Piteau (2025) indicate that the net contribution of water from the pit lake to the aquifer from May 2021 to March 2023 was 11,418,000 m^3. By that time, the pit lake level had stabilized. This net contribution represents 39% of the water added to the pit lake and highlights how the pumping system contributed to recovery of groundwater levels in surrounding aquifers.

The final pit lake elevation in 2025 is approximately 78.3 mamsl, varying from 78.0 at the end of winter to 78.4 in the spring. The pit lake is approximately circular, with a radius of between 330 and 460 m. It has a surface area of approximately 545,000 m2 and is close to 280 m deep. There is no surface water outlet for the pit lake.

Post-2023, under stable lake elevation conditions, the annual water balance for the pit lake can be calculated using the following equation and estimates:

$$P + SWin + GWin = E + SWout + GWout \pm \Delta S$$

For this equation, precipitation (P) is calculated to be 294,700 m^3/year, surface water inflow (SWin) is 605,000 m^3/year (pro-rated by area from flow data from nearby Tributary 5a), evaporation (E) is 252,280 m^3/year, surface water outflow (SWout) is zero (no outlet), and ΔS is zero (stable annual water level). These values result in net non-groundwater inputs of 647,400 m^3/year. Groundwater inflow (GWin) was estimated by Itasca (2019) in its groundwater model of post-closure conditions to be 169,700 m^3/year for the entire pit lake. This gives a total inflow in excess of evaporation of 817,000 m^3/year, which, given the lack of a surface water outlet, must be equal to groundwater outflow. Given that the volume of the lake at 78.0 mamsl is 36,818,000 m^3, the time required to flush one lake volume by the above inflows is 45 years.

Pit Lake Water and Groundwater Quality Profiles

Pit lake water quality profiles from 2020 and 2024, together with groundwater quality profiles, are compared to illustrate similarities between groundwater and pit lake water chemistry and their relationship to aquifer horizons (Fig. 3). The two pit lake profiles converge below -110 mamsl, indicating that the deepest part of the pit lake has been stable since 2020, and the 2020 pit lake profile is interpreted as representative of current water quality below this elevation.

From the surface down, the pit lake profiles reveal that the upper portion of the water column to approximately -10 mamsl contains water with much lower TDS and

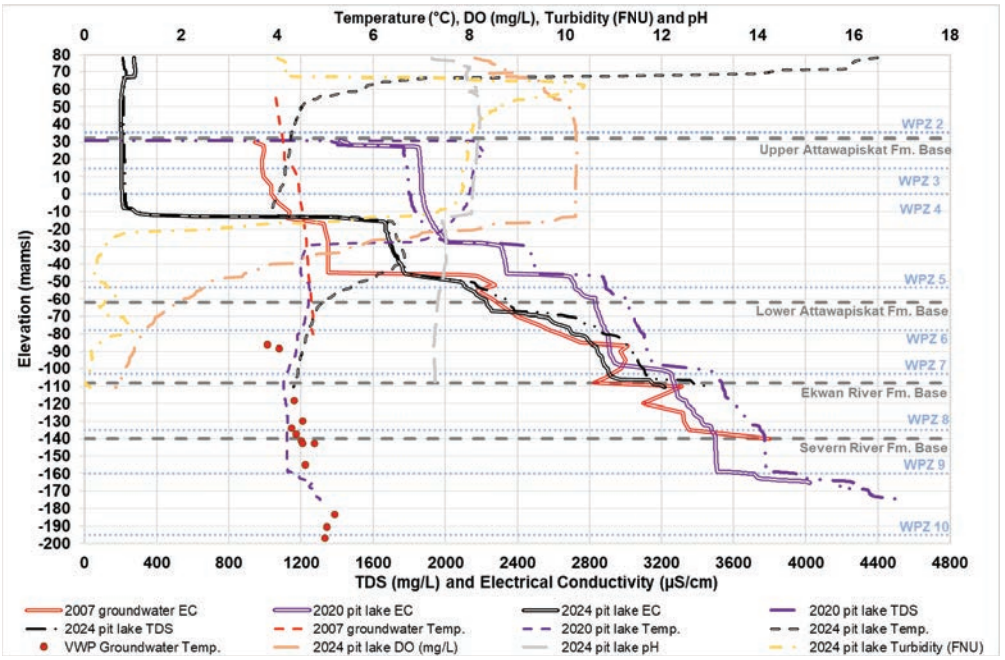

Figure 3 2020 and 2024 pit lake and pre-pit lake flooding groundwater quality profiles.

higher DO, turbidity, and pH than the deeper portions. The change at -10 mamsl is interpreted to separate an upper ≈90 m thick interval of freshwater from a lower ≈190 m thick interval of groundwater-influenced water.

The TDS and other profiles below -10 mamsl also show stepwise changes in water quality coincident with aquifers (water-producing zones, WPZ) in the pit walls. Moreover, below -45 mamsl, the 2024 pit lake electrical conductivity and groundwater profiles match (Fig. 3). These observations suggest that there is a lens of water between -10 and -45 mamsl that is influenced by the aquifers, overlying deep pit lake water that closely matches that of the adjacent aquifers.

The temperature profiles indicate that, other than a lens between -10 and -60 mamsl, the groundwater and 2024 pit lake temperature profiles are similar (Fig. 3). Between -10 and -60 mamsl, pit lake temperatures exceed those of groundwater by up to two degrees Celsius. The upper contact of this interval is sharp and coincident with the lower boundary of the freshwater interval. The lower contact is gradual, with the middle of the transition close to -45 mamsl, coincident with the boundary between the groundwater-influenced and groundwater-matching zones described above. This warm lens of pit lake water likely retains heat from when freshwater was pumped into the open pit. This lens appears to have decreased considerably in volume and cooled between 2020 and 2024, indicating that this portion of the pit lake is evolving.

Pit Lake Water and Groundwater Quality Sampling

Pit lake water samples were collected from depths between five and 130 m below lake level. This largely precluded sample collection from the deepest part of the pit lake. The results indicate pit lake chemistry is dominated by chloride, calcium, sulfate, sodium, potassium, and magnesium. Relative to groundwater data obtained at comparable depths prior to dewatering, primarily from shallow formations, the concentrations in pit lake samples are lower than the mean values of groundwater results, yet they remain within the overall range of measured concentrations.

Pre Mine-Closure Pit Lake Modelling

Itasca (formerly HCI) maintained a numerical groundwater model for the mine that was updated over the years of operation, with the final update developed prior to closure in 2019 (Itasca 2019). For the long term, the model predicted the creation of a meromictic lake. Meromictic indices for the entire 280 m deep lake and the upper 35 m of the lake were 691 and 25, respectively. These values indicate that the lake profile would be largely stable, with the possibility of turnover in the upper 35 m. Most of the stability in the full-lake profile was attributed to the higher salinity at depth.

The model did not include a scenario that is directly comparable to the current state of the pit lake, but the observed pit lake salinity at depth is higher than in the model-predicted profile, indicating that the pit lake will have equal or greater stability than predicted by the model. The model also did not include the bedding-plane aquifers, instead incorporating their flow contributions into thicker rock packages with a similar overall transmissivity. As a result, the model predicts a relatively smooth salinity profile without the stepwise changes in pit lake water quality associated with the discrete water-producing features.

Discussion

The pit lake water quality profile is still evolving following the addition of large quantities of surface water. However, the timing of the freshwater addition later in the flooding process appears to have contributed to pit lake stability. By then, the deeper 236 m portion of the pit lake was already filled with higher-TDS groundwater. As a result, the pit lake profile mimics the general pattern of water quality seen in the surrounding aquifers, with more saline water at depth.

The water quality profiles show stepwise changes coincident with the elevations of discrete bedding-plane aquifers of differing groundwater quality in the pit walls. The near-coincident occurrence of pit lake water quality changes with the aquifers suggests that, where groundwater inflow and outflow occur at similar elevations, measurable stratification of the pit lake can result. At the VDM, this effect is most noticeable in the deeper parts of the pit lake, below the augmented freshwater zone, where pit lake volume is smallest and the differences in groundwater chemistry between aquifers are most significant.

Conclusions

Pit lake water quality profiles from the Victor Diamond Mine record changes in pit lake quality coincident with the elevations of aquifers with groundwater of differing water quality. Thin, flat-lying, bedding-plane aquifers are postulated to contribute to measurable stratification of a pit lake. This requires inflow and outflow of water with distinct quality at the same horizon through a stable pit lake. Such stratification may take time to evolve where large volumes of freshwater are found in a pit lake with relatively small groundwater inflows.

Sedimentary bedrock covers 73% of the Earth's land surface (Goudie 2024). Many open pits are developed through similar flat-lying bedrock aquifers to those found at the Victor Diamond Mine. Inclusion of distinct water-producing intervals may improve predictions made with pit lake models in environments where such features are present and have distinct water chemistry.

Acknowledgements

Operating a comprehensive monitoring program under adverse conditions in a remote northern fly-in location is difficult. Staff and former staff from De Beers (Dave Ott, Rob Paterson, Lawren Wilson, Brodie Ricker, Veronique Magny, Andrew Sutherland, Jordan Edwards, Aline de Chevigny, and many others, including many members of the local communities) should be recognized for their dedication to the task.

References

Gao, C and Turon, C.L. (2025), Early Holocene marine incursion and a freshened Tyrrell Sea in Hudson Bay Lowlands, Canada. Quaternary Science Reviews, Volume 349, 1 February 2025, 109134

Gautrey, S.J. (2018). A comparison of predicted groundwater impacts to observed effects at the Victor Diamond Mine, 11 years after the start of dewatering. Proceedings of Mine Water Solutions 2018, June 12-16, 2018, Vancouver, Canada, pp 163-180.

Gautrey, S. and Desjardins, M. (2025). Groundwater recovery since the end of dewatering in 2019 at the

former Victor Diamond Mine. Proceedings of Mine Water Solutions 2018, June 16-18, 2025, Vancouver, Canada, pp 163-191.

Golder (2020). De Beers Victor Diamond Mine Detailed Current Climate Baseline.

Goudie, A. (2024). Sedimentary Rocks. In: Rocky Landscapes of the World with Google Earth. Springer, Cham. https://doi.org/10.1007/978-3-031-77418-8_5

HCI (2003). Dewatering of the Victor diamond project, predicted engineering, cost and environmental factors.

HCI (2007). Dewatering of the Victor diamond mine, predicted engineering and environmental factors.

Itasca (2019). Closure of the Victor Diamond Mine: Infilling, Hydrodynamics, and Water Chemistry of the Pit Lake. Report prepared by Hydrologic Consultants Inc., for SRK Consulting.

Kong J.M., Boucher D.R., Scott Smith B.H. (1999). Exploration and geology of the Attawapiskat kimberlites, James Bay Lowland, northern Ontario, Canada. In: Gurney JJ, Gurney JL, Pascoe MD, Richardson SH (eds), Proceedings of the 7th international kimberlite conference. Red Roof Design, Cape Town, South Africa, vol 1, pp 452–467.

Mahoney, J.J. and Howell, R.L. (2006). Presence of Tyrrell Sea Water in Deep Groundwater near James Bay, Ontario. Proceedings of the Sea to Sky Geotechnique conference, Vancouver, 2006. 1695-1700.

Piteau (2025). Victor Pit Lake Model, Analysis of results through the end of 2024.

Saving Money and Improving Data Collection When Drilling for Mining Projects

Dr R. Gebrekristos[1], Mr G. Trusler[2]

[1]*Digby Wells Environmental, Technical Lead: Hydrogeology, Johannesburg, South Africa, +27 11 789 9495, robel.gebrekristos@digbywells.com*

[2]*Digby Wells Environmental, CEO, Johannesburg, South Africa, +27 11 789 9495, graham.trusler@digbywells.com*

Abstract

Drilling provides critical data for multiple mining disciplines, yet programmes are often executed independently, leading to duplicated drilling and increased costs. This paper presents a case study where over 5,000 exploration boreholes captured only geological information, requiring additional drilling for hydrogeological, geotechnical and geochemical studies. The results show that simple multi-disciplinary observations during routine drilling could have improved data coverage and reduced follow-up drilling. An integrated drilling approach is proposed, combining early coordination, multi-disciplinary logging and shared data systems to improve efficiency, reduce costs and support more informed mine planning.

Introduction

Drilling is a primary source of data throughout the life of a mining project. Exploration, geotechnical design, hydrogeological characterisation, geochemical risk assessment, sterilisation and metallurgical testing all rely on information obtained from boreholes. Despite this shared dependency, drilling programmes are commonly planned independently by different departments, each focusing on its own objectives. This results in missed opportunities to collect useful information across disciplines during the same drilling campaign, leading to duplicated drilling, increased cost and time delays.

Exploration drilling is typically conducted at a large scale to define an ore resource, but is often limited to lithological logging. Later in the project, additional boreholes are drilled for hydrogeology investigations, geotechnical investigations or geochemical sampling, frequently in areas that have already been drilled. The issue is therefore not the availability of drilling, but how it is planned and utilised across disciplines.

The aim of this paper is to demonstrate the benefits of an integrated approach to drilling, where each borehole contributes to multiple disciplines. Using a case study from a large mining operation in Africa, the paper illustrates how thousands of exploration holes were drilled without capturing key hydrogeological, geotechnical and geochemical data, and how this resulted in additional drilling at later stages. Practical measures to improve coordination and the role of shared data systems and digital tools are also discussed.

Data requirements and case study

Different technical disciplines rely on drilling data at various stages of a mining project. Exploration geologists focus on lithology and mineralisation, geotechnical engineers require rock mass properties, hydrogeologists depend on groundwater-related observations, and geochemists require samples for assessing acid-generating potential. Although these requirements differ, they are closely related and often depend on the same boreholes.

Fig. 1 illustrates a typical sequence of model development in mining projects. While logical from a modelling perspective, this sequence often translates into discipline-specific drilling campaigns. Each discipline tends to initiate drilling only after the preceding phase has been completed, rather than identifying opportunities to collect shared data earlier.

As a result, exploration drilling is often limited to geological logging, while hydrogeological, geotechnical and geochemical investigations are carried out later through additional boreholes. In many cases, these are drilled in areas already covered by exploration, leading to duplication and increased cost. The issue is therefore not a lack of drilling, but a lack of integration in how drilling is planned and executed and what information is collected. Early integration of such datasets is widely recognised as important for reducing uncertainty in mine planning and environmental assessment (ICMM, 2019).

A case study from a large mining operation in Africa highlights the practical implications of non-integrated drilling. During the exploration phase, 5,072 boreholes were drilled to define the mineral resource. These holes provided a dense spatial dataset of lithological information across the site (Fig. 2).

Despite this extensive coverage, no hydrogeological, geotechnical or geochemical data were systematically recorded. No measurements of water levels or water strikes were taken, and observations such as weathering, fracture frequency or drill-fluid loss were not captured. Similarly, basic geotechnical parameters and geochemical indicators relevant to early AMD assessment were not recorded, despite the importance of early geochemical characterisation in mine planning (INAP, 2014).

Additional drilling was later required to support hydrogeological, geochemical and geotechnical studies. Approximately 35 boreholes were drilled for hydrogeological testing and about 8 for environmental geochemical assessment, while more than 100 additional boreholes were later drilled for geotechnical investigations. In several instances, these were located close to existing exploration holes.

The number of additional boreholes was constrained by available budgets rather than what would ideally be required to characterise a site of approximately 18 × 4 km and up to 600 m depth. Even partial integration of hydrogeological and geochemical observations within the exploration programme could have provided broader coverage and reduced reliance on a limited number of dedicated boreholes. This would have provided a broader dataset to better assess groundwater conditions, AMD risk and geotechnical stability, thereby reducing uncertainty in the overall project assessment.

In addition, reducing the need for separate drilling campaigns can lower the amount of fieldwork required, which may contribute to improved safety outcomes and

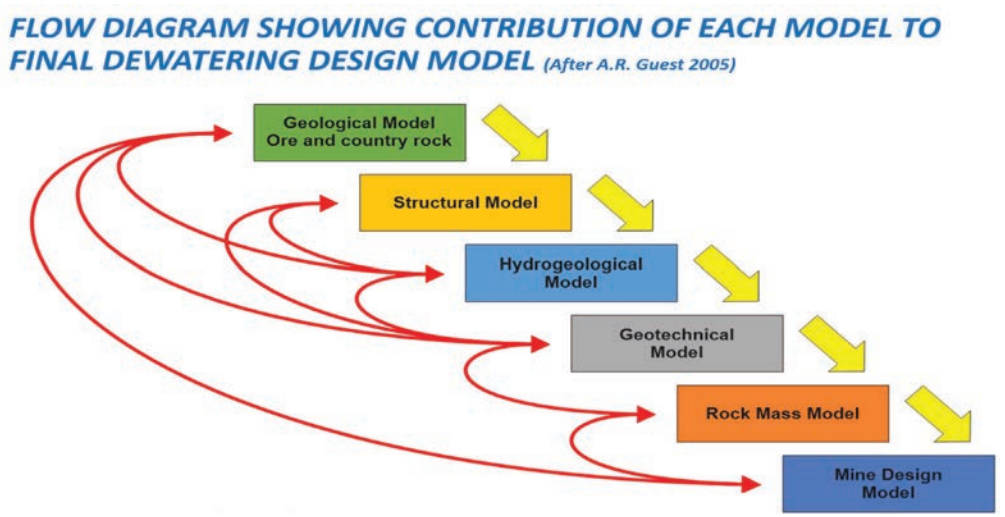

Figure 1 *Typical sequential development of mine design models (adapted from Guest, 2005, as cited in Morton, 2025).*

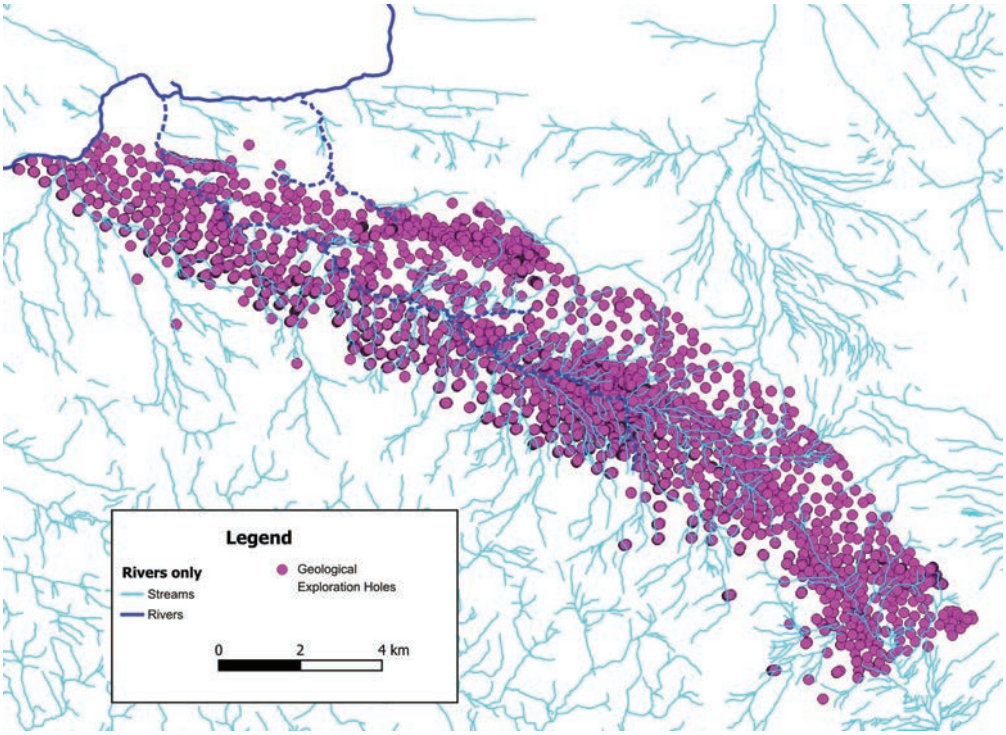

Figure 2 *Project site and distribution of the drilled exploration holes.*

Table 1 *Indicative comparison between conventional and integrated drilling approaches.*

Item	Conventional Approach	Integrated Approach
Exploration boreholes	5,072	5,072
Hydrogeological boreholes	35 additional holes	Reduced requirement
Geochemical boreholes	8 additional holes	Reduced requirement
Geotechnical boreholes	>100 additional holes	Reduced requirement
Mobilisation campaigns	Multiple	Fewer
Spatial data coverage	Limited by specialist drilling	Broader site-wide coverage
Overall drilling effort	Higher	Potentially reduced

reduce repeated disturbance to landowners and surrounding communities.

The impact of non-integrated drilling is reflected in cost, data coverage and technical uncertainty. Using a typical cost of USD 50,000 for a 100 m hydrogeological borehole, the additional groundwater investigations alone represent an expenditure exceeding USD 1 million, excluding testing and supervision costs. While such drilling is necessary, some of this cost could have been reduced if relevant data had been collected earlier.

Data coverage is also affected. Exploration drilling provides wide spatial distribution, whereas later investigations rely on relatively few boreholes. This can limit representativeness, particularly in heterogeneous settings. From a modelling perspective, fewer data points may require additional iterations to refine interpretations. Similar challenges related to limited data coverage and model uncertainty have been widely documented in groundwater studies (Anderson *et al.*, 2015). Table 1 summarises the practical differences

between the conventional and integrated drilling approaches discussed in this paper.

Integrated drilling approach

An integrated drilling approach aims to maximise the value of each borehole by aligning the data requirements of multiple disciplines before drilling begins. Rather than treating drilling as a discipline-specific activity, it is considered a shared resource that can support geological, hydrogeological, geotechnical and geochemical investigations simultaneously. The objective is not to replace specialised drilling programmes, but to ensure that routine drilling - particularly during exploration - contributes useful information to subsequent studies.

Table 2 illustrates the difference between a conventional sequential drilling workflow and a more integrated approach. In the conventional model, drilling programmes are initiated independently by each discipline, often at different stages of the project, resulting in repeated mobilisation and uneven data coverage. In contrast, the integrated approach begins with joint planning, followed by exploration drilling that incorporates multi-disciplinary logging, supported by a shared database and targeted follow-up drilling only where additional detail is required.

The first step in implementing this approach is early coordination. Prior to commencing a drilling campaign, representatives from relevant disciplines should review their data requirements and identify which parameters can be reasonably collected during exploration drilling. This typically includes low-effort observations such as recording water strikes, measuring water levels where feasible, logging weathering profiles and fracture frequency, and collecting representative samples for preliminary geochemical screening. These additions generally require only minor adjustments to logging practices rather than changes to drilling equipment or methodology.

A key component of the approach is the use of a standardised logging template that incorporates inputs from multiple disciplines. For example, an exploration log sheet can be expanded to include sections for hydrogeological observations (e.g. water strikes, fluid losses), geotechnical parameters (e.g. rock quality designation (RQD), core recovery, weathering class), and geochemical indicators (e.g. sulfide presence, visual oxidation, sample intervals). This allows field teams to capture additional information in a structured manner without increasing logging time.

Roles and responsibilities also need to be clearly defined. In many cases, exploration geologists or logging technicians can record basic multi-disciplinary observations with minimal additional training, while more specialised measurements - such as packer testing or detailed geochemical analyses - can still be conducted in selected boreholes as required. The approach therefore focuses on capturing broad, site-wide datasets during

Table 2 Integrated drilling workflow compared to conventional approach.

Current / Sequential Approach	Proposed Integrated Approach
Exploration drilling	Joint planning (all disciplines)
↓	↓
Resource definition (infill) drilling	Exploration, resource definition (infill) and sterilisation drilling (multi-disciplinary logging)
↓	↓
Hydrogeology drilling	Shared database
↓	↓
Geotechnical drilling	Targeted follow-up drilling (only where needed)
↓	↓
Sterilisation drilling	Integrated dataset (site-wide, multi-disciplinary coverage)
↓	
Multiple datasets (separate, uneven coverage)	

exploration, complemented by targeted investigations where greater detail is needed.

To ensure that the additional data are effectively utilised, they should be stored in a shared database accessible to all relevant teams. This enables different disciplines to make use of exploration data during early stages of analysis and reduces the need for separate data collection campaigns. Ongoing coordination during drilling can further support this process by allowing teams to refine data collection priorities based on preliminary findings.

When applied consistently, even partial multi-disciplinary data collection can provide broader spatial coverage than a limited number of dedicated boreholes. Over time, this can reduce the extent of follow-up drilling required and improve the efficiency of project development.

Sterilisation drilling is commonly undertaken to confirm the absence of economically viable ore in areas planned for infrastructure such as tailings storage facilities, waste rock dumps, processing plants, offices and housing. Although these drilling programmes are typically focused on geological assessment, the same areas often require geotechnical characterisation and an understanding of groundwater conditions to support infrastructure design, stability assessments and environmental management. Incorporating additional observations during sterilisation drilling can therefore provide valuable multi-disciplinary information with minimal additional effort.

Organisational challenges and data integration

While the technical aspects of integrated drilling are relatively straightforward, implementation is often constrained by organisational and communication factors within mining operations. In many cases, drilling programmes are not integrated because departments operate independently, each with its own objectives, budgets and performance targets. Exploration, hydrogeology, geotechnical engineering and environmental teams typically plan and execute their work for their respective scopes, even though they rely on the same underlying data source - drilling. Although regular meetings are held within departments to track progress, structured coordination between disciplines is less common, particularly at the level of detailed technical planning. Senior management may encourage collaboration, but they are not always involved in the day-to-day decisions that shape drilling programmes. As a result, integration is often left to departmental managers, who are primarily focused on meeting short term targets.

This structure can unintentionally discourage integrated planning. From a departmental perspective, it is often more efficient to design drilling programmes that meet immediate needs rather than coordinate with other teams and accommodate additional data collection. However, at the project level, this leads to duplication of drilling, increased costs and fragmented datasets. Improving integration therefore requires deliberate coordination mechanisms. Digital tools and shared data systems can further enhance accessibility of information across teams, but their effectiveness depends on active collaboration. Ultimately, integrating drilling programmes requires both systems and mindset - treating drilling as a shared resource rather than a discipline-specific activity, and aligning teams early to maximise the value of collected data.

Data integration is essential for maximising the value of drilling. In many operations, datasets are stored separately, limiting accessibility. Shared data platforms can allow information to be used across disciplines, improving planning and reducing duplication.

Digital tools, including artificial intelligence, can support this process by identifying patterns and extracting insights from large datasets. Their effectiveness, however, depends on collaboration between teams. Technology supports integration, but does not replace the need for communication. Integrated data systems are increasingly recognised as essential for modern mining operations (McKinsey & Company, 2020), and AI applications in geoscience are expanding rapidly (Nature Reviews Earth & Environment, 2022).

Conclusions

Drilling is widely used across mining disciplines, yet is mostly planned independently. This paper shows that the lack of integration can lead to duplicated drilling, increased cost and limited data coverage. The case study demonstrates that large exploration datasets may not fully support later studies if key observations are not recorded.

An integrated approach allows drilling to serve multiple purposes, improving data coverage and reducing reliance on additional boreholes. Achieving this requires both technical adjustments and improved coordination between departments, supported by shared data systems. In addition to these primary benefits, improved integration can contribute to better safety outcomes by reducing the extent of fieldwork, shortening project timelines, and providing a more comprehensive dataset to support decision-making. It can also reduce administrative and operational effort associated with managing multiple, separate drilling programmes.

Based on the findings of this study, several practical measures can be adopted to improve the integration of drilling programmes in mining projects:

- Plan drilling collaboratively across disciplines
- Expand exploration logging to include key multi-disciplinary observations
- Collect samples for early geochemical screening
- Use standardised logging templates to collect the many forms of data
- Maintain shared databases
- Encourage regular interdepartmental co-ordination
- Use digital tools to support integration

References

Anderson, M.P., Woessner, W.W. & Hunt, R.J. (2015). Applied Groundwater Modeling: Simulation of Flow and Advective Transport. Academic Press.

ICMM (2019). Integrated Mine Planning: Good Practice Guide. International Council on Mining and Metals.

INAP (2014). Global Acid Rock Drainage Guide (GARD Guide). International Network for Acid Prevention.

McKinsey & Company (2020). How digital innovation can improve mining productivity.

Nature Reviews Earth & Environment (2022). Artificial intelligence in geoscience applications.

Morton, T. (2025). Advances In Mine Dewatering Design and Tailings Monitoring. GWD Talk 25 June 2025.

IMWA 2026
Jeongseon

Improving Catchment Yield and Low-Flow Estimation Using HEC-HMS: Application of Loss Methods in a Case Study in Gabon

Saeed Golian[1], David Carruth[1], Mark Raynor[1]

[1]*Senior Consultant, SRK Consulting (UK), sgolian@srk.co.uk, ORCID 0000-0001-5451-3977*

[1]*Principal Consultant, SRK Consulting (UK), dcarruth@srk.co.uk*

[1]*Corporate Consultant, SRK Consulting (UK), mraynor@srk.co.uk*

Abstract

This study was focussed on low flow modelling for the purpose of estimating catchment yield in a tropical rainforest setting in Gabon using HEC HMS. It compares the Deficit and Constant (D&C) and Soil Moisture Accounting (SMA) loss methods, calibrated with limited hydrometric data from a regional catchment. The SMA method performed best, capturing baseflow and interflow contribution and providing more reliable dry season simulations. Despite limited flow records and gaps in precipitation data, calibration produced yields of 38-56 L/s/km² which were slightly higher than anticipated for the size of the study catchments in this hydrological setting and cast some doubt around the historical flows records used in this study. The work supports sustainable water resource management for mining developments and highlights the need for expanded monitoring networks to improve long term hydrological assessment and planning.

Keywords: Hydrologic modelling, HEC-HMS, soil moisture accounting (SMA), gabon

Introduction

Mining is among the most water-dependent industrial sectors where water is required for mining activities, e.g. ore processing, dust suppression and workforce supply. For many sites dewatering and water treatment are also a critical issue which should be considered in (pre-)feasibility studies. On the other hand, inadequate water management can lead to production downtime and regulatory non-compliance. At the same time, mining can alter catchment hydrology and water quality through land clearing, water abstraction, diversion works, erosion and sediment mobilisation, and mine water discharges creating risks for downstream ecosystems, stakeholders and communities. For these reasons, robust estimates of catchment yield and dry-season water availability are a basis of mine planning, environmental impact assessment, and operational water balance design, particularly where licensing decisions and environmental flow protections depend on low-flow conditions (Younger and Wolkersdorfer, 2004).

These issues are especially critical in data-scarce regions where baseline hydrometric networks are limited and projects must progress with short-duration datasets. Under such conditions, uncertainty in low-flow estimates can be material to both engineering design (e.g., sizing of raw-water storages, process-water recycle systems, and dewatering capacities) and environmental commitments (e.g., maintaining dry-season flows or setting discharge limits).

In Gabon, mining is a central pillar of economic diversification and the sector is expected to expand beyond the long-established manganese industry to include new or reactivated projects in iron ore, gold and other commodities. This strategic pivot increases the need for credible, site-relevant water resources characterisation because many prospective mining areas coincide with densely forested catchments that support high biodiversity and provide water services to local communities. At project scale, developers must demonstrate that water abstractions and discharges can be managed

within seasonal constraints, including extended dry periods when streamflow is sustained predominantly by subsurface storage. Yet, available streamflow data are sparse in many parts of Central Africa and often rely on regional or historical donor catchments, which can introduce uncertainty when transferred to a specific mine area (Kittel *et al.*, 2018; Bogning *et al.*, 2021).

Tropical rainforest hydrology further motivates careful selection of hydrological models and methods. In humid tropical forests, infiltration capacities are often high and storm runoff generation frequently involves a combination of saturation-excess mechanisms and rapid subsurface stormflow, while dry-season discharge persistence depends on the capacity of soils and shallow groundwater to store and gradually release water (Bonell, 2005). Consequently, modelling approaches used to inform mine water availability and catchment yield should be able to represent (i) quick response during high-intensity rainfall and (ii) delayed interflow and groundwater recession that controls low flows. Continuous rainfall–runoff simulation provides a useful framework because it enables explicit tracking of soil moisture storage, evapotranspiration losses, and recharge over long periods.

Hydrologic Engineering Center Hydrologic Modelling System (HEC-HMS) is widely used for both continuous and event-based simulation and offers multiple loss and baseflow methods suitable for screening-level to detailed applications. Among these, the Soil Moisture Accounting (SMA) method provides a multi-store representation (canopy, surface, soil profile, and groundwater layers) that is designed to simulate long-term water balance and recession behaviour (Bennett and Peters, 2000), whereas the Deficit and Constant (D&C) method offers a simpler conceptualisation of soil moisture deficit recovery and infiltration capacity that can be attractive when available data are limited. Comparative studies in different hydro-climatic settings indicate that SMA can better represent storage-driven runoff and recession dynamics where wet–dry contrasts are important (e.g. Halwatura and Najim, 2013; Mobarhan and Sangchini, 2021), but the additional parameterisation can also increase calibration uncertainty.

Against this backdrop of expanding mining interest and limited hydrometric coverage in Gabon, this paper evaluates and compares the performance of the SMA and D&C loss methods within HEC-HMS for catchment yield estimation, with particular emphasis on low-flow simulation that underpins dry-season water supply reliability and environmental flow protection in mine water studies.

Methodology and Study Catchments

The study applied continuous infiltration loss modules to support catchment yield estimation for regional catchments in Gabon. Catchments were delineated using available digital elevation models, and basin average precipitation and evapotranspiration inputs were derived from local gauge records supplemented by regional climate datasets.

The D&C approach represents catchment losses using a single soil layer characterised by an initial moisture deficit and a constant infiltration rate, combined with a canopy interception component. This method offers a relatively simple conceptualisation of rainfall losses and runoff generation and requires only a limited number of parameters, making it attractive for applications with short or incomplete hydrometric records (Figure1a).

In contrast, the SMA method provides a more physically based representation of hydrological processes by explicitly simulating canopy interception, surface storage, soil zone moisture, and multi layer groundwater flow. The SMA configuration applied in this study comprises ten parameters governing infiltration capacity, percolation, evapotranspiration losses, and groundwater recession from two subsurface storage zones (Figure 1b). This structure enables dynamic tracking of soil moisture and delayed subsurface drainage, which are critical controls on baseflow persistence and dry season runoff in tropical rainforest environments. Although the increased parameterisation introduces additional calibration complexity and non-uniqueness, the SMA method is expected to provide a more realistic representation of interflow

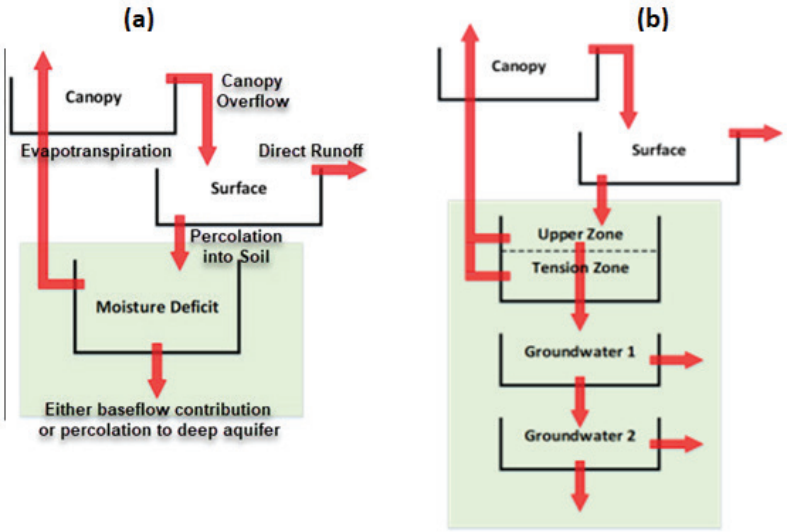

Figure 1 Model components of a) Deficit and Constant model b) Soil moisture accounting (HEC-HMS manual, 2013).

and groundwater contributions compared to simplified loss models.

Model performance was evaluated using a combination of graphical comparisons, cumulative flow analyses, and standard efficiency metrics. Particular emphasis was placed on assessing low flow simulation quality and flow recession characteristics, as these factors are most relevant for catchment yield estimation, abstraction licensing, and mine water supply reliability.

Both loss models were calibrated over a regional catchment with historical streamflow data records (ADHI 210). Figure 2 shows the distribution of the African Database of Hydrometric Indices (ADHI) hydrometry stations in Gabon. This paper presents the results for this regional hydro station in more detail.

The catchment upstream of ADHI 210 has an area of 117km2, with average annual precipitation of 1970mm and hydrometry data spanning the period 1967 to 1980.

Results and Discussion

Model parameters were calibrated and results for both loss methods are presented in Figure 3. Whilst both models have satisfactory performance, the SMA model outperforms the D&C method, especially in simulating baseflow. The performance criteria show a correlation coefficient of 0.78 and 0.85, and Nash-Sutcliffe efficiency (NSE) of 0.22 and 0.6 for D&C and SMA methods for the calibration period respectively. The SMA model performs better for baseflow and for much of the observed peak flows.

For low flows, the RMSE, correlation, logNSE and deviation from observed flow-duration-curve are 1.0, 0.48, -2.9 and -7.12% for the D&C method and 0.54, 0.6, 0.24 and -2.18% for the SMA method for the calibration period; and 1.4, 0.49, -7.3 and -52% for the D&C and 0.89, 0.36, -0.14. and -4.5% for SMA methods, respectively over the verification period. This shows the superior performance of the SMA method for low flow simulation compared to the D&C method.

Figure 3a shows SMA method slightly overestimates low flows and underestimate some historical high flows (Figure 3b) while the D&C method overestimates almost all high flows and underestimates low flow (Figure3a). Figure 4 shows the cumulative flow for observed and simulated results; the SMA model performance is much closer to the observed flow than the D&C model.

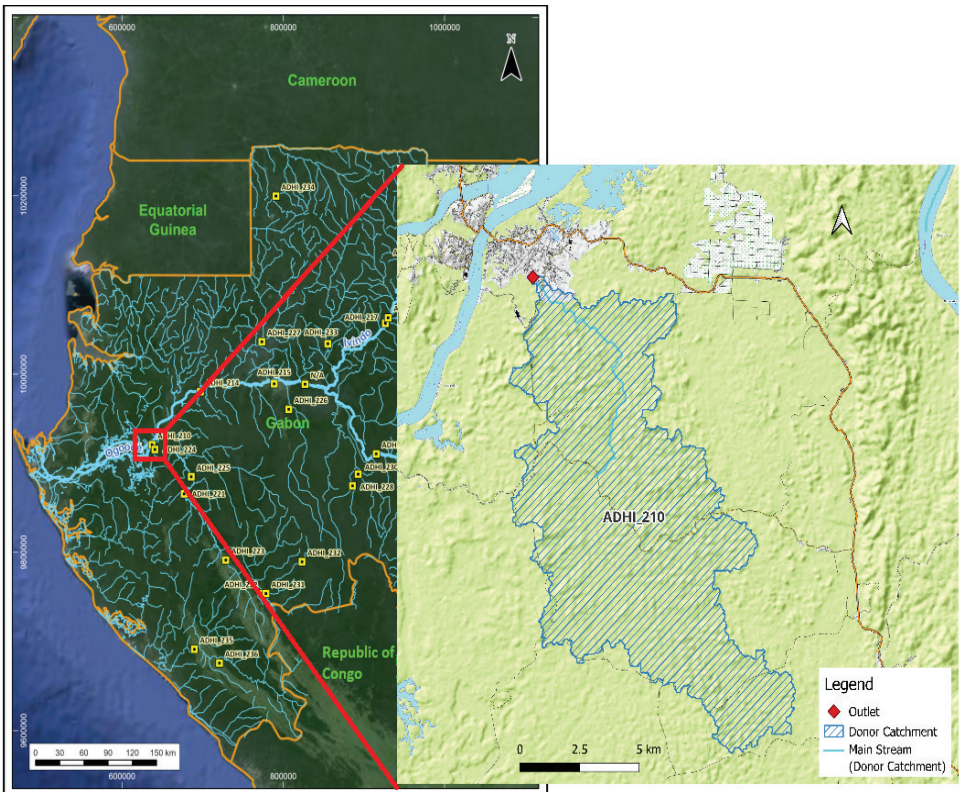

Figure 2 *Location of ADHI in Gabon and ADHI 210 catchment.*

Calibration results for the regional hydrometry station showed that there were major differences in the two methods ability to capture baseflow and dry-season runoff. The D&C method consistently underestimated late-season baseflows, resulting in abrupt reductions in simulated discharge. This behaviour is typical of simplified loss models that cannot track long-term soil storage or delayed subsurface drainage. SMA, by contrast, produced smoother recession curves, realistic groundwater contributions, and more stable low-flow representation.

The SMA approach better reproduced observed dry-season flows across ADHI-210 catchment based on performance metrics and visual goodness of fit of simulated to the observed, aligning with previous studies indicating that tropical rainforest catchments rely heavily on subsurface flow pathways and sustained soil moisture storage (Bonell, 2009). Normalised annual yield for SMA and D&C models are 37.9 and 55.6 L/s/km² respectively compared to an observed yield of 42.2 L/s/km², showing higher values compared with other regional hydrometric stations in Gabon and the Congo Basin.

It should be noted that quality assurance checks were performed on regional dataset to provide confidence in its reliability for model calibration. Table 1 indicates resulting runoff coefficient is relatively high (0.62) and evapotranspiration is likely underestimated (simulated average annual canopy evapotranspiration of 705 mm). Bruijnzeel (1990) presents actual annual evapotranspiration estimates for seven lowland tropical forest catchments in Central and West Africa which range from 1,145 mm/annum to 1,465 mm/annum with an average of 1,310 mm/annum. This indicates that the partitioning between evaporative losses and streamflow is not fully representative of expected catchment behaviour, with an excessive proportion of precipitation contributing to runoff. For similar tropical

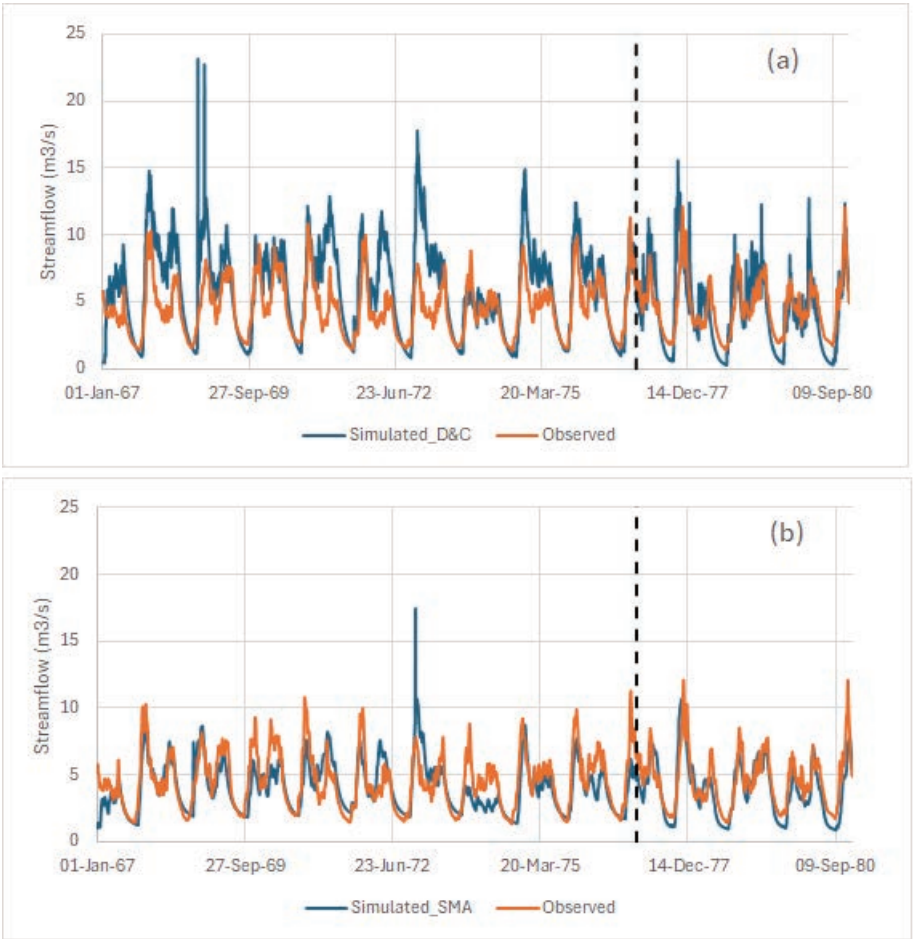

Figure 3 *Observed (black) vs simulated (blue) streamflow for a) Deficit and constant and b) SMA methods. Dashed line shows the start of verification period.*

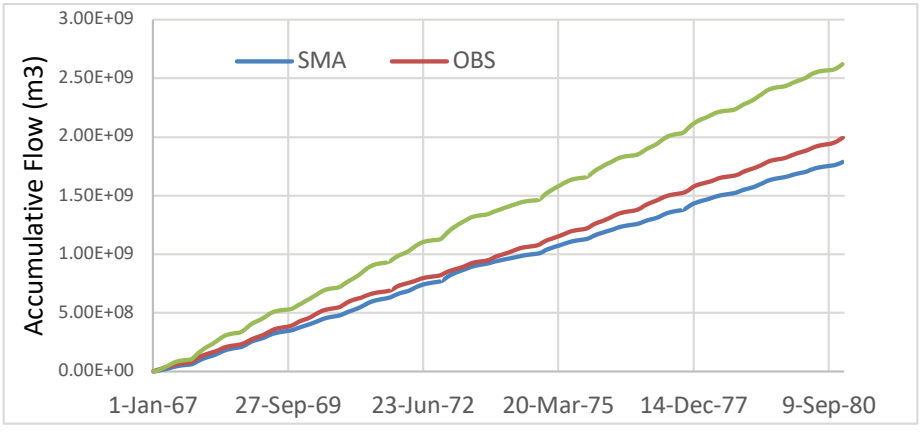

Figure 4 *Cumulative flows using Observed (red), and simulated flows (green line: Deficit and constant and blue line: SMA).*

regions, runoff coefficients of up to 0.6 and for Ogooe River at lower Ogooue, runoff coefficient of about 0.39 (Kittle *et al.*, 2018) have been reported, demonstrating the value of 0.62 lies at the upper bound of the reported range and should therefore be interpreted with caution. This finding also points towards a need for mines to establish their own local baseline monitoring network, with data quality assurance procedures established to ensure data captured is of sufficient quality, as regional historical datasets would appear to be less than ideal as potential donor catchments.

Conclusion

This study evaluated the performance of the Deficit and Constant (D&C) and Soil Moisture Accounting (SMA) loss methods within HEC HMS for continuous rainfall–runoff simulation and catchment yield estimation in a tropical rainforest catchment in Gabon, using calibration against a regional hydrometric dataset. The comparison focused specifically on the ability of each method to reproduce low flow behaviour and dry season streamflow, which are critical for water resource assessment and abstraction planning in mining contexts.

There are clear differences in the representation of baseflow and flow recession. The D&C method exhibited a tendency to underestimate late season flows, producing abrupt recessions that are inconsistent with the sustained dry season discharge observed in the regional record. This limitation reflects the simplified conceptual structure of the method, which does not explicitly account for long term soil moisture storage or delayed subsurface drainage. In contrast, the SMA method provided a more realistic simulation of interflow and groundwater contributions, resulting in smoother recession curves and improved low flow performance. This was reflected in stronger performance metrics for SMA method. The results are consistent with established understanding of tropical rainforest hydrology, where streamflow generation is strongly influenced by subsurface flow pathways and sustained soil moisture storage.

The relatively high runoff coefficient obtained from the regional catchment data assessment indicates that readily available regional historical streamflow records may not be suitable for local catchment yield analysis at mine development sites. While neglecting observed streamflow uncertainty can make calibration/evaluation conclusions inadequate, indicating a high performance metric (e.g. NSE) shows only that simulations are consistent with a plausible realisation of discharge. This issue highlights the need for expanded local monitoring networks to improve long term hydrological assessment and planning. Even a few spot flow measurements in wet/dry seasons can help to better evaluate the calibrated models

References

Bennett, T.H. and Peters, J.C., 2000. Continuous soil moisture accounting in the hydrologic Engineering Center Hydrologic Modeling System (HEC-HMS). In Building partnerships (pp. 1-10).

Bonell, M., 2009. 14 Runoff generation in tropical forests. This page intentionally left blank, p.314.

Table 1 *Modelled catchment water balance for ADHI 210.*

Parameter	Depth (mm)	% Precipitation
Precipitation (during whole simulation period)	1934	100.0%
Canopy Evaporation (including root uptake from the soil zone)	705	36.4%
Rapid Runoff	1.7	0.1%
GW1 Out	659	34.1%
GW2 Out	543	28.1%
Deep Percolation	0	0.0%
Flow	1203	
Runoff Coefficient	0.62	

Bruijnzeel, L.A., 1990. Hydrology of moist tropical forests and effects of conversion: a state of knowledge review.

Chen, X., Zhang, Z.C., Zhang, X.N., Chen, Y.Q., Qian, M.K. and Peng, S.F., 2008. Estimation of groundwater recharge from precipitation and evapotranspiration by lysimeter measurement and soil moisture model. Journal of Hydrologic Engineering, 13(5), pp.333-340.

Halwatura, D. and Najim, M.M.M., 2013. Application of the HEC-HMS model for runoff simulation in a tropical catchment. Environmental modelling & software, 46, pp.155–162.

Holberg, J.A., 2015. Downward model development of the soil moisture accounting loss method in HEC-HMS: Revelations concerning the soil profile (Master's thesis, Purdue University).

Holberg, J.A., 2015. Downward model development of the soil moisture accounting loss method in HEC-HMS: Revelations concerning the soil profile (Master's thesis, Purdue University).

Kittel, C., Nielsen, K., Tøttrup, C., BauerGottwein, P., 2018. Informing a hydrological model of the Ogooué with multi-mission remote sensing data. Hydrol. Earth Syst. Sci. 22, 1453–147

Mobarhan, E.Y. and Sangchini, E.K., 2021. Continuous rainfall–runoff modeling using HMS-SMA with emphasis on the different calibration scale. Journal of Chinese Soil and Water Conservation, 52(2), pp.112-119.

US Army Corps Engineers, 2013. HEC-HMS Technical Reference Manual

Younger, P.L. and Wolkersdorfer, C., 2004. Mining impacts on the fresh water environment: technical and managerial guidelines for catchment scale management. Mine water and the environment, 23, pp.s2-s80.

IMWA 2026
Jeongseon

Categorisation and Analysis of Flooded Mines with Regard to their Geothermal Potential

Thomas Grab[1], Tom Ebel[1], Lukas Oppelt[1], Timm Wunderlich[1], Fritz Raithel[1], Alexander Klein[1], Tobias Fieback[1]

[1]*Department of Technical Thermodynamics, TU Bergakademie Freiberg, Germany, corresponding author: Thomas.grab@ttd.tu-freiberg.de, ORCID 0000-0003-4235-5494*

Abstract

The use of heat from flooded mines via mine water represents low-emission geothermal energy with base-load capability. Despite favourable conditions, it is rarely applied in Saxony's former mining regions. A study by the Saxon State Office for the Environment, Agriculture and Geology analysed the potential of mine water for heating and cooling. Fourteen sites were selected and evaluated using underground geological and mining parameters and above-ground municipal heat demand. GIS-based potential layers combined supply and demand. Laboratory experiments at two test sites examined fouling on heat exchangers. Optimised materials reduced deposits by 30–40%, and mitigation measures were developed for future projects.

Keywords: Mine water geothermal systems, abandoned mines, heat demand analysis, heat exchanger fouling, geothermal potential mapping

Introduction

The European Green Deal aims to increase the share of renewable energy to 40% by 2030. While Germany already generates more than half of its electricity from renewable sources, the share of renewable heat remains comparatively low at around 19%, although heating accounts for more than half of total final energy consumption, AG Energiebilanzen (2024). Expanding renewable heat sources therefore represents a key element of the energy transition. One promising but still underutilised option is the use of mine water from flooded underground mines. Mining cavities provide large heat transfer surfaces and may contain considerable water volumes that can be used as geothermal energy sources. Existing shafts and galleries may reduce exploration costs compared to new drilling, Grab et. al. (2018). However, challenges include pumping requirements, underground logistics and the chemical composition of mine water, which may affect technical components through corrosion or deposit formation, Oppelt et. al. (2025). The study, conducted by the TU Bergakademie Freiberg, examines the geothermal potential of mine water in Saxony, Ebel *et al.* (2025). Based on literature research and practical investigations, selected mining sites were evaluated using a structured assessment method. The results were visualised using GIS tools. In addition, laboratory experiments and operational analyses were conducted to expand practical knowledge and to support future mine water geothermal projects.

Mine Water Geothermal Systems

Mine water geothermal systems utilise flooded underground mining structures as heat sources. The water is in thermal contact with surrounding rock masses, enabling efficient heat exchange.

Three basic system types can be distinguished:

- open systems without reinjection, return of mine water to surface waters
- open systems with reinjection of mine water to the mine
- closed systems

In open systems, mine water is pumped directly to the heat exchanger and used as the heat carrier. In closed systems, heat is transferred through a secondary fluid circulating in a

closed loop. Open systems are widely used due to their comparatively high heat output and simple design. After heat extraction, the water can either be discharged into surface waters or reinjected into the mine.

Methodology for Site Assessment

Data Basis and Site Selection

Several mining regions in Saxony contain potentially suitable mine water resources. To identify suitable sites, different information sources were evaluated, including archives of the Technical University Bergakademie Freiberg, municipal archives, the Wismut company archive and the underground cavity map of the Saxon Mining Authority, SOBA (2023). Existing geothermal projects and studies in regions such as Ehrenfriedersdorf, Freiberg, Zwickau and Marienberg provided important references. Additional information was obtained from mining museums and local authorities. Based on the available data, 14 municipalities were selected for further investigation. These locations represent a large share of the mining-related underground cavities in Saxony (Figure 1).

Underground Site Assessment

The geological and mining conditions vary significantly between the investigated sites. Therefore, a general assessment approach based on Grimm *et al.* (2001) was expanded and applied to enable a systematic comparison of all sites. Eight parameters were considered, (Tab. 1 left site). The assessment considers age, drainage system, flooded depth, and cavity volume. More recent mining periods generally provide better data availability, larger tunnel cross-sections, and improved structural conditions. Drainage systems are evaluated based on their degree of centralization and discharge rate, as higher flow rates enable greater thermal output. Smaller flooding depths reduce pumping effort. Larger cavity volumes increase the likelihood of usable water mobilization. Each parameter was evaluated using a scale from

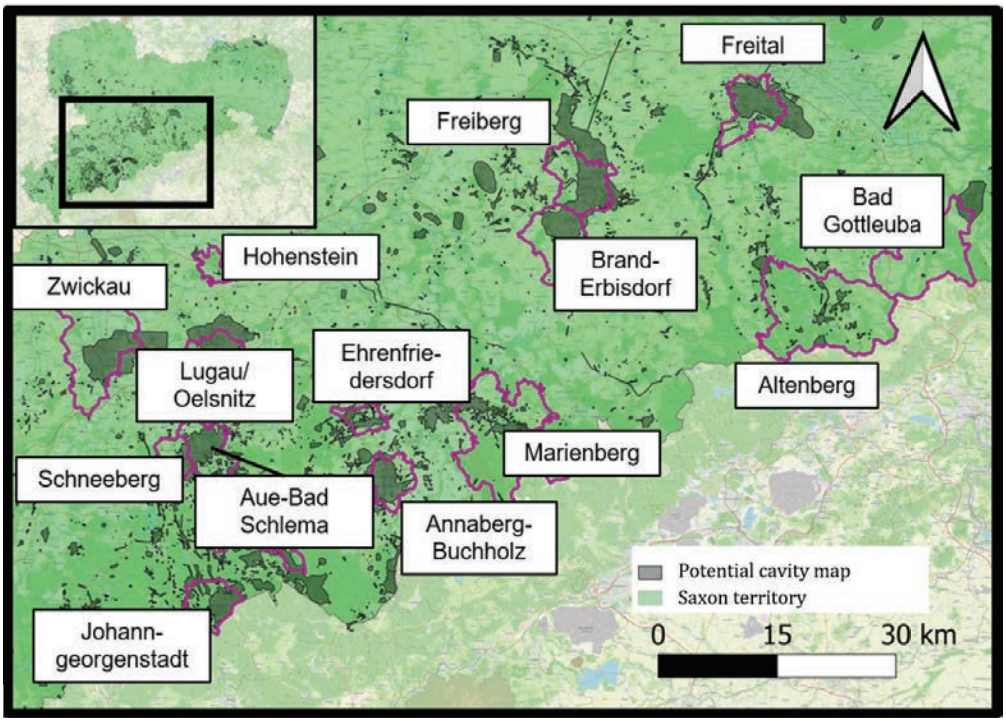

Figure 1 *Overview of the areas and municipalities included in the federal state of Saxony in Germany (according to Ebel* et al. *(2025). and Oppelt et. al. 2025).*

Table 1 Underground categories of evaluation criteria and their weighting.

Evaluation factors	Weighting
mining period and age of mine structures	3%
drainage systems and water discharge rates	17%
flooding depth and pumping requirements	11%
mine (residual) void volume	6%
availability of mining maps	22%
mine water temperature	8%
water chemistry	14%
accessibility of the mine structures	19%

1 (unfavourable) to 5 (very favourable). To account for different levels of importance, each of the eight parameters were weighted (Tab. 1 right site) using a pairwise comparison method, Wartzack (2020). The resulting weighted scores represent the underground geothermal potential of each site (Figure 2 A).

Above-Ground Site Assessment

The above-ground evaluation focuses on the heat demand structures of surrounding municipalities. Heat demand represents the most relevant indicator for the potential utilisation of mine water geothermal energy. Modelled heat demand data were spatially aggregated into demand polygons representing potential supply areas. These polygons were then classified into demand categories and evaluated using the same five-level scale applied in the underground assessment (Figure 2 B). The heat demand modelling was carried out using building-based data from the DBI building atlas, DBI GTI (2023). Georeferenced address data were combined with building parameters such as floor area, construction year, building type and specific energy demand. For residential buildings, literature values for specific energy demand were applied. Non-residential buildings were evaluated using sector-specific indicators such as energy demand per pupil, patient or sales area. Regional factors such as climate conditions and building renovation status were also considered. Climatic corrections were performed using heating degree days based on German reference values. The resulting dataset provides a house-level heat demand estimate for each building within the analysed municipalities.

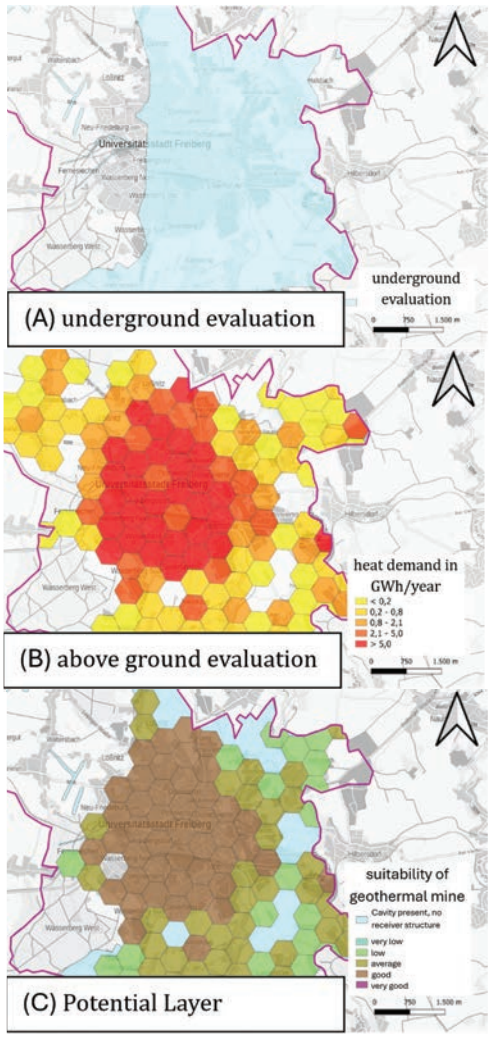

Figure 2 Illustration of the format used to present the results for each of the mining regions studied.

Potential Layer

To determine the overall geothermal potential, the underground and above-ground assessments were combined. For each polygon cell, the underground potential value of the corresponding mining district was merged with the heat demand score of the demand polygon (Figure 2 C). The overall potential was calculated as the arithmetic mean of both values. Only polygon cells located above underground cavities and belonging to the main supply area were included in the final analysis. This approach avoids overestimating small or isolated underground structures. The resulting GIS layer represents the spatial distribution of mine water geothermal potential across the analysed municipalities and will be made publicly available by the State Office for the Environment, Agriculture, and Geology of the Free State of Saxony.

Results of the Potential Analysis

All 14 analysed municipalities show at least one polygon with favourable conditions for mine water geothermal utilisation. The districts of Annaberg Buchholz (4.1 out of 5) and Freiberg, as well as Ehrenfriedersdorf, each with a score of 3.9 out of 5, receive particularly high ratings, (Table 2). High demand densities in urban areas lead to particularly favourable results, while in less populated regions favourable underground conditions can compensate for lower heat demand. The results primarily serve as a screening tool to identify promising areas. Detailed feasibility studies are required before implementing specific projects. Since not all Saxon municipalities were analysed, additional suitable sites may exist beyond the investigated regions.

Experimental Investigations

Mobile Test Facility

A major challenge in mine water geothermal systems is the formation of deposits (fouling) on heat exchangers. Fouling can be caused by mineral precipitation, suspended particles or biological growth. To investigate these processes, the Institute of Technical Thermodynamics at TU Bergakademie Freiberg developed a mobile heat pump test facility, Oppelt et. al. (2022) Oppelt et. al. (2025EGC). The system includes a 4 kW heat pump connected to plate heat exchangers that simulate heating and cooling conditions under realistic operating parameters, see Fig. 3. Two mine water sites with different temperatures (approximately 26 °C and 12 °C) were investigated. The locations differ in their water chemistry but were anonymised for confidentiality reasons.

Experimental Results

The aim of the practical measurements of the mobile heat pump test rig was to investigate the fouling behaviour of substances dissolved in mine waters on heat exchangers. Two sites with three mine waters were examined to identify materials that reduce maintenance effort. A total of 7 plate materials and 11 surface types were tested. At both sites, fouling occurred independently of the material. Site 1 showed predominantly biological fouling, promoted by high temperatures, which was reduced by stainless steel NiCr23Mo16Cu, silver, or anti-biofouling coatings. At site 2, mine water 2 caused iron-containing deposits,

Table 2 *Assessment of sites based on Saxony's flooded mine geothermal potential analysis.*

Municipalitie	Site assessment (max 5)	Municipalitie	Site assessment (max 5)
Altenberg	3.1	Freital/Gittersee	3.1
Annaberg-Buchholz	4.1	Hohenstein-Ernsttahl	3.5
Aue – Bad Schlema	3.8	Johanngeorgenstadt	3.3
Berggießhübel	3.3	Marienberg	3.9
Brand – Erbisdorf	3.0	Oelsnitz/Erzgeb.	3.3
Ehrenfriedersdorf	3.9	Schneeberg	3.7
Freiberg	3.9	Zwickau	3.1

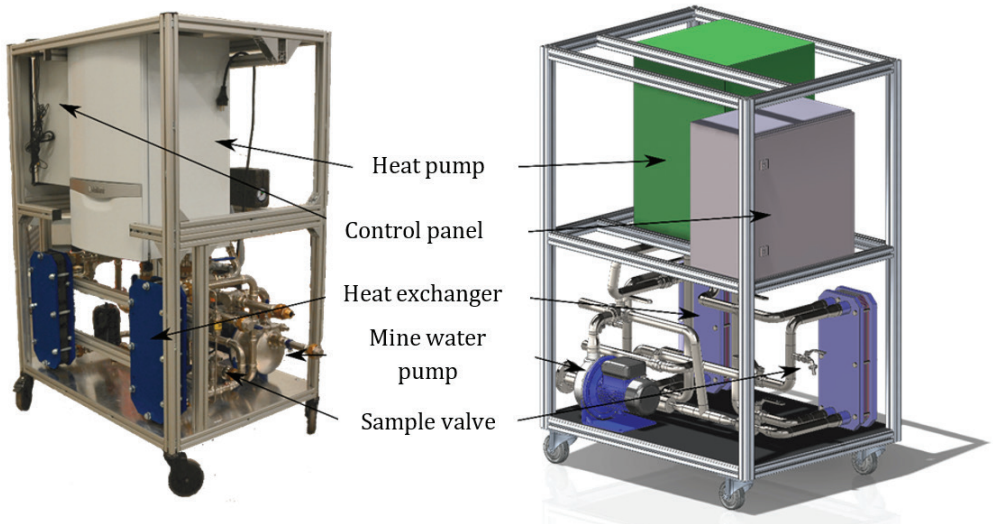

Figure 3 Mobile heat pump test rig of the Institute of Technical Thermodynamics at the TU Bergakademie Freiberg.

number of materials should be reduced and installed multiple times to increase accuracy. Thermal conductivity must be considered, as low fouling does not automatically imply high efficiency. Cleaning is relevant, as deposits adhere with varying strength; tests with chemical cleaning in place are planned.

The position of the plates in parallel-flow heat exchangers did not influence deposit formation. Analyses of the deposits showed high proportions of organic compounds and dominant iron, mainly as particulate fouling. This correlation was also demonstrated in earlier experiments by Oppelt *et al.*, (2020) and Abewywickrama *et al.*, (2021). The investigations provide practical insights, enable the preselection of suitable materials, and form the basis for further cleaning and efficiency studies.

Analysis of Existing Mine Water Plants

Existing mine water geothermal installations in Saxony were analysed to derive practical recommendations. The evaluation of permits, technical reports and operator interviews identified 14 factors that may influence project success. Key challenges include incorrect drilling, insufficient water temperatures, low flow rates, fouling of heat exchangers and technical failures of heat pumps. Mitigation measures include improved geological data, exploratory drilling, suitable material selection, filtration systems, monitoring and regular maintenance. Early coordination with authorities and potential heat consumers is also essential.

Conclusion and Outlook

Mine water geothermal energy represents a promising renewable heat source with low emissions and base-load capability. However, its application in Saxony remains limited. This study analysed 14 mining sites using a combined assessment of underground conditions and above-ground heat demand. The results were integrated into a GIS-based potential map that identifies promising areas for future projects. Additional investigations improved the understanding of mine water chemistry and heat exchanger fouling. Experimental tests demonstrated that appropriate material selection can significantly reduce deposit formation. The findings were compiled into a practical guideline supporting planning, approval procedures and funding options. Future developments should focus on the digitalisation of mining maps, improved potential calculation methods and expanded data availability. With these advancements,

mine water geothermal systems could play an important role in the sustainable redevelopment of former mining regions and contribute to the renewable heat transition.

References

AG Energiebilanzen e.V. (2023): Analysis tables for the 2024 energy balance. https://ag-energiebilanzen.de/daten-und-fakten/auswertungstabellen/ (Accessed on 4 March 2026).

Grab, T., Storch, T., Groß, U. (2018): Energetische Nutzung von Grubenwasser aus gefluteten Bergwerken, Erschienen in: Bauer, M., Freeden, W., Jacobi, H., Neu, T. (Hrsg.): Handbuch Oberflächennahe Geothermie, Kapitel 17, Springer Spektrum, ISBN: 978-3-662-50306-5, DOI: 10.1007/978-3-662-50307-2_17

Oppelt L., Grab T., Ebel T., Wunderlich T., Storch T., Fieback T. (2025): Mine Water as an Energy Source: Overview of Technical Basics, Existing Plants, and Monitoring Results. Mine Water Environ, DOI: 10.1007/s10230-025-01057-w

Ebel T., Grab T., Oppelt L., Wunderlich T., Raithel F., Krause W., Fieback T. (2025): Kategorisierung und Analyse von Grubenwässern in stillgelegten Bergwerken Sachsens hinsichtlich ihres geothermischen Potenzials. Herausgegeben vom Sächsischen Landesamtes für Umwelt, Landwirtschaft und Geologie. https://www.geologie.sachsen.de/download/Potenzialstudie_Grubenwassergeothermie_Abschlussbericht.pdf 2025, (Accessed on 4 March 2026).

SOBA: Saxon Mining Authority: Cavity map. https://www.oba.sachsen.de/hohlraumkarte-4918.html (Accessed on 4 March 2026).

Grimm, R., Jordan, H. (2001): Bewertung des Grubenwasserpotenzials Sachsens und Verifizierung umsetzbarer Standorte unter Einbeziehung des Eintrags solarer Wärmegewinne. Abschlussbericht „Grubenwasserpotenzial Sachsen". Sächsisches Landesamt für Umwelt und Geologie.

Wartzack, S. (2020): Auswahl- und Bewertungsmethoden, in: Pahl/Beitz Konstruktionslehre. Methoden und Anwendung erfolgreicher Produktentwicklung, 9. Auflage. Rostock, Bochum: Kilian Gericke, Beate Bender, 2020.

DBI GTI: Methodikbeschreibung der GIS-Analysen. unveröffentlichte Auftragsbeschreibung. Freiberg, 2023. https://www.dbi-gruppe.de/fachgebiete/energieversorgungssysteme/ (Accessed on 4 March 2026).

Oppelt L., Grab T., Pose S., Storch T., Fieback T. (2022): Innovative heat exchanger design to avoid fouling. European Geothermal Congress 2022-Proceedings, ISBN: 978-2-9601946-2-3, Berlin

Oppelt L., Wunderlich T.; Ebel T., Raithel F., Krause W., Grab T., Fieback T. (2025): Development of a fouling prediction tool and derivation of an effective heat exchanger design for geothermal utilisation of mine water, European Geothermal Congress 2025-Proceedings, Brussels, ISBN: 978-2-9601946-6-4

Abeywickrama J., Grimmer M., Hoth N., Grab, T. Drebenstedt C. (2021): Geochemical characterization of fouling on mine water driven plate heat exchangers in Saxon mining region, Germany. International Journal of Heat and Mass Transfer 176 https://doi.org/10.1016/j.ijheatmasstransfer.2021.121486

Chemical Characterization of Mine Water and Microbial Communities from the Mária Mine (Rožňava, Slovakia): Assessment of Autotrophic and Heterotrophic Bacteria after Cultivation on Liquid and Solid Media

Lenka Hagarová, Daniel Kupka

Department of Mineral Biotechnologies, Institute of Geotechnics, Slovak Academy of Sciences, hagarova@saske.sk, ORCID 0000-0002-1537-6866; dankup@saske.sk, ORCID 0000-0001-5825-9507

Abstract

The Mária Mine (Rožňava) represents an important deposit of Ag-bearing tetrahedrite rich in Cu and Sb. The mine drainage discharges into the Slaná River, underscoring the need to characterize its chemical composition and bacterial community. Mine water chemistry was evaluated by ICP spectrometry and ion chromatography. Microorganisms from the Mária mine drainage were cultivated in liquid 9K medium and on solid gelrite medium and subsequently identified using whole-genome sequencing. The mine drainage was characterized by neutral pH (6.9) and elevated sulfate, Mn and Fe concentrations. Cultivation in liquid medium revealed the iron-oxidizing bacterium *Acidithiobacillus ferrooxidans*. Solid gelrite medium yielded heterotrophic bacteria affiliated with *Pseudomonas*.

Keywords: Mária mine, Tetrahedrite, bacterial identification, *Acidithiobacillus*, *Pseudomonas*

Introduction

The Mária Mine in Rožňava, located along the Strieborná vein, represents one of Slovakia's most important deposits, characterized by Ag-bearing tetrahedrite with approximately 40–46 wt% Cu, 26 wt% Sb, and ~1 wt% Ag. This mineralization makes the site a valuable source of strategic and critical raw materials. Studying this mine drainage is particularly important, as it discharges into the Slaná River, which flows beyond the Slovak border into Hungary, underscoring the need to characterize its chemical composition and microbial community to better understand potential environmental impacts and evaluate its biotechnological relevance (Kupka *et al.* 2025; Hagarová & Kupka 2025).

Tetrahedrite represents a copper antimony sulfosalt that can be described by the simplified chemical formula $Cu_{10}(Fe,Zn)_2Sb_4S_{13}$. In natural systems, the minerals of the tetrahedrite group form a complex isotypic series with multiple iso- and heterovalent substitutions (King 2001; Moëlo *et al.* 2008). Tetrahedrite-group members may contain variable amounts of arsenic, antimony, mercury, or cadmium. Therefore, the waste from these deposits may pose environmental challenges.

Oxidative exposure of tetrahedrite and tennantite can lead to the mobilization of Sb, As, Cu, S, and other structurally bound elements. As a potentially toxic metalloid, Sb is released into the environment through multiple pathways, including mining activities, ore transport and processing, smelting operations, production and use of products, waste and sludge disposal, and industrial effluents (Liu *et al.* 2023; Stančić *et al.* 2022).

In this context, bioleaching tests were conducted to assess the behavior of the tetrahedrite concentrate under controlled acidic, oxidizing conditions at 25°C. Tetrahedrite bioleaching by acidophilic iron- and sulfur-oxidizing bacteria led to recovery of >80% Cu (>4 g L^{-1}). In addition, Sb was immobilized via precipitation of Sb(V) phases (Kupka *et al.* 2025). Although this mineral has typically been processed by alkaline

sulfide leaching due to its refractory behavior in acidic ferric media (Awe *et al.* 2010; Baláž & Achimovičová 2006), the present results demonstrate that bioleaching at ambient temperature can achieve efficient copper recovery without alkaline pre-treatment (Kupka *et al.* 2025).

To complement these process-based findings, the first comprehensive shotgun metagenomic survey of this mine drainage was conducted. The analysis generated approximately 227 million high-quality reads and revealed a community dominated by Betaproteobacteria (> 66%), with abundant lithotrophic genera *Sulfuritalea* (6.93%), *Ferrigenium* (5.45%), *Gallionella* (3.79%), and *Sideroxydans* (3.65%), alongside the heterotrophic genus *Pseudomonas* (5.2%). Among the most prevalent neutrophilic iron-oxidizing bacterial strains were *Sulfuritalea hydrogenivorans* (6.93%), *Ferrigenium kumadai* (5.45%) and *Gallionella capsiferriformans* (3.79%). Acidophilic genera (*Thiobacillus* sp. at 0.43%, *Ferrovum myxofaciens*, *Acidithiobacillus ferrivorans*, *Leptospirillum ferrooxidans*) collectively accounted for <1% of the community (Hagarová & Kupka 2025).

A key tool for mapping genomes of novel microorganisms is represented by whole-genome sequencing (WGS) that offers the ability to interrogate the entire DNA sequence of the genome without the need to use selective capture techniques to target and amplify a specific gene (Haworth *et al.* 2016). Sequencing the entire microbial genome is crucial for precise microbial identification and generation of complete reference genomes. Metagenomic data provide reliable estimates of bacterial community composition and diversity without the need to target and amplify a specific gene (Pérez-Cobas *et al.* 2020).

In this study, bacterial identification was performed following the cultivation of microorganisms originating from the Mária mine drainage in Rožňava on both liquid and solid media.

Methods

The mine water sample was collected from the outdoor discharge pipe of the Mária mine (Rožňava) (Fig. 1). Mine water chemistry was analyzed *in situ* using a pH meter (Denver Instrument UltraBasic) and a conductometer (WTW Cond 330i Set, TetraCon 325). Ion and metal concentrations were determined by ICP spectrometry and ion chromatography (Dionex ICS 5000, Sunnyvale, CA, USA).

The mine water, collected under sterile conditions, was used as an inoculum in liquid 9K medium containing 33.36 g L^{-1} $FeSO_4 \cdot H_2O$ (Silverman & Lundgren 1959) and on solid gelrite medium of similar composition but with reduced Fe^{2+} concentration (0.02 g L^{-1}) to capture heterotrophs. DNA from cultivated isolates was extracted using the QIAamp BiOstic Bacteremia DNA Kit (Qiagen, Germany).

Genomic DNA was subjected to whole-genome sequencing using an approach combining short-read sequencing (DNBSEQ platform, BGI Tech, China) and long-read sequencing (Oxford Nanopore platform). Raw reads were filtered to remove low-quality sequences, adapters, duplicated reads, and short fragments prior to assembly (Canu v2.2). For taxonomic identification and species verification, the assembled genome was aligned against the NCBI Nt (Nucleotide) database using BLAST-based similarity analysis. GC content and GC-depth correlation analysis were also performed to assess genome homogeneity and exclude potential contamination.

Results

Chemical characterization of mine water

Abiotic data revealed that the Mária mine releases a distinct neutral-pH (6.9) drainage enriched in metals, containing approximately 403.12 mg L^{-1} SO_4^{2-}, 5.58 mg L^{-1} Mn, and 4.66 mg L^{-1} Fe (Tab. 1). The temperature of the water sample was 13.9 °C, with a conductivity of 1,029 µS cm^{-1}, respectively.

Bacterial cultivation in liquid 9K medium

Cultivation in liquid 9K medium resulted in enrichment of an iron-oxidizing bacterium identified as *Acidithiobacillus ferrooxidans* (cover length 1,753,528 bp; coverage 99.09%; genomics 70%). Additional lower-percentage matches to related taxa were observed but covered substantially smaller

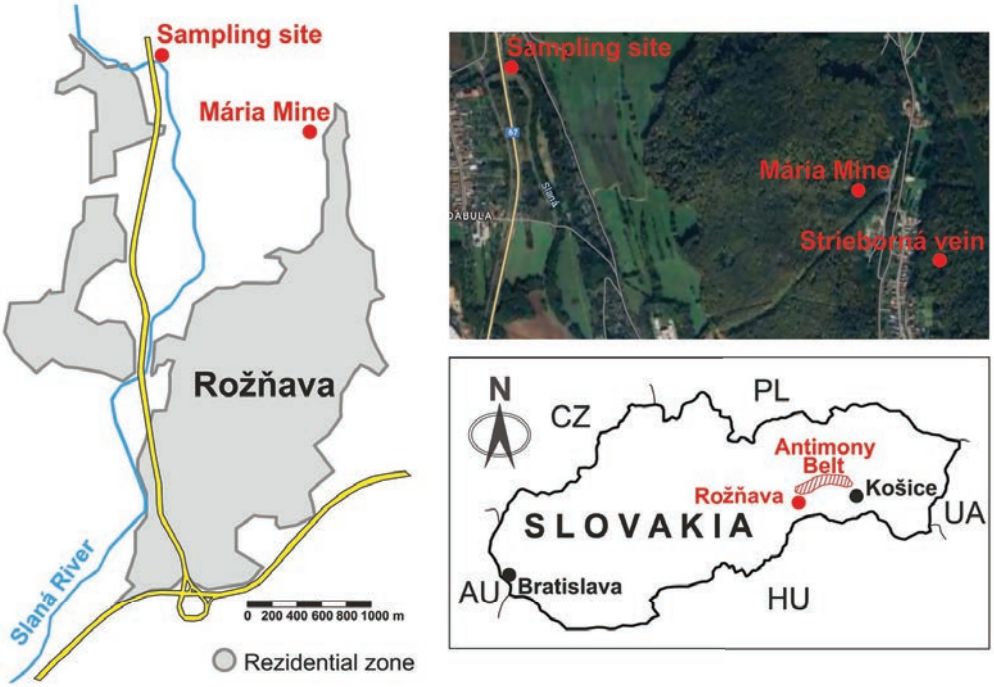

Figure 1 *Sampling site and the Mária mine in Rožňava (Hagarová & Kupka 2025).*

Table 1 *Chemical composition of the Mária mine water drainage.*

Parameter	$SO4^{2-}$	Mg^{2+}	Ca^{2+}	Cl^{-}	Na^{+}	K^{+}	Mn	Fe	F^{-}
mg L^{-1}	403.12	80.88	80.23	34.49	31.9	5.71	5.58	4.66	0.41
Parameter	NH^{4+}	Li^{+}	As	Ni	Co	Al	Zn	Sb	Cu
mg L^{-1}	0.242	0.032	0.01	0.01	0.006	0.006	0.006	0.005	0.004

genomic fractions, supporting the primary classification.

The final assembled genome had a total size of 1,850,565 bp with an overall GC content of 57.77%. The genome comprised one chromosome (1,644,415 bp; 58.04%) and five plasmids. Sequencing depth reached approximately 688x based on short-read data (1,275 Mb) and 1621x based on long-read data (3,000 Mb), providing strong support for the completeness and reliability of the genome reconstruction. The Nanopore long-read dataset was characterized by read lengths predominantly between 1-10 kb, with a maximum read length of 75,515 bp (Fig. 2).

Bacterial cultivation on solid gelrite medium

Taxonomic analysis based on Nt database comparison revealed the presence of multiple species affiliated with the genus *Pseudomonas*. Solid gelrite medium yielded heterotrophic bacteria predominantly assigned to *Pseudomonas (P.) fluorescens* (cover length 12,091,501 bp; coverage 82.66%; genomics 47.22%), together with genomic fractions closely related to *P. azotoformans* or *P. putida*, indicating the presence of more than one *Pseudomonas* species within the bacterial sample.

Genome assembly of the bacterial sample resulted in 5,258 contigs with a

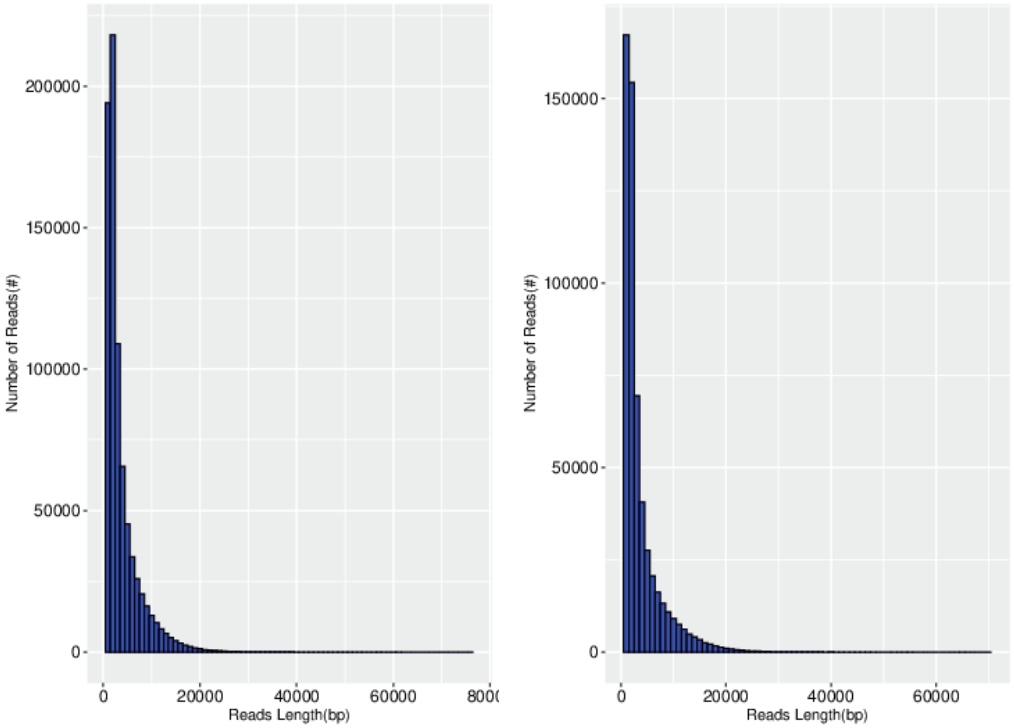

Figure 2 *Clean reads length distribution, Left – bacterial sample cultivated in liquid 9K medium; Right – bacterial sample cultivated on solid gelrite medium.*

total genome size of 30,976,816 bp and an overall GC content of 59.63%. The nanopore dataset comprised 567,178 reads, with a maximum read length of 70,102 bp (Fig. 2). The combined sequencing depth reached approximately 40x for short reads and 67x for long reads.

Conclusions

Abiotic characterization confirms that the Mária mine drainage represents a metal-enriched, neutral-pH environment that provides the geochemical framework for the development of distinct microbial functional groups.

The contrasting genomic profiles obtained from two cultivation approaches reflect the selective pressure imposed by growth conditions. Enrichment in liquid 9K medium, designed to favor iron-oxidizing chemolithotrophs, resulted in a near-complete and highly homogeneous genome of *A. ferrooxidans*, supported by high sequencing depth and a low number of replicons. In contrast, cultivation on a solid gelrite medium favored heterotrophic growth and resulted in a more genetically diverse bacterial population affiliated with multiple *Pseudomonas* species. These findings demonstrate that cultivation conditions strongly influence the composition and genomic architecture of the recovered microbial fraction.

Understanding these cultivation-driven shifts is essential for correctly interpreting microbial community structure and functional potential in mine-affected environments. In such systems, both iron-oxidizing autotrophs and metabolically versatile heterotrophs contribute to key biogeochemical processes.

The functional attributes may also indicate potential application pathways, although they are inferred from metagenomic data and require experimental validation. Under the circumneutral pH conditions of the Mária mine drainage, the dominant neutrophilic

iron-oxidizing bacteria are likely to play a more important role in iron cycling than acidophilic taxa such as *Acidithiobacillus*, whose low abundance and cultivation-based enrichment may overestimate their environmental relevance. Heterotrophic taxa such as Pseudomonas are likely to contribute primarily through the degradation of organic matter or siderophore-mediated iron mobilization. The presence of metal-resistance determinants (e.g., Czc, Ars, Aio) may also be relevant for metal tolerance and detoxification at moderate metal concentrations (Hagarová & Kupka 2025).

This work is essential for establishing the site's geochemical context and evaluating its microbial potential, particularly the presence of iron-oxidizing bacteria relevant to biohydrometallurgical processes. Such microorganisms enable the solubilization of metals from sulfide minerals (e.g., tetrahedrite) under environmentally sustainable conditions. The findings underscore the dual importance of monitoring mine water for environmental protection and exploring its microbial resources for innovative, low-impact extraction technologies.

Acknowledgements

This work was funded by the EU NextGenerationEU through the Recovery and Resilience Plan for Slovakia under the Project No. 09I03-03-V04-00271.

References

Awe SA, Samuelsson C, Sandström Å (2010) Dissolution kinetics of tetrahedrite mineral in alkaline sulphide media. Hydrometallurgy 103(1):167–172, doi:10.1016/j.hydromet.2010.03.014

Baláž P, Achimovičová M (2006) Selective leaching of antimony and arsenic from mechanically activated tetrahedrite, jamesonite and enargite. International Journal of Mineral Processing 81(1):44–50, doi:10.1016/j.minpro.2006.06.004

Hagarová L, Kupka D (2025) Insights into the microbiome of mine drainage from the Mária mine in Rožňava, Slovakia: a metagenomic approach. Frontiers in Microbiology 16 – 2025, doi:10.3389/fmicb.2025.1675058

Haworth A, Savage H, Lench N (2016) Chapter 4 – Diagnostic Genomics and Clinical Bioinformatics. In Kumar, D. & S. Antonarakis (eds) Medical and Health Genomics. Academic Press, Oxford, 37–50

King RJ (2001) The tetrahedrite group. Geology Today 17(2):77-80, doi:10.1046/j.0266-6979.2001.00268.x

Kupka D, Hagarová L, Bártová B, Majzlan J, Hredzák S, Matik M, Briančin J, Kaňuchová M, Sisol M, Ďuriška I, Jurkovič Ľ (2025) Bioleaching of Tetrahedrite by Iron- and Sulfur-Oxidizing Bacteria. Journal of Sustainable Metallurgy doi:10.1007/s40831-025-01089-0

Liu H, Zeng W, He M, Lin C, Ouyang W, Liu X (2023) Occurrence, distribution, and migration of antimony in the Zijiang River around a superlarge antimony deposit zone. Environmental Pollution 316:120520, doi:10.1016/j.envpol.2022.120520

Pérez-Cobas AE, Gomez-Valero L, Buchrieser C 2020. Metagenomic approaches in microbial ecology: an update on whole-genome and marker gene sequencing analyses. Microb Genom 6(8) doi:10.1099/mgen.0.000409

Moëlo Y, Makovicky E, Mozgova NN, Jambor JL, Cook N, Pring A, Paar W, Nickel EH, Graeser S, Karup-Møller S, Balic-Žunic TI, Mumme WG, Vurro F, Topa D, Bindi L, Bente K, Shimizu M (2008) Sulfosalt systematics: a review. Report of the sulfosalt sub-committee of the IMA Commission on Ore Mineralogy. European Journal of Mineralogy 20(1):7-46, doi:10.1127/0935-1221/2008/0020-1778

Silverman MP, Lundgren DG (1959) Studies on the chemoautotrophic iron bacterium Ferrobacillus ferrooxidans. I. An improved medium and a harvesting procedure for securing high cell yields. J Bacteriol 77(5):642-7, doi:10.1128/jb.77.5.642-647.1959

Stančić Z, Fiket Ž, Vuger A (2022) Tin and Antimony as Soil Pollutants along Railway Lines – A Case Study from North-Western Croatia. Environments 9(1):10, doi:10.3390/environments9010010

A Study on the Permeability Evolution of Self-Healing Mudstone Fracture Under Long-Term Stress

Hu Yunhao[1,2], Wu Jinxin[3], Dong Shuning[1,2], Yu Qingchun[3], Guo Xiaoming[1,2], Zhang Wenzhong[1,2], Zhang Xiyu[1,2]

[1]*Xi' an Research Institute of China Coal Technology and Engineering Group Corp, China, People's Republic of China*

[2]*State Key Laboratory of Coal Mine Hazard Prevention and Control, China, People's Republic of*

[3]*School of Water Resource and Environment, China University of Geosciences (Beijing), China, People's Republic of China*

Abstract

Self-healing capacity of roof aquitards in deeply buried coal seam goafs under long-term stress informs restoration strategies for damaged barriers. This work combines 260-day permeability tests on a mudstone fracture at 12 MPa confined pressure with fracture-scale COMSOL simulations. The decrease in permeability from transitions fast to slow. Early permeability declines rapidly due to channelization, bottlenecks, and electro-viscous effects. Dissolution–diffusion–precipitation processes and fines transport drive late-stage probable fluctuations and abrupt declines of fracture permeability. Under the tested conditions, the roof-water-region leakage barrier shows time-dependent self-healing, near-complete recovery within about three months after mining ends; late monitoring is also necessary.

Keywords: Deep-buried coal seam, mining-induced fracture, in-situ stress, water permeability, self-healing of aquiclude

Introduction

Northwest China harbors more than half of the nation's proven coal reserves, anchoring energy security for the country (Han *et al.* 2023). Yet this region is located in a dry to semi-arid climate where water resources are scarce, unevenly distributed, and groundwater system played a decisive supporting role in surface ecology (Liu *et al.* 2018). In deep goaf roofs, mining-induced disturbances fracture overburden strata, creating a water-conducting fractured zone. When these fracture networks intersect overlying aquifers, groundwater migrates toward the mined-out voids under gravity and hydraulic-head gradients, driving persistent underground inflows (Wang *et al.* 2019). Such inflows are not transient surges but long-lasting, self-healing–challenged losses that can persist for two to four years, yielding substantial groundwater depletion and ecological degradation (Yang *et al.* 2022). Remediation and reconstruction of damaged aquicludes thus emerge as essential components of sustainable, water-conscious coal development. A rigorous assessment of the self-healing capacity of damaged aquicludes under sustained formation stress is a prerequisite for deploying targeted restoration strategies with engineering precision.

Mudstone, a typical lithology of the aquiclude in the coal seam roof in the northwest coal mining area, has a high content of clay minerals and organic matter, and shows strong plasticity. Its permeability is highly sensitive to effective stress (Ju *et al.* 2020). Within geological sequences, mudstone thereby experiences prolonged, sustained stress, prompting progressive fracture closure and evolving permeability signatures. 30-day tests revealed pressure-solution and surface-erosion processes governing fracture permeability under elevated temperature (Cheng *et al.* 2021), while 60-day experiments showed rapid permeability reductions under a fixed confining pressure, with declines exceeding 90% within the first days and

continuing thereafter (Zhu and Yu 2024). Such short-duration studies inadequately capture long-term trajectories essential for engineering design and risk management, leaving a gap in understanding how mudstone fractures evolve under mining-relevant timescales.

To address this gap, we conducted permeability experiments on a single mudstone fracture for 260 days under a constant confining pressure of 12 MPa. Laboratory measurements were complemented by fracture-scale numerical simulations of water transport through the fracture. The experimental program, coupled with modeling, targets the coupled mechanical–chemical–particle-transport processes that govern self-healing under prolonged stress, with implications for roof-water-region governance and mine-water management.

Sample and Experiment

Mudstone core S1 was collected from the Anding Formation in the Ordos Basin, Northwest China at a depth of 762.6 m, yielding a dark-colored specimen. Cylindrical samples (25 mm diameter, 50 mm length) were prepared by wire-cutting. X-ray diffraction analysis identified quartz (46.8%) and clay minerals (48.5%) as the dominant phases. The water-saturated matrix permeability was measured as 2.59×10^{-18} m^2. A single longitudinal fracture was introduced at the core center using the Brazilian splitting method (Zhu and Yu 2024).

The experimental apparatus comprised a core holder, a confining-pressure loading system, a fluid-injection path, and a fluid-detection system. The core holder, with cushions at both ends, was enclosed in fluorinated rubber sleeves. A confining-pressure pump supplied water around the sleeves, with a central flow path linking the injection system to the mudstone core. Spiral grooves on the cushion cross-sections ensured uniform distribution of the injected fluid. A range of flow meters, depending on testing requirements, was employed; the instrument used in this study had a maximum full-scale of 0.5 mL and an accuracy of $\pm2.5\times10^{-3}$ mL, with a minimum range of 0.2 mL and an accuracy of $\pm1\times10^{-3}$ mL.

Saturation and permeability measurements followed a multi-step protocol. The sample was saturated in a high-pressure reactor with deionized water, using helium to pressurize the pore space to 15 MPa (Cheng and Yu 2019). Saturated samples were then placed in the core holder, and a confining pressure of 12 MPa was applied. Permeability was measured by the steady-state method (Yang *et al.* 2025). Water at 4 MPa inlet pressure was supplied, while the downstream outlet was vented to atmosphere; upon stabilization, the upstream–downstream pressure differential and flow rate were recorded synchronously to compute permeability. Each experimental set was repeated 2–3 times; individual measurement durations ranged from 2 to 6 h. If the relative deviation among measurements was ≤ 5%, the results were deemed reliable, and the mean value represented the steady-state flow rate. Matrix and fracture measurements followed the same operational protocol. Permeability generally varies with formation temperature and effective stress (Zhao *et al.* 2023); all experiments occurred in a temperature-controlled chamber with a constant temperature of 303.15 K and a confining pressure of 12 MPa to approximate deep formation conditions (Zhu *et al.* 2024). The calculation methods for matrix permeability, fracture permeability and hydraulic aperture were presented in Zhu and Yu (2024).

Simulation

Fracture flow was simulated in COMSOL Multiphysics using an initial fracture surface geometry derived from 3D surface scans. The scan data were digitized in Surfer, converting the surface into XYZ coordinates. A 3D model was constructed by embedding a rough fracture within a cylindrical rock body (25 mm diameter, 50 mm length). The computational domain was discretized into 737,229 elements, with a maximum element size of 1.33×10^{-3} m and a minimum element size of 2.51×10^{-4} m.

Boundary conditions mirrored the experimental setup. Permeability was highest along the fracture diagonal to represent the dominant flow path created by fracture roughness, while permeability was reduced

elsewhere to reflect channelized flow and aperture heterogeneity (Zhu and Yu 2024). Simulations proceeded after each adjustment to the fracture-permeability distribution until the numerically computed flow rate matched the experimental value, thereby inferring the internal fracture structure. Matrix and fracture domains employed distinct flow models. Matrix flow was described by Darcy's law:

$$\frac{\partial}{\partial t}(\epsilon_p \rho) + \nabla \cdot (\rho u) = Q_m \quad (1)$$

$$u = -\frac{k_m}{u_w} \nabla P \quad (2)$$

where ϵ_p is the porosity (-); ρ is fluid density(kg/m^3); u is Darcy velocity (m/s), and Q_m is a mass source term of matrix (kg/(m^3·s)), k_m is the matrix permeability (m^2). Fracture flow utilized a quadratic Forchheimer description to capture inertial effects in the rough channel:

$$D_h \frac{\partial}{\partial t}(\epsilon_p \rho) + \nabla_T (D_h \rho u) = D_h Q_m \quad (3)$$

$$-\nabla P = A Q_f + B Q_f^2 \quad (4)$$

$$A = \frac{u}{k_f w D_h}, B = \frac{\beta \rho}{w D_h^2} \quad (5)$$

where D_h is the hydraulic aperture (m); Q_f is a mass source term of fracture (kg/(m^3·s)), A is the viscous resistance coefficient (-), which dominant in laminar flow; B is the inertial resistance coefficient (-), which becomes important under turbulent or high-velocity conditions; and β is the Forchheimer coefficient (m^{-1}).

Results and Discussion

Temporal evolution of permeability and hydraulic aperture

Permeability and hydraulic aperture within mudstone fractures decline non-monotonically over 260 days under sustained in-situ stress (Fig. 1). The rapid-decline phase (0–21 days) exhibits the steepest reductions, followed by a slower sustained-decline phase (22–80 days), and a relatively stable phase (81–260 days) with only minor changes. Specifically, permeability and hydraulic aperture decrease by 39.7% and 63.7% during 0–21 days, by 18.0% and 18.5% during 22–80 days, and by 7.3% and 5.6% during 81–260 days, respectively. Despite continuous downward trends, changes after day 80 are modest, indicating near-equilibrium conditions for self-healing of the aquicludes in the roof of a goaf approximately three months after mining ceases. One plausible explanation is that the rapid and sustained declines reflect evolving fracture morphology and connectivity under stress, with subsequent stabilization governed by coupled mechanical and chemical processes.

Mechanistic interpretation by temporal phase

Rapid-decline phase (0–21 days). Mechanical creep and clay swelling drive the initial drop in permeability. Stress-driven contact-area evolution between fracture walls results in progressive fracture closing, consistent with stress concentration effects observed in clay-rich mudstones (Zhu *et al.* 2024). Water-

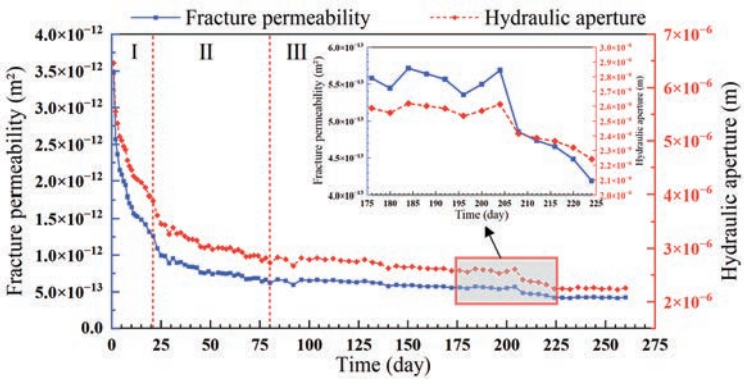

Figure 1 *The variation of water permeability in the fractured portions of the sample and the hydraulic aperture over time.*

induced clay swelling under saturation further augments closure, particularly within the early stage of exposure (van Noort and Yarushina 2019). These mechanisms collectively reduce flow pathways and enhance resistance to flow.

Sustained-decline phase (22–80 days). Flow becomes increasingly channelized within dominant fracture pathways. Bottlenecks controlling these channels dominate overall permeability; small reductions in bottleneck width yield disproportionate permeability decreases under confining stress. Water–mineral interactions also modulate transport: strongly adsorbed water can become immobile near mineral surfaces, reducing effective flow in constricted regions (Yang and Yu 2020). As stress continues, free water within wider segments diminishes, while narrower apertures compress toward the nanoscale. The narrowest bottlenecks increasingly govern transport. Electroviscous effects further suppress permeability by increasing flow resistance in these constrained regions (Li 2001).

Relatively stable phase (81–260 days). Sustained formation stress drives progressive contact-area growth between fracture surfaces, elevating fracture stiffness and rock strength while diminishing deformation capacity. The fracture approaches a new mechanical–chemical equilibrium. Persisting creep and mineral interactions yield minor fluctuations but no sustained deformation that would reopen flow paths. Permeability stabilizes as the system attains a balance among mechanical confinement, clay swelling, and dissolution–precipitation processes (Zhu and Yu 2024).

Abrupt late-stage decline (around day 205). An unforeseen, rapid drop ensues over roughly 20 days, surpassing prior trends (Fig. 1). The mechanism likely arises from the convergence of localized chemical and physical processes at fracture asperities under sustained 12 MPa confinement and flow (Huang *et al.* 2023). Asperities experience stresses well above the bulk level, elevating the chemical potential and initiating pressure solution of minerals (quartz and clays dominate the mudstone) at contact points, with dissolved material diffusing to lower-stress zones, precipitating elsewhere, or being flushed from the sample, so that dissolution–diffusion–precipitation (DDP) cycles progressively modify contact geometries and surface roughness (Sac-Morane *et al.* 2025). Concurrently, we consider that flow interacts with the rough fracture surfaces through scouring, liberating fines; these fines may deposit at bottlenecks to form bridge plugs or filter cakes that occlude channels, or be efficiently flushed to temporarily restore connectivity, yielding permeability fluctuations as the dominant pathways reorganize. The abrupt late-stage decline therefore reflects a coupled chemical–mechanical–particle-transport reconfiguration that cannot be captured by purely mechanical closure models; the observed perturbation emerges within the broader non-monotonic evolution—rapid creep and clay swelling during 0–21 days, followed by channelization-dominated reductions 22–80 days—when chemical mass transfer and fines dynamics progressively constrain flow and drive a sharp reorganization of the fracture-network permeability. This mechanism also explains discrepancies between observed trajectories and simplified simulations, underscoring the importance of incorporating DDP and fines transport in predictive models for mudstone fractures under sustained stress.

Fluid-transport dynamics from fracture-scale simulations: Simulations of fracture-flow under formation stress reveal pronounced channelization and flow reduction. Over a 120-day window, average fracture velocity declines from 0.213 m/s to 0.0202 m/s, a 90.6% decrease, signaling substantial compression, reduced effective flow area, and elevated flow resistance within the fracture network. In contrast, matrix flow remains orders of magnitude lower, near 10^{-7} m/s, and exhibits relatively small variation. During the initial compaction phase (first 12 days), dominant flow pathways contract rapidly; a limited set of channels persists and governs the fracture's bulk transport behavior. As stress persists, the initially small channels progressively close, while the originally large pathways continue to constrict and transform into smaller conduits; by day 80, flow is discernible only near those conduits that were originally large but have since narrowed to small apertures (Fig. 2).

Mechanistic synthesis and implications: One plausible explanation is that multiple processes operate in concert to produce the observed permeability evolution. In early stages, mechanical compaction and clay swelling dominate closure. In intermediate stages, flow preferentially follows a shrinking set of bottlenecks, with water–mineral interactions and electro-viscous effects further suppressing transport. In later stages, dissolution–diffusion–precipitation and pressure-solution mechanisms contribute to fluctuations in permeability by altering local mineralogy and roughness. The abrupt late-stage decline reflects a transient balance between scour-induced channel modification and fines deposition, temporarily enhancing or obstructing connectivity depending on particle transport efficiency.

Consequences for roof-water-region governance and mining practice: The non-monotonic evolution emphasizes that self-healing of mudstone fractures within deep coal-mining settings is time-dependent and path-sensitive. Short-term reductions in permeability may provide immediate leakage barriers, but long-term stability depends on sustained mechanical–chemical interactions and the fate of fines within bottlenecks. The approximately three-month timeframe for near-complete self-healing informs governance planning and strategies for water preservation in mining, enabling risk-aware design of roof-water-region protection. However, late-stage perturbations underscore the need for monitoring of fracture pathways and fines dynamics to prevent unanticipated permeability changes.

Conclusions

This study demonstrates a non-monotonic evolution of fracture permeability in mudstone under sustained in-situ stress, controlled by coupled mechanical, chemical, and particle-transport processes. In 260 days, permeability declines fastest in the rapid-decline phase (0–21 d) due to mechanical creep and clay swelling closing flow paths; a sustained-decline phase (22–80 d) is governed by channelization and bottlenecks, with water–mineral interactions and electro-viscous effects further suppressing transport; a relatively stable phase (81–260 d) approaches a new quasi-equilibrium. An abrupt late-stage decline around day 205 may reflects a synchronized reconfiguration driven by dissolution–diffusion–precipitation and fines dynamics that pure mechanical closure models cannot capture. Simulations of fracture-flow under formation stress

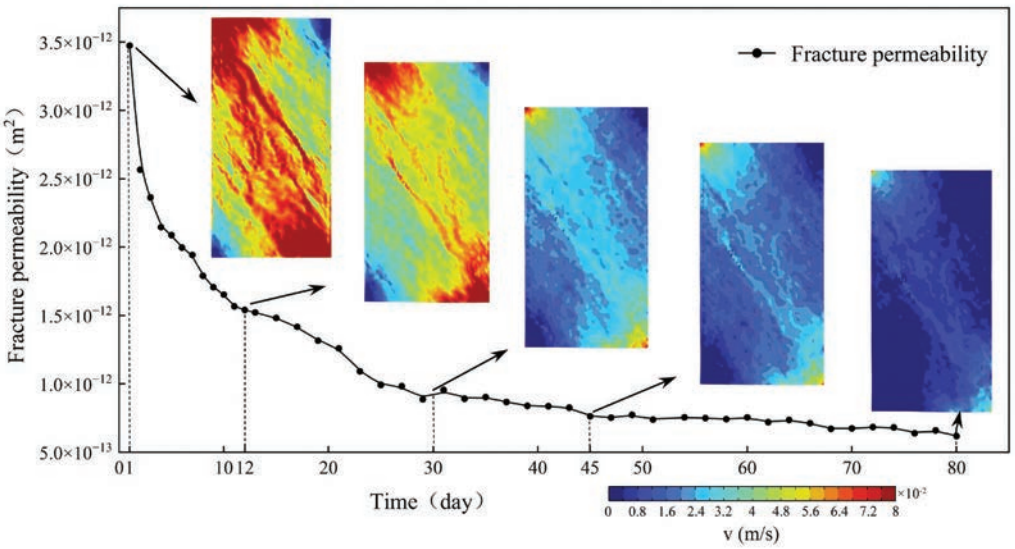

Figure 2 *Evolution of fracture permeability and the flow velocity field within the fracture during the initial 80-day experimental period (X-Y plane).*

reveal pronounced channelization and flow reduction. Practically, under the tested conditions, the roof-water-region leakage exhibits time-dependent self-healing, suggesting that it reaches its self-healing limit within about three months after mining ceases; nonetheless, late-stage late monitoring is also necessary. For modeling, incorporating DDP, fines transport, channelization, and electro-viscous effects is essential for reliable predictions. Our integrative framework clarifies the drivers of permeability trajectories and informs risk-aware strategies for roof-water-region protection. Future work should extend time scales, mineral diversity, and field-scale validation.

Acknowledgements

The authors thank all co-organisers for hosting the IMWA 2026 Conference. This study was funded by K Key Research and Development Program of Shaanxi (Program No. 2025SF-YBXM-510) and Tiandi Science and Technology Co. Ltd. Science and Technology Innovation Venture Capital Special Project (Grant No. 2025-TD-QZ030).

References

Cheng C, Herrmann J, Wagner B, Leiss B, Stammeier JA, Rybacki E, Milsch H (2021) Long-term evolution of fracture permeability in slate: an experimental study with implications for enhanced geothermal systems (EGS). Geosciences 11:443. https://doi.org/10.3390/geosciences11110443

Cheng P, Yu Q (2019) Experimental study on the relationship between the matric potential and methane breakthrough pressure of partially water-saturated shale fractures. J Hydrol 578:124044. https://doi.org/10.1016/j.jhydrol.2019.124044

Han Y, Wang Q, Li W, Yang Z, Gu T, Wang Z (2023) Predicting the height of the water-conducting fractured zone in fully mechanized top coal caving longwall mining of very thick jurassic coal seams in western China based on the NNBR model. Mine Water Environ 42:121–133. https://doi.org/10.1007/s10230-023-00918-6

Huang X, Kang Z, Zhao J, Wang G, Zhang H, Yang D (2023) Experimental investigation on micro-fracture evolution and fracture permeability of oil shale heated by water vapor. Energy 277:127677. https://doi.org/10.1016/j.energy.2023.127677

Ju J, Li Q, Xu J, Wang X, Lou J (2020) Self-healing effect of water-conducting fractures due to water-rock interactions in undermined rock strata and its mechanisms. Bull Eng Geol Environ 79:287–297. https://doi.org/10.1007/s10064-019-01550-x

Li D (2001) Electro-viscous effects on pressure-driven liquid flow in microchannels. Colloids Surf Physicochem Eng Asp 195:35–57. https://doi.org/10.1016/S0927-7757(01)00828-7

Liu S, Li W, Wang Q (2018) Height of the water-flowing fractured zone of the jurassic coal seam in northwestern China. Mine Water Environ 37:312–321. https://doi.org/10.1007/s10230-017-0501-1

Sac-Morane A, Rattez H, Veveakis M (2025) Importance of precipitation in the slowdown of creep behavior induced by pressure solution. J Eng Mech 151:04025025. https://doi.org/10.1061/JENMDT.EMENG-8360

van Noort R, Yarushina V (2019) Water, CO2 and argon permeabilities of intact and fractured shale cores under stress. Rock Mech Rock Eng 52:299–319. https://doi.org/10.1007/s00603-018-1609-8

Wang F, Xu J, Chen S, Ren M (2019) Method to predict the height of the water conducting fractured zone based on bearing structures in the overlying strata. Mine Water Environ 38:767–779. https://doi.org/10.1007/s10230-019-00638-w

Yang P, Yang W, Nie Y, Saleem F, Lu F, Ma R, Li R (2022) Predicting the height of the water-conducting fractured zone based on a multiple regression model and information entropy in the northern Ordos basin, china. Mine Water Environ 41:225–236. https://doi.org/10.1007/s10230-021-00805-y

Yang S, Yu J, Liu D, Li Y (2025) Effect of persulfate stimulation on matrix alteration and permeability enhancement of fractured shale: core-flooding experiments and numerical simulation. Gas Sci Eng 138:205612. https://doi.org/10.1016/j.jgsce.2025.205612

Yang S, Yu Q (2020) Experimental investigation on the movability of water in shale nanopores: a case study of carboniferous shale from the qaidam basin, china. Water Resour Res 56:e2019WR026973. https://doi.org/10.1029/2019WR026973

Zhao D, Chang H, Pu Y, Feng Z, Li X (2023) Study on mechanical parameters and creep seepage characteristics of different coal and rock combination samples. Geomech Geophys Geo-Energy Geo-Resour 9:25. https://doi.org/10.1007/s40948-023-00569-5

Zhu N, Cheng P, Yu Q (2024) Experimental study on the time-dependent gas permeability of fractures in shales. Rock Mech Rock Eng 57:695–718. https://doi.org/10.1007/s00603-023-03578-8

Zhu N, Yu Q (2024) Temporal evolution of fracture transport properties of fractured shales during long-term stress compaction. Eng Geol 339:107663. https://doi.org/10.1016/j.enggeo.2024.107663

The Value of Holistic Water Quality Assessment to Support Pit Lake Closure Decisions

Paul Hubbard

SRK Consulting (UK), Cardiff, phubbard@srk.co.uk

Abstract

Decisions relating to pit lake closure can exert basin-scale influence on surface water and groundwater systems. This was evaluated in a water-stressed region where a flow-through pit lake system was proposed as a community water resource. The integrated assessment considered climate, hydrology, groundwater and waste-rock seepage to test both lake viability and regional hydrological effects. The results show that closure decisions can change materially when pit lakes are assessed as part of the wider hydrological system, in-line with water stewardship principles.

Keywords: Pit lake, mine closure, water stewardship

Background and issue

Pit lakes can often act as control on the surrounding post closure water system, with potential wider impacts on water resources than just the quality of the pit lake itself. The lake will typically act as a contaminant sink or source for the immediate surrounding hydrological system to some extent, but influences can be wider reaching where pit closure involves river diversions or changes in groundwater flow regime. Under such circumstances, the pit lake interacts directly with wider hydrological pathways, and an isolated assessment of the pit lake would not capture the basin scale consequences of closure choices.

This was the case at a gold mine in sub Saharan West Africa, where rainfall is highly seasonal, evaporation greatly exceeds precipitation, and water resources are limited and strongly contested among closure objectives, local and downstream users and the broader environment. The final landform comprised three pit voids, and the closure planning concept involved diverting part of the adjacent ephemeral river through the three pits to accelerate filling and create a post closure lake resource for the benefit of local communities.

Earlier assessments had explored this closure concept, which stemmed from the original Environmental Impact Assessment for the mine. They focused on pit lake recovery and concentrations of substances in the pit lake. However, they did not evaluate the broader interaction between the pit lakes and regional groundwater and river resources. Upon review, the previous work also omitted several inputs, such as waste rock seepage and pit wall reactivity, and relied on assumed values for other inputs that appeared to be controlling the results, where dedicated parameterisation studies were needed. As a result, confidence in their conclusions was not sufficient to make updated closure decisions.

The mine was also adopting a water framework based on International Council on Mining and Metals (ICMM) water accounting/reporting and Alliance for Water Stewardship (AWS) catchment water-stewardship principles, so closure decisions needed to consider catchment-level impacts rather than only site outcomes. Given the uncertainties, it was clear a broader integrated study was needed to reassess long-term pit lake behaviour and regional water-resource consequences.

Aim

The aim of the project was to assess the long term hydrological and geochemical behaviour of the proposed pit lake system and its wider impacts, under two closure scenarios:

1. diversion of part of the river through the pits to accelerate filling and sustain higher lake levels near surface for community use [“with river scenario”], and

2. no river diversion, with pit lake levels driven by groundwater rebound, direct rainfall and runoff from adjacent waste rock dumps, where water quality was likely to be poor (Figure 1).

The study needed to provide conclusions sufficient to support closure decision making and advance the water management plan.

Approach

The assessment combined climate analysis, catchment runoff analysis, river hydrology modelling, groundwater modelling, waste rock seepage evaluation, pit wall geochemistry and a water and solute load model for the pit. A single integrated team worked across these linked components, ensuring consistent assumptions and enabling feedback between disciplines.

Climate

Climate sensitivities in this arid region would influence all parts of the assessment, particularly with the potential effects of successive dry years that had already occurred in the past and long-future climate change with potential for more intense but shorter wet seasons. Historical climate inputs were derived from regional and site rainfall gauges, site weather station data and A pan evaporation records and fitted to a climate model to fill data gaps and extend the time series, producing a daily long-term record for calibration and climate change modelling.

The site was represented by a mean annual precipitation of approximately 460 mm/year with an evaporation of around 3,500 mm/year reflecting the strongly negative climatic water balance at the site.

River flow

The ephemeral river adjacent to the mine is a regional drainage system with a catchment of over 2,500 km2 . In the wet season, flood occurs as a flashy flood of the channel and surrounding area due to the intense rains. The river passes over two shallow dams next to the mine that the mines raw water as well as water supply for the adjacent town and farmers, with the residual downstream flow supplying communities. To accurately model the function of the diversion channel, its flow into the pit lake and the lakes impact to the downstream river catchment the river diversion assessment needed to be able to mimic the wet season run-off, storm surge, and how this might change in the future.

River flows were modelled via a catchment scale hydrological and hydraulic modelling workflow. The catchment runoff was represented using a lumped basin soil moisture accounting model in HEC HMS and was calibrated against dam water level gauges. The flow intensity from the runoff was simulated using a 2D HEC RAS hydraulic model of the adjacent river corridor. The model was calibrated against the large, short duration flood events using the 15 minute spillway record that was available for the dam

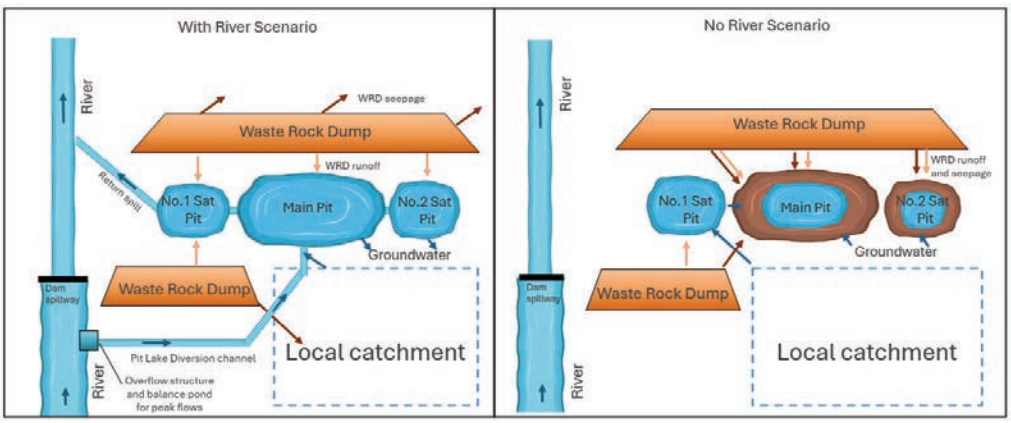

Figure 1 *Simplified conceptual model of pit lake inflows and outflows under the two closure scenarios.*

to capture the flashy hydrograph shape that is not resolved in daily simulations and also observed flood extents from satellite imagery. The proposed pit-lake diversion channel alignment was designed iterating cross section dimensions into the terrain to convey the design event without spilling.

Groundwater

In the river diversion scenario rapid filling of the pits would quickly exceed the local depressed groundwater levels. This would create outflow from the pit to the wider groundwater system, increasing the volumes of river water required to compensate for groundwater storage recovery and once the levels were near surface as intended in the closure design, permanent outflow from the lake to the wider groundwater system would occur. Conversely the no river scenario would represent constant loss from the groundwater system to the lakes and water level reduction in the aquifer and act as a sink for contaminant issues relating to the mine infrastructure. SRK had previously developed a regional scale 3D groundwater model in FEFLOW (Diersch, 2005) as part of a separate project for the mine. For this project, the regional model was cropped to the vicinity of the pit to estimate transient stage-dependent inflow and outflow relationships for the pits under variable lake conditions to use in the lake water balance simulations. Because groundwater was both a lake inflow and a potential receptor, the regional model was also used to simulate how both scenarios effected long-term groundwater levels, flow directions and the potential migration of seepage from the mine facilities

Waste Dump Seepage

The mine has a number of laterally extensive waste-rock dumps (WRD), known to readily leach metals, in particular arsenic. In dry climates, waste-rock dumps can remain under-saturated with respect to equilibrium moisture contents for years to decades, with wetting fronts progressing slowly and chemistry evolving as deeper oxidised materials are progressively wetted. Prior assessments had not taken account of this seepage source, focussing on observed solute loading from WRD runoff only. This seepage source that would potentially be released post closure was likely to be a sensitive input into the model, therefore it was decided to constrain the seepage rates and timing using unsaturated flow modelling in HYDRUS (Šimůnek, 2013). The model incorporated WRD geometry, deposition history, particle-size distribution and representative soil–water characteristic curves, with parameters adjusted to account for the coarse fraction that contributes little to storage. Residence-time analysis confirmed that downward wetting through the WRD matrix component would be slow compared to rapid macropore infiltration events, with quasi-equilibrium moisture conditions in the matrix predicted to occur well after mine closure and solute migration further delayed by the saprolite below the WRD footprints. Once quasi-equilibrium moisture conditions were reached post-closure, percolation from the WRD was estimated at around 5% of annual rainfall, based on a combined representation of long-term cover including areas of sparse shallow- and deep-rooting vegetation as per restoration plans, together with unvegetated areas where only sandy wind-blown cover was assumed to have developed.

Geochemical sources

Source terms for waste rock seepage and runoff, and pit wall inundation were derived to provide solute loading inputs into the integrated model. The derivation was based on a static and kinetic test work dataset for site lithologies including humidity cell tests (HCTs). Materials were classified as non PAG, but metal-leaching. Arsenic leaching at near neutral pH was the principal long term source concern. For WRDs, runoff source terms were developed for the exposed surface mix (typically dominated by lower risk lithologies) and calibrated to monitored WRD runoff collection pond chemistry. WRD seepage used internal dump lithologies, the long initial oxidation period and expected leaching dynamics, with evaluation in PHREEQC (Parkhurst and Appelo, 2013) to constrain oversaturated mineral phases. For pit walls, runoff contact water and first submergence flushing were treated separately;

reactive mass was estimated from 3D pit wall areas by lithology from the site's geology model. Submergence release was coupled with assumptions regarding fracture release based on fracture zone thickness, density and an oxidised rind in addition to contributions from talus on benches.

Pit lake load model

A 2D laterally averaged hydrodynamic model (CE QUAL W2) was initially planned for use in the gap analysis phase, consistent with the first of the prior assessments that suggested river inflows could generate temperature stratification. However, scoping simulations of seasonal inflows into the main pit lake were tested in 3D in TUFLOW (BMT, 2019) to check if this assumption was correct, and this indicated that persistent stratification in the main pit lake was unlikely. As a first pass, the hydrological and geochemical inputs were combined in a GoldSim (Kossik and Van Kuiken, 2006) water and solute balance model for the three pits to simulate long term water levels, solute loads and bulk concentration behaviour, with screening for oversaturation of solute in the lake using PHREEQC. GoldSim's complete mixing assumption was adopted for options appraisal because sustained stratification was not expected to be a control on long term outcomes. The model used equations to balance the flow between the lakes during river inflow events. The GoldSim approach was taken with the recommendation that if river diversion is progressed to design, lake hydrodynamics should be revisited using a 3D model once inlet/outlet structures and operating controls were better defined, particularly to understand the extent of mixing in the No2. Satellite Pit. The outputs of the pit lake model were fed back into the river and groundwater models to understand the linked effects to these systems.

Results

The results showed that both the long term behaviour of the pit lakes and closure water system was controlled by a relatively small number of dominant processes: strong evaporative loss, delayed but increasingly strengthening WRD seepage, the seasonal influx from the river (for the with river scenario) and the direction of groundwater flow as water levels changed.

No river diversion scenario

Under the no river scenario, the Main Pit and No.2 satellite pit acted as terminal evaporative basins that only partially refilled to approximately one third of the pit depths over decades. Water quality deteriorated over time through evapoconcentration and progressive loading, particularly for arsenic. The No. 1 satellite pit performed more favourably if the local catchment was directed to that pit only providing some, albeit volumetrically reduced, potential for beneficial community use post-closure. However, with this scenario inward groundwater gradients were maintained to the main pit. This contained poorer quality mine waters within the former mine site which were present from seepage in the TSF area and would be developed post closure from the WRDs situated adjacent to the pits, once full seepage potential was reached, thus limiting regional risk.

The with river diversion scenario

Under the river-diversion scenario, the main pit completed rebound to near surface in around a quarter of the time of the no river scenario, before overflowing through the linked pit system, then to the river. During filling, the diverted river inflow diluted concentrations and improved predicted water quality considerably relative to the terminal scenario. These improved outcomes were contingent on sustained throughflow for the lake back to the river. Because topography prevented direct diversion-channel connection to the No.2 satellite pit, it relied on a single connection to the Main Pit and lacked throughflow; its water quality therefore did not meet standards and continued to worsen after lake connection. Whilst the Main Pit lake quality was greatly improved compared to the no river scenario, initially achieving standards after filling, a slow gradual decline in quality was predicted over decades as continued loading outweighed dilution, meaning some water quality standards were exceeded long-term. Although water quality not achieving standards might have limited

use of the river augmented pit lake, predicted concentrations remained much better than the terminal evaporative pit lakes in the no river scenario.

Effects to groundwater quality

With the With River scenario, as lake levels rose, groundwater gradients reversed and outward seepage became possible. The main loading from this was not from the lake water itself as this was relatively near the standard, but from the change in migration direction of seepage from WRD areas. The WRDs represented a major solute loading source and with little areal recharge in saprolitic areas, the down gradient groundwater system had little capacity for dilution beyond the water seeping from the raised pit lake itself. In simulations the WRDs developed a plume in the groundwater system migrating outside the mine site. Furthermore, a plume formed by the TSF seepage that had been migrating partially to the pit in operations, also was predicted to change direction and flow outside the mine site in long-term closure under this scenario. In the context where the groundwater is the key year round water resource for surrounding and regional communities this was a key outcome outweighing any benefit from a recovered lake for community use.

Loss of water resources from evaporation

Diverting river water through the pits reduced downstream flows by approximately 10% during the filling period and by around 4% long term due to evaporation from the new permanent water surface. These were considerable for a river of such size in a water scarce region. Cutting off the top of seasonal waters to fill the pit also had implications for the extent of the river's wet-season water migration downstream. Such river systems rely on these large-scale flood waters to reach lower reaches.

The terminal lake scenario, in contrast, gave evaporative losses for groundwater and continued drawdown from the supressed lake. However, water losses were considerably lower and largely involved groundwater already compromised by seepage from the WRDs and the TSF seepage.

Discussion

From a water stewardship perspective, the river diversion scenario provided faster filling and countered wider groundwater drawdown but introduced three regional risks: additional long term evaporative losses of the river water resource, reduced river water quality (although predicted to be marginal, highly uncertain), and the long-term potential for regionalised groundwater quality derogation driven by gradient reversal for seepage from the WRDs. Whilst lake quality was vastly improved, it did not meet all standards limiting the extent of its use and its benefit did not outweigh its risk. The terminal lake scenario avoided these wider risks and therefore despite producing lake quality and levels that removed any use, it aligned more closely with basin scale sustainability that the client was implementing in their water management framework. The effect of this boundary change is summarised in Figure 2.

These findings show two relevant points transferable to other closure water management studies. First, once the system was assessed holistically, rather than just in the context of the pit lake's water quality the preferred closure option shifted. Second, the reliability of the water and solute balance depended on whether key inputs – in this case, seepage rates and chemistry, river inflows to the lake (and mixing) and evaporative losses – had been adequately defined. And after the supporting studies were completed and integrated, the environmental impacts of the pit lake and closure options could be compared more transparently and defensibly.

Conclusion

Pit lake closure decisions, particularly in water-stressed regions, can have basin-scale impacts and can benefit from integrated assessment aligned with water-stewardship principles. At this mine, linking river hydrology, groundwater flow, long-term waste-rock seepage and pit lake formation showed that the preferred option depended on broader trade-offs, not pit lake water quality alone. The concept of a beneficial pit lake resource for local communities after mine closure was relegated when this risked regional water resource derogation. Although

Boundary	No river diversion	With river diversion	Decision implication
Pit-lake-only assessment Lake level + water quality	• Partial rebound • Terminal evaporative lakes • Evapoconcentration, poor lake quality • No beneficial use	• Rapid filling to surface • Dilution + flow-through lowers lake concentrations • Local water resource benefit (but limited by concentrations) • High lake water-quality uncertainty	Pit-lake-only view **With River Diversion preferred** Because lake levels and water quality improved
Regional assessment Lake + groundwater + river resources	• Pit remains hydraulic sink • Inward gradients retain WRD /facility seepage near mine • Low loss of clean water resources to evaporation • Drawdown of local groundwater	• Near-surface lake reverses groundwater gradients • Seepage toward receptors • River loss: ~10% filling /4% long term • High lake water quality uncertainty and high risk	Holistic view **No River Diversion preferred** Because regional water resources protected

Figure 2 Summary of closure scenario outcomes under different assessment boundaries.

the terminal pit lakes had poor water quality, they helped contain mine seepage, whereas the flow-through concept redirected groundwater contaminants towards local receptors and increased evaporation losses of regional water resources. The more holistic assessment therefore changed the understanding of the risks presented by the closure options and the pit lake's role at closure.

Acknowledgements

The project was a team effort from specialists of various disciplines, including, Lorenzo Bianco (climate Assessment), David Carruth, Francis Smith and Thomas Malone (catchment, river and channel design and models) Adam Bennett (groundwater modelling), Vitor Sato (WRD seepage), Mo Walter and David Tait (geochemistry), Dr. Mike Stewart (GoldSim water and load balance and TUFLOW lake model). Thanks also to contributions from Mark Raynor and the client team.

References

BMT WBM Pty Ltd (2018) TUFLOW FV science manual. BMT WBM Pty Ltd, Brisbane

Diersch H-JG (2005) FEFLOW – Finite element subsurface flow and transport simulation system – Reference manual. WASY GmbH, Berlin

Kossik R, Van Kuiken J (2006) GoldSim: A graphical simulation environment for modelling complex systems. In: Proceedings of the Winter Simulation Conference, pp 330–336, doi:10.1109/WSC.2006.323247

Parkhurst DL, Appelo CAJ (2013) Description of input and examples for PHREEQC version 3 – A computer program for speciation, batch-reaction, one-dimensional transport, and inverse geochemical calculations. US Geological Survey Techniques and Methods, book 6, chap A43, doi:10.3133/tm6A43

Šimůnek J, Šejna M, Saito H, Sakai M, van Genuchten MT (2013) The HYDRUS-1D software package for simulating the movement of water, heat, and multiple solutes in variably saturated media, version 4.0. Department of Environmental Sciences, University of California Riverside

IMWA 2026
Jeongseon

Efficient Data Assimilation for Reactive Transport Models using Data-Space Inversion

Rui Hugman[1], Pablo Ortega[2] and Jeremy White[3]

[1]*INTERA Geosciences Pty Ltd, Faro, Portugal, rhugman@intera.com, ORCID 0000-0003-0891-3886*

[1]*INTERA Geosciences Pty Ltd, Perth, Australia, portega@intera.com*

[1]*INTERA Incorporated, Fort Collins, USA, jwhite@intera.com*

Abstract

Coupled groundwater reactive transport models are essential for water management but computationally expensive, limiting their use in ensemble-based uncertainty quantification and data assimilation. This paper demonstrates a Data-Space Inversion (DSI) surrogate modeling approach to overcome this constraint. DSI assimilates observations and conditions forecasts using statistical relationships from a prior ensemble, completely avoiding repeated full-model evaluations. Tested on a 3D groundwater system with nonlinear geochemistry (based on the DIZON pilot project), the DSI surrogate captured the physics-based model dynamics and predictive uncertainty while reducing computational costs by orders of magnitude. This approach enables rapid, probabilistic scenario evaluation, successful integration of high-fidelity models into efficient decision-support systems.

Keywords: Coupled flow and reactive transport, surrogate models, model emulation, decision support, uncertainty, data assimilation

Introduction

Coupled groundwater flow and reactive transport models (RTMs) are primary tools for assessing groundwater quality and evaluating operational risks in mine water management. However, integrating field observations into these models through data assimilation or parameter estimation is computationally demanding. Traditional inverse modelling requires iteratively evaluating the forward model to minimize the misfit between simulated outputs and field data. Because resolving non-linear geochemical reactions and multi-species transport across large three-dimensional domains is inherently resource-intensive, the repeated model executions required for parameter estimation and uncertainty quantification are frequently cost-prohibitive. While various surrogate modelling techniques exist to reduce this burden, preserving the non-linear spatiotemporal dynamics of reactive transport while maintaining a rigorous mathematical framework for uncertainty quantification remains a challenge.

This paper applies a Data-Space Inversion (DSI) (Sun and Durlofsky, 2017) surrogate modelling approach to bypass these computational constraints. DSI operates entirely within the data space, utilizing statistical relationships among model outputs to assimilate observations and condition forecasts. By constructing a surrogate from a prior ensemble of full-order model simulations, DSI removes the need for explicit parameter estimation. Consequently, no further evaluations of the forward model are required during the conditioning or forecasting phases, reducing the computational burden substantially.

We demonstrate the application of DSI within a prediction-driven decision support workflow using a three-dimensional synthetic groundwater system characterized by variable flow conditions, multiple reactive species, and nonlinear geochemical reactions. This approach provides a practical method for integrating high-fidelity RTMs into decision support systems where computational limits otherwise restrict standard inversion techniques.

Methods

We demonstrate a DSI-based surrogate modelling approach for data assimilation and predictive uncertainty analysis using a numerical model based on the DIZON (Deep well injection in Zuid-Oost Nederland) field study (Prommer and Stuyfzand, 2005). The following chapter presents the theoretical background for DSI, a summarized description of the study case, the setup of the coupled flow and reactive transport numerical model and the emulator-based data assimilation workflow.

Data Space Inversion

Initially introduced in reservoir engineering literature by Sun and Durlofsky (2017), DSI is a surrogate modelling technique that relies on the statistical properties of a model's output rather than its internal parameters. The core concept of DSI assumes that a full-order physics model M, driven by a set of uncertain input parameters k, produces a comprehensive output vector d. This output vector can be partitioned into two distinct categories: historical variables that can be directly observed (o) and future predictions required for decision-making (p):

$$\mathrm{d} = \mathrm{M(k)} = \begin{bmatrix} \mathrm{o} \\ \mathrm{p} \end{bmatrix}$$

To avoid the computationally expensive and highly dimensional process of traditional parameter estimation, DSI relies on a prior ensemble of n_{real} model realizations. By evaluating the model across a wide distribution of prior parameters, DSI establishes a direct, empirical correlation between the observable data o and the forecasts p. This approach is highly advantageous when dealing with multiple conceptual models, highly parameterized spatial structures, or numerical frameworks that are difficult to calibrate conventionally. This empirical relationship is mathematically captured by extracting a data covariance matrix, C_d from the prior ensemble of model simulated outputs. Then, Singular Value Decomposition (SVD) is employed to project the high-dimensional data space into a simplified latent-space representation:

$$\hat{\mathrm{d}} = \bar{\mathrm{d}} + \mathrm{C_d}^{1/2}\mathrm{x}$$

In this formulation, $\bar{d}$ is the ensemble mean, and x represents a vector of latent-space variables drawn from a standard normal distribution. Any new output vector $\hat{d}$ generated through this latent projection preserves the exact statistical moments of the original full-order model ensemble.

The fundamental benefit of this DSI formulation is its immense computational efficiency during the inversion process. Instead of iteratively running the complex numerical model, field observations are used to directly condition the latent-space vector x.This allows for the near-instantaneous generation of posterior predictive distributions, effectively eliminating the primary computational bottleneck of traditional history matching.

In summary, implementing a DSI surrogate based workflow requires:

- Generating an ensemble of training data by simulating a physics-based model with different random sets of model parameters (usually a few hundred model runs).
- Training the surrogate on the ensemble of model outputs.
- Calibrating the surrogate parameters.
- Obtain a posterior predictive probability distribution.

Case Study: DIZON Field Study

The foundation of our model emulation workflow is the DIZON (Deep well injection in Zuid-Oost Nederland) field study, a benchmark Aquifer Storage and Recovery (ASR) experiment originally detailed by Prommer and Stuyfzand (2005). The pilot project provides a well-documented, complex dataset of non-linear geochemical interactions triggered by artificial recharge of surface water to a deep, isolated groundwater system by means of direct injection, making it an interesting testbed for evaluating surrogate modelling efficiency.

The conceptual model involves the injection of oxic, pre-treated surface water into a deep, strictly anoxic aquifer. The native sedimentary matrix contains appreciable fractions of reactive pyrite (FeS_2) alongside minor sediment-bound organic matter. The injection of oxygen- and nitrate-rich water initiates a cascade of transient redox

reactions, dominated by pyrite oxidation. This primary reaction pathway consumes the injected oxidants and produces sulfate, acidity (H^+), and ferric iron precipitates ($Fe(OH)_3$). A critical feature of the DIZON site is the seasonal temperature variation of the injected surface water, which heavily dictates the reaction kinetics. Cold water injection suppresses reaction rates, allowing oxidants to penetrate further into the aquifer, whereas warm water drives rapid oxidant consumption immediately adjacent to the wellbore. Models must account for these temperature-dependent kinetics to accurately reproduce observed field-scale oxygen breakthrough and nitrate removal patterns.

Coupled Flow and Reactive Transport Model Setup

To demonstrate the application of DSI, the DIZON conceptual model was translated into a coupled groundwater flow and reactive transport model. Groundwater flow and transport is simulated using MODFLOW6 (Langevin *et al.* 2026), dynamically coupled to PHREEQC (Parkhurst and Appelo, 2013) using the open-source software *mf6rtm*. The numerical model couples three-dimensional groundwater flow, heat transport, and multicomponent geochemistry.

Geometry of the site is represented with a rectangular model domain approximately 120 by 300 m. A Voronoi mesh was employed to allow for refinement near injection/recovery wells. The model is divided into 12 layers, with layer elevations interpolated from borehole log data. Thirty-nine stress periods are simulated using daily time steps, for a total simulation period of 854 days. The model domain, grid and boundary conditions are shown in Fig 1.

The injection and recovery wells are placed on the southern boundary of the model reduce the overall computational demand under the assumption of radial flow. Injection and extraction was applied to model layers corresponding to screened intervals. Initial hydrogeological parameters are assigned. Horizontal and vertical conductivity were assigned a value of 1 m/d. The system is simulated as fully confined, with specific storage of 1e-4 m-1. The following parameters are assumed constant across all layers: effective porosity of 0.35; longitudinal dispersivity of 0.1; transversal horizontal and vertical dispersivity 0.01 and 0.001, respectively. The specific geochemical reaction networks explicitly included in the modelling are detailed in Prommer and Stuyfzand (2005).

FOM History Matching and Uncertainty Analysis

History matching was undertaken using the iterative ensemble smoother implemented in PEST++IES (White *et al.*, 2018). An initial ensemble of 201 samples of parameters from the prior probability distribution was generated. Each realization is comprised of randomly sampled, geostatistical correlated, model parameters, each of which reflects the conceptual understanding of the system. Each

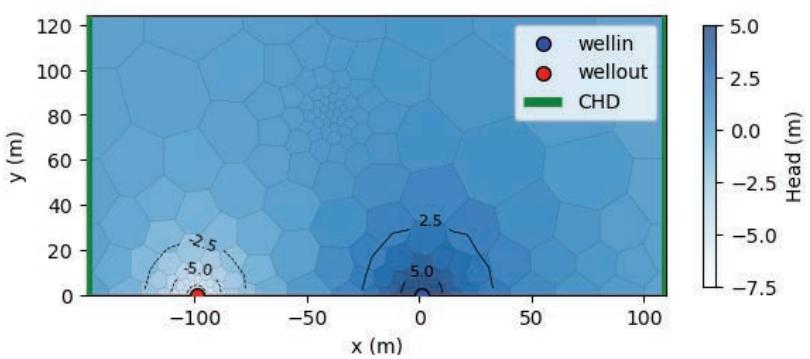

Figure 1 *Model domain, location of well boundary conditions and simulated spatial distribution of hydraulic head in layer 1after 50 days.*

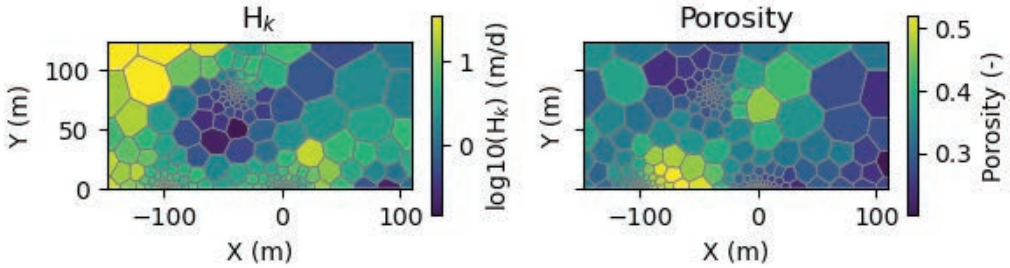

Figure 2 Example of spatial distribution of horizontal hydraulic conductivity (Hk) and porosity in model layer 6 for a single parameter realisation.

model layer has independent, spatially varying hydrogeological and geochemical parameters (e.g., hydraulic conductivity, specific storage, effective porosity), acknowledging horizontal and vertical heterogeneity and uncertainty. An example realisation of parameter spatial heterogeneity is shown in Fig.2.

A single realization was randomly selected as the "truth". Simulated values at observation wells using this parameter set were used as "measured" data during history matching. The realization was set aside and not included in the prior parameter ensemble or subsequent training data for DSI. Selected "measured" data for a few chemical species and physical parameters from the first 300 days of the simulation were used as calibration targets. The models' forecasting ability was evaluated by comparing simulated outputs to measured data during the rest of the study period.

As the synthetic model employed here is relatively fast to run (approximately 6 min), it is feasible to undertake history matching of the full-order model. Note that, in many real-world applications model computation time make this prohibitive. To compare outcomes and computational burden to the emulator-based workflow, we undertake history matching and predictive uncertainty quantification with both.

DSI History Matching and Uncertainty Analysis

A DSI surrogate model was trained on model output simulated using the same 200 parameter realisations from the FOM model prior Monte Carlo simulation. The surrogate algorithm is implemented in the open-source Python package *pyEMU*. Amongst other things, this package automates the configuration, training and set up of PEST++ for emulator-based workflows.

DSI latent parameters, x, were history matched using PEST++IES, with the same target observations obtained by simulating the "truth" model. As the computational cost is minimal (a few seconds), a large ensemble size is used (1000) to promote a more robust evaluation of predictive uncertainty.

Results

The synthetic model represents the introduction of pre-treated surface water into an aquifer, isolating how the injectate temperature and redox conditions (dissolved oxygen and nitrate) drive pyrite oxidation. The predictive variables of interest are the resulting spatial and temporal shifts in pH, iron, sulfate, and temperature. While this setup presents complex reactive transport dynamics, the primary focus of this study remains on evaluating the utility of DSI for data assimilation and uncertainty quantification. To this end, Fig 3 presents time series for selected variables, plotting the synthetic calibration targets against the prior and posterior ensembles generated by the full-order numerical model, as well as the rapidly generated DSI posterior ensemble.

Fig 3 displays time series across three distinct hydrodynamic zones: between the injection and extraction wells (wp1-f3), upgradient of the injection site (wp4-f5), and adjacent to the extraction well (pp1-f3). For all sites, data assimilation with both the full-order model and the DSI surrogate substantially reduces predictive uncertainty for SO4, TIC, and temperature. This variance

reduction is demonstrated by the tightly constrained posterior distributions compared to the wide variance of the prior ensemble.

Three iterations were employed for the full-order model history matching. This required a total of 1171 model runs, with an average run time of 8 min. Notably, approximately 70 model runs failed, likely due to numerical instability or exceeding run-time criteria. The wall-clock time that this process requires is dependent on the number of available CPUs. The 200 full-order model runs from the first iteration are used as training data for the DSI surrogate. These represent the only large compute cost of the DSI workflow. Surrogate-based history matching is accomplished in a few minutes on a high-end laptop.

Conclusions

The application of ensemble-based data assimilation to fully coupled reactive transport models (RTMs) is typically constrained by prohibitive computational costs. This study demonstrates the utility of Data-Space Inversion (DSI) as an efficient surrogate alternative to traditional parameter estimation. Using a three-dimensional synthetic model of aquifer injection and geochemical reaction networks related to pyrite oxidation, we evaluated the capacity of DSI to assimilate observations and generate conditional forecasts without requiring repeated forward model evaluations.

Results indicate that the DSI surrogate accurately reproduces the conditioning

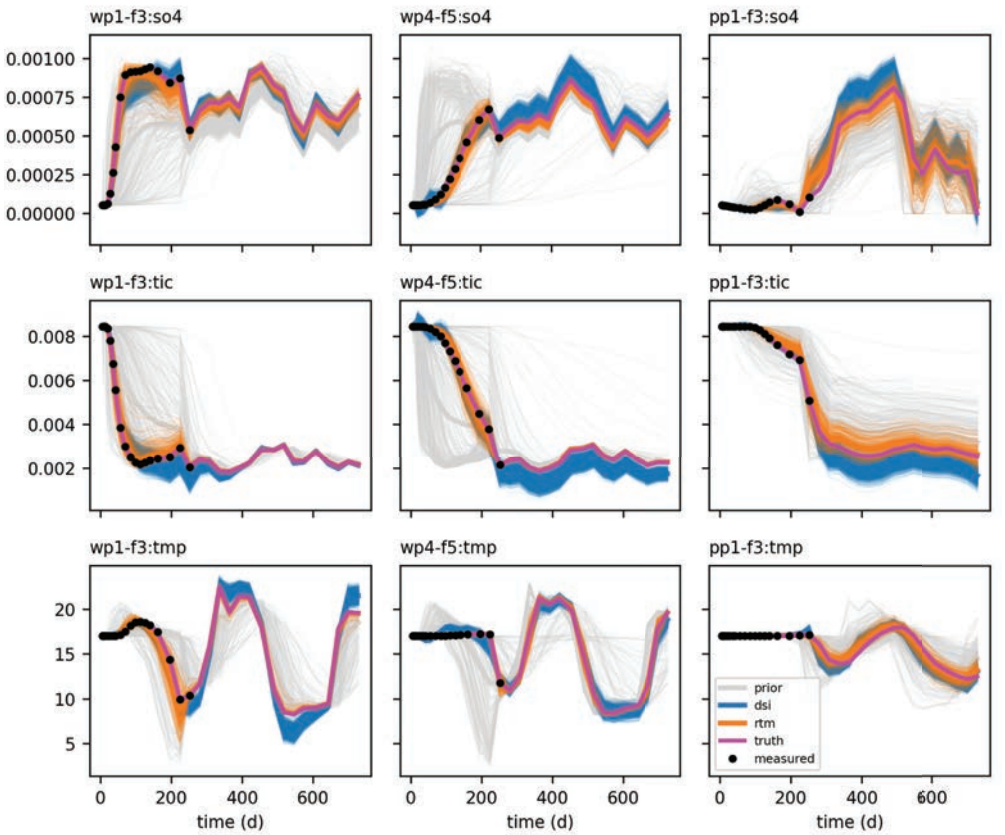

Figure 3 Time series of simulated and observed variables across three monitoring locations (columns) for sulfate (SO_4), total inorganic carbon (TIC), and temperature (rows). Each panel compares the reference synthetic truth and discrete calibration targets against three predictive ensembles: the unconditioned prior from the full reactive transport model (RTM), and the conditioned posteriors from the full RTM and the DSI surrogate.

behavior of the full-order model. Across distinct hydrodynamic zones, DSI successfully assimilated synthetic calibration targets and substantially reduced predictive uncertainty for key geochemical variables, including sulfate, total inorganic carbon, and temperature. By operating entirely in the data space, DSI bypassed the traditional computational bottlenecks associated with high-fidelity RTMs. Ultimately, this approach provides a practical framework for integrating complex geochemical models into routine uncertainty quantification, risk assessment, and decision support workflows for mine water management.

Acknowledgements

The authors thank the co-organisers for hosting the IMWA 2026 Conference. We thank the editors and reviewers for their constructive feedback.

References

Langevin CD, Hughes JD, Provost AM, Russcher MJ, Morway ED, Reno MJ, Bonelli WP, Niswonger RG, Panday S, Titus S, Merrick D, Banta ER (2026) MODFLOW6 Modular Hydrologic Model version 6.7.0: U.S. Geological Survey Software Release, 6 February 2026, DOI:10.5066/P1IJAXDZ

Parkhurst DL, Appelo CAJ, (2013) Description of input and examples for PHREEQC version 3–A computer program for speciation, batch-reaction, one-dimensional transport, and inverse geochemical calculations: U.S. Geological Survey Techniques and Methods, book 6, chap. A43, 497 p.,

Prommer H, Stuyfzand P (2005) Identification of Temperature-Dependent Water Quality Changes during a Deep Well Injection Experiment in a Pyritic Aquifer. Environmental science & technology. 39. 2200-9. doi:10.1021/es0486768.

Sun W, Durlofsky L (2017) A new data-space inversion procedure for efficient uncertainty quantification in subsurface flow problems. Mathematical Geosciences, 49, 679–715. doi:10.1007/s11004-016-9672-8. URL doi:10.1007/s11004-016-9672-8

White JT (2018) A model-independent iterative ensemble smoother for efficient history-matching and uncertainty quantification in very high dimensions. Environmental Modelling and Software, 109, 191–201. doi:10.1016/j.envsoft.2018.06.009.

Integrated Modeling Innovations for Mining and Underground Infrastructure: Dynamic Mesh Adaptation and Tunnel Boundary Conditions for Surface–Groundwater Systems

Hyoun-Tae Hwang[1,2], Young-Jin Park[2], Steven Berg[1,2], Jon Jones[2,3], Killian Miller[1], Edward Sudicky[1,2]

[1]*Aquanty Inc., Waterloo, Ontario, Canada;*

[2]*Department of Earth and Environmental Sciences, University of Waterloo, Waterloo, Ontario, Canada;*

[3]*Suncor Energy Inc., Calgary, Alberta, Canada*

Abstract

Mining and underground engineering alter coupled surface–groundwater systems, yet their representation remains limited by static meshes and simplified boundary conditions. This study presents an integrated modeling framework within HydroGeoSphere that enables continuous simulation of evolving excavation geometry without model reinitialization and improves tunnel inflow estimation under coarse regional discretization. The dynamic mesh enables continuous simulation of evolving topography during excavation and reclamation, while the boundary formulation improves inflow estimation for underground openings under coarse discretization. Verification and synthetic mining applications demonstrate that the proposed framework reduces discretization-induced inflow errors and improves representation of transient groundwater responses during excavation and reclamation. These developments enhance reliability in mine water management and support safer design of underground infrastructure.

Keywords: Integrated modeling, dynamic mesh, tunnel boundary condition, groundwater seepage, groundwater–surface water interaction

Introduction

Mining and underground construction activities substantially modify hydrologic systems by altering both land surface geometry and subsurface flow pathways. Excavation, tunnelling, and material placement processes introduce significant disturbances to the natural balance between groundwater and surface water systems. These disturbances can lead to changes in groundwater levels, redistribution of surface water, and modification of exchange fluxes between surface and subsurface domains. Such hydrologic alterations are closely linked to environmental protection, water resource sustainability, and the structural safety of engineering systems, particularly in regions where mining operations or underground infrastructure development are extensive.

Accurate prediction of these coupled processes remains challenging due to the complexity of the physical system and the limitations of conventional numerical modeling approaches. Most existing models rely on fixed spatial discretization, where the computational mesh remains unchanged throughout the simulation. While this assumption is reasonable for natural systems with relatively stable geometry, it becomes inadequate in engineering environments where topography evolves continuously due to excavation, backfilling, and landform modification. As a result, traditional approaches often require multiple sequential simulations with updated geometries, which can introduce inconsistencies in mass balance and reduce computational efficiency.

In addition to limitations in representing evolving landscapes, conventional models often simplify the representation of underground openings such as tunnels, shafts, and repositories. These features are typically approximated using coarse discretization or idealized boundary conditions, such as fixed pressure boundaries. However, such simplifications can lead to significant errors in estimating groundwater inflow, particularly when the scale of underground structures is much smaller than that of the regional model domain. This scale mismatch is a critical issue in applications such as mine dewatering, tunnel design, and safety assessment of subsurface infrastructure.

To address these challenges, this study integrates two methodological advancements within a unified modeling framework. First, a dynamic mesh adaptation scheme is introduced to represent time-dependent changes in surface and subsurface geometry, enabling continuous simulation of evolving topography without the need for model reinitialization. Second, an improved tunnel boundary condition is implemented to more accurately represent groundwater inflow into underground openings by accounting for the relationship between tunnel wall pressure and simulated nodal pressure.

These developments are incorporated into HydroGeoSphere (HGS), a fully coupled surface–subsurface modeling framework, allowing for consistent representation of hydrologic processes across spatial and temporal scales. The proposed approach is evaluated through applications relevant to mining and underground engineering, demonstrating its capability to improve predictive accuracy and provide more reliable support for water management and infrastructure design.

Methods

Integrated surface–subsurface modeling framework

This study employs HGS (Aquanty Inc., 2023) to simulate water flow dynamics under mining and underground engineering conditions. The model solves variably saturated groundwater flow and depth-integrated surface flow simultaneously, allowing for dynamic interaction between surface water and subsurface systems through exchange fluxes at the interface.

The governing equations are based on mass conservation principles and incorporate key physical processes, including hydraulic conductivity, pressure head, water saturation, and storage effects. The coupling between domains enables consistent simulation of water redistribution across different hydrologic compartments, which is essential for representing complex responses induced by excavation and subsurface infrastructure.

In the *HGS* model, areal overland flow is represented by a two-dimensional depth-integrated flow equation which is the diffusion-wave approximation of the Saint Venant equation for surface water flow:

$$\nabla \cdot d_o K_o \cdot \nabla h_o \pm Q_o + \Gamma_o = \frac{\partial h_o}{\partial t} \quad (1)$$

where d_o is the depth of flow, h_o is the water surface elevation ($= d_0 + z$), and K_o is the surface conductances that are changed with the friction slopes of the surface and is approximated by the Manning's equation in x- and y- directions. The modified form of Richards' equation describing three-dimensional transient subsurface flow under variably-saturated conditions is given by:

$$\nabla \cdot k_r \boldsymbol{K} \cdot \nabla h \pm Q + \Gamma = \frac{\partial}{\partial t}(\theta_s S_w) \quad (2)$$

where k_r is the relative permeability of the medium as a function of the water saturation S_w or the pressure head ψ, K is the hydraulic conductivity tensor, h is the total head as $\psi + z$ where z is the elevation, θ_s is the saturated water content, Q is an externally applied source or sink of water. The fluid exchange between the surface and subsurface is represented by Γ. For the exchange fluxes, separate surface and subsurface flow models can be combined by explicitly coupling the variably-saturated flow and the surface flow equations. In *HGS*, it is assumed that the two domains are separated by a thin boundary layer. Thus, Γ_o in the governing flow equation represents a first-order exchange between subsurface and surface domains as follows:

$$\Gamma_o = (k_r)_{exch} K_{exch} (h - h_o)/l_{exch} \quad (3)$$

$$\int_V \Gamma dV = -\int_{A_{\text{interf}}} \Gamma_0 dA_{\text{interf}} \quad (4)$$

where $(k_r)_{exch}$ is the relative permeability for fluid exchange, K_{exch} is the surface/subsurface conductance, and l_{exch} is the thickness of the interface layer between surface and subsurface domains. In the coupling equation, a positive Γ_0 indicates movement from the subsurface to the surface domain through the interface (A_{interf}). Note that the *HGS* model is referred to as a fully-integrated globally-implicit model, opposed to linked or iteratively coupled simulators because the governing equations are solved simultaneously with the above coupling equation.

Dynamic mesh adaptation for evolving topography

To represent time-dependent changes in land surface and subsurface geometry, a dynamic mesh adaptation scheme is implemented within the modeling framework (Hwang *et al.*, 2025). Unlike conventional approaches that rely on fixed meshes, this method updates nodal elevations and element structures during simulation to reflect excavation and material placement processes (Figure 1).

During excavation, surface nodes and corresponding subsurface layers are adjusted to represent reductions in elevation and modifications in geological structure. To maintain numerical stability, minimum element thickness is preserved to avoid degeneracy in the mesh. During material placement, additional layers or adjusted nodal positions are used to represent backfilling and restoration processes.

This approach enables continuous simulation of evolving landscapes without the need for restarting the model between different stages of engineering operations. As a result, temporal continuity is preserved, and inconsistencies associated with sequential simulations are avoided. The method is particularly suitable for representing open-pit mining, land reclamation, and other engineered landscape transformations.

Tunnel boundary condition for groundwater inflow

Groundwater inflow into underground openings is represented using an advanced head-dependent boundary condition. Conventional approaches often apply fixed pressure (Dirichlet) boundary conditions along tunnel nodes, which can lead to overestimation of inflow when tunnels are represented in coarse regional models (Figure 2).

To improve accuracy, a Cauchy-type boundary condition is introduced, which relates the tunnel wall pressure to the simulated nodal pressure through a physically based formulation derived from radial flow theory. This approach accounts for the difference between the actual tunnel wall pressure and the numerically computed pressure at model nodes, thereby reducing discretization-induced errors (Park *et al.*, 2020).

The formulation can be extended to incorporate additional engineering features, including excavation damaged zones (EDZ) and grouted zones (GZ), by modifying effective hydraulic properties around the tunnel. This allows for more realistic representation of tunnel–groundwater interactions under varying hydrogeological conditions.

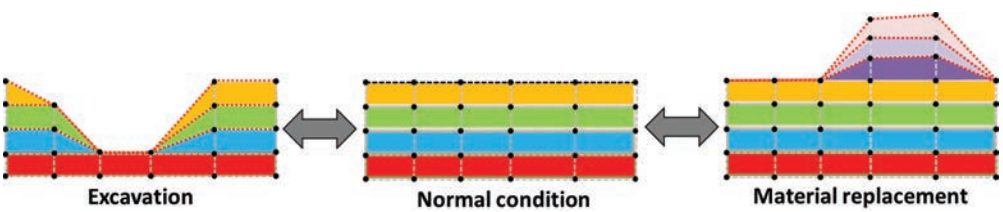

Figure 1 *Conceptual illustration of dynamic mesh adaptation for evolving topography: excavation (left), initial condition (center), and material placement (right).*

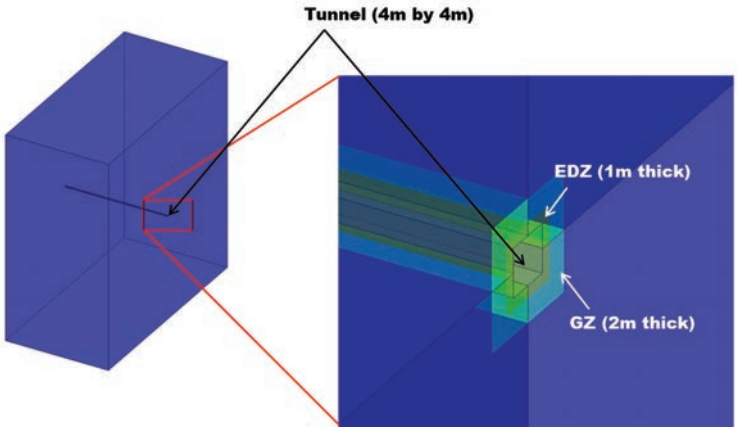

Figure 2 Conceptual representation of a tunnel with excavation damaged zone (EDZ) and grouted zone (GZ) (adapted from Park et al.*, 2020).*

Results

Hydrologic response to mining-induced landscape evolution

The integrated modeling framework was applied to synthetic mining scenarios involving excavation and material placement processes over a multi-year period. The results show that excavation induces substantial hydrologic disturbances, including increased surface water accumulation within mining areas and significant groundwater drawdown near excavation zones (Figure 3).

During excavation, surface water tends to accumulate due to localized depressions in topography, while groundwater levels decline as a result of enhanced drainage toward the excavation site. Following the material placement phase, surface water conditions recover relatively quickly; however, the groundwater system exhibits delayed recovery, reflecting the cumulative effects of hydrologic disturbance.

Sensitivity analysis of excavation and backfilling schedules indicates that shorter excavation periods produce more

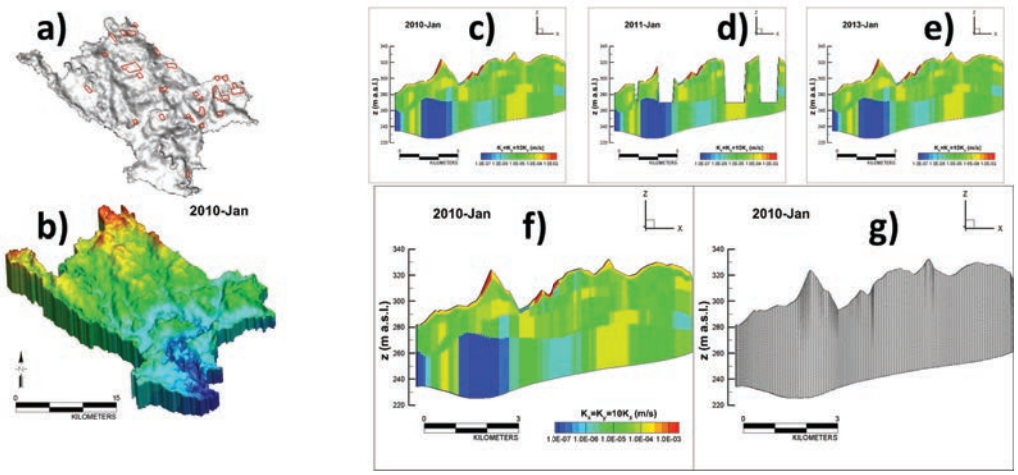

Figure 3 Model domain (a–b) and cross-sectional views showing the spatial distribution of topography and hydraulic conductivity. Temporal snapshots illustrate the evolution of the system at selected simulation times (2010–2013) (c–g).

pronounced transient responses, whereas longer material placement durations lead to more gradual recovery of groundwater levels. These results highlight the importance of operational timing in controlling hydrologic impacts in mining environments.

Evaluation of tunnel boundary condition

The improved tunnel boundary condition was evaluated by comparing simulated groundwater inflow with analytical and high-resolution numerical solutions. The results indicate that conventional fixed-head boundary conditions tend to overestimate inflow, particularly when tunnels are represented within coarse discretization (Figure 4).

Additional simulations incorporating excavation damaged zones and grouted zones demonstrate that the formulation can effectively represent engineering controls on groundwater inflow. The inclusion of these features allows for realistic evaluation of inflow reduction strategies and tunnel–groundwater interactions.

Conclusions

This study presents an integrated modeling framework that combines dynamic mesh adaptation and an advanced tunnel boundary condition to improve the simulation of hydrologic processes in mining and underground engineering environments. The results demonstrate that both methodological developments address key limitations of conventional numerical models related to static geometry representation and simplified boundary conditions.

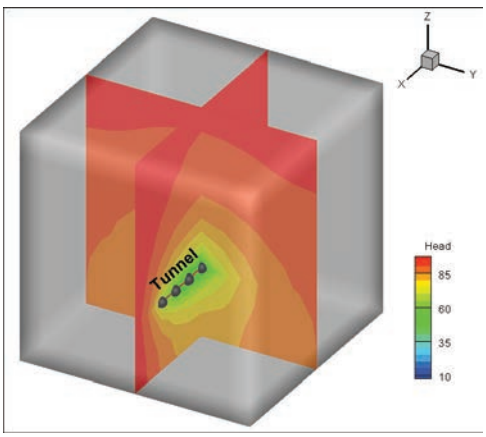

Figure 4 *Simulated groundwater head distribution around a tunnel, illustrating drawdown and flow convergence toward the tunnel.*

The dynamic mesh adaptation scheme enables continuous representation of evolving topography associated with excavation and material placement processes. By updating nodal elevations and mesh structures during simulation, the approach eliminates the need for sequential model restarts and ensures consistency in mass balance. Model verification under both surface flow and groundwater flow conditions confirms that the method accurately captures transient hydrologic responses to time-varying terrain. Applications to mining scenarios show that excavation can induce localized surface water accumulation and groundwater drawdown, while post-reclamation recovery of the groundwater system may be delayed relative to surface conditions.

The improved tunnel boundary condition enhances the accuracy of groundwater inflow estimation into underground openings, particularly in regional-scale models with coarse discretization. By incorporating a physically based relationship between tunnel wall pressure and nodal pressure, the formulation reduces errors associated with conventional fixed-head boundary conditions. The approach is also flexible in representing additional engineering features such as excavation damaged zones and grouted zones, enabling more realistic assessment of tunnel–groundwater interactions.

When combined within a fully coupled surface–subsurface modeling framework, these two advancements provide a robust and scalable approach for simulating complex hydrologic systems influenced by mining and underground infrastructure. The integrated methodology improves predictive capability for key processes such as groundwater drawdown, surface water redistribution, and tunnel inflow, which are critical for mine water management, infrastructure safety, and environmental protection.

Overall, this work demonstrates that incorporating dynamic system evolution and physically consistent boundary conditions is essential for advancing next-generation hydrologic modeling. Future research should focus on extending the framework to include coupled hydro-mechanical processes, land-use dynamics, and climate-driven variability to further enhance its applicability to real-world engineering and water resource management challenges.

Acknowledgements

This work was partially supported through collaborative research efforts with industry partners, including Suncor Energy Inc., whose contributions to project development and technical discussions are sincerely appreciated.

References

Aquanty Inc. (2023) HydroGeoSphere. A three-dimensional numerical model describing fully-integrated subsurface and surface flow and solute transport, Waterloo, ON, Canada.

Hwang, H.-T., Y.-J. Park, S. J. Berg, J. P. Jones, K. L. Miller, E. A. Sudicky (2025) A dynamic meshing scheme for integrated hydrologic modeling to represent evolving landscapes, Sci Total Environ, 976, 179129.

Park, Y. J., H. T. Hwang, S. Suzuki, H. Saegusa, K. Nojiri, T. Tanaka, P. Bruines, K. Abumi, Y. Morita, W. A. Illman (2020) Improving precision in regional scale numerical simulations of groundwater flow into underground openings, Engineering Geology, 274, 105727.

Assessing Removal Efficiencies of Mn and Ni in Mine Drainage Using a Bench-scale Slag Reactor

Dae-Gyu Im[1], Duk-Min Kim[2], Hye-Lim Kwon[3], Joon-Hak Lee[4], Seong-Taek Yun[5]

[1]*Department of Earth and Environmental Sciences, Korea University, Anam-ro 145, Seongbuk-gu, Seoul, 02841, Republic of Korea, daegull1995@korea.ac.kr, ORCID 0000-0002-7499-8403*

[2]*Department of Civil and Environmental Engineering, Sangji University, Sangjidae-gil 83, Wonju, Gangwon-do, 26339, Republic of Korea, kdukmin8@sangji.ac.kr, ORCID 0000-0002-1537-6866*

[3]*Department of Earth Resources and Environmental Engineering, Hanyang University, 222 Wangsimni-ro, Seoul 04763, Republic of Korea, ossgpfla@hanyang.ac.kr*

[4]*Korea Mine Rehabilitation and Mineral Resources Corporation, Hyeoksin-ro 199, Wonju, Gangwon-do, 26464, Republic of Korea, jun292@komir.or.kr*

[5]*Department of Earth and Environmental Sciences, Korea University, Anam-ro 145, Seongbuk-gu, Seoul, 02841, Republic of Korea, styun@korea.ac.kr*

Abstract

Mine drainage containing Mn and Ni was treated using a bench-scale slag reactor packed with steelmaking slag and limestone. The reactor was operated for 456 days across seven stages under alternating acidic and neutral inflow conditions. Under neutral conditions with residence times exceeding 3 h, removal efficiencies of both Mn and Ni exceeded 90%. PHREEQC geochemical modeling indicated that the effluent was saturated with respect to Mn (hydr)oxide minerals, while $Ni(OH)_2$ remained unsaturated. SEM–EDS analysis of precipitates revealed flower-like Mn (hydr)oxide aggregates containing Ni (9.5 at.%), providing direct evidence of Ni removal via Mn (hydr)oxide-mediated adsorption rather than direct precipitation.

Keywords: Coal mining, irrigation, green hydrogen, coal-fired power, water reuse

Introduction

Manganese (Mn) and nickel (Ni) are persistent contaminants in coal mine drainage and remain among the most challenging metals to remove by passive treatment. Conventional Mn removal requires chemical oxidation at pH > 9 using $Ca(OH)_2$ or NaOH, entailing substantial operational costs and CO_2 emissions from lime production. Ni removal is similarly difficult because direct precipitation of $Ni(OH)_2$ requires pH values above approximately 8.5–9.0, conditions that are difficult to maintain in passive systems.

Steelmaking slag has been investigated as a reactive medium for passive mine drainage treatment owing to its high alkalinity-generating capacity. In a preceding pilot-scale study, Im *et al.* (2026) assessed three slag reactor configurations (baffle-type, weir-type, vertical flow-type) using steelmaking slag mixed with limestone (4:6 v/v) for Mn removal from coal mine drainage over 316 days. All reactors reduced Mn below the South Korean effluent standard (2 mg L^{-1}) within residence times of approximately 1–2 h; XPS and SEM–EDS analysis confirmed that accumulated precipitates were predominantly Mn(III,IV) (hydr)oxides structurally similar to birnessite; and the progressive improvement in removal efficiency was attributed to autocatalytic oxidation by accumulated Mn (hydr)oxides. However, that study focused exclusively on Mn and did not investigate the co-removal of other dissolved metals.

Birnessite (δ-MnO_2) has a low point of zero charge (PZC ≈ 2.0–2.5) and carries a strong negative surface charge under circum-neutral to alkaline conditions, rendering it an effective sorbent for divalent cations such as Ni^{2+}. If birnessite forms as a secondary precipitate within slag reactors during Mn removal, it may simultaneously enable

Ni removal through surface adsorption, achieving coupled multi-metal treatment in a single process.

The objectives of the present study were to: (1) evaluate the long-term Mn and Ni removal performance of a bench-scale slag reactor over 456 days under alternating acidic and neutral inflow conditions; (2) identify the dominant Ni removal mechanism through PHREEQC geochemical modeling and SEM–EDS characterization; and (3) assess whether the Mn (hydr)oxide precipitates also function as sorbents for dissolved Ni.

Materials and Methods

The reactive media consisted of steelmaking slag (a by-product of iron and steel production with high alkalinity-generating capacity, particle diameter 2–5 mm) and limestone (3–5 cm), mixed at a volumetric ratio of 4:6. The slag was composed of Fe oxides (40.9%), CaO (36.5%), SiO_2 (9.59%), MnO (4.07%), MgO (3.51%), P_2O_5 (1.52%), and TiO_2 (0.89%) based on XRF analysis. The media composition, mixing ratio, and analytical methods followed those described in Im *et al.* (2026). Both materials were washed with distilled water before use.

The bench-scale slag reactor was used to treat mine drainage from the Taewoo coal mine in Cheongju, South Korea, for 456 days. The reactor used a downflow configuration with a porosity of 38%. Mn and Ni sulfate reagents were added to modify the mine drainage composition. Inflow Mn concentrations ranged from 0.4 to 7.7 mg L^{-1} and Ni from 1.4 to 5.8 mg L^{-1} (excluding the initial stabilization stage). Inflow pH was artificially modified through laboratory acidification of the field-collected mine drainage to simulate the seasonal acidity fluctuations commonly observed in coal mine drainages. Operational stages were defined primarily based on changes in inflow pH, while residence time was intentionally adjusted within each stage to evaluate its influence on Mn and Ni removal efficiency. A total of 74 effluent samples were collected across seven operational stages (Table 1).

Effluent temperature, pH, and oxidation–reduction potential (ORP) were measured on-site. Alkalinity was determined by titration with 0.02 N H_2SO_4. Dissolved Ca, Mn, and Ni concentrations were measured by ICP-AES after filtration (0.45 μm) and acidification. Cl^- and SO_4^{2-} were determined by ion chromatography.

Saturation indices (SI) for 11 mineral phases were calculated using PHREEQC version 3.8.6 with the wateq4f.dat thermodynamic database. This database was selected because it includes thermodynamic data for Mn(III,IV) (hydr)oxide and Ni mineral phases.

Upon completion of the 456-day operation, precipitate samples were collected from the reactive media surface. SEM–EDS analysis was performed at an accelerating voltage of 15 kV to characterize the morphology and elemental composition of precipitates.

Results and Discussion

Figure 1 shows the temporal variation of effluent Mn and Ni concentrations along with residence time over the 456-day operation. In the initial stabilization stage (days 1–35), the

Table 1 Summary of operational stages for the bench-scale slag reactor. DW = deionized water.

Stage	Designation	Period (days)	Inflow condition	n	RT range (h)
1	Initial stabilization	1–35	Neutral	3	0.10–0.32
2	Acidic-1st	36–58	Acidic (pH 4.5–7.8)	4	0.33–4.10
3	Neutral-1st-1	72–112	Neutral (pH 6.9–7.8)	6	2.90–5.80
4	Neutral-1st-2	120–191	Neutral (pH 7.1–7.6)	6	1.10–5.30
5	Acidic-2nd	203–239	Acidic (pH 4.0–8.1)	8	4.40–30.0
6	Neutral-2nd-1	255–363	Neutral (DW spiking)	34	0.28–17.5
7	Neutral-2nd-2	366–456	Neutral (mine drainage)	13	1.46–7.39

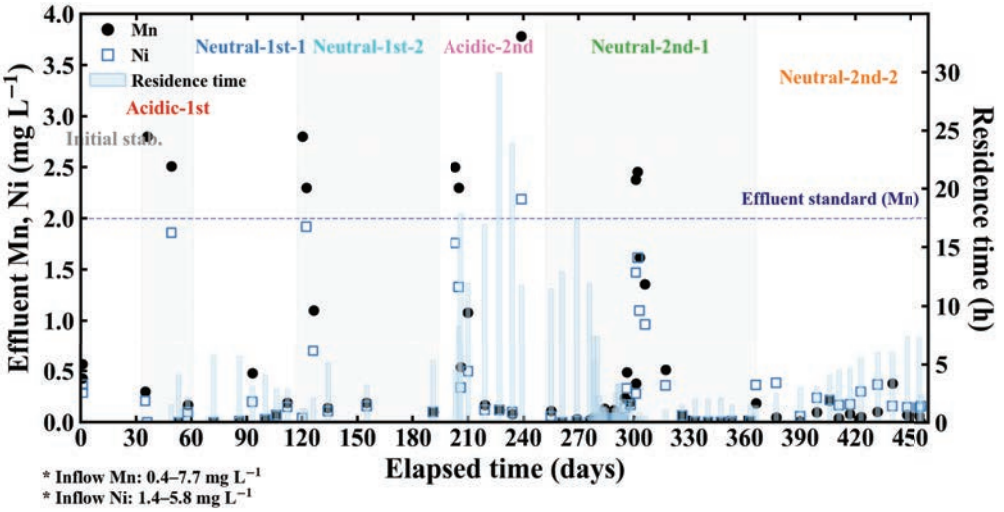

Figure 1 Temporal variation of effluent Mn and Ni concentrations with residence time across seven operational stages. Dashed line indicates the effluent standard for Mn (2 mg L^{-1}).

effluent pH remained around 9, consistent with active dissolution of CaO from the slag, resulting in effluent Mn of 0.30–0.57 mg L^{-1} and Ni of 0.21–0.37 mg L^{-1}.

During the Acidic-1st stage, Mn concentration was reduced to <2 mg L^{-1} only at residence times exceeding approximately 2 h, whereas under neutral conditions (Neutral-1st-1), effluent Mn decreased to 0–0.48 mg L^{-1} at residence times of 2.9–5.8 h, comparable to the 1–2 h reported for the pilot-scale reactors (Im *et al.* 2026).

A notable finding not addressed in previous work is the Ni removal behavior. The Acidic-2nd stage demonstrated that Ni removal from inflow concentrations of 3.7–4.5 mg L^{-1} required residence times of >20 h under acidic conditions. Effective Ni removal was observed at effluent pH values as low as ≈7, well below the theoretical pH required for $Ni(OH)_2$ precipitation (≈8.5–9.0), suggesting an adsorption-dominated mechanism rather than direct hydroxide precipitation.

In the later neutral stages (Neutral-2nd-1), the reactor achieved effluent Mn concentrations below 0.2 mg L^{-1} and Ni concentrations of 0.06 mg L^{-1} or below at residence times exceeding 2 h. The progressive improvement in removal efficiency over time is consistent with the autocatalytic effect of accumulated Mn(III,IV) (hydr)oxide precipitates enhancing subsequent metal removal.

Across the neutral-inflow stages, removal efficiency exhibited a sharp threshold around a residence time of 1 h: below this value, median Mn removal was 71% (n = 7), whereas at residence times ≥ 1 h removal plateaued at 98–99% across all longer intervals up to 17.5 h (n = 51). Effluent pH was moderately correlated with both Mn (r = 0.42) and Ni (r = 0.37) removal in the neutral stages. Notably, across all 73 samples, the inflow Mn:Ni molar ratio was strongly anti-correlated with Ni removal efficiency (r = −0.68), consistent with a coupled removal mechanism in which Mn (hydr)oxide accumulation provides sorption sites for Ni^{2+}; when the Mn supply is limited relative to Ni, the Ni removal efficiency declines accordingly.

PHREEQC geochemical modeling revealed that the effluent was frequently saturated (SI > 0) with respect to manganite (MnOOH) under neutral conditions (Figure 2), particularly in the Neutral-1st-1 stage. Calcite and rhodochrosite ($MnCO_3$) also showed SI values near or above zero, suggesting the possibility of concurrent carbonate precipitation.

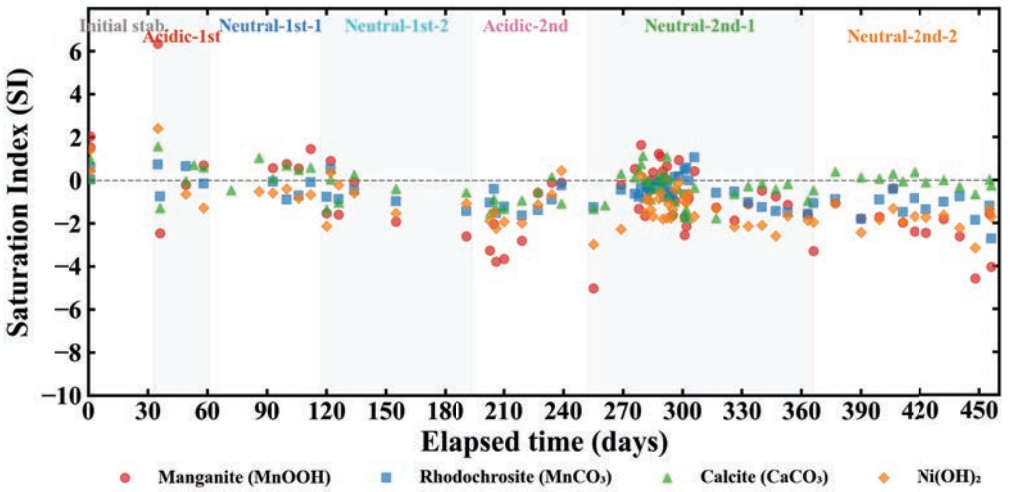

Figure 2 Saturation indices of key Mn and Ni minerals versus elapsed time. Dashed line at SI = 0 indicates equilibrium.

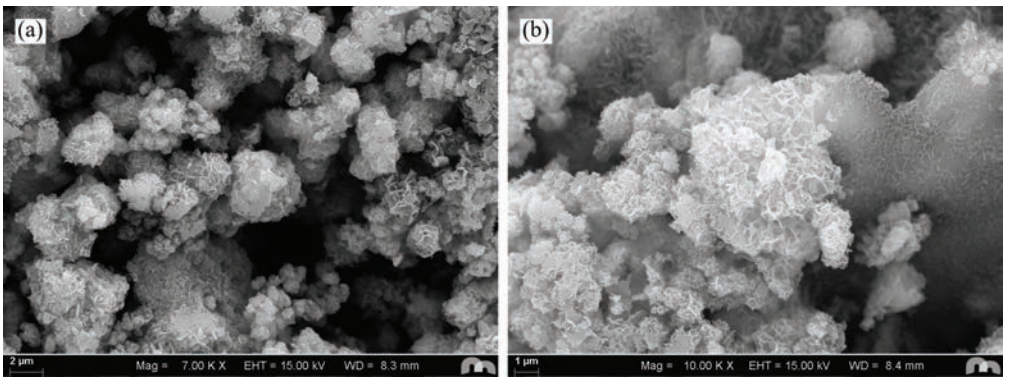

Figure 3 SEM images of precipitates: (a) fine spherical particle aggregates (×7,000); (b) flower-like crystal structures of Mn(III,IV) (hydr)oxides (×10,000).

In contrast, the SI for $Ni(OH)_2$ remained predominantly negative (SI < 0) throughout the experiment, and $NiCO_3$ was unsaturated in most samples. These results indicate that Ni removal cannot be attributed to direct precipitation of Ni hydroxide or carbonate minerals, and an alternative removal pathway, most likely adsorption onto Mn (hydr)oxide surfaces, is suggested.

A notable observation arose during the Neutral-2nd-2 stage (days 366–456), when the median saturation indices of all Mn and Ni mineral phases were negative (manganite −1.96, rhodochrosite −1.05, birnessite −5.60, $Ni(OH)_2$ −1.74) while calcite remained near saturation (SI ≈ 0). Despite this thermodynamic undersaturation, the median effluent Mn and Ni concentrations remained low (0.07 and 0.17 mg L^{-1}, corresponding to ≈98% and 95% removal). This suggests that, by the later operational stages, removal was sustained primarily through adsorption onto the Mn (hydr)oxide surfaces that had progressively accumulated during preceding stages, rather than through new bulk precipitation. The low effluent pH (median 7.5) and reduced alkalinity (mean 0.60 meq L^{-1}) in this stage were thermodynamically unfavorable for further Mn oxide precipitation; however, the low point of zero charge of pre-formed

birnessite (PZC ≈ 2.0–2.5) preserved the surface reactivity required for continued Mn^{2+} and Ni^{2+} uptake at circumneutral pH.

SEM imaging of the black precipitates revealed fine spherical particle aggregates with flower-like crystal structures (Figure 3). This morphology was characteristic of Mn(III,IV) (hydr)oxides, consistent with manganite saturation indicated by PHREEQC modeling.

EDS analysis (Table 2) confirmed that the precipitates were dominated by O (53.1 at.%) and Mn (16.3 at.%). Notably, Ni (9.5 at.%) was detected within the Mn (hydr) oxide precipitates, despite $Ni(OH)_2$ being unsaturated in the effluent. This provides direct evidence that Ni accumulated on the Mn (hydr)oxide surfaces through adsorption rather than direct precipitation. While the pilot-scale study did not assess Ni co-removal because only Mn was present in the influent, the present study extends those findings by demonstrating that Mn (hydr) oxide precipitates formed in slag reactors also function as effective sorbents for dissolved Ni.

Based on the combined evidence, the following removal mechanism is proposed. Slag dissolution raises effluent pH, promoting Mn(II) oxidation and precipitation as Mn(III,IV) (hydr)oxide phases, primarily manganite (MnOOH). The accumulated Mn (hydr)oxide precipitates then serve as autocatalytic surfaces that accelerate subsequent Mn(II) oxidation and simultaneously provide adsorption sites for dissolved Ni^{2+}, likely through surface complexation. This coupled mechanism, whereby Mn autocatalytic oxidation is followed by Ni adsorption onto Mn (hydr) oxide surfaces, explains both the progressive improvement in removal efficiency and the effective Ni removal despite $Ni(OH)_2$ remaining thermodynamically unsaturated.

Compared with other passive treatment systems for Mn-contaminated mine drainage, the slag reactor evaluated here achieved Mn removal at residence times (1–2 h) considerably shorter than those typically required for slag leach beds (SLBs) or successive alkalinity-producing systems (SAPS), in which performance is constrained by stream flow variability or limited oxidizing conditions (Im *et al.* 2026). The dual functionality demonstrated here, namely concurrent Mn oxidation and Ni adsorption onto in-situ-formed birnessite-type Mn (hydr)oxides, distinguishes the present slag reactor from earlier slag reactors that targeted Mn removal only via autocatalytic oxidation (Im *et al.* 2026) and from biological systems that rely on sulfate reduction for Ni removal. Achieving multi-metal removal without chemical reagents in a single passive unit positions the slag reactor as a competitive option among existing passive technologies, particularly for coal mine drainages containing both Mn and Ni.

Table 1 *EDS elemental analysis of Mn (hydr)oxide precipitates from the slag reactor (15 kV, × 6,190). Only selected elements are listed.*

Element	Atom %
O	53.06
Mn	16.26
Ni	9.52
C	7.55
Si	3.33
Mg	1.26
Al	0.67
S	0.31

Conclusions

This study demonstrated that a bench-scale slag reactor effectively removed both Mn and Ni from mine drainage over 456 days of continuous operation. Under neutral conditions with residence times exceeding 3 h, removal of both Mn and Ni exceeded 90%. PHREEQC modeling confirmed that the effluent was saturated with respect to manganite while $Ni(OH)_2$ remained unsaturated, and SEM–EDS analysis revealed the presence of Ni (9.5 at.%) within birnessite-type Mn (hydr)oxide precipitates. These results demonstrate that the Mn (hydr) oxides formed in slag reactors contribute not only to autocatalytic Mn oxidation but also serve as effective sorbents for dissolved Ni, enabling coupled multi-metal treatment in a single passive process.

Acknowledgements

This study was partly supported by the R&D projects of the Korea Mine Rehabilitation and Mineral Resources Corporation (KOMIR), South Korea (2020–2021; 2022–2026).

References

Im DG, Kim DM, Kwon HL, Lee JH, Kwon OH, Yun ST (2026) Pilot-scale assessment of slag reactors for manganese removal from mine drainage. Environ Geochem Health 48:173. https://doi.org/10.1007/s10653-026-03079-x

Field Demonstration of Solar-Powered Iron Electrocoagulation for Arsenic-Contaminated Mine Drainage at the Geumjeong Abandoned Mine, Korea

Sangwoo Ji[1]*, Seungil Pak[2], Chamteut Oh[3], Gil-Jae Yim[4]

[1]*Geo-Environment Research Division, Korea Institute of Geoscience and Mineral Resources, Daejeon, Republic of Korea, swji@kigam.re.kr, ORCID 0000-0003-0071-2713*

[2]*Elsetech Environment Inc., Daegu, Republic of Korea, else@elsetech.co.kr, ORCID 0009-0001-4195-6127*

[3]*Department of Environmental Engineering Sciences, University of Florida, Gainesville, USA, Chamteut.Oh@essie.ufl.edu, ORCID 0000-0002-1239-6482*

[4]*Geo-Environment Research Division, Korea Institute of Geoscience and Mineral Resources, Daejeon, Republic of Korea, gjyimi@kigam.re.kr, ORCID 0000-0002-9052-6123*

Abstract

Arsenic-rich drainage from the Geumjeong Gold Mine in Gyeongsangbuk-do, South Korea, contains 300–500 µg/L of arsenic, exceeding drinking-water standards by up to 50 times. A solar-powered iron electrocoagulation (Fe–EC) system was installed to evaluate field performance under real mine-water conditions. The modular unit, consisting of dual EC reactors and an expanded polystyrene (EPS) filtration stage, treated 8 m^3/day at 4.6 A and 2.3 V. Arsenic concentrations decreased below 10 µg/L within 20 minutes and stabilized at <5 µg/L after one hour, achieving >99% removal. Power consumption remained below 100 W, confirming suitability for decentralized, off-grid mine-water treatment applications.

Keywords: Arsenic, solar-power, electrocoagulation, mine drainage

Introduction

Arsenic (As) is a naturally occurring metalloid widely distributed in geological environments and groundwater systems (Ahn *et al.* 2007; Smedley and Kinniburgh 2002). Long-term exposure to arsenic is associated with severe health effects, leading the World Health Organization (WHO) to establish a drinking-water guideline of 10 µg/L (WHO 2004; Smith *et al.* 2002). In groundwater and mine drainage, arsenic mobility is strongly controlled by redox and pH conditions. Under reducing environments, As(III) predominates as neutral H_3AsO_3 and exhibits high mobility and low adsorption affinity. Under oxidizing conditions, As(V) forms negatively charged oxyanions ($H_2AsO_4^-$, $HAsO_4^{2-}$) that are more readily adsorbed onto iron hydroxides.

Conventional arsenic removal methods—including chemical coagulation, adsorption, ion exchange, and membrane filtration—often require chemical reagents, skilled operation, and stable power supply. Because As(III) is more difficult to remove than As(V), pre-oxidation is frequently necessary. Electrocoagulation (EC) generates iron hydroxides in situ via anodic dissolution and can simultaneously promote partial oxidation of As(III), reducing the need for chemical addition (Ji *et al.* 2011; Wan *et al.* 2011). EC systems are compact, relatively simple, and produce lower sludge volumes compared with conventional processes.

Despite promising laboratory results, field-scale validation of EC under real mine-water conditions remains limited. The Geumjeong Gold Mine in Bonghwa-gun, South Korea, discharges arsenic-rich drainage exceeding regulatory standards. This study evaluates the performance, energy efficiency, and practical applicability of a solar-powered iron electrocoagulation system for treating arsenic-contaminated mine drainage under field conditions.

Electrocoagulation Mechanism

Electrocoagulation (EC) is an electrochemical treatment process in which sacrificial metal electrodes, typically iron or aluminum, dissolve under an applied electric current to generate coagulant species in situ. In iron-based systems, anodic dissolution releases ferrous and ferric ions, which subsequently hydrolyze to form amorphous iron hydroxides with high surface area and strong adsorption capacity (Mollah *et al.* 2001; Emamjomeh and Sivakumar 2009).

At the anode, iron oxidation occurs according to:

$$Fe \rightarrow Fe^{2+} + 2e^-$$

Ferrous ions may further oxidize to Fe^{3+} in the presence of dissolved oxygen. These ions hydrolyze to produce $Fe(OH)_2$ and $Fe(OH)_3$ precipitates, forming reactive flocs capable of adsorbing and co-precipitating dissolved contaminants. In arsenic-containing waters, arsenate species (As(V)) are effectively adsorbed onto iron hydroxides through surface complexation reactions, while arsenite (As(III)) may be partially oxidized during the electrochemical process, enhancing removal efficiency (Kumar *et al.* 2004).

At the cathode, hydrogen evolution occurs:

$$2H_2O + 2e^- \rightarrow H_2 + 2OH^-$$

The generation of hydroxide ions increases local pH near the electrode surface, promoting iron hydroxide precipitation and floc formation. The combined effects of electrochemical dissolution, oxidation, adsorption, and flotation contribute to efficient contaminant removal without external chemical addition. These mechanisms make iron electrocoagulation particularly suitable for decentralized treatment of arsenic-rich mine drainage.

Methods

The field demonstration was conducted at the Geumjeong Gold Mine in Bonghwa-gun, Gyeongsangbuk-do, South Korea (Figure 1). The mine historically produced gold, silver, and iron until mining rights expired in 1988. The site currently discharges mine drainage

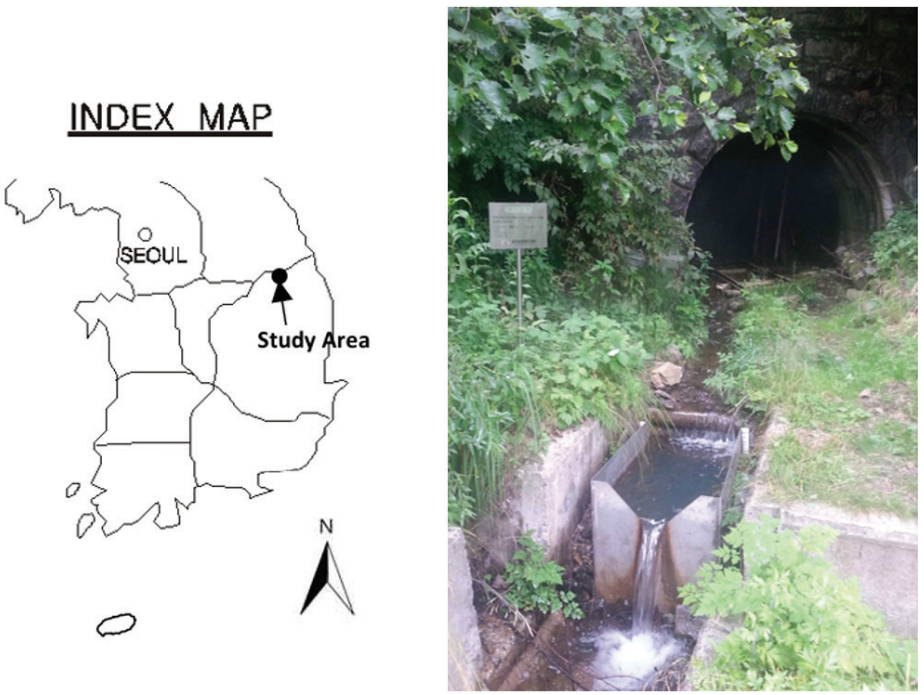

Figure 1 Study area map and mine drainage discharge at the Geumjeong abandoned mine, South Korea.

under oxidizing conditions, characterized by slightly alkaline pH (8.6–8.7), elevated oxidation–reduction potential (ORP), and high dissolved oxygen (DO) concentrations. Arsenic concentrations ranged from approximately 400 to 500 µg/L, exceeding the World Health Organization (WHO) drinking-water guideline of 10 µg/L by 40–50 times.

A stand-alone, solar-powered EC system was installed and operated as a field-scale demonstration unit under actual mine drainage conditions. The system consisted of photovoltaic panels, EC reactors, an expanded polystyrene (EPS) filtration unit, and a clean-water storage tank (Figure 2). Electricity generated by the solar panels powered a submersible pump that transferred raw mine drainage to the influent tank. To maximize energy efficiency, water movement between subsequent treatment units was driven by gravity using hydraulic head differences. The entire system was constructed in a modular, container-based configuration to facilitate transport and installation in remote mining areas lacking grid power.

Three EC reactors were installed to allow modular expansion and operational flexibility under variable mine drainage conditions. During the present field trial, two reactors were operated because the influent flow rate was sufficiently treated within the target hydraulic retention time using dual-reactor operation. Influent water was evenly distributed to the reactors in parallel flow. Each reactor contained seven iron electrodes (470 mm × 100 mm × 3 mm) arranged alternately as three anodes and four cathodes. The electrodes were mounted in a detachable cartridge structure to allow easy maintenance and replacement, with an estimated service life of approximately one year under the applied operating conditions. Mine drainage entered from the bottom of each reactor and flowed upward. During operation, anodic dissolution released iron ions that formed iron hydroxide flocs, which adsorbed and co-precipitated dissolved arsenic species.

Downstream of the EC reactors, an EPS foam filtration unit was installed to remove suspended flocs. Water flowed upward through the floating EPS media, which physically retained iron–arsenic precipitates. The filtration unit was equipped with a bottom discharge outlet to allow periodic removal of accumulated sludge without significant performance deterioration.

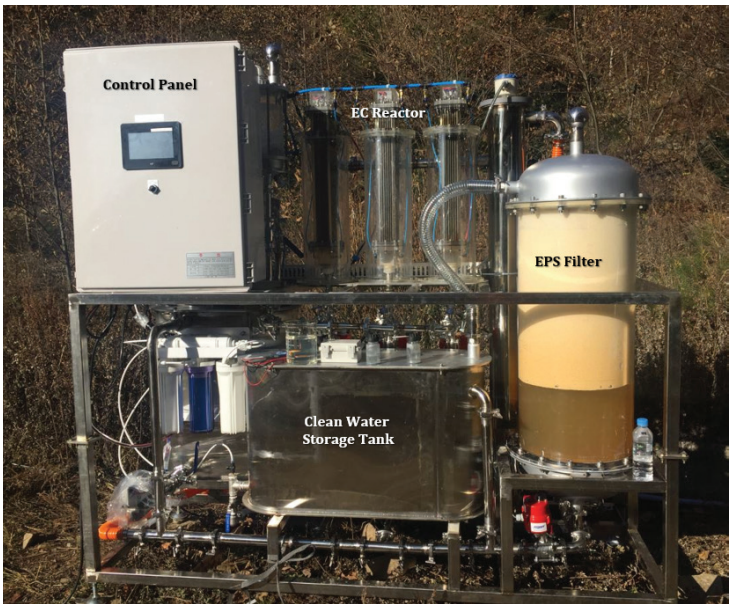

Figure 2 *Field-scale electrocoagulation (EC) system installed at the Geumjeong Gold Mine.*

During the field demonstration, the system operated at a treatment capacity of 8 m^3/day (approximately 2.8 L/min per operating line), with an applied voltage of 2.3 V and a current of 4.6 A supplied by photovoltaic power. The treatment capacity corresponded to approximately 16–80% of the mine drainage discharge (10–50 m^3/ day), depending on seasonal flow conditions. The system was therefore designed as a modular field-demonstration unit to evaluate scalability under real mine-water conditions.

Results and Discussion

Field-scale operation demonstrated rapid and stable arsenic removal performance. Within 20 minutes of system start-up, treated water arsenic concentrations decreased below the WHO drinking-water guideline of 10 µg/L (WHO 2004). After one hour of continuous operation, concentrations stabilized at <5 µg/L, confirming removal efficiencies greater than 99% from initial levels (~400– 500 µg/L). The fast stabilization indicates effective iron hydroxide floc formation and strong adsorption–co-precipitation mechanisms under slightly alkaline and oxidizing mine-water conditions, consistent with previously reported EC removal mechanisms (Mollah *et al.* 2001; Kumar *et al.* 2004).

The observed removal kinetics are comparable to previously reported electrocoagulation studies. Kobya *et al.* (2016) achieved compliance with drinking-water standards within 13 minutes under optimized current density conditions, and Das and Nandi (2021) reported similar removal efficiencies within 20 minutes in laboratory-scale systems. Notably, the present study achieved comparable reaction rates under field-scale conditions treating approximately 8 m^3/day of actual mine drainage, demonstrating the practical scalability of the system beyond laboratory validation.

The use of iron electrodes proved particularly suitable for arsenic removal. Iron hydroxide flocs are known to exhibit strong adsorption affinity for arsenate species (Smedley and Kinniburgh 2002). Comparative studies indicate that Fe electrodes perform as well as or better than aluminum electrodes for arsenic removal (Tenodi *et al.* 2024). In the present system, electrochemically generated iron ions formed dense hydroxide precipitates that effectively captured dissolved arsenic. Furthermore, electrochemical processes can promote partial oxidation of As(III) to As(V), enhancing removal efficiency without the need for external oxidants (Kumar *et al.* 2004; Emamjomeh and Sivakumar 2009). This characteristic represents a significant advantage in remote mine sites where chemical dosing is impractical.

Energy demand remained below 100 W throughout operation, confirming that the system can be fully powered by photovoltaic panels. Such low energy requirements are consistent with decentralized electrochemical treatment systems reported in recent modular water-treatment studies (Castañeda *et al.* 2024). The modular, container-based configuration further enhances field applicability by enabling rapid deployment and scalability. Compared to adsorption-based systems that require periodic media replacement, electrocoagulation continuously generates fresh coagulant in situ (Mollah *et al.* 2001). The projected electrode lifespan of approximately one year reduces maintenance frequency and operational costs, increasing suitability for long-term management of abandoned mine drainage.

Overall, the field validation confirms that solar-powered iron electrocoagulation is a technically robust, energy-efficient, and scalable solution for treating high-arsenic mine drainage. The results demonstrate that electrocoagulation can move beyond laboratory-scale research toward practical implementation in decentralized and infrastructure-limited environments.

Conclusions

This study demonstrated the field applicability of a solar-powered iron electrocoagulation (Fe–EC) system for treating arsenic-contaminated mine drainage at the Geumjeong Gold Mine, South Korea. The system reduced arsenic concentrations from 400–500 µg/L to below 10 µg/L within 20 minutes and stabilized at <5 µg/L after one hour, achieving removal efficiencies exceeding 99%.

Electrochemically generated iron hydroxide flocs effectively adsorbed and co-precipitated dissolved arsenic without the need for external chemical addition. Total energy consumption remained below 100 W, confirming the feasibility of fully photovoltaic-powered operation in remote mining areas.

The modular configuration, low maintenance demand, and projected one-year electrode lifespan highlight the practicality of this approach for decentralized remediation of abandoned mine drainage. These results support the transition of iron electrocoagulation from laboratory research to sustainable field implementation.

Acknowledgements

This work was supported by the Basic Research Program of the Korea Institute of Geoscience and Mineral Resources (KIGAM), project number 26-3414. The authors also express their sincere appreciation to Dr. Nguyen Thi Hoang Ha of Vietnam National University for her valuable assistance with the field experiments and analytical work conducted in Vietnam.

References

Ahn JS, Ko KS, Chon CM (2007) Arsenic occurrence in groundwater of Korea. J Soil Groundwater Environ 12:64–72

Castañeda LF, Baltazar A, Esquivel JP *et al* (2024) Modular electrochemical systems for decentralized water treatment: Design and scalability considerations. Electrochim Acta 470:142805

Das S, Nandi BK (2021) Removal of arsenic from drinking water by electrocoagulation: A review of process performance and mechanism. Chemosphere 286:131720

Emamjomeh MM, Sivakumar M (2009) Review of pollutants removed by electrocoagulation and electrocoagulation/flotation processes. J Environ Manag 90:1663–1679

Ghosh S, Debsarkar A, Dutta A (2019) Technology alternatives for decontamination of arsenic-rich groundwater: A critical review. Environ Technol Innov 13:277–303

Hamid NHA, Rushdan AI, Nordin AH *et al* (2024) The state-of-the-art of arsenic removal in wastewater. Water Reuse 14:279–311

Ji S, Yoo K, Dempsey BA (2011) The removal of arsenic ion in electro-coagulation cell. Geosyst Eng 14:71–78

Kanel SR, Das TK, Varma RS *et al* (2023) Arsenic contamination in groundwater: Geochemical basis of treatment technologies. ACS Environ Au 3:135–152

Kobya M, Demirbas E, Bayramoglu M (2016) Treatment of arsenic-containing drinking water by electrocoagulation using iron electrodes. J Environ Chem Eng 4:1484–1491

Kumar PR, Chaudhari S, Khilar KC, Mahajan SP (2004) Removal of arsenic from water by electrocoagulation. Chemosphere 55:1245–1252

Mollah MYA, Schennach R, Parga JR, Cocke DL (2001) Electrocoagulation (EC)—science and applications. J Hazard Mater 84:29–41

Smedley PL, Kinniburgh DG (2002) A review of the source, behaviour and distribution of arsenic in natural waters. Appl Geochem 17:517–568

Smith AH, Lopipero PA, Bates MN, Steinmaus CM (2002) Arsenic epidemiology and drinking water standards. Science 296:2145–2146

Tenodi S, Kostic M, Pavlovic M *et al* (2024) Comparative evaluation of iron and aluminum electrodes for arsenic removal by electrocoagulation. Water Res 252:120947

Wan W, Pepping TJ, Banerji T *et al* (2011) Effects of water chemistry on arsenic removal from drinking water by electrocoagulation. Water Res 45:384–392

World Health Organization (2004) Guidelines for Drinking-water Quality. WHO, Geneva

Electrocoagulation as Alternative Active Treatment for Hexavalent Chromium Removal from Nickel Mine Water in Indonesia

Umar Kasmon[1], Muhammad Sonny Abfertiawan[2], Faiz Hasan[2], Nur Latifa Ristiaramdani[3]*, Lionie Butar Butar[1], Irfa Darojat[1]

[1]*Environmental Strategic Department, PT Vale Indonesia Tbk., Indonesia*

[2]*Water and Wastewater Engineering Research Group, Faculty of Civil and Environmental Engineering, Bandung Institute of Technology, Bandung, Indonesia*

[3]*Research and Consulting Division, PT Ganeca Environmental Services, Bandung, Indonesia*

**corresponding author: latifa@ganeca.co.id*

Abstract

Indonesia, the world's largest nickel producer, faces challenges in managing mine water due to high rainfall and hexavalent chromium (Cr^{6+}) contamination. This study evaluates electrocoagulation as an alternative treatment method. A 100 L continuous reactor with iron electrodes operated for 72 hours at 5 A and 7 L/min. Results showed stable pH (6.8–7.1), with Cr^{6+} removal reaching 97% after one HRT and 99% after 72 h, reducing concentrations from 0.89 mg/L to below 0.001 mg/L. Findings suggest electrocoagulation is a promising and efficient approach for treating nickel mine water and supports further scale-up development.

Keywords: Electrocoagulation, chromium hexavalent, mine water, nickel mine

Introduction

Approximately 40% of global nickel production currently originates from laterite ores, and Indonesia is recognized as one of the countries with the largest nickel laterite resources in the world. At present, Indonesian nickel laterite ore is processed industrially using both pyrometallurgical and hydrometallurgical approaches, with a national development target of achieving 2.9 million tons of annual production by 2030 (ChuanYu *et al.* 2025). Nickel exploration in Indonesia began during the period of 1967–1976 (van Leeuwen 1994), leading to the discovery of extensive laterite nickel reserves in the eastern regions of the country, particularly in Maluku and Sulawesi

Indonesia's nickel resources are derived exclusively from surficial laterite-type ore deposits. These deposits are formed through intense chemical weathering of ultramafic massifs under tropical climatic conditions. Laterite-type deposits typically occur as tabular ore bodies characterized by extensive lateral distribution but relatively limited vertical thickness, generally less than approximately 30–40 m (Choi *et al.* 2021). Owing to their near-surface occurrence, laterite deposits in Indonesia are mined exclusively using open-pit methods (Heijlen and Duhayon 2024). Open-pit mining operations are widely acknowledged to pose potential environmental impacts on surrounding ecosystems (Abfertiawan *et al.* 2020). One of the most critical environmental concerns associated with nickel mining is mine runoff water.

Ultramafic rocks represent one of the most important geogenic sources of chromium (Cr), particularly its hexavalent form (Cr(VI)), which is a major environmental concern. Intensive weathering of ultramafic rocks in tropical regions generates substantial reservoirs of Cr(VI) (Delina *et al.* 2020). If mine water is not properly managed, dissolved metals may adversely affect biotic systems due to their non-biodegradable nature, making effective metal removal essential to prevent environmental contamination.

This issue is further exacerbated by Indonesia's high rainfall intensity. As a tro-

pical country located between the Pacific and Indian Oceans and between the Asian and Australian continents, Indonesia experiences substantial precipitation. Extreme rainfall events in Indonesia are strongly influenced by global climate variability phenomena such as the El Niño–Southern Oscillation (ENSO), the Indian Ocean Dipole (IOD), and the Madden–Julian Oscillation (MJO) (Bakri *et al.* 2021; Doyle *et al.* 2023). These climatic phenomena considerably increase the volume of mine runoff water that must be effectively managed.

The conventional treatment for Cr(VI) in mine water involves chemical reduction followed by precipitation as $Cr(OH)_3$, commonly using ferrous sulfate ($FeSO_4$) as the reducing agent (Xu *et al.* 2024). However, the use of chemical reagents presents several limitations, including inefficiency at low contaminant concentrations, generation of toxic sludge, and the requirement for pH adjustment (Itankar and Patil 2022). Alternatively, electrocoagulation offers a rapid and efficient active treatment technology capable of removing a wide range of pollutants. Despite this, electrocoagulation is frequently associated with high capital costs and energy-intensive operation (Phu *et al.* 2025; Genawi *et al.* 2025). Nevertheless, energy consumption can potentially be mitigated through integration with renewable energy systems, such as solar panels, which are particularly suitable for remote mining locations. Several studies have demonstrated that electrocoagulation can achieve high hexavalent chromium removal efficiencies, reaching up to 99% (Rusman 2024; Harahap *et al.* 2024). However, field-scale applications of electrocoagulation for Cr(VI) removal in mine water remain limited. Therefore, this study focuses on evaluating the durability and stability of Cr(VI) removal efficiency during short-term continuous operation as a step toward practical field-scale implementation of the technology.

Methods

The experiment was conducted using raw nickel mine water collected from an operating nickel mining site in South Sulawesi, Indonesia. Mine water was taken from the inlet of the sedimentation pond using a pump and stored in an Intermediate Bulk Container (IBC). From the IBC, a submersible pump was used to continuously feed the water into the electrocoagulation (EC) reactor. The electrocoagulation experiment scheme and water intake conditions for the experiment can be seen in Figure 1.

The experiment was carried out for 72 hours under continuous operation. Effluent samples were collected from the reactor outlet at nine different time points to analyze pH, total suspended solids (TSS), and hexavalent chromium (Cr^{6+}) concentrations. Sampling

Figure 1 *(a) Electrocoagulation scheme, (b) sediment pond as experimental intake, and (c) visual appearance of mine water samples for experiment.*

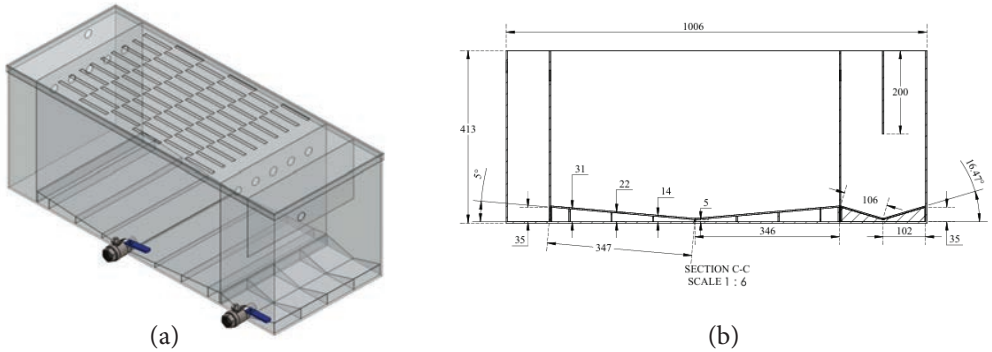

(a) (b)

Figure 2 (a) 3D reactor design and (b) reactor dimensions (in mm scale).

was performed at 15 and 25 minutes, followed by 5, 24, 29, 48, 53, and 72 hours of operation, hereafter referred to as t0, t1, t2, t3, t4, t5, t6, t7, and t8, respectively. The reactor configuration, hydraulic retention time (HRT), and applied current were adopted and scaled up from previously reported optimum conditions (Rusman *et al.* 2025). The electrocoagulation zone of the reactor had dimensions of 100 × 41.3 × 40.6 cm. The reactor was designed to ensure uniform flow distribution and high electrocoagulation efficiency. A total of 30 iron electrodes (40 cm × 10 cm × 0.2 cm) were installed with an inter-electrode spacing of 3 cm. The electrode arrangement consisted of 15 anodes and 15 cathodes configured in a monopolar connection. The electrodes were installed in a baffle configuration and connected to a DC power supply (MDB 0–60 V, 0–20 A). The reactor had a working volume of 100 L and was operated at a constant current of 5 A with an HRT of 15 minutes. The design of the electrocoagulation reactor used in this experiment can be seen in Figure 2.

No operational variations were applied, as the primary objective of this study was to evaluate the durability and consistency of electrocoagulation performance, particularly in achieving stable and sustained Cr^{6+} removal efficiency over extended operation.

Results and Discussion

Electrocoagulation operates through oxidation–reduction reactions, where oxidation occurs at the anode. At the iron anode, solid iron $Fe_{(s)}$ is oxidized to Fe^{2+} or Fe^{3+}, leading to the formation of iron hydroxides such as $Fe(OH)_2$ and $Fe(OH)_3$. The principal electrode reactions can be expressed as follows (Tabash *et al.* 2024).

Anode: $Fe \rightarrow Fe^{(2+)} + 2e^-$ (1)

Cathode: $2H_2O + 2e^- \rightarrow H_{2(g)} + 2OH^-$ (2)

The Fe^{2+} ions produced subsequently react with water to form ferrous hydroxide, $Fe(OH)_2$, which acts as a flocculant that promotes the aggregation.

$$Fe^{2+} + 2H_2O \rightarrow Fe(OH)_2 + 2H^+ \quad (3)$$

Continuous generation of Fe^{2+} enhances floc formation, as Fe^{2+} is gradually oxidized to Fe^{3+}, forming ferric hydroxide, $Fe(OH)_3$, which is recognized as a more effective coagulant.

$$4[Fe^{2+} + 2OH^-] + O_2 + 2H_2O \rightarrow Fe(OH)_3 \quad (4)$$

In addition to forming $Fe(OH)_2$ and $Fe(OH)_3$ precipitates, hexavalent chromium (Cr(VI)) removal using iron electrodes primarily occurs through chemical reduction by anodically generated Fe^{2+}. The Fe^{2+} species react with Cr(VI), reducing it to trivalent chromium (Cr(III)), which subsequently precipitates as $Cr(OH)_3$. The overall Cr(VI) removal reactions can be represented as follows (Heidmann and Calmano 2008; El-Taweel *et al.* 2015).

For 6,5 < pH < 7,5: $CrO_4^{2-} + 3Fe^{2+} + 4H_2O \rightarrow Cr^{3+} + 3Fe^{3+} + 8OH^-$ (5)

For pH > 7: $CrO_4^{2-} + 3Fe(OH)_2 + 4H_2O \rightarrow Cr(OH)_{3(s)} + 3Fe(OH)_{3(s)} + 2OH^-$ (6)

The reduction of hexavalent chromium is therefore considered the primary mechanism responsible for Cr(VI) removal in nickel mine water. Experimental results indicated that substantial Cr(VI) reduction occurred within the first 15 minutes of operation, corresponding to hydraulic retention time (HRT). At this point, the Cr(VI) concentration decreased by approximately 97%, reaching 0.028 mg/L.

This removal performance remained stable throughout the 72-hour continuous operation, with Cr(VI) concentrations consistently maintained at low levels. The sustained efficiency demonstrates that the electrocoagulation system operated reliably without performance deterioration over time. These findings indicate that the process not only achieves rapid initial reduction but also provides stable and consistent treatment performance, highlighting its potential applicability for continuous nickel mine water treatment. This rapid decline and subsequent stabilization of Cr(VI) concentration are illustrated in Figure 3a.

The formation of $Cr(OH)_3$ precipitates as a result of Cr(VI) reduction, together with $Fe(OH)_2$ and $Fe(OH)_3$ generated from the iron-based electrocoagulation process, was confirmed by the observed increase in total suspended solids (TSS) over time. The development of these flocs led to a rise and fluctuation in TSS concentrations at the reactor outlet, increasing from an initial value of 6 mg/L to a maximum of 38 mg/L.

Despite this increase, the TSS concentration remained well below the regulatory limit of 200 mg/L established by the Indonesian environmental regulation (Minister of Environment Regulation No. 09 of 2006 concerning wastewater quality standards for nickel ore mining activities). The fluctuation in TSS during the experiment is presented in Figure 3b.

The presence of visible precipitates further indicates that chromium removal was occurring. As illustrated in Figure 4, turbidity within the electrocoagulation reactor increased progressively over time, visually confirming the formation of hydroxide flocs and precipitation processes.

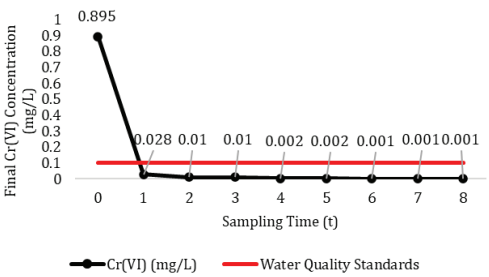

(a)

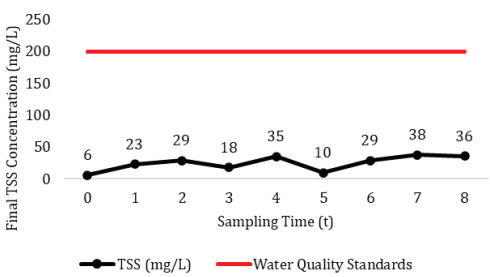

(b)

Figure 3 *(a) Final chromium hexavalent concentration (mg/L) and (b) Final Total Suspended Solid (TSS) concentration (mg/L).*

(a) (b) (c)

Figure 4 *Visual documentation of the electrocoagulation reactor: (a) initial condition at T0 (0 h), (b) reactor condition at T3 (24 h), and (c) precipitate accumulated at the reactor bottom at T3 (24 h).*

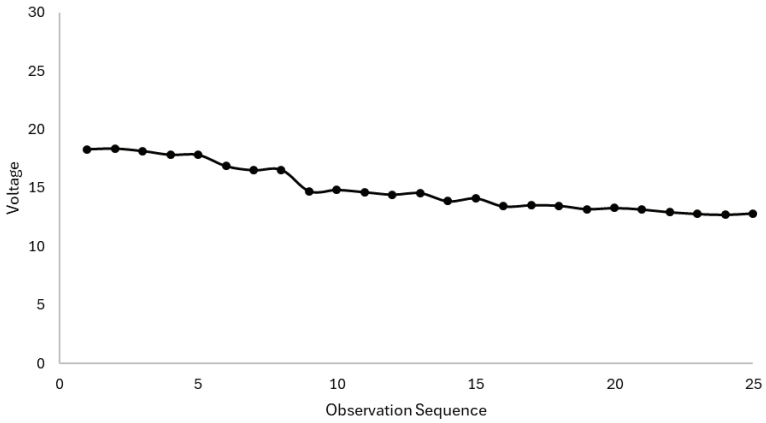

Figure 5 *Voltage profile during 72-h continuous electrocoagulation operation.*

During the 72 h electrocoagulation operation, the electrical voltage remained relatively stable, as shown in Figure 5, and did not show an increasing trend that would indicate scaling or electrode passivation. The average voltage was 14.91 V, with an average fluctuation between observation points of 7.61%. This relatively stable voltage profile suggests that the overall system resistance, including the solution, electrode, and electrode–electrolyte interface resistances, remained relatively constant throughout the operation. Therefore, the electrocoagulation process was maintained under steady operating conditions, supporting consistent energy demand.

Conclusions

This study demonstrates that electrocoagulation using iron electrodes is an effective method for treating nickel mine water containing hexavalent chromium. The process achieved rapid Cr(VI) reduction within one hydraulic retention time (15 minutes), with removal efficiency reaching approximately 97% and reducing concentrations to 0.028 mg/L. Further operation up to 72 hours increased the Cr^{6+} removal efficiency to 99%, lowering the concentration to 0.001 mg/L. Importantly, the treatment performance remained stable throughout 72 hours of continuous operation, indicating reliable and consistent system behavior.

The formation of $Fe(OH)_2$ and $Fe(OH)_3$ flocs played a dual role as coagulants and reducing agents, facilitating both chromium reduction and solid-phase precipitation. Although TSS increased due to hydroxide formation, concentrations remained well below the Indonesian regulatory limit (200 mg/L), confirming compliance with environmental standards.

Overall, the findings highlight electrocoagulation as a robust, fast, and dependable active treatment alternative for managing chromium-contaminated nickel mine water. The stable short-term continuous operation performance observed in this study supports its potential for scale-up and practical field implementation in Indonesia's nickel mining industry

Acknowledgements

The authors acknowledge the Environmental Strategic Department, PT Vale Indonesia Tbk., Indonesia, for providing access and technical support for this study. Appreciation is also extended to PT Ganeca Environmental Services, Bandung, Indonesia, for their assistance during the experimental work.

References

Abfertiawan MS, Palinggi Y, Handajani M, *et al* (2020) Evaluation of Non-Acid-Forming material layering for the prevention of acid mine drainage of pyrite and jarosite. Heliyon 6:e05590. https://doi.org/10.1016/j.heliyon.2020.e05590

Bakri B, Adam K, Rahim A (2021) SpatioTemporal Model of Extreme Rainfall Data in the Province of South Sulawesi for a Flood Early Warning System. Geomatics and Environmental Engineering 15:5–15. https://doi.org/10.7494/geom.2021.15.2.5

Choi Y, Lee I, Moon I (2021) Geochemical and Mineralogical Characteristics of Garnierite From the Morowali Ni-Laterite Deposit in Sulawesi, Indonesia. Front Earth Sci (Lausanne) 9:. https://doi.org/10.3389/feart.2021.761748

ChuanYu J, Manurung H, Anggara F, Petrus HTBM (2025) Indonesian Nickel Overview: Potential, Development and Future Prospects. In: Proceedings of the 63rd Conference of Metallurgists, COM 2024. Springer Nature Switzerland, Cham, pp 753–763

Delina RE, Arcilla C, Otake T, *et al* (2020) Chromium occurrence in a nickel laterite profile and its implications to surrounding surface waters. Chem Geol 558:119863. https://doi.org/10.1016/j.chemgeo.2020.119863

Doyle JD, Reynolds CA, Flatau M, Latos B (2023) Sensitivity and Predictability of an Extreme Rainfall Event in Sulawesi, Indonesia. SOLA 19A:19A–003. https://doi.org/10.2151/sola.19A-003

El-Taweel YA, Nassef EM, Elkheriany I, Sayed D (2015) Removal of Cr(VI) ions from waste water by electrocoagulation using iron electrode. Egyptian Journal of Petroleum 24:183–192. https://doi.org/10.1016/j.ejpe.2015.05.011

Genawi NM, Mahmud N, Hassan EA, El-Naas MH (2025) Electrocoagulation Column for the Removal of Chromium from Tannery Wastewater: Adsorption Kinetics and Sludge Recovery. ChemistryOpen 14:. https://doi.org/10.1002/open.202400497

Harahap MG, Abfertiawan MS, Syafila M, *et al* (2024) Electrocoagulation for nickel, chromium, and iron removal from mine water using aluminum electrodes. Heliyon 10:e40784. https://doi.org/10.1016/j.heliyon.2024.e40784

Heidmann I, Calmano W (2008) Removal of Cr(VI) from model wastewaters by electrocoagulation with Fe electrodes. Sep Purif Technol 61:15–21. https://doi.org/10.1016/j.seppur.2007.09.011

Heijlen W, Duhayon C (2024) An empirical estimate of the land footprint of nickel from laterite mining in Indonesia. Extr Ind Soc 17:101421. https://doi.org/10.1016/j.exis.2024.101421

Itankar N, Patil Y (2022) Assessing Physicochemical Technologies for Removing Hexavalent Chromium from Contaminated Waters—an Overview and Future Research Directions. Water Air Soil Pollut 233:355. https://doi.org/10.1007/s11270-022-05745-z

Phu TKC, Nguyen PL, Phung TVB (2025) Recent progress in highly effective electrocoagulation-coupled systems for advanced wastewater treatment. iScience 28:111965. https://doi.org/10.1016/j.isci.2025.111965

Rusman MR (2024) Distribusi Kerapatan Arus Dan Perpindahan Massa Pada Reaktor Elektrokoagulasi Kontinu Menggunakan Pendekatan Computational Fluid Dynamics Dan Pengaruhnya Terhadap Penyisihan Kromium Dan Nikel Pada Air Limbah Tambang Nikel. Thesis, Institut Teknologi Bandung

Rusman MR, Abfertiawan MS, Hasan F, *et al* (2025) Continuous-Flow Electrocoagulation for Hexavalent Chromium Reduction in Nickel Mining Wastewater: Insights into Optimization and Mechanisms. Mine Water Environ. https://doi.org/10.1007/s10230-025-01087-4

Tabash I, Elnakar H, Khan MF (2024) Optimization of iron electrocoagulation parameters for enhanced turbidity and chemical oxygen demand removal from laundry greywater. Sci Rep 14:16468. https://doi.org/10.1038/s41598-024-67425-8

van Leeuwen TM (1994) 25 years of mineral exploration and discovery in Indonesia. J Geochem Explor 50:13–90. https://doi.org/10.1016/0375-6742(94)90021-3

Xu H, Zhang H, Qin C, *et al* (2024) Groundwater Cr(VI) contamination and remediation: A review from 1999 to 2022. Chemosphere 360:142395. https://doi.org/10.1016/j.chemosphere.2024.142395

IMWA 2026
Jeongseon

Development of Design Software for Mine Drainage Treatment Facilities

Duk-Min Kim[1], Oh-Hun Kwon[2]

[1]*Department of Civil and Environmental Engineering, Sangji University, Wonju, Republic of Korea, kdukmin8@sangji.ac.kr, ORCID 0000-0002-1537-6866*

[2]*Korea Mine Rehabilitation and Mineral Resources Corporation, Wonju, Republic of Korea, ohkwon@komir.or.kr*

Abstract

A software tool was developed for the design and operation of passive, active, and semi-active mine water treatment systems. Using input parameters such as flow rate, water quality, and available area, the software generates recommended treatment trains, dimensions of individual treatment units, and operational parameters including lime dosage and sludge generation. Compared with existing tools such as AMDTreat, the present software additionally predicts Mn concentrations based on co-precipitation and sorption by Fe and incorporates a dedicated module for settling analysis. It also integrates recently published models for Fe oxidation and slag reactor performance.

Keywords: Mine drainage; treatment facilities; design software; operational factor; settling; Mn treatment

Introduction

Software tools can improve design accuracy and enhance efficiency by minimizing human error. In the design of mine drainage treatment systems, existing software such as AMDTreat (Cravotta, 2020, 2021) has been widely used to design treatment facilities and to predict key operational parameters, as well as associated costs.

The aim of this software development is to incorporate additional factors and modules based on recent findings, whereas the models are largely empirical. In particular, Mn removal is strongly influenced by co-precipitation and sorption by Fe, and recent studies addressing these processes have been integrated into the software. Furthermore, recent advances in Fe oxidation kinetics in mine drainage and the performance of slag reactors have been incorporated. A settling module has also been developed to predict settling efficiency in settling tanks based on column experiment data.

Methods

The developed software requires input parameters such as influent water quality, flow rate, and available area (Fig. 1). After selecting one of the treatment methods (passive, active, or semi-active), the program automatically generates a design, including the dimensions of the treatment facilities.

Passive Treatment

Oxidation rates of ferrous iron are calculated using newly derived equations based on experimental data and field observations from mine drainage treatment sites. The Fe oxidation algorithm determines the required oxidation time, the amount of precipitate accumulation in the SAPS (Successive Alkalinity Producing System), and the need for an oxidation pond. Within the water layer of the SAPS, the concentration of Fe(III) generated by oxidation of Fe(II) is calculated and added to the existing Fe(III) concentration. A fraction (e.g., 50%) of the resulting Fe(III) is assumed to be converted into total suspended solids (TSS), which is then added to the influent TSS. If the resulting TSS concentration is sufficiently high (e.g., >50 mg L^{-1}) to cause rapid sludge accumulation in the SAPS, an oxidation-settling pond is designed upstream of the SAPS.

The applicability of SAPS is determined by comparing the acidity and alkalinity of

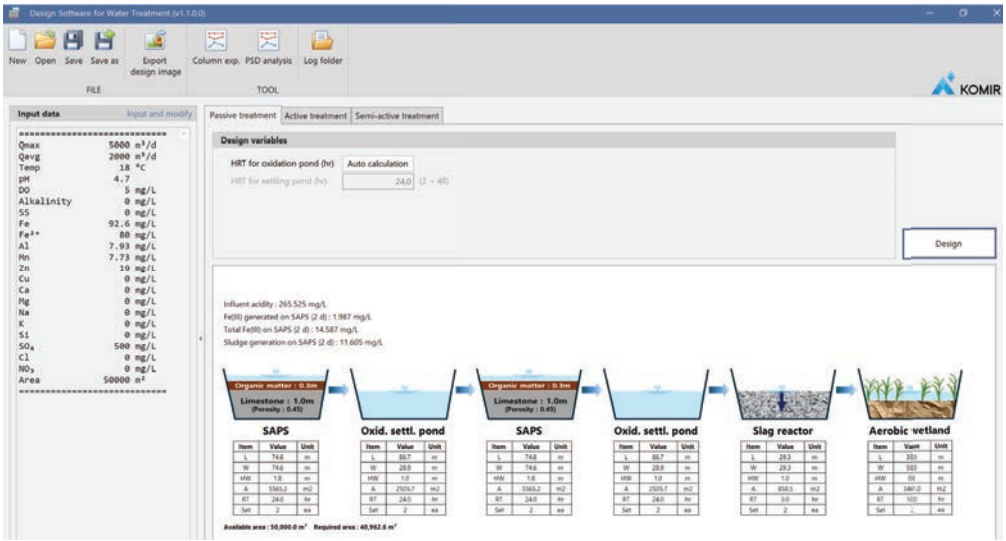

Figure 1 *Developed software for mine water treatment, showing a design example of a passive treatment system.*

the influent. The number of SAPS units is estimated using the empirical equation proposed by Zipper *et al.* (2018), which predicts alkalinity generation from limestone.

For the slag reactor, its applicability is evaluated based on the predicted Mn concentration after sequential treatment through SAPS, oxidation-settling ponds, and an aerobic wetland. The average Mn removal rates in passive treatment unit processes have recently been reported by Kwon *et al.* (2025) and were used to assess whether the passive treatment system can reduce Mn concentrations below the effluent standard (e.g., 2 mg L^{-1}).

The size of the slag reactor is estimated using an empirical relationship between hydraulic retention time (HRT) and Mn removal efficiency in slag reactors (Kim 2021). In addition, an HRT of 10 h is applied for the aerobic wetland following the slag reactor to reduce pH to meet effluent standards, as suggested by several case studies (Kim 2021).

(Semi-)Active Treatment

The optimal target pH is determined based on contaminant concentrations—primarily Mn and Fe—by considering co-precipitation and adsorption behaviors described by empirical equations (Kim *et al.*, 2022). The resulting pH value is displayed in the software output, and users can apply it as the target pH by clicking the "Apply" button (Figure 2).

The dosage of hydrated lime and the amount of precipitate generated are computed using PHREEQ-N-AMDTreat, and the results are adjusted using additional coefficients suggested by Kim *et al.* (2023). The estimated precipitate mass is then used to determine the required flocculant dosage and annual sludge production.

The required residence time for settling tanks is calculated using a module that utilizes either column test results or particle size distribution (PSD) data (Figure 3). Between the two datasets, PSD-based estimates are generally less reliable than those based on column tests. Users input measured TSS concentrations at a specific depth in the column as a function of time. In addition, the depth of the full-scale settling tank and the influent TSS concentration are provided as input parameters. After running the module, the predicted TSS concentrations corresponding to different HRTs are displayed. Subsequently, the required areas for active, semi-active, and passive treatment systems are compared with the available area to evaluate installation feasibility.

(a)

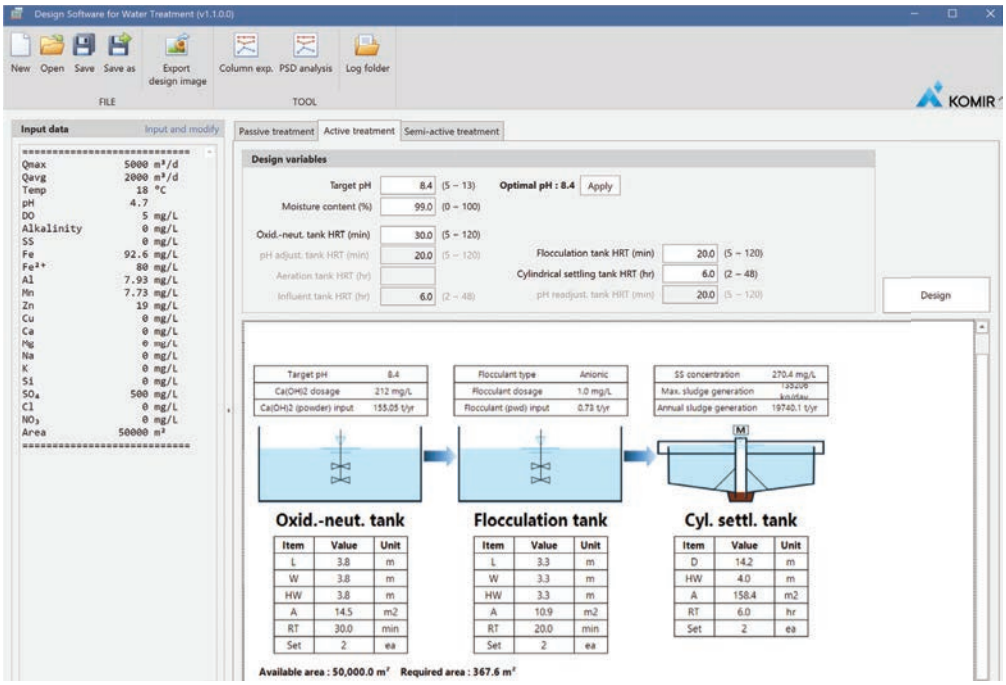

(b)

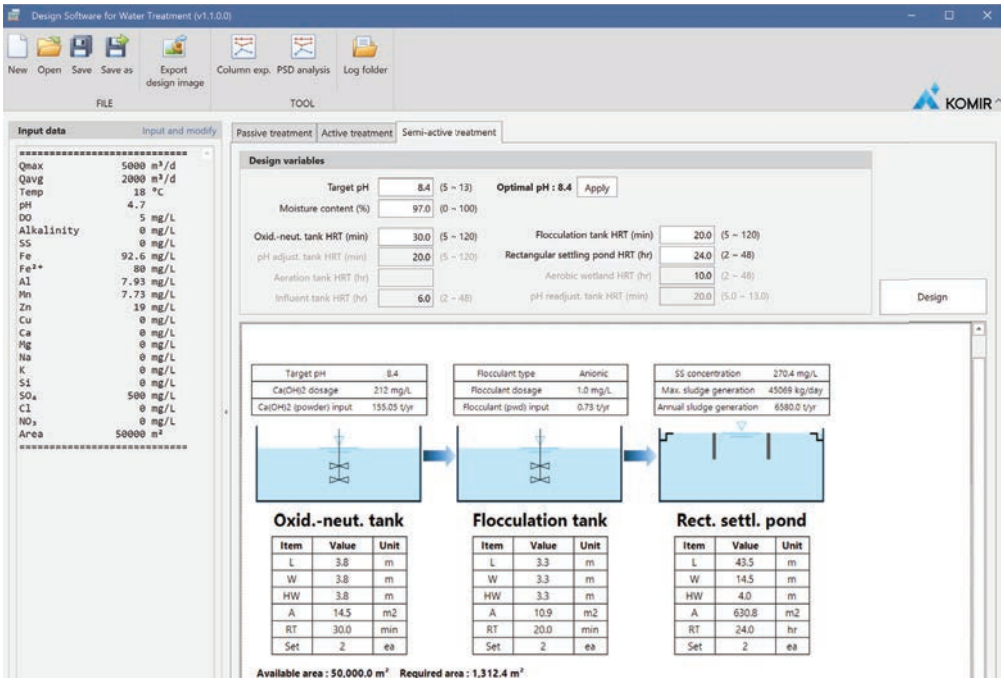

Figure 2 Developed software for mine water treatment, showing a design example of (a) an active treatment system and (b) a semi-active treatment system.

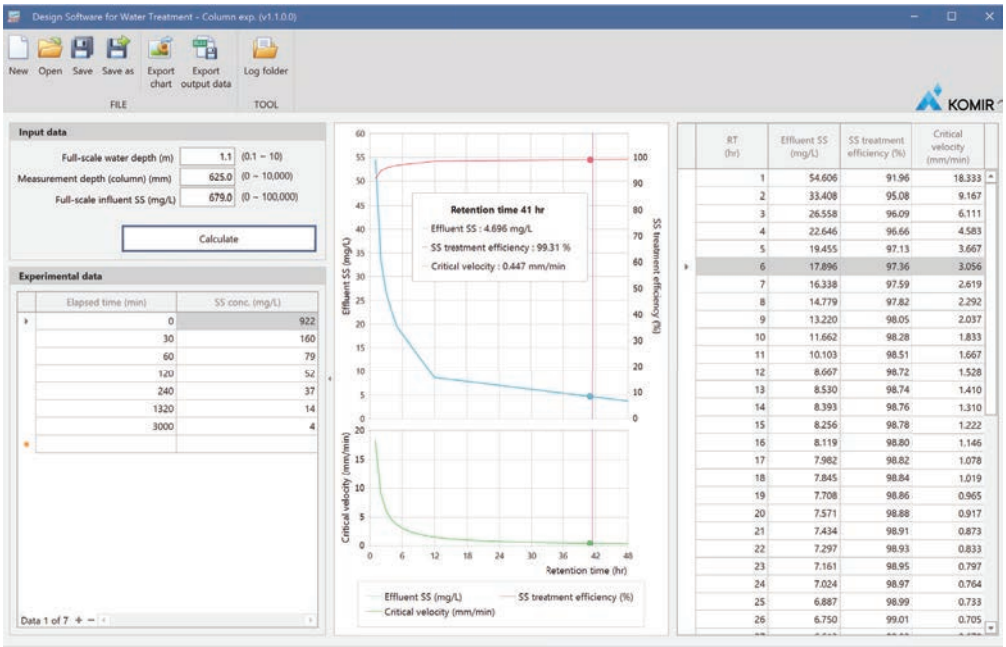

Figure 3 *Prediction module for settling efficiency in mine water treatment facilities based on column experiments*

Results and discussion

Passive Treatment

The chemical composition of adit drainage from the ET mine, Peru, was used as the input data for the software (Table 1). The modeled treatment system consisted of two sequential SAPS and oxidation–settling pond units, followed by a slag reactor and an aerobic wetland (Figure 1). A single SAPS and oxidation–settling pond sequence was insufficient to neutralize the calculated acidity (Table 2); therefore, two sequential units were recommended. In addition, because the influent pH was sufficiently low (4.7), less than 2 mg/L of Fe(III) was predicted to be generated through Fe(II) oxidation, resulting in only 11.6 mg/L of sludge accumulation in the SAPS over 2 days. Consequently, an oxidation–settling pond was not recommended prior to the first SAPS.

With an influent Mn concentration of 7.7 mg/L, the conventional treatment sequence consisting of SAPS – oxidation–settling pond – SAPS – oxidation–settling pond – aerobic wetland was predicted to reduce Mn concentration only to 6.7 mg/L, which exceeded the target concentration of 2 mg/L. Therefore, a slag reactor was additionally recommended, with a predicted hydraulic retention time (HRT) of 3.0 h based on the Mn concentration (Table 2). Subsequently, an aerobic wetland was included to reduce the effluent pH following the slag reactor. The resulting treatment train was identical to that of the pilot-scale ET mine drainage treatment facility reported by Kim *et al.* (2025), except for the As adsorption pond which was not included in the software.

(Semi-)Active Treatment

The same adit drainage from the ET mine was also used to design active and semi-active treatment facilities (Figure 2). The target treatment pH was recommended as 8.4 based on the Fe and Mn concentrations (Table 3). The required dosages of hydrated lime and flocculant (anionic PAM) were estimated to be 212 mg/L and 1.0 mg/L, respectively. Sludge generation was predicted to be 270 mg/L (Table 3).

Table 1 Chemical composition of adit drainage from the ET mine, Peru, used for model prediction (Kim et al. 2025).

pH	Al	Fe(III)	Fe(II)	Mn	Zn
(-)	(mg/L)				
4.70	7.93	12.6	80.0	7.73	19.00

Table 2 Major design parameters for the passive treatment system modeled using adit drainage from the ET mine, Peru.

Influent acidity	Fe(III) generated on SAPS (2 d)	Total Fe(III) on SAPS (2 d)	Sludge generation on SAPS (2 d)	HRT of slag reactor
(mg/L as $CaCO_3$)		(mg/L)		(h)
259.3	1.99	14.59	11.61	3.0

Table 3 Major design parameters for the (semi-)active treatment system modeled using adit drainage from the ET mine, Peru.

Target pH	Dosage of $Ca(OH)_2$	Dosage of flocculant (PAM)	Sludge generation
(-)		(mg/L)	
8.4	212	1.0	270

Additionally, Kim *et al.* (2026) investigated the prediction of settling efficiency based on column experiments by comparing predicted and measured settling efficiencies in several mine drainage treatment facilities.

Conclusions

While AMDTreat provides a range of functions, including cost estimation, the present software additionally predicts Mn concentrations based on co-precipitation and sorption by Fe and incorporates a dedicated module for settling analysis. It also integrates recently published models for Fe oxidation and slag reactor performance. This software is non-commercial and will be freely distributed. It can be applied to the practical design of mine water treatment facilities worldwide. The developed framework is expected to contribute to improving both the efficiency and the design quality of mine drainage treatment systems.

Acknowledgements

This work was supported by an R&D project of the Korea Mine Rehabilitation and Mineral Resources Corporation from 2022 to 2026 and was also partly supported by the Sangji University Research Fund in 2024.

References

Cravotta CA (2020) Interactive PHREEQ-N-AMDTreat water-quality modeling tools to evaluate performance and design of treatment systems for acid mine drainage (software download): U.S. Geological Survey Software Release. https://doi.org/10.5066/P9QEE3D5

Cravotta CA (2021) Interactive PHREEQ-N-AMDTreat water-quality modeling tools to evaluate performance and design of treatment systems for acid mine drainage. Appl Geochem 126:104845. https://doi.org/10.1016/j.apgeochem.2020.104845

Kim DM (2021) Removal of manganese from mine drainages by the passive slag reactor and active treatment system: Proposals for the design of treatment facilities. J Korean Soc Mineral Energy Resour Eng 58(3):249-257. https://doi.org/10.32390/ksmer.2021.58.3.249

Kim DM, Oh YS, Park HS, Kim DK, Lee JH (2022) Steel slag-limestone reactor for Mn removal with tolerance to Fe: experiments and mechanisms. J Environ Chem Eng 10(3):107468. https://doi.org/10.1016/j.jece.2022.107468

Kim DM, Kwon HL, Park MS (2023) Underestimation of alkaline dosage and precipitate amount during water treatment: Role of inorganic carbon and use of PHREEQ-N-AMDTreat. J Cleaner Prod 433:139683. https://doi.org/10.1016/j.jclepro.2023.139683

Kim DM, Rodriguez-Vasquez C, Bottger-Gamarra JC, Jeon JW, Choi EA, Im YJ, Kang S (2025) Passive treatment experiments including slag reactor and As adsorption reactor for mine drainages in Peru. Proceedings of IMWA 2025

Kim DM, Park SS, Lee GH, Kwon HL, Kim YM, Ko JI, Kwon OH (2026) Prediction of settling efficiencies using column tests and the role of zeta potential. Environ Sci Water Res Technol, under review

Kwon HL, Kim DM, Park SS, Hong JH, Ko JI (2025) Assessment of mechanisms and efficiencies for Mn decrease at unit processes in passive treatment facilities for mine drainage. Environ Geochem Health 47:492. https://doi.org/10.1007/s10653-025-02813-1

Zipper C, Skousen J, Jage C (2018) Passive treatment of acid-mine drainage. Powell River Project Reclamation Guidelines for Surface Mined Land, Virginia Cooperative Extension, Virginia Tech, Publication 460–133.

Facile Synthesis of Zeolite A from Molybdenum Mine Tailings and Its Potential Application in Mine Reclamation

Hyeseong Kim[1], Hyunjin In[1], Jiyun Jeong[1], Sang Yun Lee[1], Uikyu Choi[2], Youn Soo Oh[2]

[1]*Sanha Engineering & Construction Co., cometk94@naver.com*

[2]*Korea Mine Rehabilitation & Mine Resources Co., ukchoi@komir.or.kr*

Abstract

This study presents a facile and scalable synthesis of zeolite A from molybdenum mine tailings using simple alkaline fusion (550 °C) and low-temperature crystallization (30–90 °C), avoiding energy-intensive hydrothermal process. Pilot-scale production achieved a ≈90% yield. The synthesized zeolite A demonstrated a high cation exchange capacity (292 meq/100 g). In batch tests, it removed ≥99.9% of aqueous cadmium and 13.5% of fluoride, and when mixed with limestone, completely suppressed cadmium and reduced arsenic leaching in contaminated soils. This approach sustainably converts potentially problematic mine waste into functional materials for environmental remediation.

Keywords: Synthetic zeolite, mine waste, mine reclamation, adsorbent, soil stabilizer

Introduction

The global mining industry inadvertently generates massive volumes of mine tailings and waste rock. Typically stockpiled near extraction sites, these by-products pose severe environmental risks. In the Republic of Korea, exposed mining waste in abandoned areas has caused significant soil and water pollution, often involving toxic inorganic contaminants like arsenic (As), cadmium (Cd), and fluoride (F) (Lim *et al.* 2015).

Historically, mining waste management relied on physical containment such as capping. However, these methods require large land areas, do not fundamentally treat contaminants, and are vulnerable to extreme weather, leading to potential re-release of contaminants. Consequently, a transition toward fundamental solution like recycling is imperative.

Because mine waste is rich in silicon (Si) or aluminium (Al), they could be excellent precursors for synthesizing functional materials like zeolites or ceramic filters (Huang *et al.* 2024). Zeolites, with their porous structure and exceptional cation exchange capacity (CEC), are highly effective for environmental remediation. Converting these liabilities into secondary resources offers a dual benefit: mitigating environmental threats while generating functional materials.

However, conventional zeolite synthesis often relies on energy-intensive or unscalable steps, such as high-temperature hydrothermal treatment or centrifugation (Park *et al.* 2000; Jeon *et al.* 2025), hindering commercialization. Therefore, developing highly scalable methods is crucial.

In this study, we propose a facile and scalable recycling technology to convert molybdenum (Mo) mine tailings into synthetic zeolite A via a simplified alkaline fusion (550 °C) and low-temperature crystallization (30–90 °C) process. This research aims to provide a functional environmental material capable of efficiently adsorbing contaminants and stabilizing soils, offering a scalable pathway for sustainable mine reclamation.

Methods

Raw Materials and Synthesis Procedure of Zeolite A

Mo mine tailings were dried and milled to ensure a uniform particle size. The raw tailings were classified as non-hazardous general waste, with trace metal and leaching

concentrations strictly satisfying the Korean Soil Contamination Warning Standards for Area 1 and Waste Control Act thresholds, respectively (MCEE 2025a, 2025b). Zeolite A was synthesized via an alkaline fusion methods. The tailings were homogeneously mixed with NaOH using either a mortar (lab-scale) or a ribbon mixer (pilot scale), followed by heating at 550 °C for 2 h to decompose mineral phases. Sodium aluminate ($NaAlO_2$) was added to optimize the SiO_2/Al_2O_3 molar ratio. The fused mixture was hydrated and subjected to a two-stage reaction: aging at 30 °C for 3 h and crystallization at 90 °C for 3 h. The final product was washed, filtered and dried. Following lab-scale optimization of the SiO_2/Al_2O_3 and NaOH/tailings ratio (Fig. 1), the process was successfully scaled up in a pilot system, producing 10–20 kg per batch with a ≈90% yield (Fig. 2).

Characterization of Synthesized Materials

The samples were characterized using X-ray diffraction (XRD) for crystalline phases, X-ray fluorescence (XRF) for chemical composition, and scanning electron microscopy (SEM) for surface morphology. Cation exchange capacity (CEC) was measured using the standard 1 N ammonium acetate method (detection limit: 0.1 mg/L; error margin: ±20%) to assess ion-exchange potential. Commercial synthetic zeolite A was also analysed under identical conditions for comparison.

Environmental Performance Evaluation

Duplicate batch experiments were conducted to evaluate the environmental remediation performance (Fig. 3):

Batch Adsorption: To evaluate the adsorption capacity for both cationic and anionic species, Cd and F were selected as target contaminants, respectively. Separate 10 mg/L solutions with a 1 g/L adsorbent dosage were agitated at 300 rpm for 2 h before measuring residual ion concentrations.

Soil Stabilization: Batch leaching tests followed KOMIR protocols to assess As and Cd, selected for their severe toxicity, high mobility, and strict regulatory limits (KOMIR 2022). Artificially contaminated soil (120.3 mg/kg As, 23.5 mg/kg Cd) was prepared using high-purity standard

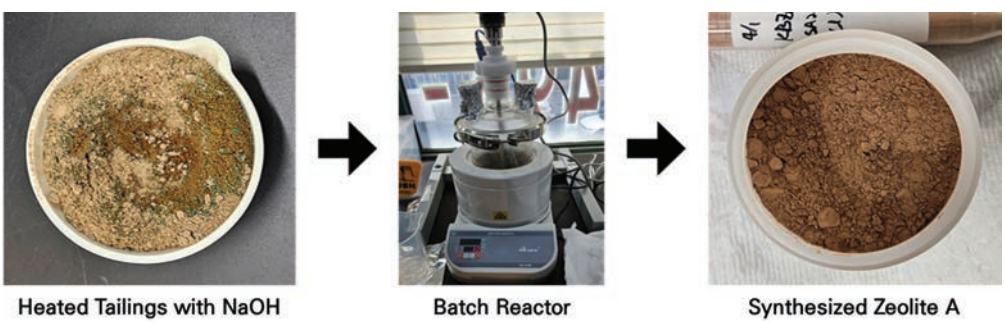

Figure 1 *Synthesis process of zeolite A by batch reactor.*

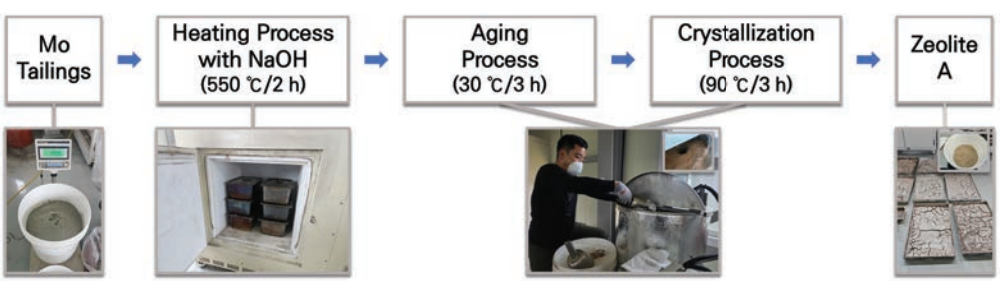

Figure 2 *Pilot production with a 200 L reactor.*

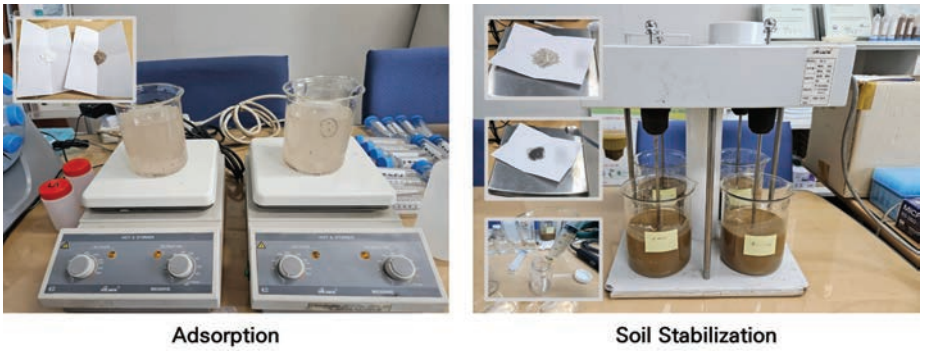

Figure 3 Batch-scale experiment of product.

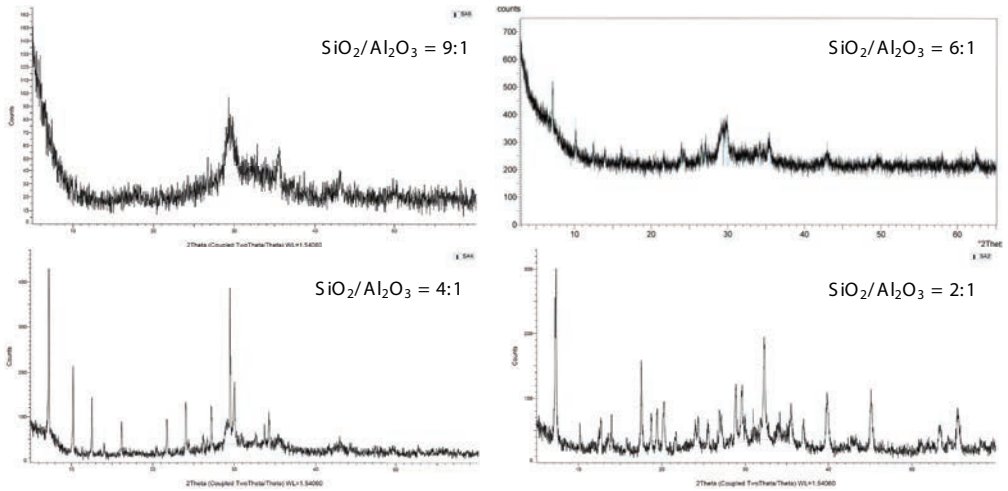

Figure 4 XRD patters of the synthesized zeolites according to SiO_2/Al_2O_3 molar ratio.

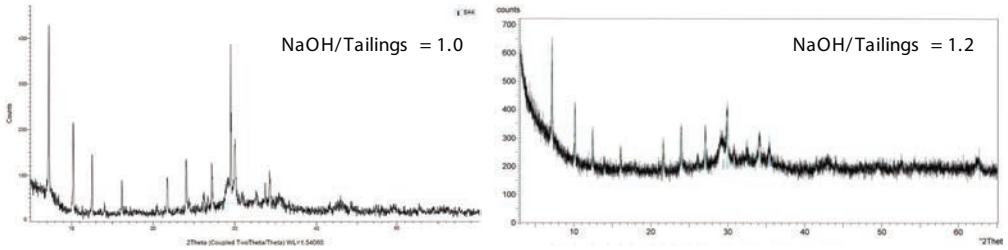

Figure 5 XRD patterns of synthesized zeolite A at different NaOH/Tailings mass ratio.

solutions and equilibrated for 24 h. Three experimental groups were compared: (1) an untreated control, (2) a limestone-zeolite A mixture (60:40 wt%), and (3) a limestone-steel slag mixture (60:40 wt%) as a reference. Stabilizers were applied at 5 wt% of the soil. Samples were periodically collected during the 36 h agitation.

Results and Discussion

XRD analysis determined the optimal SiO_2/Al_2O_3 molar ratio for zeolite A synthesis to be 4:1 (Fig. 4). Ratios ≥ 5:1 lacked sufficient aluminium for framework formation, while a ratio of 2:1 exhibited decreased peak clarity, indicating excessive alumina hindered crystallization. With the SiO_2/Al_2O_3 ratio fixed at

4:1, increasing the NaOH/tailings mass ratio to 1.2 deteriorated synthesis, likely because excessive OH- ions interfere with structure formation (Fig. 5).

Regarding the pilot-produced material, XRD confirmed the primary (7.2°) and characteristic peaks (10.2°, 12.5°, 16.1°, 21.7°, 24.0°, 27.1°, 30.0°, 34.2°) of standard zeolite A (Treacy and Higgins 2001), and SEM revealed the typical cubic morphology with sharp edges (Pan *et al.* 2025), verifying the successful pilot-scale synthesis (Fig. 6).

XRF analysis revealed residual impurities such as Fe_2O_3, CaO, and MgO from the tailings in the synthesized product (Table 1). The SiO_2/Al_2O_3 molar ratio (4.2–4.5) slightly exceeded the theoretical value of commercial zeolite A, likely due to unreacted silicate phases, residual tailings impurities, and inherent XRD instrumental variations (Pan *et al.* 2025).

To assess ion-exchange reliability, CEC was measured across three separate pilot batches, yielding an average of 292 meq/100 g (Table 2). While individual values exhibited variability (258.11-325.43 meq/100 g), this deviation falls within the analytical error margin (±20%) of the CEC measurement method, alongside minor contributions from the raw tailings' inherent mineralogical heterogeneity and pilot-scale process fluctuations. Despite these variations, the synthesized zeolite's average CEC surpassed that of commercial synthetic zeolite A (283 meq/100 g) evaluated under identical conditions.

In batch adsorption test, the product exhibited Cd removal (≈100% at 10 mg/L for 2 h) comparable to commercial zeolite (Fig. 7a). Notably, it demonstrated a 5.6-fold higher F removal efficiency (13.5% vs. 2.4%) despite the zeolite framework's inherent electrostatic repulsion toward anions (Wang and Peng 2010) (Fig. 7b). For soil stabilization, untreated soil leachates averaged 2.70 mg/L for As and 0.37 mg/L for Cd, exceeding Korean Waste Control Act limits (1.5 and 0.3 mg/L, respectively) (MCEE 2025b). The limestone-zeolite A mixture suppressed As leaching to 0.90 mg/L (Fig. 8a), and completely immobilized Cd over 36 h (Fig. 8b), matching the conventional limestone-steel slag combination. While adding limestone slightly increased soil pH from 6.3 to 7.1, pH differences between zeolite and steel slag treatments were negligible (Table 3). This confirms the immobilization efficiency is not merely due to pH-induced precipitation, highlighting the product's potential for environmental remediation.

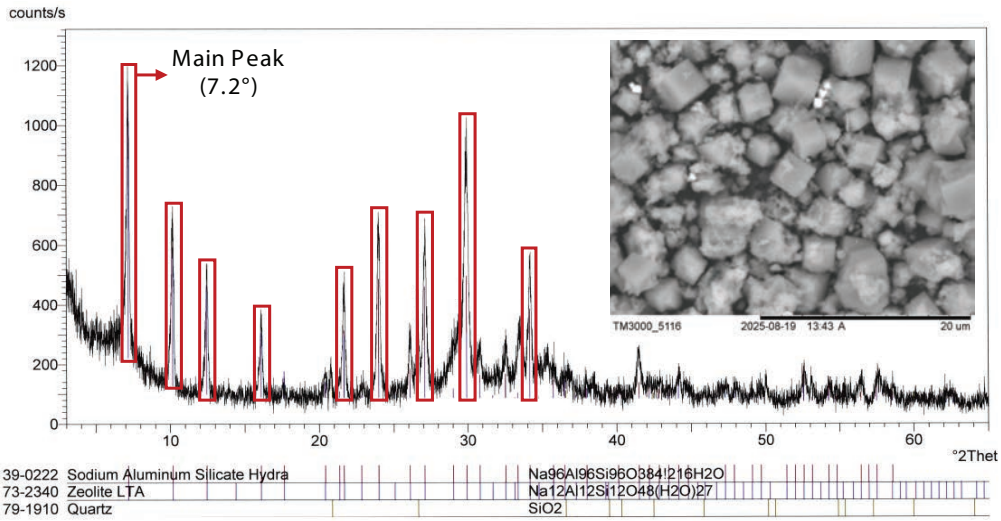

Figure 6 *XRD patterns and SEM image (inset) of synthesized zeolite A from pilot-scale production.*

Table 1 XRF analysis of fabricated zeolite A from pilot production (Unit: %, by mass).

Contents	SiO_2	Al_2O_3	Fe_2O_3	CaO	MgO	K_2O	Na_2O	TiO_2	MnO	P_2O_5
Tailings	41.80	7.83	11.99	25.47	3.08	0.78	0.23	0.30	1.02	0.08
Product(1)	37.77	14.18	8.02	12.21	1.57	0.30	11.74	0.18	0.68	0.03
Product(2)	33.18	13.36	7.99	13.04	1.45	0.30	15.88	0.18	0.68	0.04

- Minor elements were not detected as their concentrations were below the detection limit of the fusion method employed for major oxide quantification.
- Analysed from two separate pilot batches.

Table 2 CEC measurement of fabricated zeolite A from pilot production (unit: meq/100 g).

Contents	Product(1)	Product(2)	Product(3)	Average
Exchangeable-Mg	1.04	0.10	0.53	0.56
Exchangeable-Ca	5.51	0.20	1.49	2.40
Exchangeable-K	2.71	1.40	1.80	1.97
Exchangeable-Na	316.17	292.04	254.29	287.50
Total	325.43	293.74	258.11	292.43

- Measured from three separate pilot batches.
- Commercial synthetic zeolite A CEC: ~283 meq/100 g

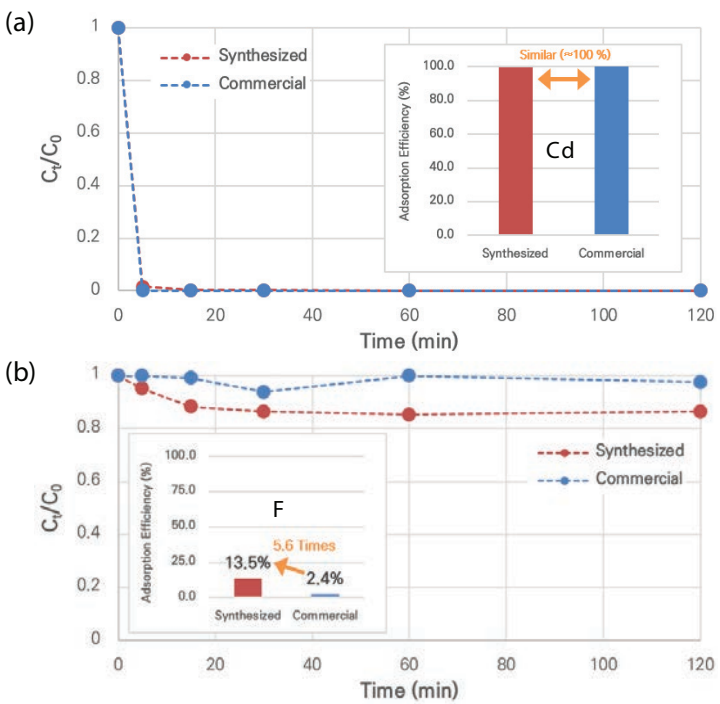

Figure 7 Batch-scale adsorption performance of the synthesized product for (a) Cd and (b) F.

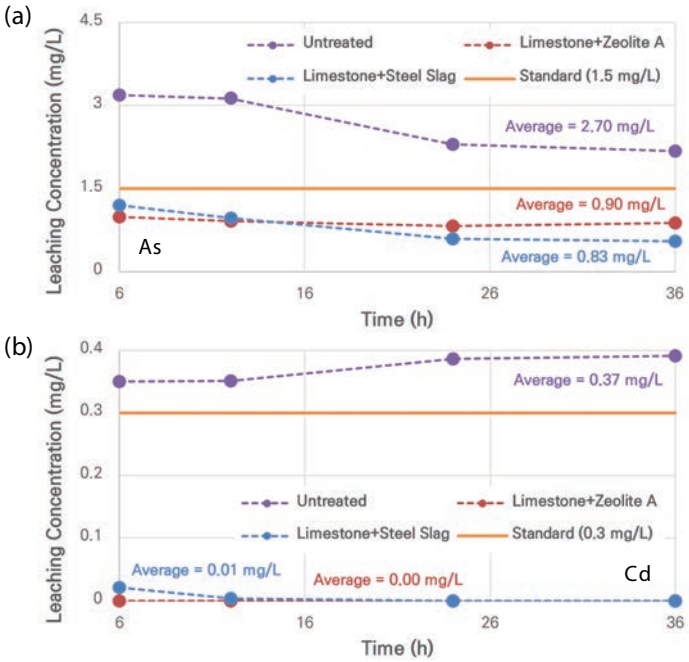

Figure 8 *Stabilization performance for (a) As and (b) Cd in soil.*

Table 3 *Changes in pH of soil leachates during the soil stabilization batch test.*

Retention Time (h)	Untreated	Limestone+Product	Limestone+Steel slag
6	6.3	6.9	6.8
12	6.4	7.0	6.9
24	6.3	7.1	7.3
36	6.1	7.2	7.3
Average	6.3	7.1	7.1

Conclusions

This study demonstrated a facile and scalable method for synthesizing zeolite A from Mo mine tailings without high-pressure hydrothermal treatment or centrifugation. By optimizing synthesis conditions (NaOH/tailings mass ratio of 1.0; SiO_2/Al_2O_3 molar ratio of 4:1), the process was successfully scaled up in a 200 L pilot reactor. This system produced 10–20 kg/batch of zeolite A with a ≈90% yield. Physicochemical analyses confirmed the crystal structure and a high CEC (292 meq/100 g), comparable to commercial product. Finally, batch-scale experiments validated the product's excellent performance and potential as an environmental remediation material for both trace metal adsorption and soil stabilization.

Acknowledgements

This work was supported by an R&D project of the Korea Mine Rehabilitation and Mineral Resources Corporation in 2025.

References

Huang Q, Wang W, Lai W, Liang B, Xiao B, Gu J, Huang Z, Zeng X, Liu H, Hu H, Yuan W (2024) Preparation of Zeolite A from Ion-Adsorbing Rare Earth Tailings for Selective Adsorption of Pb2+: An Innovative Approach to Waste Valorization. Molecules 29(21):5065

Jeon CM, Han SS, Lee SJ (2025) A review of recycling techniques for mine tailings-based zeolites. Minerals and Rocks 38(3):173–186

Korea Mine Rehabilitation and Mineral Resources Corporation (KOMIR) (2022) Mine Reclamation Technology Standards. Republic of Korea

Lim TY, Lee SW, Park MJ, Lee SH, Kim SO (2015) Comparative study on the human risk assessment of trace metal contamination between two abandoned metal mines in Korea. Journal of Korean Society of Environmental Engineers 37(11):619–630

Ministry of Climate, Energy and Environment (MCEE) (2025a) Soil Environment Conservation Act. Republic of Korea

Ministry of Climate, Energy and Environment (MCEE) (2025b) Waste Control Act. Republic of Korea

Pan J, Wang B, Liu S, Liu S, Yan W (2025) Synthesis and Application of LTA Zeolite for the Removal of Inorganic and Organic Hazardous Substances from Water: A Review. Molecules 30(3):554

Park M, Choi CL, Lim WT, Kim MC, Choi J, Heo NH (2000) Molten-salt method for the synthesis of zeolitic materials: I. Zeolite formation in alkaline molten-salt system. Microporous and Mesoporous Materials 37(1–2):81–89

Treacy MMJ, Higgins JB (2001) Collection of simulated XRD powder patterns for zeolites (4th ed). Elsevier

Wang S, Peng Y (2010) Natural zeolites as effective adsorbents in water and wastewater treatment. Chemical Engineering Journal 156(1):11–24

Factors Influencing Difference Between Theoretical and Actual Lime Dosages Including Lime Concentration and Dosing Rate

Young-Min Kim[1], Duk-Min Kim[1], Ki-Rim Lee[1], Seong-Sook Park[2], Oh-Hun Kwon[3], Jung-Sik Park[3]

[1]*Sangji University,* [2]*Hanyang University,* [3]*Korea Mine Rehabilitation and Mineral Resources Corporation*

Abstract

In the Samtan and Daedeok mine drainage treatment facilities in South Korea, lime is used as an alkaline reagent. Previous evaluations of the required lime dosage, using S/W modelling and batch tests for the influent of these facilities, showed discrepancies between the two approaches. Batch experiments were conducted to evaluate the effects of additional operational factors, specifically the concentration of the lime slurry and the dosing rate, on the required lime dosage. The results indicated that lower lime concentrations and slower dosing rates led to reduced lime consumption during the neutralization process.

Keywords: Mine drainage, hydrated lime, lime slurry concentration, dosing rate

Introduction

Hydrated lime ($Ca(OH)_2$) is widely used in mine drainage treatment to increase pH and reduce dissolved metal concentrations. Although predictive tools such as PHREEQC–AMDTreat are commonly used to estimate the required dosage of alkaline reagents, additional factors can influence the actual lime requirements. Understanding these operational factors and their underlying mechanisms is essential for optimizing lime dosage, reducing treatment costs, and lowering carbon emissions associated with hydrated lime production.

This study compared three dosage estimates: (1) predictions from PHREEQ-N–AMDTreat-based design software, (2) experimental dosages determined through batch dosing tests, and (3) actual operational dosages at two mine drainage treatment facilities in South Korea (the Daedeok treatment facility and the Samtan leachate treatment facility). To evaluate the effect of lime slurry concentration, batch tests using influent from the Samtan facility were conducted with 1%, 6%, 11%, and 17% (wt%) hydrated lime slurries to reach pH 9. In addition, dosing-rate experiments were performed using influent from the Daedeok facility and synthetic influent prepared with $FeCl_3$ and $AlCl_3$

Methods

Treatment facility investigation

During both the dry and wet seasons, water quality was measured at each unit process of the Samtan leachate treatment facility and the Daedeok treatment facility. In addition, hydrated lime consumption and sludge generation at each facility were evaluated.

PHREEQ-N-AMDTreat-based design software prediction

Based on the influent water quality data obtained from the facility investigation, the required hydrated lime dosage and the amount of sludge generated at pH 7, 8, 9, and 10 were predicted using software designed based on PHREEQC–AMDTreat.

Experimental dosage determined through batch dosing tests

Influent water collected from each facility during the treatment facility investigation was titrated to pH 7, 8, 9, and 10 using a 1% (W/V) hydrated lime solution. The lime dosage and sludge generation at each pH condition were evaluated and subsequently compared with the values predicted by the software.

Table 1 Water quality of influent water from each treatment facility.

Treatment Facility	pH	Fe (mg/L)	Al (mg/L)	Mn (mg/L)	SO_4^{2-} (mg/L)
Samtan leachate	3.51	1.0	51.3	8.3	588.8
Daedeok	2.67	416.9	230	6.5	6271.4

Table 2 Hydrated lime dosage at concentrations of 1%, 6%, and 11% to reach pH 9.

Lime concentration (wt%)	1	6	11
Lime dosage (mg/L)	110.8	168.0	187.5

Table 3 Hydrated lime dosage at concentrations of 6%, 11%, and 17% to reach pH 9.

Lime concentration (wt%)	6	11	17
Lime dosage (mg/L)	243.6	278.2	300.0

Batch test to evaluate the effect of lime slurry concentration and dosing rate

To evaluate the effect of hydrated lime concentration on lime dosage, influent water collected from the Samtan leachate treatment facility during the wet season was titrated to pH 9 using hydrated lime solutions with concentrations of 1%, 6%, 13%, and 20%. The lime dosage and sludge generation were then evaluated and compared according to lime concentration.

To evaluate the effect of lime dosing rate on lime consumption, influent water collected from the Daedeok treatment facility during the dry season was dosed with a 1% (W/V) hydrated lime solution at rates of 0.5, 1, and 5 mL/min until a total volume of 50 mL was added. The final pH reached at each dosing rate was then evaluated.

To identify the factors influencing differences in lime dosage according to dosing rate, synthetic influent prepared using $FeCl_3$ and $AlCl_3$ (Fe 400 mg/L, Al 250 mg/L) was used. A 1% (W/V) hydrated lime solution was dosed into the synthetic influent at rates of 0.5, 1, and 5 mL/min, and the pH values measured 30 minutes after dosing were evaluated.

Results and discussion

A comparison between the actual lime consumption at the treatment facilities and the lime dosage determined from batch experiments showed that, although the full-scale operational dosage was not excessive compared to the modeled dosage, it was higher than the batch experiment results. Specifically, it was approximately 36% higher for the Samtan facility and 16% higher for the Daedeok facility than the values obtained from batch experiments.

This discrepancy observed between the batch experimental results and the full-scale treatment facility dosages at both facilities was considered to be influenced by additional factors during the lime dosing process. Among these factors, hydrated lime concentration and lime dosing rate were identified as potential contributors. Therefore, additional batch experiments were conducted to evaluate the effects of these two factors.

The results of tests evaluating the effect of hydrated lime concentration on lime dosage showed that lower lime concentrations required smaller amounts of lime to achieve pH 9 (Tables 2 and 3).

The reactor dosed with 1% hydrated lime required 34% and 40% less lime than the reactors dosed with 6% and 11% lime, respectively. In addition, the reactor dosed with 6% lime required 12% and 19% less lime than the reactors dosed with 11% and 17% lime, respectively. These results indicate that lower hydrated lime concentrations require smaller amounts of lime to reach a given pH.

Batch experiments were conducted using influent from the Daedeok treatment facility to evaluate the effect of lime dosing rate on lime dosage. The results showed that lower dosing rates resulted in reduced lime consumption (Fig. 1).

Little increase in pH was observed near pH 3.0 and 4.3, whereas in other pH ranges, pH increased with different slopes under all three conditions. In addition, higher lime dosing rates required larger amounts of lime to overcome the pH plateau and further increase the pH. As a result, even when the same amount of lime was added, differences in the final pH achieved were observed depending on the dosing rate. Additionally, the increase in pH within the pH range of 5.8–9.0 became smaller as the lime dosing rate increased, even at the same lime dosage. This behavior was considered to result from the greater influence of gypsum on hydrated lime particles at higher dosing rates, which affected the pH elevation behavior. (Fig. 1).

Two possible explanations were considered for this phenomenon. First, the high sulfate concentration in the influent may lead to gypsum formation, which could coat the surface of hydrated lime particles. Second, the pH ranges around 3.0 and 4.3 correspond to the precipitation regions of $Fe(OH)_3$ and $Al(OH)_3$, suggesting that the presence of dissolved metal ions may influence the reaction behavior. To examine these hypotheses, synthetic influent with negligible sulfate concentrations was prepared using $FeCl_3$ and $AlCl_3$, and batch experiments were conducted.

Batch experiments conducted using the synthetic influent with negligible sulfate showed results similar to those obtained with influent from the Daedeok treatment facility. Little increase in pH was observed at pH 3.0 and 4.3, whereas in other pH ranges, pH increased with a similar slope under all conditions. In addition, the amount of lime required to further increase the pH differed depending on the dosing rate (Fig. 2).

The experimental results suggest that the difference in lime dosage according to dosing rate was primarily influenced by dissolved metal ions. When the pH change was evaluated 30 minutes after lime addition, the decrease in pH in the reactor dosed at 1 mL/min was smaller than that observed in the reactor dosed at 0.5 mL/min. In contrast, the reactor dosed at 5 mL/min showed a slight increase in pH. These results suggest that metal ions may coat the surface of hydrated lime particles and that higher dosing rates may lead to a greater extent of particle coating. As time passes, the coated

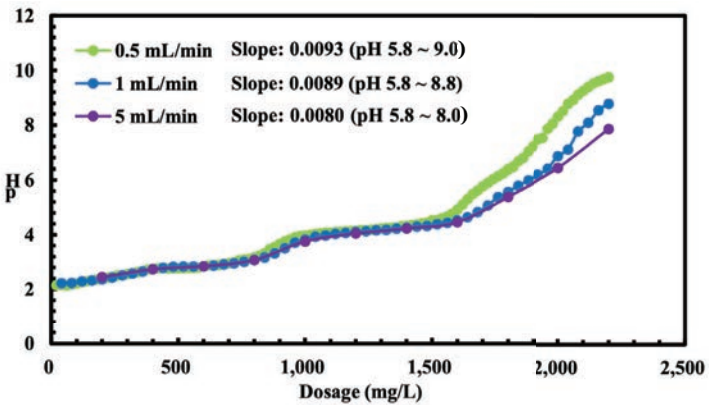

Figure 1 pH variation with lime dosage at different dosing rates for influent from the Daedeok mine drainage facility.

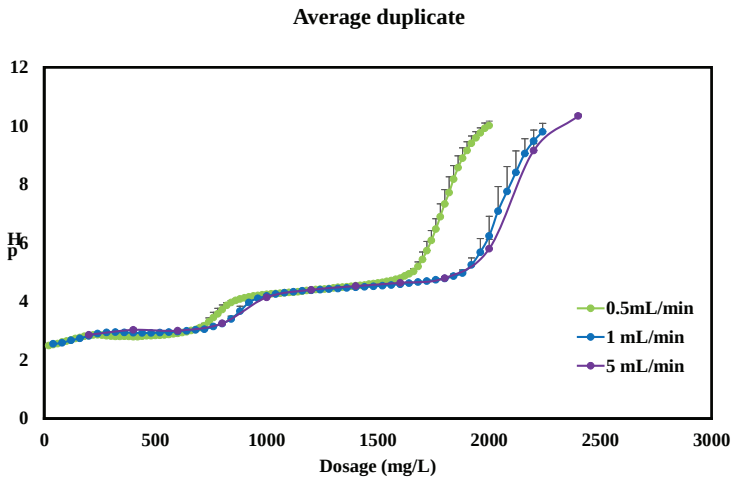

Figure 2 pH variation as a function of lime dosage at different dosing rates for synthetic influent with negligible sulfate concentrations.

Table 4 Difference in pH between immediately after lime addition and after 30 minutes at different dosing rates.

Dosage rate	pH after 0 min (A)	pH after 30 min (B)	pH change (B-A)
0.5 mL/min	10.16	9.88	-0.28
1 mL/min	10.19	9.99	-0.20
5 mL/min	10.32	10.45	0.13

lime gradually dissolves, which is considered to contribute to the observed pH behavior (Table 4).

According to the PHREEQ-N-AMDTreat modeling results, precipitation of $Fe(OH)_3$ and $Al(OH)_3$ was predicted to occur near pH 3.0 and 4.3, respectively (Figs. 3 and 4), in both the experiment using influent from the Daedeok treatment facility and the experiment using synthetic water containing negligible sulfate concentrations. These pH ranges corresponded to buffering zones in which pH elevation was temporarily inhibited, suggesting that the formation of fine metal hydroxide precipitates retarded the dissolution of $Ca(OH)_2$.

Furthermore, in the experiment using the Daedeok influent, the predicted amount of precipitated gypsum reached its maximum near the pH at which rapid pH increase begam. Differences in the pH increase gradient were also observed between the two experimental conditions. These findings suggest that gypsum formation influenced the pH elevation behavior. As shown in Figs 1 and 2, gypsum precipitation was considered to contribute to the differences in the pH elevation gradients observed between two experiments.

Conclusions

In this study, hydrated lime concentration and lime dosing rate were evaluated as key factors affecting lime consumption. The results showed that lower lime concentrations required smaller amounts of lime to reach the target pH. In addition, lower dosing rates also resulted in reduced lime consumption. The variation in lime dosage with dosing rate can be attributed to two main factors. First, the coating of hydrated lime particles by dissolved metal ions leads to a temporary stagnation in pH increase, and the amount of lime required to overcome this region varies depending on the dosing rate. Second, differences in the

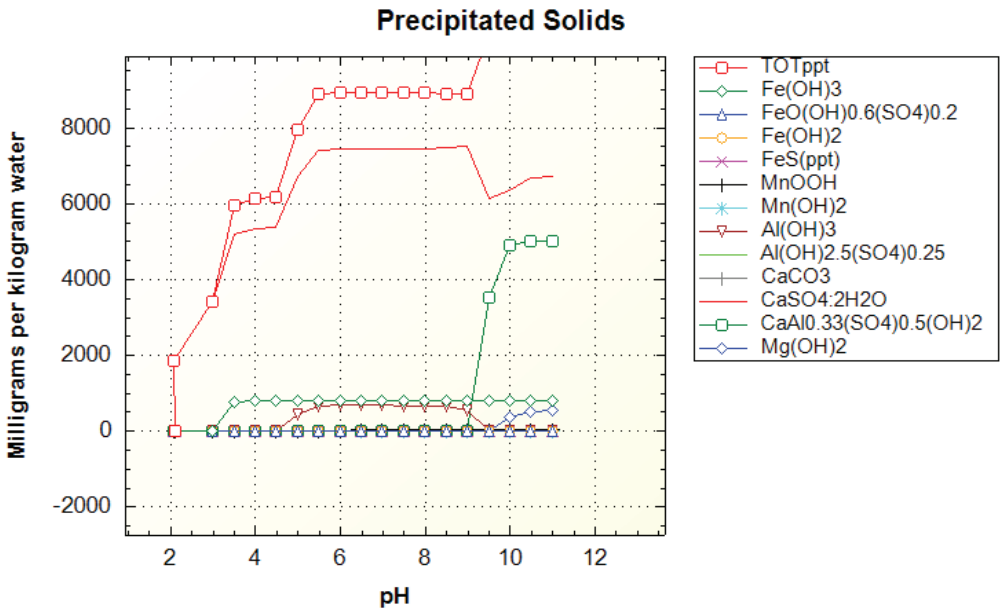

Figure 3 Amount of precipitated solids according to pH after pH after lime dosing for the Daedwok mine drainage, which was predicted using PHREEQ-N-AMDTreat.

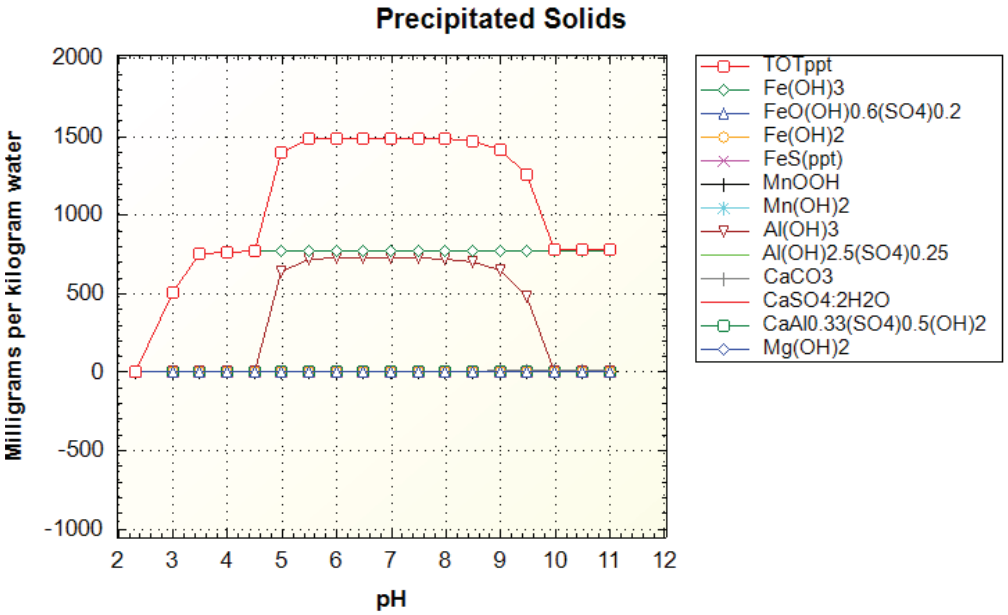

Figure 4 Amount of precipitated solids according to pH after lime dosing for synthetic influent with negligible sulfate, which was predicted using PHREEQ-N-AMDTreat.

slope of pH increase suggest that gypsum formation contributes to the coating of lime particles, thereby influencing the overall pH evolution behavior.

Acknowledgements

This work was supported by R&D Project of the Korea Mine Rehabilitation and Mineral Resources Corporation in 2025 and 2026.

Sorption of Arsenic and Fluoride in Neutral Mine Drainage Using Fe-Based Sorbents

Myoung-Soo Ko[1], Su-Jin Kim[1], Oh-Hun Kwon[2]

[1]*Kangwon National University, Korea, Republic of (South Korea)*
[2]*Korea Mine Rehabilitation and Mineral Resources Corporation (South Korea)*
msko@kangwon.ac.kr, ORCID 0000-0002-7404-7958

Abstract

Arsenic (As) and fluoride (F) are persistent contaminants in mine drainage that pose substantial environmental and health risks even at low concentrations. Unlike trace metals, As and F remain in dissolved ion under neutral pH conditions, making their removal challenging with conventional treatment methods. Adsorption is a promising alternative due to its space efficiency, operational simplicity, and cost-effectiveness. This study investigates the sorption mechanisms of As and F using two iron (Fe)-based adsorbents: AMDS (MIRESORB, E&Chem Solution) and GFH (GEH 102, Wasserchemie GmbH & Co. KG). AMDS contains 50.2 wt% of Fe, while GFH contains 73.1 wt% of Fe, with specific surface areas of 274.9 m^2/g and 316.5 m^2/g, respectively. Kinetic and isotherm sorption experiments were conducted at pH 7.4 to simulate neutral mine drainage conditions. The results showed that As sorption onto both AMDS and GFH followed the pseudo-second-order kinetic model and the Langmuir isotherm model, indicating monolayer adsorption through a chemisorption mechanism. While GFH exhibited a slightly higher maximum adsorption capacity (q_m = 42.4 mg/g) than AMDS (q_m = 32.3 mg/g), AMDS demonstrated excellent sorption efficiency relative to Fe content. The F sorption followed the pseudo-second-order kinetic model and followed the Freundlich isotherm model, suggesting multilayer adsorption via chemical interactions. The Freundlich sorption coefficient (K_F) was 0.21 for AMDS ($R^2 > 0.99$) and 0.43 for GFH ($R^2 > 0.98$), indicating that GFH had a higher fluoride adsorption capacity. Both AMDS and GFH exhibited adequate sorption performance for As and F removal. However, considering cost-effectiveness and removal efficiency, AMDS emerged as a promising sorbent for neutral mine drainage treatment. Since As and F are negatively charged ions, they would compete for adsorption sites, influencing removal efficiency. To validate the competitive sorption behavior of As and F, further research is being conducted to assess how their co-existence affects sorption mechanisms and capacity. Understanding competitive sorption dynamics is essential for developing effective mine water treatment strategies in areas where both contaminants are present.

Keywords: Arsenic, fluoride, sorption, mine drainage, iron-based sorbents

Introduction

Mine drainage, originating from abandoned mine, contains various toxic elements, including metals, metalloids, and nonmetals. Common metallic elements such as Fe, Al, and Mn in mine drainage precipitate by neutralization, however, arsenic (As) and fluoride (F) remain as dissolved anionic species under neutral pH. Thus, distinct treatment methods are required to remove As and F from mine drainage. Precipitation, coagulation, ion exchange, and electrodialysis are potential candidate methods. These methods need high operational costs and extensive areas. Sorption process is considered an applicable method for As and F removal due to operational simplicity and low energy requirement. Iron (hydr)oxides has focused notable attention as an effective sorbent for As and F, because of high reactive surface area and geochemical affinity. This study investigates the sorption behaviors of As and F

under neutral pH using iron-based materials. furthermore, competitive desorption process evaluated in the presence of both As and F to simulate the complex chemical environment of actual mine drainage.

Methods

Characterization of Adsorbents

Two iron-based adsorbents were used: MIRESORB (AMDS, E&C Solution, Korea), derived from mine drainage sludge, and granular ferric hydroxide (GFH, Wasserchemie GmbH & Co., Germany). Mineralogical properties and major element composition were determined by XRD (D2 PHASER, Bruker, Germany) and XRF (ZSX Primus II, Rigaku, Japan). Surface morphology was observed using SEM–EDS (JSM-7900F, JEOL, Japan). Specific surface area and pore structures were analyzed using BET (BELSORP MAX X, MicrotracBEL, USA). The point of zero charge (pH_{pzc}) was determined following Balistrieri LS, Murray JW (1981).

Adsorption Isotherms and Kinetics

Batch experiments were conducted in duplicate to evaluate As and F adsorption. For isotherms, initial concentrations

Table 1 *Surface area and major elements compositions of adsorbents.*

Adsorbent	Surface Area (m^2/g)	Elements composition (wt%)								
		O	Fe	Mg	Al	P	S	Mn	As	F
AMDS	274.9	36.4	50.3	2.5	8.3	0.2	1.7	0.7	-	-
GFH	316.5	26.2	73.1	-	0.2	0.1	0.3	0.2	-	-

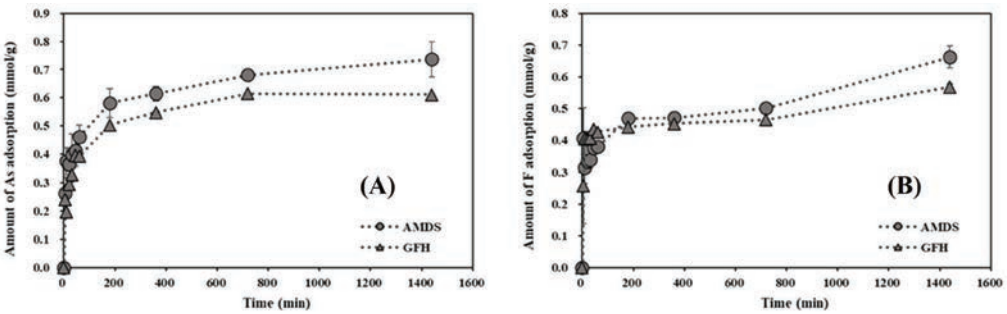

Figure 1 *Adsorption kinetics of (A) As and (B) F onto AMDS and GFH.*

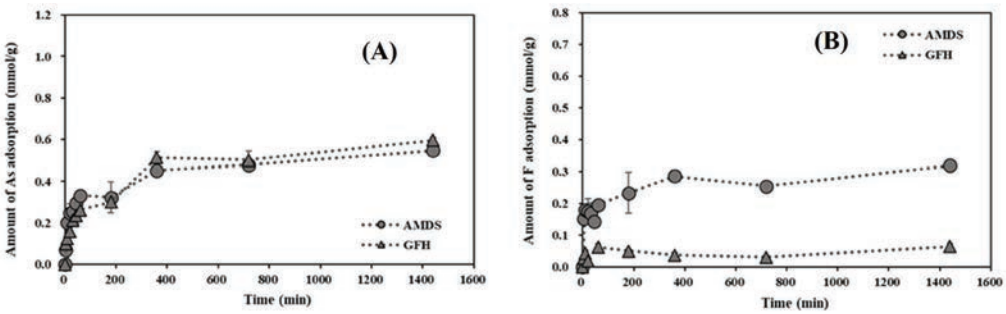

Figure 2 *Adsorption capacity of (A) As and (B) F with competitive conditions.*

(0.02–1.0 mM) were prepared in 0.1 M HEPES buffer. Adsorbent (0.01 g) was reacted with 10 mL of solution for 24 h. Kinetic studies used an initial concentration of 1.5 mM, with samples collected at intervals from 5 to 1440 min. Langmuir, Freundlich, pseudo-first order (PFO), and pseudo-second order (PSO) models were applied to describe the adsorption behavior.

Competitive Desorption

A three-step procedure, which are saturation, washing, and desorption, was performed at 25 °C and pH 7.4. Adsorbents were saturated with 10 mM As or F for 24 h, then recovered by centrifugation. Saturated adsorbent samples were washed three times with 10 mL of ethanol (99.5%) for 5 min each. Finally, desorption was induced by adding a counter-ion solution (10 mM) for 24 h, followed by filtration (0.45 μm) to assess competitive behavior.

Results and Discussion

Adsorbent Characterization

The GFH exhibited a higher Fe content (73.1 wt%) and a larger specific surface area (316.51 m^2/g) compared to AMDS (Table 1). Despite the lower Fe content in AMDS, its specific surface area remains comparable to that of GFH, suggesting a highly porous structure suitable for the sorption of dissolved ions.

Adsorption Kinetics of As and F

The adsorption of both As and F onto AMDS and GFH followed the pseudo-second order (PSO) kinetic model (R^2 > 0.99) (Figure 1). The kinetics indicate that the rate-limiting step for As and F presence during chemisorption process involving valence forces. The rapid initial sorption process observed in the first 180 min suggests that the active surface sites of the iron (hydr) oxides are readily accessible at pH 7.4.

Adsorption Isotherms and Capacity

The equilibrium results for As were described by the Langmuir isotherm model, implying monolayer adsorption on a surface with a finite number of identical sites. GFH showed a higher maximum adsorption capacity (q_m = 42.4 mg/g) than AMDS (q_m = 32.3 mg/g). However, sorption efficiency of AMDS showed higher by normalized to Fe content. Fluoride adsorption results followed the Freundlich isotherm model (R^2 0.98–0.99), indicating multilayer adsorption on heterogeneous surfaces. The Freundlich constant (K_F), representing the adsorption capacity, was 0.43 for GFH and 0.21 for AMDS. The higher K_F and q_m values for GFH can be attributed to abundant of Fe content and surface area. Both adsorbents achieved sufficient removal performance under neutral conditions.

Sorption Mechanisms and Competitive Behavior

Because As and F are negatively charged at neutral pH, the competitive reaction would occur at the same reactive sites on the adsorbent surface (Figure 2). This behavior is attributed to the formation of inner-sphere complexes with hydroxyl groups on the iron (hydr)oxide surface. The presence of As influence the F desorption from the adsorbents due to the geochemical affinity. Further investigation into the competitive sorption dynamics is currently being conducted to assess the performance of AMDS in complex mine water matrices.

Conclusions

This study evaluated the efficacy of two iron-based adsorbents, AMDS and GFH, for the removal of As and F from neutral mine drainage. Both materials demonstrated rapid adsorption kinetics, following the pseudo-second-order model, that implied rate limiting chemisorption. The equilibrium data revealed that As adsorption followed the Langmuir isotherm, indicating monolayer coverage, while F adsorption was better described by the Freundlich model, suggesting multilayer adsorption on heterogeneous surface sites. Although GFH exhibited higher maximum adsorption capacities, AMDS showed outstanding removal efficiency relative to Fe content and specific surface area. Both As and F removal were driven by the formation of inner-sphere

complexes with surface hydroxyl groups. However, since both contaminants exist as anionic species at neutral pH, competitive adsorption occurs, which may influence overall treatment performance in complex mine water matrices. In conclusion, AMDS emerged as a promising and cost-effective alternative for treating mine drainage containing both As and F.

Acknowledgements

This research was supported by R&D Project of the Korea Mine Rehabilitation and Mineral Resources Corporation (KOMIR) in 2024.

References

Balistrieri LS, Murray JW (1981) The surface chemistry of goethite (α-FeOOH) in major ion seawater. Am J Sci 281(6): 788–806. https://doi.org/10.2475/ajs.281.6.788

IMWA 2026
Jeongseon

In-Lake Water Treatment of Post-Mining Lakes – Reactivity of Lime Products

Katja Kunze[1], Felix Bilek[2]

[1]*Lausitzer und Mitteldeutsche Bergbau-Verwaltungsgesellschaft, Knappenstr. 1, 01968 Senftenberg, Deutschland, Katja.Kunze@LMBV.de*

[2]*GFI Grundwasser-Consulting-Institut, Meraner Straße 10-12, 01217 Dresden, fbilek@gfi-dresden.de*

Abstract

A new method has been developed which determines the alkalinity release of limestone powders in water under neutral conditions. This shows clear differences between the various limestone powder products. In addition, the products were also tested at different pH values. A significant decrease in alkalinity release was observed with increasing pH values, whereby product differences again came into play. The comparison with water treatment campaigns that have been carried out confirms in principle the correlations found in the laboratory. However, further influencing factors that led to the deviation from the norm can be identified in order to make future measures more efficient.

Keywords: Lime, neutralisation equivalent, post-mining lake, water treatment

Introduction

The remediation of the legacy of lignite mining became a state responsibility after the reunification of Germany. The LMBV restoration of the Lusatian water balance mainly consists of the refilling of ground water deficits, the creation of secure pit lakes, their connection to rivers and the enhancement of water quality.

Water treatment of post-mining lakes is usually carried out using in-lake technology. With this technology limestone powders are distributed by vessels into the entire lake water body thereby mixing it with the lake water to maximise lime dissolution kinetics. In this process, the entire lake water body is raised to a neutral pH value during initial treatment. Due to the continuous inflow of acidic groundwater into the post-mining lakes, repeated follow-up treatments are necessary to maintain neutral pH values. Calcium carbonate-containing neutralizing agents in the form of limestone powder are usually used for this purpose. The limestone powders available on the market are characterized by different chemical (e.g., purity) and physical (e.g., grain size) properties. When treating water in the neutral range, the various limestone powders therefore release varying amounts of alkalinity into the water body.

Until now, there has been no standard for determining the alkalinity release of carbonate lime products with respect to lake waters. On order from LMBV, a procedure for determining the reactivity of carbonate lime products was developed and a procedural specification was created.

Methods

Initial preliminary investigations to identify a practicable investigation concept have shown the titration to a stable pH value (pH-stat titration) method to be effective. This method experimentally measures the alkalinity of the lime product dissolved in solution as a neutralisation equivalent (Neq) based on acid consumption. The extensive series of experiments took into account factors that theoretically influence the dissolution kinetics of calcium carbonate particles, such as temperature, pH value, CO2 partial pressure, ionic strength, turbulence, particle diameter. The aim of developing the method was to ensure sufficient reproducibility of the measurement results.

As a result, a procedural rule was defined stipulating that a target pH value of 6.5 must be kept for titration over 90 minutes. The limestone powder sample must be homogenised and dried before testing. The

suspension is made in deionised water, which is in CO2 partial pressure equilibrium with the laboratory air. This must be stored openly in the laboratory for at least 12 hours before the test. 0.1 molar hydrochloric acid is used for titration. To ensure a defined energy input via the magnetic stirrer for the preparation of the suspension, the speed must be adjusted so that the resulting vortex occupies 1/3 of the water height in the beaker. The consumption of hydrochloric acid is recorded after 90 minutes and the neutralisation equivalent (Neq) is calculated using the mass of the tested lime product. Eleven different lime products were examined as part of the method development. The results are visualised in Fig. 1. In addition, the alkalinity content according to the product data sheet is shown for comparison. Previous experience has shown that the alkalinity content can be almost completely released in an acidic water environment. However, to fulfill legal regulations the seawater treatment must ensure a lake water pH value of at least 6.0. This is why the developed procedure focusses on alkalinity release under neutral conditions.

The Neq90 values for the limestone products examined are compared in Table 1 with their geological origin, chemical composition and mean particle diameter.

The results clearly show the product-specific differences between limestone powders in terms of alkalinity release under neutral conditions. It can be seen that geologically young limestones, known as chalk, exhibit a substantial higher alkalinity release due to their large specific surface area. Older, more compact or metamorphically altered limestones, even when finely ground, show comparatively lower dissolution and alkalinity release in neutral water.

In addition, the reactivity of four selected limestone powders, specifically lime 2, 7, 10 and 11 was examined in a pH range of 5.5 to 7.5. As expected, there is a clear pH dependence, with alkalinity release increasing clearly as the pH value decreases for all products tested. At a pH value of 5.5, between approximately 65% and 90% of the maximum possible alkalinity release was measured, depending on the respective product. At a pH value of 7.5, only 13% to 14% of the product's alkalinity could be transferred to the water phase. The differences in the Neq value between the individual lime products decrease as the pH value increases (see Fig. 2).

In a further study, the effectiveness of a total of 86 water treatment campaigns using limestone powder was investigated at

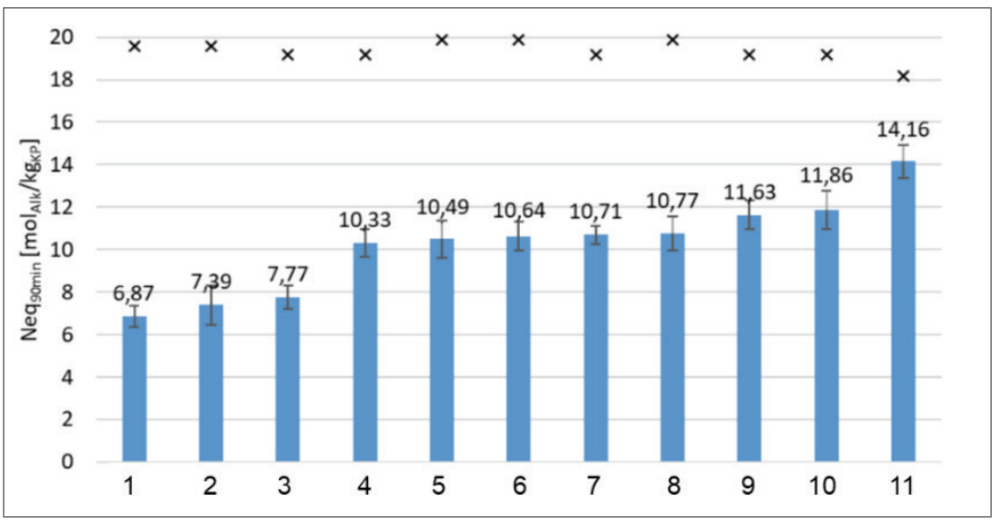

Figure 1 Neq90 values [mol/kg] (columns) of the 11 carbonate lime products used for method development compared to the alkalinity content according to the product data sheet (crosses) (BTU, GFI, 2021).

Table 1 Properties of the lime products examined.

lime	geological era	chemical composition [%]			Median particle diameter d50 [µm]	Neq90 [mol/kg]
		$CaCO_3$	$MgCO_3$	Fe_2O_3		
1	Devon	96,9	0,9	0,2	12,0	6,87
2	Devon	97,0	0,9	0,2	8,2	7,39
3	Early Palaeozoic	96,0	<1,0	0,3	3,0	7,77
4	Jura	>90,0	<1,0	<0,2	3,1	10,33
5	Jura	99,3	0,3	0,1	5,0	10,49
6	Jura	99,3	0,3	0,1	4,5	10,64
7	Jura	>95,0	<1,0	<0,2	3,1	10,71
8	Jura	99,3	0,3	0,1	3,5	10,77
9	Jura	>95,0	<1,0	<0,2	3,1	11,63
10	Jura	>95,0	<1,0	<0,2	2,9	11,86
11	Cretaceous	90,0	1,0	0,5	3,0	14,16

a total of ten post-mining lakes in Lusatia. According to [LUA, 2001], the overall efficiency η_{ges} of an in-lake process based on the mass application of the neutralising agent can be represented as the product of the material efficiency ŋ0 and the technological-chemical efficiency ŋ1 (IWB, 2025).

Equation 1: Overall efficiency of an in-lake process (LUA, 2001) .

$\eta_{ges} = \eta_0 \cdot \eta_1$

η_{ges} Overall efficiency [-]

η_0 material efficiency (active ingredient content) [-]

η_1 technological-chemical efficiency [-]

While the material efficiency η_0 is a largely stable product property of the neutralising agent (material purity), the technological-chemical efficiency η_1 is the ratio of the alkalinity that has become effective in the lake in relation to the alkalinity supplied with the material. This is influenced by various factors, such as the genesis and structure of

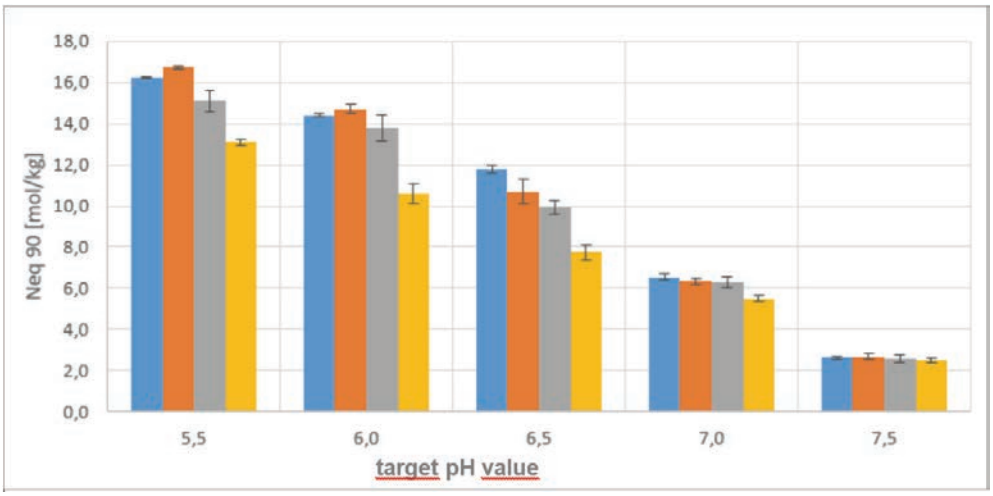

Figure 2 Neq90 values [mol/kg] of the four selected lime products at different final pH values in the pH-Stat test (GFI, 2025).

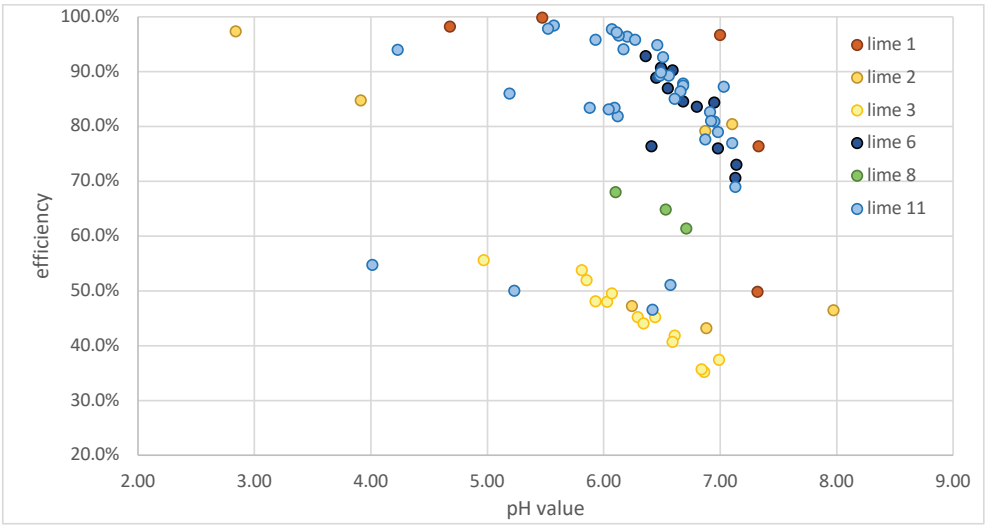

Figure 3 *Technological-chemical efficiency of in-lake treatments as a function of the pH value of six different limestone powder products.*

the limestone product (density, grain size distribution, specific surface area of the lime particles), the variable physical and hydrochemical conditions in the lake water (pH value and water temperature), the lake-specific boundary conditions (water depth, wind exposure of the post-mining lake) and technological factors such as application as a suspension or dry dosing, the distribution system and others (IWB, 2025).

The evaluation of the technological-chemical efficiency of in-lake measures at ten post-mining lakes and using six different lime products shows a clear correlation between the efficiency and the average pH value of the lake water during treatment. The correlations determined in the laboratory in Fig. 1 could in principle be found again in real-world applications (see Fig. 3). As a rule, the efficiency of lake treatment decreases as the pH value rises. This is particularly evident for lime products 3, 8 and 11 (Fig. 3) which are frequently used.

Furthermore, the evaluation shows that material with predominantly good technological-chemical efficiency levels, such as material no. 11, also appears sporadically in areas with efficiency levels <55%. These campaigns should be given special attention in the further evaluation. Here, the other influencing factors that led to the deviation from the norm must be determined. Possible causes are seen in the dosing rate, i.e. the amount of neutralising agent added per volume of water, the input energy, the water temperature and the hydrochemistry.

The in-lake treatment was carried out both by vessels and by stationary plants on the shore. The water treatment vessels either dose the lime products as a dry powder via a rotary valve or as a premixed suspension into the water. The propper distribution of the lime suspension in the lake is supported by the movement of the vessel. In the case of the shore-based systems, the lime suspension is fed through a pipeline and discharged into the water via nozzles on a discharge pontoon anchored in the post-mining lake. Mixing is primarily achieved by the impulse of the water flux. In both processes, currents within the lake contribute to further mixing.

The evaluation of the dosing technology used in 68 campaigns examined does not reveal any significant differences (see Fig. 4).

Results

The determination of the product-specific parameter neutralisation equivalent (Neq) for lime products in in-lake treatment and the model-based evaluation of the effectiveness

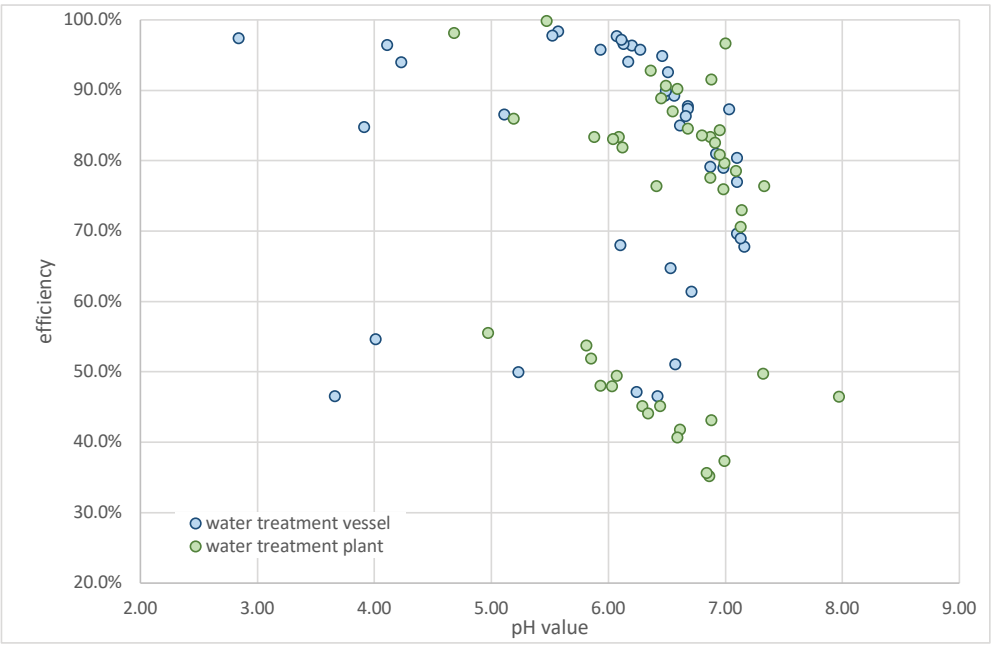

Figure 4 *Technological-chemical efficiency of in-lake treatments as a function of the pH value of two different application technologies.*

of in-lake measures in Lusatia have revealed both product-specific differences and the strong pH dependence of the dissolution of lime products. The dosing rate is also a key parameter influencing efficiency (IWB, 2025).

This suggests that the start and end of the treatment measure should be at the lower end of the pH range (pH 6.0 to 7.0) if possible. The technical prerequisite for such flexible treatment is a ready-to-use, stationary plant or vessel available in the water body. In addition, it is crucial to monitor the water quality at regular intervals and to adjust the treatment measure if too high pH values are encountered.

Conclusions and outlook

The results of this study are used for purchasing limestone powder for in-lake treatment. Suppliers are no longer asked to provide a quantity of lime product, but rather the required alkalinity. Water treatment measures for post-mining lakes with a pH value of more than 7 will also be avoided in the future. This will make in-lake treatments more cost-effective. In addition, quality monitoring and evaluation of measures is based on these more reliable laboratory data.

References

LUA (2001): Post-mining lakes. Water quality and water management remediation. Conceptual approaches and initial experiences. Brandenburg State Environment Agency (ed.). Studies and Conference Proceedings, Cottbus, Vol. 35, 2001, 77 pp.

BTU, GFI (2021): Report – Development of a procedural guideline for determining the reactivity of lime products, BTU Cottbus-Senftenberg, GFI GmbH Dresden, 15 April 2021

LMBV (2024): Procedural guideline for determining the reactivity of carbonate lime products at a pH value of 6.5 - Neq90, Version 2.0, LMBV, 4 September 2024

GFI (2025): Reactivity of lime products in the pH range of 5.5 to 7.5, GFI GmbH, 7 October 2025

IWB (2025): TA17-2: Update of the technology and efficiency comparison of in-lake processes for the neutralisation of post-mining lakes, 23 December 2025

IMWA 2026
Jeongseon

Advanced Continuous-Monitoring Column Test for Sedimentation Analysis of Mine Drainage Sludge

Dong-Kil Lee[1], Youngwook Cheong[1], Sangwoo Ji1, Giljae Yim[1]

[1]*Korea Institute Geoscience and Mineral Resources (KIGAM), 124 Gwahang-no, Yuseong-gu, Daejeon 34132, South Korea, corresponding author's phone number: +82-42-868-3228, e-mail address: ldk@kigam.re.kr, ORCID 0000-0003-3121-6405*

Abstract

Understanding the settling behavior of mine drainage sludge is critical for enhancing the performance and reliability of sedimentation systems used in acid mine drainage (AMD) treatment. Traditional settling column tests depend on discontinuous sampling, which limits their ability to capture real-time concentration changes, accurately define the hindered settling zone, and evaluate depth-specific removal efficiency. These limitations restrict effective settling pond design and hinder prediction of sludge movement and accumulation. This study introduces a column monitoring system that integrates ten turbidity sensors with periodic photometric TSS calibration to continuously measure concentration variations along a 2-m column. By converting turbidity signals into accurate TSS values and constructing a temporal–spatial TSS distribution map, the method enables high-resolution observation of sedimentation dynamics that cannot be achieved with conventional batch sampling techniques. The proposed system clearly identifies the hindered settling region as the zone where TSS remains constant over time and visualizes the downward progression of the precipitate interface. Results show that complete removal at any depth occurs only when the interface passes that location, with the highest settling velocity and removal efficiency observed between 0.4 and 1.4 m below the water surface. The maximum overflow rate achieving 100% removal occurs near 1.2 m depth, corresponding to the region of most rapid interface descent. The continuous-monitoring approach greatly improves the ability to evaluate sedimentation behavior and provides a more accurate framework for optimizing settling pond design, overflow rate selection, and sludge management strategies. Its applicability extends beyond mine drainage treatment to water purification, wastewater engineering, and industrial processes where real-time assessment of settling performance is essential.

Keywords: Mine drainage, sedimentation, column settling test, total suspended solids, hindered settling

Introduction

Sedimentation of neutralization sludge is a key unit process in acid mine drainage (AMD) treatment because it controls clarified-water quality, sludge inventory, and downstream handling. Active neutralization using lime or caustic soda produces metal-rich hydroxide precipitates that must be separated in settling ponds or clarifiers (Brown *et al.* 2002; Akcil and Koldas 2006; Wolkersdorfer 2023). Therefore, the assumed surface overflow rate (SOR) and the dominant settling regime directly affect treatment reliability and pond sizing (U.S. Environmental Protection Agency 2023).

Related studies show the need for depth-resolved observation. The settling column test was first developed to determine slime-settling tank capacity (Coe and Clevenger 1916) and is still used for sludge and wastewater solids. Recent international work has improved column-test interpretation through sludge densification experiments (Roche *et al.* 2022), while turbidity-based monitoring has been used as a practical proxy for suspended solids, although the turbidity-TSS relationship depends on particle properties and site conditions (Gao 2006). In South Korea, Lee *et al.* (2023)

characterized depth-dependent properties of mine drainage sediments in settling ponds, and Lee *et al.* (2025) demonstrated that sensor-based column monitoring can reveal temporal and spatial TSS distributions. These studies indicate that continuous, depth-resolved monitoring can provide information that conventional intermittent sampling cannot capture.

Conventional settling column tests typically rely on intermittent sampling at a limited number of depths. Such batch-style sampling can miss rapid concentration changes, obscure the spatial extent of the hindered-settling zone, and complicate the derivation of depth-specific removal and overflow criteria. These limitations become more severe for flocculent mine drainage sludge, where the turbidity-TSS relationship may drift during settling because particle size distribution, floc structure, and optical properties evolve.

Here we introduce an advanced, continuous-monitoring column test that integrates multi-depth turbidity sensing with periodic TSS calibration, enabling reconstruction of a spatiotemporal TSS distribution map. Using this map, we (i) identify the hindered-settling region consistently, (ii) quantify interface dynamics, and (iii) compute depth-specific maximum SOR values for complete (100%) removal as a design linkage to full-scale settling ponds.

Methods

Instrumentation and data logging

Ten low-cost turbidity sensors (DFRobot Gravity analog turbidity sensor, SEN0189) were used as optical proxies for suspended solids (DFRobot, accessed 2026-03-11). Sensor signals were recorded as analog voltage at 1 Hz using a multi-channel data-logging unit (Arduino Mega class) with an RTC and microSD storage. To reduce high-frequency noise, 1-Hz measurements were aggregated to 1-min means for analysis.

Settling column configuration

A transparent acrylic column (2.0 m water depth) was equipped with ten turbidity sensors and matching sampling taps installed at the same elevations (Fig. 1). A scale and thermometer were placed to visually track the precipitate interface and temperature. The column was filled to 2.0 m with mine drainage sludge generated by AMD neutralization.

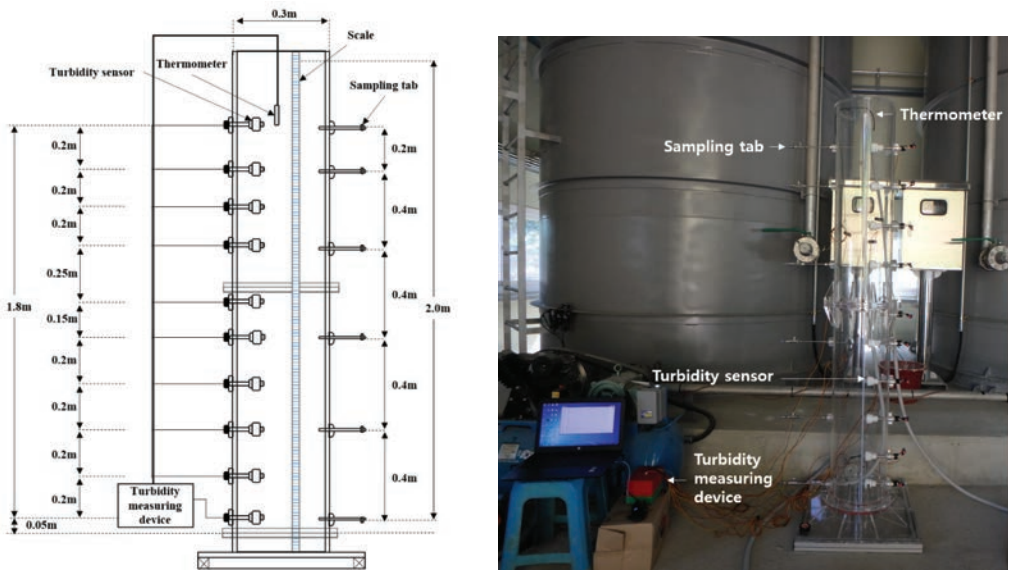

(a) Schematic diagram *(b) Photo of the equipment*

Figure 1 *Column experimental equipment.*

TSS measurement and calibration strategy

Grab samples were collected from all sampling taps every 10 minutes and analyzed for TSS using a Hach DR900 spectrophotometer following the photometric suspended-solids method at 810 nm (Hach Company 2015). Each sample was gently homogenized, transferred to a clean cell, and measured after blank correction. These periodic TSS values were used to calibrate and verify the voltage-TSS relationship at each sensor over time, enabling conversion of continuous voltage traces into quantitative TSS profiles. A preliminary response check using a coffee solution with known TSS levels (Fig. 2) was also performed to assess inter-sensor variability and sensitivity loss at high concentrations.

Spatiotemporal reconstruction and design linkage

Converted TSS profiles were interpolated in the vertical direction to obtain a continuous spatiotemporal TSS field (Fig. 3). Depth-specific removal was evaluated as a function of detention time, and the maximum SOR achieving 100% removal at each depth was derived (Fig. 4) as an actionable design/operation criterion for settling ponds.

Results and Discussions

Spatiotemporal settling behavior

The reconstructed TSS field shows that the upper and middle water column maintained quasi-constant TSS during the early stage and then declined rapidly when the precipitate interface passed each elevation. This pattern indicates collective settling of flocculent particles rather than independent discrete-particle settling. Near the bottom, TSS increased with time because solids accumulated and were compressed under the overlying precipitate. These opposite trends demonstrate the transition from hindered settling to transition/compression settling and show why continuous sensing resolves sedimentation dynamics that batch sampling can obscure.

Identification of the hindered-settling zone

In the TSS map (Fig. 3), the hindered-settling region is delineated as the zone where TSS remains approximately time-invariant and close to the initial suspension concentration. This interpretation is consistent with the concept that TSS remains nearly constant in the hindered-settling phase (DallaValle *et al.* 1958; Metcalf and Eddy *et al.* 2003). The downward migration and gradual narrowing of this constant-TSS zone show that the floc

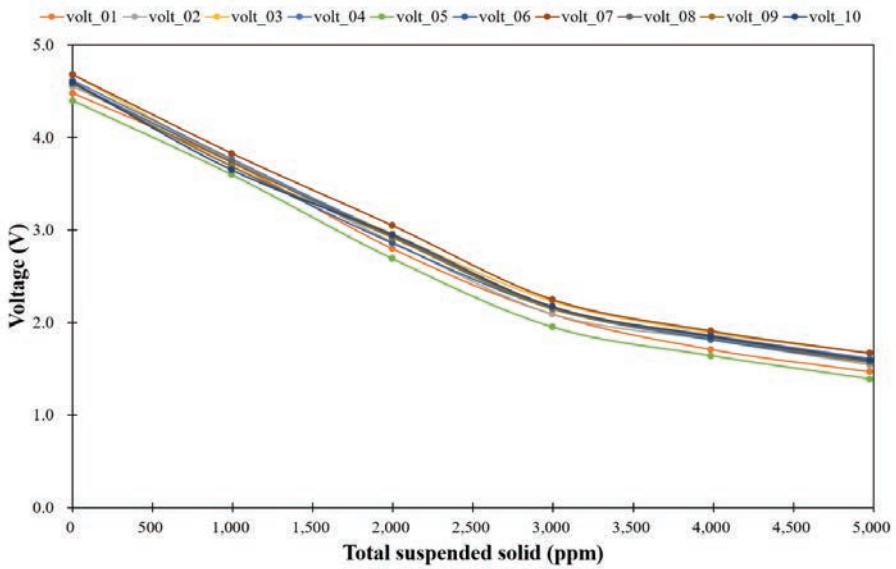

Figure 2 *Variation of voltage for each turbidity sensor according to TSS using solid coffee.*

network initially settles rapidly as a bulk suspension, but the available settling space decreases as the sludge blanket grows upward. Consequently, the highest settling velocity and removal efficiency occur between 0.4 and 1.4 m below the water surface.

Depth-specific overflow-rate criterion (SOR)

From the depth-resolved removal trajectories, the maximum SOR achieving 100% removal was computed for each depth (Fig. 4). Complete removal occurred only after the precipitate interface passed the relevant depth, confirming that clarification is controlled by interface descent rather than by local dilution alone. Values exceeded approximately 30 $m^3\ d^{-1}\ m^{-2}$ between 0.4 and 1.4 m below the surface, with a peak near 1.2 m depth. The lower SOR near the top reflects the initially diffuse interface, whereas the decrease at greater depth reflects sludge-blanket growth and compression. Thus, the optimum design interval is where the interface moves most rapidly before compression becomes dominant.

Conclusions

A continuous-monitoring settling column test was developed by integrating ten multi-depth turbidity sensors with periodic photometric TSS calibration. The method reconstructs a spatiotemporal TSS field that clarifies settling-regime transitions, identifies

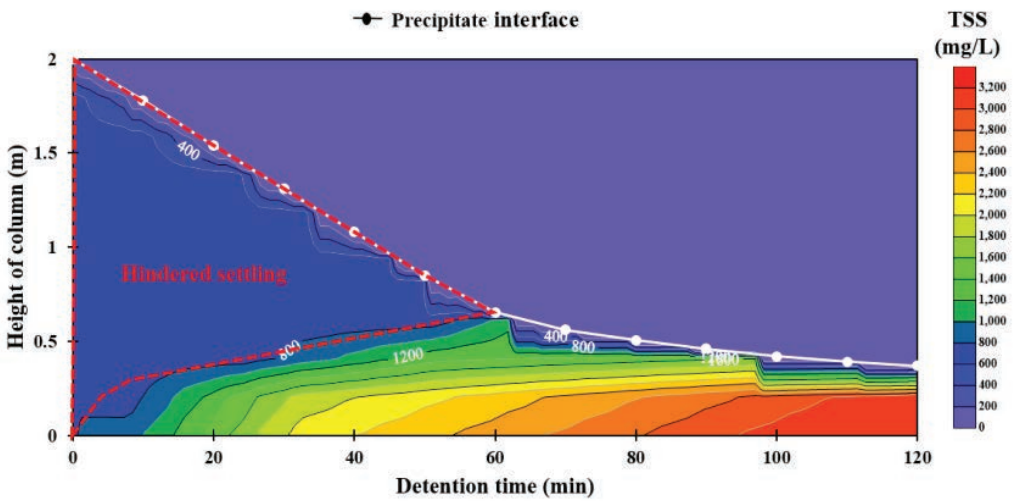

Figure 3 *TSS distribution of precipitate over time in the column.*

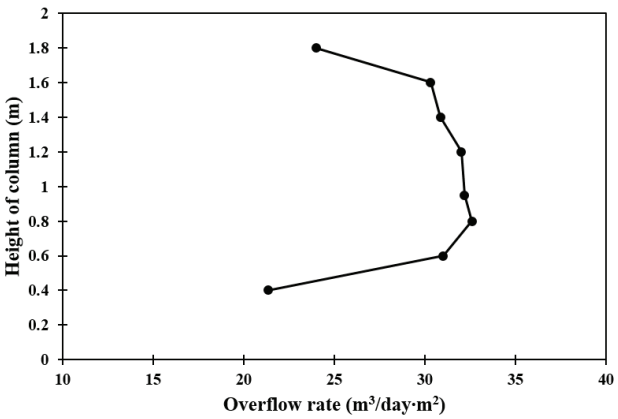

Figure 4 *Maximum overflow rate for 100% overall percent removal by column height.*

the hindered-settling region, and enables computation of depth-specific maximum SOR values for 100% removal.

For the studied mine drainage sludge, the most effective settling zone occurred between 0.4 and 1.4 m below the water surface, and the maximum SOR for complete removal peaked near 1.2 m depth. Future work should focus on standardized QA/QC, sensor-fouling mitigation, and pilot/full-scale validation.

Acknowledgements

This research was supported by the Basic Research Program of the Korea Institute of Geoscience and Mineral Resources (KIGAM), funded by the Ministry of Science and ICT, Republic of Korea.

References

Akcil A, Koldas S (2006) Acid mine drainage (AMD): causes, treatment and case studies. Journal of Cleaner Production 14(12-13):1139-1145.

Brown M, Barley B, Wood H (2002) Minewater Treatment: Technology, Application and Policy. IWA Publishing, London.

Coe HS, Clevenger GH (1916) Methods for determining the capacities of slime-settling tanks. Transactions of the American Institute of Mining Engineers 55:356-385.

DallaValle JM, McBride JP, Allred VD, Jones EV (1958) Application of hindered settling to particle size measurement. Oak Ridge National Laboratory, Tennessee.

DFRobot (accessed 2026-03-11) Gravity: Analog Turbidity Sensor for Arduino, SKU SEN0189, specifications and documentation.

Gao Q (2006) Correlation of total suspended solids (TSS) and suspended sediment concentration (SSC) test methods. New Jersey Department of Environmental Protection, Division of Science, Research, and Technology.

Hach Company (2015) Suspended Solids, Photometric Method 8006, DOC316.53.01139.

Lee DK, Lee JH, Cheong YW, Park JM (2023) Physical properties of mine drainage sediment according to depth in settling ponds. International Journal of Mining, Reclamation and Environment 37(2):148-161.

Lee DK, Cheong YW, Ji S, Yim G (2025) Evaluation of concentration distribution and settling efficiency of mine drainage precipitate through a new column settling experiment. Mine Water and the Environment 44:765-776.

Metcalf, Eddy, Tchobanoglous G, Stensel H, Ryujiro T (2003) Wastewater Engineering: Treatment and Reuse, 4th edn. McGraw-Hill, Boston.

Roche C, Medina MEV, Schmitt P, Pallarès A, Pallarès G, Meilliez M, Laurent J (2022) Densification of activated sludge for better settling performances: experimental characterization in batch column and model parameters calibration. Water Science and Technology 86(1):110-127.

U.S. Environmental Protection Agency (2023) Primary Clarifiers for Operators. EPA Operator Webinar Series slides, August 24, 2023.

Wolkersdorfer C (2023) Mine Water Treatment: Active and Passive Methods. Springer.

IMWA 2026
Jeongseon

Hydrogeochemical and Isotope-Based Assessment of Level-Specific Mine Water and Rock Characteristics in a Recently Closed Coal Mine

Ki-Rim Lee[1], Duk-Min Kim[1], Young-Min Kim[1], Jee-Hyun Jung[1], Jae-Hyun Park[1], Da-Som Kim[1], Joon-Uk Kwon[2] and Jung-Sik Park[3]

[1]*Department of Energy, Resources, and Environmental Engineering, Sangji University, Wonju, 26393, Gangwon-do, Republic of Korea, kdukmin8@sangji.ac.kr, ORCID 0000-0002-1537-6866*

[2]*GeoMirae Engineering and Construction Co., Ltd., Seoul, 08505, Republic of Korea, kwonjoonuk@naver.com*

[3]*Korea Mine Rehabilitation and Mineral Resources Corporation (KOMIR), Wonju, 26464, Republic of Korea, parkjs@komir.or.kr*

Abstract

Hydrogeochemical characteristics, acid-generating potential of rocks, and isotopic ratios were investigated to evaluate acid mine drainage (AMD) formation in a closed coal mine. Mine water, surface water, and groundwater were sampled during dry and wet seasons. Shallow mine workings showed acidic conditions with low alkalinity, indicating pyrite oxidation and depletion of carbonates, whereas deeper zones exhibited neutral conditions due dominant influence of carbonates. Most rock samples were classified as Non-Acid Forming, although several showed localized potential for AMD generation. Water isotopes indicated two different water bodies, and sulfate isotopic ratios could be used to calculate relative contributions between Fe(III) and dissolved oxygen as oxidant for pyrite.

Introduction

In abandoned mine areas, oxidation of sulfide minerals generates AMD, which is a major source of contamination for surface water and groundwater (Yun *et al.* 2001; Cidu *et al.* 2009). The acidity produced by sulfide mineral oxidation can also be neutralized through reactions with carbonate minerals, resulting in simultaneous acid generation and neutralization processes (Toran 1987). The geochemical evolution of mine drainage has been extensively investigated in various mining environments (Nordstrom & Southam 1997). After mine closure, the rise of mine water levels changes dissolution conditions of sulfide and carbonate minerals. In coal mines, sulfide minerals such as pyrite coexist with neutralizing minerals including limestone and silicate minerals, creating a complex geochemical environment where acid-generating and neutralization reactions occur simultaneously. Long-term weathering and oxidation in shallow mine levels may promote the consumption of neutralizing minerals, whereas deeper levels that were relatively recently excavated may retain greater buffering capacity under less weathered conditions. This geological heterogeneity leads to variations in water quality among different mine workings, and in some zones, active pyrite oxidation occurs together with neutralization through dissolution of carbonate minerals. In addition, acid-generating potential assessments of rock samples have shown that certain levels contain high sulfur contents, low NAGpH values, and high Fe leaching, indicating potential risks for AMD generation. Therefore, this study aimed to investigate the hydrogeochemical and geological characteristics, together with stable isotope compositions, of mine water, surface water, and groundwater in a closed coal mine with maintained drainage conditions to elucidate the mechanisms of AMD formation, to identify hydrogeochemical differences according to mine level, and to evaluate its future occurrence potential.

Study area and hydrologic setting

The study area is a recently closed coal mine located in Korea. Mining activities have ceased; however, mine drainage pumping systems are still operating to control mine water levels (Figure 1). Therefore, the mine workings have not reached completely flooded conditions, and the investigated mine levels remain partially drained. The study area consists of the Dong Tunnels and Bokam Tunnels, Active drainage conditions are still maintained in the study area. Therefore, hydrogeochemical conditions may vary according to mine level, groundwater circulation, and oxidation environment.

Methods

Mine water, surface water, and groundwater samples were collected during both the dry season (February 2025) and the wet season (August 2025). Mine water samples were obtained from representative locations within each mine level, whereas surface water samples were collected from the midstream and downstream sections of the adjacent stream. Groundwater samples were collected from nearby monitoring wells. In the field, pH, oxidation–reduction potential (ORP), electrical conductivity (EC), dissolved oxygen (DO), and temperature were measured using a portable multi-parameter water quality meter. Alkalinity was determined by field titration and expressed in mg/L as $CaCO_3$. For hydrogeochemical analysis, samples were filtered through 0.45 µm membrane filters immediately after collection. Major cations and trace elements were analyzed using ICP-AES (Inductively Coupled Plasma–Atomic Emission Spectrometry). Major anions (e.g., SO_4^{2-} and Cl^-) were quantified using ion chromatography. For stable isotope analysis, oxygen and hydrogen isotopes of water ($\delta^{18}O_{water}$ and $\delta^{2}H_{water}$) were measured using a stable isotope ratio mass spectrometer. For sulfur and oxygen isotope analysis of sulfate, filtered samples were acidified with HCl to pH < 3 to prevent carbonate precipitation, and $BaCl_2$ solution was added to precipitate $BaSO_4$. The precipitated $BaSO_4$ was recovered and used for $\delta^{34}S_{sulfate}$ and $\delta^{18}O_{sulfate}$ isotope analyses. Rock samples were collected in the field, dried, and pulverized prior to analysis. Sulfur isotopes of sulfide minerals ($\delta^{34}S_{sulfide}$) were analyzed to evaluate the origin of sulfide minerals. Net Acid Producing Potential (NAPP) and Net Acid Generation (NAG) pH tests were conducted to assess acid-generating potential, and samples were classified as Non-Acid Forming (NAF) or Potential Acid Forming (PAF). To supplement the NAPP–NAG_{pH} evaluation, sequential extraction step 3 was performed to quantify oxidized iron

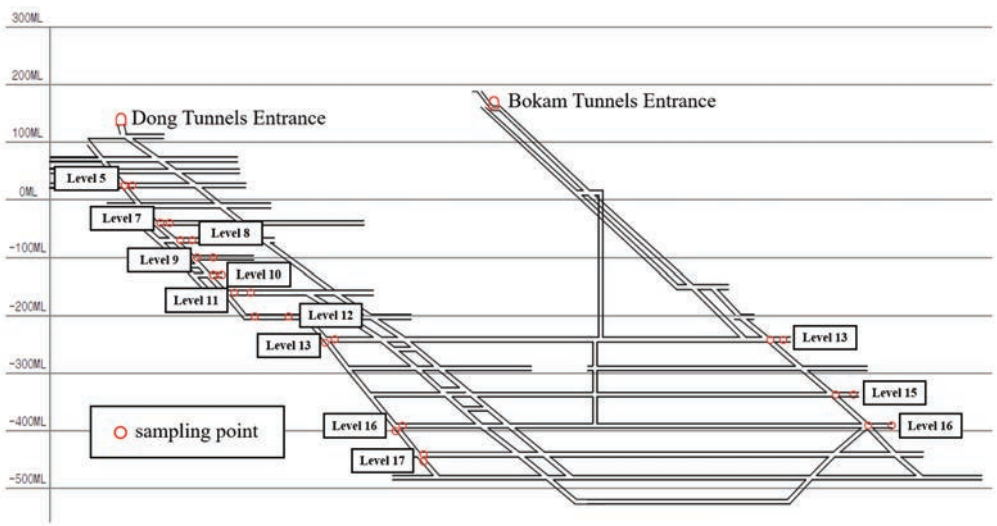

Figure 1 Mine workings and sampling locations in the recently closed coal mine.

(Fe(III)). The extracted Fe concentration was measured using ICP-AES and used as an indicator of the sensitivity of pyrite oxidation. Isotopic data were interpreted by comparison with the Global Meteoric Water Line (GMWL) and Local Meteoric Water Line (LMWL) to determine water sources. In addition, sulfur isotopes of rock samples were analyzed.

Results and discussion

Hydrogeochemical results showed that mine water in the study area could be divided into two distinct groups according to mine level and oxidation environment rather than complete flooding status. Because the mine has been closed only recently and pumping systems are still operating, all investigated levels remain partially drained and are exposed to different oxidation conditions. Therefore, the observed hydrogeochemical differences are interpreted as level-specific responses rather than development of a fully flooded mine pool. The upper-levels of the Dong Tunnels (levels 5–12) exhibited slightly acidic conditions (Table 1). In particular, levels 8–11 showed low pH values of 4.7–5.5 and high ORP values exceeding 500 mV, indicating oxidizing conditions. Alkalinity in this zone ranged from 0 to 20 mg/L as $CaCO_3$, suggesting limited buffering capacity against acid generation. Consequently, Mn and Al concentrations were relatively elevated. For example, level 11 exhibited Mn concentrations of 3.9–5.6 mg/L and Al concentrations of 5.0–13.7 mg/L, indicating enhanced mobilization associated with sulfide mineral oxidation. In contrast, levels 5, 7, and 12 showed relatively higher pH values despite elevated SO_4^{2-} concentrations and higher Ca and Mg concentrations, indicating simultaneous pyrite oxidation and neutralization by carbonate or silicate minerals. Protons generated by pyrite oxidation react with carbonate and silicate minerals, releasing Ca and Mg, and this process is typically accompanied by increasing SO_4^{2-} concentrations (Drever 1997; Kim *et al.* 2017). Level 7, in particular, maintained pH values of 6.6–6.8 with high SO_4^{2-} concentrations of 748.5–789.4 mg/L, representing active oxidation with effective buffering by carbonate minerals. These results indicate that sulfide oxidation and neutralization reactions coexist within some mine levels and produce heterogeneous geochemical environments. In contrast, deeper zones including the lower Dong Tunnels (levels 13, 16, and 17) and the Bokam Tunnels showed neutral to slightly alkaline conditions. pH values ranged from 6.9–8.0, and alkalinity reached 455–483 mg/L as $CaCO_3$ in level 16 and 628–653 mg/L as $CaCO_3$ in level 17, indicating favorable conditions for metal precipitation and adsorption. Mn and Al concentrations were generally below 0.1 mg/L, clearly contrasting with the upper-levels. However, As concentrations of 43–65 µg/L were observed in level 16, likely due to limited adsorption of dissolved As onto Fe(III) hydroxide surfaces under alkaline conditions. Samples from the Bokam Tunnels also showed stable water quality with pH values of 7.7–7.9 and low Mn and Al concentrations. Major ion composition further supported these differences. Upper-level samples were mainly classified as Ca–Mg–SO_4 or Ca–SO_4 type waters, indicating dominance of sulfate derived from sulfide mineral oxidation (Figure 2). In contrast, lower levels and Bokam Tunnel samples were characterized by Ca–HCO_3 or Na–HCO_3 type water, reflecting weaker oxidation influence and stronger carbonate dissolution and deep groundwater mixing. Some deeper samples, particularly levels 13 and 17, showed relatively higher Na compared to Ca, suggesting Ca–Na ion exchange during prolonged residence or mixing with deeper groundwater (Capuano & Jones 2020). Additionally, downstream surface water showed increased SO_4^{2-} and EC values, together with detectable Mn and Al, indicating influence from treated mine water discharge.

Acid-generating potential tests indicated that most rock samples were classified as NAF, with NAG_{pH} values greater than 4.5 and negative NAPP values, suggesting limited potential for AMD generation under current conditions. However, several samples exhibited high acid-generating potential. Sample 10-1 showed total S content of 9.17%, NAG_{pH} of 2.61, and NAPP of 280.3 kg $CaCO_3$/t, representing the highest risk

and was classified as PAF. Samples 10–2, 11–2, and 12–1 were also classified as PAF. These results indicate that localized AMD generation may occur where sulfide mineral content is high and neutralization capacity is limited. Sequential extraction (step 3) results supported this interpretation. High Fe(III) contents (> 500 mg/L) were observed in samples 7–1, 7–2, 10–1, and 10–2, indicating prolonged pyrite oxidation. Despite high Fe(III) release, samples from level 7 remained classified as NAF, suggesting sufficient neutralization capacity due to abundant carbonate minerals. Although AMD generation currently appears limited in most mine levels, continued rise of mine water levels following future termination of pumping systems may alter oxidation and neutralization conditions. Therefore, mine levels containing high sulfur contents and oxidation-sensitive materials may become important sources of future AMD generation.

Stable isotope results of water ($\delta^{18}O_{water}$ and $\delta^{2}H_{water}$) showed that most mine water, surface water, and groundwater samples plotted near the GMWL and LMWL, indicating meteoric origin (Craig 1961). Lower Dong Tunnel and Bokam Tunnel samples showed relatively lighter isotopic compositionsupper-level compared with upper-levels, suggesting differences in recharge conditions and water sources. In contrast, upper-level samples

Table 1 *Field measurements of mine water from each level during the dry season (February 2025).*

Position		pH	ORP (mV)	EC (µS/cm)	DO (mg/L)	Alkalinity (mg/L as $CaCO_3$)
Dong Tunnels	5–1	6.1	601.6	689	10.3	130
	5–2	6.2	606.2	688	10.3	128
	7–1	6.8	536.7	1327	10.3	42
	7–2	6.6	545.3	1321	10.1	52
	8–1	5.1	554.9	691	10.7	0
	8–2	5.2	544.5	688	10.5	9
	9–1	5.5	545.1	354	10.7	14
	9–2	5.5	543.2	353	10.6	20
	10–1	5.1	486.2	760	10.7	0
	10–2	5.1	474.3	743	10.7	0
	11–1	4.7	505.3	1162	11.0	1
	11–2	4.9	501.2	1403	11.1	0
	12–1	6.3	467.4	1617	10.6	208
	12–2	6.2	477.1	1608	10.6	196
	13–1	6.9	474.6	551	9.0	238
	13–2	7.0	481.2	546	9.1	224
	16–1	7.7	486.1	1094	10.7	455
	16–2	7.6	479.2	1098	10.7	483
	17–1	7.9	493.9	1595	10.0	653
	17–2	8.0	501.2	1598	10.0	628
Bokam Tunnels	13–1	7.9	486.8	283	10.6	120
	13–2	7.8	474.2	711	10.6	220
	15–1	7.7	490.1	475	8.6	187
	15–2	7.8	494.2	473	8.7	200
	16–1	7.7	408.4	1203	8.0	335
	16–2	7.8	412.5	1200	7.9	342

showed isotopic compositions similar to surface water. Wet-season samples exhibited generally lighter isotopic values compared with dry-season samples, reflecting increased recharge and dilution by isotopically depleted rainfall during the monsoon season. This tendency suggests that seasonal recharge contributes to mine water composition even under partially drained conditions.

A negative relationship was observed between $\delta^{18}O_{sulfate}$ and SO_4^{2-} concentrations, indicating isotope fractionation during pyrite oxidation (Taylor *et al.* 1984; Kim *et al.* 2019). Oxygen in sulfate is derived from both water and dissolved oxygen, and the observed $\delta^{18}O_{sulfate}$ values reflect mixing of these sources. Upper-level samples showed higher SO_4^{2-} concentrations and relatively lower $\delta^{18}O_{sulfate}$ values, indicating prolonged pyrite oxidation and higher contribution by Fe(III) as oxidant. In contrast, deeper samples showed lower SO_4^{2-} concentrations and limited variation in $\delta^{18}O_{sulfate}$, suggesting weaker oxidation influence. Additionally, differences between sulfate sulfur isotopes and sulfide sulfur isotopes ($\Delta\delta^{34}S_{sulfate-sulfide}$) were generally within ±3‰, indicating sulfate derived from the similar sulfide mineral source (Toran & Harris 1989).

Summary

Integrated analysis of hydrogeochemistry, acid-generating potential of rocks, and stable isotopes revealed distinct geochemical characteristics of mine water according to mine level and oxidation environment in the recently closed coal mine. Because pumping systems are still operating, all investigated

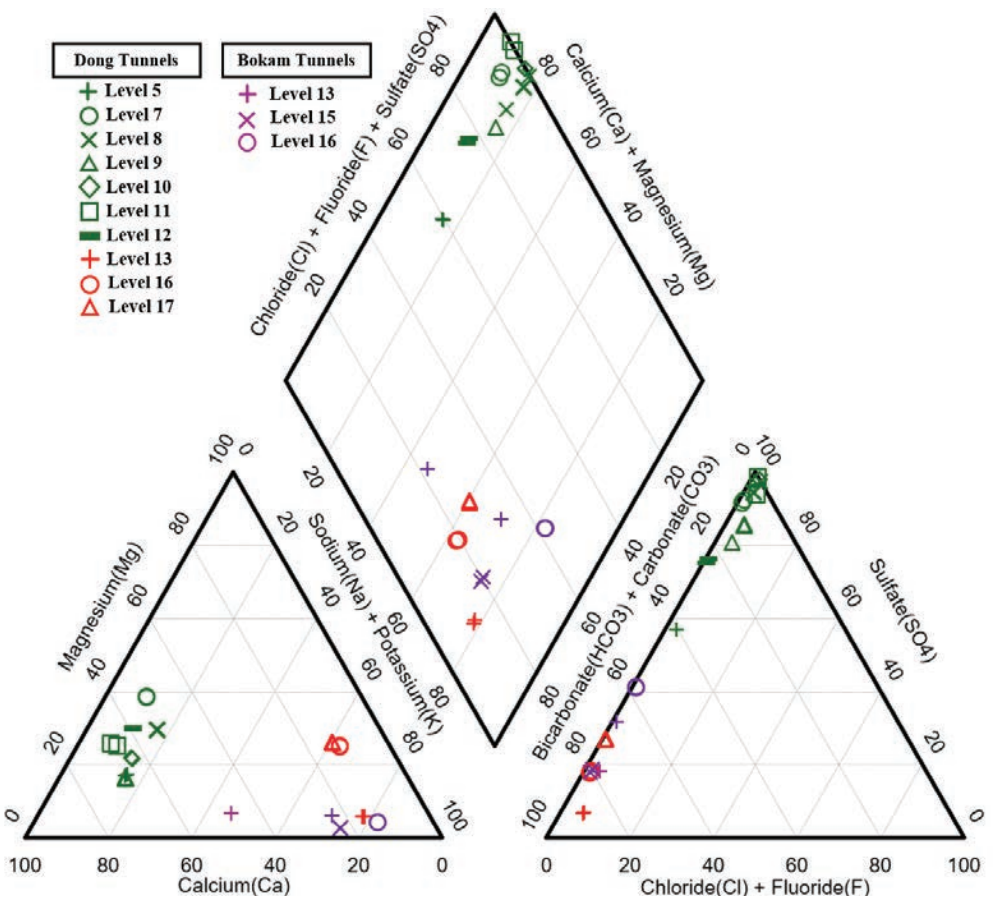

Figure 2 *Piper diagram showing hydrogeochemical facies of mine water samples.*

mine workings remain partially drained rather than completely flooded. Upper mine workings showed acidic tendencies characterized by low pH, high ORP, and low alkalinity, indicating active pyrite oxidation. In contrast, deeper workings and the Bokam Tunnels exhibited neutral conditions with high alkalinity, suggesting dominant neutralization through carbonate dissolution and mixing with deeper groundwater. Acid-generating potential tests indicated that most rock samples were classified as NAF. However, several levels showed high sulfur contents and strong oxidation sensitivity, indicating localized potential for AMD generation. Water isotope compositions indicated meteoric recharge characteristics, whereas sulfate isotopes suggested variable contributions of Fe(III) and dissolved oxygen during pyrite oxidation. Overall, the mine showed level-specific hydrogeochemical differences controlled by oxidation intensity, neutralization reactions, and lithological heterogeneity rather than development of a fully flooded mine pool. Although AMD generation is currently limited, future rise of mine water levels following termination of pumping systems may alter geochemical conditions and enhance localized AMD occurrence. Therefore, continuous monitoring is required for predicting future water quality evolution in recently closed coal mines.

Acknowledgements

This research was supported by GeoMirae Engineering & Construction Co., Ltd. in 2025 and by the Korea Mine Rehabilitation and Mineral Resources Corp. (KOMIR) through the 2026 project.

References

Craig, H (1961) Isotopic variations in meteoric waters. Science 133(3465): 1702–1703

Cidu R, Biddau R, Fanfani L (2009) Impact of past mining activity on the quality of groundwater in SW Sardinia (Italy). J Geochemical Exploration 100(2–3): 125–132

Capuano RM, Jones CR (2020) Cation exchange in groundwater-chemical evolution and prediction of paleo-groundwater flow: A natural-system study. Water Resources Research 56(8): e2019WR026318

Drever JI (1997) The Geochemistry of Natural Waters: Surface and Groundwater Environments (3rd ed.). Prentice Hall

Kim DM, Yun ST, Cho Y, Hong JH, Batsaikhan B, Oh J (2017) Hydrochemical assessment of environmental status of surface and ground water in mine areas in South Korea: Emphasis on geochemical behaviors of metals and sulfate in ground water. J Geochemical Exploration 183: 33–45

Kim, DM, Yun ST, Yoon S, Mayer B (2019) Signature of oxygen and sulfur isotopes of sulfate in ground and surface water reflecting enhanced sulfide oxidation in mine areas. Applied Geochemistry 100: 143–151

Nordstrom DK, Southam G (1997) Geomicrobiology of sulfide mineral oxidation. Reviews in Mineralogy and Geochemistry 35, 361–390

Taylor BE, Wheeler MC, Nordstrom DK (1984) Stable isotope geochemistry of acid mine drainage: Experimental oxidation of pyrite. Geochimica et Cosmochimica Acta 48(12): 2669–2678

Toran L (1987) Sulfate contamination in groundwater from a carbonate-hosted mine. J Contaminant Hydrology 2(1): 1–29

Yun ST, Jung HB, So CS (2001) Transport, fate and speciation of heavy metals (Pb, Zn, Cu, Cd) in mine drainage: Geochemical modeling and anodic stripping voltammetric analysis. Environmental Technology 22(7): 749–770

IMWA 2026
Jeongseon

The Influence of a Graben Structure on Pollution Migration from Mining and Industrial Waste Facilities

Paul Joël Havemann Lourens[1], Petrus Daniel Vermeulen[1], Josepha Simone Doris Renata Zielke-Olivier[1], Stefanus Steyn de Lange[1]

[1]*Institute for Groundwater Studies, University of the Free State, PO Box 339, Bloemfontein, 9300, South Africa, lourenspjh@ufs.ac.za, ORCID 0009-0008-0760-9907*

Abstract

Graben structures can influence both the direction and rate of groundwater flow and the migration of pollutants. The investigation aimed to determine the pollution distribution along a graben structure that extends through a mining and industrial facility. The investigation involved a desktop review of existing data, geophysical surveys, and collection of field data through drilling of analytical boreholes, complimented by aquifer tests, down-the-hole chemical profiling, and isotope analysis. The investigation indicated that the faults associated with the graben structure act as conduits for the migration of pollutants from the different waste facilities towards local river valleys.

Keywords: Graben, faults, pollution migration, industrial, waste facility

Introduction

Large-scale geological structures such as graben structures can influence both the direction and rate of groundwater flow and the migration of pollutants. Graben structures can act as preferred pathways for groundwater flow and pollution migration, or they can act as a barrier, depending on the specific characteristics of the structure and the associated lithology (geological material).

Aim and Objectives

The aim of the investigation was to determine the pollution distribution along a graben structure that extends through a mining (coal) and industrial facility (Fig. 1) The objectives of the investigation were 1) develop a conceptual understanding (model) of the geology and geohydrological processes along the graben (fault) system, 2) identify the main sources of pollution, 3) identify the distribution and/or movement of pollutants and associated risk, and 4) propose mitigation and management measures to limit/reduce pollution migration.

Materials and Methods

The methodology of the investigation was structured into three phases.

Phase 1

The initial phase involved a desktop review of existing data to identify information gaps. The desktop review was supplemented by a geophysical investigation along the graben structure to identify conductive zones and site additional analytical boreholes to address data gaps and enhance the understanding of the geological and hydrogeological characteristics of the area. The geophysical methods applied included the Electromagnetic (EM) method using a Geonics EM34–3 and the Electrical Resistivity Tomography (ERT) method using an ABEM SAS 1000.

Phase 2

Phase 2 involved the collection of primary field data through the drilling of analytical boreholes, complemented by a series of aquifer tests, down-the-hole chemical profiling, and isotope analysis. The data was used to develop a conceptual model of the groundwater system, outlining the key processes and interactions within the groundwater system and how the graben structure influences the pollution migration from the different waste facilities.

A total of 28 analytical boreholes were drilled using the air-percussion method. The boreholes drilled consisted of 13 shallow (15

m) boreholes targeting the weathered aquifer and 15 deep (40 m) boreholes targeting the mapped graben structure and associated faults (fractured aquifer).

Aquifer tests included slug tests and constant rate discharge tests. Slug tests were performed on all the boreholes to estimate initial hydraulic properties and to identify boreholes for constant rate discharge tests. Five boreholes were identified to be suitable for constant rate discharge tests to calculate hydraulic properties more accurately.

Down-the-hole chemical profiling was conducted on all the analytic boreholes with a YSI 600XLM Multi-Parameter Probe (calibration before deployment was done with the appropriate standard solutions). This allowed for the in-situ measurement of multiple parameters which included temperature, dissolved oxygen (DO), oxygen reduction potential (ORP), pH, and electrical conductivity, enabling the identification of fracture zones within the boreholes.

Water samples were collected from all the analytical boreholes, existing monitoring boreholes, and surface water sources (potential pollution sources). The samples collected were analysed for physical- and

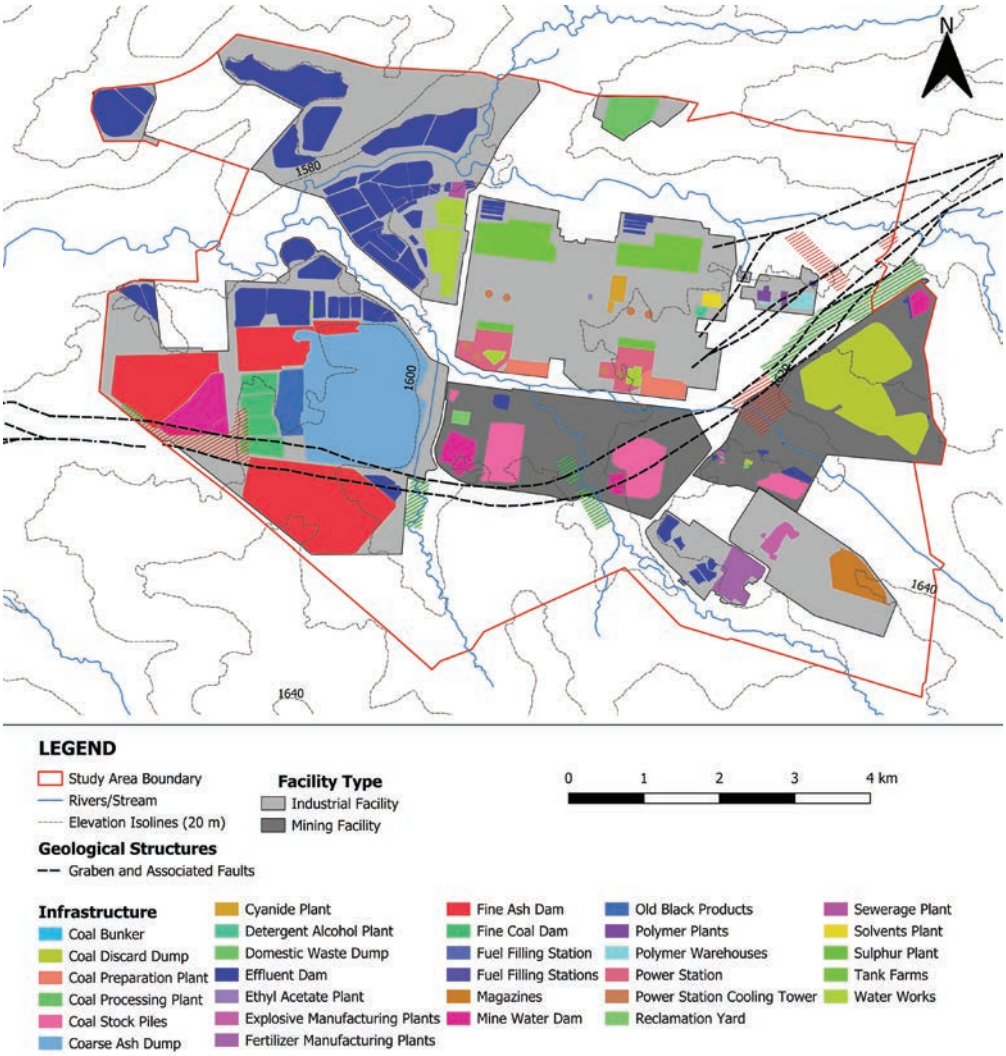

Figure 1 *Study area layout map indicating the position of the graben and associated faults.*

inorganic parameters, and stable isotopes (oxygen & hydrogen). The samples were collected using a stainless-steel specific depth sampler (bailer) at predetermined depths (flow fracture/flow zones).

Phase 3

Phase 3 synthesised all the findings to identify critical pathways for pollution movement from the various pollution sources. Identify areas of risk and recommend possible management and/or mitigation measures.

Site Description

Climate

Climate data from the South African Weather Services weather station 0478330 3 is available from 1984 to 2018. Over this period, the mean annual rainfall is 758 mm, mainly occurring in the summer months of October to March in the form of thunderstorms. It receives the highest mean rainfall in January (148 mm) and the lowest mean rainfall in the July (4 mm). The mean maximum temperature varies from 18 °C in the winter to 27 °C in the summer, whereas the mean minimum temperature varies from 1 °C in the winter to 14 °C in the summer.

Topography and Drainage

The topography of the study site forms a high of 1639 mamsl in the southeast to a low of approximately 1568 mamsl in the west of the site. The site is drained by three non-perennial streams, that enters the site from the northern and eastern boundaries and. Drainage from the north and east is expected to follow the topography towards non-perennial streams (Fig.1).

Local Geology

The geology underlying the study area mainly comprises sedimentary rocks of the Vryheid Formation that were intruded during the Jurassic period (200 to 145 Ma) by numerous interconnected dolerite saucers (sills) and dykes (Fig. 2 and Fig. 3) which frequently transgress and displace the stratigraphy (Coetzee 2016). The Vryheid Formation is assigned to the Ecca Group within the Karoo

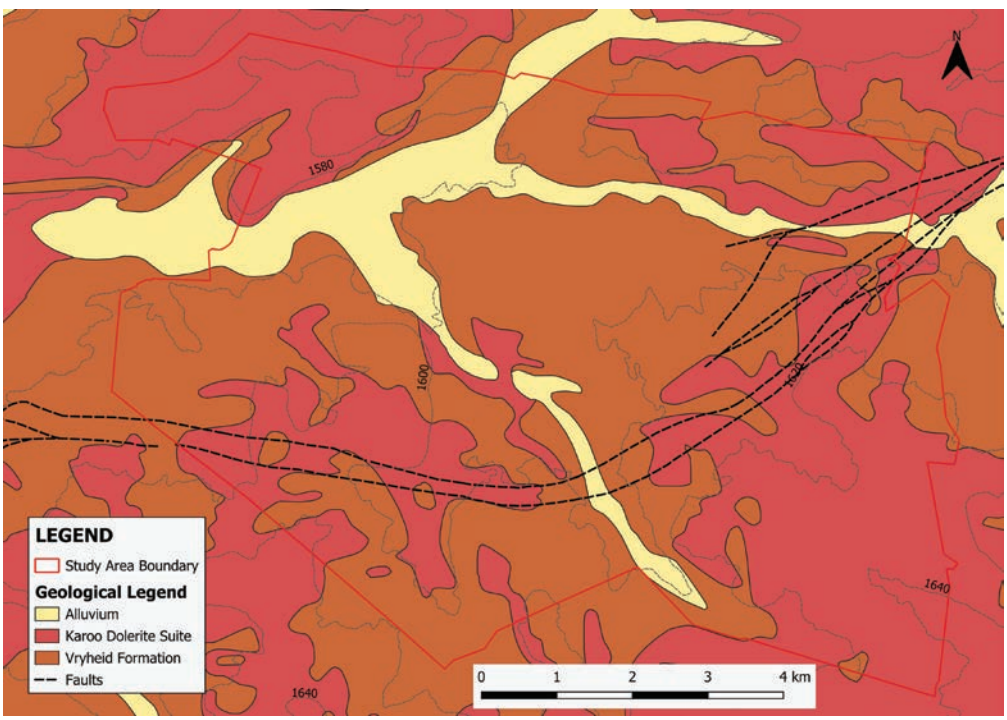

Figure 2 Study area geological map.

Supergroup. According to Johnson *et al.* (2006) the Vryheid Formation was deposited within three different environmental environments which includes a lower fluvial-dominated deltaic environment, a middle fluvial environment and an upper fluvial-dominated deltaic environment and is the host formation for the majority of South Africa's economic coal reserves (Cairncross and Cadle 1987).

Hydrogeology

The geohydrological system associated with the Vryheid Formation of the Highveld Coalfield consists of two distinct and superimposed aquifers, as described by Hodgson and Krantz (1998). They are the upper/shallow weathered aquifer and the deeper fractured rock aquifer.

The shallow weathered aquifer is associated with the weathered horizon which consists of soil and weathered rock. The depth of weathering generally ranges between five (5) and 15 metres below ground level (mbgl) and water is often intersected within a few metres below surface (Hodgson and Krantz 1998; Vermeulen and Usher 2006). The aquifer is recharged by rainfall and the recharge percentage is in the range of one to three percent of the annual rainfall (Hodgson and Krantz 1998).

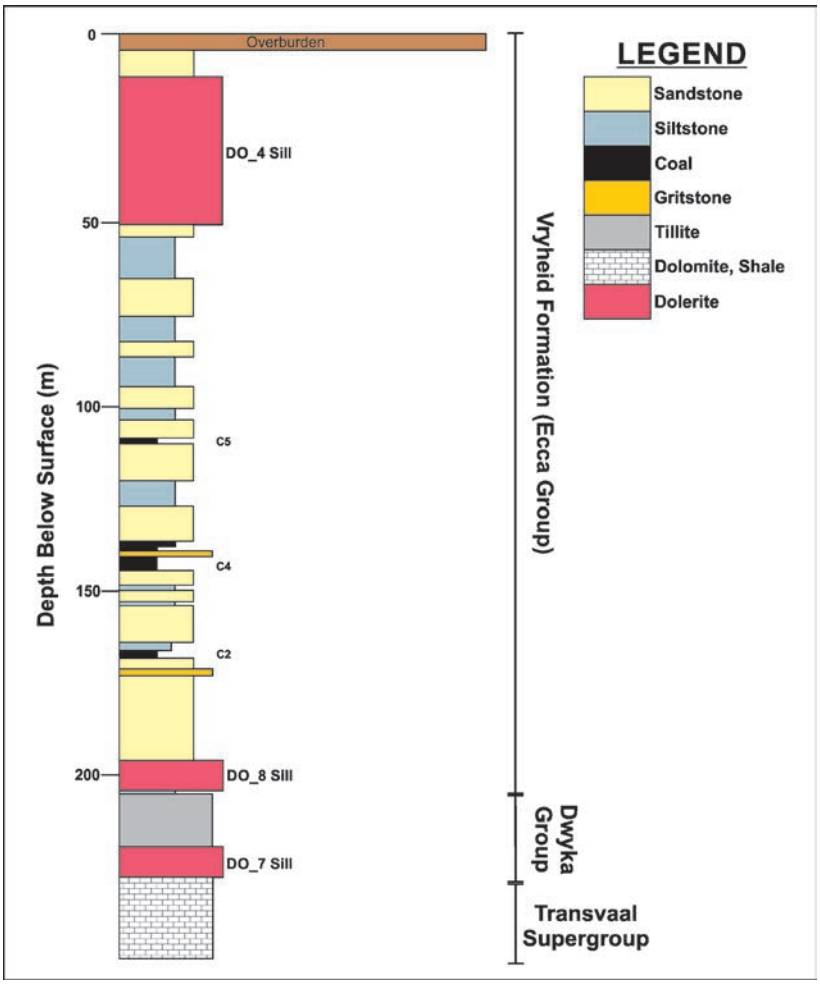

Figure 3 *Generalised stratigraphic column for the Highveld Coalfield of the study area (Modified from source: Coetzee and Kisters, 2016).*

Studies conducted by Menghistu (2010) and a geophysical survey across the graben at the mining and industrial facility indicated that the area along the graben and associated faults are underlain by a highly weathered and fractured dolerite sill. The shallow weathered aquifer could be prone to pollution from potential surface sources if leachate from these sources seeps into the subsurface via fractures and interconnected pores. The upper fractured aquifer is also likely to be affected by groundwater pollution if groundwater moves vertically along fractures, fissures and cracks and possible fault planes along the graben. The deeper lying alternating layers of sandstone, shale and siltstone are of lesser concern as the shale and siltstone layers are nearly impermeable to water movement and form a no-flow boundary (Hodgson and Krantz, 1998). Therefore, these layers can prevent pollution plumes from migrating into deeper geological strata.

Results and Discussion

The interpretation of available information indicates that at some locations along the graben structure did not contain enough information to determine groundwater flow directions within/along the graben. The following flow direction could be identified: 1) at the Coarse Ash Dump the general flow direction is north towards the local streams, 2) at the Coal Stockpiles, Effluent Dams (fertiliser) and mine water dam at the eastern coal stock pile, the general flow direction is northwest, and 3) at the eastern section (near the Coal Discard Dump), the flow direction is north.

Fig.4 displays zones of high conductivity that were identified by the geophysical survey. The resistivity survey, at some locations, could clearly identify the graben and the associated faults by a distinct change in resistivity in areas where the graben structure was often composed of less resistive material. Some of the zones of high conductivity are not confined to the graben but probably related to the shallow weathered aquifer and local dolerites sills that act as barriers to form perched aquifers that creates wetland at places.

The estimated transmissivity for the matrix was on average 0.17 m^2/d and

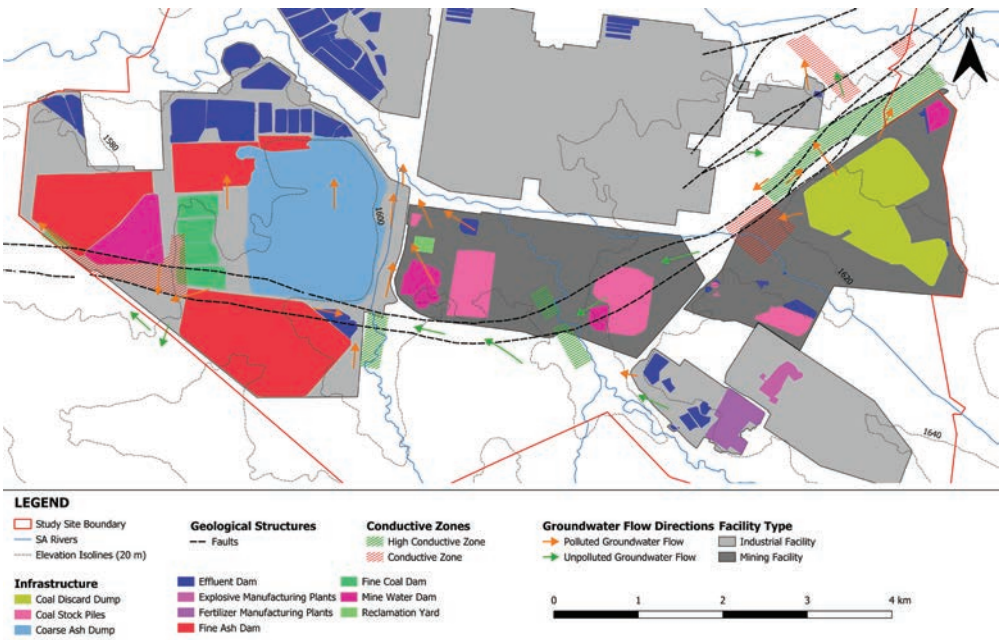

Figure 4 Study area layout map indicating the conductive zones and groundwater flow directions along the graben structure.

2 m²/d in the fracture network within the graben (weathered zone), whilst the deep boreholes, targeting the fault zone, indicated an average transmissivity of 1.9 m²/d and 123 m²/d for the matrix and fracture network, respectively. The constant rate discharge tests estimated the transmissivity to range between 0.2 m²/d to 3.7 m²/d with an average of the matrix and varied from 0.67 m²/d to 63.24 m²/d in the fractures.

The transmissivity along the fractures may vary greatly, depending on the fracture network as well as its size and extent. The similar transmissivity values calculated during the constant rate discharge tests indicates that groundwater flow is from the matrix and fracture system and it is not possible to distinguish between to the two systems. Therefore, groundwater flow occurs along a zone and not a single fracture.

The interpretation of the existing data together with the data collected during phase 2 of the investigation, identified areas of surface and groundwater pollution, and the identification of the groundwater flow paths (polluted and unpolluted) (see Fig. 4). These findings indicates that pollution from the Coarse Ash Dump and Fine Ash Dams only affects the western area of the graben, whilst it does not affect the eastern area of the graben. The groundwater pollution from the Coal Stockpiles and the Fertiliser Effluent Dams do not affect the pollution in the eastern area of the graben as flow at these sites varies from west to northwest. The groundwater pollution from the Coal Discard Dump effects the western area of the graben. Water level data, down-the-hole electrical conductivity profile data, and chemistry data suggest that groundwater flow and pollution migration occur across the graben and along the strike of the associated faults.

Conclusions

The investigation indicated that the faults associated with the graben structure act as conduits for the migration of pollutants from the different waste facilities. The groundwater flow direction within the graben structure is governed by the prevailing groundwater flow system, where pollutants in the western section of the graben flow toward the local rivers valleys in the west, and pollutants located in the eastern section flow towards the local rivers in the east.

Proposed Management/Mitigation Measures (Recommendations)

The following management and/or mitigation measures are recommended

- Re-evaluate the depth of existing cut-off trenches as well as the location of existing sumps and pumping rates from these sumps.
- Investigate the base-flow of the Coal Discard Dump during wet and dry seasons to evaluate the seepage via unlined sidewalls into the subsurface and based on the results, design and implement mitigation measures.
- Re-assess the rehabilitation of older, unlined sections of the different waste facilities.

References

Duncross B, Cadle AB (1987) A genetic stratigraphy for the Permian coal-bearing Vryheid Formation in the East Witbank Coalfield, South Africa. South African J Geol 90:219–230

Coetzee A (2016) The geometry of Karoo dolerite dykes and saucers in the Highveld Coalfield : constraints on emplacement processes of mafic magmas in the shallow crust. Dissertation (M.Sc.).Stellenbosch. Stellenbosch University

Coetzee A, Kisters A (2016) The 3D geometry of regional-scale dolerite saucer complexes and their feeders in the Secunda Complex, Karoo Basin. J Volcanol Geotherm Res 317:66–79. https://doi.org/10.1016/j.jvolgeores.2016.04.001

Hodgson FDI, Krantz RM (1998) Investigation into Groundwater Quality Deterioration in the Olifants River Catchment above the Loskop Dam with Specilised Investigation in the Witbank Dam Sub-Catchment. WRC Report No. 291/1/98

Johnson, M.R. Vuuren, C.J. Visser, J.N.J. Cole, D. I. Wickens, H. de V. Christie, A.D.M. Roberts, D.L. Brandl G (2006) Sedimentary rocks of the Karoo Supergroup. In: Johnson, M.R. Anhaeusser, C.R. Thomas RJ (ed) The geology of South Africa. Geological Society of South Africa/Council for Geoscience, Johannesburg/Pretoria, pp 461–500

Menghistu HT (2010) Development of a Numerical Model for Unsaturated/ Saturated Hydraulics in Ash/ Brine Systems. University of the Free State

Vermeulen PD, Usher BH (2006) An Investigation into Recharge in South African Underground Collieries. J South African Inst Min Metall 106:771–788

Approach for Assessing the Feasibility of Large-Scale Irrigation with Mining-Influenced Waters and Key Considerations for Implementation in the Witwatersrand Goldfields

Lesego Madiseng[1], John Annandale[1], Phil Tanner[1], Gerhard van der Burgh[2], Marion Delport[2], Helga Ottermann[2], Wiltrud Durand[2], Kai Witthüser[3] and Josepha Zielke–Olivier[3]

[1]*Department of Plant and Soil Sciences, University of Pretoria, u28424868@tuks.co.za*

[2]*Bureau of Food and Agricultural Policy (BFAP)*

[3]*Delta-H*

Abstract

An interdisciplinary study was conducted to investigate the agronomic, economic, and environmental aspects of regional-scale, long-term irrigation with mining-influenced waters in the Witwatersrand Goldfields and identify key considerations for locating and establishing such schemes, using the Eastern Basin (EB) of the goldfields as a case study. Modelling assessments indicated that irrigation with HDS-treated mine water can be productive, with <2% yield decline predicted, and profitable, with gross margin in excess of R20 000/ha for the selected cropping system. While irrigation with mine waters is expected to have some impacts on ground and surface water, groundwater modelling suggests that this practice can be sustained in the medium- to long-term with minimal environmental impacts. The key considerations for the successful implementation of large-scale mine water irrigation schemes were identified as water quality and balances, crop selection, total irrigation area, management of excess mine water, infrastructure, land availability and ownership, water costing, and the siting of irrigation schemes. The approach developed in this study can be codified into a framework for conducting feasibility assessments and providing guidance for the implementation of regional-scale mine water irrigation schemes.

Keywords: Irrigation, economics, hydrogeology, agriculture, modelling

Introduction

Mine water management is a major challenge in South Africa, particularly in the Witwatersrand Goldfields, where it is a taxpayer liability. In this region, the cessation of mining activities led to flooding of underground workings as pumping ceased. Due to the lack of mine closure regulations, many of these mines were abandoned without rehabilitation, and the management of mining-influenced water emanating from them became the state's responsibility.

Currently, up to 185 million litres per day (ML/day) of mining-influenced water are pumped and treated at three high-density sludge (HDS) plants commissioned in the Eastern, Central and Western Basins. Although HDS treatment is effective in reducing acidity and lowering the concentrations of some trace elements of concern, dissolved solute concentrations remain high. Given that the treated mine water is then released to nearby surface water courses, this results in an increased salt load to the Vaal River System (VRS), making this approach unsustainable in the long term. Therefore, long-term management strategies are sought.

Reverse Osmosis is the preferred technology for long-term management of the mining-influenced waters for regulatory compliance, as it produces potable water. However, this technology is expensive, energy-intensive and produces brine that

needs to be managed. Irrigation has been proposed as a potentially cost-effective alternative option that can make productive use of these otherwise problematic waters. Additionally, having alternative irrigation water sources will improve agricultural productivity. This is especially important in catchments where irrigation has previously been curtailed, such as the VRS, and where water supply is often prioritised for other uses (DWS, 2016).

Previous studies have demonstrated successful irrigation with mine waters in the Coalfields, and the feasibility of irrigation as a mine water management strategy in the Witwatersrand Goldfields has been explored (Annandale *et al.* 2001, 2021; Jovanovic *et al.* 1998; Annandale *et al.* 2023). However, the implications of establishing large-scale mine water irrigation in the Witwatersrand goldfields are not well understood. This study aimed to assess the feasibility of regional-scale mine water irrigation in the Witwatersrand Goldfields of South Africa and identify key considerations for locating and establishing such schemes. Three key research components were identified as necessary to address these uncertainties, and these required an interdisciplinary approach. These components were agronomic, hydrogeological, and economic.

Assessment approach

An interdisciplinary study was conducted to investigate the agronomic, economic, and environmental aspects of long-term irrigation with mining-influenced waters from the Witwatersrand Goldfields, using the Eastern Basin as a model site. The research team consisted of agronomists, agricultural economists and hydrogeologists.

The agronomic component of the study aimed to demonstrate the productivity and evaluate the sustainability of mine water irrigation, and the main responsible team was the University of Pretoria, made up of agronomists. The hydrogeological component aimed to assess the impact of mine water irrigation on groundwater and receiving surface water bodies, providing an indication of potential environmental impacts. The team responsible for this component was Delta H, made up of hydrogeologists. The economic component aimed to investigate the economic aspects of mine water irrigation, providing an indication of costs and benefits. The main team responsible for this component was the Bureau for Food and Agricultural Policy (BFAP), composed of agricultural economists.

A phased approach was used to undertake the study, with outputs from the three teams at different phases used as inputs to subsequent phases in a feedback loop process, making the assessments iterative.

Site selection

Previous studies indicated that the Eastern Basin(EB) presented the greatest opportunity in the Goldfields for successful irrigation with mining-influenced waters. Of the three basins, the water quality in this Basin was most suitable for irrigation, and it has the greatest pumping and treatment capacity, up to 110 ML/day, compared to 70 ML/day in the Central Basin and 45 ML/day in the Western Basin (Annandale *et al.* 2023; TCTA 2017). Additionally, the treatment plant in this basin is in close proximity to prime agricultural land.

Delineation of "No-go" areas

"No-go" areas were identified as areas where irrigation return flows would be conveyed towards a river course within one year, as well as areas underlain by dolomite. These areas were delineated by the hydrogeologists by performing backward calculations of transport times to surface water drainage structures using a regional-scale single-layer numerical groundwater model. Delineation of the no-go areas also considered aquifer vulnerability, as prescribed by Parsons and Conrad (1998).

Cropping system selection

Cropping system selection required input from agronomists and entailed shortlisting more than 200 potential crops to 21 suitable for the Highveld, based on the agricultural economist's knowledge and experience. Thereafter, the shortlisted crops underwent an elimination process based on their risk profile, considering susceptibility to theft,

fire, animal/bird damage, and damage due to production practices. All crops identified as high risk for these factors were eliminated, and the remaining crops were scored based on their socioeconomic inclusiveness and risk profile.

The factors contributing to socioeconomic inclusiveness were the labour multiplier and contribution to dietary diversity. The risk indicators remained the same. Scores of 1 to 3 were assigned to each indicator, with 3 indicating the highest positive score (e.g., low fire risk is assigned a score of 3, and a high contribution to dietary diversity is also assigned a score of 3). These scores were averaged to produce a combined score, and the crop ranking was assigned accordingly.

Following several iterations of the process and consultation with local farmers, maize (Zea mays), oats (Avena sativa), sweet sorghum (Sorghum bicolor), canola and soybean were selected for more detailed assessments. One objective was to maximise water use, which was addressed by selecting a double-cropping system with winter and summer crops.

Modelling scenarios

Two main scenarios were modelled, based on the area required to maximise the use of available water, either using summer or winter crop irrigation requirements to determine the total area. It was determined that a large cropping area would generally be required for the summer crop, as rainfall accounts for most of the crop's water requirements, with less irrigation needed. In contrast, irrigation requirements will increase in winter due to lower or no rainfall, requiring a smaller cropping area to utilise the available water. It was assumed that centre-pivot irrigation systems would be used.

Scenario 1, the Maximum Water Use scenario, aims to maximize water use by adding supplemental summer season irrigation, assuming that 6000 ha would be established based on summer crop requirements, while a smaller area of 2400 ha could be irrigated in winter with the available water. With this scenario, 3600 ha of monocropped maize is irrigated in summer, referred to as the "summer-only area", and 2400 ha is irrigated in both summer and winter, referred to as the "summer-winter" area. Scenario 2, the Minimum Water Use scenario, entails more intensive year-round irrigation and uses less water. This scenario assumes that 2400 ha, based on winter crop requirements, with the summer-irrigated area smaller than that required to maximise water use during the wet season. Although this scenario might have low irrigation system capital costs, it will require the management of excess mine waters in the summer season, and this may have indirect environmental impacts.

In addition to these cropping system scenarios, the potential spatial distribution of irrigation pivots (concentrated vs dispersed) was also simulated. It was expected that concentrated pivots would have a more pronounced environmental impact than the dispersed pivots. Furthermore, in the case where the minimum Area is established for irrigation, there would be some cost implications for the conveyance infrastructure as more extensive pipelines would be required if the pivots are dispersed than if they are concentrated. However, costs associated with conveyance infrastructure was not assessed in this study.

Siting of Irrigation Areas

The siting of irrigation areas was confined to a 30 km radius of the Eastern Basin treatment plant. The total available agricultural area within the region, the potential costs of establishing the infrastructure required to convey the mining-influenced water, potential receptors of return flows, and typical agricultural practices in the region were taken into account. The area required for the two scenarios, Maximum and Minimum Area, determined by the agronomists, was used as a spatial limit by the agricultural economists, who fit centre pivots within existing dryland fields using spatial and statistical algorithms, while excluding the "no-go" areas delineated by the hydrogeologists.

Agronomic modelling

The IrrigWQ Decision Support System (DSS), developed by du Plessis *et al.* (2023), was used to model long-term irrigation

with mine water from this basin, providing yield, as well as solute and water balance predictions. IrrigWQ DSS is a site-specific, risk-based software tool for assessing irrigation water quality. The software uses a simplified version of the dynamic soil water balance (SWB) model to calculate soil-crop-water interactions and includes a simplified chemical equilibrium model to simulate precipitation reactions.

Worst-case water quality for the Eastern Basin mining-influenced waters was used as input to simulate irrigation over a 45-year period. An irrigation system efficiency of 80% was assumed. Irrigation was triggered when the model detected a root-zone deficit exceeding 20 mm relative to field capacity, with irrigation applied to field capacity. Therefore, any leaching would occur due to the summer rainfall, and not through purposeful over-irrigation for salt management. A representative weather station with 50 years of daily temperature and precipitation data, located close to the basin, was selected. A summary of the water quality data used in the agronomic modelling is presented in Table 1.

It was assumed that the trace elements present in the water would generally not be mobile and would therefore be less likely to migrate into groundwater than the major cations and anions presented in Table 1. The outputs from this exercise were used to determine the irrigation return flows and the concentrations of cations and anions expected to leach to groundwater. These were then used as inputs for the hydrogeological modelling.

Economic modelling

A whole-farm model was built in FINSIM to simulate the financial performance of an existing farm intensified with a mine-water-irrigated cropping system. A typical farm owned in the Eastern Basin was assumed to cultivate 450 ha of dryland cash crops (maize and soybean. The farm was then intensified by reallocating 120 ha to a mine-water-irrigated cropping system, with the remaining 330 ha allocated to dryland cash crops.

The model accounted for revenue, direct costs, overhead costs, assets/liabilities and asset replacement costs. Revenue was calculated using 2023 crop prices and yield estimates, which accounted for modelled reductions in yield due to salinity in the irrigation water. It was assumed that the farmer does not pay for the CAPEX investment in the water infrastructure required to convey water from the water treatment plant to the farm's point-of-supply, that farmers could access water on demand, and that no storage would be required.

Hydrogeological Modelling

A numerical finite-element 3D groundwater flow model was developed using the SPRING software code from Delta h Ingenieurgesellschaft mbH, Germany (König, 2011). Model simulations assumed no retardation due to sorption, cation exchange, or any microbiological degradation in the subsurface. The simulated plumes, therefore, represent a conservative worst-case scenario for pollutant transport.

No background concentrations were assumed in the model simulations to predict and visualise the net effect of the irrigation return flows on the ambient groundwater quality. The model was run with a weekly timestep over 50 years, and simulated return-flow concentration plumes were mapped across the study area. A unit (100%) source concentration (return-flow concentration) and drainage (return flow) were used as determined by the agronomic modelling.

Table 1 *Average quantities of major constituents in Eastern Basin (EB) mine water. Concentrations are in mg/L, acidity as mg/L CaCO3 eq., EC in mS/m and pH without units.*

pH	EC	Ca	Mg	K	Na	SO42-	Cl	TDS	Acidity
7.81	257	321	97	13	188	1254	110	2314	9

Results and discussion

Suitability of mine waters for sustained irrigation

The agronomic modelling provided outputs on site-specific effects of mine water on relative crop yield, which were also used as inputs for the economic modelling. It was predicted that the mine water would be suitable for sustained irrigation of all assessed cropping systems, with little to no yield reductions due to water quality, except for the maize in the maize-oats double-cropping system. However, the yield reductions were less than 2% compared with irrigation with good-quality water. Yield estimates provided by the agricultural economists, based on typical yields in the area, were 12 t/ha for good-quality water, 11.8 t/ha for maize irrigated with EB mine water, and 8.3 t/ha for dryland maize. The yield reductions were considered negligible, particularly compared with dryland maize, which is expected to yield substantially less.

Impact of mine water irrigation on groundwater and receiving surface water

The hydrogeological model used drainage volumes from the agronomic modelling as irrigation return flows recharging the aquifer, as well as the solutes predicted to leach from return flows, to predict return flow plume concentrations over time. Return flow plumes were modelled for 110 pivots in the Minimum Water Use Scenario (2400 ha) and 273 pivots in the Maximum Area Scenario (6000 ha). Table 2 presents an example of the output results showing plume concentrations for a single pivot and is not representative of the entire output data set. It should also be noted that the model simulations assume no retardation due to, e.g. sorption, cation exchange, or any microbiological degradation in the subsurface. The simulated plumes, therefore, represent a conservative worst-case scenario for pollutant transport.

Considering the conservative (no retardation or transformation; i.e., worst-case) scenario, it was predicted that irrigation with EB mine water would increase groundwater solute concentrations over time. Plumes were also predicted to migrate up to 1km from the source; however, source concentrations that migrated that far were generally low and similar to those presented in Table 2 as source plume concentrations after 10 years. It was predicted that plumes of concentrated pivots would generally migrate further and increase in concentration faster than those of dispersed pivots, due to the convergence of plumes from nearby pivots.

It is predicted that, in all scenarios, return flow plumes will begin reaching surface water courses after 10 years of irrigation. However, this will occur within less than 5% of the plumes. After 50 years of irrigation, the proportion of plumes that reach surface water courses increases up to 43% in the Maximum Mine Water Use scenario and up to 65% in the Minimum Mine Water Use scenario when pivots are sited in a concentrated configuration.

Assuming a worst-case scenario where the receiving water body has no assimilative capacity and return flow fluxes to the surface

Table 2 *Modelled return flow plume concentrations (in mg/L) at the source after 10 and 50 years of irrigation for the most conservative scenario.*

Solute	Plume concentration at the source after 10 years	Plume concentration at the source after 50 years
Calcium as Ca	34–68	270–304
Chloride as Cl	31–63	250–282
Potassium as K	4–7	30–33
Magnesium as Mg	32–64	255–287
Sodium as Na	52–105	420–472
Sulphate as SO4	238–476	1904–2142
Total solutes	391–783	3130–3521

water bodies are similar to return flow fluxes to the saturated zone, the amount of solutes expected to migrate to surface water courses was estimated using the proportion of plumes expected to reach surface water after 50 years of irrigation. It was predicted that the Maximum Mine Water Use scenario would contribute an estimated 80 t/day of solutes to surface water courses, and irrigating 2400 ha would contribute an estimated 33 t/day, which is substantially less than the estimated 254 t/day currently being discharged with HDS-treated water.

Location and distribution of irrigated areas were identified as key factors in ensuring the sustainability of this practice and ensuring impacts remain acceptable.

Economic aspects of mine water irrigation

The economic assessments provided outputs on the profitability and cost of establishing an irrigation system at the farm level. The economic assessments indicated that irrigation with Eastern Basin mine water is economically viable and can be profitable, with an average gross margin in excess of R20 000/ha predicted for the maize-oats cropping system over the 8-year modelling period (Table 3). The Maximum Mine Water Use scenario was predicted to be less profitable than the Minimum Mine Water Use scenario due to a smaller area being planted in winter, resulting in insufficient additional income to cover the extra cost of repaying the irrigation investment. The cost of irrigation water that farmers pay is expected to play a significant role in determining its feasibility for crop production.

Conclusion

This interdisciplinary study successfully developed an approach that provided insights into the agronomic, economic, and environmental aspects of large-scale, long-term irrigation with mining-influenced waters and identified key factors to consider when implementing such schemes.

In the Eastern Basin, the mine water is expected to be suitable for sustained irrigation, provided water quality does not deteriorate over time and a suitable cropping system is selected. Some environmental impacts, particularly the transport of solutes to ground and surface water, are expected. However, it is important to determine whether these impacts are acceptable, which will depend on the type of water use (e.g., drinking, agricultural, industrial) and the baseline conditions before irrigation commences, which will require site-specific assessments. The magnitude and extent of the impacts were found to be strongly influenced by the distribution of pivots and the total irrigated area, both of which are influenced by water use. Mine water irrigation is expected to be profitable; however, its economic sustainability depends on water cost management, optimised cropping strategies, and long-term investment perspectives

The key factors to be considered for the large-scale establishment of mine water irrigation schemes were water quality and use, crop selection, total irrigation area, management of excess mine water, infrastructure, land availability and ownership, water costing, and the siting of irrigation schemes. It is evident that the successful roll-out of mine water irrigation at a regional scale requires careful planning based on in-depth, site-specific assessments, as well as adaptive management. This study developed an approach to assess the feasibility of large-scale mine water irrigation and to identify key considerations for implementing such schemes, which can be developed into a mine water irrigation feasibility assessment and implementation framework.

Table 3 *Predicted 8-year gross margins of dryland and mine water irrigated crops in rands per hectare (R/ha).*

System		2023	2024	2025	2026	2027	2028	2029	2030
Maize	Dryland	12500	13800	11600	13200	12400	12600	11900	12500
Soybeans		14500	10000	9400	9200	9400	9600	10500	10700
Maize	Irrigated	12700	16000	11500	13600	12300	12400	11300	12000
Oats		10500	12400	8700	10200	9200	9000	8000	8300

References

Annandale J, Jovanovic N, Pretorius J, Lorentz S, Rethman N, Tanner P (2001) Gypsiferous mine water use in irrigation on rehabilitated open-cast mine land: crop production, soil water and salt balance. Ecol Eng 17:153-164. DOI.org/10.1016/S0925-8574(00)00155-5

Annandale J, Tanner P, Heuer S (2021) Irrigation with poor-quality mine water in Mpumalanga. Report TT 855/1/21, Water Research Commission, Pretoria

Annandale J, du Plessis M, Tanner P, Heuer S, Madiseng L (2023) Irrigation Should be Explored as a Sustainable Management Solution to the Acid Mine Drainage Legacy of the Witwatersrand Goldfields. Mine Water and the Environment. https://doi.org/10.1007/s10230-023-00961-3

Department of Water and Sanitation-South Africa (DWS) (2016) Integrated Vaal River System- Limiting the Use of Water In Terms of Item 6 of Schedule 3 of the National Water Act of 1998 for Urban and Irrigation Purposes in the Catchment Areas of the Dams Supplying the Integrated Vaal River System and from the System

du Plessis MH, Annandale JG ,Benadé N (2023) A Decision Support System That Considers Risk and Site Specificity in the Assessment of Irrigation Water Quality (IrrigWQ). Applied Sciences 13(23): 12625. https://doi.org/10.3390/app132312625

Jovanovic N, Barnard R, Rethman N, Annandale J (1998) Crops can be irrigated with lime-treated acid mine drainage. Water SA 24:113–122

König CM (2011) Simulation of Processes in Groundwater (SPRING). delta h Ingenieurgesellschaft mbH. https://spring.delta-h.de/en/index.html

Parsons R, Conrad J (1998) Explanatory notes for the aquifer classification map of South Africa. WRC

TCTA (2017) Integrated Annual Report 2016/17. In: Trans Caledon Tunnel Authority (ed). p 39-41

IMWA 2026
Jeongseon

Crop and Soil Response to Acidic and Circum-Neutral Mine Influenced Waters

Siboniso Magwaza[1], John Annandale[1], Lesego Madiseng[1], Martin Steyn[1], Phil Tanner[1], Sakhiwo Sukati[1]

Department of Plant and Soil Sciences, University of Pretoria, Private Bag X20 Hatfield, Pretoria 0028, South Africa

E-mail: siboniso.magwaza@tuks.co.za, john.annandale@up.ac.za

Abstract

Acid mine drainage (AMD) requires treatment to circum-neutral pH using High-Density Sludge (HDS) or Biological Sulfate Reduction (BSR) processes to lower metal concentrations and reduce environmental impact. Further treatment to potable standards is very costly, making alternatives like irrigation with untreated or neutralised mine water worthy of consideration. A field trial tested the response of lucerne (*Medicago sativa*), sorghum (*Sorghum Bicolor*), soybean (*Glycine max*) and teff (*Eragrostis tef* [Zucc]) to irrigation with three mine waters [untreated AMD (pH ≈ 3.1, EC ≈ 407 mS m^{-1}), HDS-treated (pH ≈ 8.5, EC ≈ 350 mS m^{-1}), and BSR-treated (pH ≈ 7.6, EC ≈ 336 mS m^{-1})], from a treatment plant in the Mpumalanga Coalfields, South Africa. Crops performed well with HDS water, with a 25% yield penalty for untreated AMD and 50% for BSR water. Elemental concentrations increased in soil and trace elemental accumulation in plants, raising concerns about long-term continuous irrigation.

Keywords: BSR neutralised AMD, fibre and biofuel crops, food safety, HDS neutralised AMD, mine water irrigation

Introduction

The mining industry produces large volumes of mine-influenced water that must be managed responsibly (Annandale *et al.* 2006; Hutton *et al.* 2009). These waters vary widely in quality, depending on geology and the mining method used. Most are unsuitable for release into the environment without some form of treatment. A common practice is to neutralise acid mine drainage (AMD) using hydrated lime or limestone in high-density sludge (HDS) plants or using sulphate reducing bacteria in BSR plants. Such treatment raises the pH and lowers metal concentrations, but water is still too saline for direct release to natural water bodies. Further treatment is required to remove salts, which can be achieved by reverse osmosis (RO) to produce potable water, but this is very costly and energy intensive. Furthermore, HDS and RO treatment generate by-products in the form of gypsiferous sludges and brines, which also need to be managed. Therefore, alternative responsible mine water management options are sought. One being proposed is irrigation of crops on strategically limed soils with untreated acidic mine water, which, if successful, could eliminate the need for HDS or BSR treatment. If irrigation with acidic mine water proves to be problematic, then neutralisation will be essential before utilisation through irrigation, and significant savings would still be possible because there would be no need for RO and brine disposal.

Irrigation with such water has not been intensively studied. Therefore, a small-scale field trial was established at the centrally located mine water treatment plant at eMalahleni, Mpumalanga Province, South Africa. This location was strategically selected as it facilitated access to a range of mine influenced water. The specific aim of this study was to investigate crop and soil responses to irrigation with untreated highly acidic AMD with additional limestone applied to the soil, HDS neutralised AMD, and BSR treated AMD. Food and feed safety of the produce was also assessed.

Methods

Due to the limited area available, three water sources were tested alongside four cropping systems: soybean (*Glycine max*), lucerne (*Medicago sativa*), grain sorghum (*Sorghum bicolor*), and teff (*Eragrostis tef* [Zucc]), with four replicates. The main plots, representing different water treatments, had an area of 449 m2, with 1.5 m spacing between them (Figure 1). Each block had nine permanent sprinklers. One full-circle sprinkler was placed centrally, with four quarter-circle sprinklers in the corners and four half-circle sprinklers in the middle of each side. To minimize the risk of wind drift, sprinkler height was set at 1 m, necessitating the selection of short crops. Subplots, representing different cropping systems, each had an area of 24 m^2, with a 0.5 m path between them. A structure supporting dense shade netting was erected between water treatments to reduce wind drift transporting irrigation waters to adjacent water treatment plots. Netting was rolled back after irrigation to avoid edge shading for this trial. Table 1 presents the average quality of the waters tested.

Soils were analysed for pH (measured in KCl), EC in a saturated soil paste extract, P using the Bray 1 method, and K, Na, Ca, S, and Mg in ammonium acetate extracts, with Cu, Fe, and Mn in Mehlich-3 extracts. Total concentrations of trace elements were determined through microwave-assisted aqua regia dissolution and analysed by Inductively Coupled Plasma Optical Emission Spectrometry (ICP-OES) to establish baseline values (Table 2).

Crop height and canopy cover were measured weekly, and at maturity, vegetative plant biomass and yield where applicable were determined with plants cut at ground level and oven-dried at 65 °C for 48 h. Plant tissue analyses determined the concentrations of potentially toxic elements in biomass grain. Data were analysed using Microsoft Excel and GenStat, with mean separation performed using Duncan's multiple range test at a 95% probability level ($P < 0.05$).

Results and discussion

Effects of mine water on soil pH and EC.

Weekly irrigation was applied during the summer of 2024/25 for 21 weeks, with ≈471 mm irrigation and ≈229 mm rainfall. Water EC and pH were monitored with each irrigation. Untreated AMD had the highest EC (≈407 mS m^{-1}) and lowest pH (≈3.1). BSR treatment improved water quality to an EC of ≈336 mS m-1 and a pH of ≈7.6 and HDS water to an EC of ≈350 mS m^{-1}) and pH of ≈8.5. The limestone application rate was based on the total acidity (2015 mg L^{-1}) of the irrigation water, expressed as the amount of $CaCO_3$ necessary to neutralise the water to a target pH of 8.3. The estimated irrigation was 700 mm, with the soil amounting to 2 100 t ha^{-1}. The application of 14.1 t ha^{-1} of limestone effectively neutralised the pH of the untreated AMD, as the pH of the soil increased only slightly from 7.7 to 7.8 by the

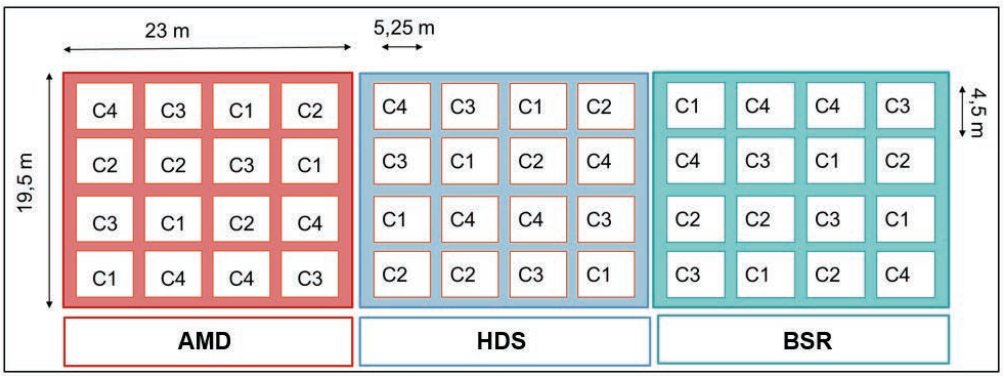

Figure 1 Trial layout design.

Table 1 Average chemical composition of the mine influenced water used for irrigation. Concentrations are in mg/L, EC in mS/m and pH is without unitless.

Constituent	AMD	HDS	BSR
pH	3.1	8.5	7.6
EC	407	350	336
Al	68	0.09	0.1
As	<0.01	<0.01	<0.01
Cd	0.004	<0.003	<0.003
Ca	412	683	264
Cl	11	31	-
Cu	0.03	<0.01	0.01
F	<0.2	0.64	0.4
Pb	<0.01	<0.01	<0.01
Mg	201	114	193
Mn	21	0.08	0.07
Hg	<0.001	<0.001	-
Ni	0.46	0.06	0.03
Se	0.02	BDL	0.00
Na	187	131	70
SO_4	2871	2394	800
Fe	638	31	1.02
Zn	1.50	0.03	0.52
TDS	4910	3752	–
TSS	200	96	–

pH was averaged using the formula $-\log_{10}[(\Sigma C_1)/(n)]$. - indicates not analysed.

end of the season. Irrigation increased the pH of the BSR and HDS blocks to 7.9. All blocks showed higher conductivities than the pre-irrigation sample (189 mS m^{-1}), with topsoil EC increasing to 230 mS m^{-1} (AMD), 224 mS m^{-1} (BSR), and 215 mS m^{-1} (HDS) after one irrigation season.

Crop response to irrigation with mine water

Sorghum and soybean irrigated with BSR water exhibited delayed seed germination, poor crop establishment, and signs of stunting compared to HDS and AMD treatments. Significant differences ($P < 0.05$) were observed in aboveground biomass production for all crops (Figure 2). Sorghum incurred yield penalties of 26% with untreated AMD and 52% for BSR-treated water relative to the HDS control. The effects on plant growth in the BSR treatment might have been caused by bicarbonate salinity which appears to be more severe than calcium sulfate dominated salinity which tends to precipitate gypsum in the soil profile, thereby lowering root-zone salinity which reduces salinity stress of crops (Ossorio *et al.* 2017).

Food safety of crops irrigated with mine water

Sorghum grain was analysed for food safety, and irrigation with mine influenced water increased elemental concentrations. The presence of Ni at a threshold of 10 mg kg^{-1} and Pb at 0.2 mg kg^{-1} in all treatments and Hg at levels above 0.1 mg kg^{-1} under irrigation AMD indicated that these levels were not safe for human consumption. However, the plant analysis data was deemed unreliable, as mass balance calculations indicated "measured" values were impossibly high. These analyses will be redone to ensure accuracy. Hg which was below the detection limit (<0.001) in

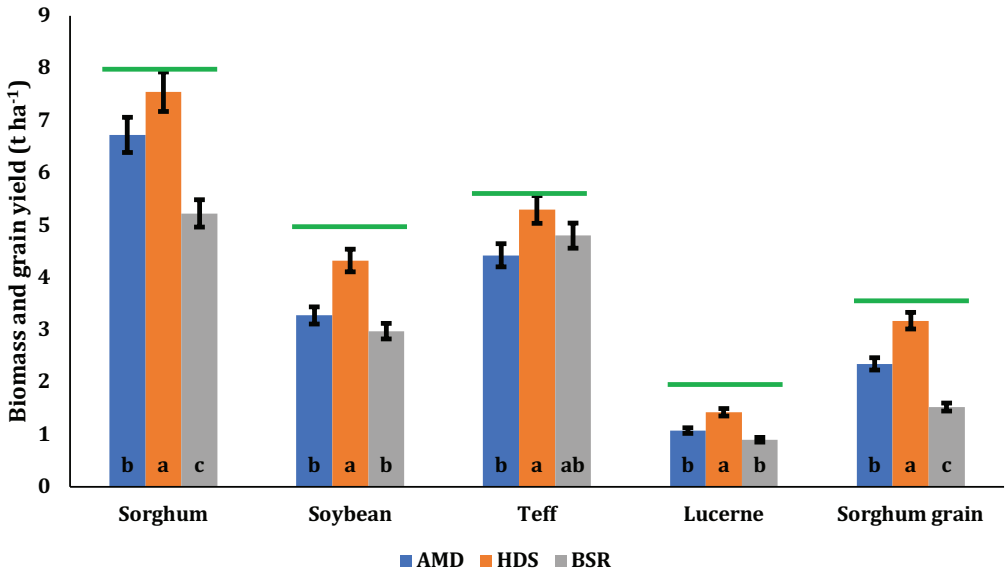

Figure 2 Aboveground biomass and grain yield of crops produced in the summer of 2024/2025. Horizontal green lines indicates published irrigated agronomic target yields for the different crops in the region. Different letters (a–c) indicate significant differences within a species ($p \leq 0.05$).

the waters, increased concentrations to 0.04 mg kg^{-1} (HDS) and 0.06 mg kg^{-1} (BSR) in circum-neutral waters. This proves that even though trace elements may be present in small amounts in the irrigation waters, when applied over prolonged periods, plus initial soil concentration, would result in increased accumulation, which is a major concern if irrigation is applied continuously. Therefore, careful monitoring is recommended to ensure that there are acceptable offsite environmental impacts and that the produce remains safe for consumption.

Conclusions

Irrigation with these mine influenced water increased soil pH and EC, with the increase in pH for the AMD treatment ascribed to limestone application. Irrigation with untreated AMD reduced aboveground biomass by 25%, and with BSR water, by more than 50%. This suggests that highly acidic AMD requires treatment prior to irrigation, and that high-bicarbonate BSR-treated water requires a polishing step to reduce bicarbonate salinity levels. Ca- and sulfate-rich HDS water, similar to that investigated by Jovanovic *et al.* (1998), demonstrated considerable potential for irrigation, with plant growth and yields comparable to those expected under irrigation with good-quality water, with limited elemental accumulation. Plant tissue analysis from this experiment resulted in increased Ni, Pb, and Hg accumulation, which is a major concern if irrigation is applied continuously. It is understandable that concerns regarding food and feed safety may arise. Therefore, it is prudent to monitor these risks, and if concerns are perceived or real, non-edible industrial crops can be considered.

Acknowledgements

The authors thank the water treatment plant in the Mpumalanga Coalfields for hosting the research team. We thank the Water Research Commission (WRC) of South Africa for funding this work (grant C2021/2023-00555), along with the Mine Water Coordinating Body (MWCB), MINTEK through the Technology Innovation Agency (TIA), and Coaltech.

References

Annandale JG, Jovanovic NZ, Pretorius JJB, Lorentz SA, Rethman NFG, Tanner PD (2001) Gypsiferous mine water use in irrigation on rehabilitated open-cast mine

land: crop production, soil water and salt balance. *Ecol. Eng.* https://www.sciencedirect.com/science/article/pii/S0925857400001555

Jovanovic NZ, Barnard RO, Rethman NFG, Annandale JG (1998) Crops can be irrigated with lime-treated acid mine drainage. Water SA 24:113-122. https://www.wrc.org.za/wp-content/uploads/mdocs/WaterSA_1998_02_apr98_p113.pdf

Annandale J, Jovanovic N, Hodgson F, Usher B, Aken M, van der Westhuizen A, Bristow K, Steyn J (2006) Prediction of the environmental impact and sustainability of large-scale irrigation with gypsiferous mine-water on groundwater resources. Water SA 32: 21-28. https://doi.org/10.4314/wsa.v32i1.5235

du Preez K (2021) *Mintek's Integrated cloSURE TM Technology for Treatment of Acid Mine Drainage.* https://www.imwa.info/docs/imwa_2021/IMWA2021_duPreez_129.pdf

Hutton B, Kahan I, Naidu T, Gunther P (2009) Operating and Maintenance Experience at the Emalahleni Water Reclamation Plant. *International Mine Water Conference, Pretoria, South Africa*, (October), 415–430. https://www.imwa.info/docs/imwa_2009/IMWA2009_Hutton.pdf

Kaksonen AH, Puhakka JA (2007) Sulfate reduction based bioprocesses for the treatment of acid mine drainage and the recovery of metals. *Eng. Life Sci,* 7(6), 541–564. https://doi.org/10.1002/elsc.200720216

Ossorio M, Stawski TM, Rodríguez-Blanco JD, Sleutel M, García-Ruiz JM, Benning LG, Van Driessche AES (2017) Physicochemical and additive controls on the multistep precipitation pathway of gypsum. *Minerals*, 7(8). https://doi.org/10.3390/min7080140

IMWA 2026
Jeongseon

Feasibility Study for Geothermal Mine Water Usage at the Mine Water Drainage Site Haus Aden, Bergkamen, Germany

Kevin Mannke, Dr. Florian Hahn, Alexander Nikolov, Roman Ignacy

Fraunhofer Research Institution for Energy Infrastructures and Geotechnologies IEG, Germany,
Kevin. Mannke@ieg.fraunhofer.de, ORCID 0009-0000-1130-8551
Florian.Hahn@ieg.fraunhofer.de
Alexander.Nikolov@ieg.fraunhofer.de
Roman.Ignacy@ieg.fraunhofer.de

Abstract

This study evaluates the geothermal potential of mine water at the Haus Aden drainage site in Bergkamen, Germany. Technical assessments, system configurations, and integration into the district heating network were analysed in collaboration with key stakeholders. Results show that mine water can provide a reliable base-load heat supply, complemented by biomass for peak demand. A phased system development reduces economic risks and improves feasibility. The project has the potential to become one of the largest mine-water geothermal systems in Europe. The study also highlights the importance of stakeholder coordination and provides transferable concepts for future mine-water-based energy systems.

Keywords: IMWA 2026, mine water, geothermal energy, district heating, heat pump, Ruhr area, coal mining

Introduction

As part of the European transition towards greenhouse gas-neutral heat supply, a transformation study was conducted for the existing district heating network in Bergkamen, Germany, to identify and evaluate potential climate-neutral supply concepts. Within this context, the assessment of locally available renewable energy sources revealed that the city and its heating infrastructure are situated above a considerable geothermal resource associated with mine water. The Ruhr area, including the city of Bergkamen, is characterised by a long history of hard coal mining, which has substantially shaped both the regional infrastructure and subsurface conditions. Following the ending of mining activities, continuous mine water management remains necessary to control groundwater levels and prevent uncontrolled discharge. Central mine water pumping sites provide long-term and reliable access to subsurface thermal energy. Despite this favourable starting point, the integration of mine water into large-scale district heating systems is still limited and requires comprehensive technical, economic, and organisational evaluation. In particular, the utilisation of centralised pumping sites offers a relevant potential for scalable and continuous heat supply but remains insufficiently explored in practice.

This study investigates the feasibility of using mine water from the Haus Aden pumping site in Bergkamen as a key component of a future climate-neutral heat supply system. The aim is to develop and evaluate technical concepts, assess their integration into the existing heating network, and identify pathways for a phased system implementation. In addition, the study considers the role of stakeholder coordination as a critical factor for successful project development.

Regional and Technical Background

Mining legacy and mine water management in the Ruhr area

Hard coal mining in Bergkamen was primarily carried out at the collieries Haus Aden and Grimberg. The first shaft at Haus Aden was sunk in 1938, followed by a second shaft in 1939. Mining activities continued at this site until 2001 and were later integrated into the colliery Ost, where operations persisted until 2010. Within the municipal area, shaft Grimberg 3 reaches a depth of 1638 m and is therefore among the deepest shafts in the Ruhr area as well as one of the deepest hard coal shafts overall (Huske J, 2006). After the ending of mining activities, the mine water management strategy in the Ruhr area was fundamentally restructured. A centralised mine water management system was established to maintain controlled mine water levels across the entire Ruhr coalfield. Today, mine water is pumped at six central locations to ensure that defined water levels are maintained throughout the system (Figure 1). The objective of this centralised approach is to prevent uncontrolled mine water rise into overlying groundwater horizons. At the same time, the concentration of pumping activities at selected sites increases operational efficiency and enables a more controlled discharge of mine water into larger receiving waters.

The central mine water pumping sites include Lohberg, Walsum, Robert Müser, Heinrich, Friedlicher Nachbar and Haus Aden. The present study focuses on the Haus Aden site, which represents one of these key locations within the regional mine water management system (RAG Aktiengesellschaft 2024).

Mine water provinces and centralised management system

Mine water provinces describe hydraulically connected mining areas that have been linked over decades of mining activities through underground connections. Within the framework of the so-called box model, created by the German company DMT by order of the RAG AG, these connections were systematically documented, including

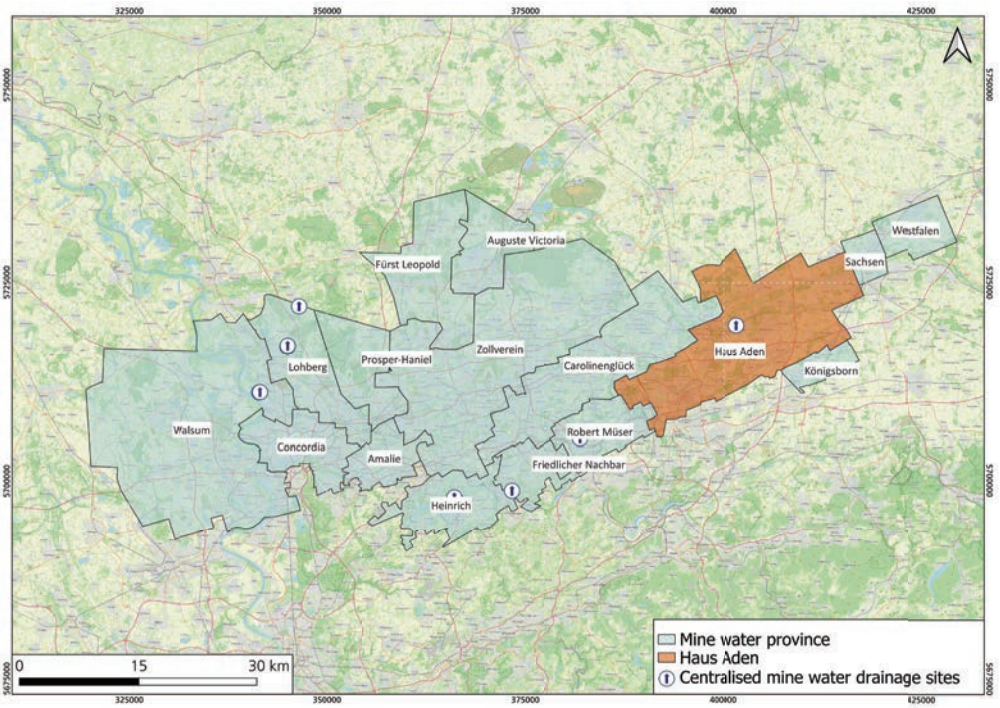

Figure 1 *Mine water provinces of the Ruhr area and centralised pumping sites (Data provided by RAG AG).*

transfer points between individual mine workings and their respective depth levels. Based on this information, water flow between the different provinces can be modelled and hydraulic interactions can be analysed. In addition, the model allows the identification of hydraulic separations between individual mine systems.

Within this system, the Haus Aden site plays a key role for the eastern part of the Ruhr area. It is responsible for pumping mine water originating not only from Bergkamen but also from adjacent areas such as Kamen, Hamm and Dortmund. To prevent a continuous rise of mine water levels within the connected provinces, a long-term balance between inflowing and extracted water volumes must be achieved. This requires that, beyond a certain point, the pumped discharge corresponds to the inflow from surrounding mine workings.

Figure 1 illustrates the spatial distribution of the mine water provinces as well as the centralised pumping sites. The investigated shaft Haus Aden 2 is highlighted, showing the area that is primarily influenced by its operation. The extracted mine water is planned to be treated and subsequently discharged into the River Lippe, located north of the site, from where it is transported further towards the Rhine.

Utilisation of mine water

For centralised pumping sites, the utilisation of the thermal energy contained in the extracted mine water represents the most relevant application pathway. At the Haus Aden site, mine water is planned to be pumped from a depth of approximately 600 m below surface level. Based on the geothermal gradient, mine water temperatures of around 20 to 22 °C are expected. The extracted mine water therefore provides continuous access to geothermal energy from depth. As mine water pumping is required as a permanent task, this resource represents a long-term and reliable energy source.

From an economic perspective, systems based on existing pumping infrastructure offer clear advantages compared to concepts requiring dedicated extraction wells. No additional investment for subsurface development is required, while large and continuously replenished water volumes are available. As a result, thermal regeneration of the underground system is not necessary.

In addition, the centralisation of pumping activities leads to substantially higher extraction rates at individual sites compared to decentralised systems. This allows for the utilisation of substantially larger thermal potentials at centralised pumping locations such as Haus Aden.

Heat demand and system integration

Heat demand and network development

The existing district heating network is located in the eastern part of Bergkamen. It has a total length of 22.7 km and a maximum peak generation capacity of 42.1 MW. Currently, approximately 600 residential and commercial units are supplied, resulting in a total annual heat demand of about 40 GWh. For the further development of the system, the heat demand of the remaining urban area was assessed. In cooperation with the local utility (GSW Gemeinschaftsstadtwerke GmbH Kamen, Bönen, Bergkamen), priority areas for network expansion as well as areas for future decentralised, non-network-based supply were identified. Based on this, a phased network expansion pathway was developed, including planned pipeline routes and a timeline for the connection of individual districts. The heat demand was determined using the spatial heating demand model of North Rhine-Westphalia (LANUV, 2024), provided by the Landesamt für Natur, Umwelt und Verbraucherschutz Nordrhein-Westfalen. The model is based on a GIS-based dataset of building-specific heat demand values derived from building characteristics, typologies, and statistical assumptions. To improve the reliability of the calculated demand, the model results were validated and refined using gas consumption data from the supply area. For the development of supply scenarios, the different energy sources available within the project area were analysed. Based on this assessment, several system configurations were defined and subsequently compared with regard to their economic performance. A key objective of this planning process was the connection of

the existing network in the eastern part of the city with the mine water pumping site at Haus Aden in order to enable the integration of a sustainable and renewable heat source. In the final expansion stage, the total heat demand of the network is expected to increase to approximately 83 GWh/a, representing nearly a doubling of the current system. Figure 2 shows the potential expansion options for the district heating grid.

The existing biomass combined heat and power plant will continue to provide renewable heat. However, its role is planned to shift from base-load supply towards peak-load coverage, while mine water is intended to gradually assume an increasing share of the base load. As an initial step, the installation of a mine water heat pump with a capacity of 2.5 MW is planned. This system is intended to cover a first share of the base load of the district heating network.

Technical integration and system concept

The extraction of mine water is planned to be implemented in a phased approach in order to control and gradually slow down the rise of mine water levels. The objective is to progressively reach the targeted long-term mine water level. In parallel, the capacity of the heat pump system can be expanded step by step. For geothermal utilisation, a partial flow of the pumped mine water is diverted from the main discharge line. The thermal energy is transferred via a heat exchanger to a secondary circuit and subsequently supplied to the heat pump system. After heat extraction, the mine water is returned to the main flow. The heat pump uses the extracted thermal energy in combination with electrical energy to provide heat at the required network temperature level. In the final expansion stage, a pumping rate of up to 24 m³/min is expected at the Haus Aden

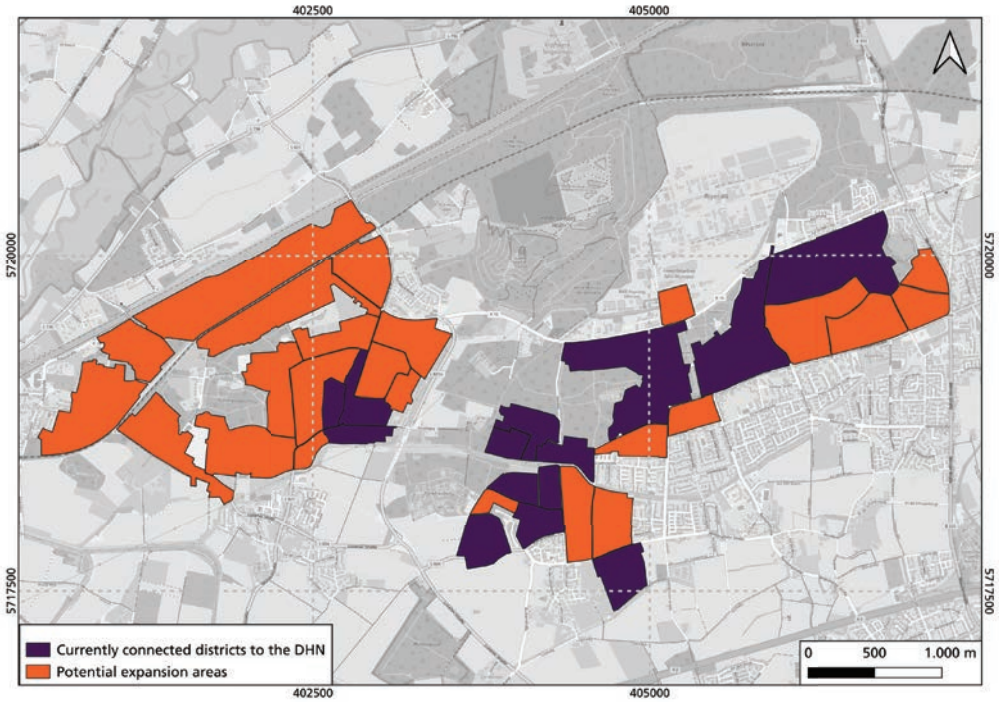

Figure 2 *Display of districts which are connected to the DHN at the moment of the study, and potential areas where the heating grid can be expanded to in the future (Expansion plan developed by Fraunhofer IEG and GSW).*

site. With a temperature difference of up to 15 K, this corresponds to a thermal output of approximately 25 MW based on the mine water alone. The use of electrical energy within the heat pump system allows for a further increase in the usable heat output. Overall, the results indicate that a large share of the urban heat demand can be covered by mine water under the described system configuration.

Discussion

During the feasibility study, the importance of close coordination between the local energy supplier and the operator responsible for mine water pumping became evident. The development of a mine-water-based heat supply system involves a number of legal and organisational aspects that require careful consideration. In particular, interface points within the system, such as heat exchangers and heat pump installations, represent critical boundaries. These points are essential for clearly defining responsibilities between the involved stakeholders and for structuring ownership and operational frameworks. Early involvement of all relevant parties proved to be a key factor for project progress. It enabled the identification of potential challenges at an early stage and allowed for the development of appropriate solutions before they could hinder further planning. If successfully implemented, the project has the potential to serve as a reference case for future mine water geothermal systems at centralised pumping sites. In this context, it may provide a transferable approach for the utilisation of mine water as a renewable heat source.

Conclusions

The results of the feasibility study demonstrate that the mine water drainage site at Haus Aden in Bergkamen has considerable potential for the expansion of its existing district heating network. This expansion is intended to be realised using renewable heat sources. Due to its specific location and its function as a centralised mine water pumping site, the Haus Aden site plays a key role in this context. The utilisation of mine water offers the possibility to provide a substantial share of the required heat and to support the transition towards a sustainable heat supply system.

The study further shows that close coordination between the mine water operator and the local energy supplier remains essential. The utilisation of mine water has to always be aligned with the existing mine water management concept in order to ensure both technical feasibility and long-term operational stability and having no negative influence on the mine water drainage concept. If successfully implemented, the project has the potential to become a reference for mine-water-based heat supply systems and to demonstrate the role of centralised pumping sites in future energy systems.

Acknowledgements

The authors thank all co-organisers for hosting the IMWA 2026 Conference. In addition, they thank the project partners at GSW for conducting this study and RAG AG for providing valuable input on the mine water utilisation aspects.

References

Huske J (2006) Die Steinkohlenzechen im Ruhrrevier – Daten und Fakten von den Anfängen bis 2005 In: Deutsches Bergbau-Museum Bochum, Bochum, p 413–690

Landesamt für Natur, Umwelt und Verbraucherschutz Nordrhein-Westfalen (LANUV) (2024) Potenzialstudie zur zukünftigen Wärmeversorgung in NRW – Kurzdokumentation: Raumwärmebedarfsmodell NRW, Version 2, Stand 17.12.2024

RAG Aktiengesellschaft (2024) Konzept zur langfristigen Optimierung der Grubenwasserhaltung der RAG Aktiengesellschaft für Nordrhein-Westfalen gemäß §4 Abs. 2 Erblastenvertrag zur Bewältigung der Ewigkeitslasten des Steinkohlenbergbaus. Essen, RAG. 33 S. (Report).

Exploring the Effects of Seawater Use in Cu-Ni-PGM Ore Flotation against Recycled Mine Water

Malibongwe S. Manono[1], Lisa L. October[2], Kirsten C. Corin[1]

[1]*Centre for Minerals Research, Department of Chemical Engineering, University of Cape Town, Private Bag X3, Rondebosch 7701, South Africa, malibongwe.manono@uct.ac.za, ORCID 0000-0002-2928-9368*

[2]*School of Chemical and Metallurgical Engineering, University of the Witwatersrand, Johannesburg 2017, South Africa*

Abstract

This study presents a comparative laboratory investigation of flotation performance using seawater and synthetic recycled mine water for a Merensky Cu–Ni–PGM ore. Batch flotation tests were conducted following standard Centre for Minerals Research protocols and complemented by three-phase froth stability tests. Seawater sourced from two coastal locations was benchmarked against synthetic plant water designed to replicate recycled process water chemistries. Key performance indicators included solids and water recoveries, froth height, froth stability (collapse time), and bubble size, alongside characterisation of water chemistry. Results demonstrate that seawater systems consistently yield higher solids and water recoveries relative to recycled process water.

Keywords: Flotation, mine water, salinity, seawater, water reuse

Introduction

Water availability has emerged as a critical constraint for mining and mineral processing operations globally, particularly in semi-arid regions such as Southern Africa, where platinum group metal (PGM) production is concentrated. Mineral flotation circuits are inherently water-intensive, often comprising up to 85% water by volume, and are therefore highly sensitive to water quality variations (Muzenda 2010). As freshwater resources become increasingly limited, the mining industry is progressively adopting alternative water sources, including recycled process water and seawater, to sustain operations and meet environmental compliance targets (Slatter *et al.*, 2009; Harrison *et al.* 2018). However, the reuse of mine water and the introduction of water of high salinity such as seawater fundamentally alter the chemical environment of flotation systems (Le *et al.* 2020). Elevated ionic strength and the presence of specific ions (e.g., Ca^{2+}, Mg^{2+}, SO_4^{2+}) influence key interfacial phenomena, including collector adsorption, bubble coalescence, froth stability, and entrainment behaviour (Manono *et al.* 2018). In particular, high ionic strength has been shown to suppress bubble coalescence, resulting in smaller bubble sizes and more stable froths, which can enhance mass pull but may also increase gangue entrainment (Craig *et al.* 1993; Manono *et al.* 2018). These competing effects introduce a critical trade-off between recovery and selectivity in flotation systems operating under saline conditions. While the effects of water chemistry on flotation have been widely studied for base metal systems (Biçak *et al.* 2012), there remains a notable gap in understanding these interactions within the context of Cu–Ni–PGM ores, particularly under seawater conditions (Cisternas and Gálvez 2018). Most existing studies have focused on recycled process water, with limited direct comparison to seawater despite its growing industrial relevance. Furthermore, the distinct ionic composition of seawater, characterised by high concentrations of Na^+, Cl^-, Mg^{2+} and SO_4^{2+}, introduces additional complexity beyond simple ionic strength effects.

This study therefore aims to provide a comparative assessment of flotation performance in seawater and synthetic recycled mine water for a Merensky Cu–Ni–PGM ore. By systematically evaluating

metallurgical responses and froth stability characteristics under controlled laboratory conditions, this work seeks to advance the understanding of water chemistry as an active metallurgical variable, with implications for water reuse strategies and sustainable processing in PGM operations.

Methods

Ore Preparation

A Cu-Ni-PGM ore from the Merensky reef situated in the Bushveld Igneous Complex (BIC) of South Africa was used for experimentation. The bulk ore sample was crushed, riffled, and then split into 1 kg samples using a rotary splitter. This ensured that the crushed ore had a consistent particle size distribution and composition for each 1 kg bag sample.

Water Quality

Recycled Mine Water

Synthetic plant water of the quality shown in Tab. 1, prepared from salts of analytical grade, was used during milling and flotation experiments. The quality of the synthetic plant water is one that mimics typical recycled mine water in Cu-Ni-PGM ore concentrators in the BIC (Manono *et al.* 2018).

Seawater

Seawater from two different coasts in Cape Town, South Africa were also used during milling and flotation procedures for comparative analysis with synthetic plant water. Seawater collection was done on the Southern Coast and the Northern Coast relative to the location of the University of Cape Town's Upper Campus. The Southern Coast Seawater (SCSW) was water collected at Rumbly Bay in Millers Point while the Northen Coast Seawater (NCSW) was collected from Silwerstroomstrand Resort off the West Coast. The water was collected in five 25 L drums at each location (125 L from each beach). To remove unwanted particles such as leaves and grass, SCSW obtained at Rumbly Bay was left to sediment. The point of collection was relatively clean hence there was no sand obtained and the few dirt particles were dense enough to remain at the bottom of the drum during use of the water. However, the water obtained in the North required filtering using the filter press because the particles present did not sink overnight. Tab. 2 shows data obtained from a microparameter water quality meter. The meter measured different parameters in the SPW, SCSW, NCSW for comparison. In this paper we report the pH, electrical conductivity, pH, and total dissolved solids.

The pH of the three water types was within the range of 7 to 8, SCSW was the most alkaline with the highest pH of 8.29. The results show that the electrical conductivity (EC) of SCSW, with SPW having the lowest electrical conductivity. The EC and TDS of the NCSW were little lower than that of the SCSW, while the EC and TDS of the SPW were the lowest.

***Table 1** Ionic Composition of Synthetic Plant Water that Mimics Recycled Mine Water.*

Water Type	Ca^{2+} (mg/L)	Mg^{2+} (mg/L)	Na^{+} (mg/L)	Cl^{-} (mg/L)	SO_4^{2-} (mg/L)	NO_3^{-} (mg/L)	CO_3^{2-} (mg/L)	TDS (mg/L)	Ionic strength (mol/L)
SPW	80	70	153	287	240	176	17	1023	0.0242

***Table 2** Summary of Data obtained from a Microparameter Water Quality Meter.*

	Unit	SPW	SCSW	NCSW
pH	–	7.61	8.29	7.94
Electrical Conductivity (EC)	µS/cm	3302	31640	21240
Total Dissolved Solids (TDS)	mg/L	1651	15820	10620

Chemical Reagents

Sodium Isobutyl Xanthate (SIBX)

To make a 1% solution of SIBX, one gram of the SIBX was measured on a scale in a weighing dish and added to 100 mL of deionised water and stirred using a spatula. The SIBX used had an activity of 94.4% and it was supplied by AECI Mining Chemicals. This solution was made daily since it decomposes quickly.

Senfroth 200

The frother used in the froth column tests and the flotation procedure is SENFROTH XP 200 provided by AECI Mining Chemicals. The chemical was provided in liquid form already hence no mixing was required; it can be used directly. The molecular weight of SENFROTH XP 200 is 205.40 g/mol and a purity of 98%.

Experimental Matrix

Table 3 shows the experimental matrix that was used. The proposed work had 5 flotation runs that were duplicated to reduce errors, making the runs accumulate to 10 experimental tests in total. The following denotions are used on Tab. 3: SPW = Synthetic Plant Water, SCSW = South Coast Seawater, NCSW = North Coast Seawater, M = Milling, F = Flotation. An experimental condition showing SPW-SPW implies ghat the water used for milling was SPW and the water used during flotation was SPW.

Batch Milling and Flotation Procedure

A 1 kg sample of the crushed ore was poured into a rod mill and 500 mL of either SPW or seawater was added to the mill depending on the experimental run being conducted to produce a slurry of 66% solids. A syringe was then used to draw 15 mL of the SIBX which was then poured into the ore and water to mix inside the mill. The mill was securely closed and allowed to run for 21 minutes as this was determined as the required time to obtain a grind of 60% passing 75 µm. The milled slurry was then transferred to a 3 L UCT Barker Flotation cell where the 3 L volume was made up by the required water type (SPW, SCSW or NCSW). This produces a slurry of 35% solids. Following the standard UCT flotation procedure described in (Wiese *et al.* 2005), The impeller was then switched on to a constant speed of 1200 rpm, and this was followed by extracting 50 mL feed sample (with no reagents except the collector added during milling). At t = 0 min, the frother was then added and allowed to condition for a minute. After the frother conditioning time, at t = 1 min the air supply is added and maintained at a flowrate of 7 L/min for all the tests. The froth height was maintained at the 2 cm mark by using top up with of the required water at regular time intervals. The concentrates were then scraped in 15 s intervals with four concentrates collected. The air supply was then turned off, and two 50 mL tailing samples were taken. The bulk tails, small tails samples, feed and concentrates filtered and left overnight in an oven to dry. Samples were thereafter weighed and analysed for Cu and Ni using a handheld XRF analyser.

Results and Discussion

Solids and Water Recoveries

Fig. 1 shows a comparison of the trends on solids and water recoveries for the selected ore milled and floated in various water qualities with the baseline condition being milling in synthetic plant water and flotation in synthetic plant water (SPW-SPW).

It can be seen from Figure 1 that the milling in SPW and flotation in SCSW resulted in an increase in solids and water recoveries compared to the baseline condition of SPW-SPW. Milling in SPW and flotation in NCSW resulted in an even greater increase in solids and water recoveries.

***Table 3** Experimental Matrix Followed during the Study.*

Experiment	SPW-SPW		SPW-SCSW		SPW-NCSW		SCSW-SCSW		NCSW-NCSW	
Point of Addition	M	F	M	F	M	F	M	F	M	F
Water Added	SPW	SPW	SPW	SCSW	SPW	NCSW	SCSW	SCSW	NCSW	NCSW

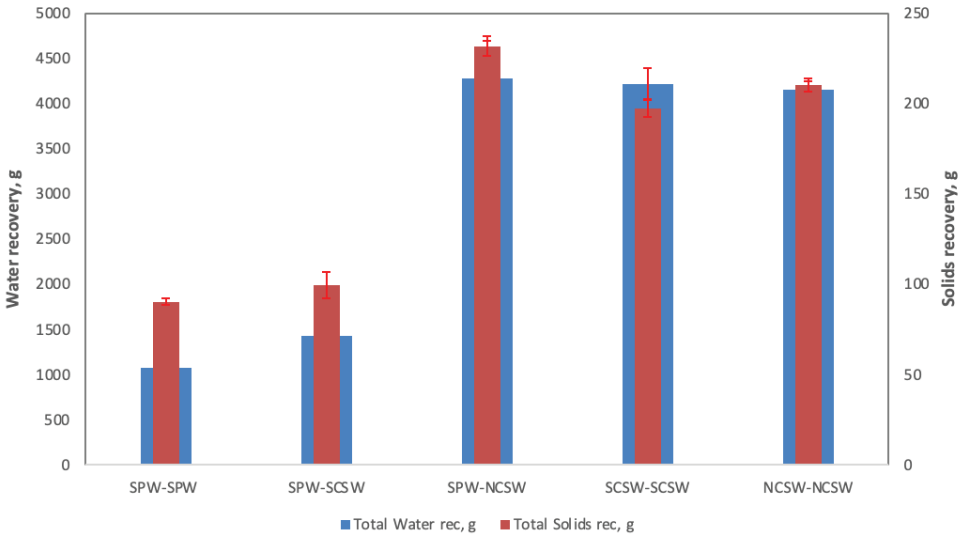

Figure 1 *Solids and water recoveries in synthetic plant water.*

Copper Recoveries and Grades

Fig. 2 shows a comparison of the flotation of copper recoveries and grades for the selected ore milled and floated in various water qualities.

It can be seen from Fig. 2 that copper recoveries follow a similar trend to that observed for solids and water recoveries, increasing as the system is changed from SPW-SPW to seawater conditions. The baseline SPW-SPW condition exhibits the lowest copper recovery, while the introduction of seawater during flotation (SPW-SCSW and SPW-NCSW) results in improved recoveries. In contrast, copper grades show an opposing trend, with higher recoveries associated with a reduction in grade.

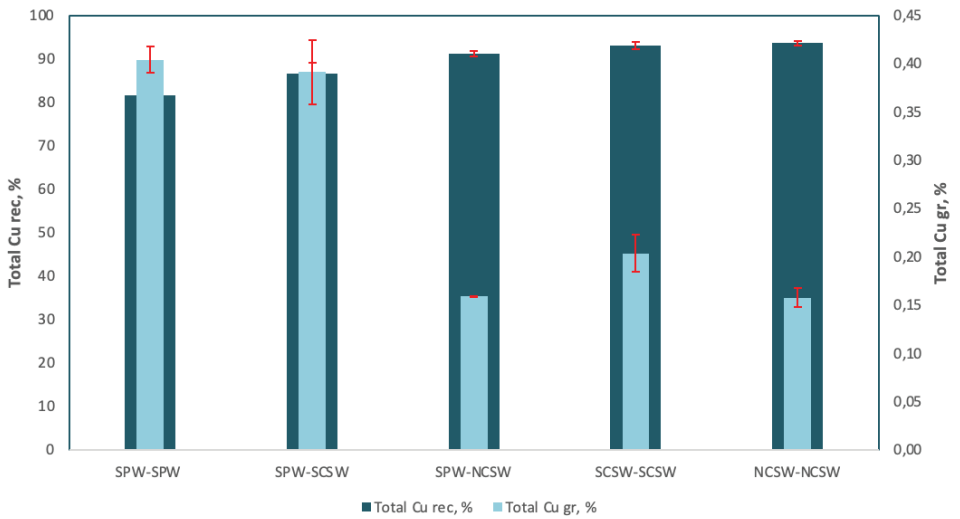

Figure 2 *Cu recoveries and grades in synthetic plant water and seawater.*

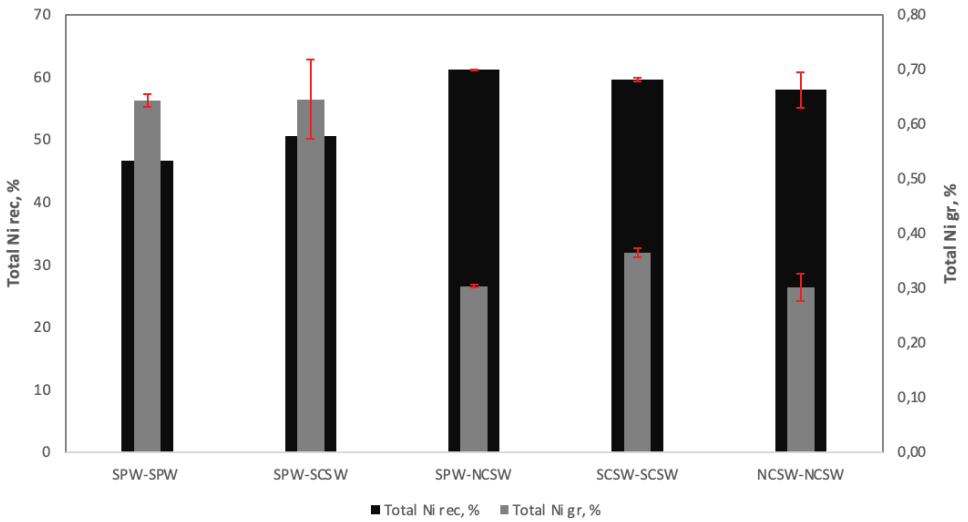

Figure 3 *Ni recoveries and grades in synthetic plant water and seawater.*

Nickel Recoveries and Grades

Fig. 3 shows a comparison of the flotation of copper recoveries and grades for the selected ore milled and floated in various water qualities.

Fig. 3 shows that nickel recoveries exhibit trends consistent with those observed for copper and overall solids recovery. Recoveries increase progressively from SPW-SPW through to seawater-dominated systems, with SPW-NCSW, SCSW-SCSW and NCSW-NCSW conditions showing the highest nickel recoveries. Similar to copper, nickel grades display an inverse relationship with recovery

Froth Properties

Fig. 4 shows the froth height and collapse time in SPW, SCSW and NCSW.

Fig. 4 shows that both froth height and froth collapse time increase significantly with

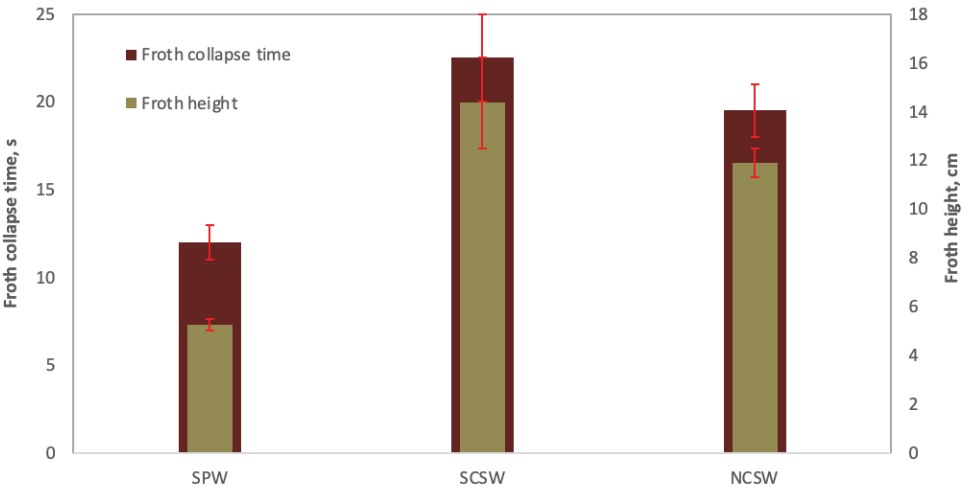

Figure 4 *Froth height and froth collapse time in SPW, SCSW and NCSW.*

increasing salinity of the water. The lowest froth height and fastest collapse are observed under SPW conditions, indicating a relatively unstable froth. In contrast, seawater systems (SCSW and NCSW) exhibit higher froth heights and longer collapse times, reflecting enhanced froth stability.

Fig. 5 shows the images of the froth phase during the flotation with the different water types. The images were captured at the beginning of the flotation process, during the collection of the first concentration.

Fig. 5 shows a clear variation in froth bubble size and distribution across the different water types. The SPW system is characterised by larger and less uniform bubbles. In contrast, seawater systems produce smaller and more uniformly distributed bubbles, with NCSW showing the finest and most homogeneous bubble structure.

Linking Flotation Performance with Froth Properties and Water Quality

The observed increase in solids, water, and mineral recoveries under seawater conditions correlates directly with the elevated electrical conductivity and total dissolved solids reported in Table 2, which reflect significantly higher ionic strength relative to SPW. Increased ionic strength is well known to suppress bubble coalescence, resulting in smaller, more stable bubbles and enhanced froth stability (Craig *et al.* 1993; Manono *et al.* 2013). This is consistent with the higher froth heights, longer collapse times, and finer bubble size distributions observed in Fig. 4 and 5. The more persistent froth phase promotes increased water recovery and entrainment, explaining the higher mass pull and corresponding increase in mineral recoveries, albeit at the expense of grade. The intermediate behaviour observed for recycled process water (SPW) reflects its lower conductivity and ionic strength, resulting in less stable froths and reduced entrainment. Furthermore, the presence of divalent ions such as Ca^{2+} and Mg^{2+} in both seawater and recycled water is known to influence interfacial properties and froth stability, reinforcing these trends (Farrokhpay and Zanin 2012; Manono *et al.* 2018). These results demonstrate that water chemistry, as captured by conductivity and TDS, exerts significant control on froth behaviour and, consequently, flotation performance.

Conclusions

The results indicate that seawater consistently produced higher solids and water recoveries than synthetic process water, attributed primarily to its substantially higher ionic strength. Enhanced froth stability, characterised by increased froth heights and longer collapse times, was observed in seawater systems, reflecting reduced bubble coalescence and smaller bubble sizes. Recycled process water showed intermediate behaviour, with flotation response influenced

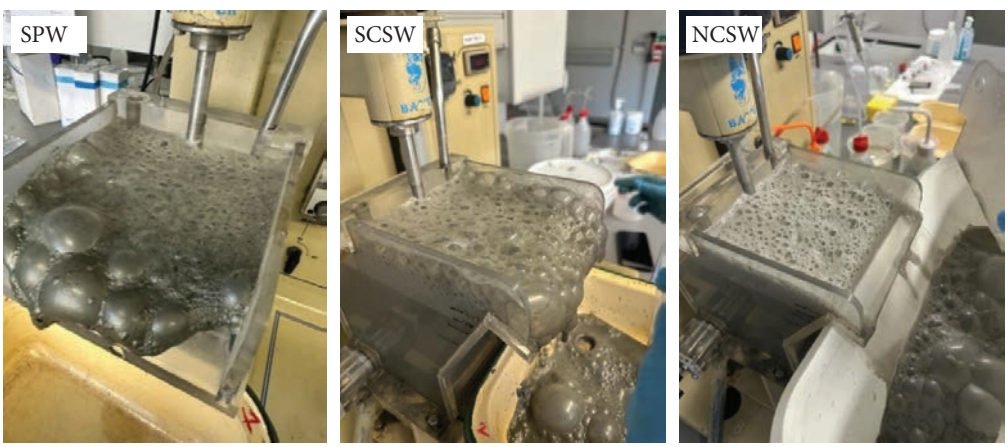

Figure 5 *Froth Bubble size comparison during flotation in SPW, SCSW and NCSW.*

by divalent ions such as Ca^{2+} and Mg^{2+}. While higher ionic strength increased mass pull, it also increased the potential for gangue entrainment, highlighting trade-offs between recovery and selectivity. The findings demonstrate that water quality should be treated as an active metallurgical variable rather than a passive process input. This work provides evidence to support informed decision-making around seawater use, mine water recycling, and closed-loop water circuits in PGM operations as seawater has not been researched in the context of PGM ores. The study further contributes to the broader understanding of how mine-affected water chemistries influence processing performance, supporting sustainable water management strategies under increasing water scarcity.

Acknowledgements

The author would like to acknowledge the University of Cape Town for supporting this work. Theresa Chibaya and Kidada Mhishi are acknowledged for conducting the test work as part of their final year project towards the degree of BSc(Eng) in Chemical Engineering at the University of Cape Town.

References

Biçak Ö, Ekmekçi Z, Can M, Öztürk Y (2012) The effect of water chemistry on froth stability and surface chemistry of the flotation of a Cu-Zn sulfide ore. Int J Miner Process 102–103:32–37. https://doi.org/10.1016/j.minpro.2011.09.005

Cisternas LA, Gálvez ED (2018) The use of seawater in mining. Mineral Processing and Extractive Metallurgy Review 39:18–33. https://doi.org/10.1080/08827508.2017.1389729

Corin KC, Reddy A, Miyen L, et al (2011) The effect of ionic strength of plant water on valuable mineral and gangue recovery in a platinum bearing ore from the Merensky reef. Miner Eng 24:131–137. https://doi.org/10.1016/j.mineng.2010.10.015

Craig VSJ, Ninham BW, Pashley RM (1993) The effect of electrolytes on bubble coalescence in water. J Phys Chem 97:10192–10197. https://doi.org/10.1021/j100141a047

Farrokhpay S, Zanin M (2012) An investigation into the effect of water quality on froth stability. Advanced Powder Technology 23:493–497. https://doi.org/10.1016/j.apt.2012.04.012

Harrison STL, Slatter-christie K, Broadhurst J (2018) Integrating competing water needs of mining and mineral processing with the environment , community and economic activity in a mining-dominated catchment

Le T, Schreithofer N, Dahl O (2020) Dissolution Test Protocol for Estimating Water Quality Changes in Minerals Processing Plants Operating With Closed Water Circulation. Minerals 10:653. https://doi.org/10.3390/min10080653

Manono M, Corin K, Wiese J (2018) Water quality effects on a sulfidic PGM ore : Implications for froth stability and gangue management. 54:1253–1265. https://doi.org/10.5277/ppmp18181

Manono MS, Corin KC, Wiese JG (2019) To Recycle or Not ? A Bench Scale Simulation of Water Recirculation in Sulfidic Cu-Ni Ore Flotation. In: Khayrulina, E.; Wolkersdorfer, Ch.; Polyakova, S.; Bogush A (ed) Mine Water – Technological and Ecological Challenges. International Mine Water Association, pp 225–231

Manono MS, Corin KC, Wiese JG (2013) The effect of ionic strength of plant water on foam stability: A 2-phase flotation study. Miner Eng 40:. https://doi.org/10.1016/j.mineng.2012.09.009

Muzenda, E (2010) An Investigation into the Effect of Water Quality on Flotation Performance. World Academy of Science, Engineering and Technology International Journal of Chemical, Molecular, Nuclear, Materials and Metallurgical Engineering 4:562–566

Slatter, K.A.; Plint, N.D.; Cole, M.; Dilsook, V.; De Vaux, D.; Palm, N.; Oostendorp B (2009) Water Management in Anglo Platinum Process Operations : Effects of Water Quality on Process Operations. International Mine Water Conference, Pretoria, South Africa, 19th – 23rd October 2009 Proceedings ISBN Number: 978-0-9802623-5-3 46–55

Wiese J, Harris P, Bradshaw D (2005) The influence of the reagent suite on the flotation of ores from the Merensky reef. Miner Eng 18:189–198. https://doi.org/10.1016/j.mineng.2004.09.013

Site-Specific Ecological Risk Assessment of Metal Mixtures in a Mining Influenced River: A Case Study of the Loddon River Basin, Australia

Mokhinabonu Mardonova[1], Ehsan Arzaghi[2], Bandita Mainali[1], Rouzbeh Abbassi[1], Muhammad Kashif Shahid[1]

[1]*School of Engineering, Macquarie University, Australia, mardonova.mokhinabonu@mq.edu.au, ORCID 0000-0001-6466-2909*

[2]*School of Mechanical, Medical & Process Engineering, Queensland University of Technology, Australia*

Abstract

Victoria, a southeastern state of Australia, has a long history of gold mining, leaving over 15,000 abandoned mine sites that continue to influence river water quality through elevated metal concentrations (Cu, Ni, Zn, Pb). Conventional guideline values (GVs) are often inadequate for mining-influenced rivers, as they do not account for site-specific water chemistry or metal bioavailability, potentially misrepresenting ecological risk.

This study presents an integrated ecological risk assessment (ERA) framework that combines bioavailability modelling and probabilistic mixture toxicity to evaluate multi-metal risks. The Loddon River basin was selected as a case study. Chronic toxicity data (NOEC) were compiled from the USEPA ECOTOX database to develop Species Sensitivity Distributions (SSDs). Site-specific HC5 values were derived using the Bio-Met tool based on local pH, DOC, and Ca conditions. Potentially Affected Fractions (PAFs) were calculated and integrated into mixture risk (msPAF) using a concentration addition (CA) approach.

Results revealed clear spatial variability, with downstream sites exhibiting greater ecological susceptibility due to increased metal bioavailability, despite comparable or lower concentrations. While HC5-based assessments indicated generally low risk, msPAF identified episodic high-risk conditions, particularly at upstream and midstream sites. These findings demonstrate a decoupling between metal concentrations and ecological risk, driven by site-specific bioavailability and mixture effects.

Overall, the proposed framework provides a more realistic and sensitive approach to ecological risk assessment by integrating bioavailability, species sensitivity, and mixture toxicity. Although demonstrated using the Loddon River, the approach is transferable to other mining-influenced catchments, supporting improved risk evaluation and water management in complex environmental systems.

Keywords: Mixture toxicity, freshwater ecosystems, ecological risk assessment, bioavailability, mining influenced river, species sensitivity distributions

Introduction

Generic water quality guideline values (GVs) are widely used to assess ecological risk by comparing measured concentrations to predefined thresholds (USEPA 1992). However, they do not account for influence of water chemistry on metal bioavailability. Key parameters such as pH, hardness, and dissolved organic carbon (DOC) can alter metal speciation and organism sensitivity, potentially leading to misrepresentation of ecological risk (Quality *et al.* 2014).

These limitations are particularly relevant in mining-influenced rivers, where metal contamination occurs under spatially variable physicochemical conditions (Macklin *et al.* 2023). While site-specific Species Sensitivity Distributions (SSDs) provide a robust probabilistic framework, their application is data-intensive(Quality *et al.* 2014; Rong

et al. 2022). Bioavailability-based tools such as Biotic Ligand Models (BLMs) and simplified approaches like Bio-Met offer a practical alternative by adjusting toxicity thresholds to local water chemistry (European Copper Institute 2023).

Conventional ecological risk assessments also assume independent metal effects, despite co-occurrence and interactions in mining systems (Nys *et al.* 2017). SSDs enable estimation of the Potentially Affected Fraction (PAF), which can be extended to mixture conditions through mixture toxicity PAF (msPAF), providing a probabilistic measure of combined toxicity (Traas *et al.* 2001; Nys *et al.* 2017; Rong *et al.* 2022).

To address these challenges, this study presents an integrated ecological risk assessment framework that combines site-specific bioavailability corrections with probabilistic msPAF. The framework is applied to the Loddon River basin (Victoria, Australia), demonstrating its broader applicability to similar mining-influenced systems.

Methods

Data sources and study area

The ecological risk assessment framework is summarised in Fig. 1. Water quality data for Cu, Pb, Ni, and Zn, along with key physicochemical parameters (pH, DOC, Ca), were obtained for the Loddon River basin (Victoria, Australia) from government database for 1997–2025. Five monitoring sites were analysed: Newstead (NS), Laanecoorie (LC), Serpentine Weir (SW), Kerang (KR), and Swan Hill (SH) (Fig.2). As concentrations were reported as totals, dissolved metals were estimated using total suspended solids (TSS) and literature-based partition coefficients (log K_d): Cu (0.768), Ni (0.255), Pb (2.07), and Zn (2.33) (Sedeño-Díaz *et al.* 2019).

Chronic toxicity data (NOECs) for freshwater species were compiled from the USEPA ECOTOX database, focusing on growth and reproduction endpoints. Based on data availability, 7–8 species per metal were included across multiple taxa (fish, crustaceans, molluscs, and insects). NOEC values ranged from 0.46–422 µg/L, with the lowest values for Cu and highest for Zn. The most sensitive records were selected, and data were normalised to site conditions.

Bioavailability adjustment and SSD development

Toxicity data were normalised to reference water chemistry using the Bio-Met tool (European Copper Institute 2023). Reference conditions were defined as pH 7.0, hardness 30 mg/L $CaCO_3$, DOC 2 mg/L, and Ca 12 mg/L. The hazardous concentration protecting 95% of species (*HC5*) was derived

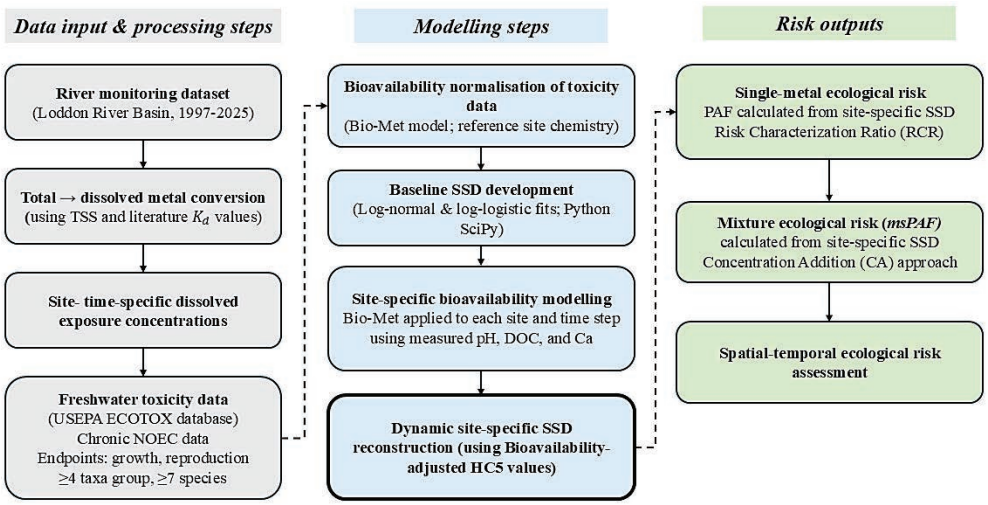

Figure 1 *Conceptual framework of the proposed ecological risk assessment methodology.*

as the 5th percentile of fitted distributions, and normalisation factors based on *HC5* ratios were applied to adjust *NOEC* values. SSDs were fitted using log-normal cumulative distribution functions in *SciPy* with parameters estimated via maximum likelihood. Sensitivity analysis confirmed robust model performance. Site- and time-specific *HC5* values were derived using measured water chemistry inputs.

Site-specific SSD reconstruction and PAF estimation

To account for spatial and temporal variability in bioavailability, *SSDs* were reconstructed for each metal across sites and time using site-specific *HC5* values, while retaining the original distribution shape. Mean μ values were derived for each site and used to reconstruct *SSDs*. Potentially Affected Fractions (*PAFs*) were then calculated from dissolved metal concentrations based on the fitted log-normal distributions (Traas *et al.* 2001).

Mixture ecological risk was quantified using the *msPAF*. Mixture ecological risk was evaluated using the Concentration Addition (CA) approach (Nys *et al.* 2017). Individual metal *PAFs* were combined as:

$$msPAF_{site\,(t)} = 1 - \prod_{i=1}^{n}(1 - PAF_{i,site\,(t)})$$

where n is the number of metals (Cu, Pb, Zn, Ni), representing the cumulative probability of species being affected by at least one toxicant.

Results and Discussion

Metal concentrations and water chemistry patterns

Dissolved metal concentrations showed clear spatial variability along the Loddon River. Zn exhibited the highest levels, particularly at LC,

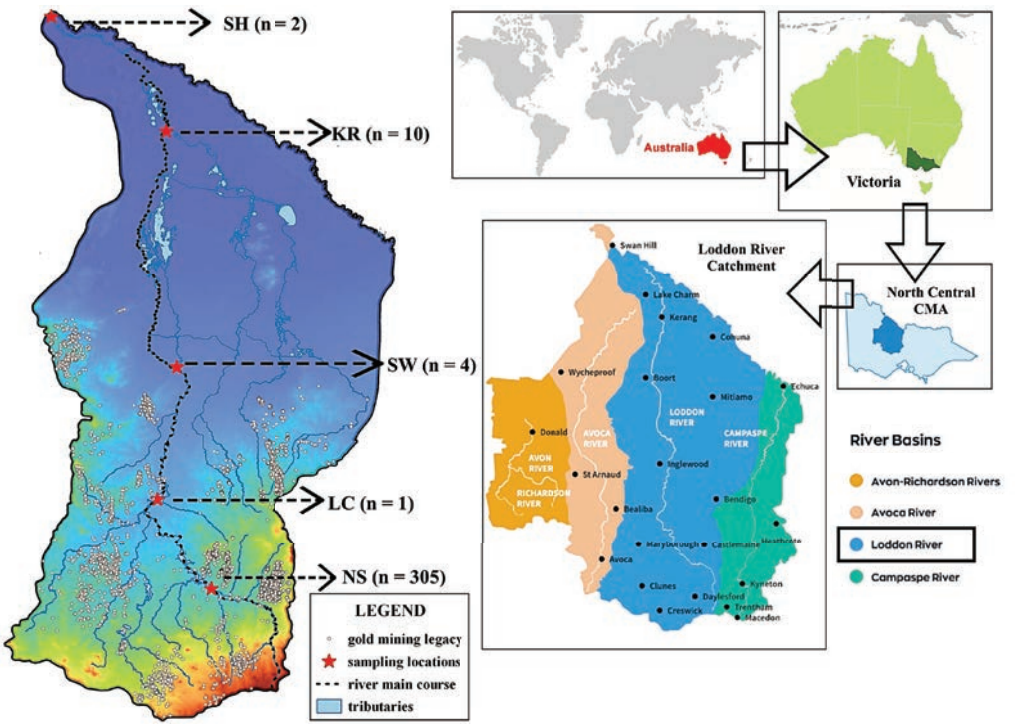

Figure 2 *Location of the Loddon River catchment (Victoria, Australia), showing historical gold mining legacy, monitoring sites (SH = Swan Hill, KR = Kerang, SW = Serpentine Weir, LC = Laanecoorie, NS = Newstead), and sampling density. The background colour gradient of the basin represents catchment topography, with elevation decreasing from brown (high elevation) to blue (low elevation).*

while Pb increased toward downstream sites (KR and SH). Cu and Ni remained relatively low. This longitudinal pattern from upstream (NS) to downstream suggests progressive metal mobilisation or accumulation along the river.

These trends align with contrasting physicochemical conditions. Upstream (NS) is characterised by higher hardness (≈210 mg/L $CaCO_3$), alkalinity (≈180 mg/L), and DOC (≈14 mg/L), which reduce metal bioavailability. In contrast, downstream sites show lower hardness (≈30 mg/L), lower DOC (≈5 mg/L), and higher turbidity (≈92 NTU), conditions that may enhance metal mobility and exposure. This highlights the role of water chemistry in controlling metal bioavailability.

SSD-derived thresholds and site-specific adjustments

SSDs produced consistent *HC5* estimates across distributions, with the log-normal model adopted. Zn showed the highest *HC5*, while Cu and Ni exhibited lower thresholds, indicating greater intrinsic toxicity (Fig. 3). Site-specific SSD reconstruction revealed a clear spatial gradient in toxicity thresholds (Fig. 3). Downstream sites exhibited lower *HC5* values, indicating higher bioavailability and ecological sensitivity, whereas the upstream NS site showed higher *HC5* values, reflecting reduced bioavailability under local water chemistry.

Comparison with guideline values (Tab. 1) demonstrated that generic thresholds may not adequately represent local ecological protection. SSD-derived HC5 threshold values for Cu and Ni were substantially lower than GVs, suggesting potential underestimation of risk when relying solely on conventional benchmarks. These differences emphasise the importance of incorporating bioavailability into ecological risk assessment and generic GVs may not adequately capture ecological risks in mining-affected river systems.

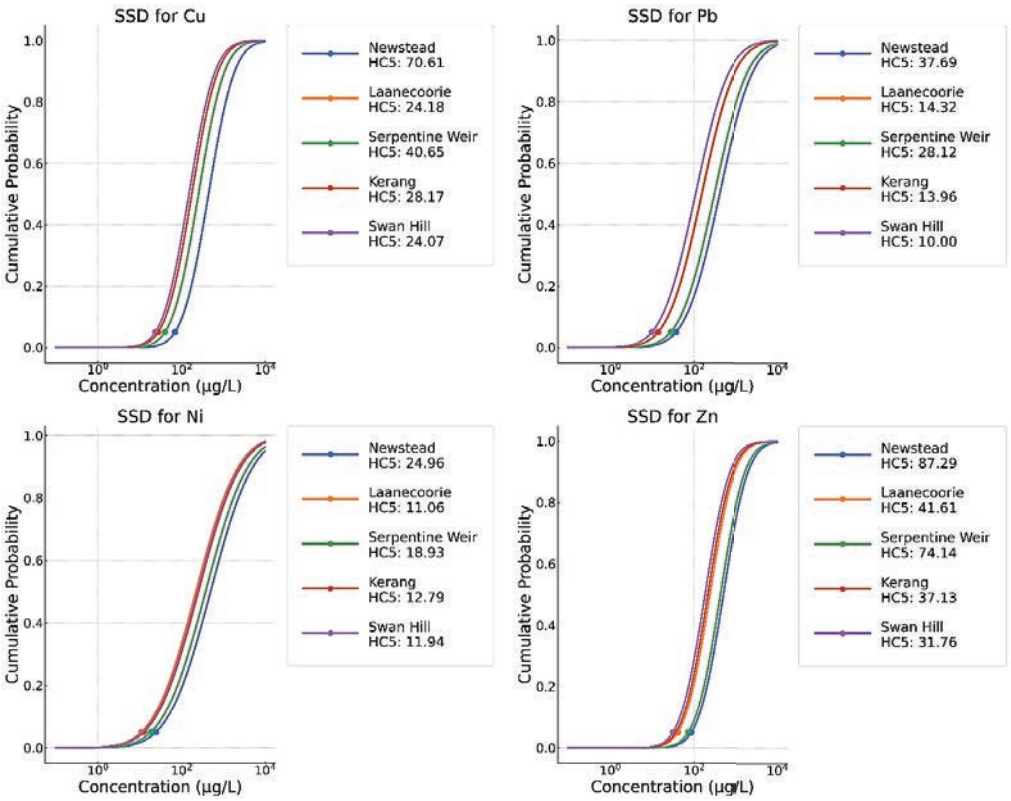

Figure 3 *Reconstructed site-specific log-normal SSDs for each metal across monitoring locations in the Loddon River.*

Table 1 Comparison of chronic protection thresholds (µg/L) derived in this study with USEPA hardness-based criteria and ANZG guideline values (hardness = 30 mg/L $CaCO_3$).

Metal	USEPA hardness-based guideline	ANZG guideline (95% protection)	This study HC5
Cu	3.2	1.0*	1.65
Pb	0.664	3.4	3.04
Ni	18.8	11.0	1.8
Zn	42.6	8.0	8.55

Mixture toxicity and msPAF patterns

Probabilistic metrics (*PAF* and *msPAF*) provided a more sensitive representation of ecological risk, particularly in identifying mixture effects and episodic risk conditions. Mean single-metal *PAF* values varied across sites, with Zn consistently contributing the highest values, followed by Ni, while Cu and Pb remained low (Fig. 4). However, *msPAF* values were consistently higher than individual-metal *PAFs*, demonstrating the importance of mixture effects.

Spatial patterns revealed low mixture risk at KR (*msPAF* < 0.001), moderate values at SW (≈0.004), and elevated levels at midstream sites such as LC and SW (up to ≈0.016). The highest variability occurred at NS, where *msPAF* ranged from near-zero to values exceeding 0.5, indicating episodic conditions under which a large proportion of species may be affected. These findings highlight that mixture toxicity can substantially amplify ecological risk beyond single-metal assessments, particularly under temporally variable conditions. A decoupling between concentration and ecological risk was observed, with some sites showing low risk despite high concentrations, highlighting the role of bioavailability and species sensitivity. Overall, ecological risk was low but spatially and temporally variable, with episodic peaks captured by *msPAF*, highlighting the importance of mixture toxicity.

The predominance of low baseline *msPAF* values with episodic high-risk events is consistent with previous studies showing that mixture effects are not captured by single-metal approaches (Nys *et al.* 2017). Spatial variability in risk along the Loddon River reflects patterns observed in other aquatic systems, where local physicochemical conditions strongly modulate toxicity. The observed decoupling between concentration and ecological risk highlights the importance of bioavailability and species sensitivity in probabilistic risk frameworks. While *msPAF* is widely applied to assess mixture toxicity, it is typically based on fixed toxicity thresholds that do not account for site-specific bioavailability (Nys *et al.* 2017; Rong *et al.* 2022; Tang *et al.* 2023). By integrating bioavailability-adjusted SSDs, this study enables toxicity thresholds to respond dynamically to local water chemistry, improving the ecological realism of mixture risk assessment in mining-influenced systems.

Conclusions

This study shows that ecological risk in mining influenced rivers is governed by site-specific bioavailability and mixture toxicity rather than metal concentrations alone. While *HC5*-based assessments indicated generally negligible risk across the Loddon River, probabilistic metrics (*PAF* and *msPAF*) revealed spatial variability and episodic high-risk conditions, particularly at upstream and midstream sites. The decoupling between concentration and ecological impact highlights limitations of conventional approaches. Overall, the proposed framework provides a more realistic and sensitive method for ecological risk assessment, with applicability to mining influenced systems beyond the case study.

Acknowledgements

This research was supported by the Commonwealth through an Australian Government Research Training Program Scholarship [DOI: https://doi.org/10.82133/C42F-K220].

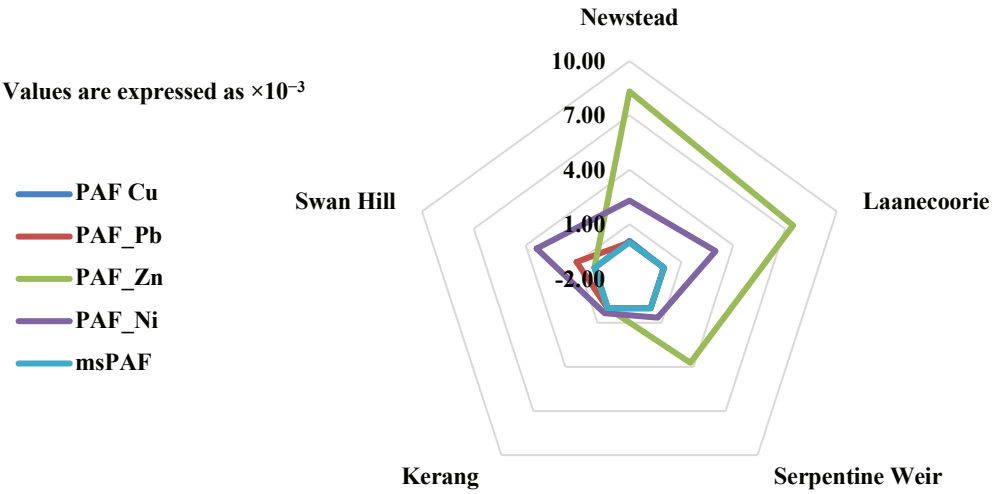

Figure 4 Mean single-metal PAF and msPAF values across monitoring sites along the Loddon River.

References

European Copper Institute (2023) bio-met tool – Bioavailability Tool for Metals in Surface Waters

Macklin MG, Thomas CJ, Mudbhatkal A, et al (2023) Impacts of metal mining on river systems: a global assessment. Science (1979) 381:1345–1350. https://doi.org/10.1126/science.adg6704

Nys C, Van Regenmortel T, Janssen CR, et al (2017) A framework for ecological risk assessment of metal mixtures in aquatic systems. Environ Toxicol Chem 37:623–642. https://doi.org/10.1002/etc.4039

Quality E, For B, Aquatic P (2014) Site-specific water quality guidelines: 1 . Derivation approaches based on physicochemical, ecotoxicological and ecological data. 118–130. https://doi.org/10.1007/s11356-013-1780-0

Rong S, Wu J, Cao X, Sun Y (2022) Comprehensive Ecological Risk Assessment of Heavy Metals Based on Species Sensitivity Distribution in Aquatic of Coastal Areas in Hong Kong. Int J Environ Res Public Health 19. https://doi.org/10.3390/IJERPH192013376

Sedeño-Díaz JE, López-López E, Mendoza-Martínez E, et al (2019) Distribution Coefficient and Metal Pollution Index in Water and Sediments: Proposal of a New Index for Ecological Risk Assessment of Metals. Water (Basel) 12:29. https://doi.org/10.3390/w12010029

Tang Z, Liu X, Niu X, et al (2023) Ecological risk assessment of aquatic organisms induced by heavy metals in the estuarine waters of the Pearl River. Scientific Reports 2023 13:1 13:9145-. https://doi.org/10.1038/s41598-023-35798-x

Traas T, de Meent D van, Posthuma L, et al (2001) The Potentially Affected Fraction as a Measure of Ecological Risk

USEPA (1992) Framework for ecological risk assessment. Washington

IMWA 2026
Jeongseon

Tailings Storage in a Disused Open Pit and the Conundrum of Explaining the Concept of a Terminal Groundwater Sink

Matthew P McGann

Director Hydrogeology Newmont Corporation. 6900 E Layton Ave, Suite 700 Denver, CO 80237 Matthew.McGann@Newmont.com

Disclaimer: This paper is provided for general informational purposes in connection with a conference presentation. The views and conclusions expressed are those of the author and do not necessarily reflect the official policy or position of Newmont Corporation or any of its affiliates. This paper may include interpretations, hypotheses, or projections subject to scientific variability and ongoing work, and may contain forward-looking statements that involve risks and uncertainties. Newmont does not guarantee the accuracy, completeness, or reliability of the information herein, and no reliance should be placed on it for investment, legal, operational, or other decision-making. Except as required by law, Newmont undertakes no obligation to update any forward-looking statements.

Abstract

Safe and efficient storage of mine tailings is a complex issue with an unfortunately checkered history. Ensuring that project stakeholders appropriately understand a potential tailings storage strategy can be a challenging task. The response to and findings from a new strategy developed to educate project stakeholders at an existing mining operation in Ghana is presented and discussed. This novel approach adopted a voiced-over animation which described in-pit tailings deposition, coupled with maintenance of a terminal groundwater sink, a potential tailings storage method. Voiced over animation as an educational tool had not been utilised in Ghana previously.

Keywords: Tailings, in-pit storage, terminal groundwater sink, voiced-over animation

Introduction

The Ahafo South mine is located in the Ahafo Region of Ghana, 290km northwest of the Ghanaian capital city of Accra. Ahafo South is the largest gold mine in Ghana and is operated by Newmont Ghana Gold Limited [NGGL], a fully owned subsidiary of Newmont Corporation. Ahafo South is a Newmont Tier-1 asset and to date has produced over 10 Moz of gold, it has Reserves of 4.1 Moz and Resources of 7.4 Moz. Advanced study and exploration work are underway to support underground growth beneath the Subika and the Apensu open pits [www.Newmont.com]. Mining at Ahafo South commenced at the Subika open pit in 2006, with open pit mining subsequently commencing at Apensu in 2007, at Awonsu in 2008 and at Amoma in 2012 Figure 1.

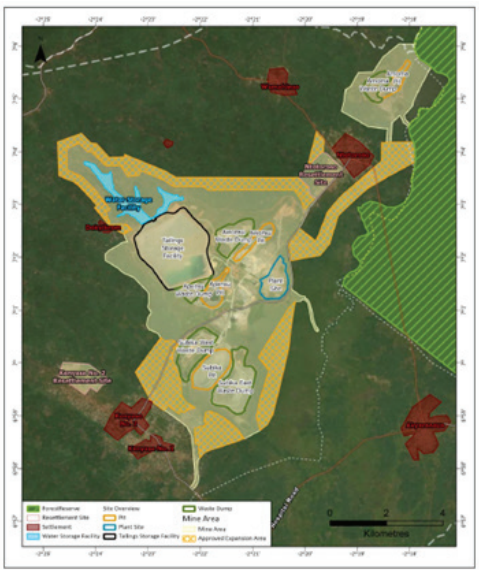

Figure 1 *Ahafo South Site Layout.*

Each of the four open pits at Ahafo South underwent various mining phases, with each phase presenting a lay-back [cut-back], typically with incremental pit floor advancement. Open pit mining was completed at Apensu in 2012, at Amoma in 2017, at Subika in 2025, and Phase 4 mining of the Awonsu open pit is currently forecast to be completed in 2032. In 2017, operations at Ahafo South expanded to include underground mining with commercial production starting at the Subika underground mine. The development of an Apensu exploration decline is currently underway, and initial plans for underground mining at Apensu are being developed, with incremental permitting studies and stakeholder engagement also underway.

The Ahafo South process plant is designed to treat approximately 10 Mt of ore per annum and utilises a conventional Carbon-in-Leach (CIL) circuit for gold recovery. Underground mining at Subika has adopted various mining methods, including longhole open stoping [LHOS] and Sub-level Shrinkage [SLS], similarly underground mine planning at Apensu is expected to utilise a range of mining methods. Ore extracted from Awonsu open pit and the Subika underground mine is stockpiled by grade classification on the Run of Mine ore pad [RoM pad] adjacent to the process plant and is blended prior to processing. Following gold extraction in the CIL circuit, the slurry is treated in a Counter-Current Decantation (CCD) circuit to recover residual cyanide back into the process and reduce Weak Acid Dissociable (WAD) cyanide to below 50 mg/L prior to discharge to a large single cell terrestrial tailings storage facility designated as Cell 1 TSF. By year-end 2025, Cell 1 contained approximately 155M tonnes of tailings, and the facility has an permitted capacity of 220M tonnes. Cell 1 is at Phase 13 of a currently projected 16 Phase construction life. A second, smaller [50Mt] terrestrial facility TSF2 has also been permitted; its footprint is centered immediately to the northeast of Cell 1 with a common embankment.

The remaining capacity of Cell 1 and the full capacity of TSF2 provide NGGL with tailings storage capacity to approximately year-end 2036. However, ongoing resource definition and exploration drilling programs are expected to confirm additional gold reserves and generate further resources, hence incremental tailings storage at Ahafo South is anticipated to be required.

Over the life of the Ahafo South mine and given the long timeframes involved in evaluating, selecting and permitting tailings storage facilities, NGGL has conducted and continues to conduct studies investigating alternative tailings management and tailings storage methods. Tailings storage methods such as thickened tailings, dry-stack tailings and the use of tailings as underground paste backfill have been investigated and remain under study; however, those potential tailings management methods are not the focus of this discussion.

Further expansion of Cell 1 beyond the currently permitted Phase 16 capacity is influenced by a number of regulatory [Ghana Minerals and Mining Regulations 2012 L.I. 2182], physical and site specific requirements, including downstream construction obligations, proximity to local communities, and the shared function of the Cell 1 northern embankment with the Ahafo South Water Storage Dam. While additional conventional terrestrial tailings storage locations have been identified and remain technically feasible, the expansion or development of incremental or additional surface facilities presents a number of challenges related to;

- construction configuration
- water management
- construction materials sourcing, and
- the timeframe of construction.

Notwithstanding these challenges, terrestrial tailings storage facilities remain a practical and important component of the Ahafo South tailings management strategy.

With the identified challenges to further surface facility construction, NGGL assessed the possibility of in-pit tailings storage at Ahafo South. Of the four open pits, Awonsu presented itself as the most viable opportunity because:

- the Amoma pit is quite small and is located some distance from the centre of operations, and
- both the Subika pit and the Apensu pit present more challenging deposition and management conditions due to existing or possible future underground mining.

While current underground mining at Subika and any possible future underground mining at Apensu do not present a fatal flaw to in-pit tailings storage, underground mining does present greater complexity to a simple open pit void without any associated underground workings.

The primary complexities with underground mining near an open pit largely revolve around the geotechnical aspects of crown pillar integrity and the management of any large seepage or inrush flows from an in-pit storage facility into the underground mining environment.

Given the challenges associated with the expansion of the existing surface facilities or the development of a new surface tailings storage facility, the concept of in-pit tailings storage at Awonsu gained support within the tailings storage assessment study team as part of a broader options assessment. This support was predicated on a number of key aspects, including:

- the use of an existing disturbed area would limit the need for any incremental site disturbance
- the Phase 4 Awonsu pit could potentially provide a considerable storage capacity
- the Awonsu pit is centrally located between the mill and the existing Cell 1
- local and district scale groundwater monitoring coupled with groundwater modelling of the Ahafo South mining district indicates that enforced terminal sink groundwater conditions are easily established and simple to maintain
- the Awonsu pit is already contained within the mining impacted area of the site-wide water balance; hence, water contained within Awonsu would simply transition from being mining impacted water to process impacted water, and there would be no increase in the total volume of water being managed at the site
- the construction effort required to utilise the Awonsu pit would be substantially less than building or expanding a surface facility and hence noise, light and dust issues would be greatly reduced, and
- stability of an in-pit facility is inherently greater than a terrestrial facility.

Given the extensive list of positive attributes, a perception developed within the tailings storage assessment study team that an in-pit tailings storage option would easily garner widespread enthusiasm with the various internal and external project stakeholders.

However, as the study progressed, three key aspects arose that presented various challenges to the in-pit tailings storage project concept:

- There is little prior experience of, and hence limited permitting of in-pit tailings storage facilities in Ghana, with AngloGold Ashanti's Iduapriem mine a rare example
- There is a lack of conceptual understanding of what a terminal groundwater sink is and how it manifests
- There is concern that the use of the open pit for tailings storage, would prevent the possibility of either an additional open pit layback or underground mining in the Awonsu area

Following engagement with various internal stakeholders, it became evident that the greater concern centered around the lack of understanding of the terminal groundwater sink concept.

Variable site conditions affecting the viability of in-pit tailings storage

In-pit storage is not always a feasible tailings management option; in some cases, the reasons behind a particular site not being feasible are straight forward, however, in other examples, the reasons are not quite as simple.

In the case of a single pit mining operation, tailings typically can't be stored in the pit that is actively being mined, as there would essentially be no storage capacity available. Hence, for single pit mine sites, a separate terrestrial tailings storage facility is likely to always be required.

With the example of a single pit operation put to the side, the key initial question to be asked or addressed when considering the concept of in-pit tailings storage is whether storage would occur above or below the groundwater surface and more specifically,

if storage would occur below the terminal sink groundwater surface. The terminal sink groundwater surface is defined as a stabilised water level within an open pit or depression that remains permanently below the surrounding regional water table [Edith Cowan University 2013]. In the case of an excavated mine pit, terminal sink conditions are typically artificially established by a dewatering pumping regime; this situation could be termed a "forced" condition. In some circumstances, evaporation from the pit can exceed minewater inflows, and the pit lake level can be more naturally maintained below the regional groundwater level. Awonsu would be an example of a forced terminal sink condition, which would require ongoing pumping. The final closure strategy for the facility would not require on-going pumping; but facility closure is outside the scope of the present discussion.

Depending on the characteristics of a mine pit, the lining of a deep, mined out, fresh bedrock open pit with either compacted clay or a Geosynthetic Clay Liner [GCL] would be at best exceedingly difficult. In these circumstances, tailings seepage management would likely become exceptionally complicated. Identifying an open-pit mine void that presents a viable terminal groundwater sink can prove to be challenging, and the storage capacity below the terminal sink must present a large enough capacity for the pit to be viable.

The hydraulic characteristics of either a natural or a forced terminal groundwater sink [i.e., constant groundwater inflow to the pit] provide for what could be referred to as a hydraulicly lined facility, at which groundwater outflow is simply not possible due to the hydraulic pressure differential.

At Awonsu, as well as more broadly across the Ahafo South operation, the presence of the very favourable geological and hydrogeological conditions makes in-pit tailings storage a viable option from a technical perspective. The Ahafo South district is characterised by the presence of a thin [20–40m] weathered horizon overlying a generally very lightly fractured bedrock. The bedrock at Ahafo South consists of metavolcanics on the hanging wall side and meta-sediments on the footwall side of the district scale Kenyase Thrust. While hydraulic

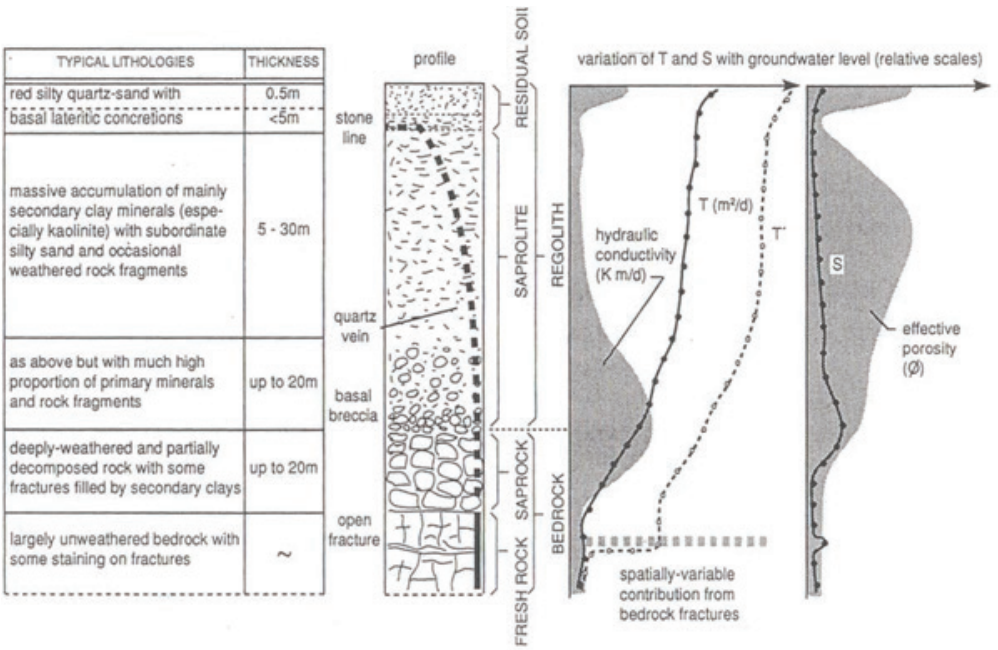

Figure 2 Generalised hydrogeological properties Ahafo South [after Chilton and Foster (1995)].

conductivity is marginally greater along strike of the Kenyase Thrust, this aspect is of no material concern. The hydrogeological characteristics of the Ahafo South district have been interpreted to essentially align with the generic hydrogeological properties, as described by Chilton and Foster (1995).

The hydrogeological properties as described by Chilton and Foster constitute a fundamental pillar of the Conceptual Groundwater Model [CGM] of the Ahafo South district. The hydrogeological properties described by Chilton and Foster have been coupled with an overall west to east groundwater flow direction from slightly elevated terrain to the west of the Ahafo South mining district, towards the principal regional surface water drainage [Tano River] to the east. These principal elements combine to form the complete CGM for Ahafo South. The CGM is the basis of a MODFLOW-USG hosted numerical groundwater flow model of the Ahafo South district [Piteau 2025], shown in Figure 3.

The Ahafo South district groundwater model was used to simulate the groundwater flow regime that would be established should Awonsu be utilised for tailings storage, and the facility decant pond was maintained below the terminal groundwater sink elevation of the pit. The numerical modelling demonstrated that the Awonsu pit could be easily maintained as a forced terminal groundwater sink by consistently abstracting water from the Awonsu pit lake [Piteau 2025].

Discussion

For the Hydrogeologists engaged in the Ahafo South tailings storage assessment study team, as well as for many others, there was and is simple recognition and acceptance of both the natural and forced terminal groundwater sink concepts. However, for some internal project stakeholders, fully grasping the theory of a terminal groundwater sink wasn't immediate, and for others, it remains challenging to visualise and hence accept the terminal groundwater sink concept.

Simply put, the fact that groundwater flows from a higher pressure environment to a lower pressure environment, isn't quite as easy to visualise or conceptualise as is the more commonly used expression that "water flows downhill". The inability to visualise

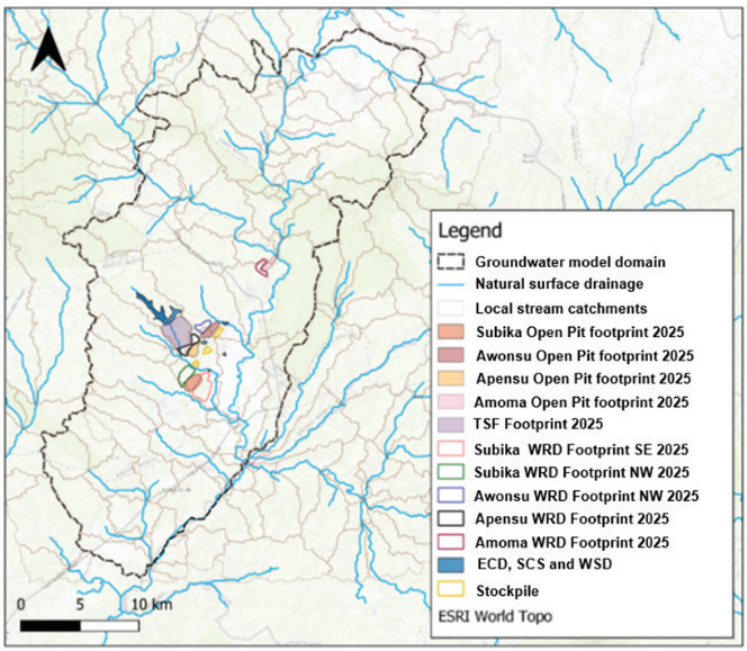

Figure 3 Ahafo South district groundwater model domain [Piteau 2025].

a groundwater surface, or a groundwater head gradient, can leave many stakeholders, including scientists and engineers, not fully understanding the terminal groundwater sink concept.

In order to provide greater clarity on the terminal groundwater sink concept and to explain why in-pit tailings storage was even being considered, NGGL turned to a company that produces video-based animations. An animated video was developed, complete with a voice-over to illustrate how an in-pit tailings storage facility would operate and how a terminal groundwater sink manifests. The video was developed so that a greater proportion of project stakeholders could better visualise both what was being imagined with in-pit tailings storage and how it might be implemented in the future.

The animation, see Figure 4 which is of five minutes duration, was originally voiced-over in English. The animation was initially presented to the broader study and operations team to help promote understanding and potentially facilitate communication with a wider stakeholder audience. The presentation was well received, and as such, the NGGL communications team developed a second voice-over in Twi; the most commonly spoken language in the project area.

The voiced-over animation provided a boost in understanding of the concept of a terminal groundwater sink and hence acceptance of the possibility of in-pit tailings storage at Ahafo South. Unfortunately, the animation did not result in universal understanding of the concept and subsequent discussions have identified improvements that need to be made to the animation. Incremental development of the animation and the education program continues.

Additional project elements

To further confound what was, and remains, a complicated issue, a significant increase in the gold price since early 2024 has dramatically changed the economics at Ahafo South and elsewhere. The potential value of incremental open pit mine laybacks and underground mining, which were lesser aspects at lower gold pricing, now present as alternate project strategies in the Awonsu area.

As a consequence of these economic aspects, much larger conventional terrestrial tailings storage facilities can retake the focus, and hence the challenge of clearly explaining the hydraulics of a terminal groundwater sink and in-pit tailings storage can be overshadowed by the possible need for a revised conceptualisation of the tailings storage project.

Conclusions

Studies conducted at the Ahafo South operation suggest that the opportunity to utilise in-pit tailings storage may, even under the best of technical circumstances, not be a simple method to implement. Reluctance to accept the in-pit terminal groundwater sink method can be caused by a difficult technical explanation of the terminal groundwater sink concept and or concerns related to geotechnical or ore recovery aspects.

The development of a voiced-over animation that describes the in-pit tailings storage concept in general, and the terminal groundwater sink concept in particular, has greatly helped to promote better understanding of the in-pit tailings storage strategy. However, refinement of the animation remains a key aspect of what is an iterative and involved process.

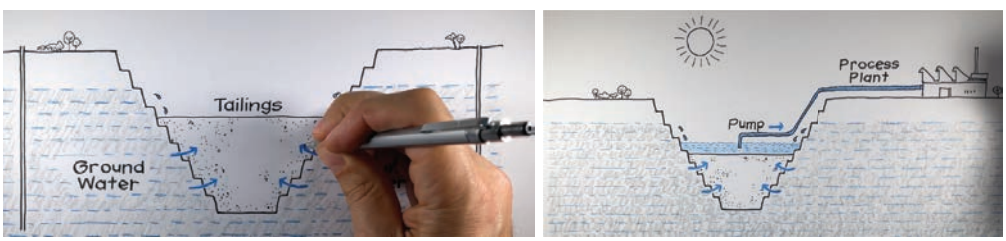

Figure 4 *Ahafo South tailings storage animation [Newmont 2025].*

References

Chilton, P.J. and Foster, S. (1995) Hydrogeological Characterisation and Water-Supply Potential of Basement Aquifers in Tropical Africa. Hydrogeology Journal, 3, 36–49.

McCullough CD, Marchand G, Unseld J, Robinson M, O'Grady B (2012) International Mine Water Association Annual Conference pg. 167–174. Pit lakes as evaporative 'terminal' sinks: an approach to best available practice mine closure.

McCullough CD, Marchand G, Unseld J, (2013)Mine Water and the Environment Vol 32, Num 4: Mine Closure of Pit Lakes as Terminal Sinks: Best Available Practice When Options are Limited?

Piteau Associates (2025). Ahafo South Mine: 2025 3D numerical groundwater model update and mine plan simulation.

Government of Ghana L.I. 2182 (2012). Minerals and Mining (Health, Safety and Technical) Regulations.

IMWA 2026
Jeongseon

Technoeconomics of the Industrial-Scale cloSURE® Biological Treatment Process

Ryan Merckel[1], Kerri du Preez[2]

[1]*Biometallurgy Division, Mintek, 200 Malibongwe Drive, Strijdom Park, Randburg, Johannesburg 2194, South Africa, ryanm@mintek.co.za, ORCID 0000-0002-1289-1598*

[2]*Biometallurgy Division, Mintek, 200 Malibongwe Drive, Strijdom Park, Randburg, Johannesburg 2194, South Africa, kerrid@mintek.co.za, ORCID 0009-0000-5097-9112*

Abstract

Mining-influenced water in South Africa's Witbank coalfields demands regulatory-compliant sulfate removal, yet reverse osmosis is energy-intensive, costly, and produces brine. A technoeconomic assessment compares Mintek's cloSURE® process, which couples microbial sulfate reduction with biological sulfide oxidation and sulfur recovery, to reverse osmosis on a normalised capacity of 5 000 m^3 d^{-1}. Discounted cash flow analysis, supported by demonstration-plant data (50 m^3 d^{-1}) and Guthrie (1974) cost estimation, indicates fixed capital investment of US$13 million for cloSURE® versus US$15 million for reverse osmosis and operating expenditure of US$2 million versus US$5 million per annum, respectively.

Keywords: Sulfate reduction, sulfide oxidation, resource recovery, capital cost, economic indicators

Introduction

Mining-influenced water containing elevated sulfate concentrations remains a major treatment challenge for the mining industry. Membrane-based technologies such as reverse osmosis are widely applied for sulfate removal, but their implementation is associated with high capital and operating costs, substantial reagent consumption for pretreatment and membrane conditioning, and the management of concentrated brines (van Rooyen *et al.* 2021; Dill *et al.* 1998), motivating continued investigation of biological sulfur cycling as an alternative (Kinnunen *et al.* 2017). Early pilot-scale studies demonstrated that sulfate-reducing microorganisms can generate alkalinity and precipitate dissolved metals while reducing sulfate concentrations (Dvorak *et al.* 1992), and subsequent work expanded this concept to passive and semi-passive treatment systems incorporating organic-substrate bioreactors (Neculita *et al.* 2007), carbon-source selection, reactor configuration (Dill *et al.* 2001), and sulfide management for stable operation (Harrison *et al.* 2014). More recently, Marais *et al.* (2024) reported a semi-passive reactor integrating sulfate reduction with biological sulfide oxidation for elemental sulfur recovery. Despite these advances, the industrial implementation of biological sulfate-reduction technologies remains limited, and technoeconomic assessments of integrated sulfate-reduction and sulfide-oxidation systems are scarce. This study therefore evaluates the technical performance and technoeconomic feasibility of the cloSURE® process using operational data from a demonstration-scale plant, estimates capital and operating costs for full-scale implementation against a reverse-osmosis benchmark, and applies discounted cash-flow modelling to assess long-term financial performance.

Site Description and Process Concept

Water Quality and Treatment Objectives

The cloSURE® process was assessed against irrigation-water quality criteria defined in the South African Water Quality Guidelines (Department of Water Affairs and Forestry 1996), with selected results summarised in Table 1. The untreated water exceeds several limits for metals and acidity indicators,

confirming the need for treatment prior to agricultural reuse. Following treatment, most regulated constituents fall within irrigation-quality limits, although manganese remains elevated and would require additional polishing for full compliance. The acidic influent (pH ≈ 3) is neutralised to near-neutral conditions (pH ≈ 7), the sodium adsorption ratio (SAR) remains below irrigation thresholds indicating low soil-sodicity risk, and increased mineral saturation reflects alkalinity generation during the coupled sulfate-reduction and sulfide-oxidation reactions.

cloSURE® Process Concept and Demonstration Plant Layout

To achieve treatment objectives aligned with irrigation-water quality criteria, the cloSURE® process integrates sequential biological sulfate-reduction and sulfide-oxidation stages within a demonstration-scale treatment train. Figure 1 shows the configuration of the cloSURE® demonstration plant. Mining-influenced water is pumped from an upstream storage dam to feed tanks and distributed to two biological sulfate-reduction ponds, where sulfate is reduced to sulfide and dissolved metals precipitate. The sulfide-rich effluent then flows through a series of biological sulfide-oxidation channels where sulfide is converted primarily to elemental sulfur. Treated water is collected in a sump and returned to the storage dam. The demonstration plant operates at a capacity of 50 $m^3 d^{-1}$.

Demonstration Plant Performance

Sulfate Reduction and Sulfide Oxidation Performance

During the stable operating period beginning at approximately day 597, influent sulfate concentrations remained near 2 500 mg L^{-1} while effluent concentrations declined from approximately 1 781 mg L^{-1} to 600 mg L^{-1}. Concurrently, dissolved sulfide increased from about 383 mg L^{-1} to 652 mg L^{-1}, which confirms sustained biological sulfate reduction. Sulfate-reduction efficiency increased from approximately 31 % (70 g m^{-3} d^{-1}) to a peak of 97 % (204 g m^{-3} d^{-1}). Sulfide concentrations entering the oxidation channels averaged 418 mg L^{-1} and decreased to an average of 235 mg L^{-1} following oxidation, with maximum oxidation rates of 29 g m^{-3} d^{-1} (≈96 %). These results confirm stable coupled sulfate reduction and sulfide oxidation during continuous operation.

Technoeconomic Assessment

Capital costs for the benchmark reverse-osmosis system were estimated using the Guthrie method, while a discounted cash-flow analysis was conducted to evaluate

Table 1 *Selected irrigation water quality criteria compared with cloSURE®-treated mining-influenced water.*

Parameter	Irrigation criterion	Untreated MIW	Treated MIW
pH	6.5–8.5	3.0	7.2
Langelier index	−0.2–0.2	−0.5	3.0
Ryznar index	≤6.5	4.2	0.1
SAR ($mmol^{0.5}$ $L^{-0.5}$)	≤1.5	0.6	0.9
Al (mg L^{-1})	≤5.0	43.6	0.1
Cu (mg L^{-1})	≤0.02	0.05	0.01
F (mg L^{-1})	≤2.0	2.7	1.0
Fe (mg L^{-1})	≤5.0	206.2	5.1
Mn (mg L^{-1})	≤0.02	17.8	19.6
N (mg L^{-1})	≤5.0	8.7	0.2
Na (mg L^{-1})	≤70	70	109
Ni (mg L^{-1})	≤0.20	0.22	0.01
Zn (mg L^{-1})	≤1.00	0.83	0.03

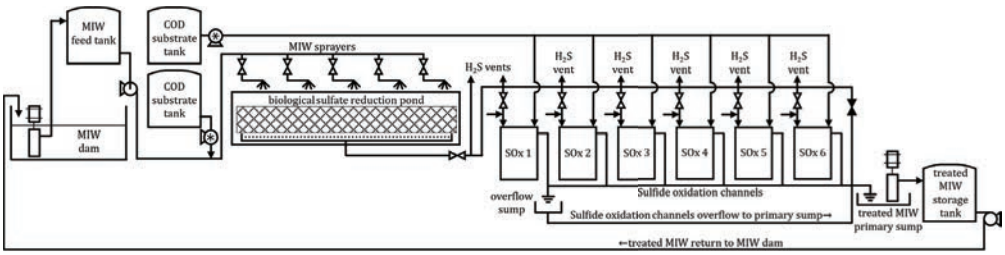

Figure 1 *Process flow diagram of the cloSURE® process.*

the financial performance of the cloSURE® process, incorporating detailed engineering data and reported operational information from both systems. The cloSURE® demonstration plant treats 50 m^3 d^{-1} using biological sulfate reduction and sulfide oxidation, whereas the benchmark reverse-osmosis system operates at approximately 5 000 m^3 d^{-1}. To enable comparison between technologies of different scale and construction period, costs were adjusted for inflation and capacity using the cost-to-capacity scaling relationship

$$C_2 = C_1 \left(\frac{P_2}{P_1}\right)^n \left(\frac{I_2}{I_1}\right)$$

where C_1 and C_2 represent plant costs at capacities P_1 and P_2, respectively, n is a technology-specific scaling exponent, and the ratio $I_2 I_1$ accounts for inflation and changes in equipment cost over time. The assessment considers four scenarios: (i) the cloSURE® demonstration plant, (ii) a scaled cloSURE® implementation at 5 000 m^3 d^{-1}, (iii) a benchmark reverse-osmosis system based on reported engineering data, and (iv) a Guthrie-method estimate of the same. Process specifications are summarised in Tables 2 and 3, and typical industrial cost data were reclassified into standard engineering cost categories to preserve confidentiality and enable direct comparison. Abattoir waste was used as the benchmark feedstock for cloSURE®. Capital costs, summarised in Table 4, reflect the modest requirements of the demonstration plant owing to its small footprint and limited mechanical complexity; at 5 000 m^3 d^{-1}, reactor packing material and civil infrastructure become the dominant cost drivers.

Capital Expenditure Comparison

Previous studies have shown that the longevity and replacement requirements of organic substrates used as bed materials can strongly influence the economic feasibility of biological sulfate-reduction systems (e.g., Neculita *et al.* 2007; van Rooyen *et al.* 2021). The present analysis similarly indicates that, at larger scales, reactor support media becomes a dominant capital component of the cloSURE® process. For the benchmark reverse-osmosis system, the owner-reported capital expenditure and the Guthrie-method estimate fall within the same order of magnitude, indicating good agreement between the datasets. Although total capital requirements for reverse osmosis and the scaled cloSURE® process are broadly comparable, their cost structures differ. cloSURE® concentrates capital in reactor support media and large treatment basins, whereas reverse osmosis requires major investment in mechanical equipment, pretreatment systems, piping, and electrical and instrumentation infrastructure. These differences become more pronounced in the operating expenditure of the two process types.

Operational Expenditure Comparison

Table 5 summarises operating costs for the cloSURE® process and the benchmark reverse-osmosis system. At demonstration scale, cloSURE® exhibits relatively high unit treatment costs due to small throughput and intensive analytical monitoring associated with research operation. When scaled to 5 000 m^3 d^{-1}, however, the unit operating cost decreases substantially as fixed costs are distributed across a larger treatment capacity.

Table 2 Process specifications for the cloSURE® plant at demonstration and scaled capacity.

Specification	Demonstration Scale	Scaled Capacity
Normal production flowrate	50.0 m^3 d^{-1}	5 000.0 m^3 d^{-1}
Design production flowrate	57.5 m^3 d^{-1}	5 750.0 m^3 d^{-1}
Influent sulfate concentration as SO_4^{2-}	2 500 mg L^{-1}	7 412 mg L^{-1}
Effluent sulfate concentration as SO_4^{2-}	400 mg L^{-1}	400 mg L^{-1}
Sulfide generated as S^{2-}	701 mg L^{-1}	2 341 mg L^{-1}
Effluent sulfide concentration as S^{2-}	200 mg L^{-1}	200 mg L^{-1}
Sulfur extraction efficiency	85.0 %	85.0 %
Sulfur net yield	7 345 kg a^{-1}	3 139 ton a^{-1}
Feedstock for sulfate reduction and sulfide oxidation	Abattoir waste	Abattoir waste
Routine sampling campaign frequency	once per week	once per week
Plant lifespan	20 years	20 years
Plant commissioning duration	9 months	9 months
Planned & unplanned maintenance	20 days $annum^{-1}$	20 days $annum^{-1}$

Table 3 Process specifications and capital cost breakdown for typical benchmark reverse-osmosis mine water treatment facilities based on reported plant data and a Guthrie-method estimate.

Specification	Engineering Estimate	Guthrie Estimate
Design treatment capacity	≈5 800 m^3 d^{-1}	≈5 800 m^3 d^{-1}
Typical operating throughput	≈5 000 m^3 d^{-1}	≈5 000 m^3 d^{-1}
Recovery ratio	≈75 %	≈75 %
Permeate production	≈3 800 m^3 d^{-1}	≈3 800 m^3 d^{-1}
Concentrate production	≈1 300 m^3 d^{-1}	≈1 300 m^3 d^{-1}
Feed sulfate concentration	≈7 400 mg L^{-1}	≈7 400 mg L^{-1}
Permeate sulfate concentration	≈400 mg L^{-1}	≈400 mg L^{-1}
Concentrate sulfate concentration	≈28 000 mg L^{-1}	≈28 000 mg L^{-1}
pH control reagents	≈4.6×10^5 kg $month^{-1}$	≈2.7×10^5 kg $month^{-1}$
Coagulation / flocculation reagents	≈1.0×10^2 kg $month^{-1}$	≈3.8×10^4 kg $month^{-1}$)
Oxidants and disinfectants	≈3.5×10^3 kg $month^{-1}$	
Membrane conditioning reagents	≈4.5×10^3 kg $month^{-1}$	≈4.5×10^3 kg $month^{-1}$)
Antiscalant dosing	≈1.4×10^3 kg $month^{-1}$	
Design plant lifespan	20 years	20 years
Commissioning duration	9 months	9 months
Planned maintenance allowance	10 d a^{-1}	10 d a^{-1}
Unplanned downtime allowance	10 d a^{-1}	10 d a^{-1}

At commercial scale, operating expenditure for cloSURE® is dominated by utilities, maintenance, waste handling, and patent royalties, while labour and administrative costs remain comparatively low due to the semi-passive nature of the process.

In contrast, the reverse-osmosis system incurs higher operating costs due to its reliance on chemical reagents, energy consumption, and mechanical maintenance. Both the engineering data and the Guthrie-method estimate for the reverse-osmosis system yield

Table 4 Capital expenditure for cloSURE® and benchmarked reverse-osmosis using engineering and Guthrie-method estimates.

Cost Category	cloSURE® Demo (Guthrie)	cloSURE® Scaled (Guthrie)	Reverse Osmosis	
			(Guthrie)	(Engineering Data)
Site & civil works	USD 219 759	USD 1 970 251	USD 5 543 158	USD 12 239 493
Equipment	USD 19 315	USD 323 219	USD 4 596 621	USD 1 515 197
Indirect costs	USD 285 550	USD 10 710 222	USD 3 447 525	USD 1 161 882
Contingencies	USD 51 588	USD 1 283 820	USD 1 358 730	USD 1 491 657
Total fixed capital	USD 576 212	USD 14 287 512	USD 14 946 034	USD 16 408 230

Exchange rate: USD 1.0000 = ZAR 16.4995, based on the South African Reserve Bank Selected Historical Rates as of 5 March 2026.

Table 5 Operational expenditure for cloSURE® and benchmarked reverse-osmosis using engineering and Guthrie-method estimates per annum.

Cost Category	cloSURE® Demo (Guthrie)	cloSURE® Scaled (Guthrie)	Reverse Osmosis	
			(Guthrie)	(Engineering Data)
Direct costs	USD 115 926	USD 836 566	USD 2 416 320	USD 3 279 004
Fixed costs	USD 43 186	USD 1 070 821	USD 1 120 176	USD 1 229 765
Overhead costs	USD 5 637	USD 79 303	USD 393 479	USD 564 740
General costs	USD 11 132	USD 107 594	USD 419 298	USD 604 113
Opex	USD 175 881	USD 2 094 284	USD 4 349 273	USD 5 677 621

Exchange rate: USD 1.0000 = ZAR 16.4995, based on the South African Reserve Bank Selected Historical Rates as of 5 March 2026.

substantially higher unit treatment costs than those calculated for cloSURE®. Although capital investment is broadly comparable, the biological process has much lower long-term operating costs, indicating a more favourable economic trajectory.

Discounted Cashflow and Financial Indicators

A discounted cash-flow analysis was conducted for the full-scale cloSURE® process to evaluate its long-term financial performance relative to reverse-osmosis treatment. The model incorporates capital investment, operating costs, revenue from elemental sulfur production, and the operating-cost savings associated with replacing membrane-based treatment. Elemental sulfur sales, valued at USD 508 070 per year, contribute appreciably to the economic performance of the process. When combined with the operating-cost advantage over reverse osmosis, these revenues drive the positive financial outcome. Based on a median South African inflation rate of 5.1 % over a 20-year operation horizon with an average real discount rate of 10.5 %, the analysis yields a net present value of approximately -USD 1.8 million, an internal rate of return of 8.5 %, a return on investment of 10.2 %, and a payback period of approximately 10.4 years. The analysis reflects only the direct economics of the cloSURE® process and does not include wider operational or environmental benefits. Abattoir waste was used as the benchmark feedstock for the technoeconomic assessment because it is produced as a disposal liability at slaughterhouses. Instead of incurring disposal costs, the producer only bears the cost of transporting the waste to the treatment facility, resulting in a net feedstock cost of approximately zero. By contrast, reverse osmosis – which generates no revenue or saleable co-products – is not amenable to payback period analysis. Assessed instead on a net present cost basis, reverse osmosis incurs a discounted lifetime expenditure of approximately -USD 48 million over

the same horizon, reflecting its character as a compliance cost rather than a value-generating asset. On a unit-cost basis, the total cost to treat mining-influenced water using cloSURE® was estimated at USD 0.92 m^{-3} (Table 6) compared to USD 2.97 m^{-3} for reverse osmosis, representing a reduction of approximately 69 %. This comparison underscores the economic advantage of the cloSURE® process, where resource recovery partially offsets treatment costs and produces a positive long-term financial outcome.

A comparison with alternative substrates shows that feedstock cost strongly influences the overall treatment economics. Fruit juice represents the lowest-cost purchasable substrate, with a feedstock price of approximately USD 21 ton^{-1}, corresponding to a treatment cost of USD 1.04 m^{-3} and annual operating expenditure of about USD 2.3 million. Ethanol and crude glycerol are substantially more expensive, with feedstock prices of approximately USD 1 578 ton^{-1} and USD 740 ton^{-1}, resulting in treatment costs of USD 7.72 m^{-3} and USD 8.14 m^{-3}, respectively. Acetate represents the least favourable option due to its high material cost (≈USD 5 818 ton^{-1}) and a treatment cost of USD 39.46 m^{-3}). These results highlight the importance of low-cost carbon sources for the economic feasibility of biological sulfate reduction processes. However, feedstock costs may vary regionally due to differences in availability, transport distance, and substrate quality. In addition, reliable supply and appropriate storage conditions are necessary to ensure continuous substrate availability and prevent premature degradation of organic feedstocks prior to use. Fruit juice was the only alternative substrate that produced favourable financial indicators, yielding an NPV of -USD 1.6 million, IRR of 8.7 %, ROI of 10.4 %, and a payback period of 10.2 years.

Conclusions

The cloSURE® demonstration plant successfully improved mining-influenced water quality through biological sulfate reduction and sulfide oxidation, increasing pH, removing metals and substantially reducing sulfate concentrations. Sulfate-reduction efficiencies of up to 97 % were achieved during stable operation, although performance was sensitive to COD availability and operational continuity. At full scale, the cloSURE® process requires capital investment comparable to reverse-osmosis treatment but exhibits substantially lower operating expenditure due to reduced chemical demand, passive operation and lower labour requirements. Financial analysis indicates favourable long-term performance: annual operating-cost savings combined with approximately USD 508 070 per year in elemental-sulfur revenue yield a net present value of about USD 4 million over twenty years at an inflation rate of 5.1 %. The resulting internal rate of return (8.2 %), return on investment (10.2 %) and payback period (~10.4 years) indicate economically viable deployment. Reverse osmosis generates no revenue or saleable co-products and is not amenable to payback period analysis; assessed on a net present cost basis, it incurs a discounted lifetime expenditure of approximately -USD 48 million over the same horizon, confirming its character as a compliance cost rather than a value-generating asset. Safety considerations are primarily associated with hydrogen

Table 6 *Operating cost estimates for cloSURE® using alternative carbon substrates.*

Scenario	Material Cost	Treatment Cost	Operational Cost
Reverse osmosis	-	USD 2.97 m^{-3}_{MIW}	USD 5 677 621 a^{-1}
cloSURE® (abattoir waste)	USD 0 ton^{-1}	USD 0.92 m^{-3}_{MIW}	USD 2 094 284 a^{-1}
cloSURE® (fruit juice)	USD 21 ton^{-1}	USD 1.04 m^{-3}_{MIW}	USD 2 305 569 a^{-1}
cloSURE® (ethanol)	USD 1 578 ton^{-1}	USD 7.72 m^{-3}_{MIW}	USD 13 819 231 a^{-1}
cloSURE® (glycerol)	USD 740 ton^{-1}	USD 8.14 m^{-3}_{MIW}	USD 14 546 477 a^{-1}
cloSURE® (acetate)	USD 5 818 ton^{-1}	USD 39.46 m^{-3}_{MIW}	USD 68 570 822 a^{-1}

sulfide exposure, mine-water handling and operational interruptions, emphasising the need for appropriate monitoring and operational support. Overall, the results demonstrate that the cloSURE® process provides a technically viable and economically competitive alternative to membrane-based mine-water treatment.

Acknowledgements

The authors acknowledge and thank the financial support provided by Mintek, the Technology Innovation Agency (TIA), and Thungela Resources for the research presented in this study.

References

Department of Water Affairs and Forestry (1996) *South African Water Quality Guidelines. Volume 4: Agricultural Use – Irrigation*. 2nd edn. Department of Water Affairs and Forestry, Pretoria.

Dill S, Kinnunen P, Puhakka J, Mäkinen T (1998) Sulphate removal technologies for mine waters – a review. Mine Water Environ 17:1–17

Dill S, Cloete TE, Coetser L, Zdyb L (2001) Determination of the suitability of alternative carbon sources for sulphate reduction in the passive treatment of mine water. Water SA 27(1):41–48

Dvorak DH, Hedin RS, Edenborn HM, McIntire PE (1992) Treatment of metal-contaminated water using bacterial sulfate reduction: results from pilot-scale reactors. Biotechnol Bioeng 40:609–616. https://doi.org/10.1002/bit.260400506

Harrison STL, van Hille RP, Rose PD (2014) Addressing the challenges facing biological sulphate reduction as a strategy for AMD treatment. Water SA 40(3):503–512. https://doi.org/10.4314/wsa.v40i3.15

Kinnunen P, Kietäväinen R, Bomberg M (2017) Sulphate removal from mine water with chemical, biological and membrane technologies. Water Sci Technol 76(1):1–12. https://doi.org/10.2166/wst.2017.204

Marais TS, Tawodzera NT, Rademeyer S, Smart M, Fernandes S, Harrison STL (2024) Development of a novel semi-passive process integrating biological sulfate reduction and sulfide oxidation for mine water treatment. Mine Water Environ. https://doi.org/10.1007/s10230-024-00977-3

Neculita CM, Zagury GJ, Bussière B (2007) Passive treatment of acid mine drainage in bioreactors using sulfate-reducing bacteria: critical review and research needs. J Environ Qual 36:1–16. https://doi.org/10.2134/jeq2006.0066

van Rooyen DJ, van Staden R, du Preez LA (2021) Sulphate removal technologies for the treatment of mine-impacted water. Mine Water Environ 40:719–737. https://doi.org/10.1007/s10230-021-00772-4

IMWA 2026
Jeongseon

Repurposing Flooded Underground Mines for Seasonal Heat Storage: Insights from the EU project PUSH-IT

Elke Mugova[1], Stefan Klein[2], Florian Hahn[3]

Fraunhofer Research Institution for Energy Infrastructures and Geotechnologies IEG, Am Hochschulcampus 1, 44801 Bochum, Germany

[1]elke.mugova@ieg.fraunhofer.de, ORCID 0000-0001-6019-9945

[2]stefan.klein@ieg.fraunhofer.de,

[3]florian.hahn@ieg.fraunhofer.de, ORCID 0009-0009-

Abstract

Flooded underground mines are increasingly recognised as geothermal resources for seasonal heat storage. In the EU funded project PUSH IT, a large-scale Mine Thermal Energy Storage (MTES) pilot site will be installed, repurposing a section of the former "Mansfeld" colliery below the Technical Centre of the Ruhr University Bochum, Germany. An isolated, estimated 10,000 m³ mine void and four 120 m boreholes will enable injection of industrial surplus heat. Initial drilling, hydro-geochemical analyses, and modelling confirm suitable conditions for heat injection and recovery. The pilot facility demonstrates MTES feasibility and supports broader deployment of mines as "geobatteries".

Keywords: mine water geothermal, mine water heat, MTES

Introduction

Seasonal discrepancies between heat production and heat demand pose a major challenge for decarbonising heating networks across Europe. Although surplus heat from industry, cooling systems, data centres, geothermal plants, and solar thermal collectors is increasingly available, demand peaks in winter, while heat supply often peaks in summer. Hence, Underground Thermal Energy Storage (UTES) technologies like Aquifer (ATES), Borehole (BTES) and Mine Thermal Energy Storage (MTES) are considered key to balancing seasonal heat availability and consumption. These systems allow seasonal storage of surplus heat in the subsurface, enabling flexible and low carbon operation of district heating networks.

Flooded underground mines are particularly promising for high temperature seasonal storage (Hahn *et al.* 2022, 2024). Former mining regions contain extensive networks of galleries, shafts and mine workings, that have been flooded after mine closure. Under suitable geological and hydraulic conditions, these voids can act as large heat storage facilities. Their substantial volumes, combined with the thermal capacity of both mine water and surrounding rock mass, allow injection of surplus heat during summer and its extraction during winter for heating applications (Oppelt *et al.* 2025). In typical MTES configurations, the system is operated as an open-loop system, where mine water is extracted, thermally conditioned via heat exchangers, and reinjected into the mine. The mine water itself is not directly used in the heating network. Former mining sites often host newly established industries with surplus heat potential or are attractive locations for future industrial development. By repurposing the underground infrastructure for seasonal heat storage, these areas become even more appealing for post mining utilisation. MTES thus offers a route to transform mining legacies into infrastructure for the energy transition.

Study site

As part of the EU funded project *Piloting Underground Storage of Heat in geoThermal reservoirs* (PUSH IT, grant no. 1011096566), a MTES pilot site is under development. The MTES pilot site is located beneath the

Technical Centre of Ruhr University Bochum (RUB), Germany, where a hydraulically isolated section of the former Mansfeld coal mine is being repurposed for thermal storage (Figure 1). The term "hydraulically isolated" refers to a section of the mine workings that is not connected to active mine water drainage systems. Instead, it represents a confined mine compartment with limited hydraulic exchange with surrounding mine voids, allowing controlled thermal storage and minimising heat losses. In the section of the Mansfeld colliery two parallel galleries on the first mine level, at approximately 120 m depth, form a mine void estimated of about 10,000 m³. These galleries are flooded and represent a confined underground space suitable for controlled heat injection and extraction (Mugova *et al.* 2026).

The site meets the three core criteria identified for successful MTES systems. First, sufficient quantities of surplus heat are available at the RUB Technical Centre, supplied by industrial cooling towers (each with an 11 MW capacity), data centre cooling processes, as well as combined heat and power units. Second, a flooded, hydraulically isolated mine working lies directly beneath the heat source, providing an ideal subsurface storage volume. Third, during winter months, the stored thermal energy can be reintegrated into the university's heating network, which currently depends largely on natural gas based systems. Well-documented mine plans make it possible to accurately plan the drilling work. Furthermore, the geological setting within the Ruhr Carboniferous strata, comprising alternating sandstones, mudstones and interbedded coal seams is well known and offers important information for designing well completions and selecting casing materials.

The planned MTES system follows an open-loop configuration, in which mine water is extracted from and reinjected into the flooded mine workings via multiple boreholes. At the surface, the extracted mine water is connected to the campus heating and cooling infrastructure via a heat exchanger and large-scale heat pumps. The overall

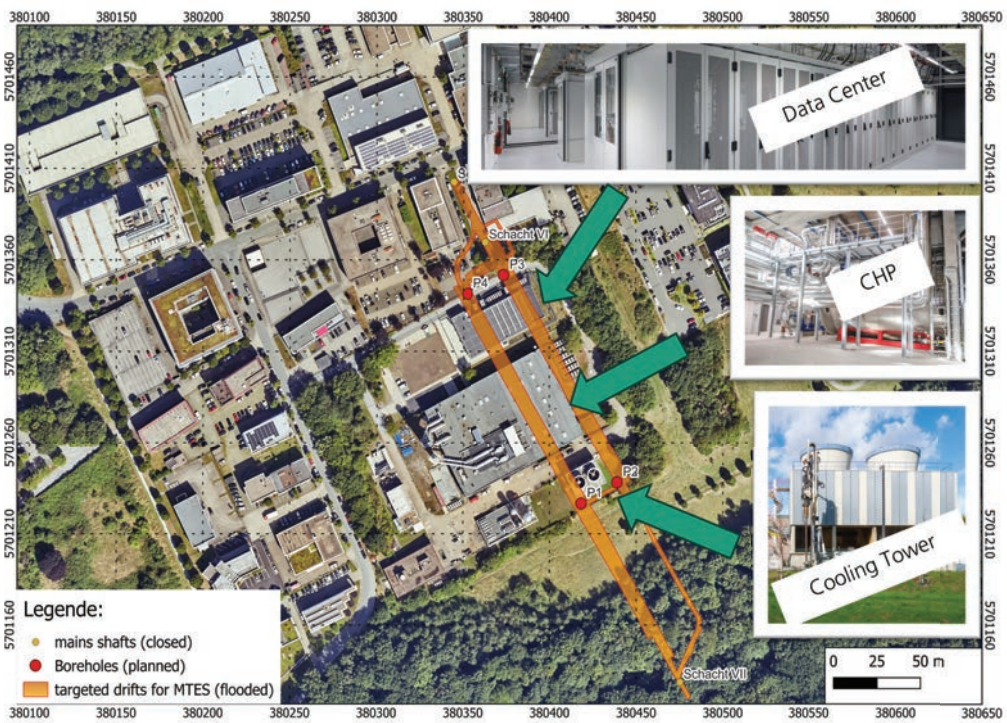

Figure 1 *Aerial view of the RUB Technical Centre. In orange, parallel mine galleries, depth 120 m.*

system design integrates surplus heat sources, a buffer storage, and the district heating network, enabling seasonal heat storage in the underground mine void and its recovery for heating purposes.

Drilling and field investigations

Since 2024, three boreholes have been drilled to depths of approximately 120 m to establish hydraulic connections to the flooded galleries. The drilling was executed using Fraunhofer IEG's Hütte HBR 207 GT drill rig and required refined technical solutions to ensure vertical well trajectories despite challenging geological conditions (Figure 2). The first borehole showed deviations of up to 5 m due to steep, alternating lithological layers. Static recalculations of the bottom hole assembly and the use of heavy weight drill collars enabled a pendulum effect that reduced deviation in subsequent boreholes to less than 0.5 m.

Advanced casing technologies were tested, including the installation of glass fibre reinforced composite tubulars (HCT casings) designed for high temperature applications and corrosion resistance in potentially mineralised mine water. Installation procedures were developed specifically for this project, making it a pioneering field test for composite casings in MTES applications. Cementation quality and borehole integrity were validated using optical and acoustic televiewer logs, distributed temperature sensing, and camera inspections. No leakage or structural issues were detected in the completed wells (Klein *et al.* 2025). The mine water sampled during drilling shows moderate temperature (~13 °C), low mineralisation, and neutral pH, indicating favourable conditions for high temperature injection (up to 85 °C) without major risks of scaling, corrosion, or biofouling. However, under elevated temperatures of up to approximately 85 °C, geochemical conditions may change. Increasing temperature can alter mineral solubility and potentially induce scaling processes or changes in microbial activity. Therefore, ongoing monitoring and geochemical modelling are essential to assess

Figure 2 *Drilling rig in front of the Technical Centre's cooling tower (on the right).*

long-term risks related to precipitation, corrosion, and biofouling under high-temperature operating conditions.

Upcoming phases include additional drilling of two boreholes, hydraulic testing (including pumping and tracer tests), and a hot push pull test to determine thermal recovery efficiencies and flow regimes within the mine workings. The Hot push–pull test will be conducted as a standardised method to evaluate the thermal recovery efficiency and hydraulic behaviour of the storage system. During these tests, heated water is injected into the reservoir and subsequently extracted from the same well, allowing the analysis of thermal breakthrough behaviour, heat transport processes, and potential short-circuit flow paths within the mine workings.

Modelling Approaches

Thermohydraulic reservoir modelling with the software SPRING is applied to simulate heat injection, storage, and recovery within the flooded mine workings. Modelling results are transferred from the WINZER project (Fraunhofer IEG, 2026). The models account for coupled fluid flow and heat transport processes, including heat exchange between the mine water and the surrounding rock mass. These models provide estimates of temperature evolution, storage capacity, and recoverable heat under cyclic operation.

Building on this, a co-simulation approach is used to evaluate the integration of the MTES system into the campus heating and cooling infrastructure (Spengler, 2025). The subsurface reservoir model is coupled with a dynamic model of the surface energy system, including heat pumps, cooling processes, and the district heating network. It is implemented in separate simulation environments and linked via an external control algorithm, enabling the exchange of thermal and operational data during runtime. Charging cycles are defined as seasonal sequences consisting of heat injection in summer and heat extraction in winter. The co-simulation framework allows the analysis of multiple consecutive cycles, providing insight into long-term system behaviour and the interaction between storage operation and energy demand.

Public Outreach and Stakeholder Engagement

Effective communication and public engagement are essential pillars of the PUSH IT project, ensuring that emerging underground heat storage technologies such as MTES are understood, trusted, and embedded within broader societal and institutional contexts. As MTES might rely on utilisation of former mining infrastructure beneath populated areas, the technology intersects with regulatory frameworks, environmental concerns, regional identity, and long term energy planning. Transparent communication therefore helps address questions around safety, environmental compatibility, and the practical implications of operating a high temperature storage system in abandoned mines.

Throughout the project, a broad range of outreach activities has been carried out to connect with key groups. Engagement with authorities and regulatory bodies has ensured that legal frameworks, environmental aspects, and permitting processes are discussed openly and informed by current scientific findings. Regular exchanges with industry representatives, utilities, and energy planners have helped align MTES development with practical needs in heat transition strategies and district heating networks. Within the scientific community, the project team contributed to knowledge exchange by presenting MTES concepts, technical progress, and preliminary results in academic and professional settings. These activities facilitated collaboration with researchers working on geothermal energy, mine water systems, and underground thermal energy storage, while also helping to establish MTES more firmly within the broader UTES research landscape. Public facing communication has been equally important. The team has consistently provided accessible explanations of MTES principles through interviews, articles, digital content, and social media communication, helping to increase general awareness of underground heat storage. Drilling site tours and on site communication with information fence banners made the project visible to local communities and provided opportunities for informal

dialogue. Educational activities for university students and early career researchers further supported long term knowledge building and created opportunities for direct interaction with the technology.

Across all formats, the overarching goal has been to ensure that MTES is understood not only as a technical innovation but also as a socially relevant component of the energy transition.

Outlook and Transferability of MTES systems

Preliminary modelling and drilling results demonstrate that the Bochum pilot site could achieve recoverable temperatures between 25 °C and 50 °C after several charging cycles, suitable for low temperature district heating, heat pumps, or hybrid heating systems. Field data from the PUSH IT site will be used to calibrate reservoir and co simulation models, improving predictions of heat dispersion, storage capacity, and long term thermal behaviour. The MTES system is intended to be connected to the university's district heating network.

The results and implications of the PUSH-IT project extend well beyond the Ruhr region. Many former mining districts worldwide, contain extensive flooded mine working that could be repurposed as MTES systems. The combination of large available void volumes, proximity to urban heat suppliers and consumers, and existing infrastructure provides unique advantages compared to other UTES systems. Scaling MTES globally depends on several enabling conditions, including advances in drilling and completion technologies for accessing flooded mine workings, the establishment of robust geochemical and hydraulic monitoring practices, the development of streamlined regulatory frameworks for underground heat storage, and the availability of validated numerical models to support engineering design. Equally important is active community engagement supported by transparent communication of risks and benefits. The Bochum pilot is among the first large scale MTES demonstrators and will provide essential operational data and best practice guidance for future sites. By converting abandoned mines into "geobatteries," MTES can deliver resilient, low carbon heating solutions, promote the circular reuse of industrial infrastructure, and contribute to socio economic revitalisation in former mining regions.

Acknowledgements

PUSH-IT is a project funded by the European Union's Horizon Europe research and innovation programme under grant agreement No 101096566, funded by the European Union. The authors thank the PUSH-IT consortium and our Fraunhofer IEG drilling team.

References

Fraunhofer IEG (2026) Abschlussbericht zum Forschungsvor-haben Winzer »Wärmespeicherung in Zechen des Ruhrgebiets« [Final report of the research project "Winzer – Thermal Energy Storage in Coal Mines of the Ruhr Area"]. Funding code: 03G0912A-D. Bochum, Germany

Hahn F, Klein S, Bussmann G, Seidel T (2022) The Mine Thermal Energy Storage project in Bochum – lessons learned from the HEATSTORE project. Available at: https://publica.fraunhofer.de/entities/publication/ede1fa5c-4672-4547-952dfc60725ec86a/details (Accessed: 10 Oct 2025).

Hahn F, Klein S, Mannke K, Verhoeven R, Güldenhaupt J, Seidel T, König T (2024) Mine thermal energy storage (MTES) systems in abandoned collieries within the Ruhr area. Proceedings of the 15th International Mine Water Association Congress 2024, Morgantown, West Virginia, USA. ISBN: 978 3 9825293 2 5.

Klein S, Mugova E, Güldenhaupt J, Wieling I (2025) Wärme aus'm Pütt – Grubenwasser als saisonaler Wärmespeicher [Heat from the mine – mine water as a seasonal heat storage facility]. bbr – Leitungsbau Brunnenbau Geothermie 12/2025.

Mugova E, Klein S, Hahn F (2026) Geothermal utilisation of flooded underground mines based on the example of a Mine Thermal Energy Storage. Mining Report 01 2026.

Oppelt L, Grab T, Ebel T, Wunderlich T, Storch T, Fieback T (2025) Mine water as an energy source: overview of technical basics, existing plants, and monitoring results. Mine Water Environ 41: https://doi.org/10.1007/s10230 025 01057 w

Spengler T (2025) Co-Simulation of a District Heating and Cooling System in Combination with Mine Thermal Energy Storage: A Case Study in Germany. Master's thesis, Delft University of Technology, Faculty of Mechanical, Maritime and Materials Engineering, Delft, Netherlands.

Mine thermal energy storage in flooded mine workings: Current status and next development Steps for a Pilot Site in Bochum, Germany

Elke Mugova, Stefan Klein, Jonas Enno Lehmann

Fraunhofer IEG, Germany

Abstract

Mine Thermal Energy Storage (MTES) offers a promising approach for using flooded underground mine workings as large-scale subsurface reservoirs for seasonal heat storage in former or active mining regions. This poster presents the current status and next development steps of an MTES pilot site in the city of Bochum, located in the Ruhr area in western Germany, one of Europe's major former hard coal mining regions.

At the site near Ruhr University Bochum, Fraunhofer IEG is developing and testing an MTES demonstration system in former mine workings at a depth of approximately 120 m. The mine workings are accessed by boreholes to investigate how the mine water occurring in the flooded underground structures can be used as a seasonal underground thermal storage system.

The poster presents the current status and next development steps of the pilot site, including drilling, monitoring infrastructure, field investigations and system integration. Two boreholes have already been completed, a third borehole is currently under construction, and a fourth borehole is planned for 2026. The boreholes are equipped with multichannel downhole sensors and fibre-optic cables to support future operational tests and to characterize the hydrodynamic and thermohydraulic behaviour of the flooded mine workings. Initial investigations include geophysical logging, camera inspection and mine water sampling. Hydrochemical measurements indicate slightly mineralized mine water with a temperature of approximately 12 to 13 °C, an electrical conductivity of about 850 µS/cm, a pH value around 7 and dissolved oxygen concentrations of approximately 5 mg/L. In parallel, thermohydraulic modelling and co-simulation approaches are being developed to evaluate the integration of underground heat storage into the existing heating and cooling network of the Technical Centre.

IMWA 2026
Jeongseon

Modeling of Pyrite Oxidation and Sulfate Reduction in Former German Hard Coal Mines

Simon E. Nikutta[1], Barbara M. A. Teichert[1], Harald Strauss[2]

[1]*Research Center of Post-Mining, Technische Hochschule Georg Agricola, 44787 Bochum, Germany, simon.nikutta@thga.de*

[2]*Universität Muenster, Institut fuer Geologie und Paläontologie, 48149 Muenster, Germany, hstrauss@uni-muenster.de, ORCID 0000-0003-2639-1225*

Abstract

Former mine workings are inaccessible today, making site-specific mine water sampling impossible. Samples are taken at pumping stations, mixing waters from large areas. To identify processes influencing mine water chemistry pyrite oxidation and sulfate reduction were modelled using PHREEQC, trying to reproduce the mine water chemistry of a former mine. The first step of modelling included pyrite oxidation with subsequent weathering of dolomite and calcite. In a second step sulfate reduction was modelled using acetate as substrate. The modelled values correspond roughly to measured values and show that further development is necessary and many processes are yet to be integrated.

Keywords: Sulfate reduction, pyrite oxidation, hydrogeochemical modelling, sulfur cycle, mine water rebound

Introduction

With the closure of the last coal mine in the Ruhr region in 2018, maintaining drainage and ventilation systems was no longer necessary for coal mining operations. However, since more than 5 million people now live in the Ruhr region, an uncontrolled mine water rise is not possible. In order to minimize the risk to the environment, the mining operator RAG AG remains obligated to pump out mine water. At the same time, these long-term tasks must be carried out as efficiently as possible. To this end, the mine water is raised to safe levels in a controlled manner (RAG 2024). Locations of the pumping stations in the Ruhr region are shown in Figure 1.

Mine water chemistry

The coal-bearing strata of the Carboniferous emerge at the surface near the Ruhr River and dip to the north. The thickness of the overlying strata increases to around 1,000 metres near the River Lippe (Wedewardt 1995). Consequently, the mine water in the southern part of the mining area originates from meteoric water and has a lower degree of mineralisation, whereas in the north the mine water is fed by deep groundwater and has a higher degree of mineralisation. In addition to the inflowing waters, the mine water chemistry is also controlled by various hydrogeochemical processes. As a result of dewatering and ventilation of the mine workings, pyrite, contained in the coal seams and surrounding rock layers, comes into contact with oxygen and is oxidised, as shown in Equation [1]:

$$[1] \quad FeS_2 + 3{,}5\,O_2 + H_2O \rightarrow Fe^{2+} + 2\,SO_4^{2-} + 2\,H^+$$

The oxidation products form secondary minerals that are water-soluble. When these secondary minerals dissolve as a result of inflows or a rise in the mine water level, sulfate and iron enter the mine water. Ferrous iron is generally less mobile in this process, as it is oxidized by oxygen to form ferric iron and iron hydroxides; see Equation [2]. Both the oxidation of sulfide and the oxidation of ferrous iron release protons. In the Ruhr region weathering of carbonate minerals buffers the pH to circum-neutral levels.

$$[2] \quad 2\,Fe^{2+} + 0{,}5\,O_2 + 5\,H_2O \rightarrow 2\,Fe(OH)_3 + 4\,H^+$$

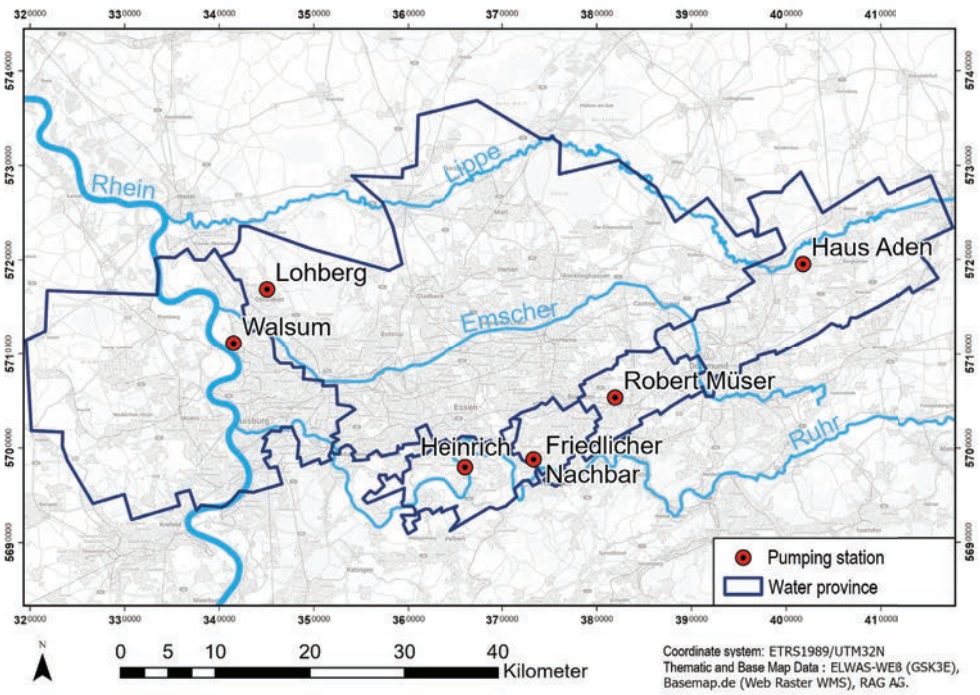

Figure 1 *Water management provinces and pumping stations between the rivers Ruhr, Rhein and Lippe in the Ruhr area, Germany. Pumping stations Lohberg and Haus Aden are currently under construction. Map provided by Dr. Benjamin Haske, 2025.*

In anoxic parts of the mine water body the sulfate is reduced by sulfate reducing bacteria (SRB). Equation [3] shows sulfate reduction using acetate as substrate. In circumneutral mine waters hydrogen sulfide is deprotonated and sulfide (HS-) is predominant.

$$[3] \quad SO_4^{2-} + CH_2COO^- + H^+ \rightarrow 2\,HCO_3^- + H_2S$$

If ferrous iron is present, it can react with the sulfide to form iron sulfides, as described in Equation [4].

$$[4] \quad Fe^{2+} + HS^- \rightarrow FeS + H^+$$

The change of the sulfate concentration can be described by a Michaelis-Menten kinetic, as shown in Equation [5].

$$[5] \quad \frac{d[SO_4^{2-}]}{dt} = R_{Michaelis-Menten} = -v_{max} \times \frac{[S]}{K_M+[S]}$$

Where [S] is the substrate concentration, t is the time, $v_{(max)}$ is the maximum growth rate, K_M is the half-saturation constant for acetate or sulfate as substrate (Ingvorsen, Zehnder, Jørgensen 1984).

Methods

Conceptual model

To model the geochemical processes of pyrite oxidation and sulfate reduction, a conceptual model was developed. Critical parameters for the assessment of the geochemical reactions are:

- Porosity and grain density of the surrounding rock
- Content of pyrite in coal seams and surrounding rock
- Content of carbonate minerals in the surrounding rock
- Fraction of Fe^{2+} which is oxidized to Fe^{3+} and immobilized as $Fe(OH)_3$
- Rates, half saturation constants and substrates for the sulfate reduction by SRB
- Transport of formed sulfate in the mine water
- Pyrite grain size and micro texture

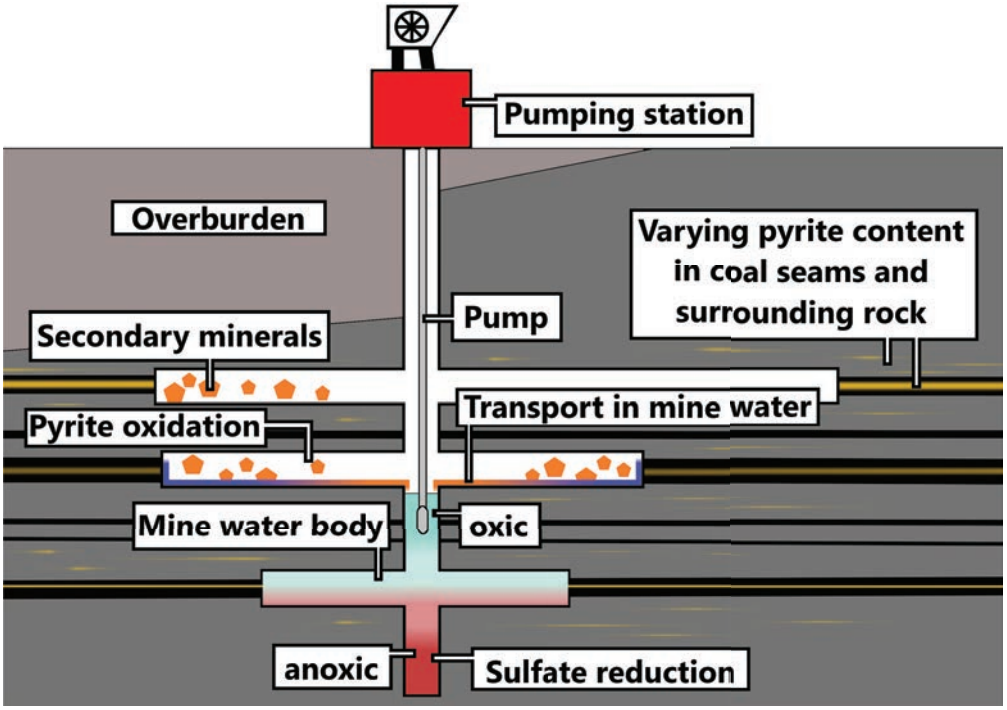

Figure 2 *Schematic drawing of the relevant geochemical processes at the water management sites.*

Since the mines are closed and no longer accessible, it proves difficult or impossible to measure these parameters in the field. Consequently, comparable values from the literature were used. At certain stages of the model development assumptions were made that are not supported by data from the literature or measurements. The geological parameters of the Ruhr Carboniferous rocks are listed in Table 1. Transport in the mine water was neglected in the calculations and it was assumed, that the mine water chemistry, that resulted from pyrite oxidation, was the initial water for the modeling of sulfate reduction. No estimations for the reactive surface of pyrite were made.

Numerical model

For numerical modeling of the mine water chemistry, the mine site RM was selected, where sulfate reduction occurs and SRB were detected using a BART-Test from Hach. Average values from this site, obtained in a monitoring campaign with two-month intervals, were used as the target function and were tried to reproduce during numerical modeling (see Table 3). PHREEQC Interactive (version 3.8.6-17100, USGS) was used for geochemical modeling. The sulfate reduction was modeled according to equation [5] with the parameters listed in Table 2.

A representative volume was defined assuming a porosity of 10%. A high value was chosen, as the surrounding rocks were impacted by mining activities and are likely to have an increased porosity. A grain density of 2.67 kg/L was assumed. Since pyrite content varies over a wide range, a conservative approach was taken, using a fraction of 0.1% pyrite for the calculation, corresponding to 222.5 mmol of pyrite. For calcite a value of 0.1% calcite was used, and dolomite was assumed to be 0.1% of the solid phase, corresponding to 266.8 mmol of calcite, and 144.7 mmol of dolomite per representative volume. The assumption of the dolomite fraction is not supported by measured data. The values from Table 3 were used to calculate the saturation index (SI) for CO_2 using PHREEQC, resulting in an

Table 1 Geological Parameters.

Parameter	Value/Range	Mean value	Source
Porosity	0.3-15.6 %	5.5 %	(Greve et. al. 2024b)
Grain density	2.6 – 2.9 g/cm3		(Bär et. al 2020, Greve et. al. 2024a)
Pyrite content	0.0 – 6.0 %	0.2 %	(Greve et. al. 2024a)
Calcite content	0.0 – 1.0 %	0.1 %	(Greve et. al. 2024a)

Table 2 Kinetic Parameters.

Parameter	Value	Source
$v_{(max,Acetate)}$	5.3×10^{-5} [mmol × L^{-1} × min^{-1} × g dry weight-1]	(Ingvorsen, Zehnder, Jørgensen, 1984)
$K_{(M,Acetate)}$	7.7×10^{-5} [mmol × L^{-1}]	(Ingvorsen, Zehnder, Jørgensen, 1984)

Table 3 Mine water chemistry of RM as target function.

Site [mg/L]	pH	Na	Ca	Mg	SO_4^{2-}	Fe(+II)	Cl	HCO_3^-
RM	7.5	1139.8	127.0	45.7	87.3	0.2	1703.3	979.1
Site [mmol/L]	**pH**	**Na**	**Ca**	**Mg**	**SO_4^{2-}**	**Fe(+II)**	**Cl**	**HCO_3^-**
RM	7.5	49.58	3.17	1.88	0.91	0.0036	48.04	16.05

SI of -1.63, assuming ideal gas behaviour. This SI was used as a proxy for log(pCO_2) and used for subsequent calculations. All calculations were initiated with neutral water at 22 °C. Additionally, it was assumed that 90% and 95% of the Fe^{2+} produced during pyrite oxidation react with O_2. Since Ca^{2+} does not react in sulfate reduction, the calculated values corresponding to the Ca^{2+}-concentration that best matched the target value of 3.17 mmol/L were selected as the basis for the subsequent sulfate reduction modelling. The sulfate reduction was carried out using the data from Table 4 as the initial solution in PHREEQC and the kinetic constants in Table 2. The calculations were carried out with and without the formation of FeS according to Equation [4]. The substrate concentration was varied between 2.0, 2.5, 3.0. 3.5 and 4.0 mmol/L acetate as substrate, respectively. Values for pH, Ca, Mg, S(+VI), Fe(+II), C(+IV) were obtained by running the simulation for 100 minutes. The results are shown in Table 5.

Results

Substrate concentrations of 2 mmol/L acetate did not reduce the S(+VI) concentration below 1.5 mmol/L and were neglected. Substrate concentrations of 3.0 mmol/L acetate and above depleted all S(+VI) and were also neglected. Calculated concentrations of the C(+IV) species were 10.77 and 10.73 mmol for $C(+IV)_{90\%Ox}$ and $C(+IV)_{95\%Ox}$, respectively. Concentrations of Mg and Ca species were unchanged from the input data in Table 4, as they do not participate as reactants in the sulfate reduction reaction. A substrate concentration of 2.5 mmol/L acetate resulted in S(+VI) concentrations of 1.01 and 1.00 mmol/L, respectively. The target HCO_3^- concentration was higher than the calculated concentrations of C(+IV) species after the sulfate reduction. Additional formation of HCO_3^- during sulfate reduction contributes to elevated concentrations of HCO_3^-, but does not reach levels of the target function with 16.05 mmol/L. Calculated concentrations of Fe(+II) species were good approximations of

Table 4 Calculated weathering processes pyrite oxidation and carbonate weathering for the location RM with 90% and 95% of Fe^{2+} reacting with O_2

90%Ox [mmol/L]	pH	Ca	Mg	S(+VI)	Fe(+II)	C(+IV)
$RM_{Wea,90\%Ox}$	7.05	3.21	2.63	3.56	0.18	5.77
95%Ox [mmol/L]	**pH**	**Ca**	**Mg**	**S(+VI)**	**Fe(+II)**	**C(+IV)**
$RM_{Wea,95\%Ox}$	7.05	3.25	2.66	3.56	0.09	5.73

Table 5 Calculated sulfate reduction with 2.5 mmol/L acetate

[mmol/L]	pH	Ca	Mg	S(+VI)	Fe(+II)	C(+IV)
90% Ox FeS	7.58	3.21	2.63	1.01	0.0051	10.77
90% Ox No FeS	7.67	3.21	2.63	1.01	0.18	10.77
[mmol/L]	**pH**	**Ca**	**Mg**	**S(+VI)**	**Fe(+II)**	**C(+IV)**
95% Ox FeS	7.67	3.25	2.66	1.00	0.0046	10.73
95% Ox No FeS	7.71	3.25	2.66	1.00	0.09	10.73

the target value of 0.0036 mmol/L if sulfate reduction was modelled with formation of FeS. With no formation of FeS calculated concentrations of Fe(+II) species remained unchanged at 0.18 and 0.09 mmol/L.

Conclusions

Initial model development shows that the basic geochemical reactions, especially the sulfur cycling processes taking place in the mine workings, can be reproduced. Low iron concentrations can be attributed to the formation of iron sulfide. High HCO_3^- concentrations in the target function of RM could be partly reproduced by weathering reactions and sulfate reduction, but the model needs further development with regards to mineralization the inflowing water.

However, the results show that this first version of the model still relies on too many assumptions. In further steps of model development, it will be important to include:

- Transport processes from sites of pyrite oxidation into the water body
  As the water chemistry from the weathering was directly used for the simulation of sulfate reduction, the reaction of ferric iron with oxygen during transport was approximated by a fraction of 90% and 95% reacting with oxygen.
- Better characterization of the SRB and their abundance
  The use of BART test proves the presence of SRB in the mine water, but is not species-specific. Here Desulfobacter postgatei was chosen as a model compound on the basis of available results. A general microbial analysis of the bacterial species in the mine water and their abundance is necessary, in order to better estimate the reduced amount of sulfate. It will also allow for a
- Incorporation of pyrite grain size and reactive surface
  The geological parameters, which were obtained from studies within the Ruhr region, were not measured in the Robert Mueser water province. It remains unclear how representative the figures are of the situation at the Robert Mueser mine.
- Mine Geometry and rising mine water levels
  The final aim is also to take the geometry of the mine into account so that rising mine water levels can be represented in the model. However, as the calculated values in this article show, there are still many stages of model development between that final step and the current model.

Acknowledgements

We sincerely thank RAG AG for their support of this project and for providing the data used in this study.

References

Bär K, Reinsch T, Bott J (2020) P3—PetroPhysical Property Database—A global compilation of lab measured rock properties. Earth Syst. Sci. Data Open Access Discuss

Greve J, Busch B, Quandt D, Knaak M, Hilgers C (2024a) The influence of sedimentary facies, mineralogy, and diagenesis on reservoir properties of the coal-bearing Upper Carboniferous of NW Germany. Pet. Geosci. 30: petgeo2023-020

Greve J, Busch B, Quandt D, Knaak M, Hilgers C (2024b) Understanding the interplay of depositional rock types, mineralogy, and diagenesis on reservoir properties of the coal-bearing Langsettian and Duckmantian strata (Bashkirian, Pennsylvanian) of the Ruhr Area, NW Germany. Int. J. Earth. Sci. 113:2275–2304

Ingvorsen K, Zehnder AJB, Jørgensen BB (1984) Kinetics of sulfate and acetate uptake by Desulfobacter postgatei. Appl. Environ. Microbiol. 47:403–408

Quandt D, Busch B, Hilgers C (2024) Evolution of Upper Carboniferous tight sandstone reservoirs in the Ruhr and Lower Saxony basins (NW Germany) of the Central European Variscan foreland. Mar. Pet. Geol. 163: 106774

RAG (2024) Konzept zur langfristigen Optimierung der Grubenwasserhaltung der RAG Aktiengesellschaft fuer Nordrhein-Westfalen. https://geodaten.rag.de/bid/tree/GenV/Grubenwasserkonzept%20NRW/Konzept%20%E2%80%93%20Grubenwasserhaltung%202024.pdf. Accessed 25 March 2025

Wedewardt M (1995) Hydrochemistry and origin of subsurface brines of the Ruhr-Basin; Hydrochemie und Genese der Tiefenwaesser im Ruhr-Revier. DMT-Berichte aus Forschung und Entwicklung, v. 39

IMWA 2026
Jeongseon

Redox Chemistry of Mine Waters – Still Misunderstood

D. Kirk Nordstrom[1]

[1]*Kwamanzi LLC, Boulder, CO, USA*

dkirknordstrom@comcast.net, ORCID 0000-0003-3283-5136

Abstract

Redox processes are critical to understanding nutrient and contaminant mobility and fate in natural waters. Solubility and toxicity of such species as Fe(II,III), As(III/V), Cr(III/VI) and Se(IV/VI) depend substantially on the dominant redox species. Unfortunately, the concept of aquatic reduction-oxidation processes is often misunderstood and misapplied. Because natural waters and mine waters contain redox species that oxidize or reduce at different rates and do not reach equilibrium, no analogy exists between pH and pE (or Eh), and a redox potential of a natural water is not meaningful. What IS meaningful is to obtain the concentrations of redox species by analysis.

Keywords: Redox species, redox processes, redox applications

Introduction

Processes of reduction-oxidation, or redox, are critical to understanding the solubility, speciation, mobility, and toxicity of redox-sensitive contaminants. Unfortunately, descriptions of redox chemistry are still burdened with decades old misconceptions when applied to natural waters. This paper reviews our knowledge of redox processes in general and some examples with acid mine drainage.

Examples of several redox-sensitive elements and their relative solubilities and toxicities are shown in Table 1. These can be useful as a qualitative guide to redox chemistry. Additional complications arise from the fact that some elements methylate or form complexes with inorganic or organic ligands which can greatly change their solubility and toxicity. The classic example is with mercury. Methylmercury is much more toxic than elemental mercury. Consequently, determining the total dissolved concentration of a redox-sensitive elements is insufficient for characterizing its solubility and toxicity. These complications are magnified when attempting to model redox transformations in natural waters because many redox processes are not amenable to equilibrium assumptions. In the absence of any direct knowledge of redox changes (by chemical analysis) at a particular site, modelling must depend on analogous studies elsewhere which has limitations because every location tends to have site-specific characteristics. It is possible to model redox chemistry using rate constants, however, the assumptions that must be made when applying simple experimental lab data to complex field situations are rarely warranted.

Table 1 *Relative solubilities and toxicities of redox species found in natural waters.*

Element	Reduced Form	Oxidized Form
Fe	Fe(II), soluble	Fe(III), insoluble
Mn	Mn(II), soluble	Mn(IV), insoluble
As	As(III), soluble, more toxic	As(V), less soluble, less toxic
Sb	Sb(III), soluble, more toxic	Sb(V), less soluble, less toxic
Se	Se(IV), less soluble, less toxic	Se(VI), more soluble, more toxic
U	U(IV), insoluble	U(VI), soluble, more toxic
Cr	Cr(III), insoluble	Cr(VI), soluble, much more toxic

This paper begins the clarification of redox by describing "redox potential," and its lack of relationship to redox couples. Examples will follow of redox species in natural waters, including mine drainage and the controlling factors.

Redox potential

The redox chemistry of an aqueous solution has often equated with the "Eh" or "pE." That mistake has been largely influenced by the adoption of the Pourbaix (or Eh-pH) diagrams by Garrels and Christ (1965) and subsequently taught in geochemistry courses for decades. I am in full agreement with the use of Eh-pH diagrams as a valuable heuristic device and should continue to be introduced in geochemistry courses. However, it has been emphasized appropriately by Hostetler (1984); Langmuir (1971, 1997); Nordstrom and Munoz (1994); Stumm and Morgan (1996); Thorstenson (1984) and Appelo and Postma (2005) that pE is not analogous to pH, that pE or Eh refers to the equilibrium between a redox couple and a conductive electrode and not a redox potential of the water, and that different redox couples do not come to equilibrium with each other. There can be a pH of an aqueous solution, but not a redox potential of an aqueous solution. There is a redox chemistry of an aqueous solution, and it can be determined analytically by measuring the redox species. Furthermore, measuring the redox species tells us far more about the redox conditions of a water than measuring the EMF (electromotive force, often mislabelled the ORP) from which the Eh (or pE) is calculated. It should be noted that Eh is best used when speaking of field measurements and pE is more appropriate for pE-pH diagrams (Truesdell 1968).

There are two situations in which the conductive electrode behaves in a Nernstian equilibrium manner. One situation is acid mine drainage (with limitations as shown below) and the other is porewaters or groundwaters undergoing sulfate reduction. In the former case, Fe(II) and Fe(III) are "electroactive" and in the latter case, sulfide (as H2S or HS-), is electroactive such that the electrode responds as if it were a sulfide ion-selective electrode (Berner 1963; Morris and Stumm 1967). In all other cases that we know about, other redox couples are not sufficiently electroactive in natural waters to give a quantitative Nernstian response.

Methods

Fe(II/III)

The sample can be filtered and acidified in the field with redistilled HCl except for waters containing sulfide which may cause some sorption or precipitation as iron sulfide. Adding 1% (v/v) to a 125 mL sample will bring the pH down to <2 and stabilize the Fe(II/III) ratio for months in the absence of nitrate.

Many "ferroin" reagents that determine Fe(II) and total Fe are quite sensitive to these species such as 1,10-phenanthroline, PTDS, TPTZ, and FerroZine. One of the most common ferroins is FerroZine because of it low cost, sensitivity and availability (Stookey 1970; Gibbs 1976). These colorimetric reagents are of similar molecular structure. FerroZine is more sensitive than 1,10-phenanthroline because of a higher absorption coefficient and a stronger ligand complex. Detection limit with FerroZine is 1−2 µg/L using a 1 cm cell. Lower detection limits are possible with a 5 or 10 cm cell. Total dissolved Fe is measured by reducing the solution with a reagent such as hydroxylamine at a buffered pH and remeasuring. The Fe(III) concentration is determined by difference and has a different detection limit of ≤ 3% of the total Fe. Because there is a need to measure Fe(III) at lower concentrations than this, a method was developed to determine Fe(III) directly (To *et al.* 1999).

As(III/V)

As with Fe(II/III), the sample can be filtered and acidified with redistilled HCl for months (McCleskey *et al.* 2004). When sulfide is present, then thioarsenites and thioarsenates can be present and the sample must be flash frozen in the field and kept frozen while transported to the laboratory. At the lab, the sample must be thawed in an oxygen-free glove box and run on an oxygen-free HPLC-ICP-MS instrument to determine thioarsenates and thioarsenates along with As(III/V) (Planer-Friedrich *et al.* 2007).

The redox species of arsenic can be determined by hydride-generation atomic absorption spectroscopy (HGAAS), ion chromatography (IC), HPLC-ICP-MS, anion-exchange chromatography ICP-MS (AEC-ICP-MS), or field separation using ion exchange columns and eluted in the lab and run on AAS, ICP-MS, or colorimetry.

Sb(III/V), Se(IV/VI)

Antimony, selenium, and other hydride-forming elements can be effectively determined by HGAAS (or hydride combined with ICP-MS). These elements also can form thio-complexes in the presence of sulfide (Planer-Friedrich and Scheinost 2011).

Cr(III/VI)

Although Cr(III) is rather insoluble as a hydroxide, these redox species can be determined in water samples by an EPA method that requires transport of sample to a laboratory within 24 hours and determination on an IC with an absorbance detector. Another common method is a colorimetric determination using diphenylcarbazone (DPC) but the sensitivity is not as good as the EPA method. Both methods are described in the third method that uses cation-exchange in the field to separate the Cr(III) on the column and Cr(VI) comes out in the eluent (Ball and McCleskey 2003). Any technique with sufficient sensitivity can be used to determine the separated Cr. With this method, the redox species are stable for several weeks and with better sensitivity than the DPC.

Mn(II, III, IV), U(IV/VI)

These aqueous redox species have rarely been determined for natural waters and could use further research. Uranium speciation has been reviewed by (Smedley and Kinniburgh 2023) and Mn(II) has been determined electrochemically with various types of voltammetry (Crapnell and Banks 2022).

N(-III, 0, I, IV, VI)

Ammonia, nitrogen gas, nitrite and nitrate are the main redox species of nitrogen and their determination by IC and gas chromatography (GC) for nitrogen gas are routine and well-established in Standard Methods and EPA methods.

Examples

One of the best examples of redox disequilibria of different redox couples in the same groundwater was demonstrated by (Lindberg and Runnells 1984). They compiled measured redox species for Fe, N, S, O, C, and the Eh and showed that they were generally out of equilibrium with each other on a plot of measured vs. calculated Eh. The calculated Eh values were, however, clustered around the standard electrode potential for each couple whereas the field measurements were spread over a large range of about 500-700 mV for any given couple. A simple example is shown from my Ph.D. thesis (Nordstrom 1977) (See Table 2).

In this example, I had measured the dissolved oxygen and calculated the Eh based on the O2/H2O redox couple and showed it bore no relation to the measured Eh. These surface waters were mountainous streams which were close to equilibrium with respect to oxygen in the atmosphere. If a measured Eh bears no relation to a calculated Eh, what does it mean to speak of a redox potential of a water? You can choose one value over the other and try to justify it, but it makes little sense. What does make sense is to ask what

Table 2 *Comparison of measured Eh values with those calculated from dissolved oxygen (D.O.) and the O_2/H_2O redox couple. Data are from Nordstrom (1977).*

Location	Spring Creek(H)	Boulder Creek(C)	Boulder Creek(G)	Spring Creek(J)
pH	6.40	3.02	1.85	2.32
D.O. (mg/L)	10.3	10.5	11.0	11.8
Eh, measured, V	0.380	0.694	0.625	0.640
Eh, calculated from D.O., V	0.948	1.156	1.227	1.197

is in the water that is "electroactive." This adjective refers to a Nernstian response at the electrode interface. For a redox couple to be electroactive the redox species must be present at high enough concentrations, and they must be able to transfer electrons rapidly across the solution/electrode interface so that equilibrium can be attained. Concentrations need to be about 10^{-5} molar or higher. Anions like arsenate, selenate, and antimonate consist of a central metalloid atom strongly covalently bonded to oxygen atoms that inhibit the transfer of electrons. These species have been shown to be insufficiently electroactive in aqueous solution, for example Runnells and Lindberg (1990).

For acid mine waters, dissolved Fe is electroactive and Nernstian equilibrium is observed. About 1510 analyses of waters contaminated with acid mine drainage from the western USA (Nordstrom 2011) were speciated to demonstrate this equilibrium. These samples were selected using several criteria: (1)the water analyses were complete for major ions with good charge balances and documented QA/QC, (2)they included analyses for Fe(II/III), and (3)they had Eh values based on field-measured EMF values that were converted to Eh based on the half-cell potential of the reference electrode (Garrels and Christ 1965; Langmuir 1971). The results for measured vs. calculated Eh based on Fe(II/III) and appropriately speciated for activities are shown in Fig. 1a below. A cluster of values at high Eh correlated quite well but at lower Eh values very few values correlated well. Detection limits for Fe(II) (<10-5 molar), Fe(III) (<3% of total dissolved iron), and for the redox electrode (Morris and Stumm 1967) were applied and used to delete any data that were below detection limits. The resulting plot is shown in Fig. 1b.

Another valuable result is that when the data from Fig. 1a is used to plot saturation indices (SIs) of freshly precipitating hydrous ferric oxides such as ferrihydrite or schwertmannite, many of the SI values are greatly supersaturated as shown in Fig. 2a. By removing data points below detection limits from the plot, the supersaturation disappears (Fig. 2b, Nordstrom 2011). The reason is that the conductive electrode only responds to dissolved Fe(II/III) and not to colloidal Fe(III) which typically is only nanometers to tens of nanometers in particle size when freshly precipitating and easily goes through the pores of filters that are usually 0.45 micrometers in pore size. Those iron colloids dissolve in the acid preservative and added to the total dissolved iron even though it is not truly dissolved. This supersaturation effect has been noted for some time by many authors and the data from Nordstrom (2011) reproduced here shows that it is caused by a filtration artifact.

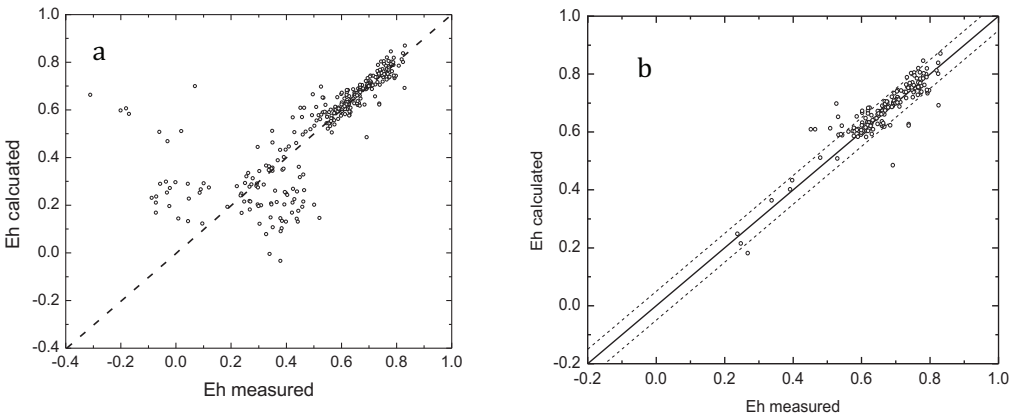

Figure 1 *(a) Eh calculated from Fe(II/III) determinations and speciated from the PHREEQC code using the wateq4f.dat database. Dashed line is the 1:1 correlation. (b) Same plot as in (a) after removing data points that were below detection with respect to Fe(II), Fe(III), and electrode potential measurements (see text). Solid line is the 1:1 correlation and the dotted lines are a ±30 mV envelope of uncertainty.*

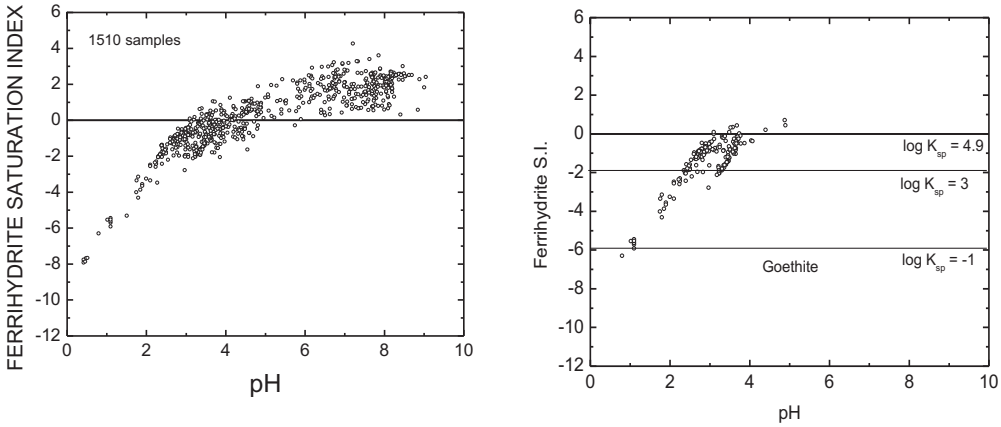

Figure 2 a. Saturation indices for freshly precipitating hydrous ferric oxides showing orders of magnitude supersaturation. b. When points based on data that are below detection limits are removed, the supersaturation disappears.

Geochemical modelling

Codes used for geochemical model computations usually allow the Eh calculations for different redox couples to be independent from each other. This would be the appropriate way of inputting and controlling redox data. Codes also allow for an input Eh or pE to determine the redox speciation for a redox element. This method is not meaningful and should not be used because it assumes redox equilibrium exists for an aqueous solution when it does not exist. Hence, modelling that assumes equilibrium between different redox couples will be incorrect.

Conclusions

These results demonstrate several important points.

1. There is no such thing as a single equilibrium redox potential of a natural water (or aqueous solution).
2. The Nernst equation applies to the equilibrium of an electroactive redox couple or species at an inert conductive electrode surface.
3. You can discuss redox chemistry of a natural water if you have measured the individual redox species, BUT disequilibrium is the rule.
4. Redox potential measurements often do not reach a stable reading because of mixed potentials, kinetic barriers, and electroactive species are too low in concentration.
5. There is no practical analogy between pE and pH (Truesdell, 1968).
6. Analytical measurements of redox species tells you far more about redox conditions of the water than any Eh measurement.
7. Redox determinations of Fe, O_2, N, S, As, Sb, Se, and Cr have been done by labs for many decades and are not very expensive; so why not determine them?
8. **Please do not plot water analyses of redox species on a pE-pH diagram** when we have much better methods (speciation and saturation index calculations). The pE-pH diagram is useful for teaching, but they are limited to one temperature, usually do not include multi-component speciation, and omit ionic strength and complexing effects.

References

Appelo CAJ, Postma D (2005) Geochemistry, Groundwater and Pollution. Balkema, Amsterdam, The Netherlands

Ball JW, McCleskey RB (2003) A new cation-exchange method for accurate determination of hexavalent chromium. Talanta 61:305–313

Berner RA (1963) Experimental studies of the formation of sedimentary iron sulfides. In: Jensen ML (ed) Biogeochemistry of Sulfur Isotopes. Yale University, p 153–168

Crapnell RD, Banks CE (2022) Electroanalytical review: The determination of manganese. Sensors and Actuators Reports 4:100110

Garrels RM, Christ CL (1965) Solutions, Minerals and Equilibria. Harper & Row, New York

Gibbs CR (1976) Characterization and application of ferrozine iron reagent as a ferrous iron indicator. Anal Chem 48:1197–1201

Hostetler JD (1984) Electrode electrons, aqueous electrons, and redox potential in natural waters. Am J Sci 294:734–759

Langmuir D (1971) Eh-pH determinations. In: Carver RE (ed) Procedures in Sedimentary Petrology. John Wiley & Sons, New York, p 597–634

Langmuir D (1997) Aqueous Environmental Geochemistry. Prentice-Hall, Upper Saddle River, NJ

Lindberg RD, Runnells DD (1984) Ground water redox reactions: An analysis of equilibrium state applied to Eh measurements and geochemical modeling. Science 225:925–927

McCleskey RB, Nordstrom DK, Maest AS (2004) Preservation of water samples for arsenic(III/V) determinations: an evaluation of the literature and new analytical results. App Geochem 19(7):995–1009. https://doi.org/10.1016/j.apgeochem.2004.01.003

Morris JC, Stumm W (1967) Redox equilibria and measurements of potentials in the aquatic environment. Advances in Chemistry Series 67. American Chemical Society, Washington, D.C., p 270–285

Nordstrom DK (1977) Hydrogeochemical and microbiological factors affecting the heavy metal chemistry of an acid mine drainage system, Ph.D. Dissert. 210 pp.

Nordstrom DK (2011) Hydrogeochemical processes governing the origin, transport and fate of major and trace elements from mine wastes and mineralized rock to surface waters. App Geochem 26(11):1777–1791. https://doi.org/10.1016/j.apgeochem.2011.06.002

Nordstrom DK, Munoz JL (1994) Geochemical Thermodynamics. 2nd edn. Blackburn Press, Caldwell, New Jersey

Planer-Friedrich B, London J, McCleskey RB, Nordstrom DK, Wallschlager D (2007) Thioarsenates in geothermal waters of yellowstone national park: Determination, preservation, and geochemical importance. Environ Sci Technol 41(15):5245–5251. https://doi.org/10.1021/es070273v

Planer-Friedrich B, Scheinost AC (2011) Formation and structural characterization of thioantimony species and their natural occurrence in geothermal waters. Environ Sci Technol 45(16):6855–6863. https://doi.org/10.1021/es201003k

Runnells DD, Lindberg RD (1990) Selenium in aqueous solutions: The impossibility of obtaining a meaningful Eh using a platinum electrode. Geology 18:212–215

Smedley P, Kinniburgh DG (2023) Uranium in natural waters and the environment: Distribution, speciation and impact. App Geochem 148:105534

Stookey LC (1970) Ferrozine - a new spectrophotometric reagent for iron. Anal Chem 42(7):779–781

Stumm W, Morgan JJ (1996) Aquatic Chemistry. 3rd edn. Wiley-Interscience, New York

Thorstenson DC (1984) The concept of electron activity and its relation to redox potentials in aqueous geochemical systems. US Geol Survey Open-File Rept 84-072:45

To TB, Nordstrom DK, Cunningham KM, Ball JW, McCleskey RB (1999) New method for the direct determination of dissolved Fe(III) concentration in acid mine waters. Environ Sci Technol 33(5):807–813. https://doi.org/10.1021/es980684z

Truesdell AH (1968) The advantage of using pE rather than Eh in redox equilibrium calculations. J Geol Educ 16:17–20

Field Application of Waste Sludge-Based Adsorbents for Arsenic Removal from Alkaline Mine Drainage in South Korea

Youn Soo Oh[1*], Hyun-Sung Park[1], Chan-Ung Kang[2], Kang Ho Kim[1]

[1]*Korea Mine Rehabilitation and Mineral Resources Corporation (KOMIR), Republic of Korea*
oys1223@komir.or.kr, ORCID : 0000-0002-4076-422X

[2]*Korea Institute of Geoscience and Mineral Resources, Republic of Korea*

Abstract

Field pilot-scale experiments were conducted over 371 d to evaluate the applicability of coal mine drainage sludge (CMDS)-derived adsorbents for As removal from alkaline mine drainage. The study site exhibited alkaline conditions (pH 8.2) and an average dissolved As concentration of 400 μg/L. Modified CMDS materials, including polyurethane-coated and pelletized forms, showed substantially improved treatment performance compared with raw CMDS. Effluent As concentrations remained below the Korean discharge limit of 50 μg/L throughout most of the operational period. This site-specific study demonstrates the applicability of mining waste-derived adsorbents as sustainable treatment materials for alkaline mine drainage systems.

Keywords: Arsenic, alkaline mine drainage, adsorption, mine drainage sludge, pilot-scale treatment

Introduction

Mine drainage generated from abandoned mine sites can contain contaminants such as Fe, Al, Mn, Zn, and As, potentially affecting nearby agricultural areas and aquatic systems (McCarthy 2011; Lechner *et al.* 2016; Worlanyo and Jiangfeng 2021). Under natural conditions, dissolved As may be attenuated through adsorption onto Fe and Al (hydr)oxides occurring downstream of mine discharges (Campbell and Nordstrom 2014; Paikaray 2015). However, in neutral or alkaline mine drainage systems, dissolved Fe concentrations are often low, limiting natural attenuation and increasing As mobility (Johnston *et al.* 2020; Rodriguez-Freire *et al.* 2014). Consequently, site-specific treatment strategies are required for effective As control.

Adsorption using Fe-rich materials is considered an effective approach for As removal from mine drainage. Coal mine drainage sludge (CMDS), generated as a by-product during active mine water treatment, contains abundant iron hydroxides and therefore has potential as a low-cost adsorbent (Kim *et al.* 2021). Reuse of CMDS may also reduce waste disposal requirements and treatment costs (Lee *et al.* 2022).

A detailed physicochemical characterization of the adsorbents and extended interpretation of the experimental results were previously reported by Kang *et al.* (2026). The present paper focuses primarily on field-scale operational performance and practical applicability under alkaline mine drainage conditions.

This study evaluated the As removal efficiency of several sludge-derived adsorbents using pilot-scale column reactors installed directly at an abandoned gold mine in South Korea.

Materials and Methods

The study area is located at the G mine, an abandoned gold mine in North Gyeongsang Province, South Korea. Mine drainage continuously discharges from a single adit and exhibits persistent As contamination exceeding the Korean discharge standard (Fig. 1). As summarized in Table 1, mine drainage pH ranged from 7.4 to 8.5, indicating alkaline conditions. Dissolved

Al, Fe, and Zn concentrations remained relatively low (<0.1 mg/L), whereas dissolved As averaged 400 µg/L, exceeding the Korean discharge criterion of 50 µg/L (Ministry of Environment in Korea 2025).

Pilot-scale column reactors were installed near the mine adit using untreated mine drainage as influent (Fig. 2a). Four Fe-based adsorbents were evaluated: raw coal mine drainage sludge (CMDS), polyurethane-coated CMDS (CMDS-PU), pelletized CMDS (CMDS-PE), and commercial granular ferric hydroxide (GFH).

CMDS was obtained from an active coal mine drainage treatment facility in South Korea. To produce CMDS-PU, pulverized sludge (<0.25 mm) was mixed with polyol, water, and methylene diphenyl diisocyanate (MDI), followed by foaming and drying. Detailed preparation procedures and physicochemical characterization were described by Kang *et al.* (2026). A schematic diagram of the experimental setup and column configuration is shown in Fig. 2b.

The packed adsorbent volumes were defined as bed volume (BV): 2.5 L for CMDS, 15.2 L for CMDS-PU, 18.5 L for CMDS-PE, and 17.4 L for GFH. Experimental durations were 371 d for CMDS-PU and GFH and 292 d for CMDS and CMDS-PE.

Column performance was evaluated using effluent As concentrations and cumulative treated BV. The breakthrough point was defined as the point where effluent As concentration exceeded the Korean discharge limit of 50 µg/L. Breakthrough behavior was additionally evaluated using the C/C_0 ratio between effluent and influent As concentrations.

Because CMDS is classified as waste material under Korean regulations (Ministry of Environment in Korea 2024), environmental assessment was also conducted using soil and waste contamination testing standards (Ministry of Environment in Korea 2023a, 2023b).

Results and Discussion

Evaluation of As Removal Performance

The CMDS column reached breakthrough most rapidly, exceeding the Korean discharge standard after treatment of 1,871 BV on day 80 (Fig. 3a). During the 292-d operational period, the column processed 12,534 BV. In contrast, CMDS-PU maintained effluent As concentrations below 50 µg/L until 5,242 BV on day 364.

The CMDS-PE and GFH columns continuously maintained effluent As concentrations below the Korean discharge criterion throughout the monitoring period. Total treated volumes were 3,353 BV for CMDS-PE and 9,550 BV for GFH.

The total As loads removed also differed substantially among the adsorbents. CMDS removed 1,677 mg As before breakthrough, whereas CMDS-PU removed 31,374 mg As. CMDS-PE and GFH removed 26,110 mg and 66,223 mg As, respectively, during the experimental period.

Figure 3b shows variations in C/C0 values with cumulative treated BV. CMDS and CMDS-PU reached breakthrough at C/C0 values of 0.24 and 0.16, respectively. These results generally agree with typical adsorption breakthrough behavior where breakthrough occurs near C/C0 ≈ 0.1 (Gutierrez-Reyna *et al.* 2024). In contrast, CMDS-PE and GFH maintained C/C0 values close to zero throughout the experiment.

Although raw CMDS exhibited relatively high Fe content and surface area, its adsorption performance declined rapidly. Field observations showed uneven wetting and preferential flow paths within the adsorbent layer. Channeling likely developed because of non-uniform packing and compaction of the sludge material, limiting effective interaction between mine drainage and the adsorbent (Haryanto *et al.* 2018).

In contrast, CMDS-PU and CMDS-PE formed more stable and permeable adsorption media, improving hydraulic distribution within the columns. Flow rates differed considerably despite identical injection pressure conditions: 67.9 mL/min for CMDS, 229.4 mL/min for CMDS-PU, and 121.5 mL/min for CMDS-PE. Corresponding empty bed contact times were 37.5, 66.3, and 152.0 min, respectively. These results indicate that hydraulic stability strongly influenced adsorption efficiency under field conditions.

Environmental Assessment of CMDS

The elemental composition results based on soil and waste contamination standards are summarized in Table 2. According to waste contamination testing standards, harmful substances in CMDS remained below the Korean regulatory limits.

Total content analysis showed detectable concentrations of F, Ni, and Zn, with F and Ni exceeding soil contamination criteria. However, monitoring of the column effluent showed no substantial release of harmful substances from the CMDS-based adsorbents during the experiment (Table 3). These results suggest that the adsorbents remained chemically stable under alkaline mine drainage conditions.

Conclusions

Pilot-scale field experiments demonstrated that modified CMDS materials effectively removed As from alkaline mine drainage under operational field conditions.

Raw CMDS showed relatively rapid breakthrough because of hydraulic instability and channeling within the adsorbent layer. In contrast, CMDS-PU and CMDS-PE exhibited improved hydraulic behavior and longer treatment performance.

CMDS-PU maintained effluent As concentrations below the Korean discharge standard until 5,242 BV, whereas CMDS-PE and GFH maintained stable treatment efficiency throughout the monitoring period.

Environmental assessment indicated limited leaching potential under alkaline conditions, supporting the applicability of mine drainage sludge as a sustainable adsorbent material for field-scale mine drainage treatment.

Acknowledgements

This study was supported by R&D project of the Korea Mine Rehabilitation and Mineral Resources Corporation (KOMIR) in 2024 and by the Basic Research Project (No. 25-3422) at the Korea Institute of Geoscience and Mineral Resources.

Figure 1 *(a) Overview of a site at G mine with a single adit discharging mine drainage, and (b) a detailed view of the mine drainage.*

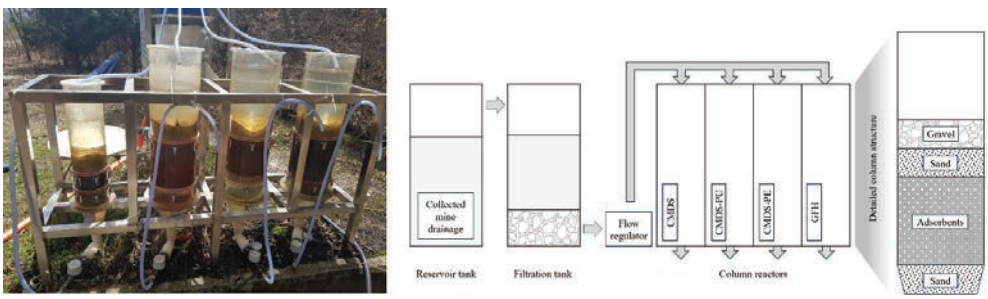

Figure 2 *The overall experimental setup installed at the G mine site and Schematic diagram of experiments and detailed structure of columns.*

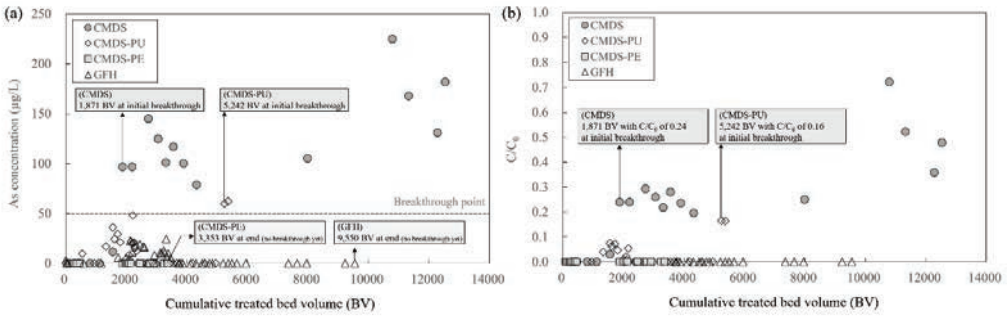

Figure 3 *Variation of (a) As concentration and (b) the ratio of the As concentration in effluent (C) to the initial As concentration in the influent (C0) with cumulative treated bed volume (BV).*

Table 1 *Flow rate and chemical properties of mine drainage monitored over a period of three years.*

Parameter	Average	Maximum	Minimum	Note (standard)[1]
Flow rate (m^3/d)	240	890	110	–
pH	8.2	8.5	7.4	5.8–8.6
Alkalinity (mg/L as CaCO3)	248	390	167	–
EC (μS/cm)	756	1217	366	–
ORP (mV)	142.6	275.9	-65.4	–
As (mg/L)	0.40	0.50	0.31	0.05
Fe (mg/L)	0.07	0.26	0.02	2
Mn (mg/L)	0.03	0.08	0.01	2
Zn (mg/L)	0.002	0.005	N.D.	1

[1]Permissible discharge limit according to Korean Ministry of Environment (2025)

Table 2 *Analysis results of elemental composition of CMDS before and after drying based on Soil Contamination Testing Standard and Waste Contamination Testing Standard*

Elements	Soil Contamination Testing Standard (Korean Ministry of Environment, 2023a)			Waste Contamination Testing Standard (Korean Ministry of Environment, 2023b)		
	Standard[1]	CMDS (before drying)	CMDS (after drying)	Standard[2]	CMDS (before drying)	CMDS (after drying)
Pb	200	4.1	4.8	3	ND	ND
Cu	150	ND3)	ND	3	ND	ND
As	25	3.57	4.00	1.5	ND	ND
Hg	4	ND	ND	0.005	ND	ND
F	400	236	439	–	–	–
Cd	4	ND	ND	0.3	ND	ND
Zn	300	211.3	229.0	–	–	–
Ni	100	122.7	134.4	–	–	–
Cr6+	5	ND3	ND	1.5	ND	ND

[1]Standards according to Ministry of Environment in Korea (2022); 2Standards according to Ministry of Environment in Korea (2024); 3ND: Not detected

Table 3 Comparison of concentrations of F, Zn, and Ni in influent (mine drainage) and effluent from CMDS-based columns.

Elements	Average concentration (mg/L)				Note (Permissible discharge standard[1])
	Influent	Effluent			
	Mine drainage	CMDS	CMDS-PU	CMDS-PE	
F	0.134	0.130	0.052	0.159	3.0
Zn	0.004	0.016	0.012	0.012	1.0
Ni	ND2)	ND	ND	ND	0.1

[1]Permissible discharge limit according to Korean Ministry of Environment (2024); 2ND: Not detected

This conference contribution is largely based on the author's publication *Kang C-U, Oh YS, Park H-S, Kwon O-H, Kim KH, Jo HY (2026) Arsenic Removal from Alkaline Mine Drainage Using Waste Sludge: Pilot-Scale Experiments at an Abandoned Mine in South Korea. Mine Water Environ. https://doi.org/10.1007/s10230-026-01115-x*

References

Arcibar-Orozco JA, Josue DB, Rios-Hurtado JC, Rangel-Mendez JR (2014) Influence of iron content, surface area and charge distribution in the arsenic removal by activated carbons. Chem Eng J 249:201–209. https://doi.org/10.1016/j.cej.2014.03.096

Campbell KM, Nordstrom DK (2014) Arsenic speciation and sorption in natural environments. Rev Mineral Geochem 79(1):185–216. https://doi.org/10.2138/rmg.2014.79.3

Gutierrez-Reyna SO, Herrera-Hernández EC, Aguilar-Madera CG, López-Ramón MV, Ocampo-Perez R, Parra-Marfil A, Garcia-Hernandez E, Bailon-Garcia E (2024) New trends in modelling of breakthrough curves to remove pollutants using adsorption on advanced monoliths geometries. Environ Res 243:117871. https://doi.org/10.1016/j.envres.2023.117871

Haryanto B, Singh W, Chang C, Chairunnisa A, Butarbutar F (2018) Loading time and channeling effect in removing copper ions from sand surface by surfactin solution in flushing column. IOP Conf Ser: Mater Sci Eng 308:012021. https://doi.org/10.1088/1757-899X/308/1/012021

Johnston SG, Bennett WW, Doriean N, Hockmann K, Karimian N, Burton ED (2020) Antimony and arsenic speciation, redox-cycling and contrasting mobility in a mining-impacted river system. Sci Total Environ 710:136354. https://doi.org/DOI.org/10.1016/j.scitotenv.2019.136354

Kang CU, Oh YS, Park HS, Kwon OH, Kim KH, Jo HY (2026) Arsenic removal from alkaline mine drainage using waste sludge: pilot-scale experiments at an abandoned mine in South Korea. Mine Water Environ. https://doi.org/10.1007/s10230-026-01115-x

Kim D, Ren Y, Cui M, Lee Y, Kim J, Kwon O, Ji W, Khim J (2021) Arsenic adsorption on two types of powdered and beaded coal mine drainage sludge adsorbent. Chemosphere 272:129560. https://doi.org/10.1016/j.chemosphere.2021.129560

Lechner AM, Baumgartl T, Matthew P, Glenn V (2016) The impact of underground longwall mining on prime agricultural land: a review and research agenda. Land Degrad Dev 27(6):1650–1663. https://doi.org/10.1002/ldr.2303

Lee Y, Ren Y, Cui M, Zhou Y, Kwon O, Ko J, Khim J (2022) Arsenic adsorption study in acid mine drainage using fixed bed column by novel beaded adsorbent. Chemosphere 291:132894. https://doi.org/10.1016/j.chemosphere.2021.132894

McCarthy TS (2011) The impact of acid mine drainage in South Africa. S Afr J Sci 107(5):1–7. https://doi.org/10.4102/sajs.v107i5/6.712

Ministry of Environment in Korea (2023a) Standard test method for soil contamination. http://www.me.go.kr. Accessed 18 Feb 2025

Ministry of Environment in Korea (2023b) Standard test method for waste. http://www.me.go.kr. Accessed 18 Feb 2025

Ministry of Environment in Korea (2024) Waste control act (No. 19126). http://www.me.go.kr. Accessed 18 Feb 2025

Ministry of Environment in Korea (2025) Enforcement rules of the water environment conservation act (No. 1020). http://www.me.go.kr. Accessed 18 Feb 2025

Paikaray S (2015) Arsenic geochemistry of acid mine drainage. Mine Water Environ 34(2):181–196. https://doi.org/10.1007/s10230-014-0286-4

Rodriguez-Freire L, Sierra-Alvarez R, Root R, Chorover J, Field JA (2014) Biomineralization of arsenate to arsenic sulfides is greatly enhanced at mildly acidic conditions. Water Res 66:242–253. https://doi.org/10.1016/j.watres.2014.08.016

Worlanyo AS, Jiangfeng L (2021) Evaluating the environmental and economic impact of mining for post-mined land restoration and land-use: a review. J Environ Manag 279:111623. https://doi.org/10.1016/j.jenvman.2020.111623

IMWA 2026
Jeongseon

MF6RTM: Flexible Reactive Transport Modeling for Mining Applications via MODFLOW 6 and PHREEQC

Pablo Ortega[1], Anthony Aufdenkampe[2], Andres Prieto-Estrada[3], Allan Foster[4], Paul Tomasula[2], Lauren Mancewicz[5], Jeremy White[3]

[1]*INTERA Geosciences, Perth, WA, Australia*

[2]*Limnotech, Oakdale, MN, USA*

[3]*INTERA Incorporated, Houston, TX, USA*

[4]*INTERA Incorporated, Denver, CO, USA*

[5]*Coastal and Hydraulics Lab, Engineer Research and Development Center, Vicksburg, MS, USA*

Abstract

Reactive transport modeling is essential for understanding the interplay between hydrogeological processes and chemical reactions in subsurface environments. This study introduces a code coupling MODFLOW-6 and PHREEQC via their respective APIs using a sequential non-iterative approach, providing a modern and open-source coupling that integrates the latest version of both codes. Implemented in Python, the tool is designed for extensibility, uncertainty analysis, and reproducible workflows. The framework handles complex processes including contaminant transport, mineral dissolution, and redox reactions, and is particularly suited to mining environments where coupled hydrogeological and geochemical processes govern metal mobilization and remediation performance, acid and metalliferous drainage migration, and in situ recovery. Its capabilities are demonstrated using an acid mine drainage benchmark problem and compared against PHT3D results.

Keywords: Reactive transport, geochemistry, software

Introduction

Reactive transport modeling is essential for understanding the intricate interplay between hydrogeological processes and chemical reactions in subsurface environments (Prommer *et al.*, 2019). In mining settings, these coupled processes directly influence operational performance and environmental risk by controlling mechanisms such as acid and metalliferous drainage migration, metal mobilization, and contaminant transport, as well as the effectiveness of remediation strategies and in situ recovery operations. Their representation remains challenging due to the complexity of predicting flow, transport, and geochemical interactions across multiple spatial and temporal scales. Therefore, there is a need for integrated and flexible modeling frameworks capable of supporting predictive and decision-relevant analyses in such environments.

Several tools have coupled flow-and-transport simulators with geochemical engines or implemented fully integrated reactive transport solutions. A few actively developed open-source and standalone (implicitly coupled) reactive transport software systems are noteworthy, including CrunchFlow (Steefel, 2014), PFLOTRAN (Hammond, 2022), and OpenGeoSys (Kolditz *et al.*, 2012). Other open-source software has explicitly coupled transport and reaction models, including PHAST (Parkhurst *et al.*, 2010), PHT3D (Prommer *et al.*, 2003), and eSTOMP (Nieplocha *et al.*, 2006). For a more comprehensive overview, see the review by Steefel *et al.*, 2015.

No open software system, however, has ever coupled the current major versions of MODFLOW (v6 released in 2017) and PHREEQC (v3 released 2013). The MODFLOW family of codes remains one

of the most widely used platforms for simulating flow and transport in real-world hydrogeologic applications for exploratory and predictive purposes among researchers and practitioners. Given the number of models and workflows built around MODFLOW, having a robust and modern reactive transport coupling is essential.

Previous couplings with PHREEQC have been developed for MODFLOW-2005/MT3DMS, known as PHT3D (Prommer *et al.*, 2003), and for MODFLOW-USG (Panday *et al.*, 2013), known as PHT-USG. PHT3D has seen extensive use in both academia and practice (Appelo and Rolle, 2010), while PHT-USG has gained traction more recently, particularly among practitioners working with MODFLOW-USG. A key limitation of both approaches is that they require modification of the underlying source code to enable the coupling. This imposes a heavy maintenance burden and increases the risk of the code falling out of date. As MODFLOW 6 and PHREEQC continue to expand in capability and adoption, there is a clear need for a modern, open-source coupling that preserves transparency, extensibility, and computational efficiency.

Here we present MF6RTM, which addresses this need by providing a fully open, Python-based, API-driven integration between MODFLOW 6 and PHREEQC-3 (Parkhurst and Appelo, 2013) using a sequential non-iterative approach (SNIA). This design eliminates custom file-based workflows, reduces opportunities for error, and enables users to construct complex reactive transport simulations directly within reproducible Python workflows. With built-in compatibility with PEST++ (White, 2018) and PyEMU (White *et al.*, 2016), the framework also supports uncertainty analysis, history matching, sensitivity analysis, and multi-objective optimization, providing a flexible and extensible platform for modern reactive transport modeling and collaborative open-source development.

Methods

MF6RTM is implemented in Python and provides a tightly coupled reactive transport workflow by linking MODFLOW-6 and PHREEQC through their respective application programming interfaces, MODFLOWAPI (Hughes *et al.*, 2022) and PHREEQCRM (Parkhurst and Wissmeier, 2015). The numerical solution follows a non-iterative sequential operator splitting approach (Figure 1), in which groundwater flow and solute transport are first solved using MODFLOW 6, followed by geochemical reactions computed using PHREEQCRM. At each transport time step, concentrations simulated by MODFLOW 6 are conditionally passed to PHREEQCRM when the time step is designated as reactive by the modeler, where equilibrium and kinetic reactions are evaluated. The updated chemical states

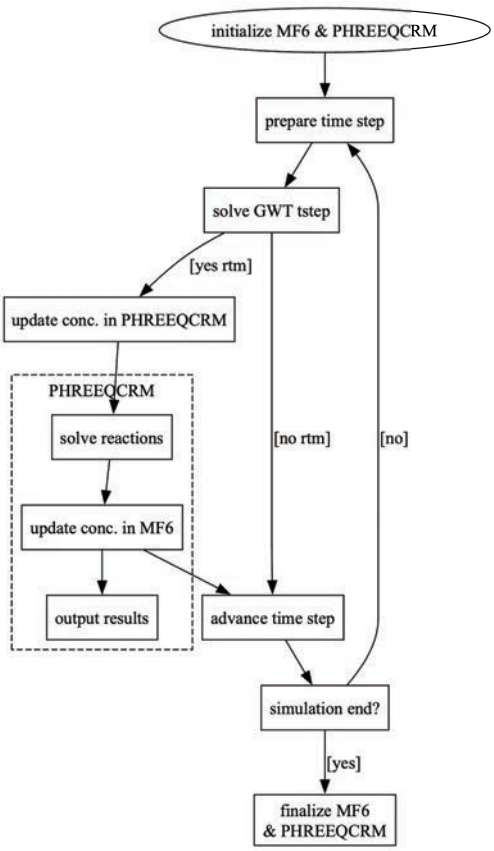

Figure 1 *Schematic of the main solution loop illustrating the sequential operator splitting workflow, including the coupling between flow and transport in MODFLOW 6 and geochemical reactions in PHREEQCRM.*

are then returned to the transport model for the subsequent time step, maintaining tight coupling while allowing flexibility in controlling when reactions are simulated and preserving computational efficiency.

Benchmark and Applied Case

To demonstrate and benchmark MF6RTM capabilities, a mining-relevant reactive transport problem is presented. Originally developed by Walter *et al.*, 1994 and later adopted as a benchmark by Guerin and Zheng (1998), the problem captures key geochemical processes arising when acidic mine tailings leach into an anaerobic carbonate aquifer. Aqueous complexation and dissolution/precipitation are treated as equilibrium reactions. Here we present the 1D benchmark as defined in Walter *et al.*, 1994.

Model Setup

The problem is configured as a 1-dimensional flow and transport domain (column), 0.4 m long, discretized into 80 grid cells. Initial geochemical conditions are summarized in Table 1 and 2. Horizontal hydraulic conductivity was 1 m/day, porosity was 0.35, and longitudinal dispersivity was 0.005 m. Temporal discretization corresponded to a total simulation time of 24 days.

Results

Results are presented in Figure 2 alongside PHT3D simulations, where breakthrough curves for 6, 12, and 24 days are presented. PHT3D (circles) and MF6RTM (lines) are compared, showing good agreement between the two software packages.

The acidic inflow is initially buffered by calcite, maintaining near-neutral pH (6.5–7), during which gypsum precipitates from calcium released by calcite dissolution and sulfate from the inflow. Where calcite is exhausted, siderite becomes the buffering mineral, followed by gibbsite where both are depleted. These three successive buffering mechanisms produce three distinct pH zones and corresponding pe levels, the latter controlled by the Fe^{2+}/Fe^{3+} redox couple, whose concentration ratio, and therefore pe, shifts as mineral buffering evolves and pH declines.

Conclusions

MF6RTM provides a modern, open-source coupling of MODFLOW 6 and PHREEQC that addresses a clear gap in the reactive transport modeling ecosystem. Benchmarking against PHT3D for an acid mine drainage front propagating into a carbonate aquifer demonstrates reliable reproduction of complex geochemical processes, including

Table 1 *Initial and boundary aqueous concentrations (Walter et al., 1994).*

Component	Aquifer conc. (mol L^{-1})	Tailings conc (mol L^{-1})
pH	6.96	3.99
pe	1.67	7.69
CO_3^{2-}	3.94×10^{-3}	4.92×10^{-4}
SO_4^{2-}	7.48×10^{-3}	5.00×10^{-2}
Fe^{2+}	5.39×10^{-5}	3.06×10^{-2}
Fe^{3+}	2.32×10^{-8}	1.99×10^{-7}
Mn^{2+}	4.73×10^{-5}	9.83×10^{-6}
Ca^{2+}	6.92×10^{-3}	1.08×10^{-2}
Mg^{2+}	1.96×10^{-3}	9.69×10^{-4}
Na^{+}	1.30×10^{-3}	1.39×10^{-3}
K^{+}	6.65×10^{-5}	7.93×10^{-4}
Cl^{-}	1.03×10^{-3}	1.19×10^{-4}
Al^{3+}	1.27×10^{-7}	4.30×10^{-3}
Si	1.94×10^{-3}	2.08×10^{-3}

Table 2 Initial mineral concentrations (Walter et al., 1994).

Mineral	Formula	Aquifer conc. (mol L^{-1}) bulk
Calcite	$CaCO_3$	6.30×10^{-3}
Siderite	$FeCO_3$	1.82×10^{-3}
Gibbsite	$Al(OH)_3$	8.81×10^{-4}
Ferrihydrite	$Fe(OH)_3$	6.51×10^{-4}
Gypsum	$CaSO_4{\cdot}2H_2O$	0.0
Amorphous silica	SiO_2	1.42×10^{-1}

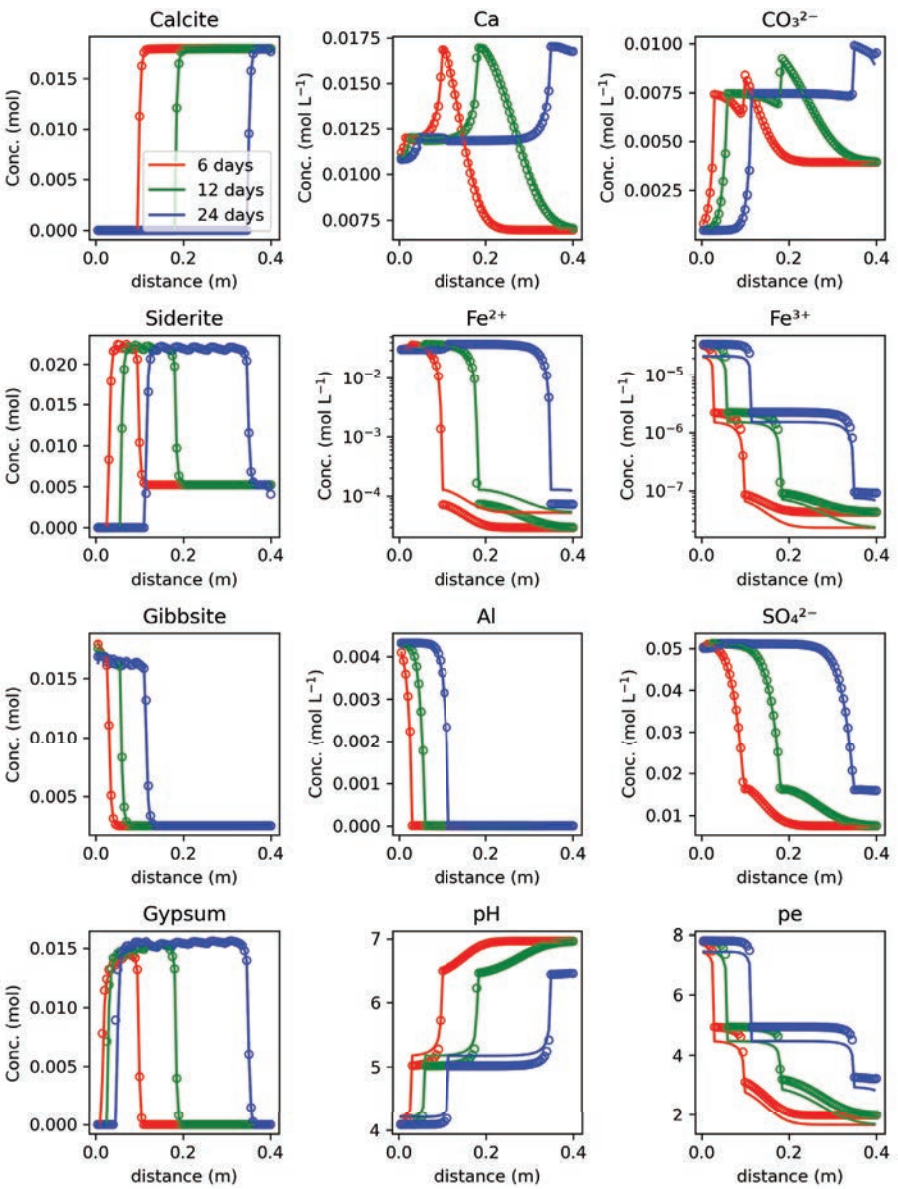

Figure 2 1D benchmark after Walter et al., 1994. Precipitation and dissolution fronts simulated with MF6RTM (lines) compared against PHT3D (circles).

mineral dissolution, precipitation, and redox reactions. The framework is particularly well suited to mining applications, where coupled hydrogeological and geochemical processes govern metal mobilization, acid and metalliferous drainage migration, and remediation and in situ recovery of metals.

Acknowledgements

The software MF6RTM was supported by INTERA INC. and its Research and Development initiative. We also thank Henning Prommer for his insights and discussions during the benchmarking of MF6RTM.

References

Appelo CAJ, Rolle M (2010) PHT3D: A reactive multicomponent transport model for saturated porous media. Ground Water 48(5):627–632. https://doi.org/10.1111/j.1745-6584.2010.00732.x

Guerin M, Zheng C (1998) GMT3D – Coupling multicomponent, three-dimensional transport with geochemistry. In: Poeter EP, Zheng C, Hill MC (Eds), MODFLOW'98, Proc. International Conference, Colorado School of Mines, Golden, CO, pp 413–420

Hammond GE (2022) The PFLOTRAN Reaction Sandbox. Geosci Model Dev 15(4). https://doi.org/10.5194/gmd-15-1659-2022

Hughes JD, Russcher MJ, Langevin CD, Morway ED, McDonald RR (2022) The MODFLOW Application Programming Interface for simulation control and software interoperability. Environ Model Softw 148. https://doi.org/10.1016/j.envsoft.2021.105257

Kolditz O, Bauer S, Bilke L, Böttcher N, Delfs JO, Fischer T, Görke UJ, Kalbacher T, Kosakowski G, McDermott CI, Park CH, Radu F, Rink K, Shao H, Shao HB, Sun F, Sun YY, Singh AK, Taron J, Zehner B (2012) OpenGeoSys: An open-source initiative for numerical simulation of thermo-hydro-mechanical/chemical (THM/C) processes in porous media. Environ Earth Sci 67(2). https://doi.org/10.1007/s12665-012-1546-x

Nieplocha J, Palmer B, Tipparaju V, Krishnan M, Trease H, Aprà E (2006) Advances, applications and performance of the Global Arrays shared memory programming toolkit. Int J High Perform Comput Appl 20(2). https://doi.org/10.1177/1094342006064503

Panday S, Langevin CD, Niswonger RG, Ibaraki M, Hughes JD (2013) MODFLOW-USG Version 1: An Unstructured Grid Version of MODFLOW for Simulating Groundwater Flow and Tightly Coupled Processes Using a Control Volume Finite-Difference Formulation. U.S. Geological Survey, Techniques and Methods 6-A45

Parkhurst DL, Appelo CAJ (2013) Description of input and examples for PHREEQC version 3: a computer program for speciation, batch-reaction, one-dimensional transport, and inverse geochemical calculations. Techniques and Methods. https://doi.org/10.3133/tm6A43

Parkhurst DL, Wissmeier L (2015) PhreeqcRM: A reaction module for transport simulators based on the geochemical model PHREEQC. Adv Water Resour 83:176–189. https://doi.org/10.1016/j.advwatres.2015.06.001

Prommer H, Barry DA, Zheng C (2003) MODFLOW/MT3DMS-based reactive multicomponent transport modeling. Ground Water 41(2):247–257. https://doi.org/10.1111/j.1745-6584.2003.tb02588.x

Prommer H, Sun J, Kocar BD (2019) Using reactive transport models to quantify and predict groundwater quality. Elements 15(2):87–92. https://doi.org/10.2138/gselements.15.2.87

Steefel CI (2014) CrunchFlow: User's manual. Department of Energy Report 6(3)

Steefel CI, Appelo CAJ, Arora B, Jacques D, Kalbacher T, Kolditz O, Lagneau V, Lichtner PC, Mayer KU, Meeussen JCL, Molins S, Moulton D, Shao H, Šimůnek J, Spycher N, Yabusaki SB, Yeh GT (2015) Reactive transport codes for subsurface environmental simulation. Comput Geosci 19(3):445–478. https://doi.org/10.1007/s10596-014-9443-x

Walter AL, Frind EO, Blowes DW, Ptacek CJ (1994) Modeling of multicomponent reactive transport in groundwater, 1, Model development and evaluation. Water Resour Res 30(11):3137–3148. https://doi.org/10.1029/94WR00955

White JT (2018) A model-independent iterative ensemble smoother for efficient history-matching and uncertainty quantification in very high dimensions. Environ Model Softw 109:191–201. https://doi.org/10.1016/j.envsoft.2018.06.009

White JT, Fienen MN, Doherty JE (2016) A python framework for environmental model uncertainty analysis. Environ Model Softw 85. https://doi.org/10.1016/j.envsoft.2016.08.017

MindMontan – Reduction of pollution in the Freiberger Mulde River in the Erzgebirge/Krušnohoří mining region through a passive water treatment plant

Jana Pinka[1], Eberhard Janneck[1], Sabrina Hedrich[2]

[1]*G.E.O.S. Ingenieurgesellschaft mbH, POB 1162, 09581 Freiberg, Germany, j.pinka@geosfreiberg.de, ORCID 0009-0009-3105-454X; e.janneck@geosfreiberg.de, ORCID 0000-0001-8013-9405*

[2]*Technische Universität Bergakademie Freiberg, Department of Biosciences, Lessingstraße 45, 09599 Freiberg, Germany, sabrina.hedrich@bio.tu-freiberg.de, ORCID 0000-0001-6125-5566*

Abstract

Many old, abandoned mines in Saxony discharge water contaminated with metals and metalloids into ground- and surface water. It is therefore foreseeable that the quality objectives of the European Water Framework Directive will not be achieved by 2027 without additional measures to reduce mining-related pollution. At the Hammerberg/Freiberg tailings pond, a cost-effective, modular passive treatment system has been successfully removing aluminium, cadmium and zinc from seepage water in several stages using combined microbial and chemical processes since July 2024. This system demonstrates that semi passive treatment can improve water quality with low energy, personnel and chemical consumption.

Keywords: Passive water treatment, tailings, acidic mine water, microbiology, sulfate reduction

Introduction

In the Ore Mountains mining region and adjacent areas, there are numerous abandoned mines and several thousand tailing heaps, of which the largest nearly 100 have a major influence on water pathways. Although large areas affected by uranium mining have already been remediated, the effect of historic mining on water systems persist for decades to centuries, for example through contamination with arsenic (As), cadmium (Cd), nickel (Ni), zinc (Zn), copper (Cu), uranium (U), and other potentially toxic elements. An efficient solution to this problem is challenging, as active technical treatment of mine water is economically feasible only at a few sites with high pollutant loads. Therefore, remediation efforts in Saxony have focused on major point sources of contaminated mine drainage, where active treatment is required to meet discharge limits.

Fig. 1 shows catchment areas of streams and rivers in Saxony that show increased levels of toxic metals and metalloids due to former ore and non-ferrous metal mining (Stevens *et al.* 2023). These discharges often cannot be treated and collectively place a substantial load on water bodies. It is foreseeable that approximately 16% of the 558 surface water bodies in Saxony will not achieve the quality objectives of the European Water Framework Directive (WFD) by 2027 without taking further steps.

The goal of passive water treatment methods is to enhance natural purification processes within a controlled treatment system, preventing pollutants from entering natural water bodies. In a review article, the pioneers of early passive mine water treatment systems (Kleinmann *et al.* 2021) describe these approaches as a cost-effective alternative to leaving many abandoned mine sites untreated. In Europe, such systems are far less widespread, although the United Kingdom plays a pioneering role (GOV UK 2016). Wolkersdorfer and Younger (2002) compiled passive treatment systems for mining-influenced waters known in Germany as of 2001.

The article presents the construction of an innovative passive treatment plant for seepage water from the Hammerberg

tailings pond in Freiberg, combining both chemical and biological treatment stages. The construction of nature-based passive systems for the treatment of contaminated mine waters requires solid interdisciplinary expertise in geochemistry, hydrochemistry, microbiology, hydraulics, and botany. Site-specific pilot studies are therefore essential for successful project development.

Methods

The Hammerberg tailings pond located in Freiberg (Fig. 2) comprising industrial flotation residues was constructed in 1964 and operated until 1969. It contains approx. 330,000 m^3 of fine-grained sludge with a thickness of 20–25 m, which was flushed into a small valley behind a dam built from coarse rock material. The main pollutants in the tailings are the elements As, lead (Pb), Cd, Cu and Zn. Underneath the tailings there is clay and weathered gneiss. At the deepest point of the pond a double-strand drainage pipe collects and drains the seepage water. Even more than 50 years after the tailings pond was closed, the seepage water still contains considerable contamination due to low pH values, high sulfate concentrations and contamination especially with the metals aluminium (Al), Cd and Zn (Tab. 1). It should be noted, that Cd is classified as a priority hazardous substance according to WFD (CAS number 7440-43-9). The remediation concept for the tailings pond includes a multi-layered cover to reduce the infiltration of rainwater and air as much as possible. However, even after covering, residual seepage is expected over a very long period. It must therefore be examined how it can be treated in order to protect the river Freiberger Mulde from the above-mentioned toxic metals in the long term.

The seepage water pilot treatment system has a modular design to separate the various pollutants in several treatment stages: First, the contaminated seepage water is pumped from the control shaft into small storage tanks (storage IBCs), from where it flows by gravity

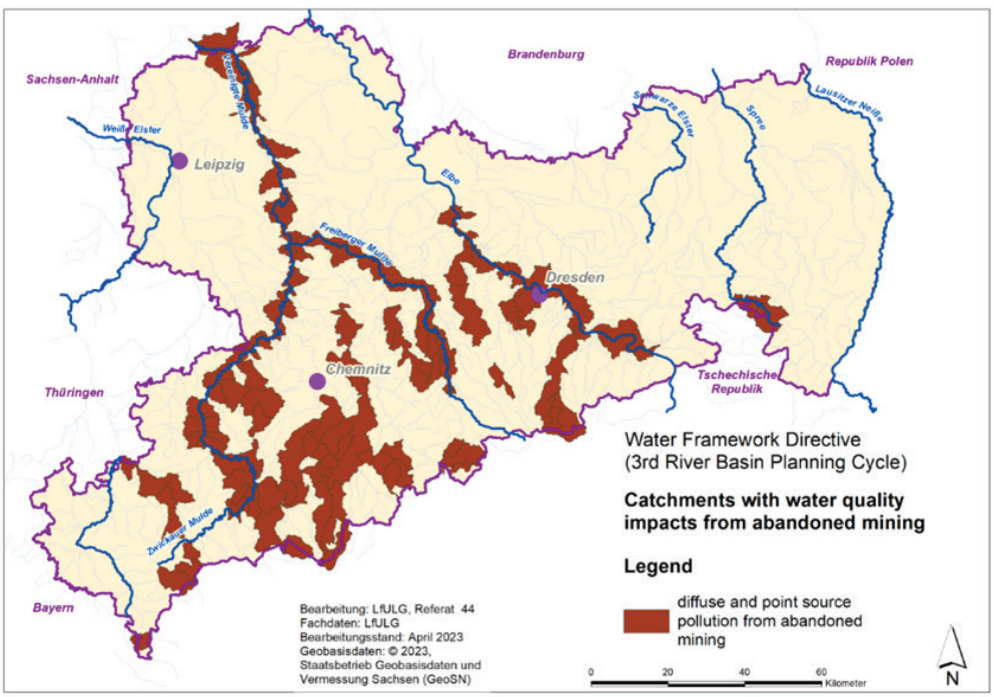

Figure 1 *Water quality influences from abandoned mines on surface water bodies in Saxony.*

Table 1 Minimum, maximum and average of selected parameters in the seepage water, shaft H, July 2024-November 2025 (without winter period November 2024-April 2025).

Element	Unit	Min	Max	Average
Aluminium	mg/L	1.01	173.0	14.8
Zinc	mg/L	11.9	62.1	33.7
Cadmium	mg/L	0.1	0.5	0.3
Sulfate	mg/L	1,000	2,087	1,578
pH	–	4.9	7.4	6.2
Redox potential (E_h)	mV	200	530	375
Oxygen content	mg/L	6.6	10.4	9.2

through the cascade-type treatment plant (Fig. 3). The electrical energy required for pumping is provided by a small photovoltaic (PV) system (sponsored by Meyer Burger Industries GmbH) with battery storage.

In the first treatment stage, the pH value of the acidic water is raised to between 6.5 and 7.0. In this pH range, the aluminium dissolved in the seepage water precipitates as $Al(OH)_3$ (Fig. 4). A special limestone (travertine Burgtonna, 93.7% $CaCO_3$) located in a filter column is used to raise the pH value. The $Al(OH)_3$ that accumulates in the travertine filter over time is flushed out with compressed air and water and collected in a filter bag (big bag).

The water then flows through a intermediate storage tank (clear water tank) into the vertically flow bioreactor (VFBR). The VFBR contains a mixture of limestone, wood chips, straw and compost, which is referred to as 'Biomix'. Sulfate-reducing bacteria grow in this mixture, producing hydrogen sulfide H_2S present as HS^- from the sulfate (SO_4^{2-}) in the

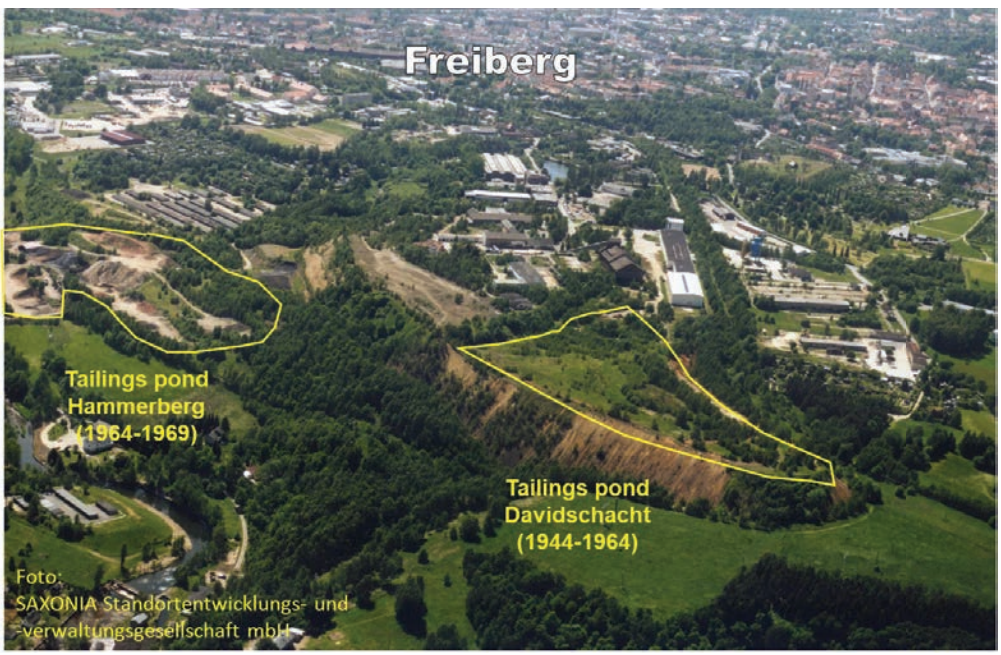

Figure 2 View of the Davidschacht and Hammerberg tailings ponds at the eastern border of Freiberg.

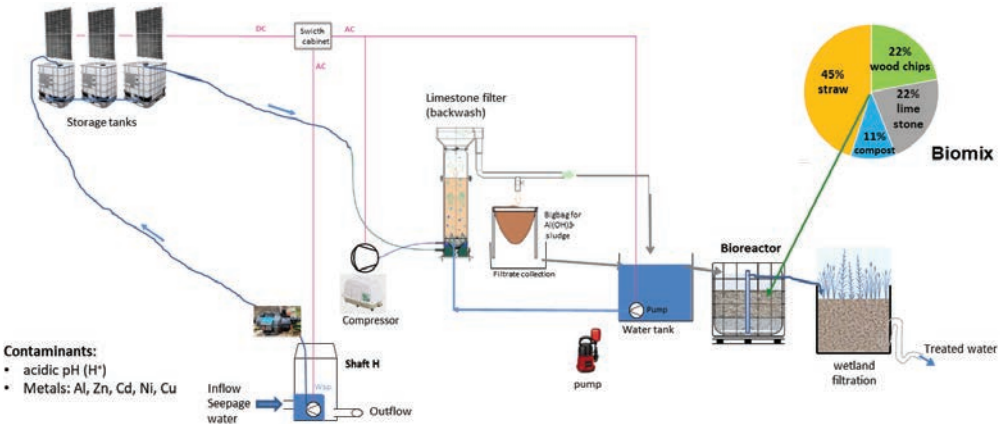

Figure 3 Pilot plant layout at Hammerberg.

leachate, which helps to precipitate the metals Zn, and Cd as metal sulfides (e.g. zinc sulfide ZnS) and retain them in the Biomix (Fig. 4).

All water samples collected were analysed both filtered and unfiltered in order to determine dissolved and particulate element concentrations.

As a final stage, the water to be treated must pass through a plant basin. Here, the water undergoes fine purification through filtration and the precipitation of any dissolved organic substances that may have been washed out of the VFBR.

Fig. 5 shows the structure of the complete pilot plant at Hammerberg. The plant is designed for a water throughput of 20–50 L/h and is being tested under various load conditions as part of the MindMontan project. The plant was commissioned in July 2024 and continuous operation was possible until the frost period at the beginning of November 2024. As the plant was not designed for winter operation for cost reasons, operation was suspended until spring 2025. In mid-April 2025, the plant was recommissioned for a new test period until winter 2025 and is scheduled to resume operation in April 2026.

Results

Fig. 6 shows the results of water treatment based on analyses of water quality at the several treatment stages. In the first treatment period in 2024, the contamination of the seepage water (shaft H) was higher than in the period from June 2025 onwards. This was particularly evident for aluminium, but also for other metals, with cadmium values shown as an example.

A reduction in the aluminium content of the seepage water can be obtained already in the storage basins. Two processes are responsible for this: (1) The degassing of dissolved carbon dioxide (CO_2), which leads to an increase in pH and thus to the partial precipitation of the dissolved Al^{3+}. (2) The settling of hydroxide sludge, which has either already been pumped up from the seepage water shaft or has subsequently precipitated in the storage basin due to the increase in pH value. The remaining dissolved Al

Neutralization: $CaCO_3 + H^+ \rightarrow Ca^{2+} + HCO_3^-$ Precipitation of of aluminiumhydroxide: $Al^{3+} + 3OH^- \rightarrow Al(OH)_3\downarrow$	Sulfate reduction: $SO_4^{2-} + 2CH_2O \rightarrow H^+ + HS^- + 2HCO_3^-$ Precipitation of metals (Cd, Zn): $Cd^{2+} + HS^- \rightarrow CdS\downarrow + H^+$

Figure 4 Simplified reactions in the limestone filter and in the VFBR.

Figure 5 Pilot plant setup: PV modules and storage IBC (left), process stages: travertine filter, intermediate storage, vertical flow bioreactor (VFBR) and plant basin (right).

is precipitated in the travertine filter and retained there. However, there were a few test phases in which the filter discharged a higher Al content than originally present in the seepage water. This occurs because the travertine contains very fine-grained clay minerals, which are washed out during the filter's initial operation phase, temporarily increasing the Al concentration. The clay minerals are retained in the next stages, VFBR and plant basin (wetland).

Fig. 6 shows also the concentrations of Cd in the seepage water shaft and in the outflow of the individual treatment stages. The logarithmic plot was chosen to make the low Cd concentrations in the VFBR and wetland treatment stages more visible. In the first two stages (IBC storage tank and travertine filter), there is no change in the Cd concentration. The concentrations drop sharply only in the bioreactor, where the poorly soluble CdS precipitates. In the outflow of the VFBR, Cd concentrations below the limit of quantification were detected. This means that the Cd concentration is definitely less than 0.01 mg/L. By improving the limit of quantification, values <0.001 mg/L were even detected in the last tests (from July 2025). Due to increased throughput and unexpected intense rainfall, increased cadmium concentrations led to inhibition of the sulfate-reducing bacteria; consequently to reactivate the sulfate reducers, a one-off addition of sodium acetate as an additional carbon source was made on 22 August 2025 to support the system. It is noticeable that with the beginning of the winter period (from November), Cd separation in the VFBR becomes worse. This is related to the decreasing water temperature (< 5 °C), which

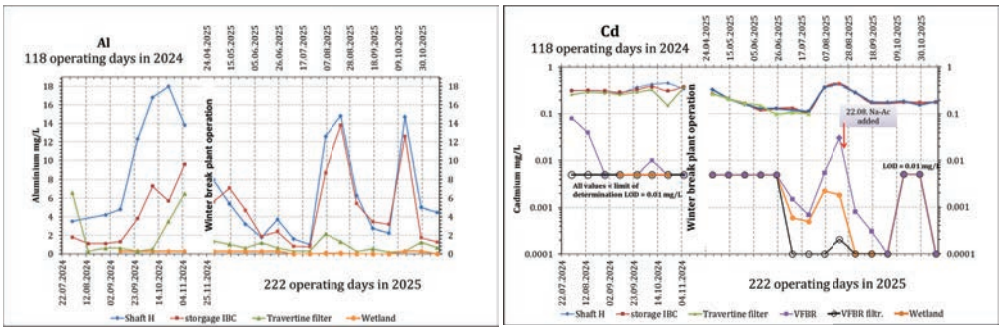

Figure 6 Al (left) and Cd (right) concentrations in the inflow water of the pilot plant (shaft H) and in the outflow of the various process stages.

leads to a slowdown in sulfate reduction and thus less HS^- is available for the formation of CdS. The hydraulic retention time (HRT) in the VFBR was estimated to vary within 17–50 hours (depending on the inflow).

Two approaches were used to evaluate the performance and efficiency of the process, treatment efficiency (TE) and volumetric metal removal rate (VMRR) (Tab. 2).

Compared to the zinc removal efficiencies published by Bailey *et al.* (2016) of up to a maximum of 11.2 g Zn/(m^3× d) in established bioreactor systems that use bacterial sulfate reduction, this system achieved an above-average efficiency rate of 21.3 g Zn/(m^3× d) in 2024 (Tab. 2).

In addition to the variables in the equations (Fig. 7), other independent parameters also have a relevant influence on the efficiency of the VFBR.

Conclusions and Outlook

The pilot plant concept was successfully validated, achieving high treatment efficiencies for Al, Zn and Cd. However, several parameters require more detailed investigation to understand their influence on the overall system. As the passive treatment system restarts in April 2026, additional data will be collected to support upscaling at the site assess transferability to other sites in Saxony. This includes determining the maximum hydraulic load capacity of the system, the treatment efficiency in the individual process stages, the temporal consumption of the Biomix and exploring option for its recycling. In addition, the general permitability and requirements beyond the research project must be clarified, as well as the expected operational expenditures (CapEx/OpEx).

Acknowledgements

We would like to thank the project and associated partners, as well as the Federal Ministry of Research, Technology and Space for funding the project and the recomine alliance.

References

Bailey MT, Gandy CJ, Jarvis AP (2016): Reducing life-cycle costs of passive mine water treatment by recovery of metals from treatment wastes. Proceedings IMWA 2016, Freiberg/Germany. Drebenstedt C, Paul M (eds.)

GOV UK (2016): The Water and Abandoned Metal Mines programme. https://www.gov.uk/government/collections/metal-mine-water-treatment. [access: 2026-02-10]

Kleinmann B, Skousen J, Wildeman T, Hedin B, Nairn B, Gusek J (2021): The Early Development of Passive Treatment Systems for Mining-Influenced Water: A North American Perspective. Mine Water and the Environment (2021) 40:818–830, https://doi.org/10.1007/s10230-021-00817-8

Moghaddam SM (2025): Assessing the performance of a passive mine water treatment system for tailings leachate at the Hammerberg dump, Freiberg. Master thesis. TU Bergakademie Freiberg. Department of Biosciences

Stevens C, Martin M, Janneck E, Greif A (2023): Reducing water quality impacts from abandoned mines on streams and rivers in Saxony – Challenges and benefits for the River Elbe Basin, Proceeding of "Magdeburger Gewässerschutzseminar 2023", https://www.ikse-mkol.org/fileadmin/media/user_upload/D/04_Themen/06_MGS/2023/MGS_2023_Tagungsband.pdf

Wolkersdorfer C, Younger PL (2002): Passive Grubenwassereinigung als Alternative zu aktiven Systemen. Grundwasser – Zeitschrift der Fachsektion Hydrogeologie 2/2002, S. 67-77

Table 2 *Treatment efficiency (TE, complete system) for Al, Zn, Cd and volumetric metal removal rate (VMRR, VFBR) for Zn in the passive pilot plant at Hammerberg.*

Element	Unit	2024	2025
TE			
Aluminium	%	97.6	97.8
Zinc	%	98.2	93.0
Cadmium	%	98.6	97.6
VMRR			
Zinc	g/m^3x d	21.3	20.8

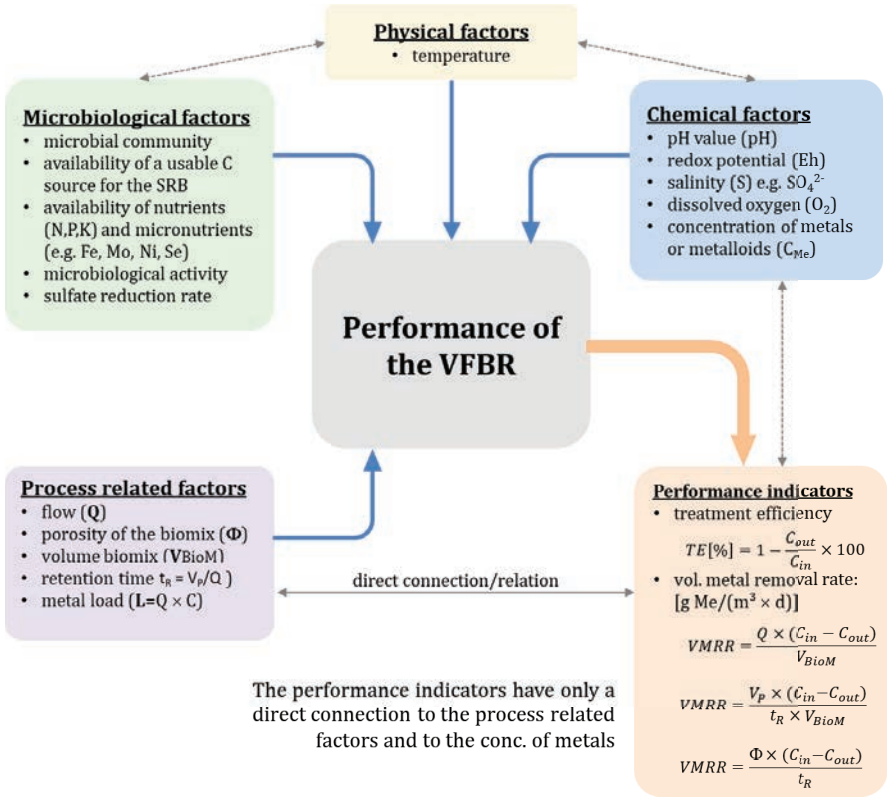

Figure 7 Parameters affecting the performance of VFBR (Moghaddam 2025).

IMWA 2026
Jeongseon

Case Study of an Environmental Remediation Project Using Technosols in São Domingos Mining Area (Portugal)

Mariana Pinto[1], Catarina Diamantino[1], Diego Aran[2,3], Erika Santos[3], Carlos Martins[1], Edgar Carvalho[1]

[1]*EDM – Empresa de Desenvolvimento Mineiro, S.A., Portugal, mariana.pinto@edm.pt, catarina.diamantino@edm.pt, carlos.martins@edm.pt, edgar.carvalho@edm.pt*

2 Inproyen Consulting, S.L., diegoaran@inproyen.com

[3]*LEAF Linking Landscape, Environment, Agriculture and Food - Research Center, Associated Laboratory TERRA, Instituto Superior de Agronomia, Universidade de Lisboa, erikasantos@isa.ulisboa.pt*

Abstract

The former São Domingos mine, located in the Iberian Pyrite Belt in southeast Portugal, is one of the country's most critical environmental legacy sites due to acid mine drainage and metal contamination. To address soil degradation, EDM – Empresa de Desenvolvimento Mineiro implemented a pilot-scale recovery strategy using engineered Technosols formulated from agro-industrial wastes. Applied over 1.5 hectares, the Technosols neutralized acidity, improved fertility, reduced metal mobility, and promoted rapid vegetation establishment. After 12 months, treated areas showed near-neutral pH, enhanced nutrient status, and stable plant cover, demonstrating that Technosols are an effective and sustainable solution for post-mining soil restoration.

Keywords: Environmental rehabilitation, acid mine drainage, degraded soils, technosols, São Domingos mine legacy site

Introduction

The São Domingos Mine, located in the Iberian Pyrite Belt in southeastern Portugal, is notable for its geological heritage and long history of mining, with periods of activity dating from the Roman period to the modern era, between 1857 and 1972 (Matos 2021). The intensive extraction of polymetallic ores, particularly copper, sulfur, and zinc, caused socioeconomic impacts and profound changes to the landscape and local ecosystems (Batista *et al.* 2003; Matos 2021).

Intense mining and metallurgical activity have resulted in extensive areas of tailings and slag deposits rich in sulfate. The oxidation of these materials, in contact with oxygen and water, generated acid mine drainage processes, characterized by the formation of hyperacidic and hyperoxidizing waters with high concentrations of potentially toxic metals and metalloids, affecting the surface water system and reservoirs constructed during the mining phase (Mendonça *et al.* 2003).

The persistence of extreme pH and redox potential conditions promote acid hydrolysis, mineral dissolution, and accelerated weathering, leading to the near-total elimination of the original soil cover. This situation, intensified by high temperatures and low precipitation, characteristics of the regional climate, favor the continuous mobilization of potentially toxic elements and delays the natural recovery of the affected systems. As a result, the soils have reduced buffering capacity, low water and nutrient retention, and limited geochemical immobilization capacity. Vegetation cover is sparse and fragmented, dominated by tolerant arbustive species such as *Cistus ladanifer L.*, reflecting an incipient stage of succession and restricted functional diversity.

Since 2001, EDM – Empresa de Desenvolvimento Mineiro, S.A., a Portuguese State-Owned Company, has been granted the responsibility for the environmental remediation of all mining legacy sites in

Portugal, under a concession contract established by the Decree-Law 198-A/2001. The environmental remediation planned for the former mining area of São Domingos covers a very large area that represents a substantial legacy of environmental, visual, and landscape changes. For this reason, these are highly complex interventions, and their implementation is expected to take place in six phases, to be carried out sequentially and in stages over time. The first two phases of the remediation, completed in 2021, consisted of recovering the existing perimeter channels for collecting runoff water, allowing clean water to be diverted from the right and left banks of the São Domingos stream valley. For the following phases, plans include the collection of various mining wastes deposits dispersed throughout the mining area and their proper concentration and technical confinement, the development of projects aimed at the collection and treatment of acid mine drainage, and the decontamination of soils in the Mosteirão stream valley, among other actions.

To address the identified challenges, associated with the remediation of soils affected by acid mine drainage, the application of Technosols emerges as a soil engineering approach aimed at the functional recover of degraded systems. Technosols are soils of technical origin that incorporate anthropogenic materials, such as waste, sludge, ashes, or other subproducts, and are designed to replicate the functions of natural soils (Aran 2017). Their development is based on adapting the proportions of its components to local conditions, in order to stimulate the biogeochemical and pedogenic processes that support medium and long term rehabilitation (Macías 2004; Macías *et al.* 2011).

In São Domingos Mine, a pilot study was conducted in 2020–2021 that included the physical-chemical and biogeochemical characterization of the treated areas, the formulation and application of Technosols adapted to conditions of extreme acidity and high metal content, and an assessment of their performance 6 and 12 months after application. The primary purpose of the formulation adopted was to mitigate the acidity associated with mine drainage, promote the geochemical stabilization of the system, and create conditions favorable to the progressive recovery of soil functions.

Characterization of the study areas

For the Technosols project, the study defined two application areas, designated as Area 1 (0.8 hectares) and Area 2 (0.7 hectares), covering a total of 1.5 hectares (Fig. 1). The difference between the two areas was related to geomorphological and hydrological conditions. The characterization of the soils to be remediated included the collection of 30 composite samples, allowing for an assessment of the current situation and the geochemical behavior of the existing elements.

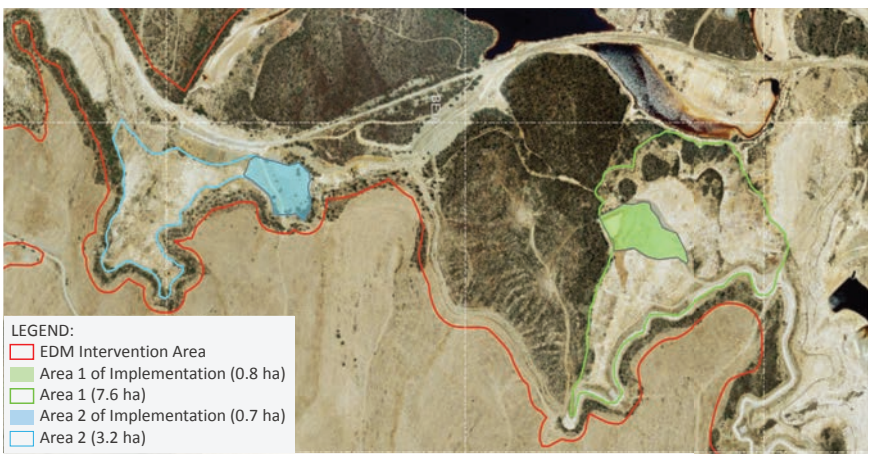

Figure 1 *Technosols implementation area. Left: Area 1; Right: Area 2.*

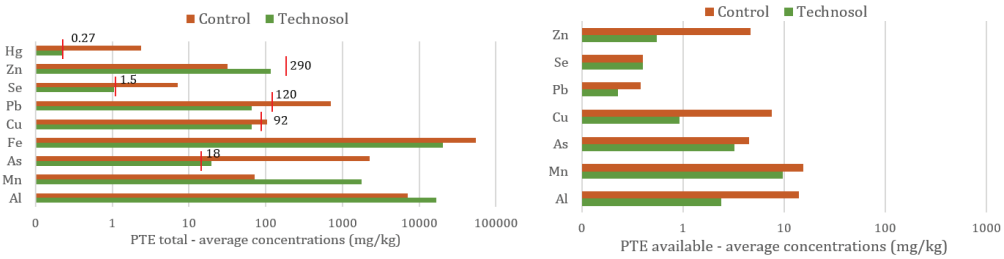

Figure 2 *Average concentrations of total and available potentially toxic elements (PTE) in control and Technosol soils samples. Reference values for urban and industrial soils in environmentally sensitive areas under Portuguese legislation in right graphic bars.*

In Area 1, the pH ranged from 3.15 to 5.23, with highly variable electrical conductivity (18.90–665.60 µS/cm). In Area 2, the pH was more homogeneous, ranging from 3.61 to 4.30, and electrical conductivity remained uniform, ranging from 72.70 to 307.20 µS/cm. Oxidation potentials range from 325 to 475 mV in Area 1 and from 332 to 422 mV in Area 2, indicating the presence of oxidizing conditions, characteristic of environments where the primary oxidizing agent is oxygen, and consistent with the redox values, which maintain the ferric equilibrium even in the worst materials. The C contents, both in the total and organic fractions, and N showed very low values (C < 7.5 g/kg; N < 1.5 g/kg). In terms of the particle size distribution of the fine fraction (<2 mm), the materials were classified as sandy loam.

The elements concentration in the total fraction were analyzed in terms of their toxicity to organisms and biogeochemical processes, and critical risk levels were identified for potentially toxic elements such as As, Hg, Pb, and Se. Regarding the available fraction analyzed in pore water, which allows for determining the potential risk of dispersion of potentially toxic elements through water and their effects on vegetation development, the concentrations reached levels considered critical for Al, As, Cu, Pb, and Zn (Fig. 2). The major elements were Fe (3.31–22.3%) and Al (0.33–1.99%), and the elements of nutritional interest (Ca, K, Mg, and P) had very low concentrations. Sulfate was the dominant anion.

Preparation of Technosols and application process

For the formulation of the Technosols, eight types of wastes mainly from the pulp and paper industry, provided by from *The Navigator Company S.A.*, were characterized: sand, *Dregs&Grits*, lime sludge, primary sludge, biological sludge, biomass ash, and wood scraps resulting from the combustion of residual forest biomass. In addition to these, waste from olive tree pruning in the São Domingos mine region and sludge from wastewater treatment plants were included. For the wastes with a dominant inorganic fraction, the forced oxidation kinetics were evaluated, and different responses were observed. *Dregs & Grits*, primary sludge, biological sludge, and biomass ash showed stability over time; in contrast, lime sludge and sand exhibited a rapid increase in initial pH due to the presence of alkaline solid phases, subsequently stabilizing without considerable changes. Using these residues, four types of Technosols (T1, T2, T3 and T4) were developed, each with different proportions of residues in their formulation. Technosol T1 is distinguished by its high alkalinity and buffering capacity; T2 and T3 have high cation exchange capacity; while T4 combines balanced pH, available phosphorus, and a loamy-clay-sandy texture, making it the formulation most favorable for immediate plant establishment. A total of 5,600 tons of waste was applied. The thickness of the Technosols ranged from 0.25 to 0.50 m. The premixes were received, homogenized, and

subjected to a controlled maturation period. Subsequently, the Technosols were applied to experimental areas according to the defined type and thickness, followed by hydroseeding and vegetation establishment. In the control areas, the seed application rate was 10 times higher than in the pilot areas with Technosols. The vegetation plan included three vegetative levels: herbaceous, arbustive and arboreal, all consisting of native species.

In general, the applied Technosols have a neutral to slightly alkaline pH (7.2 – 8.8), a high organic C content (129±31 g/kg), N total (7.7±2.1 g/kg) and a high cation exchange capacity, with average values of 82 cmolc/kg and a complex dominated by Ca. The total fraction contains metals and metalloids that meet the regulatory limits according to Portuguese legislation, and the levels of these elements in the available fraction are very low and do not pose a risk (Fig.2). The levels of Hg in available fraction for the Technosols were below the analytical detection limit.

Monitoring and analysis of the application of Technosols

The performance of the recovery system was evaluated over a 12-month period following its application through the analysis of samples from Technosols and the soils underlying these materials, as well as from the control areas. The two control areas were established in zones adjacent to the application areas, subject to the same environmental conditions. The materials were characterized by a comprehensive range of physical-chemical and biochemical parameters, including: pH, electrical conductivity (EC), redox potential (Eh), acid neutralization capacity (ANC), total carbon, organic carbon, labile carbon, total nitrogen, and available phosphorus. Multi-elemental analyses were also performed on the total fraction and pore water. The temporal evolution of vegetation cover was assessed in both the Technosol and control areas.

Results and interpretation

The application of Technosol promoted rapid and resilient vegetation cover, with germination and regeneration occurring even after dry periods. In some locations, cover exceeded 90%, with plants showing no signs of deficiency or toxicity over time. In the control areas, cover remained very low or nonexistent, with vegetation limited to spontaneous species (Fig. 3 and Fig. 4).

Twelve months after application, the control areas maintained a hyperacidic to acidic pH, with averages of 3.98 in Area 1 and 3.95 in Area 2, associated with high redox potential levels (411 mV and 436 mV, respectively) and electric conductivity between 269 to 490 µS/cm. In contrast, the Technosols maintained an alkaline pH, with 8.05 in Area 1 and 8.33 in Area 2. The electric conductivity in the Technosols ranged from 498 to 593 µS/cm and redox potentials of 222 mV and 189 mV, favoring the stabilization of sulfate and the reduction of contaminant dispersion. The material underlying the Technosols showed improvements, with a pH close to neutrality (6.30 in Area 1 and 7.04 in Area 2), electrical conductivity ranging from 201 to 588 µS/cm, and a decrease in redox potential compared to the control areas –

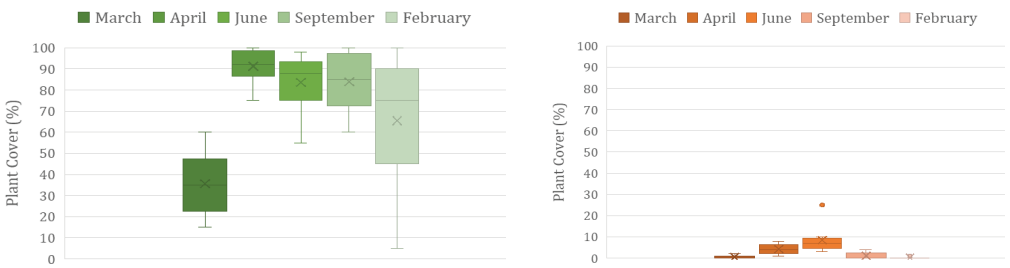

Figure 3 The evolution of vegetation cover during the different monitoring campaigns in the Technosol system (left) and the control areas (right) between 2021 and 2022.

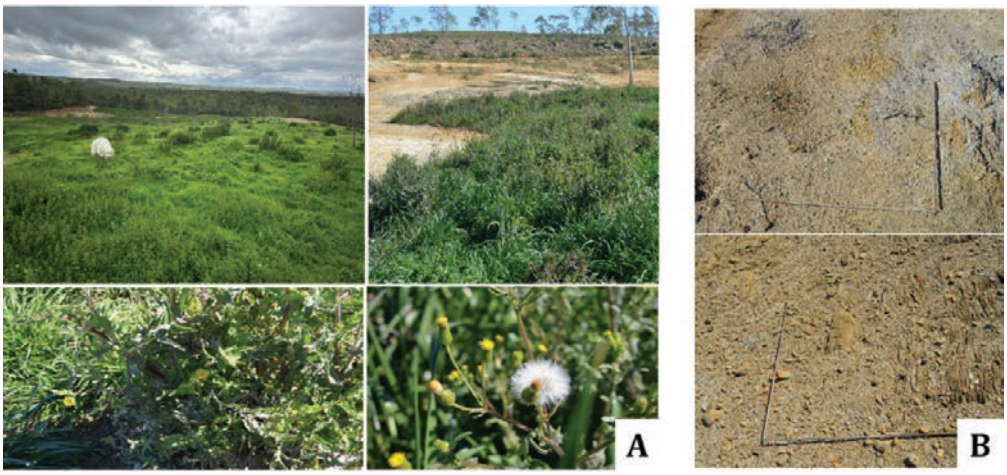

Figure 4 *State of the system's herbaceous cover. A: Area with T2 and T3 Technosols; B: Control areas 1 and 2.*

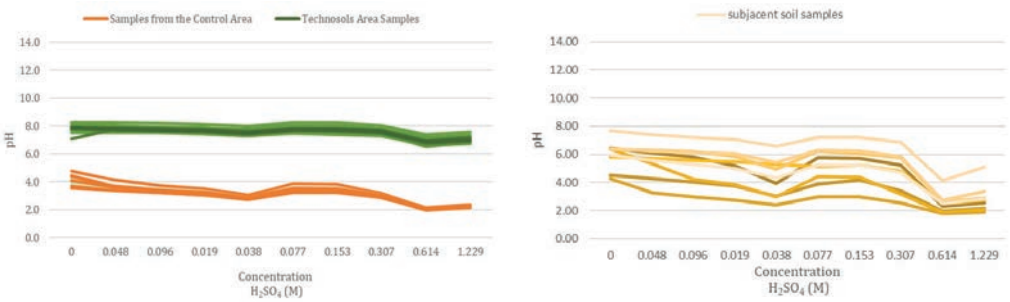

Figure 5 *Acid-Neutralizing Capacity of materials in the Control Areas and Technosols (1 and 2) (left) and subjacent soils (right).*

conditions suitable for vegetative development and promoting deeper rooting. Regarding acid neutralization capacity, the control areas remained susceptible to acidification, while the Technosols maintained high buffering potential, with a pH close to 8, even under acidic loads, functioning as an active acidity control system. In the soil samples subjacent to the Technosols, the acid-neutralizing capacity was higher than that of the control areas, demonstrating the Technosol's effectiveness in mitigating the acidification of materials at depth (Fig. 5). The carbon, nitrogen, and phosphorus contents, after 12 months, in the control areas showed low C (2.3 g/kg) and N (0.9 g/kg) contents, insufficient to sustain plant growth, with highly variable available P content (2.54 mg/kg in Area 1 and 39.52 mg/kg in Area 2). In contrast, the Technosols maintained high total C contents (74.8 g/kg in Area 1, 96% organic fraction), adequate total N (5.8–7.5 g/kg), and high available P (163.96–202.12 mg/kg), while the labile fraction of C continued to increase (10–12 g/kg). Soil samples subjacent to the Technosols showed higher values compared to the initial materials and control areas, with C concentrations 2 to 10 times higher, 50% higher N concentrations, and an increase of 10–12 mg/kg in available P concentrations, reflecting improved fertility and vegetation supporting potential.

There were reductions in the concentrations of potentially toxic elements in the available fraction analyzed in the pore water, particularly Al, Fe, As, Cu, Pb, and Sb (Fig. 6). Elements such as Cd, Se, and Cr had concentrations in the available fraction below

the detection limits of the analytical methods in all samples. Although there is considerable variability in geochemical behavior, there is a clear improvement in the characteristics of these recovered soils. With regard to the concentration of elements in the total fraction of soil samples subjacent to the Technosols, increases of more than 50%, in the levels of elements important for vegetation growth, such as Ca, Mg, Na, K, and P (Fig. 7).

Future Work and Ongoing Developments

An integrated model for the management and monitoring of mining areas contaminated with potentially toxic metals is currently being developed as part of the INCOME project - *"Inputs for a More Sustainable Region: Tools for the Management of Metal-Contaminated Sites."* This model integrates biophysical characterization tools, chemical

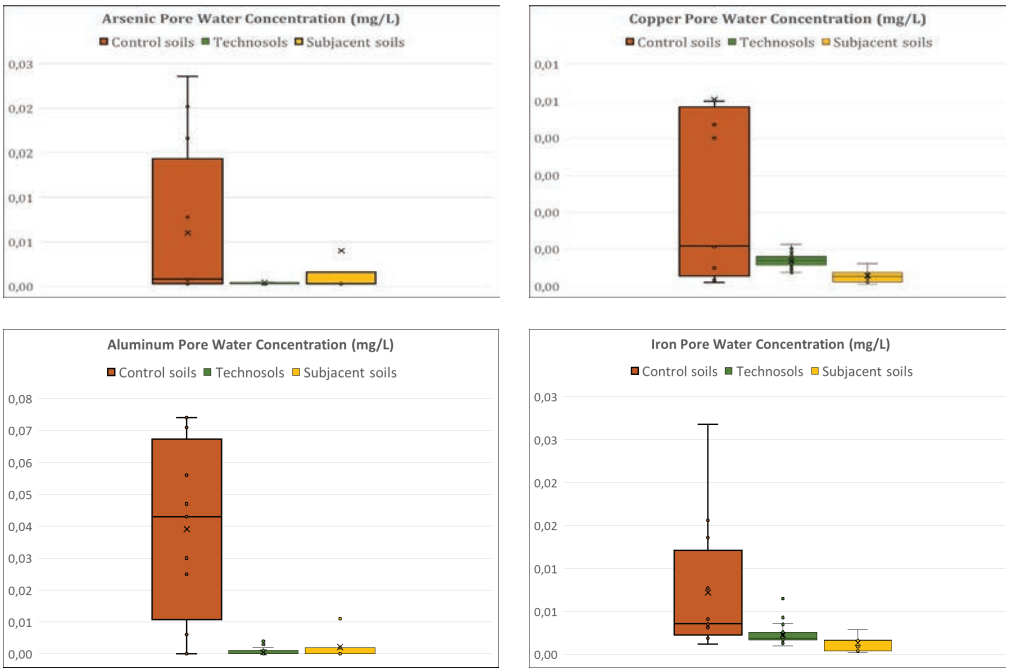

Figure 6 Concentrations of potentially toxic elements in the available fraction of control soil samples, Technosols, and subjacent soils (e.g. arsenic, copper, aluminum, iron).

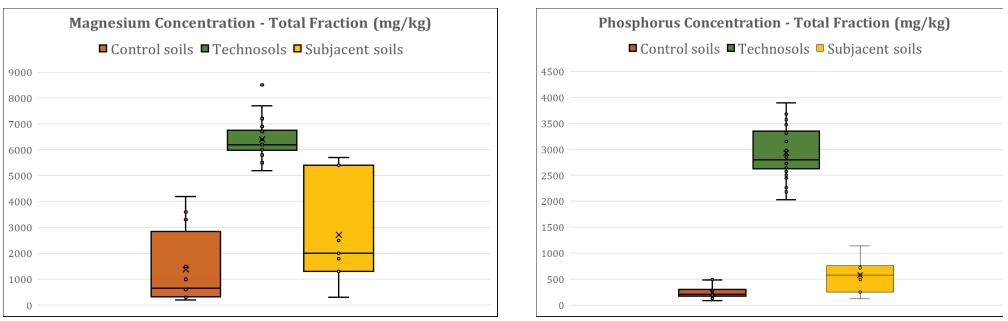

Figure 7 Nutrients concentrations in the total fraction of control soil, Technosols, and subjacent soil samples (e.g. magnesium and phosphorus).

analyses of soils and water, geophysical methods, and hyperspectral remote sensing techniques, supported by artificial intelligence algorithms. Its application will help assess degraded sites, compare their evolution with recovered areas, with and without Technosols, and support decision making, contributing to more efficient and sustainable environmental management (Oliveira *et al*. 2024).

Conclusions

In the pilot study conducted in the former mining area of São Domingos, control areas continued to pose a high environmental risk due to limited vegetation and the mobilization of potentially toxic elements, which compromised natural soil recovery. In contrast, the applied Technosols demonstrated the ability to promote rapid establishment of herbaceous cover, supported by the seed bank and spontaneous colonization, even under conditions of environmental stress. The vigorous vegetation protected the soil from erosion, promoting microbial diversity and ensuring nutrient cycling and the decomposition of organic matter. The physicochemical properties of the Technosols improved the underlying materials by limiting the upsurge of contaminant solutions, preventing salt crystallization, and stabilizing potentially toxic elements. The formulation also neutralizes acidification, increases buffering capacity, improves water and nutrient retention and promotes ecological diversity, creating favorable conditions for soil regeneration and carbon sequestration. These results demonstrate that Technosols constitute an effective strategy for mitigating environmental impacts, restoring the physical stability, chemical fertility, and biological biodiversity of the soil, and ensuring the resilience and sustainability of the ecosystems.

Acknowledgements

This work was funded by Cohesion Funds from the Operational Program for Sustainability and Efficiency in the Use of Resources (POSEUR) under the Portugal PT2020 Program. It also received support from the "la Caixa" Foundation's Promove Program, in partnership with BPI and FCT, in the scope of the INCOME Project – *Inputs for a more sustainable region: Tools for the management of metal contaminated sites*. PD23-00013.

References

Aran D (2017) Recuparación de Suelos Contaminados con Aniones Potencialmente Tóxicos y Metales Pesados mediante Tecnosoles y Bicarbones Adsorbentes. Doctoral Thesis. Univ. Santiago Compostela.

Batista M J, Brito MG, Abreu MM, Sousa AJ, Quental L, Vairinho, M (2003) Avaliação por modelação em SIG da contaminação mineira por drenagem ácida em S. Domingos (Faixa Piritosa, Alentejo). Ciências da Terra (UNL). p 6–10.

Macías F (2004) Gestión de residuos y cambio climático, in: Mosquera, MEL, Osés, MJS (Eds.), Gestión de Residuos Orgánicos de Uso Agrícola. Servizo de Publicacións e Intercambio Científico de la Universidade de Santiago de Compostela, Santiago de Compostela, p 11-24.

Macías F, Macías-García F, Nieto C, Verde JR, Pérez C, Bao M, Camps-Arbestain M (2011) Gestión de residuos y cambio climático. In Gestión de residuos orgánicos de uso agrícola. p 11–24. Servicio de Publicaciones.

Matos JX (2021) Alteração hidrotermal ácido-sulfato associada aos jazigos de sulfuretos maciços de Lagoa Salgada, Caveira, Lousal, Aljustrel e São Domingos (Faixa Piritosa Ibérica). Doctoral Thesis. Faculdade de Ciências. Universidade de Lisboa.

Mendonça JL, Silveira T, Frescata M, Pica D (2003) Contaminação dos Recursos Hídricos na área da mina abandonada de São Domingos. Jornadas Luso-Espanholas Águas Subterrâneas Sul da Península Ibérica.

Oliveira RJ, Caldeira B, Palma P, Costa MJ, Fialho A (2024) Instrumento de gestão de áreas contaminadas por metais combinando dados de Química, Geofísica, Deteção Remota, Inteligência Artificial e Gestão – Projeto INCOME. Assembleia Luso Espanhola de Geodesia e Geofísica, Évora, Portugal.

Wastewater Management in Coal Mining Operations: A Geotextile-Based Semi-Active Treatment System in South Kalimantan, Indonesia

Adhika Catra Pradhana[1], Yudha Hadiyanto Eka Saputra[1]

[1]*Environmental and Reclamation Department, PT Borneo Indobara, South Kalimantan, Indonesia*

Abstract

High-TSS mine water at PT Borneo Indobara reduces pond capacity and increases sludge handling demand. This study evaluated an integrated geotextile pool and geotextile tube system under field conditions. Fine-grained sludge was characterized by high silt-clay content. The geotextile pool reduced TSS from 92,340–150,110 mg/L to 6,424–9,307 mg/L, while the geotextile tube reduced TSS from 6,016–8,386 mg/L to 55–149 mg/L. The pool reached specific gravity 1.40 after 14 d, whereas the tube reached 1.45 after 29 d. Both systems showed complementary roles in sludge dewatering.

Keywords: Mine water, sludge dewatering, geotextile tube, geotextile pool, TSS, coal mining

Introduction

Mine water management remains a major operational and environmental challenge in open-pit coal mining, especially in tropical regions with high rainfall and fine-grained overburden. Runoff from disturbed mine surfaces transports large amounts of suspended solids into treatment ponds, reducing hydraulic retention time and accelerating sediment accumulation. Under these conditions, conventional sediment ponds must treat water and store sludge simultaneously, which lowers their operational efficiency.

In Indonesia, mine water discharge must comply with regulatory limits, including a maximum TSS concentration of 200 mg/L before discharge to natural waterways. At PT Borneo Indobara, South Kalimantan, runoff from mining areas within the Warukin Formation commonly contains very high suspended solids. Fine-grained materials derived from siltstone, claystone, mudstone, and coal-bearing strata contribute to rapid sludge accumulation in ponds and increase maintenance demand (Jamal *et al.* 2021).

Previous work from the same regional setting described quartz, kaolinite, illite, and occasional pyrite as common minerals in clay-rich materials, with SiO_2 and Al_2O_3 as dominant oxides and Fe_2O_3 and CaO also present (Sira *et al.* 2021). Those findings are consistent with the field character of sludge observed in the present study.

Geotextile-based dewatering systems are increasingly used to reduce sludge volume before final disposal or further handling. Geotextile tubes are commonly used as confined filtration units, especially when combined with polymer conditioning (Muthukumaran and Ilamparuthi 2006). At IMWA 2017, Kim and Kim (2017) reported that geotextile tubes, geotextile bags, and gunny bags could be used for mine drainage sludge dewatering through flocculation and self-filtration, and that sludge characteristics strongly influenced dewatering behaviour. Geotextile-lined pools can serve as open dewatering basins with simpler operation and easier excavation. Field-scale information comparing their operational roles within one integrated treatment train is still limited in coal mine water management.

This study aimed to evaluate the field performance of an integrated geotextile pool and geotextile tube system for sludge handling in high-TSS coal mine water treatment at PT Borneo Indobara. The objectives were to: (1) characterize sludge properties along the treatment train, (2) evaluate TSS reduction by both geotextile systems, (3) assess dewatering behaviour using specific gravity, water

content, and solid content, and (4) describe the operational role of each method in the treatment sequence.

Methods

Site Description and Treatment Process

The study was conducted at PT Borneo Indobara, an operating open-pit coal mine in South Kalimantan, Indonesia. Water and sludge from active mining areas are collected in a sump area and pumped to Karuh Pond. From there, slurry enters a geotextile-based treatment stage before passing to Sediment Pond 06 GRM and then being discharged to the receiving stream (Fig. 1).

Two geotextile systems were used in complementary roles. A geotextile pool was operated as an open pre-treatment and bulk dewatering unit without chemical addition. A geotextile tube system was operated as a secondary dewatering unit with polymer injection. In the geotextile tube arrangement, sludge was pumped from Sediment Pond 06 GRM through a dredging pump and booster pump to a mixing chamber. Polymer solution was prepared in a dosing unit using recycled filtrate water and injected into the mixing chamber during pumping. The conditioned slurry then flowed through a DN350 HDPE PN 16 pipeline into geotextile tube bags (Fig. 2).

Sludge Sampling and Characterization

Sludge samples were collected from the sump area, Karuh Pond, and Sediment Pond 06 GRM. A total of 9 samples (Tab. 1) were analysed for natural water content, specific gravity of solids, wet density, dry density, void ratio, saturated density, submerged density, degree of saturation, and grain-size distribution.

Specific gravity was measured using a density cup. Water content was calculated from the ratio between wet sample mass and oven-dried sample mass after drying at 105 °C. Grain-size analysis followed ASTM procedures. TSS was measured using a Hach DR900 instrument following the manufacturer's method and applicable international standard practice.

Geotextile Pool

The geotextile pool functioned as an open dewatering basin without chemical addition. One pool had a radius of 16 m and a height of 2.5 m, with a solid capacity of up to 1,500 m^3. The operational target was specific gravity (SG) 1.40, at which the material could be blended and excavated. Under field operation, this condition was reached after 14 d.

The geotextile pool used nonwoven polypropylene geotextile with a nominal mass of 300 g/m^2. The characteristic opening size was 0.12 mm. Manufacturer data indicate a permittivity of 0.4393 s^{-1}, UV resistance of 70%, tensile strength of 14.20 kN/m in the machine direction and 30.10 kN/m in the cross direction, and puncture resistance of 3,160 N.

During operation, slurry from the upstream treatment stage was pumped into

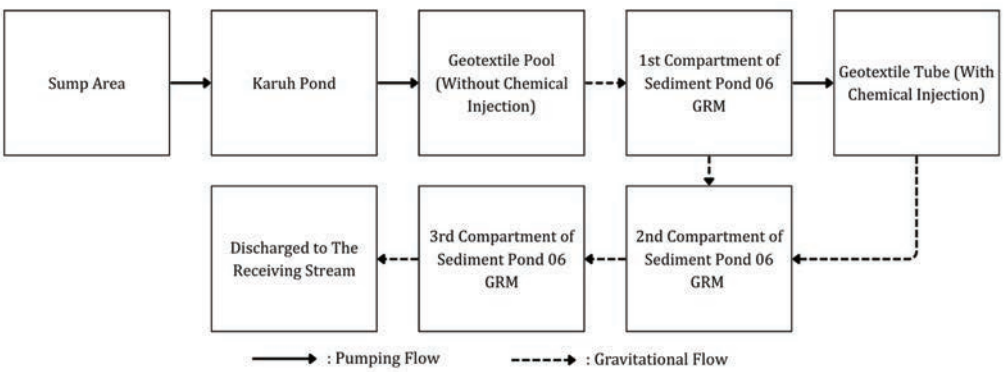

Figure 1 *Integrated mine water treatment train from sump area to discharge area.*

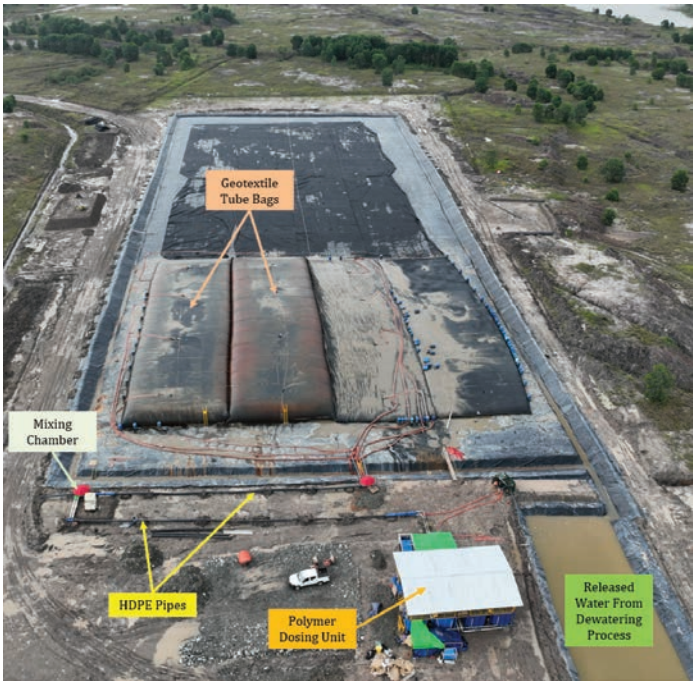

Figure 2 *Geotextile tube operating arrangement.*

the geotextile pool over one filling period. No flocculant or other chemical additive was introduced into this system. Solids settled and accumulated within the lined basin, while water gradually discharged through the geotextile and by surface drainage under gravity. Because the pool was fully exposed to field conditions, its dewatering behaviour was influenced by rainfall, evaporation, drainage capacity, and the progressive self-weight consolidation of the deposited sludge mass.

Geotextile Tube

The geotextile tube functioned as a confined secondary dewatering unit with polymer conditioning. Each tube had dimensions of 61.4 m × 18.3 m and a maximum height of about 2.4 m. One layer consisted of 12 bags. The operational target for stacking was SG 1.45, which was reached after 29 d.

The geotextile tube used woven polypropylene geotextile GT500D. Material properties provided by the manufacturer include an opening size of 0.3 mm, water permeability of 25 L/m^2/s, tensile strength of 100 kN/m in the machine direction and 125 kN/m in the cross direction, CBR puncture strength of 10 kN, and seam strength of 75 kN/m.

After the pumping stage, the geotextile tube entered a relaxation or passive dewatering stage. During this period no additional slurry was pumped, and the retained material was allowed to consolidate under self-weight while water continued to discharge through the geotextile. SG, water content, and solid content were monitored over time in order to assess densification of the sludge mass. Unlike the geotextile pool, the operational criterion for the geotextile tube was not excavation readiness but stacking readiness. The target condition was SG 1.45, which represented a denser and more stable sludge condition suitable for supporting a second layer. Under the monitored field conditions, this criterion was reached after 29 d.

Polymer Dosing and Operating Records

The geotextile tube system used Flopam AN 934 SH as flocculant. Polymer was blended with recycled filtrate water in the dosing system and injected into the mixing chamber

during pumping. Daily records included flow rate, influent TSS, chemical consumption, daily slurry volume, chemical dosage per cubic metre of slurry, and filtrate TSS.

Monitoring Datasets

Geotextile pool performance was evaluated using 10 single observations collected within one pumping batch on the same day at different hours. Each observation included influent TSS, influent SG, flow rate, and effluent TSS.

Geotextile tube performance was evaluated using 30 single observations collected from 12 bags in layer 1 on different dates during one month of operation. One zero-flow day was excluded from efficiency calculations because no slurry entered the system. Daily dewatering after the pumping stage was monitored separately using SG, water content, and solid content, together with rainfall.

The datasets represent operational field observations rather than replicated laboratory experiments. Therefore, the reported mean and standard deviation values describe field variability under actual operating conditions, including changes in flow rate, sludge condition, rainfall, and bag operation. No statistical hypothesis testing was conducted, and the comparison between systems is interpreted as a field-performance evaluation rather than a controlled experimental comparison.

Data Analysis

TSS removal efficiency was calculated as:

$$\eta = \frac{C_{in} - C_{out}}{C_{in}} \times 100$$

where C_{in} is influent TSS and C_{out} is effluent TSS. Mean, standard deviation, and range were calculated for the main TSS datasets to describe field variability. Since the observations were operational field measurements rather than replicated laboratory trials, the results are interpreted as field-performance indicators.

Results and Discussion

Sludge Characteristics

The sludge was dominated by fine material. Gravel was negligible, sand was minor, and most samples consisted mainly of silt and clay. Passing No. 200 values were generally high, commonly exceeding 90%. These results indicate that the treatment train handled fine-grained sludge that would be difficult to settle efficiently in conventional ponds alone. The observed particle-size distribution is consistent with clay-rich detrital material derived from the Warukin Formation.

Geotextile Pool Performance

The geotextile pool received highly concentrated sludge, with influent TSS ranging from 92,340 to 150,110 mg/L. Effluent TSS ranged from 6,424 to 9,307 mg/L. Mean influent TSS was 107,286.4 ± 19,753.0 mg/L, while mean effluent TSS was 7,424.4 ± 992.4 mg/L. Average TSS removal efficiency was 93.02 ± 0.46% (Tab. 2).

These results show that the geotextile pool acted effectively as a bulk solids reduction unit without chemical addition. Although the effluent remained above the final discharge criterion, the pool substantially lowered solids loading before downstream treatment. That role makes it suitable as a pre-treatment and dewatering step rather than a final polishing unit.

Geotextile Tube Performance

The geotextile tube treated slurry with influent TSS ranging from 6,016 to 8,386

Table 1 *Summary of sludge physical and grain-size characteristics by sampling location.*

Sampling Location	n	Water Content (%)	Gs	Silt (%)	Clay (%)	Passing No. 200 (%)
Sump Pit	3	13.19 ± 1.90	2.63 ± 0.01	46.98 ± 1.93	44.77 ± 5.20	91.76 ± 3.39
Karuh Pond	3	15.09 ± 5.08	2.59 ± 0.09	39.56 ± 3.10	38.66 ± 18.07	78.22 ± 19.04
Sediment Pond 06 GRM	3	13.72 ± 4.12	2.63 ± 0.04	30.88 ± 1.28	67.17 ± 2.46	98.05 ± 1.80

mg/L, excluding the zero-flow day. Filtrate TSS ranged from 55 to 149 mg/L. Mean influent TSS was 6,992.9 ± 653.6 mg/L, and mean effluent TSS was 100.9 ± 27.6 mg/L. Average TSS removal efficiency was 98.56 ± 0.34% (Tab. 2).

These results show that the geotextile tube produced much cleaner filtrate than the geotextile pool. Filtrate remained below 200 mg/L during valid monitored observations. The combined effect of woven confinement and polymer conditioning appears to be responsible for this low filtrate TSS. In operational terms, the geotextile tube served as a secondary dewatering and polishing unit.

Dewatering Cycle and Sludge Condition

The water content values in Tab. 1 are lower than those shown in Fig. 3 because they represent different material conditions. Tab. 1 summarizes laboratory characterization results from collected sludge samples, whereas Fig. 3 shows the evolution of water content in the bulk sludge mass during post-filling dewatering. Immediately after pumping, the sludge body remained highly saturated and contained large amounts of pore water, resulting in initial wet-basis water contents above 60% in both systems. This behaviour is consistent with the fine-grained nature of the sludge, which is dominated by silt and clay fractions and therefore retains water strongly. During the relaxation stage, drainage and self-weight consolidation progressively reduced water content and increased solids concentration. The geotextile tube reached a lower final water content than the geotextile pool because polymer conditioning, confined geometry, and longer dewatering time promoted denser final sludge formation.

The observed dewatering behaviour can be explained by three main mechanisms: filtration, flocculation, and consolidation. In the geotextile pool, solids were retained mainly through settling and filtration by the nonwoven geotextile layer, while water discharged by gravity and surface drainage. Because no polymer was used, fine clay-silt particles were more likely to remain dispersed, which explains why the pool reduced bulk solids effectively but still produced higher effluent TSS than the tube. In the geotextile tube, polymer conditioning promoted flocculation before the slurry entered the bag. Larger flocs were more easily retained by the woven geotextile and by the filter cake formed inside the tube. After filling, self-weight consolidation gradually reduced water content and increased solid content. This process is consistent with previous observations that sludge characteristics and polymer-assisted self-filtration influence geotextile tube dewatering performance (Kim and Kim 2017; Muthukumaran and Ilamparuthi 2006).

Post-filling monitoring showed different operational cycles for the two systems. The geotextile pool reached SG 1.40 after 14 d, which was the criterion for blending and excavation. At that stage, water content was 53.57% and solid content was 46.43% (Fig. 3).

The geotextile tube required 29 d to reach SG 1.45, which was the criterion for stacking. At that stage, water content was 49.57% and solid content was 50.43% (Fig. 3). The tube therefore required a longer dewatering period, but it produced denser final solids than the pool.

Differences in operating cycle indicate that the geotextile pool is more suitable for faster excavation readiness, whereas the geotextile tube is more suitable for staged stacking and higher final solids concentration. Rainfall during the monitoring period did not prevent gradual densification in either method, although short plateaus in SG and water content were observed.

Table 2 *TSS reduction performance of geotextile pool and geotextile tube.*

System	n	Influent TSS mean ± SD (mg/L)	Influent TSS Range (mg/L)	Effluent TSS mean ± SD (mg/L)	Effluent TSS Range (mg/L)	Removal efficiency (%) mean ± SD
Geotextile pool	10	107,286.4 ± 19,753.0	92,340–150,110	7,424.4 ± 992.4	6,424–9,307	93.02 ± 0.46
Geotextile tube	29	6,992.9 ± 653.6	6,016–8,386	100.9 ± 27.6	55–149	98.56 ± 0.34

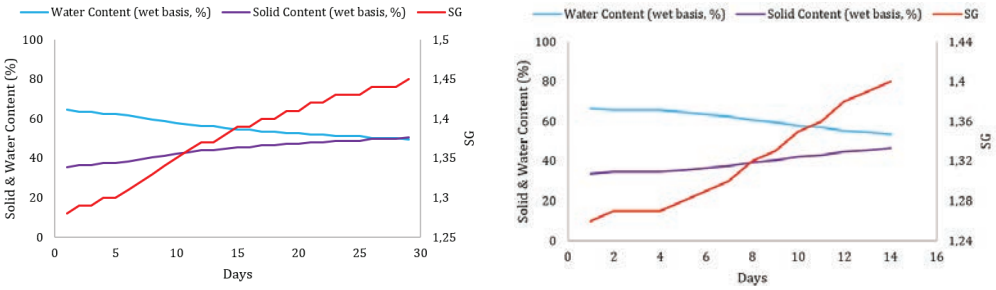

Figure 3 Changes in specific gravity (SG), water content, and solid content during post-filling dewatering for the geotextile tube (left) and geotextile pool (right).

Operational Role of Both Systems

The two systems are best understood as complementary rather than competing. The geotextile pool handled very high TSS feed and reduced solids loading rapidly, which supports its use as an open pre-treatment and bulk dewatering unit. The geotextile tube generated lower filtrate TSS and denser solids, which supports its use as a secondary dewatering unit after initial solids reduction.

From an operational perspective, the integrated system can reduce sludge-management-related cost by up to 44% compared with a conventional approach. Absolute cost values are not presented because of company confidentiality. This cost reduction is associated with lower solids loading to the main treatment ponds, reduced sludge handling frequency, and better control of concentrated material.

Conclusions

This study evaluated an integrated geotextile pool and geotextile tube system for field-scale sludge handling in high-TSS coal mine water treatment at PT Borneo Indobara.

The sludge was dominated by fine silt-clay material, which explains the difficulty of relying on settling ponds alone. The geotextile pool reduced TSS from 92,340–150,110 mg/L to 6,424–9,307 mg/L and provided an average removal efficiency of 93.02%. The geotextile tube reduced TSS from 6,016–8,386 mg/L to 55–149 mg/L and provided an average removal efficiency of 98.56%.

The geotextile pool reached excavation readiness after 14 d at SG 1.40, while the geotextile tube reached stacking readiness after 29 d at SG 1.45. Final solids concentration was higher in the tube system than in the pool system. These observations show that the geotextile pool is suitable for faster bulk dewatering and excavation, whereas the geotextile tube is suitable for lower filtrate TSS and denser final solids. Integrated use of both systems provides a practical field-scale approach for mine water sludge management under high TSS conditions.

Acknowledgements

The authors thank PT Borneo Indobara for operational support, field access, and technical data used in this study. Appreciation is also extended to site personnel involved in sampling, monitoring, and field operation.

References

Jamal J, Rijani S, Maryanto S, Cita A (2021) Clay minerals identification on Warukin Formation at Kandangan area, South Kalimantan Province based on ASD testing method. Jurnal Geologi dan Sumberdaya Mineral 22:1–7

Kim DM, Kim DK (2017) Assessment of dewatering process using flocculation and self-filtration according to the characteristics of mine drainage sludge. In: Wolkersdorfer C, Sartz L, Sillanpää M, Häkkinen A (eds), Mine Water and Circular Economy, IMWA 2017, Lappeenranta, Finland, pp 1178–1184

Muthukumaran AE, Ilamparuthi K (2006) Laboratory studies on geotextile filters as used in geotextile tube dewatering. Geotextiles and Geomembranes 24(4):210–219

Sira R, Sufriadin, Widodo S, Jaya A (2021) Analisis mineral matter dan kualitas batubara Blok Batulaki, Kecamatan Satui, Kabupaten Tanah Bumbu, Provinsi Kalimantan Selatan. Jurnal Geomine 9:206–217

Stable Isotope Evidence for Hydro-Chemical Processes in Groundwater of the Oyu Tolgoi Copper Mine, Mongolia

Tamir Puntsag[1], Tulganyam Samdanjigmed[1], Otgonbaatar Sededpurev[1], Sod-Erdene Bazardorj[1], Batdemberel Bayanzul[1], Bilguun Myagmar[2], Munkhtuya Munkhzorig[1], Sunderiya Ganzorig[1], Purevsuren Nyambuu[1], Enkhjin Naranbaatar[1]

[1]*Oyu Tolgoi LLC, Mongolia, tamirpu@ot.mn, ORCID 0000-0002-4665-1381*

[2]*Water Management LLC, Mongolia*

Abstract

Groundwater protection in mining regions requires early identification of contamination sources, though this remains challenging in complex hydrogeological settings. This study integrates major ion chemistry with stable isotopes of water ($\delta^{18}O$) and sulfate ($\delta^{34}S$, $\delta^{18}O$) to distinguish natural processes from mining influences in the Oyu Tolgoi region. Water isotopes indicate meteoric origin with strong evaporation, while sulfate isotopes reflect sulfide oxidation under open conditions. Large fractionation occurs in natural systems, whereas tailings seepage shows enriched sulfate $\delta^{18}O$ and high sulfate concentrations, indicating enhanced oxidation. Salinity is mainly driven by evaporation, while sulfate derives from dissolution and oxidation, supporting improved groundwater monitoring and sustainable management.

Keywords: Oyu Tolgoi, sulfur and water isotope signatures, sulfur oxidation, evaporation

Introduction

Early identification of groundwater contamination sources is critical in mining regions due to reliable source attribution is often complicated by the overlap of natural hydro-chemical processes and mining related influences. In complex hydrogeological settings, major ion chemistry alone is insufficient to distinguish baseline groundwater conditions from potential mining impacts. In such cases, integrating isotopic tracers with geochemical data provides an effective approach for resolving hydro-chemical processes and improving discrimination between natural background signals and anthropogenic inputs. At the Oyu Tolgoi (OT) copper mine, elevated total dissolved solids (TDS) were detected in a shallow monitoring bore screened within an alluvial aquifer downgradient of mining infrastructure. To investigate the potential causes of this salinity increase, Puntsag *et al.* (2025) applied a multivariate approach combining stable isotopes ($\delta^{18}O$, $\delta^{2}H$, $\delta^{34}S$), radiogenic isotopes ($^{87}Sr/^{86}Sr$), and major and trace element geochemistry. Their results indicated that evaporative enrichment and mineral dissolution are the dominant controls on groundwater salinity, with no clear evidence of direct mining related inputs. However, the origin and geochemical evolution of dissolved sulfate and its potential links to mining processes remain insufficiently constrained. The sulfur and oxygen isotopic composition of dissolved sulfate ($\delta^{34}S$ and $\delta^{18}O$) is widely applied to distinguish sulfate sources and oxidation processes in mining environments (Krouse and Mayer 2000; Dold and Spangenberg 2005). Sulfate derived from sulfide oxidation typically reflects the $\delta^{34}S$ signature of the parent sulfide minerals, whereas sulfate produced by evaporite dissolution generally exhibits more positive $\delta^{34}S$ values. In contrast, $\delta^{18}O$ values provide insight into oxidation pathways and groundwater mixing processes, making the combined $\delta^{34}S$–$\delta^{18}O$ isotope system an effective tool for evaluating sulfate origin and geochemical evolution in mine affected aquifer systems (Kim *et al.* 2019). In OT, the flotation circuit mineralogy is dominated by sulfide minerals, primarily chalcopyrite, with subordinate amounts of bornite, chalcocite, pyrite, and enargite.

These sulfide minerals typically exhibit $\delta^{34}S$ values ranging from negative to near zero. In contrast, associated sulfate minerals such as gypsum, anhydrite, and alunite from the Central deposit are characterized by strongly positive $\delta^{34}S$ values, reflecting distinct reduced sulfide and oxidized sulfate sulfur reservoirs (Khashgerel *et al.* 2006). Similar isotopic contrasts observed in other mine tailings and groundwater systems demonstrate the utility of $\delta^{34}S$ for discriminating sulfate derived from sulfide oxidation versus evaporite dissolution, while $\delta^{18}O$ provides complementary information on oxidation mechanisms and secondary sulfate formation processes (Dold and Spangenberg 2005; Kim *et al.* 2019; Natali *et al.* 2025). The objective of this study is to characterize the sulfur ($\delta^{34}S$) and oxygen ($\delta^{18}O$) isotopic composition of dissolved sulfate (SO_4^{2-}) in groundwater associated with copper ore processing operations at the OT mine. Isotopic analyses were conducted on precipitation, deep regional groundwater, process water components (including thickener overflow and barge water), tailings storage facility (TSF) seepage waters, and groundwater samples from multiple hydrogeological units. All samples were collected contemporaneously across the site

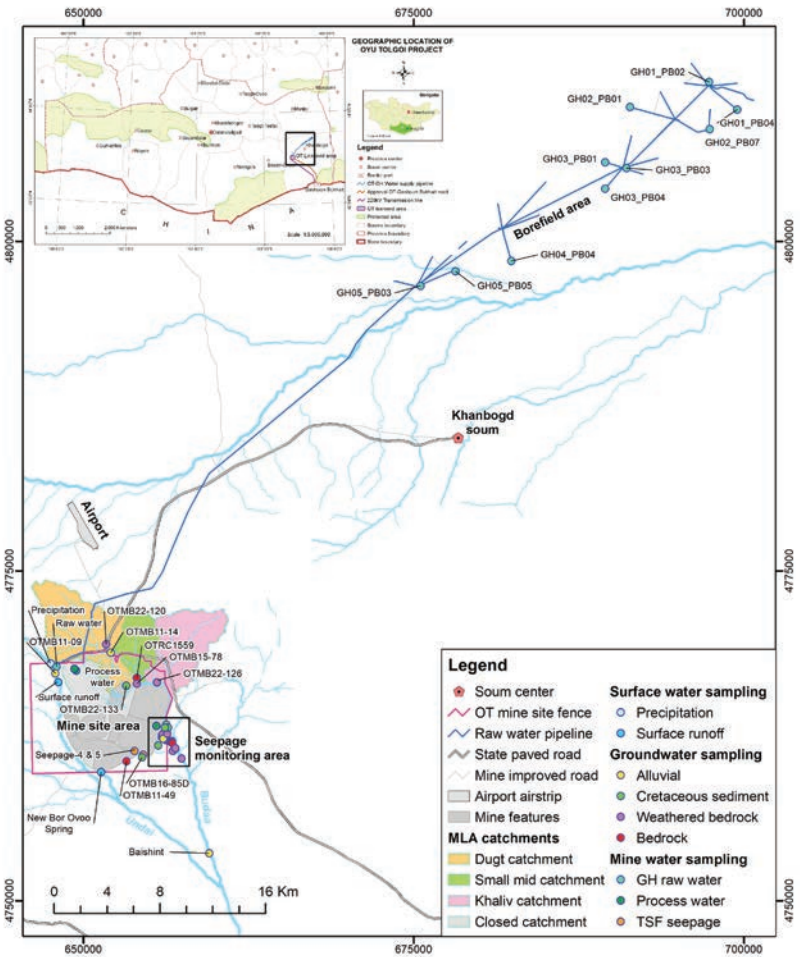

Figure 1 *OT mine site, sampling locations (from Puntsag* et al. *2025): wet precipitation, source water, process water, thickener overflow, the barge pond, seepage collection ponds, and groundwater (alluvial, Cretaceous sediments, weathered bedrock, and bedrock).*

to ensure temporal consistency. Evaluation of $\delta^{34}S$ and $\delta^{18}O$ isotopic data provides new insights into sulfate sources, mixing relationships, and transformation processes influencing groundwater chemistry at OT, thereby supporting improved assessment of mining related impacts and long-term groundwater management.

Method

This study was conducted at the OT copper mine in South Gobi, Mongolia (43000' N, 106050' E). In 2024, a two day focused sampling campaign collected more than 75 water samples along the mine water system, extending from the Gunii Khooloi borefield through the processing circuit to the downstream monitoring network east of the TSF (Fig. 1).

The study area has no notable groundwater withdrawal impacts causing sulfide oxidation or acid mine drainage, and mining-related sulfate is primarily introduced during ore processing rather than through hydrogeological disturbance. Water samples were collected in 15 mL glass vials (for hydrogen and oxygen isotopes) and 250 mL HDPE bottles (for sulfur isotope), including blanks and random duplicates with appropriate storage conditions maintained during shipment, as directed under analytical services provided by the West Australian Biogeochemistry Centre and the ICP-MS laboratory at the Centre for Microscopy, Characterization and Analysis. Hydrogen and oxygen isotope ratios were measured using a Picarro L2130 i cavity ring down spectroscopy (CRDS) analyses. All values were normalized to the VSMOW scale using three laboratory reference waters calibrated against IAEA standards (VSMOW2, SLAP2, and GISP). Sulfur isotope compositions ($\delta^{34}S$) were reported relative to the Vienna–Canyon Diablo Troilite (V CDT) scale. Analyses were undertaken on a Sercon 20 22 isotope ratio mass spectrometer coupled with an elemental analyzer. Isotopic measurements were performed using isotope ratio mass spectrometry with analytical precision better than ±0.2‰ for $\delta^{18}O$ and ±0.3‰ for $\delta^{34}S$.

The ANOVA-Analysis of Variance and other statistical analyses for the data has been performed using JMP Pro 16.2 (Hummel *et al.*, 2021).

Result and discussion

In the initial stage of this study, $\delta^{34}S$ isotopic compositions showed strong negative correlations with Ca, K, Sb, Cd, Mo, Rb, and Sr, ranging from −0.72 to −0.95. These relationships indicate that sulfur isotope variations are tightly coupled to the geochemical behavior of redox sensitive chalcophile elements (Goldschmidt, 1937; Rollinson, 2014) as well as to the mobilization and transport of alkali and alkaline earth elements. Together, these relationships underscore the dominant role of sulfur driven processes in shaping broader geochemical system responses.

As shown in Fig. 2, mean $\delta^{18}O$ of water (‰, VSMOW) differs significantly among water types ($F(8,62) = 11.08$, $p < 0.0001$), with water type explaining approximately 59% of the total variance ($R^2 = 0.59$). This result demonstrates strong isotopic differentiation between natural waters, deep groundwater, and mining related waters. Similarly, $\delta^{18}O$ of sulfate (‰ SO_4) shows significant variation among groups ($F(8,63) = 10.38$, $p < 0.0001$, $R^2 = 0.57$), indicating that sulfate oxygen isotopes are sensitive to differences in sulfur source and formation processes across water types.

$\delta^{34}S$ (‰, VCDT) also varies significantly among water types ($F(8,63) = 9.99$, $p < 0.0001$), with type accounting for 56% of the observed variance ($R^2 = 0.56$). This statistically significant separation reflects contrasts between geogenic sulfur sources and mining influenced sulfur derived from sulfide oxidation. In contrast, sulfate concentrations (SO_4^{2-}, mg/L) do not differ significantly among water types ($F(7,60) = 1.48$, $p = 0.19$), and the proportion of variance explained by type is low ($R^2 = 0.15$). This indicates substantial within group variability and highlights the limited discriminatory power of concentration data alone. Overall, the ANOVA results demonstrate that isotopic parameters provide robust and statistically significant differentiation among water types, whereas sulfate concentrations are comparatively insensitive to source

and process variability. As shown in Fig.3, $\delta^{18}O_{water}$ values are consistently negative (approximately −6 to −11‰), reflecting meteoric water signatures, whereas $\delta^{18}O_{sulfat}$e values are positive (approximately +2 to +5‰). The vertical separation between these two bars for each group corresponds to $\Delta\delta^{18}O_{sulfate}$-$\delta^{18}O_{water}$ which is uniformly large across all sample types (approximately 11–13‰). If sulfate were derived primarily from gypsum ($CaSO_4 \times 2H_2O$) dissolution, $\delta^{18}O_{sulfate}$ would largely reflect the fixed isotopic composition of the mineral and tend toward isotopic equilibrium with ambient water over time (Taylor *et al.* 1984; Dogramaci *et al.* 2001), resulting in smaller or more variable $\Delta\delta^{18}O_{sulfate}$-$\delta^{18}O_{water}$ values, typically less than 5‰.

The coupled $\Delta\delta^{18}O_{sulfate}$-$\delta^{18}O_{water}$ relationships provide definitive evidence for sulfate generation dominated by oxidative sulfide oxidation rather than gypsum dissolution. Across all water types, large and consistent $\Delta\delta^{18}O_{sulfate}$-$\delta^{18}O_{water}$ (11–13‰) persist, indicating incorporation of atmospheric O_2 into sulfate during oxidation and sustained isotopic disequilibrium with ambient water (Taylor *et al.* 1984; Dogramaci *et al.* 2001). Gypsum dissolution is ruled out because it would yield sulfate with relatively invariant $\delta^{18}O$, smaller sulfate water difference, diagnostic Ca–SO_4 stoichiometry, and minimal linkage to redox sensitive elements (Seal, 2006; Blowes *et al.* 2014). As shown in Fig. 4, background waters (deep aquifer, bedrock, weathered bedrock, and

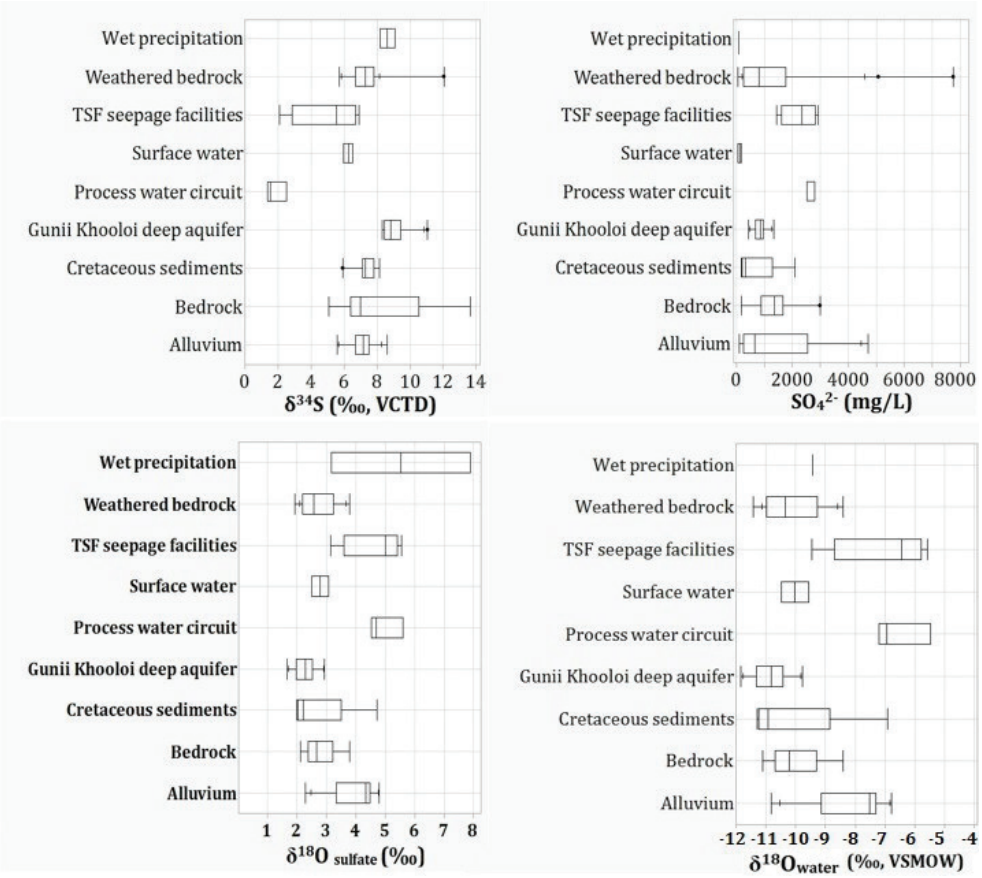

Figure 2 *Quantile box plots showing statistical distribution of $\delta^{18}O$water (‰), $\delta^{18}O$sulfate (‰), $\delta^{34}S$ (‰, VCTD), and SO_4^{2-} (mg/L) across water sources and hydrogeological units; boxes indicate the 25th–75th percentiles, the central line indicates the median, and whiskers indicate the data spread.*

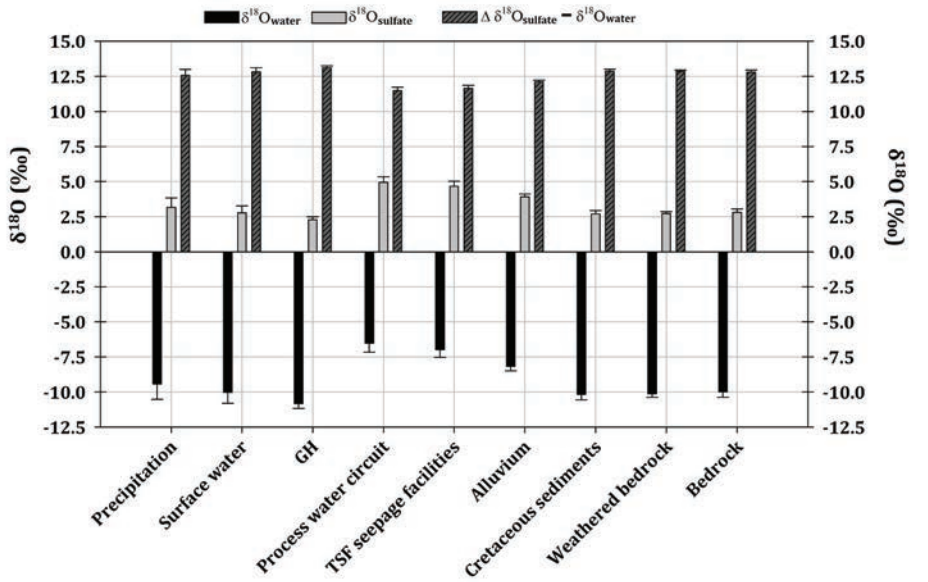

Figure 3 Mean $\delta^{18}O$ of water and $\delta^{18}O$ of sulfate, and their difference ($\Delta\delta^{18}O_{sulfate}$-$\delta^{18}O_{water}$), across water sources, process circuit water and groundwater monitoring bores of different hydrogeological units.

surface water) cluster within a relatively narrow $\delta^{34}S$ range (6–9‰) and generally at lower to moderate sulfate concentrations. These samples fall largely within the native $\delta^{34}S$ envelope, indicating minimal isotopic perturbation. In contrast, TSF seepage and process water samples plot at higher sulfate concentrations and show systematically lower $\delta^{34}S$ values, extending well below the lower limit of the native range. The strong negative trend between $\delta^{34}S$ and sulfate concentration ($\delta^{34}S = 11.2 - 0.003 \times SO_4^{2-}$, R^2adj =-0.74, p = 0.009) demonstrates that increasing sulfate is associated with progressive sulfur isotope depletion. If sulfate were derived primarily from gypsum dissolution, $\delta^{34}S$ values would remain relatively constant and constrained by the evaporite source, regardless of sulfate concentration. Instead, the observed trend reflects active sulfur redox cycling, with increasing sulfate production accompanied by isotopic fractionation during sulfide oxidation. The clear separation between background waters and process affected waters therefore indicates that mining related sulfur oxidation is the dominant control on sulfate generation in impacted zones, while natural waters retain their native sulfur isotopic signature. Most samples cluster within a $\delta^{34}S$ range of approximately 6–10‰ and $\delta^{18}O_{sulfate}$ values of 2–4‰, corresponding to background waters such as bedrock, weathered bedrock, surface water, and the Gunii Khooloi deep aquifer. In contrast, samples from the process water circuit and TSF seepage plot toward lower $\delta^{34}S$ values and higher $\delta^{18}O_{sulfate}$ values. These impacted waters define a clear inverse trend, captured by the regression $\delta^{18}O_{sulfate} = 5.66 - 0.34 \times \delta^{34}S$ (R^2adj = 0.62, p = 0.0073, n = 9), indicating that progressive sulfur isotope depletion is accompanied by enrichment in sulfate oxygen isotopes.

The observed negative relationship between $\delta^{34}S$ and $\delta^{18}O_{sulfate}$ is characteristic of oxidative sulfide weathering, where sulfate is newly generated rather than inherited from pre existing sulfate minerals. During sulfide oxidation, sulfur retains the isotopic signature of the sulfide source (often isotopically light), while sulfate oxygen incorporates a substantial proportion of oxygen from atmospheric O_2, leading to enrichment in $\delta^{18}O_{sulfat}$e. This coupled isotopic behavior cannot be explained by gypsum dissolution, which would produce relatively constant $\delta^{18}O_{sulfate}$ values largely independent of $\delta^{34}S$ and ambient water. Instead, the systematic

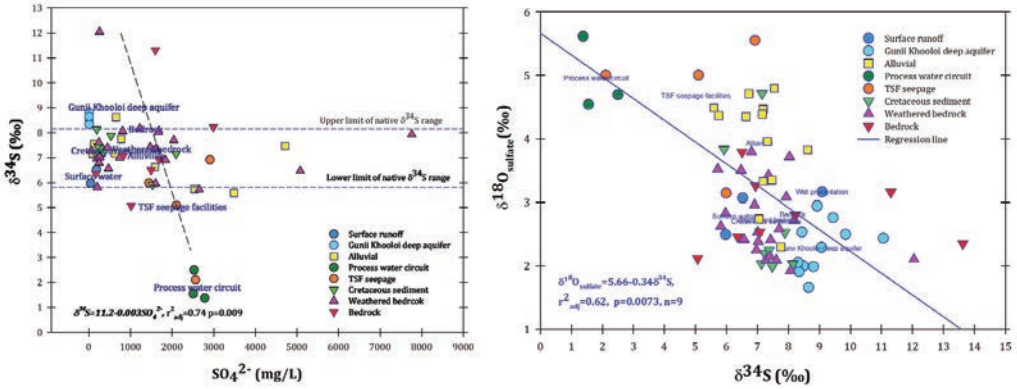

Figure 4 Relationships among variables (n = 72) for water sources, process water, and groundwater across hydrogeological units; dashed horizontal lines indicate background $\delta^{34}S$ limits, and a dashed regression line shows the $\delta^{34}S$–sulfate relationship for process-affected waters.

covariation documented in the figure demonstrates active sulfur redox cycling, with mining affected waters recording the strongest expression of oxidative sulfur processes, while background waters retain more uniform, native isotopic signatures.

The conceptual model (Fig.5) summarizes the evolution of sulfur isotopes ($\delta^{34}S$) from background waters through mining affected systems and into downgradient environment. Wet precipitation and the Gunii Khooloi deep aquifer define a narrow native $\delta^{34}S$ range (8–9‰), representing background geogenic sulfur.

In contrast, process water exhibits markedly depleted $\delta^{34}S$ values (2‰), reflecting sulfate generation dominated by oxidative sulfide weathering. As impacted waters migrate through the TSF seepage facilities, $\delta^{34}S$ values shift toward intermediate compositions (5–6‰), indicating secondary modification through evaporation, concentration, and mixing with background sulfate. Downgradient aquifers show further convergence toward native $\delta^{34}S$ values, consistent with progressive attenuation and hydrologic mixing. Overall, the isotopic evolution highlights sulfur driven redox processes as the primary control on sulfate generation in mining affected waters, with subsequent partial re equilibration during subsurface transport.

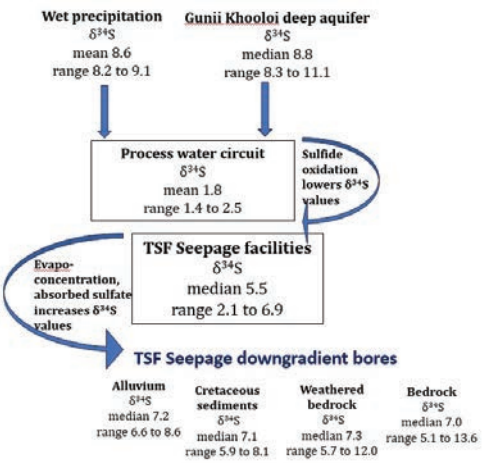

Figure 5 Summary of inputs, outputs and processes that affect $\delta^{34}S$ values. Units are ‰. Further information is provided in the text.

Conclusion

This study demonstrates that coupled sulfur and oxygen isotope systematics provide a robust framework for identifying sulfate sources and mining influences in the OT hydrogeological system. For the first time, precipitation, process water, TSF seepage, surface water, and groundwater were evaluated together using integrated $\delta^{34}S$, $\delta^{18}O_{sulfate}$, and $\delta^{18}O_{water}$ tracers. One way ANOVA shows

that isotopic compositions differ significantly among water types ($p < 0.0001$), whereas sulfate concentrations alone show limited separation. Large and consistent sulfate–water isotope offsets ($\Delta^{18}O$ =11–14‰) and negative $\delta^{34}S$–$\delta^{18}O$ relationships indicate sulfate generation dominated by open system oxidative sulfide weathering, ruling out gypsum dissolution. Mining affected waters show distinct sulfur isotopic signatures and trace element associations, confirming sulfur isotopes as effective tracers of anthropogenic influence. Overall, OT remains far from acid mine drainage conditions, with regional background processes dominating.

Acknowledgements

OT LLC funded this project. We thank Greg Skrzypek and Aleksey Sadekov for conducting the isotopic analyses, and Oyunzul Gantulga for leading the project contract and overseeing its implementation. We gratefully acknowledge the support and collaboration of the Tailings team, as well as Rio Tinto's senior hydrogeologists and geochemists, for their valuable advice, technical input, and assistance throughout the sampling campaign.

References

Puntsag T, Tulganyam S, Sededpurev O, Bazardorj S, Bayanzul B, Myagmar B, Sarangerel T, Danzan A, Natsagdorj M, Nyambuu P (2025) Water quality and potential sources in alluvial bore, downstream of the tailings storage facility, Oyu Tolgoi copper mine, Mongolia. Mine Closure 2025: Proceedings of the 18th International Conference on Mine Closure, Australian Centre for Geomechanics, doi.org/10.36487/ACG report/2515_96

Krouse HR, Mayer B (2000) Sulphur and Oxygen Isotopes in Sulphate. In: Cook, P.G., Herczeg, A.L. (eds) Environmental Tracers in Subsurface Hydrology. Springer, Boston, MA. doi.org/10.1007/978-1-4615-4557-6_7

Dold B, Spangenberg JE (2005) Sulfur speciation, and stable isotope trends of water-soluble sulfates in mine tailings profiles. Environmental science & technology 1:39(15):5650-6

Kim DM, Park HS, Hong JH, Lee JH (2022) Assessing Pilot-Scale Treatment Facilities with Steel Slag-Limestone Reactors to Remove Mn from Mine Drainage. Mine Water Environ 41(2):402–414. doi.org/10.1007/s10230-021-00819-6

Khashgerel BE, Rye RO, Hedenquist JW, Kavalieris I (2006) Geology and reconnaissance stable isotope study of the Oyu Tolgoi porphyry Cu-Au system, South Gobi, Mongolia. Economic Geology 101(3):503-22

Natali S, Franceschi L, Giannecchini R, D'Orazio M, Delgado-Huertas A, Zanchetta G, Doveri M (2025) Tracing contamination in mining areas through sulfur and oxygen isotopes in groundwater sulfates: a case study from the Apuan Alps (Italy). Environmental geochemistry and health 47(7):249

Hummel RM, Elizabeth A, Claassen RD, Wolfinger RD (2021) JMP®, SAS Institute Inc Cary, NC

Goldschmidt VM (1937) The principles of distribution of chemical elements in minerals and rocks. Journal of the Chemical Society, 655–673.

Rollinson HR (2014) Using geochemical data: evaluation, presentation, interpretation. Book, Routledge; 21

Taylor BE, Wheeler MC, Nordstrom DK (1984) Isotope composition of sulfate in acid mine drainage as a measure of bacterial oxidation. Nature 308, 538-541. doi: 10.1038/308538 a0

Dogramaci SS, Herczeg AL, Schiff S, Bone Y (2001) Controls on sulfur and oxygen isotope compositions of dissolved sulfate in aquifers of the Murray Basin, Australia. Chemical Geology, 176, 213–235.

Seal RR (2006) Sulfur isotope geochemistry of sulfide minerals. Reviews in Mineralogy and Geochemistry, 61:633–677

Blowes DW, Ptacek CJ, Jambor JL, Weisener CG, Paktunc D, Gould WD, Johnson DB (2003) The geochemistry of acid mine drainage. Environmental geochemistry, 9:149-204.

Brown MC, Wigley TC, Ford, DC (1969) Water budget studies in karst aquifers. J Hydrology 9:113–116, doi:10.1016/0022-1694(69)90018-3

Caruccio FT, Geidel G (1984) Induced alkaline recharge zones to mitigate acidic seeps. In: Groves DH, DeVere RW (Eds), 1984 Symp of Surface Mining, Hydrology, Sedimentology and Reclamation, Univ of Kentucky, p 27–36

Day TJ (1977) Field Procedures and Evaluation of a Slug Dilution Gauging Method in Mountain Streams. J Hydrol New Zealand 16(2):113–133

Gammons CH, Mulholland TP, Frandsen AK (2000) A comparison of filtered vs. unfiltered metal concentrations in treatment wetlands. Mine Water Environ 19(2):111–123, doi:10.1007/ BF02687259

IMWA 2026
Jeongseon

Inference of Green Rust Formation and Fe^{2+}/Fe^{3+} Redox Cycling in Treatment of Acid Metalliferous Drainage

Mark Roberts[1], Steven Pearce[1], Ken Grohs[2], Michael Liu[2], Azwar Satriawan[2]

[1]*Mine Environment Management, Denbigh, UK mroberts@memconsultants.co.uk*

[2]*PT Agincourt Resources, Jakarta, Indonesia*

Abstract

This paper presents field and laboratory investigations into aeration and alkaline treatment of a high-load, low-pH acid metalliferous drainage (AMD). Trials showed hydrated lime addition promoted the formation of a precipitate believed to be sulfate green rust (GR), resulting in reductive recycling of Fe^{3+} to Fe^{2+} and therefor reduced iron removal efficiency. NaOH buffering, and pre-oxidation with H_2O_2, limited GR formation but introduced operational and cost limitations. Treatment of a lower-load AMD sample exhibited no GR formation, allowing efficient lime treatment and ferric oxyhydroxide sludge generation. These findings emphasise the need to control Fe^{2+} loading and redox conditions to prevent GR-related treatment inefficiencies.

Keywords: AMD, aeration, oxidation, lime buffering, green rust

Introduction

Acid metalliferous drainage (AMD) is near-ubiquitous issue within sulfidic mining environments. If left untreated, AMD can have serious deleterious effects on local and regional receptors such as surface and groundwater quality. This in turn poses potential hazard to ecosystems and human health. To mitigate against these environmental liabilities, governing and regulatory bodies set prescriptive limits on the maximum concentrations / loads of given geochemical parameters for any waters released into local water courses from areas of mining operations. As global mining output increases to accommodate consumer demand, effective and economically sustainable AMD treatment solutions are essential to mitigate these effects and ensure regulatory compliance.

A range of active and passive treatment technologies have been developed to treat AMD, with chemical neutralisation using alkaline reagents such as hydrated lime remaining one of the most widely applied methods. However, active treatment via chemical addition can be costly, energy intensive, and generate large volumes of metalliferous sludge requiring safe disposal. Consequently, there is increasing emphasis on treatment optimisation techniques that reduce reagent consumption and lower operational costs. Aeration is one such optimisation strategy that plays a critical supporting role in many mine water treatment systems. Aeration aims to increase the concentration of dissolved oxygen (DO) within AMD whilst simultaneously degassing dissolved CO_2. By increasing the DO within the system, the oxidation of highly soluble ferrous iron (Fe^{2+}) to lower solubility ferric iron (Fe^{3+}) is accelerated. This allows the precipitation of iron at lower pH (approximately pH 4-5) and in turn reduces lime requirements.

This paper presents a case study into the use of active aeration and alkaline chemical treatment to treat a high load, low pH AMD. Due to the high manganese content of the AMD requiring treatment at the case study site, pH buffering to ≈pH 10 was required to facilitate its precipitation and removal from the aqueous phase. In an effort to avoid a high volume hazardous sludge, comprising iron oxyhydroxides, gypsum and metal hydroxides, a treatment system was developed that would generated two distinct waste sludges; 1) a high volume iron-rich relatively "clean" sludge with potential re-use applications as a sorption media elsewhere on site and 2) a low volume gypsum and metal

hydroxide (e.g. Mn) sludge for disposal as hazardous waste.

This paper will discuss observations of the formation of suspected green rust minerals during treatment and the resultant effect on system efficacy. Green rusts (GR) are a group of mixed-valence iron oxyhydroxide minerals, with a layered double hydroxide structure, that are typically meta-stable with limited stability in acidic conditions. GR typically occurs under reducing, circumneutral pH conditions where both Fe^{2+} and Fe^{3+} are present (Génin *et al.* 1998). There are numerous variants of GR but "Green Rust 2" is of particular interest in AMD settings. Within this variant, sulfate is intercalated between the positively charged iron-hydroxide sheets providing greater stability. It has also been shown to exchange and/or reduce some groundwater contaminants such as U (Latta *et al.* 2015), Se (Refait *et al.* 2000) and Cr^{6+} (Thomas *et al.* 2018) leading to their use to aid AMD remediation (Bearcock *et al.* 2011).

Methods and Materials

Testing comprised field trials of a prospective aeration-lime dosing AMD treatment system and associated laboratory scale tests. In both cases testing was performed on a low pH, high load AMD referred to henceforth as "Sample 1". A summary of the key geochemical properties of "Sample 1" is displayed in Table 1. "Sample 1" was collected after the target AMD had been passed through the venturi pump used to provide aeration within the field trial system. As such the estimation of Chemical Oxygen Demand (COD) should be conservative as oxidation provided by the venturi will have resulted in some Fe^{2+} oxidising to Fe^{3+}. A subsequent sample was acquired in the same manner 4 days after "Sample 1". Termed "Sample 1b", this represents the same source AMD after dilution by rainfall to loads more reflective of levels typically encountered at the case study site.

The field trials for AMD treatment consisted of initial runs of a bespoke designed in-line treatment system. This treatment system consists of a venturi pump to provide aeration (and oxidation) of the AMD, a dosing pump providing 20% (w/w) hydrated lime slurry prior to an in-line mixer all in series. This then outputted into a settling pond. The flow rate of AMD through the system and rate of hydrated lime dosing rates were continuously monitored with in-situ flowmeters. Measurement of pH and ORP was performed on "grab samples" acquired from the output of the in-line mixer. Samples for laboratory testing were collected in 10 L HDPE buckets with sealed lids. When collecting samples, headspace was kept to a minimum within the buckets to mitigated against potential further oxidation of samples. Prior to sealing the sample in buckets, pH and ORP was recorded. These were then verified when received at the laboratory for testing.

Laboratory bench scale testing was performed within laboratory facilities on the mine site to mitigate against sample oxidation / degradation due to excessive transportation times and the lack of suitable preservation techniques for met-stable minerals such as the suspected GR. Lab testing consisted of beaker trials performed within borosilicate glassware placed on a magnetic stirrer plate with PTFE stirrer beads to facilitate effective mixing. Sample volumes were measured gravimetrically on a balance accurate to ±0.1 g. Volumes used during titrations varied from 200 mL to 50 mL due to equipment limitations at the on-site field laboratory and due to sequential nature of testing requiring

Table 1 *Basic characterisation of "Sample 1" and "Sample 1b" AMD.*

ID	pH	ORP	Electrical Conductivity	Al	Cu	Fe	Mn	Acidity	Chemical Oxygen Demand*
		mV	mS/cm	mg/L	mg/L	mg/L	mg/L	mg/L	mg/L
Sample 1	2.30	878	8.31	198	67.4	1550	10.2	1790	225
Sample 1b	2.40	957	3.98	90.7	25.3	461	7.00	399	68.1

*Chemical Oxygen Demand calculated assuming all Fe and Mn are present in respective reduced forms

aliquots to be taken for analysis. Titrations were performed with both hydrated lime and sodium hydroxide (also referred to as "caustic"). In both cases LR grade reagents (Merck) were used to produce titrants. The hydrated lime was utilised as a 20% (w/v) slurry mixed with 18.2 MΩ deionised water. The mass of lime required was measured to 4 d.p. with a calibrated balance accurate to ±0.0001 g. When titrating with hydrated lime, the slurry was kept well mixed via the use of a magnetic stirrer and PTFE bead. The slurry was added incrementally through the use of calibrated digital pipettors. In an effort to ensure all lime was removed from the pipettor tip, small volumes of the sample were taken into the pipettor tip to rinse lime slurry out. Pipettor tips were then discarded to prevent contamination of the lime slurry reservoir.

NaOH was utilised at a concentration of 0.5 M. This was also produced with 18.2 MΩ deionised water, with the required volume of NaOH measured volumetrically using calibrated digital pipettors. NaOH was introduced to the sample via titration from a Grade A glassware burette. Where hydrogen peroxide (H_2O_2) was used to enhance oxidation of Fe^{2+}, 30% LR grade H_2O_2 was used. Volumes required are reported as 60% H_2O_2 equivalent to be reflective of industrial grades likely to be used in potential site trials.

After the pH was adjusted to the required pH, the sample was left to stir to ensure a stable pH (consistent pH reading ±0.2 pH units over 5 minute period). The resulting precipitate was removed via vacuum filtration through 0.45 µm mixed cellulose filters before being dried at 105 °C for 24 hours. An aliquot of filtrate was taken for subsequent elemental analysis by Atomic Absorption Spectroscopy at on-site Intertek® laboratory. The remnant filtrate was then, if necessary for further investigation, subjected to further pH adjustment as described above.

Results & Discussion

The initial run of the aeration treatment system field trial aimed to assess the efficacy of aeration (via venturi) with lime addition at removing metal load when the pH was raised to approximately 4.5. The system was run at 30 PSI, equating to a flow of ≈8.4 m3/h with 20% (w/v) hydrated lime at a rate of 1.18 m^3/h to raise the pH to 4.5. A distinct colour change was observed in the AMD. Rather than

Figure 1 *Green-blue colouration within treated "Sample 1" AMD, dosed with hydrated lime to pH 4.5.*

the anticipated orange brown colouration typical of iron oxyhydroxides, the AMD was observed to turn a dark blue-green colour as seen in Figure 1. Subsequent testing within the laboratory showed that when oxidised / dried the green colour changed to an orange colour typical of ferric oxyhydroxides. This was interpreted as indicative that the green colouration was due to the presence of meta-stable green rust type minerals.

The Oxidation Reduction Potential (ORP) of the AMD was observed to decrease sharply with the addition of hydrated lime. Dropping from ≈900 mV post venturi pump to ≈100 mV post lime addition. This is a result of the increased pH and subsequent shift in redox equilibria causing precipitation of ferric iron from solution, thereby removing an oxidant and contributing to lowering the ORP. Given the use of a Ag/AgCl ORP probe this equates to an Eh of ≈300 mV. The pH of the treated AMD was checked after 30 minutes and observed to have decreased to pH 3.98 from pH 4.5 suggesting either further oxidation of ferrous iron or, potentially, the reduction of ferric iron. Analysis of the AMD showed dissolved Fe concentrations had decreased from 1550 mg/L to 661 mg/L, orders of magnitude in excess of release limits (5 mg/L), and suggesting that there is still an abundance of Fe^{2+} which is contributing to the formation of suspected GR in the treated AMD. When these conditions are plotted on a Pourbaix diagram for green rust 2 and iron oxyhydroxides (Figure 2) where Fe^{2+} activity is approximately -2 we observe that whilst Fe^{2+} is stable in solution the presence of GR is not predicted as a stable phase. Despite this, observations imply that a GR-like phase may form reflecting kinetic limitations not fully captured by the diagram.

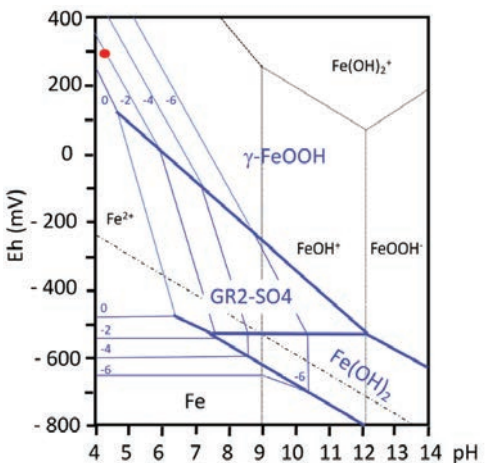

Figure 2 *Pourbaix diagram for synthetic sulfate green rust (GR2-SO4) calcualted with sulfate activity of 0.1. thin lines labelled "-n" denote Fe^{2+} activity of 10-n. Red dot represents post lime "Sample 1". Amended from Trolard* et al. *(2022).*

Beaker tests on "Sample 1" with lime addition to simulate the field trial yielded similar results to the field trial with >700 mg/L Fe remaining in solution at pH 4.3. Green colouration (interpreted as GR) was observed as in the field trials. ORP across these tests was observed to decrease as pH increased from an initial ≈460 mV to ≈170 mV after buffering, again similar to the field trial results. Addition of 30% H_2O_2 to oxidise the suspected GR and raise the ORP of the solution proved ineffective with no substantive change in dissolved Fe observed. As shown in Figure 3, the addition of H_2O_2 resulted in a rapid change in colour from blue-green to brown. However, subsequent mixing resulted in the sample returning to blue-green within a matter of seconds. This trend continued even with H_2O_2 being added in excess of 40 times calculated COD requirements. It is known that GR have the capability to reduce ferric iron back to ferrous iron (Usman *et al.* 2012). Observations of hydrated lime armoured by suspected green rust (Figure 3) lead the authors to believe that the localised high pH around the lime, in conjunction with ORP decreases from Fe^{3+} precipitation and the presence of nucleation sites for mineral formation, is resulting in higher stability for GR which are subsequently reducing Fe^{3+}. Given the high sulfate environment, the formation of gypsum within these localised high pH zones could theoretically also promote sulfate GR formation by providing further nucleation sites and a dynamic sulfate reservoir that buffers local sulfate activity, sustaining supply required for sulfate green rust formation. Testing with H_2O_2 addition prior to lime also yielded negligible improvement in Fe removal (Figure 4).

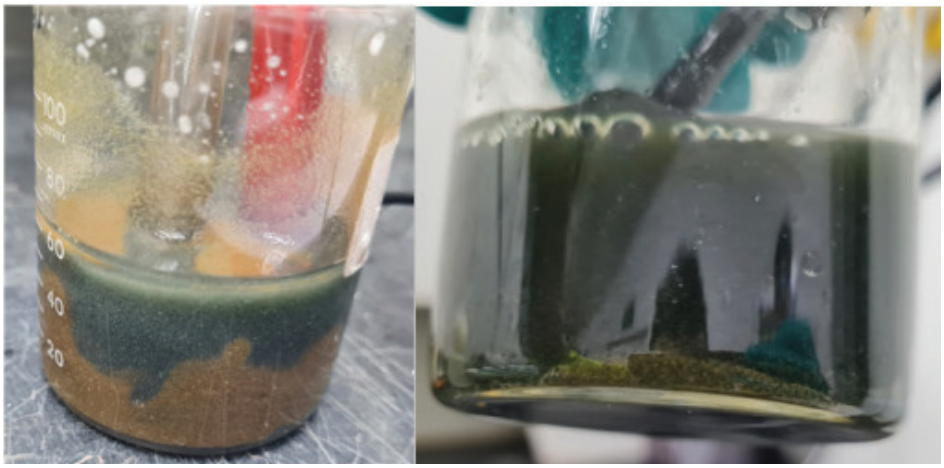

Figure 3 *"Sample 1" buffered to pH 4.3 with hydrated lime and subsequent addition of 30% H2O2 (left) and hydrated lime coated with green rust (right).*

To assess this hypothesis, hydrated lime was replaced with NaOH to buffer "Sample 1" to the desired pH. The addition of NaOH to the AMD resulted in no observable GR, supporting the hypothesis that lime addition caused the formation of suspected GR in the sample. A resulting dissolved Fe concentration of 630 mg/L demonstrates that high concentrations of soluble Fe (likely Fe^{2+}) still exist within the AMD. This again supports the assertion that the addition of lime is the causal factor to suspected GR formation rather than the presence of Fe^{2+} alone. When NaOH was utilised to buffer an aliquot of "Sample 1" that had undergone pre-treatment with the equivalent of 1 L/m³ 60% H_2O_2, a substantially lower dissolved Fe concentration was achieved (16 mg/L). This demonstrates that initial addition of H_2O_2 does result in lower Fe^{2+} concentration and that the elevated Fe observed when hydrated lime is later added is the result of suspected GR generating Fe^{2+} from the reduction of Fe^{3+} in solution. This is indicative that the formation of the suspected GR minerals introduces notable inefficiency for lime use and effectively renders H_2O_2 use as redundant.

Whilst the use of NaOH in place of hydrated lime, or the addition of high volumes of H_2O_2 have been shown to be effective, they are relatively high-cost solutions. Other methods to mitigate effects of suspected GR generation including buffering to higher pH and reducing the initial Fe^{2+} concentration to levels were also explored. Whilst buffering to pH 5 with hydrated lime yielded substantial reductions in dissolved Fe (<1 mg/L) it required a ≈30% increase in lime dosing. The resultant GR sludge is also then unstable. As the GR breaks down to form ferric oxyhydroxides, latent acidity is released potentially resulting in acid generation from the GR sludge (Legrand *et al.* 2004). This makes all forms of GR sludge unfavourable from a long-term storage viewpoint.

Given that "Sample 1" was known to represent an extreme "worst case" scenario, testing was re-run on a newer sample from the same source, post rainfall. As shown in Table 1, this "Sample 1b" had far lower Fe load and therefor COD requirements. As such when this was passed through the field trial treatment system a greater proportion of the Fe^{2+} was seemingly oxidised as no green rust was observed after the introduction of hydrated lime. In contrast to previous treatments with hydrated lime, in the absence of GR buffering to ≈pH 4.3 resulted in dissolved Fe concentrations of ≈60 mg/L. This represents an 87% reduction in with no additional oxidation via H_2O_2 required. This was comparable to the Fe removal efficiency resulting from buffering with NaOH (data

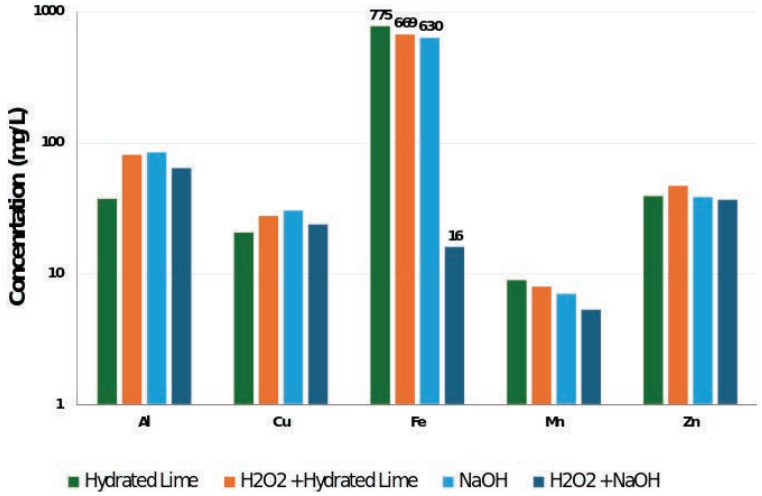

Figure 4 *Concentrations of selected analytes in "Sample 1" AMD buffered to pH 4.3 with hydrated lime and NaOH both with and without pre-treatment with 1 L/m³ 60% H_2O_2 (equiv.) and. Note: logarithmic Y axis.*

not shown) and, crucially, generated a ferric oxyhydroxide sludge which is considered less reactive from a waste disposal viewpoint. When additional oxidation was provided via the equivalent of 0.1 L/m³ 60% H_2O_2, dissolved Fe concentrations were seen to decrease to 6.6 mg/L and 0.7 mg/L with hydrated lime and NaOH respectively (data not shown). These represent Fe reductions of 99.6% and 99.8% respectively. Whilst these are impressive values, cost benefit analysis would have to be performed to assess whether it is necessary to reduce Fe to this level in the first stage or whether to accept relatively minor Fe being included in the planned secondary lower volume, gypsum & Mn oxide sludge.

Conclusions

The findings from both field trials and laboratory testing demonstrate that the formation of a suspected GR type mineral during hydrated lime treatment of high-load, low-pH AMD can hinder iron removal efficiency. It is suggested that the introduction of hydrated lime promotes localised conditions conducive to sulfate GR formation, which subsequently reduces ferric iron back to ferrous iron, counteracting oxidation efforts and limiting treatment performance. The resulting GR sludge is known to have potential for acid generation making disposal more problematic.

Alternative approaches – such as substituting lime with NaOH or implementing pre-oxidation with H_2O_2 – proved effective but come with economic and/or operational consideration. Crucially, tests on the lower load "Sample 1b" showed that when initial ferrous iron loads were consumed efficiently via the venturi pump, GR formation was avoided and hydrated lime treatment performed far more efficiently, producing a more stable ferric oxyhydroxide sludge precluding the requirements for more costly reagents like NaOH and H_2O_2.

These outcomes highlight the importance of monitoring and understanding the changing AMD characteristics on site, particularly Fe^{2+} loading and oxidation state, to optimise aeration–alkaline treatment systems and minimise the risk of undesirable GR generation. It is noted that the GR mineral phase has not been directly confirmed (e.g. by XRD, and its identification as GR is therefore based on indirect evidence. Future work intends to address this uncertainty.

Acknowledgements

The authors would like to acknowledge the diligent work of PT Agincourt Resources® MSDSE and Metallurgy teams in the commissioning and operating of the field

trial system and their support within the laboratory. Additionally, acknowledgement is made to the Intertek® laboratory team for their support with elemental analysis.

References

Bearcock, J.M., Perkins, W.T., Dinelli, E. and Wade, S.C. (2011) The use of green rust for the treatment of contaminated mine waters. British Geological Survey Internal Report, IR/11/004. Nottingham: BGS.

Génin, J.M.R., Bourrié, G., Trolard, F., Abdelmoula, M., Jaffrezic, A., Refait, P., Maitre, V., Humbert, B. and Herbillon, A. (1998) 'Thermodynamic equilibria in aqueous suspensions of synthetic and natural FeII–FeIII green rusts: occurrences of the mineral in hydromorphic soils', Environmental Science & Technology, 32(8), pp. 1058–1068. doi: 10.1021/es970547m.

Latta, D., Boyanov, M., Kemner, K., O'Loughlin, E. and Scherer, M. (2015) 'Reaction of uranium(VI) with green rusts: effect of interlayer anion', Current Inorganic Chemistry, 5(3), pp. 156–168.

Legrand, L., Abdelmoula, M., Géhin, A., Fowler, A. and Génin, J.M.R. (2004) 'The oxidation of carbonate green rust into ferric phases: solid-state reaction or transformation via solution', Geochimica et Cosmochimica Acta, 68(17), pp. 3497–3507. doi: 10.1016/j.gca.2004.04.010.

Refait, P., Simon, L. and Génin, J.M.R. (2000) 'Reduction of SeO42- anions and anoxic formation of iron(II)–Iron(III) hydroxy-selenate green rust', Environmental Science & Technology, 34(5), pp. 819–825.

Thomas, A., Eiche, E., Göttlicher, J., Steininger, R., Benning, L., Freeman, H., Diderikson, K. and Neumann, T. (2018) 'Products of hexavalent chromium reduction by green rust sodium sulfate and associated reaction mechanisms', Soil Systems, 2(4), p. 58. doi: 10.3390/soilsystems2040058.

Trolard, F., Bourrié, G., Duval, S., Refait, P. and Feder, F. (2022) 'Mineralogy, geochemistry and occurrences of fougerite in a modern hydrothermal system and its implications for the origin of life', Earth-Science Reviews, 225, p. 103910. doi: 10.1016/j.earscirev.2021.103910.

Usman, M., Hanna, K., Abdelmoula, M., Zegeye, A., Faure, P. and Ruby, C. (2012) 'Formation of green rust via mineralogical transformation of ferric oxides (ferrihydrite, goethite and hematite)', Applied Clay Science, 64, pp. 38–43. doi: 10.1016/j.clay.2011.11.006.

IMWA 2026
Jeongseon

Pit Lake Water Balance Modelling – Detail Matters

Pierre Rousseau[1], Ignacio Vernengo Lezica[2], Zip Boniecki[1],
Steven Murton[2], Marilena Stimpfl[3]

[1]*SRK Consulting (Australasia), Level 3, 18 - 32 Parliament Place, West Perth, 6002, Western Australia, prousseau@srk.com.au, ORCID 0009-0006-4651-3356, zboniecki@srk.com.au*

[2]*SRK Consulting (Australasia), Level 5, 200 Mary Street, Brisbane, Queensland, 4000, Australia, ivernengo@srk.com.au, smurton@srk.com.au*

[3]*BHP Limited, Level 30 125 St Georges Terrace, Perth, Western Australia, 6000, Western Australia, marilena.stimpfl@bhp.com*

Abstract

The influence of in-pit tailings deposition, long term salinisation and potential wind sheltering were assessed for a pit lake water balance.

Tailings slurry water content had a major influence. At 42% water content it was similar to surface water and groundwater inflow rates but at 80% water content it was about 5 times higher.

For scenarios with and without salinity and wind sheltering corrections, pit lake water levels varied by 3m to 22.5m, depending on pit morphology. Steeper slopes result in greater variability.

The work shows that operational, morphological, geotechnical and geochemical factors can have a substantial effect on outcomes.

Keywords: IMWA 2026, pit lake salinity, pit lake water balance, pit lake modelling

Introduction

SRK Consulting (Australasia) Pty Ltd was appointed to review an existing closure model for a mine pit lake, constructed in GoldSim™ software, and to construct a revised version that included in-pit tailings deposition. Additionally, an operational water balance was to be constructed, to assess the effect of in-pit tailings deposition on the operational water balance. The objective of the models was to evaluate the probability of discharge from the pit to the surrounding environment, including groundwater, if the water balance simulated water levels to exceed the pit lake flow-through level, which was obtained from the MODFLOW groundwater model for the site.

During the review process it was identified that the evaporation rate used in the original closure water balance was excessive. This was based on the use of an A-pan correction factor of 0.8 (typically a factor of 0.7 is used for fresh water). It was also identified that local groundwater was saline (>10,000 mg/L TDS), which was expected to result in a highly saline pit lake over time, due to evaporative concentration in an environment with high net evaporation. It was considered that this would result in suppression of evaporation, known to occur at high salinity concentrations (Salhotra *et al.* 2007, McJannet *et al.* 2019).

Several factors are known to influence evaporation rates in mine pit lakes, including solar shading, wind sheltering and salinity effects (McJannet *et al.* 2017, McJannet *et al.* 2019). These effects can vary widely between different mines due to pit morphology, surrounding topography, their location (latitude) and the local water balance and groundwater quality.

Methods

Salinity corrections

The existing GoldSim™ closure mine water balance model for the operation was used as a basis for constructing both an updated closure model, as well as for a separate operational model that required major modifications.

Both models were updated to include a module to calculate evaporation suppression based on salinity, specified as TDS in mg/L. This was done using the equation of Panin and Brezgunov (2007), in accordance with McJannet, *et al.* (2019). The equation was checked against other publications to evaluate its accuracy and it was found to agree satisfactorily (Salhotra *et al.*, 1987). Although evaporation suppression is affected by the ionic composition of salinity (Abdelrady, 2013), it was found that the equation was adequate to assess the effect of salinity on evaporation compared with other publications.

$$E_S = E_0 \, (0.75 + 0.25 \times e^{-0.65S\%}) \qquad (1)$$

where E_S is the evaporation rate from a saline water surface, E_0 is the evaporation rate from a freshwater surface, e is the constant 2.718 and S is the salinity in percent.

Additionally, an allowance of up to a 20% reduction in the evaporation rate, due to wind (and solar) sheltering, was also included, which was considered sufficiently conservative in the absence of a detailed wind and solar sheltering model.

Tailings deposition

The inclusion of in-pit tailings deposition for the closure water balance was limited to revising the pit lake stage-storage curve from the pit shell to the modelled tailings deposition surface (and closure pit shell above the tailings surface). This update was required in order to correctly account for the change in available water storage capacity of the pit and the change in pit lake surface area associated with the sloped tailings surface. The model was run on a daily time-step to align with daily weather data. Weather data icorporated CMIP5 Access1-0Q RCP4.5 and RCP 8.5 climate change scenarios that were carried over from the existing pit lake water quality model.

For the operational water balance, the change in water and solid volume in the pit was modelled on a daily time-step. This was required to assess the influence on the pit water storage volume and the associated pit lake water level, as well as to align with daily weather data. Weather data was updated to CMIP6 SSP 2.6, SSP 4.5 and SSP7.0 corrected daily data. Pump dewatering, at the specified pumping capacity of the dewatering system, was also included as an option. This element was used to check the duty cycle of the pumping system and to determine its capacity and the required pumping duration to remove excess water after large rainfall events.

Discussion

Salinity corrections and wind sheltering

The inclusion of detailed tracking of salinity evolution and the tailings water and solids balance provided useful insight into their influence on the water balance.

It was found that inclusion of wind sheltering and salinity in the evaporation calculation resulted in an effective A-pan correction factor to between 0.50 and 0.58 for the base case (no in-pit tailings deposition). This assessment was based on an initial correction for an open water body of between 0.7 and 0.8, maximum salinity correction of 0.9 (over the modelled period to 2400) and a wind sheltering correction of 0.8 (an assumed conservative value). With in-pit tailings deposition, salinity increases much quicker due to a lower in-pit water volume, reaching a salinity of >250,000 mg/L by 2400 and an evaporation reduction factor of 21%. Over the modelled period, average salinity changes from around 10,000 mg/L to >250,000 mg/L for this case, through evaporative concentration (Fig. 1). Over the very long term, salinity would be expected to continue increasing at the study site, due to relatively high magnesium concentrations in local groundwater. Magnesium salts are known to be highly soluble relative to NaCl salinity, thereby resulting in higher salinity than solutions where salinity is controlled by salt precipitation, e.g. Na^+ and Cl^- forms halite. The evaporation rates (E*s*) may be reduced by more than 20% relative to fresh water if salinity exceeds about 250,000 mg/L, potentially resulting in a pan correction factor of as low as about 0.45 (assuming a 0.2 wind sheltering factor). Evaporation reduction over the modelled period is shown in Fig. 2. The salinity correction factor as modelled is shown in Fig. 3 and versus salinity according to Panin & Brezgunov (2007) in Fig. 4.

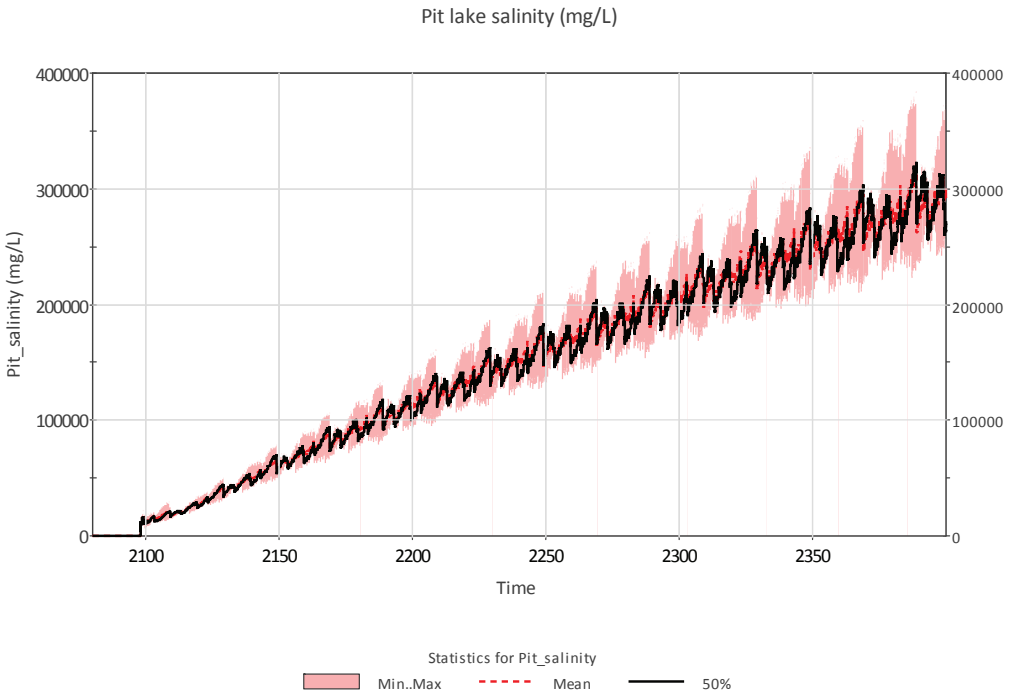

Figure 1 Pit lake salinity evolution over the modelled period to year 2399.

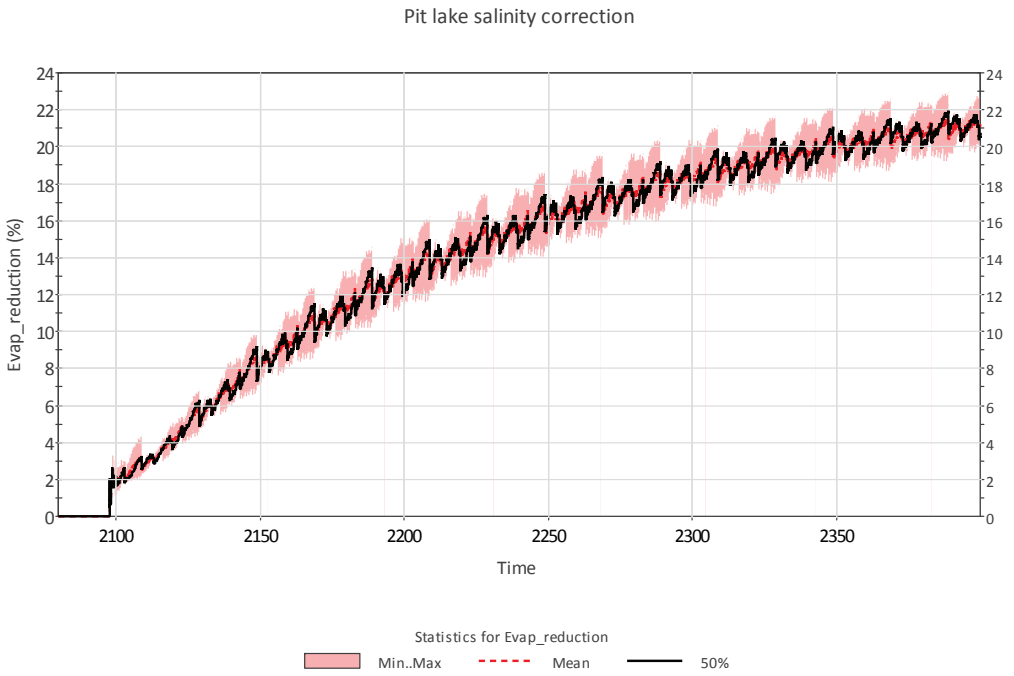

Figure 2 Reduction in the evaporation rate with increasing salinity, as a fraction relative to fresh water by year.

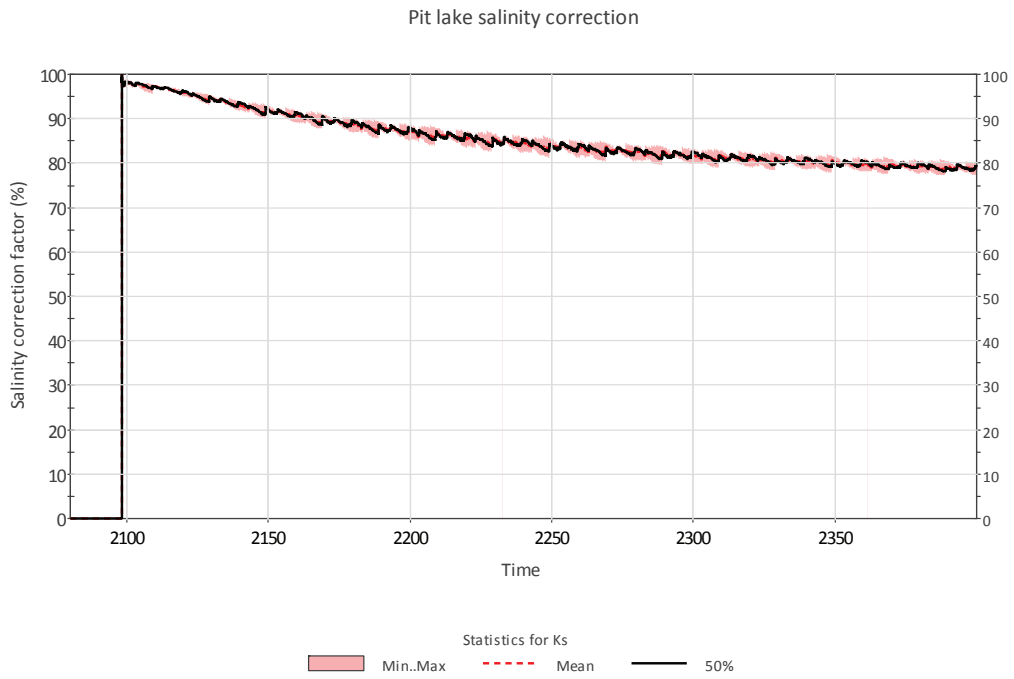

Figure 3 Evaporation rate relative to fresh water, as a result of salinity correction, over the modelled period.

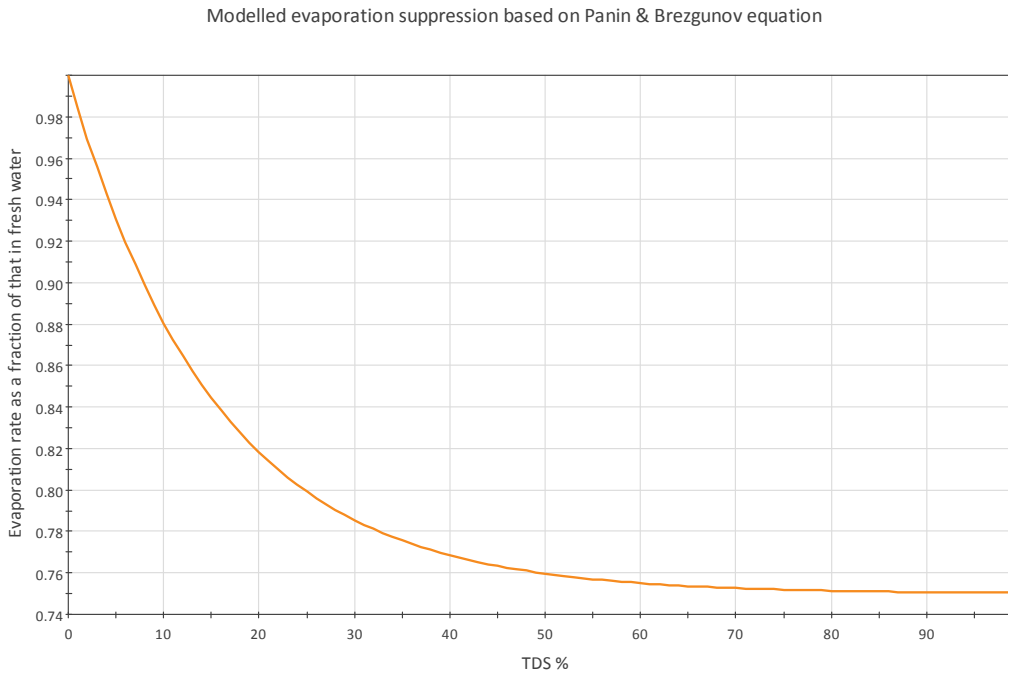

Figure 4 Correction factor vs salinity based on Panin & Brezgunov (2007), as a function of total dissolved solids, in weight %.

When including the adjusted evaporation factors in model calculations, the morphology of the pit was found to be an important influence on the outcome. Pits with relatively flat slopes (about 15° on average) were not affected by dramatic changes in pit lake elevation, with a change of only 3m calculated for the closure model. In a pit with steep slopes (about 35° on average), a change of up to 22.5m in the pit lake elevation was calculated. This is attributed to flat slopes resulting in large changes in evaporative surface area with small changes in water elevation, whereas the opposite is true for steep slopes. Factors such as surface water catchments and groundwater inflow rates versus pit lake elevation must also be taken into account to calculate the pit lake water level, hence it is not possible to generalise the extent of these impacts.

In-pit tailings disposal

Modelling of in-pit tailings disposal showed that accurate representation of the elevation – volume stage curve can be an important factor in calculating the water balance, particularly post closure when dewatering has ceased.

In the case of the project under discussion, a single-point discharge was specified for tailings disposal. This would create a sloping tailings surface, with a sump (decant pond) on the opposite end of the pit from the discharge point. An initial calculation was done assuming a flat tailings surface at the approximate crest height of the tailings. It was found that spills (overtopping) would occur from the pit during large rainfall events, due to limited water storage capacity above the tailings. The model was adjusted to include the modelled tailings surface, as used in deposition modelling for estimation of total tailings storage. The model results indicated that the sloping tailings surface would create sufficient additional storage to hold a probable maximum precipitation event within the pit, without creating spill events. This was complemented by an evaporative surface that remained active below the tailings crest as the water receded. On a flat tailings surface evaporation would effectively cease, or would be much lower than from open water, once the pit lake water level intercepts it, as tailings would be exposed over the whole area.

For the operational phase, a flat tailings surface was modelled, but to a lower elevation to accommodate an equivalent quantity of tailings to the final tailings surface. This was done to estimate the effect of tailings deposition on the water balance, in particular the probability of creating spills from the pit and to evaluate pumping requirements. Simulations were run using 58% solids content (42% water content) and 20% to 40% (60% to 80% water content) for the tailings stream to be deposited. It was found that the change in solid content of the tailings made a major difference to the overall pit water balance. For the higher solid content, free water (defined as total water minus entrained water trapped in deposited tailings) was of a similar magnitude to groundwater and surface water inflows. For the lower solid content, free water generated was about 5 times higher on average. With the higher solid content, only 5% to 10% of maximum pumping capacity would be required, reducing to virtually zero at mine closure due to evaporative losses. For the low solid content scenario, pump utilisation was generally between 30% and 35% of maximum capacity, reducing to a mean of about 10% at closure (see Figs. 5 and 6).

Conclusions

The results of the GoldSim water balance model showed that oversimplification of the modelled scenario had major effects on the simulated results. Where groundwater inflowing to a pit lake is highly saline, there is the potential for significant reduction of the pit lake evaporation rate in the long term. This can result in an evaporative sink becoming a flow-through system due to reduced water losses. The potential for wind and solar sheltering to reduce the evaporation rate should also be considered in modelling, particularly for deep pits and those with north-south orientation, as these factors would also impact on evaporation rates.

Where in-pit tailings disposal is practiced, a sloped tailings surface may have an important influence on the long-term pit lake water balance, due to increased storage and evaporation relative to a flat surface.

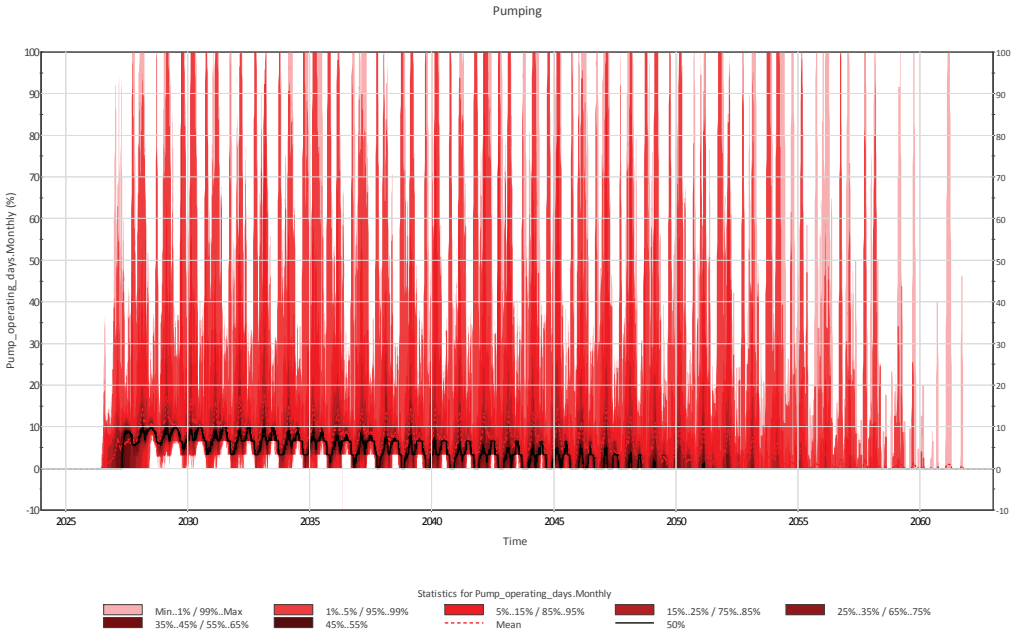

Figure 5 *Modelled pumping requirements with 58% solids.*

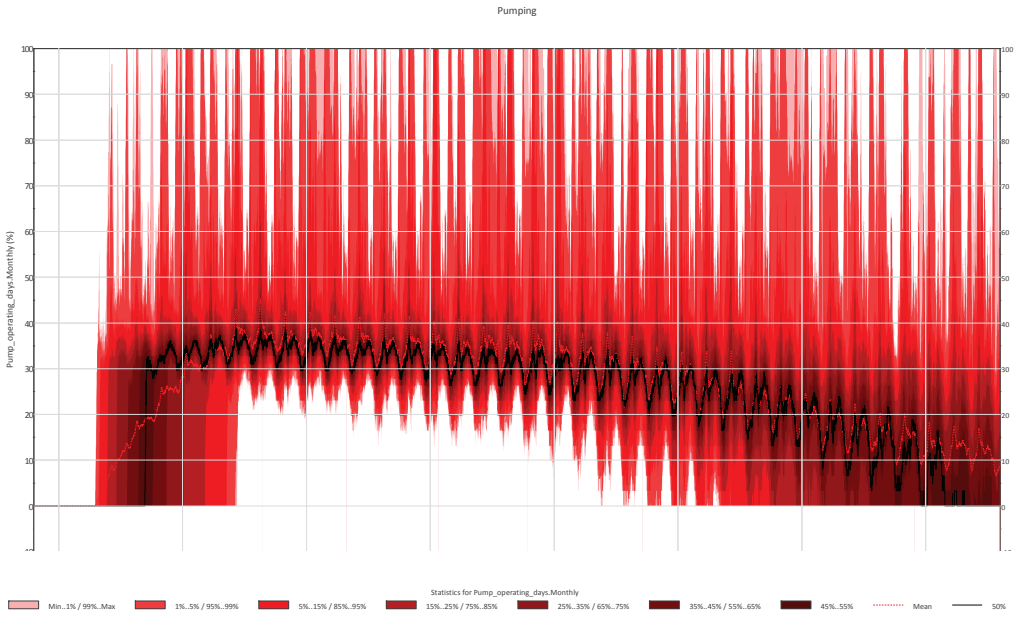

Figure 6 *Modelled pumping requirements for 20% to 40% solids.*

Acknowledgements

The authors thank SRK Consulting (Australasia) for their support in presenting this paper and also colleagues who assisted us.

References

Abdelrady AR, (2013) Evaporation over fresh and saline water using SEBS. M.Sc. thesis, University of Twente.

McJannet D, Hawdon A, van Niel T, Boadle D, Baker B, Trefry M, Rea I (2017) Measurements of evaporation from a mine void lake and testing of modelling approaches, Journal of Hydrology, Vol 555, pp 631-647.

McJannet D, Hawdon A, Baker B, Ahwang K, Gallant J, Henderson S, Hocking A (2019) Evaporation from coal mine pit lakes: measurements and modelling. Mine Closure Conference Proceedings, Perth, Australia, Australian Centre for Geomechanics, pp. 1391 - 1404.

Panin GN, Brezgunov VS, (2007) Influence of the Salinity of Water on Its Evaporation. Izvistiya, Atmospheric and Oceanic Physics, pp. Vol. 43, No. 5, pp 663-665.

Salhotra AM, Adams EE, Harleman RF, (1987) The Alpha, Beta, Gamma of Evaporation from Saline Water Bodies. Water Resources Research, Vol 23, No 9, pp1769-1774.

IMWA 2026
Jeongseon

A Quantitative ESG-Based Framework for Evaluating Tailings Reprocessing and Resource Recovery

Abeer Sajid[1], Seyed Mostafa Taghavi[1], Moeen Hamedi[1],
Hernán Anticoi[1], Marc Bascompta[1]

[1]*Department of Mining, Industrial and ICT Engineering,*
Universitat Politècnica de Catalunya (UPC) – Barcelona Tech, 08242, Spain

Abstract

Mine tailings pose environmental risks but also offer a secondary source of critical raw materials for the energy transition. Conventional tailings reprocessing assessments focus mainly on metal recovery, often overlooking environmental, social, and governance (ESG) considerations. This study presents a quantitative ESG-based framework that integrates measurable indicators within the Analytic Hierarchy Process (AHP) to generate a Composite ESG Index for systematic project evaluation. The primary contribution is the framework itself: a quantitative, AHP-weighted ESG evaluation structure with geometric aggregation preventing compensatory masking of critical failures, anchored scoring rubrics for social and governance indicators, and a recalibration protocol enabling jurisdictional transfer. An illustrative application using secondary data from Chilean tailings operations demonstrates that water protection, carbon emission reduction, and energy demand receive high priority under Chilean mining conditions.

Keywords: Critical raw materials, analytic hierarchy process, indicator weighting, mine waste management, composite sustainability index

Introduction

The global mining industry faces a dual challenge of addressing the environmental legacy of past operations while meeting the rising demand for critical materials essential for the energy transition (Kursunoglu, 2025). Mine tailings present persistent risks, including catastrophic dam failures such as those at Mount Polley (2014), Fundão (2015) and Brumadinho (2019) resulted in loss of life, extensive environmental damage, and long-term disruptions to communities (Samadi *et al.*, 2025). Beyond structural instabilities, tailings are major sources of acid mine drainage and long-term land degradation, leading to widespread contamination of ecosystems and posing serious threats to human health (Araya *et al.*, 2020).

These environmental and social consequences emphasize the need for more integrated management approaches that move beyond risk mitigation toward responsible and sustainable resource recovery. At the same time, declining global primary ore grades are reshaping resource strategies. Historical mine tailings often contain higher concentrations of valuable metals than many newly exploited deposits, positioning tailings reprocessing as both a remediation strategy and a strategic resource opportunity (Alajoki *et al.*, 2024). This dual role, risk reduction and resource recovery, demands a more systematic and sustainability-oriented evaluation framework.

Despite progress in mining sustainability assessment, no unified quantitative framework currently exists to specifically evaluate ESG performance in tailings reprocessing projects. While circular economy principles and the 3R approach (reduce, reuse, recycle) support resource recovery and waste minimization, a structured method to quantitatively assess ESG performance within this context remains underdeveloped (Segura-Salazar *et al.*, 2019). The study addresses this gap by developing and applying a quantitative ESG-based framework to systematically evaluate tailings reprocessing alternatives. The framework's

primary contribution is a literature-informed AHP weight set for tailings reprocessing ESG evaluation, calibrated to the Chilean context and aligned with the Global Industry Standard on Tailings Management (GISTM), which constitutes the main new research output of this study. Four structural advances underpin this contribution: an AHP-weighted indicator hierarchy purpose-built for tailings reprocessing scope; geometric aggregation that reduces excessive pillar-level compensability; anchored scoring rubrics for social and governance indicators; and a recalibration protocol enabling transfer to other jurisdictions without structural change.

Methods

Analytic Hierarchy Process

Analytic Hierarchy Process methodology is applied to determine the relative weights of the selected ESG indicators. Indicator weights are derived from a structured literature-informed judgment process, drawing on published Chilean tailings ESG priorities, decarbonisation targets, and regional water scarcity constraints (Araya et al., 2020; Garcia-Zavala *et al.*, 2023; Luo et al., 2024). This approach follows established practice for methodological framework papers in mining sustainability research (Bascompta *et al.*, 2022; Garcia-Zavala *et al.*, 2023). Weights are presented as an illustrative configuration intended for recalibration by practitioners using site-specific expert input. The relative importance of each criterion against every other is assessed based on Saaty's 9-point fundamental scale (Luo *et al.*, 2024). Because indicators are expressed in heterogeneous units, tCO_2e, kWh/t, m^3, ha, and ordinal scores, all raw values are rescaled to a common [0,1] interval using min-max normalisation (Pollesch and Dale, 2016). For positive indicators:

$$x'_{ij} = \frac{x_{ij} - x_{min}}{x_{max} - x_{min}}$$

For negative indicators such as GHG emissions and LTIFR:

$$x'_{ij} = \frac{x_{max} - x_{ij}}{x_{max} - x_{min}}$$

ensuring a score of 1 always represents best ESG performance. Boundary values for normalisation were defined as follows. For GHG emissions and energy demand, maximum values were set at the highest reported figures across comparable Chilean tailings reprocessing operations, with minimum values representing best available technology benchmarks reported in the literature (Araya *et al.*, 2020; Garcia-Zavala *et al.*, 2023). For water consumption, boundaries reflect the range of specific water consumption reported across hyperarid mining operations in the Atacama and Antofagasta regions (Garcia-Zavala *et al.*, 2023). For land rehabilitation, minimum and maximum values correspond to the lowest and highest percentage reductions in disturbed land area reported in peer-reviewed Chilean tailings studies (Araya *et al.*, 2020). For safety, the 2024 ICMM industry-average TRIFR of 2.29 serves as the normalisation benchmark, with zero representing best achievable performance. For stakeholder engagement and transparency, boundaries correspond to the GRI defined scoring rubric endpoints: 0 representing absent or unverifiable performance and the maximum score representing full compliance with all defined criteria. For regulatory compliance, boundary values are defined by the rubric itself, ranging from 0% to 100% adherence, with targets aligned to national and international mining standards (Anani *et al.*, 2025). The weighted indicators are then aggregated into a Composite ESG Index using weighted geometric aggregation expressed in logarithmic form for each reprocessing alternative under evaluation (Munda, 2005; OECD *et al.*, 2008). The ESG Index for alternative j is calculated as equation 1.

$$ESG\ Index_j = exp\left(\sum_{i=1}^{n} w_i \times \ln\left(x'_{ij} + \varepsilon\right)\right) \quad (1)$$

where w_i is the global weight of indicator i, x'_{ij} is the normalised score of indicators i for alternative j, and ϵ is a small constant introduced to avoid undefined logarithmic values when normalised scores equal zero. In this study, $\epsilon = 0.001$ was used. This value

is small relative to the 0–1 normalised scale and preserves the penalty for very low indicator scores.

Weighted geometric aggregation, expressed in logarithmic form, was selected over additive weighted averaging because it reduces full compensability among ESG indicators. In an additive index, strong performance in some indicators can offset very poor performance in others, even when the weak indicator represents a critical risk. This is problematic for tailings reprocessing, where poor performance in areas such as water protection, safety, regulatory compliance, or tailings facility integrity may have severe and potentially irreversible consequences. Under the logarithmic aggregation structure, a very low normalised score produces a strong penalty in the overall index, limiting the ability of high scores in other indicators to compensate for critical weaknesses. This aggregation approach is therefore more suitable than additive weighted averaging for evaluating tailings reprocessing alternatives involving potentially catastrophic or irreversible ESG risks (Munda, 2005; OECD et al., 2008).

Quantifiable ESG Indicators

Indicators were selected based on established international sustainability reporting guidelines, relevant regulatory requirements including those from the EU, and systematic review of peer-reviewed tailings sustainability literature, to ensure both comprehensiveness and local relevance. The chosen indicators are designed to be quantifiable and reflective of critical performance aspects across all three ESG dimensions. For each indicator the following information is provided: indicator name, measurement unit, preference scale (indicate a better performance for lower or higher indicator values), and a short description.

The environmental dimension comprises four indicators that relate to greenhouse gas emissions, energy demand, water consumption and land rehabilitation.

Greenhouse Gas Emissions: GHG emissions are quantified in CO_2 equivalents (tCO_2e) using standard life cycle assessment methodologies for energy consumption, process chemicals, and transportation activities. This involves calculating Scope 1 (direct emissions), Scope 2 (indirect emissions from purchased energy), and relevant Scope 3 (other indirect emissions) emissions, acknowledging that improved recovery can reduce GHG emissions (Araya *et al.*, 2020; Padilla-Rivera *et al.*, 2025).

Energy Demand: Energy demand is measured as energy intensity, expressed in kilowatt-hours per tonne (kWh/t) or gigajoules per tonne (GJ/t) of reprocessed material. This metric accounts for all forms of energy consumption, including electricity, heat, and fuel, during the reprocessing stages (Araya *et al.*, 2020; Bascompta *et al.*, 2022; Karu and Kekkonen, 2025).

Water Consumption: Water consumption is evaluated using metrics such as cubic meters of water recovered (m^3), the percentage of process water recycled (%) within the operation, and specific water consumption per tonne of material processed. Emphasis is placed on minimizing fresh water intake and maximizing reuse for remining, especially in hyperarid locations (Araya *et al.*, 2020; Garcia-Zavala *et al.*, 2023).

Land Rehabilitation: This is quantified by the area of land restored in hectares (ha), the percentage reduction in disturbed land area post-reprocessing, and the measured increase in biodiversity indices. These metrics assess the ecological recovery and future land use potential following reprocessing activities, often aiming to improve environmental safety and reduce site rehabilitation costs (Karu and Kekkonen, 2025; Kursunoglu, 2025).

The indicators in the social dimension integrate different societal aspects like employment, safety and stakeholder engagement.

Employment: This is measured by the number of local jobs created or maintained, the percentage of local hires in skilled and unskilled positions, and the financial investment in local skills development and training programs, often considering the unemployment rate of a community (Bascompta *et al.*, 2022).

Safety: Safety performance is measured using industry-standard metrics such as the LTIFR and TRIFR, both expressed per million hours worked per the ICMM safety protocol.

Stakeholder Engagement: Stakeholder engagement is quantified through an index based on the frequency and quality of

interactions (e.g., public meetings, workshops), the number and resolution rate of recorded grievances, and the extent of participatory decision-making instances, scored on the five-level IAP2 Public Participation Spectrum (1=Inform, 2=Consult, 3=Involve, 4=Collaborate, 5=Empower), with each level requiring documented evidence to be assigned. This index is derived from structured interviews, surveys, and content analysis of engagement records, with a focus on prioritizing stakeholder concerns and values (Manjengwa *et al.*, 2023; Nehring and Knights, 2024). While ordinal in nature, this scoring approach is compatible with AHP-based composite indexing when anchor points are explicitly defined and consistently applied across all evaluated alternatives (Ishizaka and Labib, 2011).

The indicators of the governance dimension reflect the political and regulatory environment.

Regulatory Compliance: This is assessed by the percentage (%) of adherence to environmental and social regulations, with a target of zero instances of non-compliance, demonstrating commitment to national and international standards. This includes adherence to corporate policies and international mining standards (Di Guimarães *et al.*, 2025).

Transparency: Transparency is evaluated by the clarity and accessibility of project information to stakeholders, and the demonstrable robustness and effectiveness of grievance mechanisms, scored against a seven-item GRI 102 disclosure checklist (0=absent, 1=present and verifiable), rescaled to [0,1]. This includes public reporting and clear communication strategies (Jagrič *et al.*, 2025; Padilla-Rivera et al., 2025). Similarly, the GRI 102 checklist scoring is ordinal but consistently anchored, ensuring comparability across alternatives within the same evaluation (Ishizaka and Labib, 2011).

Framework demonstration using secondary data

Chile is selected as a critical case: it produces approximately 24% of global mined copper, hosts over 740 registered tailings storage facilities, and operates predominantly in the Atacama and Antofagasta regions where 93% of mining operations face high or very-high water scarcity risk (Cacciuttolo and Atencio, 2022; Garcia-Zavala *et al.*, 2023). This concentration of tailings volume, water stress, and decarbonisation pressure represents the most demanding available test context for the proposed framework. Following established practice for methodological framework papers in mining ESG research (Bascompta *et al.*, 2022; Garcia-Zavala *et al.*, 2023), the framework is demonstrated through illustrative validation using secondary data compiled from peer-reviewed tailings reprocessing studies in Chile and comparable contexts (Araya *et al.*, 2020; Garcia-Zavala *et al.*, 2023; Luo *et al.*, 2024). The original contribution of this conference paper lies in the development, calibration, and illustrative application of the ESG evaluation framework, rather than in the generation of new primary field measurements. Primary field validation across multiple jurisdictions is identified as the next research phase to further strengthen transferability. The objective is to demonstrate four framework properties: discriminant capacity, non-compensatory behaviour, contextual weight sensitivity, and diagnostic utility. The demonstration assessed whether the selected indicators appropriately reflect sustainability priorities in the Chilean context and whether the weighting distribution aligns with prevailing ESG challenges, such as water scarcity, energy intensity, decarbonisation targets and regulatory oversight. Indicator values reported in the literature were normalised to ensure comparability across different scales, allowing consistent integration within the Composite ESG Index structure. The resulting weighting distribution is presented in Table 1.

Global Weights represent the final contribution of each indicator to the Composite ESG Index. The distribution reflects that in the Chilean context, environmental factors associated with energy and emissions carry the highest priority to ensure that tailings reprocessing contributes to national decarbonisation goals (Adrianto and Pfister, 2022; Luo *et al.*, 2024). Land Rehabilitation and Water Consumption

Table 1 ESG Dimension, indicators, and the weights of the ESG framework applied to the Chilean tailings reprocessing context (Garcia-Zavala et al., 2023)

Dimensions	Indicators	Weights (%) per dimension	Weights (%) per Indicator	Global Weight (%)
Environmental	GHG emission	70	34.3	24
	Energy demand		28.6	20
	Water consumption		18.6	13
	Land rehabilitation		18.5	13
Social	Safety	25	50	12.5
	Stakeholder engagement		30	7.5
	Employment		20	5
Governance	Regulatory compliance	5	70	3.5
	Transparency		30	1.5

follow, which is a reflection of the industry's need to address long-term geotechnical liabilities and the extreme water scarcity prevalent in the Atacama and Antofagasta region (Araya *et al.*, 2020; Luo *et al.*, 2024).

Within the social dimension, safety is prioritized as the most critical indicator to prevent catastrophic tailings failure and ensure a safe workplace (Kursunoglu, 2025). This is followed by Stakeholder Engagement and Employment, ensuring that reprocessing initiatives maintain a social license to operate by providing local community benefits and resolving grievances (Garcia-Zavala *et al.*, 2023; Nehring and Knights, 2024). Governance factors are distributed between Regulatory Compliance and Transparency, serving as essential thresholds for institutional accountability and public reporting (Garcia-Zavala *et al.*, 2023; Karu and Kekkonen, 2025).

Quantitative aggregation of these indicators reveals a critical trade-off inherent in the Chilean context. The transition to energy-intensive water solutions, such as desalination, to address local scarcity can increase the energy demand and GHG components of the index. However, the framework can identify whether such trade-offs are offset by improvements in long-term geotechnical liability reduction and land-footprint reduction (Adrianto and Pfister, 2022; Araya *et al.*, 2020). The application confirms all four properties: the framework produces differentiated scores, geometric aggregation penalises critical weaknesses, the weight distribution reflects Chilean priorities, and pillar-level sub-scores provide diagnostic information. Empirical validation using primary field data constitutes the next research phase.

Conclusions

This study developed and demonstrated a quantitative ESG-based framework for the evaluation of tailings reprocessing. By integrating measurable environmental, social, and governance indicators within the Analytic Hierarchy Process (AHP), the research generated a Composite ESG Index that enables comparative assessment of resource recovery options. The framework addresses a critical gap in tailings reprocessing evaluation, where technical and economic criteria have traditionally dominated while ESG dimensions remained secondary considerations.

Results demonstrate that environmental indicators, particularly greenhouse gas emissions, energy intensity, and water consumption, carry the greatest influence in the Chilean context, reflecting national decarbonisation goals and regional water scarcity constraints. At the same time, social and governance dimensions, especially safety

and regulatory compliance, function as essential boundary conditions for responsible operation.

The framework is adaptable to different regulatory and geographical contexts through recalibration of indicator weights, enhancing its broader applicability. This research advances the operationalization of ESG principles in tailings reprocessing by aligning resource recovery with water protection, emissions reduction, and institutional accountability. The framework has three limitations: the weight configuration is Chilean-specific and requires recalibration for other jurisdictions using the protocol described herein; social and governance indicators rely on anchored ordinal scoring rather than continuous measurement; and the application uses secondary data, with primary field validation across multiple jurisdictions constituting the critical next research phase.

Acknowledgements

This research has received funding from the European Union's Horizon Europe research and innovation programme under the Marie Skłodowska-Curie Actions Doctoral Network (HORIZON-MSCA-2023-DN-01) within the CRITERIA Project (Grant No. 101169238). The authors gratefully acknowledge this financial support and the institutional support of Universitat Politècnica de Catalunya. The authors also thank all co-organisers for hosting the IMWA 2026 Conference.

References

Adrianto, L.R., Pfister, S., 2022. Prospective environmental assessment of reprocessing and valorization alternatives for sulfidic copper tailings.

Alajoki, J., Karppinen, A., Rinne, T., Serna-Guerrero, R., Lundström, M., 2024. Leaching strategies for the recovery of Co, Ni, Cu and Zn from historical tailings. Miner. Eng. 217, 108967. https://doi.org/10.1016/j.mineng.2024.108967

Anani, A., Adewuyi, S.O., Gonzales, C.G., 2025. Sustainable copper supply chains: Evaluating ESG risks through the lens of regulatory compliance and risk assessment strategies. Extr. Ind. Soc. 23. https://doi.org/10.1016/j.exis.2025.101662

Araya, N., Kraslawski, A., Cisternas, L.A., 2020. Towards mine tailings valorization: Recovery of critical materials from Chilean mine tailings. J. Clean. Prod. 263, 121555. https://doi.org/10.1016/j.jclepro.2020.121555

Bascompta, M., Sanmiquel, L., Vintró, C., Yousefian, M., 2022. Corporate Social Responsibility Index for Mine Sites. Sustainability 14, 13570. https://doi.org/10.3390/su142013570

Cacciuttolo, C., Atencio, E., 2022. Past, Present, and Future of Copper Mine Tailings Governance in Chile (1905–2022): A Review in One of the Leading Mining Countries in the World. Int. J. Environ. Res. Public. Health 19, 13060. https://doi.org/10.3390/ijerph192013060

Di Guimarães, L., Araújo, U.P., Lima, H.M.D., 2025. Mine closure transparency and disclosure: An open-source evaluation of financial, technical, and social reporting. Resour. Policy 107. https://doi.org/10.1016/j.resourpol.2025.105644

Garcia-Zavala, C., Ordens, C.M., Pagliero, L., Lébre, É., Aitken, D., Stringer, M., 2023. An approach for prioritising environmental, social and governance (ESG) water-related risks for the mining industry: The case of Chile. Extr. Ind. Soc. 14. https://doi.org/10.1016/j.exis.2023.101259

Ishizaka, A., Labib, A., 2011. Review of the main developments in the analytic hierarchy process. Expert Syst. Appl. S0957417411006701. https://doi.org/10.1016/j.eswa.2011.04.143

Jagrič, T., Mumel, D., Skaza, A., 2025. Evaluation of Environmental, Social, and Governance Risks? A Critical Literature Review with Practical Implications. Sustainability 17, 8451. https://doi.org/10.3390/su17188451

Karu, V., Kekkonen, A., 2025. Integrating ESG and Sustainability in the Raw Materials Sector, in: Environ. Technol. Resour. - Proc. Int. Sci. Pract. Conf. RTU PRESS, pp. 267–274. https://doi.org/10.17770/etr2025vol1.8692

Kursunoglu, S., 2025. A Review on the Recovery of Critical Metals from Mine and Mineral Processing Tailings: Recent Advances. J. Sustain. Metall. 11. https://doi.org/10.1007/s40831-025-01126-y

Luo, C., Liu, Y., Pan, L., Yang, F., 2024. Navigating mineral policy development challenges in the global south using analytic hierarchy process. Resour. Policy 90. https://doi.org/10.1016/j.resourpol.2024.104797

Manjengwa, E.R., Dorfling, C., Tadie, M., 2023. Development of a conceptual framework to evaluate factors that affect drivers for stakeholder engagement in mine waste management. Resour. Policy 81, 103280. https://doi.org/10.1016/j.resourpol.2022.103280

Munda, G., 2005. "Measuring Sustainability": A Multi-Criterion Framework. Environ. Dev. Sustain. 7, 117–134. https://doi.org/10.1007/s10668-003-4713-0

Nehring, M., Knights, P., 2024. A Systems Engineering Approach to Incorporate ESG Risks and Opportunities in Early-Stage Mine Design and Planning. Mining 4, 546–566. https://doi.org/10.3390/mining4030031

OECD, European Union, Joint Research Centre - European Commission, 2008. Handbook on Constructing Composite Indicators: Methodology and User Guide. OECD. https://doi.org/10.1787/9789264043466-en

Padilla-Rivera, A., Hannouf, M., Assefa, G., Gates, I., 2025. Enhancing environmental, social, and governance, performance and reporting through integration of life cycle sustainability assessment framework. Sustain. Dev. 33, 2975–2995. https://doi.org/10.1002/sd.3265

Pollesch, N.L., Dale, V.H., 2016. Normalization in sustainability assessment: Methods and implications. Ecol. Econ. 130, 195–208. https://doi.org/10.1016/j.ecolecon.2016.06.018

Samadi, M., Gilani, S.-O., Abdollahisharif, J., Bakhtavar, E., 2025. Towards sustainable mine closure and reclamation through strategic tailing disposal sites evaluation: A causality-based Dempster-Shafer framework. Resour. Policy 108, 105676. https://doi.org/10.1016/j.resourpol.2025.105676

Segura-Salazar, J., Lima, F.M., Tavares, L.M., 2019. Life Cycle Assessment in the minerals industry: Current practice, harmonization efforts, and potential improvement through the integration with process simulation. J. Clean. Prod. 232, 174–192. https://doi.org/10.1016/j.jclepro.2019.05.318

Fallen Rocks: A Participatory Land Art Installation for Community Engagement in Bergslagen's Past and Present Mining Landscape

Lotta Sartz[1,2], Mattias Bäckström[1], Stefan Sädbom[1], Veronika Geiger[1], Monika Andersson[3]

[1]*Bergskraft Bergslagen AB, Södra Kungsvägen 49, SE-692 30 Kumla, Sweden, lotta.sartz@bergskraft.se*
[2]*Örebro University, Department of Communication and Collaboration, SE-701 82 Örebro, Sweden*
[3]*Boliden Zinkgruvan, Centrumvägen 1, SE-696 81 Zinkgruvan, Sweden*

Abstract

Mining regions with long industrial histories face ongoing challenges related to community development, environmental legacies, and generational renewal, even where mining remains active. This paper presents *Fallen Rocks*, a land art installation in Bergslagen, Sweden, as an approach to community engagement in mining-related sustainability issues. Around forty locally sourced rocks form a labyrinth-like structure designed for physical interaction. The installation is complemented by digital experiences introducing mining processes, resource use, and environmental aspects such as energy, emissions, and water-related challenges. The project illustrates how cultural and participatory approaches can support dialogue on mining effects, resource management, and long-term environmental responsibility.

Keywords: Lindesberg municipality, digital tools, science education, STEM

Introduction

Bergslagen – Historical context

Bergslagen region in south-central Sweden has a long and well-documented mining history dating back to at least the 15th century, forming one of Sweden's most important early industrial landscapes. In small Bergslagen municipalities like Lindesberg, iron ore mining and copper extraction supported the development of local communities and contributed significantly to Sweden's economic and technological growth. Mining shaped not only the physical landscape but also social structures, cultural identity, and patterns of settlement, with generations of miners and their families forming the backbone of these communities (Fig. 1).

Over time, the region has undergone major transformations, from small-scale medieval operations to industrialized mining in the 20th century, followed by closures during the 1970s and 1980s driven by economic restructuring, global competition, and technological change. But mining has not disappeared from the region. Active operations such as Boliden Zinkgruvan (Askersund), Boliden Garpenberg (Hedemora), and Lovisagruvan (Lindesberg), as well as ongoing limestone extraction, demonstrate continued importance of mineral production in Bergslagen.

This coexistence of historical mining environments and active operations makes Bergslagen a place where past, present, and future intersect in a tangible way. In this context, the introduction of a site-specific, land art-inspired installation offers a way to connect these different time perspectives through physical experience and reflection. The installation, *Fallen Rocks*, builds on the region's visible geological and industrial heritage and invites reflection on both the legacy of mining and its ongoing role in shaping sustainable futures. This perspective is also reflected in local political support. At the inauguration of *Fallen Rocks*, the Chair of the Municipal Executive Board in Lindesberg stressed the importance of preserving the region's history and described the integration of art into this context as "excellent" (pers. comm., inauguration of *Fallen Rocks*, 2025).

Figure 1 *Mine workers in Stripa Mine in the 1930s. Photo source: Lindesberg Cultural Heritage Archive.*

Metals, minerals and geoscience literacy for sustainable futures

Future societies will depend heavily on access to raw materials for the energy transition, digitalization, and the development of sustainable infrastructure. This creates a need not only for technical solutions, but also for public understanding and engagement in questions related to mining, land use, and resource management. At the same time, to secure competence, attracting future generations to the mining sector is essential.

However, public perceptions of the mining sector remain challenging. A national Swedish survey showed that almost six out of ten respondents could not imagine working in the mining industry, while more than seven out of ten perceived a conflict between mining and environmental issues (SGU 2025). These attitudes are problematic in a context where society increasingly depends on responsibly produced metals and minerals, and where the industry is working continuously to improve environmental performance and sustainability practices.

Education therefore plays a key role in strengthening understanding of mineral resources, and the role of mining in sustainable development. Introducing children and young people to these perspectives at an early stage can help build both knowledge and engagement around complex sustainability challenges. Research also shows that learning is strengthened when information is connected to sensory experience and emotional engagement (Boström and Svantesson 1998; Dunn *et al.* 1992). Visualization and experiential learning approaches can help make otherwise abstract scientific concepts more tangible and meaningful (Cook 2006; Wu and Shah 2004).

Artistic and interactive approaches can hence complement traditional education by engaging multiple senses and inviting curiosity-driven exploration. By allowing visitors to physically and intuitively engage with geological materials, understanding of the role of metals and minerals in society can be deepened and support more informed discussions about sustainable resource use.

Artistic perspective and conceptual foundation

The artistic concept of *Fallen Rocks* is rooted in the land art tradition, where artworks are created in direct relation to a specific landscape and often use natural materials found on site. For the artist Veronika Geiger, this approach is closely connected to an interest in geology, deep time, and the relationship between humans and the earth.

The idea of the installation emerged through visits to mining environments in Bergslagen, particularly the underground spaces of Boliden Zinkgruvan. These spaces were experienced as labyrinth-like structures, both fascinating and disorienting, leading to the development of a spatial concept where visitors move through an open maze of stones. The labyrinth becomes a metaphor for how humans navigate and try to understand the world, inspired in part by literary references and reflections on how children intuitively engage in complex environments.

The title *Fallen Rocks* carries multiple meanings. It refers both to the physical material, rocks that have been moved and reassembled, and to the often-overlooked human experiences connected to mining, including risk, labor, and loss. In this way, the installation introduces an existential dimension to the mining landscape, acknowledging that the materials underpinning modern society come at a cost. At the same time, the work remains open to interpretation, allowing each visitor to form their own understanding.

Methods

Development of artwork

The development of *Fallen Rocks* was based on a close collaboration between artistic practice and scientific knowledge. The conceptual framework, spatial design, and material composition were led by the artist, while geological and contextual knowledge was contributed by the project partners. This transdisciplinary approach allowed different forms of understanding, analytical and experiential, to coexist within the same installation.

A central aspect of the artistic process was the strong connection to place. In land art practice, the location is an integral part of the work itself. The installation was therefore developed in direct relation to the Bergslagen landscape, its geological conditions, and its mining history. Through site visits, dialogues with miners, and field observations, the artist built an understanding of both the physical environment and the human experiences connected to it.

The design of the installation as an open, labyrinth-like structure reflects both the spatial experience of underground mining and a conceptual interest in movement, perception, and orientation. The intention was to create a space that visitors can enter from multiple directions, move through freely, and experience from within. Physical engagement is considered essential, as it enables a more immediate and sensory connection to the materials and the environment. The installation is intended to be used: walked through, touched, explored, and even played in, especially by children and young people, who are seen as naturally inclined to engage intuitively with such environments. By encouraging this type of interaction, the artwork aims to create conditions for reflection, curiosity, and personal interpretation.

Rock collection and installation process

Collection of rocks was carried out during the summer of 2025. All materials were sourced from the area surrounding Zinkgruvan in Askersund municipality, where the active mine operated by Boliden Zinkgruvan is located (Fig. 2).

Rocks were selected to represent a wide range of mineralogical compositions, as well as variation in size and shape. Following collection, the materials were temporarily placed in the parking area outside Zinkgruvan Mine Museum. At this stage, the artist documented each rock through photography and recorded characteristics such as colour, size, and form, forming the basis for a detailed layout plan and spatial design of the installation.

The rocks were transported from Zinkgruvan to Lindesberg in November 2025 and temporarily stored near the installation site. Ground preparation was carried out over one day, during which the topsoil was removed and replaced with a base layer of coarse rock material (20–50 mm), followed by a layer of gravel (0–16 mm).

Digital tools

In parallel with development of the artwork, a set of digital tools consisting of games and interactive environments were developed through collaboration between geoscientists, educators, and digital designers with the aim of translating complex mining-related concepts into accessible and engaging formats.

The work focused on identifying key themes in the mining value chain and exploring how these could be communicated through interactive and experience-based learning. Attention was given to lowering barriers to engagement, by emphasizing interactivity, and curiosity-driven learning. The digital layer was integrated into the artwork using QR codes (Tab. 1).

Together, these tools broaden the understanding of mining beyond extraction, addressing the full lifecycle of materials and introducing environmental aspects such as energy use, emissions, mine water management, contamination risks, and long-term stewardship of former and active mining areas.

Results and Discussion

Installation and inauguration as a social process

Fallen Rocks was assembled according to plan during one working week in mid-November 2025, and inauguration took place in December (Fig. 3). The inauguration event brought together residents and representatives from the regional mining sector. It began with presentations at the local library, followed by a joint visit to the installation site, where the artwork was formally introduced through a ribbon-cutting ceremony.

The event can be understood as both a symbolic and practical handing over of the installation to the community of Lindesberg. Notably, the artwork was immediately taken into active use, with visitors entering and exploring the labyrinth. Digital components also attracted notable interest during the inauguration, with many visitors asking questions about their content and use. This early interaction suggests the potential of the installation to function as an open and shared space.

Experiential engagement and accessibility

This type of interaction aligns with previous research emphasizing the importance of physical accessibility and participation in shaping visitor experiences in art–science contexts. Such environments can facilitate states of 'flow', characterized by immersion

Figure 2 *Collection of rocks and documentation, summer 2025, Zinkgruvan, Askersund municipality.*

Table 1 *Name of games, area they cover and QR-code to access the game.*

Drillrunner	Mine Rider	Connect Rush	Slingshot Savant	Periodic Slingshot	Ore Scanner
Exploration, underground mining practices.	Exploration, underground mining practices.	Large-scale mining systems, connectivity.	Metals in society and global distribution.	Metals in society and global distribution.	Links to everyday life.

and engagement (Renowden *et al.* 2022), and support learning processes where understanding emerges through movement, sensory experience, and reflection.

Research on art–science practices also shows that immersive and participatory approaches can strengthen both cognitive and emotional engagement with complex environmental issues, making abstract concepts easier to relate to and reflect upon (Xu 2025). In *Fallen Rocks*, the possibility to move through, touch, and explore the installation creates similar conditions, particularly for children and young people, who often engage intuitively with materials and spatial environments.

Participatory and aesthetic approaches such as *Fallen Rocks* may also broaden participation by reaching audiences who are less likely to engage with traditional forms of science communication. Similar observations have been reported in school-based environmental projects in Bergslagen, where pupils showed increased interest in science and sustainability issues when working with local mining-related environmental challenges through practical and participatory activities (Sartz and Bäckström 2014). Previous studies further indicate that science-based art exhibits can increase interest in scientific topics, particularly among visitors without a formal STEM background, suggesting that such formats can lower barriers to engagement (Ricci *et al.* 2023).

At the same time, arts-based and outdoor learning approaches have been shown to strengthen individuals' sense of connection to the natural environment and foster emotional engagement with environmental issues (Gray and Birrell 2015). Within environmental ethics, similar ideas are reflected in discussions of land art, where working with natural materials and landscapes can contribute to a deeper appreciation of nature and encourage more reflective attitudes towards environmental responsibility (Brady 2007).

It is anticipated that *Fallen Rocks* may contribute to increased awareness of the relationship between natural resources, industrial activity, and everyday life, although these longer-term educational and community effects remain to be evaluated.

Future work and long-term engagement

Future work will focus on evaluating how the installation functions over time as a platform for dialogue, learning, and community engagement. Planned activities include collaborations with local schools, recurring public events connected to Geology Day, and continued dialogue with the municipality and regional stakeholders. Future studies could also explore how participatory and place-based art installations influence young people's interest in geoscience, mining, and environmental sustainability, as well as perceptions of mining-related environmental challenges such as land and water management.

Conclusions

This paper presents *Fallen Rocks* as a transdisciplinary approach that combines art, science, and local collaboration to engage communities in mining-related sustainability issues. By integrating a site-specific land art installation with digital educational tools,

Figure 3 *Fallen Rocks in Lindesberg, Sweden, December 2025.*

the project demonstrates how physical experience, materiality, and interactive learning can contribute to dialogue on resource use, environmental responsibility, and the societal role of mining.

An important insight from the project is the value of creating open and accessible spaces for dialogue, where different perspectives, local, industrial, scientific, and societal can meet. Such approaches may support increased understanding of complex issues related to mining, including environmental impacts, mine water challenges, legacy issues, and long-term stewardship of land and water. At the same time, the project highlights practical considerations that should not be overlooked, such as long-term maintenance, safety aspects, and the integration of public installations into everyday environments.

The installation is intended to function as a lasting meeting place in Lindesberg, offering opportunities for reflection, learning, and engagement over time. Through the combination of physical and digital elements, *Fallen Rocks* may contribute to a broader understanding of the importance of metals, minerals, and geoscience in modern society, while encouraging more informed and inclusive dialogue on sustainable mining and future resource management.

Acknowledgements

The authors thank the participants of Metals4U+ project, funded by Swedish Mining Innovation and supported by Vinnova, Formas, and the Swedish Energy Agency. Special thanks to the Epiroc team for development of digital tools: Katarina Öquist, Bengt Parkedal, Björn Syse, Hanna Gustafsson and Vignesh Rajkumar.

References

Boström L, Svantesson I (1998) Learning styles in practice. Jönköping: Brain Books AB [in Swedish]

Brady E (2007) Aesthetic regard for nature in environmental and land art. Ethics Place Environ 10(3): 287–300

Cook MP (2006) Visual representations in science education: the influence of prior knowledge and cognitive load theory on instructional design principles. Sci Educ 90(6): 1073–1091

Dunn R, Dunn K, Treffinger DJ (1992) All children are talented – in their own way. Wiley [in Swedish]

Gray T, Birrell C (2015) 'Touched by the Earth': a place based outdoor learning programme incorporating the Arts. J Advent Educ Outdoor Learn 15(4): 330–349

Renowden C, Beer T, Mata L (2022) Exploring integrated ArtScience experiences to foster nature connectedness through head, heart and hand. People nat 4(2): 293–587

Ricci K, McLauchlin B, Hua J (2023) Impact of a science art exhibit on public interest and student comprehension of disease ecology research. J Microbiol Biol Educ 24(1): 1–8.

Sartz L, Bäckström M (2014) Chemistry and environmental research as a part of education – an example from Sweden. In: Oral AY, Bahsi ZB (eds) 1st Int Con Exhib Curr Trends Sci Tech Educ, p 27-32, SCITEED 2014

SGU (2025) Attityder till svensk gruvnäring 2024 – Novusrapport. Geological Survey of Sweden (SGU), Uppsala, Sweden [in Swedish]

Wu HK, Shah P (2004) Exploring visuospatial thinking in chemistry learning. Sci Educ 88(3): 465-492

Xu C (2025) From art to action: Case studies of art–science in creative practices. J Mus Educ 50(2): 210–224

IMWA 2026
Jeongseon

Implementation of Operative Monitoring During Flooding of the Königstein Mine – First Experiences from Hydraulic Test 2

Nadja Schmidt, Sven Eulenberger, Ulf Jenk

Wismut GmbH, Jagdschänkenstraße 29, 09117 Chemnitz, Germany, nadja.schmidt@wismut.de

Abstract

At the Königstein site, final flooding of the former uranium mine is taking place according to a stepwise flooding concept. The process is accompanied by an intensive, site-specific monitoring program, which is subject to continuous adaptation and optimization as remediation progresses. In preparation for flooding beyond 140 m a.s.l., the existing monitoring system was extended by the construction of new wells as well as equipping permanent probes with wireless network modules for continuous transmission of water level and EC. This paper discusses first outcomes from adapted monitoring and provides an overview of the current state of flooding.

Keywords: Mine flooding, uranium mining, groundwater monitoring, Königstein mine

Introduction

Situated inside the Elbe Sandstone Mountains and surrounded by important groundwater resources, the Königstein uranium deposit is located in the lowermost of four cretaceous sandstone aquifers within the Pirna sedimentary basin. About 6 km² of the total 25 km² uranium deposit were subject to mining activities by the former Wismut SDAG. Due to decreasing uranium grades in the mineralized sedimentary rock, conventional mining shifted towards an underground in situ block leaching technology in 1984. In total, some 130,000 t of sulfuric acid were brought into the mine until mine closure due to the German reunification in 1990. By this process, more than 50 million tons of sandstone came into contact with the acid, triggering follow-up reactions as the release of easily soluble contaminants as metals and radionuclides (Jenk *et al.* 2011).

Following a longstanding and thorough phase of preparation, stepwise controlled flooding of the mine was initiated in 2001. The basic principle is to reduce leachate-related pollutants in the mine whilst ensuring the greatest possible protection of the surrounding aquifer areas (aquifers #3 and #4). Main elements of flood control are two extraction wells (FBL), which are connected to the northernmost and deepest mine workings, the so-called control drifts, which have no direct connection to the remaining mine by open mine workings or boreholes (Figure 1). By these wells, the contaminated water is pumped from the mine, cleaned in the treatment plant on site, and finally discharged into the river Elbe or re-injected into the mine. Continuous pumping of the flooding water maintains a hydraulic gradient from the host sandstone towards the control drift and prevents acidic flooding water from flowing into the surrounding aquifer #4. Controlled flooding of mine section I until the water level of 140 m a.s.l. was completed in 2013.

Although the applied remediation technology of pump and treat led to a major decrease of acid and radionuclide concentrations during the last three decades, contamination potential persists at a high level. In 2025, the extracted mine water had a pH of 3.3 and was characterized by average concentrations of SO4 = 620 mg/L, Fe = 39 mg/L, U = 6.3 mg/L, Zn = 4.2 mg/L and Ra 226 = 6.5 Bq/L.

Stepwise permanent flooding above the level of 140 m a.s.l. was preceded by years of planning and preparation. During this time, several large-scale tests were conducted, the findings of which served to further develop the hydraulic and hydrochemical models.

Specifically, since 2017, the following measures and tests have been carried out as prerequisites to continue the final flooding above 140 m a.s.l. in form of the so called "hydraulic test 2":

- Hydraulic test 1: It involved a controlled short term flooding to a level of 150 m a.s.l., which took about 6 months, followed by immediate return to the initial level of 140 m a.s.l.. The test was accompanied by an intensified monitoring program for the early detection of mine water encroaching into the upper aquifer #3. The results of hydrochemical monitoring during and after the test provided no indication of mine water influence on the water quality of the surrounding aquifers #3 and #4 (Frenzel *et al.* 2018, Schmidt *et al.* 2022)
- Hydrochemical field test: In 2020, a single borehole test was carried out at an existing monitoring well (k-77018) in the mine. Over a period of eight months, a reactive solution consisting of potassium hydroxide and butanol was injected directly into the mine (17 times in total) and re-pumped after a reaction time of 1–2 weeks. Analyses of the extracted water effectively demonstrated the suitability of the reactive solution for an efficient reduction of the acid potential. After approximately two months, decreasing iron concentrations and an increase in sulfide indicated enhanced bacterial sulfate reduction in the vicinity of the test well (Bilek *et al.* 2023).
- Construction of an injection borehole in the southern part of the mine: For the implementation of supporting measures for acid reduction and contaminant precipitation in the mine using reactive solutions, a strategically located injection borehole (k-77045) was drilled into upstream open mine voids near the sealed shaft 398 in 2023 (see Figure 1).

In contrast to hydraulic test 1, in hydraulic test 2 the water level in the former mine is plan-ned to be kept at the target level of 150 m a.s.l. for at least two years. Flooding is accompanied by the injection of reactive solutions directly in-to the mine. Hydraulic test 2 started in Mai 2024 with the first injection of NaOH at k 77045, one year later lifting of the mine water level began. If the current operation is maintained, the tar-get level of 150 m a.s.l. will be reached in late summer 2026.

Adaption of the monitoring network to further flooding steps

The existing monitoring network, consisting of approximately 140 groundwater monitoring wells in the 3rd and 4th aquifers, was designed to reliably monitor any effects of mine flooding at least to a level of 140 m a.s.l. To accommodate higher water levels beyond this, the monitoring network was gradually expanded starting in 2018.

The construction of new monitoring wells for flooding beyond 140 m a.s.l. mainly serves for supervising potential mine water encroachments in the vicinity of incompletely backfilled ventilation shafts (k-66039) and along the north fault (k-66040), as well as monitoring of potential contaminant mobilisation from the unmined uranium deposit Thürmsdorf (k-77041). Thereby, the exact location of a planned monitoring well depends not only on the geological conditions underground and their position downstream of potential locations of mine water encroachment, but also on surface factors such as accessibility and land ownership. The extension is done step by step, in accordance with the flooding strategy and based on the latest findings, in order to account for high installation costs due to the great depth and the need for hydraulic sealing of overlying aquifers. Groundwater monitoring wells and injection boreholes required to expand the monitoring network for further flooding, which have already been constructed or are currently under construction, are listed in Table 1.

New measuring points are used for collecting water samples in order to expand and improve the data basis for site-specific downstream and transport models (Eulenberger *et al.* 2021). At the same time, core material obtained from the boreholes is used to carry out for example column tests to investigate the reaction of unmined ore horizons to the inflow of acidic mine water.

A further expansion of the measurement network is also planned for the further

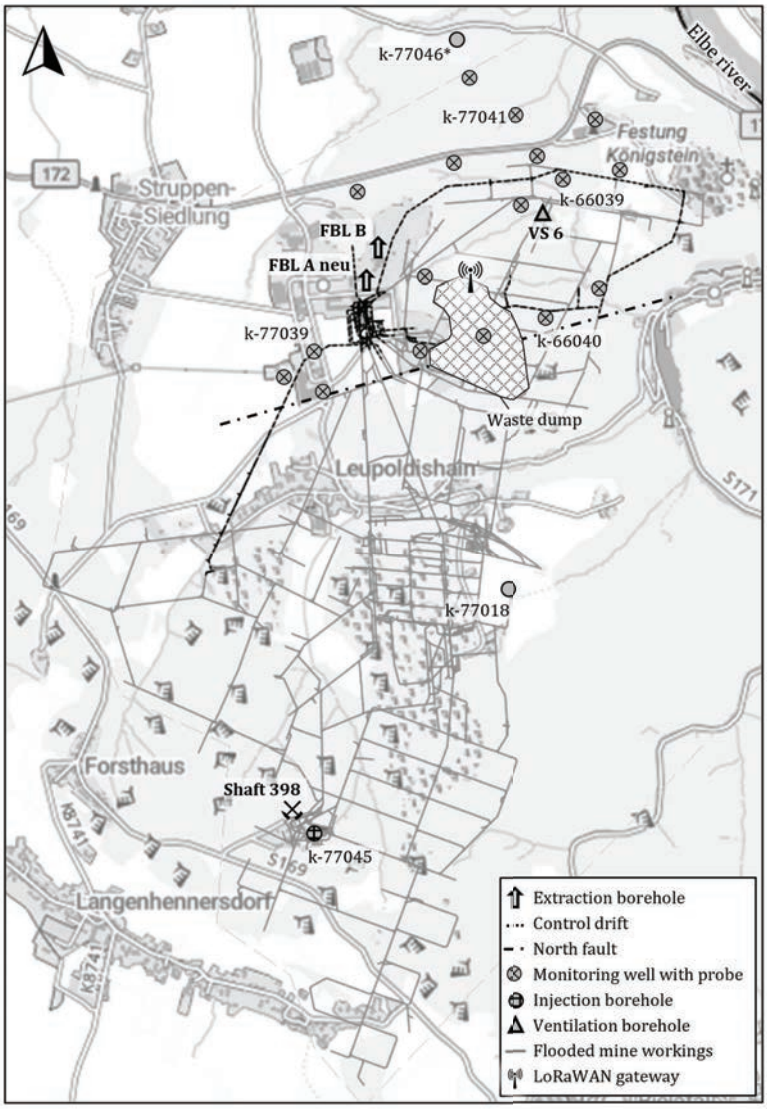

Figure 1 *Map of the Königstein uranium mine with relevant elements discussed in this paper.*

Table 1 *Overview of monitoring wells build in recent years for the stepwise extension of the monitoring network for the adaption to further flooding of the Königstein mine.*

Monitoring well	Aquifer	Year of construction	Depth	Function
k-66039	#3	2018	200	Monitoring downstream of ventilation shaft
k-66040	#3	2020	192	Monitoring along north fault
k-77039	mine	2022	283	Monitoring the hydraulic connection of control drifts north and west
k-77041	#4	2024	273	Monitoring of unmined deposit
k-77045	mine	2023	259	Injection of reactive fluids into the mine
k-77046	#4	2026	272*	Monitoring of unmined deposit

* planned depth

progress of flooding. The necessity and exact positioning of the measuring points to be established will be determined by the findings gained from the flooding process in the coming years. The evolving flooding strategy sets the framework for the gradual expansion of the current measurement network.

Using electrical conductivity as early indicator for mine water influence

Criteria for event-related intensification of monitoring, for initiating measures to limit the spread of hydrochemical influence, and ultimately for the termination of hydraulic test 2 are defined in a response plan. The response plan specifies an increase in EC of 100 µS/cm over a period of one month, measured by probe or sampling in wells of aquifer #3, as a criterion for the intensification of sampling. In a first step, an additional sample will be taken for verification, followed by monthly sampling and the comparison with indicator values which have been specified in the response plan for indicating an influence from flooding water.

The electrical conductivity is continuously observed using permanent probes (*SEBA Hydrometrie*) in 17 monitoring wells of aquifers #3 and #4. The mine waters EC is approximately 1.5 mS/cm, which is about 10 times that of regional unaffected, low mineralized groundwater, so that the possible influence of mine water but also secondary processes can be detected at an early stage.

During flooding up to 140 m a.s.l. and the subsequent holding of the water level, permanent probes were read at regular intervals of 2-4 weeks and data were uploaded to the environmental database for evaluation. To ensure an instant detection of changes in electrical conductivity in the monitoring wells of aquifers #3 and #4 during hydraulic test 2, online data transmission was established. Due to unfavorable local conditions in mountainous terrain and with dense forestation, reliable mobile network coverage is limited in the Königstein region. Therefore, a local wireless network based on LoRaWAN technology was installed. LoRaWAN (=long range wide area network) is a network protocol designed for the wireless connection of battery-operated devices to the internet. Being independent from the mobile network and having a very low power consumption, it is possible to transmit small amounts of data over long distances, which is why the technology is very suitable for use in remote areas.

The path taken by the probe data from the measurement on-site via online transmission into the process control system to the final presentation in the environmental database is shown in figure 2. The process control system of Königstein, where all data are collected, performs an initial valuation of transmitted data. Failures in data transmission, increases in EC and potential differences compared to the control drift trigger an automated notification of the staff responsible. Following the ongoing transfer of data from the process control system to the probe database, the data is validated and approved, and finally transferred to the environmental database.

In 2022/2023, the LoRaWAN technology was tested at the Königstein site over a period of one year as part of a feasibility study. It

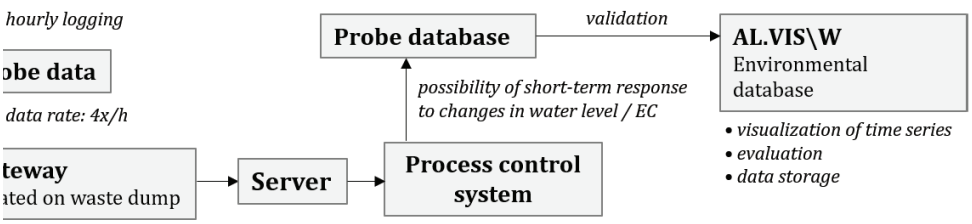

Figure 2 Dataflow for continuous online transmission of probe data by LoRaWAN technology at the Königstein site.

revealed that all measuring points to be equipped could be reached via the wireless network standard if the gateway was located on the northeastern edge of the former mine operating area (Figure 1). During the test period, it was also observed that the transmission rate highly depends on external factors. For example, precipitation leads to a substantial reduction in the transmission rate. Generally, transmission rate is clearly better in winter, due to the lack of foliage on the trees, high cloud cover, and snow- or ice-covered surfaces, which promote the reflection of radio waves and thus signal transmission. Due to the positive results of the feasibility study, all existing permanent probes observing the aquifers #3 and #4 were equipped with LoRaWAN transmission modules prior to the beginning of hydraulic test 2.

After more than one year of operating the technology at the Königstein site, it has been shown that the principle works reliably at over 90% of the monitoring wells equipped with probes. Depending on the weather, minor data gaps of few hours may occur, which are acceptable due to change dynamics of the measured parameters. At few monitoring wells, due to their location and position (underfloor, situated in a valley), data transmission is unreliable and insufficient, with data gaps of up to several days. Therefore, manual probe readout remains necessary at these locations. Measurable reactions related to the beginning of hydraulic test 2 were evident after few months of rising the flood level. The following section describes the observations made at the affected monitoring well k-66040 in more detail and explains the derived steps.

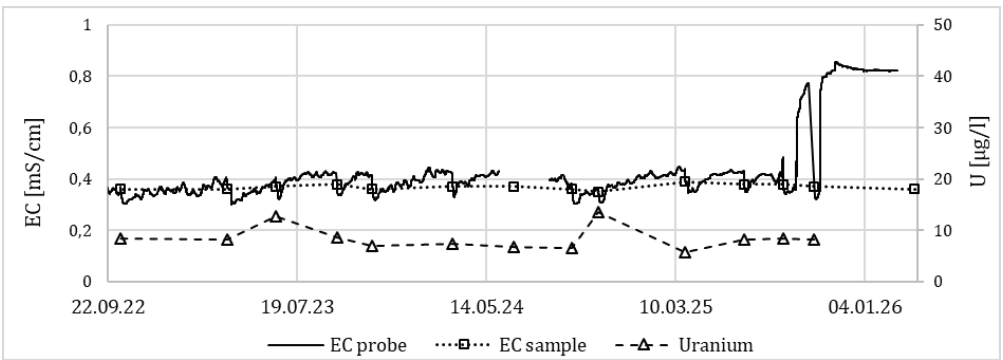

Figure 3 EC profile measured at monitoring well k-66040 using a permanent probe compared to EC and uranium values in pumped samples.

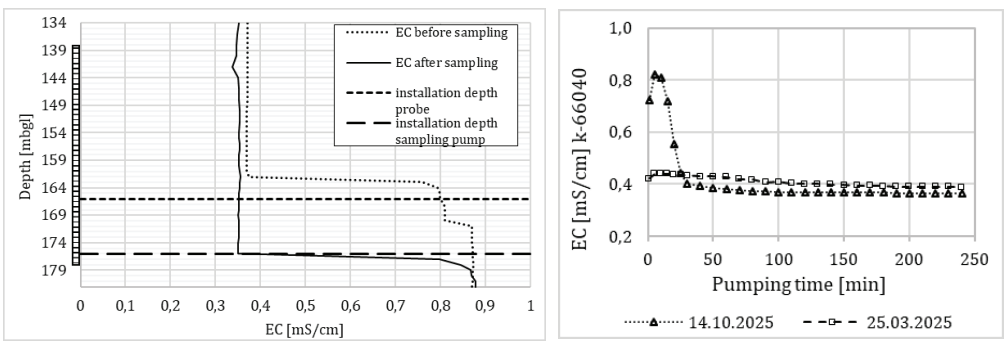

Figure 4 EC depth profile of k-66040 from October 9, 2025 - before sampling, compared to October 15, 2025 after sampling (left); EC profiles of k-66040 measured during pumping prior to sampling (right).

After its construction in 2020, the water in the monitoring well k-66040, which exposes the Lower Turonian sandstone of aquifer #3 at a depth of 90 to 180 m, had a total mineralization of 230 mg/L, with a slightly acidic environment (pH 6). The concentrations of mine water typical parameters were considerably below background values in this region, thus showing no influence by mine water. In September 2025, a sudden increase in EC to 0.7 mS/cm occurred, with a maximum of 0.85 mS/cm finally (see figure 3). Representative sampling at the monitoring well is carried out by pumping once the borehole water has been removed and in-situ parameters (EC, pH, temp.) in the pumped water have stabilised. Figure 3 shows that, for all samples taken in this way, the electrical conductivity remained at a consistently low level, and also uranium showed no upward trend.

Electrical conductivity profiles recorded, using a cable-based light probe with EC sensor (*Hydrotechnik GmbH*), a few days before and after sampling in October 2025 showed that there is a clear stratification in the monitoring well with a higher mineralized layer underlying the typical low mineralized groundwater. The interface level was lowered by 14 m due to sampling (Fig. 4, left). The continuous EC measurements taken during the pumping process prior to sampling showed that the volume of higher mineralized water was completely pumped out at a pumping rate of 2.0 m^3/h within less than 30 minutes (Fig. 4, right). This equals to a maximum volume of 1 m^3 of higher mineralized water. The results of water analyses also remained unchanged compared to the initial values with regard to parameters typical for floodwater. Results thus indicate that the upwelling water with higher EC is not representative for the hydrochemical character of the surrounding aquifer. The change in pressure conditions, and thus altered hydraulics caused by raising the water level during the hydraulic test 2, leads to a changing convection within the monitoring well. Hence, a direct inflow of mine water cannot be assumed so far, based on the available results. A similar effect was also observed after hydraulic test 1. As long as the volume of higher mineralized water can be completely pumped out within short time during the sampling process and chemical analysis shows no abnormalities, an encroachment of mine water to aquifer #3 along the north fault is not to be assumed.

Conclusions

The permitted increase in water level during hydraulic test 2 as part of the complete flooding of the Königstein mine is in progress and accompanied by an intensive monitoring program. Initial hydrochemical effects can be observed at surrounding groundwater monitoring wells. It became evident, that the transmission of probe data via LoRaWAN technology is well suited for the early detection of hydrochemical changes in remote areas. Investigations of initial changes at monitoring wells show, that an increase in the electrical conductivity does not necessarily indicate mine water influence, but rather that the causes can be multifaceted and complex. Conducting supplementary investigations, such as creating electrical conductivity profiles and intensifying sampling, can provide insights into the relevant reactions in the aquifer, and provides data for further hydraulic and hydrochemical modelling. Hydrochemical signals during the process of mine flooding should therefore not only be viewed as a problem regarding the risks to the surrounding aquifer. They also essentially contribute to validating and further developing the model assumptions for predictions and optimization of further flooding steps.

Acknowledgements

This work is part of Wismut's Königstein mine closure program. The authors would like to thank all persons actively involved in the outcome of this unique and long-lasting project.

References

Bilek F, Jenk U, Uhlig U (2023) Field test to control the hydrochemical conditions in the Königstein uranium mine by injecting a reactive solution. In: WISSYM 2023 – Re-thinking mining remediation. – p. 161–162; Dresden, Germany

Eulenberger S, Frenzel M, Metschies T, Kleditz N, Brix U, Jenk U (2021) Konzept zur Errichtung zusätzlicher Grundwassermessstellen und Aufgabebohrlöcher im Zusammenhang mit der geplanten Fortführung der Grubenflutung über das Niveau von 140 m NN. Internal report, Wismut GmbH, 14 pp

Frenzel M, Jenk U, Metschies T (2018) Flooding of the Königstein mine - Documentation of the execution of the hydraulic test (in German). Internal Report, 42 pp.

Jenk U, Zimmermann U, Paul M, Uhlig U, Schöpke R (2011) Development of an in-situ mine water treatment approach for the flooded Königstein Uranium mine (Germany) – Field experiment. – In: Rüde R. T., Freund A., Wolkersdorfer Ch.: Mine Water – Managing the Challenges. – p. 365–369; Aachen, Germany

Schmidt N, Eulenberger S, Jenk U (2022) Final Flooding of the Königstein Uranium Mine – Supporting Activities and Implications for Monitoring. – In: Pope J., Wolkersdorfer C., Rait R., Trumm D., Christenson H., Wolkersdorfer K.: IMWA 2022 – Reconnect. – p. 453–458; Christchurch, New Zealand

IMWA 2026
Jeongseon

Modelling a Moving Disaster: A Novel Approach to Modelling Non-Newtonian Flow Post Tailings Dam Breach

Nadia Skifa, James McKenna, Vassilis Glenis

School of Engineering, Newcastle University, United Kingdom

Abstract

Tailings dam failures cause catastrophic loss of life, environmental degradation, and economic damage. Contemporary industry-standard models typically rely on simplified solvers that fail to capture the non-Newtonian behaviour of tailings under rapid dynamic conditions, limiting hazard assessment accuracy and weakening emergency preparedness. This paper presents a finite-volume shock-capturing solver incorporating a quadratic viscoplastic rheology, an Osher-type approximate Riemann solver, and a hydrodynamic reconstruction technique preserving stationary and moving equilibria. Benchmarks against the idealised viscoplastic dam-break of Hungr and the 2019 Brumadinho disaster, show good agreement with published modelling results and observed data.

Keywords: Tailings flow, non-Newtonian, Riemann solver, Brumadinho failure

Introduction

When a tailings dam breaches, the released slurry behaves as a non-Newtonian fluid with a finite yield stress and shear-dependent resistance. This behaviour governs the sharp deceleration, progressive deposition, and localised arrest that define real events. Existing models struggle to represent this behaviour with sufficient fidelity for credible consequence analysis. Current approaches to tailings breach-runout modelling address only part of this challenge. Empirical volume-area relationships (Ghahramani *et al.*, 2020; Rico *et al.*, 2008) provide rapid screening but can be highly uncertain. Landslide models such as DAN3D and RAMMS use robust shock-capturing numerics yet represent tailings as purely frictional materials, rather than viscoplastic slurries (Sreekumar *et al.*, 2024). Shallow-water models, such as FLO-2D (FLO-2D Software Inc), MadFlow (Chen & Lee, 2003), and HEC-RAS (Brunner, 2016) implement adequate rheological formulations, however their diffuse numerical schemes tend to struggle to resolve sharp flow fronts, wet-dry transitions, and the steep depth gradients (Kheirkhah Gildeh *et al.*, 2021). In fact, many implementations rely on non-conservative formulations that do not rigorously satisfy the conservation laws and lead to convergence towards incorrect solutions, as noted by Hou & Le Floch (1994). The practical consequence is that models may reproduce the gross inundation footprint whilst misrepresenting the arrival time and proximal tailings wave height. This is crucial for emergency planning and determination of contamination zones and downstream water quality impacts. This paper presents a finite-volume shock-capturing solver that combines a quadratic viscoplastic rheology with an Osher-type approximate Riemann solver and a well-balanced hydrodynamic reconstruction. The solver is validated against the idealised viscoplastic dam-break of Bryant *et al.* (1983) and benchmarked against Iber-NNF (Sanz-Ramos *et al.*, 2024) and DAN (Hungr, 1995). The Brumadinho 2019 tailings dam failure is then used as a case study to demonstrate the model's applicability to a real catastrophic event, with predictions compared against published modelling results.

Numerical model

To preserve the physical integrity of this moving disaster, the numerical scheme must resolve sharp fronts and rapid flow transitions without spurious oscillations. The mudflow is therefore modelled using the 2D depth-averaged incompressible flow equations in conservative form with a non-Newtonian source term:

$$\frac{\partial U}{\partial t}+\frac{\partial F}{\partial x}+\frac{\partial G}{\partial y}=S(U)$$

where U = [h, hu, hv]^T are the conserved variables, F = [hu, hu^2 + 0.5gh^2, huv]^T and G = [hu, huv, hv^2 + 0.5gh^2]^T are the flux vectors, and S(U) accounts for the source terms including bed-slope and non-Newtonian shear stress.

The rheological behaviour of the tailings is described by the O'Brien & Julien quadratic model (O'Brien *et al.*, 1985), in which the total shear stress is:

$$\tau=\tau_Y+\eta\frac{du}{dy}+C\left(\frac{du}{dy}\right)^2$$

The three terms represent distinct physical contributions. The yield stress τ_y, is the finite stress required for flow to initiate. The viscous stress is characterized by the dynamic viscosity η. The turbulent-dispersive stress $C\ (du/dy)^2$ accounts for inertial and grain-collision forces, with coefficient $C = \rho_m l^2 + f(\rho_m, C_v)\ d_s^2$, where d_s is the representative particle diameter and ρ_m is the mixture density and C_v the concentration by volume. Collectively, the three stresses contribute to describe the full rheology of tailings behaviour from fluid-like behaviour at high shear rates near the breach, through viscous deceleration in the channel, to plastic arrest at the deposit boundary where the local stress falls below τ_y. The computational domain is discretized into a uniform Cartesian grid of rectangular finite-volume cells, over which the conserved variables are assumed piecewise constant within each cell. Intercell fluxes are computed using a generalised Osher-Solomon approximate Riemann solver (Dumbser *et al.*, 2010; Osher & Solomon, 1982). The solver valuates the numerical flux by integrating the flux Jacobian along a straight-line path in phase space via three-point Gauss–Legendre quadrature. This approach is entropy-satisfying and conservative, resolves sharp flow discontinuities and accurately captures the material interfaces and moving wet-dry fronts. The path-integral formulation avoids the need for explicit wave-speed estimates or flux limiters and remains well-defined across the full range of flow regimes encountered in a dam-break event. In addition, well-balanced treatment of the bed-slope source term is achieved through a hydrodynamic reconstruction (Berthon & Michel-Dansac, 2024) at cell interfaces, which ensures non-negativity of the mixture depth over irregular terrain and preserves dynamic and stationary equilibria. This property is essential for simulations on real topography, where bathymetric irregularities would otherwise generate spurious flows in dry or stationary regions. The full framework of the model is described in (Skifa *et al.*, 2026).

Test Cases

Idealized dam-break for viscous-plastic fluid

The numerical scheme is benchmarked against the semi-analytical one-dimensional viscoplastic dam-break problem on a horizontal plane of Bryant *et al.* (1983). Similar benchmarking exercises have been performed by many studies such as Hungr (1995) and Sanz-Ramos *et al.* (2024), which provides a semi-analytical reference solution for the runout of a finite volume of viscoplastic material released on a horizontal plane. This test case is widely used to assess the ability of depth-averaged solvers to reproduce the time evolution of flow depth and front position under purely viscoplastic resistance, without the complicating influence of topographic irregularities.

Tailings dam failure of Brumadinho

On January 25th, 2019, the B1 dam at the Córrego do Feijão iron ore mine near Brumadinho, Minas Gerais, Brazil (Figure 1), underwent a sudden and complete failure triggered by static liquefaction of the tailings material (Robertson *et al.*, 2019). The entire structure collapsed, releasing approximately 9.7 Mm^3 of material, roughly 75% of the stored tailings volume, within five minutes (Robertson *et al.*, 2019). The resulting flow

Table 1 Key Parameters and values used in the model for Brumadinho mine tailings flow.

Parameter	Value
Mixture specific density ρ_m	26 kN/m^3
Yield stress τ_y	800 Pa
Dynamic viscosity η	100 Pa·s
Manning roughness n	0.167
Volumetric concentration C_v	55%
Roughness flow parameter K	2,285

travelled approximately 10 km downstream, inundating the mine's canteen, swiping the railway bridge and reaching the Paraopeba river, ultimately claiming 270 lives. The outflow from the failed dam was a mixture of the embankment itself, stored tailings, and water, producing a hyperconcentrated non-Newtonian mudflow (Robertson *et al.*, 2019; Lumbroso *et al.*, 2021). Since no direct field or laboratory measurements of the Brumadinho tailings rheology are publicly available, the parameter values listed in Table 1 were derived from three complementary sources: (i) the Robertson *et al.* (2019) expert panel report, which provides estimates of in-situ volumetric concentration and material density; (ii) satellite imagery processed to delineate the final inundation extent; and (iii) parameter ranges reported in comparable numerical studies using MIKE21 (Lumbroso *et al.*, 2021), RiverFlow2D (Palu *et al.*, 2019) and TUFLOW HPC (TUTFLOW modelling team, 2021).

Unlike Lumbroso *et al.* (2021) and (Gibson *et al.*, 2022), who used a time-varying breach hydrograph as inflow, the present model adopted a dam-break initial condition, releasing the full tailings volume instantaneously at t = 0, under the assumption of an initial constant mixture free surface elevation of 960m with depths between 0 and 95m in the reservoir area. This is a more conservative assumption avoiding the additional uncertainty associated with breach parameter estimation. The computational domain was discretized into a regular grid based on a 12.5 m resolution ALOS PALSAR RTC DEM. The computational domain extent was obtained by adding a buffer of 200m of the observed inundation extent, which captures the flow from the dam toe to the Paraopeba River including the Dam VI near the TSF dam.

Results and Discussion

Idealized dam-break for viscous-plastic fluid

Figure 2 presents the simulated flow depth profiles at t = 0, 30, 60, 90, and 130 s alongside the Hungr (1995) analytical solution at arrest. The predicted final deposit extent, in Table 2, of 1883 m agrees with the Hungr (1995) analytical solution of 1892.8 m to within 0.5%, comparing favourably against DAN (1875 m) and Iber-NNF (1850 m).

The overprediction of proximal deposit depth relative to the analytical value of 7.36 m is attributed to the breakdown of the shallow water long-wave assumption in the near-dam region, where vertical accelerations are non-negligible, a known limitation shared by all depth-averaged viscoplastic solvers.

Tailings dam failure of Brumadinho

The results of the Brumadinho simulation are reported in Figure 3, showing the mudflow depth at 0 s, 90 s, 300 s, 600 s, 3600 s and 6600 s following the instantaneous dam-break. The results demonstrate that the solver captures the wave spread of the Brumadinho failure, though with limitations that are discussed below. The simulation reproduced the sequential inundation of three reference locations documented in post-event investigations. Predicted arrival times are compared against estimated arrival times from Lumbroso *et al.* (2021) in Table 3.

The flow reaches the canteen (black marker) by t = 120 s, consistent with video evidence and with Lumbroso *et al.* (2021), whose MIKE 21 Bingham simulation places canteen inundation within the first two

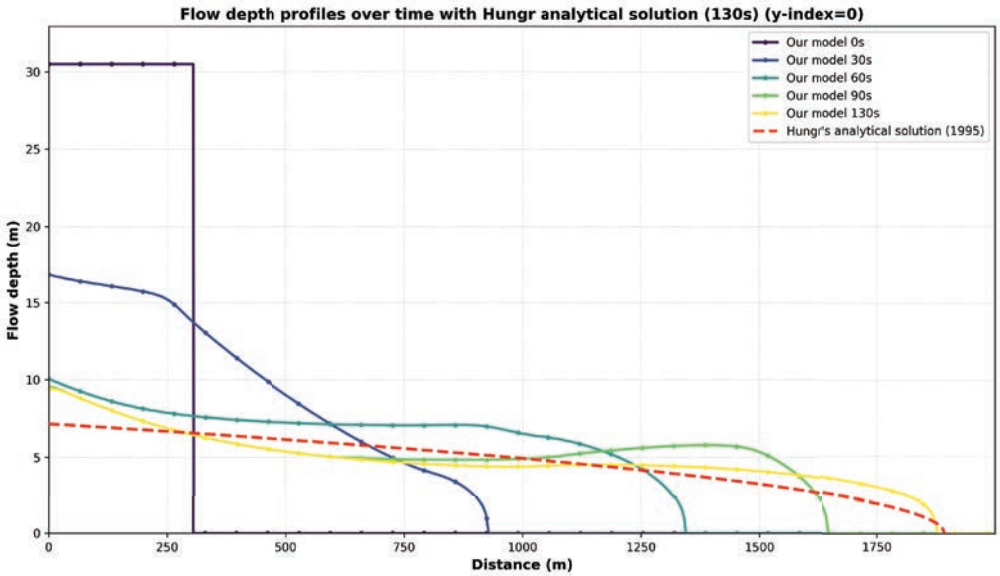

Figure 1 *Comparison of the modelled mudflow depth and the observed mud extent. The back marker is the Canteen, and the red cross is the Railway bridge.*

Table 2 *Comparisons of final deposit extent between models.*

Model	Final wave deposit extent (m)
Analytical solution	1892.80
Our model	1883.00
DAN	1875.00
Iber-NNF	1850.00

Table 3 *Arrival times of observed and simulated flow at key locations.*

Location	Estimated arrival time	Modelled arrival time
Mine canteen	≈ 2 min (observed)	2 min
Railway bridge	9 min 10 s	16 min 10 s
Paraopeba River	> 1.5 h	1 h 49 min 40 s

minutes of failure. The flow reaches the railway bridge (red marker) at t = 970 s (16 min 10 s). The estimated observed arrival time at the bridge, from video analysis by Lumbroso *et al.* (2021), is 9 min 10 s. The later predicted arrival in the present simulation, despite the dam-break initial condition producing a faster initial wave celerity than the time-varying hydrograph used by Lumbroso *et al.* (2021), could be attributed to the additional resistance introduced by the turbulent-dispersive stress term $C(du/dy)^2$ of the quadratic model, which is absent from the Bingham formulation used in Lumbroso *et al.* (2021) and becomes significant at the high shear rates in the confined valley reach between the canteen and the bridge. At t = 6580 s the modelled flow has reached the Paraopeba River (yellow marker), approximately 10 km downstream. Lumbroso *et al.* (2021) report

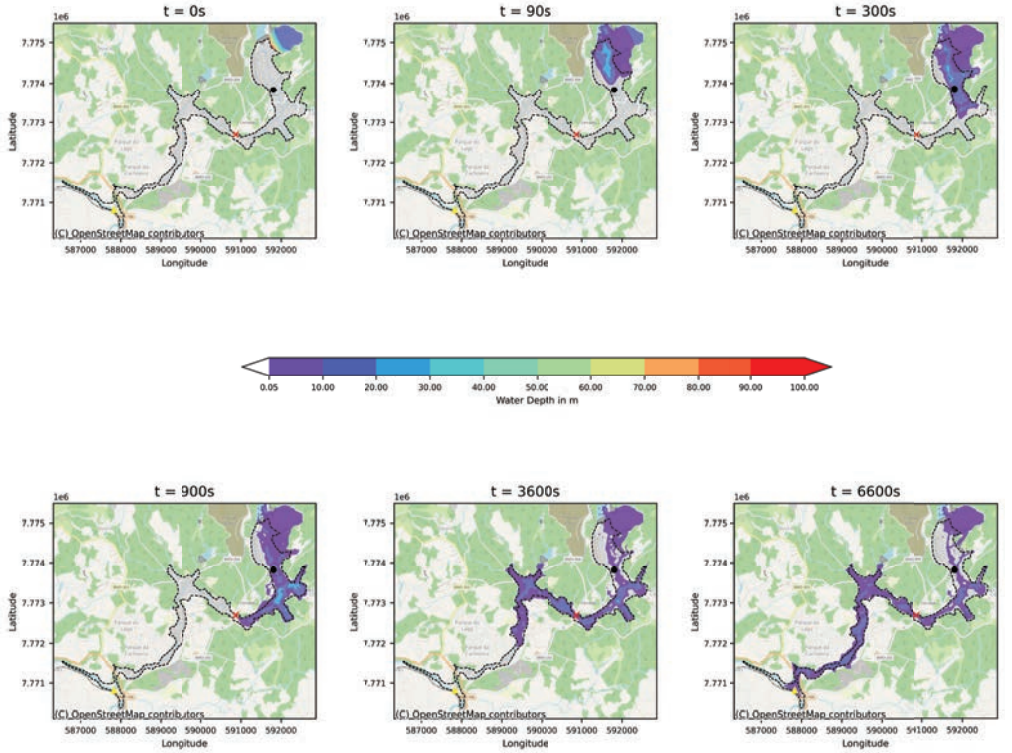

Figure 2 Comparison of the modelled mudflow depth and the observed mud extent. The back marker is the Canteen, the red cross is the Railway bridge, and the yellow triangle is the river.

a modelled river arrival of 1 h 26 min 05 s against an estimated observed arrival of approximately 1hour 30min to 2hours 30min (TUTFLOW modelling team, 2021). The small overprediction of runout arrival time in the present simulation is compounded by two factors not reported in other studies: a portion of the simulated volume was diverted into a neighbouring reservoir, reducing the volume propagating toward the river, a behaviour consistent with satellite imagery showing tailings reaching the adjacent reservoir, and the use of Bingham-calibrated parameters in a quadratic formulation introduces structural parameter mismatch. The dam-break initial condition was adopted on physical grounds, as documented in video evidence and confirmed by Robertson *et al.* (2019) of the of the Feijão dam that failed by near-instantaneous liquefaction across the full reservoir, making this assumption a physically appropriate representation of the mobilisation mechanism rather than a simplifying convenience. Whilst Lumbroso *et al.* (2021), Gibson *et al.* (2022), Ligier (2020), and Raman & Liu (2019) adopted time-varying hydrographs, they were not directly measured but derived from geotechnical breach models requiring several input parameters, dam geometry, erodibility, and pore pressure distribution, that are not publicly available for Brumadinho failure, introducing a new source of uncertainty. The dam-break assumption avoids this uncertainty whilst remaining consistent with the observed failure mode. A systematic comparison between both approaches would help isolate any sensitivity of predicted arrival times and runout extent to the initial conditions.

Conclusion

The results presented in this paper demonstrate that the proposed finite-volume solver, reproduces the essential physical behaviour of a large-scale tailings dam failure.

The solver is numerically stable, conservative, and correctly enforces the yield criterion throughout the domain, producing the sharp flow fronts and abrupt flow arrest that are characteristic of tailings materials. The Brumadinho case study demonstrates that a physically consistent numerical model is a necessary condition for reliable tailings flow predictions. Without correct enforcement of the shock-capturing numerics and well-balanced treatment of topography, the rheological parameters cannot be correctly translated into physically consistent flow behaviour. Moreover, rheological parameters are a dominant source of uncertainty in tailings breach modelling, with runout distance, arrival time, and inundation extent all shown to be strongly sensitive to yield stress and viscosity (Lumbroso *et al.*, 2021; Palú and Julien, 2019). Several limitations and directions for future work are identified. The present model does not account for breach initiation or erosion-progressive failure, and the 2D depth-averaged formulation neglects the vertical flow component; extension to a multilayer framework is therefore identified as a future priority. In addition, the sensitivity of the model to rheological parameters needs to be quantified, future work will conduct a formal sensitivity and uncertainty analyses to produce probabilistic intervals on predicted inundation extents. Addressing these limitations will enable better determination of inundation and contamination zones and downstream water quality impacts.

Acknowledgements

This research is developed as part of the PhD project of the primary author and is funded by the Engineering and Physical Science Research Council (EPSRC) within the Geospatial Systems CDT (EPSRC Reference: EP/S023577/1).

References

Berthon, C., & Michel-Dansac, V. (2024). A fully well-balanced hydrodynamic reconstruction. https://irma.math.unistra.fr/~micheldansac

Bryant, S., Duncan, J. M., & Bolton Seed, H. L. (1983). Application of Tailings Flow Analyses to Field Conditions.

Chen, H., & Lee, C.F. (2003). A dynamic model for rainfall-induced landslides on natural slopes, Geomorphology, 51(4), 269-288. ISSN 0169-555X, https://doi.org/10.1016/S0169-555X(02)00224-6.

Dumbser, M., & Toro, E. F. (2010). A Simple Extension of the Osher Riemann Solver to Non-conservative Hyperbolic Systems. Journal of Scientific Computing 2010, 48(1), 70–88. https://doi.org/10.1007/S10915-010-9400-3

FLO-2D Software Inc. (1986). Retrieved https://flo-2d.sharefile.com/share/view/s52897e9457fb46949a92bb7e15ab580a/fo694c04-a524-420b-92d7-e3346e384135

Ghahramani, N., Adria, D. A. M., Rana, N. M., Llano-Serna, M., McDougall, S., Evans, S. G., & Take, W. A. (2024). Analysis of Uncertainty and Sensitivity in Tailings Dam Breach-Runout Numerical Modelling. Mine Water and the Environment, 43(1), 87–103. https://doi.org/10.1007/s10230-024-00970-w

Gibson, S., Moura, L. Z., Ackerman, C., Ortman, N., Amorim, R., Floyd, I., Eom, M., Creech, C., & Sánchez, A. (2022). Prototype Scale Evaluation of Non-Newtonian Algorithms in HEC-RAS: Mud and Debris Flow Case Studies of Santa Barbara and Brumadinho. Geosciences (Switzerland), 12(3), 134. https://doi.org/10.3390/GEOSCIENCES12030134/S1

Hungr, O. (1995). A model for the runout analysis of rapid flow slides, debris flows, and avalanches. Canadian Geotechnical Journal, 32(4), 610–623. https://doi.org/10.1139/t95-063

Kheirkhah Gildeh, H., Halliday, A., Arenas, A., & Zhang, H. (2021). Tailings Dam Breach Analysis: A Review of Methods, Practices, and Uncertainties. In Mine Water and the Environment (Vol. 40, Issue 1, pp. 128–150). Springer Science and Business Media Deutschland GmbH. https://doi.org/10.1007/s10230-020-00718-2

Ligier, P.-L., Okumura, N., & Alderman, C. (2022). Overview and lessons learned from performing tailings dam breach modelling with TELEMAC-2D. 28th TELEMAC User Conference.

Lumbroso, D., Davison, M., Body, R., & Petkovšek, G. (2021). Modelling the Brumadinho tailings dam failure, the subsequent loss of life and how it could have been reduced. Natural Hazards and Earth System Sciences, 21(1), 21–37. https://doi.org/10.5194/nhess-21-21-2021

O'Brien, J. S., Julien, P. Y., & Laboratory, U. S. U. U. W. R. (1985). Physical Properties and Mechanics of Hyperconcentrated Sediment Flows.

Osher, S., & Solomon, F. (1982). Upwind difference schemes for hyperbolic systems of conservation laws. Mathematics of Computation, 38(158), 339–374. https://doi.org/10.1090/s0025-5718-1982-0645656-0

Palu, M. C., S. M., & Julien, P. Y. (2019). Modeling the Sediment Load of the Doce River after the Fundão Tailings Dam Collapse, Brazil. https://doi.org/10.1061/(ASCE)HY.1943-7900.0001582

Raman, A., & Liu, F. (2019). An investigation of the Brumadinho Dam Break with HEC RAS simulation. http://arxiv.org/abs/1911.05219

Rico, M., Benito, G., & Díez-Herrero, A. (2008). Floods from tailings dam failures. Journal of Hazardous Materials, 154(1–3), 79–87. https://doi.org/10.1016/J.JHAZMAT.2007.09.110

Sanz-Ramos, M., Bladé, E., Sánchez-Juny, M., & Dysarz, T. (2024). Extension of Iber for Simulating Non–Newtonian Shallow Flows: Mine-Tailings Spill Propagation Modelling. Water (Switzerland), 16(14). https://doi.org/10.3390/w16142039

Skifa, N, McKenna, J & Glenis, V 2026, 'A robust numerical framework for non-Newtonian tailings flows in dam breach scenarios', in AB Fourie, M Horta, M Oliveira & S Wilson (eds), Paste 2026: Proceedings of the 28th International Conference on Paste, Thickened and Filtered Tailings, Australian Centre for Geomechanics, Perth, pp. 1-12, https://doi.org/10.36487/ACG_repo/2655_36

Sreekumar, U., Gildeh, H. K., Mohammadian, A., Rennie, C., & Nistor, I. (2024). Tailings Dam Breach Outflow Modelling: A Review. Mine Water and the Environment 2024 43:4, 43(4), 563–587. https://doi.org/10.1007/S10230-024-01015-Y

TUTFLOW modelling team. (2021). Modelling the Brumadinho Tailings Dam Failure with TUFLOW HPC's Non-Newtonian Solver. https://www.tuflow.com/insights/2021_04-brumadinho-tailings-dam-failure/

US Army Corps of Engineers. (2023). HEC-RAS Mud and Debris Flow Mud and Debris Flow.

Microencapsulation for Suppressing Acid Mine Drainage Formation: Applications in Mineral Processing and Metallurgical Operations

Itsuki Sugiura[1], Ilhwan Park[1], Sanghee Jeon[2], Carlito Tabelin[3], Mayumi Ito[1]

[1]*Division of Sustainable Resources Engineering, Faculty of Engineering, Hokkaido University, Japan*

[2]*Department of Earth Resource Engineering, Faculty of International Resources Science, Akita University, Japan*

[3]*Department of Materials and Resources Engineering and Technology, College of Engineering and Technology, Mindanao State University-Iligan Institute of Technology, Philippines*

Abstract

Acid mine drainage (AMD, and acidic leachate generated by the oxidation of sulfide minerals and enriched with toxic metal(loid)s, recognized as a persistent and widespread environmental threat to the mining industry. To suppress the AMD formation, microencapsulation techniques that limit the oxidation of AMD-forming minerals by creating surface protective coatings have been developed. Microencapsulation using aluminum (Al)-catecholate complexes created Al-oxyhydroxide coatings on the arsenopyrite surface, resulting in an approximately 70% reduction in arsenopyrite oxidation compared to the uncoated sample. In addition, the application of microencapsulation techniques has been proven effective in improving mineral processing and hydrometallurgical processes.

Keywords: Acid mine drainage, microencapsulation, sulfide passivation

Introduction

Mining and processing are essential activities for metal production, which is indispensable for sustaining modern living standards. However, these anthropogenic activities have resulted in the generation of large amounts of wastes, such as mine tailings. As a simple example, processing a copper (Cu) ore with a grade of 0.5% Cu, assuming 100% Cu recovery and a concentrate grade of 30%, would generate approximately 98.3 t of tailings per 100 t of ore processed. Since tailings generally have no economic value, they are disposed of in the tailings storage facilities (TSFs) located near mine sites. In TSFs, non-valuable sulfide minerals such as pyrite (FeS_2) and arsenopyrite (FeAsS) undergo oxidation upon exposure to oxygen and water, leading to the formation of acid mine drainage (AMD) – an acidic effluent enriched with toxic metal(loid)s. If not properly treated, AMD can cause severe environmental impacts on receiving water bodies.

The most widely used AMD treatment technique is chemical neutralization, in which AMD is mixed with alkaline materials (e.g., limestone ($CaCO_3$), quicklime (CaO), and slaked lime ($Ca(OH)_2$)) to increase the pH and induce the precipitation of metal ions (Johnson and Hallberg, 2005). This approach can be applied to a wide range of AMD conditions regardless of flow rate and water chemistry (Taylor *et al.*, 2005). However, AMD formation generally lasts for several decades to millennia, necessitating long-term treatment and resulting in high operational costs due to the continuous consumption of neutralizing agents and energy (Tabelin *et al.*, 2022). Furthermore, the generation of large volumes of sludge poses an additional challenge.

To overcome the above-mentioned drawbacks of chemical neutralization, microencapsulation (ME) techniques have been investigated to suppress AMD formation by passivating AMD-forming minerals. Microencapsulation is a technique that forms coatings to protect the core materials (e.g., particles or droplets) from environmental factors (e.g., light, moisture, temperature,

and oxygen), extend shelf-life, and improve the release properties of core material (Jyothi *et al.*, 2012; Peanparkdee *et al.*, 2016). The first application of ME technique for suppressing AMD formation was reported by Evangelou (1995), who attempted to passivate pyrite using phosphate ions and hydrogen peroxide. Following ME treatment, the pyrite surface was coated with a ferric phosphate layer, effectively suppressing its oxidation.

The authors' research group has developed an advanced ME technique, termed carrier microencapsulation (CME), which utilizes metal–organic complexes to form metal oxyhydroxide coatings on the surfaces of AMD-forming minerals (Jha *et al.*, 2012; Li *et al.*, 2019, 2021; Park *et al.*, 2018a, 2018b, 2021; Satur *et al.*, 2007). A key advantage of this technique is its ability to selectively target electrochemically reactive minerals, particularly sulfide minerals, thereby reducing unnecessary reagent consumption in complex systems such as tailings. In this paper, CME technique for passivating pyrite and arsenopyrite to suppress AMD formation is introduced. Furthermore, its potential applications not only in supressing AMD formation but also in improving the efficiency of mineral processing and metallurgical operations are discussed.

Microencapsulation for the Suppression of AMD Formation

In CME, various metal ions (e.g., Ti^{4+}, Si^{4+}, Fe^{3+}, and Al^{3+}) complexed with organic ligand – pyrocatechol (1,2-dihydroxylbenzene, $C_6H_4(OH)_2$) – forming metal-organic complexes $[Me(cat)_n]^{m-2n}$; where Me: metal ion, cat: catechol, m: valency of metal ion (3 for Fe^{3+} and Al^{3+}; 4 for Ti^{4+} and Si^{4+}), n: the number of catechol molecules complexed) have been examined to suppress the oxidation of pyrite and arsenopyrite (Jha *et al.*, 2012; Li *et al.*, 2019, 2021; Park *et al.*, 2018a, 2018b, 2021; Satur *et al.*, 2007). Among them, this paper introduces CME using aluminum (Al)-catecholate complexes to passivate arsenopyrite. Figure 1 shows the working principle of CME on how Al-catecholate complexes passivate sulfide minerals.

As can be seen, Al-catecholate complexes are electrochemically sensitive, and thus they are oxidatively decomposed on the surface of semiconducting minerals like arsenopyrite (Eqs. 1–3):

$$[Al(cat)_3]^{3-} \rightarrow [Al(cat)_2]^{-} + Q + 2e^{-} \quad (1)$$

$$[Al(cat)_2]^{-} \rightarrow [Al(cat)]^{+} + Q + 2e^{-} \quad (2)$$

$$[Al(cat)]^{+} \rightarrow Al^{3+} + Q + 2e^{-} \quad (3)$$

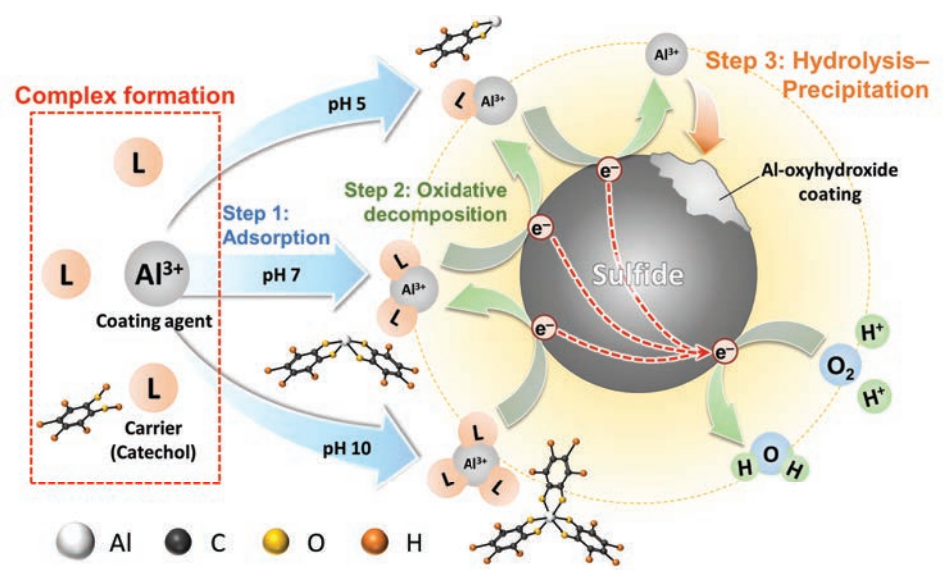

Figure 1 A schematic illustration of CME technique for sulfide passivation. Reproduced with permission from Park et al., 2018b.

where Q denotes 1,2-benzoquinone ($C_6H_4O_2$) – an oxidation product of catechol. As a result, Al^{3+} is released from the complex and precipitated as Al-oxyhydroxide under appropriate pH conditions (i.e., pH 5–8) (Eq. 4).

$$Al^{3+} + 3H_2O \rightarrow Al(OH)_3 + 3H^+ \quad (4)$$

Through the complex decomposition followed by metal precipitation reactions, sulfide minerals are passivated by Al-oxyhydroxide coatings.

Figure 2(a) shows the changes in dissolved Al concentration after CME treatment of arsenopyrite using 5 mM Al^{3+} in the form of mono-, bis-, and tris-catecholate complexes, which predominantly form at pH 5, 7, and 10, respectively. The amounts of Al^{3+} precipitated after CME treatment were 83 mg/L for $[Al(cat)]^+$, 53 mg/L for $[Al(cat)_2]^-$, and 10 mg/L for $[Al(cat)_3]^{3-}$. This trend indicates that increasing catecholate coordination number decreases Al precipitation due to the enhanced stability and solubility of higher-order Al-catecholate complexes. The concentrations of Fe, As, and S released from arsenopyrite during CME treatment increased in the order $[Al(cat)]^+ < [Al(cat)_2]^- < [Al(cat)_3]^{3-}$ (data not shown), indicating that a strong correlation between the amount of Al precipitated and the suppression of arsenopyrite oxidation. These results suggest that among the three complex species, $[Al(cat)]^+$ is the most effective one in suppressing the arsenopyrite oxidation.

In addition to the complex species, the complex concentration also showed a significant effect on arsenopyrite oxidation; specifically, the release of S from arsenopyrite decreased from ≈90 mg/L with no complex to <10 mg/L with 15 mM $[Al(cat)]^+$, due to the greater amount of coating formed at higher complex concentrations (date not shown).

Figure 2(b) shows the XPS Al 2p spectra of untreated and CME-treated arsenopyrite using $[Al(cat)]^+$. The Al 2p spectrum of untreated arsenopyrite showed no discernible peak, whereas three distinct peaks corresponding to boehmite (γ-AlO(OH)) at 73.9 eV, gibbsite (γ-$Al(OH)_3$) at 74.3 eV, and bayerite (*y*-$Al(OH)_3$) at 74.8 eV were observed for the CME-treated arsenopyrite. These results indicate that Al-based CME forms Al-oxyhydroxide coatings on the arsenopyrite surface.

The effect of CME treatment on suppressing arsenopyrite oxidation was evaluated by a weathering cell test. The procedure for the weathering cell test followed that described by Bouzahzah *et al.* (2014). Two samples were tested: (i) arsenopyrite leached in deionized (DI) water for 7 days (control), and (ii) arsenopyrite treated with 15 mM $[Al(cat)]^+$ for 7 days. As shown in Fig. 2(c), both samples continued to oxidize, releasing sulfur species into the leachate; however, the extents of dissolved S release differed significantly between the two. After 6 weeks of the weathering cell tests, the cumulative S concentration reached ≈700 mg/L for the control and ≈200 mg/L for the CME-treated sample; that is, CME treatment suppressed arsenopyrite oxidation by approximately 70%.

Application of Microencapsulation in Mineral Processing and Metallurgical Operations

As confirmed in the previous section, the ME technique is effective in suppressing the oxidation of AMD-forming minerals. Although the ME technique can be applied to wastes generated after mineral processing and metallurgical operations, its optimum application would be prior to ore processing, aiming to separation and extraction efficiencies while simultaneously suppressing AMD formation. In the subsequent sub-sections, the application of the ME technique to coal cleaning and gold hydrometallurgy is presented.

Microencapsulation for Coal Cleaning

Pyrite is a common gangue mineral associated with coal and is removed by gravity concentration technique like jigging due to the different specific gravities of pyrite (≈5 g/cm^3) and coal (1.1–1.5 g/cm^3). The appropriate particle size for coal cleaning by the conventional jig is > 10 mm, so its efficiency dramatically decreased when processing 1 mm size fraction (Phengsaart *et al.*, 2023).

To improve the separation efficiency of fine particles, the authors developed the hybrid

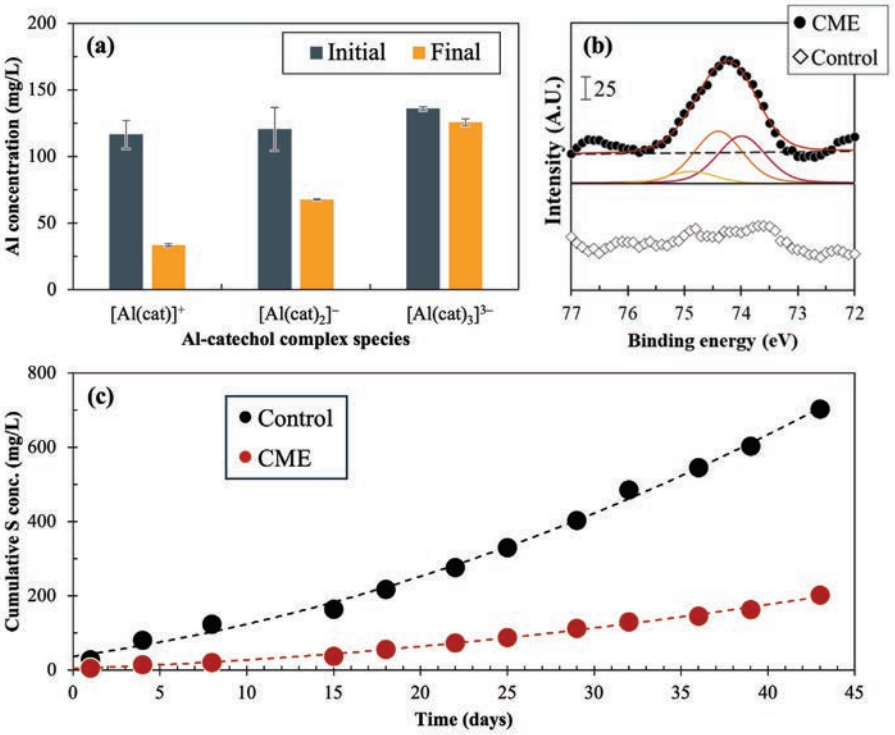

Figure 2 (a) Changes in dissolved Al concentration before and after CME treatment, (b) XPS Al 2p spectra of untreated and CME-treated arsenopyrite, and (c) weathering cell test results of control and CME-treated arsenopyrite. Reproduced with permission from Park et al., 2018b, 2020.

jig, which combines the principles of jigging and flotation (i.e., jigging while introducing air) (Hori *et al.*, 2009). In order for hybrid jig to work, air bubbles should be selectively attached to coal particles. However, the selective bubble attachment is impossible due to the fact that both coal and pyrite are inherently hydrophobic. To overcome this problem, ME treatment was applied to selectively render pyrite hydrophilic, while coal particles remain hydrophobic to be able to attach air bubbles (Phengsaart *et al.*, 2023). Pyrite and coal were each treated with a solution containing 1 mM ferrous (Fe^{2+}) and phosphate (PO_4^{3-}) ions at pH 3 for 1 h. Ferrous ions are selectively oxidized to ferric ions on the pyrite surface, after which ferric ions react with phosphate ions to precipitate as ferric phosphate.

The XPS analysis of untreated and ME-treated pyrite and coal showed that the peaks of Fe(III–PO_4 and P(V–O were observed only in the spectrum of ME-treated pyrite. Figure 3 shows the distribution of coal and pyrite (particle size: −1.4+1.0 mm) in each layer after conventional jig, hybrid jig and hybrid jig with ME treatment. The conventional jig result at the separation time of 0.5 min (Fig. 3(a-1)) showed that pyrite content in the middle layer was ≈11%. Although pyrite content in the middle layer decreased to 4.2% by extending the separation time to 5 min, the sulfur content of the product exceeded the criterion for low-sulfur coal (Fig. 3(b-1)). In the case of hybrid jig, the result was worse compared to the conventional jig due to non-selective bubble attachment (Figs. 3(a-2) and 3(b-2)). When ME treatment was applied, however, the efficiency of hybrid jig separation was improved (Figs. 3(a-3) and 3(b-3)); that is, pyrite content in the middle layer was 1% and 0% at the separation time of 0.5 min and 5 min, respectively, indicating low-sulfur coal could be produced by ME treatment followed by hybrid jig separation and the separation time can be shortened.

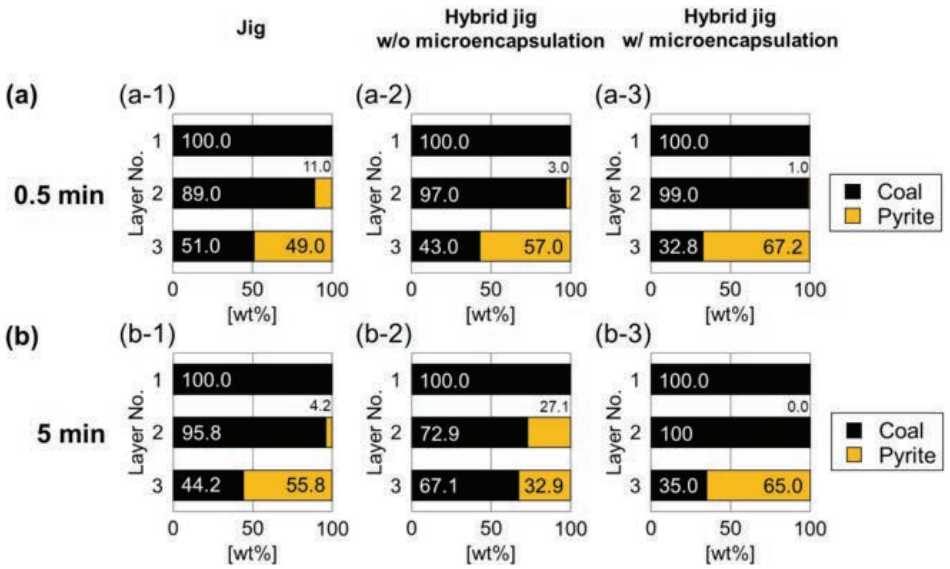

Figure 3 *Distribution of coal and pyrite in each layer after jig separation for 0.5 min (a-1) and 5 min (b-1), hybrid jig separation for 0.5 min (a-2) and 5 min (b-2), and hybrid jig separation with ME treatment for 0.5 min (a-3) and 5 min (b-3) (Phengsaart et al., 2023).*

Microencapsulation for Gold Hydrometallurgy

The conventional method to extract gold from ores is the cyanidation process. Although cyanide is inexpensive and highly effective for gold extraction, its use in gold processing has been increasingly challenged by environmental organizations and governments due to its toxicity (Bocse, 2021). Because of this drawback of cyanide, many studies have been conducted to find alternative lixiviants to cyanide, the candidates of which are thiourea, thiocyanate, halogen-based, and thiosulfate solvents (Mhandu *et al.*, 2023). Among them, thiosulfate is considered the most promising lixiviant due to its high selectivity, fast leaching rate, low toxicity, and low corrosivity. However, the applicability of thiosulfate medium is challenging when processing arsenopyritic gold ores because of unwanted thiosulfate decomposition occurring on the arsenopyrite surface (Mhandu *et al.*, 2023). To solve this problem, the applicability of the ME treatment using ferrous and phosphate prior to thiosulfate leaching of gold was investigated. As can be seen in Fig. 4, when processing with untreated arsenopyrite, only 16% of gold was extracted, whereas it was improved to 72% by employing the ME treatment. This proved that $FePO_4$ coating formed on the arsenopyrite surface reduced thiosulfate decomposition, thus improving gold extraction efficiency.

Conclusions

The ME technique was demonstrated to be effective in suppressing the oxidation of AMD-forming minerals by forming protective coatings on their surfaces. In

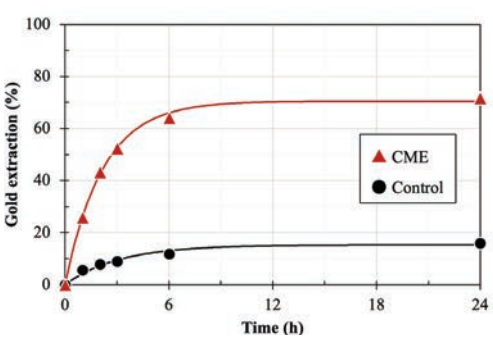

Figure 4 *Gold extraction by thiosulfate in the presence of untreated and ME-treated arsenopyrite.*

addition to its environmental benefits, ME was shown to enhance separation efficiency in coal cleaning and improve gold extraction in hydrometallurgical processes. These findings highlight the potential of ME as a versatile pre-treatment strategy that not only mitigates environmental risks but also enhances the efficiency of mineral processing and metallurgical operations.

Acknowledgements

This research was funded by the Japan Society for the Promotion of Science (JSPS) grant-in-Aid for Early-career Scientists (JP24K17639).

References

Bocse A (2021) Hybrid transnational advocacy networks in environmental protection: banning the use of cyanide in European gold mining. Int Environ Agreements 21:285–303. doi: 10.1007/s10784-020-09492-6

Bouzahzah H, Benzaazoua M, Bussiere B, Plante B (2014) Prediction of acid mine drainage: Importance of mineralogy and the test protocols for static and kinetic tests. Mine Water Environ 33:54–65. doi: 10.1007/s10230-013-0249-1

Evangelou VP (1995) Potential microencapsulation of pyrite by artificial inducement of ferric phosphate coatings. J Environ Qual 24:535–542. doi: 10.2134/jeq1995.00472425002400030021x

Hori K, Tsunekawa M, Ueda M, Hiroyoshi N, Ito M, Okada H (2009) Development of a new gravity separator for plastics – a hybrid-jig. Mater Trans 50(12):2844–2847. doi: 10.2320/matertrans.M-M2009825

Jha RKT, Satur J, Hiroyoshi N, Ito M, Tsunekawa M (2012) Suppression of pyrite oxidation by carrier microencapsulation using silicon and catechol. Miner Process Extr Metall Rev 33(2):89–98. doi: 10.1080/08827508.2011.562946

Johnson DB, Hallberg KB (2005) Acid mine drainage remediation options: a review. Sci Total Environ 338(1–2):3–14, doi:10.1016/j.scitotenv.2004.09.002

Jyothi SS, Seethadevi A, Prabha KS, Muthuprasanna P, Pavitra P (2012) Microencapsulation: A review. Int J Pharma Bio Sci 3:509–531.

Li X, Hiroyoyshi N, Tabelin CB, Naruwa K, Harada C, Ito M (2019) Suppressive effects of ferric-catecholate complexes on pyrite oxidation. Chemosphere 214:70—78. doi: 10.1016/j.chemosphere.2018.09.086

Li X, Park I, Tabelin CB, Naruwa K, Goda T, Harada C, Jeon S, Ito M, Hiroyoshi N (2021) Enhanced pyrite passivation by carrier-microencapsulation using Fe-catechol and Ti-catechol complexes. J Hazard Mater 416:126089. doi: 10.1016/j.jhazmat.2021.126089

Mhandu TJ, Park I, Jeon S, Hamatsu S, Elakneswaran Y, Ito M, Hiroyoshi N (2023) A pretreatment of refractory gold ores containing sulfide minerals to improve gold leaching by ammonium thiosulfate: a model experiment using gold powder and arsenic-bearing sulfide minerals. Metals 13:1357. doi: 10.3390/met13081357

Park I, Tabelin CB, Magaribuchi K, Seno K, Ito M, Hiroyoshi N (2018a) Suppression of the release of arsenic from arsenopyrite by carrier-microencapsulation using Ti-catechol complex. J Hazard Mater 344:322–332, doi: 10.1016/j.jhazmat.2017.10.025

Park I, Tabelin CB, Seno K, Jeon S, Ito M, Hiroyoshi N (2018b) Simultaneous suppression of acid mine drainage formation and arsenic release by carrier-microencapsulation using aluminum-catecholate complexes. Chemosphere 205:414–425, doi:10.1016/j.chemosphere.2018.04.088

Park I, Tabelin CB, Seno K, Jeon S, Inano H, Ito M, Hiroyoshi N (2020) Carrier-microencapsulation of arsenopyrite using Al-catecholate complex: nature of oxidation products, effects on anodic and cathodic reactions, and coating stability under simulated weathering conditions. Heliyon 6(1):e03189. doi: 10.1016/j.heliyon.2020.e03189

Park I, Higuchi K, Tabelin CB, Jeon S, Ito M, Hiroyoshi N (2021) Suppression of arsenopyrite oxidation by microencapsulation using ferric-catecholate complexes and phosphate. Chemosphere 269:129413. doi: 10.1016/j.chemosphere.2020.129413

Peanparkdee M, Iwamoto S, Yamauchi R (2016) Microencapsulation: A review of applications in the food and pharmaceutical industries. Rev Agric Sci 4:56–65. doi: 10.7831/ras.4.56

Phengsaart T, Park I, Pasithbhattarabhorn J, Srichonphaisarn P, Kertbundit C, Phumkokrux N, Juntarasakul O, Tabelin CB, Hiroyoshi N, Ito M (2023) Development of microencapsulation-hybrid jig separation technique as a clean coal technology. Energies 16(5):2432. doi: 10.3390/en16052432

Satur J, Hiroyoshi N, Tsunekawa M, Ito M, Okamoto H (2007) Carrier-microencapsulation for preventing pyrite oxidation. Int J Miner Proc 83(3–4):116–124. doi: 10.1016/j.minpro.2007.06.003

Tabelin CB, Uyama A, Tomiyama S, Vilacorte-Tabelin M, Phengsaart T, Silwamba M, Jeon S, Park I, Arima T, Igarashi T (2022) Geochemical audit of a historical tailings storage facility in Japan: Acid mine drainage formation, zinc migration and mitigation strategies. J Hazard Mater 438:129453, doi:10.1016/j.jhazmat.2022.129453

Taylor J, Pape S, Murphy N (2005) A summary of passive and active treatment technologies for acid and metalliferous drainage (AMD). In Proceedings of the 5th Australian Workshop on Acid Drainage, 29–31 August 2005, Fremantle, Austral

IMWA 2026
Jeongseon

Identifying the Sustainability Efficiency Peak in Tailings Reprocessing: An Entropy–TOPSIS Assessment of Restorative Mining

Seyed Mostafa Taghavi[1], Abeer Sajid[1], Moeen Hamedi[1], Hernan Anticoi[1], Marc Bascompta[1]

[1]*Department of Mining, Industrial and ICT Engineering, Universitat Politècnica de Catalunya (UPC) – Barcelona Tech 08242, Spain*

Abstract

Reprocessing of historical sulfidic tailings is evaluated as a circular economy strategy using a multi-criteria decision-making framework. Using Entropy-TOPSIS, six reprocessing alternatives were analyzed integrating technical, economic, environmental, and social indicators. Results identify 80% tailings reprocessing as the sustainability-optimal restorative mining pathway, achieving a closeness coefficient of 0.844. Although full reprocessing maximizes copper recovery, exponential increases in freshwater stress and community disturbance penalize performance. Findings reveal a non-monotonic relationship between reprocessing intensity and sustainability. Moderate reprocessing provides a resilient balance between resource efficiency and regional socio-environmental stability.

Keywords: Restorative mining, circular economy, tailings reprocessing

Introduction

Strategic European policy initiatives now frame mine tailings as vital secondary resource reservoirs rather than mere environmental liabilities (European Commission 2023). Such a paradigm shift is essential, given that annual global production of mineral waste exceeds 10 billion tonnes (Araya et al. 2020; Johansson *et al.* 2024). Reprocessing these deposits represents a restorative mining strategy capable of mitigating acid mine drainage (AMD) and reducing reliance on primary extraction (Blannin *et al.* 2023; Kursunoglu 2025). Evaluating the viability of tailings re-mining requires balancing technical feasibility, economic performance, and environmental-social impacts through structured sustainability assessment frameworks integrating multi-dimensional indicators (Adiansyah et al. 2015; Figueiredo *et al.* 2019; Bascompta *et al.* 2025). Current decision-making often lacks formal quantitative models that integrate environmental, social, and governance (ESG) metrics directly into strategic planning. This absence of a structured multi-dimensional framework creates uncertainty in determining the most sustainable operating scale for secondary resource projects (Araya et al. 2021).

To address this gap, this study introduces an integrated multi-criteria decision-making (MCDM) framework based on technical, economic, environmental, and social (TEES) dimensions. Objective indicator weights are derived using the Entropy method, while strategic alternatives are ranked through the Technique for Order of Preference by Similarity to Ideal Solution (TOPSIS) (Jiang *et al.* 2020; Kaneesamkandi *et al.* 2020). To demonstrate its practical applicability, the proposed framework is applied to a large-scale historical tailings facility in the Iberian Pyrite Belt (Spain).

Central to this research is determining the sustainability-optimal level of historical tailings reprocessing and evaluating whether sustainability increases proportionally with extraction intensity or if intermediate reprocessing provides a more balanced trade-off.

Research boundaries are limited to a site-specific assessment under current technological and regulatory conditions. Conventional flotation is assumed as the reference processing technology, and copper

represents the primary recovered product. Results represent a strategic evaluation of defined scenarios ranging from 0–100% tailings reprocessing.

Methods

This study applies a structured multi-criteria decision-making (MCDM) framework to evaluate the sustainability of historical tailings reprocessing at Atalaya Mining within the Iberian Pyrite Belt. The assessment utilizes a site-specific database derived from Atalaya Mining's 2023–2025 Sustainability Reports and the Proyecto Riotinto NI 43-101 Technical Report (Noble *et al.* 2018; Noble 2022; Atalaya Mining Plc 2023, 2024, 2025). This ensures that the 14 indicators across technical, economic, environmental, and social (TEES) dimensions reflect the real-world operational constraints of the Iberian Pyrite Belt. All objective weighting and ranking were performed via the Entropy-TOPSIS method implemented in Microsoft Excel.

Scenario Definition

Six discrete alternatives (A0–A5) represent varying degrees of tailings reprocessing, ranging from a "no-action" baseline (A0) to 100% full reprocessing (A5) (Table 1). These scenarios assume proportional scaling of operational flows based on the percentage of tailings treated.

Indicator Selection and Justification

Fourteen indicators across technical, economic, environmental, and social (TEES) dimensions were operationalized to reflect site-specific risks and strategic priorities (Table 2). Indicators were selected based on reliable site-specific data availability and operational relevance (Noble *et al.* 2018; Atalaya Mining Plc 2023, 2024, 2025), ensuring methodological transparency while avoiding speculative assumptions. Technical indicators (T1–T2) capture resource recovery efficiency and geotechnical safety factor improvements in alignment with the Global Industry Standard on Tailings Management (GISTM). Economic indicators (E1–E3) evaluate net present value (NPV), capital expenses (CAPEX), and operational efficiency (OPEX), while environmental indicators (ENV1–ENV5) address regional water scarcity, electricity demand, carbon footprint, and acid mine drainage (AMD) load reduction. Social indicators (S1–S4) measure employment generation, social investment, heritage conservation, and a community disturbance index representing noise and traffic effects.

Although certain indicators may exhibit operational correlation (e.g., electricity demand and carbon emissions), they represent distinct sustainability dimensions and were therefore retained to capture independent environmental pressures within the TEES framework.

Indicators were calculated on a project-life basis, assuming proportional scaling of material throughput, energy demand, water consumption, and associated operational flows across reprocessing scenarios. To ensure a strict evaluation of regional impacts, the analysis incorporates site-specific environmental constraints, including a regional freshwater concession limit of 4.93 $Mm^3/year$. This is operationalized by applying an exponential stress factor ($x^{1.2}$) to scenarios approaching or exceeding this

Table 1 Definition of reprocessing alternatives.

Alternative	Tailings Reprocessed (%)	Description
A0	0	No action – environmental liability
A1	20	Very low reprocessing
A2	40	Low reprocessing
A3	60	Medium reprocessing
A4	80	High reprocessing
A5	100	Full reprocessing

Table 2 Indicator system and TEES framework parameters.

Dimension	Code	Indicator	Unit	Benchmark	Rationale
Technical	T1	Copper recovery	kt	52.3 (Atalaya Mining Plc 2023)	Reflects resource recovery efficiency and contribution to supply
	T2	TSF safety factor improvement	–	1.88 (Global Tailings Review 2020; Noble 2022; Atalaya Mining Plc 2023)	Indicates geotechnical risk reduction
Economic	E1	CAPEX	$ M	94.90 (Noble *et al.* 2018)	Represents upfront investment requirement
	E2	OPEX	$/t	6.13 (Noble 2022)	Reflects operational efficiency
	E3	NPV (10% rate)	$ M	915 (Ramírez Rodríguez 2023)	Measures long-term financial viability
Environmental	ENV1	Total water intensity	m^3/t	1.91 (Atalaya Mining Plc 2025)	Captures regional water pressure
	ENV2	Electricity intensity	kWh/t	22.66 (Atalaya Mining Plc 2025)	Reflects energy demand
	ENV3	Carbon footprint	t CO_2-eq	98,447 (Noble 2022)	Indicates greenhouse gas emissions
	ENV4	AMD load reduction	%	Proportional to the reprocessed tailings	Reflects mitigation of acid mine drainage risk
	ENV5	Freshwater withdrawal	m^3/t	0.22 (Atalaya Mining Plc 2025)	Measures freshwater consumption
Social	S1	Total employment influence	jobs	2,355 (Atalaya Mining Plc 2023)	Measures local job creation
	S2	Social investment	$ k/y	1,107 (Atalaya Mining Plc 2025)	Indicates community development contribution
	S3	Heritage conservation	M$	3.11 (Atalaya Mining Plc 2023)	Reflects cultural preservation contribution
	S4	Community disturbance	-	index	Captures local nuisance and disruption

threshold to reflect increased water scarcity risk. Benchmark values were proportionally scaled across the six reprocessing scenarios (A0–A5).

Entropy Weight Method (EWM) and TOPSIS Ranking Procedure

Objective indicator weights were determined using the Entropy Weight Method (EWM) to eliminate subjective bias. Shannon entropy theory evaluates the dispersion of each indicator across alternatives; indicators with greater variability provide more discriminatory information and receive higher weights (Kaneesamkandi *et al.* 2020). Raw data were standardized into dimensionless values using min–max normalization for benefit-type and cost-type indicators (Kaneesamkandi *et al.* 2020). Computation of entropy values utilized the normalized TEES indicator matrix derived from the scenario dataset for the six reprocessing alternatives (A0–A5).

Subsequent ranking was performed using the Technique for Order of Preference by Similarity to Ideal Solution (TOPSIS). This procedure identifies the optimal alternative by calculating the Euclidean distance from both the Positive Ideal Solution (PIS) and the Negative Ideal Solution (NIS) (Adibi *et al.* 2015; Jiang *et al.* 2020). Relative closeness coefficients (C_i) ranging from 0 to 1 were determined for each scenario, where higher values indicate superior multi-dimensional sustainability performance (Kaneesamkandi *et al.* 2020).

Table 3 Entropy weights and objective indicator utility.

Code	Indicator	Type	Σ(yij)	Entropy (Ej)	Utility (dj)	Weight (Wj)
T1	Copper recovery	Benefit	3.006	0.8327	0.1673	7.16%
T2	TSF safety factor improvement	Benefit	3.008	0.8351	0.1649	7.06%
E1	CAPEX	Cost	2.435	0.9084	0.0916	3.92%
E2	OPEX	Cost	3.006	0.8327	0.1673	7.16%
E3	NPV (10% rate)	Benefit	3.006	0.8327	0.1673	7.16%
ENV1	Total water intensity	Cost	3.284	0.8041	0.1959	8.38%
ENV2	Electricity intensity	Cost	3.175	0.8149	0.1851	7.92%
ENV3	Carbon footprint	Cost	3.272	0.8052	0.1948	8.33%
ENV4	AMD load reduction	Benefit	3.006	0.8327	0.1673	7.16%
ENV5	Freshwater withdrawal	Cost	3.472	0.7853	0.2147	9.19%
S1	Total employment influence	Benefit	3.105	0.8224	0.1776	7.60%
S2	Social investment	Benefit	3.324	0.8001	0.1999	8.55%
S3	Heritage conservation	Benefit	3.402	0.7932	0.2068	8.85%
S4	Community disturbance	Cost	3.008	0.8711	0.1289	5.52%
Total					2.3364	100.00%

Results and Discussion

Entropy analysis quantifies the objective information utility of each indicator based on its dispersion across the six reprocessing scenarios (Table 3). The weighting structure indicates that environmental and social indicators exert the strongest influence within the decision framework. Freshwater withdrawal (ENV5) receives the highest weight (9.19%), reflecting both its strong variability across scenarios and the operational sensitivity of the Iberian Pyrite Belt to water resource constraints (Rosario-Beltré *et al.* 2023). Social indicators, particularly heritage conservation (S3, 8.85%) and social investment (S2, 8.55%), also demonstrate high discriminatory power, emphasizing the importance of socio-cultural considerations in long-term tailings management strategies.

Environmental indicators related to electricity demand and carbon emissions (ENV2–ENV3) maintain consistently high influence, confirming that resource and energy intensity are critical constraints for large-scale reprocessing systems. In contrast, CAPEX (E1) receives the lowest weight (3.92%), indicating comparatively lower variability between alternatives and suggesting that long-term operational and environmental trade-offs dominate over initial investment costs within the entropy-based framework. Geotechnical stability (T2) retains moderate influence (7.06%), ensuring that alignment with the Global Industry Standard on Tailings Management (GISTM) remains integrated into the sustainability assessment.

Defining A0 ("No Action") as the baseline demonstrates that maintaining an untreated TSF is not a neutral pathway; its negative NPV (–$74.1 M) (Noble *et al.* 2018), zero material recovery, and lack of safety improvements result in a closeness coefficient of 0.000 (Rank 6). This outcome highlights tailings reprocessing as a liability-reduction strategy rather than solely a production-oriented activity.

Alternative A4 (Ci = 0.844) represents the optimal sustainability balance within the evaluated system. The scenario achieves substantial copper recovery and significant TSF stabilization benefits while avoiding the disproportionate increases in freshwater demand and electricity consumption observed under full-scale reprocessing. Consequently, A4 maintains the most favorable balance between the Positive Ideal Solution (PIS) and Negative Ideal Solution (NIS) within the entropy–TOPSIS framework. Although

Table 4 Entropy-weighted TOPSIS ranking of reprocessing scenarios.

Alternative	Tailings Reprocessed	C_i	Rank
A4	80%	0.844	1
A3	60%	0.754	2
A5	100%	0.741	3
A2	40%	0.560	4
A1	20%	0.330	5
A0	0%	0.000	6

Table 5 Sensitivity analysis under varying policy priorities.

Scenario	Weighting Adjustment	Top Ranking	Stability
Base Case	Objective Entropy Weights	A4 > A3 > A5	–
Economic Priority	+20% Economic Weight (E1–E3)	A4 > A5 > A3	Stable
Environmental Priority	+20% Env. Weight (ENV1–ENV5)	A4 > A3 > A2	Highly Stable
Social Priority	+20% Social Weight (S1–S4)	A3 > A4 > A2	Moderate

Alternative A5 (100% reprocessing) generates the highest economic return, with an NPV of $1,043.5 M, it ranks third overall (Ci = 0.741). However, the scenario is penalized by marked increases in freshwater stress (70.4 Mm^3 over the project life) and community disturbance impacts (Supplementary Material). These additional environmental and social burdens offset the economic gains associated with maximum copper recovery. These results demonstrate that maximum production does not necessarily correspond to optimal sustainability performance within resource-constrained regional systems.

TSF safety factor (T2) and AMD reduction (ENV4) drive the restorative mining narrative by transforming potentially liquefiable impoundments into stabilized landforms aligned with GISTM. While safety factor improvements from 1.88 to 2.29 are substantial, the results indicate that geotechnical stabilization alone is insufficient to achieve overall sustainability. Alternative A4 demonstrates that optimal performance is achieved when safety improvements are balanced with responsible environmental management and acceptable community impacts.

Sensitivity Analysis

Structural sensitivity analysis confirms the robustness of the identified "sweet spot" across various policy scenarios (Table 5). Under an Economic Priority scenario, A5 improves its rank but fails to overtake A4, as extreme CAPEX and OPEX requirements act as a financial drag. Environmental Priority scenarios penalize A5 further due to its high carbon footprint and energy intensity. Shifting to a Social Priority favors Alternative A3 (60% reprocessing), highlighting the critical trade-off between job creation and local nuisance effects. Results suggest an optimal operating range between 60% and 80% reprocessing.

Adjusting economic weights (E1–E3) promotes A5 to second rank, as full-scale extraction maximizes production and NPV (Bascetin and Nieto 2007; Araya *et al.* 2020). Nevertheless, A4 remains optimal by avoiding the extreme capital and operational costs characterizing the 100% scenario. Elevating environmental weights to 50% penalizes A5 for high carbon and energy intensity (Marín *et al.* 2022; Adrianto *et al.* 2023), while moderate reprocessing (A2–A4) proves more resilient. Prioritizing social factors (S1–S4)

favors A3 (60% reprocessing), highlighting critical trade-offs between employment and community disturbance. Medium-scale operations appear most sustainable for securing a Social License to Operate.

Conclusion

This study demonstrates that the sustainability of historical tailings reprocessing is characterized by a non-monotonic relationship between extraction intensity and overall performance. Entropy–TOPSIS analysis identifies 80% reprocessing (A4) as the sustainability efficiency peak. This optimal scenario maximizes the trade-off between restorative gains, such as copper recovery, acid mine drainage (AMD) load reduction, and geotechnical stabilization, and the constraints of regional water scarcity and social acceptance.

Analysis confirms that the "no-action" baseline is neither a neutral nor a sustainable option, as it perpetuates long-term environmental liabilities and economic loss. However, the study also identifies a clear sustainability ceiling; moving from 80% to 100% reprocessing triggers disproportionate penalties in water withdrawal, electricity demand, carbon footprint, and community disturbance that marginal economic gains cannot offset.

These findings suggest that "restorative mining" projects should be managed within a strategic operating envelope rather than pursuing maximum volume. By aligning mineral recovery with the Global Industry Standard on Tailings Management (GISTM), operators can transform legacy risks into stabilized landforms while maintaining their Social License to Operate. While the results are site-specific to the Iberian Pyrite Belt, the TEES-based MCDM methodology provides a transparent, data-driven model for evaluating secondary resource projects worldwide, ensuring they contribute effectively to the green energy transition without shifting environmental burdens.

Acknowledgments

This research has received funding from the European Union's Horizon Europe research and innovation programme under the Marie Skłodowska-Curie Actions Doctoral Network (HORIZON-MSCA-2023-DN-01) within the CRITERIA Project under Grant Agreement No. 101169238. The authors gratefully acknowledge this financial support, as well as the institutional support provided by the Universitat Politècnica de Catalunya (UPC). Additionally, the authors would like to thank the organizers and co-organizers for hosting the International Mine Water Association (IMWA) 2026 Conference.

Reference:

Adiansyah JS, Rosano M, Vink S, Keir G (2015) A framework for a sustainable approach to mine tailings management: disposal strategies. J Clean Prod 108:1050–1062. https://doi.org/10.1016/j.jclepro.2015.07.139

Adibi N, Ataee-pour M, Rahmanpour M (2015) Integration of sustainable development concepts in open pit mine design. J Clean Prod 108:1037–1049. https://doi.org/10.1016/j.jclepro.2015.07.150

Adrianto LR, Ciacci L, Pfister S, Hellweg S (2023) Toward sustainable reprocessing and valorization of sulfidic copper tailings: Scenarios and prospective LCA. Sci Total Environ 871:162038. https://doi.org/10.1016/j.scitotenv.2023.162038

Araya N, Kraslawski A, Cisternas LA (2020) Towards mine tailings valorization: Recovery of critical materials from Chilean mine tailings. J Clean Prod 263:121555. https://doi.org/10.1016/j.jclepro.2020.121555

Araya N, Ramírez Y, Kraslawski A, Cisternas LA (2021) Feasibility of re-processing mine tailings to obtain critical raw materials using real options analysis. J Environ Manage 284:112060. https://doi.org/10.1016/j.jenvman.2021.112060

Atalaya Mining Plc (2023) Sustainability Report 2022. Atalaya Mining Plc

Atalaya Mining Plc (2024) Sustainability Report 2023. Atalaya Mining Plc

Atalaya Mining Plc (2025) Sustainability Report 2024. Atalaya Mining Plc

Bascetin A, Nieto A (2007) Determination of optimal cut-off grade policy to optimize NPV using a new approach with optimization factor. 107:

Bascompta M, Yousefian M, Vintró C, *et al* (2025) Sustainability Assessment in Mining: A CSR-Based Analysis Model for Social and Environmental Impact. Fudan J Humanit Soc Sci 18:329–345. https://doi.org/10.1007/s40647-024-00419-y

Blannin R, Frenzel M, Tolosana-Delgado R, *et al* (2023) 3D geostatistical modelling of a tailings storage facility: Resource potential and environmental implications. Ore Geol Rev 154:105337. https://doi.org/10.1016/j.oregeorev.2023.105337

European Commission (2023) Proposal for a Regulation of the European Parliament and of the Council establishing a framework for ensuring a secure and sustainable supply of critical raw materials (Critical Raw Materials Act)

Figueiredo J, Vila MC, Fiúza A, *et al* (2019) A Holistic Approach in Re-Mining Old Tailings Deposits for the Supply of Critical-Metals: A Portuguese Case Study. Minerals 9:638. https://doi.org/10.3390/min9100638

Global Tailings Review (2020) Global Industry Standard on Tailings Management. International Council on Mining and Metals (ICMM); United Nations Environment Programme (UNEP); Principles for Responsible Investment (PRI), Geneva, Switzerland

Jiang F, Wu H, Liu Y, *et al* (2020) Comprehensive evaluation system for stability of multiple dams in a uranium tailings reservoir: based on the TOPSIS model and bow tie model. R Soc Open Sci 7:191566. https://doi.org/10.1098/rsos.191566

Johansson L, Bahrami A, Wallhagen M, Cehlin M (2024) A comprehensive review on properties of tailings-based low-carbon concrete: Mechanical, environmental, and toxicological performances. Dev Built Environ 18:100428. https://doi.org/10.1016/j.dibe.2024.100428

Kaneesamkandi Z, Rehman AU, Usmani YS, Umer U (2020) Methodology for Assessment of Alternative Waste Treatment Strategies Using Entropy Weights. Sustainability 12:6689. https://doi.org/10.3390/su12166689

Kursunoglu S (2025) A Review on the Recovery of Critical Metals from Mine and Mineral Processing Tailings: Recent Advances. J Sustain Metall 11:2023–2050. https://doi.org/10.1007/s40831-025-01126-y

Marín OA, Kraslawski A, Cisternas LA (2022) Estimating processing cost for the recovery of valuable elements from mine tailings using dimensional analysis. Miner Eng 184:107629. https://doi.org/10.1016/j.mineng.2022.107629

Noble A (2022) Technical Report On the Riotinto Copper Project

Noble, Bouza B, Pickarts (2018) Technical Report on the Riotinto Copper Project. Ore Reserves Engineering (prepared for Atalaya Mining Plc), Highlands Ranch, CO

Ramírez Rodríguez G (2023) Preliminary Economic Assessment Proyecto Riotinto | Riotinto District Huelva Province, Spain

Rosario-Beltré AJ, Sánchez-España J, Rodríguez-Gómez V, *et al* (2023) Critical Raw Materials recovery potential from Spanish mine wastes: A national-scale preliminary assessment. J Clean Prod 407:137163. https://doi.org/10.1016/j.jclepro.2023.137163

IMWA 2026
Jeongseon

Global Copper Supply Under Climate-Driven Water Stress: A Proof of Concept

Mariam Taki[1], Nicolas Flipo[2], Damien Goetz[3]

[1]*Department of Geosciences, Paris School of Mines, PSL University, France, mariam.taki@minesparis.psl.eu, ORCID 0009-0007-3864-1611*

[2]*Department of Geosciences, Paris School of Mines, PSL University, France, nicolas.flipo@minesparis.psl.eu, ORCID 0000-0002-8099-2104*

[3]*Department of Geosciences, Paris School of Mines, PSL University, France, damien.goetz@minesparis.psl.eu, ORCID 0009-0007-4740-4255*

Abstract

A global framework assessing climate-driven hydrology for mineral production was applied to evaluate water availability for porphyry copper production. Using validated historical simulations and SSP2-4.5 projections, extractable water from rivers, lakes, and aquifers was quantified, and monthly mining water stress was calculated under a grade-based production schedule. Results identified temporal and spatial hotspots where water demand approached or exceeded local availability, with peak stress exceeding 100% in northern Chile. The framework demonstrated the feasibility of linking climate-driven hydrology to mineral-specific production and highlighted the importance of integrating water resources into mine planning under changing climatic conditions.

Keywords: Water stress, climate change, copper, hydrology, mine water management

Introduction

Water availability constrains mining operations through its role in mineral extraction, processing, dust suppression, and tailings management (Gunson *et al.* 2012). For large-scale metal production, sustained access to water is required over multi-decadal timescales, making mining systems sensitive to long-term changes in hydrological conditions. Climate change alters precipitation patterns, evapotranspiration, runoff generation, groundwater recharge, and surface water storage, directly affecting the volume and timing of water that can be physically extracted for industrial use.

Copper is central to electrification and energy system transitions, and porphyry deposits account for the majority of global copper supply. Assessing whether climate-driven changes in water availability may constrain copper extraction therefore represents a relevant problem for mine water management and long-term supply planning.

Existing assessments of mining water risk often rely on static water stress indicators that do not reflect climate-driven variability or low-flow conditions relevant to mine operations (Lakshman 2024) (Northey 2017). At the global scale, few approaches combine physically based hydrology, historical validation against observations, and mineral-specific water demand in a single framework. This limits the ability to identify when and where water availability may act as a binding constraint on production under evolving climatic conditions.

Climate-driven changes in water availability were evaluated at the global scale using HyIR, a hydrological aggregation framework developed to translate climate projections into physically based estimates of extractable water. Outputs from the hydrological framework were then combined with a process-based model of water demand for porphyry copper extraction to assess mining water stress. This application provided a proof of concept for linking climate-informed water availability with mineral-specific production requirements.

Methods

Climate-driven water availability was assessed using the HYdrological and Industrial Resilience (HyIR) framework, a global-scale hydrological aggregator developed to translate outputs from the Coupled Model Inter-comparison Project Phase 6 (CMIP6) general circulation models into physically interpretable indicators of extractable water (Eyring *et al.* 2016). The framework was forced with outputs from the first Taiwanese Earth System Model TaiESM1 for the historical period and under the Shared Socioeconomic Pathway SSP2-4.5, reflecting moderate greenhouse gas emissions scenario also referred to as "Middle of the road" scenario, and was applied at the native spatial resolution of the climate model (1.25° × 0.9°) with monthly time steps (Lee *et al.* 2020).

HyIR represents water evolution through three coupled components: storage in lakes and reservoirs, groundwater storage in aquifer systems, and river discharge including explicit routing (Fig. 1). The framework produces gridded time series of gross extractable water, defined as the volume of water that could be withdrawn from each component while remaining physically sustainable, without accounting for infrastructure constraints, sectoral allocation, or water rights. Reservoir and lake availability was based on a fixed fraction of stored volume ensuring a minimum persistence of 10 years without recharge, river availability on flows exceeding a 30-day low-flow threshold defined from long-term quantiles, and groundwater availability on accessible aquifer storage limited by permeability and a 50-year depletion constraint. Indicators evolved dynamically in response to climate forcing and were aggregated at the climate model grid scale.

To better represent basin-scale hydrology and improve agreement with observed river discharge, three correction factors were introduced and calibrated: a redistribution factor controlling the fraction of infiltration redirected to surface runoff, a seasonal baseflow multiplier adjusting groundwater contribution through the year, and a time-of-concentration multiplier affecting river discharge routing. These corrections were evaluated against observed discharge from the Global Runoff Data Centre (GRDC 2026) using a modified drought-focused Kling-Gupta Efficiency metric KGE-d (Schaefli and Gupta 2007). The metric ranges from $-\infty$ to 1, where 1 indicates perfect agreement between simulated and observed discharge, and is defined as:

$$KGE_d = 1 - \sqrt{(r-1)^2 + (\beta-1)^2 + (\gamma-1)^2}$$

where r is the linear correlation coefficient, β is the ratio of simulated to observed mean discharge, and γ is the ratio of QMNA5 low-flow quantiles. QMNA5 represents the minimum 30-day mean discharge with a 5-year return period, used here to characterize low-flow conditions. Following Knoben *et al.* (2019), a value of –0.41 was adopted as the threshold for acceptable performance, corresponding to the score obtained when simulated discharge is equal to the observed mean value, meaning that values above this threshold perform better than a mean-flow benchmark. Validation was performed over the historical period 1850–2015 using observed and simulated daily discharge for large river basins with available data.

Water demand for porphyry copper production was estimated using a process-based, bottom-up model representing on-site mining and mineral processing operations up to the production of copper concentrate. The model accounted for water inputs, internal recycling, and losses primarily associated with tailings management and evaporation (Fig. 2). Copper production was represented using a publicly available global database of porphyry copper deposits (Magnin *et al.* 2025), with water demand computed using deposit-specific parameters, empirically derived production scheduling rules, processing configurations, and a conceptual representation of tailings-related water flows.

Copper production was scheduled to meet demand trajectories from the International Energy Agency Stated Policies Scenario STEPS, reflecting a moderate energy transition scenario consistent with the SSP2-4.5 climate pathway, over the period 2025-2050 (IEA 2024). Scheduling followed a descending ore-grade order and

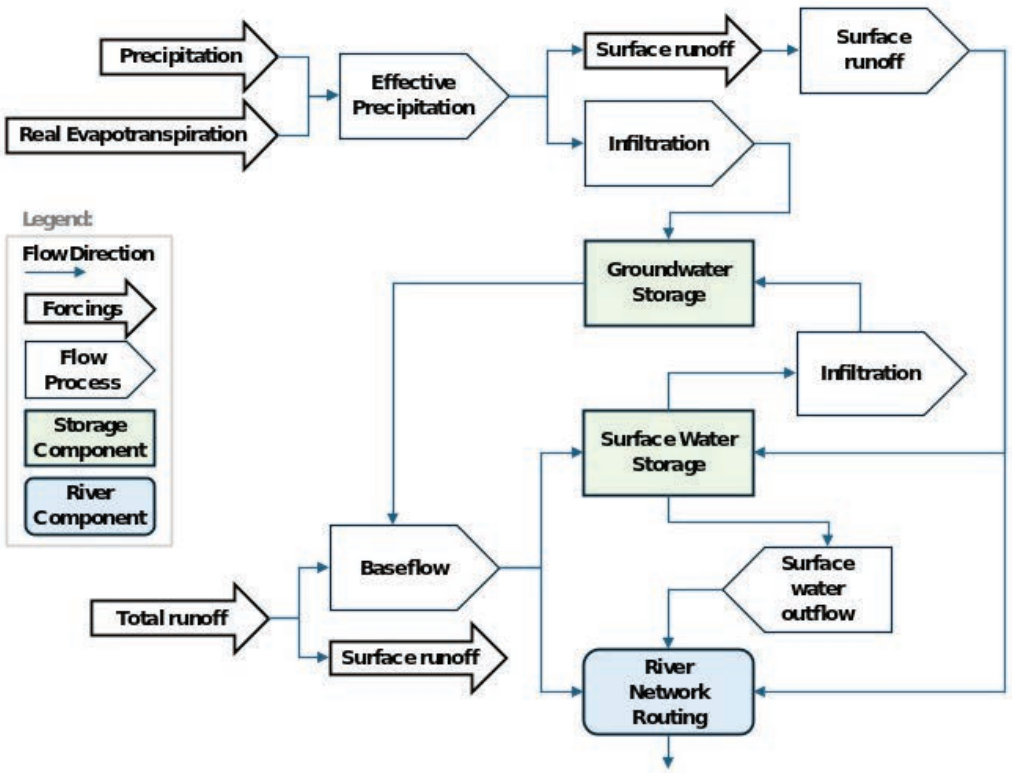

Figure 1 Schematic overview of HyIR.

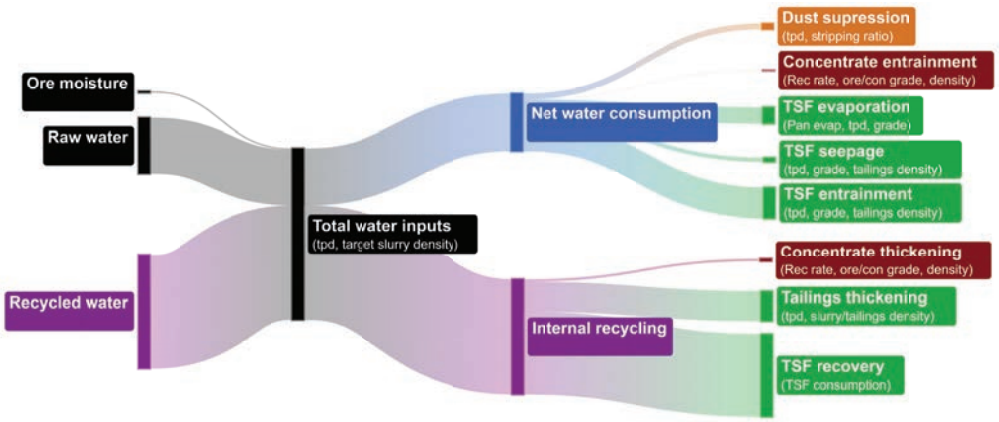

Figure 2 Water flows considered in the model.

was scaled to represent global copper supply by scaling demand to porphyry deposits, assumed to continuously account for 82% of identified copper resources. New deposits were activated as existing operations were exhausted to reduce the demand–supply gap.

Monthly mining water stress was quantified as the ratio of monthly water demand associated with scheduled copper production, aggregated spatially to the hydrological grid, to a fixed fraction of monthly gross extractable water allocated for mining

within the corresponding grid cell. Where extractable water availability approaches zero, the ratio loses interpretability, such cases were therefore flagged.

Results

Simulated river discharge from HyIR, forced with historical TaiESM1 data, was compared to GRDC observations across South America for the period 1850–2015 (Fig. 3a). Observations were available for large basins covering 71.6% of the continent. Using the −0.41 performance threshold, 69.9% of the assessed area exhibited KGE-d values above the benchmark, indicating that HyIR simulations forced with historical TaiESM1 data reproduced hydrological variability more effectively than assuming stationary mean flows. Lower scores representing 30.1% of the assessed area were mainly observed in relatively small coastal basins characterized by extreme precipitation (>2600 mm a^{-1}), where forcing precipitation exceeded observed discharge by more than 1000%, indicating unrealistically wet forcing conditions in TaiESM1 rather than structural limitations of the HyIR framework.

Using the validated HyIR configuration, extractable water availability was simulated from TaiESM1 projections under the SSP2-4.5 moderate scenario. Monthly extractable water was computed at the climate model grid scale as the aggregate contribution from lakes and reservoirs, river discharge, and groundwater storage (Fig. 3b). The resulting fields represented physically based estimates of gross extractable water availability derived from climate forcing and hydrological storage dynamics and formed the hydrological input for subsequent mining water stress calculations.

Scheduled copper production under the IEA Stated Policies moderate scenario was simulated over 2025–2050, producing a temporal profile of active deposits and corresponding production (Fig. 4a), with a total simulated production of 702 Mt compared to 731 Mt of demand, corresponding to the depletion of 30.3% of the studied copper resources. Periods where demand exceeded the supply capacity of available deposits were highlighted in the schedule. Of the 852 porphyry deposits considered, 699 met the minimum mine-life threshold of 10 years and

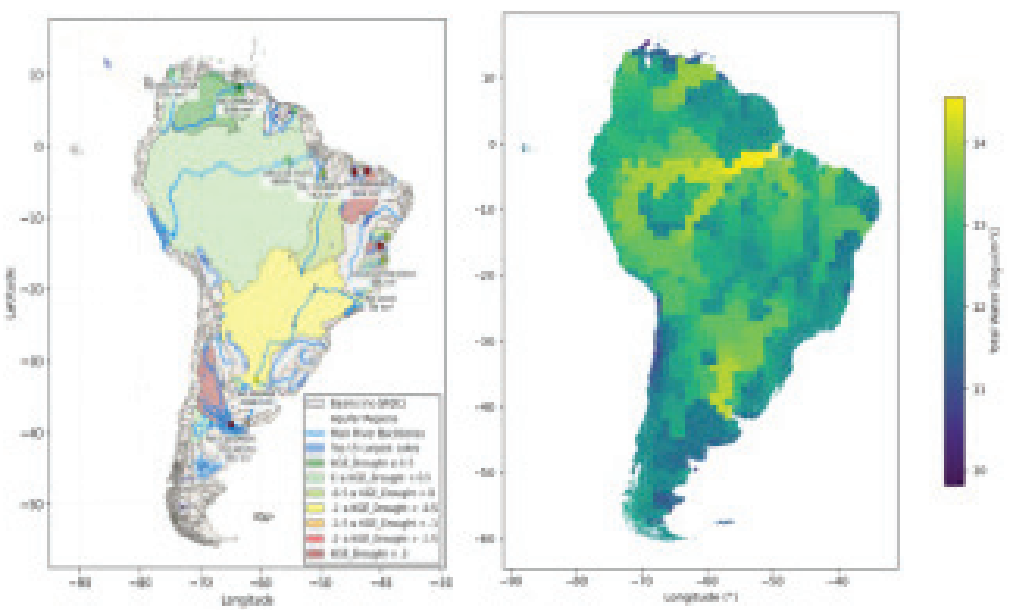

a) Historical validation results *b) Future total extractable water*

Figure 3 *(a) Historical validation of HyIR using the drought-KGE metric in South America, and (b) projected extractable water availability under SSP2-4.5, computed as the sum of lake, river, and aquifer contributions.*

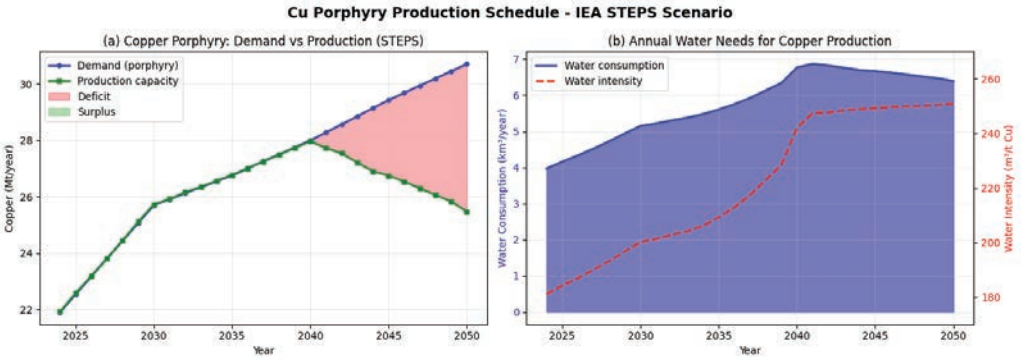

Figure 4 Global production scheduling (a) and associated annual water demand (b).

were therefore included in the production assessment, representing 2318 Mt of contained copper (99.7% of 2326 Mt identified across all deposits). The 153 excluded deposits accounted for 7.9 Mt of copper (0.3% of identified copper). Water requirements for the activated deposits were simulated (Fig. 4b), the deposit-level water intensity had a mean of 365 m^3 t^{-1} of copper and a median of 265 m^3 t^{-1}, with the 10th and 90th percentiles at 123 and 608 m^3 t^{-1} respectively, variability being primarily controlled by differences in ore grade.

Monthly mining water stress was evaluated for 2030, 2040, and 2050 under TaiESM1 SSP2-4.5 forcing and the applied production schedule (Fig. 5). Stress levels exceeding 20% were identified in multiple hydrological grid cells across the assessment period. The stress classification (<10%, 10–20%, 20–40%, 40–80%, >80%) was adapted from the Water Stress Indicator framework (Pfister et al. 2009). However, as only mining water demand was considered, the demand values represented partial withdrawal pressure and therefore underestimated total water stress. In mining-intensive, water-scarce countries such as Australia, Chile, and South Africa, mining accounted for only 2–4.5% of national water withdrawals (Brown, 2003), but local demands could be higher. For this reason, a representative allocation of 10% of gross extractable water was applied to mining, reflecting the coarse spatial resolution and allowing for meaningful assessment of mining-related water stress.

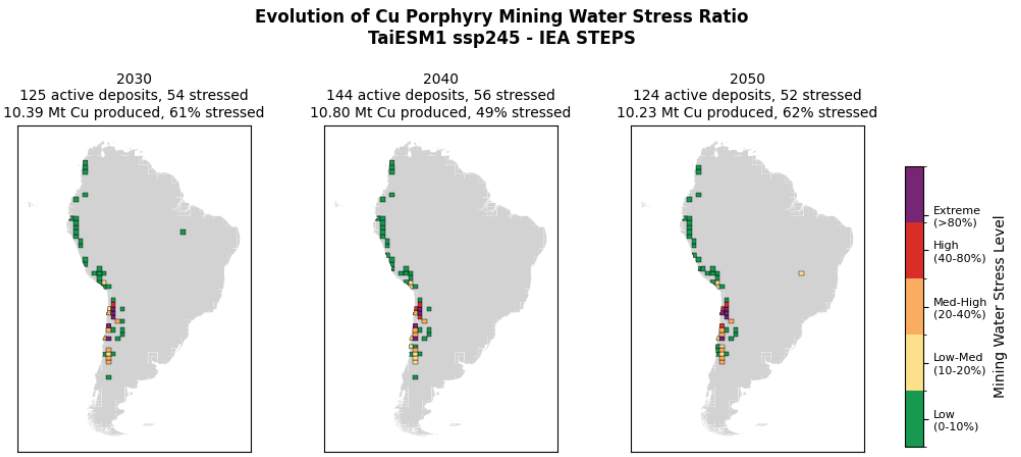

Figure 5 Mining water stress under SSP2-4.5 and STEPS scheduling.

Peak mining-related stress reached 580% in northern Chile in 2034, reflecting the concentration of high-production deposits within a single hydrological grid cell combined with limited local extractable water availability. The same cell exhibited a continuous period above the 20% threshold for 279 months (around 23 years), corresponding to the duration over which deposits in this cell were activated. Thus, highlighting a hotspot where copper production demands reached up to 58% of the total extractable water for all uses in the region. Across South America, the fraction of copper produced from regions exceeding the 20% stress threshold consistently ranged between 49% and 66% of total production throughout the assessment period, indicating that more than half of future copper production in the continent was exposed to medium-to-extreme mining water stress.

Conclusions

Coupling climate projections, hydrological aggregation, and mining production models demonstrated the feasibility of assessing the evolution of water availability for global mineral production. Application of the framework to porphyry copper illustrated its ability to identify spatial and temporal hotspots where production could be constrained by local water resources. Results indicated that a substantial share of future copper production may occur in regions exposed to moderate-to-extreme water stress. Results also indicated the hydrological limitations of grade-based scheduling, highlighting the importance of integrating resource planning with local water availability when evaluating mining operations under changing climatic conditions. Extension of the framework aims to support decision-making by identifying regions where mineral production is most viable under combined production and water availability constraints.

Acknowledgements

The authors thank all co-organisers for hosting the IMWA 2026 Conference.

References

Brown E (2003) Water for a sustainable minerals industry – A review. In Proceedings of the Water in Mining 2003, The Australasian Institute of Mining and Metallurgy

Eyring V, Bony S, Meehl GA, Senior CA, Stevens B, Stouffer RJ, Taylor KE (2016) Overview of the Coupled Model Intercomparison Project Phase 6 (CMIP6) experimental design and organization. *Geoscientific Model Development*, 9(5), 1937–1958. https://doi.org/10.5194/gmd-9-1937-2016

Global Runoff Data Centre (2026) GRDC database. Federal Institute of Hydrology (BfG), Koblenz, Germany. Available at: https://www.bafg.de/GRDC (Accessed 3 March 2026)

Gunson AJ, Klein B, Veiga M, Dunbar S (2012) Reducing mine water requirements. Journal of Cleaner Production 21:71–82. https://doi.org/10.1016/j.jclepro.2011.08.020

International Energy Agency (2024) Global critical minerals outlook 2024. IEA, Paris. Available at: https://www.iea.org/reports/global-critical-minerals-outlook-2024

Knoben WJM, Freer JE, Woods RA (2019) Technical note: Inherent benchmark or not? Comparing Nash–Sutcliffe and Kling–Gupta efficiency scores. Hydrology and Earth System Sciences 23:4323–4331. https://doi.org/10.5194/hess-23-4323-2019

Lakshman S (2024) More critical minerals mining could strain water supplies in stressed regions

Lee W-L, Wang Y-C, Shiu C-J, et al (2020) Taiwan Earth System Model Version 1: description and evaluation of mean state. Geoscientific Model Development 13:3887–3904. https://doi.org/10.5194/gmd-13-3887-2020

Magnin BP, Graham GE, Huston DL, Eglington BM (2025) A global database of porphyry copper deposits and prospects

Northey SA, Mudd GM, Werner TT, et al (2017) The exposure of global base metal resources to water criticality, scarcity and climate change. Global Environmental Change 44:109–124. https://doi.org/10.1016/j.gloenvcha.2017.04.004

Pfister S, Koehler A, Hellweg S (2009) Assessing the environmental impacts of freshwater consumption in LCA. Environmental Science & Technology 43:4098–4104. https://doi.org/10.1021/es802423e

Schaefli B, Gupta H (2007) Do Nash values have value? Hydrological Processes 21:2075–2080. https://doi.org/10.1002/hyp.6825

Impacts of Extreme Precipitation Events on Abandoned Mines: A Case Study from North Rhine-Westphalia, Germany

B.M.A. Teichert[1], S.E. Nikutta[1], H. Strauss[2], S. Weinand[3], S. Westermann[1]

[1]*Research Center of Post-Mining (FZN), Georg Agricola University of Applied Sciences (THGA), Herner Str. 45, Bochum, Germany*

[2]*Institute for Geology and Paleontology, University Münster, Corrensstr. 24, Münster, Germany*

[3]*RAG Aktiengesellschaft, Im Welterbe 10, 45141 Essen, Germany*

Abstract

An exceptional precipitation period from October 2023 to March 2024 in North Rhine-Westphalia, Germany, caused pronounced changes in mine water chemistry at abandoned hard coal mines. Bimonthly monitoring at pumping stations of 'Robert Müser' (RM) and 'Friedlicher Nachbar' (FN) revealed that sulfate concentrations increased by up to 160 % (RM) and 60 % (FN), peaking between September and November 2024. The sulfur isotopic composition ($\delta^{34}S$) of dissolved sulfate in the mine water initially indicated ongoing microbial sulfate reduction, but subsequently decreased by up to 10 ‰ reflecting the input of sulfate from pyrite oxidation in the hard coal and possibly surrounding rocks. The inverse relationship between $\delta^{34}S$ and sulfate concentration highlights dynamic biogeochemical and hydrological responses to extreme infiltration of surface waters within the upper, unsaturated zones of the mine workings. These results demonstrate that extreme winter precipitation can mobilize significant amounts of sulfate and other soluble compounds in shallow, partially flooded abandoned mines. Understanding such processes is critical for predicting the impacts of future extreme climatic events on post-mining environments.

Keywords: Mine water, precipitation, climate, sulfate, sulfur isotopes

Introduction

In North Rhine-Westphalia, Germany, a very remarkable and unprecedented precipitation period occurred between October 2023 and the end of March 2024. The region recorded its highest rainfalls since meteorological observations began in 1881. As part of an ongoing hydrochemical monitoring program, mine water from abandoned hard coal mines was sampled at least every two months from standpipes through which it is pumped to the surface and analysed for its geochemical composition. To identify ongoing processes in the inaccessible underground mine workings, sulfur isotopes of the dissolved sulfate was measured.

Study Area

Hard coal, formed from extensive Carboniferous swamps, defines the geology of the Ruhr Area, having been buried and tectonically deformed over geological time. This sequence was later covered by younger Permian, Mesozoic, and Cenozoic sediments, marking a complex history of geological uplift and subsidence. Today, these Carboniferous rocks mostly lie beneath thick overburden, dipping towards the northwest, with exposures limited to the southern part of the region.

Methods

Water samples were collected every 2 months and at higher resolution starting April 2023. The samples represent mine water that is being pumped from two water provinces (Robert Müser (RM), Friedlicher Nachbar (FN)) in the southern Ruhr Area in the city of Bochum, Germany (Figure 1). Precipitation data obtained from the German Weather

Service (DWD) station in Bochum were used to compare with mine water geochemistry (Deutscher Wetterdienst, 2026).

Sulfate was measured with ion chromatography. For sulfate sulfur isotope measurements, dissolved sulfate was first filtered (cellulose nitrate filter, 0.45 µm pore diameter) and subsequently precipitated as $BaSO_4$ at subboiling temperature (80 °C) and pH 2 using an 8.5% $BaCl_2$ solution following Dogramaci *et al.* (2001). Sulfur isotopic measurements ($\delta^{34}S$) were performed using Flash EA IsoLink CN Elemental Analyzer interfaced to a ThermoScientific Delta V Advantage (EA-IRMS). For this, approximately 200 µg of BaSO4 precipitate was mixed with an equal amount of V_2O_5 and placed in a tin cup. Results are reported in the standard delta notation as permil difference to the Vienna Canon Diablo Troilite (V-CDT). Reproducibility (1σ) as determined from replicate measurements was generally better than ±0.3 ‰. Accuracy was monitored with internal lab standards and international reference materials (IAEA S1, S2, S3, and NBS127).

Results and Conclusions

Precipitation

Following a rather wet summer in 2023, precipitation showed a remarkable period between October 2023 and March 2024 in Bochum, North Rhine-Westphalia. Daily precipitation was as high as 26.6 Lm^{2-} at the end of December 2023. The monthly precipitation values also reflect the high precipitation values during winter 2023/2024. The sum of the monthly mean precipitation values between October 2023 and March 2024 in Bochum was 669.6 Lm^{2-} (Deutscher Wetterdienst, 2026). In comparison, the sum of the monthly mean values for the same time period (October – March) was 378.7 Lm^{2-} from 1991 to 2020 and 363.5 Lm^{2-} from 1961 to 1990. Therefore, precipitation during the winter of 2023/24 was approximately 177 % to 184 % of the long-term average recorded between 1961 and 2020 for the same period.

Sulfate concentration in mine water

Sulfate concentration at the pumping stations 'Robert Müser' (RM) and 'Friedlicher Nachbar' (FN) has been monitored every 2 months since the end of 2021. The mean sulfate concentration at RM until the end of 2023 was about 88 mgL^{-1} (Figure 2). In January 2024, the sulfate concentration was significantly elevated by about 50 mgL-1 and continued to rise until September 2024 (Figure 2). The mean sulfate concentration at FN until the end of 2023 was about 224 mgL^{-1}. In April 2024, the sulfate concentration was significantly elevated by about 49 mgL^{-1} and continued to rise until November 2024

Figure 1 *Map showing the mine water sampling locations 'Friedlicher Nachbar' and 'Robert Müser'.*

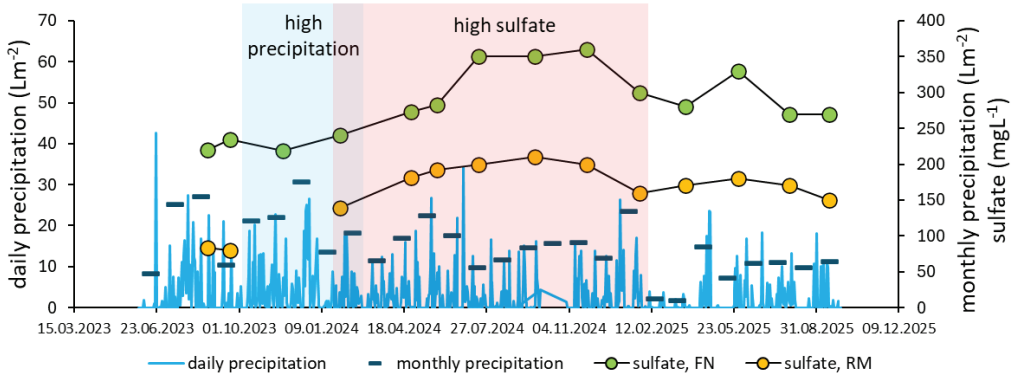

Figure 2 Graph showing the daily and monthly precipitation at Bochum (Deutscher Wetterdienst, 2026) together with sulfate concentration at the pumping stations 'Friedlicher Nachbar' (FN) and 'Robert Müser' (RM) from June 2023 to September 2025. The blue box indicates the high precipitation period in winter 2023/24. The red box indicates the time interval of high sulfate concentration in the mine water.

(Figure 2). At both pumping stations, sulfate concentrations slowly decreased afterwards but did not return to pre-winter 2023/24 values until September 2025.

Sulfur isotopic composition of sulfate in mine water

The sulfur isotopic composition of sulfate in the mine water at 'Robert Müser' (RM) shows rather high values between 20 ‰ V-CDT and 25 ‰ V-CDT at the end of 2023 (Figure 3). Such high $\delta^{34}S$ values are typical for ongoing sulfate reduction (Kaplan & Rittenberg 1964). Within the monitored time interval, sulfate sulfur isotopic composition and sulfate concentration exhibit an inverse relationship (Figure 3). The $\delta^{34}S$ values decrease by about 10 ‰.

A similar observation can be made at 'Friedlicher Nachbar' (FN). At the end of 2023, the sulfur isotopic composition of sulfate in the mine water at FN shows values between 15 ‰ V-CDT and 20 ‰ V-CDT (Figure 4). The $\delta^{34}S$ values decrease quickly by about 7 ‰ and start rising again in May 2024 which is four months earlier than at RM (Figure 4). Thus, the inverse relationship is less pronounced at FN compared to RM.

The sulfur cycle in the mine waters of the Ruhr Area is largely governed by the presence of iron sulfide minerals in the hard coal deposits. Iron sulfide, predominantly

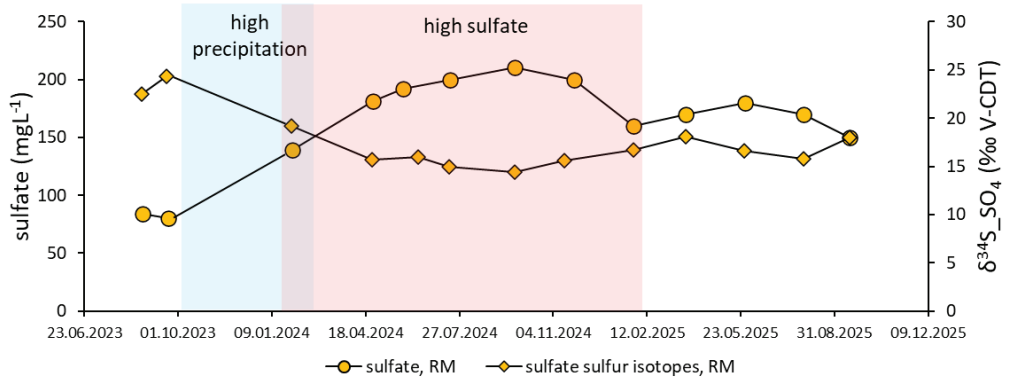

Figure 3 Sulfate concentration (circles) and sulfur isotopic composition of dissolved sulfate (diamonds) at 'Robert Müser' (RM). The blue and red boxes correspond to those shown in Figure 2.

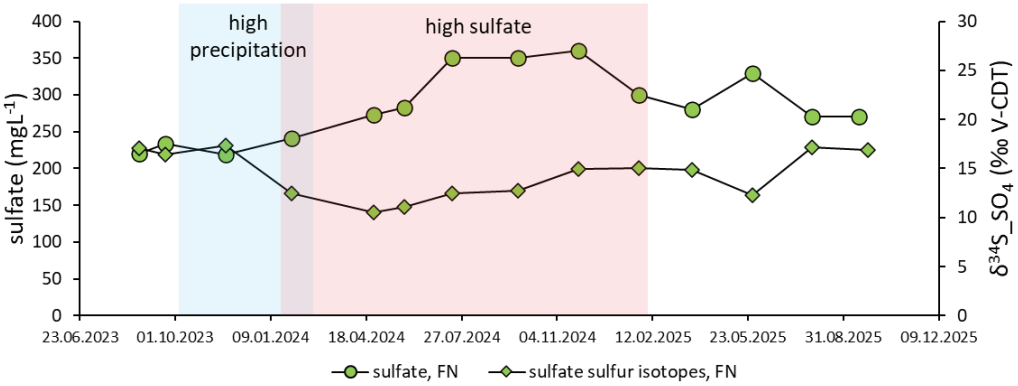

Figure 4 *Sulfate concentration (circles) and sulfur isotopic composition of dissolved sulfate (diamonds) at 'Friedlicher Nachbar' (FN). The blue and red boxes correspond to those shown in Figure 2.*

occuring as pyrite, is oxidized under aerobic conditions through a complex biogeochemical process (Singer & Stumm 1970). The sulfate formed during iron sulfide oxidation exhibits a characteristic isotopic fingerprint as negligible fractionation occurs during the oxidation. Consequently, the sulfur isotopic composition of the resulting dissolved sulfate reflects the original iron sulfide source. Sulfur isotopic values around 10 ‰ V-CDT are typical for pyrite (Puchelt & Nielsen 1967). Such low $\delta^{34}S$ values are observed at FN and nearly at RM, indicating that substantial quantities of sulfur derived from pyrite oxidation were released into the mine water following the precipitation anomaly of 2023/24.

Conclusion and Outlook

The precipitation anomaly 2023/24 led to a distinct change in mine water chemistry at the former hard coal mines 'Friedlicher Nachbar' and 'Robert Müser'. Sulfate concentrations showed the most prominent changes. Starting in January 2024, these increased by about 60 % (FN) to 160 % (RM), reaching a maximum between September and November 2024, before subsequently decreasing. The sulfur isotopic composition of sulfate in the mine water provides evidence for the origin of the sulfate. Both former mining sites are characterized by a thin or absent Cretaceous overburden allowing precipitation water to directly infiltrate the mine workings. Within the upper, unsaturated zones of the mine workings, sulfate from oxidized pyrite in the hard coal and possibly also the wall rock was dissolved during the extensive infiltration of surface water and transferred into the deeper, flooded part of the ancient mine workings. This process is reflected by a distinct decrease in δ34S values of the dissolved sulfate by up to 10 ‰ resulting from the release of lighter sulfur isotopes during pyrite oxidation.

The precipitation anomaly 2023/24 in western Germany provides a unique opportunity to assess the potential consequences of extreme climatic conditions on post-mining environments. Mine waters from shallow, abandoned underground mines that are only partially flooded and receive infiltration from precipitation may contain substantial amounts of soluble compounds originating from the upper mine levels or the overburden. As climate models predict more extreme weather events in the future with increasing precipitation during winter and prolonged dry periods in summer it is crucial to understand the potential consequences for such abandoned mining systems.

Acknowledgements

The authors would like to thank A. Fugmann for assistance in the laboratory (Univ. Münster) and T. Trieb (RAG AG) during mine water sampling. We greatly appreciate financial support of the RAG AG for this project. The authors thank two anonymous reviewers for providing critical comments on an earlier version of this abstract.

References

Deutscher Wetterdienst (2026) Monatliche Niederschlagswerte. https://www.wetterkontor.de/wetter-rueckblick/monats-und-jahreswerte.asp?id=H432. Accessed 11 March 2026

Dogramaci SS, Herczeg AL, Schiff SL, Bone Y (2001) Controls on δ34S and δ18O of dissolved SO4 in aquifers of the Murray Basin, Australia and their use as indicators of flow processes. Applied Geochemistry 16: 475–488. DOI:10.1016/S0883-2927(00)00052-4

Kaplan I R, Rittenberg, SC (1964) Microbiological fractionation of sulphur isotopes. Journal of General Microbiology 34: 195–212. DOI:10.1099/00221287-34-2-195

Puchelt H, Nielsen, H (1967) Untersuchungen über die Verteilung der Schwefelisotope in den Grubenwässern des Ruhrreviers. Glückauf-Forschungshefte 6: 303–310.

Singer PC, Stumm W (1970) Acidic mine drainage: the rate-determining step. Science 167: 1121–1123. DOI:0.1126/science.167.3921.1121

IMWA 2026
Jeongseon

How Long Is Long Enough? Assessing the Critical Storm Duration for Non Discharge TSFs

Heather Thomson[1], Joanna So[2], Justin Walls[3]

[1]*SRK Consulting (Australasia) Pty Ltd., hthomson@srk.com.au*
[2]*SRK Consulting (Australasia) Pty Ltd., jso@srk.com.au*
[3]*SRK Consulting (Australasia) Pty Ltd., juwalls@srk.com.au*

Abstract

Weather hazards are a leading cause of tailings storage facility (TSF) failures, with weather-triggered flow incidents increasing (Rana *et al.* 2021). While spillways are a common means of providing TSF flood discharge capacity, many facilities are designed as 'non-discharge' systems which contain all inflows within the basin. Designing non-discharge TSFs requires an understanding of the critical storm duration, yet guidance is inconsistent and practice often defaults to 24–72-hour events with limited justification. This paper presents a practical method for identifying the critical storm duration for non-discharge TSFs using water-balance modelling in parallel with emergency response assumptions.

Keywords: Tailings, mine waste, freeboard, critical duration, water balance, risk management

Introduction

Weather hazards are the most common contributing factor to TSF failures, with the number of tailings flow incidents triggered by weather events steadily increasing over time (Rana *et al.* 2021). A key aspect of mitigating this risk is designing and operating TSFs to safely manage inflow design floods.

For non-discharge TSFs where all flood-water is retained, the concept of a critical storm duration is nuanced. Industry practice often defaults to adopting 24-hour or 72-hour storm durations, but there is little justification for whether these represent the critical duration for non-discharge TSFs, leaving a gap in both practice and regulation. As such, the objectives of this paper are to:

- Investigate the critical duration storm for non-discharge TSFs using water balance modelling combined with operational and emergency response considerations.
- Undertake sensitivity analyses to explore the influence of tailings properties and climatic conditions.
- Propose a practical method for assessing and selecting the critical duration that can be used to inform TSF design and operational planning.

There are many uncertainties inherent in TSF water management, and the way these are addressed varies significantly between jurisdictions and site settings. This paper is not intended to challenge existing guidance or regulatory requirements, where present, but rather to propose a general framework that practitioners can adapt, expand upon and apply to their specific context.

Background

TSFs are complex systems that must safely manage variable inflows from tailings deposition, runoff and direct rainfall, while maintaining sufficient freeboard to mitigate the risk of overtopping and run-on stability problems. To add further complexity, TSF structures are typically constructed gradually (i.e., raised in stages), resulting in a permanent landform that must function safely in perpetuity under a changing climate.

Water is typically removed from TSFs via operational discharge infrastructure (pumped decant or gravity penstock), which – in flood scenarios – can be (and for design purposes is generally assumed to be) rendered inoperable. Thus, it is good practice to include a spillway to passively

pass significant design floods in emergency scenarios. However, spillways can be complex and costly to construct and can inherently introduce additional risks, particularly for facilities raised in multiple stages or those lacking a viable spillway location.

As a result, in many situations it is considered more cost and/or risk effective to design non-discharge TSFs, relying on the impoundment's basin storage capacity to contain floodwater. This is particularly common in Western Australia (WA) and similar semi-arid to arid regions, where evaporation can exceed rainfall by an order of magnitude, and flat terrain lends itself to large, paddock-style TSFs with limited catchment areas. TSF ponds can remain well below operating limits, and design storm ponds remain distant from the embankment by hundreds of metres. Similarly, in-pit TSFs are commonly designed as 'non-discharge facilities' as the risk of overtopping or instability inducing a catastrophic failure can be negligible. This is acknowledged in WA regulatory guidance (DMP 2015), which states that *'the use of spillways is not encouraged, particularly for paddock or ring-dyke type facilities with perimeter retaining structures constructed using tailings.'*

In contrast, guidance from ICOLD (2025) and ANCOLD (2019) recommend that an emergency spillway or controlled overflow pathway should always be considered as a fail-safe. Therefore, the decision to exclude a spillway must be a well-justified, risk-based decision that considers the risks associated with storing additional water.

For TSFs with spillways, the critical duration of the design flood can be readily determined by routing the inflow hydrograph through the basin and identifying the duration that produces the maximum outflow and/or water level. However, for non-discharge TSFs where all floodwater must be retained, the concept of a critical storm duration is more nuanced. Under storm conditions, active discharge systems are assumed to be unavailable due to power outages, access constraints or operational risk controls. As such, the longer the storm duration, the greater the accumulation of water in the impoundment. The critical duration is governed by a balance between increasing inflow, limited passive losses and decreasing storage availability over time. If a reliable and proven emergency response plan is in place, the critical duration can be bounded by the period over which the plan can be enacted.

Most industry guidance and standards, such as the Global Industry Standard on Tailings Management (GISTM) (GTR 2020), refer to inflow design floods without prescribing a specific duration for non-discharge TSFs. In practice, designers frequently adopt 24-hour or 72-hour events as a default. However, there is limited justification for these choices in the context of non-discharge TSFs where all floodwater must be retained.

Methods

The approach presented in this paper is based on simple water balance modelling to account for inflows from longer duration, multi-day storms and passive outflows. This can be readily expanded to account for uncertainties and superimposed with assumptions about operational status and emergency response during extreme events, forming a framework to identify the storm durations that govern maximum pond levels in non-discharge facilities.

The hydrological inflow to the model is based on rainfall time series that are representative of the local climate. The rainfall input should be representative of a range of storm durations associated with the design annual exceedance probability (AEP), selected considering the tolerable risk level. It is noted that 'long' duration events are typically comprised of several embedded short duration rainfall bursts, thus a long duration design storm implicitly accounts for the probability of sequential events.

Practically, this involves constructing a series of synthetic design hyetographs of different durations, consistent with design intensity–duration–frequency relationships and relevant climate change predictions. These design hyetographs (graphical representation of rainfall intensity over time) are then embedded within a longer continuous record or applied to representative antecedent moisture conditions and transformed to runoff

over the contributing catchment. For extreme design events, runoff is typically represented using conservative loss assumptions (i.e., negligible or very low losses).

Model outflows are limited to passive losses from evaporation and infiltration. As with rainfall, evaporative losses are represented by time series that are characteristic of the local climate, noting that actual evaporation during storm events can be significantly lower than average conditions.

Infiltration into tailings is a complex process, as hydraulic behaviour varies and evolves over time with spatial variability due to beaching, consolidation, deposition history and desiccation. A fully coupled unsaturated flow model is not practical to incorporate into the proposed framework. Instead, infiltration is represented using simple physically based formulations, or by prescribing effective loss rates derived from available site data or representative parameter ranges.

The TSF storage characteristics are represented through a stage–storage relationship that reflects the geometry of the basin, including the tailings beach and supernatant pond area. This relationship may be developed from survey data or idealised design geometry and should reflect the expected operating configuration at the time the design event is assumed to occur, or the configuration that results in the most critical outcome. Where tailings are actively being deposited and beach geometry is continually evolving, a conservative representation of beach slope and pond area should be adopted.

To identify the critical storm duration, the model is run for a set of scenarios in which storms of varying duration, but common AEP, are applied. By comparing the predicted maximum pond levels across durations, the storm or sequence of storms that produces the highest pond level is identified as the critical duration for the modelled conditions and assumptions. The resulting maximum pond levels should then be assessed in the context of overall TSF performance and risk criteria, including freeboard, stability, erosion and other site-specific operational limits.

Emergency response plans should specify intended measures such as siphons, pumps or emergency excavated spillways. Where such measures are demonstrated to be reliable and are explicitly relied upon, their effect can be superimposed on the water balance model, potentially limiting the critical storm duration. This must consider both the influence of storm intensity on site access and the time required to initiate and implement the emergency response actions.

Monte Carlo simulations or sensitivity analyses can be used to account for, and explore, the influence of key parameters and assumptions on the model results and resulting critical duration. Key uncertainties may include tailings beach slope and the resulting stage–storage relationship, catchment size and runoff characteristics, infiltration and evaporative losses, climatic conditions, antecedent conditions and emergency response assumptions. By varying these parameters within plausible ranges, the robustness of the analysis and its dependence on site conditions can be assessed.

From a design perspective, it is not recommended to rely on infiltration and evaporation losses when calculating required storage capacity, as these losses are often negligible during the peak of the event and can be highly uncertain. However, incorporating realistic passive losses allows practitioners to identify a meaningful, physically justifiable critical duration, while still sizing storage allowances on a conservative basis.

Application

The proposed method was applied to a paddock-style TSF in the Goldfields region of WA. A simplified approach was adopted to inform the selection of appropriate design criteria at an early design stage, before the facility was constructed and in the absence of observation data. The facility is designed to have a downstream-raised embankment, a small supernatant pond (operationally discharged via a pump), no spillway, and 0.5% beach slopes. The climate is semi-arid, with low but highly variable rainfall dominated by infrequent, high-intensity short-duration storms and occasional multi-day events, and very high potential evaporation across most of the year.

A simplified water balance model was constructed in which a design storm is applied above the maximum operating level, assuming that both tailings deposition and reclaim pumping are ceased at the onset of the event, no controlled releases from the TSF occur, and pumping can only resume after a prescribed recovery period once weather conditions improve and access is restored. Infiltration into the tailings beach is assumed to decrease exponentially from an initial capacity of 1 mm/h to a constant minimum rate of 0.5 mm/h as the tailings becomes saturated over time. An average evaporation rate of 10 mm/day is applied, reducing to 40% of this during the storm event.

A 1% AEP design storm is selected and assessed for durations ranging from 24 to 168 hours (selected as required to reveal the critical duration). The design rainfall depth is obtained from the Australian Bureau of Meteorology and included climate change adjustments as recommended in Australian Rainfall and Runoff Guidelines. An example of the model results for a 24-hour storm is shown in Figure 1, illustrating a drain down period of approximately 18 days to return to the original pond level, relying only on passive outflows (infiltration and evaporation) and assuming no further rainfall occurs in the days following the design storm.

The model was then run for a set of scenarios in which storms of varying duration but common exceedance probability were applied to the TSF. Given the uncertainties inherent at the early design stage, alternative scenarios were also considered in which key assumptions were varied, including beach slope, evaporation and infiltration capacity. The results for the full range of durations assessed are shown in Figure 2. In this case, the infiltration capacity of the tailings beach both largely controls the outflows and represents a substantial uncertainty at the design stage (which could reasonably vary by an order of magnitude). A 1% AEP event with a duration of 120 hours was conservatively selected for design.

However, in this scenario the absolute difference between the design storms is relatively modest. The additional freeboard allowance required between a 72-hour and 120-hour 1% AEP event is in the order of 25 mm, which is within both the accuracy of the assessment and adopted design tolerances. Thus, for this facility, adopting a 'default' 72-hour storm duration for storage calculations would not have materially underestimated the risk of exceeding the available freeboard provision.

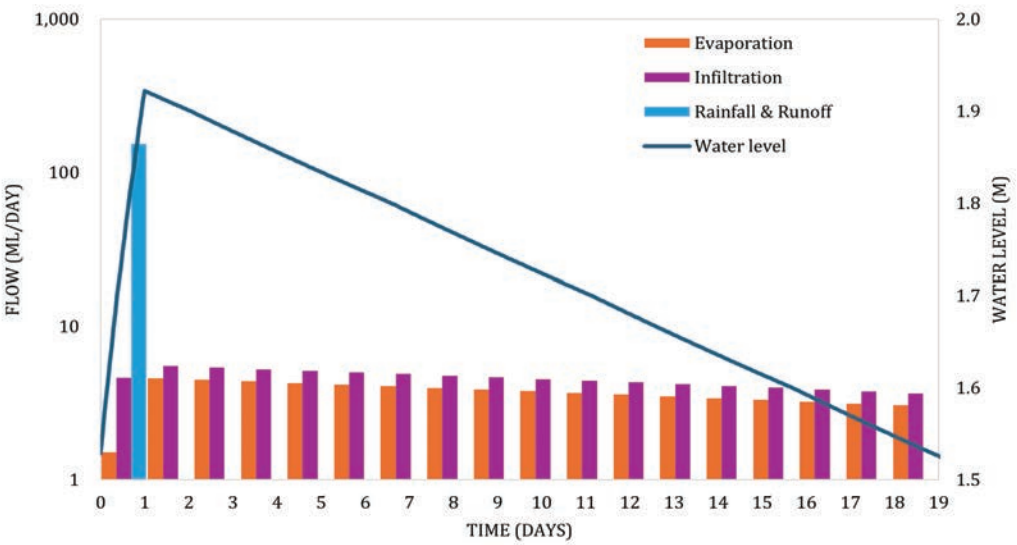

Figure 1 24-hour duration simplistic water balance result.

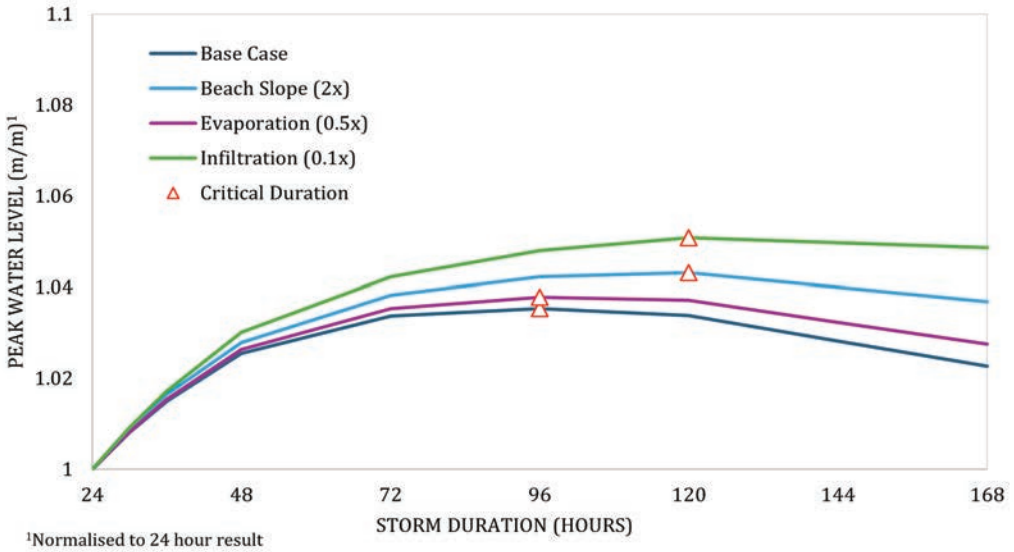

Figure 2 Scenario analysis results.

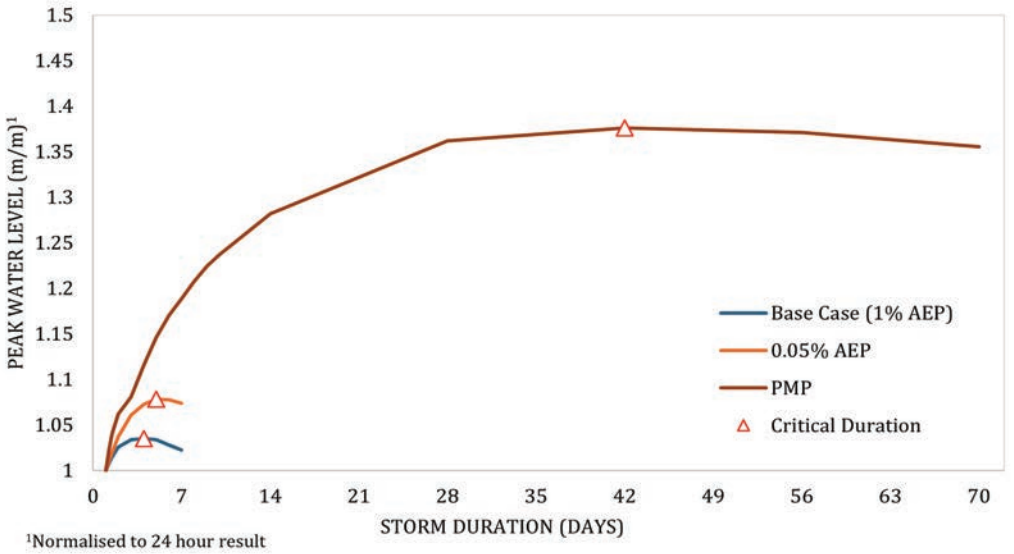

Figure 3 Alternative AEP results.

To enable stress testing and inform a risk assessment, the model was then run for a range of alternative AEPs. The results are shown in Figure 3. The results illustrate that the critical duration increases as the AEP decreases, which is expected given the relationship between inflow intensity and the rate-limited outflows, which are assumed constant. Accordingly, and in contrast to the base case (1% AEP) assessment above, adopting a default 72-hour storm duration for probable maximum precipitation (PMP) storage calculations would significantly underestimate the risk of exceeding the available freeboard, especially in closure designs which commonly adopt design storms from 0.01% AEP events up to the PMP.

Practical guidance for practitioners

For practitioners, the key is to embed critical storm duration assessment within routine TSF design and review, rather than relying on default 24–72 hour events for non-discharge TSFs. A practical workflow is to:

1. select the design AEP (or AEPs) consistent with risk tolerance, best practice and regulatory criteria
2. construct a simple but defensible water balance model that represents a range of realistic operating conditions before, during and after a design storm event
3. apply a suite of design storms of varying duration for the chosen AEP
4. use sensitivity analysis to test uncertainties in critical parameters such as stage–storage relationships, infiltration capacity and evaporation
5. select the critical storm duration to be adopted for the chosen design event
6. if required, and where there is a demonstrably reliable plan, superimpose credible emergency response actions (for example, deployment of siphons or pumping to adjacent storages) to bound the critical duration.

The selected critical duration should then be used to assess storm storage requirements (generally ignoring all losses) and translated into operational freeboard criteria and trigger levels (e.g. maximum allowable pond volume prior to the wet season). The assessment should be clearly documented alongside the underlying assumptions so they can be revised as observation data and site conditions evolve.

It is acknowledged that determining design rainfall depths for long duration, rare events can be challenging. Where long duration estimates are required, practitioners may need to extrapolate beyond standard guidance or consider more complex analyses.

Conclusions

This paper presents a practical framework for identifying the critical storm duration for non-discharge TSFs using a simple water balance model. The example application demonstrates that relying on a default storm duration without justification can underestimate the risk of freeboard exceedance, particularly for design storms of increasing rarity.

The results emphasise that the critical duration is inherently site-specific. It is governed by the relationship between the intensity and duration of the design storm inflows and the rate-limited passive outflows (infiltration and evaporation). Because this balance changes with storm severity, the critical duration is not constant across different AEPs or storm intensities. In the example application, the difference between 72-hour and 120-hour storms at the 1% AEP was modest and within design tolerances, but for rarer events (e.g., 0.05% AEP and PMP) the critical durations increased significantly.

Finally, even where a non-discharge configuration is selected, the decision to not include a spillway should be made on a risk-informed basis. The example application shows that large paddock-style TSFs in highly evaporative climates can, in some cases, safely operate without a spillway, provided adequate storage capacity and freeboard provisions are in place. Nonetheless, a spillway or controlled overflow pathway remains an important fail-safe that should always be actively considered in design, consistent with contemporary TSF guidance and good practice.

References

Australian National Committee on Large Dams (ANCOLD) (2019) Guidelines on Tailings Dams-Planning, Design, Construction, Operation and Closure-Revision 1

Global Tailings Review (GTR) (2020) Global Industry Standard on Tailings Management

Government of Western Australia Department of Mines and Petroleum (DMP) (2015) Guide to the preparation of a design report for tailings storage facilities (TSFs), Department of Mines and Petroleum, August 2015

International Commission on Large Dams (ICOLD) (2025) Tailings Dam Safety. ICOLD Bulletin 194

Rana NM, Ghahramani N, Evans SG, McDougall S, Small W, Take WA (2021) Catastrophic mass flows resulting from tailings impoundment failures. Engineering Geology 292:106262

Hydrogeological and Hydrogeochemical Characteristics of the Lo Tri Coal Mine in Cam Pha, Vietnam

Tuan Quang Tran[1], Hien Thu Vu[1], Bang Duc Dao[1], Thao Bach Nguyen[1]

[1]*Department of Hydrogeology, Faculty of Geosciences and Geoengineering, Hanoi University of Mining and Geology, No. 18, Vien Street, Dong Ngac Ward, Hanoi, 100000, Vietnam, tranquangtuan@humg.edu.vn, ORCID 0000-0001-9614-126X*

Abstract

This study investigated the hydrogeological and hydrogeochemical characteristics of the Lo Tri coal mine in the Cam Pha coalfield, Vietnam. Groundwater levels, flow directions, hydrostratigraphic units, and temporal hydrogeochemical variations were analyzed using historical and recent monitoring data, including 57 water samples and pumping-test results from exploration boreholes. Three hydrostratigraphic units were identified: a Quaternary porous aquifer, a fractured aquifer within coal-bearing Triassic sediments, and water-bearing fault zones. Groundwater generally flows in a north-to-south direction. Hydrogeochemical analyses revealed that the groundwater was generally fresh, but locally acidic, dominated by Na-Mg-Ca-SO_4-HCO_3 and Na-Mg-SO_4 types. These results provide a scientific basis for mine water management and environmental effect assessment in the Lo Tri coal mine.

Keywords: Hydrogeology, hydrogeochemistry, underground coal mining, Lo Tri coal mine, Cam Pha

Introduction

Coal mining in Cam Pha, Quang Ninh province, Vietnam, has been conducted on a large scale since the late 19th century and is one of the country's most important coal production areas (Nguyen 2025). In recent decades, mining activities have progressively extended to deeper levels, raising considerable hydrogeological and hydrogeochemical challenges. Groundwater inflow into underground workings, water-rock interaction processes, and the quality of mine drainage are increasingly critical issues affecting mining safety, operational costs, and the surrounding environment (Le 2021). The present study focuses on the Lo Tri coal mine, operated by Thong Nhat Coal Company-TKV, covering approximately 2.91 km2 in the Hon Gai-Cam Pha coalfield (Fig. 1).

Underground coal extraction is currently conducted at depths ranging from approximately -35 to -150 m and to -350 m in the next few years (Thong Nhat Coal Company-TKV 2023). The terrain is characterized by coastal mountains and extensive waste dumps, with elevations generally between 200 and 300 m, and a maximum elevation of 439.6 m above sea level (a.s.l.). The southwestern part of the mine area is relatively lower, forming a valley shaped by historical and ongoing open-pit mining activities. A large waste dump with variable thickness ranging from 1.0 to 50 m is distributed in the central area. Vegetation cover is sparse due to long-term mining. Surface drainage in the area is controlled by watershed divides in the north of the mine. An artificial freshwater reservoir (Bara Lake) is located in the northeastern part of the mine area and serves industrial and domestic purposes. The mine is situated in a tropical monsoon climate zone with distinct rainy (from April to October) and dry (from November of the previous year to March of the following year) seasons. Air temperature ranges from 37–38 °C (in summer) to 8-15 °C (in winter) (Cua Ong Meteorological Station 2025). Geologically, the mine area is dominated by the Hon Gai Formation (T_3n-r*hg*), which is divided into the lower unit (T_3n-rhg_1) and upper unit (T_3n-rhg_2) (Vu 1987). The lower unit mainly consists of conglomerate and breccia interbedded with sandstone, siltstone, and claystone.

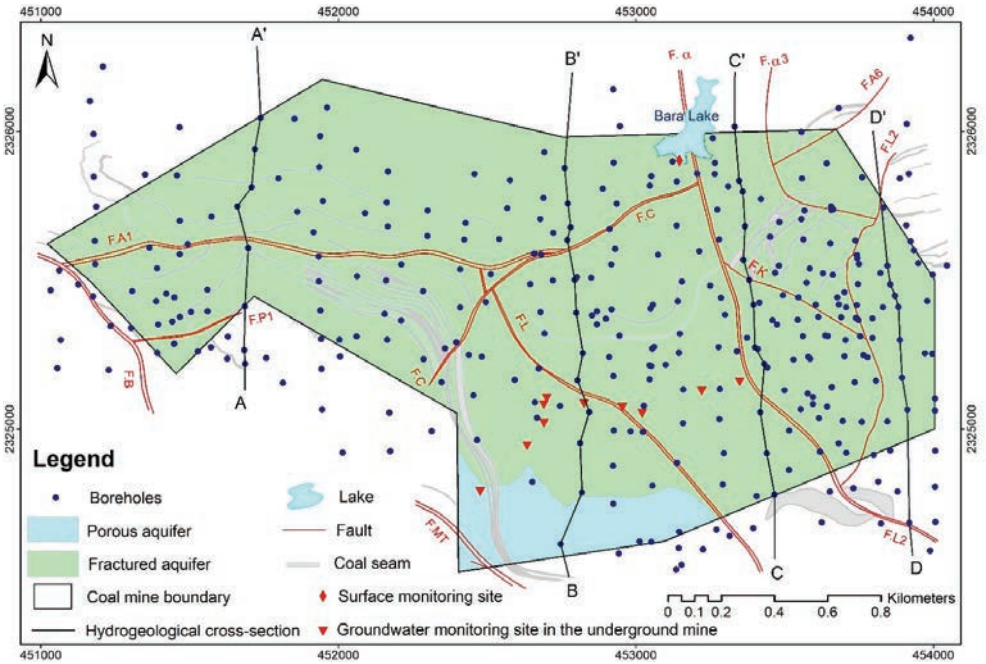

Figure 1 *The hydrogeological map of the Lo Tri coal mine with cross-sections (after Dao* et al. *2023).*

The upper unit is widely distributed and comprises conglomerate, breccia, sandstone, siltstone, claystone, and industrial coal seams (Le 1997; Nguyen *et al.* 2022). Quaternary sediments are locally distributed along faults, slopes, and valleys and consist of pebble, gravel, sand, clay, and organic matter. The geological structure of the Lo Tri mine is complex, with multiple folds and fault systems dividing the area into northern, central, and southern structural blocks (Thong Nhat Coal Company-TKV 2023). These structural features play an important role in controlling the occurrence and flow patterns of groundwater. Although mining operations have been ongoing for decades, studies that address both hydrogeological conditions and groundwater chemistry at the Lo Tri mine remain limited. Thus, this study aims to characterize the hydrogeological conditions and hydrogeochemical properties of groundwater in the Lo Tri coal mine, which is important for supporting future deeper mining activities. The results are expected to provide a scientific basis for improved mine water management and to contribute to a better understanding of groundwater behavior in the area.

Methodology

Data collection

Data were collected from an exploration project conducted to upgrade the Lo Tri coal mine (Thong Nhat Coal Company-TKV 2023). These included geological and hydrogeological reports, borehole logs, and an exploration report, all prepared by Thong Nhat Coal Company-TKV and Vinacomin Information, Technology, and Environment Joint Stock Company (VITE). The data included pumping test results, borehole stratigraphy, water levels, and water analysis results. This study used monitoring data from one surface monitoring site (Bara Lake) and ten groundwater monitoring sites in the underground mine (located along the drainage channels in the underground mine galleries, flowing towards the pumping stations) (Fig. 1). The static water level was measured in 65 boreholes, including 37 boreholes before 2020 and 28 boreholes from 2020 to 2022. Water samples were analyzed at

the VITE laboratory using titration methods, an atomic absorption spectrophotometer (AA-7000, Shimadzu, Japan), and a UV-Vis spectrophotometer (UV-1900i, Shimadzu, Japan).

Data processing

The lithological units, their depths, and hydrogeochemical data were processed using Excel, AutoCAD, ArcGIS 10.8, and Geochemist's Workbench software. Based on lithological units, the respective hydrostratigraphic units were verified and classified. The borehole data, which included XY coordinates, depth, elevation, and thickness for each hydrostratigraphic unit, were imported into ArcGIS. Moreover, to determine groundwater flow, water level data were processed and interpolated in ArcGIS using the Kriging technique. Potential metric maps were derived from the interpolated heads to determine the flow direction. Aquifer hydraulic characteristics were calculated from pumping tests.

Results and Discussion

Aquifer characterization

Three hydrostratigraphic units were identified in the Lo Tri coal mine area: a porous aquifer in Quaternary sediments (q), a fractured aquifer in the Hon Gai Formation (T_3), and a fault-related water-conducting zone. The porous aquifer is primarily distributed in the southern part of the area (Fig. 1). Four hydrostratigraphic cross-sections were constructed across the mine area to illustrate the hydrostratigraphic framework (Figs. 1 and 2). The cross-sections show the spatial configuration of the hydrostratigraphic units. For instance, the fractured aquifer in the T_3 sediments can be divided into three layers: (1) the fractured aquifer in the overlying strata of the Day coal seam, (2) the fractured aquifer in the Day coal seam, and (3) the fractured aquifer in the underlying sediments beneath the Day coal seam (Fig. 2). The porous aquifer pinches out northward against the fractured aquifer (e.g., cross-section BB').

Cross-sections show that the strata overlying the Day coal seam (1) are widely distributed, extending from the central part of the mine towards the north and northeast. This distribution has been locally modified by open-pit mining and waste disposal activities (Fig. 2). The north-south cross-sections (BB´, CC´, and DD´) reveal the presence of fault zones. Fractured conglomerate and sandstone constitute the main water-bearing formations, in which groundwater is primarily stored and transmitted through fracture systems. In contrast, siltstone and claystone contain only minor fractures, which are commonly filled with clay minerals. Therefore, they exhibit poor water-bearing capacity and generally act as aquitards or aquicludes. Several layers of fractured conglomerate and sandstone form aquifers up to 70 m thick. Due to unstable sedimentary conditions, impermeable and water-bearing layers occur as discontinuous lenses. Consequently, the groundwater in these layers is hydraulically connected through hydrogeological windows, resulting in unconfined or weakly confined conditions. Moreover, based on the pumping test results obtained from borehole TN146 in this layer, three pumping stages were conducted with different flow rates. The pumping rates (Q) were 0.38, 0.35, and 0.32 L s^{-1}, corresponding to specific discharge (q) values of 0.0189, 0.0238, and 0.0315 L s^{-1} m^{-1} and permeability coefficients (K) ranging from 0.0105 to 0.0142 m d^{-1} for tests 1, 2, and 3, respectively. These values suggest that the formation is weak water-bearing and has very low permeability (Bindeman 1963; Kruseman and de Ridder 1994; Singhal and Gupta 2010).

In the Day coal seam (2), the coal seams rarely crop out at the surface (Figs. 1 and 2). This sequence is characterized by well-developed cyclothems, with a lithology dominated by siltstone, mudstone, and coal seams. According to the results of pumping tests, the specific discharge (q) ranges from 0.00406 to 0.320 L s^{-1} m^{-1} (Table 1), indicating that, according to Bindeman's classification (Bindeman 1963), the aquifer varies from very poor to poor in terms of groundwater abundance. The permeability coefficient (K) ranges from 0.0015 to 0.013958 m d^{-1}, indicating very low permeability (Kruseman and de Ridder 1994; Singhal and Gupta 2010). In addition, water inflow from mine roadways excavated at the +13 and -35 m levels in this stratigraphic unit is minimal.

Table 1 Results of pumping tests from boreholes in the Day coal seam sediments.

Borehole ID	Borehole collar elevation (m)	Static water level (m)	S (m)	Q (L s^{-1})	q (L s^{-1} m^{-1})	K (m d^{-1})
1071	248.6	131.4	1.21	0.178	0.320	0.006
196b	371.4	1.5	7.1	0.021	0.147	0.0015
TN121	157.2	92.9	16.7	0.0679	0.00406	0.00375
			11.7	0.0538	0.00460	0.00400
			6.6	0.0346	0.00524	0.00410
TN160	154.5	121	10.8	0.0553	0.00512	0.012929
			7.4	0.0428	0.00580	0.013958
				0.0272	0.00648	0.013684

In many locations, water is either absent or present only as minor seepage (Thong Nhat Coal Company-TKV 2023). These observations indicate that the rock and coal layers in this unit generally function as a water-poor formation due to their low water-bearing capacity.

The strata underlying the Day coal seam (3) are exposed in the southeastern and southern parts of the mine (Figs. 1 and 2). Field observations and previous drilling data suggest the presence of a siltstone layer directly beneath the coal seam. From a hydrogeological perspective, this siltstone layer is laterally continuous across the region, acting as an aquitard that restricts groundwater flow. Beneath this layer are coarse-grained rocks such as conglomerate and sandstone, which are locally interbedded with thin lenticular layers of fine-grained siltstone and claystone. Currently, no borehole pumping tests have been conducted in these sediments. However, observations from an inclined shaft at the -35 m level suggest that, where the shaft intersects conglomerate layers, groundwater flows continuously along the shaft walls and floor. At the -140 m level, the inflow of water into the underground workings was

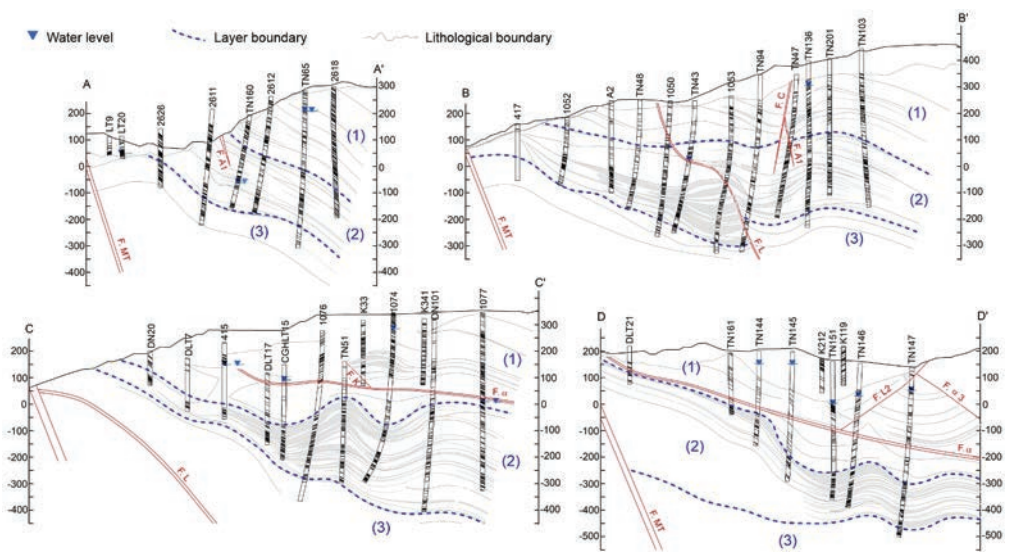

Figure 2 Hydrogeological cross-sections from the transects in Figure 1: (1) the strata overlying the Day coal seam, (2) the Day coal seam, and (3) the strata underlying the Day coal seam.

most pronounced. The maximum inflow into the mine during the rainy season reaches 839 $m^3 h^{-1}$, causing flooding of mine workings that disrupts production and results in economic losses. Overall, this aquifer has relatively high groundwater potential.

Also, a fault-related water-bearing zone occurs in relatively wide tectonic fault damage zones, e.g., F.A1, F.C, F.L (Figs. 1 and 2). In addition to being encountered in exploration boreholes, these fault zones have also been exposed in underground roadways during coal mining operations (Thong Nhat Coal Company-TKV 2023). No pumping tests have been conducted in boreholes intersecting this zone in the Lo Tri coal mine. Potential recharge sources for the mine might be water from the overlying strata, previously mined-out areas, and precipitation. Therefore, the hydrogeological characteristics of these fault zones require further investigation.

Regional groundwater flow pattern and dynamics

Groundwater flow shows temporal variations and is influenced by mining activities. In general, groundwater flows from north to south in the central part and from west to east in the eastern part (Fig. 3). In the central part of the mine, the groundwater flow pattern during 2020-2022 was similar to that observed before 2020, with flow predominantly directed from north to south. Groundwater levels increase progressively towards the north due to the topographic influence of Khe Sim Mountain. However, during the upgrade exploration period (2020–2022), the groundwater flow pattern in the eastern part of the mine differed from that observed before 2020 (Fig. 3a and 3b).

In addition, faults, such as F.C and F.L, act as conduits for the downward flow of groundwater in the overlying strata of the Day coal seam. Mining activities, including blasting in the longwall face and controlled roof caving, have fractured the strata immediately above the Day coal seam. This process creates hydraulic connections between aquifer layers, allowing groundwater to flow into the mine workings at the +13 and -35 m levels. According to mine water monitoring data collected at drainage points in the mine, the average inflow at the -35 m level was 116.6 m^3 h-1 in 2021 (Thong Nhat Coal Company-TKV 2023).

Regarding groundwater dynamics, monitoring results from mine workings indicate that both groundwater levels and mine inflow increase during the rainy season and decrease during the dry season. For example, at the +13 m adit, the coefficient of variation (CV) of annual discharge in the hydrological year ranged from 1.51 in 2015 to 18.58 in 2019. The CV was 6.84 in 2020 and 8.13 in 2021. At the -35 m level, monitoring of monthly mine drainage discharge shows that the CV of flow rate in the hydrological year increased from 1.61 in 2016 to 5.38 in 2021. Surface water monitoring results indicate that the water volume of Bara Lake ranged from approximately 508.4 m3 to about 146.6 m3. However, the lake's water level fluctuates only slightly, ranging from 328.3 m in the dry season (2013) to 328.9 m in the rainy season (2014). Precipitation is considered the main source of recharge for

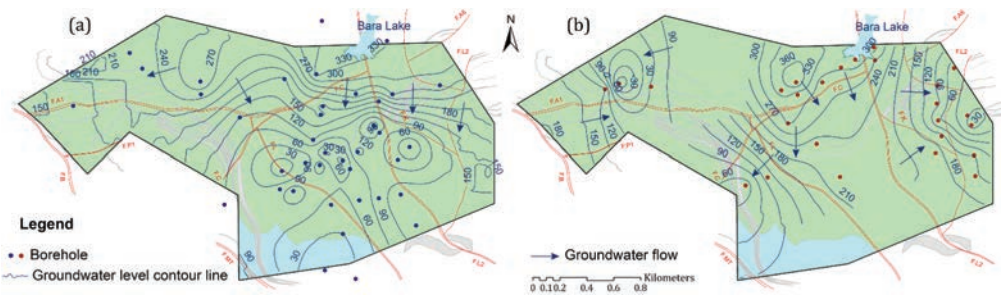

Figure 3 *Groundwater potentiometric surface and flow pattern in the Lo Tri coal mine area: (a) before 2020 and (b) during the exploration upgrading period 2020–2022.*

the lake (Bara Lake monitoring statistics; Thong Nhat Coal Company-TKV 2023).

Hydrogeochemical characteristics

Hydrogeochemical facies

In general, the pH values of the groundwater at the Lo Tri coal mine ranged from 2.15 to 6.60, indicating acidic water. A Durov diagram (Durov 1948) was plotted for the groundwater samples to categorize the hydrogeochemical types (Fig. 4). The dominant cations follow the order of $Mg^{2+} > (Na+K)^{+} > Ca^{2+}$, whereas the major anions follow the order of $SO_4^{2-} > Cl^{-} > HCO_3^{-}$.

However, as mentioned above, the water type differed between water-bearing layers. For example, in the Day coal seam, the average pH value of the groundwater was 6.5, indicating slightly acidic water. The TDS value was 0.77 g L^{-1}, corresponding to fresh water (Freeze and Cherry 1979). The water was characterized as Na-K-Mg-SO_4-HCO_3 water type. In contrast, the average pH value of the groundwater was 4.3, indicating acidic water, and the TDS value was 0.34 g L^{-1}, corresponding to fresh water, with the Na-K-Mg-SO_4 type in the underlying strata beneath the Day coal seam. The low pH values were likely related to the oxidation of sulfide minerals associated with the coal seams. The Fe^{2+} concentration also differed between the strata (Table 2).

Engineering implications of groundwater chemistry

In the Day coal seam, the average water hardness was 17.9 °dH, indicating hard water. The water exhibited strong effervescence and contained a considerable amount of sediment with hard deposits. It was also corrosive and had a high soap consumption capacity, ranging from 6,905 to 10,283 g m¬¯³. In contrast, groundwater in the underlying sediments of the Day coal seam had an average hardness of 6.37 °dH, which is classified as soft water. The water exhibited normal foaming characteristics, produced little residue, and had a low tendency for scale formation. Its soap consumption capacity ranged from 986.4 to 8,832 g m-3 (Fig. 5). These characteristics may influence mine drainage operations, pumping equipment performance, underground water systems, and maintenance conditions in underground mine workings.

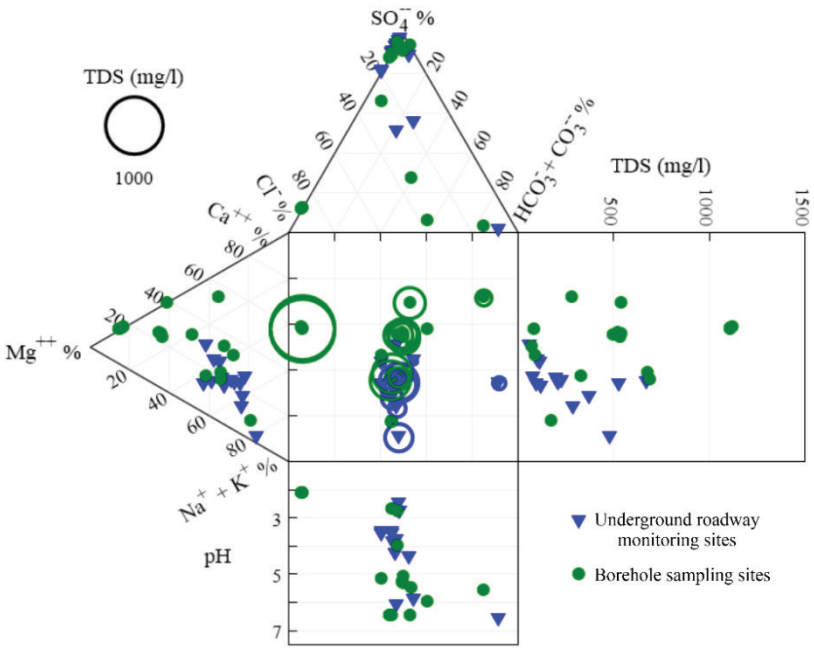

Figure 4 *Durov diagram of groundwater hydrogeochemistry in the Lo Tri coal mine.*

Table 2 The chemical characteristics of groundwater.

Parameter	Unit	Concentration (Day coal seam)			Concentration (below the Day coal seam)		
		Average	Max	Min	Average	Max	Min
pH	-	6.5	6.5	6.5	4.3	6.6	2.5
TDS	g L^{-1}	0.73	0.77	0.70	0.34	0.876	0.095
Cl^-	mg L^{-1}	27.9	44.55	0	10.4	19.85	0.92
SO_4^{2-}	mg L^{-1}	422.2	446.4	378.9	176.5	493.8	1.23
HCO_3^-	mg L^{-1}	12.2	30.51	3.05	35.3	192.82	0
Ca^{2+}	mg L^{-1}	48.1	61.52	38.88	15.0	38.65	2.95
Mg^{2+}	mg L^{-1}	48.4	58.96	42.7	19.1	60.05	2.74
$(Na + K)^+$	mg L^{-1}	73.6	114.37	0.925	33.8	130.53	0.069
Fe^{2+}	mg L^{-1}	2.67	8	0	4.31	40.2	0.55

Conclusions

This study provided an integrated hydrogeological and hydrogeochemical characterization of the groundwater conditions at the Lo Tri underground coal mine. The results revealed that the occurrence and flow of groundwater were mainly controlled by fractured Triassic coal-bearing strata and tectonic fault zones, whereas the Quaternary porous aquifer plays only a limited role locally. Mining activities and fault structures created hydraulic connections that facilitated the inflow of groundwater into the underground workings. Hydrogeochemical analyses revealed that the groundwater is generally fresh, albeit slightly to moderately acidic. These findings improved the understanding of groundwater behavior in the mine, providing useful information for mine water management and future deeper mining operations in the Cam Pha coalfield.

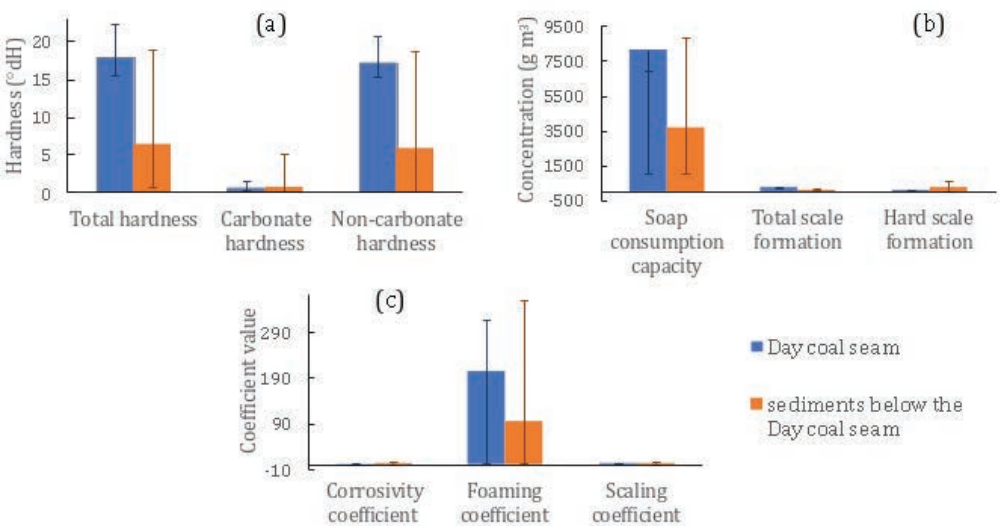

Figure 5 Engineering-related groundwater characteristics in the Lo Tri mine: (a) hardness indices, (b) scale formation potential, and (c) corrosion-related coefficients for groundwater in the Day coal seam and underlying sediments.

Acknowledgements

This research was funded by the National Foundation for Science and Technology Development (NAFOSTED), Vietnam, under grant number 105.99-2025.40. The authors would like to thank Hanoi University of Mining and Geology and Thong Nhat Coal Company-TKV for their support. The authors also thank Dr. Phuc Quang Le (Hanoi University of Mining and Geology) for his assistance with the field investigation.

References

Bindeman NN (1963) Hydrogeology of Ore Deposits. Gosgeoltekhizdat, Moscow (in Russian)

Cua Ong Meteorological Station (2025) National Hydro-Meteorological Monitoring Center, Automated Meteorological and Hydrological Monitoring System. https://kttvtudong.net/kttv. Accessed on 25.12.2025

Dao MH, Nguyen DL, Pham TT, Nguyen TM, Nguyen HH (2023) The hydrogeological map of the Lo Tri coal mine, the scale of 1:2,000. Vinacomin Information, Technology, and Environment Joint Stock Company

Durov SA (1948) Classification of natural waters and graphic presentation of their composition. Dokl Akad Nauk SSSR 59(1):87-90

Freeze RA, Cherry JA (1979) Groundwater. Prentice-Hall, Inc., Englewood Cliffs, New Jersey

Kruseman GP, de Ridder NA (1994) Analysis and Evaluation of Pumping Test Data. Netherlands, 1994

Le H (1997) Geology and Mineral Resources Mapping of Cam Pha on a 1:50,000 Scale. Vietnam Institute of Geosciences and Mineral Resources, Hanoi, Vietnam

Le TTH (2021) Assessing impacts of mining activities on land use/land cover change using remote sensing and GIS techniques: A case study in Campha city, Vietnam. J. Polish Miner. Eng. Soc. 1, 467–477. https://doi.org/10.29227/IM-2021-02-44

Nguyen X, Li J, Zhuang X, Li B, Querol X, Moreno N, Cordoba P (2022) Significant enrichment of Rb and Cs in the Late Triassic coals from the Coc Sau surface mine, Cam Pha Coalfield, Quang Ninh Province, Vietnam. Ore Geol. Rev. 142, 104700. https://doi.org/10.1016/j.oregeorev.2022.104700

Nguyen TL (2025) Mining Patterns and the Pacification of the Coal Mining Frontier. In: Vietnam's Coal Frontier: Mining, Environment, and Empire, pp. 44–67. Cambridge University Press. https://doi.org/10.1017/9781009638005

Singhal BBS, Gupta RP (2010) Applied Hydrogeology of Fractured Rocks. 2nd edition Springer

Thong Nhat Coal Company-TKV (2023) The exploration report on upgrading the Lo Tri coal mine. Cam Pha City, Quang Ninh Province, 24 April 2023, Thong Nhat Coal Company-TKV (in Vietnamese)

Vu NK (1987) Hydrogeological conditions in the main coal basins of Vietnam. In: IMWA Proceedings 1987. International Mine Water Association 2012. pp. 415–419

IMWA 2026
Jeongseon

The Lusatian Mining Area Water Management Centre: A Case Study in Successful, Forward-Looking, Cross-Border Water Management in a Mining Region with Limited Water Resources

Maik Ulrich[1], Oliver Totsche[2]

[1]*LMBV, Knappenstraße 1, 01968 Senftenberg, Germany, maik.ulrich@lmbv.de*

[2] *LMBV, Knappenstraße 1, 01968 Senftenberg, Germany, oliver.totsche@lmbv.de*

Abstract

This case study describes the challenges posed by mining, the rehabilitation of open-cast mines, and the flooding of former pits. It shows how these challenges were overcome through targeted cooperation between the rehabilitation mining company, the state and federal authorities and the active mining company. It also shows how the parties involved are preparing for future challenges resulting from the end of lignite mining and climate change. The article follows a case study approach in which Lusatia is examined as a model region. It is based on the experience of a publicly funded mining rehabilitation company LMBV in water management over the past 25 years and considers the cooperation with ministries, specialist authorities, and companies. The insights gained are intended not only to provide an understanding of the transformation of water management in Lusatia, but also to identify starting points for other former mining regions.

Keywords: Pit lake flooding, water management, river basin management, cross-border water coordination

Introduction and historical context

Due to lignite mining, Lusatia is one of the regions in Germany that has undergone the most significant transformation in terms of water management. The history of lignite mining in Lusatia goes back over 200 years, with its beginnings in the 18th century and large-scale expansion since the second half of the 19th century. Active mining has resulted in rivers being straightened, channels being expanded and relocated, and groundwater being lowered over large areas in order to drain the mines.

One of the greatest challenges in Lusatia was and still is to restore the water balance, which has been significantly disrupted by mining, to a largely self-regulating state. At the peak of the lignite industry in the former socialist eastern Germany, up to 190 million tons of lignite were mined in Lusatia each year. This required the extraction of a total of approximately 1.2 billion cubic meters of water per year. In some places, the groundwater level was lowered by up to 100 meters. By 1990, this had resulted in mining-induced groundwater lowering over an area of around 2,000 square kilometres and a total deficit of approximately 13 billion cubic meters of water. Part of this area is still used today for active lignite mining.

With the closure of individual opencast mines since the 1990s, the restoration of the land in accordance with mining law has begun, coordinated by the publicly funded LMBV, a private company owned by the German federal government. The central objectives are to restore the water balance, flood the opencast mining pits to create post-mining lakes, secure embankments, prevent landslides, and limit iron and sulphate pollution through water management measures.

At that time, the region was undergoing a period of turmoil following political change: numerous mines were being closed down, and flooding the huge mine pits was a key objective in order to create new landscape and water structures. In Lusatia, which

otherwise has relatively little runoff, this project posed a considerable planning and technical challenge and laid the foundation for today's water management. This created the need to establish water management networks to coordinate both the technical processes of flooding and the cross-border interactions in the water balance. Against this backdrop, the first transformation of water management began.

The founding of the Lusatia Flooding Centre in 2000 was a decisive step for the situation at the time, which today proves to be an important starting point for the upcoming structural change. The aim of the LMBV was to flood the opencast mines as effectively as possible and create stable hydrological conditions in the remediation areas, while the federal states remained responsible for maintaining minimum water flows and managing the river basins. In order to combine both levels and advance the flooding process as quickly as possible, the Lusatian Flooding Centre was ultimately established as a technical unit within the LMBV.

Its main task was to coordinate the flooding of former opencast mines across state borders, regulate water levels, and ensure water quality. In Germany water management is generally considered to be a sovereign task of the federal states. In the mining area, however, the LMBV, as a private company, albeit owned by the state, has de facto taken over parts of these sovereign tasks. However, this primarily concerns the technical aspect, i.e., the assessment of the hydrological situation, the calculation of scenarios, and the formulation of control measures. The management proposals of the Flooding Control Centre were then discussed with the authorities of the two federal states. Once an agreement had been reached, the Flooding Control Centre initiated the control measures.

Study area

The area of activity of the Flooding Control Centre, which has since been renamed the Water Management Centre, covers a region in which a large number of former opencast mines, mining lakes, reservoirs, and watercourses interact with each other in a complex network system and across different federal states.

The Water Management Centre is in charge of 18 inlet structures, 12 outlet structures, 13 transfer channels, 65 weir systems, 47 pumping stations, 16 water treatment plants and three horizontal filter well systems. Additionally, the system incorporates numerous other water management facilities overseen by different federal states.

A characteristic feature of the region is the close interconnection between mining lakes, dams, reservoirs, and connecting canals and rivers and tributaries. The area is naturally a rather water-poor lowland area with sandy soils and low natural runoff and comprises the catchment areas of the Spree, Schwarze Elster, and parts of the Lausitzer Neiße rivers.

The main focus of management in the Spree river is on protecting the Spreewald Biosphere Reserve wetland and on the city of Berlin, where the water is used to produce drinking water. The primary concern in the Schwarze Elster river, on the other hand, is ensuring minimum ecological flows and facilitating tourist use of the post-mining lakes.

In addition to the issues of groundwater lowering and large-scale flooding related to mining, there are problems such as low water levels in watercourses, ensuring the supply of water for use, complying with minimum ecological flows, maintaining limit water levels in post-mining lakes and improving water quality, which is negatively affected by acid-mine-drainage.

Flooding of the Pit Lake Chain

The Pit Lake Chain consists of four interconnected, navigable opencast mining lakes and is located in the Schwarze Elster catchment area. Two of these lakes are divided by the border between two federal states, which means that two water authorities and two mining authorities are responsible for issuing permits.

The lakes were designed to help support the flow of the Schwarze Elster river when necessary. They are also very important for tourism in the region. Active flooding began in 2004 via the introduction of water from the Schwarze Elster river. A supply structure with a capacity of up to 10 m^3/s is available for this

purpose. However, as the Schwarze Elster has only very low flow rates, inflows from the Lausitzer Neiße and the Spree can be used via a transfer channel and two pumping stations. The flooding of all four lakes was completed in 2025. Together, they cover a water area of around 40 km² and have a total volume of approximately 580 million m³.

The flooding phase for these lakes, which lasted over 20 years, required complex water management and close coordination between various stakeholders. The Flooding Centre acted as a connecting element between the geotechnical remediation carried out by LMBV and the relevant approval, technical and supervisory authorities. A key challenge was distinguishing between the responsibilities of mining law and water law. As the flooding progressed, the opencast mines gradually transformed into recognisable water management facilities. This also altered the responsibilities and approval procedure requirements and responsible authorities over time. The Lusatia Flooding Centre played a pivotal role in communicating these changes to the LMBV and incorporating them into ongoing planning and remediation processes.

Coordination with the relevant authorities takes place primarily via an established committee structure, the River Basin Management Working Group (Fig. 1). This working group consists of a decision-making body, regularly convening specialist working groups, and topic-specific expert committees.

In contrast to traditional dam construction, the creation and restoration of opencast mining lakes takes place in parallel with flooding. It was therefore unusual for the water authorities to approve flooding, even though the final lake structure had not yet been completely established. Only through close cooperation between LMBV and the water authorities was it possible to repeatedly find compromises to ensure that the restoration work progressed.

The flooding occurred in stages. Due to geotechnical specifications, there were temporary limits on the water level that could not be exceeded. This meant that some of the water had to be pumped out. Before being discharged into the Schwarze Elster river, the drained water was chemically treated, neutralised and its iron content removed. As the Schwarze Elster river often has low discharge rates in summer, the

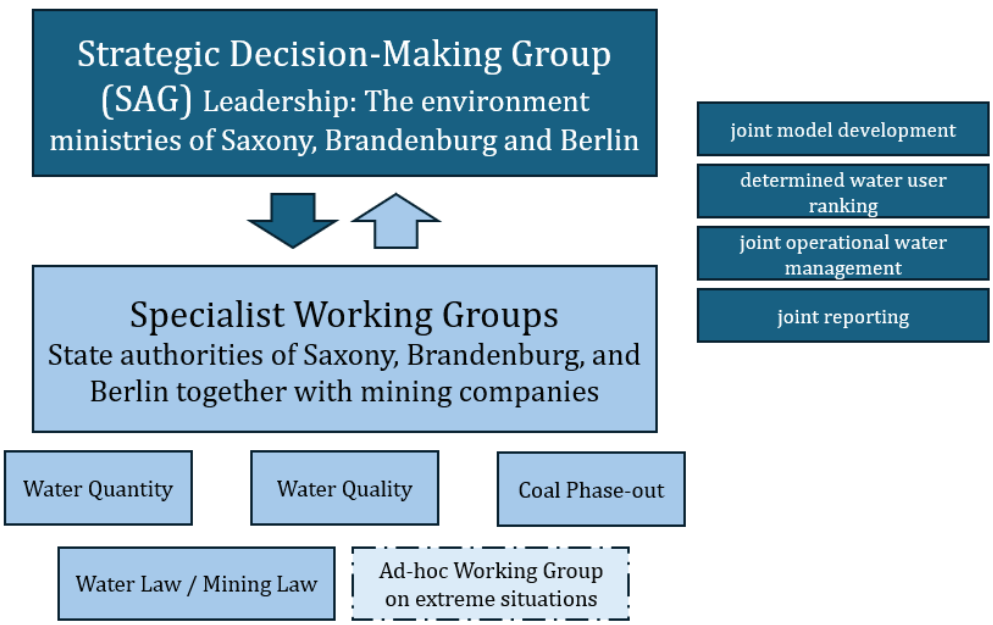

Figure 1 *River Basin Management Working Group Scheme.*

water authorities decided from early on that the Pit Lake Chain would have to provide a permanent water supply to support the river. To avoid jeopardising the remediation process, scenarios were developed using a joint management model that would allow simultaneous flooding and river support.

Similar coordination processes were required again in 2023, when a nearly constant water level in a pit lake was needed for several months for earthworks and compaction measures. The state authorities involved then examined whether temporary storage could be provided in the neighbouring lakes. The issue was raised early on in the Water Quantity working group and prioritised as a short-term measure. Various solution scenarios were calculated using the management model, and ultimately, a variant was approved that ensured the success of the remediation.

Dry period

Between 2018 and 2020, Lusatia experienced a pronounced dry period, which posed considerable challenges for water management. Not only was 2018 the warmest year since weather records began in 1881, but with a precipitation deficit of 36%, it was also one of the driest. Over the course of the entire dry period, this deficit amounted to around -612 mm, which is comparable to the average annual precipitation in the region (DWD 2026). The high temperatures also led to exceptionally high evaporation.

Consequently, several sections of waterway dried up and the water supply to the UNESCO Spreewald Biosphere Reserve wetland was sometimes severely compromised. Fortunately, thanks to the existing institutional structure, the Ad Hoc Working Group on extreme situations could be convened quickly to develop appropriate management strategies and make optimal use of the available water resources.

As part of these measures, the existing management rules were temporarily adjusted. For instance, lower minimum flows were permitted in watercourses to ensure the storage reserves in reservoirs remained available for longer. To conserve water reserves in the reservoirs, guideline values for sulphate concentration in the Spree were also temporarily increased. Additionally, water from the management lamellae of pit lakes undergoing remediation was used to support watercourses. Overall, the LMBV pit lakes provided over 210 million m^3 of water to the rivers during the three dry years (Scholz and Lucke 2019, Scholz and Totsche 2020, Scholz and Totsche 2021). Furthermore, the active mining company reduced the amount of drainage and thus also the discharge of particularly sulphate-rich water into the Spree during particularly critical periods in order to maintain water quality.

To systematically record the hydrological situation, a large-scale, cross-state flow measurement campaign was carried out in 2019. Around 150 measurements were taken in the Spree river and the UNESCO Spreewald Biosphere Reserve during this campaign. Thanks to the close collaboration of the environment ministry representatives in the Ad Hoc Working Group, these measures were implemented swiftly and without bureaucracy. This was followed by a joint cross-state evaluation of the events and the preparation of a comprehensive low water report (Creutzfeld *et al.* 2023). The data and findings from the measurement campaigns formed the basis for the development of a low water concept. Without the close coordination of the parties involved and the targeted use of water from the opencast mining lakes still undergoing remediation, the effects of the dry period on land use and aquatic ecosystems would have been much more severe.

Future challenges

Restoring the over many decades severely depleted water balance is one of the core tasks of the LMBV. By 2025, the original water deficit of 7 billion m^3, consisting of 2.5 billion m^3 in pit lakes and 4.5 billion m^3 in groundwater depressions, had been reduced by 6.4 billion m^3 within the LMBV's area of responsibility.

After 30 years of successful work, the flooding of the Lusatian opencast mining pits has largely been completed and the resulting pit lakes are now being used for water management and tourism purposes.

This reflects the fact that water management, rather than flooding, is now the main focus. The Lusatian Flooding Centre was renamed the Lusatian Water Management Centre in 2025. Despite the successes already achieved, restoring the water balance in Lusatia will be a task for generations to come.

The impending phase-out of coal will directly impact the water balance of the watercourses in Lusatia. Currently, around half of the summer discharge originates from active mining operations. In the Spree river, discharges from active mining are almost constant at 150 million m^3/a (5 m^3/s). Once coal has been phased out by 2038, these discharges will cease over the following years. This will significantly impact the water balance in Lusatia. At the same time, huge new opencast mines will need to be flooded. The expected water deficit in 2038 will be around 1.7 billion m^3 in the opencast mines, and an additional 3.1 billion m^3 will be lost from the groundwater.

Climatic changes are already noticeable. Temperatures are rising and precipitation patterns are changing. Heavy rainfall events that are intense but short-lived are becoming more frequent. Long-lasting, steady precipitation is becoming less common, however. These changes are already impacting groundwater recharge and, consequently, runoff formation throughout the entire area. While the pit lakes can partially compensate for the outflow in summer, the likelihood of the storage capacity being refilled in winter and spring is declining.

The Lusatian mining region has become accustomed to high water availability due to the long-standing oversupply of mine-water. However, increasing periods of drought are showing that there is no longer enough water in Lusatia for all uses. The phase-out of coal by 2038 and the subsequent end of water extraction will further reduce the water supply. At the same time, huge new opencast mining pits will need to be flooded, creating additional competition for water resources. These developments are further compounded by climate change, which is bringing longer dry periods and lower precipitation.

State authorities and mining companies are therefore collaborating intensively within the River Basin Management Working Group to develop new strategies. Models are being updated extensively, and studies on storage optimisation, as well as the maintenance and expansion of the technical networking of watercourses, are being commissioned. Additionally, investigations are being conducted to ascertain whether new storage locations can be identified within the catchment areas, or if transfers from other regions are feasible.

Conclusion

The case study demonstrates that the added value of the Lusatian approach lies not only in technical water management, but in the establishment of a permanently coordinated governance and management system. The establishment of the Flood Control Centre, which brought with it additional responsibilities for the LMBV in terms of watercourse management, was a win-win situation for both the LMBV and the authorities. The authorities were supported in their work by a group of highly qualified specialists with sophisticated models for forecasting and water management. The LMBV, on the other hand, obtained optimal water control to implement its remediation tasks. Over time, both the state authorities and the LMBV began to view their respective areas of responsibility, i.e., the authorities' responsibility for rivers and water distribution and the LMBV's remediation tasks, as a joint task. Neither side waited for the other to make proposals, but worked together to find a joint solution.

The existing close cooperation in both strategic planning and the development and updating of model bases creates the conditions for overcoming the current challenges in the best possible way. Key instruments include coordinated reporting systems, documented decision-making processes, and the joint use of storage management models to evaluate different scenarios. It is essential to involve all relevant institutions at an early stage in order to streamline approval procedures and identify potential conflicts between mining law and water management requirements at an early stage. The advantage of the committee work lies in

its structural anchoring, high transparency, and interdisciplinary continuity. This creates trust, supports a common understanding of complex interrelationships, and enables coordinated and legally secure decisions to be made even under exceptional conditions such as droughts or remediation constraints.

The establishment of a water management unit at a mining (remediation) company and the close cooperation with the authorities, structured through committees, can serve as a model for other mining areas with demanding water management requirements. Transferable principles include: (i) the early institutional integration of mining and water authorities, (ii) the use of shared data and modeling frameworks as a basis for decision-making, (iii) the establishment of flexible regulatory frameworks for extreme situations, and (iv) the active use of opencast mining lakes as strategic water reservoirs within larger river basin systems.

Acknowledgements

We would like to thank all our colleagues at the Water Management Centre, the authorities, and the rest of the LMBV for their contribution to ensuring that, water management in Lusatia can serve as a prime example of good cooperation and a model region for joint water management.

References

DWD (2026) Climate Data Centre, Deutscher Wetterdienst 2026, Offenbach am Main, https://opendata.dwd.de/climate_environment/CDC/

Scholz E, Lucke B (2019) Wasserwirtschaftlicher Jahresbericht der LMBV für den Zeitraum 01. Januar–31. Dezember 2018. Lausitzer und Mitteldeutsche Bergbau Verwaltungsgesellschaft, Senftenberg 03/2019, p 10

Scholz E, Totsche O (2020) Wasserwirtschaftlicher Jahresbericht der LMBV für den Zeitraum 01. Januar–31. Dezember 2019. Lausitzer und Mitteldeutsche Bergbau Verwaltungsgesellschaft, Senftenberg 03/2020, p 17

Scholz E, Totsche O (2021) Wasserwirtschaftlicher Jahresbericht der LMBV für den Zeitraum 01. Januar–31. Dezember 2020. Lausitzer und Mitteldeutsche Bergbau Verwaltungsgesellschaft, p 19

Creutzfeld B *et al.* (2023) Auswertung Niedrigwasser 2018, 2019 und 2020 – Spree, Schwarze Elster und Lausitzer Neiße, Sächsisches Landesamt für Umwelt, Landwirtschaft und Geologie (LfULG), Dresden 24.02.2023

Microbial Systems for Sustainable Resource Recovery

Denys Villa Gomez[1,2,3], Rosie Gillane[1,2,3], Luke Webster[1,2,3], Fernanda Soto[1,2,3] and Esteban Marcellin[1,3]

[1]*ARC Centre of Excellence in Synthetic Biology (CoESB), The University of Queensland, Brisbane, Queensland, Australia*

[2]*School of Civil Engineering, The University of Queensland, 4072 QLD, Australia*

[3]*Australian Institute for Bioengineering and Nanotechnology, The University of Queensland, 4072, QLD, Australia*

Abstract

The mining industry supplies critical metals essential for the net-zero transition but generates challenging alkaline wastes like red-mud tailings. SynBiomining develops modular biotechnologies that integrate microbiome discovery, extremophile bioleaching, and protein-based biorecovery to selectively extract metals while neutralising residues. High-throughput omics and validation workflows establish reusable pipelines that accelerate bioprocess design across diverse mine wastes. This framework enhances circularity in mining, transforming liabilities into critical-metal resources and minimising environmental impacts.

Keywords: Critical metal recovery, mine waste, extremophile isolation, fungal bioleaching, metal-binding proteins

Introduction

The mining industry occupies a paradoxical position in the global drive toward net-zero emissions: it is simultaneously a major source of greenhouse gases and a critical supplier of the metals required for electrification, renewable energy and advanced manufacturing (Lord, 2019). Meeting rapidly growing demand for critical and strategic elements such as rare earth elements (REEs), nickel and cobalt while reducing environmental impacts is a formidable challenge. Conventional hydrometallurgical and pyrometallurgical routes for metal production are energy-intensive, chemically aggressive and often poorly suited to low-grade ores, complex residues and legacy mine wastes. At the same time, mine waters and solid wastes frequently contain significant inventories of dissolved or mineral-bound metals that remain under-utilised, representing both a contamination risk and a lost resource.

Biotechnological approaches offer an attractive alternative by harnessing the metabolic capabilities of microorganisms to mobilise, transform and recover metals under comparatively mild conditions (Nancharaiah *et al.*, 2016). Classical biomining has already demonstrated the viability of microbially assisted leaching at industrial scale, particularly for sulfide ores and base metals (Kaksonen *et al.*, 2020). However, these applications have remained largely focused on a narrow set of autotrophic acidophiles and have not been broadly extended to the recovery of many critical metals or to more diverse, heterotrophic and extremotolerant microbial communities. This constrains the applicability of biomining to other waste streams with critical-metal recovery potential such as red-mud tailings, alkaline tailings and complex mine waters.

In response to these challenges, we are advancing biomining through a framework that combines microbiome characterisation, omics-driven discovery and high-throughput screening with targeted bioprocess development. Within the UQ Biosustainability Hub, our work focuses on two key application areas, bioleaching and biorecovery, and uses genome- and proteome-resolved microbiome analyses to identify candidate organisms, pathways and metal-binding functions from mining environments.

Extremotolerant fungi are developed for bioleaching of critical metals from alkaline and saline wastes, while proteomic mining of metal-resistant strains yields metal-binding proteins and biomaterials for selective recovery from leachates. Synthetic biology provides a forward-looking layer to enhance these systems by improving strain performance and tailoring binding specificity (Capeness and Horsfall, 2020), while the present study demonstrates how omics and high-throughput tools can accelerate the development and optimisation of biomining processes across these two domains.

The aim of this paper is to demonstrate how microbiome-informed, omics-driven and high-throughput techniques can be used to build and refine biomining pipelines for critical-metal recovery (Figure 1). By showing how these tools guide the development of extremotolerant fungal bioleaching systems and protein-based biorecovery platforms, we highlight a methodology for accelerating bioprocess design rather than a single, fixed process configuration. In doing so, this work outlines how SynBiomining (Synthetic biology and mining) approaches can expand biomining beyond classical organisms and commodities, contribute to circular-economy strategies that transform mine wastes into sources of critical metals while reducing their environmental footprint.

Materials and Methods

Microbiome characterisation. Metagenomic sequencing was used to characterise microbial communities associated with red-mud tailings and related mine wastes and to identify candidate taxa, functions and strains. Approximately 250–500 mg

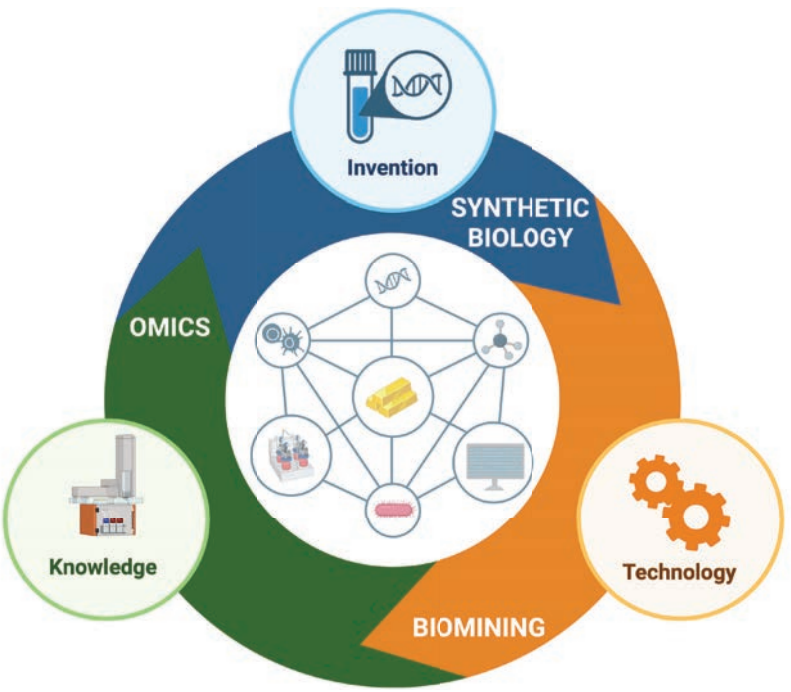

Figure 1 *Conceptual overview of the SynBiomining framework, highlighting how omics driven knowledge generation, synthetic biology enabled invention, and biomining technology are coupled in a cyclical design build test learn loop to recover critical metals from mine wastes. The central panel depicts engineered microbial systems and process units connected in a network around a critical metal product, while the surrounding colored segments emphasize the integration of (i) omics platforms that generate mechanistic insight and design rules, (ii) synthetic biology tools that create and optimise new biomining functions, and (iii) biomining technologies that implement and validate these functions at process scale.*

of material per sample was submitted for DNA extraction and shotgun sequencing, followed by high-stringency quality control, assembly, binning and taxonomic assignment to obtain medium- to high-quality metagenome-assembled genomes and a non-redundant protein catalogue annotated with DRAM. Community profiles derived from MAGs and single-copy marker genes resolved bacterial and archaeal lineages associated with metal resistance, organic-acid production and extracellular polymer formation, providing a reusable template for microbiome-informed strain and target selection in other mining residues. In parallel, microorganisms were isolated from red-mud tailings on a suite of alkaline and general media, purified, and identified by 16S rRNA gene amplicon sequencing; a subset of unique isolates was further subjected to PacBio whole-genome sequencing and functional annotation.

Fungal bioleaching of critical metals. *Aspergillus niger* (DSM 2466) and *Penicillium oxalicum* (DSM 898) were used to develop an extremotolerant bioleaching pipeline for red-mud tailings that can be adapted to other alkaline wastes. Initial screening assessed pH (7–12), salinity (5–20% w/v NaCl) and red-mud tolerance (2–40% w/v) on modified Vogel's minimal medium (1.5% sucrose, 1.5% agar). Both strains showed high neutralisation capacity, decreasing pH by 0.6–2.7 units (*A. niger*) and 0.2–0.9 units (*P. oxalicum*), and prior work showed that their organic acids outperform mineral acids for V and REE recovery from red mud (Soto-Montandon, 2025). To extend tolerance, fungal strains were subjected to adaptive laboratory evolution by chemical and physical mutagenesis (EMS at 75, 150, 300 µg/mL; UV exposure for 10, 15, 20 min) and then adaptively passaged to increasing red-mud loadings.

Discovery and testing of metal-binding proteins. To establish a discovery pipeline for metal-binding proteins that can be used to extract critical metals from mine influenced waters and leachates, we applied a common metal-induced proteomics, REE-IMAC enrichment and bioinformatics workflow across biomining organisms (*Pseudomonas putida, Geobacter metallireducens, Shewanella oneidensis, A. niger, P. oxalicum*). Metal-tolerance ranges were first determined in microplate cultures in defined minimal media, and sub-inhibitory exposure concentrations, for example 100 µM La and Dy, 2 µM Ga, 2000 µM Ge for *P. putida* were selected for proteomic analysis (Webster *et al.*, 2025). Triplicate shake-flask cultures were grown to mid-exponential phase, harvested, and cell lysates passed through a custom rare-earth–immobilised metal affinity chromatography (REE-IMAC) column to enrich putative metal-binding proteins before S-Trap™ digestion and Orbitrap Exploris 480 LC–MS analysis against species-specific UniProt reference proteomes. Differentially abundant and/or REE-enriched proteins were identified at false discovery rate <5% and $|\log_2$ fold-change$|$ >0.58 (~1.5-fold). A composite metal-binding protein database was built from UniProt, the Metal-binding Protein Atlas and MetalPDB, and each proteome was aligned against it, integrating metal-binding motifs, subcellular localisation (PSORTb, CELLO, UniProt) and domain information (InterProScan). Cross-referencing these annotations with the REE-IMAC-enriched proteomics in R yielded a short list of candidate metal-binding scaffolds that can be carried forward to functional testing for a range of leachates and residues, not only the systems studied here.

Results and Discussion

Native extremophile pipelines from red mud microbiomes

Across red mud tailings, over 1,000 colonies were screened, with 60 isolates subjected to 16S whole operon identification and 19 to whole genome sequencing, yielding 18 assembled genomes with functional and secondary metabolite annotations. Key isolates included *Priestia megaterium*, *Halomonas spp.*, *Aliidiomarina haloalkalitolerans*, *Nesterenkonia salmonea* and *Bacillus spp.*, several of which may represent novel taxa. Growth and tolerance tests showed that strains affiliated with *Halomonas, Bacillus* and *Nesterenkonia* maintained colony formation even at 15% red mud loading and under elevated Na^+, Fe^{2+} and lanthanide concentrations. *Halomonas sp.* (RG49) in particular displayed consistent growth across ionic stresses, whereas *Bacillus subtilis* responses were more variable, especially

in the presence of lanthanides. Although mechanisms were not resolved here, these patterns are consistent with haloalkaliphilic strategies and demonstrate that red mud tailings harbour native, extremotolerant communities. From a pipeline perspective, this microbiome work establishes a strain and genome resource that can be reused as chassis or community members for future bioleaching and biorecovery processes in mine waste streams.

Scalable fungal bioleaching for alkaline residues

A. niger and *P. oxalicum* bioleaching agents for red mud tailings were adapted through mutagenesis and stepwise exposure to increasing red mud loadings to further improved growth, tolerance to red mud tailings and capacity to produce organic acids that both decreased pH and complex REE. Both fungal strains were capable to decrease the pH and to improve tolerance to red mud, but more importantly, they allowed the creation of a protocol using high throughput tolerance screens and iteratively improving strains for operation on chemically challenging residues, with output solutions tailored for downstream selective recovery.

High-throughput metal-binding protein discovery

A biorecovery pipeline was established based on metal induced proteomics, REE IMAC enrichment and informatics across P. putida, G. metallireducens, S. oneidensis, A. niger and P. oxalicum. Across La, Dy, Ga and Ge exposures, 434 proteins showed significant abundance changes, with La and Dy sharing 125 differentially expressed proteins and strong up regulation of periplasmic cation ABC transporters and TonB dependent receptors, traits consistent with enhanced metal trafficking at the cell surface. Integration of these data with a curated metal binding database indicated that ~300 responsive proteins carried predicted metal binding functions, many located in membranes or periplasm and therefore well positioned for biosorption or transport. Gene set enrichment analysis showed, for example, that 78% of predicted Ni binding proteins were enriched under Dy exposure, pointing to overlapping machinery for lanthanide and transition metal handling that could be co-opted for critical metal recovery. Cloning of the most promising candidates will allow to test these proteins for biorecovery of REE, Ni, Co and other critical metals. These outcomes illustrate how the pipeline moves from broad proteomic reprogramming to a short, rationally selected list of protein scaffolds ready for engineering and deployment.

Conclusions

This study demonstrates modular, transferable pipelines for recovering critical metals from mine wastes. These results show how microbiome informed strain discovery, extremotolerant fungal bioleaching, and protein based biorecovery are being developed as modular, reusable pipelines. Each module is demonstrated on red mud tailings and selected mine water chemistries but is explicitly structured so it can be transferred to other residues, metals and sites as the SynBiomining program expands.

References

Capeness, M.J., Horsfall, L.E., 2020. Synthetic biology approaches towards the recycling of metals from the environment. Biochemical Society Transactions 48(4), 1367-1378.

Kaksonen, A.H., Deng, X., Bohu, T., Zea, L., Khaleque, H.N., Gumulya, Y., Boxall, N.J., Morris, C., Cheng, K.Y., 2020. Prospective directions for biohydrometallurgy. Hydrometallurgy 195, 105376.

Lord, M., 2019. From mining to making - Australia's future in zero-emissions metal, Energy Transition Hub. The University of Melbourne.

Nancharaiah, Y.V., Mohan, S.V., Lens, P.N., 2016. Biological and bioelectrochemical recovery of critical and scarce metals. Trends in Biotechnology 34(2), 137-155.

Soto-Montandon, F., Webster, Luke, Gillane, Rosemary, Marcellin, Esteban, Harrison, Susan T. L., and Villa-Gomez, Denys, 2025. Valorisation of bauxite residue for critical metal recovery using fungal bioleaching: a pathway toward circular economy., Global Bioeconomy Alliance Annual Conference 2025. Copenhagen, Denmark, p. 45.

Webster, L.J., Palfreyman, R., Gillane, R., Soto, F., Marcellin, E., Villa-Gomez, D., 2025. Protein Identification and Binding Capacity of Pseudomonas putida to Critical Metals, in: Metallurgy, Materials Society of, C.I.M. (Eds.), Proceedings of the 63rd Conference of Metallurgists, COM 2024. Springer Nature Switzerland, Cham, pp. 1185-1188.

A Linear Flow Channel Reactor for High Sulphate Water Treatment: A Simple and Practicable AMD Treatment System for Rural Communities in South Africa

JB Witbooi[1], IG Mkhize[2]*, FB Waanders[1], AC Eloka-Eboka[1], SKO Ntwampe[2]

[1]*School of Chemical and Mineral Engineering, Faculty of Engineering and the Built Environment, North-West University, Potchefstroom, 2531, South Africa, witbooijan40@gmail.com, Frans.Waanders@nwu.ac.za, fadafounder@gmail.com*

[2]*Department of Chemical Engineering, Faculty of Engineering and the Built Environment, Durban University of Technology, Durban, 4001, South Africa, InnocentiaM2@dut.ac.za, SetenoN@dut.ac.za*

Abstract

AMD remains a major challenge posed by both abandoned and active mines. A 12 L LFCR was operated for 110 d using a floating sulphur biofilm (FSB) supported by ethanol. Across Periods I (40 d), II (30 d), and III (40 d), sulphate and COD removal reached 99%, 92%, and 94%, and 95%, 77%, and 78%, respectively. Sulphide production was 195, 144, and 233 mg L-1. Fe, Cu, Ni, and Zn removal exceeded 95% within days, with Mn reduced over longer operation, while pH stabilised at 6.8-7.5. A feed-forward network predicted sulphate removal (R^2 = 0.75), with overall strong reactor stability.

Keywords: Acid mine drainage, biological sulphate reduction, sulphate-reducing bacteria, linear flow channel reactor, hydraulic retention time, feed forward network

Introduction

One of the threats to freshwater resources is acid mine drainage (AMD) (Baloyi *et al.* 2024). In South Africa (SA), AMD is generated by the mineral production industry, primarily through mining. AMD is produced by the oxidation of sulphide-rich gangue and coal deposits. Specific environmental problems, such as high sulphate concentrations, elevated dissolved metal concentrations, and low pH, are associated with AMD. Biological sulphate reduction (BSR) (Mafane *et al.* 2025) is a process that employs sulphate-reducing bacteria (SRB) to treat AMD by removing sulphate and metal contaminants and producing sulphide.

A linear flow channel reactor (LCFR) (Marais *et al.* 2022b) capable of integrating both the biological sulphate reduction (BSR) process and partial sulphide oxidation, can treat AMD. The reactor demonstrated satisfactory performance in removing sulphates from AMD and can handle the more toxic sulphide by developing a floating sulphur biofilm (FSB). Furthermore, the LFCR presents a practical, low-cost, and low-energy solution for rural communities affected by AMD. Its simple design and minimal operational requirements make it ideal for areas with limited technical capacity, while still achieving high removal efficiency for sulphate and metal contaminants. Importantly, the FSB enables safe sulphide management and supports potential recovery of elemental sulphur (S^0) (Marais et al, 2022a), offering circular-economy opportunities for agriculture-based livelihoods. By relying on naturally occurring microbial processes and inexpensive organic carbon sources, the LFCR provides a sustainable alternative to chemically intensive and energy-dependent AMD remediation operations. Implementing such systems in rural communities can protect freshwater resources, improve public health, and stimulate community-level economic value from AMD streams.

Methods

An LFCR with total volume 12 L, operational volume 9 L, dimensions 800 mm × 100 mm × 150 mm, 11 mm thick Perspex, and 15 sampling ports was used – see Fig. 1. AMD (Quality characteristics are listed in Table 1) was supplied in 25 L containers by the Council

for Mineral Technology (Randburg, Gauteng province, South Africa), hereafter referred to as Mintek. Ethanol was used as a sole carbon source. The reactor was operated for 110 d, divided into Period I (40 d), Period II (30 d), and Period III (40 d).

LFCR Sampling, Monitoring, Process Control, and Operational Adjustments

The operation of the LFCR followed a structured strategy designed to sustain BSR, maintain a stable FSB, and ensure robust performance under varying feed conditions over time. The reactor influent comprised a controlled mixture of AMD and an SRB-rich inoculum supplied by Mintek (developed as reported elsewhere by Preez and Marumo, 2024), together with a fixed ethanol dose as the electron donor (Table 1). To stabilize biological activity and interrogate system resilience, the AMD-to-inoculum ratio was deliberately varied across three operating periods: during Period I, a high inoculum fraction promoted rapid SRB acclimation and strong early sulphate reduction; in Period II, an increased AMD load and reduced inoculum concentration spiked Mn imposed more acidic and metal-rich conditions to stress the system; and in Period III, the inoculum fraction was increased to facilitate performance recovery following the stressed regime, Period II. Ethanol was supplied at a constant dosage throughout all periods to ensure a consistent carbon source irrespective of feed composition. Sampling ports (n=15) were distributed along the reactor length, with nine central ports routinely used to avoid zones affected by surface biofilm formation or bottom sediment accumulation. Sampling was conducted daily by withdrawing 30 mL of reactor fluid into 50 mL tubes for analysis of pH, sulphate, sulphide, COD, and dissolved metals, with rubber septa replaced regularly to prevent leakage and preserve anaerobic conditions. Over the 110-day operational campaign, intentional step changes in feed composition and hydraulic retention time were applied to evaluate system resilience, inducing stress during Period II and enabling recovery during Period III. In parallel, routine visual inspection of the biofilm, assessing colour, thickness, and structural integrity, provided qualitative insight into sulphide oxidation behaviour and potential oxygen ingress.

Reactor Loading and Hydraulic Retention Time

The LFCR was filled using a low-flow peristaltic pump operating at a fixed rate, thereby providing the desired hydraulic residence time (HRT). The operational plan deliberately shifted the HRT across periods: 3 d in Periods I and III, 2 d in Period II. These changes were used to examine how reduced contact time affects SRB performance and

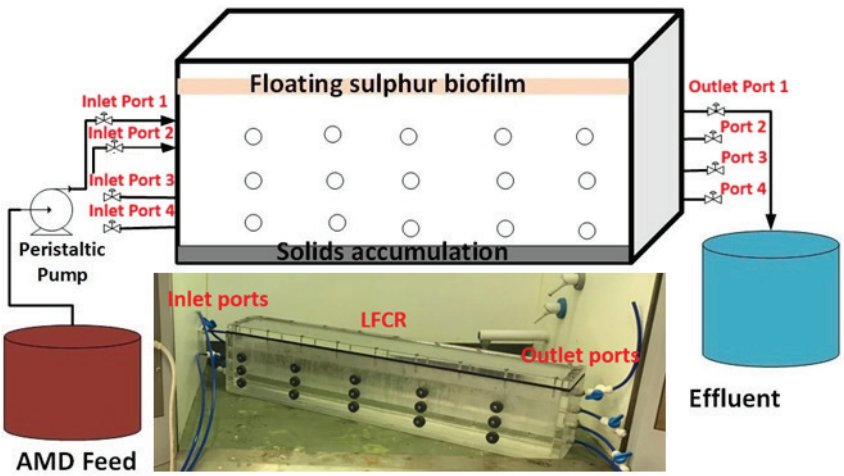

Figure 1 *The complete LFCR design and operation setup.*

sulphate-reduction efficiency. The reactor remained closed to mixing, allowing the LFCR's characteristic laminar-like, stratified flow regime to develop. This flow pattern was essential for maintaining anaerobic conditions within the biofilm while sustaining a microoxic zone at the liquid-biofilm interface.

Establishment and Management of the Floating Sulphur Biofilm

Once the reactor was filled, it was left unoperated for 2 to 3 d to allow the FSB to form at the air–AMD interface. As the operation continued, the biofilm thickened progressively as SRB biofilm became established (see Figure 2). The FSB served dual roles: (i) restricting oxygen transfer into the bulk liquid and enabling potential partial oxidation of sulphide to S0, which subsequently accumulated in the biofilm. Later in the run (Period III), signs of biofilm ageing and structural weakening, i.e., sloughing, appeared, indicating the need for periodic harvesting or maintenance in long-term operation. Maintaining the integrity of this biofilm was central to the reactor operation strategy.

Feed Forward Network Methodology

The feed-forward network (FFN) was used to predict effluent sulphide concentration from routinely measured process variables, with effluent sulphide as the dependent variable and influent COD, bulk pH, and sulphate concentration as inputs. The full dataset collected over the 110-day campaign was cleaned to remove outliers, normalised, and partitioned into training (70%) and testing (30%) subsets to enable validation and avoid overly optimistic performance estimates. The FFN had a single hidden layer (3 neurons) and a linear output. As in Fig. 3, the hidden units used tan-sig (hyperbolic tangent) activation, while the output layer used purelin (linear).

Training employed the Levenberg–Marquardt optimisation, chosen for its fast convergence in small - to medium-sized regression problems. Implementation was done in MATLAB (R2020a). To benchmark non-linear learning against a simpler alternative, a multiple linear regression (MLR) model using the same inputs was also developed. Model validity was assessed using R^2, RMSE, and MAE on both training and test partitions.

Routine Analyses

The pH of the influent, reactor samples, and effluent was measured using a calibrated glass electrode on a Metrohm 744 pH meter. The 10 mL samples were filtered and sent for analysis using Thermo Fisher Scientific's 6200 inductively coupled plasma optical emission spectrometry (ICP-OES) to determine the presence of, amongst others, Mn, Fe, Ni, Cu, and Zn. COD was measured using a HI83399 Hanna multiparameter photometer.

Table 1 *Operating conditions for the three periods during which the LFCR was in operation.*

Parameter	Period I	Period II	Period III
AMD volume (L)	6	7	5
Inoculum volume	2	1	3
Ethanol volume (mL)	30	30	30
Reactor liquid volume (L)	9	9	9
Oxygen requirement	Anaerobic	Anaerobic	Anaerobic
Influent pH	5.84	5.13	5.72
Influent sulphide concentration (mg L^{-1})	55	41	3.4
Influent sulphate concentration (mg L^{-1})	4179	5050	2761
Temperature (°C)	25	25	25
Hydraulic residence time (HRT) (d)	3	2	3
Sulphate:COD ratio	0.7	0.9	0.6

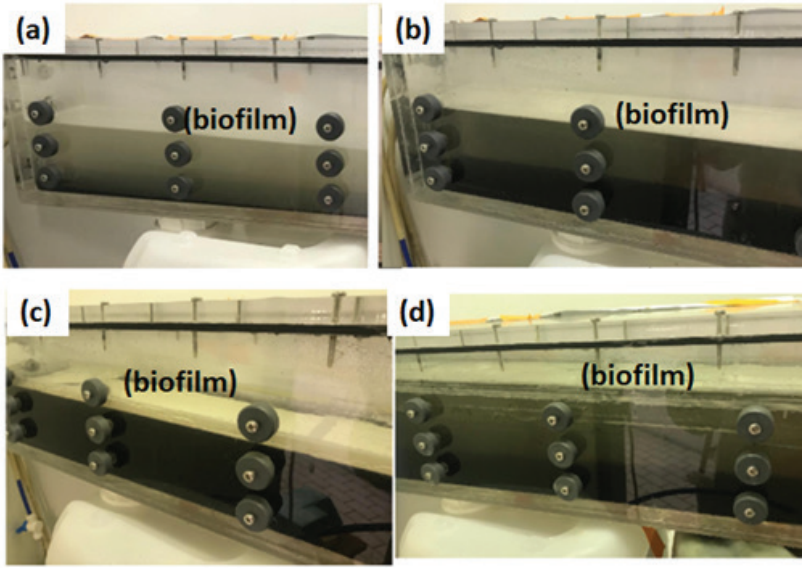

Figure 2 Formation and maturing of the biofilm throughout the reactor operation, at (a), 3, (b) 40, (c) 70 (c) and (d) 90 d.

The sulphides present in the samples were measured using the Methylene Blue method. The sulphate content in the samples was measured using a Shimadzu UVmini-1240 UV spectrophotometer.

Results

LFCR Performance Analysis

The LFCR's performance indicators, sulphate removal, COD reduction, dissolved metal contaminants, and sulphide production, showed robust but period-dependent performance. Sulphate removal reached 99% in Period I, decreased to 92% in Period II, and recovered to 94% in Period III, while COD reduction declined from 95% to 77–78% under stressed conditions. Peak sulphide concentrations (195, 144, and 232 mg L^{-1}, respectively) reflected biological activity coupled with oxidation and precipitation (Baloyi *et al.* 2023; Horn *et al.* 2022). These trends are consistent with expectations that reduced HRT and elevated sulphate:COD ratios suppress sulphidogenesis, whereas sufficient HRT and carbon availability restore performance. Reactor pH rapidly stabilised near neutral during Period I (≈7.0–7.5) due to alkalinity generation during BSR, declined and became more variable in Period II (≈6.0-6.5) under increased acid loading, and recovered to 6.8–7.0 in Period III, although late-stage biofilm ageing was evident. Metal contaminants removal exhibited a two-timescale response: (i) rapid attenuation of Fe, Cu, Ni, and Zn to near-nondetectable levels within 10-15 days, a response seen elsewhere (Baloyi *et al.* 2024), (ii) followed by slower Mn removal governed by its stronger pH dependence (Smičiklas *et al.* 2023). A transient Mn increase following the addition of fresh AMD (30-37 days) was subsequently stabilised at ≈2.8 mg L^{-1} as the SRB community acclimated, consistent with

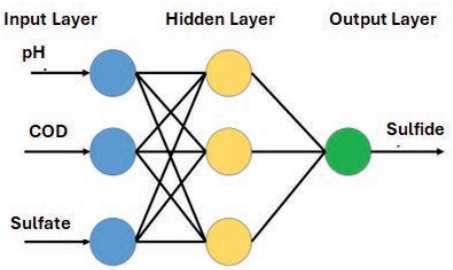

Figure 3 The FFN model structure used for modelling.

Table 2 Period-wise pH stabilisation and trace metal removal.

Period (d)	pH stabilisation	Performance evaluation
I (1–40)	Stabilised around pH 7.0-7.5 as SRB adapted.	Ni, Cu, Zn: ≈0.9 mg L^{-1} initially to nondetectable by 15 d. Fe: ≈37 mg L^{-1} to ≈1 mg L^{-1} by 10 d. Mn: fell from ≈12 mg L^{-1}; extended tracking reached ≈0.1 mg L^{-1} by 30 d, then later fluctuated (Period II).
II (41–70)	Fluctuated around pH 6.0-6.5 with higher AMD load and lower inoculum.	Mn: after reaching ≈ 0.1 mg L^{-1} by 30 d, spiked to ≈12 mg L^{-1} with new AMD addition (30–37 d), then declined to ≈2.8 mg L^{-1} as SRB re-adapted.
III (71–110)	Stabilised around pH 6.8-7.0 with higher inoculum; some biofilm ageing noted late	Overall, sulphate and COD removal performance remained high and consistent with Period I and II trends.

the known requirement for higher pH and longer HRT for effective Mn removal (Zhao *et al.* 2024). A summarised performance evaluation is listed in Table 2.

Overall, alkalinity generation moderates influent acidity, thereby promoting metal sulphide precipitation and the rapid removal of Fe, Cu, Ni, and Zn. The transient Mn increase following the addition of fresh AMD reflects an acid-metal pollutant shock, followed by stabilisation as pH and sulphide speciation recover and the FSB's buffering role takes effect. From a process-control perspective, the period-wise data reinforce established LFCR behaviour, (i) reducing HRT from 3 to 2 days curtailed contact time and carbon utilisation, lowering sulphate and COD removal, whereas restoring HRT improved performance. Increasing the sulphate-to-carbon ratio constrained SRB activity and sulphide production, while lowering it relieved carbon limitation. Increasing the inoculum fraction in Period III restored near-neutral pH and sulphate removal, offsetting the mid-campaign decline.

Several features distinguish this study and strengthen the case for decentralized rural AMD treatment: (i) integration of BSR and partial sulphide oxidation in a single unit enables sulphide control without downstream reactors, reducing energy and chemical inputs while possibly generating recoverable elemental sulphur; (ii) semi-passive open-channel operation minimizes mechanical requirements, easing operation where power and skilled labour are limited; (iii) effective metal pollutant removal, combined with near-neutral pH, demonstrates that compact LFCRs can achieve regulatory-relevant discharge water requirements under realistic feed conditions; and (iv) ethanol, with potential substitution by low-cost local organics, provides flexibility in carbon sourcing. The constraint associated with biofilm ageing late in Period III indicates the need for maintenance, such as periodic FSB harvesting.

Long Term Performance: Operational Sustainability

While the LFCR demonstrated sustained sulphate and metal removal over 110 days, the late Period III performance decline highlights long-term sustainability challenges associated with biofilm ageing and excess sulphur accumulation, which impair mass transfer and sulphide oxidation. Stable long-term operation can be achieved through conservative loading conditions, routine monitoring, and simple biofilm management such as periodic manual harvesting, consistent with the system's semi-passive, low-energy design. Operational stressors, including reduced hydraulic residence time and high sulphate-to-COD ratios, were shown to accelerate performance loss via carbon limitation and microbial stress. Crucially, performance recovery after reinoculation and restoration of HRT demonstrated LFCR resilience, supporting their suitability for decentralised AMD treatment and confirming that biofilm ageing is a manageable maintenance issue rather than a fundamental limitation

Feed-Forward Network Performance.

BSR-FNN integrates microbially mediated redox reactions, alkalinity generation, sulphide production and oxidation, and metal precipitation, all of which respond non-linearly to pH, electron-donor availability, and chemical speciation (Yao *et al.* 2024). Because FFNs learn non-linear input-output relationships, the FFN captured interactions that linear regression could not, yielding higher test-set R^2 values and lower error metrics (Karadurmuş *et al.* 2024). The choice of COD, pH, and sulphide as predictors was physically justified: COD represents electron-donor supply to the SRB, pH governs microbial activity and precipitation equilibria, and sulphide is both a BSR/LFCR product and a reactant in partial oxidation and metal sulphide formation. The compact FFN architecture (one hidden layer with three neurons) achieved a practical bias–variance trade-off, remaining sufficiently expressive to model the non-linear behaviour of the LFCR while limiting overfitting for the available dataset. Model performance was FFN: R^2 (train/test) = 0.93/0.75, RMSE = 389/483 mg L^{-1}, MAE = 228/305 mg L^{-1}; and MLR: R^2 = 0.83/0.42, RMSE = 589/735 mg L^{-1}, MAE = 425/541 mg L^{-1}, confirming substantially better generalisation by the FFN, consistent with the inherent non-linearity of sulphidogenic systems.

The residual train-test gap indicated potential for improvement through the inclusion of additional process variables (e.g., HRT, sulphate: COD ratio, inoculum fraction, temperature), expansion of the dataset across additional operating regimes, or the use of regularisation strategies. The superior FFN performance aligns with prior wastewater and bioprocess modelling studies, where neural networks outperform linear models for variables governed by multi-factor kinetics. In LFCRs, where sulphate reduction beneath the FSB is coupled with potential partial sulphide oxidation at the interface, real-time sulphate soft sensing could help identify carbon limitation, detect acid or metal shocks, and schedule FSB maintenance to prevent LFCRs' underperformance. While the present dataset spans a single 110-day campaign with three operating periods, broader generalizability would benefit from additional campaigns covering wider ranges of HRT, sulphate/COD ratio, temperature, and inoculum conditions.

Conclusions

The campaign showcases a compact, low-energy LFCR that can stably neutralise pH, achieve high sulphide and COD removal, and rapidly clear metals (with Mn requiring additional residence time and pH control), all while converting sulphide to elemental sulphur within the reactor. The data are consistent with recent LFCR literature on HRT sensitivity, FSB-mediated sulphur recovery, and microbial adaptation across reactor zones, consolidating the case for semi-passive, circular-economy AMD treatment in resource-constrained settings. Lastly, FNN outperformed linear regression, achieving better generalisation to unseen data (test $R^2 \approx 0.75$ with lower RMSE/MAE) and thus is the preferred model for predicting effluent sulphate concentration in the LFCR.

Acknowledgements

I am grateful to my supervisors, laboratory staff, technical colleagues, and my family for their continuous guidance, assistance, and encouragement throughout this research journey. I also thank North-West University and Sasol for the financial support that made the successful completion of this study possible.

Declaration

The research reported herein was the subject of a master's thesis at the North-West University, South Africa, in 2025.

References

Baloyi J, Ramdhani N, Mbhele R, Simate GS (2024) Acid mine drainage from gold mining in South Africa: Remediation, reuse, and resource recovery. Mine Water and the Environment 43:418–430.

Baloyi J, Ramdhani N, Mbhele R, Ramutshatsha-Makhwedzha D (2023) Recent progress on acid mine drainage technological trends in South Africa: Prevention, treatment, and resource recovery. Water 15(19):3453.

Marais TS, Huddy RJ, Harrison STL (2022a) Elemental sulphur recovery from a sulphate-rich aqueous stream in a single hybrid linear flow channel reactor

is mediated through microbial community dynamics and adaptation to reactor zones. FEMS Microbiology Ecology 98:fiac059.

Marais TS, Huddy RJ, Van Hille RP, Harrison STL (2022b) Effect of temperature change on the performance of the hybrid linear flow channel reactor and its implications on sulphate-reducing and sulphide-oxidising microbial community dynamics. Frontiers in Bioengineering and Biotechnology 10:908463.

Horn EJ, van Hille RP, Oyekola OO, Welz PJ (2022) Functional microbial communities in hybrid linear flow channel reactors for desulfurization of tannery effluent. Microorganisms 10(11):2305.

Mafane D, Ngulube T, Mphahlele-Makgwane MM (2025) Anaerobic bioremediation of acid mine drainage using sulphate-reducing bacteria: Current status, challenges, and future directions. Sustainability 17(8):3567.

Smičiklas I, Janković B, Jović M, Maletaškić J, Manić N, Dragović S (2023) Performance assessment of wood ash and bone char for manganese treatment in acid mine drainage. Metals 13(10):1665.

Yao Y, Li Y, Shi Y, Shi K, Bai Y, Gao Y, Jiang Q, Xue J, Cheng D (2024) Prediction of artificial neural network for sulfate removal from wastewater and analysis of key factors in an anaerobic biological system. Journal of Environmental Chemical Engineering 12:112085.

Karadurmuş E, Göz E, Keleş C, Yüceer M (2024) Utilizing artificial neural networks (ANN) for predictive modeling of sulfate removal from water. Sigma Journal of Engineering and Natural Sciences 42(6):1866–1875.

Preez, K. D., Marumo, M. (2024). Feasibility of the scale-up of a semi-passive biological sulfate reduction process treating high sulfate mine-influenced water. In West Virginia Mine Drainage Task Force Symposium, International Mine Water Association Congress: Morgantown, VA, USA.

Zhao P, Zhang R, Hu M (2024) Alkaline chemical neutralization to treat acid mine drainage with high concentrations of iron and manganese. Water 16(6):821.

IMWA 2026
Jeongseon

Hydrodynamic Investigations in the Abandoned Havelock Asbestos Mine, Eswatini, by Means of Tracer Tests

Christian Wolkersdorfer[1], Elke Mugova[2], Kagiso More[3], Leshego Molaba[4], Joané Botha[1], Valentina Utkin[5]

[1]*South African Research Chair for Acid Mine Drainage Treatment, Tshwane University of Technology (TUT), Private Bag, X680, Pretoria, 0001, South Africa, christian@wolkersdorfer.info, ORCID 0000-0003-2035-1863*

[2]*Fraunhofer IEG, Competence Center for Post-Mining-Exploitation, Am Hochschulcampus 1, 44801 Bochum, Germany, elke.mugova@ieg.fraunhofer.de, ORCID: 0000-0001-6019-9945*

[3]*Centre of Excellence for Sustainability and Food Security, University of Doha for Science and Technology, Doha, Qatar, Kagiso.More@udst.edu.qa, ORCID: 0000-0003-2803-7983*

[4]*Tshwane University of Technology (TUT), 213532570@tut4life.ac.za, ORCID: 0000-0002-7795-6487*

[5]*Ruhr Universität Bochum, Germany*

Abstract

Understanding the hydrodynamics of flooded underground mines is important for assessing residence times, hydraulic connectivity and the movement of dissolved constituents within abandoned mine systems. This paper presents the results of four artificial tracer tests conducted in the flooded Havelock Asbestos Mine near Bulembu, eSwatini. The tests were designed to investigate flow paths, travel times and the degree of hydraulic connection between selected injection points and the mine water discharge. Sodium chloride (NaCl), sodium fluorescein (uranine) and eosin y were used as tracers, and monitoring was undertaken by continuous electrical conductivity (EC) measurements and field fluorometry at the discharge point. The NaCl test did not produce a usable breakthrough curve, which is attributed to the comparatively low tracer mass, the elevated background EC and probable downward movement of the denser tracer into deeper parts of the flooded workings. In contrast, the uranine tests yielded clear breakthrough curves with first arrivals after approximately 1.0 to 1.5 days over distances of 1.1 to 1.4 km. Mean residence times ranged from about 8 to 9 days, and maximum flow velocities ranged between 0.6 and 1.3 m/min. Eosin y was not detected. The results indicate that substantial parts of the flooded mine are hydraulically well connected and that fluorescent dye tracer tests are a suitable method for hydrodynamic investigations in abandoned underground mines.

Keywords: Abandoned mine, asbestos mine, tracer test, uranine, eosin y, hydrodynamics, eSwatini

Introduction

Flooded underground mines are hydraulically complex and evolving subsurface systems rather than static underground reservoirs (Wolkersdorfer 2008; Younger *et al.* 2002). Even after mining has ceased, the voids, stopes, drives, winzes and raises of the mine, as well as fractures, may remain hydraulically connected over long distances (Wolkersdorfer 2008). These flow patterns determine the length of time that water remains in the mine, its contact with reactive rock surfaces, the distribution of dissolved constituents and ultimately the quality and quantity of water discharged from the flooded mine pool (Mugova *et al.* 2024).

Therefore, hydrodynamic investigations form a central part of mine water studies. However, compared to hydrochemical sampling and water level monitoring, direct

hydraulic investigations in abandoned mines are still relatively rare. Among the available methods, tracer tests are one of the most robust tools for identifying flow paths, estimating mean residence times and assessing hydraulic connectivity. In flooded mines, however, tracer tests are far from trivial. Density stratification, inaccessible injection points, uncertain flow geometry, tracer losses and restricted access to discharge points can all complicate the design of the test and interpretation of the results. The overall intention of the mine water tracer tests described here was to provide additional background data for the question of whether underground mines can be modified such that artificial density stratification occurs, which can then be used for in situ mine water remediation (Melchers *et al.* 2015; Mugova and Wolkersdorfer 2025; Wolkersdorfer 2025).

The abandoned Havelock Asbestos Mine near Bulembu in eSwatini offered a rare opportunity to investigate hydrodynamic processes in an environmentally relevant and logistically challenging flooded mine system. This mine is interesting because it is an abandoned asbestos mine, the mine workings are flooded and mine water discharge from the system may affect the quality of water downstream (Wolkersdorfer *et al.* 2025). As the mine water composition is similar at the point of discharge and a distant location in the mine pool (10E service raise), it was of interest if this results from a hydraulic connection. Furthermore, understanding how mining influenced water (MIW) moves through the mine is crucial for any future considerations regarding flow control, water level management or potential in situ treatment options in flooded underground mines in general.

This paper presents the results of artificial tracer tests conducted at the Havelock mine using sodium chloride (NaCl), sodium fluorescein (uranine) and eosin y. The main objectives were to evaluate if hydraulically distant parts of the mine are connected, to estimate travel times and flow velocities and to identify whether injection locations and tracer type influence the observed breakthrough behaviour. Particular attention was given to whether mine water flow follows a topographic gradient or whether flooded workings also permit counterintuitive flow directions.

Site Background

The Havelock Asbestos Mine, located in eSwatini (Barton 1986; Hall 1931), is one of the country's best-studied abandoned mine sites. Following its closure in 2001, parts of the underground workings flooded to form a hydraulically connected body of mine water with a volume of 8–11 million m^3. The mine's geometry is complex and includes various access points, including an incline shaft and a main vertical shaft. The horizontal projection of the spatial separation between the injection and sampling points is around 1.1 to 1.4 km (Wolkersdorfer *et al.* 2025).

As with many abandoned underground mines, the Havelock mine cannot be treated as a simple pipe system. The actual flow field in the mine pool is instead controlled by the mine's geometry, partial collapses, local constrictions, flooded stopes, possible density differences and the hydraulic gradients prevailing between connected mine sectors and discharge points. In such a system, assumptions based on maps alone can be misleading. Direct tracer-based evidence is therefore required to identify flow paths (Mugova and Wolkersdorfer 2022; Wolkersdorfer 2002, 2008; Younger *et al.* 2002).

Another complicating factor is that the flooded mine likely contains bodies of water with different hydraulic behaviour at different depths. Previous measurements were inconclusive in this regard, which became one reason for selecting two different injection locations in the mine pool. One tracer (eosin y) was introduced to the surface of the mine water via access through an incline shaft (10 E). The other tracer (uranine) was injected through the main vertical shaft (HVS) into the mine water body at a depth of 107 m below shaft collar (Fig. 1), enabling an initial assessment of the effect of injection position within the water column on the subsequent tracer response.

Materials and Methods

Four separate tracer tests were conducted, each using a different tracer substance, mass combination or injection configuration. One of the reasons for repeating the tracer test was that the tracer breakthrough took more time than the battery in the online fluorimeter lasted or that a tracer could not be detected. No pH adjustment of the MIW was applied, as online detection of fluorescent dyes in the MIW discharge does not permit such a procedure. However, as the pH of the MIW is between 8.6 and 8.7, the recovery of the uranine and eosin y signals would theoretically exceed 100% anyway (Cao *et al.* 2017).

The first test used 2 kg of NaCl as an artificial tracer. The advantages of salt are that it is inexpensive, readily available and easy to detect using electrical conductivity EC (Käß 1998; Leibundgut *et al.* 2009). However, in large, flooded mine pools, substantial quantities of the tracer are often required, particularly where background EC is already high or dilution volumes are large (Wolkersdorfer 1996).

The second test used 503.55 g of uranine injected into the Havelock vertical shaft. This well-established fluorescent dye has been used successfully in surface water, karst and mine water studies and is particularly suited to systems with large dilution volumes due to its low detection limit (Aley *et al.* 2025; Goldscheider and Drew 2007; Käß 1998; Leibundgut *et al.* 2009).

The third test combined 1 kg of uranine and 1 kg of eosin y to test two fluorescent tracers simultaneously and obtain additional information on flow behaviour from different injection locations. One tracer was introduced via the 10E incline shaft onto the surface of the mine water at location 5A, while the second tracer was injected through the main vertical shaft to the mine water surface at a depth of 107 m below shaft collar.

In the fourth test, the same configuration as in test three was used except that the tracer masses were increased to 3,020.09 and 5,026.81 g for uranine and eosin y, respectively. At the underground injection location 10E, the injection was moved 25 m to the south of 5A, into a West–East drift that is better connected to the mine pool.

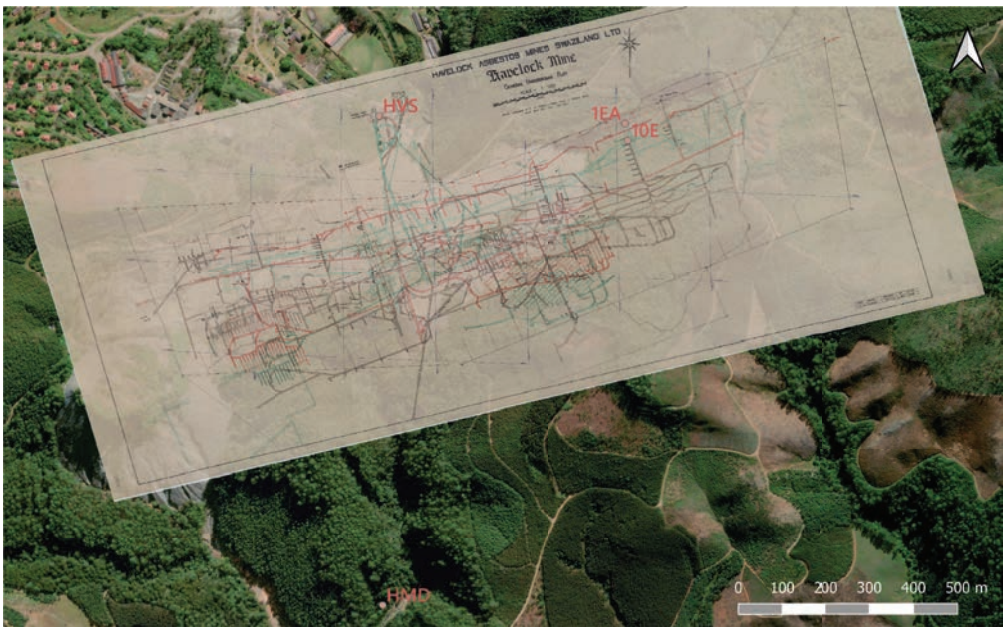

Figure 1 *Injection (HVS, 10E) and sampling location (HMD) for the tracers at the Havelock asbestos mine. Mine map overlay from Archive Bulembu Mining Museum, base map World Imagery 1.9cm Resolution Metadata.*

Tracer monitoring focused on the only accessible discharge location of the mine, south of the asbestos tailings. Continuous on-site fluorometry (GGUN FL-30, Albillia, Switzerland) was used to establish breakthrough curves for the fluorescent tracers (Lemke *et al.* 2013). For the salt test, EC measurements (van Essen CTD Diver, Netherlands) were used to identify any increase in tracer-related EC values above background levels. Travel times were derived from the time of the first detectable arrival and the mean residence time of the recovered tracer signal. Maximum flow velocities were then estimated by relating the horizontal flow distance of 1.1–1.4 km to the observed travel times using QTRACER2 (Field 2002).

Tracer recovery was calculated from the monitored tracer concentrations. As with all tracer tests, these recovery rates must be interpreted with caution because they are influenced by analytical precision, incomplete mixing in the mine pool, temporary storage in stagnant zones, sorption and uncertainties in the measured discharge volumes.

Results

Sodium chloride test

The NaCl tracer test did not result in a usable breakthrough curve. This was because no tracer response could be distinguished from the natural EC variability, though an increase of about 50 µS/cm would have been expected. There are several possible explanations for this outcome: Firstly, the amount of tracer used may have been insufficient for the size of the flooded mine and the resulting dilution. Secondly, the salt may have sunk into deeper parts of the mine pool and thus not reached the point of discharge within the observation period. Thirdly, the monitoring period may have been too short to detect a delayed response. In the flooded Havelock mine with its complex void geometry, all three explanations are plausible, and they are not mutually exclusive. Based on the uranine tracer results, the most likely explanations are insufficient tracer mass and sinking of the tracer into deeper parts of the Havelock vertical shaft.

Fluorescent dye tests

In contrast to the salt test, the fluorescent dye tracer tests were successful (Fig. 2). Uranine was clearly detected at the monitoring location in all investigations using fluorescent tracers. The first arrivals appeared after approximately 1–1.5 days. This comparatively rapid response time for a flooded underground mine over the given travel distance already indicates a good hydraulic connection between the injection and the sampling locations.

The calculated mean residence times ranged between 8 and 9 days. Despite the rapid initial arrival after one day, these values

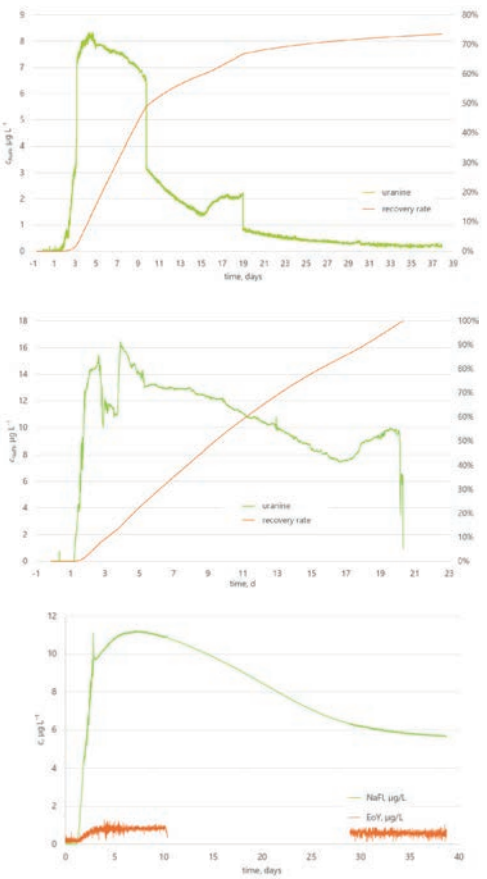

Figure 2 *Results of the 2023, 2024 and 2026 dye tracer tests at the Havelock mine, eSwatini (missing 2026 data interpolated).*

show that the tracer remained in the flooded mine for a much longer period. This is typical for a mine with a combination of preferential pathways and slower exchange with less mobile zones in stopes or other galleries.

Recovery rates were high, though the battery of the data logger only lasted for about 4 to 6 weeks. The 2023 investigation yielded a recovery rate of 74%, while the 2024 investigation yielded one of 99%. At the time of writing this paper, the 4th test was not finished. These values suggest that the monitored discharge point captured most of the tracer mass during the observation period of the fluorescent tests. They also support the interpretation that the mine levels, stopes and drifts involved in the test were hydraulically well connected.

Maximum flow velocities between 0.6 and 1.3 m/min were calculated for the uranine tracer on the basis of the horizontal distance of 1.1 to 1.4 km and the observed arrival characteristics. The average flow velocity was around 0.1 m/min. This is close to the worldwide median flow velocity of 0.15 m/min reported for flooded underground mines, placing the Havelock results well within the range observed elsewhere.

No eosin y was detected during the four-week observation period of the second test and none in the first weeks of the 4th tracer test. This result may indicate that the tracer followed a different flow path, remained in a less mobile part of the mine, underwent stronger retardation or attenuation, or that the injection point was hydraulically less well connected to the monitored discharge. The absence of an eosin y signal despite successful uranine detection therefore suggests that the vertical position of the injection point and the local hydraulic setting can strongly influence tracer behaviour.

Discussion

The Havelock tracer tests show that the flooded mine workings are well connected hydraulically over distances exceeding one kilometre. This is an important finding in itself, as mine maps and topographic gradients often suggest a simpler hydraulic picture than is present. At Havelock, dye tracer tests demonstrated that water could move rapidly through the mine, showing that the effective hydraulic connection between distant mine locations is stronger than one might assume from the geometry alone.

It could be shown that mine water can flow both downstream and upstream within flooded mine workings. This does not contradict hydraulic principles. Rather, it reflects the fact that, in abandoned mines, the flow field is governed by local hydraulic heads, submerged connections, internal mine geometry, and density-related effects. In practice, this means that contaminants released in one part of the mine may flow in unexpected directions. For mine water management, this is a relevant consideration.

The contrast between the unsuccessful salt tracer test and the successful dye tracer tests highlights a methodological point. In large, flooded mine systems with not too acidic mine water, fluorescent dyes are generally preferable to salt tracers when dilution volumes are uncertain and only a few observation points are accessible. Their low detection limits make them more robust under such conditions. At the same time, the failure of the salt tracer test should not simply be viewed as a failure of field execution. It highlights the complexity of the system and the need to carefully adapt tracer choice to site-specific hydraulic conditions.

The non-detection of eosin y in test two is also informative. This suggests that not every injection point within the mine accesses the same active flow domain. This observation is consistent with layered or compartmentalised flow behaviour and may also indicate partial stratification or weak hydraulic exchange between different depths (Wolkersdorfer *et al.* 2007a, 2007b). Since this part of the Havelock mine is not fully accessible, no specific reasons could be determined. Previous studies of other flooded mines have shown that even minor density variations can affect vertical exchange, tracer dispersion and residence time behaviour. The Havelock results fit well within this broader understanding, even though the studies were not primarily designed as a density stratification experiment.

From an applied perspective, the Havelock tracer test results support the view that open

discharge adits and controlled discharge points are essential for maintaining a stable mine water level. If such outlets become blocked or restricted, however, water levels may rise and previously disconnected mine sectors may become activated, resulting in unwanted flooding of built-up areas. In this sense, the tracer results are not merely of academic interest. They provide a hydraulic basis for practical mine water management decisions at abandoned mine sites.

Conclusions

The tracer tests at the abandoned Havelock asbestos mine yielded several conclusions:

The study demonstrated that fluorescent dye tracer tests can be successfully conducted in a flooded, abandoned asbestos mine despite the logistical constraints at Havelock. We found no published record of an earlier fluorescent dye tracer test in eSwatini or in an asbestos mine. In addition, the mine workings were found to be hydraulically well connected over distances of 1.1 to 1.4 km. Uranine arrived within 1–1.5 days, with mean residence times of 8–9 days. Maximum flow velocities ranged from 0.6 to 1.3 m/min, averaging about 0.1 m/min. Furthermore, the unsuccessful NaCl test and the successful dye tests demonstrate the importance of tracer selection. For large, flooded mine pools with an uncertain dilution behaviour, fluorescent tracers are clearly preferable. Furthermore, the absence of detectable eosin y during the four-week monitoring period suggests that different injection points within the mine may access distinct hydraulic domains. This suggests internal complexity within the flooded workings, which reflects variable connectivity at different depths.

Finally, the tests confirm that mine water in flooded workings can flow in directions that cannot be predicted based on surface topography alone. Rather, it is important to identify the points of discharge with the lowest hydraulic potential. This has direct consequences for interpreting contaminant transport, hydraulic control measures, and the management of abandoned mine discharges. The Havelock results therefore provide both site-specific knowledge and broader methodological insights for hydrodynamic investigations in flooded underground mines.

Acknowledgements

We acknowledge the financial support of our institutions and the colleagues who were involved in the field investigations, tracer preparation, sampling and laboratory analyses. We gratefully acknowledge access to the Havelock Mine site and the logistical support provided during the field campaigns by the Bulembu Ministries, specifically Kurt Puttkammer. Tsebo Lamula assisted in injecting the tracers during the 4th test. Funding was provided by the NRF (NRF Grant UID 86948) and the German Forum Bergbau und Wasser via the International Giving Foundation.

References

Aley T, Osorno T, Devlin JF, Goers A (2025) Practical Groundwater Tracing with Fluorescent Dyes. The Groundwater Project, Guelph. https://doi.org/10.62592/mfwe5297

Barton CM (1986) The Havelock Asbestos Deposit in Swaziland, Barberton Greenstone Belt. In: Anhaeusser CR, Maske S (eds) Mineral Deposits of Southern Africa. vol I. Geol. Soc. S. Afr., Johannesburg, p 395–407

Cao V, Schaffer M, Jin Y, Licha T (2017) Preservation of commonly applied fluorescent tracers in complex water samples. Grundwasser 22(2):127–133. https://doi.org/10.1007/s00767-017-0356-1

Field MS (2002) The QTRACER2 Program for Tracer-Breakthrough Curve Analysis for Tracer Tests in Karstic Aquifers and Other Hydrologic Systems. vol EPA/600/R-02/001. U.S. Environmental Protection Agency – Office of Research and Development, Washington

Goldscheider N, Drew DP (2007) Methods in Karst Hydrogeology. Taylor & Francis, London. https://doi.org/10.1201/9781482266023

Hall AL (1931) The Havelock asbestos mine. S Afr Mining and Eng J 42(1):85 & 87

Käß W (1998) Tracing Technique in Geohydrology. Balkema, Rotterdam. https://doi.org/10.1201/9780203735282

Leibundgut C, Małoszewski P, Külls C (2009) Tracers in Hydrology. Wiley-Blackwell, Oxford. https://doi.org/10.1002/9780470747148

Lemke D, Schnegg P-A, Schwientek M, Osenbrück K, Cirpka OA (2013) On-line fluorometry of multiple reactive and conservative tracers in streams. Environ Earth Sci 69(2):349–358. https://doi.org/10.1007/s12665-013-2305-3

Melchers C, Goerke-Mallet P, Henkel L, Coldewey WG, Wesche D (2015) Density stratification in Mine Water Bodies as a Contribution to Better Long-

Term Water Management [Dichteschichtungen in Flutungswasserkörpern als Beitrag zur Optimierung der langzeitigen Wasserhaltung]. Mining Rep 151(6):503–510

Mugova E, Molaba LE, Wolkersdorfer C (2024) Understanding the Mechanisms and Implications of the First Flush in Mine Pools: Insights from Field Studies in Europe's Deepest Metal Mine and Analogue Modelling. Mine Water Environ 43(2):73–86. https://doi.org/10.1007/s10230-024-00969-3

Mugova E, Wolkersdorfer C (2022) Density Stratification and Double-Diffusive Convection in Mine Pools of Flooded Underground Mines – A Review. Water Res 214:118033. https://doi.org/10.1016/j.watres.2021.118033

Mugova E, Wolkersdorfer C (2025) Understanding the influence of stratification for mine water management: a comparative study. Nat Sci Reports 15(1):2757. https://doi.org/10.1038/s41598-024-82293-y

Wolkersdorfer C (1996) Hydrogeochemische Verhältnisse im Flutungswasser eines Uranbergwerks – Die Lagerstätte Niederschlema/Alberoda. Clausthaler Geowiss Diss 50:1–216

Wolkersdorfer C (2002) Mine water tracing. Spec Publ – Geol Soc London 198:47–61. https://doi.org/10.1144/GSL.SP.2002.198.01.03

Wolkersdorfer C (2008) Water Management at Abandoned Flooded Underground Mines – Fundamentals, Tracer Tests, Modelling, Water Treatment. Springer, Heidelberg. https://doi.org/10.1007/978-3-540-77331-3

Wolkersdorfer C (2025) Hydrodynamic Investigation of a density-stratified Underground Mine – Tracer Test Challenges and Results in the Georgi-Unterbau Mine, Tyrol, Austria. Paper presented at the International Mine Water Association Conference – Time to Come, Braga, Portugal; Oviedo/Uviéu, Spain:1011–1016.

Wolkersdorfer C, More KS, Mugova E, Nchabeleng N, Sotiralis AJ (2025) Hydrogeochemical and hydrogeological baseline study following the mining of asbestos at the Havelock Mine, Bulembu, eSwatini. J Afr Earth Sci:105533. https://doi.org/10.1016/j.jafrearsci.2024.105533

Wolkersdorfer C, Neumann C, Hasche-Berger A (2007a) Hydrodynamics of the flooded Freiberg/Saxony Underground Mine. Water in Mining Environments. Mako Edizioni, Cagliari

Wolkersdorfer C, Neumann C, Hasche-Berger A (2007b) Tracer Tests in the flooded Himmelfarth Fundgrube Underground Mine (Freiberg/Saxony). Wiss Mitt Inst Geol 35:157–162

Younger PL, Banwart SA, Hedin RS (2002) Mine Water – Hydrology, Pollution, Remediation. Kluwer, Dordrecht. https://doi.org/10.1007/978-94-010-0610-1

IMWA 2026
Jeongseon

From Pit to Lake: UAV-Assisted Tracking of Hydrological and Geomorphological Transformation in the Stanisław-Południe Clay Mine, SW Poland

Magdalena Worsa-Kozak[1], Krzysztof Chudy[1], Damian Kasza[1], Jarosław Wajs[1]

[1]*Faculty of Geoengineering, Mining and Geology, Wroclaw University of Science and Technology, Wybrzeże Wyspiańskiego 27, 50-370 Wrocław, Poland. magdalena.worsa-kozak@pwr.edu.pl*

Abstract

The progressive flooding of the former Stanisław-Południe open-pit clay mine in Lower Silesia, SW Poland, provides a unique opportunity to document the hydrological and geomorphological evolution of a mid-scale post-mining excavation undergoing natural refilling. Annual monitoring from 2022 to 2025 integrated direct discharge measurements, in-situ physicochemical profiling, and high-resolution UAV-based photogrammetry (DJI M3M, 0.02 m GSD). Water levels rose from 171.98 m a.s.l. in 2022 to 177.23 m a.s.l. in 2025, a cumulative rise of 5.25 m. Annual inflow rate accelerated from ≈1 m/a to over 2.1 m/a after 2023. Eight active inflow points delivered 2.34 L/s in 2025. Internal slope reshaping was ongoing but confined to areas destined for submersion, with no destabilisation of the external pit rim detected.

Keywords: Post-mining lake, pit lake formation, UAV photogrammetry, water balance, slope stability, Lower Silesia

Introduction

The transition of exhausted open-pit mines into pit lakes constitutes an increasingly recognised pathway for post-mining land reclamation across Central Europe (Major *et al.* 2025; McCullough *et al.* 2020). As surface dewatering ceases, former excavations refill naturally through groundwater recovery, direct precipitation, and surface runoff. The resulting water bodies may serve ecological, recreational, or water-retention functions. Yet, their formation is accompanied by significant geomorphological adjustments, including slope erosion and mass movements, which require careful long-term monitoring (Castendyk and Eary 2009).

The Stanisław-Południe site, operated by JARO S.A. in the Jaroszów area of the Świdnica County (Lower Silesia, SW Poland), was an open-pit clay mine extracting refractory clays and sub-coal Oligocene-Miocene-Pliocene clays until the cessation of mining operations. The excavation, located approximately 8 km east of Strzegom and 60 km west of Wrocław, covers approximately 54.7 ha with a total void volume of ca. 9.79×10^6 m^3 above the 2022 reference water level of 171.98 m a.s.l. The geological setting comprises Oligocene-Miocene-Pliocene sequences of silts and clays, with two lignite seams, overlying Precambrian metamorphic schists, capped by Quaternary fluvioglacial sands and gravels that constitute the primary aquifer supplying the forming lake (Trentowski 2021).

Previous water-balance modelling (Worsa-Kozak *et al.* 2023) forecast complete flooding within 30 to 130 years depending on precipitation scenario, with a maximum expected water level of ca. 200-201 m a.s.l., constrained by the hydraulic head of the surrounding Quaternary aquifer. The observed filling rate, however, had not yet been validated against real multi-year data. This paper presents the first four years of integrated monitoring (2022-2025), regarding outer-slope stability, water-chemistry classification, the water-balance model, pit-lake morphology, and the georeferencing approach, and demonstrates the replicability of the UAV-geomatics methodology for post-mining environmental assessment.

Study Area and Geological Setting

The Stanisław-Południe excavation is situated in the southern part of the Strzegom Hills mesoregion within the Sudeten Foreland macroregion. The terrain shows a gentle northward slope from ca. 210 m a.s.l. to ca. 190 m a.s.l. beyond the pit rim. Land use in the surrounding area is predominantly agricultural, with the village of Rusko located to the north-east. The site drains into the Dąbia stream, a tributary of the Strzegomka River, within the Odra River catchment.

The stratigraphy of the deposit (Trentowski 2021; Cwojdziński *et al.* 2017) includes: (i) a Quaternary overburden of fluvioglacial sands and gravels (aquifer) underlain by till, (ii) Oligocene-Miocene-Pliocene silty-sandy deposits transitioning into refractory clays with two lignite seams, and (iii) a Precambrian schist and phyllite basement. The hydraulically most significant unit is the Quaternary sand-gravel aquifer in the southern sector, which is in direct hydraulic connection with the forming pit lake through a ca. 10 m thick saturated zone at elevations of ca. 195-205 m a.s.l. (Herbowy and Mądrala 2021). This southern aquifer is the dominant source of groundwater inflow and controls the eventual equilibrium water level. The pit floor lies at approximately 165-167 m a.s.l.

The climate of the Jaroszów area is oceanic-continental with mountain influence from the adjacent Sudeten Range. Mean annual precipitation at the nearby Dobrogoszcz station (1956-2022 series) is 595.5 mm/a, with annual extremes of 419.8 mm/a (1969) and 909.9 mm/a (1977). Mean annual air temperature for 1990-2014 was 9.2 °C (Klein Tank 2002). These values informed the water-balance model developed in the 2023 forecast report (Worsa-Kozak *et al.* 2023)

Methods

Monitoring Design

Annual monitoring campaigns were conducted in the autumn of each year from 2022 to 2025, in compliance with the statutory monitoring framework. Each campaign combined hydrological and hydrogeological mapping with UAV-based terrain surveying. Two additional campaigns were performed in spring (May 2022) and autumn (October 2022) during the baseline year.

Hydrological and Hydrogeological Mapping

Surface inflow points above the water-table surface were identified by systematic traversal of accessible pit faces. At each active seepage point, discharge was measured three times using the volumetric bucket method (volume 0.2-4.2 L collected per measurement; time 1.4-40 s), and the mean value $\bar{Q}$ was recorded. Basic physicochemical parameters – water temperature (T), pH, electrical conductivity (specific electrical conductance, PEW in µS/cm), redox potential (E^h, mV), dissolved oxygen (mg/L), and chloride concentration (mg/L) – were measured in situ with a portable multi-parameter probe. All measurement locations were recorded on a georeferenced mine survey plan. Water-level elevation was determined by GNSS measurement at the shoreline.

UAV-Based Photogrammetric Surveying

Terrain data were acquired using multirotor UAV platforms: DJI Phantom 4 Pro (2022–2023 campaigns, flight altitude 70 m, ground sampling distance ≈2–3 cm) and DJI M3M (2024–2025 campaigns, flight altitude 70 m, ground sampling distance ≈2–3 cm, resulting in a post-filtering point cloud of ca. 119 million points). Eight photogrammetric ground control points (GCPs) were surveyed per campaign using RTK-GNSS in the ETRS89/Poland CS2000 Zone 6 coordinate reference system, yielding horizontal geolocation accuracy of ±2–3 cm and vertical accuracy of ±3–5 cm in EVRF2007 datum. Point clouds were processed in Agisoft Metashape and exported as Digital Terrain Models (DTMs) at 0.2 m resolution after ground-point filtering.

The georeferencing process used permanent benchmark markers installed within the mining area, measured at the start of the monitoring programme and re-occupied at each subsequent campaign. RTK measurements were obtained with base corrections from the nearest ASG-EUPOS CORS station. This approach ensures inter-annual comparability.

Volumetric and Change-Detection Analysis

DTM-derived hypsometric curves were computed in QGIS by intersecting the DTM with horizontal planes at 1 m intervals. Inundated volumes were calculated as the void space between the DTM and each plane. Inter-annual surface deformation was quantified using a Cloud-to-Mesh (C2M) signed-distance analysis in CloudCompare, yielding vertically oriented displacement maps. Change zones were classified by genesis as natural (slope wash, instability, and erosion) or anthropogenic (surface grading). Uncertainty was highest near the water surface due to waterlogged conditions, which reduced GCP availability; these levels are flagged accordingly in the volumetric output.

Water Balance Model

A water balance model (Worsa-Kozak *et al.* 2023) was applied with the equation $P + D = H + S \pm \Delta R$, where P is atmospheric precipitation, D is groundwater inflow, H is surface outflow (zero during the filling phase), S is actual evapotranspiration estimated by the Pardé nomogram, and ΔR is the change in storage. Three precipitation scenarios were adopted: maximum (P = 910 mm/a), neutral (P = 604 mm/a), and minimum (P = 420 mm/a). The model was constrained by field-measured inflow rates and the known excavation hypsometry. The present paper compares observed water-level rises with model predictions as a four-year validation dataset.

Results

Water Level and Filling Rate

Water levels recorded at each autumn campaign demonstrate a consistent and accelerating rise (Tab. 1). From October 2022 to September 2023 (≈11 months), the surface rose by 0.97 m, equivalent to ≈0.3 cm/d. Between September 2023 and October 2024 (≈13 months), the rise was 2.11 m (≈0.53 cm/d). Between October 2024 and October 2025 (≈12 months), the rise was a further 2.17 m (≈0.59 cm/d). The cumulative rise over the entire monitoring period is 5.25 m, from 171.98 m a.s.l. to 177.23 m a.s.l. The acceleration beyond 2023 corresponds qualitatively to the increasing water-surface area intercepting precipitation and the growing volume of subaqueous inflow as formerly exposed seepage faces became submerged.

Inflow Characteristics and Water Chemistry

The number and spatial distribution of measurable inflow points above the water surface varied between campaigns, reflecting seasonal precipitation conditions and the progressive submersion of lower-elevation seepage faces. In May 2022, seven measurement points yielded a total of 4.04 L/s, dominated by a single high-discharge point (P2, 3.00 L/s) in the southern sector. By October 2022, total inflow had decreased to 1.54 L/s (eleven points), consistent with lower autumn precipitation following a dry winter. September 2023 recorded the highest measured total inflow at 6.93 L/s (eight points), with two major contributors (P3: 2.53 L/s; P8: 3.15 L/s) associated with concentrated drainage from the Quaternary sand-gravel aquifer outcropping in the southern wall. October 2024 and October 2025 returned lower totals of 1.92 L/s and 2.34 L/s, respectively, both reflecting drier autumn conditions.

Table 1 *Water level and inflow summary for the Stanisław-Południe monitoring campaigns, 2022–2025.*

Campaign date	Water level (m a.s.l.)	Rise since the previous (m)	Measured inflow (L/s)	Annualised inflow (m^3/a)
May 2022	–	–	4.044	127 540
Oct 2022	171.98	baseline	1.535	48 407
Sep 2023	172.95	0.97	6.932	218 612
Oct 2024	175.06	2.11	1.915	60 383
Oct 2025	177.23	2.17	2.340	73 819

The inflow waters are consistently slightly alkaline. In October 2022, pH ranged from 6.9 to 8.2, specific electrical conductance (PEW) ranged from 536 to 1717 µS/cm, and dissolved oxygen ranged from 64.5 to 100.6 mg/L. In September 2023, pH ranged from 7.8 to 8.7 and PEW from 491 to 1230 µS/cm. In October 2025, pH ranged from 7.56 to 8.05 and PEW from 879 to 1345 µS/cm. Water temperatures ranged from 10.5 to 11.6 °C in October 2025 and from 12.4 to 25.8 °C in warmer-season campaigns. The slightly alkaline reaction and moderate mineralisation are consistent with shallow groundwater circulation through Quaternary sandy-gravelly deposits with calcareous cement. The elevated temperatures in summer/autumn campaigns and the rapid thermal equilibration with ambient air confirm that these are shallow-circulation waters with short aquifer transit times. No acidic drainage indicative of sulfide mineral oxidation was detected in any campaign, reflecting the essentially non-sulfidic clay lithology. The slight alkalinity (pH 7.6-8.7) is attributed to the dissolution of carbonate cements within Quaternary sands and gravels in the southern sector, rather than to any deep hydrothermal influence. In situ profiling was the measurement modality used to record all physicochemical parameters at the inflow points.

Morphological Change and Slope Behaviour

C2M difference maps revealed progressive internal reshaping in each monitoring interval (Tab. 2). In 2022–2023, two zones of accelerated vertical change were identified in the southern pit sector, both immediately above the contemporaneous water line: Sub-area #1 (ca. 6000 m², maximum vertical displacement ≈1.5 m) displayed characteristics of a translational slide whose snout reached the water surface, with the main scarp extending to approximately 192 m a.s.l.; Sub-area #2 (ca. 1500 m²) showed shallower instability across two benches directly beneath a seepage point, with a maximum vertical displacement ≈1.1 m. In 2023-2024, four zones of morphological change were documented, all in the southern sector, associated with bench-face sliding at individual extraction levels. In 2024–2025, eight change zones were identified, of which seven were of natural origin (primarily slope wash and sliding, concentrated in the southern sector) and one was anthropogenic (surface grading in the north-western portion of the mining area) (Figure 1).

Critically, in all four monitoring periods, no morphological change attributable to slope instability was detected along or outside the external pit rim (Worsa-Kozak *et al.* 2022-2025). All identified displacement zones were confined to interior pit faces at elevations that will be fully submerged as the lake continues to fill. The absence of external rim deformation is consistent with the geological control: the outer pit walls above the future maximum water level (ca. 200-201 m a.s.l.) are composed predominantly of firm, low-permeability Oligocene-Pliocene clay, which has not experienced significant changes in pore pressure during the monitored period. The internal instabilities are driven by: (i) concentrated groundwater seepage through the Quaternary sand-gravel unit outcropping in the southern faces, undercutting clay benches; and (ii) wave-action and waterline-parallel erosion as the lake surface rises. The slopes above the pit rim are not in direct hydraulic contact with the active seepage zone, because the thick clay series acts as

Table 2 *Summary of morphological change zones identified by Cloud-to-Mesh analysis, 2022–2025.*

Period	Change zones (total)	Natural origin	Anthropogenic origin	Location of changes
2022–2023	2	2	0	Southern sector, above waterline
2023–2024	4	4	0	Southern sector, bench faces
2024–2025	8	7	1	Southern + eastern; NW grading

an aquitard. Nonetheless, the water-balance model (Worsa-Kozak *et al.* 2023) identified the northern pit rim (ca. 200-201 m a.s.l.) as the lowest-elevation sector; therefore, long-term monitoring of that rim remains warranted.

Volumetric Change and Initial Pit-Lake Morphology

The total void volume of the excavation above the 2022 baseline level (171.98 m a.s.l.) is ca. 9.79 × 10^6 m^3, as derived from the 2022 photogrammetric survey. Between 2024 and 2025, the flooded volume increased by ca. 370 000 m^3 (Scenario 2: 124 885 m^3 of net geometric change attributable to morphological adjustment, excluding the flooded volume). The excavation hypsometry shows a bowl-shaped profile: bathymetric cross-sections in the SW-NE and NW-SE directions demonstrate near-vertical to steeply dipping walls down to ca. 170–175 m a.s.l., widening progressively upward. The minimum rim elevation in the northern sector is ca. 200–201 m a.s.l., defining the maximum feasible lake level.

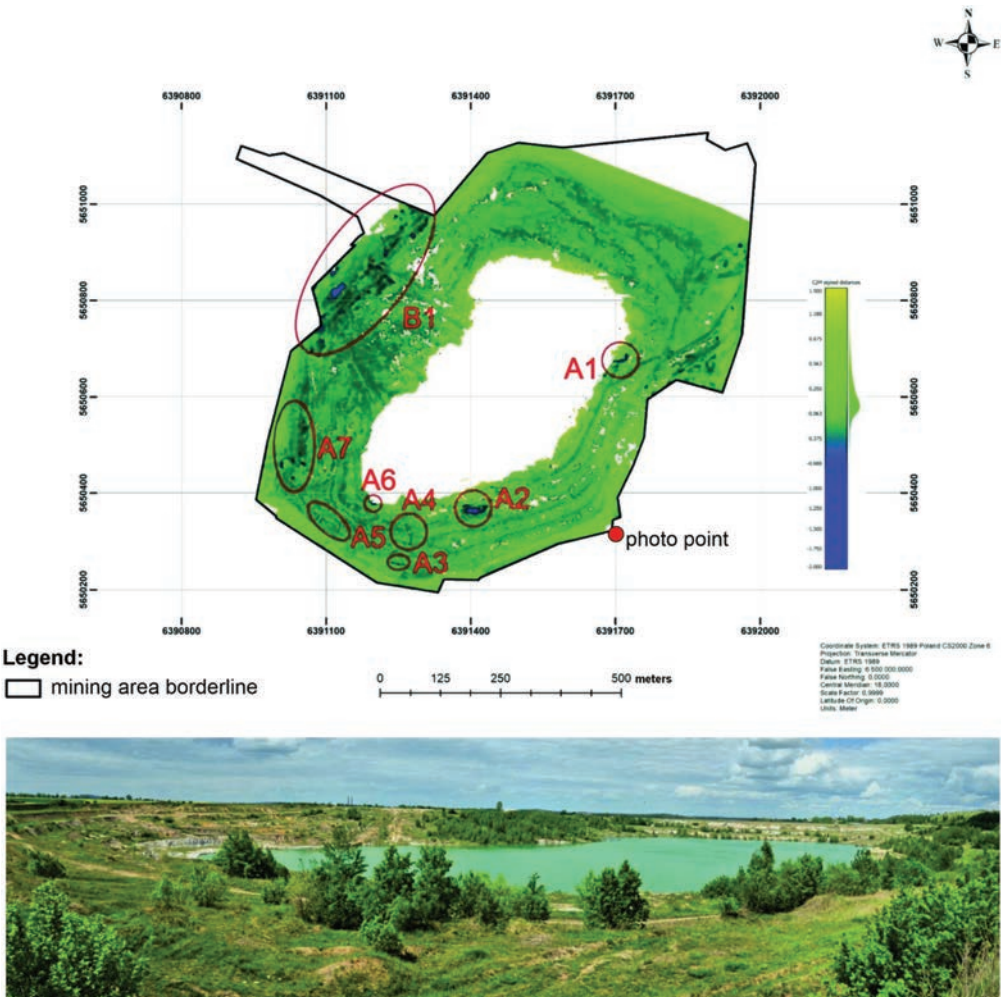

Figure 1 *The results of the difference analysis showing morphological changes 2024-2025 in the reclaimed excavation area. Locations of visible morphological changes: (A) of natural origin; (B) of anthropogenic origin. Source: Worsa-Kozak* et al.*, 2022-2025, Photo by: M. Worsa-Kozak.*

The initial pit-lake morphology at 177.23 m a.s.l. (October 2025 water level) shows an elongated, asymmetric basin. The deepest accessible area is in the central-northern zone, while the southern zone features the active seepage faces and erosion scarps. As the lake level rises, the water surface will progressively cover the lower benches of the southern wall, reducing exposed seepage-face area and likely moderating internal erosion. The development of a shoreline morphology through wave action and nearshore erosion is already visible in the 2025 difference map (Figure 1) along the northern waterline. A quantitative hypsometric curve was available from the 2022 photogrammetric baseline survey and served as the basis for the water-balance model calculations.

Water Balance: Model Validation

The Water balance model (Worsa-Kozak *et al.* 2023) is based on: (i) annual precipitation data from Dobrogoszcz station (1956-2022); (ii) actual evapotranspiration estimated by Pardé nomogram using a mean annual temperature 9.2 °C; (iii) groundwater inflow measured at field campaigns; and (iv) the excavation hypsometry from UAV photogrammetry. The four-year observed record now available constitutes the first empirical validation dataset for this model, and its expansion will enable progressive refinement of the inflow parameters. The 2023 water-balance forecast (Worsa-Kozak *et al.* 2023) predicted annual water storage increase (ΔR) of 57 084 m^3/a (Scenario III, low precipitation), 126 780 m^3/a (Scenario II, mean precipitation), and 249 548 m^3/a (Scenario I, high precipitation). The predicted water-level rise for Scenario II from the baseline of 172 m a.s.l. was approximately 1 m in the first year. Observed rises of 0.97 m (Year 1) and 2.11 m (Year 2) are consistent with Scenario II and Scenario I, respectively, suggesting that 2023-2024 was a significantly wetter-than-average period. The long-term neutral-scenario forecast of ca. 59 years to reach 200 m a.s.l. remains a reasonable central estimate.

Discussion

The Stanisław-Południe case demonstrates that integrated UAV photogrammetry and hydrogeological mapping provide a cost-effective, technically robust approach for real-time monitoring of pit-lake formation. The methodology is replicable at comparable post-mining sites and offers regulatory authorities evidence-based documentation of slope behaviour and water-body formation, as required by Polish mining reclamation law.

The accelerating filling rate observed after 2023 (from ca. 1 m/a to ca. 2.1–2.2 m/a) is an important departure from the initially estimated neutral-scenario rate. Two factors may explain this acceleration. First, as the lake surface area expands with rising water level, the effective precipitation catchment area increases proportionally, augmenting direct recharge. Second, submerged seepage faces contribute to the hydraulic head balance in ways not fully captured by surface-only inflow measurements. Once seepage points fall below the water surface, their discharge is no longer directly measurable, but they continue to contribute to lake volume. The good agreement between the observed Year 1 rise and the Scenario II prediction confirms the model's validity under average conditions. In contrast, the Year 2-4 acceleration suggests that wetter-than-average conditions or the progressive expansion of the effective recharge area should be incorporated into future model updates, as recommended by Worsa-Kozak *et al.* (2023) at 5-year intervals.

The internal slope instabilities documented in each monitoring period are geotechnically consistent with the hydrogeological setting. The southern pit wall, where the Quaternary aquifer directly contacts the excavation face through a ca. 10 m saturated sand-gravel unit, experiences the highest pore-pressure gradient. As the pit lake rises, the saturated thickness between the lake water surface and the free-water table in the southern aquifer decreases, reducing the hydraulic gradient and, consequently, the seepage velocity. This mechanism predicts a self-limiting character to the southern-wall instabilities: as the lake approaches equilibrium with the surrounding groundwater table, seepage forces will diminish. The consistently observed absence of deformation at the outer pit rim supports this interpretation. It is physically explained

by the presence of the thick, low-permeability Oligocene-Pliocene clay series, which isolates the outer rim from the hydraulically active southern aquifer.

Based on the four years of data, the monitoring and geotechnical analyses indicate potential future slope stability beyond the mining area borderline. The outer-rim geology (firm clays, low hydraulic conductivity, minimal pore-pressure change) and the absence of any measurable surface displacement along the rim in any campaign support this conclusion. However, it is acknowledged that pore-pressure monitoring within the outer-rim embankment has not been conducted; this constitutes a limitation of the current monitoring scope. Installation of piezometers in the outer rim area would provide a more definitive assessment of this risk.

The water chemistry data reveal a consistent pattern of slightly alkaline, low-TDS groundwater with no indication of acid generation, consistent with the absence of reactive sulfide minerals in the clay lithology. The elevated summer campaign temperatures (up to 25.8 °C at P8 in September 2023) reflect the short subsurface residence time of near-surface recharge water during warm periods rather than any anthropogenic thermal influence. The seasonally variable chloride concentrations (range 77-279 mg/L) are consistent with agricultural land use in the catchment (fertiliser application) and road de-icing.

Conclusions

Four years of integrated UAV photogrammetric and hydrogeological monitoring at the Stanisław-Południe pit lake have yielded the following principal findings:

(I) Water levels rose cumulatively by 5.25 m (from 171.98 m a.s.l. in 2022 to 177.23 m a.s.l. in 2025), with the annual rise accelerating from ca. 1 m/a in 2022-2023 to ca. 2.1 m/a in 2023-2025, broadly consistent with the neutral to wet precipitation scenarios of the water-balance model. (II) Eight active inflow points were identified in October 2025, supplying a total of 2.34 L/s. Inflow waters are consistently slightly alkaline (pH 7.56-8.05 in 2025), with moderate mineralisation (PEW 879-1345 µS/cm), characteristic of shallow Quaternary aquifer circulation with no indication of acid-mine drainage. (III) Internal slope reshaping is ongoing, with a progressive increase in identified change zones. All instability is confined to benches destined for submersion in the southern and eastern pit sectors; the external pit rim remains unaffected. (IV) The absence of outer-rim deformation is attributable to the isolating effect of the thick Oligocene-Pliocene clay series, which prevents hydraulic connection between the active southern aquifer and the outer-rim slope. (V) The 2023 water-balance model is validated as broadly accurate for the first year of observation and points to wetter-than-average conditions or an increasingly effective catchment area as explanations for the post-2023 acceleration. (VI) The integrated UAV-geomatics plus hydrogeological methodology constitutes a replicable reference framework for monitoring flooded post-mining excavations in Central European geological settings.

References

Castendyk DN, Eary LE (Eds) (2009) Mine Pit Lakes: Characteristics, Predictive Modeling, and Sustainability. Society for Mining, Metallurgy and Exploration, Littleton, CO

Cwojdziński S, Przybylski B, Ihnatowicz A (2017) Szczegółowa Mapa Geologiczna Polski 1:50 000. Ark. Świdnica (798) (Detailed Geological Map of Poland, scale 1:50,000. Sheet: Świdnica (798)). Państwowy Instytut Geologiczny, Warszawa

Herbowy K, Mądrala D (2021) Mapa Hydrogeologiczna Polski w skali 1:50 000 - pierwszy poziom wodonośny, arkusz 798 Świdnica (Hydrogeological Map of Poland at a scale of 1:50,000 – first aquifer, sheet 798 Świdnica). PIG-PIB, Warszawa

Klein Tank AMG and Coauthors (2002). Daily dataset of 20th-century surface air temperature and precipitation series for the European Climate Assessment. Int J Climatol 22:1441-1453. https://doi.org/10.1002/joc.773

Major, V., Svarcova, V., Hendrychova, M. *et al.* (2025) Water quality of reclaimed lakes in post-mining locations of Czech Republic. Environ Monit Assess 197, 1073. https://doi.org/10.1007/s10661-025-14478-5

McCullough CD, Schultze M, Vandenberg J (2020) Realising beneficial end uses from abandoned pit lakes. Minerals 10:133. https://doi.org/10.3390/min10020133

Trentowski J (2021) Dodatek nr 3 do dokumentacji geologicznej złoża glin ogniotrwałych Rusko-Jaroszów (Appendix 3 to the geological documentation for the Rusko-Jaroszów refractory clay deposit). Usługi Geologiczno-Kartograficzne Janusz Trentowski, Walbrzych (in Polish, unpublished)

Worsa-Kozak M, Chudy K, Kasza D, Wajs J (2022-2025) Realizacja usługi badawczo-rozwojowej p.t. Monitoring okresowy zalewanego wyrobiska Stanisław-Południe wraz z raportem rocznym (R&D service entitled 'Periodic monitoring of the flooded Stanisław-Południe excavation site', including an annual report) - parts I-IV, years 2022-2025. Reports: W06/2022, W06/2023/S-53, W06/2024/S-23, Report W06/2025/S-26. Katedra Górnictwa, Politechnika Wrocławska, Wrocław (in Polish, unpublished)

Worsa-Kozak M, Chudy K (2023) Prognoza wypełniania wodą wyrobiska poeksploatacyjnego Stanisław-Południe wraz z określeniem maksymalnej rzędnej zwierciadła wody. (Forecast of flooding of the Stanisław-Południe post-mining excavation, including the determination of the maximum water table elevation.) Report W06/2023/S-04. Katedra Górnictwa, Politechnika Wrocławska, Wrocław (in Polish, unpublished)

IMWA 2026
Jeongseon

Designing the Post-Mining Future: Hydrological Modeling as a Foundation for Sustainable Pit Lake Management

Heksantia Rahmadinda Yasya[1]*, Muhammad Sonny Abfertiawan[2], Aditia Adyanugraha Arfan[1], Nur Latifa Ristiaramdani[1], Bagja Mulyana[1]

[1]*Research and Consulting Division, PT Ganeca Environmental Services, Bandung, Indonesia*

[2]*Water and Wastewater Engineering Research Group, Faculty of Civil and Environmental Engineering, Bandung Institute of Technology, Indonesia*

**corresponding author: heksantia@ganeca.co.id*

Abstract

Sustainable post-mining management is essential to mitigate environmental impacts and ensure that disturbed landscapes transition into safe and productive land uses. Coal extraction often leaves deep mining voids that evolve into pit lakes, requiring careful hydrological assessment. This study applies a water-balance model to predict water-level dynamics and filling scenarios for ex-mining voids at a coal mine in East Kalimantan, Indonesia. Results show that filling a 290 m deep pit lake through direct precipitation takes 37.5 years, but river diversion could reduce it to 10.3 years. The study highlights the importance of hydrological modelling in supporting sustainable post-mining land-use planning.

Keywords: Post-mining, hydrology, water balance model, pit lake, sustainability

Introduction

Post-mining landscapes, particularly pit lakes, have been widely studied due to their long-term environmental and hydrological implications. Pit lakes are commonly formed in deep mining voids and function as terminal water bodies within modified catchment systems, where hydrological inputs largely determine water balance, stratification, and water quality evolution (Castendyk & Webster-Brown, 2007; McCullough & Lund, 2006). Their sustainability depends on the interaction between catchment processes, groundwater exchange, and climatic conditions, making hydrological assessment a critical component of post-mining management. Moreover, in this case, technical sustainability also could be done by hydrological engineering design related to river diversions during pit lakes' filling period until a stable post-mining landscape is achieved.

Previous studies emphasize that water balance modeling is essential for predicting pit lake filling rates and long-term stability. Conceptual rainfall–runoff models have been widely applied in data-limited regions due to their ability to estimate streamflow using limited input data (Smakhtin, 2001). In tropical environments, where hydrological data are often scarce, such models provide a practical approach to simulate inflow conditions and evaluate management scenarios. Additionally, environmental flow frameworks highlight the importance of maintaining downstream ecological integrity when implementing water diversion strategies (Bunn & Arthington, 2002; Richter *et al.*, 1996).

International experiences further demonstrate the potential for integrated pit lake management. In Germany, large-scale post-mining lake systems have been successfully developed through controlled flooding strategies, improving water quality while enabling socio-economic utilization such as tourism and regional water management (Schultze *et al.*, 2010). Similar approaches have been explored in Australia, where pit lakes are increasingly recognized as potential assets rather than liabilities (McCullough & Lund, 2006).

Despite these advancements, limited studies explicitly integrate hydrological modeling with decision-making for pit lake filling strategies under data-constrained conditions, particularly in tropical regions such as Indonesia. This gap highlights the need for applied modeling approaches that link hydrological prediction with sustainable post-mining land-use planning.

The post-mining plans are designed to be constructed primarily once the pit lake has filled to capacity to ensure the physical and chemical stability of the pit lake is maintained. The chemical stability is supported by minimizing contact between factors that trigger AMD: water isolation that limits contact between oxygen and material containing sulfide mineral (Gautama et al., 2013). These plans also incorporate environmental, hydrological, geochemical, socio-economic, and regulatory dimensions within a unified planning framework. Decree of Ministry of Energy and Mineral Resources No. 1827 of 2018 on Guidelines for the Implementation of Good Mining Practices and No. 344 of 2025 on Technical Guidelines for the Implementation of Land Reclamation and Post-Mining Activities in Mineral and Coal Mining Operations require every mining industry in Indonesia to develop comprehensive reclamation and post-mining plans which emphasizes the importance of incorporating socially and economically sustainable programs to support long-term community development. In this study, a few land-use recommendations were developed to become mine closure success criteria, allowing the mining company to be responsible to the government and the community. The recommendations applied SMART (Specific, Measurable, Achievable, Relevant, and Time-bound) principle to create the master plan. This master plan will be discussed in a Focus Group Discussion (FGD) with local stakeholders.

Methods

The hydrological water-balance model used in this study was an Excel-based modelling, conducted by calculating the balance between inputs and outputs from a pit lake. From the hydrological model, pit lake filling duration and pit lake final volume was generated and was used as a basis of analysis in determining water infrastructure requirements and post-mining land-use planning. Water recovery in a pit lake should have a greater inputs than outputs to ensure a surplus and the pit lake will be filled eventually. A water quality model was also developed using PHREEQC to analyse annual pit lake water quality until the end of the filling period, which includes the geochemical impact of the exposed mining seam. The model was supported by exposed lithological data combined with rainwater and groundwater quality, generating stratified water quality in the pit lake.

Two scenarios were conducted as an alternative for pit lake filling method. The first scenario relied on direct precipitation only. Rainfall data series of 16 years were collected from a local ground station. Around

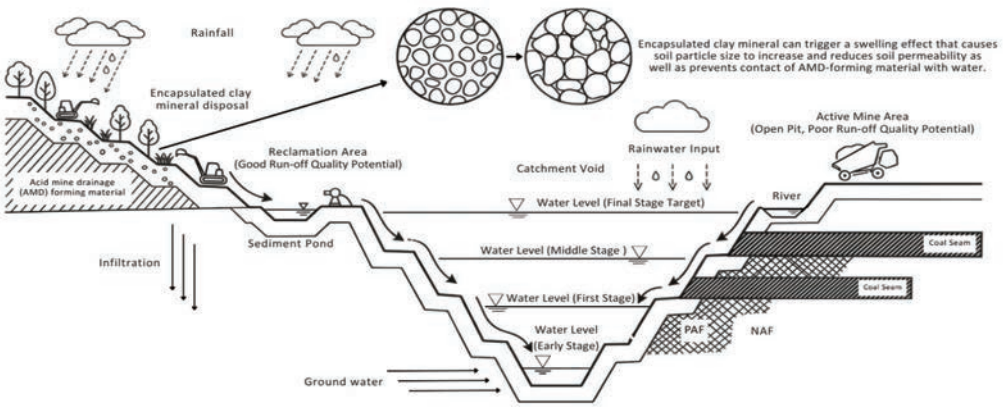

Figure 1 Pit lake modelling concept illustration.

East Kalimantan, Indonesia, the climate type based on Schmidt-Ferguson classification was considered as type A, which is a tropical rainforest area with a really wet character with annual rainfall around 1.935 to 3.733 mm/year. The second scenario of pit lake filling method included river diversion as an additional inflow that allows faster pit lake filling duration which is favorable by the company since backfilling is impractical to reclaim a large void and complete backfilling is not feasible because coal mining creates a material deficit. Evapotranspiration rate using Penman method was also accounted as an output for the water-balance model. The climatology data from Sultan Aji Muhammad Sulaiman Sepinggan International Airport meteorological station was used, resulting in a monthly evapotranspiration rate ranged between 4.49 to 6.79 mm/day.

Results and Discussion

This study focuses on one of two mining blocks at a coal mine company in East Kalimantan, Indonesia, and mainly on one examined void. The assessed void was the biggest one, reaching the depth of 292 m, with a partial backfilling conducted on the northern side of the void. There was a nearby river that had the potential to be an additional input in filling the void, allowing the increase in water inflow that could shorten the pit lake filling period. This strategy could be considered as controlled flooding management, as applied in other international mining practices.

Based on hydrological analysis using the NRECA method in Figure 2, monthly runoff discharge and reliable river discharge (Q_{80}) were estimated to represent dependable water availability throughout the year using the same rainfall data from a nearby airport. The Q_{80} discharge was selected as it reflects flow conditions that can be maintained with 80% reliability and is widely used in water resource planning to ensure supply sustainability without compromising environmental requirements (McMahon & Adeloye, 2005; Smakhtin, 2001). To maintain the hydrological balance, only 30% of the river discharge was allocated for pit lake filling, while the remaining flow was preserved within the natural river. This approach aligns

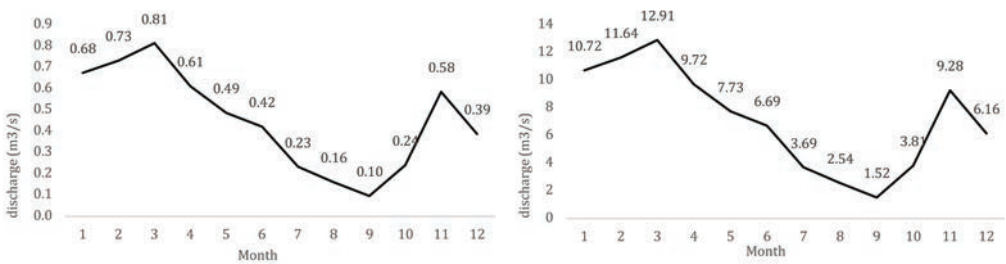

(a) Local catchment runoff discharge (b) River discharge

Figure 2 *Comparison of Flow Discharge Calculations Using NRECA Method.*

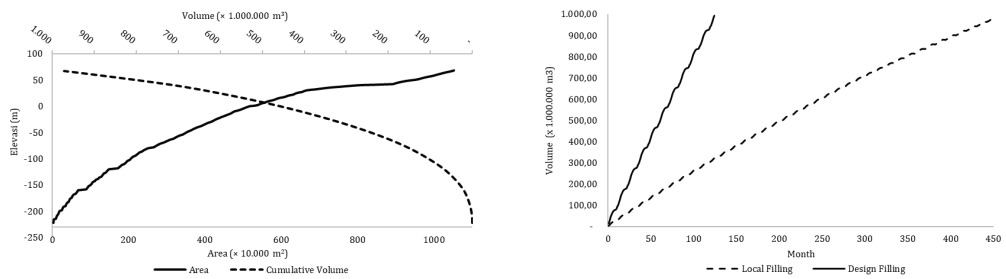

(a) Area-storage capacity curves (b) Filling duration chart

Figure 3 *Area-storage capacity curves and Filling duration chart.*

with environmental flow principles, which emphasize the need to maintain sufficient natural flow to sustain aquatic ecosystems and downstream water users (Acreman & Dunbar, 2004; Poff *et al*., 2009).

The void has a surface area of 10.56 km², with a base elevation of −222 m and a crest elevation of 68 m, resulting in a total storage capacity of approximately 982,602,164 m³. Based on modelling results, two filling scenarios were evaluated. Under the first scenario, relying solely on local catchment runoff, the pit lake would require approximately 450 months (37.5 years) to reach full capacity. In contrast, the second scenario, the local catchment inflow was supplemented by water diversion from the nearby river, significantly reduces the filling duration to approximately 124 months (10.3 years). The storage capacity curve of the void can be seen in Figure 2a and the filling curves for each scenario are presented in Figure 2b.

In Indonesia, mining companies are required to hold a specific legal document known as a mining business permit, which includes mining exploration business permits and mining production operation business permits. The maximum duration for both types of permits is stipulated in Government Regulation of the Republic of Indonesia No. 96 of 2021, which is also determined based on a feasibility study previously approved by the minister. For a coal mining company, mining exploration business permits is limited up to 7 years and mining production operation business permits is limited up to 20 years. On the other hand, mining companies are also required to prepare a post-mining plan document. This document must be approved by the national authorities, such as the Ministry of Energy and Mineral Resources, and companies must already have it approved no later than 2 years before the end of the mining operation period. In this document, the maximum duration of the post-mining period is not explicitly specified but is aligned with the company's post-mining plan. However, this duration is tied to the company's responsibilities. The sooner the post-mining period ends—provided the success criteria have been met—the company's responsibilities regarding that area are considered fulfilled. The Ministry of Energy and Mineral Resources will verify whether the reclamation has been completed. Once the reclamation is confirmed to meet the required criteria, the reclamation guarantee will be paid back.

Hydrological engineering, as the primary aspect analyzed in this study, also plays a role in the development of the company's strategy for complying with regulations regarding these post-mining obligations. Based on the hydrological analysis described above regarding the reduced duration of void filling, the post-mining period for which the company is responsible will automatically be shortened as well. This provides benefits such as reduced daily operational costs, reduced potential AMD generation through limiting the presence of oxygen to an exposed sulfide material (Younger, 2002), and also accelerates the utilization of water bodies for the local community.

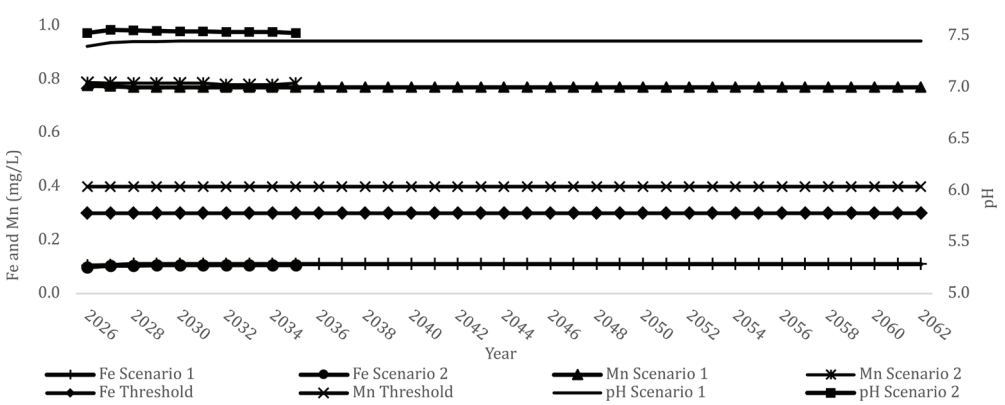

Figure 4 *Water quality prediction for scenario 1 and 2.*

The results of the pit lake water quality model generated from PHREEQC are shown in Figure 3, showing the model for two scenarios on pH, iron (Fe), and manganese (Mn) concentration. These parameters were selected according to Minister of Environment Decree No. 113 of 2003 concerning Wastewater Quality Standards for Coal Mining Businesses and/or Activities. Meanwhile each of the thresholds were selected according to Republic of Indonesia Government Regulation Number 22 of 2021 concerning lake water quality standards for Class I water quality standard, which can be utilized as raw water for drinking water, and/or other uses. The threshold for pH is 6 – 9, Fe concentration is 0.3 mg/L, and Mn concentration is 0.4 mg/L. Based on the model, pH and Fe concentration during the filling period complied within the threshold, meanwhile Mn concentration remained above the quality standard, averaged in 0.77 mg/L. Therefore, water treatment is needed to make sure the pit lake could be utilized properly in the future.

Beyond hydrological recovery and water quality model, the study evaluates potential post-mining land uses, including industrial zones, agroforestry, renewable energy development, and urban expansion. These opportunities highlight the need to integrate hydrological modeling with long-term spatial, social, and economic planning. Although deep mining voids present serious technical and environmental challenges, they also offer opportunities to reimagine post-mining landscapes as multifunctional assets that contribute to a regional development that is environmentally and economically sustainable.

The allocation of water during the void/pit lake filling process is closely linked to the dynamic evolution of land use, which develops progressively in line with increasing water volume and water level, as illustrated in Figure 4. In the early stage, when water volume and elevation remain relatively low and unstable, water utilization is primarily focused on basic functions that support land conservation and ecosystem recovery, such as vegetation irrigation (agroforestry) and dust control. This approach aligns with the principle that the initial post-mining phase should prioritize biophysical stabilization and the control of environmental degradation (McCullough & Lund, 2006). As the system progresses into the first stage, with increasing water volume and the emergence of initial hydrological input, water allocation is gradually expanded to support biodiversity enhancement and the early development of land-based tourism, providing ecological water usage and begins to accommodate socio-economic needs, albeit at a limited scale. In the middle stage, as storage capacity and water levels increase significantly and become more stable, water utilization evolves toward productive, water-based activities such as freshwater aquaculture, as well as environmental education and food security

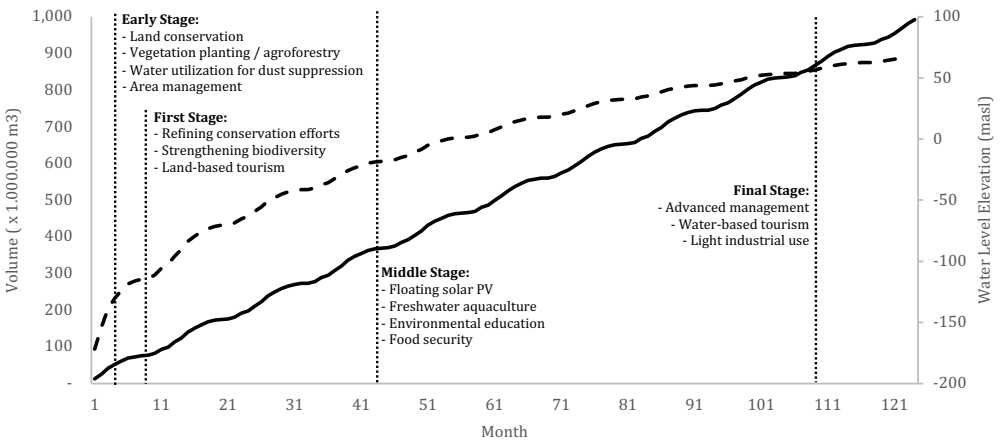

Figure 5 *Land-use recommendations based on water level, volume, and filling duration design.*

functions. This stage represents a transition from rehabilitative functions to sustainable productive uses, where the water body begins to serve as an economic resource without neglecting ecological considerations (Schultze *et al.*, 2010).

Finally, in the final stage, when long-term hydrological stability is achieved and water levels approach their maximum elevation, water allocation is optimized for higher-value activities such as floating solar photovoltaic (PV) systems and water-based tourism and light industrial use. At this stage, the integration of environmental, economic, and social functions becomes more pronounced, reflecting a multifunctional landscape approach in post-mining pit lake management (McCullough *et al.*, 2009). Through this staged framework, pit lake utilization can be progressively optimized from the initial filling phase to full capacity, ensuring sustained and evolving benefits ranging from fundamental ecological functions to more complex socio-economic applications.

Conclusion

This study demonstrates that the integration of hydrological analysis, water quality modeling, and post-mining land-use planning is an effective approach for optimizing the management of voids into sustainable pit lakes. Analysis results using the NRECA method indicate that utilizing 30% of the river's 80th percentile flow (Q_{80}) can significantly reduce the void filling duration from 37.5 years to 10.3 years without disrupting the downstream ecosystem balance. Moreover, water quality modeling shows that pH and Fe parameters met the national quality standards, while Mn concentrations still require further treatment. This hydrological approach is also expected to showcase a need in either passive or active treatment of pit lake water.

This hydrological engineering strategies also helped the company for complying with regulations regarding post-mining obligations. Through this approach, the responsibility of the company to realize the post-mining phase will be shortened in time, also providing benefits such as reduced operational costs and achieving stable, safe, and self-sustaining mine conditions more quickly. Furthermore, a phased approach to water allocation enables the progressive optimization of pit lake functions, ranging from ecological conservation to more complex economic and social uses. This study initiates the idea that post-mining voids have the potential to be developed into multifunctional landscapes that not only support environmental restoration, but also provide sustainable benefits for regional development. This study confirms that pit lake filling duration can be accelerated when additional input, such as river diversion, is used.

Acknowledgements

The authors acknowledged PT Ganeca Environmental Services, for providing access and unlimited opportunities to learn from this project. Appreciations are also extended for the specialists involved in developing the post-mining plans.

References

Acreman, M., & Dunbar, M. J. (2004). Defining environmental river flow requirements - A review. Hydrology and Earth System Sciences, 8(5), 861–876. https://doi.org/10.5194/hess-8-861-2004

Bunn, S. E., & Arthington, A. H. (2002). Basic Principles and Ecological Consequences of Altered Flow Regimes for Aquatic Biodiversity. Environmental Management, 30(4), 492–507. https://doi.org/10.1007/s00267-002-2737-0

Castendyk, D., & Webster-Brown, J. (2007). Sensitivity analyses in pit lake prediction, Martha mine, New Zealand 2: Geochemistry, water–rock reactions, and surface adsorption. Chemical Geology - CHEM GEOL, 244, 56–73. https://doi.org/10.1016/j.chemgeo.2007.06.005

McCullough, C. D., Hunt, D., & Evans, L. (2009). Sustainable development of open pit mines: Creating beneficial end uses for pit lakes. In Castendyk, D.N., & Eary, L.E. (eds) Mine pit lakes: characteristics, predictive modelling, and sustainability. Society for Mining, Metallurgy, and Exploration.

McCullough, C. D., & Lund, M. A. (2006). Opportunities for Sustainable Mining Pit Lakes in Australia. Mine Water and the Environment, 25(4), 220–226. https://doi.org/10.1007/s10230-006-0136-0

McMahon, T. A., & Adeloye, A. (2005). Water Resources Yield. Water Resources Publications.

Poff, N. L., Richter, B. D., Arthington, A. H., Bunn, S. E., Naiman, R. J., Kendy, E., Acreman, M., Apse, C., Bledsoe, B. P., Freeman, M. C., Henriksen, J., Jacobson,

R. B., Kennen, J. G., Merritt, D. M., O'Keefee, J. H., Olden, J. D., Rogers, K., Tharme, R. E., & Warner, A. (2009). The ecological limits of hydrologic alteration (ELOHA): a new framework for developing regional environmental flow standards. Freshwater Biology, 55(1), 147–170. https://doi.org/10.1111/j.1365-2427.2009.02204.x

Richter, B. D., Baumgartner, J. V, Powell, J., & Braun, D. P. (1996). A Method for Assessing Hydrologic Alteration within Ecosystems. Conservation Biology, 10(4), 1163–1174. https://doi.org/https://doi.org/10.1046/j.1523-1739.1996.10041163.x

Schultze, M., Pokrandt, K.-H., & Hille, W. (2010). Pit lakes of the Central German lignite mining district: Creation, morphometry and water quality aspects. Limnologica - Ecology and Management of Inland Waters, 40(2), 148–155. https://doi.org/10.1016/j.limno.2009.11.006

Smakhtin, V. U. (2001). Low flow hydrology: a review. Journal of Hydrology, 240(3), 147–186. https://doi.org/https://doi.org/10.1016/S0022-1694(00)00340-1

Younger, P. (2002). Mine water pollution from Kernow to Kwazulu-Natal: Geochemical remedial options and their selection in practice. Geoscience in South-West England, 10, 255–266.

Hydrogeological significance of a buried polje on dewatering of karst aquifers for a diamond mine in Northern Ontario, Canada

Wanfang Zhou

Hana Engineers and Consultants, LLC., United States of America
wanfang.zhou@hanaengineers.com

Abstract

A series of diamond-bearing kimberlite pipes were emplaced through Paleozoic carbonates during the Jurassic Period in the peatland of Northern Ontario, Canada. One of these kimberlite pipes was mined using a 220-m deep open pit. Borehole drilling and geophysical surveys were conducted during diamond exploration and feasibility study and revealed a unique geologic feature that abutted steeply the northeast side of the kimberlite. The geologic feature encompassed an area of approximately 3 km^2 and cut through most of the carbonates to a depth of at least 250 m. Because dissolution of the carbonate rocks created karst aquifers characterized with sinkholes, caves, and voids in the study area, this geologic feature was likened to an internally drained karst polje, although its formation mechanism was unknown. Because the polje could potentially provide a vertical pathway through which the karst aquifers were hydraulically connected, it was recognized as an essential component in the hydrogeological conceptual site model, and understanding of its hydrogeological properties was critical for predicting groundwater flow, designing dewatering wells, and mitigating water related risks.

Detailed sediment coring from boreholes indicated that the polje was filled with unconsolidated materials including glacial diamictons at the bottom, glaciolacustrine silt and sand in the middle, and silt and clay with fine lamination at the top. Such a deposition sequence was indicative of gradual infilling of the polje. Two constant-rate pumping tests, one 4-day test at 1,830 m^3/day and one 60-day test at 16,350 m^3/day, were conducted in the primary karst aquifer. The log-log plots of drawdown data in monitoring wells installed in the polje followed the classic Theis curves for porous-medium aquifers with minor deviations. No evidence was observed to suggest strong hydraulic connections between the polje and the karst aquifers. Calibration of a numerical groundwater flow model to the 60-day pumping test data resulted in average horizontal and vertical hydraulic conductivities of 0.01 and 0.001 m/day, respectively, for the polje deposits, which were orders of magnitude less than the average hydraulic conductivity of 5 m/day for the karst aquifers. The pumping test and modeling results suggested that the polje was not an impactful pathway for groundwater flow, and the lack of hydraulic connections between karst aquifers was also supported by groundwater geochemistry data that showed a stratification pattern in the polje deposits.

Multiple lines of evidence suggested that the hydrostratigraphic complexities of the buried polje would not have substantial effects on mine dewatering effectiveness and would not pose substantial risks to mining-induced water hazards by functioning as a preferential flow path, as proved by successful operations of the open pit mine for approximately 12 years.

IMWA 2026
Jeongseon

Integrating Geochemical and Hydro(geo)logical Modelling to Predict Long-Term Water Quality in Pit Lakes

Ziukelis, L.A*., Colston, R.E.[1] & Robinson, J.R.[2]

SLR Consulting Ltd, Summit House, 12 Red Lion Square, London, WC1R 4QH

**Corresponding Author: lziukelis@slrconsulting.com*

[1]ORCID: 0000-0002-1876-3474. [2]ORCID: 0000-0001-5218-4321

Abstract

Developing reliable predictions of water quality in post-mining pit lakes supports long-term environmental protection and helps determine whether water reuse schemes are feasible. Integrating hydro(geo)logical and geochemical modelling provides robust predictions of future water quality and helps identify treatment options that support closure objectives. By coupling two industry-leading modelling software packages, GoldSim and PHREEQC, a comprehensive framework has been developed to assess long-term water quality and guide effective, sustainable solutions, that protect water resources during the transition to post-mining land use.

Introduction

SLR Consulting Ltd (SLR) was appointed to provide geotechnical and hydro(geo)logical support to a client redeveloping a site within a mining-legacy area in Europe. The site includes a pit lake, which will be pumped out and enlarged to support a hydroelectric power plant (HEP). This project is subject to non-disclosure agreements, therefore no mention of the site is made herein, and diagrams do not represent the actual site. This modelling study used data gathered as part of the Environmental Impact Assessment (EIA) and historic data collected during operation and closure.

This paper discusses geochemical and hydro(geo)logical modelling to predict the fill rate and water quality of the new pit lake referred to as the 'Lower Reservoir'. This long-term prediction enables assessment of the scaling and corrosion risk to HEP impellers and discharge water quality to maintain the operational water balance. The modelling required the integration of individual technical components (surface water, groundwater, climate and geochemistry) using a GoldSim model, which was adapted to include the geochemical modelling software, PHREEQC. The approach and dependencies of each technical element are presented in Figure 1. This approach can be adapted to specific site or project requirements.

Methodology

A desk-based review of previous historic site studies and environmental impact assessments supported development of a conceptual model for the site (Figure 2), from which source terms (inputs) for the hydro(geo)logical and geochemical model were defined. Data used in the model included primary sources collected during SLR's field work (environmental monitoring) and historic data from previous studies. A strong conceptualization of the site hydrodynamics (above and below ground) is fundamental for accurate predictive modelling.

GoldSim is an industry-leading Monte Carlo simulation software for dynamically modelling complex systems for mining projects and other hydrochemical systems (GoldSim Technology Group, 2026) (GoldSim Technology Group, 2026). GoldSim supports decision-making and risk analysis by simulating future performance while quantitatively representing the uncertainty and risks inherent in all complex systems associated with pit lake closure situations.

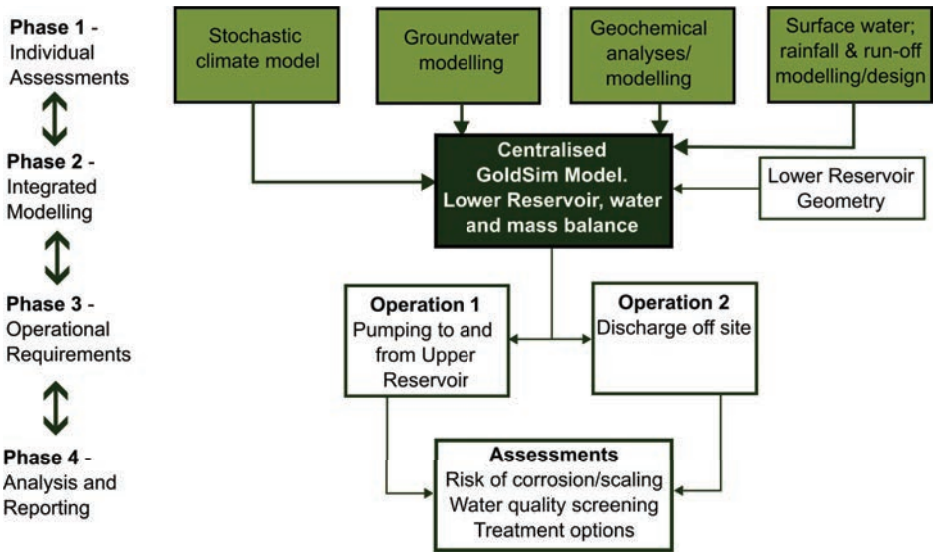

Figure 1 *Integrated modelling approach, adapted from (Robinson, Klimczak and Smyth, 2023).*

Monte Carlo methods are especially useful for simulating systems with many coupled degrees of freedom, such as water. To model the complex chemical processes of equilibration, speciation and sorption, GoldSim's external element with dynamic link library (DLL) was used to communicate with a PHREEQC script and extension (Eary, 2007) and more recent updates in 2018 (Johnson, Rohal and Eary, 2018). PHREEQC stands for 'pH-redox-equilibrium', developed by the US Geological Society to simulate chemical reactions and transport processes (Parkhurst and Appelo, 2013). It has been widely used to predict chemical species, mineral solubility, redox equilibrium and reactive transport. PHREEQC can be linked to a variety of thermodynamic databases, which inform the chemical processes undertaken in PHREEQC. In this exercise, the Wateq4F.dat database was used as it is a comprehensive database for low-temperature geochemical processes.

An iterative approach for both models was adopted, to calibrate and check for errors in the model's function and dynamically link between them. The model was developed with built in flexibility to system changes, as data is collected with subsequent site investigations. The DLL was written using C++ coding language and compiled with Microsoft Visual C++ Studio. This approach has the advantage of providing a generalized procedure to model complex chemical processes at each time step.

Conceptual Site Model

The site lies within a limestone formation in which barite was extracted by open-cast mining. Sulfide deposits were also mined underground for zinc, lead and nickel ore, and these are hosted in a dolomitised zone beneath the limestone formation. The current pit geometry sits within the limestone bedrock (Lithology 1, Figure 2). Historic maps of the area showed several surface water channels draining towards the pit prior to mining. The understanding at the beginning of the project was that upstream drainage had been culverted and channelled around the open pit. However, SLR's site investigation proved one surface water input had formed, which helped determine accurate hydrological catchments alongside topographical data from LiDAR surveys. The groundwater is understood to follow the topography within the site, going from south to north. No groundwater studies have been conducted in recent history post-2000. SLR has plans to conduct a detailed ground investigation in which groundwater assumptions can be tested. Groundwater flows into the pit and is either discharged through a surface water point or as seepage.

Historic mine waste dumps are located upstream, within which massive sulfide has been observed (Figure 2). Further assessment of these dumps is needed to understand the longevity of any potential source material. Current monitoring includes runoff from the mine waste dumps. The proposed geometry for the HEP reservoirs is shown in Figure 2. The lower reservoir will be developed further underground from the existing pit lake and will expose the dolomitised, sulfide ore body (Lithology 2). There has been limited geochemical characterisation of the lithologies and waste dumps exposed on site, and it has been recommended that more detailed geochemical analysis be undertaken to test the surface water inputs used in the current model.

Source Definition and Hydro(geo)logy Modelling Results

The current conceptual site model and data available has been used to populate the GoldSim and PHREEQC models. There are planned site and ground investigations to test the assumptions made in this initial modelling.

Water Inputs/Outputs

Rainfall and Evaporation

Direct rainfall to the water surface is a small but important part of assessing the long-term water quality. In addition, the gaseous exchange between the water level surface and the atmosphere will influence the long-term water chemistry. Rainwater chemistry was ascertained by sampling the rain gauge on site and analysing for a range of parameters. Local climate data has been used for the evapotranspiration from the water surface.

Surface Water (including contact water)

As part of the EIA, monthly surface water samples were collected, including water levels of the existing pit lake. Observed site rainfall runoff behaviour was used to inform surface water inputs to the pit lake. The upstream water quality in catchments discharging to the pit lake have been averaged for input chemistry at this stage, it is assumed these represent long-term water quality from contact with mine waste dumps. As the model progresses, the monthly water quality measurements will allow GoldSim to select monthly surface water chemistry through each timestep to account for variability in surface water quality.

Groundwater

At the time of writing, SLR has not collected groundwater data or geochemical data of Lithology 1 and Lithology 2. The geochemical characterisation of the host lithologies are scheduled in future works using static and kinetic testing to understand and predict the long-term groundwater quality from them. Therefore, groundwater flow and chemistry from historical studies between

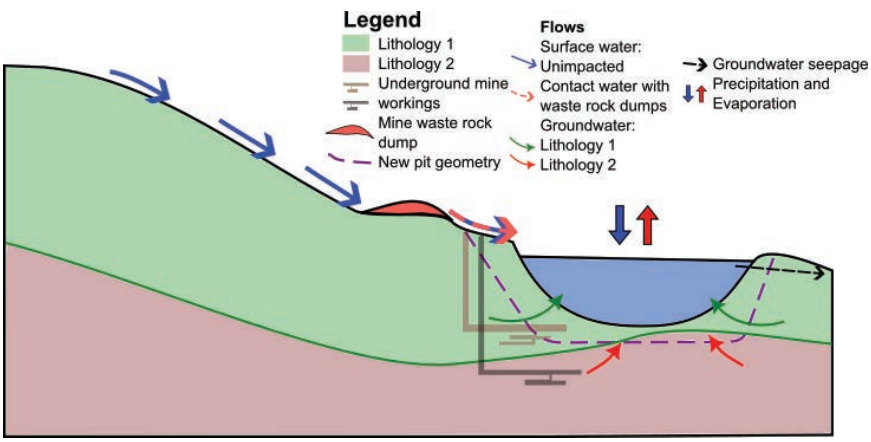

Figure 2 *Conceptual site model, dashed line represents Lower Reservoir geometry.*

1997 and 2001 have been used to develop the model. The new reservoir geometry has been imposed onto the geological model for the site, which will expose Lithology 2 (Figure 2). SLR's planned ground investigation will validate and update the assumptions made in the modelling process so far.

Results

To model the dynamic hydro(geo)chemical processes, a calibration model for the water level using the hydro(geo)logical inputs discussed above was developed, versus the measured pit lake water levels. This provides an opportunity to update inputs that support observed water levels whilst awaiting more site-specific data. Further, a static geochemical model was created to understand the hydro(geochemical) processes within the pit lake currently occurring. These findings helped inform the initial set up of the working GoldSim-PHREEQC model.

Calibration Model

Using the groundwater inflow rates from the historic groundwater studies, results of the calibration showed a large overestimate in pit water level, leading to a rapid water level rise relative to the rate observed on site. As a result, the groundwater inflows were reduced by between 30% and 45% for summer groundwater inflows and 80% to 85% for winter groundwater inflows. In addition, runoff rates within the upstream catchment were lowered. These new groundwater inflows resulted in a better fit for modelled water levels compared to measured water levels between July 2024 and March 2025 (Figure 3). This highlights the importance of obtaining hydrodynamic data for the site which is ongoing at the time of writing.

Static Geochemical Model

The water quality inputs were mixed and equilibrated in PHREEQC using a mixing ratio determined from the calibration model. The resultant chemistry was compared with SLR's measured chemistry of the pit lake. This indicated several modelled metals/metalloids elevated above their baseline concentrations and exceeding general acceptance criteria (GAC) for the site. The GAC at this stage, uses local regulatory water quality standards. Review of the saturation indices showed iron hydroxide minerals were super-saturated. Iron hydroxide was allowed to precipitate, and the mass of precipitate formed was calculated using the change in iron (II) and stoichiometric principles. This mass of precipitated iron hydroxide was used in PHREEQC's sorption command. The water chemistry after precipitation of, and sorption with, iron hydroxides was akin to the measured pit lake chemistry. To test this modelling step, SLR plan to sample sediments in the pit lake to validate the step further. An additional consideration is the stratification

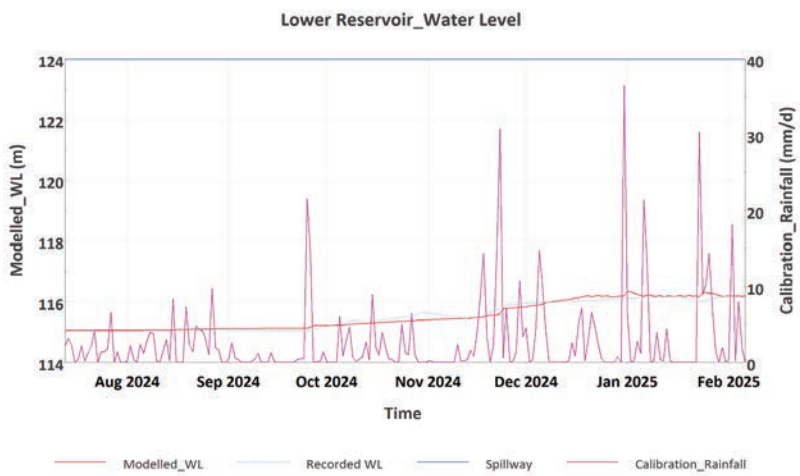

Figure 3 *Calibrated Lower Reservoir Water Level.*

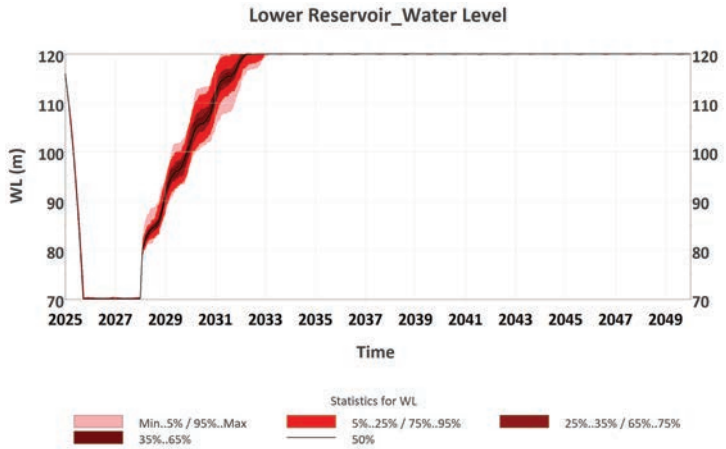

Figure 4 *Lower Reservoir Filling Rate, WL = Water Level.*

of the pit lake. SLR conducted conductivity, depth, temperature surveys on three locations within the pit lake. This showed no stratification within the pit lake and has not been considered further at this stage.

Water Balance

The water levels in the Lower Reservoir were modelled based on the stage-storage curve provided by the client, local rainfall data and calibrated groundwater/runoff flows, modelled on a daily time step (allowing unscheduled sub-daily timesteps in GoldSim where needed). A number of operational phases were modelled in the lower reservoir to simulate HEP operations. The new reprofiled and lined pit comes online in 2028, with groundwater outflows and seepage removed. The pit rebounds over a period of 4-5 years and reaches the new spillway depth, intermittently spilling and lowering below the spillway level. The water level and rebound rate was used to inform geochemistry concentrations and operational pumping rates. The spillway volumes were calculated by the model and would be used to inform the viability of passive wetland systems downstream of the reservoir.

Water Quality

At each timestep of the water balance model the mass balanced chemistry was exported from GoldSim into the PHREEQC model, to equilibrate, precipitate and sorb. It was found that pumping between the Lower and Upper Reservoirs by-passed areas of the PHREEQC export, leading to chemical concentration build up within the water balance, which was not realistic. As a result, the water balance between the Lower and Upper Reservoirs was considered a single cell to communicate with PHREEQC. The chemical equilibrium for major ions is reached by 2035. The pH at equilibration is roughly 7.1 in the sorbed model, compared to 6.1 from the GoldSim model and 8.5 after equilibration. Alkalinity stabilises at roughly 85 mg $CaCO_3$/L after sorption. Chloride was also modelled as a hydrochemical check on the model due to its conservative nature and showed no changes in any modelling step.

The lead concentrations across all three outputs are presented in Figure 5. The lead concentration does not change between the GoldSim output and the equilibrated chemistry and exceeds the GAC. After the precipitation of iron hydroxides and sorption, the lead concentration is several orders of magnitude lower and now below the GAC as observed in the static model. In comparison, zinc (Figure 5) decrease slightly after sorption, but not enough to fall below the GAC. This indicates there is a risk zinc will exceed the GAC in discharge from the site, highlighting that more detailed risk assessment is required. Further, it allows for a suitable treatment options study to be defined. This also provides evidence for local

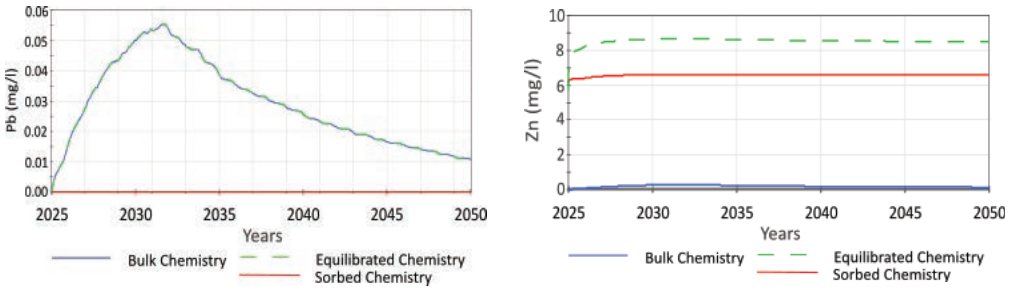

Figure 5 Modelled chemistry trends for the HEP Water Balance.

permitting requirements which provides rationale to exclude lead or other metals/metalloids in permitting requirements, as they have been shown to be removed by geochemical processes in the pit lake.

Scaling and Corrosion Assessment

As part of the phase 3 assessment of the model outputs, a preliminary assessment of the risk of corrosion and scaling to the HEP impellers was conducted. This used the long-term average of the modelled water quality of the HEP water balance. This is widely used across materials assessments and risks based on environmental conditions (Singley, 1981; Roberge, 2007) and will help identify whether corrosion or scaling is a long-term risk.

These indexes assess the likelihood of carbonate scaling or dissolution (Langelier-Saturation Index (LSI, (Langelier, 1936)), Ryznar Stability Index (RSI, (Ryznar, 1944)), Puckorius Scaling Index (PSI, (Puckorius and Brooke, 1991))) and corrosion (Riddick Index (RI, (Riddick, 1941)) and Larson-Skold Index (LSI, (Larson and Skold, 1958))). These indices are founded on either laboratory experiments or site-specific studies such as the Larson-Skold Index, which has been developed using the corrosion potential of waters from the Great Lakes (Roberge, 2007). Results show the modelled water quality will dissolve carbonate scaling i.e. the LSI (-1.37), RSI (9.85) and PSI (9.62). The risk of corrosion based on the model outputs to date indicates the potential for corrosion is unlikely.

Conclusion

A robust modelling approach has enabled prediction of the long-term water balance and water quality for a planned redevelopment of a legacy mining site. The outcomes will help define operational limits for the HEP operators. The dynamic chemical modelling results show that several parameters exceed the GAC when a mass balancing approach was used. The field observations informed the modelling approach, indicating sorption of chemical species was needed within the model. This step reduces the list of potential contaminants based on the mining legacy alone. This can be used to inform the development of passive treatment options.

The modelling approach has assisted in developing the conceptual understanding of the site without detailed site investigations at the prefeasibility stage of the project. This helps inform the site and ground investigations needed to validate and test the assumptions made in the model. An iterative modelling approach allows new data to be input to the model structure to improve the outputs.

References

Eary, T. (2007) "Linking GoldSim with the PHREEQC Geochemical Model with a Dynamic Link Library Element GoldSim 2007 User Conference, San Francisco," in. San Francisco: GoldSim User Conference.

GoldSim Technology Group (2026) GoldSim, GoldSim User's Guide. Available at: https://www.goldsim.com/Web/Customers/Education/Documentation/ (Accessed: March 9, 2026).

Johnson, B.C., Rohal, P. and Eary, T. (2018) "Coupling PHREEQC with GoldSim for a More Dynamic Water Modeling Experience," in Wolkersdorfer, C. *et al*. (eds) 11th ICARD | IMWA | MWD Conference – "Risk to Opportunity". IMWA, pp. 1081–1086.

Langelier, W.F. (1936) "The analytical control of anti-corrosion water treatment," American Water Works Association, 28(10), pp. 1500–1521.

Larson, T.E. and Skold, R.V. (1958) "Laboratory studies relating mineral quality of water to corrosion of steel and cast iron," Corrosion, 14(6), pp. 285–288.

Parkhurst, D. and Appelo, C. (2013) Description of Input and Examples for PHREEQC Version 3-A Computer Program for Speciation, Batch-Reaction, One-Dimensional Transport, and Inverse Geochemical Calculations. Available at: http://www.hydrochemistry.eu (Accessed: March 9, 2026).

Puckorius, P.R. and Brooke, J.M. (1991) "A New Practical Index for Calcium Carbonate Scale Prediction in Cooling Tower Systems," Corrosion, 47(4), pp. 280–284.

Riddick, T.M. (1941) "Notes on Current Corrosion Problems," American Water Works Association, 33(5), pp. 903–907.

Roberge, P.R. (2007) "Appendix B," in Corrosion Inspection and Monitoring. Wiley, pp. 373–376. doi:10.1002/9780470099766.app2.

Robinson, J., Klimczak, P. and Smyth, N. (2023) "An innovative approach to accommodate the draft National Mine Closure Strategy in South Africa by predicting pit lake water quality and generating a post closure resource using passive treatment," in Proceedings of the International Conference on Mine Closure. Australian Centre for Geomechanics. doi:10.36487/ACG_repo/2315_003.

Ryznar, J.W. (1944) "A new index for determining amount of calcium carbonate scale formed by a water," American Water Works Association, 36(4), pp. 472–483.

Singley, J.E. (1981) "The search for a corrosion index," Journal AWWA, 73(11), pp. 579–582. doi:10.1002/j.1551-8833.1981.tb04802.x.

IMWA 2026
Jeongseon

Mine Water Sharing for Sustainable Water Security - A Strategy for a Water-Scarce Region

John Ngoni Zvimba[1], Pieter Holtzhausen[2], Kym Morton[2]

[1]*Water Research Commission, South Africa*
[2]*KLM Consulting Services Pty Ltd, South Africa*

Abstract

The study investigated mine water sharing as a strategy to address water scarcity in Rustenburg, South Africa. Active and abandoned mines store water creating subsurface reservoirs that supplement municipal, agricultural, and mining demands thereby supporting economic development. The research developed a legally aligned, implementation framework supported by stakeholder engagement, hydrochemical analyses and hydrogeological modelling. Results show most mine water requires minimal treatment, with hardness and nitrates as primary concerns. Numerical models estimated sustainable yields and a prioritisation tool identified high-potential areas. A case study and financial analysis will confirm feasibility and then support replication across other mining regions.

Keywords: Water scarcity, mine water sharing, underground reservoirs, water-scarce region, modelling

Introduction

South Africa has a rich heritage of over 150 years of deep mining across all provinces. The Rustenburg area, northwest and west of the main industrial areas of Johannesburg and Pretoria, has been mined for Chrome and Platinum since the 1950's. Mining creates underground and surface voids, which then fill with water, creating new underground reservoirs, aka aquifers and surface storage.

The Rustenburg region of South Africa is water-scarce with a fast-growing population, and numerous socio-economic and infrastructural challenges undermine equitable, reliable access to high-quality water. Seasonal rainfall variability and aging infrastructure (RLM 2022) exacerbate these issues. Within the region, active Chrome and Platinum mines generate excess water that requires safe management or disposal. Moreover, closed underground workings create underground mine voids and storage zones that are not depleted by evaporation. These mine voids present an untapped opportunity to augment supplies for nearby communities and water-stressed sectors such as agriculture and other mining operations. Their incorporation into the regional water supply will reduce demand on an overstretched municipal supply system. This study, funded by the Water Research Commission of South Africa, is investigating how this unused asset can be integrated in a regional water supply and conservation strategy.

Figure 1 shows the area of the study, comprising parts of four quaternary catchments in the Rustenburg and Madibeng Local Municipalities, and the geology. Figure 2 shows the mines in the area and their proximity to villages and towns, all of which require reliable water supply to enable them to support economic growth and generate income for the area.

Methods

This study is developing a step-by-step, implementable mine water sharing strategy aligned with local legislation. Adoption by stakeholders, including mining companies, municipalities, water authorities, and government will facilitate the sustainable distribution of excess mine water stored in abandoned workings. Successful implementation of the mine water sharing strategy requires evaluating the quality and quantity

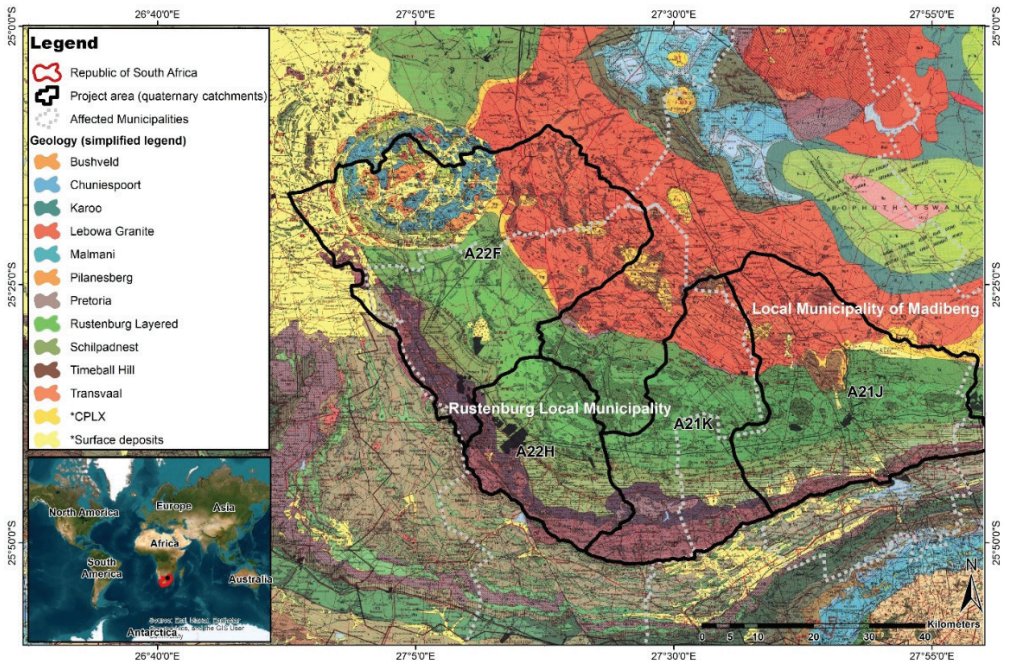

Figure 1 Location of the study area and its geology, Rustenburg, South Africa (GSSA 1981).

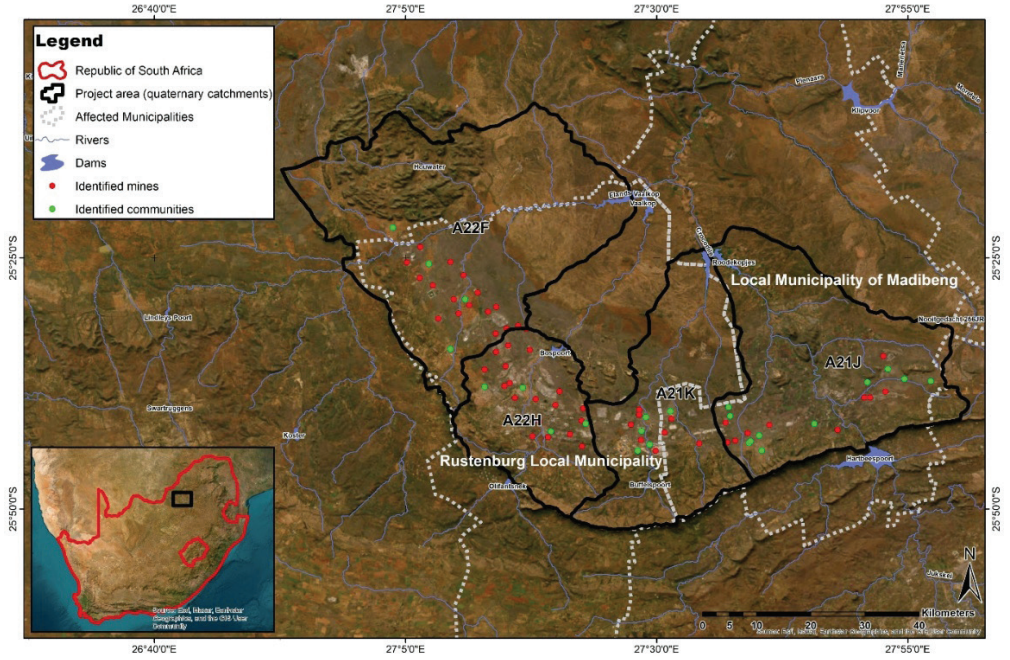

Figure 2 Mines in the study area and their proximity to villages.

of mine water, identifying potential treatment and reticulation options, and assessing local demand.

The scope of work comprised: a desk top study, stakeholder engagement, geochemical analysis, and numerical hydrogeological modelling followed by prioritisation of an area for use in a case study.

Desktop assessment

Information was collected and reviewed to support a mine water sharing strategy, understand the legal compliance requirements, and to collate the geological, hydrogeological, and other relevant environmental factors. Key national and spatial datasets were obtained including long-term meteorological records from the South African Weather Service (SAWS), topographic data, borehole records from the National Groundwater Archive, surface-water quality and quantity data from the Department of Water and Sanitation's (DWS) National Integrated Water Information System. The DWS also provided water use data and spatial data from the 2012 Water Resources of South Africa study. Literature on the geology and hydrogeology, as well as open-source data about mine water quantity and quality were also reviewed

A legislative review was done to identify statutory constraints and institutional roles for implementation. This included water needs evaluation and a review of historic augmentation efforts. The desk study also compiled an inventory and assessment of legacy, active and planned underground mine workings and their inflows, water balances and post-closure scenarios. Finally, the desk top study characterised and summarised the climate, topography, drainage, land cover, geology and hydrogeology to establish preliminary recharge estimates and hydrogeological parameters for the area.

Stakeholder engagement

A structured, top-down approach guided the stakeholder engagement process, beginning by engaging the water use authorities then municipalities, water services providers, and mining companies. On-line and in person consultations were used to introduce the project, gather feedback and sentiment, receive suggestions, and request data for the overall study.

Geochemical analysis

Mine water chemistry determines the methods used for treatment to ensure the water is fit for purpose. Open-source mine water quality data was collected and compiled into a consolidated water quality database. Water quality data was also provided by Tharisa Minerals from their active Chrome mine. Low-flow verification sampling was done at the Tharisa Mine. The quality of water being used by villages and townships was assessed through spot sampling within selected communities to identify background usage.

Piper trilinear diagrams were used to characterise and group different water types at each mine, while Stiff diagrams were used to map the water quality variations across the project area. Results were benchmarked against the South African National Standards (SANS) 241-1 2015 (drinking water) and DWS Target Water Quality Guidelines (agricultural use), to identify the need for treatment. Time-series graphs and regression models were used to identify long-term trends and to identify parameters of concern. Hardness and Nitrate were the main parameters identified as requiring reduction.

Numerical hydrogeological modelling and prioritisation

High-level numerical hydrogeological models for each catchment have been developed in a FEFLOW™ to estimate the volume of groundwater inflow and storage within the reservoirs created by mining. An Excel-based analytical water balance model was used to estimate preliminary groundwater inflows and outflows as input to the numerical models. The groundwater models included all relevant flow boundaries as translated from the desktop conceptualisation.

An Excel-based prioritisation tool was developed to weight and rate criteria to identify areas for potential sharing of water. The criteria included: proximity of source to potential water users, water quality and treatment requirements, reticulation options,

accessibility of the resources, groundwater inflow and volume stored in the potential sources, and the needs of potential recipients. The results will be used to select a high-priority area for use as a case study. The next phase will draft a step-by-step implementable water sharing strategy, apply it to a prioritised area, and then conduct an economic evaluation for the case study area to determine the financial feasibility.

Results and Discussion

Desktop assessment

The Rustenburg area is characterised by a semi-arid climate, with low, variable rainfall and high evaporation rates (SAWS 2024). The topography is diverse, with several notable drainage systems and runoff patterns that influence water availability. Geologically, the area has key structural features such as faults and dykes that influence groundwater flow. The rocks consist of a diverse set of lithologies belonging to the Pretoria Group (Transvaal Supergroup), the Bushveld Igneous Complex, and the Pilanesberg Complex. There have also been multiple phases of dyke and sill emplacement. Four main sets of faults have been identified. The most noteworthy fault set is NNW-oriented faults that parallel the Brits Graben, probably formed in an extensional regime, and can be substantial carriers of groundwater. The major natural aquifers include alluvial, shallow intergranular, and fractured systems.

The desktop assessment established the need for additional water sources. The Rustenburg (RLM) and Madibeng (MLM) Local Municipalities suffer severe water scarcity, driven by increasing demand from rapidly growing urban and rural populations. Table 1 and 2 show the population's access to water infrastructure and the reliability of the water supply in the RLM and MLM, respectively.

52% to 60% of both rural and urban populations (about 500 000 people in both areas) in the Rustenburg and Madibeng areas have reliable access to water infrastructure and reliable supplies. This water is primarily supplied by the municipality from some boreholes and three supply systems:

1. Magalies Water (Vaalkop System): This is a primary source, providing approximately 80 Mℓ (megalitres) per day to the towns and mines.
2. Rand Water (Barnardsvlei System): Supplies approximately 120 Mℓ per day to the municipality and mining sector.
3. Bospoort Dam (via Bospoort Water Purification Works): Managed by the Rustenburg Local Municipality, this source provides approximately 12 Mℓ per day.

The population is growing rapidly meaning that additional sources of water are required. Old and new mines, mainly Platinum Group Metals (PGM's) and Chrome, may provide additional storage and can be used as supplementary water supplies.

Table 1 *Population with access to water infrastructure and reliable supply in the RLM (DWS n.d.).*

Area Type	Population	Population with Water Access	Population with Reliable Supply	% Population with Water Access	% Population with Reliable Access
Rural	191 996	183 653	99 773	96	52
Urban	372 167	351 367	191 842	94	52

Table 2 *Population with access to water infrastructure and reliable supply in the MLM (DWS n.d.).*

Area Type	Population	Population with Water Access	Population with Reliable Supply	% Population with Water Access	% Population with Reliable Access
Rural	341 921	257 307	204 004	75	60
Urban	187 739	141 200	111 971	75	60

An inventory of 53 mines and mine shafts was created and their potential contribution calculated. Inflows into mines across quaternary catchments A22F, A22H, A21K, and A21J range from 100 to 4 000 m^3/d which can be used to meet domestic and industrial demand.

Several key pieces of legislation that affect the implementation of a bulk water-sharing strategy were reviewed, notably the National Water Act (1995). No legal obstacles for the implementation of this mine water sharing strategy were identified, and the mine water sharing strategy will be further developed to detail the specific legislative requirements.

Stakeholder engagement

The most complex aspect of this study is getting all the different water authorities and suppliers to contribute. The DWS provided guidance as the Competent and National Water Use Authority. RLM and MLM (local Water Services Authorities) highlighted water scarcity and infrastructure challenges. Mining companies, including Sibanye Stillwater and Implats (combined they own 75% of operations in the study area), provided operational insights. Concerns were raised regarding liability and community trust when sharing water. The Royal Bafokeng Nation (RBN), Magalies Water (a local Water Service Provider), and the South African Minerals Council offered to facilitate connections with relevant departments. Overall, these entities emphasised the need to confirm the scientific feasibility for the area to develop a mine water sharing project, before engaging farmers and communities to prevent raising false hope. The approaches to the Department of Mineral and Petroleum Resources and Rand Water (the largest bulk water supplier in Africa) have yet to yield a response.

Geochemical analysis

Hydrochemical data show that minimal treatment of mine water will be required to meet the SANS for domestic use (SABS 2015). Hardness and nitrate concentrations are the principal concerns, while trace metals were detected only sporadically. Mine water quality in the Rustenburg region can typically be classified as magnesium-bicarbonate dominant or mixed (Fig. 3). At numerous sites, samples had to be taken from pre-filled buckets, as water was not available from the taps 24 hrs a day. In communities, nitrate was

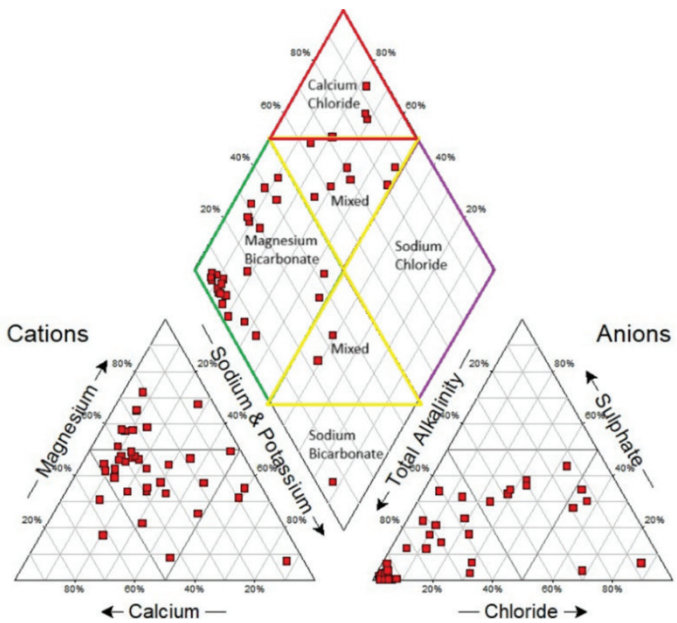

Figure 3 Typical water quality from mines in the Rustenburg project area.

identified as a parameter of concern at 71% of the sites and poses chronic health risks to domestic users. E. coli, manganese, fluoride, and turbidity posed localised risks.

Numerical hydrogeological modelling and prioritisation

The analytical water balance showed that all catchments exhibit a positive net water balance, confirming the presence of usable groundwater resources. Recharge through rainfall dominates the inflow component of the water budget, mine sites such as pits, backfilled areas, and waste rock dumps have enhanced recharge and increase water storage. The numerical model indicated a reliable and stable regional groundwater system, with a balanced water error of only 0.1%. The numerical model results show:

- Quaternary catchment A21K indicated the highest cumulative pit inflows, typically ranging between 10 000 to 30 000 m^3/day with distinct sharp peaks during high-recharge periods
- Quaternary catchment A22H indicated the highest cumulative underground reservoir inflows, stabilising at 12 000 to 13 000 m^3/day

This data will be fed into the prioritisation tool to select an area for a detailed case study.

Further Work

In the next phase, a comprehensive, step-by-step implementable mine water-sharing strategy will be developed. This will be supported by a detailed case study that conceptualises the implementation of mine water sharing within a prioritised zone. The case study will include financial models quantifying the costs and benefits over defined timeframes. Insights from the case study will be used to refine the overall strategy, promoting its implementation and potential replication across other South African mining regions.

Conclusions

Early findings conclude that it will be feasible to use water stored in old underground workings of PGM and Chrome mines to supplement the water supply to the Rustenburg area. The hydrochemistry indicates that it will require minimal treatment to meet the SANS for domestic use. Hardness and nitrate concentrations represent the principal concerns, while trace metals were detected only sporadically. Numerical modelling indicated high daily inflows into underground voids and increased storage.

We are confident that the financial modelling will show that it will be cost-effective to use mine storage water to contribute to the long-term planning for the development of the Rustenburg area. The strategy can then be applied to other mining regions world wide taking into account the hydrochemistry of each different metal mined.

Acknowledgements

We would like to acknowledge the support of the Water Research Commission under project C2024.2025-01616.

References

Department of Water and Sanitation (DWS n.d.) National Integrated Water Information System. https://niwis.dws.gov.za/niwis2/

Geological Survey of South Africa (GSSA 1981) Geological Sheet Rustenburg 2526. GSSA, Pretoria, Gauteng, RSA

Rustenburg Local Municipality (RLM 2022) Rustenburg Local Municipality 5-Year IDP 2022/2027. https://www.rustenburg.gov.za/wp-content/uploads/2022/07/IDP-2022-2027-FINAL.pdf

South African Bureau of Standards (SABS 2015) SANS 241-1:2015 Drinking water - Part 1: Microbiological, physical, aesthetic and chemical determinants. Pretoria, South Africa: SABS

South African Weather Service (SAWS 2024) Daily and Hourly Weather Data. https://www.weathersa.co.za/

Water Resources of South Africa study https://waterresourceswr2012.co.za/

IMWA 2026
Jeongseon

Exploring a New Water Economy Post Mining in a Coal Mining Region

John Ngoni Zvimba[1], Mavis Dineo Makate[2], Resego Bernice Macquela[2]

[1]*Water Research Commission of South Africa, Lynnwood Manor, Pretoria 0081, South Africa; johnz@wrc.org.za, ORCID 0000-0002-3687-7432*

[2]*Prime Africa Consult, 274A Brander Street, Jan Niemand Park, Pretoria, 0081, South Africa, d.makate@primeafrica.net; b.macquela@primeafrica.net*

Abstract

The study investigated the opportunity for a new water economy in Mpumalanga, South Africa, as coal mines close and coal-fired power generation is decommissioned. Study findings indicate that about 434 Mm^3/a of water will become available. This includes 117 Mm^3/a raw water from coal-fired power operations, 224 Mm^3/a of mining-influenced water and 93 Mm^3/a of treated municipal effluent. This water exhibits variable qualities due to mining and industrial impacts and is unsuitable for direct use without treatment. Reuse of treated water for irrigation offers the most immediate and cost-effective pathway while green hydrogen production represents a promising long-term opportunity.

Keywords: Coal mining, irrigation, green hydrogen, coal-fired power, water reuse

Introduction

For over a century, coal has driven South Africa's economic development by supporting electricity generation, industrialisation, mining, manufacturing, and urbanisation. Affordable coal-based energy has enabled economic growth and employment but also contributed to significant environmental and water management challenges including structural dependence on coal-based energy systems (Staffell *et al.*, 2019).

Mpumalanga plays a central role in South Africa's coal economy, producing most of the country's coal and hosting the majority of coal-fired power stations. This coal-dependent development pathway has supported economic growth, employment, and infrastructure but increased resource dependency and environmental pressures, particularly on water resources. As South Africa transitions from coal, the province faces major economic, social, and environmental restructuring challenges.

Water is central to Mpumalanga's coal-based economy, as coal mining and coal-fired power generation require substantial volumes for mining, beneficiation, dust suppression, cooling, and emissions control. Historically, extensive surface water, groundwater, and inter-basin transfers supported these activities, increasing long-term dependence on imported water and altering natural hydrological systems.

Mining-influenced water (MIW) is among the most significant and persistent environmental legacies of coal mining in Mpumalanga, posing long-term risks to water quality, ecosystem health, and sustainable water resource management. However, several studies have demonstrated that a number of treatment technologies, sustainable management strategies and regulatory measures addressing the magnitude and complexity of MIW management have been developed (Mogashane *et al.* 2025). A significant milestone was achieved in 2005 with the completion of the eMalahleni Water Reclamation facility, the world's first plant to supply purified MIW to a municipality (Gunther & Mey, 2008).

As part of South Africa's Just Energy Transition (JET) seeking to decarbonise industrial operations while addressing social equity, regional inequality and environmental restoration, the Integrated Resource Plan projects the retirement of approximately

10 GW of coal-fired generation capacity by 2030, with further decommissioning thereafter, leaving only 2 operational coal-fired power stations by 2040 (DMRE, 2023). Such developments are expected to result in the closure of coal mines supplying coal-fired power operations and reduced water abstraction associated with mining and power generation.

This study assessed the emergence of a new water economy as coal mines close and coal-fired power generation is decommissioned in Mpumalanga. The study advances existing mine water research by integrating water release from energy decommissioning with regional economic modelling, enabling direct comparison of water reuse pathways in a post-coal context.

Study Area

Figure 1 shows the case study area (Mpumalanga Province), located on the northeastern part of South Africa. Mpumalanga falls within three major water management regions: the Upper Olifants Catchment Area, Upper Vaal Catchment Area, and the Inkomati–Usuthu Water Management Area. Each region has distinct hydrological and economic characteristics and management challenges, yet collectively they underpin the provincial water economy and provide the spatial framework for this study.

Methods

An assessment was undertaken to identify various water resources that will become available as coal mines close and coal-fired power stations are decommissioned. Data on the water resources were obtained from different water users within the case study province, with three primary water resources identified for the assessment. Each water resource was assessed in terms of its potential quantity, quality and reuse for productive purposes.

An economic modelling approach was applied to assess the economic value of water in supporting an irrigation pathway and estimate how increased water inputs could contribute to regional GDP growth and employment

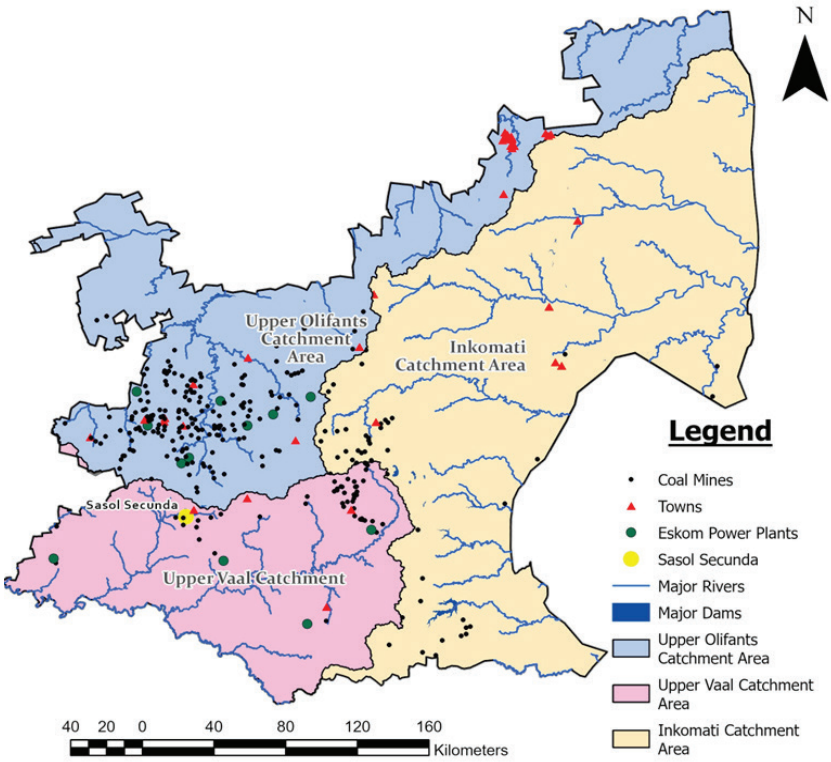

Figure 1 Study area and its land use activities.

creation through sectoral multiplier effects. This model was based on a Social Accounting Matrix (SAM) framework, which tracks the flow of income and expenditure between different sectors of the economy, including intersectoral transactions, taxes, value added, and compensation to employees. The modelling assumes that historical economic relationships and multipliers represented within the SAM remain broadly applicable under future development conditions. Employment impacts were estimated based on changes in compensation to employees and therefore represent aggregate employment related benefits rather than disaggregated job categories or skill levels.

Results and Discussion

Current water use patterns in Mpumalanga

Mpumalanga's water governance is challenged by weak institutional capacity, delayed water licensing, fragmented regulation, and competing demands from mining, agriculture, and municipalities. Historical users retain dominant access to water, while enforcement and monitoring remain inadequate. These governance gaps hinder equitable allocation, pollution control, and effective management of water and water scarcity (Helen Suzman Foundation, 2026).

Agriculture remains the largest water user, accounting for approximately 1 434 Mm^3/a, with the Inkomati–Usuthu WMA alone responsible for about 1 069 Mm^3/a. Irrigated agriculture in this region is dominated by sugarcane, citrus, and other subtropical crops that is highly dependent on regulated river abstractions and dam releases. Forestry constitutes a further major water consumer, with an estimated 450 Mm^3/a lost primarily through evapotranspiration, significantly reducing runoff and groundwater recharge, especially within the Inkomati–Usuthu WMA. Power generation has historically been a major strategic water user in Mpumalanga. Coal-fired power stations currently consume approximately 214 Mm^3/a for cooling, boiler feed, and flue gas desulfurisation. Manufacturing uses a further 179 Mm^3/a, largely concentrated in the Upper Vaal Catchment Area and driven by large industrial operations, which are expected to increase their direct water demand in the medium term (Sasol Limited, 2023).

Municipal and domestic water use amounts to approximately 202 Mm^3/a, but system inefficiencies significantly reduce effective supply. Non-revenue water losses of around 40%, largely due to ageing infrastructure and operational challenges, represent a major opportunity for demand management and water recovery (DWS, 2024).

Water release through coal-fired power stations decommissioning

The decommissioning of coal-fired power stations under South Africa's JET presents a substantial opportunity for reallocating released raw water. Table 1 provides a breakdown of the projected water demand associated with power generation up to 2035. From Table 1 the total water demand is projected to reduce to 97.4 Mm^3/a by 2035 compared to a demand of 214.1 Mm^3/a in 2024, thereby releasing about 117 Mm^3/a. By 2050, cumulative releases from all decommissioned stations are projected to reach between 200 and 245 Mm^3/a. Individual power stations such as power stations A, B, E, and H are projected to reduce water use by more than 90%, highlighting the scale of potential reallocation (Eskom, 2024). This positions power generation released water as a strategic input into a future water economy that can potentially support economic diversification and regional resilience.

Raw water is generally of relatively high quality, having been supplied through regulated inter-basin transfer schemes and managed bulk water systems. Typical raw water quality in these systems includes pH values ranging from approximately 6.5 to 8.5, total dissolved solids (TDS) concentrations between 150 and 400 mg/L, sulphate concentrations generally below 250 mg/L, and relatively low concentrations of iron and manganese (Ngamlana *et al*, 2024). These characteristics mean that the water is generally suitable for irrigation with minimal treatment requirements, although localized salinity or hardness adjustment may occasionally be necessary depending on crop sensitivity and irrigation method.

Table 1 Coal-fired power stations projected water demand for the year 2035 (Eskom, 2024).

Power station	Coal-fired power stations water demand estimates (Mm^3/a)	
	2024	2035
A	13.3	1.3
B	25.3	1.9
C	26.1	10.0
D	2.6	2.6
E	29.6	3.1
F	37.6	14.5
G	8.7	13.3
H	16.1	0.4
I	20.0	14.7
J	26.7	24.5
K	8.1	11.1
Total	214.1	97.4

Table 2 Mining-influenced water discharge in Mpumalanga by catchment (WARMS, 2023).

Discharge Method	Upper Olifants (Mm^3/a)	Upper Vaal (Mm^3/a)	Inkomati-Usuthu (Mm^3/a)
Discharge into rivers	163.5	11.5	35.1
Point Source Discharge	13.3	0.17	0.40
Total	176.8	11.7	35.5

Coal mining and mining-influenced water as a recoverable resource

Although coal mining uses a relatively modest volume of raw water compared to agriculture and power generation, its legacy impact on water resources is substantial. Coal mining in Mpumalanga generates approximately 224 Mm^3/a of MIW with the Upper Olifants Catchment Area recording the highest volumes, followed by the Inkomati–Usuthu WMA and then the Upper Vaal catchment Area as given in Table 2 (WARMS, 2023). While only a small proportion is discharged directly into rivers, extensive use of rivers for discharging excess MIW creates cumulative water quality risks and long-term environmental liabilities.

MIW in Mpumalanga coalfields typically exhibits substantially poorer water quality due to prolonged interaction with exposed geological materials, underground workings, and mine residue deposits. Typical MIW quality includes pH values between approximately 2.5 and 7.5, TDS concentrations ranging from about 1 500 to 6 000 mg/L, sulphate concentrations between 500 and 3 500 mg/L, hardness concentrations between 300 and 2 000 mg/L as $CaCO_3$, iron concentrations ranging from 1 to 200 mg/L, and manganese concentrations between 0.5 and 50 mg/L (Matebese *et al.*, 2024). These concentrations commonly exceed irrigation and industrial reuse thresholds. For irrigation reuse, South African water quality guidelines generally recommend long term TDS concentrations below approximately 450 mg/L and sulphate concentrations below approximately 200 mg/L for sensitive crops (Du Plessis *et al.* 2017). Elevated sulphates and TDS may contribute to soil salinisation and reduced crop productivity, while elevated metals may create toxicity risks and long-

term accumulation in soils. Consequently, untreated MIW is generally unsuitable for irrigation and requires treatment before reuse.

Treated municipal wastewater effluent

Mpumalanga province hosts about 76 municipal wastewater treatment plants (WWTPs) treating and discharging approximately 93 Mm^3/a into the water resource (DWS Green Drop Report, 2022). This water can be redirected for reuse purposes, however, the effluent quality is highly variable (Malakane & Maphanga 2024), with many plants not fully compliant due to operational inefficiencies, therefore requiring additional treatment for reuse purposes.

Treatment technologies and cost implications

The assessment of treatment technologies confirms that available water resources can be transformed into usable resources across a range of applications. Neutralisation using lime and limestone was identified as the most cost-effective option for treating large volumes of MIW at an estimated cost of R5.68/m^3 (USD 0.34/m^3) for non-potable uses. Biological sulphate removal offers enhanced sulphate reduction and broader industrial reuse potential, albeit at higher operational complexity and costs of around R7.40/m^3 (USD 0.45/m^3). Reverse osmosis (RO) remains essential for high-purity applications, including green hydrogen production, but at a significantly higher cost of approximately R18.61/m^3 (USD 1.13/m^3). In this regard, the eMalahleni Water Reclamation Plant represents a full scale RO plant implemented in Mpumalanga, and is currently recovering potable water from MIW sourced from several mines in the eMalahleni area (Gunther & Mey, 2008).

Economic opportunities and strategic pathways

Overall, an estimated 434 Mm^3/a of water is expected to become available in Mpumalanga through the combined effects of coal-fired power generation decommissioning, mine closure, and treated municipal effluent discharges.

The results of the economic modelling based on the SAM framework indicates that redirecting treated water to irrigation offers the most immediate and cost-effective development pathway. In this regard, reusing approximately 224 Mm^3/a for irrigation has the potential to create more than 16 000 jobs, generate R3 billion worth of direct value addition and a total economic output exceeding R26 billion when multiplier effects are considered. However, these results should be interpreted as indicative ranges of potential economic outcomes rather than precise forecasts, as they remain subject to uncertainty associated with future market conditions, infrastructure availability, policy developments, technological change, and limitations in the availability and quality of economic and water use data. Nonetheless, the irrigation pathway presents an option that supports food security, economic revitalisation and employment creation in areas affected by mine closures.

Green hydrogen production represents a longer-term strategic opportunity aligned with low-carbon industrial development. However, its feasibility depends not only on water availability and quality but also on the parallel development of renewable energy, electrolyser capacity, and supporting infrastructure. While Mpumalanga's existing grid and industrial base provide advantages for green hydrogen as a pathway, irrigation remains the most practical near-term option for maximising socio-economic benefits.

Conclusions

Mpumalanga is expected to face significant economic, environmental and social changes as South Africa moves away from coal-based energy. The study shows that water currently used in coal mining and power generation, including mining-influenced water and treated municipal effluent, could support future economic activities through productive reuse. Irrigation presents the most immediate opportunity, while green hydrogen may offer longer-term industrial potential. Achieving this transition will however require careful planning across water, energy and land-use sectors, together with improved governance,

regulatory reform, and investment in water treatment and reuse infrastructure to support sustainable regional development and long-term water security.

Acknowledgements

The authors thank the Water Research Commission for funding the project under project C2023.2024-01243. This text was language improved by using ChatGPT.

References

Department of Mineral Resources and Energy (DMRE) (2023) Integrated Resource Plan, IRP 2019. https://www.gov.za/sites/default/files/gcis_document/202401/49974gon4238.pdf

Department of Water and Sanitation (DWS) (2022) Green Drop Report. https://ws.dws.gov.za/iris/releases/Report_DPW_Rev02_29Mar22_MN%20web.pdf

Department of Water and Sanitation (DWS) (2024) National State of Water Report. https://www.dws.gov.za/Projects/National%20State%20of%20Water%20Report/Documents/National%20State%20of%20Water%20Report%202024_Final%20(002).pdf

Du Plessis M, Annandale J, Benadé N, Van der Laan M, Jooste HS, Du Preez C, Barnard J, Rodda N, Dabrowski JM, Genthe B (2017) Risk Based, Site-specific, Irrigation Water Quality Guidelines: Description of decision support system, Water Research Commission, Pretoria.

Eskom (2024) Sustainability report. https://www.eskom.co.za/wp-content/uploads/2024/12/Eskom-sustainability-report-2024.pdf

Gunther P, Mey W (2008) Selection of mine water treatment technologies for the eMalahleni (Witbank) water reclamation project. In: Proceedings of the Water Institute of Southern Africa Biennial Conference, Sun City, South Africa, 18—22 May.

Helen Suzman Foundation (2026) The institutional structure of water resource management in South Africa. https://hsf.org.za/about/about-helen-suzman/

Malakane KC, Maphanga T (2024) An assessment of the quality of effluent discharged from several wastewater treatment plants into the Crocodile River of Mpumalanga, South Africa, J. Applied Research in Water and Wastewater, 11(1) 15—23.

Matebese F, Mosai AK, Tutu H, Tshentu, ZR (2024) Mining wastewater treatment technologies and resource recovery techniques: A review, Heliyon, 10(3).

Mogashane TM, Maree, JP, Mokoena L, Tshilongo J (2025) Research Activities on Acid Mine Drainage Treatment in South Africa (1998–2025): Trends, Challenges, Bibliometric Analysis and Future Directions, Water 17, 2286. https://doi.org/10.3390/w17152286

Ngamlana Z, Malherbe W, Gericke G (2024) Association of coal fired power plants with river water quality in South Africa, Limnologica 104, 126140, https://doi.org/10.1016/j.limno.2023.126140.

Sasol Limited (2023) Water Security, CDP Water Security Report. https: //www.sasol.com/sites/default/Files/2023-2/Sasol%20CDP%20Water%20Security%202023.pdf

Staffell I, Scamman D, Velazquez Abad A, Balcombe P, Dodds PE, Ekins P, Shah N, Ward KR (2019) The role of hydrogen and fuel cells in the global energy system. Energy & Environ Sci 12(2) 463—491.

Water Use Authorisation and Registration Management System (WARMS) (2023) Coal Mining Water Use and Discharge Data for Mpumalanga, Department of Water and Sanitation, Pretoria.

Author Index

A

Abbassi, Rouzbeh 322
Abfertiawan, Muhammad Sonny 1, 248, 509
Alakangas, Lena 7, 149
Álvarez-Mejías, Lucía 23
Álvarez, Rodrigo 23
Anaya-Hilario, Isabel Magaly 74
Andersson, Monika 418
Annandale, John 298, 305
Antelo, Juan 28
Anticoi Sudzuki, Hernan Francisco 411, 445
Aquino, Norberto Jr 7
Arán, Diego 377
Arfan, Aditia Adyanugraha 509
Arzaghi, Ehsan 322
Aufdenkampe, Anthony 365

B

Bäckström, Mattias 12, 418
Bamforth, Selina Mary 18
Barrio-Parra, Fernando 23, 97
Barroso, Ana Raquel 28
Bártová, Zuzana 35, 91
Bascompta Massanes, Marc 411, 445
Batbayar, Uugankhuu 41
Bayanzul, Batdemberel 390
Bazardorj, Sod-Erdene 41, 390
Benson, David 47
Berg, Steven 231
Bernasconi, Rachele 110
Berry, Luke 66
Bettoni, Laura Nina 54
Bilek, Felix 276
Boniecki, Zip 404
Botha, Joané 494
Bottger-Gamarra, Joyce Carol 74
Boucher, Sebastien 182
Bowell, Rob 104
Briančin, Jaroslav 35
Butar Butar, Lionie 248

C

Canavessi, Juana María 104
Carabante, Ivan 28
Carruth, David 195
Carvalho, Edgar 377
Castillo, Mariel 85
Cheong, Youngwook 281
Chikanda, Frances 60
Chipakwe, Vitalis 66
Choe, Yonghwan 72
Choi, Euna 74
Choi, Uikyu 260
Choo, Tai Ho 76, 80
Choo, Yeon Moon 76, 80
Chudy, Krzysztof 501
Chun, Chan Lan 85
Čičáková, Claudia 91
Colston, Rob 517
Conde, Eduardo 97
Corin, Kirsten Claire 315
Cox, Nick 18

D

Dano, Dayle Tranz 98
Dao, Bang Duc 469
Darojat, Irfa 248
De Lange, Stephanus Steyn 292
de los Hoyos, Camilo Raúl 104
De Miguel, Eduardo 23, 97
Delport, Marion 298
Dendup, Tshewang 110
DePriest, Nathan 117
Desjardin, Mathieu 182
Diamantino, Catarina 377
Ding, Jia 124
Dogan, Tansel 169
Dong, Donglin 129
Dong, Shuning 124, 129, 213
du Plessis, Gert 157
du Preez, Kerri 136, 335
Du, Guri 142
Dufresne, Kevin 85
Dzimbanhete, Vimbainashe Lorraine 149

E

Ebel, Tom 202
Edytya, Agventy Nuranis 1
Eloka-Eboka, Andrew 487
Eulenberger, Sven 425

F

Fabián, Martin 35
Fahle, Marcus 156
Fairgray, Marlese 157
Febriana, Adithyanti 162

Fernández-Gutiérrez del Álamo, Luis 97
Fieback, Tobias 202
Fiol, Sarah 28
Flipo, Nicolas 452
Flores, Hernan 169, 176
Foster, Allan 365

__G

Ganzorig, Sunderiya 390
Gautrey, Simon 182
Gebrekristos, Robel 189
Geiger, Veronika 418
Gillane, Rosie 483
Glenis, Vassilis 432
Goetz, Damien 452
Golian, Saeed 195
Gomez, Denys Villa 162
González, Claudina 104
Grab, Thomas 202
Grohs, Ken 397
Gunathunga, Samadhi 162
Guo, Xiaoming 124, 129, 213

__H

Hagarová, Lenka 91, 208
Hahn, Florian 310, 342
Hallin, Sara 54
Hamai, Takaya 142
Hamedi, Moeen 411, 445
Hasan, Faiz 1, 248
Hedrich, Sabrina 370
Hellman, Maria 54
Herbert, Roger 54
Ho, Hsing-Jung 142
Holtzhausen, Pieter 524
Horta Ribeiro Antunes, Isabel Margarida 28
Hu, Yunhao 213
Hubbard, Paul 219
Hugman, Rui 225
Hwang, Dong Shin 76, 80
Hwang, Huijeong 72
Hwang, Hyoun-Tae 231

__I

Ignacy, Roman 310
Iizuka, Atsushi 142
Im, Dae Gyu 237
In, Hyunjin 260
Ito, Mayumi 98, 439
Izquierdo-Díaz, Miguel 23, 97

__J

Jannneck, Eberhard 370
Jenk, Ulf 425
Jeon, Jong-Wook 74
Jeon, Sanghee 439
Jeong, Jiyun 260
Ji, Sangwoo 72, 243, 281
Johansson, Maria Elisa 54
Johansson, Thomas 12
Jones, Jon 231
Jung, Jee-Hyun 267, 286
Jung, Youngkook 74

__K

Kang, Chan-Ung 360
Kang, Seyoung 74
Karlsson, Torbjörn 149
Kasmon, Umar 248
Kasza, Damian 501
Kim, Da-Som 286
Kim, Duk-Min 74, 237, 254, 267, 286
Kim, Hee Dae 76, 80
Kim, Hyeseong 260
Kim, Kang Ho 360
Kim, Su-Jin 272
Kim, Yo-Han 74
Kim, Young-Min 267, 286
Klein, Stefan 310, 342, 347
Ko, Myoung-Soo 272
Kolka, Randy 85
Kondo, Masataka 142
Krzemień, Alicja 169
Kunze, Katja 276
Kupka, Daniel 91, 208
Kwon, Hye-Lim 237
Kwon, Joon-Uk 286
Kwon, Oh-Hun 254, 267, 272
Kwon, Soondong 72

__L

Larson, Britta 85
Lau, Maximilian P. 156
Layton-Matthews, Daniel 104
Lee, Dong-Kil 281
Lee, Hayeon 72
Lee, Joon-Hak 237
Lee, Ki-Rim 267, 286
Lee, Sang Yun 260
Lee, Seon-Yong 72
Lehmann, Jonas Enno 347
Leybourne, Matthew 104
Li, Peitao 129
Licht, Gero 156
Liu, Feng 124, 129
Liu, Michael 397
Lourens, Paul Joël Havemann 292
Lund, Mark 110
Lundell, Peter 66

M

Mačingová, Eva 91
Macquela, Resego Bernice 530
Madiseng, Lesego 298, 305
Magwaza, Siboniso 305
Mainali, Bandita 322
Makate, Mavis Dineo 530
Mancewicz, Lauren 365
Mannke, Kevin 310
Manono, Malibongwe Shadrach 315
Månsson, Erik 7
Marcellin, Esteban 483
Mardonova, Mokhinabonu 322
Marinho Reis, Amélia Paula 28
Marquez, Antonio 169
Martins, Carlos 377
Masaki, Yusei 142
Mazadiego, Luis 97
McGann, Matthew P. 328
McKenna, James 432
Merckel, Ryan 136
Merckel, Ryan David 335
Miller, Killian 231
Miller, Savannah 47
Mkhize, Innocentia Gugulethu 487
Molaba, Leshego 494
Montalvo-Piñeiro, Jaime 23
More, Kagiso 494
Morton, Kym 524
Mugova, Elke 342, 347, 494
Mulyana, Bagja 509
Munkhzorig, Munkhtuya 390
Murton, Steven 404
Myagmar, Bilguun 390

N

Nakamura, Fugo 60
Ñancucheo, Iván 162
Naranbaatar, Enkhjin 390
Nguyen, Thao Bach 469
Nikolov, Alexander 310
Nikutta, Simon E. 176, 348, 458
Nordstrom, Darrell Kirk 354
Novikova, Ksenia 7, 66
Ntwampe, Seteno Karabo Obed 487
Nyambuu, Purevsuren 390

O

October, Lisa Louise 315
Oh, Chamteut 243
Oh, Jung Geun 76, 80
Oh, Youn Soo 260, 360
Oppelt, Lukas 202
Ordoñez, Almudena 23
Ortega, Pablo 225, 365
Otake, Tsubasa 60
Ottermann, Helga 298

P

Pak, Seungil 243
Park, Hyun-Sung 360
Park, Ilhwan 98, 439
Park, Jae-Hyun 286
Park, Jeong Sik 72, 267, 286
Park, Seong-Sook 267
Park, Young-Jin 231
Păsculescu, Vlad Mihai 169
Paulsson, Oscar 149
Pearce, Steve 397
Pinka, Jana 370
Pinto, Mariana 377
Potter, Hugh 18
Pradhana, Adhika Catra 384
Prieto-Estrada, Andres 365
Puntsag, Tamir 41, 390
Purevsuren, Uuganbayar 41

R

Raithel, Fritz 202
Raynor, Mark 195
Reina, Pablo 97
Reker, Bastian 169
Requena-Mendizabal, Manuel 74
Resabal, Vannie Joy 98
Ristiaramdani, Nur Latifa 248, 509
Rivera Blanco, Edward 74
Roberts, Mark 397
Röder, Eric 156
Rodriguez-Vasquez, Carmen 74
Ronne, Erik 7
Ronne, Ksenia 66
Rousseau, Pierre 404
Rudolph, Tobias 176

S

Sädbom, Stefan 12, 418
Säfström, Maria 12
Sajid, Abeer 411, 445
Salifu, Musah 7
Salmi, Tomas 54
San, Hkaung 60
Santos-Conde, Alina Liliana 74
Santos, Erika 377
Sapsford, Devin 18
Saputra, Yudha Hadiyanto Eka 384
Sartz, Lotta 12, 418
Sato, Tsutomu 60
Satriawan, Azwar 397
Schmidt, Nadja 425
Sededpurev, Otgonbaatar 390

Serrano-García, Humberto 23, 97
Servan-Vargas, Mario 74
Shahid, Muhammad Kashif 322
Shi, Hongjie 129
Skifa, Nadia 432
So, Joanna 463
Sokolova, Ekaterina 54
Soto, Fernanda 483
Southam, Gordon 162
Spirnak, Rachel 117
Steyn, Martin 305
Stimpfl, Marilena 404
Strauss, Harald 348, 458
Sudicky, Edward 231
Sugiura, Itsuki 439
Sukati, Sakhiwo 305
Sun, Wenjie 129
Suup, Malin 66
Syafila, Mindriany 1

__T

Tabelin, Carlito 98, 439
Taghavi, Seyed Mostafa 411, 445
Taki, Mariam 452
Tanner, Phil 298, 305
Teichert, Barbara M. A. 176, 348, 458
Thompson, John 85
Thomson, Heather 463
Tomasula, Paul 365
Torres-Aguilar, Carlos Cheito 74
Totsche, Oliver 477
Tran, Tuan Quang 469
Trusler, Graham 189
Tulganyam, Samdanjigmed 390
Tuncer, Elif 54

__U

Ulrich, Maik 477
Utkin, Valentina 494

__V

Valente, Teresa Maria 28
van der Burgh, Gerhard 298
Vasques, Isabela 28
Vermeulen, Petrus Daniël 292
Vernengo Lezica, Ignacio 404
Verri Kozlowski, Alejandro 104
Villa Gomez, Denys 483
Vu, Hien Thu 469

__W

Waanders, Frans Boudewijn 487
Wajs, Jarosław 501
Walls, Justin 463
Wang, Tiantian 129
Washburn, Spencer 85
Weber, Anne 156
Webster, Luke 483
Weinand, Svenja 458
Westermann, Sebastian 458
White, Jeremy 225, 365
Witbooi, Jan Bonakele 487
Witthüser, Kai 298
Wolkersdorfer, Christian 494
Worsa-Kozak, Magdalena 501
Wu, Jinxin 213
Wu, Qiang 129
Wunderlich, Timm 202

__Y

Yadamsuren, Oyunchuluun 390
Yasya, Heksantia Rahmadinda 509
Yim, Gil-Jae 72, 243, 281
Ylipää, Mattias 54
Yoon, Daewan 76, 80
Yu, Qingchun 213
Yun, Seong-Taek 237

__Z

Zeman, Josef 91
Zeng, Yifan 129
Zhang, Wenzhong 124, 213
Zhang, Xiyu 129, 213
Zhou, Wanfang 516
Zielke-Olivier, Josepha Simone Doris Renata 292, 298
Ziukelis, Laurence 517
Zug, Sebastian 156
Zvimba, John Ngoni 524, 530

Keyword Index

A

abandoned mine areas 76
abandoned mine lands 117
abandoned mine 494
Acid Metalliferous Drainage (AMD) 162
Acid Mine Drainage Measure 97
Acid mine drainage see AMD
acidic mine water see AMD
Acidithiobacillus ferrooxidans 208
Acidophiles 35
active treatment 267
adaptation 477
Adsorbent 260
adsorption 28
Agriculture 298
airborne survey 501
Alginate beads 72
algorithm 254
Alkaline mine drainage 360
alkalinity 276
AMD treatment 397
AMD 72, 76, 370, 404
Analytic Hierarchy Process 411
aquifer testing 47
arsenate 28
arsenic adsorption 74
Arsenic 7, 243, 272, 360
Artificial neural network 487
asbestos mine 494
autonomous surface vehicle (ASV) 156

B

Bayesian isotope mixing 104
bioavailability 322
Biological sulfate reduction 54, 136, 335, 487
biological treatment 85
bioprocess engineering 483
Bioreactor efficiency 54
bioremediation 162
birnessite 237
Brumadinho failure 432
BSR neutralised AMD 305

C

Cam Pha 469
carbon flow 142
carbon neutrality 142
Carbon sequestration 60
Catchment 195
chalk 276
chemical dosage 267
chemical neutralization 80
chemical stabilization 80
chromium hexavalent 248
circular economy 35, 98, 445, 483
climate change 452
climate 458
CO_2 emission 142
Coal mining 530
Column settling test 281
complexation 149
Compliance to legislation 41
Composite Sustainability Index 411
conservative tracers 110
copper 452
Critical metals recovery see Critical Raw Materials
Critical Raw Materials 169, 411, 445, 483

D

Data Acquisition Systems 97
data assimilation 225
data integration 169
data space 169
Deep-buried coal seam 213
degraded soils 377
depth profiles 12
design 254
Dewatering 516
Diamond mine 182, 516
discharge 12
disequilibrium 354
Dissolved organic matter 129
District heating network 310
Drilling 189
drone sampling 157
dry tailings 1
Dynamic mesh adaptation 231

E

Ecological Risk Assessment 322
Education 418
Eh 354
Electrification 66

Electrochemical treatment/approach 66, 85
electrocoagulation 243, 248
Electrodialysis 66
endmember mixing analysis 110
Enhanced Rock Weathering 60
Entropy 445
environmental monitoring 156, 501
Environmental Rehabilitation 377
eosin y 494
eSwatini 494
evaporation 390
Evolving topography 231
exploration 189

F

Faults 292
feasibility study 347
Fenton treatment 7
Fe-oxidizing bacteria 91
field demonstration 243
Field operation 54
Flotation 315
flow 365
Fluoride 272
free draining column leaching 1
freshwater ecosystems 322
Fuzzy Delphi 445

G

geochemical modelling 348
geochemistry 189, 365
Geotextile pools 384
Geotextile tubes 384
Geothermal Energy 347
Geothermal potential 202
Geothermal 310
Gobi Desert 41
goethite 28
GoldSim 517
Graben 292
Green hydrogen 530
Green rust 397
groundwater monitoring 425
Groundwater–tunnel interaction 231

H

hard coal mining 347
HDS neutralised AMD 305
Heat Exchangers 202
Heating and Cooling 202
HEC-HMS 195
hexavalent chromium 1
high-sulfidation 104
Hindered settling 281
hydrated lime 267
Hydraulic retention time 487
Hydrochemical evolution 129
hydrodynamics 494
hydrogeochemistry 110, 469
hydrogeological conceptual site mode 516
hydrogeology 189, 365, 469
Hydrologic modelling 195
hydrology 452
hyperspectral imaging 176

I

Indicator Weighting 411
Industrial 292
In-lake 276
In-situ stress 213
Integrated surface–subsurface modeling 231
integration 189
iron electrode 243
iron oxidation 35, 91
iron oxyhydroxides 397
Irrigation 530

J

Just Energy Transition 530

K

Karst 516
kinetic study 1
Königstein mine 425

L

land reuse 169
leaching 149
limestone 276
Linear flow channel reactor 487
Lo Tri coal mine 469

M

machine learning 225
Managed Aquifer Recharge 129
Manganese sludge 72
manganese treatment 74
Mária mine water 208
MCMC 47
meromictic 182
metal mine water 18
metal recycling 98
metals recovery 91
microbiology 370
microencapsulation 439

mine closure 219, 501
Mine dewatering 231
Mine drainage sludge 360
mine drainage treatment design software 267
mine drainage treatment facilities 254
Mine drainage 60, 243, 281
mine flooding 425, 501
Mine Reclamation 260
Mine Waste Management 411
Mine waste valorisation 483
mine wastewater 7
mine water chemistry 286
mine water disaster 124
mine water energy 347
Mine Water Geochemistry 348
mine water geothermal 342
mine water heat 342
mine water irrigation 305
mine water management 452
Mine water potential study 202
mine water rebound 348
Mine water sharing 524
Mine water treatment 384
Mineral Pigments 35
mining environment management 80
mining lakes 110
Mixture toxicity 322
Mn oxides 237
modelling 517, 524
Monitoring 157
MTES 342

N

Neutral pH 272
neutralization 66, 76
Ni adsorption 237
nickel extraction waste 1
nickel mine 248
nickel slag 1
non-Newtonian 432

O

open pit 501
oxidation 397
Oyu Tolgoi mine 41

P

passive treatment 18, 237, 335, 370
Peru 74
PHREEQC 517
PHREEQ-N-AMDTreat 267
Pilot-scale experiment 360
Pit Lakes 156, 157, 182, 219, 509, 517
Pollution Migration 292
post-mining 176, 347, 509
precipitation 76, 458
prevention 439
Pseudomonas fluorescens 208
Pumping test 516
pyrite oxidation 286

R

redox 354
reducing the potential for secondary contamination 80
remediation 98, 117
remote sensing 176
Renewable Energy 310
resource estimation 169
Resource utilisation 66
restoration 117
Reuse 517
Rhine-Ruhr-Region 310
Riemann solver 432
Rožňava 208

S

Salinity 315
São Domingos mine legacy site 377
schwertmannite 28
Seawater 315
secondary metal resources 98
Sediment management 384
Sedimentation 281
Sediments 23
Self-healing of aquiclude 213
sequential extraction 7
signatures for water tracing pathways 390
slag reactor 74
sludge 7
SMA loss method 195
Social license to operate 418
socioeconomics 298
software 254
soil in abandoned mine areas 80
Soil Stabilizer 260
solar power 243
Sorption 72, 272
South Africa 136
Species Sensitivity Distributions 322
stabilization 76
stable isotopes 104, 286, 390
storm storage 463
sulfate reduction 348, 370
sulfate source proportions 104
sulfate-reducing bacteria 162

sulfide oxidation 390
sulfide passivation 439
Sulfur Cycling 348
sulfur isotopes 458
sulfur recovery 335
Sulfur 85
Surface Runoff Modeling 23
surrogate 225
sustainability 509
sustainable future strategies 477
Sustainable mine drainage treatment 360
Sustainable mining 445
Sweden 418
Synthetic biology 483
Synthetic Zeolite 260

T

Tailings 60, 370, 404, 463
tailing ponds 176
Tailings flow 432
Tailings reprocessing 445
tailings sludge 169
Tailings storage 328
techno-economics 335, 445
Technosols 377
Temperature 54
terminal groundwater sink 328
testing 97
tetrahedrite 208
TOPSIS 445
Total suspended solids 281
Trace Elements 23
tracer test 494
transport 365
treatment 12

U

UAV see uncrewed aerial vehicle
uncertainty 47, 225
uncrewed aerial vehicle (UAV) 156, 157, 176
underground mining 469
Underground reservoirs 524
unmanned aerial system see uncrewed aerial vehicle
upscaling 85
uranine 494
uraninite 149
Uranium mining 425
Uranium 149

V

Valdarcas mine 28
Valorization 72
Vertical Flow Reactor 18
VFR 74
Victor Mine 182

W

Waste Facility 292
water balance model 509
Water balance 404
Water management 41, 477
Water monitoring 41
Water permeability 213
water quality evolution 124
Water reuse 315
Water scarcity 524
water stewardship 219
Water stress 452
water treatment 276
Water Use 530
water-rock interaction 124
Water-scarce region 524
watersheds 117
weathering 149
well performance 47
Western China mining area 124
Woodchips 54

Z

zinc 18

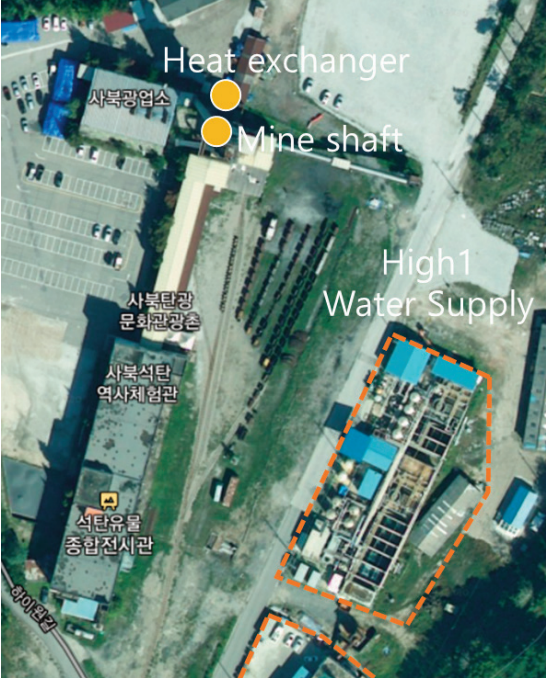

Dear IMWA 2026 Participant, dear Reader!

We are delighted to welcome you to IMWA 2026 in South Korea, only the second IMWA conference to be held in Asia during the Association's 47-year history.

The presentations and discussions at IMWA 2026 reflect the latest advances in mine water science and engineering, including innovative modeling approaches, software applications and emerging technologies for mine water management. Through these contributions, IMWA 2026 aims to support the development of smarter, more sustainable and more efficient solutions for mine water challenges worldwide. Several presentations also address climate change, carbon sequestration and carbon accounting, highlighting the growing importance of environmental sustainability in the mining sector. At the same time, hydrogeology, geochemistry, mine water control and treatment, water reuse and geothermal applications remain central themes of the conference.

Ninety-two presentations were included in the conference program, comprising 75 oral presentations and 17 poster presentations, with more than 200 participants representing around 30 countries. This broad international participation demonstrates the continued strength and diversity of the global mine water community.

All papers included in this volume have undergone rigorous peer review to ensure a high scientific standard. We sincerely thank all authors, reviewers, organizing committee members, sponsors and participants whose contributions made IMWA 2026 possible.

We hope that this conference and its proceedings will further strengthen international collaboration in mine water research and practice, while encouraging greater participation from Asia and other emerging regions. We trust that the knowledge shared through IMWA 2026 will contribute to the advancement of sustainable mine water management for years to come.

Duk-Min Kim | Conference Chair
Ritva Mühlbauer | IMWA 2026 Proceedings Editor
Christian Wolkersdorfer | IMWA President

ISBN: 978-3-9825293-4-9